

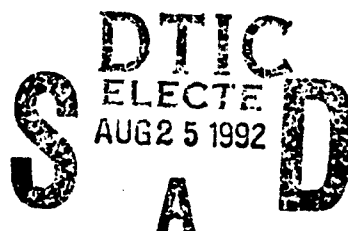
WL-TR-92-3063

AD-A255 527



**QUANTITATIVE FEEDBACK THEORY  
SYMPOSIUM PROCEEDINGS**

Constantine H. Houpis  
Phillip R. Chandler



August 1992

Final Report for August 1992

Reproduced From  
Best Available Copy

Approved for Public Release: Distribution Is Unlimited.

**20000410151**

FLIGHT DYNAMICS DIRECTORATE  
WRIGHT LABORATORY  
AIR FORCE SYSTEMS COMMAND  
WRIGHT-PATTERSON AIR FORCE BASE, OHIO 45433-6553

422730  
618 92-23492


92 8 24 001

## NOTICE

WHEN GOVERNMENT DRAWINGS, SPECIFICATIONS, OR OTHER DATA ARE USED FOR ANY PURPOSE OTHER THAN IN CONNECTION WITH A DEFINITELY GOVERNMENT-RELATED PROCUREMENT, THE UNITED STATES GOVERNMENT INCURS NO RESPONSIBILITY OR ANY OBLIGATION WHATSOEVER. THE FACT THAT THE GOVERNMENT MAY HAVE FORMULATED OR IN ANY WAY SUPPLIED THE SAID DRAWINGS, SPECIFICATIONS, OR OTHER DATA, IS NOT TO BE REGARDED BY IMPLICATION, OR OTHERWISE IN ANY MANNER CONSTRUED, AS LICENSING THE HOLDER, OR ANY OTHER PERSON OR CORPORATION; OR AS CONVEYING ANY RIGHTS OR PERMISSION TO MANUFACTURE, USE, OR SELL ANY PATENTED INVENTION THAT MAY IN ANY WAY BE RELATED THERETO.

THIS TECHNICAL REPORT HAS BEEN REVIEWED AND IS APPROVED FOR PUBLICATION.

  
Phillip R. Chandler  
Project Engineer

  
JAMES K. RAMAGE, Chief  
Control Systems Development Branch  
Flight Control Division



WILLIAM E. GABEL, Col, USAF  
Chief, Flight Control Division

IF YOUR ADDRESS HAS CHANGED, IF YOU WISH TO BE REMOVED FROM OUR MAILING LIST, OR IF THE ADDRESSEE IS NO LONGER EMPLOYED BY YOUR ORGANIZATION, PLEASE NOTIFY WL/FIGXI, WRIGHT-PATTERSON AFB, OH 45433-6553 TO HELP MAINTAIN A CURRENT MAILING LIST.

COPIES OF THIS REPORT SHOULD NOT BE RETURNED UNLESS RETURN IS REQUIRED BY SECURITY CONSIDERATIONS, CONTRACTUAL OBLIGATIONS, OR NOTICE ON A SPECIFIC DOCUMENT.



**REPORT DOCUMENTATION PAGE**Form Approved  
OMB No. 0704-0188

Public reporting burden for this collection of information is estimated to average 1 hour per response, including the time for reviewing instructions, searching existing data sources, gathering and maintaining the data needed, and completing and reviewing the collection of information. Send comments regarding this burden estimate or any other aspect of this collection of information, including suggestions for reducing this burden, to Washington Headquarters Services, Directorate for Information Operations and Reports, 1215 Jefferson Davis Highway, Suite 1204, Arlington, VA 22202-4302, and to the Office of Management and Budget, Paperwork Reduction Project (0704-0188), Washington, DC 20503.

<b>1. AGENCY USE ONLY (Leave blank)</b>		<b>2. REPORT DATE</b> August 1992	<b>3. REPORT TYPE AND DATES COVERED</b> Final, August 1992	
<b>4. TITLE AND SUBTITLE</b> Quantitative Feedback Theory Symposium Proceedings			<b>5. FUNDING NUMBERS</b> PE: 62201F PR: 2403 TA: 00 WU: 23	
<b>6. AUTHOR(S)</b> Constantine H. Houpis Phillip R. Chandler				
<b>7. PERFORMING ORGANIZATION NAME(S) AND ADDRESS(ES)</b> Flight Control Division Flight Dynamics Directorate Wright Laboratory Air Force Systems Command Wright-Patterson AFB OH 45433-6553 Dept of Electrical Engineering Air Force Institute of Technology Wright-Patterson AFB OH 45433			<b>8. PERFORMING ORGANIZATION REPORT NUMBER</b>  WL-TR-92-3063	
<b>9. SPONSORING / MONITORING AGENCY NAME(S) AND ADDRESS(ES)</b> Flight Control Division, Flight Dynamics Directorate Wright Laboratory Air Force Systems Command Wright-Patterson AFB OH 45433-6553			<b>10. SPONSORING / MONITORING AGENCY REPORT NUMBER</b>	
<b>11. SUPPLEMENTARY NOTES</b>  Prepared in cooperation with Purdue University, School of Mechanical Engineering.				
<b>12a. DISTRIBUTION / AVAILABILITY STATEMENT</b>  Approved for public release, distribution is unlimited.			<b>12b. DISTRIBUTION CODE</b>	
<b>13. ABSTRACT (Maximum 200 words)</b>  This document contains the proceedings of Quantitative Feedback Theory (QFT) Symposium at Hope Hotel, WPAFB, OH on 2-4 August 1992. Included are QFT tutorials, and session papers on application to a wide variety of physical systems. The sessions include (1) Theory and Design, (2) Aerospace, and (3) Industrial applications. QFT is a Multiple-Input Multiple-Output (MIMO) frequency based synthesis technique that explicitly employs quantitative performance standards and plant uncertainty during controller design.				
<b>14. SUBJECT TERMS</b> Robust Control, Multivariable Control, QFT, Control Theory, Feedback, Flight Control, Computer-Aided Control System Design, Synthesis, Quantitative			<b>15. NUMBER OF PAGES</b> 624	
			<b>16. PRICE CODE</b>	
<b>17. SECURITY CLASSIFICATION OF REPORT</b> Unclassified	<b>18. SECURITY CLASSIFICATION OF THIS PAGE</b> Unclassified	<b>19. SECURITY CLASSIFICATION OF ABSTRACT</b> Unclassified	<b>20. LIMITATION OF ABSTRACT</b> UL	

# FOREWORD

Since 1980 there has been a tremendous advance in the state-of-the-art of QFT. This is due primarily to the association of Wright Laboratory's Flight Dynamics Directorate (WL/FIG) with the Department of Electrical and Computer Engineering of the Air Force Institute of Technology (AFIT/ENG) and with Professor Issac M. Horowitz, the founder of QFT. Numerous technical publications by WL/FIG and AFIT/ENG researchers have resulted from this association. This symposium is a testimonial to these researchers and is intended to transfer many of their results to the general public.

DTIC QUALITY INSPECTED 5

Accession For	
NTIS CAA&I	<input checked="" type="checkbox"/>
DTIC TAB	<input type="checkbox"/>
Unannounced	<input type="checkbox"/>
Justification	
By	
Distribution /	
Availability Codes	
Dist	Avail and/or Special
A-1	

# TABLE OF CONTENTS

Participating Institutions .....	1
Operating Committee .....	2
Plenary Address	
I. M. Horowitz .....	9
Banquet Speech	
E. Eitelberg .....	15
List of QFT Symbols	
C. H. Houpis .....	19
Air Force Sponsorship of QFT	
P. Chandler .....	25

## QFT TUTORIALS CHAIRMAN: C. H. Houpis

Overview of MISO Quantitative Feedback Theory (QFT) Technique	
C. H. Houpis .....	31
Synthesis of Uncertain MIMO Feedback Systems by QFT - A Tutorial	
Oded Yaniv .....	39

## SESSION 1A - THEORY AND DESIGN CHAIRMAN: F. N. Bailey, University of Minnesota VICE-CHAIRMAN: Y. Chait, University of Massachusetts

A Delta Transform Approach to Loop Gain-Phase Shaping Design of Robust Digital Control Systems	
A. J. Punyko, F. N. Bailey .....	49
QFT, the UHB, and the Choice of the Template Nominal Point	
D. J. Ballance, P. J. Gawthrop .....	74
Stability Analysis Using Nichols Charts	
N. Cohen, Y. Chait, O. Yaniv, C. Borghesani .....	80
QFT: Methods for Synthesis of Optimal Controls	
D. F. Thompson .....	104
Quantitative Feedback Design of Robust Control Systems	
O. D. I. Nwokah, S. Jayasuriya, D. F. Thompson .....	125

**SESSION 2A - AEROSPACE APPLICATIONS**  
**CHAIRMAN: F. Barfield, Wright Laboratory**  
**VICE-CHAIRMAN: P. Chandler, Wright Laboratory**

<b>A Robust Digital Flight Control System for an Unmanned Research Vehicle Using Discrete Quantitative Feedback Theory</b>	
D. J. Lacey, I. M. Horowitz, C. H. Houps, S. N. Sheldon .....	154
<b>Combined QFT and LQG/LTR Approach to AIAA Controls Design Challenge</b>	
C-Y Chang, T-S Chang, S. H. Wang, C. W. Chen.....	164
<b>Vehicular Longitudinal Control Using Quantitative Feedback Theory</b>	
S. Gardner, S. Fadali .....	170
<b>Multi-Input Multi-Output Flight Control System Design For the YF-16 Using Nonlinear QFT and Pilot Compensation</b>	
R. B. Miller, I. M. Horowitz, C. H. Houps, F. Barfield .....	178
<b>Robust Crossfeed Design for Hovering Rotorcraft</b>	
D. R. Catapang, M. B. Tischler, D. J. Biezad .....	190

**SESSION 3A - INDUSTRIAL APPLICATIONS**  
**CHAIRMAN: A. E. Bentley, Sandia National Laboratories**  
**VICE-CHAIRMAN: M. Franchek, Purdue University**

<b>Arc Welding Penetration Control Using Quantitative Feedback Theory</b>	
A. E. Bentley .....	212
<b>Pinch Weld Quality Control Using Quantitative Feedback Theory</b>	
A. E. Bentley .....	238
<b>Storage Size from Process Control Bandwidth Specification and the Other Way Around</b>	
E. Eitelberg .....	264
<b>QFT and Robust Process Control</b>	
P. S. V. Nataraj .....	275
<b>QFT-Like Design of an Idle Speed Controller for an Uncertain Fuel-Injected Engine</b>	
S. Rober, S. Koffman, M. Franchek.....	285
<b>Applying QFT to Benchmark Problems</b>	
B. Azvine, R. J. Wynne .....	296

### **SESSION 1B - MULTIVARIABLE SYSTEMS**

**CHAIRMAN: M. B. Tischler, NASA Ames Research Center**

**VICE-CHAIRMAN: O. Yaniv, Tel-Aviv University**

<b>General Sensitivity Expressions for MIMO Systems</b>	
C. Verde .....	315
<b>A MIMO P.M. System Synthesis Theory with Plant Uncertainties</b>	
J-L Lai, B-C Wang .....	334
<b>A MIMO Uncertain System with Nonlinear Compensator</b>	
R-C Chu, B-C Wang .....	355
<b>Direct Quantitative Feedback Theory Design for Multi-Input Multi-Output Systems</b>	
M. S. Park, Y. Chait, J. Rodrigues .....	383
<b>QFT Design of Earthquake Simulator Machines</b>	
A. J. Clarke .....	398
<b>A Model Reference Quantitative Feedback Design Theory and Aircraft Engine Application</b>	
C. H. Yau, J. E. Gallagher, O. D. I. Nwckah .....	399

### **SESSION 2B - THEORY AND DESIGN**

**CHAIRMAN: S. Jayasuriya, Texas A & M University**

**VICE-CHAIRMAN: D. F. Thompson, Ford Motor Corporation**

<b>Control System Design for Parametric Uncertainty</b>	
L. H. Keel, S. P. Bhattacharyya .....	435
<b>Design of Feedback Systems Using Kharitonov's Segments in Quantitative Feedback Theory</b>	
I. Fialho, V. Pande, P. S. V. Nataraj .....	457
<b>QFT and Irrational Transfer Functions: The Design of Feedback for Distributed-Parameter Structures</b>	
M. McCormick, J. W. Brewer, M. Hafez .....	471
<b>Stability of Quantitative Feedback Designs and the Existence of Robust QFT Controllers</b>	
S. Jayasuriya, Y. Zhao .....	503
<b>Quantitative Design of a Class of Nonlinear Systems with Parameter Uncertainty</b>	
S. Odlak, C. Bari, P. O. Gutman .....	542

**QFT CAD TUTORIAL**  
**CHAIRMAN: Gary B. Lamont**

<b>The Loop Gain-Phase Shaping Design Programs</b> F. N. Bailey, C. H. Hui, A. Punyko .....	565
<b>Development of an Analog MIMO QFT CAD Package</b> R. R. Sating, I. M. Horowitz, C. H. Houpis .....	575
<b>Multiple Input Single Output QFT CAD User Manual</b> O. Yaniv .....	585
<b>Object-Oriented Design and Programming of QFT CAD Environment</b> W. E. Bell, R. L. Ewing, I. M. Horowitz, G. B. Lamont, F. L. Trevino .....	595

## **PARTICIPATING INSTITUTIONS**

**AIR FORCE INSTITUTE OF TECHNOLOGY  
C. H. Houpls**

**AIR FORCE WRIGHT LABORATORY  
S. Sheldon, P. Chandler**

**UNIVERSITY OF MINNESOTA  
F. N. Bailey**

**WAYNE STATE UNIVERSITY  
R. D. Barnard**

**UNIVERSITY OF MASSACHUSETTS  
Y. Chait**

**FMC CORPORATION  
C. W. Chen**

**ISRAEL INSTITUTE OF TECHNOLOGY  
P. O. Gutman**

**UNIVERSITY OF CALIFORNIA-DAVIS  
J. Brewer, S. H. Wang**

**OAKLAND UNIVERSITY  
M. Zohdy**

**TEXAS A & M UNIVERSITY  
S. Jayasuriya**

**PURDUE UNIVERSITY  
O. Nwokah**

**SANDIA NATIONAL LABORATORIES  
L. N. Tellerico**

**TEL-AVIV UNIVERSITY  
O. Yaniv**

**UNIVERSITY OF GLASGOW  
P. Gawthrop**

**UNIVERSITY OF DURBAN-WESTVILLE  
E. Eitelberg**

# **QFT SYMPOSIUM**

## **OPERATING COMMITTEE**

### **GENERAL CHAIRMAN**

**Constantine H. Houpls**  
School of Electrical Engineering  
AFIT/ENG  
WPAFB, OH 45433

### **ARRANGEMENTS CHAIRMAN**

**Captain Stuart Sheldon, USAF**  
WL/FIGL  
WPAFB, OH 45433

### **PAPERS CHAIRMAN**

**Osita D. I. Nwokah**  
School of Mechanical Engineering  
Purdue University  
West Lafayette, IN 47907-1288

### **REGISTRATION CHAIRMAN**

**Robert L. Swisher**  
Universal Technology Corporation  
4031 Colonel Glenn Highway  
Dayton, OH 45431-1600

### **CAD CHAIRMAN**

**Gary Lamont**  
School of Electrical Engineering  
AFIT/ENG  
WPAFB, OH 45433

### **PUBLICATIONS CHAIRMAN**

**Phillip R. Chandler**  
WL/FIGX  
WPAFB, OH 45433

### **FINANCE CHAIRMAN**

**Bruce Clough**  
WL/FIGL  
WPAFB, OH 45433

### **PUBLICITY CHAIRMAN**

**Matt Franchek**  
School of Mechanical Engineering  
Purdue University  
West Lafayette, IN 47907-1288





**GENERAL CHAIRMAN**  
**Dr. Constantine H. Houpis**



**CAD CHAIRMAN**  
**Dr. Gary Lamont**



**PAPERS CHAIRMAN**  
**Dr. Osita D. I. Nyokshi**

# PROGRAM COMMITTEE



**Captain S. Sheldon**



**Finley Barfield**



**Peggy Cassidy**



**Matt Franchek**



**Phillip Chandler**



**Lynn Merica**



**Bruce Clough**



**Jim Coughlin**

## PLENARY SPEAKER



**Dr. I. M. Horowitz**

Dr. Horowitz is the originator and developer of the Quantitative Feedback Theory (QFT) for control systems design. He is a professor at the University of California, Davis and the 1992 recipient of the ASME Dynamic Systems and Control Division "Rufus Oldenburger Award". As a Distinguished Visiting Professor at the Air Force Institute of Technology for the past 7 years, he has been co-advisor on numerous thesis research efforts. His past achievements include engineering professorships at the Weizmann Institute of Science, Israel, University of Colorado-Boulder, and City University of New York.

QFT is the first quantitative feedback design in control history. QFT is widely used in Japan and Russia. Dr. Horowitz has extended QFT from SISO, to MIMO, to discrete time, to non-minimum-phase plants, to time-varying plants, to nonlinear systems, and to the use of non-LTI compensation.

## BANQUET SPEAKER



**Dr. E. Eitelberg**

Dr. Eitelberg is a Professor and Head of the Department, Electrical Engineering, at the University of Durban-Westville, Durban, South Africa.

Dr. Eitelberg is a native of Tartu, Estonia and received his Dr. Ing. habil. in 1982 at the University of Karlsruhe, Karlsruhe, West Germany. He is a researcher in control engineering and has performed extensive research on power plant detailed modeling and computer simulation for KWU/Siemens, Germany. He developed a new numerical "absolutely" stable modular simulation method for very large nonlinear systems.

Dr. Eitelberg has over 60 publications; including 6 books, 40 scientific journal papers, and two patents.

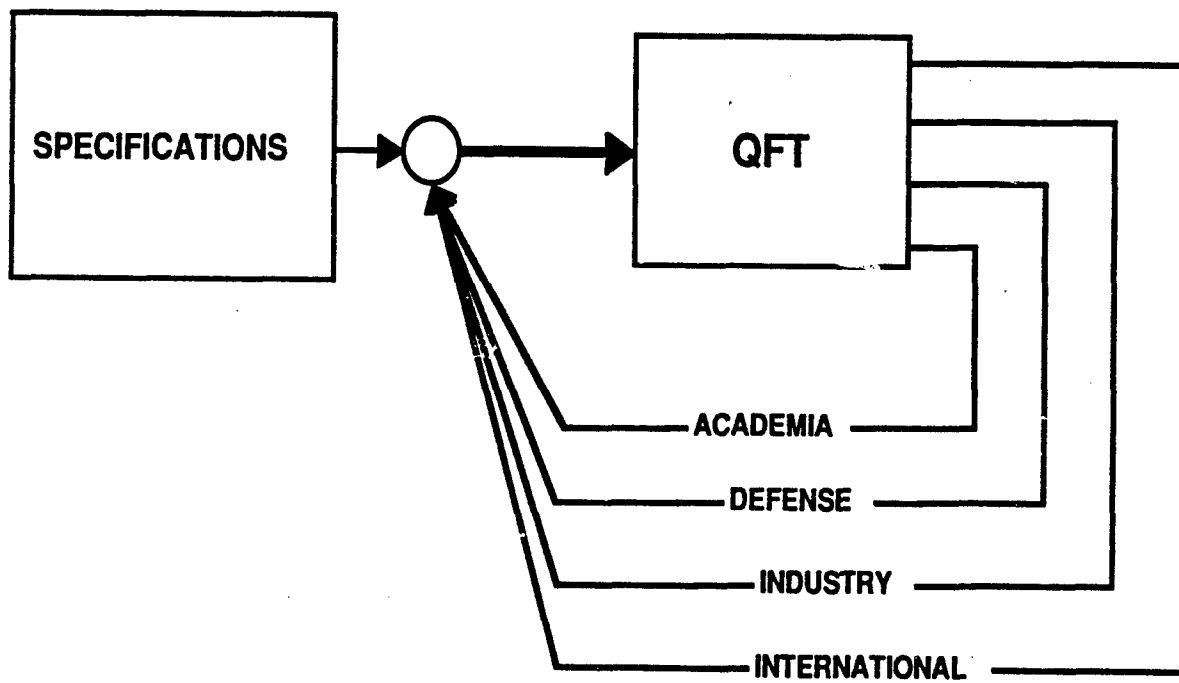
# MIMO QFT TUTORIAL



**Dr. Oded Yaniv**  
**Faculty of Engineering**  
**Electrical Engineering-Systems**  
**Tel-Aviv University, Tel-Aviv, Israel**

Dr. Yaniv received his Ph.D. from Weizmann Institute of Science under the guidance of Dr. Horowitz. He has been with Tel-Aviv University since his graduation. He is active in QFT research and computer aided design tools.

# TECHNOLOGY TRANSFER



# PLENARY ADDRESS

## QFT - PAST, PRESENT AND FUTURE

Isaac Horowitz, Professor Emeritus

University of California, Davis

Davis, CA 95616

and

Weizmann Institute of Science

Rehovot, Israel

### ABSTRACT

Quantitative feedback theory (QFT) is an engineering science devoted to the problem of achieving precise performance specifications, despite high uncertainty in the means of producing the desired outputs. It was an outgrowth of the author's work in Active Network Synthesis. Early in its history it chose the input-output system description, frequency response and the loop transmission as its principal and natural design tools. QFT is especially oriented towards the practical designer in its emphasis on the cost of feedback, design transparency, and the mathematical simplicity of its design methods. QFT has developed such techniques for SISO, MIMO, single and multiple loop, linear and nonlinear, lumped and distributed plants. But it is as yet in its infancy, pointing to vast, available problem areas.

### 1. Network Synthesis Origin

My role in the development of QFT was influenced by my prior work in Modern Network Synthesis, especially Active Network Synthesis. A set of building blocks is assumed available: resistors (R), inductors (L), capacitors (C) in passive network synthesis; R, C and transistors in active RC synthesis. One is to design a function, usually the transfer function, by combining these elements in a systematic manner. Modern type "existence" theorems were rare in those days because it was assumed that primarily engineering research was supposed to show how to build practical systems rather than just prove that systems could be built with idealized elements. So the theorems were mostly implicit, constructive in nature, usually presenting design techniques based on canonical structures. As the subject advanced, the practicality of the design constraints was increased such as element size, value spread and dissipation factors.

My interest was in Active RC synthesis. The poles of RC transfer functions are confined to the negative real axis. Feedback around the active element can move them into the complex plane. But active element parameters usually have much greater variation than passive elements. So in the problem statement I would list their maximum variation ( $v_a$ ), and the assigned tolerances ( $v_d$ ) on the desired transfer function. In a narrow band filter,  $v_d$  would be very small. Find a synthesis technique for this purpose, assuming some R, C elements could be built with arbitrary small variation. There are two problems here. One is the filter problem, to obtain the desired nominal transfer function. The second is the sensitivity problem, to obtain the desired small  $v_d/v_a$  ratio. Here, feedback is intentionally used in the filter problem and introduces the second problem which it has a major role in solving. Active network synthesis had heretofore not incorporated sensitivity to such an extent.

It is an obvious transition from such an approach, to feedback control where the sensitivity problem is paramount and the filter problem is mostly secondary. The sensitivity aspect is easier in SISO feedback control because uncertainty is lodged in the plant function  $P(s)$ , which appears

as a single block in the transfer function  $T(s) = FPG/(1 + PG)$ . It is more complicated in active synthesis: the low-frequency model of the active element has four resistances and a controlled source. In the more challenging structures, these five parameters are scattered about in the system transfer function, so unlike feedback control it is not simply a matter of making the loop transmission large enough over a large enough frequency range.

## 2. PRINCIPAL FEATURES OF QFT

The principal features of QFT almost all appear in the first QFT work in 1959 [1]. Major considerations were: time domain vs transform domain, input-output vs detailed internal modelling, frequency response vs state-space, sensitivity function vs loop transmission, global optimization vs detailed quantitative design. The transform domain was chosen because of the great difficulty of satisfying specifications and stability directly in the time domain. Professor Barnard [2] is working in the latter area. Input-output seemed obvious because systems theory in general focuses on the relation between blocks, rather than on the internal design of the individual blocks. So why bother with the unnecessary complexity of detailed internal descriptions when the information is irrelevant for our purpose? In a 20<sup>th</sup> order system, why use 20 equations when 19 of them are only definitions? Controllability, observability and hidden oscillations are easily handled in a proper input-output description, i.e., which considers parameter uncertainty. For several decades it was rather lonesome in the frequency domain, which was derided by the dominant modern control society. However, times are changing and "the stone which the builders scorned has become the corner stone" [3].

The sensitivity function  $S = (1 + L)^{-1}$  seems to be the natural design tool because it gives directly

$$\frac{\text{effect with feedback}}{\text{open-loop effect}} = S$$

and offers hope for analytical, automatic design. However it is very cumbersome for detailed quantitative design, although it may be suitable for global measures and global optimization wherein one throws a variety of factors into a single cost function. But in multivariable design, one is interested in detailed control of  $n^2$  input-output relations. It is difficult to discern and achieve such detailed control via a single scalar cost function. It has additional disadvantages. A practical  $L = PG \rightarrow k/s^e$  as  $s \rightarrow \infty$ , so the first  $e$  leading numerator coefficients of  $S$  must equal those of its denominator. If degree of  $S$  is  $e + m$ , only  $2m$  free parameters are available for design. This seems to be the reason why its compensation functions turn out so impractical in terms of bandwidth, which is the principal cost of feedback.

Another important factor is high-frequency sensor noise effect at plant input,  $T_N = (1 - S)/P$ . In this range  $|L| \ll 1$ ,  $S \rightarrow 1$ ,  $P \rightarrow 0$ , so  $T_N$  is highly insensitive to  $S$ . But written as  $T_N = L/P(1 + L) \doteq L/P$ , it is very sensitive to  $L$ , and one sees the importance of fast decrease of  $|L|$  at large  $\omega$ . At  $|L| = 10^{-3}$ , an increase to  $10^{-2}$  (tenfold) changes  $|S|$  at best from .999 to .99 (1%), i.e., an insensitivity factor of 1000. Thus the sensitivity function is highly insensitive to two important costs of feedback: sensor noise and loop bandwidth.

It is instructive too that Bode, the pioneer of feedback theory and the definer of the sensitivity function  $S$ , did not use  $S$  for actual design, but instead used  $L$ , the loop transmission function [4]. This was the choice of QFT at the outset [1]. Our commitment to detailed quantitative design drove us to use  $L$  because of the vagueness of the global figures of merit. In fact, I believe that once the decision was made that plant uncertainty was the problem and practical quantitative design the objective, then the problem structure led QFT into the direction it has taken



since its beginning in 1959 [1]. An additional gift nature has awarded to QFT is its design transparency, which is so often emphasized by its practitioners. One clearly sees and has in his grasp the important trade-offs between bandwidth, design complexity, sensor noise effects, etc. This property and the close relation of QFT to Bode's work were sustaining sources during the long, lonely period when QFT was confined to the wilderness by academia and by government funding agencies.

For about half a century feedback control concentrated on the filter problem, and neglected its ability to cope with uncertainty. The following quotations are illustrative:

"... it is generally taken for granted that the dynamic characteristics of the process will change only slightly under any operating conditions encountered during the lifetime of the control system. Such *slight* changes are foreseen and are usually counteracted by using feedback. Should the changes become large, the control equipment as originally designed may fail to meet performance specifications."

(Kalman [5])

"Conventional control systems are designed to meet certain specifications under certain given conditions of the environment and the system parameters, but should these conditions change, the performance will change as a result."

(Gibson and McVey [6])

The above was the natural outcome of classical feedback's concentration on the filter problem. They were used to justify use of nonlinear compensation (so-called adaptive systems) in problems amenable to relatively simple linear time-invariant (LTI) compensation. I believe that I showed most of these arguments were invalid [7]. Successful QFT design for huge plant uncertainties (1000 to 1) were published. It is also worth noting that this lack of appreciation of the power of LTI compensation is widespread even today. Recently a student auditing a QFT course did an example with plant uncertainty factor of only 10. His advisor was skeptical of his results and performed the simulations himself. Modern control theory for many years appeared to be concerned with the same problem as classical feedback control, the filter problem. However, classical feedback control dealt in a relatively practical manner with the filter problem, whereas modern control theory, with its apparent primary interest in existence theorems, often emerged with unrealistic results. QFT was a pioneer in its re-definition of the basic purpose of feedback control. QFT is "classical" only in that it uses the classical tool of frequency response, whereas in the much more important sense of design objectives, it is modern feedback control which is classical, actually 'distorted classical,' because practicality is secondary to existence theorems. After many years, some universities have caught up with this fundamental truth.

### 3. PROGRESS OF QFT

Following the single-loop SISO design technique, two directions were obviously open. One was to consider use of internal variables available for feedback, as in the SISO cascade-loop structure. Frequency response and the Nichols chart as the synthesis tools were overwhelmingly vindicated. One sees almost by inspection how the feedback burden should be allotted among the loops, and the trade-offs between the loops, their bandwidths and their sensors. This is due to the "pointwise synthesis" nature of QFT. Thus the actual plant uncertainty and the desired much smaller closed-loop system uncertainty obviously impose constraints on the loop transmission operator  $L(s)$ , or equivalently on the sensitivity function  $S(s) = (1 + L)^{-1}$ . In QFT these are translated into bounds on  $L(j\omega)$ , separately at each  $\omega$  rather than on a global operator, following the ancient technique of breaking a difficult problem into smaller easier problems. In a multiple-

loop system this feedback burden can be divided among several available loops. By doing so separately at each  $\omega$  it is relatively easy to see the important trade-offs involved in this apportionment of the "feedback burden." It is very easy to see that it is overwhelmingly in favor of the major burden on the outer loop in the low- $\omega$  region with respect to sensor noise effects, compensator complexity and bandwidth, and that the opposite is true in the high- $\omega$  region. Also, it is easy to locate the critical  $\omega$ -range in which the transition should be made, and how to do so. It is enormously more difficult to do so by means of the more mathematically sophisticated global operator technique. Furthermore, the transparency available in the pointwise technique, easily seen by the ordinary engineer, is lost in the process. This is another major difference between QFT and  $H_\infty$  with its use of a global sensitivity function.

In this manner, systematic QFT design procedures were developed for a number of SISO multiple-loop structures. However, the general SISO multiple-loop problem has not as yet been solved in the QFT sense. It is an important problem over and above its own sake, because the general MIMO system with available internal feedback variables, can be rigorously transformed into SISO multiple-loop problems whose solutions are guaranteed to solve the original MIMO problem.

A second direction of QFT was in design optimization for the single-loop system. A reasonable definition was made, and it was shown that the optimum exists and lies on its bounds for all  $\omega$  values. It became obvious even then and much more so later, that there is ample room in QFT for the mathematically oriented researcher whose primary interest is in existence theorems.

QFT has proceeded step by step to nonminimum-phase (NMP) systems, digital compensation, multivariable plants with and without internal feedback variables. It was proven that despite contrary opinion, digitally compensated feedback systems are inherently inferior, in the sensitivity sense, than analog feedback systems. An especially important QFT breakthrough was made in time-varying and nonlinear feedback plants wherein the problem is reduced to rigorously equivalent LTI problems. Two design techniques have been developed. In one, the nonlinear and/or time varying uncertain plant set is replaced by a LTI set which is equivalent with respect to the set of desired plant outputs. The following modelling is necessary for the nonlinear MIMO case: Given a set of output  $n$ -vectors  $\mathcal{Y} = \{y\}$  and associated set of plant input vectors  $\mathcal{U} = \{u\}$ , find the set of  $n \times n$  matrices  $\mathcal{P} = \{P\}$  such that  $y = Pu$ . This is quite tricky in feedback because it can be very important whether  $P$  is MP or NMP. But suppose both models appear to give equally good results in the time domain? This problem is avoided to a large extent in the second technique where the nonlinearities become equivalent disturbances. They have been successfully applied to many multivariable problems, including man-in-the loop flight control. The reader is referred to Reference 8 for a more detailed exposition of QFT progress.

#### 4. FUTURE OF QFT

If one accepts the feedback problem in the QFT sense of design to achieve quantitative performance specifications despite uncertainty, then the research problems are limitless. We are living in a sea of uncertainty, and nature depends on its myriads of self-correcting feedback loops. Nature is far from delicately, fragilely balanced, as espoused by many. Thanks to its feedback loops it is highly robust. History, especially recent history, has dramatically shown that it is some of man's economic and social systems which are delicately fragile. One might attribute this to (1) ideological rather than empirical assessment of the plant (nature of man), and (2) woeful ignorance of quantitative feedback theory.

There are very many open areas of research even in LTI feedback theory: SISO and MIMO internal variable feedback even with all feedback returned to plant inputs, but more important with

feedback returned to internal plant points, thereby introducing 'plant modification' [8]. The latter has hardly been touched and is extremely important in biological, economic and organizational systems. It can greatly reduce the cost of feedback in typical control problems if it is considered in the original plant design. There is needed much more extensive, intimate experience in the design of MIMO systems in order to achieve greater insight into the trade-offs between the loops and the cost of feedback. I would urge much greater involvement of the theoretical researcher in actual design. That is, in my opinion, the only way for deep understanding and consequent practical research usefulness, and for formulation of deep, realistic research problems. QFT has made its greatest progress by such interaction with practicality. There is hardly a single QFT topic which is totally completed. In the NMP SISO system, is it possible to obtain better, simpler criteria for the existence of a solution? A versatile loop-shaping program would be very useful in general. We need more detailed tools for trade-off between loop bandwidth economy and design complexity. I have not mentioned as yet distributed plants with input, output and control all distributed, and the design tolerances are also distributed, very important in traffic control and transportation.

QFT has only opened a door into feedback design for nonlinear, time-varying uncertain plants. But the techniques may be far from the last word in design economy. Much more design experience is needed with such plants. QFT has at least provided rigorous design techniques enabling such experience to be attained. Consider the vast amount of work in LTI feedback theory, which is nevertheless far from complete, and the much greater complexity and importance of nonlinear plants.

The most critical and challenging area is in non-LTI compensation. We have a pretty good idea of the power and limitations of LTI compensation, whether for linear or nonlinear plants. The only way to beat the game is by non-LTI compensation, and therein is the challenge. Adaptive systems with their emphasis on identification are only one means of non-LTI compensation. Consider the huge support it has received since its inception in the late 1950s. Yet, I am not aware of any such adaptive design techniques which quantify their advantages, if any, over LTI compensation. The only such techniques I know of have been done by QFT for oscillating adaptive systems, and to some extent for a specialized nonlinear element FORE (first order reset element). In both, the design theory enables one to see beforehand the advantages, if any, of non-LTI compensation and therefore if it is worth the extra complexity. In some problem classes there is no option, as the problem is not solvable by LTI compensation.

Linear time-varying (LTV) compensation is an intermediate stage between LTI and nonlinear compensation. The following QFT result is fascinating and provocative [9]. Consider a lumped (ODE) uncertain nonminimum-phase, unstable SISO plant whose finite number of RHP poles and zeros are close together. With LTI compensation a stable design is always possible for a nominal case, but even in an optimal design [10], it remains stable for only very small departures from nominal. LTV compensation permits its stabilization over a large class of arbitrarily large uncertainty. However, the normally acute sensitivity to the plant is transferred to the compensation. Very small variation in the latter renders the system unstable. This is a fantastic result. It is far easier to build a compensator (say a digital controller) with very narrow tolerances than a plant whose power level can be billions of times greater. But even more fascinating is this means of transfer of razor-edge sensitivity from one part of a system to another. This is only a glimpse into the power of non-LTI compensation and a suggestion of how much more powerful nonlinear compensation may be.

Non-LTI compensation is the means for radically changing the relation between cost of feedback and its benefits, and of achieving results otherwise totally unattainable. Its potentialities are unlimited. However, I would advise the researcher to first obtain deep knowledge of LTI feedback theory and its limitations. Also, do not attack this formidable opponent on too wide a

front. It has been tried unsuccessfully for decades by many brilliant researchers in adaptive control. Try first to squeeze out just a bit of profit in some area where the limitation of LTI compensation is clearly delineated.

## 5. CONCLUSIONS

It is suggested that QFT is essentially what feedback control theory is all about. It is only in its infancy at present. Unlimited opportunities face the enthusiastic researcher in the unending quest for achieving highly precise results, despite large uncertainty in the means of producing the results. There is room in QFT for highly diverse talents: the nonmathematical practical engineer with physical insight and inventive talent, the skilled mathematician interested in existence theorems and abstract generalizations, up to the stubborn, even plodding researcher who by hard dedicated work acquires deep understanding of his subject.

## REFERENCES

- (1) I. Horowitz, Fundamental Theory of Linear Feedback Control Systems, Trans. IRE on Auto. Control, AC-4, Dec. 1959, 5-19.
- (2) S. Jayasuriya, M. Rabins and R. Barnard, Guaranteed Tracking Behavior in the Sense of Input-Output Spheres for Systems with Uncertain Parameters, Journal of Dynamic Systems Measurement and Control, 106, Dec. 1984, 273-279.
- (3) Psalms 38, 22.
- (4) H.W. Bode, Network Analysis and Feedback Amplifier Design, Van Nostrand, 1945.
- (5) R.E. Kalman, Design of a Self-Optimizing Control System, Trans. ASME, Feb. 1958.
- (6) J.E. Gibson, E.S. McVey, Multidimensional Adaptive Control, Proc. NEC, 15, 1959.
- (7) I. Horowitz, Plant Adaptive Systems vs Ordinary Feedback Systems, Trans. IRE on Auto. Control, AC-7, Jan. 1962, 48-56.
- (8) I. Horowitz, Survey of Quantitative Feedback Theory (QFT), Int. J. Control, 53, 1991, 225-291.
- (9) I. Horowitz, O. Yaniv, Quantitative Design for SISO NMP Unstable Plants by the Singular G Method, Int. J. Control, 46, 1987, 281-294.
- (10) I. Horowitz, Design of Feedback Systems with Nonminimum-Phase Unstable Plants, Int. J. Sys. Sci., 10, 1979, 1025-1040.

# BANQUET SPEECH

## QFT INDUSTRIAL APPLICATIONS: PAST, PRESENT, AND FUTURE

Dinner-Speech by Dr Eduard Eitelberg

Ladies and Gentlemen!

It is an exceptional honour to have been asked by Professor Isaac Horowitz and the conference organizers to speak at this important meeting of people that have either grown up with or been converted to QFT.

I assume that the number of QFT opponents or indifferents present is insignificant. Hence my aim is not to bore you with what you know anyway – that the QFT is the best control system design strategy and philosophy today. Having thus established my loyalties, I will try to stay on the topic of my speech.

I would like to restrict attention to industry that produces goods, excluding for example the tourism industry. Due to often vastly different financing philosophies I would like to distinguish between the military or defence industry and the non-socialist non-monopolistic (?) market-related industry, whose product must be marketable at a profit although sometimes there is very little difference in the actual production activity. It may not be a commonly accepted classification, but there are practical differences in control theory applications where the control system is an inherent part of the manufactured product on the one hand and where the control system is part of the production process (hence "process control").

I am not qualified to survey the defence industry applications for various reasons. One is the extreme confidentiality in this field. The other is that many of you know more than I do. Hence I shall concern myself with the non-military industrial applications.

At another level, if "past" is what was before now, and if "future" is after now, then there is no need to talk about "present." Hence, for the purpose of this speech, I would like to consider the last five years as "present" – this is in the order of magnitude that an idea may need to become a marketable product.

With these clarifications, I can say that the QFT non-military industrial applications do not yet seem to have a past. It has a presence in a few products, such as earthquake instrumentation, welding machines and a few other confidential/classified machines. I actually requested data from 23 QFT related researchers and their acquaintances. To those 10 who responded – a big thank you! Not one of them has reported process control applications of QFT. What is more, I do not foresee in the near future significant QFT applications in the process control industry, the way QFT is understood at the universities, unless dramatic changes of attitudes occur among all concerned groups. I would not be surprised if more and more products included feedback loops designed with the QFT (or if there were fewer of them), this depends mostly on the attitude of the academics.

In the following I shall explain the reasoning for both of these statements and for the difference in process control and control in products. Let us address the products first.

Designing a product usually involves experimentation in a laboratory-type environment. Most of the respondents to my survey did not report laboratory application of QFT although some had product development experience. I am convinced that if students are forced to control realistic

laboratory experiments, some of them will be able to apply QFT in industrial products. There are at least four academic institutions known to me where efforts are made in this QFT direction – two are in the R.S.A. (at UDW and Wits) and two are in the U.S.A. (at AFIT and UMass)

What do I mean by a realistic experiment? I mean an experiment that is not finished in an afternoon. I mean an experiment where the student will have to specify the sensor and actuator and will have to justify his control system specification by the currently available technology. The experiment must educate the student to modify or build systems that facilitate the controller's performance. I realize that this may be too expensive for many universities and one may have to use post-graduate supervised industrial training before a graduate becomes an engineer. At least two such places are known to me – El-Op in Israel and Sandia National Laboratories in the USA. There certainly are others. This engineering experience cannot be replaced by QFT-CAD.

Process control is much more difficult to learn in a laboratory than control in a product, because of the sheer size and expense of the usual plants. Furthermore, in my experience, QFT knowledge and application skill has almost nothing to do with the chance of its application in the process industry. Most industrial decision makers do not understand control theory of any kind and frankly find control theoreticians to be a nuisance.

Let me try to put the above statements into some perspective.

The hardware and associated software in controlled systems can be classified as indicated in Figure 1.

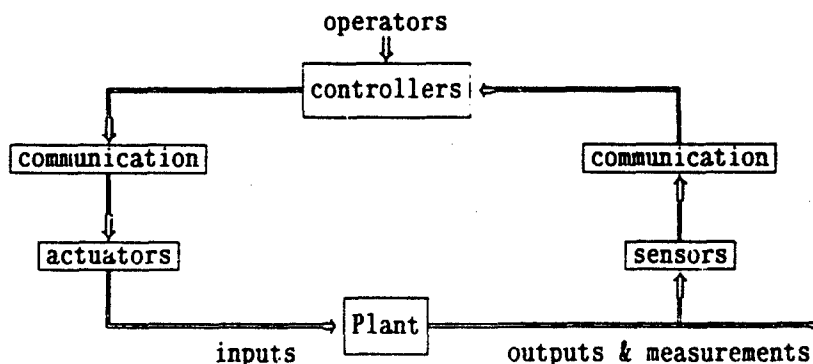


Figure 1: Hardware in (process) control systems.

Sensors, actuators, communication hardware (e.g. transmitters, I-to-P converters, signal conditioners, multiplexers), and power supplies are called instrumentation in process control circles.

A lot has been published in recent years about the design and reliability of (digital) controllers, about their programming, hardware and software maintenance, operator interfaces, Distributed Control System (DCS) communication via bus systems (as opposed to instrumentation communication) and so on.

Concurrently, the application design aspects of instrumentation have been neglected by the academic control community with the result that almost the complete field of instrumentation in many areas of process industry is often handled by technicians and vendors. Universities, generally, do not graduate instrumentation engineers (McMillan, G.K. and Weiner, S.: *How to*

*Become an Instrument Engineer – The Making of a Prima Donna, ISA, 1987).*

The U.S. market for instruments and controllers was in 1989 about (US) \$6 billion, it was probably twice that in the world (*Control Engineering*, Oct. 1991). Total U.S. automation spending was \$33 billion. [Compare this to G.E. (U.S.) yearly turnover of \$60 billion (*Control Engineering*, Nov. 1991). Of this control spending only 3% was spent in the aerospace industry (*Control Engineering*, Oct. 1991).]

In process industry, probably most control related projects are carried out on existing plants as retrofits. In an unpublished ICI presentation a typical "control" project cost break-down was given as:

Contract Engineering:	11%
Own Engineering:	8%
Civil/Mech/Elec. Eng:	25%
DCS:	40%
Instruments:	15%
Benefits Analysis:	1%

Hence in an "average" (few hundred thousand U.S. dollar) control project, just over 50% is spent directly on the control loop hardware and associated (configuration) software – controllers (DCS) and instrumentation. Only the benefits analysis actually deals with feedback control system design aspects and specifications. In my experience there is not even a separate heading in a project for this activity, the management does not know about it and cannot care less, there is nobody to talk to about QFT or any other control system design techniques. Often even the Ziegler-Nichols tuning rules are not handled at the engineering level, the technicians use them for better or for worse.

Of course, there are engineers who know better. But I am pretty convinced that QFT will have to be sneaked into process control projects – and keep quiet, don't frighten anybody.

I would like to tell you a little personal story. During a 10 month sabbatical leave from the academic world, I acted as the coordinator between electrical, instrument, computer and boiler building companies for about one month during commissioning of a chemical recovery boiler. That meant 20 hour work-days and sometimes sleeping in my car on site.

Once, because it was not spelled out in the contract, because of incompetence of the computer control contractor and because the paper company was loosing about \$100 000 of production per day, I volunteered to tune the control systems. There was no possibility of system identification or literature study and the control contractors said that it was impossible to get it right in less than a week. I told them, "Watch me!" and tuned 26 loops in about half a day and a night. That included running between the control room and the various actuators at the top of the boiler or down at the fuel heaters in order to check if the valves were limit cycling or why some outputs reacted wrongly (mostly because of faulty equipment or manual by-passes). I succeeded, thanks to QFT helping me to interpret what I saw. This all happened at about 30% load. Some time later, at full load almost no retuning was necessary.

Some people have suggested that more QFD-CAD is needed for its success. I think that good CAD is needed in learning stages until one memorizes the individual moves of loop shaping etc. graphically. During commissioning there is no time for elaborate designs and after commissioning, "outsiders" are most unwelcome in the vicinity of the control room. If one could design a plant like a product then the whole situation would be easier for QFT, but this is improbable because of the cost and because most process plants are built by a combination of (sometimes rather uncooperative) manufacturers.

How can QFT be sneaked into process control? Firstly the "sneakers" must be educated with realistic laboratory experiments and designs. This will lead to the recognition that in order to apply QFT one does not have to design to uncertainty specifications. In the process industry one can very seldom extend the loop bandwidth over the plant bandwidth, hence loop shaping proceeds backwards from the stability margins to steady state. The PI control structure with measures against integrator wind-up is eminently suited for this approach — mostly fix the gain and then find the shortest possible integrator time. One may have to design to specified regulating behaviour, but it must be recognized that this requires process redesign or finding and eliminating limit-cycling loops in other parts of the plant more often than fancy controller design.

In relation to MIMO control, the processes are mostly designed so that single loops and their common sense combinations are justified and can be tuned individually or in a common sense sequence. Remember, "ordinary" people must be able to maintain these systems.

In both cases, SISO and MIMO, the most crucially neglected part of the control system is the instrumentation. Instrumentation must be handled in QFT and alongside it. Instrumentation limits the achievable performance and hence should be specified (at least) partly by the control system designer in a quantitative manner. Furthermore, instrumentation fails very often and (speaking to the younger generation) a successful control engineer must be able to use QFT for extending instrument and plant life and reduce maintenance costs, down time and accidents. Failure mode and process interlocking designs have yet to enter (seriously) the QFT-club. These are presently important activities under the instrumentation and DCS headings of a project

Therein lies hope. Control engineers with QFT background must become instrument and "DCS" experts or stick to these experts in order to apply QFT. One could try and become a project manager in order to be able to decide what is done during a project, but there seems to be a universal incompatibility between simultaneous managerial and design engineering mind sets.

Finally, let me entertain you with a story about how important a single \$2000 instrument can be. A few million U.S. dollar boiler rebuild project in Africa was won by a world-leading Scandinavian company. Their base price was close to cost, but a substantial premium was payable if they managed to increase the fuel (black liquor) throughput by 20%. Their commissioning engineers could not achieve this goal during the normal commissioning. During an extended stay they almost achieved this, but just before they were at the goal they set the precipitators on fire and in addition melted or burnt substantial parts of the ducting and machinery. It took over a year for the respective lawyers to sort this mess out. The "culprit" was a reputedly 0.5% accurate magflowmeter measuring the fuel flow rate. It had its regular so-called calibration certificates (for the electronics, mind you) but its primary sensor had not been visually checked for at least two years, before I checked it. I found that due to lining deformation this flowmeter measured about 7% less and hence the plant had already had 7.5% more throughput before upgrade than conveyed to the unsuspecting contractors, who in effect were trying to achieve 29% performance improvement. This was constructively impossible.



LIST OF QUANTITATIVE FEEDBACK THEORY (QFT) SYMBOLS

Version 1.0

Prepared by

Professor C. H. Houpis

Air Force Institute of Technology

and

Flight Dynamics Directorate, Wright Laboratory

Wright-Patterson AFB, Ohio

July 11, 1991

Revised March 12, 1992

---

The awareness of the power of QFT to solve real world problems has evoked the interest and involvement of a greater number of control engineers and researchers. At the recent IFAC ACE and the ACC meetings in Boston, MA, the QFT participants stated that this increased involvement necessitates the establishment of a list of standard QFT symbols. They suggested the publication of this list in order to avoid confusion to those trying to learn and understand QFT and to enhance its acceptance and development into fertile research areas and the solving of real world control problems.

This list is based upon the following:

1. The articles written by Professor I. M. Horowitz that are listed in the References listing in "Quantitative Feedback Theory (QFT)," Dr. C. H. Houpis, AFWAL-TR-86-3107, Flight Dynamics Laboratory, AF Wright Aeronautical Laboratories, AFSC, Wright-Patterson AFB, OH.
2. Chapter 21 of "Linear Control System Analysis & Design" by D'Azzo & Houpis, McGraw-Hill Book Co., 3rd Edition, 1988.
3. Chapter 16 of "Digital Control Systems: Theory, Hardware, Software," by Houpis & Lamont, McGraw-Hill Book Co., 2nd Edition, 1992.
4. Master Theses by the flight control students of the Air Force Institute of Technology, Wright-Patterson AFB OH

This is the first attempt in establishing a standard list of QFT symbols. Based upon the use and the reviews and comments that are obtained of this list a new version, hopefully, will be published periodically.

<u>Symbol</u>	<u>Defintion</u>
$\alpha_p$	-- The specified peak magnitude of the disturbance response for the MISO system
a.l.	-- Arbitrarily large
a.s.	-- Arbitrarily small
$a_{ij} = \text{Lm } \tau_{ij}$	-- The desired lower tracking bounds for the MIMO system
$b_{ij} = \text{Lm } \tau_{ij}$	-- The desired upper tracking bounds for the MIMO system
$a_{ii}'$	-- The desired modified lower tracking bound for the MIMO system: $a_{ii}' = a_{ii} + \Delta\tau_{Dii}$
$b_{ii}'$	-- The desired modified upper tracking bound for the MIMO system: $b_{ii}' = b_{ii} - \Delta\tau_{Dii}$
$B_D(j\omega_i)$ $B_R(j\omega_i)$ $B_O(j\omega_i)$	-- The bounds on $\text{Lm } L(j\omega_i)$ for disturbance, $B_D$ , and tracking bounds, $B_R$ , respectively, and the optimal bounds, $B_O$ , for the MISO system
$B_h$	-- Ultra high frequency boundary (UHFB) for analog design
$B_h'$	-- Ultra high frequency boundary (UHFB) for discrete design
$B_U = \text{Lm } T_{RU}$	-- The $\text{Lm}$ of the desired tracking control ratio for the upper bound of the MISO system
$B_L = \text{Lm } T_{RL}$	-- The $\text{Lm}$ of the desired tracking control ratio for the lower bound of the MISO system
$B_s$	-- Stability bounds for the discrete design
BW	-- Bandwidth
$\Delta\tau_D$	-- allotted portion of the $ij$ output due to a disturbance input
$\delta_D(j\omega_i)$	-- The (upper) value of $\text{Lm } T_D(j\omega_i)$
$\delta_{hf}(j\omega_i)$	-- The dB difference between the augmented bounds of $B_U$ and $B_L$ in the high frequency range

$\delta_R(j\omega_i)$	-- The dB difference between $B_u$ and $B_l$ for a given $\omega_i$
$d_{ij}$	-- The interaction or cross-coupling between the of a MIMO system
$D$	-- MISO system disturbance input
$D = \{d_{ij}\}$	-- The $\ell \times \ell$ MIMO disturbance control ratio matrix
$\mathcal{D} = \{D\}$	-- Script cap dee to denote the set of disturbance inputs for a MIMO system $\mathcal{D} = \{D\}$
$F, F = \{f_{ij}\}$	-- The prefilter for a MISO system and the $\ell \times \ell$ prefilter matrix for a MIMO system respectively
FOM	-- Figures of merit (see the D'Azzo & Houpis text)
$G, G = \{g_{ij}\}$	-- The compensator or controller for a MISO system and the $\ell \times \ell$ compensator or controller matrix for a MIMO system, respectively. For a diagonal matrix $G = \{g_i\}$
$\gamma, \gamma_i$	-- The phase margin angle for the MISO system and for the $i^{\text{th}}$ loop of the MIMO system, respectively
$\gamma_{ij}$	-- A function only of the elements of a square plant matrix $P$ (or $P_e$ )
$k$	-- A running index for sampled-data systems where $k = 0, 1, 2 \dots$
$kT$	-- The sampled time
$\lambda$	-- The excess of poles over zeros of a transfer function
$L_o, L_{oii}$	-- The optimal loop transmission function for the MISO system and the $ii$ loop of the MIMO system, respectively
LHP	-- Left half-plane
LTI	-- Linear time-invariant

MIMO	-- Multiple-input multiple-output; more than one tracking and disturbance inputs and more than one output
MISO	-- Multiple-input single-output; a system having one tracking input, one or more disturbance inputs, and a single output
$M_L, M_{Li}$	-- The specified closed-loop frequency domain overshoot constraint for the MISO system and for the $i^{\text{th}}$ loop of a MIMO system, respectively. This overshoot constraint may be dictated by the phase margin angle for the specified loop transmission function
mp	-- Minimum phase
nmp	-- Nonminimum phase
NC	-- Nichols chart
$\Xi$	-- The number of plant transfer functions for a MISO system or plant matrix for a MIMO system that describes the region of plant parameter uncertainty where $\xi = 1, 2, \dots, \Xi$ denotes the particular plant case in the region of plant parameter uncertainty
$\omega_b$	-- the symbol for bandwidth frequency of the models for $T_{RU}$ , $T_{RL}$ , and $T = \{t_{ij}\}$
$\omega_\phi, \omega_{\phi i}$	-- phase margin frequency for a MISO system and for the $i^{\text{th}}$ loop of a MIMO system, respectively
$\omega_s$	-- Sampling frequency
P	-- MISO plant with uncertainty
$P_\xi = (p_{ij}^\xi)$	-- $\ell \times m$ MIMO plant matrix where $p_{ij}^\xi$ is the transfer function relating the $i^{\text{th}}$ output to the $j^{\text{th}}$ input for plant case $\xi$
$\Phi$	-- Script cap pee to denote a set that represents the plant uncertainty for $\Xi$ cases in the region of plant uncertainty, i.e., $\Phi = \{P\}$ for a MISO system and $\Phi = \{P_\xi\}$ for a MIMO system

$P_{\xi}^{-1} = (p_{ij}^{\xi})$	-- The inverted plant matrix for plant case $\xi$ where $\ell = m$
$P_{\xi}^{\ell} = P_{\xi} W$	-- The $\ell \times \ell$ effective plant matrix when $P_{\xi}$ is not a square plant matrix and $W$ is an $m \times \ell$ weighting or a squaring-down matrix
QFD	-- Quantitative feedback design based on quantitative feedback theory
$Q_{\xi} = (q_{ij}^{\xi})$	-- An $\ell \times \ell$ matrix whose elements are given by $q_{ij}^{\xi} = 1/p_{ij}^{\xi}$
$\mathcal{Q}$	-- Script cap que to denote a set that represents the plant uncertainty for a MIMO system, i.e., $\mathcal{Q} = \{Q_{\xi}\}$
$R, R = \{r_i\}$	-- The tracking input for a MISO system and the tracking input vector for a MIMO system, respectively
RHP	-- Right half-plane
$T$	-- Sampling time
$\mathcal{T}P(j\omega_i)$	-- Script cap tee inconjunction with $P$ or $(q_{ij})$ denotes a template, i.e., $\mathcal{T}P(j\omega_i)$ and $\mathcal{T}q_{\xi}(j\omega_i)$ represent the templates, for a given frequency, for a MISO and MIMO plants respectively
$T_{RU}$	-- The desired MISO tracking control ratio that satisfies the specified upper bound figures of FOM
$T_{RL}$	-- The desired MISO tracking control ratio that satisfies the specified lower bound FOM
$T_D$	-- The desired MISO disturbance control ratio whichsatisfies the specified FOM
$T_{R}^{\xi}, T_D^{\xi}$	-- The MISO tracking and disturbance control ratios for case $\xi$
$T_{\xi} = (t_{ij}^{\xi})$	-- The $\ell \times \ell$ MIMO tracking control ratio matrix for plant case $\xi$

$T_R$	-- The script cap tee denotes the set that represents the tracking control ratios for $E$ cases, i.e., $T_R = \{T_R^k\}$ for the MISO system and $T_R = T\{T_R^k\}$ for the MIMO system
$T_n$	-- The script cap tee denotes the set that represents the disturbance control ratios for $E$ cases. i. e., $T_D = \{T_D^k\}$ for the MISO system and $T_D = T\{T_D^k\}$ for the MIMO system
$\tau_{ij}$	-- A set of assigned tolerances on $t_{ij}$ : $\tau_{rij}$ and $\tau_{dij} = 2\Delta\tau_{dij}$ , the assigned tolerances for tracking and disturbance, respectively
$U$	-- The $\ell \times \ell$ controller input vector
UHFB	-- The ultra high frequency boundary
$v, \mathbf{v}$	-- The MISO prefilter output and the $\ell \times \ell$ MIMO prefilter output vector, respectively
$V$	-- $\lim_{\omega \rightarrow \infty} [Lm P_{max} - Lm P_{min}]$ is the dB limiting value for a MISO plant
$V_i$	-- $\lim_{\omega \rightarrow \infty} [Lm (q_{ii})_{max} - Lm (q_{ii})_{min}]$ is the $i^{th}$ loop template dB limiting value for a MIMO plant
$W = (w_{ij})$	-- The weighting or squaring-down matrix
$w' = u + jv$	-- $w'$ -domain variable; the use of $u$ and $v$ must be interpreted in context
$Y, \mathbf{Y} = (y_{ij})$	-- The output of a MISO system and the output matrix of a MIMO system, respectively, where $Y_{ij} = Y_{ri} + Y_{di}$
$Y_{ri}$	-- Is that portion of the $i^{th}$ output due to the $i^{th}$ input
$Y_{dij}$	-- Is that portion of the $i^{th}$ output due to the disturbance input $d_{ij}$ (cross-coupling effect or interaction of the other loops)

# Air Force Sponsorship of Quantitative Feedback Theory

P. Chandler  
Flight Control Division  
Flight Dynamics Directorate  
Wright Laboratory  
Wright-Patterson AFB, OH 45433

## Introduction

This paper is an attempt to present, in approximate chronological order, the support provided to Dr. Horowitz by the Air Force for his research into control theory. It is not intended to be complete, but to document the major milestones in the development of QFT achieved under this support. The Air Force has provided real problems and this has resulted in significant enhancements to the theory.

## Air Force Support Prior to '76

Air Force sponsorship of Dr. Horowitz's work extends back almost 20 years. The earliest this author could locate was from 1973. He was funded under a grant from Air Force Office of Scientific Research (AFOSR) through their arm European Office Aerospace Research and Development (EOARD) under grant number 73-2549. Indeed, much of the early Air Force support for Dr. Horowitz came through EOARD.

Under this grant he published the milestone paper entitled "Synthesis of Feedback Systems with Nonlinear Time-Varying Uncertain Plants to Satisfy Quantitative Performance Specifications", that appeared in the IEEE Proceedings in 1976. This paper presents an approach to solve feedback control problems with uncertain nonlinear plants by means of an equivalent linear time invariant (LTI) plant set. Schauder's fixed point theorem is applied to prove that the *equivalent* LTI plant set satisfies the original nonlinear problem. This important milestone turns an uncertain nonlinear problem into an uncertain linear problem, which is then solved in a conventional manner. Prior to this there was no rigorous theory for treating uncertain nonlinear control systems with quantitative performance specifications.

## Air Force Support From '76-'77

During this period, sponsorship of Dr. Horowitz was provided by a grant, number AFOSR-76-2946 from AFOSR to the University of Colorado, Boulder. At this time he held a chair at the Weizmann Institute of Science, Israel and was also professor at University of Colorado. His work on quantitative synthesis during this period is best described in the review paper "Quantitative Feedback Theory", which was published in IEE proceedings in '82.

He also worked in two other areas that are significant advances, one in adaptive control - the other in plant modification.

One research area not normally associated with QFT is "adaptive control". However, of the various adaptive design techniques which have been proposed, the only one for which there exists *quantitative* systematic design to specifications was done by Dr. Horowitz and his students. This is the class of Oscillating Adaptive Systems developed in a series of doctoral theses. Furthermore, the design theory tells the developer if and to what extent the adaptive system is superior to a LTI design. Part of the work in adaptive control is documented in "A Synthesis Theory for Multiple-Loop Oscillating Adaptive Systems" and published in International Control in '79. This work presents the first quantitative design effort in adaptive control.

Also during this period, Dr. Horowitz worked on plant modification. This is documented in the paper "Synthesis of Multiple Loop Feedback Systems with Plant Modification" in IJC in '79. This approach is for cascaded plants; for example, process plants and robotic manipulators. For a cascaded plant, the feedback is permitted to proceed directly to internal plant variables, constituting *plant modification*. This permits a drastic reduction in the *cost of feedback*, in terms of loop bandwidth and effect of sensor noise. This is the first quantitative work of its kind. The designer can achieve the desired trade-off between increased plant signal level and cost of feedback.

Dr. Horowitz's coauthors and students have not been mentioned, and this, by no means, is intended to slight their efforts. Dr. Horowitz significantly contributed to controls education. He has had a great number of students, and it is not possible to acknowledge them all in so short a document.

## Air Force Support From '77-'78

This period signifies the first involvement of the Flight Control Division of the then Air Force Flight Dynamics Laboratory (AFFDL) and now the Flight Dynamics Directorate. This work was sponsored under grant AFOSR-77-3355 to Weizmann Institute of Science, Rehovot, Israel. This work is documented in the report AFFDL-TR-79-3120 entitled "Research in Advanced Flight Control Design". The monitors for this effort were in turn Capt. Terry Tarr, Bob Poyneer, Bob Lemble, and Phil Chandler.

The objective of this effort was to investigate feedback design techniques which can work when the plant has significant uncertainty and there are exacting performance requirements.



Design techniques were to be developed for nonlinear systems and applied to a F-4B 3-axis nonlinear control problem.

This effort is a landmark in the development of QFT. Before this time there was no synthesis theory for control design that could incorporate uncertainty and performance bounds quantitatively. Two breakthroughs were achieved yielding precise quantitative synthesis for both linear and nonlinear time-varying, single and multiple input-output systems containing plants with large uncertainties.

The first breakthrough was the development of the concept of LTI plant sets that, for given inputs, are *precisely equivalent* to the nonlinear plant. This converts a nonlinear problem into a set of linear ones.

The second breakthrough was in converting a complex Multiple-Input Multiple-Output (MIMO) problem into a number of Single-Input Single-Output (SISO) control problems. The tolerances on the output of one SISO loop appear as *disturbances* in another loop. A specified degree of decoupling is achieved in the process. This effort was applied to a F-4B nonlinear 3-axis flight control problem. All of the performance specifications were completely satisfied. Any other approach, at this time, would have been very conservative and required numerous iterations.

## Air Force Support From '80-'83

During this period, the Air Force, through AFOSR (EOARD), sponsored an effort entitled "Flight Control Design based on Multiple Input-Output Nonlinear Model with Uncertain Parameters" at the Weizmann Institute of Science. This effort was initiated under grant AFOSR-80-0213 and joint funded by EOARD (Maj Powell) and under the 2304N3 task managed by Bob Schwanz, then later, Frank George. This effort is documented in AFWAL-TR-83-3036 entitled "Multivariable Flight Control Design with Uncertain Parameters".

This effort was to develop pitch pointing, yaw pointing, and direct side force control laws for a YF-16 CCV model. The objective was to decouple the pitch, roll, and yaw axes so that, for example, a yaw pointing command will have a small specified effect on roll and lateral acceleration. In addition, the pitch pointing mode would decouple pitch angle from normal acceleration.

This is a major milestone in the development of QFT, for, in its application to the YF-16 CCV, it is the first *practical* application of the design technique of decomposing the MIMO problem into a number of SISO feedback loops. This demonstrated the great flexibility of QFT in controlling three outputs that are highly coupled. A significant step forward was made when it was discovered that the YF-16 CCV did not satisfy the theoretical high frequency condition. This event forced a significant advance in the theory, which demonstrates the importance of applying theory to real problems by the academic researcher. The YF-16 CCV effort was first presented at NAECON, '81 in the paper entitled "A Synthesis Technique for Highly Uncertain and Interacting Multivariable Flight Control Systems".

This period of time saw major advances in the theory. These advances were first presented in the paper "Improved Design Techniques for Uncertain Multiple Input-Output Feedback

Systems" in International Journal of Control, '82. It was shown that fixed point theory was not needed to justify the theory. Simpler matrix algebra would suffice. Significant overdesign was wrung out of the theory. The original theory is used for the first loop, then the exact system equations are used for the other loops. This was motivated by the YF-16 CCV high frequency bound problem. Also, arbitrarily small sensitivity constraints were taken out of the design theory for those problems that did not require it in the specifications.

Also in this time frame, the Laboratory sponsored, and Dr. Horowitz conducted, a short course in QFT. This course was entitled "Practical Design Techniques for Nonlinear and Multiple Input-Output Feedback Systems with Large Uncertainty". The course was 14 hours long over two days with 45 attendees from throughout Wright Patterson AFB. It was conducted and video taped in the candid classroom at AFIT in Mar '82. The agenda included: 1) quantitative LTI SISO problem, 2) example nonlinear problem  $\dot{y} + ay^2 \text{sign}(y) = kx$ , 3) nonlinear F-4B short period response, and 4) YF-16 CCV direct side force mode.

## Air Force Support From '83-'87

### Robust Multivariable Control

This was a very productive period in the development of QFT. A number of papers were written, of which only three are discussed. This period was typified by the variety of issues delved into. The work came under the heading Robust Multivariable Control in the Flight Control Division and was supported under contract F33615-83-C-3000.

Saturation: Control surface actuator rate and amplitude limiting is a real and critical problem in flight control and for an unstable aircraft can result in departure. In the paper "Quantitative Non-linear Design for Saturating Unstable Uncertain Plants", International Journal Control, '86, a nonlinear saturating element is introduced in the feedback loop. This loop prevents saturation of the actuator. Unlike most techniques used today, the design accepts large signals and can work close to maximum capacity. The system responds to the large input signals with virtually no delay. There are many tricks developed over the years for this problem, but this approach is one of the few with a good engineering-theoretical foundation.

Non-Minimum Phase: It is well known that non-minimum-phase (NMP) plants restrict the potential benefits of feedback. In the SISO case, a plant right half plane (RHP) zero constrains the system transfer function to have a RHP zero at the same location. Modern fighter aircraft are typically NMP in the longitudinal axis. The system can be stabilized, but the stability margins may be quite small. In the paper "An Important Property of Non-Minimum-Phase Multiple-Input Multiple-Output Feedback Systems", IJC, '86, this led to the apparently hitherto unknown, but important fact that not all the  $n \times n$  transfer functions need suffer from the NMP liability. The MIMO capability allows the NMP liability to be placed on a less important output, and the critical outputs can be minimum phase.

Discrete: All flight control systems today are implemented digitally, i.e. are sampled-data systems. Heretofore nearly all of the theoretical work in QFT has been continuous. In the

paper "Quantitative Feedback Design for Sampled-Data Systems", IJC, '86, the theory is developed for design in the  $\omega'$  domain. The detailed design procedure parallels very closely that for continuous systems. Because of sampling, all digital control systems are NMP. The design shows how this effect can be minimized with the sampling frequency for minimum phase plants. For NMP plants the constraints are the same as in continuous time, which is demonstrated quantitatively.

## X-29 Study

The X-29 has very strong non-minimum-phase properties at some points in the envelope. This results in a reduced benefit of feedback, and robustness (or stability margins) to parameter variations can be very small. Dr. Horowitz performed a brief study under contract F33615-81-3201, problem number 426, to examine the robustness properties of the X-29. As a result of these investigations, he rediscovered the singular loop transmission approach for control design for NMP plants. The technique (which he calls singular  $G$ ) has been used in the past in an ad hoc manner, but he was the first to put it on a theoretical footing and thoroughly explore its properties. The singular  $G$  name is derived from a  $G$  compensation matrix that is not full rank. This means that at least one of the outputs is not independent, i.e. two outputs have a fixed ratio. Ordinarily, this means giving up some design freedom, but the NMP problem is eliminated and robustness to parameter variations is much greater and the need for scheduling reduced.

## Inherent Reconfiguration

The Self-Repairing Flight Control System (SRFCS) Program Office retained Dr. Horowitz as a consultant to investigate *inherent reconfiguration*. The SRFCS program objective was to develop and flight demonstrate a flight control system that would identify and isolate control surface failures and damage, then reconfigure the control laws to maintain performance and stability. Dr. Horowitz's task was to explore control design techniques so that, even under severe control surface failures, the tolerances can be satisfied automatically, with no need of explicit identification and switching in of new (a priori designed) compensators. This is denoted as *inherent reconfiguration*.

The primary motivation for this effort is that the control laws need to be sufficiently robust for the period during which the identification is isolating the failure. The approach taken by Dr. Horowitz is a natural extension of QFT, and clearly reveals the cost of feedback needed. This enables the designer to make intelligent trade-offs between fixed compensation, scheduling, and adaptation-identification. Identification, when it is necessary, can be done more slowly and accurately when the design is stable over as many failures as possible. The designs performed by Dr. Horowitz proved to be remarkably robust.

A SRFCS contractor, Lear Astronics, applied QFT to their design to maximize robustness to failures. Elements of this design were flown in the real-time simulator.

## **Air Force Institute of Technology Involvement - '82 to Present**

During this time, Dr. Horowitz began his association with the Air Force Institute of Technology (AFIT). Based upon the success of his earlier work, the laboratory requested that AFIT, through Professor C. H. Houpis, become involved with Professor Horowitz in a joint QFT research and development effort. Since the early eighties, Professor Horowitz has been an AFIT Distinguished Visiting Professor under the financial sponsorship of the laboratory (now directorate). A number of AFIT Masters of Science thesis students have been involved in this research and development effort, and has resulted in a number of journal and conference publications.

## OVERVIEW OF

### MISO QUANTITATIVE FEEDBACK THEORY (QFT) TECHNIQUE

Constantine H. Houppis

Air Force Institute Of Technology  
Wright-Patterson AFB, Ohio, 45433, USA

#### INTRODUCTION<sup>1-6</sup>

Quantitative feedback theory (QFT) has achieved the status as a very powerful design technique for the achievement of assigned performance tolerances over specified ranges of plant uncertainties without and with control effector failures. This paper presents an overview of the MISO QFT analog design technique<sup>1</sup>. The MISO QFT PC CAD package demonstration on Tuesday afternoon will reinforce this overview.

#### 1. The MISO Control System

The overview of the QFT design technique is presented in terms of the minimum-phase (m.p.) LTI MISO system of Fig. 1. The control ratios for tracking ( $D = 0$ ) and for disturbance rejection ( $R = 0$ ) are, respectively,

$$T_r(s) = \frac{F(s)G(s)P(s)}{1 + G(s)P(s)} = \frac{FL}{1 + L} \quad (1)$$

$$T_d = \frac{P(s)}{1 + G(s)P(s)} = \frac{P}{1 + L} \quad (2)$$

or

$$T_d = a \text{ constant} = \alpha_p \quad (3)$$

The tracking thumbprint specifications, based upon satisfying some or all of the step forcing function figures of merit for underdamped ( $M_p$ ,  $t_p$ ,  $t_r$ ,  $t_s$ ,  $K_m$ ) and overdamped ( $t_r$ ,  $t_s$ ,  $K_m$ ) responses, respectively, for a simple-second system, are depicted in Fig 2(a). The Bode plots corresponding to the time responses  $y(t)_u$  and  $y(t)_l$  in Fig. 2(b) represent the upper bound  $B_u$  and lower bound  $B_l$ , respectively, of the thumbprint specifications; i.e., an acceptable response  $y(t)$  must lie between these bounds. Note that for the m.p. plants, only the tolerance on  $|T_r(j\omega_i)|$  need be satisfied for a satisfactory design. For nonminimum-phase (n.m.p.) plants, tolerances on  $\angle T_r(j\omega_i)$  must also be specified and satisfied in the design process.<sup>7,8</sup> It is desirable to synthesize the tracking control ratios

corresponding to the upper and lower bounds  $T_{RU}$  and  $T_{RL}$ , respectively, so that  $\delta_v(j\omega_i)$  increases as  $\omega_i$  increases above the 0 dB crossing frequency of  $T_{RU}$ . This characteristic of  $\delta_R$  simplifies the process of synthesizing a loop transmission  $L_o(s) = G(s)P_o(s)$ , where  $P_o$  is the nominal plant transfer function, that requires the determination of the tracking bounds  $B_R(j\omega_i)$  which are obtained based upon  $\delta_R(j\omega_i)$ . The simplest disturbance control ratio model is  $T_D(s) = Y(s)/D(s) = \alpha_p$ , a constant (the maximum magnitude of the output based upon a unit step disturbance input).

## 2. Plant Templates of $P_j(s)$ , $\mathcal{GP}(j\omega_i)$

With  $L = GP$ , Eq. (13) yields

$$Lm T_R = Lm F + Lm \left[ \frac{L}{1 + L} \right] \quad (4)$$

The change in  $T_R$  due to the uncertainty in  $P$  is

$$\Delta(Lm T_R) = Lm T_R - Lm F = Lm \left[ \frac{L}{1 + L} \right] \quad (5)$$

By the proper design of  $L = L_o$  and  $F$ , this change in  $T_R$  is restricted so that the actual value of  $Lm T_R$  always lies between  $B_U$  and  $B_L$  of Fig. 2. The first step in synthesizing an  $L_o$  is to make templates which characterize the variation of the plant uncertainty, as described by  $j = 1, 2, \dots, J$  plant transfer functions, for various values of  $\omega_i$  over a specified frequency range. For the simple plant

$$P(s) = \frac{Ka}{s(s + a)} \quad (6)$$

where  $K \in \{1, 10\}$  and  $a \in \{1, 10\}$ , is used to illustrate how the templates are obtained for a plant with variable parameters. The region of plant uncertainty is depicted in Fig. 3. The boundary of the plant template can be obtained by mapping the boundary of the plant parameter uncertainty region as shown on the Nichols chart (NC) in Fig. 4. A curve is drawn through the points A, B, C, and D and the shaded area is labeled  $\mathcal{GP}(j1)$ , which can be represented by plastic a template. Templates for other values of  $\omega_i$  are obtained in a similar manner.

## 3. U-Contour

The specifications on system performance in the frequency domain [see Fig. 2(b)] identify a minimum damping ratio  $\zeta$  for the dominant

roots of the closed-loop system which becomes a bound on the value of  $M_p = M_m$ . On the NC this bound on  $M_m = M_L$  [see Fig. 2(b)] establishes a region which must not be penetrated by the template of  $L(j\omega)$  for all  $\omega$ . The boundary of this region is referred to as the universal high-frequency boundary (UHFB), the U-contour, because this becomes the dominating constraint on  $L(j\omega)$ . Therefore, the top portion, efa, of the  $M_L$  contour becomes part of the U-contour. For a large problem class, as  $\omega \rightarrow \infty$ , the limiting value of the plant transfer function approaches

$$\lim_{\omega \rightarrow \infty} [P(j\omega)] = \frac{K}{\omega^\lambda} \quad (7)$$

where  $\lambda$  represents the excess of poles over zeros of  $P(s)$ . The plant template, for this problem class, approaches a vertical line of length equal to

$$\Delta \triangleq \lim_{(\omega \rightarrow \infty)} [Lm P_{max} - Lm P_{min}] = Lm K_{max} - Lm K_{min} = V \text{ dB} \quad (8)$$

If the nominal plant is chosen at  $K = K_{min}$ , then the constraint  $M_L$  gives a boundary which approaches the U-contour abcdefa of Fig. 5.

#### 4. Bounds $B_o(j\omega)$ on $L_o(j\omega)$

The determination of the tracking  $B_R(j\omega_i)$  and the disturbance  $B_D(j\omega_i)$  bounds are required in order to yield the optimal bounds  $B_o(j\omega_i)$  on  $L_o(j\omega_i)$ . The solution for  $B_R(j\omega_i)$  requires that the actual  $\Delta T_R(j\omega_i) \leq \delta_R(j\omega_i)$  dB in Fig. 2(b). Thus it is necessary to determine the resulting constraint, or bound  $B_R(j\omega_i)$ , on  $L(j\omega_i)$ . The procedure is to pick a nominal plant  $P_o(s)$  and to derive the bounds, by use of templates or a CAD package, on the resulting nominal transfer function  $L_o(s) = G(s)P_o(s)$ . The disturbance bounds can be determined by the method described in Reference 2. For the case shown in Fig. 6  $B_o(j\omega_i)$  is composed of those portions of each respective bound  $B_R(j\omega_i)$  and  $B_D(j\omega_i)$  that have the largest dB values. The synthesized  $L_o(j\omega_i)$  must lie on or just above the bound  $B_o(j\omega_i)$  of Fig. 6.

#### 5. Synthesizing (or Loop Shaping) $L_o(s)$ and $F(s)$

The shaping of  $L_o(j\omega)$  is shown by the dashed curve in Fig. 6. A point such as  $Lm L_o(j2)$  must be on or above  $B_o(j2)$ . Further, in order to satisfy the specifications,  $L_o(j\omega)$  cannot violate the U-contour. In this example a reasonable  $L_o(j\omega)$  closely follows the U-contour up to  $\omega = 40$  rad/sec and must stay below it above  $\omega = 40$  as

shown in Fig 6. It also must be a Type 1 function (one pole at the origin). Synthesizing a rational function  $L_o(s)$  which satisfies the above specification involves building up the function

$$L_o(j\omega) = L_{ok}(j\omega) = P_o(j\omega) \prod_{k=0}^W [K_k G_k(j\omega)] \quad (9)$$

where for  $k = 0$ ,  $G_o = 1/\angle 0^\circ$ , and  $K = \prod_{k=0}^W K_k$ .  $L_o(j\omega)$  is built up term-by-term or by a CAD loop shaping routine,<sup>9</sup> in order to stay just outside the U-contour in the NC of Fig. 6. The design of a proper  $L_o(s)$  guarantees only that the variation in  $|T_R(j\omega_i)|$  is less than or equal to that allowed, i.e.,  $\delta_R(j\omega_i)$ . The purpose of the prefilter  $F(s)$  is to position  $Lm [T(j\omega)]$  within the frequency domain specifications, i.e., that it always lies between  $B_U$  and  $B_L$  [see Fig. 2(b)] for all  $J$  plants. The method for determining  $F(s)$  is discussed in the next section.

## 6. Prefilter Design<sup>1,7,8</sup>

Design of a proper  $L_o(s)$  guarantees only that the variation in  $|T_R(j\omega)|$  is less than or equal to that allowed, i.e.,  $\delta_R(j\omega) \leq \Delta[Lm T_R(j\omega)]$ . The purpose of the prefilter  $F(s)$  is to position

$$Lm T(j\omega) = Lm \frac{L(j\omega)}{1+L(j\omega)} \quad (10)$$

within the frequency domain specifications. A method for determining the bounds on  $F(s)$  is as follows: Place the nominal point of the  $\omega_i$  plant template on the  $L_o(j\omega_i)$  point of the  $L_o(j\omega)$  curve on the NC (see Fig. 7). Traversing the template, determine the maximum  $Lm T_{max}$  and the minimum  $Lm T_{min}$  values of Eq. (10) obtained from the M-contours. Based upon obtaining sufficient data points, for various values of  $\omega_i$ , and in conjunction with the data used to obtain Fig. 2(b) the plots of Fig. 8 are obtained. Utilizing Fig. 8, the straight-line Bode plot technique, and the condition

$$\lim_{s \rightarrow 0} F(s) = 1 \quad (11)$$

for a step forcing function, an  $F(s)$  is synthesized that lies within the upper and lower plots in Fig. 8.



## **7. Simulation**

The "goodness" of the synthesized  $L_o(s)$  and  $F(s)$  is determined by simulating the QFT designed control system for all  $J$  plants. MISO QFT CAD packages are available that expedite this simulation phase of the complete design process (see Appendix).

## **8. MISO QFT Discrete Design Technique<sup>3,6</sup>**

The bilinear transformation,  $z$ -domain to the  $w'$ -domain and vice-versa, is utilized in order to accomplish the QFT design for both MISO and MIMO sampled-data control systems in the  $w'$ -domain. This transformation enables the use of the MISO QFT analog design technique to be readily used, with minor exceptions, to perform the QFT design for the controller  $G(w')$ . If the  $w'$ -domain simulations satisfy the desired performance specification then by use of the bilinear transformation the  $z$ -domain controller  $G(z)$  is obtained. With this  $z$ -domain controller a discrete-time domain simulation is obtained to verify the goodness of the design.

### **Appendix -- QFT CAD PACKAGES**

#### **A. INTRODUCTION**

The first useable MISO QFT CAD package was developed, in 1986 for the analog design and in 1991, for the discrete design at the Air Force Institute of Technology (AFIT). This CAD package has been a catalyst in assisting the newcomer to QFT to understand the fundamentals of this powerful design technique.

**A.1 MISO QFT CAD --** The AFIT package is called "ICECAP/QFT" which is designed for the VAX. Those desiring a copy of this package can contact: Professor Gary B. Lamont, AFIT/ENG, Wright-Patterson AFB, OH 45433. Currently Professor Lamont is developing a PC version of this package. These packages have been designed as an "educational tool."

**A.2 MISO QFT PC CAD --** Dr. Oded Yaniv, Tel-Aviv University, Israel, has a MISO QFT PC CAD package for both analog and discrete system design.

**A.3 OTHERS --** Professor F. Bailey, University of Minnesota, Minneapolis, Minnesota, has also developed QFT CAD packages. The QFT CAD packages mentioned in this Appendix will be demonstrated Tuesday afternoon during the symposium.

## B. MIMO QFT CAD

A MIMO PC QFT CAD package was developed by Mr. Richard R. Sating as a Master thesis, under the direction of Professor C. H. Houpis, for his AFIT MS degree. This package was designed to handle MIMO control problems of arbitrary dimensions for both the analog and the digital case with the option to use the improved method during the design. This package will also be demonstrated on Tuesday afternoon.

## REFERENCES

1. D'Azzo, J. J., and C. H. Houpis: "Linear Control System Analysis and Design," McGraw-Hill, NY, 3rd Ed., 1988.
2. Houpis, C. H.: "Quantitative Feedback Theory (QFT): Technique for Designing Multivariable Control Systems," AFWAL-TR-86-3107, AF Wright Aeronautical Laboratories, Wright-Patterson AFB, OH, 1987. (Available from Defense; Technical Information Center, Cameron Station, Alexandria, VA 22314, document number AD-A176883.)
3. Houpis, C. H. and G. Lamont: "Digital Control Systems: Theory, Hardware, Software," McGraw-Hill, NY, 2nd Ed., 1992.
4. Horowitz, I. M. and M. Sidi: "Synthesis of Feedback Systems with Large Plant Ignorance for Prescribed Time Domain; Tolerances," Int. J. Control, vol. 16, pp 287-309, 1972.
5. Horowitz, I. M., and C. Loecher: "Design of a 3x3 Multivariable Feedback System with Large Plant Uncertainty," Int. J. Control, vol. 33, pp. 677-699, 1981.
6. Horowitz, I. M. and Y. K. Liao: "Quantitative Feedback Design for Sampled-data Systems," Int. J. Control, vol. 38, May, 1986.
7. Horowitz, I. M.: "Optimum Loop Transfer Function in Single-Loop Minimum Phase Feedback Systems," Int. J. Control, vol 22, pp. 97-113, 1973.
8. Horowitz, I. M. and C. Loecher: Design of a 3x3 Multivariable Feedback Systems with Large Plant Uncertainty," Int. J. Control, vol. 33, pp. 677-699, 1981.
9. Thompson, D. F. and O. D. I. Nwokah: "Optimal Loop Synthesis in Quantitative Feedback Theory," Proceed. of the American Control Conference, San Diego, CA, pp. 626-631, 1990.

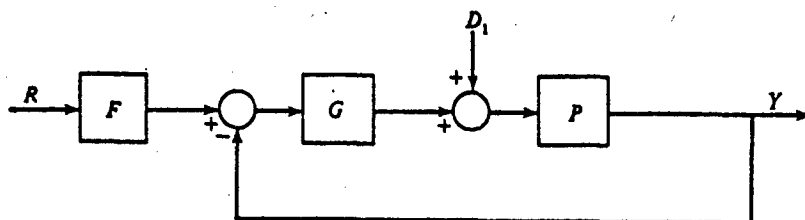


Fig. 1 A MISO plant

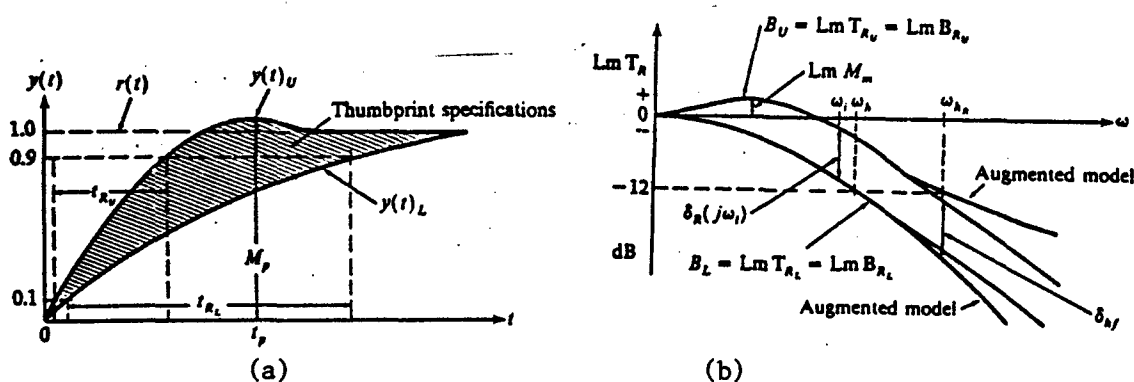


Fig. 2 Desired response characteristics: (a) thumbprint specifications, (b) Bode plots of  $T_R$

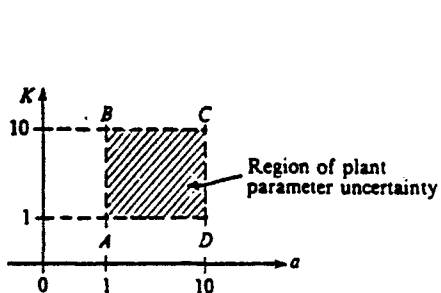


Fig. 3 Region of plant uncertainty

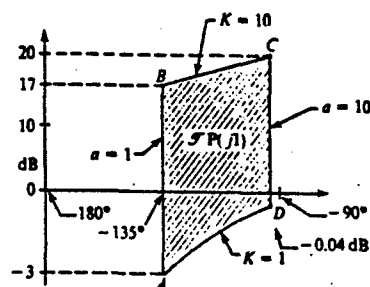


Fig. 4 The template  $SP(j1)$  characterizing Eq. (6)

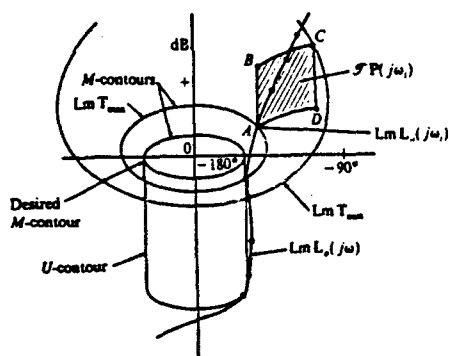
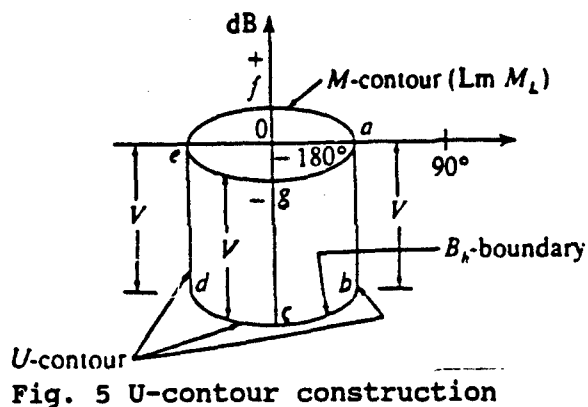
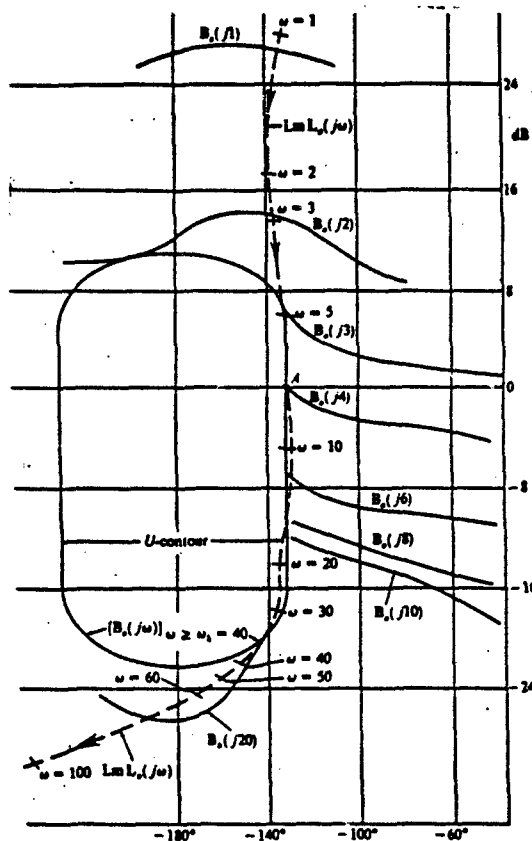
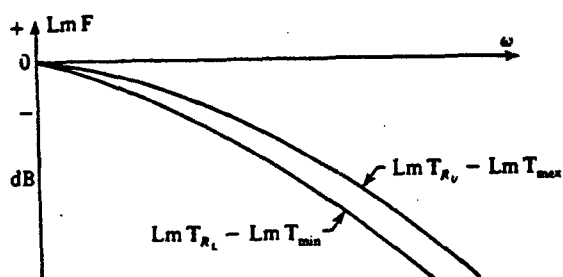


Fig. 7 Prefilter determination



# SYNTHESIS OF UNCERTAIN MIMO FEEDBACK SYSTEMS BY QFT - A TUTORIAL

ODED YANIV\*

## Abstract

In the QFT design technique for MIMO uncertain feedback systems, the objective is to design the controller and prefilter such that given closed loop specifications are achieved over a given range of plant uncertainty. This tutorial uses a two input two output plant to explain the properties of the QFT technique for linear time invariant systems, which are: (1) Design to plant uncertainties both in model and disturbances, (2) Design to performance specifications, (3) Emphasize 'cost of feedback', (4) Elimination of underdamped closed loop behavior if possible, and (5) the design procedure is always reduced to a sequential SISO and/or MISO design process whose bounds can be calculated in a closed form.

---

\*Faculty of Engineering, E.E.-Systems, Tel-Aviv University, Tel-Aviv 69 978, Israel.

## 1 Introduction

The synthesis of MIMO feedback systems with uncertain plants (Wendell, 1988) is a problem which has aroused a great deal of interest. Some of the most important synthesis methods are  $H_\infty$  (Francis, 1987), Adaptive Control (Astrom, 1985), the British school (Mayne 1979, Rosenbrock 1974) and the QFT method (Yaniv and Horowitz, 1986). In addition to robust stability and performance, a good synthesis technique should meet the demands of low cost of feedback solution, no internal conditionally stable loops if possible, and gain and phase margin specifications. The last property has been discussed in several papers using various definitions of gain and phase margin, for example (Davison 1986, Sobel 1983 and Tannenbaum 1986). The definition adopted by QFT emphasizes the distance from the critical point -1 of the loop transfer function at different channel breaking points. In general terms, this implies a smooth, not underdamped, time response for tracking commands as well as disturbances at the plant output.

The tutorial is set out as follows: The problems QFT solves are defined in Section 2, while Section 3 develops the design process for the basic tracking problem, and Section 4 is devoted to a design example.

## 2 Definition of the Problem

In Fig. 1  $P = [p_{ij}(s)]^1$  is a linear time invariant plant model. Due to plant uncertainty  $P$  can be any member of a given set denoted by  $\mathcal{P}$ . For all  $i, j = 1, \dots, n$ , let the following definitions hold:

- $a_{ij}(\omega)$  - a non-negative function of  $\omega$ .
- $b_{ij}(\omega)$  - a positive function of  $\omega$ ,  $b_{ij} > a_{ij}$ .
- $m_i(\omega)$  - a positive function of  $\omega$ , exists  $\omega_1$  and  $\alpha_i$  such that  $m_i(\omega) < \alpha_i < 1$  for  $\omega \geq \omega_1$ .
- $y_i^d(\omega)$  - a positive functions of  $\omega$ .
- $F = [f_{ij}]$  - a prefilter.
- $G = \text{diag}(g_i)$  - a strictly proper controller.
- $T_R = [t_{ij}] = [I + PG]^{-1}PGF$  - the transfer function from  $r_j$  to  $y_i$  in Fig. 1.
- $T_D = [d_{ij}] = [I + PG]^{-1}P$  - the transfer function from plant input  $j$  to  $y_i$  in Fig. 1.
- $D = \{D\}$ , a set of disturbances at the plant input.
- $L_i^n$  - the true loop transmission from the input at  $e_i$  (of Fig. 2), where only the channel at  $e_i$  is disconnected, derived as follows: feed an impulse into  $e_i'$  and measure the signal returned to  $e_i$ , the transfer function of the latter is  $L_i^n$ .
- $\omega_0$  - this frequency is defined as the frequency above which the disturbances are of low magnitude and sensitivity to plant variations is not important (since at high frequencies the benefits of feedback are negligible).

The problem QFT solves: find  $F$  and  $G$  to satisfy (1-4) below for all  $P \in \mathcal{P}$ :

- Stability: the closed loop system

$$T_R = [I + PG]^{-1}PGF \quad (1)$$

is internally stable.

<sup>1</sup>Throughout this paper, all matrices are  $n$  by  $n$  whose elements are proper rational transfer functions.

- Closed loop performance: For a given  $\omega_0$ ,  $a_{ij}$  and  $b_{ij}$

$$a_{ij}(\omega) \leq |t_{ij}(i\omega)| \leq b_{ij}(\omega); \text{ for } i, j = 1, \dots, n, \text{ and } \omega \leq \omega_0, \quad (2)$$

- Margin performance: For  $i = 1, \dots, n$ , the  $i$ -th loop stability margin satisfies:

$$|1 + L_i^n| \geq m_i(\omega); \quad i = 1, \dots, n. \quad (3)$$

- Disturbance rejection performance: For each member  $D$  of  $\mathcal{D}$

$$(T_D D)_i < y_i^d, \quad i = 1, \dots, n. \quad (4)$$

**Remark 2.1** Inequality (3) used by Horowitz (1972) is not identical to the gain and phase margin found in classic control texts (See D'Azzo and Houpis, 1988), but rather the 'closest distance to the critical point -1' of the transfer function  $L_i^n$ , which is given by the value  $D_i(\omega)$ . For example if  $D_i(\omega) = 0.5$ , the gain and phase margin are 6dB and 30° respectively.

**Remark 2.2** For  $F = I$  and for a diagonal controller  $G$ ,  $t_{ii} = L_i^n / (1 + L_i^n)$ , is the transfer function from input  $r_i$  to output  $y_i$  (O'Reilly, 1991). A proper choice of  $m_i(\omega)$  will eliminate any underdamped behavior of  $t_{ii}$ , so that the uncertain MIMO system will then exhibit a better time response similar to that seen in SISO systems. The same is valid for output  $y_i$  due to disturbance at the plant output  $i$ , since its transfer function is  $(1 + L_i^n)^{-1}$ .

### 3 The Design Procedure

The Horowitz MIMO design method (Yaniv and Horowitz, 1986) which is concerned with satisfying (1-2), turns the design process into a sequence of MISO problems. The solution of each MISO problem is the controller  $g_i$  and the prefilters  $f_{ij}$ ,  $j = 1, \dots, n$  (each  $f_{ij}$  being due to the closed loop specifications from input at  $j$  to output at  $i$ ), giving a combined solution  $G = \text{diag}[g_i]$  and  $F = [f_{ij}]$  for the MIMO system. The main task during the design of each MISO problem is to find bounds on an open loop transfer function. Each bound is a closed curve on the complex plane dividing the latter into two regions, one of which is called  $\sigma(\omega)$ , so that if the open loop transfer function at frequency  $\omega$  belongs to  $\sigma(\omega)$  and satisfies the Nyquist stability criterion, the synthesis procedure must work. In order to satisfy each of the performances (1-4), more constraints are placed on each of the MISO problems. Thus the permissible region  $\sigma(\omega)$  is reduced, which in turn implies a solution for the MIMO system, if a solution is found. This is a kind of simultaneous stabilization problem with constraints, i.e., at each step,  $g_i$  is designed so that the bounds are satisfied and the same controller  $g_i$  stabilizes a given set of plants.

#### 3.1 Stability and Closed Loop Performance

Consider the feedback system shown in Fig. 1. Let  $(i_1, \dots, i_n)$  be a given order of the integers  $(1, \dots, n)$ , and  $P^k = [p_{ij}^k]$  be defined recursively as follows:

$$\begin{aligned} [p_{ij}^1] &= P^{-1}; \\ [p_{ij}^k] &= \begin{bmatrix} p_{ij}^{k-1} - \frac{p_{i i_k}^{k-1} p_{i_k j}^{k-1}}{p_{i_k i_k}^{k-1} + g_{i_k}} \end{bmatrix}; \quad h = i_{k-1}, \quad i = i_k, \dots, i_n \end{aligned} \quad (5)$$

Based on the sequential loop closure technique of Mayne (1979) and Rosenbrock (1974), it is shown that (for the sake of clarity  $i_k = k$  and the superscript  $k$  denotes the recursive step

number):

$$t_{ij} = \frac{f_{ij}g_i q_i^k}{1 + g_i q_i^k} - \frac{d_{ij}^k q_i^k}{1 + g_i q_i^k}; \quad i = k, \dots, n; \quad j = 1, \dots, n \quad (6)$$

where

$$d_{ij}^k = \sum_{u=1, \dots, k-1} p_{iu}^k f_{uj} + \sum_{u=k+1, \dots, k} p_{iu}^k t_{uj}; \quad q_i^k = 1/p_{ii}^k. \quad (7)$$

Clearly,  $t_{ij}$  does not depend on  $k$  or on the chosen recursive order  $(i_1, \dots, i_n)$  and  $q_i^k$  does. Hence (6) gives  $(n - k + 1)$  equations for  $t_{ij}$  as a function of  $q_i^k$ . Equations (6-7) reduce the MIMO problem into  $n^2$  MISO problems in the following way. At step  $m$ , ( $m = 1, \dots, n$ ), the designer obtains the scalar transfer function  $g_m$  and  $f_{mj}$  ( $j = 1, \dots, n$ ) so that for all  $P \in \mathcal{P}$

$$a_{mj}(\omega) \leq \left| \frac{f_{mj}g_m q_m^m}{1 + g_m q_m^m} - \frac{d_{mj}^m q_m^m}{1 + g_m q_m^m} \right| \leq a_{mj}(\omega); \quad \omega \leq \omega_0$$

$$\frac{1}{1 + g_m q_m^m} \text{ is internally stable.} \quad (8)$$

where  $d_{mj}^m$  is assumed (in the Horowitz MIMO technique) bounded by

$$\left| \sum_{u=1, \dots, k-1} p_{iu}^k f_{uj} \right| + \sum_{u=k+1, \dots, k} |p_{iu}^k b_{uj}|$$

**Remark 3.1** The  $g_m$  and  $f_{mj}$  designed for  $j = 1, \dots, n$ , are used to define the parameters of the next step (step  $m + 1$ , Equations (6-7) for  $i = m + 1$ ). After  $n$  steps, all  $g_i$  and  $f_{ij}$  are known and the design process comes to an end.

**Remark 3.2** Step  $m$  is equivalent to solving  $n$  uncertain MISO problems with the same controller  $g_m$  and  $n$  prefilters  $f_{mj}$ , which can be solved within the framework of the QFT technique. Moreover, a parameter  $x$  can be chosen, generally between 0.5 and 0.8, so that  $|(1 + g_m q_m^m)| > x$ .

### 3.2 Margin Performance

In order to satisfy the margin conditions 3, i.e.,

$$|1 + L_i^n| \geq m_i(\omega); \quad i = 1, \dots, n. \quad (9)$$

the bounds for  $g_k$  should also guarantee [15]

$$|1 + L_i| \geq m_i(\omega); \quad i = 1, \dots, k. \quad (10)$$

The solution of these inequalities, to find bounds on  $g_k$  such that (10) is true, is a closed curve in the complex plane which can be calculated for each case and phase of  $g_k$  by solving a quadratic equation. The bound on  $g_k$  will be the union of bounds due to all the constraints. In the trivial  $2 \times 2$  case this may decrease the allowed region for the second step (say design  $g_2$ ) such that

$$\left| 1 + \frac{g_1}{p_{11} - p_{12}p_{21}/(p_{22} + g_2)} \right| > d_1(\omega); \quad \left| 1 + \frac{g_2}{p_{22} - p_{12}p_{21}/(p_{11} + g_1)} \right| > d_2(\omega) \quad (11)$$

The solution of these inequalities, to find bounds on  $g_2$  such that (11) is true, is a closed curve in the complex plane which can be calculated for each case and phase of  $g_2$  by solving a quadratic equation. The bound on  $g_2$  will be the union of bounds due to all the constraints.



## 4 A 2x2 Example

### 4.1 Plant and Performance definition

- Plant Model:

$$P = \frac{1}{s} \begin{bmatrix} k_{11} & k_{12} \\ k_{21} & k_{22} \end{bmatrix} \quad (12)$$

- Plant Uncertainty:  $k_{11}$  and  $k_{22}$  in  $[2 - 6]$ ,  $k_{12}$  and  $k_{21}$  in  $[0.5 - 1.5]$
- Closed Loop Performance: Are given on  $[t_{ij}]$ , off diagonal tracking elements less than  $-20dB$  and the diagonal satisfy the constraints given in the following table:

$\omega$	$b_{11}, b_{22}$	$a_{11}, a_{22}$
1	1.1	0.9
2	1.1	0.8
3	1.0	0.6
5	0.7	0.2
10	0.1	0

### 4.2 Design Execution

#### 4.2.1 Design step #1

Find a solution to the two MISO feedback systems described schematically in Fig. 3, i.e., find  $g_1$ ,  $f_{11}$  and  $f_{12}$  such that for all plant cases and  $|t_{ij}| < b_{ij}$

$$a_{11} < |t_{11}| < b_{11}, \text{ and } a_{12} < |t_{12}| < b_{12}. \quad (13)$$

Since the off-diagonal should be as small as possible, the choice  $f_{12} = 0$  and  $f_{21} = 0$  is reasonable. Thus the solution of the MISO problems

$$a_{11} < \left| \frac{f_{11}g_1q_{11}}{1+g_1q_{11}} \right| + \left| \frac{b_{21}q_{11}/q_{12}}{1+g_1q_{11}} \right| < b_{11}, \quad \left| \frac{b_{22}q_{11}/q_{12}}{1+g_1q_{11}} \right| < b_{12} \quad (14)$$

is a solution to step #1. The bounds and nominal loop transmission are given in Fig. 4. The controller and prefilters are:

$$g_1 = \frac{5(1+s/45)}{(1+s/5)(1+s/140+s^2/140^2)}; \quad f_{11} = \frac{1}{1+1.4s/2.5+s^2/2.5^2}; \quad f_{12} = 0. \quad (15)$$

#### 4.2.2 Design step #2

Find a solution to the two MISO feedback systems described schematically in Fig. 5, i.e., find  $g_2$ ,  $f_{21}$  and  $f_{22}$  such that for all plant cases and  $|t_{ij}| < b_{ij}$

$$a_{21} < |t_{21}| < b_{21}, \text{ and } a_{22} < |t_{22}| < b_{22}. \quad (16)$$

where

$$p_{2i}^2 = p_{2i}^1 - \frac{p_{1i}^1 p_{21}^1}{p_{1i}^1 + g_1}, \quad d_{2i}^2 = -\frac{p_{21}^2}{p_{22}^2} f_{1i} \quad (17)$$

and

$$q_{22}^2 = 1/p_{2i}^2 \quad (18)$$

The bounds and nominal loop transmission are given in Fig. 6. The controller and prefilters are:

$$g_2 = \frac{25(1 + s/25)}{1 + s/90 + s^2/90^2}; f_{22} = \frac{1}{1 + 1.4s/3 + s^2/3^2}; f_{21} = 0. \quad (19)$$

#### 4.2.3 Frequency Domain Simulations

The next table gives upper and lower values for the closed loop transfer function diagonal elements and upper values for the off-diagonal values.

$\omega$	1	2	3	5	10
$t_{11}$	0.99-0.99	0.86-0.85	0.59-0.58	0.26-0.25	
$t_{12}$	1.00-1.00	0.94-0.92	0.75-0.52	0.39-0.35	
$t_{21}$	0.02	0.04	0.05	0.05	
$t_{22}$	0.04	0.07	0.08	0.07	

## References

- [1] Astrom, K. J. (1985). 'Adaptive Control - A Way to Deal with Uncertainty', in Ackerman J: 'Uncertainty and Control Lecture Notes in Control and Information Science', 70, Springer-Verlag, Berlin.
- [2] Francis, A. B. (1987). 'A Course in H Control Theory', Lecture Notes in Control and Information Sciences, 88, Springer-Verlag.
- [3] Davison, E.J. (1986). 'Robust Control for Industrial Systems', Proc. of 25th CDC, WP1, Athens, Greece.
- [4] D'Azzo J. J. and C.H. Houpis (1988). 'Linear Control Systems Analysis and Design', 3rd edition Mc-Graw Hill student edition.
- [5] Horowitz, I. and M. Sidi (1972). 'Synthesis of Feedback Systems with Large Plant Ignorance for Prescribed Time-Domain Tolerances', Int. J. Con. Vol. 16, No. 2, pp. 287-309.
- [6] Horowitz, I. (1979). 'Quantitative Synthesis of Uncertain Multiple Input Output Feedback Systems', Int. J. Con., Vol. 30, No. 1, pp. 81-100 Appendix 1.
- [7] Mayne, D. Q. (1979) 'Sequential Design of Linear Multivariable Systems', Proc. IEE, Vol. 126, No. 6, pp. 568-572.
- [8] Nwokah, O.D.I, D.F Thompson and R.A. Perez (1990). 'On Some Existence Conditions for QFT Controllers', Recent Developments in Quantitative Feedback Theory, edited by O.D.I. Nwokah, DSC-Vol. 24, pp 1-10.
- [9] O'Reilly, J. and E.W. Leithead (1991). 'Multivariable Control by Individual Channel Design', Int. J. Cont., Vol. 54, No. 1, pp. 1-46.
- [10] Rosenbrock, H. H. (1974). 'Computer Aided Control System Design', Academic Press, London.
- [11] Sobel, K.M., J.C. Chung and E.Y. Shapiro (1983). 'Application of MIMO Phase and Gain Margins to the Evaluation of a Flight Control System', ACC, Vol. 3, pp. 1286-1287.
- [12] Tannenbaum, A. (1986). 'On the Multivariable Gain Margin Problem', Automatica, Vol. 22, No. 3, pp. 381-383.
- [13] Wendell H. F. (1988), 'Future Directions in Control Theory - A Mathematical Perspectives', SIAM, Philadelphia, 1400 Architects Build. 117 South 17th St. Phil., PA 19103.
- [14] Yaniv, O. and I. Horowitz (1986), 'A Quantitative Design Method for MIMO Linear Feedback Systems Having Uncertain Plants', Int. J. Con., Vol. 43, No. 2, pp. 401-421.
- [15] Yaniv, O. (1992), 'Synthesis of Uncertain MIMO Feedback Systems for Gain and Phase Margin at Different Channel Breaking Points', Automatica, to appear.

## List of Figures

1	Two degree of freedom MIMO structure. . . . .	9
2	$L_i^n$ is the transfer function from $e_i'$ to $e_i$ . . . . .	9
3	MISO problems for design step #1 . . . . .	9
4	Solution of step #1 . . . . .	9
5	MISO problems for design step #2 . . . . .	9
6	Solution of step #2 . . . . .	9

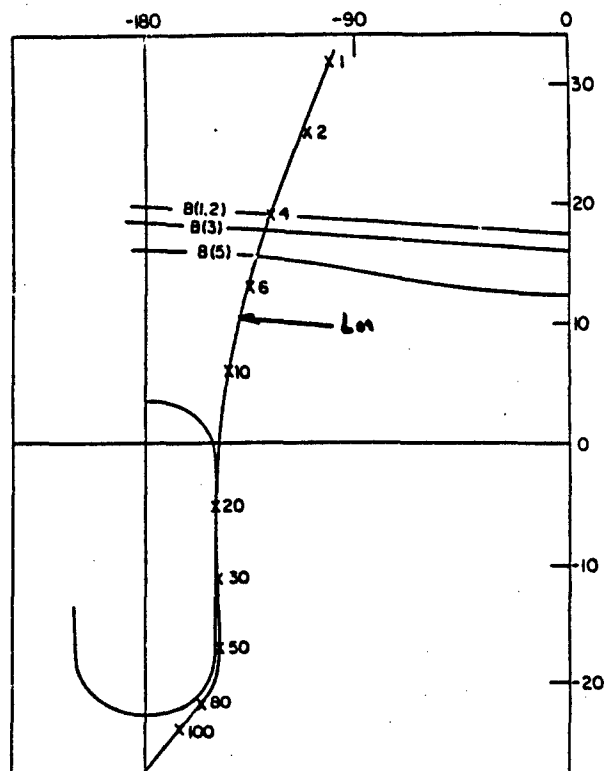
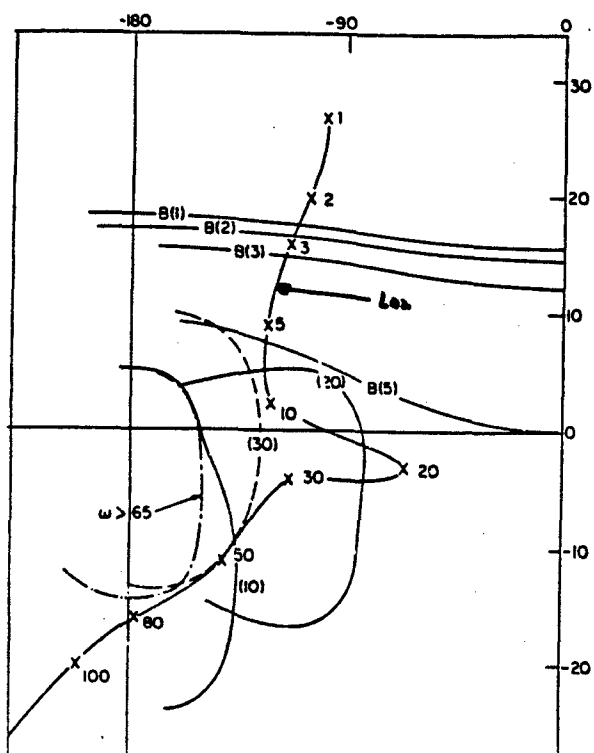


Figure 4: Solution of step #1



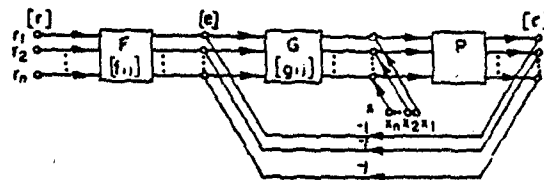


Figure 1: Two degree of freedom MIMO structure.

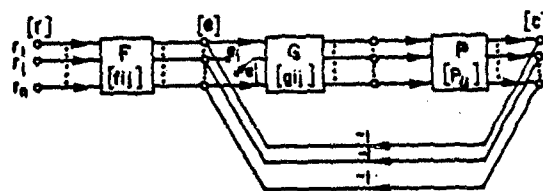


Figure 2:  $L_i^n$  is the transfer function from  $e_i'$  to  $e_i$ .

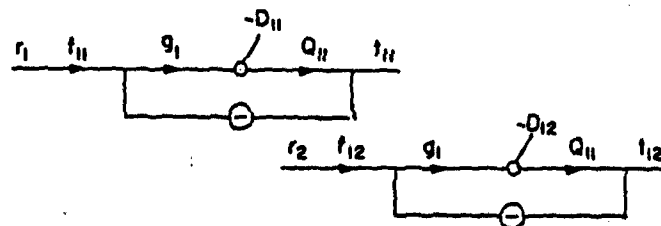


Figure 3: MISO problems for design step #1

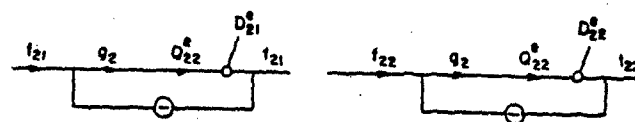


Figure 5: MISO problems for design step #2

# A Delta Transform Approach to Loop Gain-Phase Shaping Design of Robust Digital Control Systems\*

A.J. Punyko\*

F.N. Bailey\*

**Abstract:** This paper addresses the existence of loop gain-phase shaping (LGPS) solutions for the design of robust digital control systems for SISO, minimum-phase, continuous time processes with parametric uncertainty. We develop the frequency response properties of LGPS for discrete time systems using the  $\Delta$ -transform, a transform method that applies to both continuous and discrete time systems. A theorem is presented which demonstrates that for reasonable specifications there always exists a sampling period such that the robust digital control problem has a solution. Finally, we offer a procedure for estimating the maximum feasible sampling period for LGPS solutions to robust digital control problems.

## 1. INTRODUCTION

The Loop Gain-Phase Shaping (LGPS) approach to robust control system design uses closed loop performance and relative stability specifications, combined with a model of process uncertainty, to define complex plane gain-phase constraints on the nominal open loop gain function. The designer then "fits" a realizable nominal loop gain function  $L_o(s)$  to these constraints and uses  $L_o(s)$  to obtain descriptions of the necessary compensation networks. The LGPS concept for single-loop, analog, robust control system design was originally proposed by Horowitz in (Horowitz 1963) and later combined in the general framework of quantitative feedback theory, or QFT (Horowitz 1982). In (Bailey and Hui 1991) it was shown that for SISO robust control system design, LGPS has performance advantages over traditional loop gain shaping and its derivatives (LQG/LTR,  $H_\infty$ -Optimization, etc.). Moreover, LGPS allows the control system designer to directly attack the robust performance problem, unlike other methods which indirectly address robust performance by solving a stabilization problem.

The fitting of a realizable nominal loop gain function to specification/uncertainty generated gain-phase constraints is the difficult part of the LGPS design procedure. Although several iterative search approaches have been demonstrated, no closed form solution exists (Gera and Horowitz 1980; Thompson 1990). An important unresolved question involves the existence of solutions to the fitting problem. If one plans to use an iterative search approach to the solution of this problem, it is important to know whether a solution exists. In (Bailey and Cockburn, 1991), a mathematical formalization of LGPS was used to study the existence of solutions to the fitting problem in the continuous time case. There it was shown that in the case of minimum phase (but possibly unstable) processes with only parametric uncertainty, a fitting solution (and thus a solution to the LGPS design problem) always exists if there are no constraints on the open and/or closed loop bandwidth. However, fitting solutions in the case of non-minimum phase processes is problematical (Horowitz and Sidi 1978).

The increasing popularity and flexibility of digital controllers has lead to the adaptation

---

\*This work was supported in part by a grant from FMC Corporation.

\*Department of Electrical Engineering, University of Minnesota, 200 Union St. S.E., Minneapolis, MN 55455, USA, 612-625-7808.

of LGPS concepts to the design of digital control systems. This problem was considered in (Horowitz and Liao 1986). However, these authors merely present a design example in order to show the effects of sampling on the continuous time LGPS problem. Additional papers on QFT design of digital controllers (Yaniv and Chait 1991; Lamont, Houppis, and Ewing 1991) have primarily focused on design techniques. Unfortunately, none of these papers discuss the existence of discrete time LGPS solutions. In fact, because discrete time plant models are generally non-minimum phase, for a fixed sampling period there may be no solution to discrete time LGPS problems.

In this paper we adapt the mathematical formalization of the LGPS problem as described in (Bailey and Cockburn 1991) to address questions about the existence of solutions to discrete time LGPS problems in the case of parametric uncertainty. We will assume that the discrete time robust control problem arises in the context of digital control of a continuous time process. Thus, we will assume that the discrete time process is the step-invariant equivalent (or zero-order hold equivalent) of a continuous time process which is finite-dimensional, linear, time-invariant, minimum phase, but possibly unstable. A glossary of notation and definitions is provided in the Appendix.

## 2. THE CONTINUOUS TIME ROBUST CONTROL PROBLEM

Given a process model with uncertainty, a model of external disturbances, and desired stability and performance specifications, the goal of the general robust feedback control problem is to design a controller such that the closed loop system meets the desired stability and performance specifications.

Because the LGPS approach assumes that only the process inputs and outputs are available, the most general controller configuration is the two-degree-of-freedom structure (TDF) (Horowitz 1963). Given the particular TDF structure shown in Fig. 1, the LGPS approach to the robust control problem is to choose a loop compensator  $G(s)$  and pre-compensator  $F(s)$  such that the closed-loop transfer function  $T(s)$  meets the desired stability and performance specifications.

In the next sections, we outline the continuous time LGPS robust control problem and then summarize the continuous time LGPS existence conditions detailed in (Bailey and Cockburn 1991).

### 2.1 Problem Description

#### The Process Model

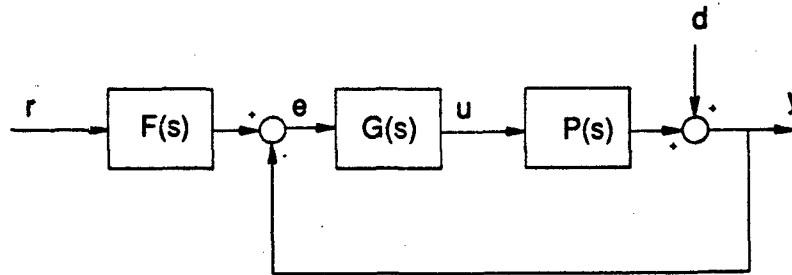
Throughout this paper, we model the continuous time process as an arbitrary SISO dynamic system with parametric uncertainty. Formally, we have this set of assumptions about the process model,  $P(s)$ .

**Assumption 1C:** We assume that the continuous time process model  $P(s; \alpha)$  is finite-dimensional, linear, time-invariant (FDLTI) and has only parametric uncertainty. We assume a transfer function model of the process in the form



$$P(s) = P(s; \alpha) := \frac{\sum_{i=0}^m b_i(\alpha) s^i}{\sum_{j=0}^n a_j(\alpha) s^j} \quad \text{with } \alpha \in A_p \subset \mathbb{R}^p, n > m$$

where the coefficients  $b_i(\alpha)$  and  $a_j(\alpha)$  are uncertain due to underlying uncertainty in some model parameters  $\alpha$  (e.g., masses, gains, inertias, etc.) and  $A_p$  is a compact set of parameter variations. We also assume that there is a nominal parameter vector  $\alpha_0 \in A_p$  which defines the nominal process model:  $P_0(s) := P(s; \alpha_0)$ . Also, we consider only those processes that are minimum-phase (i.e., no closed RHP zeros), have no uncertain poles on the  $j\omega$ -axis for all  $\alpha \in A_p$ , and assume that  $a_n(\alpha)b_m(\alpha) > 0$  for all  $\alpha \in A_p$ . We define the pole-excess of the process as  $r = n - m > 0$ .



$F(s)$  = Pre-compensator  
 $G(s)$  = Loop Compensator  
 $P(s)$  = Process Model  
 $L(s) = P(s)G(s)$  = Loop Gain  
 $T(s) = F(s)L(s)/[1+L(s)]$  = Closed Loop Transfer Function

Fig. 1. A TDF Feedback Control Structure.

### Performance Specifications

We assume that the closed loop performance specifications<sup>1</sup> are given in terms of bounds on allowable variation of  $|T(j\omega)|$ :  $0 \leq a(\omega)c(\omega) \leq |T(j\omega)| \leq b(\omega)c(\omega) \leq \infty$ , where  $a(\cdot)$ ,  $b(\cdot)$ , and  $c(\cdot)$  are real-valued functions of  $\omega$ . Thus, for each  $\omega$  we define  $\delta T(\omega) := \ln[b(\omega)/a(\omega)]$  as the allowable logarithmic gain variation in  $|T(j\omega)|$ .

**Assumption 2C:** We assume that the performance specifications  $\delta T(\omega)$  satisfy the fact that  $\delta T(\omega) \geq \tau(\omega)$ , where  $\tau(\omega)$  is real-valued, non-negative, non-decreasing, and  $\tau(\omega) \rightarrow \infty$  as  $\omega \rightarrow \infty$ .

<sup>1</sup>For simplicity we will consider performance boundaries related to robustness in the presence of process uncertainty. Similar performance boundaries can be developed for robustness in the presence of external disturbances. The results of this paper easily generalize in the case where both types of performance boundaries are considered.

The above assumption means that closed loop performance is required only for "low" frequencies.

### Stability Specifications

Throughout this paper, we assume that the stability (and/or relative stability) specifications are given in terms of a desired Nichols plane gain-phase region surrounding the  $(-180^\circ, 0 \text{ dB})$  point. For simplicity, this specification will be described by a rectangular region,  $S_s = (G_m^+, G_m^-, \Phi_m^+, \Phi_m^-)$ , as shown in Fig. 2.

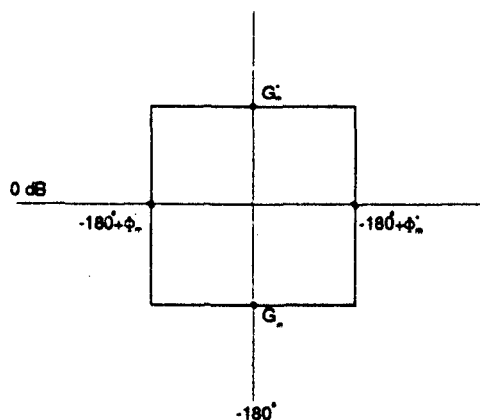


Fig. 2. Stability Specification Region  $S_s = (G_m^+, G_m^-, \Phi_m^+, \Phi_m^-)$ .

**Assumption 3C:** We assume that the stability specifications  $S_s$  satisfy the restrictions that  $G_m^-$  and  $G_m^+$  are bounded, while  $\Phi_m^+ \in [0^\circ, 180^\circ]$  and  $\Phi_m^- \in [-180^\circ, 0^\circ]$ .

## 2.2 The Continuous Time LGPS Solution

Given a process model  $P(s)$  and specifications on desired performance and relative stability, the loop compensator  $G(s)$  and the pre-compensator  $F(s)$  of Fig. 1 are chosen through a procedure based on the following six steps:

- 1) Development of process uncertainty templates describing process gain and phase variations due to (parametric) uncertainty.
- 2) Use of these templates, closed-loop performance specifications, and a model of the external disturbances to develop "performance boundaries" describing gain-phase constraints on acceptable nominal loop gain functions,  $L_o(s)$ .
- 3) Use of the templates, along with system stability and/or relative stability specifications to develop "stability boundaries" describing additional gain-phase constraints on acceptable  $L_o(s)$ .
- 4) Fitting a realizable, nominal loop gain function  $L_o(s)$  to the gain-phase constraints

represented by the performance and stability boundaries.

- 5) Manipulation of the resulting  $L_o(s)$  to extract a description of the loop compensator  $G(s)$ .
- 6) Selection of the pre-compensator  $F(s)$  to shape the closed-loop transfer function,  $T(s)=F(s)L(s)/[1+L(s)]$ .

The mathematical objects and procedures described above (e.g., templates, boundaries, fitting, etc.) are all based on modifications of classical frequency domain design procedures which reflect the LGPS assertion that both gain and phase information should be used where available. Moreover, these objects can be represented in either the  $C$ -plane (the complex plane) or the  $N$ -plane (the Nichols or gain-phase plane). Both of these representations have their advantages at certain steps in the development of LGPS theory. A complete discussion of these issues can be found in (Bailey Cockburn 1991). A brief summary of that discussion follows.

### Uncertainty Templates

For each frequency  $\omega \in [0, \infty)$ , the process uncertainty region or template<sup>1</sup>  $Q(\omega)$  is a set of points in the  $N$ -plane representing all possible uncertainty induced values of the normalized process transfer function  $P(j\omega)/P_o(j\omega)$ . A useful viewpoint is that, for each  $\omega$ , the set  $Q(\omega)$  represents a region of gain-phase uncertainty about the nominal process  $P_o(j\omega)$ . Thus, for each  $\omega \geq 0$ , we define  $Q(\omega)$  as

$$Q(\omega) := \{(\phi, g) \in N: \phi = \arg[P(j\omega; \alpha)/P_o(j\omega)], g = \ln|P(j\omega; \alpha)/P_o(j\omega)| \text{ for all } \alpha \in A\}$$

Use of the normalized process causes all of the templates to have their nominal points located at the point  $(0^\circ, 0 \text{ dB})$  in the  $N$ -plane. Since  $G(j\omega)$  is assumed to have no uncertainty, the template  $Q(\omega)$  also represents the gain-phase uncertainty of  $L(j\omega)=P(j\omega)G(j\omega)$ .

In the limit case as  $\omega \rightarrow \infty$ , the parametric uncertainty templates approach a vertical line in the  $N$  plane. This template is called the "high frequency uncertainty template" and is denoted by  $Q(\infty)$ . In the  $N$ -plane,  $Q(\infty)$  is a bounded vertical line with nominal point located at  $(0^\circ, 0 \text{ dB})$ . The high frequency template plays a major role in the demonstration of the existence of both continuous and discrete time LGPS solutions.

### Performance Sets and Boundaries

Given a template  $Q(\omega)$  and performance specifications  $\delta T(\omega)$ , for each  $\omega$ , the performance set  $B_p(\omega)$  describes an  $N$ -plane region that acceptable nominal loop gain functions,  $L_o(j\omega)=G(j\omega)P_o(j\omega)$ , must avoid in order to satisfy the robust performance specifications. The boundary of  $B_p(\omega)$  is called the performance boundary and is denoted  $\partial B_p(\omega)$ .

It is also known that, for all  $\omega \geq 0$ , the performance sets  $B_p(\omega)$  are bounded in magnitude

<sup>1</sup>The uncertainty templates  $Q(\omega)$  generated by the normalized process  $P(j\omega)/P_o(j\omega)$  are LGPS versions of the multiplicative uncertainty terms  $1+D_m(j\omega)$  in  $P(j\omega)=P_o(j\omega)[1+D_m(j\omega)]$ .

and enclose the N-plane point  $(-180^\circ, 0 \text{ dB})$ . In the limit case as  $\omega \rightarrow \infty$ , the performance sets  $B_p(\omega)$  converge to a high frequency performance set  $B_p(\infty)$ , which is itself a vertical line located at the point  $(-180^\circ, 0 \text{ dB})$ . This property arises from the facts that  $\delta T(\omega) \rightarrow \infty$  and  $Q(\omega) \rightarrow Q(\infty)$ , as  $\omega \rightarrow \infty$ .

### Stability Sets and Boundaries

Given a template  $Q(\omega)$  and the stability specifications  $S_s$ , the stability set  $B_s(\omega)$  describes, for each  $\omega$ , another N-plane gain-phase region that any acceptable  $L_o(j\omega)$  must avoid in order to satisfy the robust stability specifications. The boundary of the stability set is called the stability boundary and is denoted  $\partial B_s(\omega)$ .

The stability sets  $B_s(\omega)$  are also bounded in magnitude and enclose the N-plane point  $(-180^\circ, 0 \text{ dB})$ . In the limit case as  $\omega \rightarrow \infty$ , the stability sets  $B_s(\omega)$  approach a single high-frequency stability set, denoted  $B_s(\infty)$ . This high frequency stability set will also have a rectangular shape in the N-plane. In addition, there is a frequency  $\omega_1 > 0$  such that  $B_p(\omega) \subset B_s(\omega)$  for all  $\omega > \omega_1$ . Thus, at frequencies greater than  $\omega_1$ , any  $L_o(j\omega)$  satisfying  $B_s(\omega)$  automatically satisfies  $B_p(\omega)$ .

### Existence Results

While the performance and stability sets  $B_p(\omega)$  and  $B_s(\omega)$  are more conveniently defined in the N-plane, equivalent C-plane sets are needed for later use in the proof of existence theorems. In Fig. 3 below, we show the shape of the high frequency C-plane performance and stability constraints, denoted  $C_p(\infty)$  and  $C_s(\infty)$  respectively. Note that  $C_p(\infty) \subset C_s(\infty)$ .

Given the above results it is possible to prove the following theorem on the existence of continuous time LGPS solutions. A formal proof is given in (Bailey Cockburn 1991).

**Theorem 1:** If the process model  $P(s; \alpha)$  satisfies Assumption 1C, the performance specifications  $\delta T(\omega)$  satisfy Assumption 2C, and the stability specifications  $S_s$  satisfy Assumption 3C with  $\Phi_m^+ < 180^\circ$ , then one can always find a realizable, rational loop-gain function  $L_o(s)$  such that  $L_o(j\omega)$  meets these closed loop specifications.

\* *Proof Sketch:* By choosing  $L_o(j\omega)$  to have large gain and bandwidth, it can avoid the performance and stability constraints,  $C_p(\omega)$  and  $C_s(\omega)$ . At some large frequency  $\omega_1 > \omega_0$ ,  $C_p(\omega)$  and  $C_s(\omega)$  will closely approximate  $C_p(\infty)$  and  $C_s(\infty)$  and  $C_p(\omega) \subset C_s(\omega)$ . Since  $\Phi_m^+ < 180^\circ$ , there is a negative "gap" angle  $\Gamma < 0$  between  $C_s(\infty)$  and the positive real axis (see Fig. 3). For  $\omega > \omega_1$ ,  $L_o(j\omega)$  is chosen to fit through this gap area until it is inside the stability constraint  $C_s(\infty)$ . At this point,  $L_o(j\omega) \rightarrow 0$  as required by its pole excess.  $\square$

In summary, the above theorem shows that in the minimum-phase case, the continuous time LGPS robust control problem described above is underspecified. Thus, before beginning an iterative search technique to find an LGPS solution, one knows that a solution exists. In addition, since the problem is underspecified, additional design criteria such as bandwidth minimization can be considered.

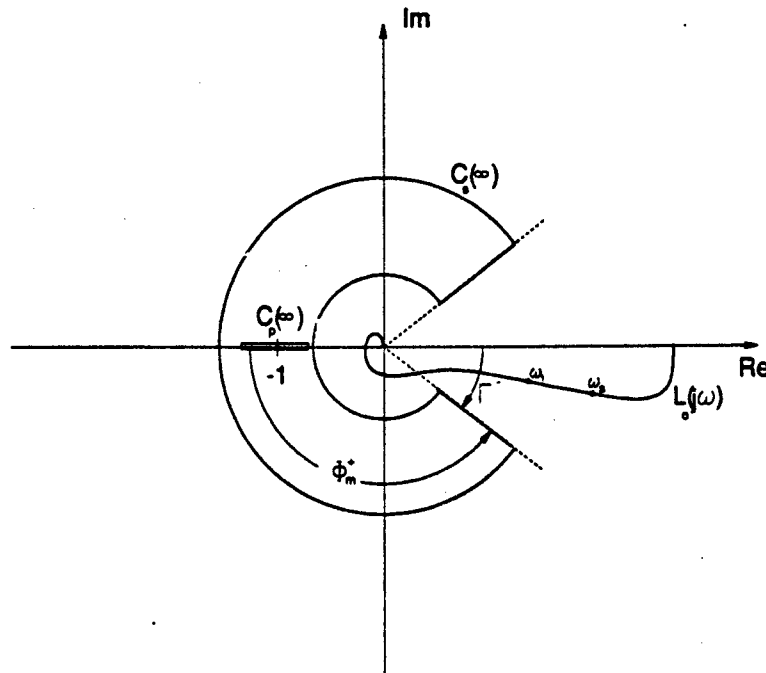


Fig. 3. Fitting  $L_o(j\omega)$  to the Constraints  $C_p(\infty)$  and  $C_s(\infty)$ .

### 3. BACKGROUND ON $\Delta$ -TRANSFORMS

In the past, control system designers have used several different transform techniques in the design process (e.g., the Laplace-transform, Z-transform, and W-transform). In recent work, Middleton and Goodwin have proposed an alternative transform, the  $\Delta$ -transform, that unifies the treatment of continuous and discrete time systems. The  $\Delta$ -transform has several advantages including the facts that (1) it provides a single unified framework for describing all known control system design techniques (2) it has better numerical properties than the Z-transform and (3) it converges to the Laplace transform as the sampling period goes to zero. As will be shown, the  $\Delta$ -transform is a "corrected" Laplace transform, with the corrections on the order of the sampling period ( $\Delta$ ). Moreover, in the case when fast sampling is employed, these corrections become "insignificant" (Middleton and Goodwin 1990).

#### 3.1 Discrete Time Models

Although we assume the reader is familiar with the linear difference equations and Z-transforms, in this section we present a brief review of these topics in order to facilitate a clearer presentation of the discrete time  $\delta$ -model and the  $\Delta$ -transform.

### Shift Operators and Z-Transforms

The standard description of discrete models uses the forward shift operator  $q$  defined by the relation

$$qx_k := x_{k+1}$$

These models are useful because they exactly describe a linear difference equation and are easily implemented in digital control or signal processing algorithms.

The Z-transform is the traditional transform technique used to analyze a time series  $\{x_k\}$  which is described by a shift-operator model. Given a time series  $\{x_k\}$ , the one-sided Z-transform of  $\{x_k\}$  is given by

$$Z\{x_k\} = X(z) := \sum_{k=0}^{\infty} x_k z^{-k}$$

where  $Z$  denotes the Z-transform operator. In elementary texts (Franklin and Powell 1980), it is shown that if there exist constants  $M, \sigma \in \mathbb{R}$  such that  $|x(k)| < Me^{\sigma k}$  for all  $k$ , then the one-sided Z-transform exists for all  $|z| > e^{\sigma}$ .

### Delta Operators and $\Delta$ -Transforms

The discrete time delta operator  $\delta$  performs a forward difference operation and is defined by

$$\delta x_k = \frac{x_{k+1} - x_k}{\Delta}$$

where  $\Delta$  is the sampling period. It is directly related to the forward shift-operator  $q$  by the relation

$$\delta := \frac{q - 1}{\Delta}$$

As the complex variable  $z$  is a frequency domain representation of the shift operator  $q$ , the transform variable associated with  $\delta$ -operators is the complex variable  $\gamma$ . Given a time series  $\{x_k\}$ , the  $\Delta$ -transform of  $\{x_k\}$  is obtained as

$$T\{x_k\} = X_{\Delta}(\gamma) := \Delta \sum_{k=0}^{\infty} x_k (1 + \Delta\gamma)^{-k}$$

where  $T$  denotes the  $\Delta$ -transform operation.

From this definition it is clear that  $\gamma = (z-1)/\Delta$ . Thus, one can obtain a table of  $\Delta$ -transforms from a table of Z-transforms by noting that

$$X_{\Delta}(\gamma) = \Delta X(z)|_{z=\Delta\gamma+1}$$

$$X(z) = \frac{1}{\Delta} X_{\Delta}(\gamma)|_{\gamma=\frac{z-1}{\Delta}}$$

Finally, it can be shown that as  $\Delta \rightarrow 0$ ,  $T\{x(\cdot)\}$  converges to the Laplace transform (herein denoted by  $\mathcal{L}$ ). For a complete discussion of Unified Transform Theory, which includes delta transforms, see (Middleton and Goodwin 1990).

### Discrete Time $\delta$ Models

In view of the relation between the shift operator  $q$  and the delta operator  $\delta$ , one can directly compute a  $\delta$ -model from a shift operator model, Z-transfer function, or difference equation. However, if this discrete time model was obtained from an underlying continuous time process, there are significant numerical advantages in determining the  $\delta$ -model directly from the continuous time state equations (Middleton and Goodwin 1990).

To derive a discrete time step-invariant equivalent model, we assume a zero-order hold at the input of the continuous time process and an ideal sampler at the output. Then, if the continuous time model is

$$P: \begin{aligned} \dot{x} &= Ax + Bu \\ y &= Cx \end{aligned}$$

the corresponding step-invariant discrete time  $\delta$  operator model is given by

$$P_{\Delta}: \begin{aligned} \delta x_k &= Fx_k + Gu_k \\ y_k &= Cx_k \end{aligned}$$

where,

$$\begin{aligned} F &= \left( \frac{1}{\Delta} \int_0^{\Delta} e^{A\tau} d\tau \right) A = \frac{e^{A\Delta} - I}{\Delta} \\ G &= \left( \frac{1}{\Delta} \int_0^{\Delta} e^{A\tau} d\tau \right) B \end{aligned}$$

The corresponding  $\Delta$ -transform of this step-invariant discrete time model is

$$P_{\Delta}(\gamma) := \frac{\gamma}{1+\Delta\gamma} T \{ \mathcal{L}^{-1}[P(s)/s] \} = C(\gamma I - F)^{-1} G$$

### Stability Analysis and Frequency Response Using $\Delta$ -Transforms

In the complex  $\gamma$ -plane, sinusoids of frequency  $\omega$  correspond to points  $\gamma = (e^{j\omega\Delta} - 1)/\Delta$ . For  $\omega \in [-\pi/\Delta, \pi/\Delta]$ , these points describe a circle with its center at  $-1/\Delta$  and radius  $1/\Delta$  as shown in Fig. 4. This circle (herein called the  $\beta$ -circle) represents the stability boundary in the  $\gamma$ -plane and stable poles of  $P_\Delta(\gamma)$  will lie inside this circle with  $|1 + \Delta\gamma| < 1$ . For convenience we define  $\beta := (e^{j\omega\Delta} - 1)/\Delta$  as the complex parameter along the stability boundary, which is analogous to the continuous time complex variable  $j\omega$ . Thus, one can express the frequency response of  $P_\Delta(\gamma)$  by  $P_\Delta(\beta)$ , where  $\beta = (e^{j\omega\Delta} - 1)/\Delta$ . An important point on the  $\beta$ -circle is the fold-over frequency  $\beta_f$ , where  $\beta_f = -2/\Delta$  corresponding to  $\omega = \omega_f = \pi/\Delta$ .

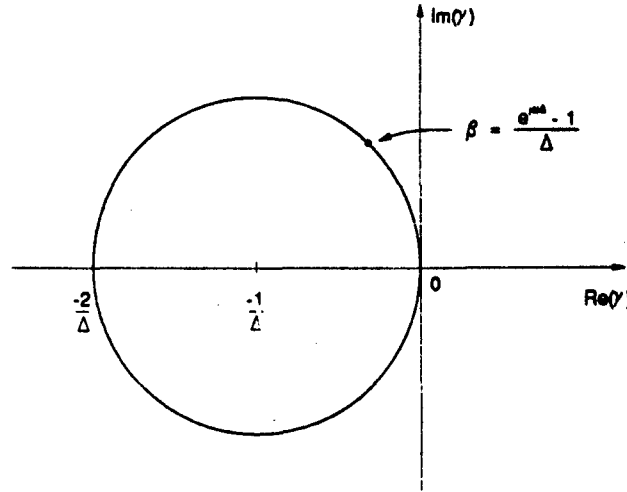


Fig. 4. Stability region for the  $\gamma$ -plane.

### 3.2 Results From $\Delta$ -Transform Theory

Given a discrete time signal  $\{x_k\}$  which is a sampled version of a continuous time signal  $x(t)$ , one can obtain the Laplace transform of the underlying continuous time signal  $x(t)$  by taking the limit  $\Delta \rightarrow 0$  of the  $\Delta$ -transform of  $\{x_k\}$ . The following lemma shows that this property of  $\Delta$ -transforms hold for all signals  $x(t)$  that have a Laplace transform.

**Lemma 1:** (Middleton and Goodwin 1990)

Suppose  $x(\cdot)$  ( $\mathbb{R} \rightarrow \mathbb{R}$ ) satisfies

- (i) There exist  $M, \lambda \in \mathbb{R}$  such that  $|x(t)| \leq Me^{\lambda t}$  for all  $t$ ; and
- (ii) For any  $\text{Re}\{\gamma\} > \lambda$ ,  $x(t)e^{-\gamma t}$  is Riemann integrable.

If  $X_\Delta(\gamma)$  is the  $\Delta$ -transform of  $\{x(k\Delta)\}$ , then for any  $\text{Re}\{\gamma\} > \lambda$ ,

$$\lim_{\Delta \rightarrow 0} X_\Delta(\gamma) = \int_0^\infty x(t)e^{-\gamma t} dt = X(s)|_{s=\gamma}$$

where the above integral is a Riemann integral.



Another important feature of the  $\Delta$ -transform is its ability to reveal connections between continuous and discrete time equivalent process models as the sampling period is varied. The following lemma illustrates this property.

**Lemma 2:** If  $P(s) = C(sI - A)^{-1}B$  is a linear, time-invariant, continuous time process, the step-invariant equivalent discrete time model  $P_\Delta(\gamma) = C(\gamma I - F)^{-1}G$  satisfies

$$\lim_{\Delta \rightarrow 0} P_\Delta(\gamma) = P(s)|_{s=\gamma}$$

\* Proof: If  $F$  and  $G$  are given as above, it is easy to show that

$$\lim_{\Delta \rightarrow 0} P_\Delta(\gamma) = C(\gamma I - A)^{-1}B.$$

Note that Lemma 2 has the following obvious Corollary.

**Corollary 1:** If  $P_\Delta(\gamma)$  is the step-invariant equivalent, discrete time model of  $P(s)$ , then

$$\lim_{\Delta \rightarrow 0} P_\Delta(\beta) = P(j\omega).$$

where  $\beta = (e^{j\omega\Delta} - 1)/\Delta$  and  $\omega \in [0, \pi/\Delta)$ .

In addition to the above results, there are other advantages in the use of  $\Delta$ -transforms in the study of discrete time control systems. Some of these are:

- (1) For fast sampling, the poles and zeros of the  $\delta$ -model are approximately invariant with respect to the sampling period. However, the extra zeros arising from sampling (Astrom, Hagander, Sternby 1984) vary with  $\Delta$  and converge to  $-\infty$  as  $\Delta \rightarrow 0$ . This means that for fast sampling the system dynamics stay approximately constant, while the sampling zeros move towards  $-\infty$ .
- (2) The delta operator has superior numerical properties compared to the equivalent shift form. The main reason for this is that the delta operator moves the  $z$ -plane point  $(1+j0)$  to the origin in the  $\gamma$ -plane and thus eliminates the offset associated with the shift operator pole-zero locations.

For those interested in using the  $\Delta$ -transform for system design or analysis, there is a set of numerical tools in MATLAB called the Delta Toolbox (Middleton Goodwin 1990).

#### 4. THE DISCRETE TIME ROBUST CONTROL PROBLEM

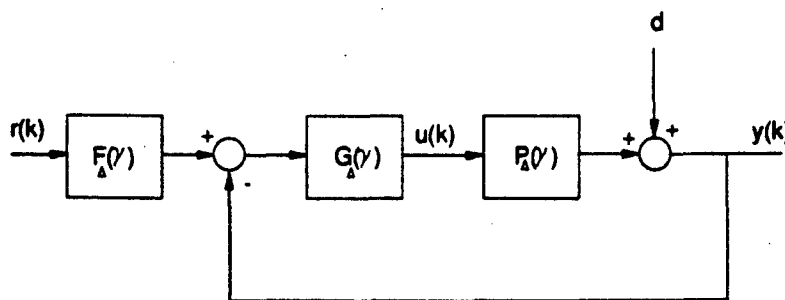
In this section, we describe a discrete time robust control problem that arises in the design of a robust digital controller to satisfy the continuous time LGPS problem outlined in Section 2. We then prove the existence of a discrete time TDF controller which meets the related  $\gamma$ -plane frequency response specifications and the corresponding continuous time specifications.

#### 4.1 Problem Description

As in the continuous time case, the discrete time LGPS approach assumes the TDF structure, shown in Fig. 5. The problem we address is the LGPS design of a robust digital controller for the uncertain discrete time process  $P_\Delta(\gamma, \alpha)$  described below.

##### Process Model

The first step in the discrete time LGPS solution is to identify the equivalent discrete time process model and the discrete time closed loop performance and stability specifications.



$F_\Delta(\gamma)$  = Digital Pre-compensator  
 $G_\Delta(\gamma)$  = Digital Controller  
 $P_\Delta(\gamma)$  = Step-Invariant Discrete Time Process Model  
 $L_\Delta(\gamma) = P_\Delta(\gamma)G_\Delta(\gamma)$  = Loop Gain  
 $T_\Delta(\gamma) = F_\Delta(\gamma)L_\Delta(\gamma)/[1+L_\Delta(\gamma)]$

Fig. 5 An SISO Discrete Time System with TDF Structure.

**Assumption 1D:** The discrete time process  $P_\Delta(\gamma, \alpha) := \gamma/(1+\Delta\gamma)T\{\mathcal{L}^{-1}[P(s; \alpha)/s]\}$  is the step-invariant discrete time equivalent of a continuous time process  $P(s; \alpha)$  that satisfies Assumption 1C. (Note:  $T$  in this definition is the delta transform operator defined in Section 3.) We also assume a sampling period  $\Delta$  such that all poles of  $P(s; \alpha)$  are inside the primary strip  $[-\omega_r, \omega_r]$ , where  $\omega_r = \pi/\Delta$ , all the sampling zeros of  $P_\Delta(\gamma, \alpha)$  are real, and all other *non-sampling* zeros of  $P_\Delta(\gamma, \alpha)$  are stable<sup>1</sup>.

##### Performance Specifications

We assume that the discrete time closed loop performance specifications are given in terms of bounds on the allowable variation of the closed loop transfer function,  $T_\Delta(\beta)$  (see Fig. 5). These performance specifications are given in the form  $0 \leq a(\beta)c(\beta) \leq |T_\Delta(\beta)| \leq b(\beta)c(\beta) < \infty$  for  $\beta < \beta_r$ . Thus for each  $\beta < \beta_r$ , we define the allowable logarithmic gain variation as

<sup>1</sup> Further research into the behavior of *non-sampling* zeros is needed. However, for fast sampling, we know that the non-sampling zeros of  $P_\Delta(\gamma, \alpha)$  will approach the zeros of  $P(s; \alpha)$ .

$$\delta T_{\Delta}(\beta) := \ln[b(\beta)/a(\beta)].$$

In addition, we assume that these discrete time performance specifications  $\delta T_{\Delta}(\beta)$  converge to the continuous time specifications  $\delta T(\omega)$  as  $\Delta \rightarrow 0$ . Moreover, we require that the discrete time performance specifications relax completely as  $\beta \rightarrow \beta_r$ . These assumptions are given below<sup>1</sup>.

**Assumption 2D:** We assume that  $\delta T_{\Delta}(\beta) \rightarrow \delta T(\omega)$  as  $\Delta \rightarrow 0$  and that  $\delta T_{\Delta}(\beta) \rightarrow \infty$  as  $\beta \rightarrow \beta_r$ .

This assumption merely states that the performance specifications are reasonable: one should not expect to achieve performance near or at the foldover frequency.

### Stability Specifications

As in the continuous time case, the stability and/or relative stability specifications are given in terms of a rectangular N-plane gain-phase margin region:  $S_r := (G_m^+, G_m^-, \Phi_m^+, \Phi_m^-)$ . This region was shown previously in Fig. 2.

**Assumption 3D:** We assume that the stability specifications  $S_r$  satisfy the restriction that  $G_m^+$  and  $G_m^-$  are bounded, while  $\Phi_m^+ \in [0^\circ, 180^\circ]$  and  $\Phi_m^- \in [-180^\circ, 0^\circ]$ .

## 4.2 The Discrete Time LGPS Solution

As will be shown, the basic elements of discrete time loop gain-phase shaping are very similar to the continuous time case and the procedure for demonstrating the existence of LGPS solutions in the discrete time case is similar to the one described in Section 2.

### 4.2.1 Discrete Time LGPS Definitions

#### Discrete Time Uncertainty Templates

Let  $P_{\Delta}(\gamma, \alpha)$  be a step-invariant, discrete time plant model that satisfies Assumption 1D. For each  $0 \leq \beta \leq \beta_r$ , we define the discrete time gain-phase uncertainty template  $Q_{\Delta}(\beta)$  as

$$Q_{\Delta}(\beta) := \{(\phi, g) \in \mathbb{N} : \phi = \arg[P_{\Delta}(\beta; \alpha)/P_{\Delta}(\beta; \alpha_0)], g = \ln |P_{\Delta}(\beta; \alpha)/P_{\Delta}(\beta; \alpha_0)|, \text{ for all } \alpha \in A_{\beta}\}.$$

As before, these are normalized templates and thus will have their nominal points at  $(0^\circ, 0 \text{ dB})$ . Given the above definition of  $Q_{\Delta}(\beta)$ , we can prove the following properties of the uncertainty templates.

**Property 1:** If  $P_{\Delta}(\gamma, \alpha)$  satisfies Assumption 1D, then for each  $\beta \in [0, \beta_r)$  the uncertainty templates  $Q_{\Delta}(\beta)$  are gain bounded above and below in the N-plane.

\* **Proof:** Let  $P(s; \alpha) = C(\alpha)[sI - A(\alpha)]^{-1}B(\alpha)$  for some state variable representation of  $P(s; \alpha)$ . Then, Assumption 1D implies that the matrices  $A(\alpha)$ ,  $B(\alpha)$ , and  $C(\alpha)$  have elements that are bounded,

<sup>1</sup> If the performance specifications are given in terms of a continuous function  $\delta T(\omega)$ , the use of the Bilinear Transformation to map  $\delta T(\omega)$  into discrete time specifications  $\delta T_{\Delta}(\beta)$  will satisfy Assumption 2D.

continuous functions of  $\alpha \in A_p \subset \mathbb{R}^p$ . Thus, the matrix

$$\Omega = \frac{1}{\Delta} \int_0^{\Delta} e^{A\tau} d\tau$$

also has elements that are bounded, continuous functions of  $\alpha \in A_p$ . This implies that the coefficients of the transfer function  $P_{\Delta}(\gamma, \alpha) = C(\alpha)[\gamma I - F(\alpha)]^{-1}G(\alpha)$ , where  $F = \Omega A$  and  $G = \Omega B$ , are bounded, continuous functions of  $\alpha \in A_p$ . From Assumption 1D,  $P_{\Delta}(\gamma, \alpha)$  can have no uncertain poles or zeros on the  $\gamma$ -plane stability boundary for all  $\alpha \in A_p$  and the sampling zeros are on the real axis. Thus  $P_{\Delta}(\gamma, \alpha)$  is a continuous function of  $\alpha$  and maps the compact set  $A_p$  into a compact set in  $\mathbb{C}$  which does not contain the origin. Thus,  $0 < |P_{\Delta}(\beta; \alpha)| < \infty$  for all  $\alpha \in A_p$ , where  $\beta \in [0, \beta_r)$ .

**Property 2:** Let  $Q(\omega)$  be the continuous time uncertainty template for  $P(s; \alpha)$ . Then, the discrete time template  $Q_{\Delta}(\beta) = Q_{\Delta}((e^{j\omega\Delta} - 1)/\Delta)$  will converge to the continuous time template  $Q(\omega)$  as  $\Delta \rightarrow 0$ , for  $\omega \in [0, \pi/\Delta)$ .

\* Proof: This result follows from Corollary 1.

In the continuous time case, the high-frequency uncertainty template  $Q(\infty)$  plays a fundamental role in the proof of the existence of LGPS solutions. In the discrete time case, there is a similar high-frequency template  $Q_{\Delta}(\beta_r)$ , where  $\beta_r$  is the discrete time fold-over frequency defined in Section 3.1.

**Property 3:** At the frequency  $\beta = \beta_r$ , the uncertainty template  $Q_{\Delta}(\beta_r)$  is a vertical line in the N-plane located at  $(0^\circ, 0 \text{ dB})$ .

\* Proof: Since  $\beta_r \in \mathbb{R}$ , it follows that  $P_{\Delta}(\beta_r; \alpha) \in \mathbb{R}$ .

**Property 4:**  $Q_{\Delta}(\beta_r) \rightarrow Q(\infty)$  as  $\Delta \rightarrow 0$ .

\* Proof: This also follows from Corollary 1.

### Performance Sets and Boundaries

Given an template  $Q_{\Delta}(\beta)$  and performance specifications  $\delta T_{\Delta}(\beta)$ , the performance set  $B_{p\Delta}(\beta)$  describes an N-plane region that any acceptable  $L_{\Delta o}(\beta) = G_{\Delta}(\beta)P_{\Delta}(\beta; \alpha_o)$  must avoid in order to satisfy the performance specifications. Since the gain-phase uncertainty of  $L_{\Delta}(\beta)$  is the same as the gain-phase uncertainty of  $P_{\Delta}(\gamma, \alpha)$ , a performance set is obtained by shifting the uncertainty template over the M-contours<sup>1</sup> in the N-plane simulating alternative choices of  $|G_{\Delta}(\beta)|$  and  $\arg\{G_{\Delta}(\beta)\}$ .

Given a template  $Q_{\Delta}(\beta)$  with its nominal point shifted to the location  $q_{nom} \in N$ , there is an associated total closed loop gain variation over the entire template denoted  $\delta M(\beta; q_{nom})$  given by

<sup>1</sup>M-contours are  $\mathbb{C}$  plane loci of constant  $M = |z/(1+z)|$ . See [do89] for details.

$$\delta M(\beta; q_{nom}) := \max_{Q_A(\beta)} M - \min_{Q_A(\beta)} M$$

By Property 1, as the template nominal point  $q_{nom}$  is shifted toward larger gain (in the N-plane), the value of  $\delta M$  decreases to zero. And, as  $q_{nom}$  is shifted toward the point  $(-180^\circ, 0 \text{ dB})$  the value of  $\delta M$  increases toward  $\infty$ . Thus, given a performance specification requirement  $\delta T_\Delta(\beta)$ , it is possible to find a set of nominal point locations  $q_{nom} \in N$  such that  $\delta M(\beta; q_{nom}) \geq \delta T_\Delta(\beta)$ . For each  $\beta$ , we define the performance set  $B_{pd}(\beta)$  as

$$B_{pd}(\beta) = \{q_{nom} \in N: \delta M(\beta; q_{nom}) \geq \delta T_\Delta(\beta)\}.$$

The boundary of the performance set  $B_{pd}(\beta)$  is denoted  $\partial B_{pd}(\beta)$ .

**Property 5:** As  $\Delta \rightarrow 0$ , the discrete time performance sets  $B_{pd}(\beta)$  converge to the continuous time performance sets  $B_p(\omega)$ , where  $\beta = (e^{j\omega\Delta} - 1)/\Delta$ .

\* Proof: This follows from Assumption 2D and Property 2.

**Property 6:** The discrete time performance sets  $B_{pd}(\beta)$  will converge to the continuous time high frequency performance set  $B_p(\infty)$ , as  $\beta \rightarrow \beta_r$  and  $\Delta \rightarrow 0$ .

\* Proof: Follows from Assumption 2D and Property 4.

#### Stability Sets and Boundaries

Given specifications on relative stability,  $S_s := (G_m^+, G_m^-, \Phi_m^+, \Phi_m^-)$ , the stability set  $B_{sd}(\beta)$  describes for each  $\beta$ , a gain-phase (N-plane) region that all nominal loop functions  $L_o(\beta) = G_\Delta(\beta)P_\Delta(\beta)$  must avoid in order to satisfy the stability specifications. We define the stability set  $B_{sd}(\beta)$  as the set of all template nominal point locations  $q_{nom} \in N$  such that the gain-phase template intersects the stability specification region. That is,

$$B_{sd}(\beta) = \{q_{nom} \in N: S_s \cap Q_\Delta(\beta) \neq \emptyset\}.$$

The boundary of this set is denoted  $\partial B_{sd}(\beta)$ .

**Property 7:** As  $\Delta \rightarrow 0$ , the discrete time stability sets  $B_{sd}(\beta)$  will converge to the continuous time performance sets  $B_s(\omega)$ , where  $\beta = (e^{j\omega\Delta} - 1)/\Delta$ .

\* Proof: Follows from Property 2 and Assumption 3D.

**Property 8:** The discrete time stability sets  $B_{sd}(\beta)$  will converge to the continuous time high frequency stability set  $B_s(\infty)$ , as  $\beta \rightarrow \beta_r$  and  $\Delta \rightarrow 0$ .

\* Proof: Follows from Property 4 and Assumption 3D.

**Property 9:** The sets  $B_{pd}(\beta_r)$  and  $B_{sd}(\beta_r)$  have the property that  $B_{pd}(\beta_r) \subset B_{sd}(\beta_r)$ .

\* Proof: This follows from the fact that  $B_{pd}(\beta_r) = \{(\phi, g) \in N: Q_\Delta(\beta_r) \cap (-180^\circ, 0 \text{ dB}) \neq \emptyset\}$ . Since the point  $(-180^\circ, 0 \text{ dB})$  is contained in  $S_s$ , we see that  $B_{pd}(\beta_r) \subset B_{sd}(\beta_r)$ .

Property 9 indicates that the discrete time stability sets will enclose the performance sets, as  $\beta \rightarrow \beta_r$ . This is a crucial argument in the continuous time LGPS existence theorem given in [bc91] and we see that it is also valid for the discrete-time case. This result simplifies the loop fitting procedure because it shows that for  $\beta$  sufficiently large one needs only satisfy the high-frequency stability set.

As in the continuous time case, a complex plane description of the discrete time loop gain constraint sets  $B_{\beta\Delta}(\beta)$  and  $B_{\beta\Delta}(\beta)$  facilitates the proof of the LGPS existence theorem. The equivalent  $C$ -plane discrete time performance sets and stability sets are denoted by  $C_{\beta\Delta}(\beta)$  and  $C_{\beta\Delta}(\beta)$ , respectively. These discrete time  $C$ -plane constraints have the same convergence properties as the  $N$ -plane constraints, i.e.,  $C_{\beta\Delta}(\beta) \rightarrow C_{\beta\Delta}(\beta_r)$  and  $C_{\beta\Delta}(\beta_r) \subset C_{\beta\Delta}(\beta_r)$ , etc.

#### 4.2.2 An LGPS Existence Theorem for Discrete Time Systems

From Section 2, we know that if the continuous time process is minimum-phase and has only parametric uncertainty, the LGPS problem normally has a solution. As long as  $\Phi_m^* < 180^\circ$ , there exists an  $L_o(s)$  that meets arbitrary performance and stability specifications. Theoretically, there is no limit on the "bandwidth" of the solution in this case and the use of large gain and bandwidth allows us to meet arbitrary specifications for processes with parametric uncertainty. However, when the process is non-minimum phase, the existence of a feasible LGPS solution is problematical. In this case, the non-minimum phase zeros place an upper limit on the allowable bandwidth of the solution (Freudenberg and Looze 1988). Thus, in some cases it is *impossible* to find a real, rational loop function that will meet the given specifications.

In the discrete time robust control problem, the step invariant discrete time process model typically has non-minimum phase zeros. Thus, in general the existence question of discrete time LGPS solutions also appears problematical.

However, for the discrete process  $P_\Delta(\gamma)$ , we also know that as  $\Delta \rightarrow 0$ , the zeros due to sampling will separate from the "non-sampling" zeros (Middelton and Goodwin 1990). Moreover, the  $\Delta$ -transform description of the sampled process reveals the fact that the sampling zeros move towards  $-\infty$ , as  $\Delta \rightarrow 0$ . Thus, for arbitrarily fast sampling, we can move the "bandwidth limitations" due to the non-minimum phase zeros to arbitrarily high frequencies. This suggests that as  $\Delta \rightarrow 0$ , there exists a real, rational discrete time nominal loop function  $L_{\Delta 0}(\gamma)$  such that the closed loop system satisfies arbitrary performance and stability specifications. This reasoning is justified in Theorem 2 below.

**Theorem 2:** Let  $P_\Delta(\gamma)$  be a discrete time process model that satisfies Assumption 1D. Then, if the performance specifications  $\delta T_\Delta(\beta)$  satisfy Assumption 2D and the stability specifications  $S_\Delta$  satisfy Assumption 3D with  $\Phi_m^* < 180^\circ$ , there exists a sampling period  $\Delta > 0$  and a realizable, rational nominal loop function  $L_{\Delta 0}(\gamma)$  such that  $L_{\Delta 0}(\beta)$  that will satisfy these specifications.

\* Proof: Let  $L_{\Delta 0}(\gamma) = \gamma / (1 + \Delta \gamma) T\{\mathcal{L}^{-1}(L_o(s)/s)\}$ , where  $L_o(s)$  is a solution to the continuous time LGPS robust control problem. From Section 4.2.1, we know that  $C_{\beta\Delta}(\beta) \rightarrow C_\beta(\omega)$  and  $C_{\beta\Delta}(\beta) \rightarrow C_\beta(\omega)$  as  $\Delta \rightarrow 0$ . We also know that the high frequency constraint sets  $C_{\beta\Delta}(\beta_r)$  and  $C_{\beta\Delta}(\beta_r)$  converge to  $C_\beta(\infty)$  and  $C_\beta(\infty)$ , respectively, as  $\Delta \rightarrow 0$ . Since  $\Phi_m^* < 180^\circ$ , there exists a negative "gap" angle  $\Gamma < 0$  between  $C_\beta(\infty)$  and the real axis such that  $L_o(j\omega)$  can fit through the gap and roll-off as necessary. Now, if  $L_{\Delta 0}(\beta)$  is the frequency response of  $L_{\Delta 0}(\gamma)$ , Corollary 1 says that

the function  $L_{\Delta 0}(\beta)$  also satisfies these constraints as  $\Delta \rightarrow 0$ .  $\square$

Theorem 2 tells us that by choosing  $\Delta$  arbitrarily small, we can approximate the gain-phase constraints of the continuous time LGPS problem,  $C_i(\omega)$  and  $C_p(\omega)$ , arbitrarily close with equivalent discrete time gain-phase constraints,  $C_{i\Delta}(\beta)$  and  $C_{p\Delta}(\beta)$ . Moreover, we can approximate  $L_o(j\omega)$  with a discrete time  $L_{\Delta 0}(\beta)$  as close as necessary. Thus, we can always find a solution to the discrete time LGPS robust control problem described above.

## 5. ESTIMATING THE MAXIMUM FEASIBLE SAMPLING PERIOD

The above results show that given reasonable specifications there exists a sampling period  $\Delta$  for which one can solve the discrete time robust control problem using LGPS. While these results represent a contribution to the theory of QFT they are not very satisfying as they give no hint to the range of acceptable  $\Delta$ . A control systems designer would like to know that the specifications can be met for all  $\Delta$  less than some maximum value  $\Delta_M$ . Unfortunately, this problem and others related to existence of LGPS solution of non-minimum phase processes is quite difficult. In this section we outline this problem and offer a technique which is useful in estimating  $\Delta_M$ .

To begin, we note that the estimation of  $\Delta_M$  involves all of the elements of the LGPS design problem. That is, the feasibility of the LGPS fitting problem for non-minimum phase processes depends on the specifications, the process uncertainty, and details of the minimum phase behavior of the process. To date only rough rules-of-thumb exist in the problem of estimating feasibility in these cases. However, in the discrete time case, we have two advantages: 1) the non-minimum phase nature of the problem is somewhat limited by the structure of the discrete time process model and 2) we can influence the "non-minimum phase effects" by the choice of  $\Delta$ .

### 5.1 Fast Sampling

In most digital control problems, the step-invariant discrete time process model  $P_\Delta(\gamma)$  has added zeros. That is, if  $P(s)$  has  $n$  poles and  $m$  zeros then  $P_\Delta(\gamma) = [\gamma/(1+\Delta\gamma)]T\{\mathcal{L}^{-1}P(s)/s\}$  typically has  $n$  poles and  $n-1$  zeros. The additional  $n-m-1$  zeros of  $P_\Delta(\gamma)$  are commonly termed sampling zeros (Astrom, et. al. 1984). As  $\Delta \rightarrow 0$  in the  $\gamma$ -plane, the poles and "non-sampling" zeros of  $P_\Delta(\gamma)$  cluster around the origin  $\gamma=0$ , imitating the pattern of  $P(s)$ , while the sampling zeros of  $P_\Delta(\gamma)$  are real (assuming no aliasing) and cluster around the point  $\gamma=-2/\Delta$  (Middleton and Goodwin 1990).

In the case of parametric uncertainty where  $P(s)=P(s;\alpha)$  for  $\alpha \in A_p$ , the resulting step invariant equivalent  $P_\Delta(\gamma;\alpha)$  will have poles and zeros dependent on  $\alpha$ . In addition, as  $\Delta \rightarrow 0$  the poles and "non-sampling" zeros of  $P_\Delta(\gamma;\alpha)$  converge to the  $\alpha$ -dependent poles and zeros of  $P(s;\alpha)$ . However, as  $\Delta \rightarrow 0$  the sampling zeros of  $P_\Delta(\gamma;\alpha)$  converge to  $\alpha$ -independent locations. Thus, we will use the term *fast sampling* to denote situations where  $P_\Delta(\gamma;\alpha)$  can be approximated as

$$P_\Delta(\gamma) \approx \hat{P}_\Delta(\gamma;\alpha) N_\Delta(\gamma)$$

where  $\hat{P}_\Delta(\beta;\alpha) \approx P(j\omega;\alpha)$  and  $N_\Delta(\gamma)$  contains all of the sampling zeros of  $P_\Delta(\gamma)$  (See Fig. 6). Also note that when  $\omega\Delta$  is small,  $\beta = (e^{j\omega\Delta} - 1)/\Delta \approx j\omega$  and thus there is a significant frequency range where

$$P_{\Delta}(\beta) \approx P(j\omega).$$

In our estimation of  $\Delta_M$ , we will assume that these fast sampling properties hold: 1) the separation of the sampling zeros from the remaining pole-zero cluster, 2) the  $\alpha$ -independence of the sampling zero locations and 3) the assumption that  $P_{\Delta}(\beta) \approx P(j\omega)$  for a significant frequency range.

### 5.2 Phase Deviation of $L_{\Delta\alpha}(\beta)$

The LGPS fitting procedure outlined in Section 4 assumed that there was a phase margin gap  $\Gamma$  and that a minimum phase, rational  $L_0(s)$  could be found such that  $L_0(j\omega)$  fit through this gap. The difficulty of the discrete time LGPS fitting problem is the fact that the sampling zeros contribute additional phase shift to  $P_{\Delta}(\beta)$  and thus to  $L_{\Delta\alpha}(\beta)$ . For any fixed  $\Delta$ , this additional phase shift may prevent  $L_{\Delta\alpha}(\beta)$  from conforming to the  $\Gamma$  gap and the high frequency stability constraints. In this section we estimate the additional phase angle  $\phi_s(\beta)$  contributed by the sampling zeros. We assume that this phase shift  $\phi_s(\beta)$  will represent the deviation in  $L_{\Delta\alpha}(\beta)$  from  $L_0(j\omega)$  for  $\beta = (e^{j\omega\Delta} - 1)/\Delta$ .

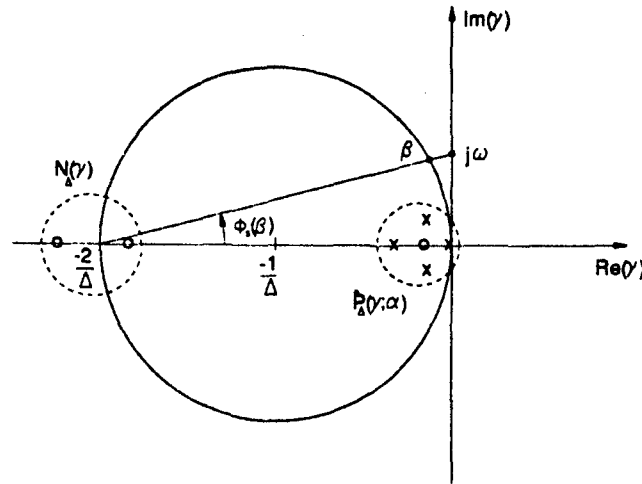


Fig. 6. Fast Sampling Conditions in the  $\gamma$ -plane.

As shown in Fig. 6, when the  $\beta$ -circle is close to the imaginary axis, the additional phase contribution of  $n_s$  sampling zeros at frequency  $\beta \approx j\omega$  can be estimated as

$$\phi_s(\beta) = \tan^{-1}(\omega\Delta n_s/2)$$

Note that we have assumed that the sampling zeros are all located at the point  $\gamma = -2/\Delta$ . They are in fact distributed on both sides of this point.

### 5.3 The Allowable Phase Deviation in $L_{\Delta\alpha}(\beta)$

By choosing  $\Delta$  small, the above relation shows that we can make  $\phi_s(\beta)$  small and thus make  $L_{\Delta\alpha}(\beta)$  close to  $L_0(j\omega)$ . The next question is the allowable range of  $\phi_s(\beta)$  when solving the



LGPS fitting problem.

As implied in Sections 2 and 5.2, there are two critical elements in the LGPS fitting problem: one is the existence of a negative gap angle  $\Gamma$  and the other is the existence of a  $\omega_i$  such that  $C_p(\omega) \subset C_s(\omega)$  for all  $\omega > \omega_i$ . Since some of this gap is used by the phase angle of  $L_o(j\omega)$  as it is rolled-off to enter the region where  $\omega > \omega_i > \omega_s$ , the designer must decide how much of the gap is available for  $\phi_s(\beta)$ . We will denote this "available" gap  $\phi_s$  and note that  $\phi_s < \Gamma$ , as shown in Fig. 7. Thus, we will require that

$$\phi_s(\beta_s) \leq \phi_s < \Gamma = 180^\circ - \Phi_m^*.$$

The above result indicates that part of the gap  $\Gamma$  will be used for the roll-off of  $L_o(j\omega)$  and the other part for the phase lag due to sampling zeros. This suggests a trade-off between the bandwidth of  $L_{\Delta o}(\beta)$  and  $\Delta_M$ : the designer has a choice of using the available gap to provide phase shift for rapid roll-off of  $L_{\Delta o}(\beta)$  near  $\beta_s$ , or sampling zero phase shift in  $\phi_s$ .

#### 5.4 Estimation of the Frequency $\omega_i$

To minimize loop gain-bandwidth, the loop gain function  $L_{\Delta o}(\beta)$  must fit through the  $\Gamma$  gap at frequencies  $\beta$  near  $\beta_s \approx \omega_i$ . Implementation of the  $\Delta_M$  estimate implied in Section 5.3 requires an estimate of the frequency  $\beta_s \approx \omega_i$ . This is complicated by the fact that  $\omega_i$  depends on the details of both the specifications  $\delta T(\omega)$  and the size of the template  $Q(\omega)$ .

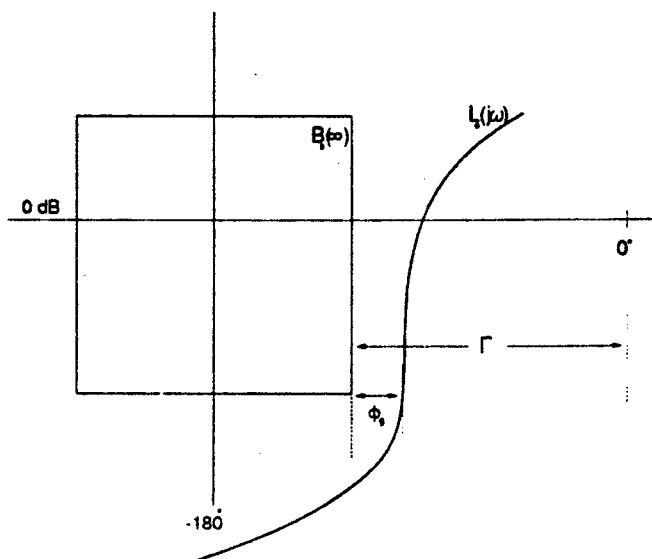


Fig. 7. N-Plane Depiction of the Allowable Phase Tolerance  $\phi_s$  in  $L_o(j\omega)$ .

One estimate of  $\omega_i$  may be obtained by noting that  $B_p(\omega) \subset B_s(\omega)$  only when  $B_p(\omega)$  is closed in the N-plane. Moreover,  $B_p(\omega)$  is closed only at frequencies where  $|Q(\omega)| < \delta T(\omega)$ . Since we require that  $\delta T(\omega) \rightarrow \infty$  as  $\omega \rightarrow \infty$ , and we know that  $Q(\omega) \rightarrow Q(\infty)$  which is finite, we are

assured that such frequencies always exists. Thus, we can estimate  $\omega_i$  as the smallest frequency  $\hat{\omega}_i$  such that  $|Q(\omega)| < \delta T(\omega)$  for all  $\omega > \hat{\omega}_i$ .

### 5.5 Estimation of $\Delta_M$

Given the above development we now conclude that  $\Delta_M$  should be sufficiently small such that the fast sampling conditions hold and

$$\Delta_M \leq 2/(\hat{\omega}_i n_i) \tan(\phi_g)$$

where  $\hat{\omega}_i$  is an estimate for the frequency  $\omega_i$ . This result is intuitively attractive because it includes all of the features one would expect in such an estimate: the template size, the performance specifications, and the stability specifications. However, note that some amount of continuous time LGPS design is needed to determine  $\hat{\omega}_i$  and to select  $\phi_g$ .

## 6. AN EXAMPLE: A DC Motor with Uncertain Load

This example illustrates the utility of the above estimate for the maximum feasible sampling period  $\Delta_M$  for a specific discrete time LGPS robust control system design problem. In this example, we find a discrete time LGPS solution to the continuous time robust control problem discussed in (Bailey and Hui 1991).

### Process Model

A DC motor with an uncertain inertial load can be modeled by the following transfer function

$$P(s; J_L) = \frac{K_m}{L(J_m + J_L)s^2 + R(J_m + J_L)s + K_m^2}$$

where  $J_L \in [7 \times 10^{-5}, 1.4 \times 10^{-2}]$  and  $J_{L0} = 1.4 \times 10^{-3}$ . The remaining constants (in SI units) have the values

$$\begin{aligned} L &= 2.2 \times 10^{-3} & K_m &= 0.2 \\ R &= 0.4 & J_m &= 1.4 \times 10^{-3} \end{aligned}$$

### Specifications

- (i) The continuous time performance specifications for the closed loop system are given as follows:

$\omega$ (rad/sec)	$ T(j\omega) $ (dB)	$\delta T(\omega)$ (dB)
$\omega \leq 10$	$0 \pm 0.05$	0.1
$\omega \in [10, 100]$	$0 \pm 0.20$	0.4
$\omega = 300$	$-20 \pm 2.00$	4.0
$\omega = 3000$	$-40 \pm 20.0$	40.0

(ii) The closed-loop stability specifications  $S_c$  are given as the gain-phase region enclosed by the 5 dB  $M$ -contour in the Nichols plane. This corresponds to a gain margin of about 4 dB and a phase margin of about  $35^\circ$ .

(iii) As additional specifications,  $L_o(s)$  is required to be Type 1 (i.e., one pole at  $s=0$ ) and the loop compensator must have a pole excess of one.

#### Solution 1

The first step in the design of a digital controller is the selection of the sampling period  $\Delta$ . From the continuous time uncertainty templates in (Bailey and Hui 1991), we see that  $|Q(\omega)| \approx 20$  dB for all  $\omega \geq 1000$  (rad/sec). Given this information and the shape of the specifications  $\delta T(\omega)$ , one can estimate that  $|Q(\omega)| < \delta T(\omega)$  for all  $\omega \geq 2000$  (rad/sec) and thus the estimate<sup>1</sup> for  $\omega_c$  is chosen to be  $\omega_c = 2000$  (rad/sec). From the continuous time solution  $L_o(j\omega)$  given in Fig. 9, notice that  $\phi_p \approx 10^\circ$ . Thus, from Section 5 the estimate for the maximum feasible sampling period is  $\Delta_M = 1.76 \times 10^{-4}$  (sec). Initially, we will use  $\Delta = \Delta_M = 1.76 \times 10^{-4}$  sec.

Given  $\Delta$ , the next step is to develop discrete time process uncertainty templates  $Q_d(\beta) = Q_s((e^{j\omega\Delta} - 1)/\Delta)$ , several of which are shown in Fig. 8. Note that these discrete time templates are almost identical in size to the continuous time templates shown in (Bailey and Hui 1991). In fact for this choice of  $\Delta$ , the discrete time templates were identical to the continuous time templates for frequencies up to the foldover frequency,  $\omega_f = 1.785 \times 10^4$  (rad/sec).

Given the templates, the performance specifications, and stability specifications, the next step is to find the discrete time performance and stability boundaries. Because  $\Delta$  is small, the discrete time performance specifications  $\delta T_d(\beta)$  and the continuous time specifications  $\delta T(\omega)$  are nearly identical. Thus, we will use the continuous time specifications given above. For these reasons the discrete time performance and stability constraints are also identical to the continuous time constraints, i.e.,  $B_{sA}(\beta) \approx B_s(\omega)$  and  $B_{pA}(\beta) \approx B_p(\omega)$ . Fig. 9 shows the performance boundaries for  $\omega = 3, 10, 30, 100, 300$ , and  $3000$  (rad/sec), and the high frequency stability boundary  $B_s(\infty)$ .

Fig. 9 shows a typical minimum phase continuous time LGPS solution  $L_o(j\omega)$  and a discrete time solution  $L_{do}(\gamma)$ . Note that both loop functions satisfy the performance and stability constraints.

<sup>1</sup> For this particular example, it careful analysis shows that  $\omega_c \approx 2600$  (rad/sec).

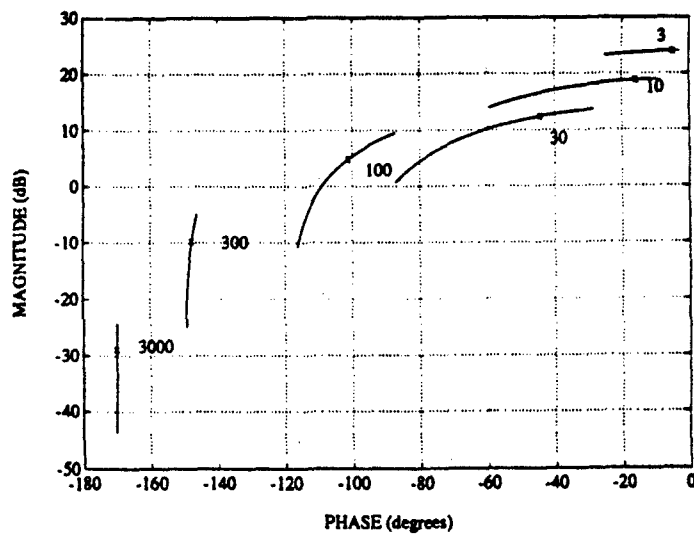


Fig. 8. Discrete Time Process Uncertainty Templates  $Q_{\Delta}((e^{j\omega\Delta}-1)/\Delta)$  for  $\omega=3, 10, 30, 100, 300$ , and  $3000$  (rad/s) with  $\Delta=0.176$  msec.

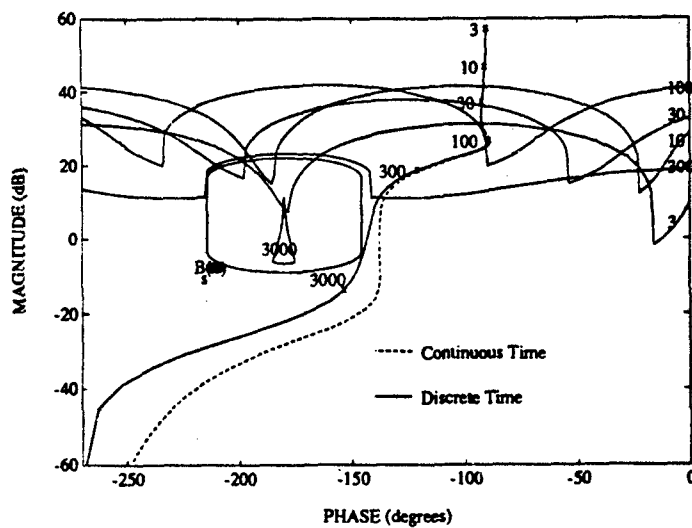


Fig. 9. Continuous Time and Discrete Time ( $\Delta=0.176$  msec) LGPS Solutions.

## Solution 2

In Fig. 10, another continuous time LGPS solution is shown with  $\phi_s = 25^\circ$ . Thus, given  $\hat{\omega}_1 = 2000$  as found above, the estimate is  $\Delta_M = 4.663 \times 10^{-4}$  sec. However, for this example, if  $\Delta = \Delta_M$ , no realizable, minimum phase, discrete time loop function  $L_{\Delta_0}(\gamma)$  was found that fits the constraints. Experimentation suggests that the absolute maximum sampling period for this particular example is  $\Delta = 0.33$  (msec). With  $\Delta = 0.32$  (msec) one can satisfy the loop constraints with the minimum phase loop function  $L_{\Delta_0}(\gamma)$  shown in Fig. 10. The process uncertainty templates for  $\Delta = 0.32$  (msec) are identical to those shown in Fig. 8. Note that in this case, the estimated  $\Delta_M$  is high but reasonably close to what appears to be the *true*  $\Delta_M$ .

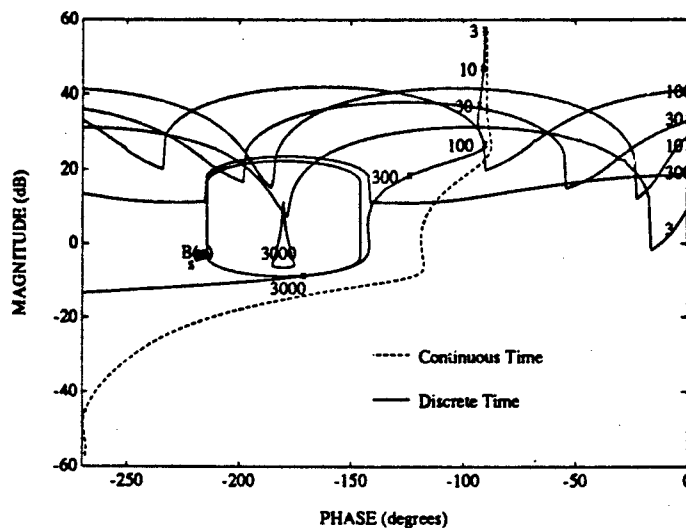


Fig. 10. Continuous Time and Discrete Time ( $\Delta = 0.32$  msec) LGPS Solutions.

## 7. CONCLUSIONS

In this paper we have developed the frequency domain properties of loop gain-phase shaping for discrete time processes. With these properties, we have demonstrated the existence of discrete time LGPS solutions to robust digital control of SISO, minimum-phase, continuous time processes. The properties of discrete time LGPS were developed using the  $\Delta$ -transform discussed in (Middleton and Goodwin 1990). The  $\Delta$ -transform allowed us to explicitly relate the continuous time LGPS results given in (Bailey and Cockburn 1991) to the more difficult (and usually non-minimum phase) discrete time LGPS robust control problem presented in this paper. The results show that for reasonable specifications there always exists a sampling period  $\Delta > 0$  such that the robust digital control problem has a solution.

In addition we presented an estimate for the maximum feasible sampling period for robust digital control problems. It was shown that the question of maximum feasible sampling period is related to the LGPS fitting problem for non-minimum phase processes. For step-invariant equivalents of minimum phase continuous time processes, the non-minimum phase behavior (caused by sampling zeros) is determined by the relative degree of the continuous time process

$P(s)$  and the sampling period  $\Delta$ . By assuming fast sampling and by estimating the locations of the sampling zeros, we estimate the additional phase lag introduced by the sampling zeros. We then use this estimate of additional phase shift, along with partial information about the continuous time LGPS solution, to estimate the maximum feasible sampling period  $\Delta_M$ .

In general, the existence of discrete time LGPS solution for problems where the sampling period is fixed a priori is problematical. Additional results in the area of LGPS feasibility for non-minimum phase processes are needed in this area.

## 8. REFERENCES

- ASTROM, K.J., HAGANDER, P., and STERNBY, J., 1984, Automatica, **20**, 21.
- BAILEY, F.N., and COCKBURN, J.C., 1991, in O.D. Nwokah (ed.), Robust Control of Mechanical Systems: Theory and Applications, ASME-WAM, **27**.
- BAILEY, F.N., COCKBURN, J.C., and HOWARD, P.J., "The Existence of Loop Gain-Phase Shaping Solutions for Problems with Parametric and Mixed Uncertainty", submitted to Automatica.
- BAILEY, F.N., and HUI, C.H., 1991, IEEE Control Syst. Mag., **11**, 93.
- BEKE, H.W., 1992, PhD Thesis, University of Minnesota.
- CHEN, T., and FRANCIS, B., 1990, Lecture notes from "EE 8451-2: Sampled-Data Control Systems", University of Minnesota.
- DORF, R.C., 1989, Modern Control Systems 5th ed. (Addison-Wesley).
- FRANKLIN, G.F., and POWELL, J.D., 1980, Digital Control of Dynamic Systems (Addison-Wesley).
- FREUDENBERG, J.S., and LOOZE, D.P., 1988, Frequency Domain Properties of Scalar and Multivariable Feedback Systems, Lecture Notes in Control and Information Sciences (Springer-Verlag).
- GERA, A., and HOROWITZ, I.M., 1980, Int. J. Control, **31**, 389.
- HOROWITZ, I.M., and LIAO, Y.K., 1986, in Houpis, C.H., Quantitative Feedback Theory, AFWAL-TR-86-3107, Appendix C.
- HOROWITZ, I.M., 1963, Synthesis of Feedback Systems (Academic Press); 1982, Proc. IEE, **129**, 215.
- HOROWITZ, I.M., and SIDI, M., 1978, Int. J. Control, **27**, 361.
- LAMONT, G.B., HOUPIS, C.H., and EWING, R.L., 1991, in O.D. Nwokah (ed.), Robust Control of Mechanical Systems: Theory and Applications, ASME-WAM, **27**.
- LEUNG, G.M.H., PERRY, T.P., and FRANCIS, B.A., 1991, Automatica, **27**, 699.
- MIDDLETON, R.H., and GOODWIN, G.C., 1990, Digital Control and Estimation (Prentice-Hall).
- THOMPSON, D.F., 1990, PhD Thesis, Purdue University.
- YANIV, O., and CHAIT, Y., 1991, Amer. Control Conf., 1987.

## APPENDIX

The following is a glossary of the notation and definitions used above.

$\beta$	Discrete time frequency response variable (analog of $j\omega$ in continuous time)
$\beta_f$	Discrete time fold-over frequency
$\beta_1$	Discrete time frequency such that $C_{pd}(\beta) \subset C_{\Delta}(\beta)$ for all $\beta \geq \beta_1$
$B_p(\omega), B_{pd}(\beta)$	Continuous and discrete time N-plane performance constraint sets
$B_1(\omega), B_{\Delta}(\beta)$	Continuous and discrete time N-plane relative stability constraint sets
$B_1(\infty), C_1(\infty)$	Continuous time high-frequency stability sets (N-plane and C-plane)
$B_p(\infty), C_p(\infty)$	Continuous time high-frequency performance sets (N-plane and C-plane)
$C_p(\omega), C_{pd}(\beta)$	Continuous and discrete time C-plane performance constraint sets
$C_1(\omega), C_{\Delta}(\beta)$	Continuous and discrete time C-plane relative stability constraint sets
$\Gamma$	Negative gap angle between real axis and the edge of $C_1(\infty)$
$\Delta$	Sampling period in seconds
$\delta T(\omega), \delta T_{\Delta}(\beta)$	Performance specifications of allowable variation in $ T(\omega) $ or $ T_{\Delta}(\beta) $
$G_m^-, G_m^+$	Lower and upper gain margins
$L_o(j\omega), L_{\Delta o}(\gamma)$	Continuous and discrete time nominal loop gain function
$Q(\omega), Q_{\Delta}(\beta)$	Continuous time and discrete time process uncertainty templates
$Q(\infty), Q_{\Delta}(\beta_f)$	Continuous time and discrete time high-frequency uncertainty templates
$S_1$	Relative stability specifications
$\Phi_m^-, \Phi_m^+$	Lower and upper phase margins
$\omega_f$	Continuous time fold-over frequency ( $\omega_f = \pi/\Delta$ )
$\omega_1$	Frequency such that $C_p(\omega) \subset C_1(\omega)$ for all $\omega \geq \omega_1$

# QFT, the UHB, and the Choice of the Template Nominal Point

D.J. Ballance and P.J. Gawthrop,  
Control Group,  
Department of Mechanical Engineering,  
University of Glasgow,  
Glasgow.  
G12 8QQ.  
Tel: 041-339-8855 ext 5187/4960  
Fax: 042-330-4343  
Email: D.Ballance@uk.ac.glasgow

## Abstract

Recent developments in the use of computers for QFT design have concentrated in automating the various aspects of the standard QFT design procedure. This paper examines one aspect of the standard design technique which could, and perhaps should, be altered by the use of computing power. This is the use of the UHB and the choice of nominal point. It is argued that more exact criteria are now usable given the increase in computation power available, and that the simplification of using the UHB is no longer necessary.

Additionally a view on the need for additional restraints within the QFT procedure is shown; namely some constraints on the loop gain to ensure that the perceived good performance in theory is not the result of eliminating the "nasty" dynamics by using a pre-filter.

## 1 Introduction

Since the introduction of the Nichols chart for the implementation of the graphical approach to QFT little has changed in the basic approach to design of controllers for single-input single-output (SISO) linear time-invariant systems. This paper looks at some of the assumptions and simplifications used and considers whether they are still useful given the vast increase in computing power now available.

The four main areas that are considered are the assumption that there are no unmodelled high frequency dynamics, the purpose of the Universal High-frequency Bound (UHB), the choice of the nominal point for the templates, and the requirement for additional constraints on the loop transfer function, other than the re-



quirement that the *variation* of the closed loop transfer function is smaller than a given bound.

This paper is designed to promote discussion of the fundamental design process of QFT, and to determine whether changes should be proposed in the techniques used.

## 2 High frequency shape of templates

It is generally assumed within the standard QFT design theory (Horwitz and Sidi, 1972, Horowitz, 1982) that at high frequency as  $\omega \rightarrow \infty$  that the templates of plant uncertainty tend to a vertical lines with length given by the magnitude of the uncertainty in the gain of the system. This assumption leads to the statement (Horwitz and Sidi, 1972) that the ideal loop transfer function should follow the UHB exactly for all frequencies greater than  $\omega_x$ , the frequency at which optimum loop transfer function  $L(j\omega)$  first touches the UHB. This statement is based upon the assumption that at high frequency there is only uncertainty in magnitude, and no uncertainty in phase. This is clearly not true for the case of unmodelled high-frequency dynamics. This criticism was raised by Doyle (1986), and a reply was given by Yaniv and Horwitz (1987), however the fundamental problem of the assumption that the templates tend to a vertical line as  $\omega \rightarrow \infty$  remains. This causes problem because the current usage of the UHB is based upon this principle. Other problems with the current usage of the UHB are tackled in the next two sections.

## 3 The purpose and accuracy of the UHB

There are a number of related interpretations of the purpose of the Universal High-frequency Bound (UHB) but its main use is to ensure that at high frequencies the controlled system cannot go unstable and has sufficient noise-rejection properties. More specifically, it attempts to ensure that the system obeys the Nyquist stability criterion, and that all of the templates remain outside a given  $M$ -circle; typically the  $M = \sqrt{2}$   $M$ -circle is chosen to ensure a minimum amount of damping.

In the standard QFT design technique the nominal point of the templates to be manipulated on the Nichols chart is a point with the highest phase and lowest gain. It is then fairly simple to determine the UHB by ensuring that, even at the highest frequencies when the uncertainty, as mentioned above, is assumed to be in magnitude only, the template does not intersect with the required  $M$ -circle. Thus the UHB of normal QFT design is typically a vertical line in the Nichols chart extending from the  $M = \sqrt{2}$   $M$ -circle down a distance given by the uncertainty of the magnitude at high frequency. The main historical reason for the development of this UHB seems to be the saving in the time required to compute and manipulate a large number of high-frequency templates on the Nichols chart. Given the increase in computational power available it is now possible to calculate the templates at many more frequencies than before and thereby eliminate the need for the UHB.

What is required is a condition at each frequency that ensures the template does not intersect the specified  $M$ -circle. Example 1 takes a simple system and

shows how, for a particular frequency, the UHB and the true bound on the nominal loop transfer function  $L(j\omega)$  differ.

**Example 1:** Consider the plant

$$P(s) = \frac{K}{(1 + as)} \quad \text{where} \quad \begin{array}{l} 0.5 \leq K \leq 4 \\ 0.5 \leq a \leq 2 \end{array}$$

at a frequency of  $\omega = 1$ . Figure 1 shows the true template (solid line) with its nominal, with  $K = 0.5$ , and  $a = 2$  marked by \*. It also shows the  $M = \sqrt{2}$   $M$ -circle (dashed line) and the region into which the nominal must not pass at this frequency to avoid the template intersecting the  $M = \sqrt{2}$   $M$ -circle (dotted line). The figure also shows the UHB for this plant marked by the dot-dashed line, which has a vertical section of 30.1 dB (The magnitude of the high-frequency uncertainty).

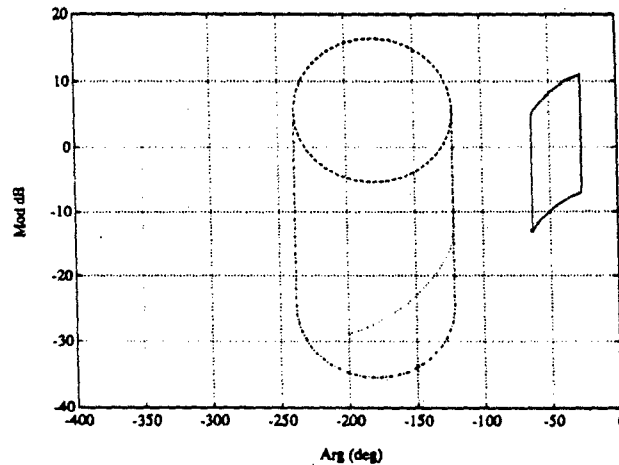


Figure 1: The  $M = \sqrt{2}$   $M$ -circle, the corresponding UHB, the true boundary and the uncertainty template.

It should be noted that not only does the bound on the template have a higher gain for the nominal point, but it would, if continued, also extend considerably further to the left, i.e., a greater phase lag, than does the standard UHB. This is related to the choice of the nominal point of the templates, a point discussed in the next section.

## 4 Choice of the nominal point

It is generally assumed that the choice of the nominal point is not fixed in the QFT design technique. However because of the current usage of the UHB it is essential that the nominal point of the templates is chosen for minimum gain, maximum phase-lag, thus ensuring that all of the template, however large, is to the right of the nominal in the Nichols chart, and hence all of the template avoids the specified

$M$ -circle. If this condition is not met then the UHB becomes useless, because the template specified can intersect the  $M$ -circle while the nominal remains outside the UHB.

This can be illustrated by using Example 1 again but choosing the nominal to be the point where  $K = 0.5$ , and  $a = 0.5$ . Figure 2 shows the template with the nominal marked by \*. It can clearly be seen that while the nominal remains outside the UHB, for some choices of parameters (e.g.,  $K = 4$ ,  $a = 0.5$ ) the plant is inside the  $M = \sqrt{2}$   $M$ -circle. This aspect of the choice is not clearly specified in the standard QFT design procedure. Additionally this problem arises when other template shapes are considered. This problem also appears in the work of East (1981, 1982), where the use of circular templates is considered (Ballance, 1992).

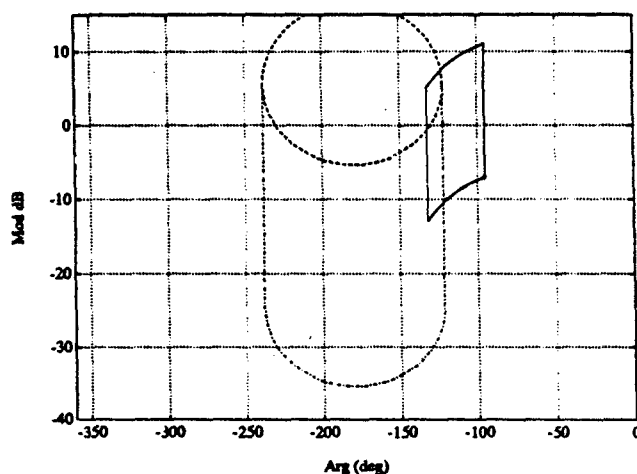


Figure 2: The  $M = \sqrt{2}$   $M$ -circle, the corresponding UHB, and a template with nominal outside the UHB while intersecting the  $M = \sqrt{2}$   $M$ -circle.

## 5 Specification of QFT problem

The final point to be raised in this paper is the specification of the QFT problem. The emphasis in the QFT design procedure is in meeting the tolerances of the closed-loop specification. This is generally achieved by the use of the two-degree-of-freedom controller structure, ensuring that the loop controller reduces the spread or variation of the closed loop transfer-function envelope, and using by the pre-filter to ensure that the closed loop response falls within the specified tolerances. Except for the simple use of the UHB, or more preferably ensuring that the templates cannot intersect with the  $M = \sqrt{2}$   $M$ -circle, there is generally little specification or constraint on the form of the resultant loop transfer-function. Any undesirable responses may be eliminated by the choice of the pre-filter to ensure the tolerances are achieved. However, the result of this is that, while the tolerances on the closed loop transfer function may be achieved, large gains may exist at sensitive

frequencies within the loop that are not considered in the input/output analysis, because they are cancelled by the pre-filter. This can cause problems in systems where measurement noise is a particular problem at a frequency close to that at which it is desired to control the system. In order to achieve the required performance of the system in terms of noise suppression and disturbance rejection, it is normally necessary to undertake some post-design evaluation of the noise problem and re-design if required. An alternative to this procedure is to directly include requirements or specifications on the sensitivity function  $S(j\omega) = [1 + L(j\omega)]^{-1}$ . The treatment of such specifications can be incorporated in the standard QFT design technique quite easily, however their use is not yet widespread.

## 6 Conclusions

This paper should serve as a basis for consideration of the fundamental principles underlying the QFT design procedure. Its aim is to question whether the advances in computational power available to the control system designer should alter the assumptions and simplifications that are inherent in the QFT design procedure. It has outlined four areas in which consideration should perhaps be given to altering the basis upon which QFT computer aided design packages are based. These are the effect of high frequency unmodelled dynamics on the template shape, the use of the UHB, the choice of the nominal point of the templates, and the need for additional specifications on the sensitivity of the loop frequency response.

## References

- BALLANCE, D. J., 1992, Comments on the papers "A new approach to optimum loop synthesis" and "On the determination of plant variation bounds for optimum loop synthesis", *Int. J. Control*, 55(1), 241-248.
- DOYLE, J. C., 1986, Quantitative feedback theory (QFT) and robust control, In *Proc. American Control Conf., Seattle, Washington, USA*, pages 1691-1698.
- EAST, D. J., 1981, A new approach to optimum loop synthesis, *Int. J. Control*, 34(4), 731-748.
- EAST, D. J., 1982, On the determination of plant variation bounds for optimum loop synthesis, *Int. J. Control*, 35(5), 391-908.
- HOROWITZ, I. M., 1973, Optimum loop transfer function in single-loop minimum-phase feedback systems, *Int. J. Control*, 18, 97-113.
- HOROWITZ, I. M., 1982, Improved design technique for uncertain multiple-input multiple-output feedback systems, *Int. J. Control*, 36(6), 977-988.
- HOROWITZ, I. M., 1982, Uncertain multiple-input-multiple-output systems with internal variable feedback, *Int. J. Control*, 36(6), 989-1009.
- HOROWITZ, I. M., 1982, Quantitative feedback theory, *Proc. IEE*, 129 Pt. D.(6), 215-226.

HOROWITZ, I. M., 1983, Some properties of delayed controls (Smith regulator), *Int. J. Control*, 38(5), 977-990.

HOROWITZ, I. M. and SIDI, M., 1972, Synthesis of feedback systems with large plant ignorance for prescribed time-domain tolerances, *Int. J. Control*, 16, 287-309.

HOROWITZ, I. M. and YANIV, O., 1985, Quantitative cascaded multiple-input multiple-output synthesis by an improved method, *Int. J. Control*, 42(2), 305-331.

LONGDON, L. and EAST, D. J., 1979, A simple geometrical technique for determining loop frequency response bounds which achieve prescribed sensitivity specifications, *Int. J. Control*, 30(1), 153-158.

YANIV, O. and HOROWITZ, I. M., 1986, A quantitative design method for mimo linear feedback systems having uncertain plants, *Int. J. Control*, 43(2), 401-421.

YANIV, O. and HOROWITZ, I. M., 1987, Quantitative feedback theory—reply to criticisms, *Int. J. Control*, 46(3), 945-962.

# STABILITY ANALYSIS USING NICHOLS CHARTS

by

Nir Cohen<sup>1</sup> Yossi Chait<sup>2 3 4</sup> Oded Yaniv<sup>5</sup> Craig Borghesani<sup>6</sup>

April 14, 1992

## Abstract

In this paper, a rigorous formulation is presented for stability analysis of closed-loop linear, time-invariant, single input/output systems using Nichols charts. This formulation is based on the celebrated Nyquist stability criterion, the simplified criterion that employs the notion of crossings, and the properties of the mapping from the complex plane to the Nichols chart. An extension of this criterion for a class of uncertain systems is also presented.

---

<sup>1</sup>Senior Research Associate, Electrical Engineering Department, The Technion, Israel

<sup>2</sup>Assistant Professor, Mechanical Engineering Department, University of Massachusetts, USA

<sup>3</sup>Author to whom all correspondence should be made to

<sup>4</sup>Research supported in part by an NSF grant No. MSS-8920628

<sup>5</sup>Assistant Professor, Department of Electrical Engineering, Tel Aviv University, Israel

<sup>6</sup>Graduate Student, Mechanical Engineering Department, University of Massachusetts, USA

## 1 Introduction

In this paper we develop a graphical stability criterion using a Nichols chart rather than the standard complex plane. The motivation for this development is that use of Nichols charts can often simplify control design. Chief among the techniques that employ Nichols charts is the Quantitative Feedback Theory (QFT) [1]. Numerous examples demonstrated that the design procedure used in single-input/single-output QFT does indeed lead to a stable design and even to robust stability in case of uncertain plants. However, a rigorous proof for the stability of this, and for that matter of any other Nichols chart based techniques, has never been formulated. Indeed, in [2] it was remarked that in some cases it may be difficult to define the closed-loop stability using Nichols plots. In this note we present a simple and natural proof that is based on the celebrated Nyquist criterion.

## 2 Preliminaries

Before describing our main results (Theorems 3,4), we need to take a closer look at some of the technicalities involved with the Nyquist criterion.

The classical Nyquist stability criterion for rational functions ([3]) has been extended to include certain classes of distributed parameter, nonlinear and time-varying systems. In this paper we shall consider the class  $\mathcal{L}$  of distributed parameter, linear time-invariant plants whose impulse response  $p(t)$  has the form [4]

$$p(t) = p_a(t) + p_s(t) \quad (1)$$

where  $p_a(t)$  is the inverse Laplace transform of a proper rational function  $P_a(s)$  that has no poles on the extended  $j\omega$ -axis, and  $p_s(t)$  is an absolutely integrable function on

$t \in [0, \infty)$  (i.e.,  $p_s \in L_1[0, \infty)$ ). The Laplace transform of  $p(t)$  will be denoted by  $P(s)$ .

Define the loop transmission as  $L(s) = P(s)G(s)H(s)$ , where both the forward  $G(s)$  and the feedback  $H(s)$  functions are rational and fixed. Assume that there are no unstable cancellations between poles and zeros when forming  $L(s)$ . Define the standard Nyquist contour,  $\Gamma$ , as in Fig. 1, where  $j\omega$ -axis indentations are added as necessary to account for imaginary poles of  $L(s)$ . We assume that  $\Gamma$  is chosen big enough to include all unstable poles of  $L(s)$ . Let  $n$  denote the total multiplicity of these poles. The *Nyquist plot* is the image of  $L(s)$  under  $\Gamma$ . The Nyquist stability criterion for the feedback system shown in Fig. 2 with  $P \in \mathcal{L}$  is the following [4].

**Theorem 1:** *The feedback system in Fig. 2 is stable if and only if the Nyquist plot of  $L(s)$  does not intersect the point  $(-1, 0)$ , and encircles it  $n$  times in the counterclockwise direction.*

Such encirclements are related to the net change of the *argument* of  $L(s)$  as  $s$  completes a full counterclockwise (or clockwise) revolution around  $\Gamma$ . Hence, Nyquist criterion is an immediate consequence of the argument principle of complex analysis [5].

A recent article [6] presented the following simplification of the Nyquist criterion. Let  $R'_0$  be the ray  $(-\infty, -1)$ . A *crossing* occurs when the plot of  $L(s)$  intersects  $R'_0$ . The crossing is said to be *positive* if the direction of the plot is upward, and *negative* otherwise, as shown in Fig. 3.

**Theorem 2:** *The feedback system in Fig. 2 is stable if and only if the Nyquist plot of  $L(s)$  does not intersect the point  $(-1, 0)$ , and the net sum of its crossings is equal to  $n$ .*



It is this simplification of the Nyquist stability criterion which we use in our Nichols chart stability result.

Note in passing that in Theorem 2 the ray  $R'_0$  may be replaced by any complex ray emanating from the point  $(-1, 0)$ . More generally, it may be replaced by an arbitrary curve connecting this point and the point at infinity, under a suitable definition of crossing orientation.

### 3 The Nichols Chart and Main Result

The Nichols chart  $NC$  represents complex numbers in terms of their magnitudes and phases. Each complex number,  $s$ , has a cartesian representation  $(x, y)$  and a polar representation  $(r, \phi)$ . For historical reasons, we shall assume a non-principal choice for the phase:  $-360 < \phi \leq 0$ . The coordinates of the Nichols chart are  $(\phi, \log r)$ , in this order. The horizontal coordinate  $\phi$  ranges between  $-360^\circ$  and  $0^\circ$ , while the vertical coordinate  $\log r$  ranges theoretically from  $-\infty$  to  $+\infty$ . In practice, the actual Nichols chart is naturally limited to a finite range of log amplitudes. For simplicity, we use here  $\log r$  instead of the  $20 \log r$  used in control studies.

The map

$$\Upsilon : (x, y) \longrightarrow (\phi, \log r) \quad (2)$$

transforms the Nyquist plot into the Nichols chart, and will be used to derive the Nichols result. To have a better understanding of this map, we consider it as the composition of two maps  $f \circ g$ , where

$$1. g : (x, y) \longrightarrow (\log r, \phi)$$

$$2. f : (r, \phi) \longrightarrow (\phi, r)$$

The map  $g$  amounts to taking the logarithm of a complex number. It is a bijection from the punctured complex plane  $\mathbb{C}_x$  onto the bi-infinite strip

$$S := \{(r', \phi) : -\infty \leq r' \leq \infty, -360^\circ \leq \phi < 0\}.$$

(A bijection is a one-to-one and onto map). It is orientation preserving: a clockwise plot in  $\mathbb{C}_x$  (say, not crossing the positive real axis) is transformed by  $g$  to a clockwise plot in  $S$ . As defined, it is an analytic map at any point  $(x, y)$  not on the positive real axis. On this ray, it is not even continuous.

The map  $f$  is evidently a continuous bijection from the bi-infinite strip  $S$  into the Nichols chart. It is orientation reversing: a clockwise contour in  $S$  will be transformed into a counterclockwise contour in  $NC$ . In particular, it is not an analytic mapping (to see this apply the Cauchy-Riemann conditions).

The map  $\Upsilon$  is thus seen to be an orientation reversing, one-to-one map from  $\mathbb{C}_x$  onto the Nichols chart  $NC$ , which is continuous except for a jump across the positive ray.

Mathematically speaking, the Nichols chart should have been drawn with the phase as its vertical abscissa and the log magnitude as its horizontal abscissa. For unknown reasons, Nichols [7] who introduced this  $20 \log r / \text{phase}$  chart, added the map  $f$ , and chose a non-principal branch for the angle  $\phi$  in  $NC$ ; and this format has since been adopted as a standard.

Let us now consider the action of  $\Upsilon$  on a closed curve  $\Psi$  in  $\mathbb{C}_x$ . Of course, the case we have in mind is when  $\Psi$  is the Nyquist plot of  $L(s)$ .

The image curve  $\Upsilon(\Psi)$  in the Nichols chart may fail to be closed, due to the discontinuity of  $f$  on the positive real axis. Each time  $\Psi$  hits the positive real axis,  $\Upsilon(\Psi)$  disappears at the right or left margin of the vertical strip  $NC$  and reappears on the opposite margin. In particular, due to orientation reversal, each clockwise winding of  $\Psi$  around the origin will result in  $\Upsilon(\Psi)$  traversing  $NC$  from right to left, i.e. from  $\phi = 0^\circ$  to  $\phi = -360^\circ$ .

Each of the continuous pieces of  $\Upsilon(\Psi)$  formed this way will be called a *Nichols branch*. The *single-sheeted Nichols plot* is merely the union of these branches, drawn on a single copy of the Nichols chart.

If one wishes to retain continuity of the Nichols plot, one has to extend  $S$  and  $NC$  periodically in the angular coordinate. A Nyquist curve winding  $k$  times around the origin would be transformed this way into a continuous (but not closed!) curve drawn along a scroll of at least  $k$  Nichols sheets. This curve will be called the *multiple-sheeted Nichols plot*.

Using the established properties of the map  $\Upsilon$ , we can now proceed to describe the Nichols stability criterion. We emphasize that this criterion can be equally performed on a single-sheet plot or a multiple-sheet plot. The decision to use the one or the other is a matter of convenience only.

**Theorem 3:** *The following are equivalent:*

1. *The feedback system in Fig. 2 is stable.*
2. *The one-sheeted Nichols plot of  $L(s)$  does not intersect the point  $q := (-180^\circ, 0dB)$ , and the net sum of its crossings of the ray  $R_0 := \{(\phi, r') : \phi = -180^\circ, r' > 0dB\}$  is equal to  $n$ .*
3. *The multiple-sheeted Nichols plot of  $L(s)$  does not intersect any of the*

points  $(2k+1)q$ ,  $k = 0, \pm 1, \pm 2, \dots$ , and the net sum of its crossings of the rays  $R_0 + 2kq$  is equal to  $n$ .

**Proof.** This is a straightforward adaptation of Theorem 2 to the Nichols chart. The bijection  $\Upsilon$  takes the ray  $R'_0 := [-\infty, -1) \subset \mathbb{C}_x$  onto the ray  $R_0 \subset NC$ , and the point  $(-1, 0)$  into the point  $q$ . Orientation reversal means that each counterclockwise crossing of  $R'_0$  is mapped into a crossing from left to right of  $R_0$ . We can now quote Theorem 2. QED

Some remarks on Theorem 3 are in order:

1. The choice of  $-180^\circ$  in Theorem 3 is canonical, and cannot be altered; on the other hand, the ray  $R_0$  may be replaced by an arbitrary curve that connects the point  $q$  with the upper boundary of the Nichols chart and maintains positive distance from its left and right margins. This follows from the remark following Theorem 2.

2. It has become customary in control design to use only half of the Nyquist plot (i.e. the Bode plot). Because of conjugate symmetry, if there is a crossing at some  $s_0 \in \Gamma$  then there will be another crossing at  $\bar{s}_0$ , and of the same sign. That is, each crossing of the half plot is tantamount to two crossings of the complete plot.

### 3.1 Examples

To illustrate the Nichols chart stability criterion, let us consider several examples that cover various cases, stable and unstable, minimum phase and non minimum phase, and of varying types. In all the examples below, for simplicity, the feedback system is the one shown in Fig. 2 with unity feedback,  $H(s)=1$ . The Nyquist contour is the one shown in Fig. 1.

*Example 1.* This example is stable and minimum phase

$$L(s) = \frac{k}{s+1}$$

The full and half Nyquist plots on a NC are shown on Figs. 4-5 with  $k = 2$ . Because there are no crossings of the rays  $R_0 + 2kq$  for any positive gain  $k$  and the open-loop system is stable, the closed-loop system is stable. Note that the same conclusion can be arrived at using either half or full plot.

*Example 2.* This example has the same  $L(s)$  of Example 1, however, the range of the gain is  $k < 0$ . The sign of the feedback loop remains unchanged, negative, and we use  $k = -2$  for plotting. Let us first consider the full plot shown in Fig. 6. One can observe a positive crossing (i.e., from left to right) of the ray  $R_0$  at  $\omega = 0$ . This crossing occurs below or above 0 dB if  $k > -1$  or  $k < -1$ , respectively. If  $k = -1$ , the plot crosses the point  $q$  and hence we cannot deduce stability from the criterion. Therefore, the closed-loop system is unstable for any  $k < -1$ . Similar conclusion can be arrived at using the half plot (Fig. 7). Note that if the half plot touches but not actually crosses the ray  $R_0$ , the full plot will show a single crossing there. However, if the half plot is tangential to this ray, there is no crossing there.

*Example 3.* This example has three stable poles and no zeros.

$$L(s) = \frac{k}{(s+1)(s+5)(s+10)}$$

The gain used for plotting is  $k = 3000$ . When drawing the NC plot, one can use a single chart or several as needed. As described earlier, any portion of the NC plot can be shifted left or right by  $k360^\circ$ . Based on a shifted (i.e., using a single NC sheet) full plot (Fig. 8),

two positive crossings are identified. Hence, the closed-loop system is stable if and only if  $0 < k < 1000$ . The non-shifted full plot (Fig. 9) indicates the same conclusion. Based on the half plot (Fig. 10), a single positive crossing is identified at  $\omega = 8.11$  and  $|L(j8.11)| = 3$  (or 9.5 dB). This implies two positive crossings of the full plot.

*Example 4.* This example is taken from [6]. The system is open-loop stable

$$L(s) = \frac{k(s+50)^2(s+1000)}{(s+1)(s+2)(s+5)(s+200)(s+500)}.$$

The full and half NC plots are shown in Figs. 11-12. The gain used for plotting is  $k = 1$ . In the half plot there are several crossings at  $-18$  dB (negative),  $-67$  dB (positive) and  $-98$  dB (negative). Note, however, that these are not counted for stability analysis since  $|L(s)| < 0$  dB. Because the system is open-loop stable, we have closed-loop stability if and only if the sum of all crossings is zero. Therefore, the closed-loop system is stable if and only if  $0 < k < 8$  or  $2240 < k < 80000$ . More specifically,

- if  $k < 8$  there are no crossing above 0 dB; stable
- if  $8 < k < 2240$  there are 2 positive crossings; unstable
- if  $2240 < k < 80000$  there are 2 positive and 2 negative; stable
- if  $80000 < k$  there are 4 positive and 2 negative crossings; unstable

*Example 5.* Consider a stable type 1 system

$$L(s) = \frac{k}{s(s+1)(s+10)}.$$

The full and half NC plots are shown in Figs. 13-14 for  $k = 1$ . Based on the full plot there are two positive crossings at  $-40$  dB. Therefore, closed-loop system is stable if and only if

$0 < k < 100$ . The same conclusion can be reached using the half plot. Note, however, that if the system type is greater than zero, the half plot must include the segment corresponding to the indentation about the origin. In the complex plane, each integrator contributes to the Nyquist plot a semi-circle of infinite radius. On a NC, each integrator contributes a  $180^\circ$  wide horizontal segment at magnitude of  $\infty$  dB. This segment will always end at the start of the half plot, i.e. at the point corresponding to  $\omega = \epsilon$ . Clearly, in this example the segment does not cross the ray  $R_0$ . Hence, we conclude that the half plot has a single positive crossing at  $-40$  dB. This implies two positive crossings of the full plot at  $-40$  dB.

*Example 6.* Consider a type 1 unstable system

$$L(s) = \frac{k}{s(s-1)}.$$

The shifted full, non-shifted full, and half NC plots are shown in Figs. 15-17, respectively. The gain used for plotting is  $k = 1$ . Based on either the shifted or non-shifted full plots there is a single positive crossing of the ray  $R_0$  at  $\infty$  dB due to the  $j\omega$ -indentation in  $\Gamma$ . The plot is not closed on the NC, but as mentioned earlier this does not influence the analysis. At any rate, there is one open-loop unstable pole and together with the single positive crossing we conclude that the closed-loop system will have two closed-loop unstable poles for any  $k > 0$ . The half plot shows single positive crossing due to the integrator. Such a crossing will not be counted as any other crossing two in the full plot because it already reflects the map of the complete  $j\omega$ -indentation by  $L(s)$ .

*Example 7.* Consider a non minimum phase type 1 system

$$L(s) = \frac{k(1-s)}{s(s+1)}.$$

The full and half NC plots are shown in Figs. 18-19 for  $k = 1$ . Based on the either plot one concludes that there are two negative crossings at 0 dB. Hence, the closed-loop system is stable if  $0 < k < 1$ .

the  $\infty$  dB segment. Again, the fact that the plot is not closed on the NC is not important for stability analysis.

## 4 Robust Stability

Having derived the Nichols chart stability criterion for a fixed plant, let us turn our attention to uncertain plants. In many physical situations, the actual plant response is not known precisely. Rather, it is known to belong to a connected set  $\mathcal{P}$  of plants. The idea of robust stability amounts to checking stability using one *randomly chosen* nominal loop  $L_0 = G(s)H(s)P_0$ , where  $P_0 \in \mathcal{P}$  is termed the nominal plant, and then demonstrating stability of the whole set  $\mathcal{P}$  by some argument involving the connected nature of  $\mathcal{P}$ . This in particular implies the stability of the actual plant  $P$ . Note that the attributes of the set  $\mathcal{P}$  are passed to  $L(s)$  because both  $G(s)$  and  $H(s)$  are fixed.

In the Nyquist level, this is done as follows: at each frequency on the Nyquist contour,  $\Gamma$ , the responses of the  $L(s)$  fill in a neighborhood of the nominal response  $L_0(s)$ . This neighborhood, which is typically an open connected region, is called the *template* at  $s$ . As  $s$  travels along the Nyquist contour, the union of these templates becomes a connected region, which we shall call the Nyquist envelope. The following robust stability result is a minor modification of a well known result [8] (Theorem 1), where we do not explicitly assume connectedness of  $\mathcal{P}$ , but add a crucial assumption on the number of unstable poles:

**Theorem 4:** *Let  $\mathcal{P}$  be a set of admissible plants that share the same number of*



unstable poles. Assume that each template is connected. Let  $P_0(s) \in \mathcal{P}$ . Then the feedback system in Fig. 2 is robustly stable iff the fixed system corresponding to  $L_0(s)$  is stable and the Nyquist envelope does not intersect the point  $(-1, 0)$ .

A similar picture is seen on the Nichols chart. Connectedness raises a small technicality: if a connected Nyquist template intersects the ray  $R'_0$ , its singly-sheeted image in the Nichols chart may fail to be connected. In this case, we shall find it necessary to assume horizontal connectivity across the margins.

Similarly, the singly-sheeted Nichols envelope is not necessarily connected even if the Nyquist envelope is. However, one can reconstruct a connected multiple-sheeted Nichols envelope, with connected templates.

Under the map  $T$ , and taking connectedness into consideration, the following Nichols stability criterion is obtained:

**Theorem 5:** Let  $\mathcal{P}$  be a set of admissible plants that share the same number of unstable poles. Assume that each template in the multiple sheeted Nichols chart is connected. Namely, each template in the single sheeted chart is connected or connected across the margins. Let  $P_0(s) \in \mathcal{P}$ . Then the following are equivalent:

1. The feedback system in Fig. 2 is robustly stable.
2. The fixed system corresponding to  $L_0(s)$  is stable and the single-sheeted Nichols envelope does not intersect the point  $q$ .
3. The fixed system corresponding to  $L_0(s)$  is stable and the multiple-sheeted Nichols envelope does not intersect any of the points  $(2k + 1)q$ ,  $k = 0, \pm 1, \pm 2, \dots$

The proof is again routine, using the map  $T$  and Theorem 4. The condition that the plot does not intersect any of the points  $(2k+1)q$  is in fact the one used in the Quantitative Feedback Theory.

## References

- [1] Horowitz, I.M., and Sidi, M., (1972). "Synthesis of Feedback Systems with Large Plant Ignorance for Prescribed Time-Domain Tolerances," *International J. of Control*, 16(2), pp. 287-309.
- [2] D'Azzo, J.J., and Houpis, C.H., (1988). *Linear Control System Analysis & Design*, 3rd edition, Sec. 8-20.
- [3] Nyquist, H., (1932). "Regeneration Theory," *Bell Systems Technical J.*, Vol. 11, pp. 126-147.
- [4] Desoer, C.A., and Vidyasagar, M., (1975). *Feedback Systems: Input-Output Properties*, Academic Press, New York.
- [5] Churchill, R.V., and Brown, J.W., (1980). *Complex Variables and Applications*, McGraw-Hill, New York.
- [6] Vidyasagar, M., Bertschmann, R.K., and Sallaberger, C.S., (1988). "Some Simplifications of the Graphical Nyquist Criterion," *IEEE Transactions on Automatic Control*, Vol. 33(3), pp. 301-303.
- [7] James, H.M., Nichols, N.B., and Philips, R.S., (1947). *Theory of Servomechanisms*, McGraw-Hill, first edition.

- [8] Chen, M.J., and Desoer, C.A., (1982). "Necessary and Sufficient Condition for the Robust Stability of Linear Distributed Feedback Systems," *International J. of Control*, 35(2), pp. 255-267.

## **List of Figures**

- Figure 1: The Nyquist contour**
- Figure 2: The feedback system**
- Figure 3: The notion of crossing**
- Figure 4: Full Nichols plot of Example 1**
- Figure 5: Half Nichols plot of Example 1**
- 
- Figure 6: Full Nichols plot of Example 2**
- Figure 7: Half Nichols plot of Example 2**
- Figure 8: Full Nichols plot (shifted) of Example 3**
- Figure 9: Full Nichols plot (non-shifted) of Example 3**
- Figure 10: Half Nichols plot of Example 3**
- Figure 11: Full Nichols plot of Example 4**
- Figure 12: Half Nichols plot of Example 4**
- Figure 13: Full Nichols plot of Example 5**
- Figure 14: Half Nichols plot of Example 5**
- Figure 15: Full Nichols plot (shifted) of Example 6**
- Figure 16: Full Nichols plot (non-shifted) of Example 6**
- Figure 17: Half Nichols plot of Example 6**
- Figure 18: Full Nichols plot of Example 7**
- Figure 19: Half Nichols plot of Example 7**

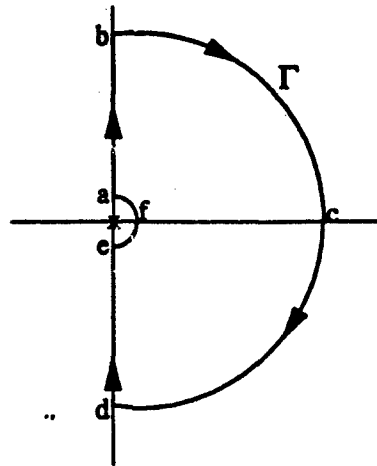


Figure 1: The Nyquist contour

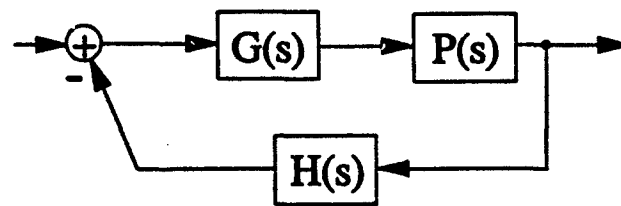


Figure 2: The feedback system

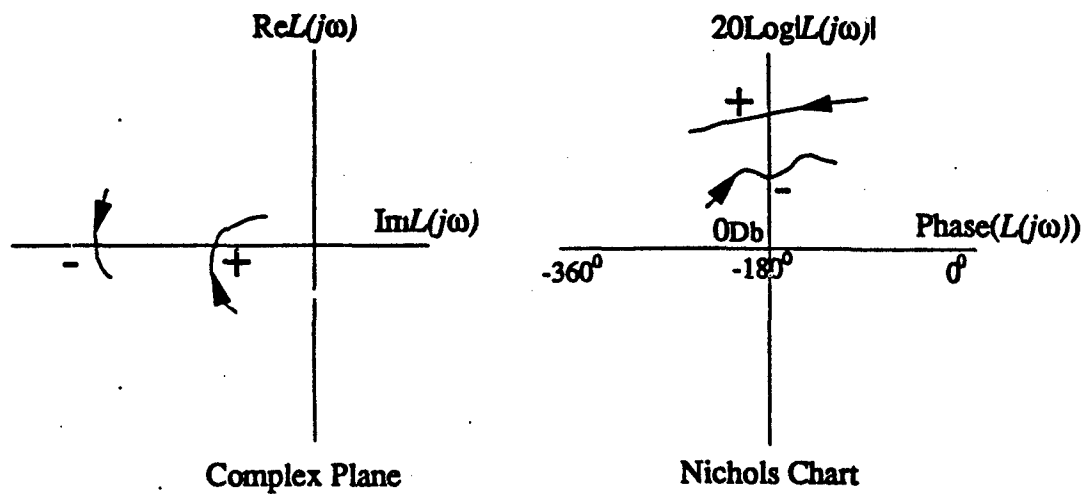


Figure 3: The notion of crossing.

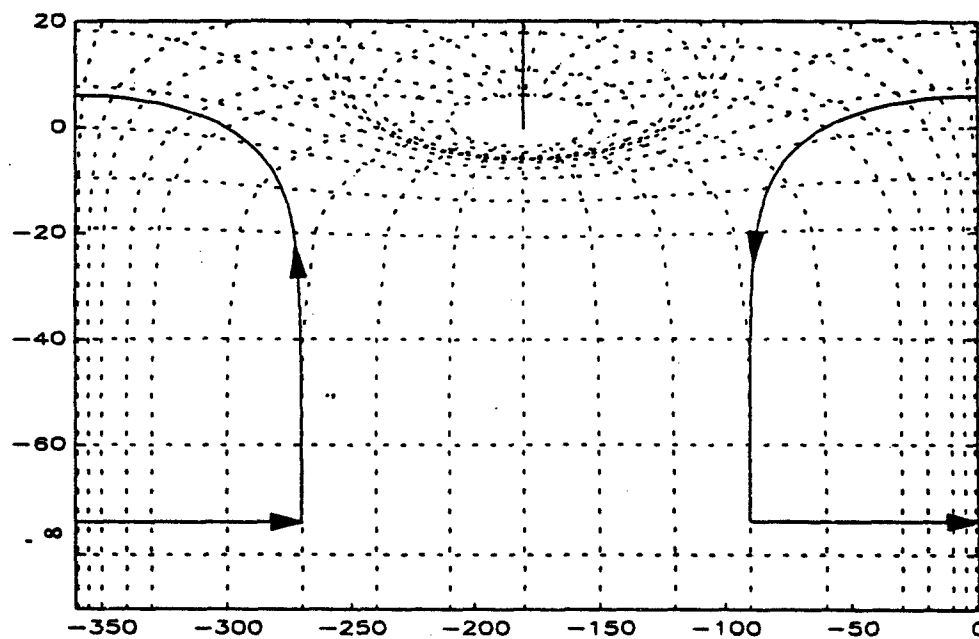


Figure 4: Full Nichols plot of Example 1

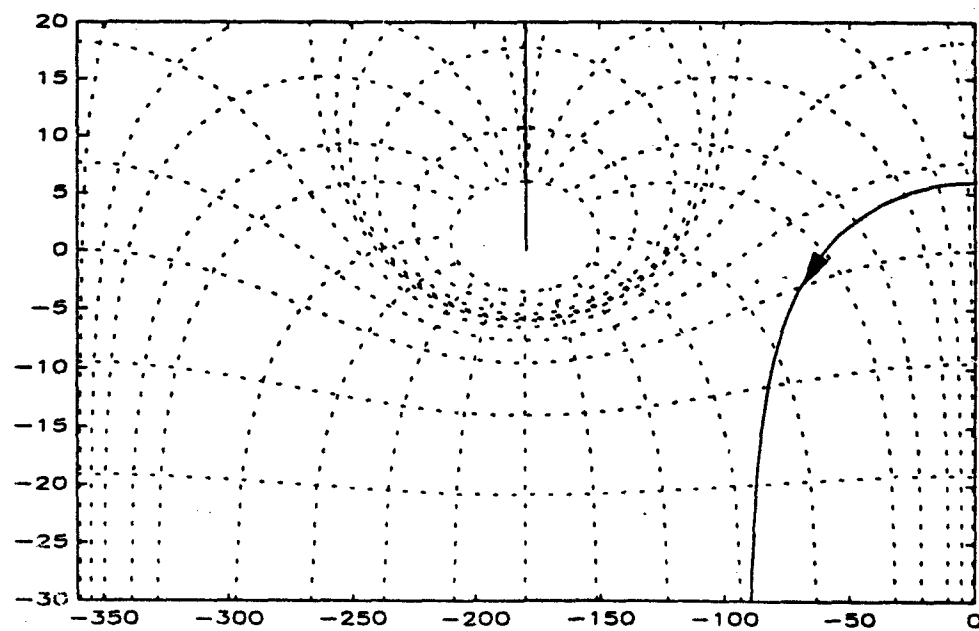


Figure 5: Half plot of Example 1

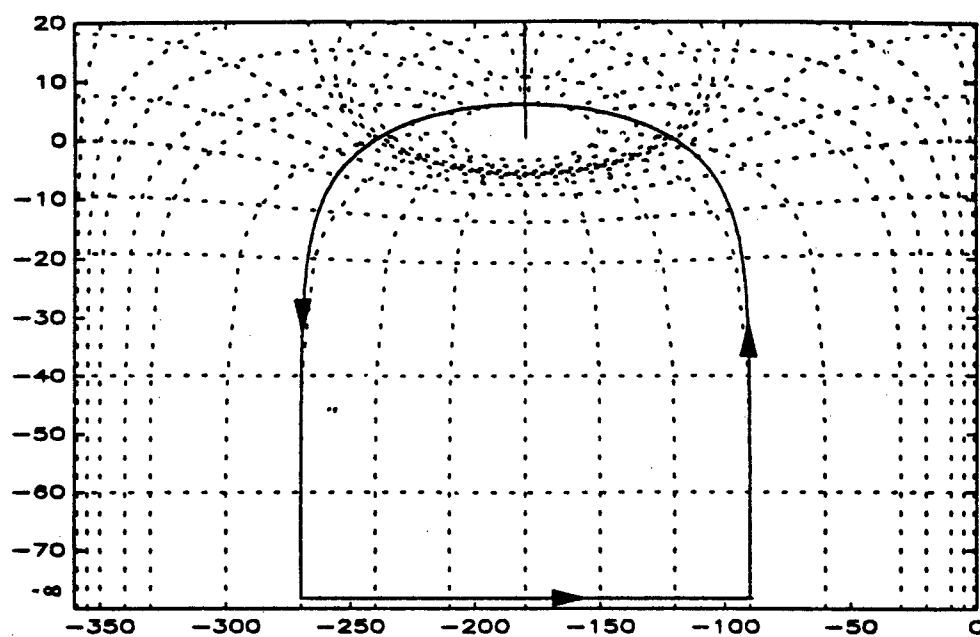


Figure 6: Full Nichols plot of Example 2

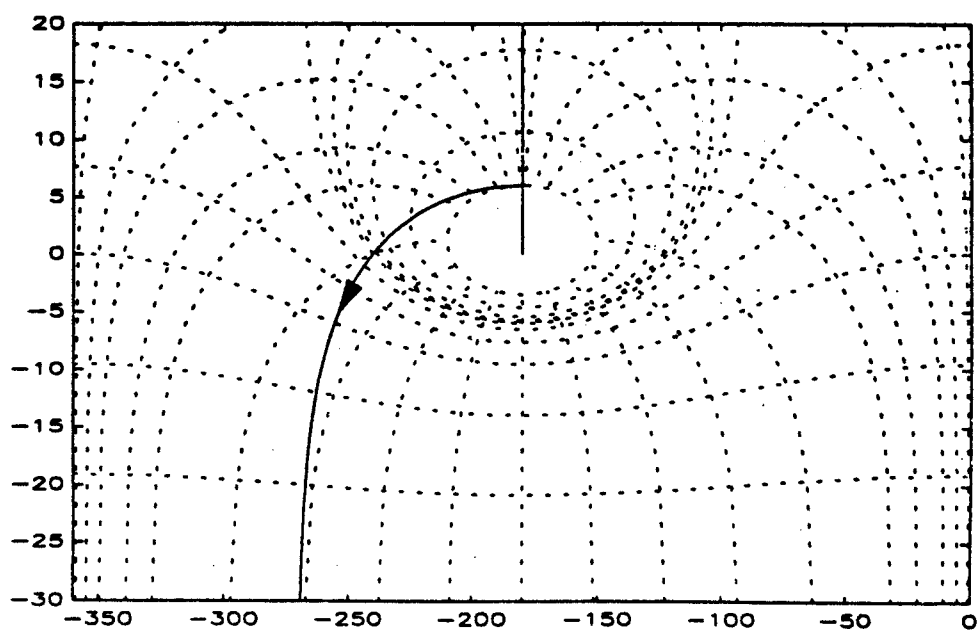


Figure 7: Half plot of Example 2

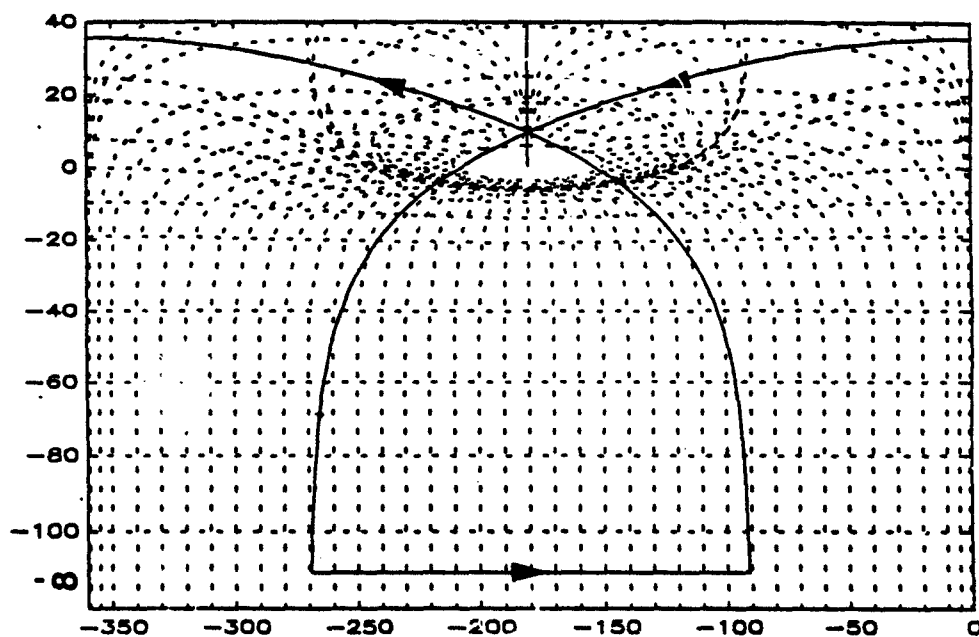


Figure 8: Full Nichols plot (shifted) of Example 3

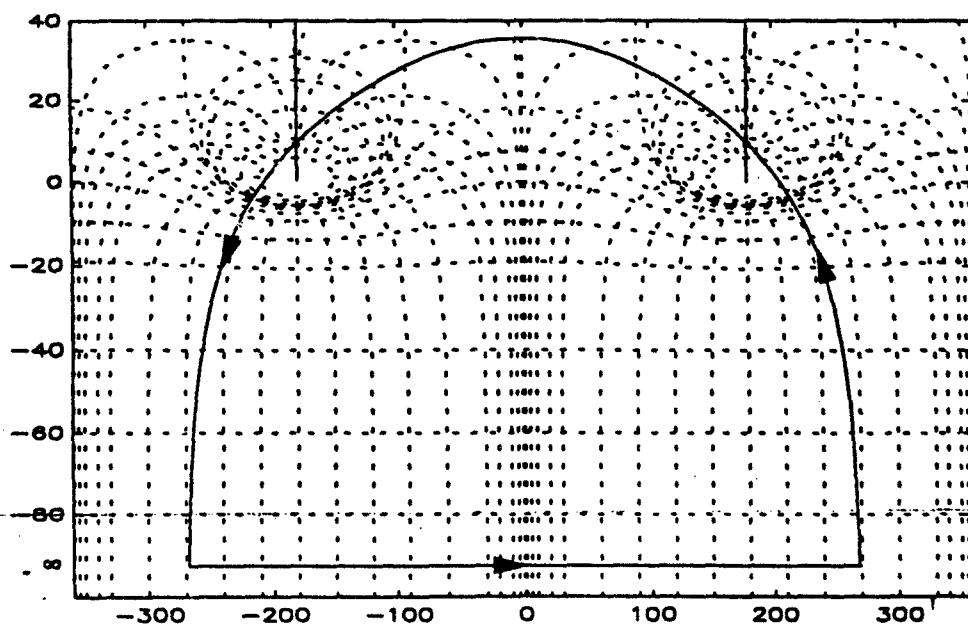


Figure 9: Full Nichols plot (non-shifted) of Example 3



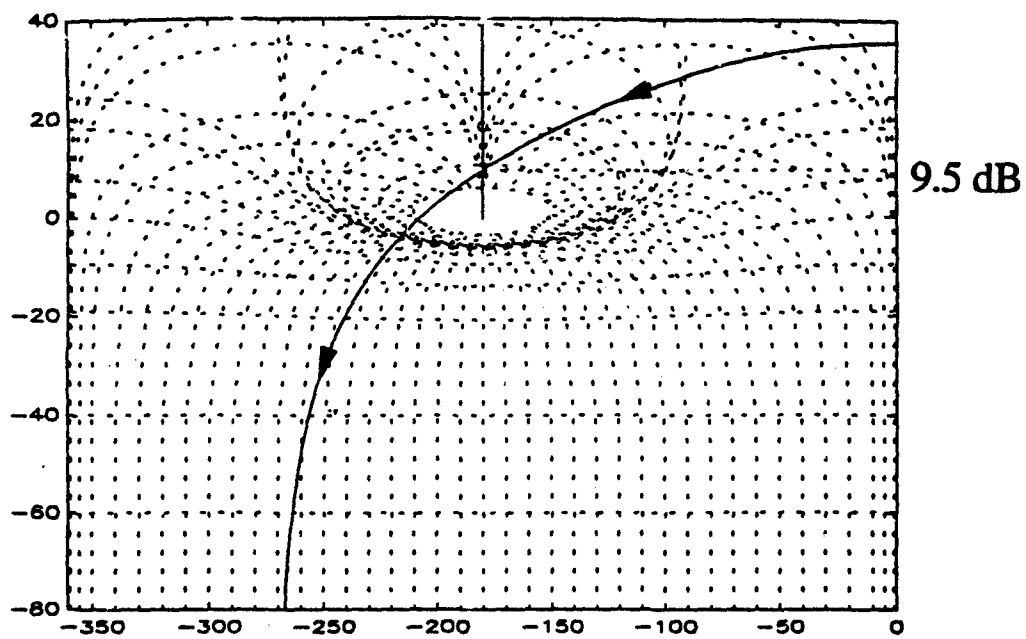


Figure 10: Half plot of Example 3

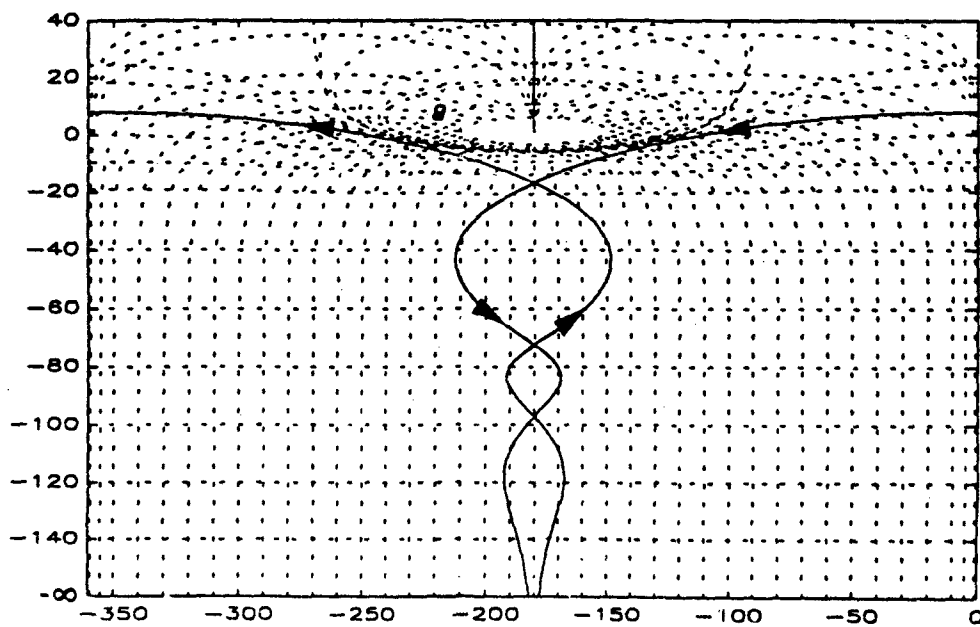


Figure 11: Full Nichols plot of Example 4

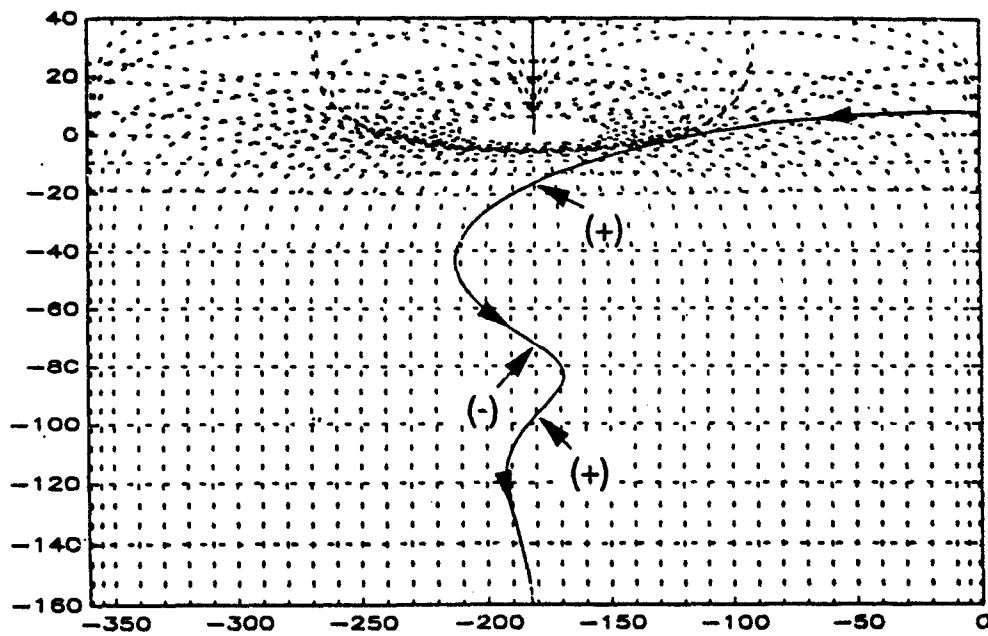


Figure 12: Half plot of Example 4

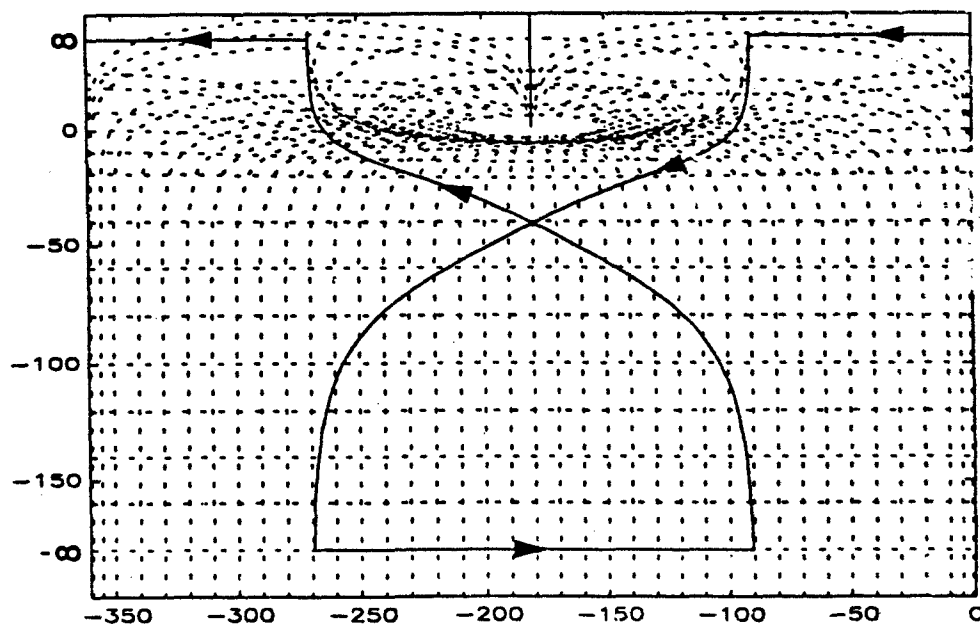


Figure 13: Full Nichols plot of Example 5

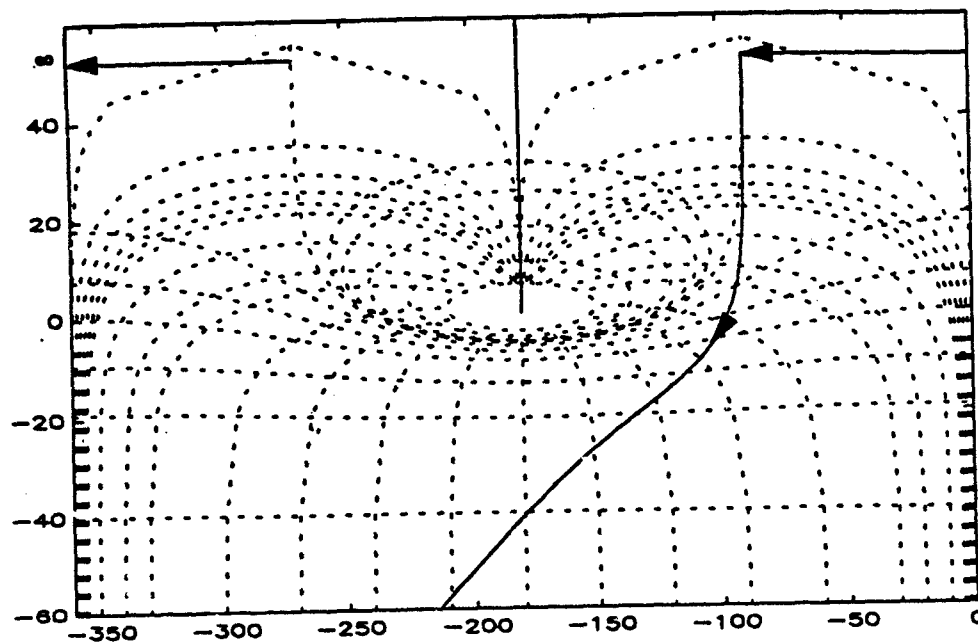


Figure 14: Half plot of Example 5

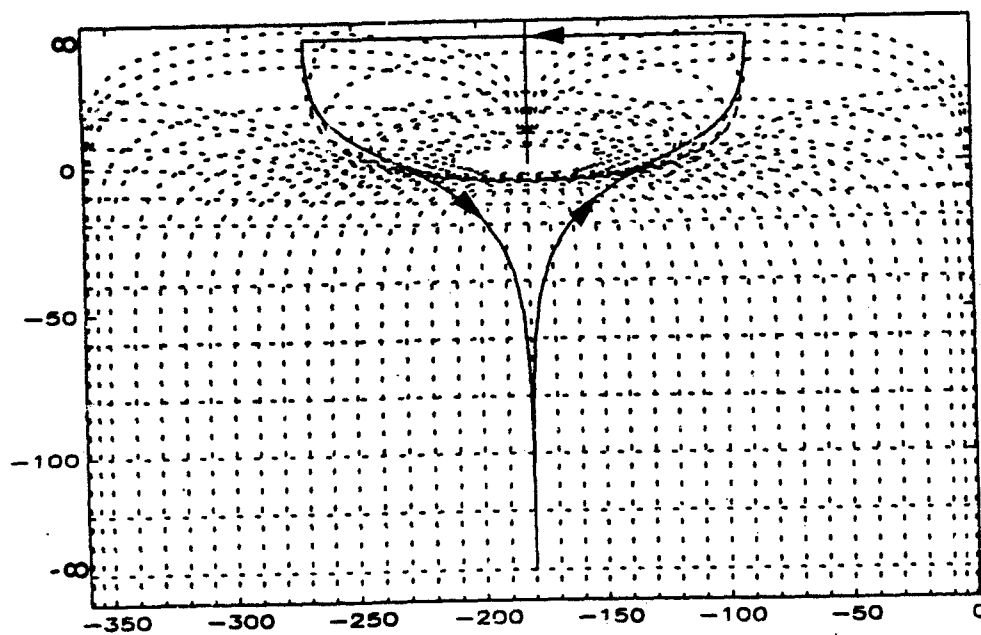


Figure 15: Full Nichols plot (shifted) of Example 6

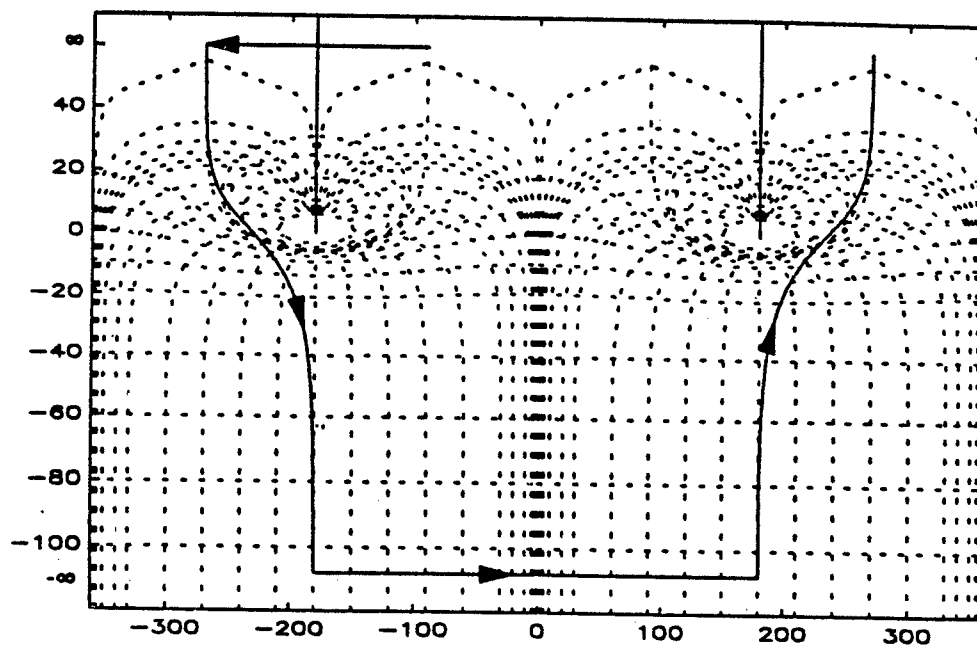


Figure 16: Full Nichols (non-shifted) plot of Example 6

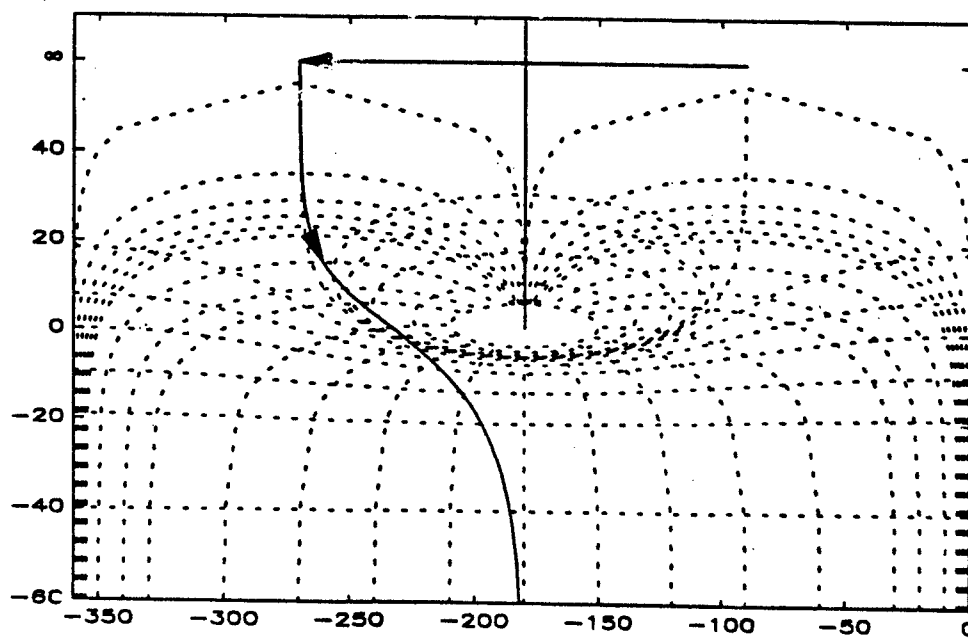


Figure 17: Half plot of Example 6

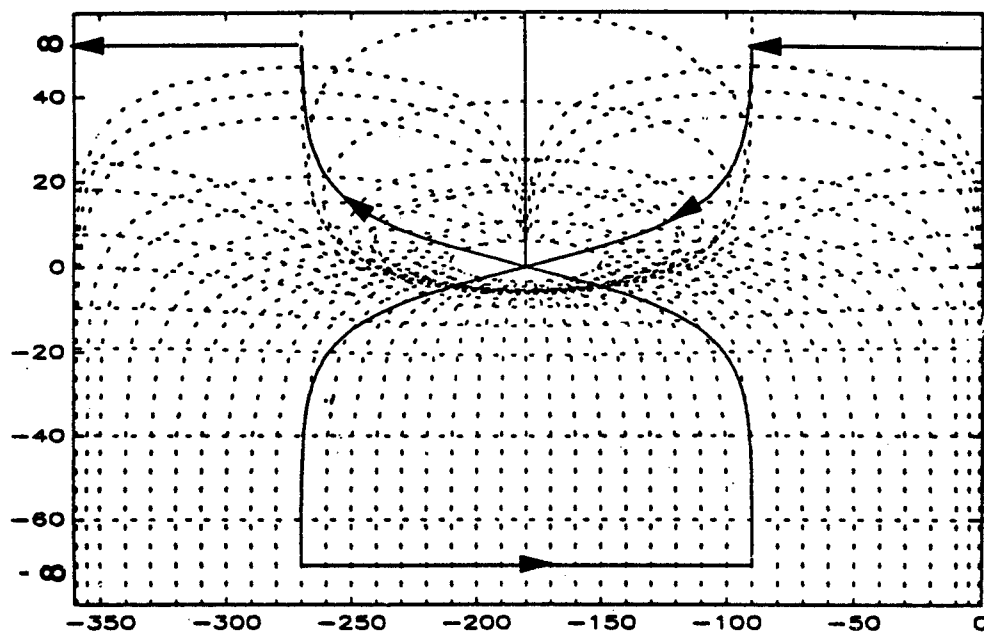


Figure 18: Full Nichols plot of Example 7

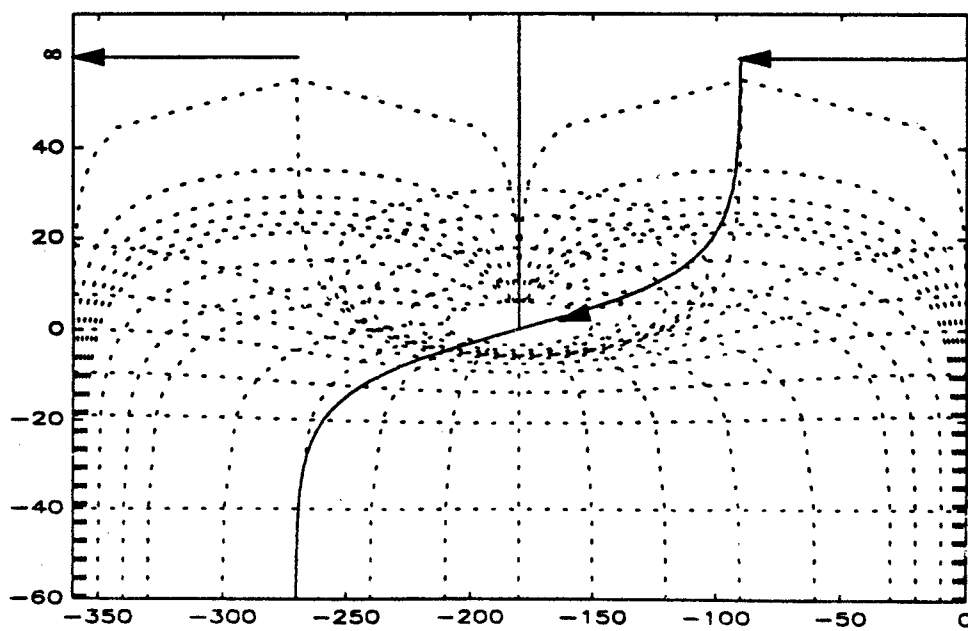


Figure 19: Half plot of Example 7

QFT: Methods for Synthesis  
of Optimal Controls

David F. Thompson  
Ford Motor Company  
Transmission and Chassis Operations  
36200 Plymouth Rd., Box 26  
Livonia, MI 48150

ABSTRACT

Recent interest in robust control has been focused upon the issue of performance robustness, particularly in the frequency domain. Of the various techniques, Quantitative Feedback Theory (QFT) has often been recognized as more transparent, with a formulation of the greatest engineering significance in many applications. In the QFT problem, it is sought to obtain an admissible set of complex functions which, evaluated along the  $j\omega$  axis, meet open loop magnitude and phase constraints. (These constraints are the image of closed loop transfer function bounds which are to be met in the face of parametric, and possibly non-parametric plant uncertainty.) From this set of admissible controllers, an appropriate optimum is to be chosen. Although boundaries of the admissible set are readily available (as gain-phase contours), the optimization is not straightforward. Furthermore, a more fundamental issue is raised as to which of two figures of merit, sensitivity or controller bandwidth, represents with the most fidelity the "true" QFT design objective: minimization of the *cost of feedback*. In this expository paper, we begin to examine these questions. In addition, candidate formulations for the synthesis problem are proposed including nonlinear programming, a real-function optimal control formulation, as well as complex extremal methods. As a benefit of these formulations, a definitive link is established between the traditional QFT problem formulation, sensitivity functions, and  $H_2$ - $L_2$  optimization theory.

---

This research was sponsored in part by a grant from the Air Force Office of Scientific Research/Universal Energy Systems under contract No. F49620-88-C-0053, and by the School of Mechanical Engineering, Purdue University, West Lafayette, IN.

## 1. Introduction

Much of the current interest in frequency domain robust stability and robust performance dates from the work of Bode (1945), and Horowitz (1963). Techniques developed by Horowitz, which characterize closed loop performance specifications against parametric plant uncertainty, mapped into open loop design constraints, have come to be known as *Quantitative Feedback Theory* (QFT). In this paper, it is sought to present the QFT problem in its very simplest form in order to illustrate the key points of the controller synthesis problem. Most all simplifying assumptions, such as those of minimum-phase and/or single-input, single-output (SISO) plants, impact only the structure of the admissible set. However, the nature of the optimization problem is more broadly applicable. Although the structure of this admissible set is the subject of recent study (Bailey and Hui, 1991), it is the formulation and solution of the optimization problem which remain as key unresolved issues.

In fact, the underlying issues are much greater than that of simply identifying computational techniques. One principal goal of recent work in robust design, and in QFT in particular, has been to make precise and mathematically rigorous many of the applicable design goals and "rules of thumb" that have often been known to classical designers. Of these, we shall attempt to define and make precise the idea of *cost of feedback* in the context of the QFT problem, and to examine two candidate measures of this cost: controller bandwidth, and sensitivity integrals.

### 1.1. Structure of the SISO Problem

For illustration, consider a two degree-of-freedom SISO system (Figure 1) with plant  $P$ , forward loop controller  $G$ , and prefilter  $F$ . The problem is posed in continuous time and in the  $s$ -domain. Let the plant  $P(\alpha, s)$  of known structure be described by parametric uncertainty, where the parameter vector  $\alpha \in \mathbb{R}^n$  is contained in a compact set. Furthermore, let the plant  $P$  be stable and minimum phase over this set. (More general assumptions would have the plant set be path connected and stabilizable by a single controller  $G$  over all  $\alpha$ . Combined parametric/non-parametric representation of uncertainty is also appropriate.)

For the open loop system, let

$$L(\alpha, j\omega) \triangleq P(\alpha, j\omega)G(j\omega) \quad (1.1)$$

and define a "nominal" system

$$L_o(j\omega) \triangleq P_o(j\omega)G(j\omega) \quad (1.2)$$

where

$$P_o(j\omega) \triangleq P(\alpha_o, j\omega) \quad (1.3)$$

for a nominal parameter value  $\alpha_o$ . Then,

$$T(\alpha, j\omega) \triangleq \frac{L(\alpha, j\omega)}{1 + L(\alpha, j\omega)} \quad (1.4)$$

represents closed loop. Later we consider the effect of a noise signal  $N(j\omega)$  entering the feedback path (Figure 1).

## 1.2. Statement of Closed Loop Transfer Function Bounds

The QFT robust performance problem is then, for some appropriate bounding functions  $|T_U(j\omega)|$ ,  $|T_L(j\omega)|$ , find (if possible) a set of admissible controllers  $\{G\}$ , and then for some  $G \in \{G\}$  a suitable prefilter  $F$ , such that

$$|T_L(j\omega)| \leq |F(j\omega) T(\alpha, j\omega)| \leq |T_U(j\omega)| \quad \text{for all } \omega \in [0, \infty) \quad (1.5)$$

and for all  $\alpha$ . Then find (if possible) some  $G^* \in \{G\}$  which is optimal by some measure. Note here that (1.5) is, precisely stated, a system of constraints dictating a given level of *performance* robustness in the face of parametric plant uncertainty. This stands in contrast to methodologies in which performance, performance robustness, and/or stability robustness measures are themselves optimized, without auxiliary conditions.

Equation (1.5) is furthermore a pointwise, hard constraint, specifying that closed loop responses are bounded in an "acceptable envelope" at all frequencies. For real-rational, strictly proper controllers, feedback proves ineffective at high frequencies (where  $|L_o(j\omega)| \ll 1$ ). Therefore, a more realistic re-statement of the specification (1.5) would be in a split-frequency form

$$|T_L(j\omega)| \leq |F(j\omega) T(\alpha, j\omega)| \leq |T_U(j\omega)| \quad \text{for all } \omega \in [0, \omega_c) \quad (1.6)$$



$$|T(\alpha, j\omega)| \leq |T_U(j\omega)| \quad \text{for all } \omega \in [\omega_C, \infty) \quad (1.7)$$

where  $\omega_C$  is part of the designer's specification (subject to iterative refinement) identifying the bandwidth over which feedback is likely to be effective. Alternatively, the frequency  $\omega_C$  may indicate a crossover point at which robust stability requirements (not stated explicitly here) dominate the robust performance constraints.

In a split parametric/non-parametric plant model there is, in general, another transition frequency  $\omega_H$  above which the parametric model is irrelevant. This  $\omega_H$  is sometimes referred to as the *Horowitz high frequency*. A related, more general notion is that of the *normal bandwidth* of a plant, presumably intended to indicate the frequency range over which plant transfer function magnitude is above some useful value. (In some cases, this may also indicate the range over which the structured portion of the plant model is significant.) These frequencies  $\omega_H$  and  $\omega_C$  will not, in general, be coincident; it is, in fact, the *difference* between the controller bandwidth and the normal plant bandwidth which becomes a significant issue in the QFT formulation. We shall address these ideas subsequently. However, for the purposes of this initial discussion, the formulation will be in terms of the original specification (1.5); the implications of (1.6) and (1.7) will be noted, as applicable. We now introduce the synthesis problem.

## 2. Open Loop Synthesis

From the known structure of (1.1)-(1.4), it is possible to map the constraint set (1.5) into a system of constraints on the *nominal* open loop transfer function  $L_o(j\omega)$ . This step is part-and-parcel of the QFT method and is well documented (Horowitz and Sidi, 1972, 1978). The effective result may be viewed as generating a system of constraints of the form:

$$B(L_o(j\omega), \omega) \geq 0, \quad \omega \in [0, \infty). \quad (2.1)$$

Under some conditions, this may be given in the more explicit form:

$$|L_o(j\omega)| - b(L_o(j\omega), \omega) \geq 0, \quad \omega \in [0, \infty). \quad (2.2)$$

Analytic expressions for (2.2), and its gradients, have been developed by Thompson (1990), Thompson and Nwokah (1991).

There is the additional requirement of closed loop stability (over all  $\alpha$ ) that is somewhat implied by (1.5). The mapping to open loop conditions (2.1) or (2.2) does not, however, preserve this property, and it must be added as side condition (usually an encirclement condition, commonly known in QFT as the "U-Contour"). Furthermore, these constraint sets must pass certain necessary conditions (e.g., in terms of allowable sensitivity reduction) in order for admissible controllers to exist; see Bailey and Cockburn (1991), Bailey and Hui (1991), Thompson and Nwokah (1991), Nwokah, et al. (1992).

### 3. Optimization Criteria and Techniques

If a non-empty set of admissible controllers  $\{ \bar{G} \}$  exists, we then wish to formulate an appropriate objective function, ideally one which makes more precise the controller bandwidth ideas introduced in the previous section. We begin with an interpretation of the traditional QFT objectives.

#### 3.1. High Frequency Gain, Bandwidth, and the Cost of Feedback

For illustration, consider  $L_o$  with a known (fixed) pole-zero excess  $e$ . Then the high frequency gain  $k_\infty$  of  $L_o$  is given by:

$$k_\infty \triangleq \lim_{\omega \rightarrow \infty} (j\omega)^e L_o(j\omega) \quad (3.1)$$

This is simply the gain constant of a transfer function in standard form. *Example:* Suppose  $L_o(j\omega)$  is given as

$$L_o(j\omega) = \frac{k(a + j\omega)}{j\omega(p + j\omega)(b + j\omega)} \quad (3.2)$$

then  $e = 2$  and  $k_\infty = k$ .

Minimization of the open loop  $k_\infty$  within the performance bounds (2.1) was the criterion originally proposed by Horowitz and Sidi (1972,1978) as a suitable measure of cost of feedback. This is often interpreted as minimization of the open loop bandwidth, an analogy which stems from the classical servo-design problem. Although this statement is not precise, the two concepts are rooted in the same philosophy.

As stated, the objective in QFT is to meet closed loop performance (1.5) and stability robustness specifications while minimizing some measure of cost of feedback. This can be viewed as an extension of the classical servo-design problem, but where the additional

constraints provide *guaranteed* closed loop robustness margins; always the implicit intent in classical design, but which for years was never formulated explicitly. Note that these constraints (2.1) essentially *fix* the level of performance, thus fixing what would be considered the usual definition of open loop bandwidth:  $\{ \omega : |L_o(j\omega)| = 1 \}$ . In fact, the system of constraints on  $L_o$  (e.g., 2.2) could be viewed as a phase-dependent *prescribed rolloff* on  $\omega \in [0, \infty)$ . This leaves the remaining degrees of freedom in the phase of  $L_o(j\omega)$ , as well as its high frequency gain; we shall find subsequently that there is a definitive link between these two quantities as well.

Within these remaining degrees of freedom, it was argued (Horowitz and Sidi, 1972, 1978) that amplification *at the plant input* of high frequency noise  $N(j\omega)$  entering the feedback path (Figure 1) became the principal concern in many high-performance feedback systems. As an illustration, for the feedback system of Figure 1 consider the transfer function from noise input  $N(j\omega)$  to the plant input  $U(j\omega)$ :

$$\frac{U(j\omega)}{N(j\omega)} = \frac{G(j\omega)}{1 + G(j\omega)P(j\omega)} \quad (3.3)$$

In certain applications, design objectives may lead the loop transfer function  $L_o(j\omega)$  to be pushed far beyond its normal bandwidth, as suggested by Figure 2. In such cases there exists a frequency range, indicated by  $[\omega_1, \omega_2]$ , over which  $|L_o(j\omega)| = |P_o(j\omega) G(j\omega)| \ll 1$ , but yet  $|G(j\omega)| \gg 1$ . Over this frequency range, the loop gain is transferred almost entirely to the controller; the noise transfer function (3.3) becomes

$$\frac{U(j\omega)}{N(j\omega)} = G(j\omega) \quad (3.4)$$

which, depending upon noise bandwidth, would likely imply saturation of the plant inputs. The implication within this context is that excess controller bandwidth reflects the cost of feedback, and furthermore, it was argued that high frequency open loop gain is a readily available measure of this quantity.

To make a connection between the ideas of bandwidth and high frequency gain, consider the open loop transfer function as effectively

$$L_o(j\omega) = \frac{k}{(j\omega)^s} \quad (3.5)$$

over some frequency range of importance. In this simple case, open loop bandwidth (by any definition) is directly proportional to  $k_\infty = k$ . For more complex systems, the analogy is less direct. However, Horowitz and Sidi (1972,1978) argued that the frequency range "of importance" from a cost-of-feedback standpoint is at high frequency (more specifically, on the interval  $[\omega_1, \omega_2]$  of Figure 2) for which (3.5) must hold for all strictly proper plants. Thus, to complete the formulation let us state the traditional QFT cost-of-feedback objective as minimization of controller bandwidth, with measure  $k_\infty$ .

We shall return to build upon these ideas shortly. What we wish to accomplish first is to establish a connection between the QFT criteria and objectives, and the more familiar concepts of sensitivity functions.

### 3.2. Sensitivity and the Cost of Feedback

We assume that the reader has some knowledge of the motivation for and properties of sensitivity functions; for a more detailed treatment, see Freudenberg and Looze (1988). For the closed loop system of Figure 1, recall the definition of the sensitivity function  $S$

$$S(\alpha, j\omega) \triangleq \frac{1}{1 + L(\alpha, j\omega)} \quad (3.6)$$

Now, for small perturbations in  $\alpha$  about the nominal condition  $\alpha_0$ , consider the nominal sensitivity function  $S_0(j\omega) = S(\alpha_0, j\omega)$ . The benefit of feedback is achieved at all frequencies for which  $|S_0(j\omega)| < 1$ , while feedback is detrimental at all frequencies for which  $|S_0(j\omega)| > 1$ . When  $|S_0(j\omega)| = 1$ , sensitivity is equal to that of the open loop system.

For illustration, let there be some frequency  $\omega_s$  such that  $|S_0(j\omega)| < 1$  for all  $\omega \in [0, \omega_s)$ , and  $|S_0(j\omega)| \geq 1$  for all  $\omega \in [\omega_s, \infty)$ . The cost of feedback in this formulation would typically be given as the area of sensitivity increase; i.e.,

$$\int_{\omega_s}^{\infty} \log |S_0(j\omega)| d\omega \quad (3.7)$$

However, a well known fact for stable, minimum-phase systems is the following (Bode, 1945):

$$\int_0^{\infty} \log |S_o(j\omega)| d\omega = 0 \quad (3.8)$$

thus implying

$$\int_{\omega_1}^{\infty} \log |S_o(j\omega)| d\omega = - \int_0^{\omega_1} \log |S_o(j\omega)| d\omega \quad (3.9)$$

Hence the well known property that for stable, minimum-phase systems, the area of sensitivity reduction *equals* the area of sensitivity increase. Freudenberg and Looze (1986) showed that for unstable and/or non-minimum phase open loop systems, the area of sensitivity increase *exceeds* the area of sensitivity reduction by a fixed amount dependent upon the RHP factors.

What we wish to illustrate here within the integral sensitivity framework is the *direct* link between the notions of robustness and cost of feedback. Here, the feedback design objective is interpreted to be that of obtaining a certain level of sensitivity reduction on the interval  $\omega \in [0, \omega_1]$ . If a desired nominal sensitivity characteristic were somehow known (pointwise) on this interval, then the value of  $|S_o(j\omega)|$  could simply be *assigned* (assuming certain realizability and closed loop stability requirements were met). However, this would then *fix* the area of sensitivity reduction

$$\int_0^{\omega_1} \log |S_o(j\omega)| d\omega \quad (3.10)$$

which, by (3.9), fixes the cost of feedback (3.7). In other words, no additional degrees of freedom exist.

In practice, admissible sensitivity functions are not known *a priori*, but rather are obtained based upon various synthesis criteria. One such method is that of a  $H^\infty$  sensitivity minimization problem, which can be posed in the general form:

$$\min_{G \in G} \sup_{\omega \in [0, \infty)} \left\{ \rho(\omega) |S_o(j\omega)| \right\} \quad (3.11)$$

where  $\rho$  represents a scalar, frequency dependent weighting function and  $G$  represents an

appropriate set of admissible controllers. In this case, the optimal controller  $G$  is that which minimizes the *worst case* nominal sensitivity on  $\omega \in [0, \infty)$ . From our standpoint this is viewed as an *unconstrained* minimization problem; i.e., there are no auxiliary conditions on  $S$ , such as (2.1). This problem has also been well-studied; see Helton (1985), Francis (1987). However, the notion of robust performance within this framework differs markedly from that of traditional QFT. What we now wish to suggest is that there exists an alternative, sensitivity-domain synthesis formulation based upon QFT.

### 3.3. QFT Robustness Bounds and Sensitivity Functions

Traditional QFT design bounds (e.g., 1.5) are predicated on the possibility of *large* parameter uncertainty. To establish a connection between sensitivity functions and QFT, it is possible to state synthesis criteria (e.g., 2.2) alternatively in terms of *sets* of admissible sensitivity functions  $\{ S(\alpha, j\omega) \}$  induced by parametric uncertainty (Nwokah, et al., 1992). In fact, the closed loop bounds (1.5) can be mapped into upper and lower magnitude bounds on the *worst-case* sensitivity function (over  $\alpha$ ), *pointwise* at each  $\omega \in [0, \infty)$ . Such bounds are the sensitivity domain analog of the traditional QFT bounds (2.1) and (2.2).

An admissible sensitivity function  $|S_o^*(j\omega)|$  which minimizes the area of sensitivity increase (3.7) can (if it exists) be shown to lie on the boundary for all  $\omega \in [0, \infty)$ , analogous to the result of Horowitz and Sidi (1972, 1978). Note that these bounds must not violate (3.9). From this standpoint, the magnitude of the optimal nominal sensitivity function is known on  $\omega \in [0, \infty)$ , and a strictly proper, real-rational approximant of desired order and accuracy may be synthesized. The primary benefit of the sensitivity-based QFT formulation is in simplification, particularly in the MIMO case. Since this formulation neglects *some* phase information, simplification is achieved at the cost of some increased conservatism over traditional QFT.

However, this formulation also differs from traditional QFT in its notion of cost of feedback. Here the cost of feedback was essentially fixed, in terms of the area of sensitivity increase (3.7), and no additional degrees of freedom exist. The controller bandwidth question, as discussed in Section 3.1, remains as a separate issue. In the case of an optimal nominal sensitivity function, the controller bandwidth must necessarily be fixed. But for real-rational approximants to this solution, the resulting controller bandwidth is embedded in the order and accuracy of the approximation.

Therefore, it appears that gain/bandwidth optimal controller synthesis methods may be necessary for sensitivity-based QFT problems as well. In the discussion of the synthesis problem to follow, we shall base our developments primarily upon traditional QFT, while drawing upon the commonality between the two formulations. Before proceeding, let us summarize

our review of the traditional and sensitivity-based QFT problems by presenting an outline of their prominent features *vis-a-vis* some competing methodologies.

### 3.4. Comparison of Feedback Design Methodologies

Here we compare, in spirit, some of the significant points of the four feedback design paradigms discussed. In particular, we are interested in the handling of robustness to plant uncertainty:

#### Classical Design:

*Objectives:* Meet various performance and stability figures of merit (e.g., gain margin, phase margin, overshoot, etc.), no explicit optimization. *Characterization of plant uncertainty:* implicit. *Treatment of stability robustness:* implicit. *Treatment of performance robustness:* implicit. *Advantages:* designer can make tradeoffs between multiple objectives. *Drawbacks:* dependent upon experienced designer, concepts only applicable to SISO systems, no guaranteed closed loop margins.

#### H-infinity Sensitivity Minimization:

*Objectives:* Minimize worst-case nominal sensitivity on  $\omega \in [0, \infty)$ ; unconstrained minimization (no pointwise conditions). *Characterization of plant uncertainty:* non-parametric. *Treatment of stability robustness:* in terms of nominal sensitivity. *Treatment of performance robustness:* in terms of nominal sensitivity. *Advantages:* Straight-forward extension to MIMO systems. *Drawbacks:* Conservatism due to neglected phase information, notion of performance robustness linked to stability.

#### Sensitivity-Based QFT:

*Objectives:* Minimize area of sensitivity increase on  $\omega \in [\omega_s, \infty)$  subject to magnitude bounds on worst case sensitivity (over  $\alpha$ ) pointwise, on  $\omega \in [0, \omega_s]$ ; constrained minimization. *Characterization of plant uncertainty:* parametric, retain partial phase information. *Treatment of stability robustness:* pointwise, in terms of worst-case sensitivity. *Treatment of performance robustness:* pointwise, in terms of closed loop hard constraints. *Advantages:* Less conservative than  $H^\infty$ , more applicable to MIMO systems than traditional QFT. *Drawbacks:* More conservative than traditional QFT.

#### Traditional QFT:

*Objectives:* Minimize high frequency bandwidth subject to explicit closed loop

magnitude bounds, mapped into open loop gain-phase contours; constrained minimization. *Characterization of plant uncertainty*: Parametric, retain all phase information. *Treatment of stability robustness*: pointwise, in terms of worst-case sensitivity. *Treatment of performance robustness*: pointwise, in terms of closed loop hard constraints. *Advantages*: guaranteed closed loop robustness margins with no conservatism. *Drawbacks*: computationally intensive, no known globally convergent solutions.

#### 4. Traditional QFT Synthesis Formulation

Now having motivated the traditional, as well as the sensitivity-based QFT formulations, we wish to focus on optimal synthesis for the traditional problem. However, we expect to find some commonality with the methods of optimal sensitivity as well.

##### 4.1. Parametric Optimization

To begin our discussion, take the objective function for QFT as high frequency gain within the framework of the traditional problem (2.1) or (2.2). Historically, an admissible controller was found by trial-and-error, and successful completion of this step was normally considered acceptable; explicit minimization of high frequency gain of a given design within the performance constraints was generally not considered practical. This ideology generally lacked constructive existence conditions and convergent algorithms, although steps have been taken in this direction via Hilbert transforms; see Gera and Horowitz (1980), Sobhani and Jayasuriya (1992).

However, with discretization of the constraint set (2.2) by taking  $\omega \in [0, \infty)$  into  $\omega \in \{\omega_1, \dots, \omega_{n_\omega}\}$ , and by choice of a controller  $G(x, j\omega)$  of fixed structure with free design vector  $x \in \mathbb{R}^n$ , a constrained nonlinear programming problem may be posed. Analytic forms for the constraints (2.2) may be obtained which are, in general, piecewise smooth. This philosophy for QFT synthesis was proposed by Thompson (1990). More general frequency domain optimal design methods are due to Polak, et al. (1984), Boyd, et al. (1990), Boyd and Barratt (1991).

Based upon previous work, it is found that a number of drawbacks to the nonlinear programming formulation for QFT exist:

- In general, the constraint set (2.2) is non-convex; only local optima are found.
- Robust stability constraints tend to be frequency-independent, not of the form (2.2). With limited computational effort, the best way to cope with this constraint is to review designs graphically, at each iteration, to check for violation of stability bounds.



- Computations become badly scaled with open loop poles in the vicinity of the  $j\omega$  axis.
- Considering only a collection of constraints (2.2) at discrete frequencies, high frequency gain minimization becomes ill-posed; i.e., this gain can be made arbitrarily small as some controller parameters become arbitrarily large. In this case, it becomes necessary to augment the cost function with additional terms to penalize controller gain-bandwidth area.

Despite these drawbacks, parametric optimization techniques are successful in many cases. However, it appears desirable to explore alternative formulations to this problem.

#### 4.2. Function-Analytic Methods

As an alternative to parametric optimization of open loop high-frequency gain, consider the following minimization problem:

$$\min_{L_o \in L \subset RH^2} \int_0^{\infty} \rho(\omega) |L_o(j\omega)|^2 d\omega \quad (4.1)$$

i.e., minimization of what is essentially a weighted  $H^2$  norm of the open loop transfer function  $L_o$ , with scalar weighting function  $\rho$ . The admissible set  $L$  is a subset of all  $RH^2$  functions which *also* satisfy the QFT performance robustness constraint

$$B(L_o(j\omega), \omega) \geq 0, \quad \omega \in [0, \infty) \quad (4.2)$$

where the set  $RH^2$  is (for now) comprised of all real-rational, strictly proper, minimum-phase functions bounded in the closed right half-plane.

This formulation can be considered a *constrained  $H^2$  minimization problem*. The traditional QFT problem of high frequency gain minimization is a special case which can be recovered (symbolically) by the choice of weight  $\rho(\omega) = \delta(\frac{1}{\omega})$  \*.

#### 4.3. Properties of $H^2$ Norms, High Frequency Gain, and Rules of Thumb

At this point, we argue that (4.1) is a natural generalization of the high frequency gain objective function. To illustrate an important property, given a simple  $L_o \in RH^2$  it can be shown that the unweighted  $H^2$  norm of  $L_o$ , denoted as  $\|L_o\|_2$  is a product of the DC and high

\*  $\delta(\cdot)$  is the Dirac Delta function.

frequency gains.

*Example:* take

$$L(s) = \frac{k}{s+a} \quad (4.3)$$

in which case  $k_{DC} = \frac{k}{a}$  and  $k_{\infty} = k$ . Now,

$$\|L_o\|_2 = \int_0^{\infty} |L_o(j\omega)|^2 d\omega = \int_0^{\infty} \frac{k^2}{\omega^2 + a^2} d\omega \quad (4.4)$$

$$= \frac{k^2}{a} \tan^{-1} \frac{\omega}{a} \Big|_0^{\infty} \quad (4.5)$$

$$= \frac{k^2}{a} \left[ \frac{\pi}{2} \right] \quad (4.6)$$

Note that this can be written as:

$$\|L_o\|_2 = \left| k_{DC} k_{\infty} \left[ \angle L_o(j\infty) - \angle L_o(j0) \right] \right| \quad (4.7)$$

Properties of this nature were noted by Horowitz (1963), including a dual result linking the high frequency gain  $k_{\infty}$  with the integral of phase angle. In fact, Horowitz used this property extensively as a rule of thumb to argue that the  $L_o(j\omega)$  with minimal high frequency gain must have minimal phase angle (i.e., greatest allowable phase lag) for all  $\omega \in [0, \infty)$ . In practice, the competing objective is stability. Previously, these concepts were little more than rules of thumb, but we now wish to retain these ideas as we develop a more precise formulation.

#### 4.4. QFT Synthesis by Variational Methods

In view of the preceding arguments, let us now consider an alternative formulation for traditional QFT. Let the original robust performance criterion, as in (1.5), be specified in terms of  $RH^2$  functions  $T_L$ ,  $T_U$ , with pole-zero excess  $e_L$  and  $e_U$ , respectively,  $e_L > e_U$ , and let there be a non-empty set of admissible controllers  $\{G\}$  leading to satisfaction of the closed loop problem

$$|T_L(j\omega)| \leq |F(j\omega) T(\alpha, j\omega)| \leq |T_U(j\omega)| \quad \text{for all } \omega \in [0, \infty) \quad (4.8)$$

over all  $\alpha$ . Now consider the system of open loop constraints of the explicit form:

$$|L_o(j\omega)| - b(\angle L_o(j\omega), \omega) \geq 0, \quad \omega \in [0, \infty), \quad (4.9)$$

and, for illustration, consider the case where the constraint (4.9) is active (i.e., equality holds) for all  $\omega$ . Now, write  $L_o(j\omega) = R(\omega)e^{j\phi(\omega)}$ . From (4.9), this leads to the constraint equation

$$R(\omega) - b(\phi(\omega), \omega) = 0, \quad \omega \in [0, \infty). \quad (4.10)$$

Then for the objective function (4.1), subject to (4.10), the following *variational* problem may be posed:

$$\min_{\{R, \phi, \lambda\}} \int_0^\infty \rho(\omega)[R(\omega)]^2 + \lambda(\omega)[R(\omega) - b(\phi(\omega), \omega)]^2 d\omega \quad (4.11)$$

with multiplier  $\lambda$  and weighting function  $\rho$ . Boundary conditions should be specified in this case as  $\phi(0) = 0$ , and, if possible,  $R(\infty) = 0$ ,  $\phi(\infty) = -\frac{\pi}{2}e$ .

*Remark:* The variational problem suggested by (4.11) could be considered a frequency-domain analog of the time-varying optimal control problem with a *state-space constraint*, particularly for treatment of the inequality (4.9). Such a problem, for choice of weight  $\rho(\omega) = \delta(\frac{1}{\omega})$  is *precisely the traditional QFT problem*.

Again, we make this statement symbolically; we do not expect to obtain a solution to (4.11) for  $\rho(\omega) = \delta(\frac{1}{\omega})$ , although we might hope to do so under more reasonable assump-

tions. However, in the statement of (4.11) the following additional points have been neglected:

1.  $L_o(j\omega) = R(\omega)e^{j\phi(\omega)}$  must be realizable by a strictly proper, real-rational function.
2. The real functions  $R$  and  $\phi$  must be Bode gain-phase compatible; i.e.,  $\phi$  must be the Hilbert image of  $R$ , given as

$$\log R(\omega) = \frac{1}{\pi} \int_0^{\infty} \frac{\phi(\zeta)}{\zeta - \omega} d\zeta . \quad (4.12)$$

3. Closed loop stability margins must be maintained; i.e.,  $\phi(\omega)$  must be bounded away from  $-\pi$  in the vicinity of  $\{\omega : R(\omega) = 1\}$ .

Item 3 is somewhat beyond the scope of this treatment, although robust stability bounds are ultimately incorporated into a system of constraints such as (4.9). However, inclusion of the gain-phase compatibility condition (4.12) would be difficult. Instead, let us examine the following.

*Proposition:* Compute (if possible) an optimum  $R^*(\omega)$  and  $\phi^*(\omega)$  from (4.11), and form a candidate  $L_o^*(j\omega) = R^*(\omega) e^{j\phi^*(\omega)}$ . Then, choose a real-rational approximant  $L_o$  of the desired order, one which also meets closed loop stability margins. The approximation error could then be given as

$$\|L_o^* - L_o\|_2 = \int_0^{\infty} |L_o^*(j\omega) - L_o(j\omega)|^2 d\omega . \quad (4.13)$$

Various real-rational interpolation and approximation techniques have been well studied and are often employed in  $H^\infty$  frequency domain synthesis.

However, the wisdom and feasibility of optimizing  $R$  and  $\phi$  independently, as in (4.11), is open to question and is to be the subject of further studies. It is thought possible that the known structure of the constraint set (4.9), itself derived from magnitude ratios of real-rational functions and their extrema over compact parameter sets may, under certain conditions, provide sufficient structure to yield gain-phase admissible optima  $R^*$  and  $\phi^*$  without auxiliary conditions. Some commonality with the Hilbert boundary value methods of Gera and Horowitz (1980) is also sought.

In our final full section, we review some important results from the theory of complex extremals which may provide yet another direction in optimal synthesis techniques.

## 5. Direct Complex Extremal Methods

A number of developments in complex variational methods arise as possible tools for the QFT synthesis problem. We introduce them here.

In the development of complex analysis results, it is frequently convenient to work in the unit disk  $|z| < 1$ . A suitable mapping  $z = e^{sT}$  can be established between the axis  $s = j\omega$  and the unit circle  $|z| = 1$ .

### 5.1. Interpolation Problem of Ahlfors

The following problem has been solved explicitly by Ahlfors (1953) using variational techniques:

*Problem:* Find a function  $f(z)$ , analytic in the unit disk, which solves

$$\min_f \frac{1}{2\pi} \int_0^{2\pi} |f(e^{j\theta})|^2 d\theta \quad (5.1)$$

subject to:

$$f(z_i) = A_i, \quad |z_i| = 1, \quad i = 1, \dots, n \quad (5.2)$$

The function  $f$  is constructed as

$$f(z) = L(z) + P(z)\psi(z) \quad (5.3)$$

where  $L(z)$  solves the interpolation problem (5.2),  $\psi(z)$  represents a variation, analytic in the unit disk, and  $P(z_i) = 0$  (chosen as a Blaschke product).

The desired minimizing function  $f^*(z)$  is given as

$$f^*(z) = \prod_{i=1}^n \left[ \frac{z - z_i}{1 - \bar{z}_i z} \right] \sum_{i=1}^n \left[ \frac{A_i}{z - z_i} \right] \frac{\prod_{k=1}^n (1 - \bar{z}_k z_i)}{\prod_{\substack{k=1 \\ k \neq i}}^n (z_i - z_k)} \quad (5.4)$$

Here  $\bar{z}_i$  represents the complex conjugate of  $z_i$ . To apply this result directly to the QFT problem, the following conditions would be required:

1. Discretization of the constraint set on  $\omega \in [0, \infty) \rightarrow \omega \in \{\omega_1, \dots, \omega_n\}$ .
2. *A priori* assignment of the closed loop gain and phase at these frequencies; i.e.,

$$L_o(j\omega_i) = A_i, \quad i = 1, \dots, n \quad (5.5)$$

Thus, the degrees of freedom of  $L_o(j\omega)$  along the constraints  $B(L_o(j\omega), \omega)$  at these frequencies would be eliminated, and essentially unconstrained loop optimization would be performed over the set of frequencies defined by the difference:

$$\omega \in [0, \infty) - \{\omega_1, \dots, \omega_n\} \quad (5.6)$$

This clearly is *not* the desired solution. Instead, it is clear that an extension of Ahlfors' problem (5.1) and (5.2) must be developed.

*Proposition* (extended complex extremal problem): Find a function  $f(z)$ , analytic in the unit disc, which solves:

$$\min_f \frac{1}{2\pi} \int_0^{2\pi} |f(e^{j\theta})|^2 d\theta \quad (5.7)$$

subject to:

$$B(f(e^{j\theta}), \theta) = 0, \quad \theta \in [0, 2\pi] \quad (5.8)$$

Solutions to this problem, which would lead to a closed form solution to the traditional QFT optimal synthesis problem, are currently sought.

## 5.2. Complex Euler-Lagrange Equations

In other relevant work, Euler-Lagrange equations for extremal holomorphic mappings of the unit disk have been developed by Poletskii (1983). This approach can accommodate a finite number of  $N$  bounded, real-valued functionals  $\Phi_i$ ,  $i = 1, \dots, n$ .

The extremal problem is stated as follows: Given a bounded domain  $D \in \mathbb{C}$ , find  $f^*$  such that

$$f^* = \min_{f \in D} \Phi_0(f) \quad (5.9)$$

subject to

$$\Phi_i(f) = a_i, \quad i = 1, \dots, N. \quad (5.10)$$

Formulation of the QFT synthesis problem within this framework is also under investigation.

## 6. Conclusions

In this introductory paper, the traditional QFT performance robustness problem has been posed in sufficient detail to state the optimal synthesis problem. In order to motivate this formulation, some of the aspects and common features of traditional QFT, sensitivity-based QFT, and  $H^\infty$  sensitivity minimization were reviewed. The issue of cost of feedback was addressed, both in terms of controller bandwidth implications, as well as in terms of sensitivity functions.

Once the optimization problem was posed, it was found that a nonlinear programming approach was appealing in some cases, but presented specific limitations. Providing certain questions can be addressed, the approaches of real and complex variational methods appear to hold promise to provide a more direct and insightful solution to this very practical control synthesis problem. These issues are to be the subjects of future development.

## REFERENCES

- Ahlfors, L.A., "Variational Methods in Function Theory," course notes, Dept. of Mathematics, Harvard University, 1953. Transcribed by E.C. Schlesinger.
- Bailey, F.N., and J.C. Cockburn, "Loop Gain-Phase Shaping for SISO Robust Controllers," *Proc. Amer. Control Conf.*, Boston, 1991.
- Bailey, F.N., and C.H. Hui, "Loop Gain-Phase Shaping Design for Single Input Single Output Robust Controllers," *IEEE Control Systems Magazine*, V. 11, pp. 93-101, 1991.
- Bode, H.W., *Network Analysis and Feedback Amplifier Design*, Princeton, NJ: Van Nostrand, 1945.
- Boyd, S., C. Barratt, and S. Norman, "Linear Controller Design: Limits of Performance via Convex Optimization," *Proc. IEEE*, V. 78, No. 3, pp. 529-574, 1990.
- Boyd, S., and C. Barratt, *Linear Controller Design: Limits of Performance*, Englewood Cliffs, NJ: Prentice Hall, 1991.
- Francis, B.A., *A Course in  $H^\infty$  Control Theory*, Lecture Notes in Control and Information Sciences, New York: Springer-Verlag, 1987.
- Freudenberg, J.S., and D.P. Looze, "Right Half Plane Poles and Zeros and Design Tradeoffs in Feedback Systems," *IEEE Trans. Auto. Control*, V. AC-30, No. 6, pp. 555-565, 1985.
- Freudenberg, J.S., and D.P. Looze, *Frequency Domain Properties of Scalar and Multivariable Feedback Systems*, Lecture Notes in Control and Information Sciences, New York: Springer-Verlag, 1988.
- Gera, A., and I.M. Horowitz, "Optimization of the Loop Transfer Function," *Int. J. Control*, V. 31, No. 2, pp. 389-398, 1980.



- Helton, J.W., "Worst-Case Analysis in the Frequency Domain: The  $H^\infty$  Approach to Control," *IEEE Trans. Auto. Control*, V. AC-30, No. 12, pp. 1154-1170, 1985.
- Horowitz, I.M., *Synthesis of Feedback Systems*, New York: Academic Press, 1963.
- Horowitz, I.M., and M. Sidi, "Synthesis of Feedback Systems with Large Plant Ignorance for Prescribed Time-Domain Tolerances," *Int. J. Control*, V. 16, No. 2, pp. 287-309, 1972.
- Horowitz, I.M., and M. Sidi, "Optimum Synthesis of Non-Minimum Phase Feedback Systems with Plant Uncertainty," *Int. J. Control*, V. 27, No. 3, pp. 361-386, 1978.
- Nwokah, O.D.I., S. Jayasuriya, and D.F. Thompson, "Quantitative Feedback Design of Robust Control Systems," submitted for publication, *Automatica*, special issue on robust control, 1992.
- Polak, E., D.Q. Mayne, and D.M. Stimler, "Control System Design via Semi-Infinite Optimization: A Review," *Proc. IEEE*, V. 72, No. 12, pp. 1777-1794, 1984.
- Poletskii, E.A., "The Euler-Lagrange Equations for Extremal Holomorphic Mappings of the Unit Disk," *Michigan Math J.*, V. 30, pp. 317-333, 1983.
- Sobhani, M., and S. Jayasuriya, "An Algorithm for QFT Loop Shaping," *Proc. Amer. Control Conf.*, Chicago, 1992 (to appear).
- Thompson, D.F., "Optimal and Sub-Optimal Loop Shaping in Quantitative Feedback Theory," Ph.D. Thesis, School of Mechanical Engineering, Purdue University, West Lafayette, IN, August, 1990.
- Thompson, D.F., and O.D.I. Nwokah, "Frequency Response Specifications and Sensitivity Functions in Quantitative Feedback Theory," *Proc. Amer. Control Conf.*, pp. 2015-202, Boston, 1991.
- Thompson, D.F., and O.D.I. Nwokah, "Analytic Loop Shaping Methods in Quantitative Feedback Theory," accepted for publication, *ASME J. Dynamic Systems, Measurement, and Control*, 1992.

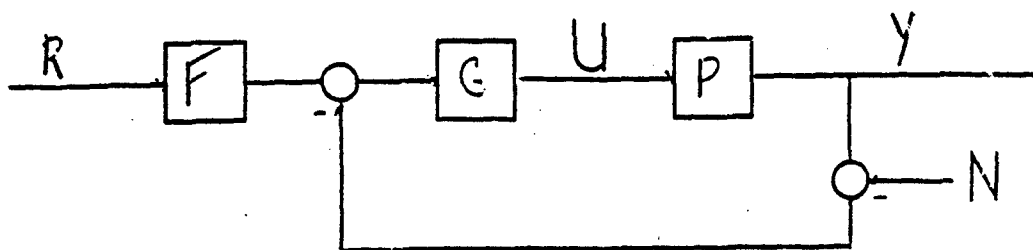


Fig. 1

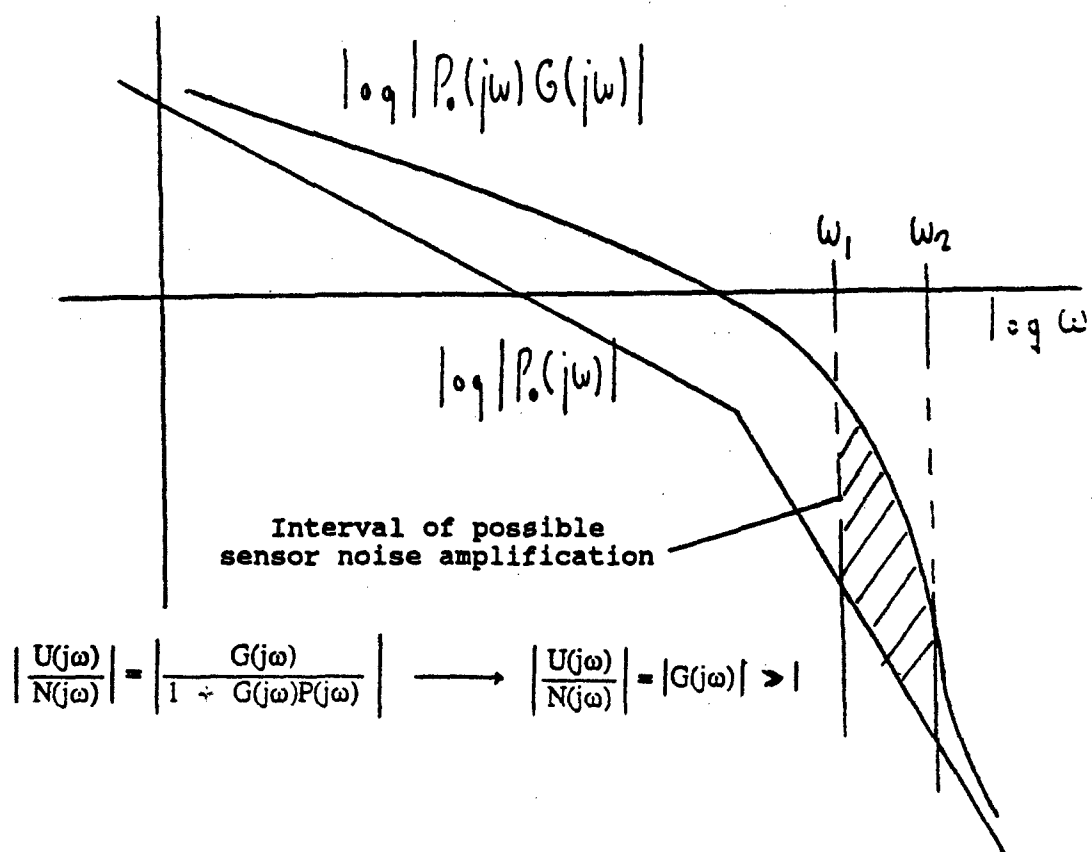


Fig. 2

# QUANTITATIVE FEEDBACK DESIGN OF ROBUST CONTROL SYSTEMS

Osita Nwokah  
School of Mechanical Engineering  
Purdue University  
West Lafayette, Indiana 47907

Suhada Jayasuriya  
Department of Mechanical Engineering  
Texas A&M University  
College Station, Texas 77843-3123

David Thompson  
Transmission and Chassis Division  
Ford Motor Company  
Livonia, MI 48150

**Keywords:** Parametric uncertainty, QFD, robust control.

## ABSTRACT

The problem of performance robustness, especially in the face of significant parametric uncertainty, has been increasingly recognized as a predominant issue of engineering significance in many design applications. Quantitative feedback design (QFD) is very effective for dealing with this class of problems even when there exist hard constraints on closed loop response. In this paper, SISO-QFD is viewed formally as a sensitivity constrained multi objective optimization problem whose solution cannot be obtained analytically but (when feasible) can be obtained graphically. In contrast to the more recent robust control methods where phase uncertainty information is often neglected, the direct use of parametric uncertainty and phase information in QFD results in a significant reduction in the cost of feedback. An example involving the unscheduled bank angle control for the C-135 military transport aircraft is included for completeness.

# List of Symbols Used.

$L_\infty$ : Banach space of essentially bounded Baire functions

$\| \cdot \|_\infty$ : norm on  $L_\infty$

$H^\infty$ : Banach space of bounded analytic functions.

$\|A\|_\infty$ :  $\sup\{ |A(i\omega)| : \omega \in \mathbb{R} \}, A \in H^\infty$

$RH^\infty$ : Banach space of bounded analytic functions with elements from the ring of stable, proper real rational functions.

Unit of  $RH^\infty$ : An element of  $RH^\infty$  whose inverse  $\in RH^\infty$ .

$e, r$ : relative degree of transfer function

SISO: single input, single output

MIMO: multi-input, multi-output

$\omega, \lambda$ : radian frequency

$\Omega$ : compact parameter space with elements  $\alpha$ .

QFD: Quantitative Feedback Design

$A := B$ : A is defined by B

$A \simeq B$ : A is approximately equal to B.

$G_H$ :  $H^\infty$  controller

$G_Q$ : QFD controller

$S_H$ :  $H^\infty$  sensitivity function

$S_Q$ : QFD sensitivity function

$\mathbb{R}_+$ : Positive real line

RHP: Right half plane

RHS: Right hand side

LHP: Left hand side

LHS: Left hand side

## 1. Introduction

The last decade has witnessed a steady and growing research effort in robust control; see for example the recent book (Dorato and Yedavalli 1990). The majority of this effort has been devoted to systems that are assumed to have unstructured uncertainty. This allows such problems to be transformed into a form where the small gain theorem (Zames 1981) and powerful recent mathematical techniques from functional analysis and operator theory (Francis 1987, Maciejowski 1989) can be successfully employed for system analysis and synthesis. However many problems of practical interest appear as models with both large parametric uncertainty and high frequency non-parametric uncertainty. Typical examples include flight control and tubomachinery control over a flight envelope parametrized by power level, height and mach number, as well as general automotive engine control problems. All these problems yield a collection of linear models obtained by a linearization of a parametrically dependent nonlinear differential equation set about a finite number of different operating points. This problem class is often endowed with hard stability and performance constraints such as on rise time and overshoot. This problem class also requires plant uncertainty to be expressed as variations in both gain and phase. Traditional control of this problem has relied on gain-scheduling or the on-line switching of controllers designed for models obtained at the different operating points; as and when due. The design of the switching logic and some resulting stability problems are nontrivial. When feasible; parametric robust control makes gain scheduling redundant. A non-parametric description of uncertainty is of course possible but will almost always result in loss of phase information. This often leads to higher bandwidth controllers. The quantitative feedback design (QFD) robust control methodology (more usually called quantitative feedback theory) introduced by Horowitz (Horowitz 1959, 1979, 1982, Horowitz and Sidi, 1972, 1980, Shaked and Horowitz 1976) is perhaps the only known technique that considers both large parametric uncertainty and phase information simultaneously. The major pay-off is the ability to satisfy both robust stability and multi-objective hard performance constraints, with the minimum possible cost of feedback. The downside is that the method though systematic and powerful in the hands of an experienced control engineer has not until recently lent itself easily to formal mathematization as in the more recent paradigms such as  $H^\infty$  control and  $\mu$ -synthesis. The present effort is an attempt to bridge the gap. A key aim of the present work is to systematize the QFD design process. The QFD problem can be posed as a formal sensitivity constrained optimization problem (Jayasuriya, Nwokah, Yaniv 1991) which reduces to the problem statements in  $H^\infty$ -control when the hard performance constraints and parametric uncertainty descriptions are relaxed. Consequently the newer methods may be viewed as restricted quantitative feedback design methods (Perez, Nwokah, Thompson 1991).

This paper is divided into six sections of which this is the first one. In section two, we develop a complete description of the representation of plant uncertainty. In section three we formally state the QFD problem and subsequently convert it into a constrained sensitivity optimization problem whose general analytic solution is unknown. In section four we translate these requirements into the classical QFD format and use graphical search techniques and  $H^\infty$  design methodology to generate sub-optimal solutions to the sensitivity optimization problem. In section five we give a nontrivial example with the

corresponding  $H^\infty$  solution. This example clearly demonstrates the more aggressive controller bandwidth problem which is called for whenever there is a loss of phase uncertainty information. Finally in section six we give some concluding remarks.

## 2. Representation of Plant Uncertainty

We assume that the process to be modelled is uncertain due to both parametric and unstructured, non-parametric uncertainty. Parametric uncertainty is uncertainty that can be represented by parameter variations, in an appropriately structured process model, while non-parametric uncertainty is any process uncertainty which cannot be explained adequately in the context of the structured uncertainty. Typical sources of non-parametric uncertainty are unmodelled dynamics, unmodelled parameter variations and measurement errors. The process consists of the union of parametric and non-parametric components.

We may therefore represent the uncertain process as follows:

$$\{P(s)\} = P(\alpha, s) \cdot P_n(s) \quad (1)$$

Here,  $\{P(s)\}$  is the plant set,  $P(\alpha, s)$  is the parametric plant subset, while  $P_n(s)$  is the corresponding non-parametric plant subset, (Bailey, Hui, 1991). The parametric plant set is described by:  $\{P(\alpha, s), \alpha \in \Omega \subset \mathbb{R}^m\}$  where  $\alpha$  is an  $m$ -dimensional parameter vector that ranges over the compact parameter space  $\Omega$ . Each nominal parameter point  $\alpha_0 \in \Omega$  generates a nominal plant  $P_0(s) = P(\alpha_0, s) \in P(\alpha, s)$ . The set  $P(\alpha, s)$  is represented as:

$$P(\alpha, s) = \frac{k \prod_i (s + z_i) \prod_k (s^2 + 2\zeta_k \omega_k s + \omega_k^2)}{s^\tau \prod_{j=1}^n (s + p_j) \prod_\ell (s^2 + 2\zeta_\ell \omega_\ell s + \omega_\ell^2)} \cdot e^{-s\tau} \quad (2)$$

Here,  $\tau$  represents a possible time delay. Each of the parameters,  $k, z_i, \zeta_k, \omega_k, p_j, \zeta_\ell, \omega_\ell$ , is uncertain, continuously dependent on  $\alpha \in \Omega$ , and lies in a specific compact interval. However the order and relative degree of  $P(\alpha, s)$  is fixed. This representation is most appropriate for the process behavior in the low to mid frequency range. On the other hand, the unstructured plant subset  $P_n(s)$  is assumed to affect the process dynamics significantly only at high frequencies. We may then suppose that the plant set admits the following "split frequency" representation:

$$\{P(s)\} = \begin{cases} P(\alpha, s), & \forall \omega < \omega_h, s = i\omega \\ P_h(s) \cdot P_n(s), & \forall \omega \geq \omega_h, s = i\omega \end{cases} \quad (3)$$

where  $P_h(s)$  is the high frequency model of  $P(\alpha, s)$ . The frequency  $\omega_h$  marks the beginning of the high frequency region. For  $\omega \geq \omega_h$  the overall plant set  $\{P(s)\}$  degenerates to the high frequency model  $P_h(\alpha, s) \cdot P_n(s)$ . In this paper we shall assume that  $P_n(s) \equiv 1$ , for  $\omega < \omega_h$ , and use a relative stability bound to constrain its effect at high frequencies  $\omega \geq \omega_h$ . In practice  $P_n(i\omega)$  is only given as a gain and phase deviation about some nominal high frequency gain of 1 and phase of  $0^\circ$ . So that the so called universal high frequency boundary becomes a function of frequency  $\omega \geq \omega_h$ . In traditional QFD,  $P_n(i\omega) \equiv 1 \forall \omega$ , thus insuring that the universal high frequency

boundary is independent of frequency for  $\omega > \omega_h$ . Let  $P_h(\alpha, s) = \frac{k}{s^e}$ . Then for our present purposes, assume:

$$|P_h(\alpha, s) P_n(i\omega)| \leq \frac{k m(\omega)}{\omega^e}, \forall \omega \geq \omega_h \quad (4)$$

where  $m(\omega) = |P_n(i\omega)|$ ,  $\forall \omega > \omega_h$ , and

$$|P(\alpha, i\omega_h)| \leq \frac{k}{\omega_h^e}, \forall \alpha \in \Omega \quad (5)$$

where  $e$  is the relative degree of  $P(\alpha, s)$ , and  $k$  represents the parametric plant high frequency gain defined by:

$$k := \lim_{|s| \rightarrow \infty} s^e P(\alpha, s). \quad (6)$$

We also assume that:

- (i)  $P_n(s)$  is stable but may have high frequency non-minimum phase zeros. Furthermore, it is totally without structure, in the sense that the relative degree of its members are finite but may not be fixed.
- (ii) On the other hand the structured model  $P(\alpha, s)$  may be unstable from some or all  $\alpha \in \Omega$ , but has a fixed relative degree for all  $\alpha \in \Omega$ . Furthermore, every member of  $P(\alpha, s)$  has the same number of unstable zeros.
- (iii) The plant set  $\{P(s)\}$  is topologically path connected (Nwokah 1988, Foo and Postlethwaite 1988).

A consequence of this assumption is that:

$$\lim_{|s| \rightarrow \infty} P_o(s) P^{-1}(\alpha, s) = \frac{k_o}{k} > 0, \forall \alpha \in \Omega \quad (7)$$

Write

$$B_z(\alpha, s) = \prod_{i=1}^{N_z} \left( \frac{s - z_i}{s + z_i} \right) \quad (8)$$

for the Blaschke product of the unstable zeros for  $P(\alpha, s)$ , and

$$B_p(\alpha, s) = \prod_{j=1}^{N_p} \left( \frac{s - p_j}{s + p_j} \right) \quad (9)$$

for the Blaschke product of the unstable poles of  $P(\alpha, s)$ .

Then factor  $P(\alpha, s)$  as:

$$P(\alpha, s) = P_m(\alpha, s) \cdot P_z(\alpha, s) \quad (10)$$



where  $P_m(\alpha, s)$  represents the stable and minimum phase factor and  $P_a(\alpha, s)$  is the all pass factor given by:

$$P_a(s) = B_r(\alpha, s) \cdot B_p^{-1}(\alpha, s) e^{-sr}.$$

In the present description of plant uncertainty, it is perfectly legal for the poles of  $P(\alpha, s)$  to migrate to and fro across the imaginary axis, or indeed for all the poles to lie entirely in the open right half complex plane as  $\alpha$  ranges over  $\Omega$ . However all the zeros of  $P(\alpha, s)$  are constrained not to migrate across the  $i\omega$  axis and the unstable zeros are to stay in the interior of the closed right half complex plane. This extremely realistic description of plant uncertainty was originally proposed by Aström, Neumann and Gutman (1989), and used by Nwokah (1988), and has recently been implicitly used by Bailey and Hui (1991), Bailey and Cockburn (1991). On the other hand the unstructured uncertainty description mandated by the  $H^\infty$  methodology dictates that there be no criss-crossing of poles across the imaginary axis, or equivalently that every member of the plant set  $\{P(s)\}$  must have exactly the same number of unstable poles (Morari and Zafriou 1989). For our present sensitivity based QFD design to work, we shall impose the same restriction on the unstable poles of  $P(\alpha, s)$ . However, we retain the full sensitivity uncertainty description as in standard QFD formulations (Horowitz and Sidi 1972).

### 3. The QFD Problem Specification and Solution Feasibility

The QFD problem can now be stated as follows. There is given an uncertain family of linear time-invariant finite-dimensional plants  $\{P(s)\}$  as described in section 2. There is also given an ideal target closed loop transmission function  $T_o(s)$  and an ideal disturbance response transfer function  $T_D^0(s)$ . The QFD problem is to find (if possible) an admissible pair of strictly proper, real rational, and stable functions  $\{G(s), F(s)\}$  in the two degree-of-freedom feedback arrangement shown in Fig. 1, such that the following conditions are satisfied with some measure of optimality:

$$a) \quad T(\alpha, s) \text{ is stable } \forall \alpha \in \Omega \text{ (robust stability)} \quad (11)$$

$$b) \quad |T(\alpha, s) - T_o(s)| \leq \delta_T(s), \forall s, \forall \alpha \in \Omega \text{ (robust performance)} \quad (12)$$

$$c) \quad |T_D(s)| \leq |T_D^0(s)| = \delta_D(s), \forall s, \forall \alpha \in \Omega \text{ (disturbance attenuation)} \quad (13)$$

$$d) \quad \sup_{\omega} |H(\alpha, i\omega)| \leq M_p, \forall \alpha \in \Omega \text{ (relative stability margin)} \quad (14)$$

where  $\delta_T(s) \geq 0$  and  $\delta_D(s) \geq 0$  are specified a priori, and

$$T(\alpha, s) = H(\alpha, s) \cdot F(s), \quad T_o(s) = H_o(s)F(s) \quad (15)$$

$$H(\alpha, s) = \frac{L(\alpha, s)}{1 + L(\alpha, s)}, \quad H_o(s) = \frac{L_o(s)}{1 + L_o(s)} \quad (16)$$

$$L(\alpha, s) = P(\alpha, s) \cdot G(s), \quad L_o(s) = P_o(s) \cdot G(s) \quad (17)$$

under the constraint that  $G(s)$  is an internally stabilizing controller (Freudenberg and

Looze 1988) for the plant set  $\{P(s)\}$ . Because of internal stability all non-minimum phase zeros of  $L(\alpha, s)$ , including those from the rational approximation of  $e^{-sT}$  are required to appear in  $T(\alpha, s)$ .  $P_o(s)$  is the nominal plant model and unlike the traditional QFD methodology cannot be chosen arbitrarily. The robust performance specification given in (12) is slightly different from the one originally defined by Horowitz and Sidi (1972) but is in an analytic form (Doyle 1987) which enables direct time domain to frequency domain conversions via Parseval's theorem (Robinson 1962). Krishnan and Cruickshanks, (1977) have argued that there is insignificant practical difference between the traditional measure and the one used here. Our design example to follow also confirms this viewpoint. We next convert the system design data into equivalent sensitivity constraints.

From Bode's sensitivity equation, suitably normalized for large uncertainty (Cruz and Perkins 1964, Nwokah, Jayasuriya and Chait 1991), we can write:

$$\frac{T(\alpha, s) - T_o(s)}{T_o(s)} = S(\alpha, s) \cdot \frac{P(\alpha, s) - P_o(s)}{P_o(s)}, \quad \forall \alpha \in \Omega \quad (18)$$

where  $S(\alpha, s) := \frac{1}{1 + L(\alpha, s)}$ . Therefore:

$$|T(\alpha, s) - T_o(s)| = \left| T_o(s) S(\alpha, s) \left[ \frac{P(\alpha, s) - P_o(s)}{P_o(s)} \right] \right|, \quad \forall \alpha \in \Omega \quad (19)$$

Define the nonnegative function  $\delta_G(s)$  by

$$\max_{\alpha \in \Omega} \left| \frac{P(\alpha, s) - P_o(s)}{P_o(s)} \right| = \delta_G(s), \quad \forall s. \quad (20a)$$

Now,

$$\left| T_o(s) S(\alpha, s) \frac{P - P_o}{P_o} \right| \leq |T_o(s)| \delta_G(s) \max_{\alpha \in \Omega} |S(\alpha, s)|. \quad (20b)$$

Now put  $s = i\omega$ . If the RHS of (20b) is upper bounded by  $\delta_T(\omega)$ , the tracking constraint (12) reduces to:

$$|S(\alpha, i\omega)| \leq \frac{\delta_T(\omega)}{\delta_G(\omega) |T_o(i\omega)|} := M_T(\omega) \quad \forall \omega \geq 0, \quad \forall \alpha \in \Omega \quad (21)$$

Notice that  $S(\alpha, i\omega)$  carries both gain and phase uncertainty information with it, but the phase uncertainty information embodied in the variations of  $P(\alpha, i\omega)$  is lost when we take the bound  $\delta_G(\omega)$ . From Fig. 1, it is clear that the disturbance transfer function  $T_D(s)$  is given by

$$T_D(\alpha, s) = \frac{1}{1 + L(\alpha, s)} = S(\alpha, s). \quad (22)$$

Thus, the requirement (13) reduces to:

$$|S(\alpha, i\omega)| \leq |T_D^0(i\omega)| := M_S(\omega) \quad \forall \omega \geq 0, \quad \forall \alpha \in \Omega \quad (23)$$

Finally, the constraint  $M_p$  on the allowable maximum dynamic magnification of the frequency response of  $H(\alpha, i\omega)$ , translates to a worst case phase stability margin  $\phi_m$  given by:

$$\sin \phi_m \geq \frac{1}{M_p}, \forall \alpha \in \Omega, \quad (24)$$

or equivalently:

$$|S(\alpha, i\omega_h)| \leq M_p, \forall \alpha \in \Omega \quad (25)$$

This is easy to establish from a simple analysis of M-circles (Netushil 1973). Consequently, the system specifications (11)-(14) have now been converted to sensitivity inequalities. It then follows that all the QFD constraints are simultaneously satisfied if there exists an internally stabilizing controller  $G(s)$  for the plant set  $\{P(s)\}$ , such that  $S(\alpha, s)$  is stable  $\forall \alpha \in \Omega$  and satisfies, for  $s = i\omega$ , equation 25 and:

$$|S(\alpha, i\omega)| \leq \min \{M_T(\omega), M_s(\omega)\} = M(\omega) \quad \forall \omega \geq 0, \forall \alpha \in \Omega \quad (26)$$

Here,  $M(\omega)$  is a bounded continuous function that satisfies

$$(i) \quad \lim_{\omega \rightarrow \infty} M(\omega) = 1$$

$$(ii) \quad M(\omega_h) = M_p$$

$$(iii) \quad \sup_{\omega} M(\omega) = M_D \quad (27)$$

$$(iv) \quad 1 \leq M_p \leq M_D < \infty$$

Bode's sensitivity integral (Frue denberg and Looze 1988) shows that if  $S(\alpha, i\omega)$  is stable  $\forall \alpha \in \Omega$ , then

$$\int_0^{\infty} \left\{ \log |S(\alpha, i\omega)| \right\} d\omega = \sum_{i=1}^{N_2} \operatorname{Re} \left\{ P_i(\alpha) \right\}, \quad \forall \alpha \in \Omega, \quad (28)$$

where  $P_i(\alpha)$  is an unstable pole of  $P(\alpha, s)$ . Since in our present formulation the poles of  $P(\alpha, s)$  are not allowed to migrate across the imaginary axis, we may choose as our nominal model  $P_o(s) \in \{P(s)\}$ ; the plant with the worst instability. That is to say, the nominal model must be chosen such that

$$\sum_{i=1}^{N_p} \operatorname{Re}(P_i^o) \geq \max_{\alpha \in \Omega} \sum_{i=1}^{N_p} \operatorname{Re} P_i(\alpha) \quad (29)$$

where  $P_i^o, i = 1, 2 \dots N_p$  are the unstable poles of  $P_o(s)$ , which is the transfer function for the parameter combination that generates the worst instability. On the other hand, the

unstable zeros of the nominal model are chosen as those with real parts nearest the imaginary axis, i.e.

$$\sum_{j=1}^{N_z} \operatorname{Re}(z_j^0) \leq \max_{\alpha \in \Omega} \sum_{j=1}^{N_z} \operatorname{Re} z_j(\alpha) \quad (30)$$

All the QFD specifications are now satisfied if  $S(\alpha, i\omega)$  is stable  $\forall \alpha \in \Omega$  and also satisfies:

$$|S(\alpha, i\omega)| \leq M(\omega), \quad \forall \omega \geq 0, \quad \forall \alpha \in \Omega. \quad (31)$$

Let  $\omega_s$  be the first finite frequency at which  $S(\alpha, i\omega) = 1$  for all  $\alpha \in \Omega$ . This is called the sensitivity cut-off frequency (Rosenbrock 1974). Bode's sensitivity integral then gives:

$$\int_0^\infty \log |S(\alpha, i\omega)| d\omega = \int_0^{\omega_s} \log |S(\alpha, i\omega)| d\omega + \int_{\omega_s}^\infty \log |S(\alpha, i\omega)| d\omega, \quad \forall \alpha \in \Omega. \quad (32)$$

The benefits of feedback are only obtained in the interval  $0 \leq \omega < \omega_s$ , while the cost of feedback is paid for in the frequency interval  $\omega_s \leq \omega \leq \infty$ . Feedback is said to be beneficial (Bode 1945) at the frequencies where  $|1 + L(\alpha, i\omega)| > 1$ , or equivalently  $|S(\alpha, i\omega)| < 1$  and is non-beneficial otherwise. Using Bode's sensitivity integral, we may then define the cost of feedback as  $\int \log |S(\alpha, i\omega)| d\omega$  over the frequency interval where feedback is not beneficial. It follows that the required cost function to be minimized is given by:

$$\int_{\omega_s}^\infty \log |S(\alpha, i\omega)| d\omega = \left| \int_0^{\omega_s} \log |S(\alpha, i\omega)| d\omega \right| + \sum_{i=1}^{N_p} \operatorname{Re}(P_i^0) \geq 0 \quad (33)$$

As the number of unstable poles is fixed by the plant, the cost of feedback is minimized by minimization of  $\left| \int_0^{\omega_s} \log |S(\alpha, i\omega)| d\omega \right|$ , over all  $\alpha \in \Omega$ . It turns out that this is equivalent to the minimization of the gain-bandwidth area of  $\log |1 + L|$ . Let  $G$  be the set of all robust stabilizing controllers for  $\{P(s)\}$ . The QFD optimization problem is then set up as follows:

$$\min_{G \in G} \left[ \max_{\alpha \in \Omega} \int_0^{\omega_s} \log |S(\alpha, i\omega)| d\omega \right] \quad (34)$$

subject to the sensitivity constraint:

$$(i) \quad |S(\alpha, i\omega)| \leq M(\omega), \quad \forall \omega, \quad \forall \alpha \in \Omega. \quad (35)$$

From (33), it is clear that (34) is also equivalent to:

$$\min_{G \in G} \left| \max_{\alpha \in \Omega} \int_0^{\omega_s} \log |S(\alpha, i\omega)| d\omega \right|. \quad (36)$$

This agrees with the classical notion that tracking performance should be achieved if possible with the minimum amount of feedback, or minimal value of the gain-band width area of the loop transmission function.

**Theorem 3.1.**

Subject to the constraint  $|S(\alpha, i\omega)| \leq M(\omega), \forall \omega,$

$$\min_{G \in \mathcal{G}} \left[ \max_{\alpha \in \Omega} \int_{\omega_0}^{\infty} \log |S(\alpha, i\omega)| d\omega \right] = \int_{\omega_0}^{\infty} \log M(\omega) d\omega.$$

**Proof:**

The result is well known and follows from the principle in statistical decision theory for example (Kwakernaak 1985) that equalizers yield min-max solutions.

Any admissible optimal sensitivity solution  $S_0(s)$  to the QFD problem must be analytic in the closed right half complex plane and satisfy:  $|S_0(i\omega)| = M(\omega)$  almost everywhere.

**Theorem 3.2.**

There exists an  $S_0(s) \in H^\infty$  and satisfying the QFD constraints (i.e. constraints of Theorem 3.1) if and only if  $M(\omega) \geq 0, M(\omega) \in L_\infty$  and:

$$\int_{-\infty}^{\infty} \log M(\omega) d\omega > -\infty. \quad (37)$$

**Proof:**

This follows easily from Hoffman (1962) and Robinson (1962).

Combining Theorems (3.1) and (3.2), produces existence conditions for solvability of the QFD problem.

**Theorem 3.3.**

An  $H^\infty$  solution to the QFD problem exists if and only if:

- (i) There exists some  $G(s) \in H^\infty$  such that  $S(\alpha, s) = \frac{1}{1 + P(\alpha, s) G(s)} \in H^\infty, \forall \alpha \in \Omega$
- (ii)  $|S(\alpha, i\omega)| \leq M(\omega) \forall \omega \geq 0, \forall \alpha \in \Omega$
- (iii)  $M(\omega) \in L_\infty, M(\omega) \geq 0$  and satisfies  $\int_{-\infty}^{\infty} \log M(\omega) d\omega > -\infty.$

In other words, if an optimal sensitivity function  $S_0(s)$  exists, its magnitude  $|S_0(i\omega)|$  lies on the sensitivity boundary  $M(\omega)$  almost everywhere. This conclusion was also arrived at by Gera and Horowitz (1980) from a different route. However, as pointed

out by Gera and Horowitz (1980), a finite order  $S_{opt}(s) \in RH^\infty$  that simultaneously satisfies the bounds on  $M(\omega)$  with equality does not exist. Consequently, the existence of a theoretically admissible optimal sensitivity function  $S_o(s) \in H^\infty$  does not necessarily imply the corresponding existence of a realizable (feasible) sensitivity function  $S_{opt}(s) \in RH^\infty$ . Of the three conditions of Theorem 3.3, condition (i) is the most difficult to establish. Bode's sensitivity integral equation (Freudenberg and Looze 1988) shows that for the bounding function  $M(\omega)$  to be feasible, it is necessary for the following inequality to hold:

$$\sum_{i=1}^{N_p} \operatorname{Re}(P_i) \leq \frac{1}{\pi} \int_0^\infty \log M(\omega) d\omega \geq 0 \quad (38)$$

A sufficient condition for this to be satisfied is that (Thompson and Nwokah 1991):

$$\lim_{\omega \rightarrow \infty} M_T(\omega) = \infty,$$

a condition that has traditionally been assumed in QFD work without any particular mathematical justification, and succinctly expresses the well known fact that the benefits of feedback cannot be obtained over an infinite frequency band (Bailey and Cockburn 1991). Observe from (34) and (35) that the optimum cost of feedback now reduces to

$\int_0^\infty \log M(\omega) d\omega$ . Any sub-optimal sensitivity function  $M_o(\omega)$  which satisfies:

$M_o(\omega) \leq M(\omega)$  in the frequency interval  $0 \leq \omega \leq \omega_s$ , will clearly satisfy the QFD performance specifications, but will also necessarily satisfy  $M_o(\omega) \geq M(\omega)$  in some range in the frequency interval  $\omega_s \leq \omega \leq \omega_\infty$ . The optimal bounding function  $M(\omega)$  is shown in Fig. 2. Notice that if  $\{P\}$  is stable, so that  $\sum_{i=1}^{N_p} \operatorname{Re}(P_i) = 0$ , feasibility merely requires

that:  $\int_0^\infty \log M(\omega) d\omega = 0$ . When this fails, use of a suboptimal  $M_o(\omega)$  involving a relaxation of the original performance specifications but which meets the condition is mandatory. When  $\{P\}$  has no unstable inverse  $\forall \alpha \in \Omega$ , a feasible finite bounding function  $M_o(\omega)$  always exists (Bailey and Cockburn 1991). After the feasibility condition is satisfied, it becomes necessary that  $M_o(\omega)$  satisfies the Bode gain-phase rules (Bode 1945) in order for a realizable  $S_{opt}(s)$  to exist.

When all the necessary feasibility conditions are satisfied, the QFD problem then effectively reduces to the synthesis of a suitable approximation of  $S_o(s)$  with a finite order unit  $S_{opt}(s) \in RH^\infty$  such that:

$$\|S_{opt}(s) - S_o(s)\|_\infty < \epsilon, \quad (39)$$

for any arbitrarily small  $\epsilon > 0$ . If so, then a feasible sub-optimal sensitivity function  $S_{opt}(s)$  which, satisfies the inequality constraints on  $M(\omega)$ , can be written as:

$$S_{opt}(s) = A(s) S_a(s) = B_p(s) S_a(s), \quad (40)$$

where  $A(s)$  can be suitably approximated as:

$$A(s) \simeq B_p(s) \quad (41)$$

and  $B_p(s)$  represents the Blaschke product of the unstable poles of  $P_o(s)$ . A mathematical solution of this optimization and approximation problem does not exist because in general  $S_o(s)$  is not continuous on the boundary, i.e., the imaginary axis (Robinson 1962). In practice the actual sensitivity function may be oscillatory, displaying several resonance peaks, none of which must exceed  $M(\omega)$  if the specifications are to be met.

#### 4. Solution Via Automatic Analytic Loop Shaping

Although constructive general existence conditions for the problem posed in section 3 are unknown, QFD has employed graphical techniques to obtain acceptable solutions for the same problem for a very long time (Horowitz and Sidi, 1972). From (22), write:

$$S(\alpha, i\omega) = \frac{1}{1 + L(\alpha, i\omega)} = \frac{1}{1 + L_o \cdot \frac{P(\alpha, i\omega)}{P_o(i\omega)}} \quad (42)$$

where  $L_o := P_o \cdot G$ . Suppressing the arguments  $\alpha, i\omega$ , temporarily, the above equation can be rewritten as:

$$S = \frac{\frac{P_o}{P}}{L_o + \frac{P_o}{P}} \quad (43)$$

Here,

$$P_o(s) = P_{mo}(s) \cdot B_{zo}(s) B_{po}^{-1}(s) e^{-s\tau_o} \quad (44)$$

where  $\tau_o$  is the maximum time lag, and  $P_{mo}(s)$  is the nominal minimum phase and stable transfer function that contains the stable conjugate symmetric factors of the unstable terms in  $B_{zo}(s)$  and  $B_{po}(s)$ . Consequently,  $L_o$  can also be written as:

$$L_o = L_{mo} \cdot L_a \quad (45)$$

where

$$L_{mo} = P_{mo} \quad (46)$$

and

$$L_a = B_{zo} B_{po}^{-1} e^{-s\tau_o} \quad (47)$$

Assume that  $M(\omega)$  is a feasible sensitivity bounding function. The QFD performance and stability specifications now translate to:

$$|S| = \left| \frac{\frac{P_o}{P}}{L_o + \frac{P_o}{P}} \right| \leq M(\omega), \forall \omega \geq 0, \forall \alpha \in \Omega. \quad (48)$$

Define the admissible loop transmission set as:

$$B_p(\omega, \phi) = \left\{ L_o : \left| \frac{\frac{P_o}{P}}{L_o + \frac{P_o}{P}} \right| \leq M, \forall \phi \in [0, -2\pi], \forall \omega \in [0, \infty), \forall \alpha \in \Omega \right\} \quad (49)$$

and  $\partial B_p(\omega, \phi)$  as the boundary of  $B_p(\omega, \phi)$ . This boundary represents the set of all  $\{L_o\}$  where (48) is satisfied with equality. Any optimum loop transmission function  $L_{opt}$  which solves the QFD optimization problem (27-29) must lie on  $\partial B_p(\omega, \phi) \forall \omega \in [0, \infty)$ , (Gera and Horowitz 1980, Thompson and Nwokah 1991). The generation of  $\partial B_p(\omega, \phi)$  proceeds as follows: From (31), it is clear that feedback is effective in controlling sensitivity only in the semi-open frequency interval  $[0, \omega_h)$ . Note that when  $\omega = \omega_h$ ,  $P(\alpha, s)$  is assumed to satisfy:

$$P(\alpha, s) = \frac{k(\alpha)}{s^e} \quad (50)$$

Define the nominal high frequency plant as:

$$P_o(s) = \frac{k_o}{s^e}, \text{ where } k_o \in k(\alpha), \alpha \in \Omega \quad (51)$$

Hence

$$\frac{P_o(s)}{P(\alpha, s)} = \frac{k_o}{k(\alpha)} > 0, \forall \omega \geq \omega_h, \forall \alpha \in \Omega, \quad (52)$$

follows from the path connectedness assumption for  $P(\alpha, s)$ . Let

$$\max_{\alpha \in \Omega} k(\alpha) = k_{max} \quad (53)$$

and

$$\min_{\alpha \in \Omega} k(\alpha) = k_{min} \quad (54)$$

Then  $\forall \omega \geq \omega_h$ ,  $\frac{P_o}{P}$  is real and represents a vector from the origin to any point on the



closed compact interval:  $[\frac{k_o}{k_{\max}}, \frac{k_o}{k_{\min}}]$

For any  $\omega \in [0, \omega_h)$ ,  $\frac{P_o}{P}$  describes a complex vector from the origin to a contour surrounding the point  $(1 + i0)$  in the complex plane. This contour lies entirely in the RHP, does not touch or enclose the origin, and transitions to the real interval  $[\frac{k_o}{k_{\max}}, \frac{k_o}{k_{\min}}]$  at  $\omega = \omega_h$  and thereafter.

Therefore write:

$$\frac{P_o}{P} = a(\alpha) + i b(\alpha) \quad (55)$$

and

$$L_o = x + iy \quad (56)$$

Then equation (48) reduces to

$$\left| \frac{a(\alpha) + ib(\alpha)}{x + iy + a(\alpha) + i b(\alpha)} \right| \leq M, \forall \omega \geq 0 \quad (57)$$

Suppressing the argument  $\alpha$  temporarily and squaring both sides of (57), the above gives:

$$(x + a)^2 + (y + b)^2 \geq \frac{a^2 + b^2}{M^2}, \forall \omega \geq 0, \quad (58)$$

When the inequality in (58) is replaced by an equality, we can obtain as a condition for satisfaction of (48), the equation of a circle with center  $(-a, -ib)$  and radius  $r_m = \frac{\sqrt{a^2 + b^2}}{M}$

Let the union of the set of circles generated at any given frequency  $\omega$ , and any  $M$  for all  $\alpha \in \Omega$  be denoted by  $C_p(\alpha, \omega)$ . Then  $B_p(\omega, \phi)$  is defined by:

$$B_p(\omega, \phi) = C \setminus C_p(\alpha, \omega), \quad (59)$$

and

$$\partial B_p(\omega, \phi) = \partial C_p(\alpha, \omega) \quad (60)$$

where  $\partial C_p(\alpha, \omega)$  is the external boundary of  $C_p(\alpha, \omega)$ . The radial line from the origin to  $\partial C_p(\alpha, \omega)$  at an angle of  $-\phi$  from the positive real line gives the minimum (optimum)  $|L_o|$  at the given frequency and angle  $\phi$  for which (48) is satisfied with equality. By sweeping through  $\phi \in [0 - 2\pi]$  the optimum  $|L_o|$  at the given  $\omega$  and any

phase angle  $\phi \in [0, -2\pi]$  can thus be determined. Note that  $\partial C_p(\alpha, \omega)$  divides  $C$  into two disjoint regions: an interior and an exterior region. Any admissible  $|L_o|$  is required to lie (preferably) on the boundary  $\partial B_p(\omega, \phi)$  or at least in the exterior region  $B_p(\omega, \phi)$  in order for the corresponding sensitivity function to satisfy the QFD specifications at  $\omega$ . For feasibility, the interior region is a forbidden region. By repeating the same procedure at a finite number of frequencies, a series of non-intersecting performance boundaries are generated on the complex plane. These boundaries are easily translated to the Nichols chart. The relative stability specification  $|S(\alpha, i\omega_h)| \leq M_p$  also translates to a corresponding (closed) region  $C_s(\alpha, \omega)$  surrounding the critical point  $(-1 + i0)$  called the relative stability region with boundary  $\partial C_s(\alpha, \omega)$ , which is determined as follows:

From  $\omega \geq \omega_h$ ,  $\frac{P_o}{P}$  is a vector based at the origin and terminating at any point  $\in [\frac{k_o}{k_{\min}}, \frac{k_o}{k_{\max}}] \subset R_+$ . Consequently in the inequality (58),  $b(\alpha) \equiv 0, \forall \omega \geq \omega_h$ .

$$\text{At } \omega = \omega_h, \quad M(\omega_h) = M_p. \quad (61)$$

Hence the inequality (58) at  $\omega = \omega_h$  reduces to

$$(x + a)^2 + y^2 \geq \left( \frac{a}{M_p} \right)^2, \quad M_p \geq 1 \quad (62)$$

Again, if the inequality in (62) is replaced with an equality, we obtain the equation of a circle with center  $(-a, i0)$  and radius

$$r_m = \frac{a}{M_p} \quad (63)$$

The centers of these sets of circles for all  $\alpha \in \Omega$  lie between

$$-\frac{k_o}{k_{\max}} \leq a \leq -\frac{k_o}{k_{\min}} \quad (64)$$

Call these sets of circles  $C_s(\alpha, \omega)$  with boundary  $\partial C_s(\alpha, \omega)$ .

Observe that

$$C_p(\alpha, \omega) \subseteq C_s(\alpha, \omega) \quad \forall \omega \geq \omega_h; \quad (65)$$

which gives a further justification for terminating feedback after  $\omega = \omega_h$ . The region  $C_s(\alpha, \omega)$  is called the high frequency forbidden region while  $\partial C_s(\alpha, \omega)$  is called the universal high frequency boundary. Notice that  $(-1 + i0) \in C_s(\alpha, \omega)$ . Since for feasibility,  $L_o \notin C_s(\alpha, \omega) \quad \forall \omega \geq 0$ ,  $C_s(\alpha, \omega)$  effectively forms a forbidden relative stability region that is derived directly from the stability constraint  $M_p$ . Any admissible

$L_0$  is also required to avoid the interior of  $C_s(\alpha, \omega)$ . All these sets and boundaries which are displayed in Fig. 3 are easily translated to the Nichols chart as shown in Fig. 4. If equation (63) is replaced with  $r'_m = \frac{am}{M}$  to take account of the high frequency plant gain  $|P_n(i\omega)| = m(\omega)$ ; then  $\partial C_s(\alpha, \omega)$  becomes a function of frequency, (see Fig 4a). Observe that  $\partial C_s(\alpha, \omega)$  expands with increasing  $\omega$  because  $M$  decreases towards 1 and  $m$  increases as  $\omega \rightarrow \infty$ , so that  $r'_m$  increases. Define

$$\partial C_s(\alpha, s) := \partial B_s(\omega), \quad (66)$$

where  $\partial B_s(\omega)$  is symmetrical about the  $\phi = -180^\circ$  line. However its position along this line is completely determined by the choice of  $k_0 \in k(\alpha)$ , subject only to the constraint:

$$(-1 + i0) \subset C_s(\alpha, \omega) \quad (67)$$

This would appear to suggest that an 'optimal' choice of a nominal model  $P_0(s)$  may be possible but the exact criteria of optimality are unknown at present. For example if maximization of the gain margin of  $L_0$  in the classical control sense is desired, then it can be shown that an optimal choice of  $P_0(s)$  is that for which  $\frac{k_0}{k_{\min}} = 1$ . This choice has fortuitously been made in most traditional QFD work (Horowitz and Sidi 1972). On the other hand if a full unstructured description is used for  $P(\alpha, s)$  as in  $H^\infty$  control say, then  $P_0(s)$  must necessarily be chosen so that  $\frac{k_0}{k_{\max}} \simeq 1$ , for only then are

we guaranteed that:  $\left| \frac{P - P_0}{P_0} \right| = \delta_G \leq 1 \forall \alpha \in \Omega$ . Having generated the performance sets  $B_p(\phi, \omega)$  and the universal high frequency boundary  $\partial B_s(\omega)$ , the design problem reduces to fitting a feasible  $L_0$  (if one exists) to satisfy the QFD specifications without violating either of the boundaries  $\partial B_p(\phi, \omega)$  and  $\partial B_s(\omega)$  for all  $\omega \in (0, \infty)$ , or the Bode sensitivity integral constraints and the gain-phase rules. Note that condition (i) of Theorem 3.3 is automatically satisfied if such an  $L_0$  exists and satisfies the Nyquist stability criteria.

Write

$$L_a = (-1)^{N_s - N_p} \prod_{i=1}^{N_s} \left( \frac{1 - \frac{s}{z_i}}{1 + \frac{s}{z_i}} \right) \prod_{j=1}^{N_p} \left( \frac{1 + \frac{s}{P_{oj}}}{1 - \frac{s}{P_{oj}}} \right) e^{-sr_0} \quad (68)$$

Then,

$$\log L_0 = \text{Log } L_{m0} + \log L_a$$

and

$$= \arg L_o \arg L_{mo} + \arg L_a \quad (69)$$

$$= \arg L_{mo} + 2 \left\{ \sum_{j=1}^{N_p} \tan^{-1} \frac{\omega}{P_j} - \sum_{i=1}^{N_z} \tan^{-1} \frac{\omega}{Z_i} \right\} - \omega \tau_o - \pi_{-1} \quad (70)$$

where

$$\pi_{-1} = \begin{cases} 0, & \text{if } N_z - N_p \text{ is zero or even} \\ -\pi & \text{otherwise.} \end{cases}$$

Since internal stability dictates that  $G$  be stable, we aim to loop shape on  $L_{mo}$ . But  $|L_{mo}| = |L_o|$  and as

$$L_{mo} = L_o L_a^{-1} \quad (71)$$

it follows that:

$$\arg L_{mo} = \arg L_o + 2 \left\{ \sum_{i=1}^{N_z} \tan^{-1} \frac{\omega}{Z_i} - \sum_{j=1}^{N_p} \tan^{-1} \frac{\omega}{P_j} \right\} + \omega \tau_o + \pi_{-1} \quad (72a)$$

$$= \arg L_o + \phi_m \quad (72b)$$

Consequently by translating the boundaries  $B_p(\omega)$  and  $B_s(\omega)$  on the Nichols chart by  $\phi_m(\omega)$  at every frequency  $\omega$ , we obtain the design boundaries  $B_{pm}(\omega)$  and  $B_{sm}(s)$  on which actual loop shaping will be done. When the new boundaries  $B_{pm}(s)$  and  $B_{sm}(s)$  indicate that loopshaping is impossible, a stable non-minimum phase controller  $G$  is called for whenever  $\phi_m$  is very negative. This puts the boundaries back into the phase region  $[0 - \pi]$ . Once  $L_{mo}$  is designed, we recover  $L_o$  from  $L_o = L_{mo} \cdot L_a$ .

The process of selecting an appropriate  $L_o$  from the set of all admissible  $L$ 's that satisfies the boundary conditions with minimum controller gain and minimum controller bandwidth is the very essence of QFD loop shaping. Traditionally this aspect of the design involves trial and error procedures. In an attempt to systematize the process, we make the loop shaping procedure automatic by first solving an associated  $H^\infty$  optimization problem. The  $H^\infty$  optimal controller is then used as an initializing controller in a nonlinear optimization automatic loop shaping algorithm developed by Thompson (1990). The initializing  $H^\infty$  controller is needed in the routine because unless an initial controller is "near" to the optimum in the low frequency region, the optimization scheme may converge to some unacceptable local optimum. The  $H^\infty$  controller often satisfies the "nearness" condition and hence avoids the problem. The determination of the appropriate  $H^\infty$  initializing controller using suitable  $H^\infty$  approximations to the QFD specifications  $\frac{\delta_G |T_o|}{\delta T}$ , and  $\delta_G$  as appropriate weighting functions respectively for the sensitivity and complementary sensitivity functions is developed in detail in (Nwokah, Jayasuriya and Chait 1991,1992).

Denote the resulting  $H^\infty$  controller by  $G_H$ . Once  $G_H$  is determined, we draw the graph of  $L_H(i\omega) = P_o G_H(i\omega)$  on the Nichols chart. This forms the initializing loop transmission function for the QFD optimization algorithm. On the same Nichols chart is superimposed the standard QFD performance and stability boundaries obtained from equations (58) and (62). The over-design in the  $H^\infty$  solution will usually be graphically apparent. The QFD optimization routine strives to reduce the gain-bandwidth area of  $L_H$  by moving  $L_H(i\omega)$  towards the boundaries at every frequency. Once the boundary conditions are satisfied, the loop transmission function can be rolled off as rapidly as possible in order to reduce the controller bandwidth as shown in Fig. 5. The resultant loop transmission function is designated as  $L_Q$ . It is not difficult to show that

$$|L_H(i\omega)| \geq |L_Q(i\omega)| \quad \forall \omega \geq 0. \quad (73)$$

Starting with the same nominal models  $P_o$ , equation (73) then establishes that:

$$|G_H(i\omega)| \geq |G_Q(i\omega)|, \quad \forall \omega \geq 0. \quad (74)$$

Thus, although general existence conditions for solvability of the QFD optimization problem (34) are unknown, the existence of an  $H^\infty$  solution to the resultant unstructured uncertainty problem is certainly a sufficient condition for solvability of the corresponding QFD problem. The reason for this lies in the different descriptions of the relative uncertainty  $\frac{P_o}{P}$  in (37). In QFD,  $\frac{P_o}{P}$  is some contour centered at  $(1 + i0)$  in the complex plane. On the other hand the corresponding  $H^\infty$  description of  $\frac{P_o}{P}$  is a disk centered at  $(1 + i0)$  whose radius is given by the maximum distance from  $(1 + i0)$  to the boundary of  $\frac{P_o}{P}$ . Consequently the  $H^\infty$  uncertainty template at any frequency entirely contains the corresponding QFD uncertainty template at that frequency. Or equivalently, the performance boundary  $B_p(\omega, \phi)$  generated by the  $H^\infty$  disk surrounding  $\frac{P_o}{P}(i\omega)$  will enclose the corresponding  $B_p(\omega, \phi)$  generated from the contour  $\frac{P_o}{P}(i\omega)$  at every  $\omega$ , i.e.

$$B_p(\omega, \phi)|_{H^\infty} \geq B_p(\omega, \phi)|_{QFD} \quad \forall \omega$$

Since admissible loop transmission functions must lie on or above their corresponding boundaries at every  $\omega$ , the inequality (73) can easily be established.

### 5. The Design Example

The following QFD design example is based upon the formulation for the C-135 lateral autopilot (Thompson 1990). The three flight conditions considered in this example, with relevant information, are given in Table 1.

Table 1: Flight conditions for the C-135 aircraft (Thompson 1990).

Flight Condition	Altitude (ft.)	Mach Number	Gross Wt. (lbs.)	Velocity (ft./sec.)
1. Cruise 1	42,000	0.75	190,000	726
2. Cruise 2	25,000	0.65	250,000	660
3. Power Approach	Sea Level	-	165,000	275

Equivalent plants  $P_i(s)$ ,  $i = 1, 2, 3$  for the above flight conditions are given as follows:

Flight Condition 1.

$$P_1(s) = \frac{0.7278(s + 22.35)(s + 15.66)}{(s + 0.5295)(s + 16.52)(s + 23.27)(s - 0.01572)} \quad (75)$$

Flight Condition 2.

$$P_2(s) = \frac{0.7088(s + 30.3)(s + 0.8731)}{(s^2 + 1.57s + 0.6179)(s + 28.71)(s - 0.032)} \quad (76)$$

Flight Condition 3.

$$P_3(s) = \frac{1.434(s + 4.12)(s + 1.37)}{(s^2 + 2.56s + 1.6913)(s + 3.42)(s - 0.04)} \quad (77)$$

A connected set  $P(\alpha, s)$  can be constructed from the 3-plant set (75)-(77) (Thompson 1990). Observe that the least stable plant arises from flight condition 3. Assuming flight condition 3 as the nominal model,  $\delta_G(\omega)$  was generated as in Table 2 below.

Table 2: Relative plant uncertainty; C-135.

$\omega(\text{rps})$	$\delta_G(\omega = \max_{\alpha \in \Omega} \left  \frac{P(\alpha, i\omega) - P_o(i\omega)}{P_o(i\omega)} \right  \text{ (db)})$
0.01	-7.80
0.02	-8.53
0.05	-4.17
0.1	-3.11
0.2	-1.83
0.5	-1.98
1.0	6.23
3.0	10.45
8.0	11.24

$\delta_G(\omega)$  is bounded above by the  $\text{RH}^\infty$  function:

$$\delta_G \leq |W_2(s)| = \left| \frac{0.38(1 + \frac{s}{0.02})(1 + \frac{s}{0.2})(1 + \frac{s}{1.1})}{(1 + \frac{s}{0.032})(1 + \frac{s}{0.55})(1 + \frac{s}{3.0})} \right| \quad (78)$$

which is obtained by a Bode approximation of the data in Table 2, where  $W_2(s)$  is the complimentary sensitivity weighting function in  $H^\infty$  control. The tracking specifications are given by (Thompson 1990):

$$T_o(s) = \frac{1 + \frac{s}{2}}{(1 + \frac{s}{0.5})(1 + s)(1 + \frac{s}{10})} \quad (79)$$

and

$$\delta_T(s) = \left| \frac{0.5s}{(1 + \frac{s}{0.5})(1 + s)(1 + \frac{s}{10})} \right| \quad (80)$$

Combination of all the performance specifications then yield:

$$\max_{\alpha \in \Omega} |S(\alpha, i\omega)| \leq M_T(\omega) = W_1^{-1}(s) = \frac{\delta_T}{\delta_G |T_o|} = 1.31 \left| \frac{s(1 + \frac{s}{0.032})(1 + \frac{s}{0.55})(1 + \frac{s}{3.0})}{(1 + \frac{s}{2})(1 + \frac{s}{0.02})(1 + \frac{s}{0.2})(1 + \frac{s}{1.1})} \right| \quad (81)$$

where  $W_1(s)$  is the sensitivity weighting function in  $H^\infty$  control. Stability and disturbance requirements are constrained by  $M_p \leq 1.41$  or equivalently,  $\max_{\alpha \in \Omega} |S(\alpha, i\omega_b)| \leq 1.41$ . Using the above sensitivity inequalities, the performance boundaries were generated. The nonlinear optimization package developed in

(Thompson 1990) was applied to an initial controller as shown in Fig. 5, and four iterations yielded the controller:

$$G_Q(s) = \frac{12.877(1 + \frac{s}{0.091})(1 + \frac{s}{0.071})(1 + \frac{s}{0.714})(1 + \frac{s}{2.29})}{(1 + \frac{s}{0.034})(1 + \frac{s}{0.185})(1 + \frac{s}{0.525})(1 + \frac{s}{14.01})}, \quad (82)$$

with the corresponding prefilter given by:

$$F(s) = \frac{1}{(1 + \frac{s}{0.55})(1 + \frac{s}{1.7})}. \quad (83)$$

The response to a step input command in bank angle for different flight conditions is given in Fig. 6. Note that the performance specifications are completely satisfied for every flight condition.

## 6. Conclusions

Quantitative feedback design is a very useful robust control methodology whenever large parametric uncertainty and hard constraints on closed loop response are indicated. Until recently however, the technique relied almost entirely on semi-analytical and graphical methods, making comparison with  $H^\infty$  control at best indirect. By using  $H^\infty$  control as an initial trial design however, the QFD methodology can be systematized. The formalization of the QFD process such as is presented here makes comparison with  $H^\infty$  and  $\mu$ -synthesis straightforward. The result of the non inclusion of phase information in these methods is the inevitability of a higher cost of feedback, as shown by the example. The extension of these ideas to multivariable systems is not difficult (Nwokah, Thompson, Perez 1990). Investigations into the adaptation of this approach to nonlinear control design along the lines originally suggested by Horowitz is in progress.

## 7. References

1. Åström, K.J., L. Neumann, and P.O. Gutman, "A Comparison of Robust and Adaptive Control," Proc. ICCON'89 Conference, Jerusalem, Israel, September 1989.
2. Bailey, F.N. and C.H. Hui "Loop Gain-Phase Shaping For Single-Input-Single-Output Robust Controllers," *IEEE Control System Magazine*, 11, 93-101, 1991.
3. Bailey, F.N. and J.C. Cockburn, "Loop Gain Phase Shaping Design for SISO Robust Controllers with Mixed Uncertainty", *Proceedings of the American Control Conference*, Boston, MA, June 1991.
4. Chait, Y., Hollot, C.V., A Comparison Between  $H^\infty$  Methods and QFD for a SISO Plant with Both Plant Uncertainty and Performance Specifications, ASME Winter Annual Meeting, Dallas, TX, November 1990.



5. Cruz, J.B. and W.R. Perkins, "A New Approach to the Sensitivity Problem in Multivariable Feedback System Design," *IEEE Trans. Automatic Control*, AC-9, 218-223, 1964.
6. Dorato, P., Yedavali, R. (Eds.), *Recent Advances in Robust Control*, IEEE Press, New York, 1990.
7. Doyle, J.C. "Quantitative Feedback Theory and Robust Control," *Proceedings of the American Control Conference*, Minneapolis, MN, 1987.
8. Foo, Y.K. and I. Postlethwaite, "Extensions of the Small  $\mu$ -Test for Robust Stability," *IEEE Trans. Automatic Control*, AC-33, 172-176, 1988.
9. Francis, B.A., *A Course in  $H^\infty$  Control Theory*, Lecture Notes in Control and Information Sciences, No., Springer-Verlag, New York, 1987.
10. Freudenberg, J.S. and D.P. Looze, *Frequency Domain Properties of Scalar and Multivariable Feedback Systems*. New York: Springer-Verlag, 1988.
11. Gera, A., and I.M. Horowitz, "Optimization of the Loop Transfer Function," *International Journal of Control*, 31, 389-398, 1980.
12. Hoffman, K., *Banach Spaces of Analytic Functions*, Prentice-Hall, New Jersey, 1972.
13. Horowitz, I.M., Fundamental Theory of Linear Feedback Control Systems, *Trans. IRE Prof. Group on Automatic Control*, AC-4, 5019, 1959.
14. Horowitz, I.M., Quantitative Feedback Theory, *IEE Proc. pt. D*(6), 129, 215-226, 1982.
15. Horowitz, I.M., Quantitative Synthesis of Uncertain Multiple Input-Output Feedback Systems, *Int. J. Control*, 30, 81-106, 1979.
16. Horowitz, I.M., Sidi, M. Synthesis of Feedback Systems with Large Plant Ignorance for Prescribed Time-Domain Tolerances, *Int. J. Control*, 16(2), 287-309, 1972.
17. Horowitz, I.M., Sidi, M., Practical Design of Multivariable Feedback Systems with Large Plant Uncertainty, *Int. J. System Science*, 12, 851-875, 1980.
18. Jayasuriya, S., Nwokah, O.D.I., Yaniv, O., The Benchmark Problem Solution by Quantitative Feedback Theory, *Proc. ACC*, Boston, MA, 1991. Also in *AIAA Journal of Guidance and Control* (To Appear).
19. Krishnan, K.R. and A. Cruickshanks, "Frequency-Domain Design of Feedback Systems for Specified Insensitivity of Time-Domain Response to Parameter Variation," *International Journal of Control*, Vol. 25, No. 4, pp. 609-620, 1977.
20. Kwakernaak, H. Minimax Frequency Domain Performance and Robustness Optimization of Linear Feedback Systems *IEEE Trans. Autom. Control* AC-30, 994-1004. 1985.
21. Maciejowski, J., *Multivariable Feedback Design*, Addison-Wesley, Reading, MA, 1989.

22. Morari, M., Zafriou, E., *Robust Process Control*, Prentice-Hall, NJ, 1989.
23. Netushil, A. (Ed.) *Theory of Automatic Control Systems*, MIR Publishers, Moscow, USSR, 1973.
24. Nwokah, O.D.I., "Strong Robustness in Uncertain Multivariable Systems," *Proceedings of IEEE Conference Decision and Control*, Austin, TX, 1988.
25. Nwokah, O.D.I., Jayasuriya, S., Chait, Y., "Parametric Robust Control by Quantitative Feedback Theory," *Proceedings of the American Control Conference*, Boston, MA, June 1991. Also in *AIAA J. Guidance, Control and Dynamics*, Vol. 15, pp. 207-214, 1992.
26. Nwokah, O.D.I., Thompson, D. F., Perez, R. A., On the Existence of QFD Controllers, ASME-WAM, Dallas, TX, 1990.
27. Perez, R.A., Nwokah, O.D.I., Thompson, D.F., Almost Decoupling by Quantitative Feedback Theory, *Proceedings of the American Control Conference*, Boston, MA, 1991. Also *ASME Journal of Dynamic Systems Measurement and Control* (To Appear).
28. Robinson, E.A., *Random Wavelets and Cybernetic Systems*, Hafner Publishers, New York, 1982.
29. Rosenbrock, H.H., *Computer Aided Control System Design*, Academic Press, London, 1974.
30. Shaked U., Horowitz, I.M., Synthesis of Basically Non-interacting Systems with Significant Plant Uncertainty, *Automatica*, 12, 61-73, 1976.
31. Thompson, D.F., Nwokah, O.D.I., Frequency Response Specifications and Sensitivity Functions in Quantitative Feedback Theory, ACC, Boston, 1991. Also *ASME J. Dynamic Systems Measurement and Control* (To Appear).
32. Thompson, D.F., Optimal and Sub-optimal Loop Shaping in Quantitative Feedback Theory, Ph.D. Thesis, Purdue University, August 1990.
33. Verma, M. Jonckheere, E.  $L^\infty$  Compensation with Mixed Sensitivity as a Broadband Matching Problem, *Systems and Control Letters*, 4, 125-129, 1984.
34. Zames, G., Feedback and Optimal Sensitivity: Model Reference Transformation, Multiplicative Semi Norms, and Approximate Inverses, *IEEE Trans. Autom Control*, AC-26, April 1981.

#### **8. Acknowledgments**

Financial support from AFOSR under contract #F49629-88-C-0053, from the Allison Gas Turbine Division of General Motors Corporation under contract #530-1288-0875 and from the National Science Foundation under contract #MSS90-19531 is greatly appreciated. Dr. David F. Thompson developed the loop optimization software.

--

### List of Figure Captions

- Figure 1:** Standard 2-D of Feedback Structure
- Figure 2:** Bounding Sensitivity Functions  $M(\omega)$  and  $M_o(\omega)$
- Figure 3:** Performance and Stability Boundaries in the Complex Plane
- Figure 4:** Performance and Stability Boundaries on the Gain-Phase Plane
- Figure 5:** Sequential Controller Optimization from Initial  $G_H$ .
- Figure 6:** Bank Angle Response For Different Flight Conditions.

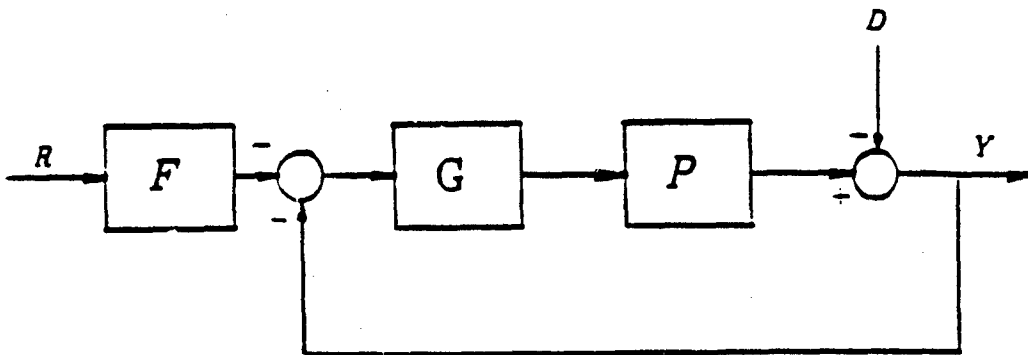


Figure 1: Standard 2-D of Feedback Structure

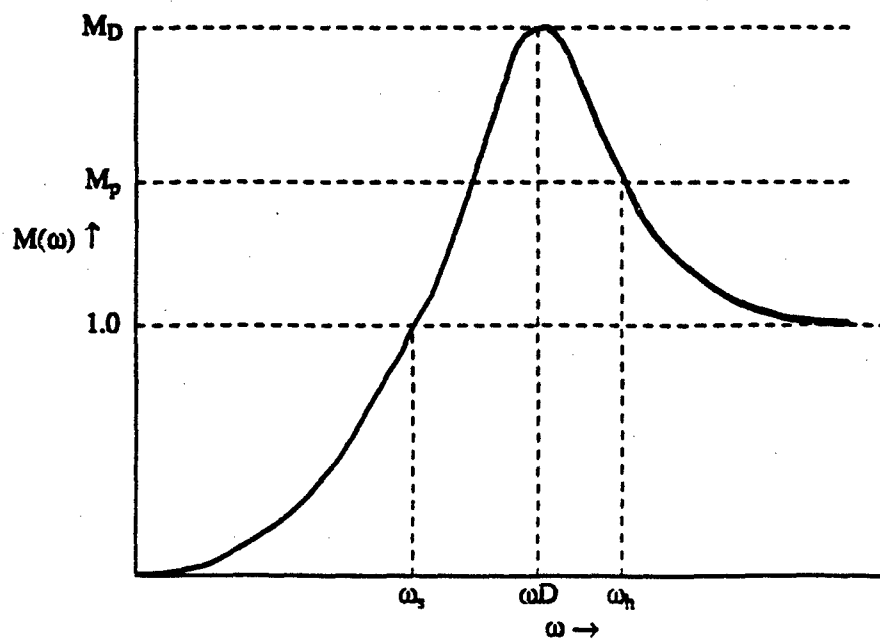


Fig. 2: Bounding Sensirvity Function

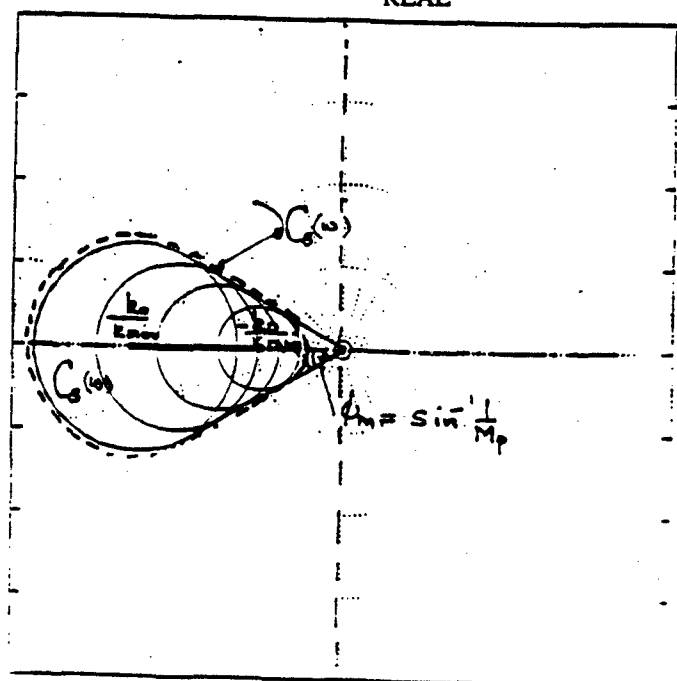
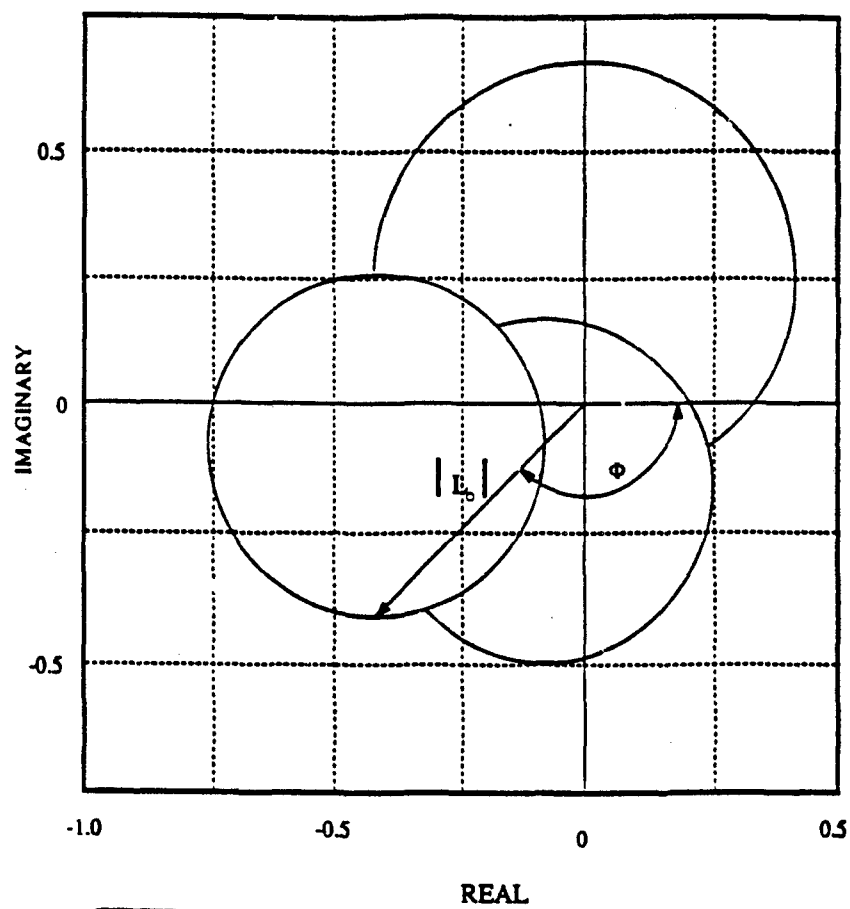


Figure 3: Performance and Stability Boundaries in the Complex Plane

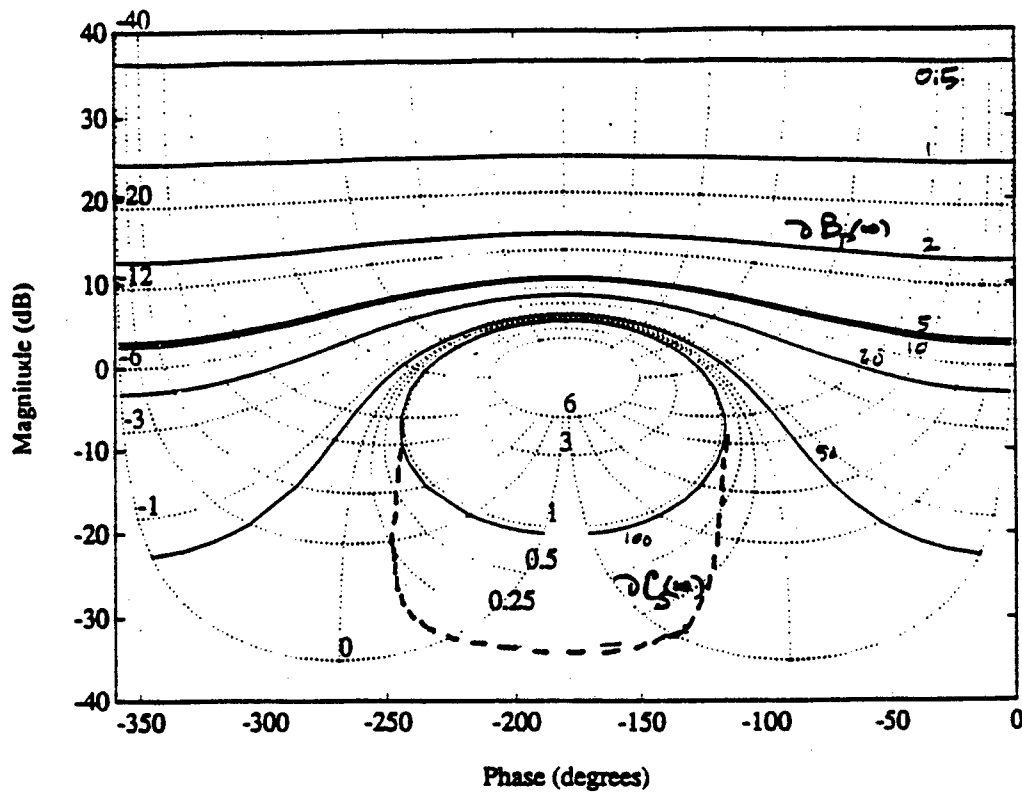


Figure 4: Performance and Stability Boundaries on the Gain-Phase Plane

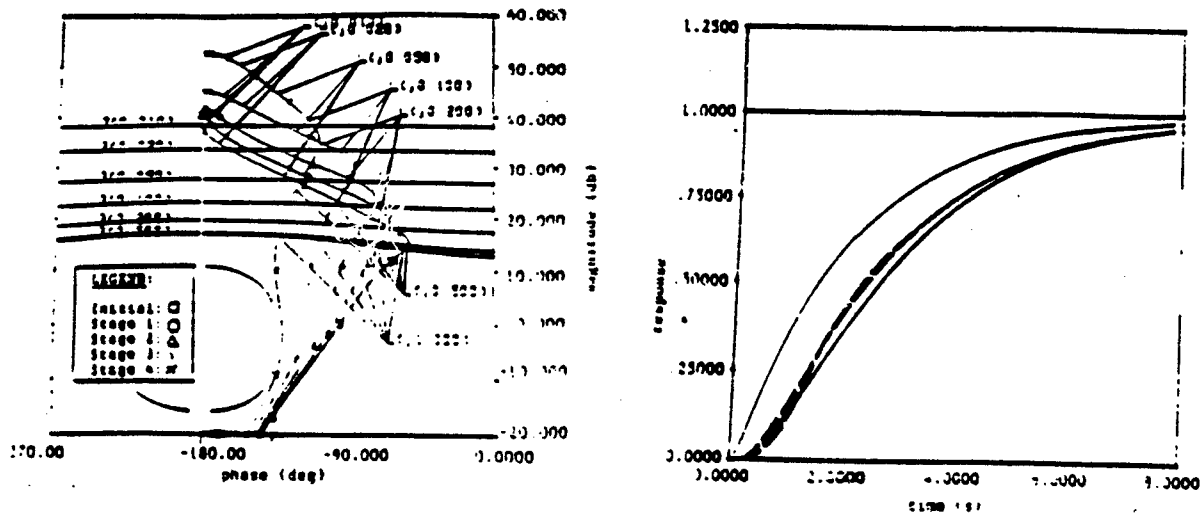


Figure 5: Sequential Controller Optimization from Initial  $G_H$ .

Figure 6: Bank Angle Response For Different Flight Conditions.

# A ROBUST DIGITAL FLIGHT CONTROL SYSTEM FOR AN UNMANNED RESEARCH VEHICLE USING DISCRETE QUANTITATIVE FEEDBACK THEORY

D.J. Lacey, Jr.<sup>\*</sup>, I.M. Horowitz<sup>\*</sup>, C.H. Houppis<sup>\*</sup>, S.N. Sheldon<sup>†</sup>

## Abstract

This paper synthesizes the application of digital multiple-input multiple-output Quantitative Feedback Theory technique to the design of a three axis rate controller for the Lambda Unmanned Research Vehicle. Simulations show that the resulting robust controller performs well throughout the flight envelope without gain scheduling. A small perturbation linear model developed from flight test data is used for the design. Nineteen separate plants are used to represent the flight envelope of the aircraft resulting from variations in speed, altitude, center of gravity location, and weight. The design employs the Nichols Chart and is accomplished in the  $w'$ -domain.

## 1 INTRODUCTION

The Control Systems Development Branch of the Wright Laboratory at Wright Patterson Air Force Base, OH (WL/FI GL) developed the Lambda unmanned research vehicle (URV) for in-flight testing of experimental aircraft (A/C) control hardware and software. In order to provide the necessary test data, Lambda requires a stable, robust flight control system which performs well throughout the entire flight envelope.

Quantitative Feedback Theory (QFT) is a frequency design technique incorporating plant uncertainty early in the design process resulting in a robust controller [1]. In this design effort [2] the variations in plant parameters come from different flight conditions. Robust automatic flight control systems in a URV, and unmanned aerial vehicles in general, are important to their mission because they reduce pilot work load, increase safety, and aid in the recovery of the vehicle.

<sup>\*</sup>Air Force Institute of Technology

<sup>†</sup>Wright Laboratory

This design was created and tested on Sun SPARCstation 2 workstations. All development and testing was done using MATRIX<sub>X</sub>.

## 2 PROBLEM DEFINITION

The challenge was to produce a robust digital flight control system for Lambda using QFT and deliver a set of controller difference equations. This controller aims to uncouple the roll, pitch and yaw responses. The system must meet all performance specifications throughout the entire flight envelope which includes speeds from 45 to 110 knots, center of gravity locations between 21.8 and 32.4% Mean Aerodynamic Cord (MAC), vehicle weights from 181 to 215 pounds, and altitudes up to 5000 feet. Air speeds may vary between 76 and 185 feet-per-second.

### 2.1 Assumptions

Several assumptions were used to simplify the design procedure. The design uses a linear time-invariant (LTI) model of Lambda which is known to be a non-linear system. Further, the equations of motion and the A/C dynamics are assumed to be Laplace transformable. In addition, the following conditions are assumed:

- Small-angle perturbation models are valid.
- Aircraft mass is constant.
- The aircraft is rigid: that is, no bending or flutter modes.
- The commanded inputs and the commanded outputs are measurable.
- Three-axis rate signals—pitch rate ( $q$ ), roll rate ( $p$ ) and yaw rate ( $r$ )—and the Euler angles—pitch angle ( $\theta$ ), roll angle ( $\phi$ ), and yaw angle ( $\psi$ )—are available on the Lambda URV.
- A digital sampling rate of 50 Hz is used.



## 2.2 Scope

The design is limited to the development of the set of controller difference equations needed to control Lambda throughout the expected flight envelope. Eventually, the success of the design will be proven when the automatic flight control system is installed and flown on Lambda.

## 2.3 Standards

The controller is required to have a 45° phase margin throughout the flight envelope in all three axes—pitch, roll, and yaw. In addition, the A/C is required to meet figures-of-merit including specific rise time and overshoot requirements shown in Table (1) [3].

Table 1: Design Figures-of-Merit

Model	$T_r$ (sec)	$T_s$ (sec)	$M_p$ ( $\frac{rad}{deg}$ )
$\frac{q_{LB}(s)}{q_{cmd,r}(s)}$	0.84	1.56	1.0
$\frac{q_{UB}(s)}{q_{cmd,r}(s)}$	0.15	2.05	1.25
$\frac{p_{LB}(s)}{p_{cmd,r}(s)}$	0.87	1.56	1.0
$\frac{p_{UB}(s)}{p_{cmd,r}(s)}$	0.44	0.78	1.0
$\frac{r_{LB}(s)}{r_{cmd,r}(s)}$	3.48	6.22	1.0
$\frac{r_{UB}(s)}{r_{cmd,r}(s)}$	1.76	3.13	1.0

## 3 DESIGN APPROACH

### 3.1 Approach/Methodology

Beginning with a mathematical description of the A/C, followed by definition of the flight envelope, individual flight conditions are selected using variations in flight speed, center of gravity location, vehicle weight, and altitude. Analysis of the model reveals the lateral-directional dynamics can be separated from the longitudinal dynamics. Thus, the design reduces to a single-input single-output (SISO) QFT system design for the longitudinal channel and a two-by-two multiple-input multiple-output (MIMO) QFT system design for the lateral channel. In addition, unstable and nonminimum phase conditions exist. Inversion of the plant matrix is necessary [1], therefore the plants must be square. In this case, flight data used for the mathematical model produced square (three-by-three) plants.

A two-by-two MIMO system QFT design requires the synthesis of two separate transmission loops. Design should start with the loop with the smallest bandwidth. Once obtained, the first loop is used in develop-

ing the second loop. The technique of designing loops using elements of previously designed loops is part of the QFT improved method (Method Two). Method Two takes into account the reduction in uncertainty resulting from the compensation of the previous loops [4]. Once the loops are shaped, the design is simulated on the computer to validate the performance expectations. The steps used for application of the discrete QFT technique are:

- Choose the Flight Conditions
- Determine the Plant Transfer Function Matrix,  $P(s)$
- Invert  $P(s)$

$$P^{-1}(s) = \begin{bmatrix} p_{11}^{-1}(s) & p_{12}^{-1}(s) \\ p_{12}^{-1}(s) & p_{22}^{-1}(s) \end{bmatrix} \quad (1)$$

- Calculate the  $Q(s)$  Matrix

$$Q(s) = \begin{bmatrix} \frac{1}{p_{11}^{-1}(s)} & \frac{1}{p_{12}^{-1}(s)} \\ \frac{1}{p_{12}^{-1}(s)} & \frac{1}{p_{22}^{-1}(s)} \end{bmatrix} = \begin{bmatrix} q_{11} & q_{12} \\ q_{21} & q_{22} \end{bmatrix} \quad (2)$$

- Transform  $Q(s)$  to the  $w'$  Domain,  $Q(w')$  which includes the necessary zero order hold (ZOH).
- Determine the Frequency Response Data
- Extract the Template Data from the Frequency Response Data
- Plot the Templates for One Input-Output Pair
- Choose a Nominal Plant
- Use the Templates to Form the Stability and Performance Bounds
- Shape the Nominal Loop,  $L_o(w')$
- Extract the Compensator,  $G(w')$ , from  $L_o(w')$
- Synthesize the Prefilter,  $F(w')$
- Shape the Remaining Loops
- Form the Remaining  $G(w')$ 's and  $F(w')$ 's
- Verify Loop Shaping in the  $w'$ -plane
- Transform the  $F(w')$ 's to  $F(z)$ 's and the  $G(w')$ 's to  $G(z)$ 's
- Simulate using the  $G(z)$ 's,  $F(z)$ 's, and  $P(s)$ 's

### 3.2 The Aircraft Model

Lambda is a small remotely-piloted airplane with a 14 foot wing span and weight of approximately 200 pounds. It uses a pusher propeller behind the fuselage and in front of a conventional aft tail. The horizontal tail consists of a horizontal stabilizer and a split elevator. A vertical tail is located on either end of the horizontal tail, and consists of a vertical stabilizer and rudder. The wings are slightly tapered; each has three trailing, movable control surfaces.

Table 2. Lambda Descriptive Data

<b>Dimensions</b>	
Wing Span .....	14 ft
Wing Area .....	19 sq ft
Length .....	9.6 ft
Height With Landing Gear .....	3 ft
Propeller Diameter .....	2.3 ft
<b>Weights</b>	
Maximum Fuel .....	14 lb
Maximum Payload .....	15 lb
Maximum Flight Weight .....	200 lb
<b>Performance</b>	
Maximum Level Speed at Sea Level .....	115 mph (100 knots)
Stall Speed .....	63 mph (55 knots)
Stall Speed With Flaps .....	52 mph (45 knots)
<b>Engine</b>	
Power .....	18 hp
Type .....	2 cycle 2 cylinder
<b>Control Limits</b>	
Elevator Deflection Limit .....	$\pm 15^\circ$
Rudder Deflection Limit .....	$\pm 25^\circ$
Flap Deflection Limit .....	$20^\circ$ down
Aileron Deflection Limit .....	$\pm 15^\circ$

Lambda closely resembles the Pioneer UAV successfully employed by the United States Navy in the Persian Gulf War. The Pioneers are slightly larger and twice as heavy but share the configuration of an aft tail, center mounted engine, and pusher propeller. Lambda has ten separate control surfaces. They are:

- Left Elevator
- Right Elevator
- Left Rudder
- Right Rudder
- Left Aileron
- Right Aileron
- Left Outer Flap
- Right Outer Flap
- Left Inner Flap
- Right Inner Flap

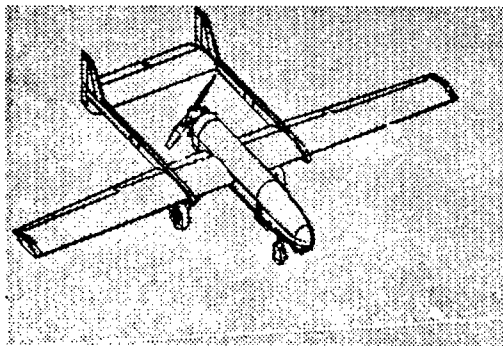


Figure 1: Lambda URV

Even though each control surface can be operated independently, the flight data, used to create the mathematical model upon which this design is based, were obtained using the control surfaces together. All four of the flap control surfaces were operated together as were the two rudders. The split elevators were deflected together while the ailerons were operated differentially. Since the mathematical model does not include flap actuator dynamics, the flaps are not used as a control surface.

It is expected that Lambda will gain weight. Indeed, today's model of Lambda is heavier than it was when first built, which was heavier than specified. The weight increase results from adding equipment, such as video cameras and additional sensors. For this reason, this design includes weights up to 215 pounds. Additionally, since Lambda is designed to fly at speeds up to 100 knots, speeds up to 110 knots are included to encompass all of the expected plant variation. The heavier weights are very demanding of the technique and contribute greater plant variation compared with the higher speeds which contribute little variation.

The small perturbation model is based on a series of test flights and was developed by Swift [5]. The model incorporates the traditional stability derivatives into a state space representation of the A/C. A MATLAB macro file creates the state space representation along with the stability derivatives when given a set of flight conditions. The A/C, excluding actuator and sensor dynamics, is described using nine states. They are:  $q$ ,  $p$ ,  $r$ ,  $\theta$ ,  $\phi$ ,  $\psi$ ,  $\alpha$ ,  $u$ ,  $\beta$ . Of these,  $q$ ,  $\theta$ ,  $\alpha$ , and  $u$  are used to describe the longitudinal channel, while the states  $p$ ,  $r$ ,  $\phi$ ,  $\psi$ , and  $\beta$  describe the lateral-directional dynamics. The A/C model state space representation is:

$$\dot{\mathbf{x}}(t) = \mathbf{A}(t)\mathbf{x}(t) + \mathbf{B}(t)\mathbf{u}(t) \quad (3)$$

$$\mathbf{y}(t) = \mathbf{C}\mathbf{x}(t) \quad (4)$$

Assuming zero initial conditions ( $\mathbf{x}_0 = 0$ ) and a trim condition ( $\dot{\mathbf{x}}_0 = 0$ ), the Laplace transform of the plant is the perturbation model:

$$\mathbf{\dot{X}}(s) = \mathbf{A}(s)\mathbf{X}(s) + \mathbf{B}(s)\mathbf{U}(s) \quad (5)$$

$$\mathbf{Y}(s) = \mathbf{C}(s)\mathbf{X}(s) \quad (6)$$

where:

$$\mathbf{A}(s) = \begin{bmatrix} \mathbf{A}(s)_{long} & 0 \\ 0 & \mathbf{A}(s)_{lat} \end{bmatrix} \quad (7)$$

$$\mathbf{B}(s) = \begin{bmatrix} \mathbf{B}(s)_{long} \\ \mathbf{B}(s)_{lat} \end{bmatrix} \quad (8)$$

$$\mathbf{C}(s) = [\mathbf{C}(s)_{long} \quad \mathbf{C}(s)_{lat}] \quad (9)$$

The Lambda longitudinal and lateral-directional dynamics are modelled as decoupled. Actually, some unmodelled coupling exists, however, this design uses the best model available.

The actuators used in the model are second-order in the pitch and roll channels and first-order in the yaw

channel. The model used for the pitch channel actuator is:

$$\frac{87}{s^2 + 18s + 120} \quad (10)$$

The model used for the roll channel is:

$$\frac{84}{s^2 + 18s + 120} \quad (11)$$

The model used for the yaw channel is:

$$\frac{5.58}{s + 6.2} \quad (12)$$

The sensors used to measure the rates are identical gyroscopes with transfer functions modelled as:

$$\frac{50}{s + 50} \quad (13)$$

This paper covers the only design of the longitudinal channel of Lambda using QFT. The entire design, including the lateral directional channel along with additional autopilot functions, is covered in [2].

### 3.3 Flight Conditions

Lambda is to fly within the flight envelope:

- Speeds from 45 to 100 Knots
- Maximum Flight Weight 200 Pounds
- Altitude up to 5000 Feet

The flight conditions are selected from the design flight envelope of Lambda with considerations given to the growth of the program and expected changes. There are four variables considered in the selection of flight conditions. They are:

- Center of Gravity Location
- Flight Speed
- Altitude
- Aircraft Weight

The minimum and maximum values of each variable create a set of 16 flight conditions. The 16 flight conditions produce two widely spaced plant groupings. The difference in speed contributes the most to the wide plant variation, with the other variables contributing smaller variations. Three additional speeds are added to fill in the gap between the lower and higher speeds. A weight of 200 pounds, a center of gravity location in the center of the range, along with the lowest altitude, are chosen for the additional conditions. A total of 19 separate plants are used as shown in Table 3.3.

Table 3: The Aircraft Flight Conditions

Plant #	cg (% MAC)	Speed (kts)	Q <sub>∞</sub> (lbs/ft <sup>2</sup> )	Weight (lbs)
1	21.8	110	35.05	181
2	21.8	110	35.05	215
3	21.8	110	40.08	181
4	21.8	110	40.08	215
5	32.4	110	35.05	181
6	32.4	110	35.05	215
7	32.4	110	40.08	181
8	32.4	110	40.08	215
9	27.1	61	12.61	200
10	27.1	77	20.08	200
11	27.1	93	29.90	200
12	32.4	45	5.915	181
13	32.4	45	5.915	215
14	32.4	45	6.765	181
15	32.4	45	6.765	215
16	21.8	45	5.915	181
17	21.8	45	5.915	215
18	21.8	45	6.765	181
19	21.8	45	6.765	215

### 3.4 s Plane Transfer Functions

The longitudinal plant transfer functions are developed from MATRIX<sub>X</sub> using the System Build capability. Each condition is used as an input into the MATLAB macro file. The outputs include **A** and **B** matrices for the longitudinal and lateral directional dynamics of Lambda. The **A**<sub>long</sub> and **B**<sub>long</sub> matrices for the longitudinal channel are respectively of the form:

$$\begin{bmatrix} X_u & X_\alpha & 0 & -g \cos \theta \\ \frac{Z_u}{u} & \frac{Z_\alpha}{u} & \frac{u+Z_A}{u} & -g \sin \theta \\ \frac{M_u + M_A Z_A}{u} & \frac{M_\alpha + M_A Z_A}{u} & \frac{M_A + M_u u + Z_A}{u} & -g M_A \sin \theta \\ 0 & 0 & 1 & 0 \end{bmatrix} \quad (14)$$

$$\begin{bmatrix} X_{\delta_{flap}} & X_{\delta_{flap}} \\ \frac{Z_{\delta_{flap}}}{u} & \frac{Z_{\delta_{flap}}}{u} \\ \frac{M_{\delta_{flap}} + M_u Z_{\delta_{flap}}}{u} & \frac{M_{\delta_{flap}} + M_u Z_{\delta_{flap}}}{u} \\ 0 & 0 \end{bmatrix} \quad (15)$$

Since the flaps are not used as a control input, the second column of **B**<sub>long</sub> is discarded which results in:

$$\begin{bmatrix} X_{\delta_{flap}} \\ \frac{Z_{\delta_{flap}}}{u} \\ \frac{M_{\delta_{flap}} + M_u Z_{\delta_{flap}}}{u} \\ 0 \end{bmatrix} \quad (16)$$

The longitudinal matrices, A, B, C, and D are then assembled into a state space representation:

$$\begin{bmatrix} \mathbf{A} & \vdots & \mathbf{B} \\ \dots & \dots & \dots \\ \mathbf{C} & \vdots & \mathbf{D} \end{bmatrix} \quad (17)$$

The state space representation is used in a MATRIX<sub>X</sub> System Build simulation to produce a linearized state space model which includes the actuators and sensors. The resulting state space representation is then transformed to a transfer function which relates the output to the input. The transfer functions are used in the design of the QFT controller which includes a compensator as well as a prefilter (Fig. 2). A complete set of transfer functions used in the design is included in the appendix of [2].

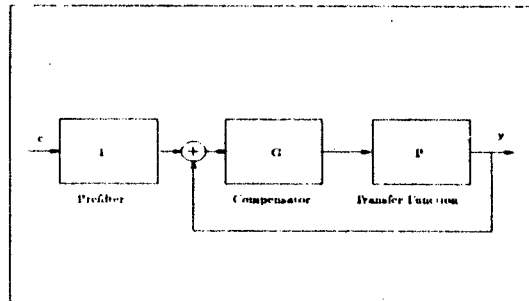


Figure 2: QFT Controller Block Diagram

### 3.5 $w'$ Plant Transfer Functions

Lambda uses digital flight control hardware requiring a digital flight control system design. Although an additional transform is necessary, the  $w'$ -plane is used in this design because it allows use of a plane development tools, such as the Nichols Chart. Designing either in the  $w'$  plane or the  $s$  plane, the pseudo continuous approach (PCT), produces some "warping" when transforming the  $s$  or  $w'$  plane controller into the  $z$  domain. The degree of "warping" decreases as the sampling time decreases as shown in [6].

The  $w'$  plane representation is normally obtained by transforming the  $s$  plane plant, with a zero order hold (ZOH), into the  $z$  plane then performing the bilinear transformation:

$$z = \frac{2 + w'T}{2 - w'T} \quad (18)$$

$$w' = \frac{2}{T} \left[ \frac{z-1}{z+1} \right] \quad (19)$$

where  $T$  is equal to the sampling interval. From:

$$T = \frac{1}{\text{Sampling Frequency}} \quad (20)$$

Lambda has a sampling frequency of 50 Hz which is equivalent to a sampling interval of 0.02 seconds. The relationships between  $s$ ,  $z$ , and the  $w'$  plane are presented in [6].

In this design, the  $w'$ -plane representation of the plants are found using the Hofmann algorithm [7]. The Hofmann algorithm allows conversion of the  $s$  domain representation through the  $z$ -plane and into the  $w'$  plane without the normal numerical difficulties [3]. An important feature of Hofmann's algorithm is the automatic inclusion of the zero order hold. A ZOH is assumed to exist between the digital controller and the analog A/C. The Hofmann algorithm allows conversion of:

$$s\mathbf{X}(s) = \mathbf{A}\mathbf{X}(s) + \mathbf{B}\mathbf{U}(s) \quad (21)$$

and:

$$\mathbf{Y}(s) = \mathbf{C}\mathbf{X}(s) + \mathbf{D}\mathbf{U}(s) \quad (22)$$

to:

$$w'\mathbf{X}(w') = \mathbf{A}^*\mathbf{X}(w') + \left[1 - \frac{w'T}{2}\right] \mathbf{B}^*\mathbf{U}(w') \quad (23)$$

and:

$$\mathbf{Y}(w') = \mathbf{C}\mathbf{X}(w') + \mathbf{D}\mathbf{U}(w') \quad (24)$$

where:

$$\mathbf{A}^* = \mathbf{A} \left[ \frac{\mathbf{A}T}{2} \right]^{-1} \tanh \left( \frac{\mathbf{A}T}{2} \right) = \mathbf{A}_e \quad (25)$$

$$\mathbf{B}^* = \left[ \frac{\mathbf{A}T}{2} \right]^{-1} \tanh \left( \frac{\mathbf{A}T}{2} \right) \mathbf{B} = \mathbf{A}_e \mathbf{B} \quad (26)$$

A six term Taylor series approximation of  $\mathbf{A}_e$  is used in this design. Since there are 19 plants included in this design, the Hofmann algorithm is performed 19 times by using the programming capability of MATRIX<sub>X</sub> and placing the program code [3] in an iterative loop.

The  $w'$  plane representation of the transfer function at the nominal conditions contains non-minimum phase (NMP) zeros at 100 and 130 resulting from the  $w'$  transformation, which always produces a transfer function with the same number of zeros as poles. The NMP zero at 100 is due to the sampling rate and the NMP zero at 130 is due to the excess number of poles over zeros in the  $s$  domain transfer function. If the number of poles exceeding the number of zeros is two, there will be two additional zeros created and one will be NMP. A complete set of  $w'$  plane transfer functions is included in the appendix of [2].

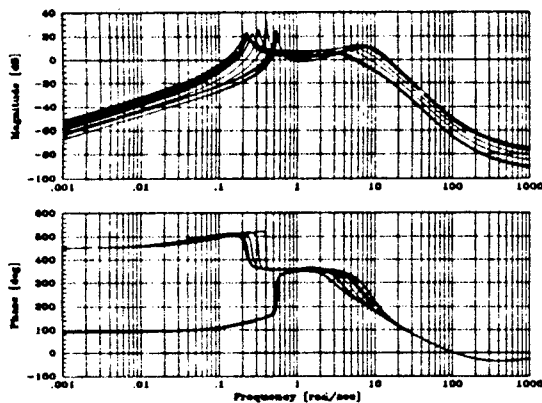


Figure 3: Frequency Response of the 19 Longitudinal Plants

### 3.6 Frequency Response Data

The QFT technique uses templates that represent the plant parameter uncertainty, at the specified design frequencies. The plant uncertainty is represented by the 19 LTI plants. For this reason, the frequency response information for all of the plants at the design frequencies is necessary. The frequency response data of the 19 longitudinal plants are summarized in Fig. 3.

### 3.7 Plant Templates

Plant templates are developed from the frequency response data. First the template frequencies are chosen on the basis of plant variation. Where the plants vary significantly, the template frequencies must be closely spaced. For this design the frequencies  $v = 0.001, 0.005, 0.01, 0.05, 0.1, 0.2, 0.3, 0.4, 0.5, 0.6, 0.7, 1, 2, 3, 4, 5, 6, 8, 10, 20, 50, 100$  (rad/sec) are used; where  $v$  is the  $w'$  analog of  $\omega$  in the  $s$ -plane.

Next, the template data are "stripped out" of the frequency response data. Twenty two sets of template data are formed, a set for each template frequency. Each set contains magnitude and phase information for the 19 plants at the template frequency. Only the magnitude and phase differences are important to the QFT technique. In plotting the templates, the data are normalized by subtracting the smallest phase from the phase data and the smallest magnitude from the magnitude data. The templates are then plotted. The template is defined by a set of points, each representing a plant. The spread of the points is due to the plant variation at the template frequency.

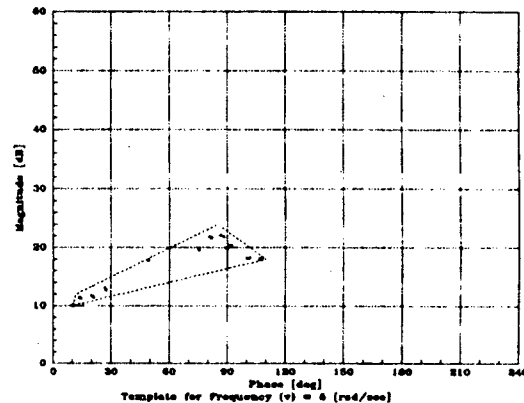


Figure 4: Example of Template Used in Longitudinal SISO Design

### 3.8 Nominal Plant

Any one of the plants can be chosen as the nominal plant; however, choosing the plant with the least number of right-half-plane (RHP) poles and zeros may make the loop shaping easier. The location of the nominal plant on each of the templates is needed before the bounds—tracking, disturbance, and stability—can be plotted on the Nichols Chart (NC). Plotting the bounds on the NC is key to the QFT technique. Because the plant uncertainty is captured in the templates and the templates are used to form the bounds, the single transmission loop shape meeting or exceeding the plotted NC bounds guarantees each plant considered will meet or exceed the tracking, disturbance, and stability performance specifications. The nominal plant chosen for the longitudinal SISO design is flight condition one. Additionally, the same flight condition is used in the lateral-directional MIMO system design.

### 3.9 Stability Bounds

A benefit to the designer using a predetermined (fixed) sampling rate is the need to consider only the stability bounds during the transmission loop shaping. The maximum gain in the loop is primarily constrained by the NMP zeros. Therefore, the objective is to "pack in" as much transmission loop gain as possible. If the tracking and performance specifications are not met, a change in the sampling rate must be made to allow higher loop transmission gain. The military standard requirement [8] specifies a phase margin  $\gamma = 45^\circ$  to be used to form the NC stability contour  $M_L$ . The  $\gamma = 45^\circ$  requirement corresponds to a 3 dB  $M_L$  contour on the NC.

Table 4: All-Pass-Filter Used in the Longitudinal SISO System Design

Template Frequency $\nu$ (rad/sec)	Phase $\phi_A$ (deg)
0.001	0.002
0.005	0.01
0.05	0.10
0.10	0.20
0.20	0.40
0.30	0.61
0.40	0.81
0.50	1.01
0.60	1.21
0.70	1.41
1.00	2.02
2.00	4.04
3.00	6.06
4.00	8.08
5.00	10.1
6.00	12.1
8.00	16.1
10.0	20.2
20.0	40.0
50.0	94.9
100	165

### 3.10 The All-Pass-Filter Technique

The all-pass-filter (apf) technique is used throughout this design [9] to remove the NMP elements from the design while still accounting for their effects. The apf technique complicates the design; however, it allows the designer to rapidly determine the maximum possible loop transmission. The phase of the apf  $\phi_A$  is included when plotting the stability bounds. The apf used in the longitudinal SISO design is:

$$\text{apf} = \frac{(w' - 100)(w' - 130)}{(w' + 100)(w' + 130)} \quad (27)$$

The amount of phase associated with the template frequencies is summarized in Table 4. At low frequencies, below  $\nu = 0.5$  (rad/sec) ( $\omega = 0.4999958$  rad/sec), the shift is negligible. At higher frequencies, above  $\nu = 0.5$  (rad/sec), the shift must be incorporated in the stability bounds. The moving Nichols chart technique, which is slightly different from the method usually employed, is used to plot the stability bounds on the NC. For a discussion of the moving Nichols chart technique, see [2].

The stability bounds are used in shaping the loop transmission where the design can proceed using a variety of techniques. The two techniques used in this design are the "backward loop shaping technique" and "minimum order compensator design technique". A high order compensator is not desirable for Lambda and the "backward loop shaping technique" may pro-

duce a high order compensator, however, both loop shaping design techniques are used in this design.

Although the final design is based on the "minimum order compensator technique", the "backward loop shaping technique" is used to determine the theoretical maximum loop transmission. In the lateral-directional MIMO design the "backward loop shaping technique" is used as a performance baseline. An illustrative discussion of the techniques are included in [2]. Loop shaping produces the following minimum phase transmission loop ( $L_{mo}$ ):

$$\frac{0.0183(w' + 2)(w' + 5)(w' + 10)(w' + 50)P_{mo}}{(w')^2(w' + 160 \pm j120)(w' + 300)} \quad (28)$$

Figure 5 is the MP loop transmission  $L_{mo}$  plotted on the NC. A NC showing a plot of all the plants including the NMP elements is shown in Fig. 6.

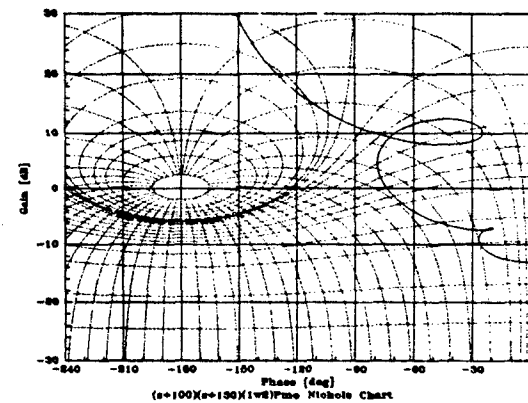


Figure 5: NC Showing MP Transmission Loop After Loop Shaping

### 3.11 $w'$ Compensator

The  $w'$  compensator,  $G(w')$ , is found by dividing the loop transmission by the nominal plant. If the loop transmission includes the plant,  $G(w')$  is simply the poles, zeros, and gain added during loop shaping. If the nominal plant is not included in the transmission loop, the zero and poles not absorbed in  $L_{mo}$  become poles and zeros, respectively, of  $G(w')$ . The longitudinal SISO  $G(w')$  for this design is:

$$\frac{0.0183(w' + 2)(w' + 5)(w' + 8)(w' + 10)(w' + 50)}{(w')^2(w' + 160 \pm j120)(w' + 300)} \quad (29)$$

### 3.12 Prefilter Design

The prefilter,  $F(w')$ , is obtained by plotting the frequency response data of the closed loop system:

$$\left( \frac{L(w')}{1 + L(w')} \right) = \left( \frac{G(w')P(w')}{1 + G(w')P(w')} \right) \quad (30)$$

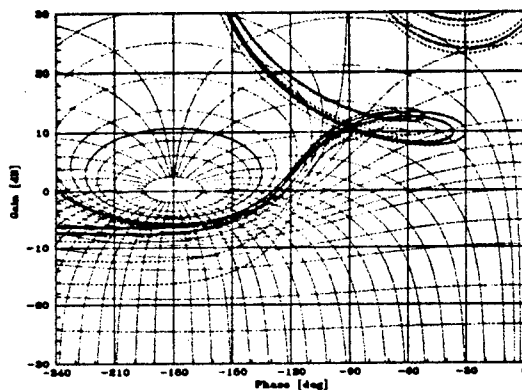


Figure 6: NC Including All 19 Plants and NMP Elements

The frequency response bounds, developed from the specifications, are plotted over the closed loop response producing a family of curves. See the first plot in Fig. 7. Poles and zeros are placed in front of the closed loop system until all of the responses are contained within the performance bounds, as in the second plot in Fig. 7.

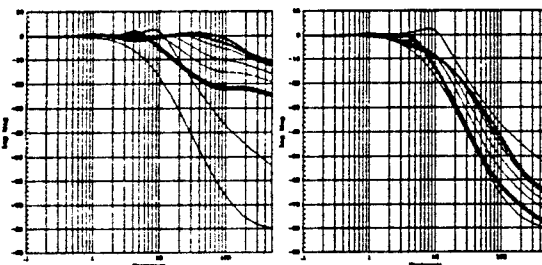


Figure 7: Closed Loop Response Without and With Prefilter,  $F(w')$

The prefilter for the longitudinal SISO QFT design is:

$$F(w') = \frac{0.001875(w' + 200)^2}{(w' + 5)(w' + 15)} \quad (31)$$

where:

$$\lim_{w' \rightarrow 0} F(w') = 1 \quad (32)$$

### 3.13 $w'$ Simulation

The  $w'$ -plane design is simulated to verify the performance before proceeding with the design. The  $w'$  simulations are performed using the System Build capability of MATRIX<sub>x</sub>. Time domain step responses are plotted along with the performance bounds (see Fig. 8)

which indicate that a robust design is achieved, that is, all responses lie between the upper and lower specified tracking bounds.

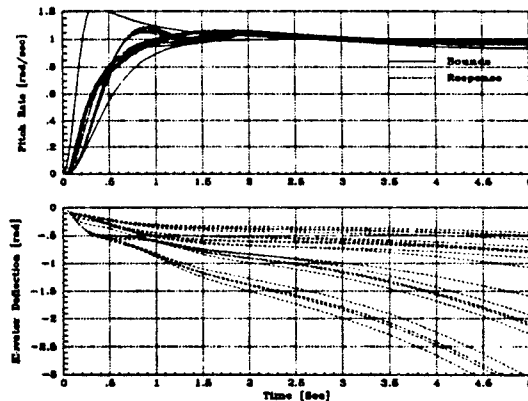


Figure 8: System Build  $w'$  Simulation Frequency Response

### 3.14 $z$ -Plane Transformations

$F(w')$  and  $G(w')$  are transformed to the  $z$ -plane for digital implementation on Lambda. The  $z$ -plane representations are obtained by performing the bilinear transformation; see Eq. (19). In addition to performing the transformation, the user function divides the numerator and denominator by the denominator leading coefficient resulting in a normalized  $z$ -plane representation of  $F(z)$  and  $G(z)$ :

$$\frac{.013975z^2 + 0.0093168z + 0.0015528}{z^2 - 1.6439z + 0.66874} \quad (33)$$

$$\frac{96.749z^5 - 374.31z^4 + 566.96z^3 - 417.22z^2 + 147.36z - 19.538}{z^5 - 0.76829z^4 - 0.87805z^3 + 0.17073z^2 - 0.36585z + 0.10976} \quad (34)$$

### 3.15 Comparison of $w'$ and $z$ -Plane $F$ 's and $G$ 's

The  $w'$ -plane and  $z$ -plane compensators and filters must be comparable up to frequencies greater than  $\frac{1}{3}\omega_s$  (rad/sec). The sampling frequency on Lambda is 50 Hertz, therefore  $\omega_s = 314$  (rad/sec) and the  $w'$  and  $z$ -plane representations must be fairly close up to  $\omega = 105$  (rad/sec). The frequency response of  $F(w')$  and  $F(z)$  are plotted in Fig. 9 where a good comparison exists within the required frequency bandwidth  $0 \leq \omega \leq 105$  (rad/sec). Similarly, a good comparison exists between  $G(w')$  and  $G(z)$  [2].

The synthesis of the QFT compensators and prefilters for the two-by-two lateral-directional MIMO plants follows the same steps. The first transmission loop and thereby the prefilters and compensators are done

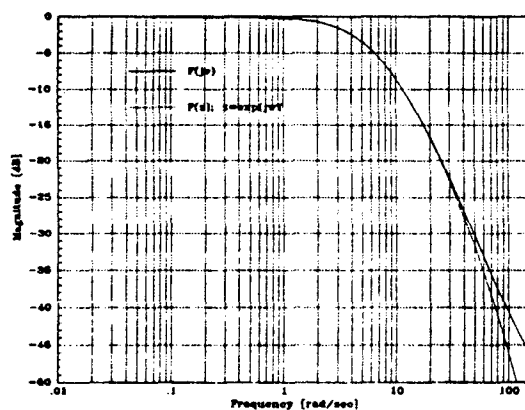


Figure 9: Comparison of  $F(w')$  and  $F(z)$  Magnitude Frequency Response

exactly as the same as a SISO design. However, in forming the second transmission loop the compensation of the first loop is used to reduce the amount of uncertainty.

#### 4 SIMULATION RESULTS

The design is simulated using the best model available, in this case the same one used in the design with the additional nonlinear elements added. The nonlinear elements are due to the software and hardware limiters. MATRIX<sub>X</sub> has the ability to simulate a system with both continuous and discrete elements. This "hybrid" simulation capability is used to verify the performance of the design. Adding the limiters produces the simulation results shown in Fig. 10. The simulations predict the performance expected from Lambda in actual flight. They show good performance at all flight conditions for a step command of  $10^\circ$  per second for at least two seconds. After two seconds, the deflection limits on the actuators begin to affect the response.

#### 5 SUMMARY, CONCLUSIONS, AND RECOMMENDATIONS

##### 5.1 Summary

A single QFT controller is synthesized that produces satisfactory performance throughout the flight envelope. It is important to note that no gain scheduling is necessary. Response of the system remains stable in spite of the inherent nonlinearities present due to hardware and software control limiters. The hybrid simulation with nonlinear elements (see Fig. 10) is the final test of the design as it includes all that is known about the plant. Some of the performance limitations

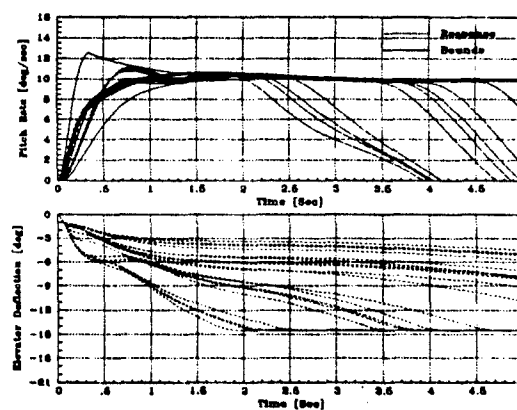


Figure 10: Hybrid Simulation With Non-Linear Elements

can be overcome if Lambda's speed is held constant. In the simulations, Lambda can hold a pitch rate constant until the speed drops. As the speed drops, more elevator is needed than is available to the controller. Since the simulation results are good, within the performance limitations of Lambda, it is assumed that the A/C will perform well with this controller design.

With the exception of generating the MISO equivalent transfer functions, the QFT design for the lateral-directional MIMO portion of Lambda follows the same procedure as the longitudinal SISO channel. The design is effective but somewhat limited by the low-order compensator requirement. Again, adding the nonlinear elements in the model limited the response but did not produce instabilities. Better performance could be obtained through faster sampling, higher bandwidth actuators, and higher-order compensation, all of which would allow higher loop transmission gain. In spite of the physical and imposed limitations, the QFT controller performs well.

In contrast with previous efforts that used models developed from computer predictions from design specifications, this design employs a model developed from flight test data. In the model, A/C dynamics separate into two independent channels—the longitudinal channel and the lateral-directional channel. The longitudinal channel is a SISO system while the lateral-directional channel is a two-by-two MIMO system.

##### 5.2 Conclusions

The QFT design technique is powerful and useful for the design of a rate controlled autopilot for URVs requiring robust autopilot systems. Lambda simulations show a single QFT controller can perform well throughout the entire flight envelope of Lambda with-



out additional sensors. The technique is straightforward. Synthesis and simulations can be performed using a computer aided design package such as MATRIX<sub>x</sub> using minimal computer resources. The method is completely transparent, in that the designer is able to predict the ultimate performance early in the design. More importantly, the designer is able to make engineering tradeoffs during loop shaping. For example, performance at certain frequencies can be increased by reducing the performance at frequencies of lower interest to the designer.

### 5.3 Recommendations

Working on a controller for Lambda is a unique opportunity. Simply knowing that the controller design will be used is highly motivating. Wright Laboratory should continue to challenge AFIT students with thesis proposals involving Lambda. The students benefit by facing a real life challenge and the laboratory gets needed research.

This design is to be implemented on Lambda and the performance to be compared with predictions. The Lambda model should be improved as more information becomes available and should be extended to include the effects of operating the ten flight control surfaces independently. The weight of Lambda should be reduced or, at least, held to its current value since the heavier weights are the main source of plant variation and contain open loop unstable poles. Additionally, other QFT controllers should be synthesized for Lambda.

This design is aimed at stability throughout the envelope assuming no failures. Future efforts should consider the effects of component failure or battle damage on the controllability of the A/C. Because of limited computer resources aboard Lambda, this controller is limited to fifth order compensation. Superior performance is achieved in simulation with higher order compensation due to higher available loop transmission gain. Future efforts might add the computer resources, without additional weight, to Lambda to allow higher order compensation and a faster sampling rate.

Finally, Lambda's performance could be improved by installing faster actuators since the present actuators severely limit the loop transmission gain.

### References

- [1] Horowitz, I. and A. Ioinovici, "Quantitative Feedback Theory for Multiple-Input Multiple-Output Feedback Systems with Control Input Failures," *Int. J. of Control*, vol. 43, pp. 1803-1821, June 1986.
- [2] D. J. Lacey, "A Robust Digital Flight Control System for an Unmanned Research Vehicle Using Discrete Quantitative Feedback Theory," Master's thesis, Air Force Inst. of Tech., Wright Patterson AFB, OH, Dec. 1991.
- [3] D. G. Wheaton, "Automatic Flight Control System Design for an Unmanned Research Vehicle Using Discrete Quantitative Feedback Theory," Master's thesis, Air Force Inst. of Tech., Wright Patterson AFB, OH, Dec. 1990.
- [4] Horowitz, I., "Improved Design Technique For Uncertain Multiple-Input-Multiple-Output Feedback Systems," *Int. J. of Control*, vol. 36, no. 6, pp. 977-988, 1982.
- [5] G. A. Swift, "Model Identification and Control System Design for the Lambda Unmanned Research Vehicle," Master's thesis, Air Force Inst. of Tech., Wright Patterson AFB, OH, Sep. 1991.
- [6] Houpsis C. H. and G. B. Lamont, *Digital Control Systems—Theory, Hardware, Software*. McGraw-Hill, 1988.
- [7] Hofmann, L. G. and R. E. Michael., "Technique for Analysis of Digital Control Systems." General Electric Company, Avionic and Electronic Systems Division. Binghamton, New York.
- [8] Military Specification—Flying Qualities of Piloted Aircraft. MIL-STD-1797A. 30 Jan. 1990.
- [9] Houpsis, C. H., "Quantitative Feedback Theory (QFT)—Technique for Designing Multivariable Control Systems," Tech. Rep. AFWAL-TR-86-3107, Flight Dynamics Laboratory, Wright-Patterson AFB, OH, Jan. 1987.

## Combined QFT and LQG/LTR Approach to AIAA Controls Design Challenge

Chu-Yin Chang Tsu-Shuan Chang Shih H. Wang  
University of California, Davis, CA 95616

Cheng W. Chen  
FMC Corporate Technology Ctr  
Santa Clara, CA 95050

### ABSTRACT

The QFT and LQG/LTR techniques are applied to design flight control laws for the AIAA Control Design Challenge nonlinear aircraft model. In this approach, the nonlinear aircraft model is first linearized and the LQG/LTR technique is used to obtain a baseline control law. Then the QFT technique is applied to enhance robustness of the baseline control law in order to account for nonlinearities of the system. The QFT enhancement is used in the inner loop control to achieve good flying qualities. The outer loop control laws are designed for the low order aircraft model using the LQR technique to accomplish hands-off autopilot for the specified maneuvers.

### 1. INTRODUCTION

One of the demands for modern advanced fighter aircraft is high maneuverability. In order to achieve this objective, we can trade some degrees of stability robustness for maneuverability. In addition to this trade-off, certain maneuvers (e.g. flight with high angle of attack) introduce significant amount of nonlinearities. However, in practice, linearized aircraft models are often used to approximate the short period aircraft dynamics for designing control laws. Thus, errors between nonlinear aircraft dynamics and its linear approximation become critical, and the control law design techniques which better account for nonlinearities are needed.

In this paper, the QFT approach is explored to design flight control laws for the AIAA Control Design Challenge nonlinear aircraft model. The nonlinear aircraft model is first linearized and the LQG/LTR technique is used to obtain a baseline control law. Then the QFT technique is applied to enhance the robustness of the baseline control law in order to account for the modeling errors.

### 2. CONTROL DESIGN OBJECTIVES

In order to achieve good flying qualities, design goals for the inner loop control laws are specified by first and second order transfer functions as shown below.

(a) Longitudinal Axis

$$\frac{N_z}{F_s} = \frac{G\omega_s^2}{s^2 + 2\zeta_s\omega_s s + \omega_s^2}$$

where  $N_z(g)$ ,  $F_s(\text{inch})$ ,  $G(g/\text{inch})$ ,  $\omega_s$  (rad/sec) and  $\zeta_s$  denote normal acceleration, stick input, stick gain, short period frequency and short period damping ratio, respectively.  $\zeta_s$  is set to be 0.7 at all flight conditions and  $\omega_s$  varies at each flight condition as shown in table 1.

Flight Condition.	$\omega_s$
0.5M/9,800 ft.	3.6
0.9M/9,800 ft	7.3
0.6M/30,800 ft	2.2
1.4M/39,800 ft	7.0

Table 1. Short Period Frequency

The stick gain  $G$  converts the longitudinal stick input to normal acceleration command to achieve a desired 2nd order response.

(b) Lateral/Directional Axis

$$\frac{P}{F_s} = \frac{G \cos \alpha_0}{s+a}$$

$$\frac{r}{F_s} = \frac{G \sin \alpha_0}{s+a}$$

$$\frac{\beta}{F_s} = 0$$

where  $P$ (deg/sec),  $r$ (deg/sec),

$\beta$ (deg),  $\alpha_0$ (deg),  $G$ (deg/sec.inch) and  $a$  denote roll rate, yaw rate, side slip angle, trimmed angle of attack, stick gain and bandwidth, respectively. The values of  $a$  are shown in table 2.

Flight Condition	$a$
0.5M/9,800 ft	2.2
0.9M/9,800 ft	2.4
0.6M/39,800 ft	1.7
1.4M/39,800 ft	2.2

Table 2. Bandwidth

For normal acceleration control, collective stabilators are used as the control effectors and ailerons and differential stabilators are used for roll rate and yaw rate control. Outer loop control laws are designed to generate the commands in the longitudinal and lateral/directional axes for the specified maneuvers so that the error responses of the aircraft are within the specified error tolerances.

### 3. LINEAR QFT METHOD

The aircraft model of the AIAA control design challenges is linearized around the four given trim conditions. To demonstrate our design approach, the flight condition 0.5M/9800ft is considered in the following to illustrate the main ideas.

### Longitudinal Control

The longitudinal dynamics at the flight condition 0.5M/9800ft is a nonminimum-phase single-input/single-output transfer function. The nonminimum-phase appears at +6.6465. The reference command is the desired normal acceleration and the input control is the symmetrical collective stabilator. To accommodate the flight regime in the neighborhood of the flight condition and model errors induced in linearization, various degrees of parameter variations are introduced intentionally. The longitudinal controller is designed to tolerate these uncertainties without significant performance degradation from the given specifications. The intention is to obtain a longitudinal control which works for the nonlinear aircraft model in a reasonable large flight regime about the given flight condition.

### Longitudinal Control Design

The design approach taken here follows three steps:

- Use LQG/LTR to generate a baseline design which is stable and performs reasonably well.
- Use QFT to generate the loop transmission constraints or bounds to define the potential robust compensators to achieve the desired specifications.
- Use the classical loop shaping techniques to enhance the LQG/LTR compensator to meet the QFT bounds.

#### (1) LQG/LTR Baseline Design

The standard LQG/LTR techniques are used to find a stable, reasonably good yet not fully satisfactory compensator

$$G_{LQG}^{long}(s) = 70 \frac{(s+19.6824)(s+5.8356)}{(s+1459.47)(s+8.8769)} \times \frac{(s+0.8821+j2.1527)(s+0.8821-j2.1527)}{(s+7.5082)(s+5.0158)(s+0.02)}$$

The time response of the design is very satisfactory except the steady state

error and large control bandwidth (refer to Figs.1&4 ).

## (2) QFT Bounds

The LQG/LTR design does not take the model uncertainties and variations into account explicitly. Based on the QFT theory, given a quantified model uncertainty, for example a 10% aerodynamic coefficient variation, one set of the so called tracking loop transmission bounds, which characterize the lower bounds for potential loop transmissions, is produced to guarantee the closed loop system performs uniformly well within the allowed performance tolerance with respect to the given amount of variations. Another set of stability bounds which characterize the forbidden regions for loop transmissions, is derived to guarantee the closed loop system stability. For this longitudinal control problem, the allowed tolerance on the magnitude of the closed loop response is shown in Fig. 2 , where the upper and lower bounds are added to the desired specification discussed in Sec. 2 to indicate the tolerance. The 10% aerodynamic coefficient variation leads to the frequency response variations portrayed by templates for a number of frequencies as indicated in QFT [3]. These templates and their associated tolerances determine the tracking and stability bounds. The algorithms developed in [4],[5] are used to construct these bounds as shown in Fig.3.

## (3) Enhancement

This baseline design is overlayed on the Nichols Chart to check against the QFT bounds. Figure 3 displays both the QFT bounds and the LQG/LTR design loop transmission. Under the 10% variation of the aerodynamic coefficients, the LQG design satisfies most QFT bounds but a few. It implies the LQG/LTR design would not behave as robustly for the 10% parameter variation as a QFT design. Noticeably, the LQG design lacks an integrator and thus causes a steady

state error. This can be easily fixed by classical loop shaping by adding a small zero and an integrator. The further analysis of the LQG design reveals that the LQG/LTR controller contains a small pole and a very large pole. The small pole can be cancelled by the small zero just mentioned without affecting the performance much. That very large pole causes excessively large control bandwidth. This can be easily corrected by replacing with a relatively small pole around 100. Thus an enhanced compensator with an integrator is obtained:

$$G_{LQG}^{long}(s) = 4.75 \frac{(s+19.6824)(s+5.8356)}{(s+100)(s+8.8769)} \times \frac{(s+0.8821+j2.1527)(s+0.8821-j2.1527)}{(s+7.5082)(s+5.0158)s}$$

Fig.3 also shows the enhanced loop transmission against the QFT bounds. The envelopes for the variations of the time and frequency responses are shown in Figs.5 & 6 for 5%,10% and 20% parameter variations.

## Lateral/Directional Control

The lateral dynamics at the flight condition 0.5M/9800ft is a 3x3 multiple-input/multiple-output transfer function matrix. The reference commands are the desired sideslip, yaw and roll rates and the control variables are the unsymmetrical differential stabilator, rudder and aileron. The intention is to obtain a lateral control which works for the nonlinear aircraft model in a reasonable large flight regime about the given flight condition.

## Lateral/Directional Control Design

The same 3-step approach will be followed for lateral compensator design. The details will be included in the final paper.

## 4. AUTOPILOT DESIGN

Autopilot control laws are designed for altitude hold, bank angle hold and velocity hold modes to provide pilot relief automatic

flight control. The longitudinal and lateral/directional command inputs to the inner loop control laws are generated to achieve the specified maneuvers with precision. The closed loop flight control system consisting of the airframe and the inner loop controller are approximated with the low order systems specified in the design objectives and the LQR technique was employed to design controller gains for each autopilot mode (see Figure 7).

The velocity hold mode autopilot is achieved by commanding the throttle to regulate the error between the commanded velocity and the fed back velocity, ( $V_{com} - V$ ), and to regulate acceleration  $N_z$  to regulate the error between the commanded altitude and the fed back altitude, ( $h_{com} - h$ ), and to regulate vertical velocity,  $dh/dt$ . The bank angle hold mode autopilot is achieved by commanding the roll rate to regulate the error between the commanded bank angle and the fed back bank angle, ( $\phi_{com} - \phi$ ).

## 5. SIMULATION RESULTS

Nonlinear simulation was performed using the inner loop control laws designed with the LQG/LTR plus QFT technique at each specified flight condition to evaluate the resulting designs against the design specifications. The time response of the normal acceleration with the control laws designed by the LQG/LTR plus QFT technique at a flight condition of 0.5 Mach at 9,800 feet is shown in Figure 8. Using the autopilot control laws designed for the altitude hold maneuver together with the inner loop control laws, the nonlinear simulation was performed. At 9,800 feet, 0.5 Mach, a vertical velocity of 50 feet/sec was commanded and held for 4 seconds. Then the altitude hold mode was engaged. The aircraft vertical velocity response is shown in Figure 9. The altitude command input and the resulting aircraft altitude are shown by the dashed and the solid line, respectively in Figure 10. The results show very good aircraft responses. In order to quantify the error between the commanded and the achieved altitude, the error response is shown in Figure 11.

## REFERENCES

- [1] I. Horowitz, "Feedback Systems with Nonlinear Uncertain Plants," *Int. J. Control*, Vol.36, No.1, pp.155-171, 1982.
- [2] I. Horowitz and M. Breiner, "Quantitative Synthesis of Feedback Systems with Uncertain Nonlinear Multivariable Plants," *Int. J. Systems Sci*, Vol.12, No.5, pp.539-563, 1981.
- [3] Horowitz, I. and M. Sidi, "Synthesis of Feedback Systems for Large Plant Ignorance," *Int. J. Ctrl*, v.16, pp.287-309, 1972.
- [4] C.Y. Chang, T.S. Chang and C.W. Chen, "Loop Transmission Bounds for Multivariable Diagonal Control in Quantitative Feedback Theory," to be presented in 1992 American Control Conference, June 1992.
- [5] G.G. Wang, C.W. Chen and S.H. Wang, "Loop Transmission Bounds in Quantitative Feedback Theory," submitted to *I. J. Control*.

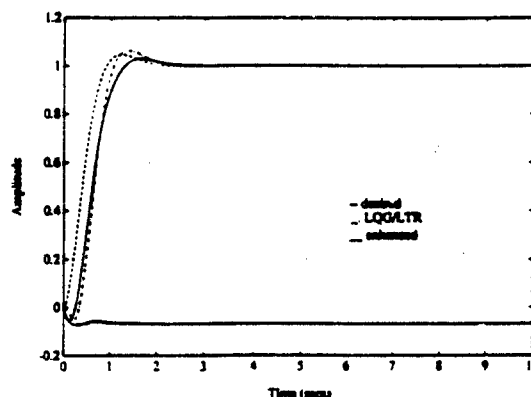


Figure 1. Step Responses

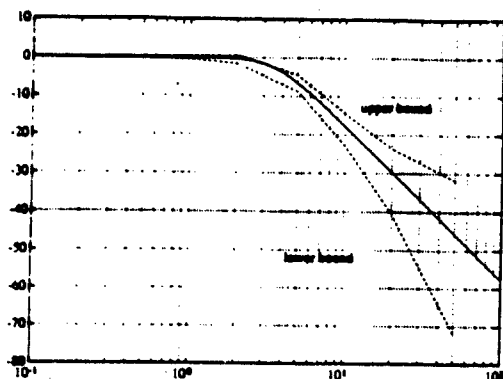


Figure 2. Design Specifications

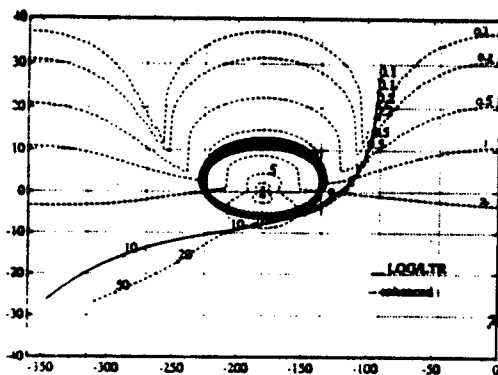


Figure 3. Loop Transmission

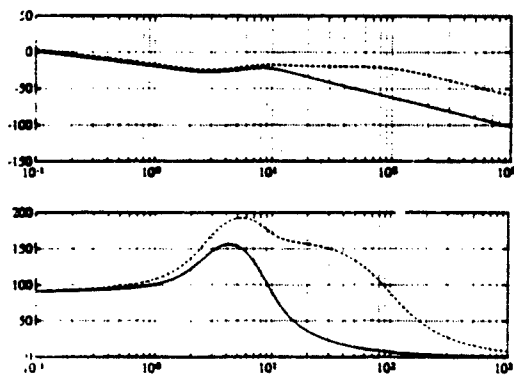


Figure 4. Compensator Frequency Responses

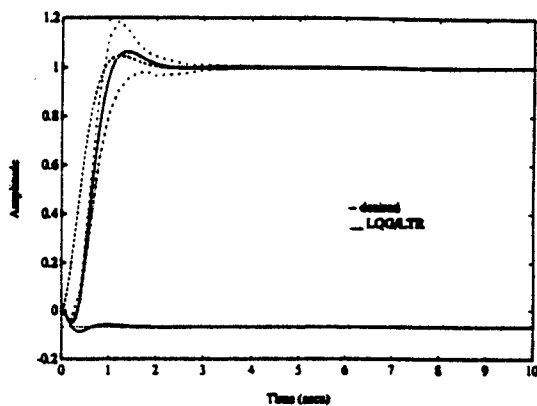


Figure 5. Step Response Variation of LQG/LTR Controller for 5% Plant Variation

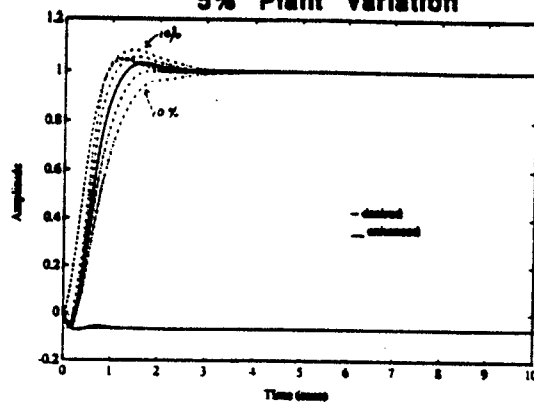


Figure 6. Step Response Variation of QFT Enhanced Controller for 5 & 10% Plant Variation

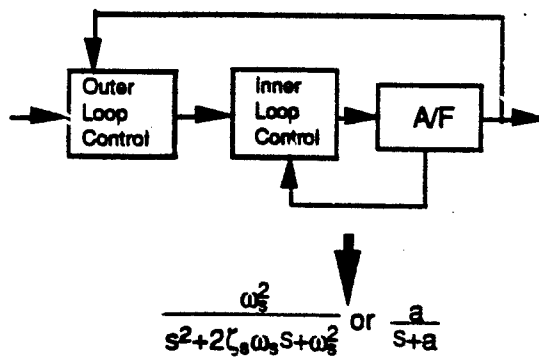


Figure 7. Flight Control System

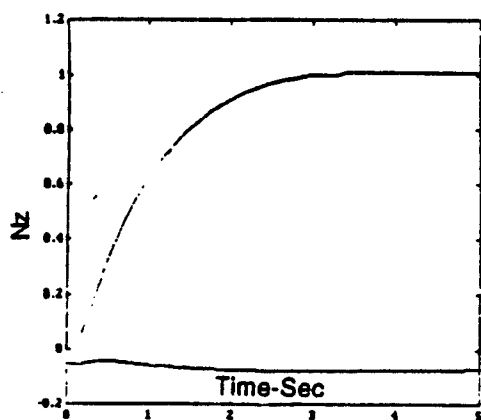


Figure 8. Longitudinal Nonlinear

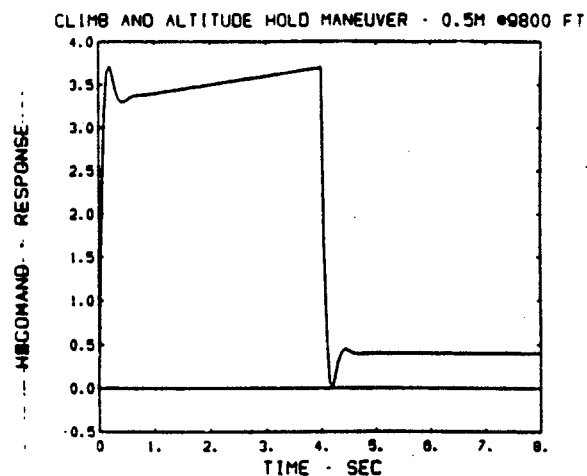


Figure 11. Altitude Error Response

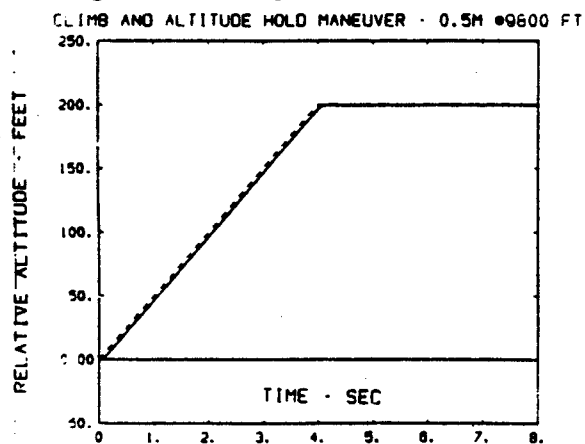


Figure 9. Vertical Velocity Response

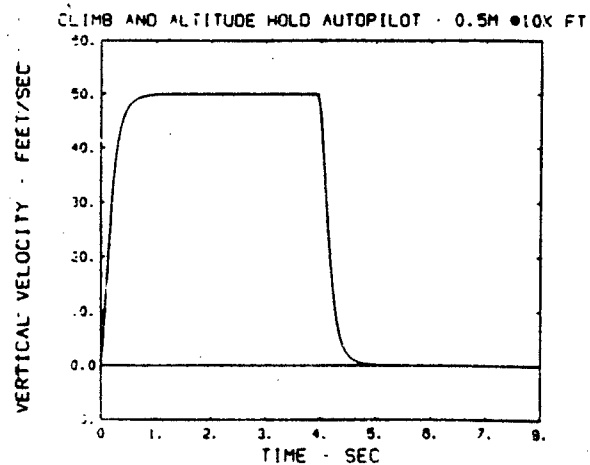


Figure 10. Altitude Response

# VEHICULAR LONGITUDINAL CONTROL USING QUANTITATIVE FEEDBACK THEORY

Susan J. Gardner and Sami Fadali  
Electrical Engineering Department, University of Nevada-Reno

## Abstract

Quantitative Feedback Theory (QFT) has proven itself as one of the most viable methods of control for systems with large parameter variations. These large variations are prevalent in modern automobiles and trucks. The vehicle dynamic model is the sum of the forces, propulsion force, air drag force and gravitational force ( $F_d - F_a - F_g$ ). The propulsion force ( $F_d$ ) includes saturation constraints and varying masses and time delays in engine and brakes. Gravitational force ( $F_g$ ) is a function of the highway terrain. The air drag force ( $F_a$ ) is both constant (due to steady velocities and wind) and incidental due to wind gusts and will be addressed in a later paper. To allow more vehicles/hour on existing roadways, it is evident that an automated controller must operate very dissimilar vehicles in changing environments (topographies, weather, emergencies, etc.) to control speed, spacing and lateral positioning. A requirement for a controller for this purpose is smooth (comfortable) operation during maneuvers such as stopping or entrainment with rejection of environmental disturbances. Speed and spacing (longitudinal control) is the emphasis of this paper in which QFT is offered as one possible solution.

## Introduction

Today, roadways have become overburdened and congested worldwide. In California alone, three million more cars are expected on its roads and highways by the turn of the century (California Senate Research 1991). Not only are the number of autos increasing but the number of miles traveled is growing due to the extreme dependence on the auto and the growing separation of work, home and shopping. The purpose of the "smart highway" or Intelligent Vehicle Highway System (IVHS) is to improve existing highway efficiency. Expected added benefits are greater safety, convenience and a decrease in fuel consumption and pollution from the largest source of air pollutions. By eliminating stop-and-go driving, emissions/mile will be reduced.

One aspect of the automated highway is the "platooning" a number of vehicles as a group. This entails control, both longitudinal and lateral, being surrendered by the drivers so that a shorter distance between cars may be maintained than would be safe for manual control. This compresses the area of highway necessary to transport these vehicles and ultimately increase the highway's vehicles/mile capacity.

Several approaches have been used to effect the longitudinal control. Due to the performance variations in individual vehicles caused by maintenance, weather or loading and the changing roadways (wind and topography), QFT seems a viable solution.



### Representation of the Dynamic Model

The simplified analog transfer function model for the throttle-torque response of the power plant is shown in Figure 1 (Morris 1983, Frank 1990).

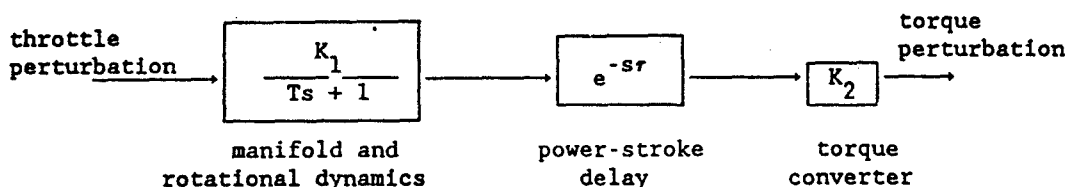


Figure 1. Block Diagram of Propulsion Plant

The Laplace representation of the force due to the propulsion system,  $F_d$ , is a first-order transfer function:

$$F_d = \frac{C e^{-sr}}{Ts + 1}$$

where  $C$ , the driving coefficient, is the product of the gains of the manifold and rotational dynamics and the torque converter. The variable,  $T$ , represents engine dynamics and  $r$  is the time delay inherent in the system.

The dynamic formula is the sum of the forces both internal and external, i.e. air drag,  $F_a$ , and gravitational force,  $F_g$ , exerted from an uneven terrain.

$$\Sigma F = F_d - F_a - F_g$$

where

$$F_a = C_a (V + V_w)^2 \text{sgn}(V + V_w) \quad (1)$$

$$F_g = m g \sin \theta \quad (2)$$

In equation (1),  $C_a$  is a function of the air drag coefficient, air density and vehicle frontal area. The variables,  $V$  and  $V_w$ , are the vehicular and wind velocity, respectively. Equation (2) is the horizontal component of the gravitational force which is the product of the mass,  $m$ , the gravity constant,  $g$ , and the sine of the angle of the road with respect to horizontal,  $\theta$ . The sum of the dynamic forces is shown in Figure 2.

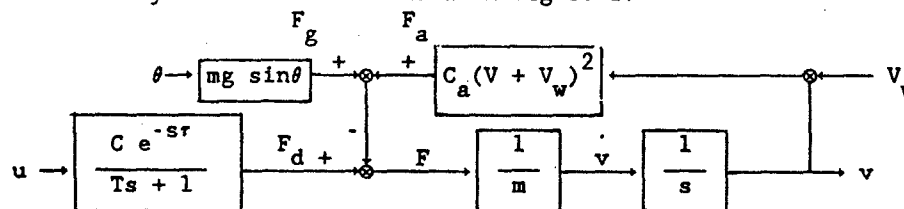


Figure 2. Dynamics Block Diagram

### Objectives

The purpose of longitudinal control is twofold:

- 1) To maintain a desirable speed (velocity)
- 2) To maintain a proper headway between vehicles (spacing)

These two objectives must be met during normal operation while rejecting disturbances such as gravitational forces and wind resistance (addressed in a future paper). Also special maneuvers such as speed changes or vehicles entering and exiting the platoon (entrainment) must be performed while still maintaining the desired speed and spacing. The performance of the controller is also limited by requirements of energy conservation and comfort over all speeds from 0-30 m/s (0-67 mph).

### Controller Design

There are two outputs, velocity and spacing, and therefore two controllers for this system. The one system is divided into two SISO systems where the speed regulating system is nested within the space controlling system, Figure 3.

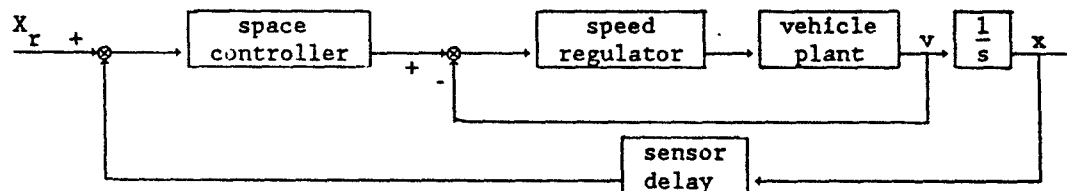


Figure 3. Control System Block Diagram

It is intended that there be a fast response to changes in velocity requirements while the outer loop should be slower so that it is less sensitive to changes in space between cars. This will allow a compression of the platoon when a hill is approached or when adjustments are made for the entrainment of another vehicle. Without this compression, the platoon might spread out during the process and thus use more highway area that could lead to a domino effect on following platoons.

### Speed Controller

The inner loop controls the velocity which is limited by the requirements for comfort and fuel economy, that is, no more than a .2g acceleration and a .2g/s jerk. In the case of a mid-sized car, this means a speed of response between 20 and 60 seconds with a maximum slope of  $1.5\text{m/s}^2$ . An overshoot of 10% is arbitrarily chosen with a steady state error of 5%. These constraints are shown in Figure 4.

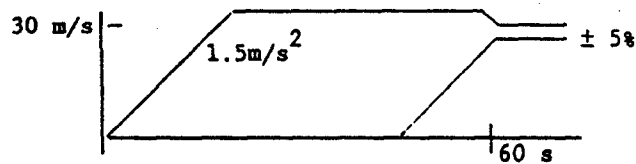


Figure 4. Constraints on Closed Loop Response

Using standard templates which lie within these constraints, the bounds are identified in the frequency domain about the approximate cut-off frequency,  $\omega_c$ , of .07, Figure 5.

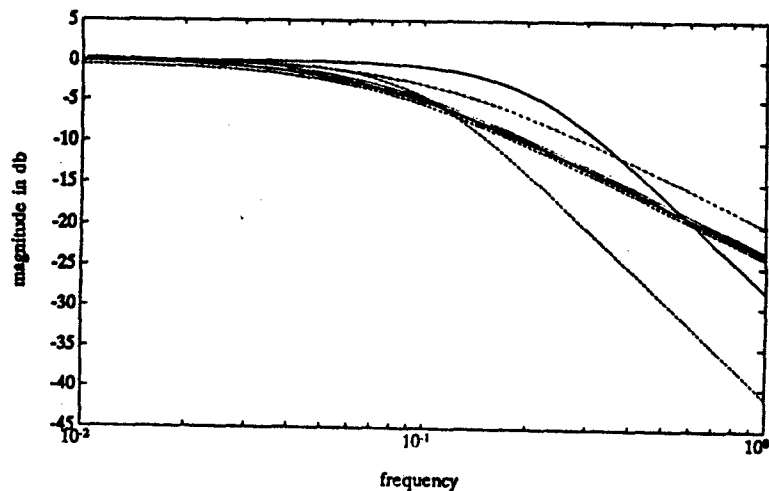


Figure 5. Frequency Response of Standard Templates Satisfying Constraints

The plant equation is:

$$\frac{V(s)}{U(s)} = \frac{F_d(s) + F_g(s)}{ms} \\ = \frac{\frac{C e^{-\tau} 1^s}{Ts + 1} + m g \sin \theta}{m s}$$

Since the time delay term is not multiplicative it cannot be transformed into a simple phase shift in the frequency domain. Being additive, it was necessary to substitute the second-order Pade' approximation, which introduced the effects of a non-minimum phase zero into the equations:

$$e^{-\tau s} = \frac{12 - 6\tau s + \tau^2 s^2}{12 + 6\tau s + \tau^2 s^2}$$

The parameter variations are:

$$T = 1 \text{ to } 2$$

$$\tau_1 = .3 \text{ to } .6 \text{ s}$$

$$m = 750 \text{ to } 1750 \text{ kilograms}$$

$$g \sin \theta = -.06 \text{ to } .06 \text{ grade}$$

Using these values to produce the Horowitz templates, the familiar QFT boundary curves are produced at frequencies 3 octaves above and below  $\omega_c$ .

Figure 6.

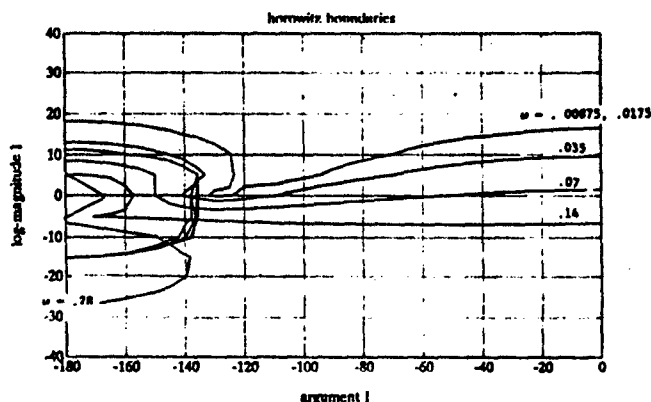


Figure 6. Boundary Curves for Speed Regulator

During this process, the zeros created by the time delay moved back and forth across the imaginary axis as the various parameters were varied. This had the effect of causing instability for which it was impossible to compensate, that is, the critical circle moved across the Nichols Chart as in Figure 7. Since this is inherent in the plant, it meant that certain vehicles were unable to perform at specific loads, on specific grades with this time delay. Although in this application, this is a more concern of the auto designer than the control engineer, it did give some insight into how a sensor with a similar time delay, as in the case of the outer space regulating loop, may effect stability and that is a concern of the control designer. For this application, the workable curves of Figure 6 were obtained by putting a smaller load variation, i.e. those given.

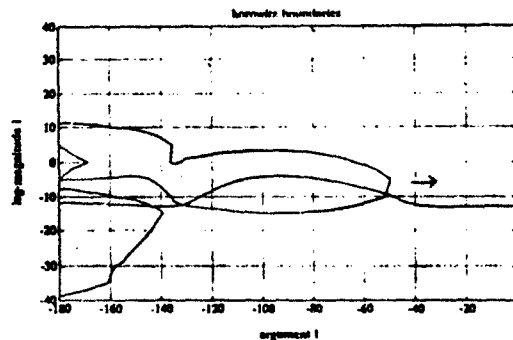


Figure 7. Instability Caused by Varying Parameters

Using the curves produced in Figure 6, a compensator,  $G_c(s)$ , was designed to bring the return ratio to a close proximity to the bounding curves.

$$G_c(s) = \frac{.32 (s + .02)}{(s + .05)}$$

The resulting bode plots were obtained by varying the parameters over the compensated plant with feedback,  $H(s) = 1$ , Figure 8.

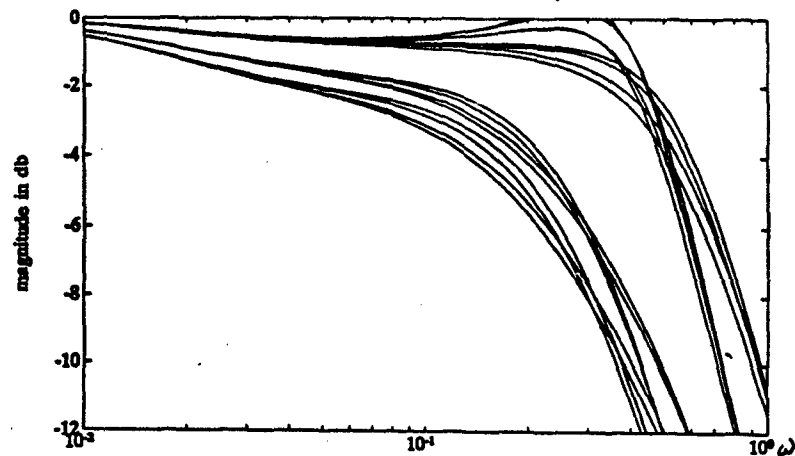


Figure 8. Bode Plots of Compensated Plant

A precompensator,  $P(s)$ , of  $.16/(s + .15)$  further shaped the curves to align within those templates of Figure 5. The step response for the velocity controller is shown in Figure 9.

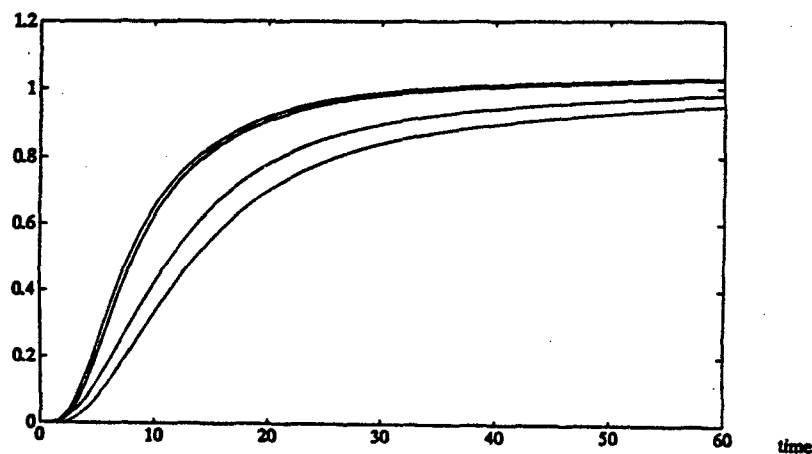


Figure 9. Step Response of the Speed Controller

### Space Controller

The outer loop controls spacing between vehicles. The spacing information is obtained by a radar mounted on the front of the autos. This necessitates a rather lengthy time delay which appears in the feedback loop. For this application, the Pade' approximation for  $e^{-s\tau}$  is again used, this time in the feedback loop. The time constraints on the space controller are not rigorous, due to the desire for a slow response time to allow for compression of the platoon during operations such as entrainment or approaching a hill. A response time 4 times slower than the velocity controller, 240 seconds, achieves this spring effect in the platoon. An overshoot of 10%, and a steady state error of 5% is arbitrarily chosen. Such a large steady state error is appropriate since a "spacing policy" for each vehicle based upon their mass and performance. This "spacing policy" determines the target position for the spacing controller and allows a safety margin.

Again in the method of QFT, frequency constraints were determined from the time constraints in which appropriate standard templates lie. The  $G_p(s)$  equation for the outer loop was the entire closed loop compensated transfer function of the inner loop. The Horowitz boundaries were calculated using

this new  $G_p(s)$  convolved with the feedback function,  $H(s) = e^{-s\tau_2}$  to obtain the return ratio,  $L(s)$ . The four parameters of the inner loop were again varied, with the additional one of  $\tau_2$ , which varied from .05 to .2 seconds.

Due to the difference in response times between the two loops, the boundaries for all the frequencies 3 octaves below and above  $\omega_c$  were closed curves such that the critical curve was the only consideration. Because there were no boundary restrictions except for stability, it was only necessary to compensate with a simple gain of .01778 to obtain Bode plots which lie within the appropriate area within the frequency domain. Figure 10 shows the step response to the outer loop (no precompensator was necessary).

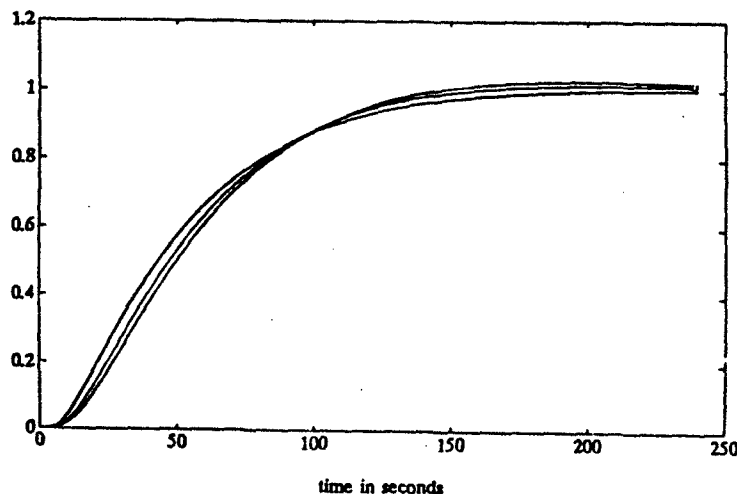


Figure 10. Step Response of the Space Controller

### Conclusion

The disparity in the response times between the inner loop and the outer loop trivialized the outer loop. However, in real practice, it may be found that the outer loop may need both a faster response time and a longer time delay. (It may take longer than .2 seconds to determine the space between two moving vehicles.) In that case a balance between the two loops may be harder to achieve. Also one controller that may substitute for these two must be designed in the case of loss of either feedback loop. With this design, when the inner feedback loop is opened, the space controller causes the vehicle to become wildly unstable in which an accident is entirely probable. The QFT method has proven as a method of design and stability analysis that could be implemented in all these cases.

This is just a beginning design which, to become workable, must be considered in the MIMO case. The speed controller must have an external input from a traffic controller,  $V_r$ , for the reference. The space controller must have not only information about the space between vehicles but needs velocity data from the car in front,  $V_f$ , to determine what change in velocity will effect a spacing between them, making this a tracking problem. Without considering such things as emergency stopping, etc. there are at least two inputs and two outputs. In any future practical application, the MIMO case must be considered.

### References

1. California Senate Office of Research, Meeting the Challenge of California's Growth, 1991.
2. Morris, R.L., Borcherts, R.H., Warlick, M.V., Hopkins, H.G., Spark Ignition Engine Model Building, Int. J. of Vehicle Design, 1983.
3. Frank, A.A. Longitudinal Control Concepts for Automated Automobiles and Trucks Operating on a Cooperative Highway, submitted to SAE, 1990.
4. Horowitz, Issac. Survey of Quantitative Feedback Theory, Int. J. Control. vol.53, no.2, 1991.
5. Horowitz, Issac. Appendix on Loop Shaping, unpublished 1992.
6. Brewer, John. "Notes on Feedback Control Theory". unpublished 1992.
7. Freudenberg, J.S., Looze, D.P., "Frequency Domain Properties of Scalar and Multivariable Feedback Systems", 1988 Springer-Verlag, New York.

# MULTI-INPUT MULTI-OUTPUT FLIGHT CONTROL SYSTEM DESIGN FOR THE YF-16 USING NONLINEAR QFT AND PILOT COMPENSATION

R B Miller\*, I M Horowitz\*, C H Houppis\*, and F Barfield\*\*

## 1. Introduction

This paper asserts the validity and value of both nonlinear (NL) QFT and man-in-the-loop modelling to the application of aircraft (A/C) flight control system design. Nonlinear QFT is basically a standard linear QFT design with the exception that the NL characteristics of the plant over the desired range of operation are included in the range of plant uncertainty. In previous work [5], NL QFT was used for a single-input single-output (SISO) design that developed a technique to design pilot compensation for tracking tasks with the goal of reducing the pilot's workload. This workload reduction provides the pilot with the opportunity to focus maximum attention on mission accomplishment as opposed to simply maintaining stable flight. This technique was applied and validated for a NL SISO design for the YF-16 A/C. This paper presents a multi-input multi-output (MIMO) design on the same plant [6].

## Assumptions, Scope, and Standards

The assumptions utilized are: 1) Only the modelled inputs are of interest for final performance, and 2) All inputs and outputs are Laplace transformable. Assumption #1 is required to reduce the workload involved with the design. A sufficiently large number of inputs are used to ensure that this is a reasonable assumption. The second assumption does not place any real limitations on the analysis since Laplace transformability requires only that either (1) the function is smooth, continuous and bounded, or (2) the function is unbounded and there exists a  $\delta$  such that  $\int_0^t f(t)e^{-\delta t} dt$  exists. This flight control problem involves the design of a pitch and roll control system for the YF-16. The plant model is a 6-DOF NL FORTRAN simulation. For this design the only independent commanded controls are symmetric horizontal tail (elevator) and aileron deflections. The simulation includes rudder and leading edge flap compensation which were left intact. The rudder controls are required for lateral stability, but the decision to leave in the flap controls is rather arbitrary. As long as the design model is the same as the simulation model, treatment of additional control surfaces is not a significant issue. Response specifications are based on guidelines presented in MIL-STD-1797A, *Flying Qualities of Piloted Aircraft*.

## Approach

Nonlinear QFT is used to design a 2x2 flight controller whose outputs, elevator and aileron command, are used to control  $C^*$  and roll rate,  $p$ .  $C^*$  is a blend of normal acceleration and pitch rate as felt at the pilot station, given by  $C^* = N_{zp} + 12.4q$ . The design is based on obtaining satisfactory responses for step commands in both  $C^*$  and roll at the two flight conditions 0.9 mach, 20,000 feet (0.9M,20K) and 0.6M,30K. The maximum commands on which the design is based are 2.2 g's for  $C^*$  and 30°/s for roll rate.

**Inner Loop Design.** The inner loop design consists of the development of the stability augmentation system (SAS) compensator, designated G in Fig. 1.1. For this design, G and F are 2x2 diagonal transfer function matrices. The compensator, G, stabilizes the A/C and ensures appropriate outputs to pilot inputs. The prefilter F is developed following the completion of the SAS compensator, for simulation and verification of the inner loop design.

**Pilot Compensation.** The outer loop design consists of choosing a pilot compensation filter,  $F_p$  in Fig. 1.2, to provide satisfactory system response with minimal pilot work load. The outer loop design is based on the Neal-Smith (NP) pilot model of Eq. (1.1) which consists of a gain, a time delay, and a first order filter. The basic

$$K_p e^{-\tau_p s} \left( \frac{\tau_p s + 1}{\tau_p s + 1} \right) \quad (1.1)$$

design strategy is to model the pilot by parameters which have been shown to result in satisfactory pilot ratings [8:10,15], and synthesize pilot compensation that results in the appropriate system response while it is being driven by these optimal pilot characteristics. Thus, the pilot model simulates an actual human pilot in the loop, "flying" the system in a manner which he considers to be acceptable. Designs which do not consider the pilot may be capable of producing the appropriate A/C responses, but if the pilots do not like the way they "feel", time consuming and expensive modifications must be made. These modifications can be avoided by the development of a design technique that considers the pilot-aircraft interaction in the early design phase so that the completed product is always satisfactory to the pilots.

\* Air Force Institute of Technology

\*\* Flight Dynamics Directorate, Wright Laboratory



**Simulation.** A linear inner loop MATRIXx simulation is performed, followed by a full NL simulation on a VAX with the FORTRAN YF-16 simulator. Comparison of the two simulations indicate the validity of the equivalent LTI design models. Finally, the outer loop design is simulated on the NL FORTRAN simulator.

**Equivalent Linear Time Invariant Plant Models.** A set of equivalent linear time invariant (LTI) plant models that rigorously represent the NL plant are generated by a MATRIXx program [6] based on Golubev's method and extended to the MIMO case. This program, given an input-output time history of a 2x2 plant generates an equivalent LTI transfer function set that represents the NL plant used to generate the time history. This equivalent plant is valid for the specified inputs only. Thus, given a NL model, by generating input-output time histories for all realistic inputs into the plant, a set of equivalent LTI transfer functions  $\mathcal{P}_e = \{P(s)\}$  are developed that represent the single NL plant. This set of plants represents the parameter uncertainty for which the QFT design method was developed, and includes the NL effects of the plant. It has been proven that for a very large problem class the solution to the  $\mathcal{P}_e$  uncertainty problem is guaranteed to solve the original NL uncertainty problem [4].

#### *Generation of Equivalent LTI Plants*

Both the Golubev technique for SISO systems (SISOTF) and the modified technique for MIMO systems (MIMOTF) are implemented in MATRIXx. These programs have been significantly tested with known transfer functions, and give excellent fits. Fits for all of the actual equivalent transfer functions used in the design and their errors are shown in App. B of ref [6].

The YF-16 simulator is used to generate sets of input-output time histories for plant generation, which utilizes the full NL six degree of freedom equations of motion. The original simulator control system is significantly modified to ease the task of filling the response envelopes. Since this design is limited to a 2x2 system, 1) the original rudder and leading edge flap controls are left intact, and 2) the connections to the elevator and ailerons are broken and controlled independently of the original control system. The use of pure gain compensators as shown in Fig. 1.3 results in tight loops whose outputs are very similar to the commanded inputs, which makes it a relatively simple task to fill the desired response envelope. Additionally, since the gains  $K_c$  and  $K_p$  do not affect the equivalent plant, they can be altered from run to run. During the simulator runs, surface commands to the actuators (inputs) and A/C responses (outputs) are recorded. These input-output histories are used with MIMOTF to generate a set of equivalent LTI plants which represent the A/C for the full range of desired responses.

The inputs used for plant generation are  $\delta_{c\text{cmd}}$  and  $\delta_{a\text{cmd}}$  (see Fig. 1.3) while the outputs are  $C^*$  and  $p$ . Notice that the elevator and aileron trim values are not included in the plant input as far as linear plant generation is concerned. Theory requires that the inputs used for equivalent plant generation should include only the inputs which are directly responsible for the obtained outputs [3]. In the case of  $C^*$ , the addition of the trim value is enough to make the input appear as a negative step, which results in stable plants for the YF-16's longitudinal axis. Since this axis is well known to be unstable, these plants obviously cannot be equivalent to the actual system. Fig. 1.4 clarifies the difference in the plant generation with and without including the trim value. In the figure, "delta  $\delta_c$ " represents the change in elevator only (no trim), and " $\delta_c$ " includes the trim value. Note that when the trim value is included, the input looks like a negative step with significant overshoot. A relatively slow, stable transfer function can easily be matched to the resulting input-output pair. Without the trim value right half plane poles (rhp) are required to match the input output pair, as is expected for a longitudinal F-16 transfer function. Note that the plant used in this design is defined with the original rudder and leading edge flap compensation in place, and open-loop simulations verify that the leading edge flap compensation is not sufficient to stabilize the longitudinal axis.

For the  $C^*$  loop, an interesting technique is used to drive the system to the desired output set. Since the system outputs closely resemble the commanded inputs, weighted averages of the response envelope are used to drive the system. As a result, the response envelope is filled rather nicely. Problems are encountered in determining equivalent plants for most of the cases with overshoot and no undershoot that do not violate the requirements of (qii) having no phase uncertainty at infinity. Therefore, those responses are not used in the design. Instead, underdamped responses which contain both undershoot and overshoot are used to fill the upper area of the response bounds. For the roll rate responses, the driving inputs consist of filtered steps of varying speeds formed in MATRIXx, and the step responses of those filters used as inputs to the roll channel. A total of 22 equivalent LTI plants are developed for the design using MIMOTF with actual simulator responses. These plants represent the A/C at the two flight conditions 0.9 M, 20,000 feet and 0.6 M, 30,000 feet. The maximum commands are 2.2 g's for  $C^*$  and 30°/s for roll rate. At the second flight condition (FC), the system reaches moderately high angles of attack up to approximately 15°. These system responses enclosed in their respective bounds are shown in Fig. 1.5, and the plant transfer functions are given in App. A of Ref [6]. Note that the original thumbprints were somewhat less severe, but are tightened around the achieved responses to provide for a more stringent test on the design.

#### *Cautions and Pitfalls*

The generation of equivalent plants for the MIMO problem requires an additional consideration. For a response of the form  $y_1 = y_{11} + y_{12}$  there exists an infinite number of solutions because of the addition involved. It is not

sufficient, however, to get a good fit on only the response  $y_1$ , but is also important to accurately model the individual components  $y_{11}$  and  $y_{12}$ . In the NL problem, superposition does not apply, and the individual components of the response are not available. To ensure that the individual elements of the equivalent plant matrix are correctly weighted, the inputs are staggered by one second. That is, for each set of commanded inputs, one is commanded at time  $t = 0$ , while the second input is not applied until  $t = 1$ s. Some runs have  $C^*$  first, while others have  $C^*$  as the delayed response. The delay is applied to each of the variables with the intent that the range of plant uncertainty includes the case of simultaneous responses. This staggering effect forces MIMOTF to reasonably weight the individual components of the response since during the first second one of the inputs is zero and there exists a substantial response on only one of the outputs. An analysis of the individual components of the responses of the generated plants when simulated with the input with which they were derived, shows them to all be reasonable at least for the majority of the run. In some plant cases, toward the end of the run the individual components of  $y_{11}$  and  $y_{12}$  begin to diverge in opposite directions with a cancelling effect. In reality [2], the control system forces the plant input to contain rhp zeros to exactly cancel the rhp poles of the plant, so this apparent divergence from reality is not necessarily a real problem. In some cases, the "equivalent" plants are only valid for the first 80 or 90% of the run. Three second responses are considered to be sufficient for the desired outputs, but the plant generation runs are extended to five seconds to prevent premature divergence of the unstable longitudinal equivalent plants.

## II. Inner Loop Design

### Introduction

Since the designs are based on the equivalent MISO systems, in this section the term 'plant', or  $P$  refers to the equivalent MISO plant,  $q_{ij}$ . In both designs, overdesign is neglected and the only criteria considered is stability and the requirement for a maximum open-loop crossover frequency of 30 rad/s to ensure sufficient attenuation of structural modes. That is, maximum loop transmission is obtained while meeting the crossover and stability requirements. The reason for neglecting tracking and disturbance boundaries is that experience [2] suggests that the 30 rad/s crossover requirement is the dominant constraint, which means that a detailed QFT design to satisfy the tracking and disturbance requirements with minimum overdesign would result in higher crossover frequencies. The decision is made to design the roll rate compensator first because of lesser uncertainty present.

### Design Requirements

The requirements on the completed design are: 1) the time domain responses fall within the specified envelopes, 2) stability margins of 6 dB and 45° are maintained, and 3) a maximum crossover frequency of 30 rad/s is maintained for all plant cases. By obtaining maximum loop transmission, the tracking and disturbance requirements are automatically satisfied if they are obtainable. The expectation that the crossover requirement will be dominant is substantiated by the simulation results. Note that the increased loop transmissions are helpful for gust alleviation and robustness over a larger range of uncertainty.

### Templates

Templates which represent the entire plant uncertainty in the frequency domain are obtained for a set of frequencies [6] based on the appearance of the composite frequency response plots of Fig. 2.1. When little variation exists in the templates of a certain frequency range they result in very similar boundaries and only the most restrictive (highest frequency) need be drawn on the Nichols chart (NC). The plots of Fig. 2.1 provide insight into the characteristics of  $q_{11}$  and  $q_{22}$  that are worth mentioning. For instance, they bring out the fact that both  $q_{11}$  and  $q_{22}$  have an excess of one pole, since all cases have a final slope of -20 dB/dec. One case for  $q_{11}$  has a very large zero, and the -20 dB/dec final slope is not entirely obvious from the figure. Also,  $q_{11}$  contains two rhp poles in some cases, and only one in others. Since  $q_{22}$  has a -20 dB/dec final slope, indicating the one excess pole, but 270° of phase change, it can be noted that in all cases  $q_{22}$  contains one rhp zero.

### Loop Shaping

In order to minimize the complexity of the compensator  $G$ , the nominal plant is included in the loop transmission function  $L_0$  as shown in Eq. (2.1)

$$L_0 = GP_0 = \frac{K_m \left( \frac{s}{z_1} + 1 \right) \left( \frac{s}{z_2} + 1 \right) \dots \left( \frac{s}{z_m} + 1 \right)}{\left( \frac{s}{p_1} + 1 \right) \left( \frac{s}{p_2} + 1 \right) \dots \left( \frac{s}{p_n} + 1 \right)} = \frac{K \left( s^m + c_{m-1}s^{m-1} + \dots + c_1s + c_0 \right)}{\left( s^n + d_{n-1}s^{n-1} + \dots + d_1s + d_0 \right)} \quad (2.1)$$

By beginning the loop shaping with the nominal plant poles and zeros, the complexity of the compensator is reduced since  $G = L_0/P_0$ . Compensator poles and zeros are added to bring the loop down the edge of the stability bounds. A high frequency complex pair of poles is generally added at the end to provide maximum attenuation for high frequencies where the design model may no longer be valid.

### P Loop Compensator

The stability contour is determined by the required gain and phase margins. The 3 dB contour corresponds to a 45° phase margin, but to ensure the 6 dB gain margin requirement, it must be extended on the lower half. The designs are made in order to provide maximum loop transmission at all frequencies while meeting the stability and crossover frequency requirements. Since the template at 30 rad/s is 13 dB in magnitude and the nominal plant is located at the bottom of the template, the nominal loop must fall at -13 dB at 30 rad/s to guarantee a 30 rad/s crossover for all plant cases. The compensator  $g_p$  used for the final loop shape of Fig. 2.2a is

$$g_p(s) = \frac{-259.2(s + 4)(s + 25)(s + 30)}{s(s + 10)(s^2 + 140s + 30,625)} \quad (2.2)$$

### C\* Loop Compensator

The stability requirements for this loop are the same as in the roll channel, 3 dB and 45°. In this design the frequency response for  $q_{22eq}$  is identical to that of the original  $q_{22}$ , thus the second loop design is based on the original equivalent plants derived previously. The completed loop shape of Fig. 2.2b is achieved with the compensator

$$g_c(s) = \frac{-1665(s + 2)(s + 15)(s + 26)}{s(s + 10)(s^2 + 75s + 5,625)} \quad (2.3)$$

### Prefilters

Fig. 2.3 shows the frequency domain thumbprints with the frequency response for the completed inner loop design without prefilters. The prefilters,  $f_{11}$  for  $C^*$ , and  $f_{22}$  for roll rate are determined in the usual manner, and are respectively

$$f_{11}(s) = \frac{30(s + 40)}{(s + 4)(s + 300)} \quad f_{22}(s) = \frac{3.5}{(s + 3.5)} \quad (2.4)$$

The frequency response with prefilters are shown for both cases in Fig. 2.4. Note that in both cases the responses are adequately enclosed within the thumbprints.

## III. Simulation of the Inner Loop

### Introduction

A MATRIXx simulation with the equivalent linear design models, and a full NL simulation with the original FORTRAN simulator used to generate the design models are performed. The first simulation is used to validate the design, while the second is used to determine the validity of the design models. Also, modifications made to the roll compensator to improve the NL performance are detailed.

### Linear Simulations

**C\* Linear Simulation.** The first linear simulation is that of the  $C^*$  compensation with the equivalent LTI design models via MATRIXx system build. For the linear simulations, the response is independent of the input magnitudes and only unit step simulations are performed. The linear simulation of all plant cases is shown in Fig. 3.1. The responses are all predominantly within the bounds with only minor excursions toward the end of the run. These excursions are from the plants at FC 2 and are due to small complex zeros in the linear plants. These zeros result in nearby closed-loop poles with very large time constants and small residues. These linear responses are judged to be satisfactory, and the simulation phase is continued.

**Roll Linear Simulation.** The roll channel unit step responses are also shown in Fig. 3.1. In this case, more pronounced boundary violations are noted. A small, oscillatory component of the time response prevents the responses from being completely enclosed within the bounds. Note that these oscillations are present only in the cases of FC 2. A look at the Bode plots of  $q_{22}$  (Fig. 2.1) at these conditions indicate a peak at approximately 2.5 rad/s. An inspection of the  $q_{22}$  transfer functions reveals the existence of a pair of complex poles and zeros in this frequency range that nearly cancel, but not completely. Since the final objective is the NL response, the linear simulation is considered acceptable and the NL simulation performed. Note that the roll compensator was modified to the form of Eq. (2.2) following the NL simulations and these simulations are based on an earlier version [6].

### Nonlinear Simulations

**Nonlinear Simulation of the SISO Systems.** First, NL simulations are performed on each channel separately. As opposed to the linear simulation where simple step commands are sufficient simulations, the NL system must be evaluated with commands of varying magnitudes. For the SISO  $C^*$  simulation,  $C^*$  is commanded from 1 to 5 g's at each FC for a total of 10 runs. The response on roll rate for the SISO  $C^*$  simulations is essentially zero for all cases. The SISO simulations for roll rate consist of step commands from 10 to 40°/s in increments of 10°/s. In these simulations, the  $C^*$  response is negligible. The normalized responses enclosed in the thumbprints are shown for both cases in Fig. 3.2. Both sets of responses are completely satisfactory.

**Nonlinear MIMO Simulations Over the Design Range.** The true test of the NL design consists of simulations over the range of input magnitudes on which the design is based. As mentioned earlier, it is essential that in the

equivalent plant generation phase, equivalent plants are generated for the full range of desired outputs. Figure 3.3 shows the normalized responses of the NL plant over the full range of input magnitudes on which the design is based. The only significant boundary violations are in the roll rate response, and are similar to those of the linear simulation. Before attempts are made to eliminate these boundary violations, the NL system is simulated over a wider range of input magnitudes to provide additional insight into corrective measures. The results of those simulations can be found in Ref [6]. The roll rate responses show troublesome oscillations very similar to those seen in the linear simulation, but they are somewhat more pronounced. Again, the only problem responses are at the second FC, 0.6M, 30K, and the oscillations get progressively worse as the commanded magnitude grows from the original design range. The frequency of oscillation is approximated to be between 2 and 5 rad/s. This value is consistent with the peaking of the Bode plots of  $q_{22}$  at 2.5 rad/s discussed previously. One attempt to eliminate this oscillation is to include an exact cancellation of the troublesome pair of complex poles and zeros of the nominal plant ( $q_{22}$ ). This additional compensation eliminates the upper violations in the response, but oscillations are still present and significant 'dips' are present before the response reaches its final value. The most obvious solution to the problem is to increase the loop transmission in this frequency range. A second look at the loop shape of the completed roll loop shows that increased loop transmission can be obtained in this critical frequency range without violating the 30 rad/s crossover requirement by the implementation of the modified compensator given by Eq. (2.2). Simulations of the roll system with this modified compensator at 0.6M, 30K over the original design range are shown in Fig. 3.4. The  $C^*$  responses are virtually unchanged from those with the original roll compensator. The resultant responses are located predominantly within the bounds, but could stand improvement.

In designing a fixed compensator, it is expected that there be a trade off in quality of performance at the various parameter values. By examining the templates for both loops, it is apparent that superior performance is obtained at the first FC. In both cases, the responses at the first FC are predominantly located at the top of the templates, implying a higher loop transmission for that condition. The general appearance of the template for  $p$  at 30 rad/s is shown by Fig. 3.5, where points marked by 'o's are for 0.9M, 20K, and 'x's represent responses at 0.6M, 30K. In order to design a fixed compensator, the specified criteria must be met for all cases. Therefore, the loop transmission for the plants represented by the bottom of the template is always less by the height of the template at any given frequency. Hence, there is a trade off between the use of a fixed compensator and optimal performance for all parameter values. The constraining criteria in this design is the 30 rad/s open loop crossover requirement, resulting in lower loop transmission in that vicinity of approximately 13 dB for roll rate, and 12 dB for  $C^*$ . Note that in a case such as this where the two flight conditions represent the extreme ends of the templates, scheduling of the compensator gain could be used to provide comparable loop transmission for all cases. An additional 7 dB of gain in the roll channel, and 3 dB in the  $C^*$  channel, for the second FC results in the responses of Fig. 3.6 for the extended simulation range. With gain scheduling, the gain values used for Fig. 3.6 can be achieved without violating any of the design specifications. Additional simulations would be required for this scheduling to determine whether the dominant factor causing this separation is velocity, altitude, or a combination of the two.

**Additional Simulations.** Additional NL simulations are given in App. C of Ref [6]. Included are the full A/C outputs and surface deflections for: 1) simultaneous pitch and roll commands for a few of the cases of Fig. 3.4, 2) roll out of a coordinated turn, and 3) a  $120^\circ/s$  roll command from straight and level flight.

#### Summary

This section presents both linear and NL simulations of the compensated inner loop. There are strong correlations between the two simulations, indicating that the equivalent LTI plants are at least reasonable. There are some coupling effects between the two outputs that can not be overcome with fixed compensation, but a gain scheduling option is suggested which can result in satisfactory responses over the entire design range and beyond without violations in any of the system requirements.

### IV. Pilot Compensation

#### Introduction

This section describes the development of the Pilot Compensation filters,  $f_{pc}$  and  $f_{pp}$  shown in Fig. 4.1 to augment or replace the prefilters  $f_{11}$  and  $f_{22}$ . The purpose of this pilot compensation is to reduce the pilot's workload while ensuring acceptable responses. Essentially, the technique is to model the pilot with parameters known to give good pilot ratings and design the pilot compensation such that it shapes the responses to their desired forms. Note that the darker lines in Figure 4.1 represent feedback paths which are not physically connected. Kobylarz [5] designed pilot compensation based on a single equivalent plant of the designed inner loop. This paper considers an equivalent plant set as in the inner loop design to shape the loop to ensure satisfactory response over a range of flight conditions, but the pilot compensation is designed as two independent SISO systems. That is, when equivalent plants for the  $C^*$  inner loop are generated, the roll command is zero and vice versa. The decision to synthesize the pilot compensation in this manner is based solely on time constraints, and the method used for the MIMO SAS design can be used for pilot compensation with the only difference being the requirement for more plants and the conversion to the MISO equivalent loops.

Criteria for pilot in the loop pitch response is fairly well defined and can be found in the NS report [7] as well as MIL-STD 1797A. Criteria for roll response, however is very limited. Therefore, an approach very similar to the one used by Kobylarz is used for the longitudinal compensator, and a new approach is introduced for the lateral design. Because of the differences in the two designs, they are presented separately.

#### Plant Generation for Pilot Compensation

After the inner loop designs are completed, SISOTF is used to generate a new set of equivalent LTI plants that represent the closed inner loop system as shown in Fig. 4.2. Plants are generated for  $C^*$  commands of 1, 3, and 5 g's at 0.9M, 20K, and 1 and 2g's at 0.6M, 30K. For the roll channel, plants are generated in  $10^\circ/s$  increments from 10 to  $30^\circ/s$  at both flight conditions. Templates representing the magnitude and phase uncertainty are then generated for both loops as in the inner loop design. The uncertainty has been considerably reduced by the inner loop design, thus templates are required for moderate and high frequency regions only.

#### Pilot Model

Since the ideal pilot input is one of pure gain [8], the pilot model used in the design includes only the inherent time delay and unity gain. The selection of unity gain is somewhat arbitrary, because the total gain of the inner loop is given by the product of the pilot gain and the respective compensator gain. Hence, any value of pilot gain could be achieved from the designed system by adjusting the compensator gain such that the total gain is the same as that of the original compensator. For instance, if the optimal pilot gain for a certain application is 2 instead of 1, the compensator should be implemented with half the gain determined from the design process.

#### Longitudinal Pilot Compensation

The NS report [7] clearly lays out frequency domain characteristics for closed loop  $C^*$  response that result in satisfactory pilot ratings. Specifically, the report calls for a closed loop bandwidth of 3.5 rad/s and a maximum of 3 dB of droop for  $\omega < \omega_{BW}$ . The report defines the closed loop bandwidth as the frequency at which the closed loop response has a phase lag of  $90^\circ$ . The final specification is for maximum closed loop resonance of 3 dB. These criteria are readily displayed on the NC of Fig. 4.3. Pilots of the NS study generally preferred responses with overshoot but no undershoot so that the droop for  $\omega < \omega_{BW}$  should be held as close to zero as possible [5]. The frequency criteria of Fig. 4.3 can be modified by manipulating the templates around them in order to develop a new set of bounds as in the QFT technique so that by satisfying the modified bounds with the nominal loop the criteria would be met for all plant cases. Instead, because the templates are very small in the frequency range of primary interest, the decision is made to shape the nominal loop based on the original criteria, with the templates occasionally being placed over the nominal loop to ensure that no plant case violates the specified requirements.

The synthesized longitudinal pilot compensator,  $f_{pc}$ , is given by

$$f_{pc}(s) = \frac{55(s+7)^2(s+300)}{s(s+40)(s^2+100s+10,000)} \quad (4.1)$$

where one of the poles and zeros cancel a pole and zero from the original prefilter derived previously. Therefore, the total outer loop compensation is given by

$$f_c(s) = \frac{1650(s+7)^2}{s(s+4)(s^2+100s+10000)} \quad (4.2)$$

Note that in shaping this loop, the phase lag of the pilot model must be included. The compensated loop shape is shown in Fig. 4.4. Note that this compensation results in a slight violation of the bandwidth specification. The reasons for allowing this violation are given in the simulation results section.

#### Lateral Pilot Compensation

As mentioned earlier, specifications for closed loop roll specifications are somewhat limited. Guidelines are primarily limited to rise times and damping factors. MIL-STD 1797A (sec 4.5.1.1) indicates that rise times of the roll rate response between 0.33 and 1s generally result in satisfactory pilot ratings. Barfield [1] has indicated that desirable roll rate responses have high damping factors. Since the purpose of this design is to introduce pilot compensation techniques, and not to meet a prespecified set of requirements, the decision is made to adopt a general criteria of

- 1)  $0.33 < T_R < 1.0$ , and
- 2)  $0.8 < \zeta < 1.0$

The first step in the synthesis technique is to develop simple-second-order transfer functions which exhibit the desired closed loop response. For this design, four transfer functions are used, representing the four extremes of damping factors and rise times, given by

$$\frac{5.29}{s^2 + 3.68s + 5.29} \quad \zeta=.8, TR=1 \qquad \frac{56.25}{s^2 + 12s + 56.25} \quad \zeta=.8, TR=0.33$$

$$\frac{10.24}{(s^2 + 6.4s + 10.24)} \quad \zeta=1, TR=1 \qquad \frac{100}{(s^2 + 20s + 100)} \quad \zeta=1, TR=0.33 \quad (4.3 \text{ a-d})$$

If these transfer functions are designated  $M_T(s)$ , then it can be easily derived from Figs. 4.1 and 4.2 that

$$M_T(s) = \frac{L(s)}{1 + L(s)} \quad (4.4)$$

where  $L(s) = e^{-sT} L_1(s)$ .  $L_1$  represents the desired transfer function of the closed inner loop plus compensation. Solving Eq. (4.4) for  $L_1$  (including the closed loop effect of the pilot's delay) gives

$$L_1(s) = \frac{M_T(s)}{1 - e^{-sT} M_T(s)} \quad (4.5)$$

The next step is to plot the frequency response of  $L_1(s)$  for all cases in Eq. (4.3) on a NC. It is reasonable to expect similar time responses from any system which has a similar Nichols plot [2]. Therefore, by using the four cases of  $L_1$  as an approximate set of bounds, the open loop Nichols plot can be directly shaped to develop the pilot compensation which results in the desired response. Again, the templates are used to ensure that the resultant loop falls within the desirable range for all plant cases. Note that in this case, the phase lag of the pilot model has already been accounted for in  $L_1$ , and it is not included in the loop shaping process. The four "bounds" are shown in Fig. 4.5. Because of the radical behavior of the faster response models, the decision is made to emulate the slower response models. It is noted from the bounds, that larger damping factors tend to move the Nichols plot to the right, and that higher loop transmission correlates with faster responses. The compensated loop is therefore shaped to be similar in shape to the slower bounds, but to the right of the left-most bound with slightly higher loop transmission to get a response reasonably within the chosen specs. The designed lateral compensator is given by

$$f_{pp}(s) = \frac{0.314(s + 6)}{s(s + 5)} \quad (4.6)$$

In this case, the roll prefilter designed previously is cancelled out, so Eq. (4.6) represents the complete compensator,  $f_p$  for the roll system outer loop. The completed loop shape with this compensation is shown in Fig. 4.6.

#### *Simulation of the Pilot Compensation*

The only simulations performed on these designs are with the actual NL simulator. Originally, the fourth order Pade' approximation for the pilot model is used in the simulations. However, simulations with the designed compensator and pilot model shows periodic peaking after the response has appeared to be settled down. This peaking effect is shown in Fig. 4.7. Extensions on Kobylarz's simulation of Fig. 6.8 [5] to eight seconds showed the same problems as are experienced with this design. After the Pade' approximation is replaced with a true delay, these peaks disappear. The normalized pilot in the loop simulations are given in Fig. 4.8. The  $C^*$  responses are enclosed in the original bounds, but since the roll synthesis is based on a new set of general requirements those responses are displayed without bounds. The  $C^*$  simulations extend from 1 to 5 g's at 0.9M, 20K, and 1 to 3 g's at 0.6M, 30K, and the roll responses are from 10 to 30°/s at each FC. The  $C^*$  responses are clearly bounded by the original thumbprint, and contain overshoot without significant undershoot as desired [5]. It is difficult to obtain these desirable responses over both flight conditions while satisfying the bandwidth requirement of 3.5 rad/s. Attempts to satisfy the bandwidth requirement with fixed compensation result in at least one of the responses containing 10% or larger undershoot. As in the design of the inner loop, gain scheduling can be used to provide the desired responses while meeting all specs. It is interesting to note that in this case, however, the second FC requires less compensator gain to give the desired response, which is the opposite of the case in the inner loop design. The roll rate responses have relatively high damping factors, but are slightly less than 0.8 for the responses at 0.6M, 30K. An equivalent second order plant fit with SISOTF indicates that the worst case corresponds to  $\zeta = 0.78$ . The settling times for roll rate are within the specified criteria, given by  $T_R = 0.81s$  at 0.9M, 20K, and  $T_R = 0.73s$  for 0.6M, 30K. In both loops, there is essentially one response form at 0.9M, 20K and a distinctly different response at the condition 0.6M, 30K. These differences indicate that even with the decreased uncertainty after closure of the inner loop the two flight conditions are significantly different. Additional pilot in the loop simulations are included in App. C of Ref [6], including simulations as the full MIMO system.

#### *Summary*

This section presents the pilot compensation techniques used in this design. The paper covers the entire design process, from method to simulation. Additional simulations and details are provided in App. C of Ref [6].

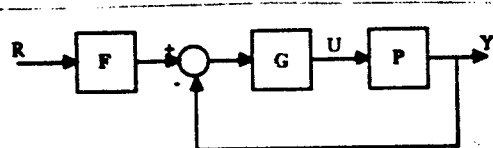


Figure 1.1. Closed Loop Control System

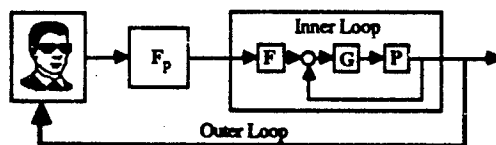


Figure 1.2. Closed Loop Control System Including Man in the Loop

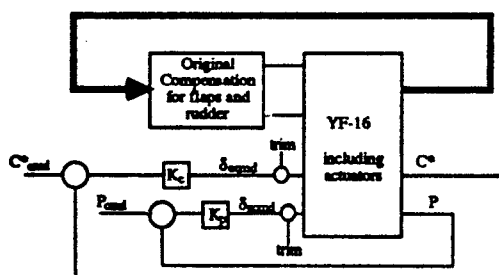


Figure 1.3. Modified YF-16 Simulator

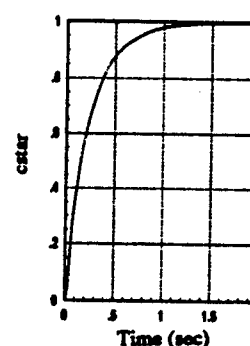
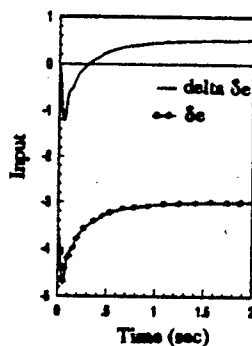


Figure 1.4. Effects of Including Trim

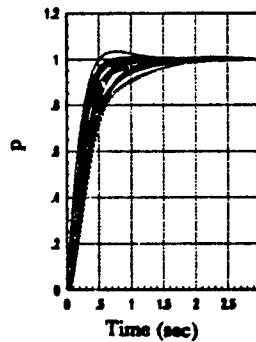
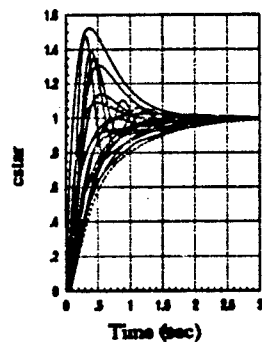


Figure 1.5. System Responses Used for Equivalent Plant Generation

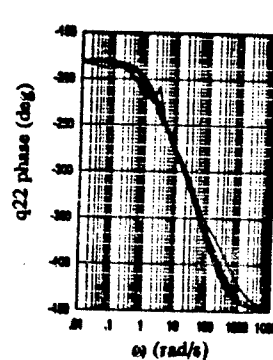
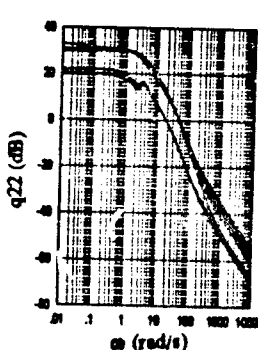
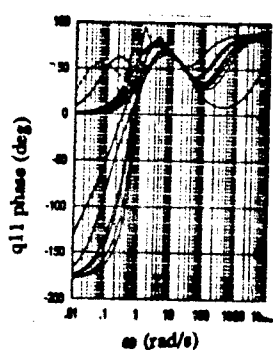
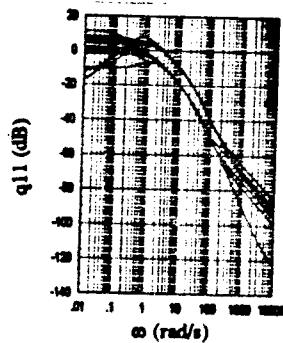
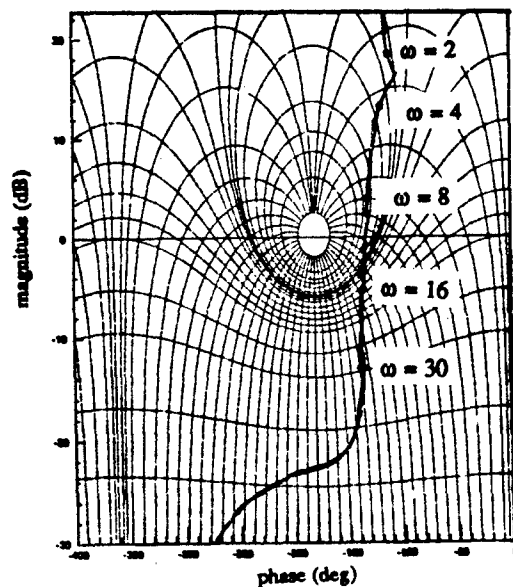
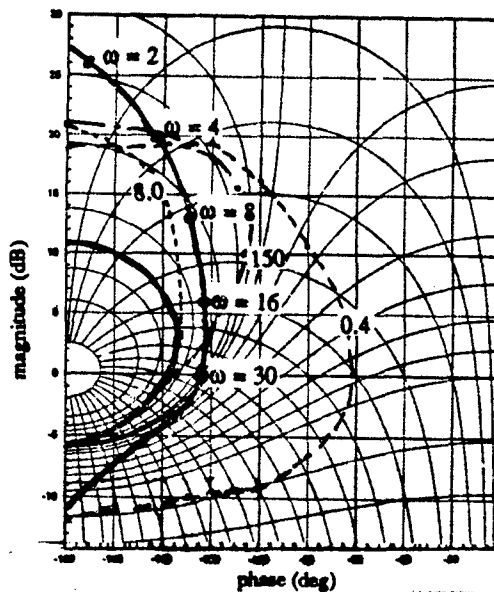


Figure 2.1. Uncertainty of the Uncompensated System



(a) Roll Loop



(b) C\* Loop and Stability Bounds

Figure 2.2. Compensated Loops

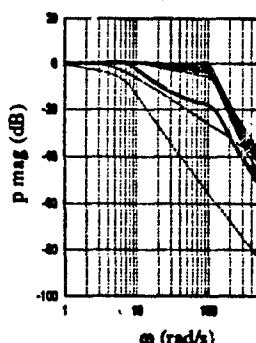
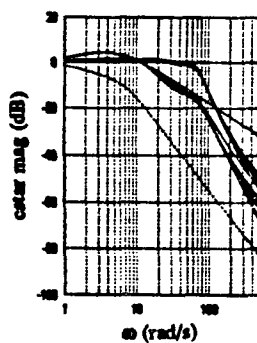


Figure 2.3. Compensated Responses Without Prefilters

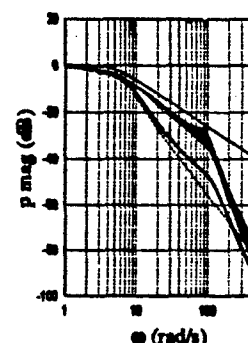
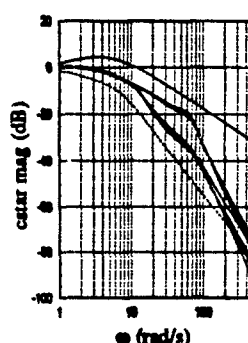


Figure 2.4. Compensated Responses With Prefilters

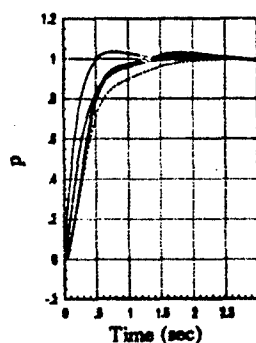
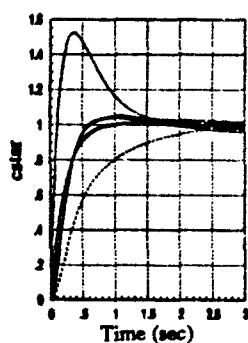


Figure 3.1. Linear Simulations of the Inner Loop

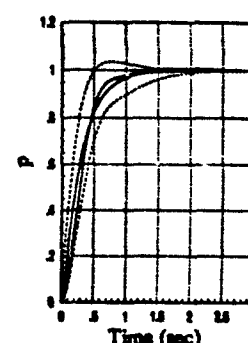
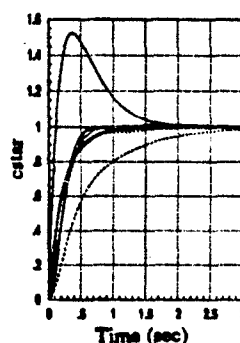


Figure 3.2. Nonlinear SISO Simulations of the Completed Design



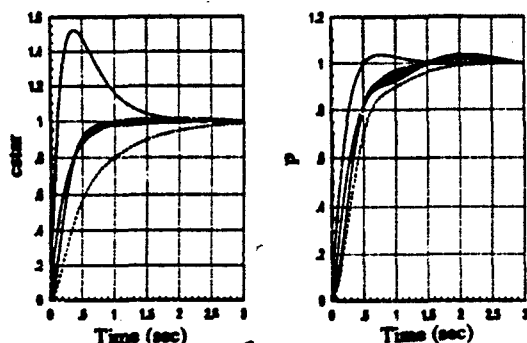


Figure 3.3. Nonlinear MIMO Responses Over the Design Range

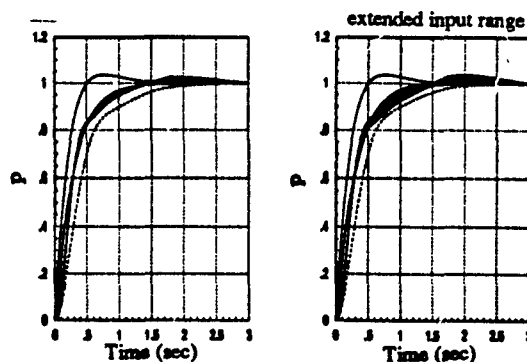


Figure 3.4. Nonlinear MIMO Simulation with the Modified Roll Compensator

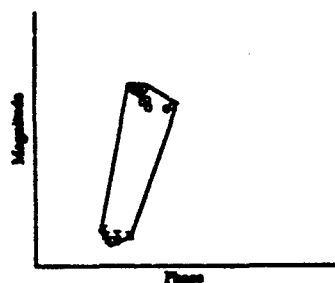


Figure 3.5. Template of  $q_{c2}$  at 30 rad/s

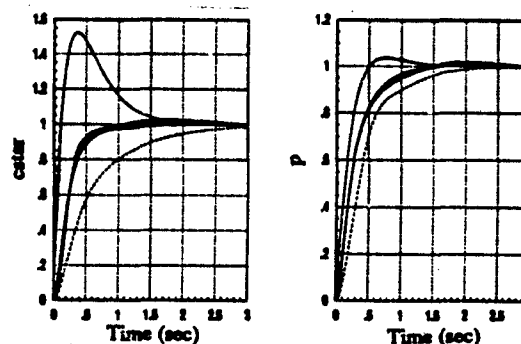


Figure 3.6. Nonlinear MIMO Simulations at 0.6M, 30K with Increased Gain

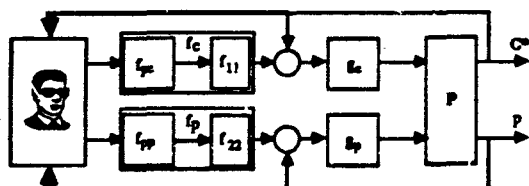


Figure 4.1. Closed Loop Control System Including Man-in-the-Loop



Figure 4.2. Equivalent Plants for Outer Loop Design

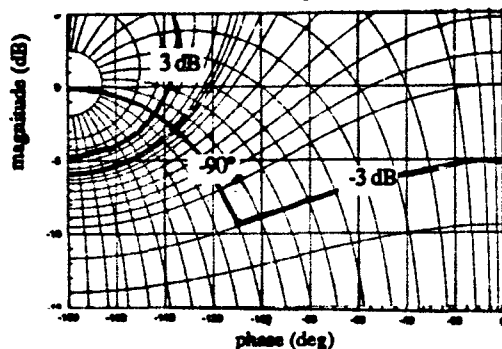


Figure 4.3.  $C^*$  Pilot in the Loop Criteria

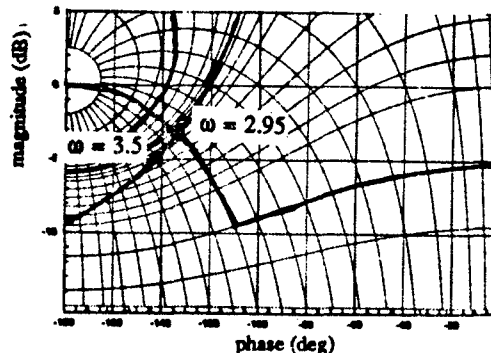


Figure 4.4. Compensated  $C^*$  Loop

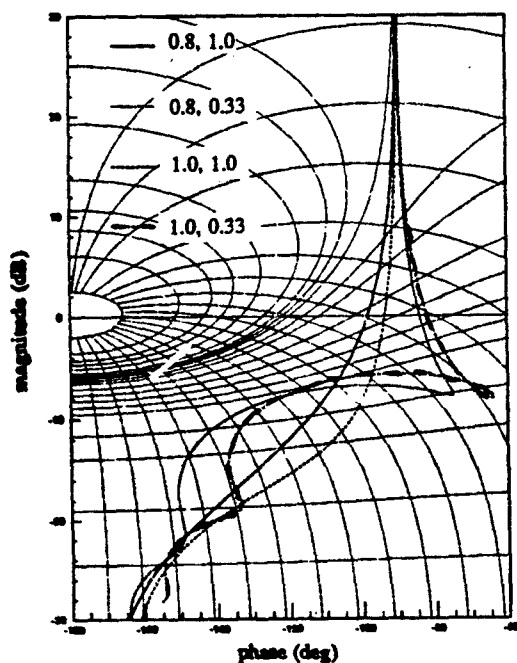


Figure 4.5. Pilot in the Loop Roll Criteria

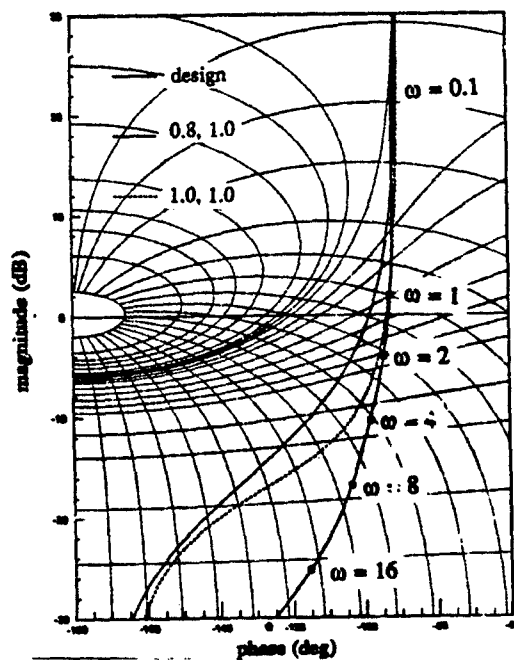


Figure 4.6. Compensated Roll Response

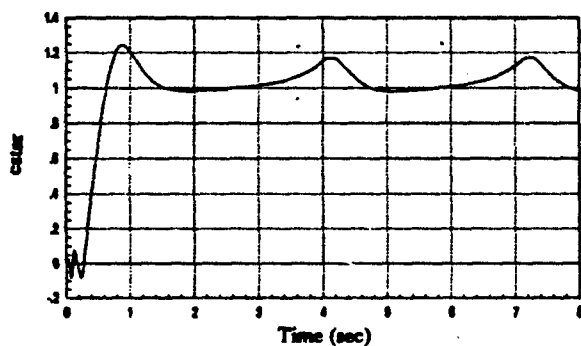


Figure 4.7. Problems Caused by the Pade' Approx

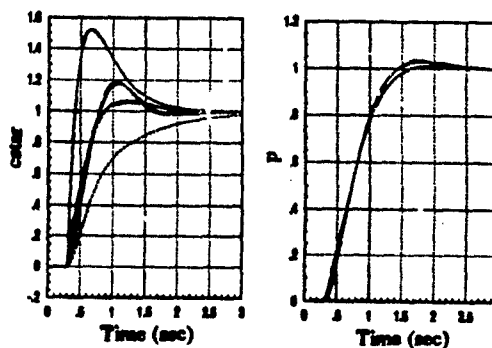


Figure 4.8. Pilot in the Loop SISO Simulations

#### Bibliography

1. Barfield, F. Head Control Engineer AFTI/F-16. Interviews. AF Flight Dynamics Labs, Wright-Patterson AFB, OH, Jan through Nov 1990.
2. Horowitz, I.M. Interviews. Air Force Inst of Tech, Wright-Patterson AFB OH, Jan through Nov 1990.
3. Horowitz, I.M. "Nonlinear Uncertain Feedback Systems with Initial State Values," *IJOC*, 34: 749-764 (1981).
4. Horowitz, I.M. "Synthesis of Feedback Systems with Nonlinear Time-Varying Uncertain Plants to Satisfy Quantitative Performance Specifications," *Proceedings of the IEEE*, 64: 123-130 (1976).

5. Kobylarz, 1Lt T. J. *Flight Controller Design with Nonlinear Aerodynamics, Large Parameter Uncertainty, and Pilot Compensation*. MS thesis, AFIT/GE/ENG/88D-19. School of Engineering, Air Force Inst of Tech (AU), Wright-Patterson AFB Ohio, Dec 1988 (AD-202 727).
6. Miller, 2Lt R.B. *Multi-Input Multi-Output Flight Control System Design for the YF-16 Using Nonlinear QFT and Pilot Compensation*. MS thesis, AFIT/GE/ENG/90D-42. School of Engineering, Air Force Inst of Tech (AU), Wright-Patterson AFB Ohio, Dec 1990.
7. Neal, T. Peter, and Rogers E. Smith. *An In-Flight Investigation to Develop Control System Design Criteria for Fighter Airplanes*, AFFDL-TR-70-74, Vol. I, AF Flight Dynamics Laboratory: Wright-Patterson AFB Ohio, Dec 1970.
8. Roskam, Jan. *Flight Dynamics of Rigid and Elastic Airplanes*. Lawrence KS: Roskam Aviation and Engineering Corp, 1972.

# Robust Crossfeed Design for Hovering Rotorcraft<sup>1</sup>

David R. Catapang  
Aeronautical Engineering Department  
California Polytechnic State University, San Luis Obispo, CA.

Mark B. Tischler  
U.S. Army Aeroflightdynamics Directorate  
Ames Research Center, Moffett Field, CA.

Daniel J. Biezd  
Aeronautical Engineering Department  
California Polytechnic State University, San Luis Obispo, CA.

## I. ABSTRACT

Control law design for rotorcraft fly-by-wire systems normally attempts to decouple the angular responses using fixed-gain crossfeeds. This approach can lead to poor decoupling over the frequency range of pilot inputs and increase the load on the feedback loops. In order to improve the decoupling performance, dynamic crossfeeds should be adopted. Moreover, because of the large changes that occur in the aircraft dynamics due to small changes about the nominal design condition, especially for near-hovering flight, the crossfeed design must be "robust." A new low-order matching method is presented here to design robust crossfeed compensators for multi-input, multi-output (MIMO) systems. The technique minimizes cross-coupling given an anticipated set of parameter variations for the range of flight conditions of concern. Results are presented in this paper of an analysis of the pitch/roll coupling of the UH-60 Black Hawk helicopter in near-hovering flight. A robust crossfeed is designed that shows significant improvement in decoupling performance and robustness over the fixed-gain or single point dynamic compensators. The design method and results are presented in an easily-used graphical format that lends significant physical insight to the design procedure. This plant pre-compensation technique is an appropriate preliminary step to the design of robust feedback control laws for rotorcraft.

## II. NOMENCLATURE

$G_{in}^{out}(\#1_{LO})$	Low order (LO) fit to crossfeed relating "out" to "in" for configuration #1
IDEAL	Refers to exact analytical decoupling solution for a specific configuration.
$J_{AVG, \#1 LO}$	Average decoupling in dB for all configurations using $G_{in}^{out}(\#1_{LO})$ .
MSW	Mean-Square Weighted.
$M_{on,i,j}$	Mag. in dB of the on-axis frequency response at $\omega_i$ for configuration "j".
$M_{off,i,j}$	Mag. in dB of the off-axis frequency response at $\omega_i$ for configuration "j".
NAVFIT	Computer program used to compute low-order "fits" to transfer functions.
TARGET	Refers to a heuristic decoupling crossfeed solution for a class of configurations.
TEMPLATE	Gain and phase values for "ideal" crossfeeds at a specific frequency.
$W_{i,j}$	Weight for a point at $\omega_i$ for configuration "j"
(a)	Short form for (s+a).
$(\zeta, \omega)$	Short form for $(s^2 + 2\zeta\omega s + \omega^2)$ .
$\Delta M_{i,j}, \Delta \phi_{i,j}$	Differences in gain and phase at $\omega_i$ for configuration "j"

<sup>1</sup> Paper presented at the Symposium and Tutorial on Quantitative Feedback Theory, Aug 3-4, 1992, Dayton, Ohio.

### III. INTRODUCTION

#### Background.

Cross-coupling is a characteristic problem for helicopter flight control system design. The UH-60 Black Hawk, shown in figure 1, is representative of such a helicopter with highly coupled motion because of its single main rotor and canted tail rotor that is located above the center of gravity. The Black Hawk will be used as the Rotorcraft Aircrew Systems and Controls Airborne Laboratory (RASCAL), a joint U. S. Army / NASA program to evaluate advanced controls and systems concepts (ref 1). A key goal of the flight control design for RASCAL is to achieve high bandwidth and decoupled response characteristics as required by the current helicopter handling-qualities specification (ref 2). This same goal is needed to operate RASCAL as an in-flight simulator.

The achievable level of feedback is severely limited in rotorcraft flight control design due to rather large inherent system delays. Among the most important delays are those associated with the rotor dynamics, actuator dynamics, and sensor filters (ref 3). The needed feedback gain levels can be substantially reduced when the decoupling requirement is achieved largely using crossfeeds ("feedforward"), rather than relying heavily on feedback. This approach has been applied in the design of a number of rotorcraft flight control systems (ref 4) and was notably successful in the flight tests of the in-flight simulation control system for the BO-105 helicopter (ref 5), an airframe that exhibits very high levels of open-loop cross-coupling. Substantial emphasis was placed on a sophisticated multivariable crossfeed design and flight test validation as the first step in development of a high-bandwidth flight control system for the BO-105. Excellent decoupling of the mid- and high-frequency characteristics was achieved for the forward flight condition (80 kts), thus reducing the need to use high-gain feedbacks. At low frequency, the feedbacks yielded higher loop gains and ensured closed-loop performance robustness, stability, disturbance rejection, and long-period modal decoupling. Feedback gains were kept to a minimum in order to avoid closed-loop instabilities and control limiting that were encountered with earlier high-feedback gain designs for the BO-105 and had been problematic in earlier flight control designs for the UH-60 (ref 6). A successful high-bandwidth, highly-decoupled, but *low-gain* in-flight simulator was achieved for the BO-105 based on a point design at 80 kts. The BO-105 experience highlights the value of a careful crossfeed design as a precursor to feedback design, regardless of the feedback synthesis method.

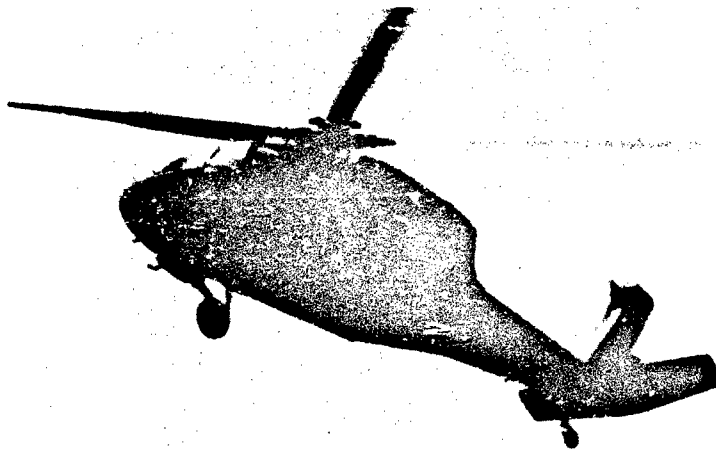


Figure 1 - RASCAL UH-60 Black Hawk

A comprehensive study of rotorcraft flight control was conducted by Takahashi (ref 7), who used advanced H-2 loop shaping methods to synthesize a multi-variable flight control system for the RASCAL in hover. Takahashi based the H-2 synthesis on a nominal hover condition design point, and then evaluated the robustness of the design based on a large family (72) of off-nominal conditions. The work was especially thorough in its use of comprehensive linear and nonlinear simulations of the RASCAL UH-60 -- including the dynamics of the rotor system, rotor wake, airmass, actuators, and fly-by-wire system elements. Handling-qualities that were satisfactory without improvement were achieved for the most aggressive helicopter missions in the synthesis study. Later piloted simulation evaluations of the control system design indicated some unexpected loss of performance robustness for the off-design points. The multivariable nature of the feedback structure made it somewhat cumbersome to tune the system gains to isolate and correct these deficiencies. Current work is aimed at simplifying the H-2 approach to achieve a control system structure that is more easily adjusted.

Another of the proposed concepts for the RASCAL flight control system is based on the application of Quantitative Feedback Theory (QFT). QFT is a classically-based feedback control design method for robust compensation of uncertain plant transfer functions (ref 8,9). The method is well suited to the rotorcraft flight control problem as described above because it directly addresses costs include actuator limiting, sensor noise amplification, and loss of stability robustness. The benefits of feedback are performance robustness, stability, and disturbance rejection. In QFT, aircraft dynamics uncertainties are modeled in direct terms of gain and phase response variation ("uncertainty templates") associated with the family of design points to be included in the design. As such, the QFT problem formulation is very well suited to the helicopter problem, where sophisticated simulations provide a large family of single point dynamic models as a function of physical parameters such as wind speed and direction, weight at hover, center of gravity location, moments-of-inertia, main rotor speed, and aircraft turn rate. It is impractical to gain schedule the control system compensation as a function of the many parameters which affect aircraft dynamics; furthermore, many of these parameters are not measurable in-flight. Therefore, a large degree of uncertainty of aircraft dynamics will exist that must be included in the design. Dynamics variations are generally most significant for helicopter near-hovering flight, while control power is generally at a minimum level due to the lack of airspeed. These factors combine to make the hover condition flight control design a most challenging problem for the application of QFT techniques.

The classical approach to crossfeed design uses coupling numerator theory, as explained in detail by McRuer et al. (ref 10-12). The concept of "constrained variables" (see also reference 3) is an important aspect of this approach. This concept allows the crossfeed design to take into account the approximate effects of the feedback loops not yet synthesized at this stage of the control system formulation. In the cited references, coupling numerator techniques were applied either to obtain crossfeeds for single design point models or to gain schedule as a function of key flight condition variables (e.g., airspeed, air density, gross weight, and vertical velocity as in reference 11) but did not consider the problem of crossfeed design for highly uncertain systems. The current work combines coupling numerator theory with the QFT concept of uncertainty templates to yield an approach for robust crossfeed design.

The coupling numerator approach for crossfeed synthesis is first reviewed and demonstrated for a single point design problem (nominal hover condition). The current work treats the pitch-roll coupling problem, which is a key source of coupling for most helicopter flight near hover. The new robust crossfeed design is explained and then applied to a design problem that considers five near-hover flight conditions. The performance of the robust crossfeed is shown to be superior to the conventional crossfeed based on a single point design model. The formulation and computer implementation of the new method allows the direct generalization to a relatively large number of flight conditions. Since, as discussed above, crossfeed pre-compensation is commonly used in helicopter flight control synthesis, the techniques presented in this paper are also applicable to design approaches other than QFT.

#### IV. METHODOLOGY

##### Overview of Control System Structure and Design Approach

The overall control system structure for the QFT RASCAL design is shown in figure 2. The vertical channel is not shown since it generally has a much lower bandwidth than the angular channels and thus is considered as an open-loop response for this study. The current study considers only the key roll-to-pitch control crossfeed  $G_{\delta_{lon}^{\delta_{lat}}}$  (referred to herein as "pitch axis crossfeed") and pitch-to-roll control crossfeed  $G_{\delta_{lat}^{\delta_{lon}}}$  (referred to herein as "roll axis crossfeed"), but it does account for the presence of the yaw feedback compensation ( $G_r$ ). The method can be extended to include yaw axis crossfeeds, in which case the full 3-input/3-output architecture would require 6 crossfeeds (ref 11). Using the robust techniques discussed in this paper, the crossfeeds are optimized for effectiveness in the frequency range of 2-10 rad/sec (at and above the crossover frequency), which will reduce the feedback load associated with the decoupling requirement. The crossfeed designs of this study are included in the bare-airframe dynamics to yield the "compensated open-loop response." With the mid- and high-frequency cross-coupling now effectively suppressed by the crossfeeds, QFT techniques can then be applied to the compensated open-loop response to synthesize feedback and prefilter elements of the control system that satisfy the remaining design specifications. Cross-coupling suppression at low frequency (i.e. below 2 rad/sec) will be accomplished in the completed system by the large loop gains (feedback\*plant) which are effective below the crossover range.

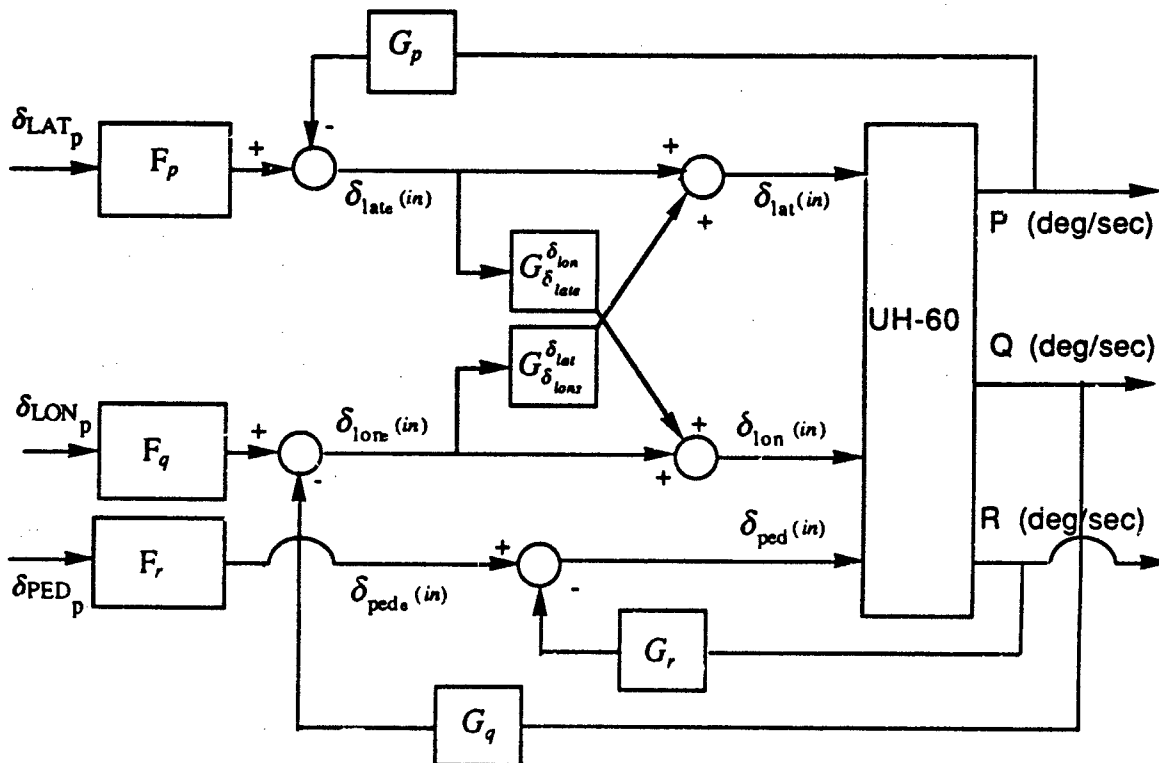


Figure 2 - Control System Block Diagram

## Rotorcraft Models

High-order linear models of the UH-60 dynamics near hover are extracted from a comprehensive nonlinear simulation program (UMGENHEL- ref 13). UMGENHEL is a methodically restructured and upgraded version of the original GENHEL helicopter blade-element simulation program (ref 14). The UMGENHEL linear models include dynamics of the fuselage, rotor, airmass, engine, and governor. Also represented is the control mixing, which provides limited decoupling through static crossfeeds. Since the control system actuators and digital component dynamics are symmetric in the pitch and roll axes, they do not affect the crossfeed calculations and therefore are not included in the model at this stage of the design.

Results presented in this paper are for a 6 degree-of-freedom (DOF), reduced-order (quasi-steady) UMGENHEL model. The use of the complete high-order UMGENHEL model is critical for the design of the feedback-loop elements (ref 3) but is of less importance for the crossfeed design at this stage. The simulation is capable of efficiently generating large families of linear models over a wide range of flight and configuration conditions. The current study includes the nominal hover operating point plus 24 off-nominal points. Each off-nominal point represents an expected near-hover trim condition within the desired operating range of a constant-gain QFT controller. The 24 configurations include variations in trim airspeed (longitudinal and lateral), rotor RPM, aircraft weight and center of gravity, turning rate, climb speed, and descending speed. For this paper, only four off-nominal conditions were considered:

- Config.#1: (Nominal) hover
- Config.#2: 15 kts forward speed
- Config.#3: 15 kts rearward speed
- Config.#4: 15 kts right sideward flight
- Config.#5: 15 kts left sideward flight

The final crossfeed design will be based on the complete high-order UMGENHEL model using the entire family of 25 configurations.

## Decoupling the Pitch and Roll Axes

This section presents the crossfeed methodology for pitch/roll decoupling. First, the ideal decoupling relationships for full-order crossfeeds are presented and illustrated with results for the UH-60 at the nominal hover condition. Lower-order approximations to these ideal crossfeeds are shown to be much simpler yet still effective in the frequency-range of concern (2-10 rad/sec). Then, the effect of variations in the plant dynamics are shown on the decoupling performance of the nominal crossfeed. A new graphical method based on the QFT concept of templates concludes the section.

**"Ideal" decoupling relationships.** The "ideal" roll-to-pitch and pitch-to-roll crossfeeds ( $G_{\delta_{lon}}^{\delta_{lat}}$  and  $G_{\delta_{lat}}^{\delta_{lon}}$ ) are determined that cause the off-axis responses ( $\frac{q}{\delta_{lat}}$  and  $\frac{p}{\delta_{lon}}$ ) to be zero without the pitch and roll-rate feedback loops. Although the pitch and roll-rate feedback loops are dropped, yaw-rate feedback is included and accounted for in the crossfeed calculation. In the development that follows, the prime symbol (') denotes that the yaw loop closure is included in the input-output relationship.



The crossfeed-compensated off-axis pitch response  $\left(\frac{q}{\delta_{lat.}}\right)'$  is determined from fig 2 as follows:

$$\left(\frac{q}{\delta_{lat.}}\right)' = \left(\frac{q}{\delta_{lat.}}\right)' \left(\frac{\delta_{lat.}}{\delta_{lat.}}\right) + \left(\frac{q}{\delta_{lo.}}\right)' \left(\frac{\delta_{lo.}}{\delta_{lat.}}\right) \quad (1)$$

where

$$\left(\frac{\delta_{lo.}}{\delta_{lat.}}\right) \equiv G_{\delta_{lat.}}^{\delta_{lo.}}$$

$$\left(\frac{\delta_{lat.}}{\delta_{lat.}}\right) \equiv 1$$

The "ideal crossfeed" exactly eliminates the off - axis response :

$$\left(\frac{q}{\delta_{lat.}}\right)' = 0$$

from which the ideal roll - to - pitch crossfeed is obtained :

$$G_{\delta_{lat.}}^{\delta_{lo.}} = - \frac{\left(\frac{q}{\delta_{lat.}}\right)'}{\left(\frac{q}{\delta_{lo.}}\right)'} \quad (2)$$

Following references (10-12,3)

$$\left(\frac{q}{\delta_{lat.}}\right)' = \frac{N_{\delta_{lat.}}^q + G_r N_{\delta_{lat.}}^q \delta_{lat.}'}{\Delta + G_r N_{\delta_{lat.}}^q} \quad (3)$$

where,

$\Delta$  = denotes:  $\text{Det}(sI - A)$  ; and A is the matrix of stability derivatives.

$N_{\delta_{lat.}}^q$  denotes the "conventional" numerator obtained by substituting the forcing function column for lateral control input ( $\delta_{lat.}$ ) into the column of the system matrix ( $sI - A$ ) associated with the q response and then evaluating the determinant.

$N_{\delta_{lat} \delta_{ped}}^q$  denotes the "coupling numerator" obtained by simultaneously substituting the forcing function columns for lateral and pedal control inputs ( $\delta_{lat}$  and  $\delta_{ped}$ ) into the columns of the system matrix (sI - A) associated with the q and r responses, respectively, and then evaluating the determinant.

When the yaw feedback is tight, then the yaw response is "constrained" to zero, and the effective cross - coupling response becomes:

$$\left( \frac{q}{\delta_{lat}} \right)' = \frac{N_{\delta_{lat} \delta_{ped}}^q}{N_{\delta_{ped}}^r} \quad (4)$$

Similarly, the effective on - axis pitch response with the yaw response constrained by the yaw feedback loop is:

$$\left( \frac{q}{\delta_{lo}} \right)' = \frac{N_{\delta_{lat} \delta_{ped}}^q}{N_{\delta_{ped}}^r} \quad (5)$$

Substituting (4) and (5) into (2) yields the final result for the ideal roll - to - pitch crossfeed:

$$G_{\delta_{lat} \delta_{ped}}^{\delta_{lat}} = - \frac{N_{\delta_{lat} \delta_{ped}}^q}{N_{\delta_{lat} \delta_{ped}}^q} \quad (6)$$

Similarly, the off - axis roll response with the yaw response constrained is:

$$\left( \frac{p}{\delta_{lo}} \right)' = \frac{N_{\delta_{lat} \delta_{ped}}^p}{N_{\delta_{ped}}^r} \quad (7)$$

The on - axis roll response with the yaw constrained is:

$$\left( \frac{p}{\delta_{lat}} \right)' = \frac{N_{\delta_{lat} \delta_{ped}}^p}{N_{\delta_{ped}}^r} \quad (8)$$

and the pitch - to - roll ideal crossfeed is obtained as:

$$G_{\delta_{lat} \delta_{ped}}^{\delta_{lat}} = - \frac{N_{\delta_{lat} \delta_{ped}}^p}{N_{\delta_{lat} \delta_{ped}}^p} \quad (9)$$

**Ideal Decoupling for the Nominal Configuration.** The on-axis frequency responses

$\left(\frac{p}{\delta_{lat}}\right)$  and  $\left(\frac{q}{\delta_{lon}}\right)$  are shown for the five configurations in figures 3 and 4, and the

uncompensated off-axis responses  $\left(\frac{p}{\delta_{lon}}\right)$  and  $\left(\frac{q}{\delta_{lat}}\right)$  in figures 5 and 6. Overall variability is significantly greater for the off-axis responses than for the on-axis responses. Variability in all responses is greatest at the lower frequencies (below 1 rad/sec), due to the sensitivity of the speed dynamics (e.g. phugoid mode) to trim rotor flapping angles.

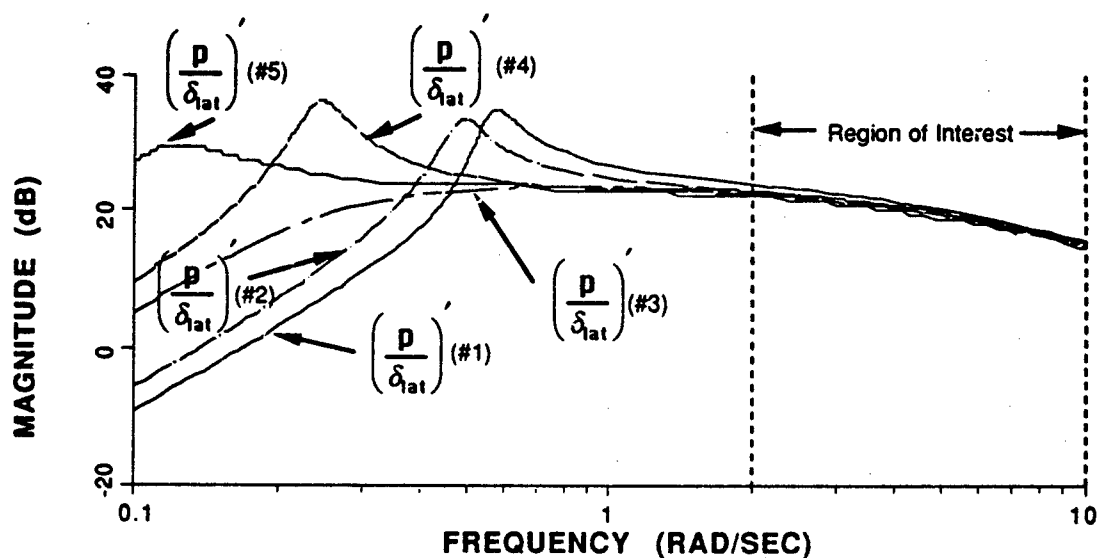


Figure 3 - On-axis Roll Rate Frequency Response

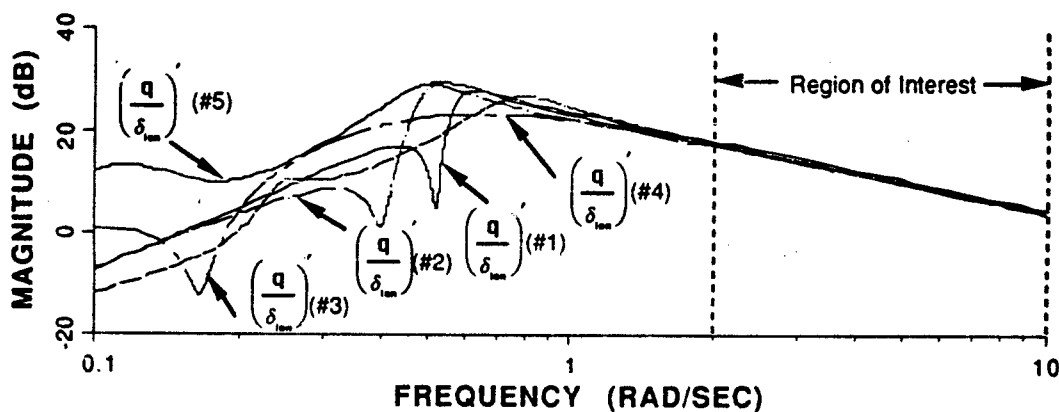


Figure 4 - On-axis Pitch Rate Frequency Response

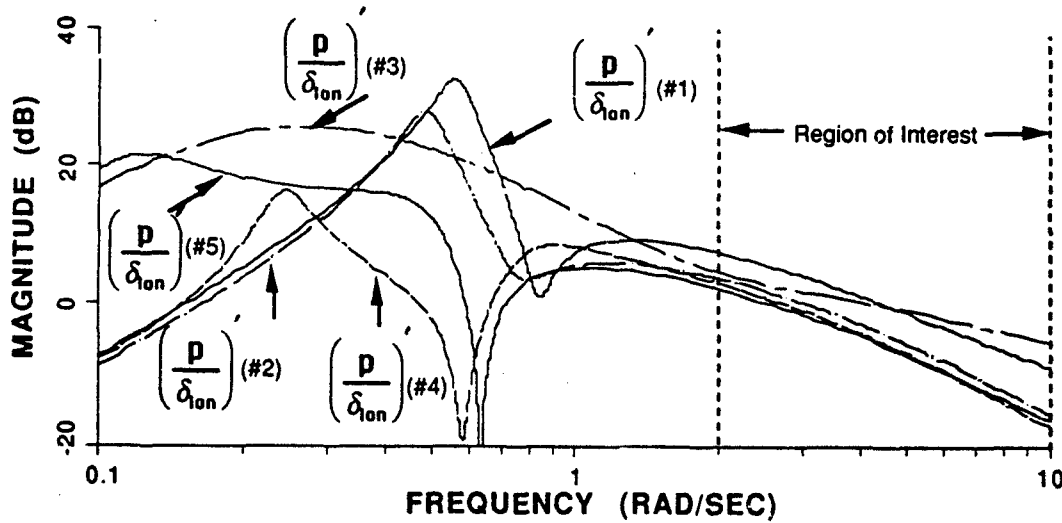


Figure 5 - Uncompensated Off-axis Roll Rate Frequency Response

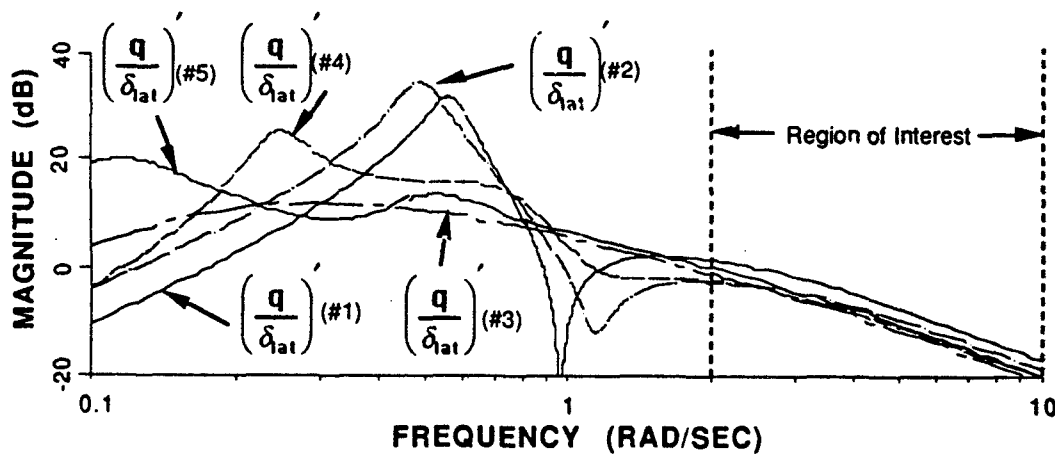


Figure 6 - Uncompensated Off-axis Pitch Rate Frequency Response

The on-axis and off-axis time responses (yaw constrained) for configuration 1 (nominal), following a doublet input, are depicted in figure 7. The doublet was tuned to a natural frequency of 3 rad/sec to highlight the cross-coupling dynamics at and above the crossover frequency range, where the crossfeeds must be effective. As seen in figure 7 for the nominal configuration with no crossfeed, the magnitude of the off-axis coupling responses are about 30-40% of the magnitude of the on-axis responses. This indicates rather significant cross-coupling.

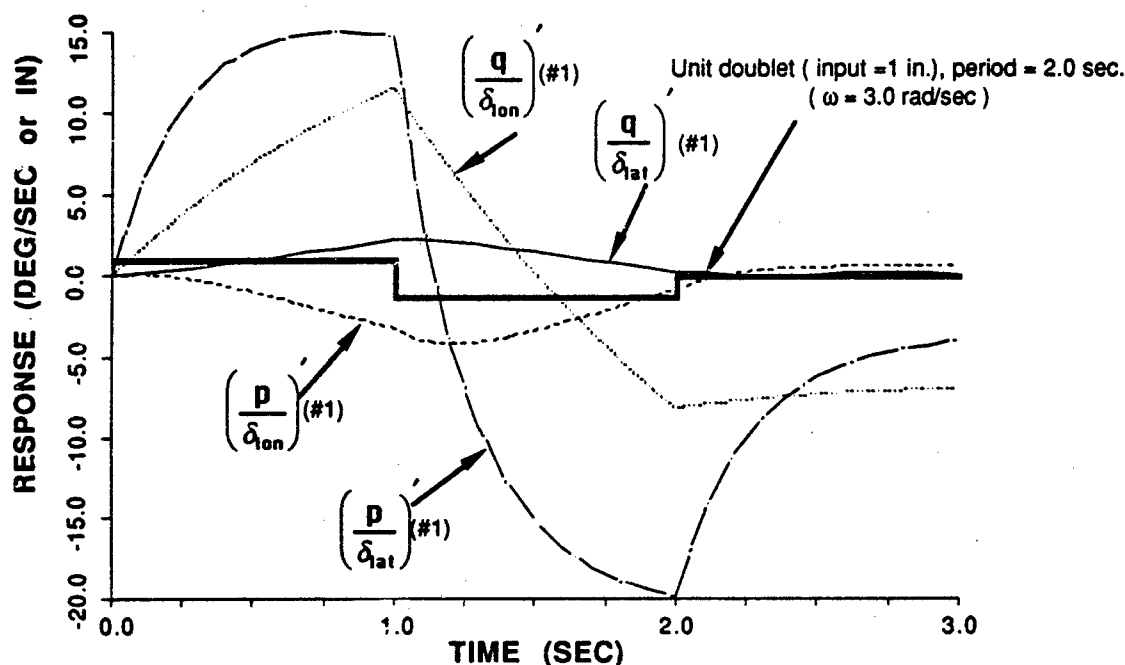


Figure 7 - Time Responses for Nominal Configuration with Doublet Input

Using the coupling numerator relationships (6) and (9) above, the ideal crossfeeds for the nominal (#1) configuration are

$$G_{\delta_{10n}}^{\delta_{1a1}}(\#1) = -\frac{N_{\delta_{10n}}^{\delta_{1a1}}}{N_{\delta_{1a1}}^{\delta_{10n}}} = \frac{-0.571(0.966)(.503E-03)(-.695E-02)(.26)(23.6)}{16.6(-.143E-01)(.519)(-.171E-03)(-.26E-01)(.263)(4.06)} \quad (10)$$

and

$$G_{\delta_{1a1}}^{\delta_{10n}}(\#1) = -\frac{N_{\delta_{1a1}}^{\delta_{10n}}}{N_{\delta_{10n}}^{\delta_{1a1}}} = \frac{2.98(.0541)(.833)(.0362)(.264)(-8.16)(0)}{65.6(-.253)(.489)(.0222)(.264)(.949)(0)} \quad (11)$$

which were obtained using the LCAP controls analysis program (refs 3,15). Note that these "ideal" crossfeeds have unstable poles, and so are not practical. Practical, stable dynamic crossfeeds are obtained by approximating the ideal crossfeeds with low-order equivalent transfer functions over the frequency range of interest (2-10 rad/sec). The low-order crossfeed fit results obtained from NAVFIT (refs 16, 17) are summarized for the nominal configuration in table 1. These crossfeeds are simple first and second order functions with stable (i.e. physically practical) dynamic modes.

Note that static crossfeeds used in helicopter flight control are commonly obtained from the high frequency gain of the "ideal" solutions of equations 10 and 11. These solutions presume existence of a closed high-gain yaw-rate feedback loop. Another common alternative is to use the static crossfeed solutions determined by inverting the control distribution matrix (C\*B). In that case the solutions presume an open yaw-rate feedback loop (ref 4,5). These static gains were obtained from LCAP and are shown in table 1. This approach, as will be shown, yields solutions that are poor approximations of the "ideal" crossfeeds in the 2-10 rad/sec frequency range of interest.

In QFT loop-shaping terminology, the performance characteristics of a crossfeed apply not only to a single design configuration but to a "specified set" of configurations. This single crossfeed, appropriately selected for a set of configurations, is called in this study the "target" compensation, and the low-order (LO) approximation to this "target" is called the "achieved" compensation.

TABLE 1. Approximations to the Ideal Crossfeeds for the Nominal Configuration

Type of Fit	$G_{\delta_{iat}, \delta_{iat}}^{\delta_{iat}} (\#1) = -\frac{Z_{\delta_{iat}, \delta_{iat}}^{\delta_{iat}}}{Z_{\delta_{iat}, \delta_{iat}}^{\delta_{iat}}}$	$G_{\delta_{iat}, \delta_{iat}}^{\delta_{iat}} (\#1) = -\frac{Z_{\delta_{iat}, \delta_{iat}}^{\delta_{iat}}}{Z_{\delta_{iat}, \delta_{iat}}^{\delta_{iat}}}$
$G(\#1_{STATIC})$	-2.35E-02	-5.00E-02
$G(\#1_{LO})$ NAVFIT Ref 9	$\frac{-0.0275(29.7)}{(4.54)}$	$\frac{49.5}{(0.351, 11.8)(0.2)}$

Figure 8 is a Bode plot for configuration #1 showing the accuracy of the static and lower-order dynamic approximations to the ideal crossfeed  $G_{\delta_{iat}, \delta_{iat}}^{\delta_{iat}} (\#1)$ . The static crossfeed, commonly used because of the simplicity of its determination and implementation (a matrix mixing function), matches the ideal result only at very high frequency, and so can be expected to perform poorly. The simple low-order dynamic crossfeed  $G_{\delta_{iat}, \delta_{iat}}^{\delta_{iat}} (\#1_{LO})$  matches the ideal result very well over the frequency range of concern (2 to 10 rad/sec).

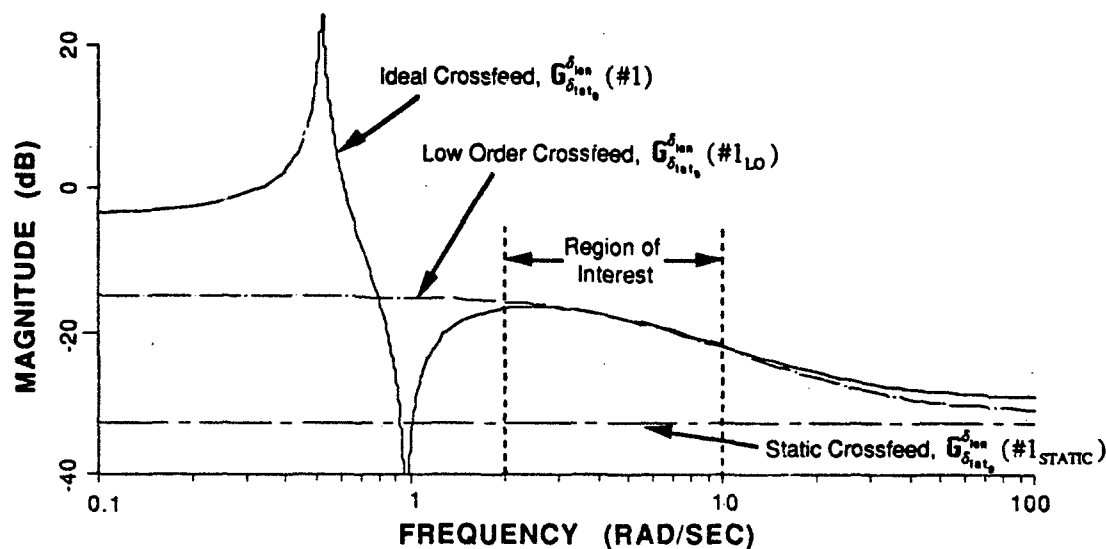


Figure 8 - Frequency Response Accuracy of Fit for  $G_{\delta_{iat}, \delta_{iat}}^{\delta_{iat}} (\#1)$

**Nominal Decoupler Applied to Off-nominal Configurations.** Consider the results of using the low-order crossfeeds in the last row of table 1 as decouplers for all of the off-nominal configurations. The off-axis responses obtained by such a strategy are shown in figure 9. The resulting decoupling performance for each off-nominal configuration is *still improved* relative to the uncompensated cases. Performance between 2 and 10 rad/sec as shown in figure 9 may be compared with figure 6 to illustrate this. Note that performance below 2 rad/sec is not improved significantly using the nominal crossfeeds. However, it is presumed that pitch and roll feedback loops (not presented here) will accomplish decoupling at the lower frequencies.

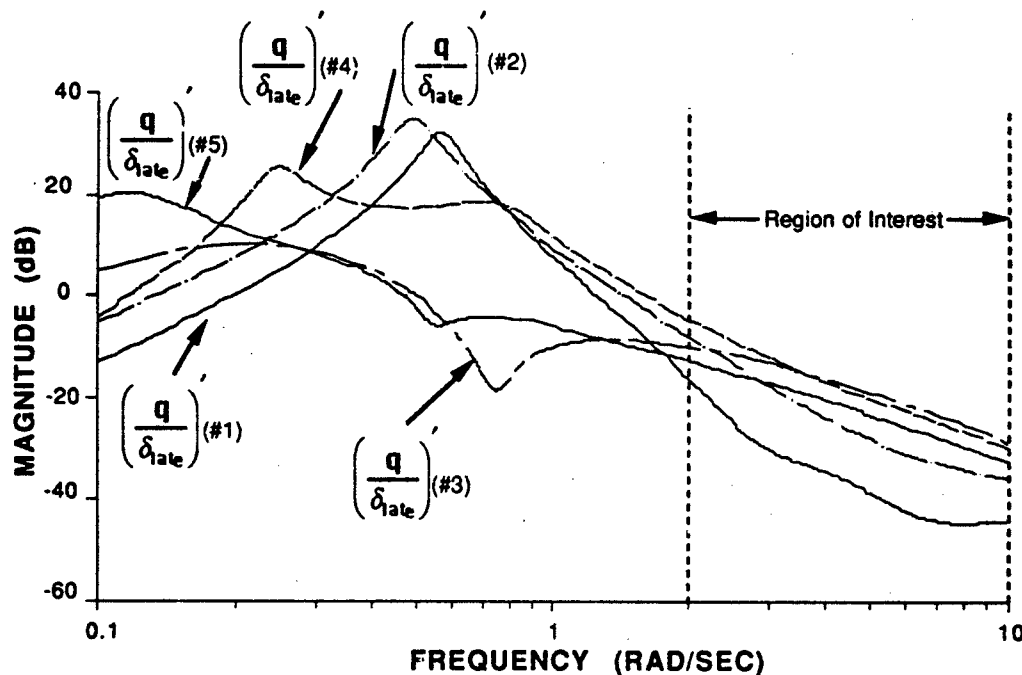


Figure 9 - Off-axis Pitch Rate Responses Using  $G_{\delta_{lat}}^{\delta_{lat}} (\#1_{LO})$

Since the choice of an "ideal" crossfeed so far has been arbitrarily chosen as the mathematical decoupling solution for configuration #1, a few questions now arise. First, would a design based on the "ideal" crossfeed solution for one of the other configurations (#2 through #5) result in more "robust" decoupling for the entire family? "Robust" here implies significant improvements in decoupling across all configurations. For example, a low-order approximation for configuration #2,  $G_{\delta_{lat}}^{\delta_{lat}} (\#2_{LO})$ , might be a more robust solution for decoupling the entire family of configurations than is  $G_{\delta_{lat}}^{\delta_{lat}} (\#1_{LO})$ . Crossfeed templates are introduced in the following section to better visualize the range of possible design solutions.

#### **Graphical Basis for Robust Crossfeed Design.**

The strategy developed in this study is patterned after QFT graphical techniques that use the Nichols chart for presentation of "target" compensation, "achieved" compensation, and configuration variations in gain and phase ("templates"). For example, figure 10 compares the Nichols chart representation of the low-order crossfeed  $G_{\delta_{lat}}^{\delta_{lat}} (\#1_{LO})$  with that of the "ideal" crossfeed  $G_{\delta_{lat}}^{\delta_{lat}} (\#1)$  for the nominal hover configuration. This figure is simply a re-plot of the

lower-order dynamic crossfeed results from fig 8 (including the phase data). The "ideal" crossfeed based on the nominal configuration is shown with the symbol "+" for five frequency points over the 2-10 rad/sec frequency range of interest. The five frequency points are logarithmically-spaced,  $(\omega_1) = \{2.0, 3.0, 4.47, 6.68, 10.0 \text{ rad/sec}\}$ . The (small) mismatches of the ideal and lower-order crossfeeds are clearly visible for this frequency range. Gain and phase values for "ideal" crossfeeds based on the other remaining four configurations may also be depicted on the Nichols chart at each of the frequency points. Figure 10 shows the result for a frequency of 2 rad/sec. This collection of "ideal" gain and phase values at a specified frequency is called a "crossfeed template" and may be connected with lines for useful visual effect.

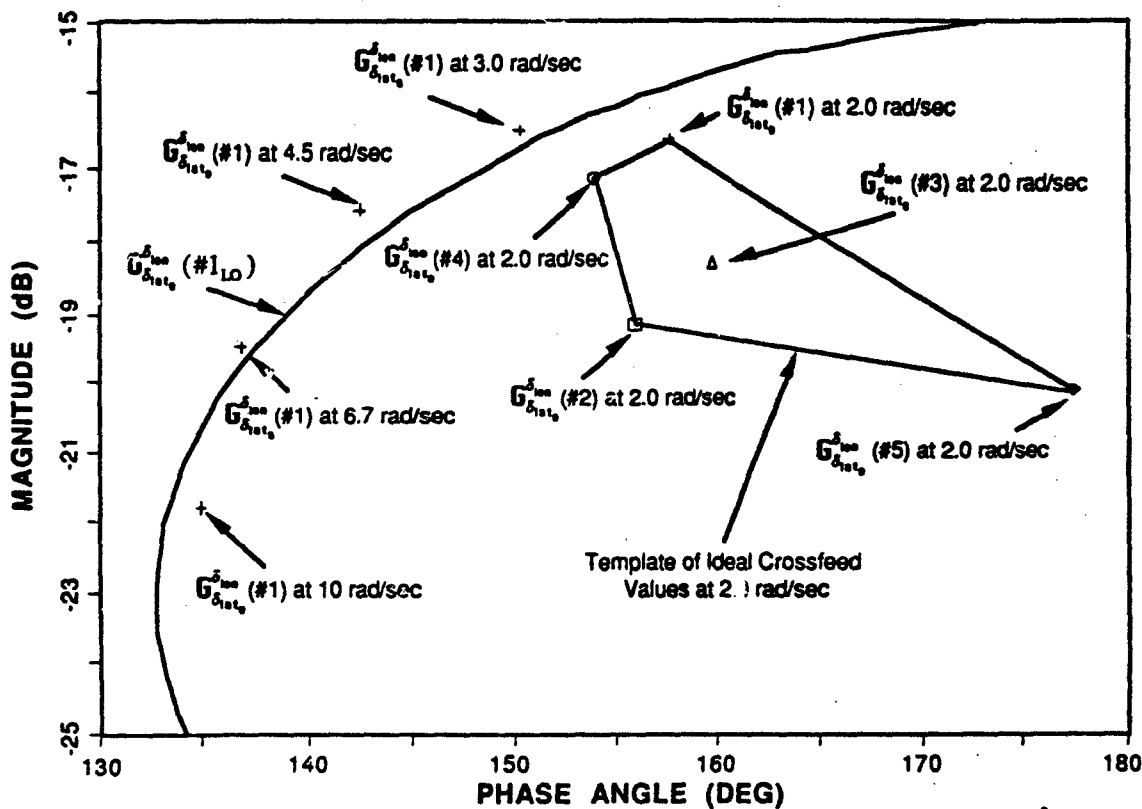


Figure 10 - Nichols Chart Representation of Low-Order Approximation,  $G_{s_{11}}^{f_{10}} (\#1_{LO})$

The  $G_{s_{11}}^{f_{10}}$  crossfeed template for each of the five frequency points is shown in figure 11. Each template depicts the variability of the "ideal" crossfeeds over the family of plant configurations. In the earlier crossfeed design, the "target" gain and phase values used in the low-order fit process were those associated with the ideal solution for the nominal configuration (#1) denoted with the symbol "+" on each template. This is obviously the best solution for decoupling the nominal plant dynamics. However, an inspection of figure 11 shows that a design that closely tracks the ideal crossfeed solution for configuration #1 ( $G_{s_{11}}^{f_{10}} (\#1)$ ) will be quite far from the crossfeed solution for configuration 5, and may in fact worsen the coupling behavior for this configuration. Therefore, the question now is whether there is a better strategy for selecting a "target" point in each template that will result in improved overall decoupling performance. The



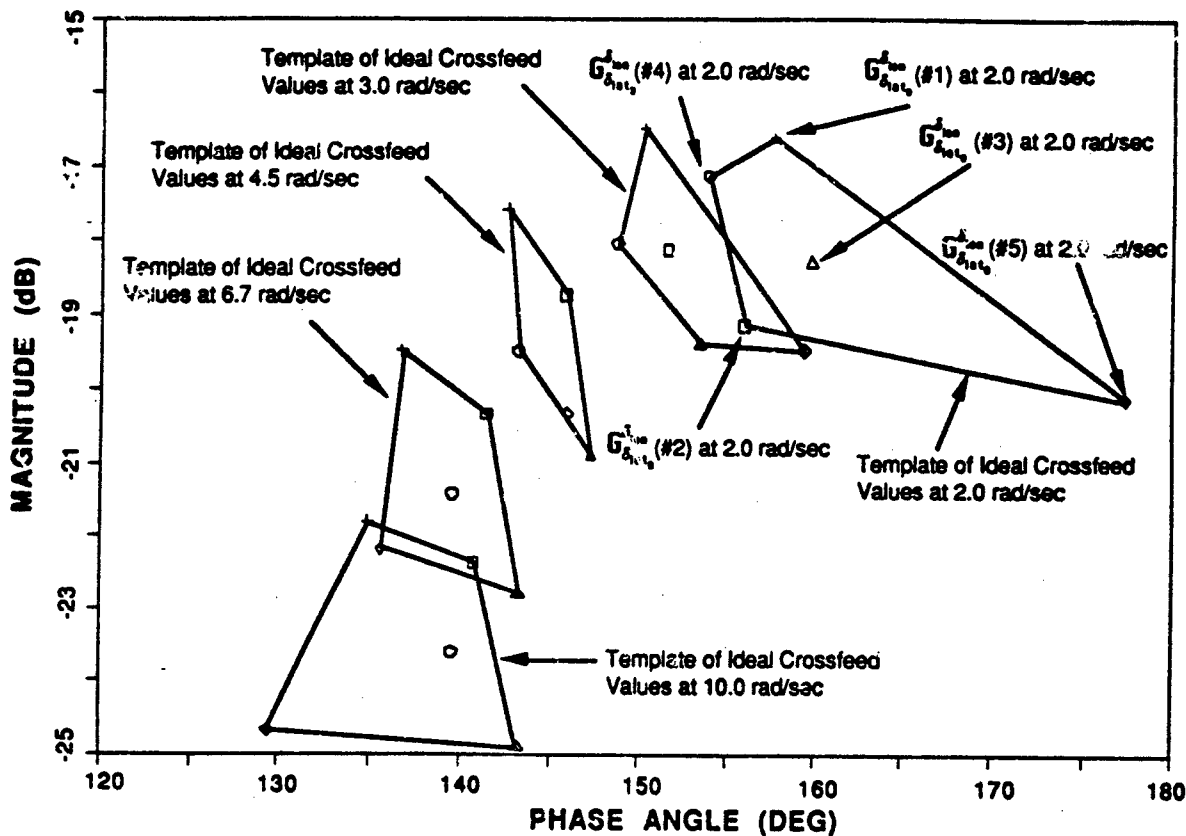


Figure 11 - Frequency Templates of Ideal Crossfeeds  $G_{\delta_{i,j}}^{j_{avg}}$

quality of overall decoupling for the family of configurations is assessed via the decoupling performance metric discussed in the next section.

#### Decoupling Performance Metric

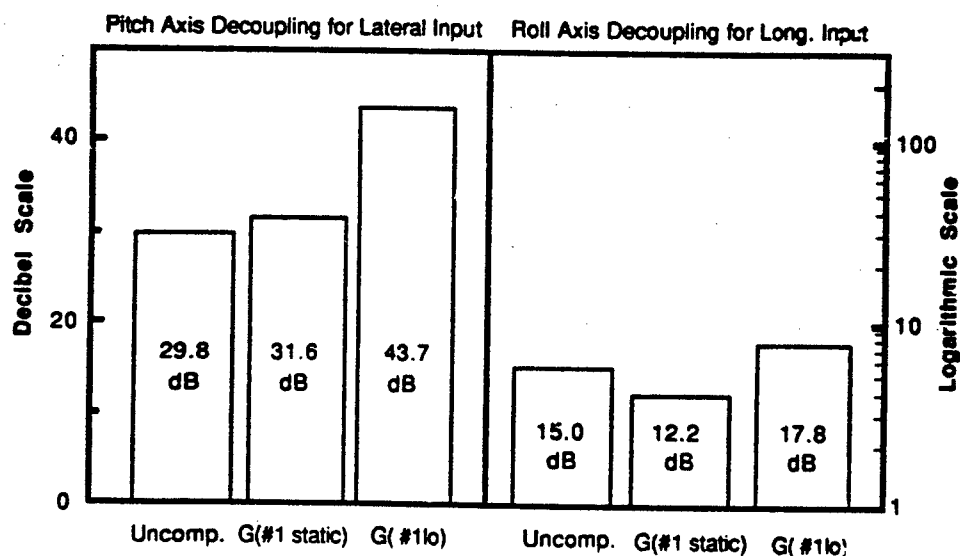
If a crossfeed is doing its job properly, then the off-axis frequency responses of the family of configurations will be substantially attenuated over the frequencies of concern " $\omega_i$ ". The array of off-axis response magnitudes for each of the " $j$ " configurations are obtained at these " $i$ " frequencies and denoted by  $M_{off,i,j}$  in dB. The magnitude of the off-axis response is conveniently normalized relative to a baseline *on-axis* response to yield a measure of relative decoupling. The choice of which configuration to use for this baseline is arbitrary since we are mostly concerned with comparative improvements in decoupling for various strategies. In this paper the nominal configuration (#1) is established as the baseline configuration, and is denoted by  $M_{on,i,1}$  dB at each frequency " $\omega_i$ ". The decoupling at each of the five frequencies "averaged" over all of the configurations is expressed (for each axis) by the metric:

$$J_{AVG} = \sum_{Conf=j=1}^5 \sum_{\omega_i=1}^5 (M_{on,i,1} - M_{off,i,j}) / 25 \quad \text{dB} \quad (12)$$

The decoupling performance results for the uncompensated case and the two crossfeeds of the previous section (static and low-order) are shown in table 2. The baseline pitch decoupling for lateral inputs with no crossfeed is obtained by using the data from figure 6 for the uncompensated off-axis response  $M_{off,i,j}$ . The on-axis roll response data from configuration #1 ( $M_{on,i,1}$ ) is obtained from figure 3. Using these data, the baseline decoupling with no crossfeed is  $J_{AVG, Uncomp} = 29.8$  dB, or a linear attenuation factor of roughly 30 dB. In other words with no crossfeed, the pitch response coupling is about 3% of the on-axis roll response in the frequency range of concern. This high level of decoupling reflects the action of the mixer box (included in the bare airframe model) which decouples the control moments. The mixer box is effective for the pitch axis which has low relative aerodynamic damping specific moments due to the high relative pitch inertia. The static gain crossfeed  $G(\#1 \text{ static})$  does little to further improve the decoupling. If nominal crossfeed compensation  $G_{s_{m}}^{s_{m}}(\#1_{LO})$  is implemented, then the  $M_{off,i,j}$  values would be taken from the plots in figure 9 instead of from figure 6 to compute  $J_{AVG, \#1_{LO}} = 43.7$  dB. There is a large improvement in decoupling when the low order fit to the "ideal" nominal crossfeed is used.

The results for the roll axis decoupling for longitudinal inputs are also shown in table 2. Here the uncompensated coupling is significant (15.0 dB=18%) due to the lower roll axis inertia. The static crossfeed solution actually worsens the overall cross-coupling (12.2 dB) while the nominal lower-order crossfeed shows an improvement in decoupling  $J_{AVG} = 17.8$  dB (13%), although the coupling is still significantly above desired levels (25dB=5%).

**Table 2 - Decoupling Performance Summary Using Approximations to Ideal Solution for Nominal Configuration**



This metric is easily extended for a large number of configurations and strategies. A computer program was developed to automatically scan configuration frequency files and tabulate the results. A single value of the metric may even be used (cautiously) to summarize decoupling performance for more than one axis (the average, for example). The safest procedure, however, is to apply the metric individually to each degree of freedom.

**Choosing a Strategy.** In the previous examples, the "target" crossfeed values used in the fitting process were chosen based on the "ideal" crossfeed solutions for configuration #1 (nominal). The average decoupling performance metric using this strategy,  $J_{AVG, \#1 LO}$ , was improved relative to the static crossfeed,  $J_{AVG, \#1 Static}$  for both the pitch and roll cases. Many heuristic strategies for selecting appropriate target values were also considered in this study. Referring to figure 11, one obvious method would be to select target values based on the average or centroid of each crossfeed template.

The heuristic strategy recommended in this paper, which balances simplicity of implementation with excellent decoupling performance, is called "mean-square weighting" (MSW) decoupling. The first step in this strategy is to find a "target" crossfeed point (gain/phase location) on each template that is a weighted-average which favors a cluster of points within a given template. Then, the lower-order fitting technique is used to design a crossfeed to best match these target points. Weights in the fitting program are chosen so that the crossfeed design matches more closely the target points associated with the templates having a smaller size -- where the proper choice of desired target value is well defined and should be ensured. When the template is large in size, the weights are reduced since the exact location of the crossfeed is not as well defined. This is illustrated in figure 12 for a set of artificially constructed templates.

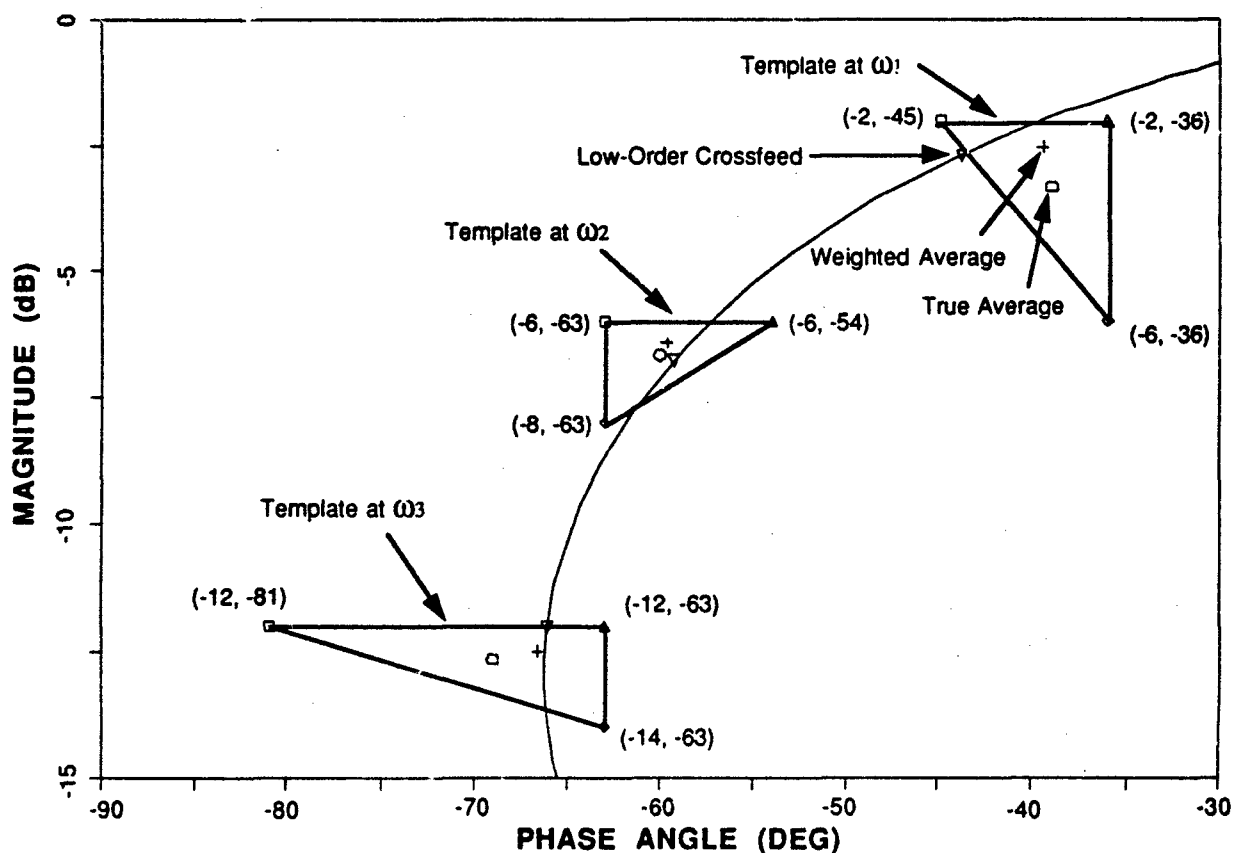


Figure 12 - Illustration of the MSW Strategy with Synthesized Templates

To implement the MSW strategy, first determine the average gain and phase point (dB and degrees) for each template  $|G(\text{avg})|$  and  $\angle G(\text{avg})$ . The difference between the average gain and phase of a template and the "ideal crossfeed" gain and phase for each configuration (j) in the template gives the gain and phase deviations for the template "i". Now looping over all the template frequencies gives arrays as a function of i and j:

$$\Delta M_{i,j} = \{|G(\#j)| - |G(\text{avg})|\}_i \quad \text{dB} \quad (13)$$

$$\Delta \phi_{i,j} = \{\angle G(\#j) - \angle G(\text{avg})\}_i \quad \text{deg} \quad (14)$$

The mean square weight for the point (i,j) is defined as:

$$W_{i,j} = \min[1, \{ \frac{1}{\Delta M_{i,j}^2 + 0.01745(\Delta \phi_{i,j})^2} \}] \quad (15)$$

where the weighting of 7.6 deg of phase to 1dB is adopted as recommended in practice (ref 17).

The MSW "target" crossfeed point for the template "i" is defined as:

$$M_{\text{MSW},i} = \frac{\sum_{\text{Conf } j} W_{i,j} |G(\#j)|_i}{\sum_{\text{Conf } j} W_{i,j}} \quad \text{and} \quad \phi_{\text{MSW},i} = \frac{\sum_{\text{Conf } j} W_{i,j} \angle G(\#j)_i}{\sum_{\text{Conf } j} W_{i,j}} \quad (16)$$

The lower-order "fit" to the above "target" crossfeed points is found by using the following weights in the NAVFIT program at frequency "i":

$$W_{\text{NAVFIT},i} = \min[1, \{ \frac{1}{\sigma_{\text{mag},i}^2 + 0.01745(\sigma_{\text{phase},i}^2)} \}] \quad (17)$$

where

$$\sigma_{\text{mag},i}^2 = \frac{1}{5} \sum_{\text{Conf } j=1,5} \{|G(\#j)| - |G(\text{avg})|\}_i^2 \quad \text{and} \quad \sigma_{\text{phase},i}^2 = \frac{1}{5} \sum_{\text{Conf } j=1,5} \{\angle G(\#j) - \angle G(\text{avg})\}_i^2 \quad (18)$$

A sample calculation of weights is provided in table 3 for the artificial data in figure 12. Template 2 has the highest relative weighting because the template points are more highly clustered than the other templates.

Table 3 - Sample Target Crossfeed Values

Template "i"	$ G(\text{avg}) $	$\angle G(\text{avg})$	$M_{\text{MSW},i}$	$\phi_{\text{MSW},i}$	$W_{\text{NAVFIT},i}$
1	-3.33	-39.0	-2.52	-39.5	.51
2	-6.67	-60.0	-6.42	-59.6	1.00
3	-12.67	-69.0	-12.50	-66.6	.92

## V. ANALYSIS

### Mean-Square Weighted Decoupling Improvement

The "mean-square weighting" (MSW strategy) was applied to design pitch and roll crossfeeds which are robust for all five configurations. The following low-order MSW crossfeeds are obtained:

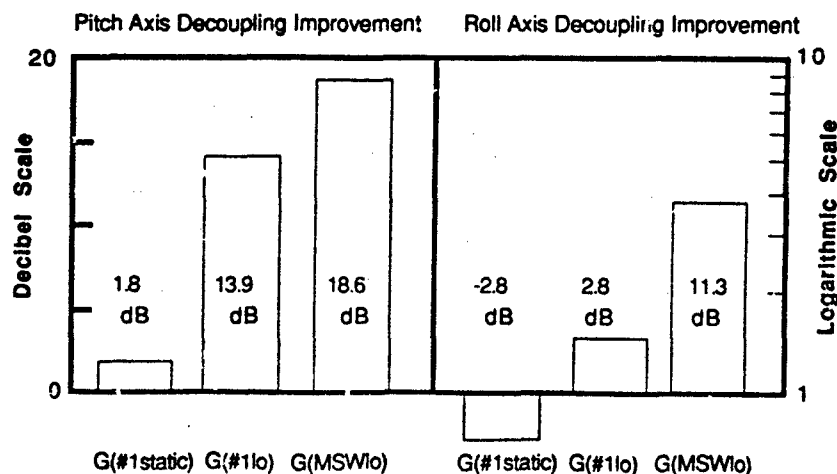
$$G_{\delta_{tot}}^{\delta_{tot}}(MSW_{LO}) = \frac{-0.0272(24.5)}{(4.62)} \quad (19)$$

$$G_{\delta_{tot}}^{\delta_{tot}}(MSW_{LO}) = \frac{0.275(1.61)}{(2.51)(0.292)} \quad (20)$$

These crossfeeds may be compared with those in table 1 which approximated only the nominal "ideal" crossfeed. The weighting did not change the pitch decoupling crossfeed significantly, which already exhibited satisfactory decoupling. The MSW roll decoupling crossfeed has been considerably adjusted relative to the earlier result.

The performance improvement of the three crossfeed approaches (static, nominal, MSW) are compared in table 4. Here the results are referenced to the uncompensated decoupling performance to highlight the differences between the decoupling strategies. In table 4 a value of 0 dB would indicate no relative improvement over the uncompensated case. As shown before, the static crossfeed slightly improves the robust decoupling in the pitch axis, but degrades the decoupling in the roll axis. With the MSW crossfeeds, significant performance improvements are achieved. The pitch rate decoupling improves by 4.6 dB relative to the nominal crossfeed, yielding an overall relative attenuation of 18.6 dB. An even larger improvement in roll rate decoupling is shown. The MSW result is 8.5 dB improved over the nominal crossfeed for an overall relative attenuation of 11.3 dB. Absolute decoupling of both axes (pitch axis decoupling = 48.4 dB; roll axis decoupling = 26.3 dB) is well within the desired goal of 25 dB.

**Table 4 - Decoupling Performance Improvement Summary**



Figures 13 and 14 show a carpet plot of the off-axis longitudinal and lateral frequency responses for all five configurations using the MSW crossfeeds. In both axes, the improved performance of the MSW crossfeeds are clearly apparent. Most of the improvement is gained for frequencies of 1-3 rad/sec which is the critical range for reducing the cross-coupling impact on the bandwidth of the feedback loops. The improvement in roll axis decoupling is especially significant (20 dB) in the crossover frequency-range (1-3 rad/sec).

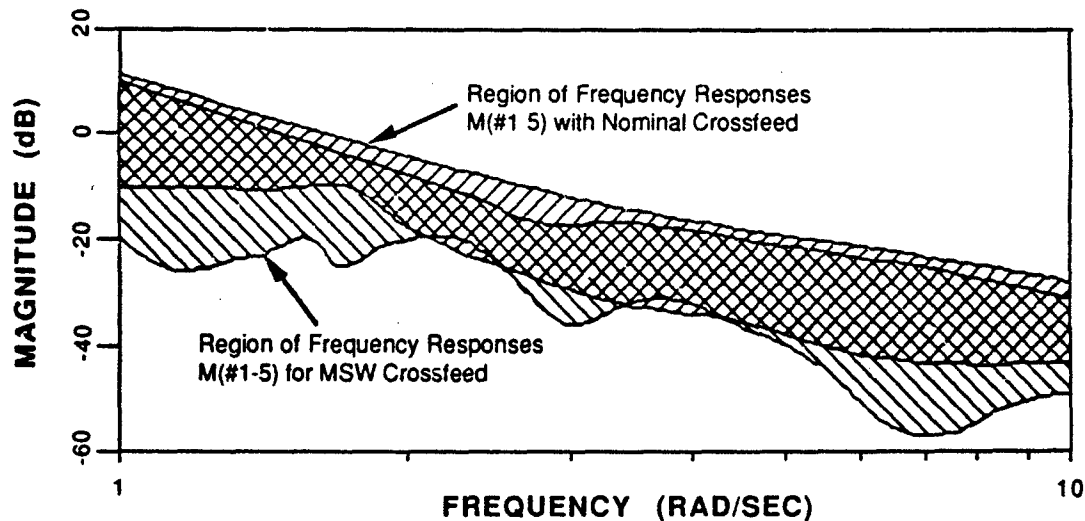


Figure 13 - Comparison of Frequency Response Bounds for Nominal and MSW Compensation - Longitudinal Axis

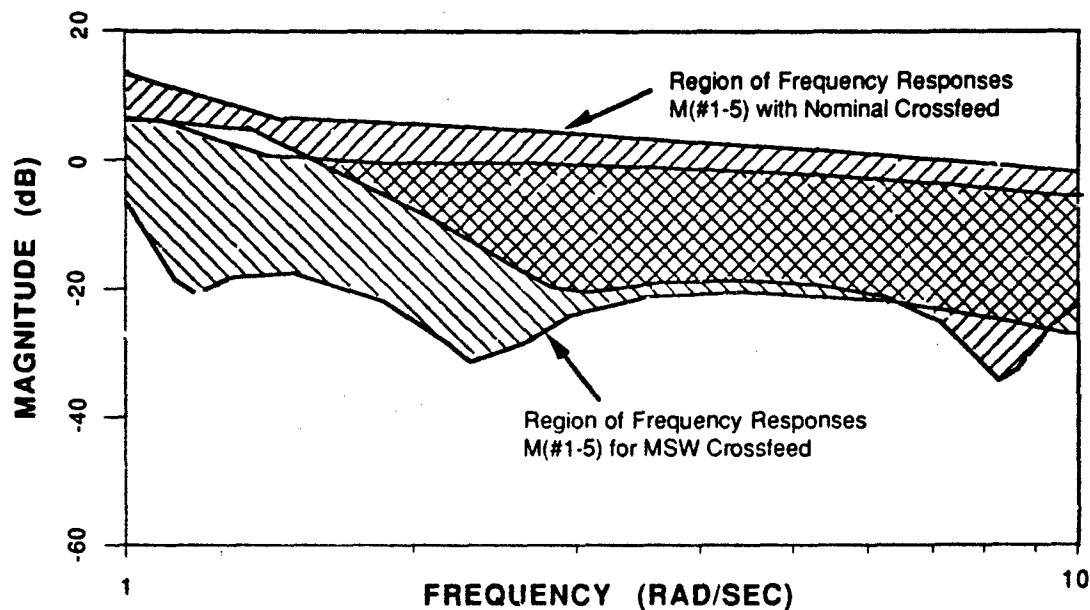


Figure 14 - Comparison of Frequency Response Bounds for Nominal and MSW Compensation - Lateral Axis

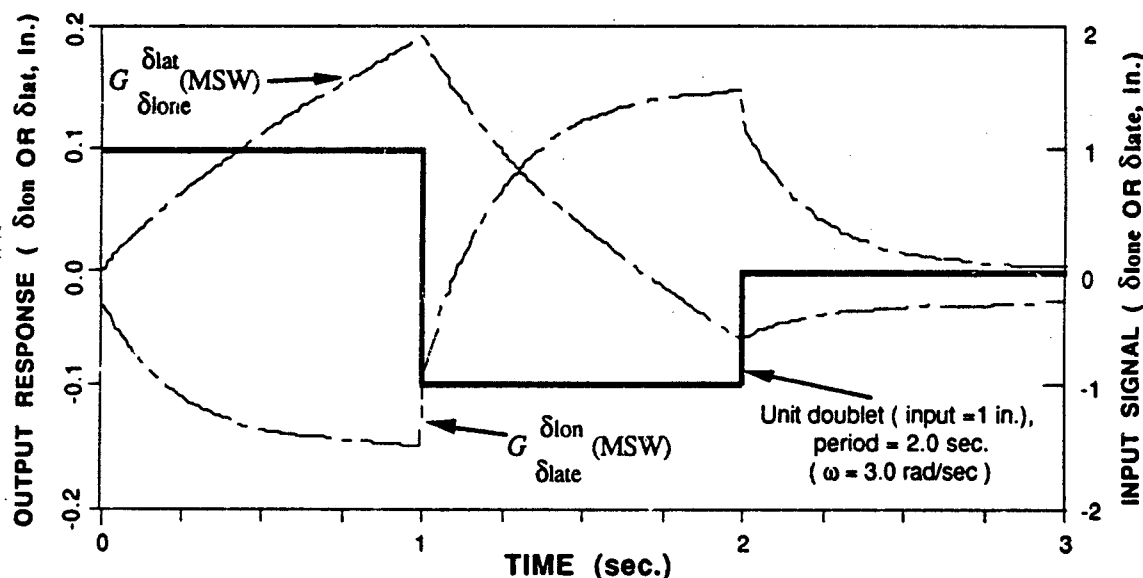


Figure 15 - MSW Crossfeed Time Responses with Doublet Input

Off-axis control activity commanded by the MSW crossfeed is shown in figure 15 for the doublet input to the primary axis. The MSW crossfeeds are seen to command smooth and low bandwidth cross-coupled inputs. These commands would be practical for implementation.

### Metric Robustness.

The average performance metric presented previously does not contain information about the decoupling achievable for a specific configuration. It would be undesirable, for example, for average improvement to be achieved at the expense of severe degradations in specific configurations. To evaluate the extent that this may be a problem, let the off-axis magnitude response of the most improved or "best" configuration be

$$J_{\text{BEST, Strategy}} = \sum_{\omega_i=1}^5 (M_{\text{on},i,1} - M_{\text{B off},i}) / 5 \quad \text{dB} \quad (21)$$

and the least improved or "worst" configuration be

$$J_{\text{WORST, Strategy}} = \sum_{\omega_i=1}^5 (M_{\text{on},i,1} - M_{\text{W off},i}) / 5 \quad \text{dB} \quad (22)$$

where  $M_{\text{B}}$  and  $M_{\text{W}}$  are the dB values from the off-axis performance curves for the best (most improved) and "worst" (least improved) configurations, respectively. These metrics for specific configurations should be compared with the average improvement over all of the configurations as a check for relatively uniform improvement. This check was done for all the crossfeed strategies described in this paper and no anomalies were observed in any of the data sets.

## VI. CONCLUSIONS

1. A new method for the design of robust crossfeeds for rotorcraft flight control systems has been developed. The objective of the design approach is to decouple the family of anticipated dynamic responses over the frequency range of 2-10 rad/sec. This reduces the load on the feedbacks at mid and high-frequencies, and thereby allows a desired reduction in feedback loop bandwidths.
2. The design method makes extensive use of frequency-domain graphical techniques (Bode and Nichols plots analysis) which lends significant physical insight to the design procedure. The approach easily lends itself to computational implementation and computer graphics tools.
3. The method was applied to a reduced order model of the UH-60 Black Hawk helicopter in near-hover flight. Reduced-order (quasi-steady) models and a limited set of configurations (5) were examined. Crossfeed were designed to attenuate the pitch/roll coupling. The new robust crossfeeds were found to provide a significant improvement in the roll coupling from longitudinal inputs as compared to static or fixed operating point dynamic crossfeeds.

Future work will expand the present analysis to include all 24 off-nominal configurations for near-hovering flight and will also include the full-order helicopter dynamics. Crossfeed connections to the yaw and heave channels will also be included. Final crossfeed design will be included in the UH-60 dynamic response as a precompensator for a RASCAL QFT control law design.

## REFERENCES

- 1) Aiken, E. W., Hindson, W. S., Lebacqz, J. V., Denery, D. G., Eshow, M. M., "Rotorcraft In-Flight Simulation Research at NASA Ames: A Review of the 80s and Plans for the 90s," presented at the International Symposium on In-Flight Simulation for the 1990s, Braunschweig, Federal Republic of Germany, July 1-3, 1991.
- 2) Anonymous, "Aeronautical Design Standard - Handling Qualities Requirements for Military Rotorcraft," ADS-33C, Aug 1989.
- 3) Tischler, M. B., "Digital Control of Highly Augmented Combat Rotorcraft," NASA-TM 88346 and USAAVSCOM TR 87-A-5. Ames Research Center, Moffett Field. May 1987.
- 4) Osder, S., Caldwell, D., "Design and Robustness Issues for Highly Augmented Helicopter Controls," AIAA-91-2751-CP, AIAA Guidance and Navigation, and Control Conference, Aug 12-14, 1991, New Orleans, LA.
- 5) Pausder, H. J., Bouwer, G., von Grunhagen, W., "A Highly Maneuverable Helicopter In-Flight Simulator: Aspects of Realization," 14th European Rotorcraft Forum, 20-23 September 1988, Milano, Italy.
- 6) Tischler, M. B., Fletcher, J. W., Morris, P. M., Tucker, G. E., "Flying Quality Analysis and Flight Evaluation of a Highly Augmented Combat Rotorcraft," Journal of Guidance, Control, and Dynamics, Vol 14, Number 5, pg 954-964, Sept-Oct 1991.
- 7) Takahashi, M. D., "Helicopter Flight-Control Design Using an H<sub>2</sub> Method", AIAA Guidance, Navigation, and Control Conference, Aug 12-14, 1991, New Orleans, LA.
- 8) Horowitz, I., "Survey of Quantitative Feedback Theory (QFT)," International Journal of Control, Vol. 53, No. 2, 1991, pp. 255-291.



9) Houpis, C. H., "Quantitative Feedback Theory (QFT): Technique for Designing Multivariable Control Systems," AFWAL-TR-86-3107. Air Force Wright Aeronautical Laboratories, Wright-Patterson AFB, Ohio. January 1987.

10) McRuer, D. T., Ashkenas, I. L., and H. R. Pass, "Analysis of Multi-loop Vehicular Control Systems," ASR-TDR-62-1014. Wright-Patterson Air Force Base, Ohio. March 1964.

11) Jewell, W. F., Clement, W. F., "Crossfeed Compensation Techniques for Decoupling Rotorcraft Responses to Control Inputs," TR-1229-1, Systems Technology, Inc., Sept 1985.

12) Hoh, R. H., Myers, T. T., Ashkenas, I. L., Ringland, R. R., and S. Craig, "Development of Handling Quality Criteria for Aircraft with Independent Control of Six Degrees of Freedom," TR-81-3027. Air Force Wright Aeronautical Laboratories, Ohio. April 1981.

13) Kim, F. D., Celi, R. Tischler, M. B., "Higher-Order State-Space simulation models of Helicopter Flight Mechanics," 16th European Rotorcraft Forum, Sept, 1990, Glasgow, UK.

14) Howlett, J. J., "UH-60A Black Hawk Engineering Simulation Program: Volume I -- Mathematical Model," NASA CR-166-09, 1981.

15) Lee, Eugene A., "LCAP2 - Linear Controls Analysis Program." IEEE Control Systems Magazine, Vol. 2, No. 4, December 1982. pp. 15-18.

16) Hodgkinson, J., and Buckley, J., "NAVFIT - General Purpose Frequency Response Curve Fit Program (Arbitrary Order)," October 1978.

17) Tischler, M. B., "Frequency-Response Identification of XV-15 Tilt-Rotor Aircraft Dynamics," NASA TM 89428, ARMY TM 87-A-2, May 1987.

# **Arc Welding Penetration Control** **Using** **Quantitative Feedback Theory**

**Anthony E. Bentley**

Process Development and Fabrication Division  
Sandia National Laboratories, Livermore, California

## ***Abstract***

Quantitative Feedback Theory was used to design a control system for arc weld penetration control. The feedback signal is obtained by measuring the amount of visible and near-infrared light emitted from the back side of the weld. The system is sensitive enough to use a fiber-optic cable for transmitting the light from the weld to the sensor. This facilitates welding assemblies with limited access to the underside of the weld. Welds of constant penetration have been demonstrated in tests with travel speeds varying from 1.5 to 6 inches per minute (0.64-2.54 millimeters per second), and with 200 percent changes in part thickness. The system also compensates for sharp discontinuities in heat sinking and arc length.

## ***Introduction***

Arc welding encompasses a group of several joining techniques that use an electric arc to melt and join metals. The arc is established between the workpiece and the tip of an electrode, which can be either a consumable wire or a nonconsumable carbon or tungsten rod. When a nonconsumable electrode is used, filler metal can be added by a separate wire not carrying the welding current. Shielding gases (usually inert) are often added to protect the arc and weld zone from oxidation, and provide the desired arc characteristics<sup>1</sup>.

- 
1. American Welding Society, *Welding Handbook* Volume 1, Eighth edition, edited by L. P. Connor, (American Welding Society, Miami, Florida, 1987), pp 4-7.

The feedback technique described in this paper was developed for the girth weld of a stainless steel pressure vessel using the Gas Tungsten Arc (GTA) welding process (shown in Figure 1)—since GTA welding is used extensively throughout the nuclear defense industry. However, the system is applicable to virtually any type of arc welding, and for any part geometry, provided that there is some degree of access to the back side of the weld. For the components designed at Sandia in Livermore, the GTA girth weld is one of the most complicated and critical fabrication processes. If the bond is not of sufficient quality, often the entire assembly must be discarded.

Modern commercial GTA welding equipment operates under the direction of a welding operator who determines proper machine settings. In more advanced systems, individual weld parameters (weld process inputs) such as arc voltage, weld current, travel speed and wire feed speed, are held reasonably constant with feedback control loops; however, set points for the individual weld parameters are selected based on the results of narrow experimental parameter searches, which are expensive even for statistically designed experiments. Characteristics of the back side of the weld such as weld width, depth and surface appearance are used as acceptance criteria during the parameter selection process. In this case however, (since visual inspection of the back side of the weld is difficult) these visual cues are supplemented by nondestructive examination with X-rays or ultrasound, and by destructive sectioning, tensile testing, and bend testing. While these methods are useful, they do not **improve** quality, but simply **inspect** quality, and in the process add tremendous cost to the product.

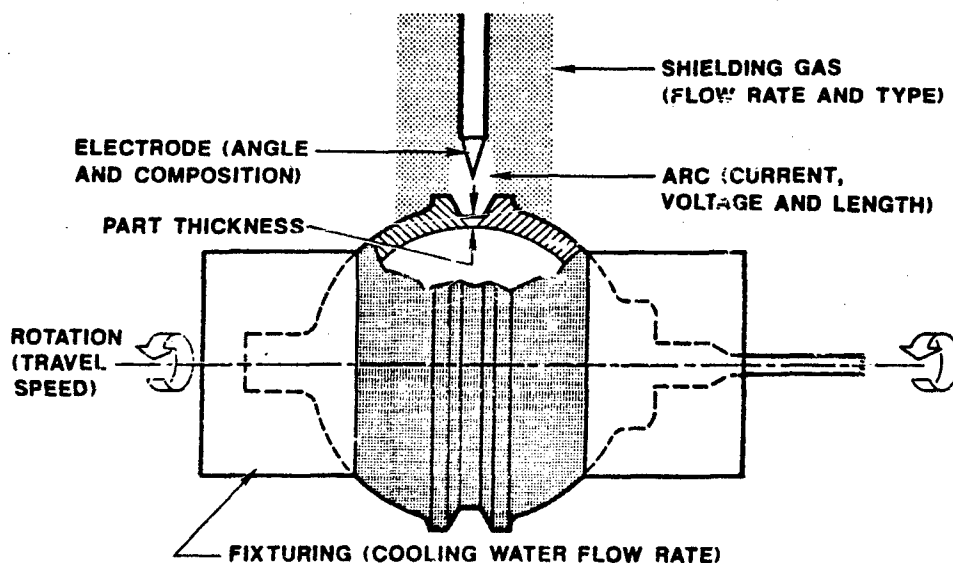


Figure 1. Gas Tungsten Arc (GTA) welding parameters

The goal of this work is to reduce the need for post weld inspection by implementing real time penetration control. This can be viewed as replacing destructive testing with in-process **nondestructive** testing. That is, by utilizing feedback control, weld quality variation can be minimized to the point that inspection becomes unnecessary. Achieving this requires sensor systems capable of accessing weld quality in real-time. As noted by Richardson below, there is currently enormous effort in this area of weld penetration control, yet results have been met with limited success:

Unfortunately, the development of reliable penetration sensors cannot at this time be considered to be broadly successful. This is certainly related to shortcomings of current sensor technologies themselves, but also to the lack of knowledge of how to control penetration once detected. That is, we do not have a good **quantitative** understanding, in engineering terms, of how control is achieved by manipulation of process parameters in the face of a multiplicity of disturbing variables<sup>2</sup>.

Since visual inspection of the back side of the weld is often impossible, the ideal weld penetration sensor would only require access to the top side of the weld. Currently several top-side penetration sensors have been investigated by other researchers; however, all except two use indirect assessments of weld penetration, and therefore introduce uncertainty into the feedback measurement<sup>3</sup>.

The two top side direct penetration measurement methods consist of ultrasonic sensing and a newly patented method involving a video camera. The ultrasonic method uses shear waves through the base metal to determine the location of the fusion interface. This method is difficult to implement because of the necessity to couple the transducers to the workpiece and synchronize sensor movement with the electrode motion<sup>4</sup>. The second method is used in the joining of metal pipes. A small gap is left between the two pipes and a video camera is positioned ahead of the electrode, almost tangent to the workpiece at the weld pool<sup>5</sup>. This gives a "side view" of the weld and allows the controller to actually "see" the depth of penetration for the first weld pass. It works well for the root pass, but gives no penetration information for the remaining fill passes. One problem we have encountered in the fabrication of pressure vessels is called "double-drop-through", when full penetration occurs on a fill pass. This is undesirable because it has been found to cause hot cracking in some alloys and may also produce a concave underbead surface. Therefore, for our application it was necessary for the penetration assessment to apply not only to the root pass, but to the fill passes also.

---

2. Richard W. Richardson, Paul Taylor, "An Experimental System for Full-penetration Gas Tungsten-Arc Welding", Edison Welding Institute Research Brief, B9007, September 1990, p 1. (Emphasis Added.)

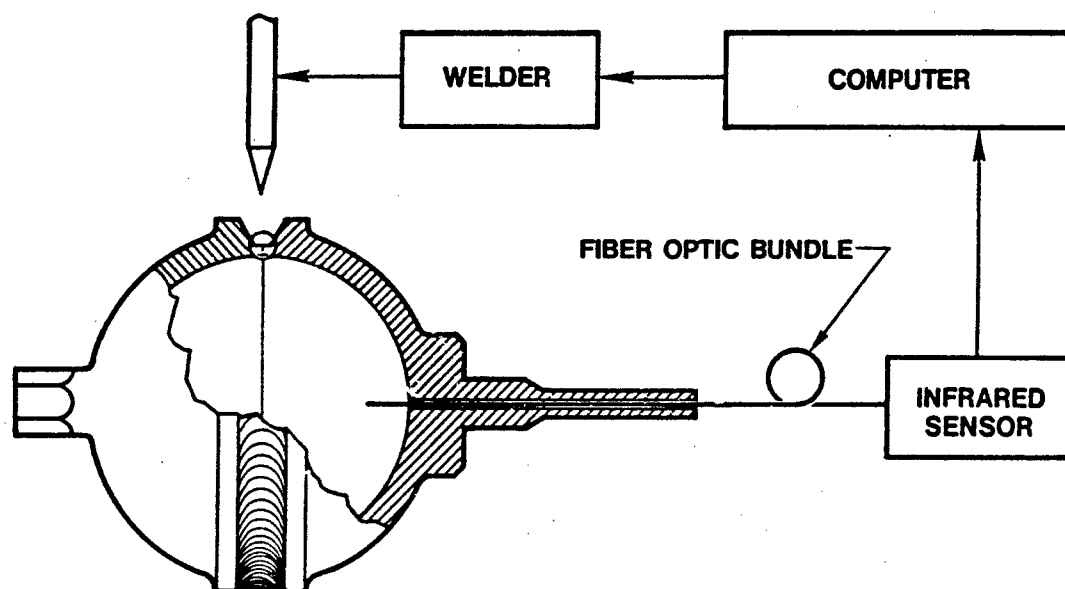
3. R. B. Madigan, H. R. Castner, "Survey of Weld Penetration Techniques", Edison Welding Institute Research Report, MR9002, January 1990

4. Ibid., Page 4.

5. F. Nadeau, P. Fafard, G. Patenaude, J. Tremblay, "Method and Apparatus for Controlling Root Pass Weld Penetration in Open Butt Joints", United States Patent number 4,733,051, March 22, 1988.

For our purposes, then, the ideal feedback technique would measure penetration directly (including partial penetration) for both root and fill passes. Other investigators have explored two methods for direct measurement from the back side of the weld. The first uses a video camera, or a fiber-optic bundle coupled to a video camera, to obtain an image of the underbead. It then uses elaborate processing techniques to determine the fusion zone width. This not only requires synchronization between the optics and the electrode, but also requires enough access to the back side of the weld to position the camera or insert and position the fiber bundle<sup>6</sup>.

The other back side measurement technique uses a simple photo-sensor to measure radiation which is related to penetration. The sensor does not have to be located directly behind the weld if fiber-optic cables are used to direct the light to the photo-diode. This is the method that was used for this study since it has the advantage of being the simplest technique to implement, and yet is considered a direct measurement of penetration<sup>7</sup>. The high-temperature fiber optic cable used is only one sixteenth of an inch in diameter so it can be inserted into the pressure vessel through the fill tube. (See Figure 2.) Also note that the vessel doubles as an "integrating sphere" so that the cable does not have to be aimed at the weld. This improves reliability and greatly decreases measurement complexity by eliminating the need for alignment and synchronization with the electrode.



**Figure 2. Weld penetration control scheme**

6. Madigan, Ibid. pp. 3-4.

7. Ibid, p 3.

At Sandia National Laboratories, this technique was pioneered by Marburger<sup>8</sup>. Initial results were extremely encouraging. The empirically designed feedback system was able to make real-time corrections for large variations in weld parameters to achieve welds of constant penetration. It was found, however, that the relationship between penetration and radiation changed as a function of travel speed. This was attributed to the change in width to length ratio of the molten pool for different travel speeds.

This present study more clearly defines the correlation between back-side radiation and weld penetration, and accounts for the effect of travel speed on the penetration measurement. Also, with the redesigned feedback control system, welds of more consistent penetration were produced with wider variations in weld parameters including travel speed.

Welding systems are inherently uncertain, nonlinear, and time varying in their input/output relationships. Historically, controls have been designed by linearization of system behavior over a narrow range about some operating point. This has produced controllers that are not optimized or even unstable away from the linearization point. To avoid instabilities away from the linearized region, designers often settle for a reduction in open loop gain—not realizing the maximum benefits of feedback. For this work, the control algorithms were developed using Quantitative Feedback Theory (QFT) that does not require linearization<sup>9</sup> and is the ideal tool for design of highly uncertain systems such as welding.

Quantitative Feedback Theory easily handles the design of systems with multiple transfer functions describing the uncertain dynamic characteristics of the process under control. Thus input/output information obtained under a wide variety of weld process conditions to characterize the static as well as dynamic behavior of the welding process, was used in the design. This characterization encompasses the welding system as a whole, not just the arc, weld pool, power supply nor any state variables within the process. This global approach yields a controller that is optimized over the entire range of weld performance explored during the process characterization phase, and has proved able to control well beyond the optimized range.

---

8. S. J. Marburger, "Feedback Control of Penetration in Gas Tungsten Arc Welding", Master of Science Project Report, Spring Quarter 1983, Department of Mechanical Engineering at University of California at Berkeley.

9. Isaac Horowitz, "Application of Fixed Point Theory To Uncertain Nonlinear and MIMO Feedback Problems", Dynamic Systems and Control Division, ASME, Vol. 24, [1990:ASME] pp 45-49.

### Process Characterization

A simplified block diagram for the control system is shown in Figure 3. The elements in the diagram are shown as functions of 's'—implying the use of Laplace transforms. Laplace domain system analysis assumes linearity and time invariance, yet as stated above, the welding process is nonlinear and time-varying. It has been shown, however, that frequency domain techniques (Such as Laplace) can be successfully applied to a large class of nonlinear, uncertain and time varying processes<sup>10-12</sup>.

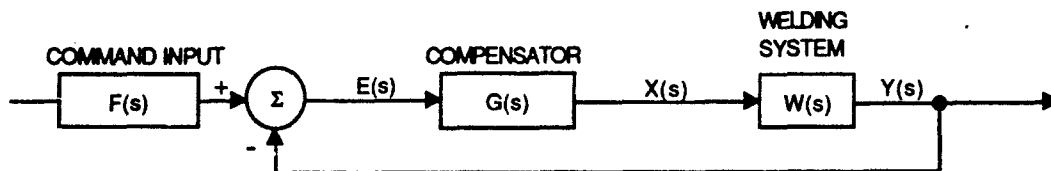


Figure 3. Block diagram of feedback system

For this project it was decided to use weld current as the control variable  $X(s)$  to compensate for process disturbances. Varying only the weld current while holding all other inputs constant, reduces the system to a single-input/single-output system and the transfer function becomes:  $W(s) = Y(s)/X(s)$ , where  $Y(s)$  is the Laplace transform of penetration (measured in volts on the photo-diode) and  $X(s)$  is the Laplace transform of the weld current control signal. All other inputs are considered to be process disturbances—which add uncertainty to the system equation.

To our knowledge, the transfer function  $W(s)$  is not available in the welding literature, but it can be estimated by calculating the ratio of input to output signals (weld current to light reading.) This was done by varying the weld current with sinusoids of various frequencies, and recording the ratio between the radiated light\* and weld current command signal. (See Figure 4.) Collecting this information at several different frequencies+ produces a Bode plot which represents a transfer function of the welding system.

10. Horowitz, M. Sidi, "Synthesis of Feedback Systems With Large Plant Ignorance for Prescribed Time Domain Tolerances", *International Journal of Control*, Vol. 16, pp 287-309, 1972.

11. Horowitz, "Synthesis of Feedback Systems With Nonlinear Time-varying Uncertain Plants to Satisfy Quantitative Performance Specifications", *Proceedings of IEEE*, Vol. 64, No. 1, January 1976.

12. Horowitz, *Synthesis of Feedback Systems*, Academic Press, 1963.

\* Note: The object of this project is to control penetration. Since no purely direct measure of penetration exists, we measure the amount of light from the back side of the weld. This light is measured by amplifying the voltage on the photo-diode—no attempt was made to correlate that voltage to units of light energy, since weld penetration is the really the variable we want to measure, not light energy.

+ Figure 4 shows the input/output information for a single frequency and is not actual data. The actual input data used to test the system was a waveform consisting of several frequencies superimposed together at random phase. Frequency correlation was used to separate out the magnitude and phase information for each frequency individually.

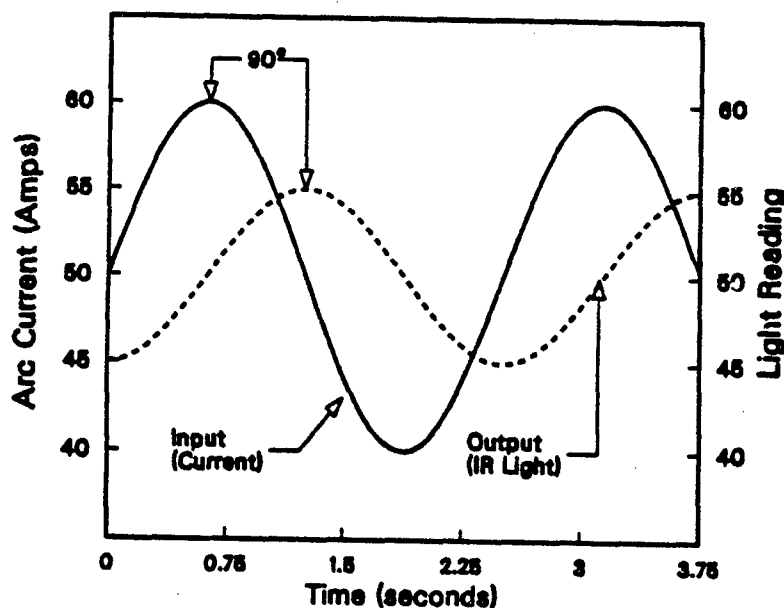


Figure 4. Arc weld input (current) and output (light) data.

Because welding processes are uncertain, each test (even under identical conditions) will produce a different Bode plot. Nonlinearities in the process produce further uncertainties. For example, in arc welding the amount of heat produced (and consequently the amount of glowing metal) is roughly proportional to the square of the weld current. Thus the back side radiation  $R \approx \alpha \cdot I^2$ . Now suppose we test the system with some current waveform whose average value is  $I$ , and then repeat the test with the same current waveform that is scaled by some constant  $\beta$ . Then:  $R_1 \approx \alpha \cdot I^2$ ,  $R_2 \approx \alpha \cdot \beta^2 \cdot I^2$ , and the zero frequency magnitude of the two bode plots will be:

$$\frac{R_1}{I_1} \approx \frac{\alpha \cdot I^2}{I} = \alpha \cdot I \quad \text{and} \quad \frac{R_2}{I_2} \approx \frac{\alpha \cdot \beta^2 \cdot I^2}{\beta \cdot I} = \alpha \cdot \beta \cdot I \neq \frac{R_1}{I_1}$$

Were the welding process linear, with no uncertainty, then the two tests would have produced identical results that is:  $\frac{R_1}{I_1}$  would be equal to  $\frac{R_2}{I_2}$ . But since it is not,

each test will produce its own unique representation of the system dynamics—its own Bode plot. Thus, the system nonlinearities have simply increased the system uncertainty. By testing the system over the entire range of operation, all nonlinearities can be accounted for as increases in uncertainty. However, the system need not be tested for each and every possible condition—only those conditions that produce acceptable outputs. This is because, if the system is designed correctly, only acceptable outputs will be produced by the closed-loop system—any condition which causes the process to head for an unacceptable output will be avoided via feedback control. Therefore, calculating the Laplace transform of all acceptable outputs, and dividing those by the Laplace transform of the corresponding input, gives a set of transfer functions that span the range of uncertainty inherent in the system.



Four such transfer functions are represented in the Bode plots shown in Figure 5. The data was gathered by making full penetration welds on 1.5 inch (3.8 cm) outside diameter stainless steel tubes\* while modulating the weld current at various frequencies. The datum in Figure 5 are from welds made on tubes of three different wall thicknesses. Note that while the phase information seems to be independent of part thickness (possibly due to the fact that all welds were full penetration), the magnitude changes significantly. This is because it takes less current to penetrate the thinner tubes—and minor fluctuations in current will thus yield much greater variations in weld penetration. To further quantify the process uncertainty, more frequency data was obtained for welds made with fifty different combinations of the parameters shown below:

<u>Weld Parameter</u>	<u>Low Setting</u>	<u>High Setting</u>
Transformer tap setting <sup>+</sup>	Low	Medium
Travel speed (inches/min)	2.5 (1 mm/s)	4.4 (2 mm/s)
Part thickness (inches)	1/32 (0.8)	1/16 (1.6 mm)
Arc length (inches)	1/16 (1.6 mm)	7/64 (2.8 mm)

All welds were autogeneous, (with no filler metal). Material composition was not varied in this initial experiment, but was explored later. Data was taken on both single and multiple pass welds of full and partial penetration. The fifty Bode plots produced (shown in Figure 6) constitute a set of weld transfer functions, that span the range of uncertainty in the welding system. (Each weld transfer function will hereafter be referred to as a "plant".) The goal of this project is to design one compensator,  $G(s)$ , that will produce good welds for any plant within the set of weld transfer functions. That is: at any time the weld may "take on" the dynamic characteristics of any one of the plants in the set, and the feedback system must adjust the current to maintain constant penetration.

---

\* The tubes used were readily available and much less expensive than machined pressure vessels of Figures 1 and 2. The dynamics of the relationship between the light emitted from the back side of the molten pool and the radiation measured at the sensor is the same for welds made on the pipes as on the actual pressure vessels. The only difference between the two is in the reflections of the light inside the vessel—a function of vessel or tube geometry—resulting in a steady state shift in the light reading.

+ Changing the transformer tap setting from low to medium results in twice as much arc current and four times as much power for the same input signal.

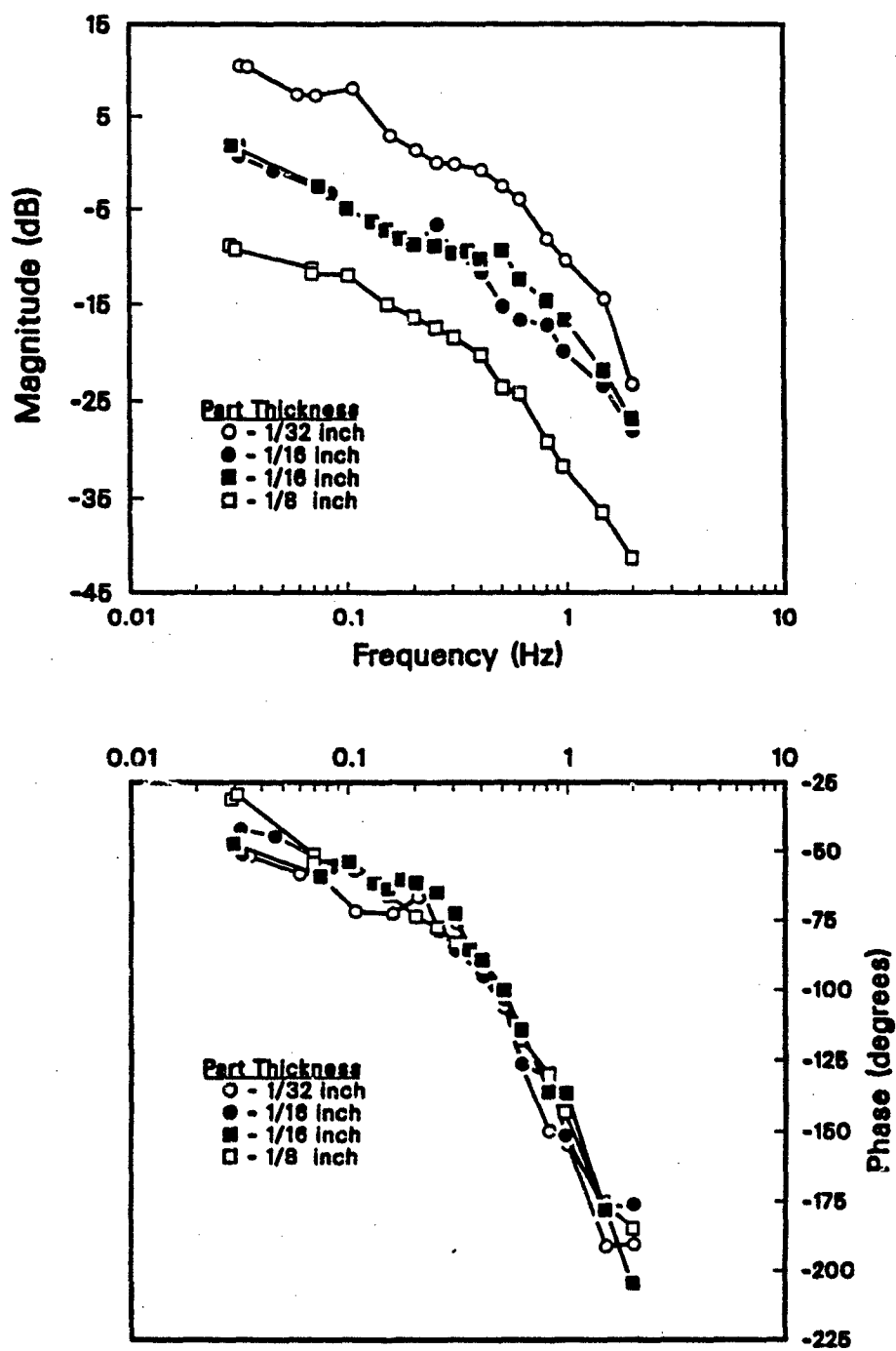


Figure 5. Effect of part thickness on arc weld Bode plots

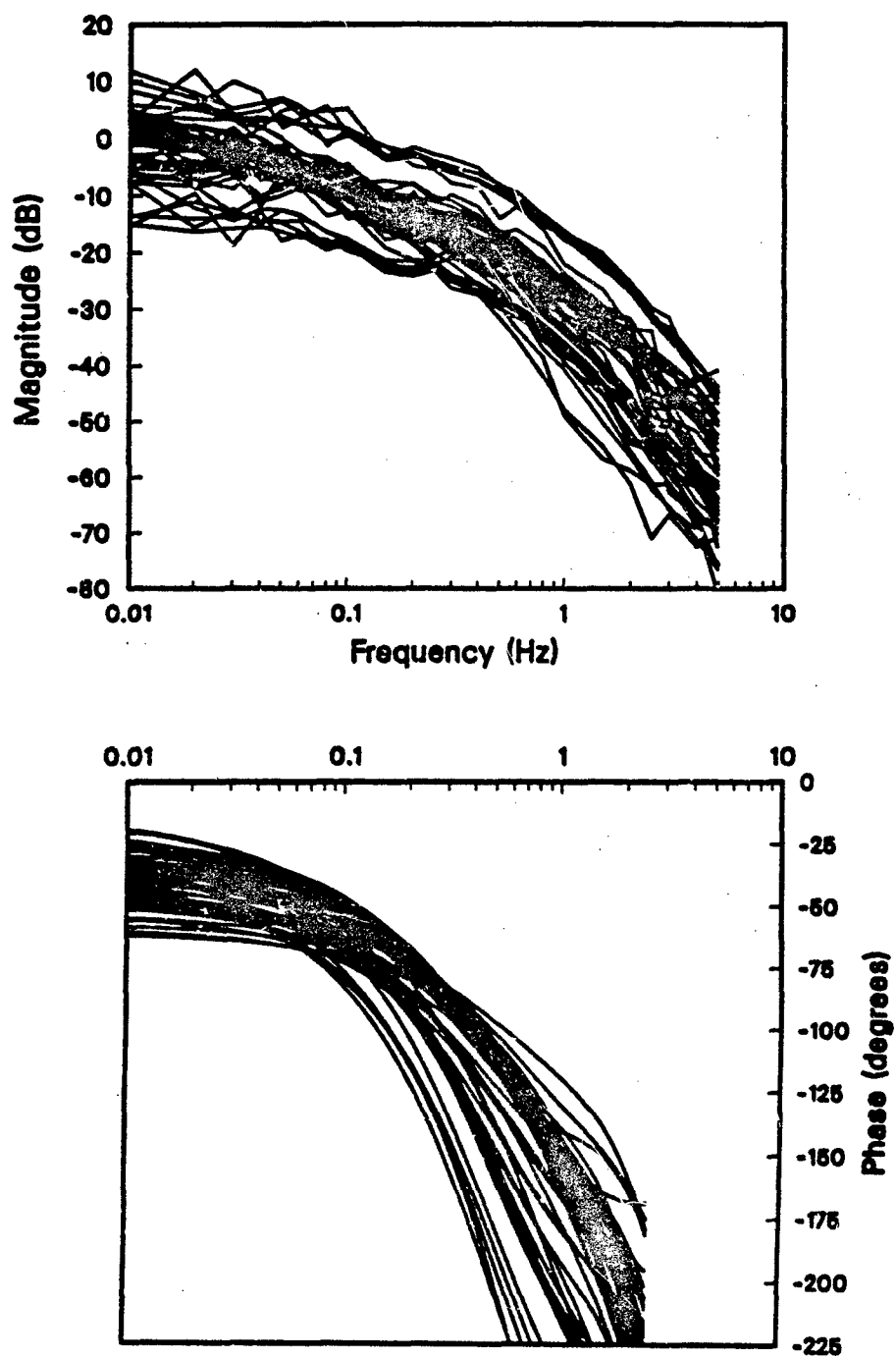


Figure 6. Bode plots for fifty arc welds

### Design Procedure

The feedback system was designed for maximum disturbance attenuation, and minimum response time, overshoot and complexity. The ideal tool for designing a control system to the above specifications is the Nichols chart. The Nichols chart provides a convenient way to graphically "close the loop" on a feedback system. The straight horizontal and vertical lines on the Nichols chart are lines of constant magnitude and phase for the open loop system, and the curved lines represent contours of constant magnitude for the closed loop system. Thus one can quickly get an idea of the relationship between the open and closed loop system response from the Nichols chart.

The frequency information for the fifty welds can easily be plotted in Nichols chart form for a discrete set of frequencies. This produces a set of plant "templates", three of which are shown in Figure 7. These templates give a quantitative measure of the amount of uncertainty in the plant  $W(s)$ . For each frequency, there are fifty points plotted (one for each plant in the set), and they are connected by straight lines. Any plant not represented by one of the fifty points, but within the range of weld uncertainty tested, should fall inside the area bounded by the lines connecting the fifty points.

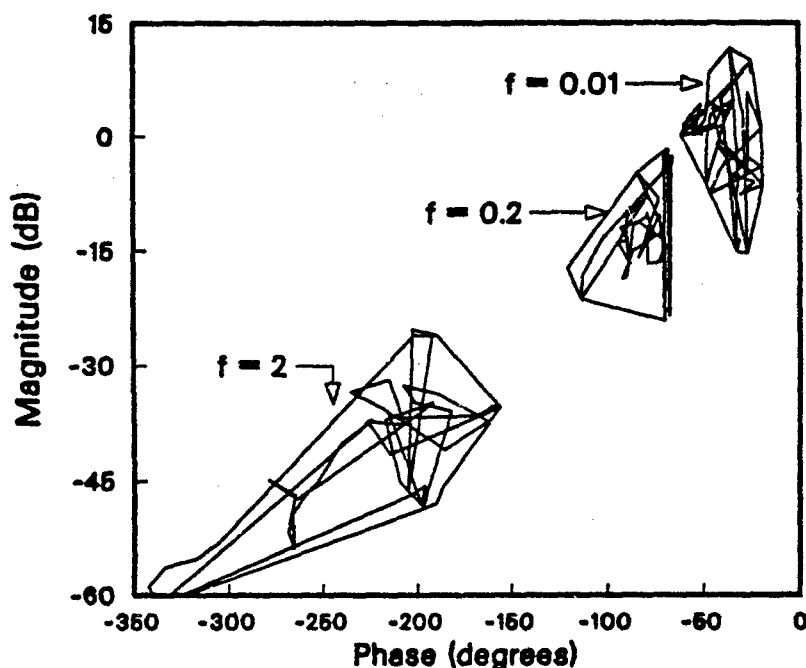


Figure 7. Plant Templates for  $f = 0.01, 0.2$  and  $2$  Hz.

\* As material is melted, a permanent change in the microstructure and geometry occurs. Therefore, the weld underbead is only controllable in the positive direction—there is no mechanism for causing the fusion zone to "un-melt". Because of this nonlinearity, overshoot must be minimized.

If the plant templates are printed on transparent paper, and superimposed onto a Nichols chart of the same scale, the magnitude and phase of the closed-loop transfer functions  $T(f)$  can be read directly from the Nichols chart. This makes it possible to design for all plants in the set at the same time. Any compensation added to the system from  $G(s)$  will affect all plants equally, and thus translate the plant template to another location on the Nichols chart. To guarantee closed-loop stability, it is necessary to ensure that the compensated plant  $L(f)$  [ where:  $L(f) = G(f) \cdot W(f)$  ] stays away from the region on the Nichols chart about  $-180^\circ$ , until the gain is well under 0 dB. The closer a system comes to this area of instability, the more overshoot the closed-loop system will have.

By insuring that the magnitude of the closed-loop transfer function  $|T(f)|$  (where:  $T(f) = L(f) / [1 + L(f)]$ ) is less than some value  $\gamma$  for all plants in the set, one can control the amount of overshoot in the output responses. A typical practice is to design for  $\gamma = 2.3$  dB—which is associated with minimum overshoot and optimum response times. The frequency bounds for the compensator  $G(s)$  (which guarantee a stable closed-loop system with  $|T(f)| \leq \gamma$  for all plants in the set) can be determined by moving the template over the range of the Nichols chart.

Shown in Figure 8 are the Nichols chart frequency bounds in dashed lines. To determine the bounds, one of the plants was chosen as the "nominal", and a hole was made in each template at the location of the nominal. Each template was then moved around the Nichols chart (taking care to keep the template square with the coordinate axes) and the regions were found where all of the plants on the template satisfied the criteria:  $|T(f)| \leq \gamma$ . The boundary where  $|T(f)| = \gamma$  is marked on the Nichols chart (through the hole at the nominal) so that if the compensated nominal plant falls above and to the right of the bound, then  $|T(f)| \leq \gamma$  for all plants in the set.

Assuming the significant process disturbances are primarily low frequency, insensitivity to process disturbances is maximized by minimizing steady state error—that is: minimum variation in magnitude of the closed-loop transfer functions  $\Delta|T(f)|$  at zero frequency. The smallest frequency for which the input/output data was collected was 0.01 Hz, so the system was designed for a maximum error of 1 dB at  $f = 0.01$  Hz. That is:  $\Delta|T(0.01)| \leq 1$  dB.

Also shown in Figure 8 is the "trajectory" of the uncompensated nominal plant  $W_n(f)$  (shown in solid) as the frequency is varied from 0.01 to 1 Hz. The uncompensated system is stable and satisfies all of the bounds except at  $f = 0.01$  Hz. It would therefore not provide the desired level of disturbance attenuation. If the gain were raised to satisfy the bound at  $f = 0.01$  Hz, then it would violate the higher frequency bounds and become unstable. The purpose of  $G(s)$  is to "shape" or compensate the open loop system response so that the closed-loop system meets all design objectives. The trajectory of the compensated nominal plant  $L_n(f)$  is also shown (in solid) in Figure 7 where:

$$G(s) = \frac{53.4 (s + 0.6) (s + 2.2)}{(s + 0.016) (s + 1.3) (s + 36)} \quad (1)$$

The compensated system meets the stability bounds comfortably. The Bode plot of the compensator  $G(s)$  is shown in Figure 9 and that of the compensated nominal plant  $L_n(s)$  in Figure 10. The closed-loop Bode plot for the fifty welds is shown in Figure 11. Note that both design criteria were satisfied.

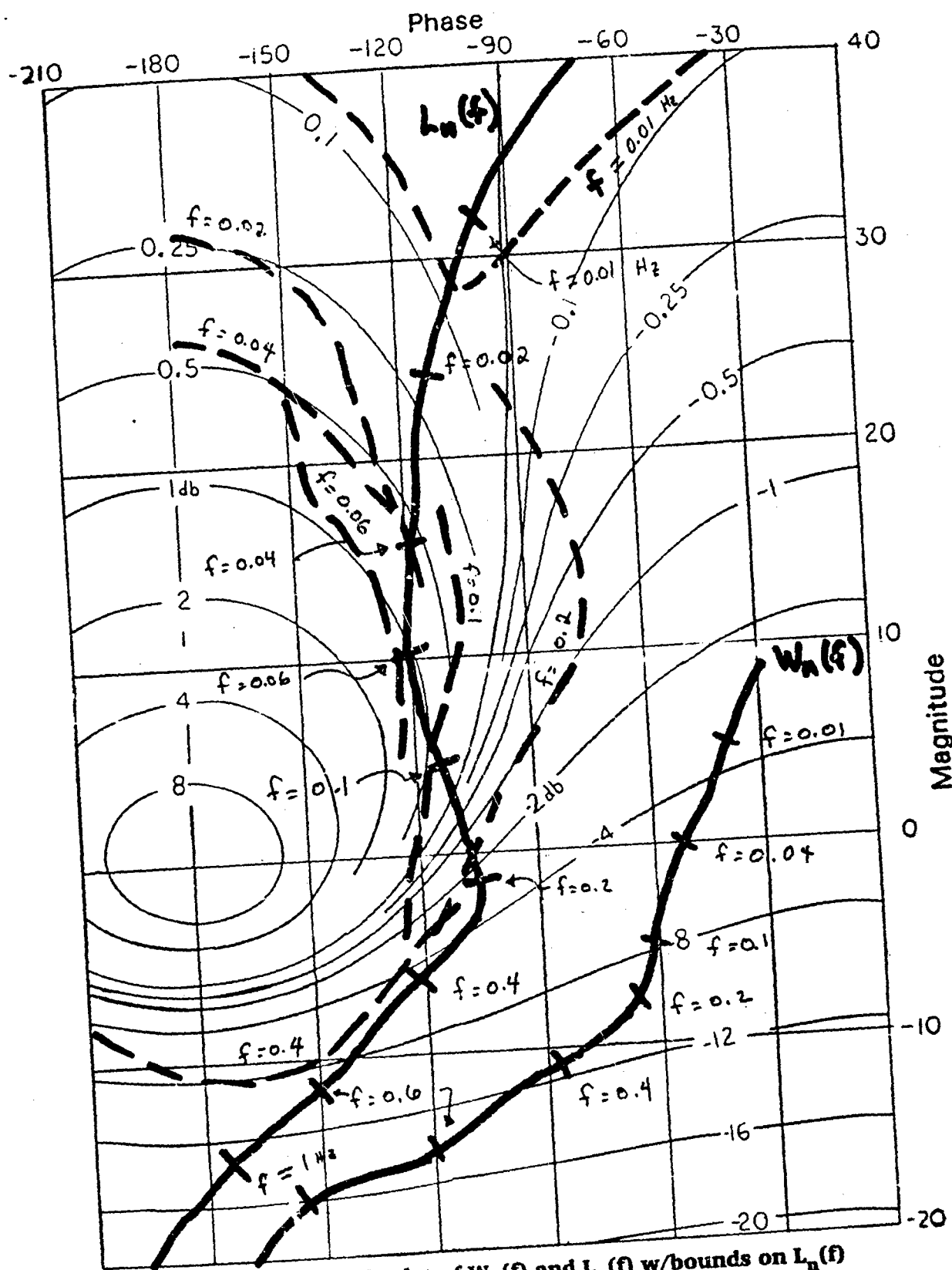


Figure 8. Nichols plot of  $W_n(f)$  and  $L_n(f)$  w/bounds on  $L_n(f)$

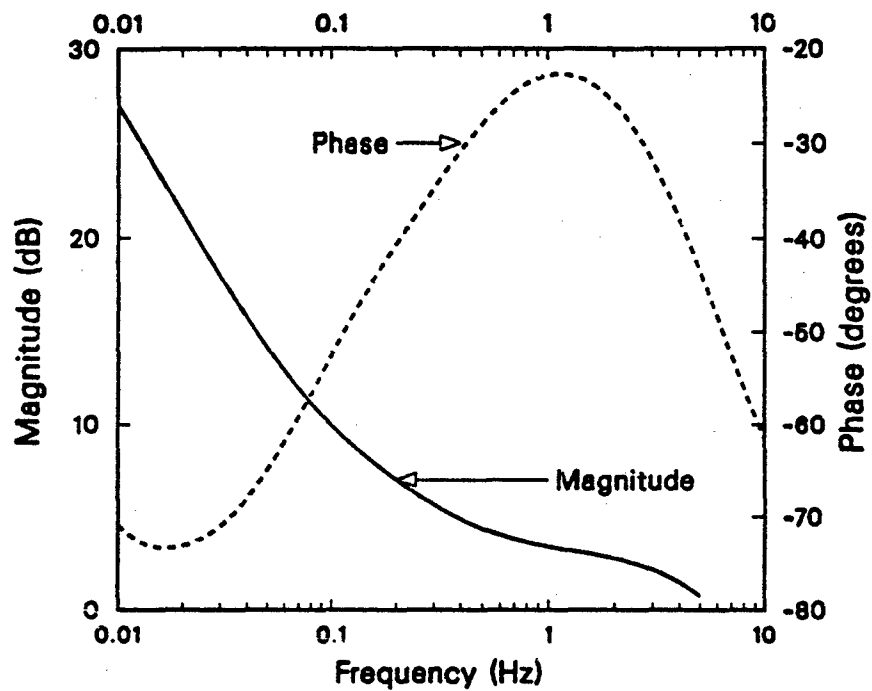


Figure 9. Bode plot of compensator  $G(s)$

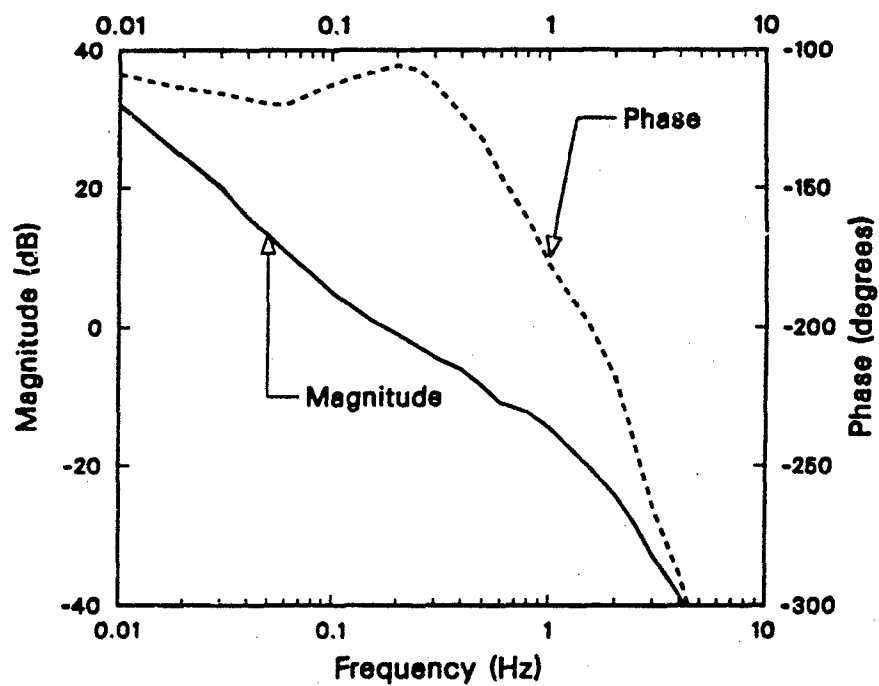


Figure 10. Bode plot of the compensated nominal plant  $L_n(f)$

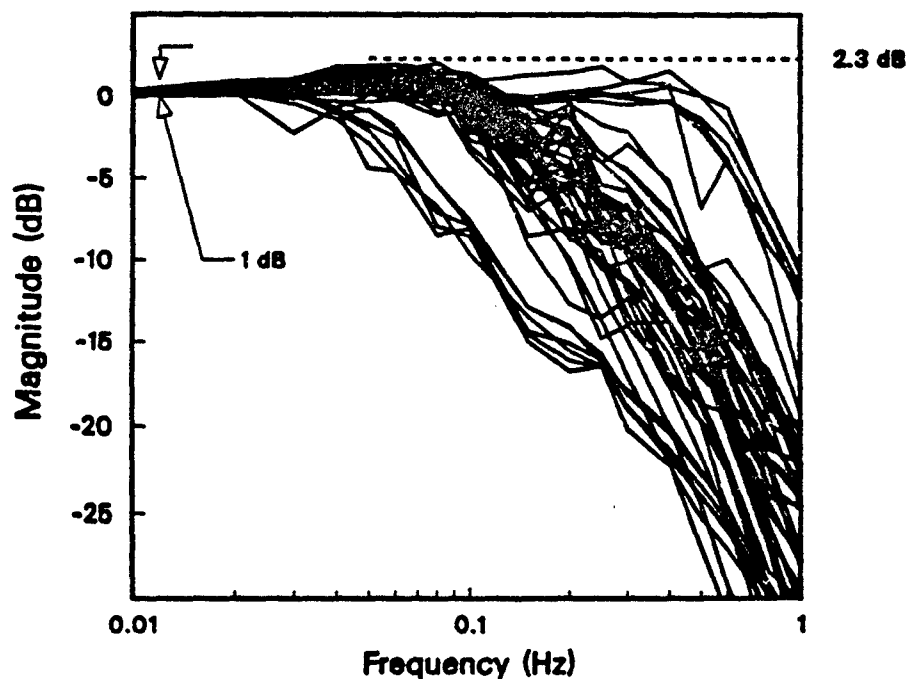


Figure 11. Closed loop Bode plots of welds in Figure 6

The design so far has considered only those control elements needed to minimize system sensitivity to outside disturbances. We now turn our attention to those special provisions needed to establish a stationary full penetration weld and transition into a moving weld while maintaining constant penetration. These provisions, namely the Pre-filter  $F(s)$ , the Set Point Feed Forward loop, the Travel Speed Feedback loop, and the Start Travel Comparator (see Figure 12), also expand the range of disturbances over which the controller can maintain consistent weld quality. The design and operation of these special provisions is best explained by detailing their operation in the complete control system.

In manual welding, the operator first establishes a weld pool, then starts the part rotating, whilst increasing weld current to maintain the pool size. This is emulated by the expanded control system shown in Figure 12.\* Notice the addition of a set point feed forward loop and a travel speed feedback loop.

The system works as follows: At the start, both the travel speed and radiated light signals are zero (since there is no weld to emit light and the part is not rotating.) The controller initiates the weld with a 'step function' change in weld current—a sharp change from zero to a pre-defined nominal current.+ Initially, the feedback signals,

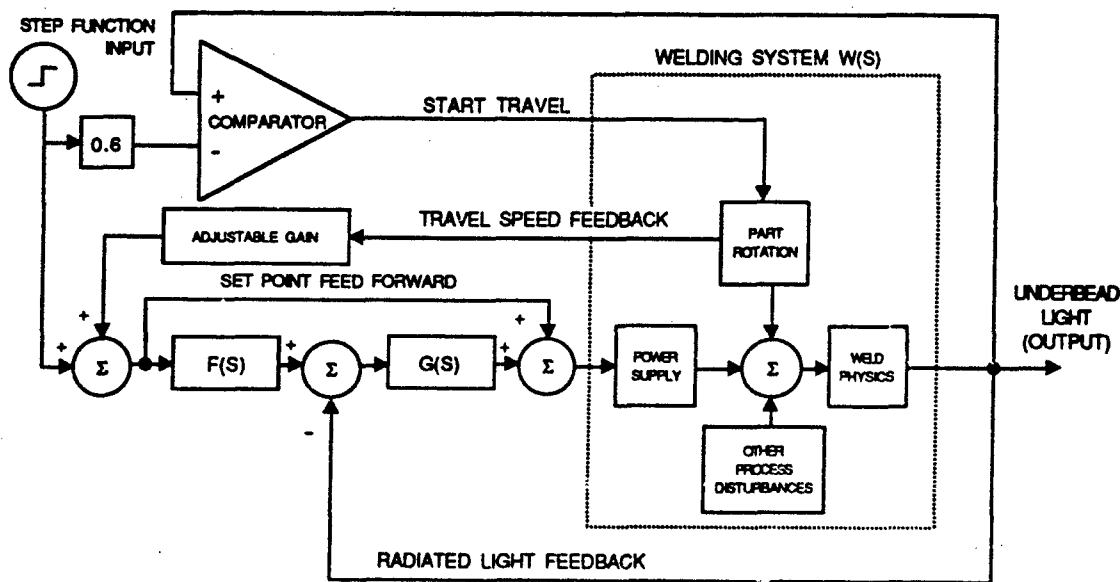
\* Figure 12 is an expansion of Figure 3. The welding system  $W(s)$  has been broken up into four components: The power supply, part rotation motor, weld process uncertainty (disturbances) and the remainder is lumped together under the label 'weld physics'.

+ The nominal weld current can be predetermined for each part by the welding operator, or if desired, the operator could guess a nominal current and allow the controller to automatically adjust to the true nominal setting.



along with the start-up filter output, are zero, so the Step Function Input drives the power supply with the nominal current and the weld pool begins to form. As the weld penetrates the joint, the photometer begins to register light. This signal is fed back and compared to the output of the start-up filter  $F(s)$ . The start-up filter smooths the Step Function Input to a signal that more closely approximates the process of an establishing and growing weld pool. The difference between the approximated start-up signal and the actual Radiated Light is called the error signal and is processed by the compensator  $G(s)$  and added to the nominal current setting to adjust the weld current control signal. If the weld is responding nominally, the error signal will be small, and the controller will continue to weld at the nominal current. Changes are made to the weld current only when there is a difference between the actual and desired penetration.

When weld penetration reaches the appropriate depth, the controller should start the part rotating. This is accomplished by the Start Travel signal and Travel Speed Feedback loop. When the light reading reaches 60% of the set point, the Comparator starts the part rotating, and the Travel Speed Feedback increases the set point (thereby increasing weld current) to maintain penetration. The magnitude of this adjustment was determined empirically, and is proportional to travel speed. Travel speed variations during welding are also handled in the same manner.



**Figure 12. Expanded block diagram of feedback system**

- \* However, the width-to-length ratio of the molten region decreases as travel begins. That is: a traveling weld will produce a molten region that is longer and narrower than a stationary weld. The light signal may be the same, but the weld will be narrower. To maintain constant underbead width, the controller must increase the set point for traveling welds.

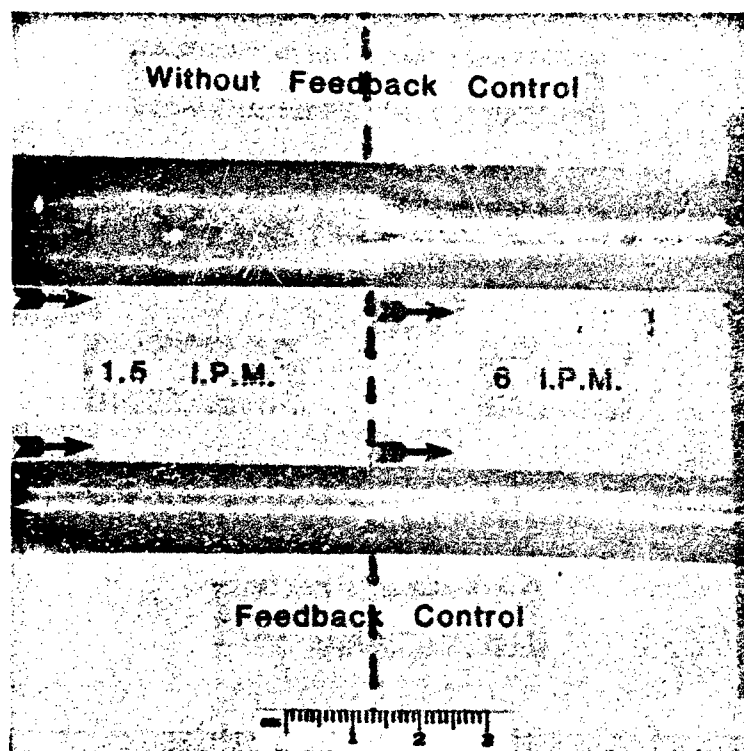
## **Experimental Results**

The system was tested with various disturbances to the welding process to determine how well the controller would be able to maintain penetration. Figure 13 shows two welds made with a step change in travel speed from 1.5 to 6 inches per minute (0.64 to 2.54 mm/s). (All of the test welds were made on tubes. After welding, the tubes were cut longitudinally and flattened-out.) Figure 14 shows that the controller had no problem compensating for step-changes in heat-sinking, while this disturbance caused large variations in the welds made without feedback. Figure 15 shows the end view of a pipe that was welded to test the system tolerance to changes in part thickness. The system had no trouble welding this part, so in order to further disturb the system, step-changes in heat-sinking was also added. (See Figure 16.)

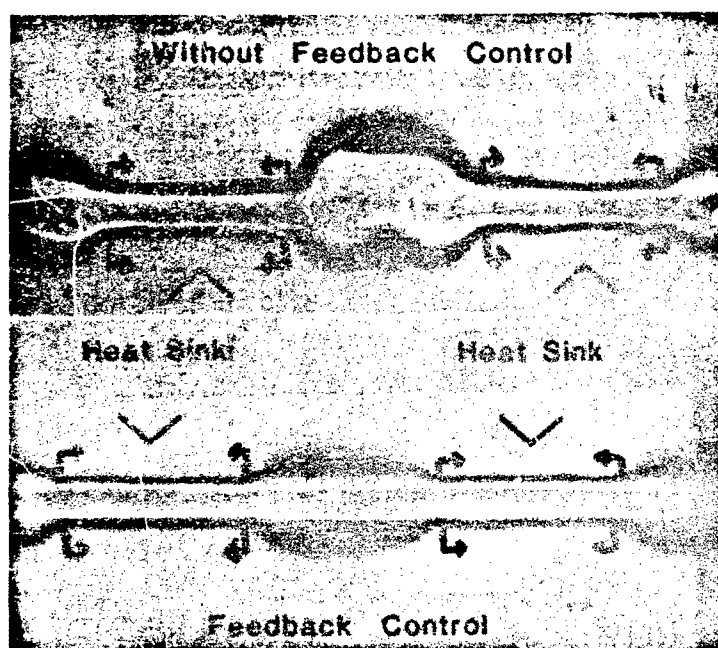
The system was next tested on the tube shown in Figure 17, which not only introduces step-changes in part thickness, but also step-changes in arc voltage—which is related to arc length. (An Arc Voltage Controller [AVC] is normally used that adjusts the position of the electrode up and down to maintain constant arc voltage. The AVC was not used in this test.) The tube was difficult to flatten out, so the results are shown with two photographs of the same part, taken at different angles. See Figures 18 and 19. The first weld (Weld A in Figures 18 and 19) compensated remarkably well, except when the weld was coming off the bottom plate where it pulled away from the tube causing light to come from between the bottom plate and the tube, and be interpreted as penetration. The next weld (Weld B) did much better, because the first weld had sealed the bottom plate to the tube, thus preventing the above mentioned problem. Weld C was made without feedback control.

In order to assess the system sensitivity to sensor positioning, twelve welds were made, on the same tube, at the same set-point, but at different distances from the light cable. The width for each weld was measured and is plotted versus distance in Figure 20. Although the underbead width variation as a function of distance from the fiber cable was significant, it is clear that positioning the sensor accurately enough to maintain constant penetration will not be difficult. Also note that there is an optimum distance for maximum sensor input, at about three inches (7.6 cm) from the end of the light cable.

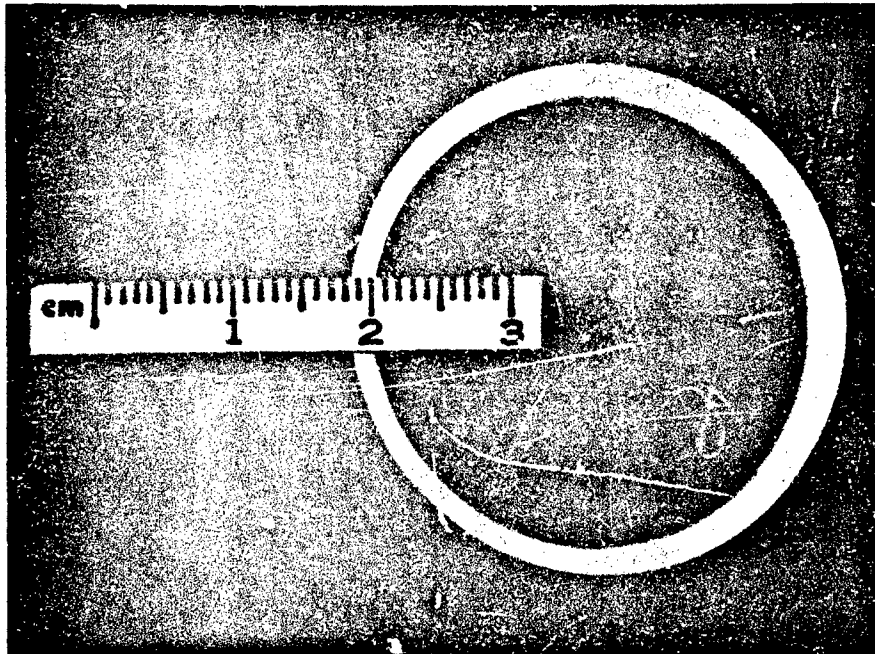
Originally there was some concern that with open groove butt welds, the arc light would shine through and be interpreted as penetration. To address this question several welds were made on tubes with open grooves from 0.03 to 0.09 inches (0.76 to 2.3 mm) wide. For the tubes with the 0.03 inch gap, weld penetration was unaffected by the presence of the gap. This is most likely because any light coming through the gap enters the vessel at a right angle to the fiber cable—and therefore is not well coupled to the photo-diode. The system did have trouble keeping constant penetration with larger gaps because a greater portion of arc light was being picked up by the sensor.



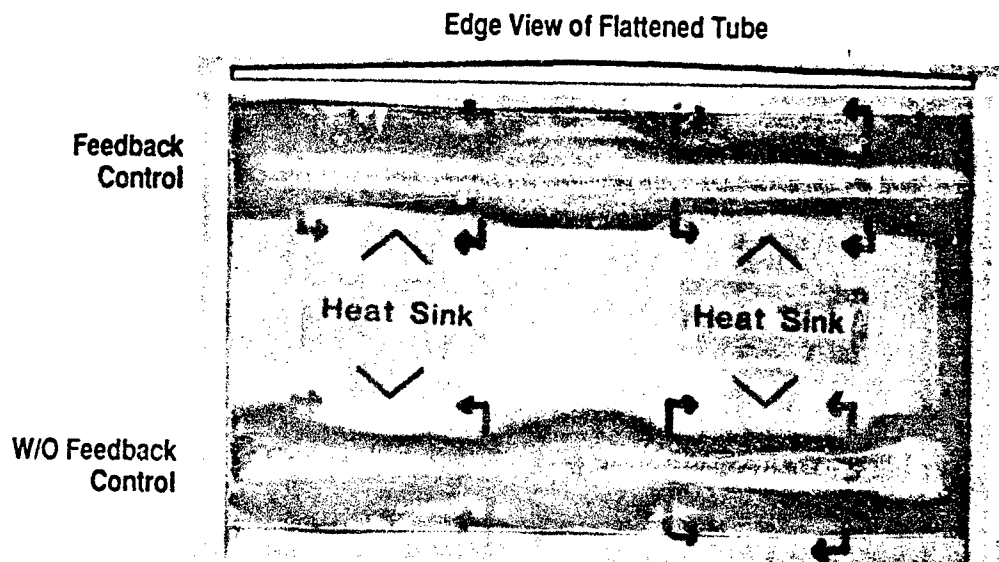
**Figure 13. Welds made with step changes in travel speed from 1.5 to 6 inches per minute (0.64-2.54 mm/sec)**



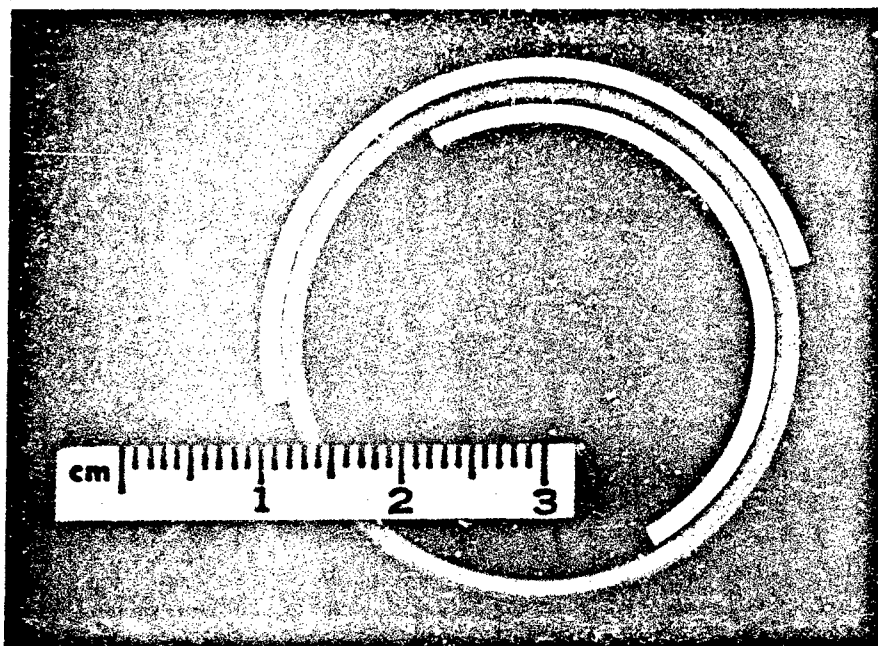
**Figure 14. Welds made with sudden changes in heat sinking**



**Figure 15. End view of variable thickness tube**



**Figure 16. Welds made on Figure 15 tube with changes in heat sinking**

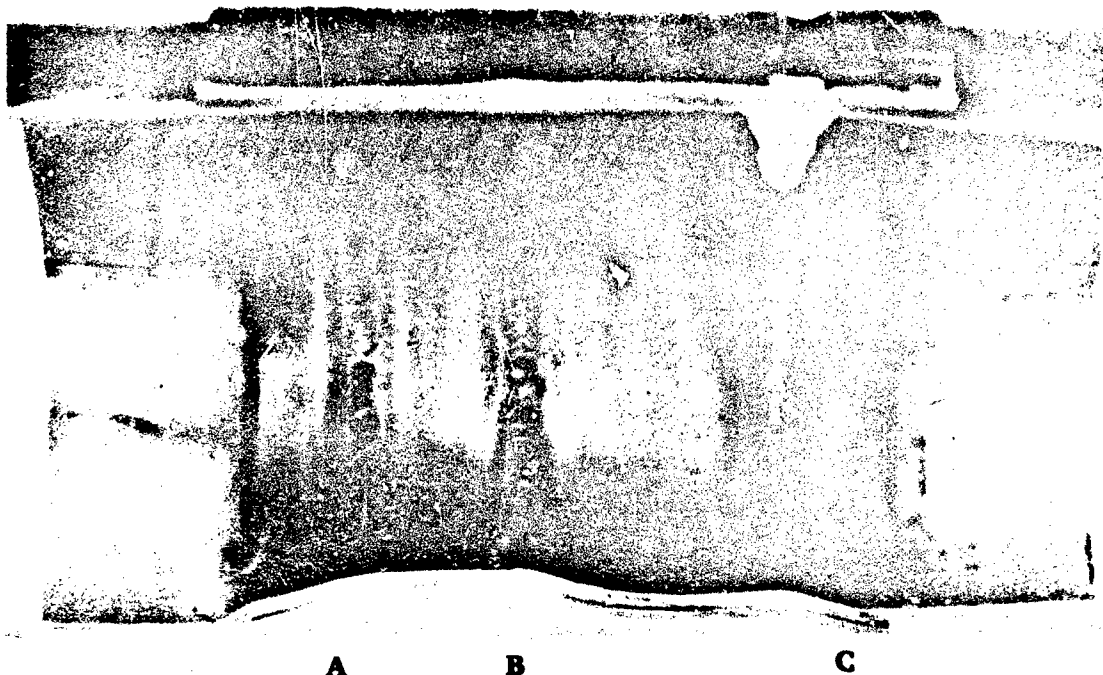


**Figure 17. Tube with step changes in thickness and arc length**

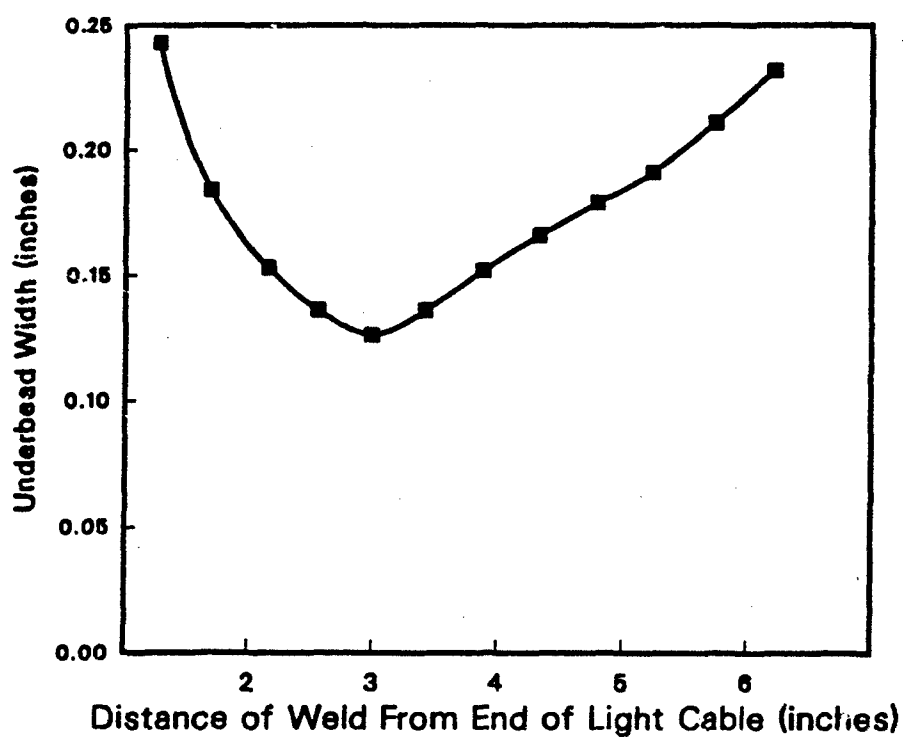


**A                      B                      C**

**Figure 18. Welds on Figure 12 tube (A & B with—C without feedback)**



**Figure 19. Welds on Figure 12 tube (A & B with—C without feedback)**



**Figure 20. The effect of distance on light reading**

### Controller Refinements

Once the control system was built, it was possible to make welds of constant back-side radiation, and the relationship between travel speed, radiation and underbead width was more accurately quantified. As would be expected, travel speed has a nonlinear effect on the penetration measurement. This is illustrated in Figure 21. Figure 21 plots underbead width versus back-side radiation for three different travel speeds. Assuming that radiation is proportional to the area of the molten pool, the effect of travel speed on this relationship can be modeled. Since the area of an ellipse is proportional to the width "W" times the length "L", the radiation "R" is also proportional. The width can be measured after the weld is made, but the length must be calculated. For zero travel speed the length is equal to the width, and increasing the travel speed will cause the length to increase proportionally to the width. Therefore:

$$L = \beta \cdot W \quad (2)$$

Where  $\beta$  is greater than or equal to one, and is a function of travel speed. Then the area (and thus the radiation) is proportional to the width squared. That is:

$$R = \alpha \cdot W^2 \quad (3)$$

The solid lines in Figure 21 are the result of a least-mean-square fit of Equation 3 to the data from several welds made at 1.5, 3 and 6 inches per minute (0.64, 1.3 and 2.54 mm/s). The set point adjustment needed to maintain constant penetration with variations in travel speed is different depending on the desired underbead width, and is not simply proportional to travel speed.

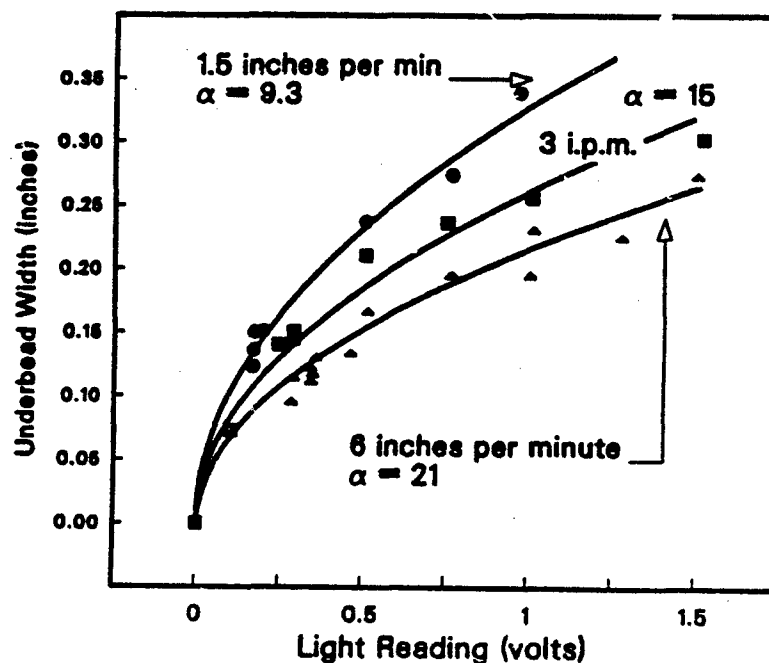
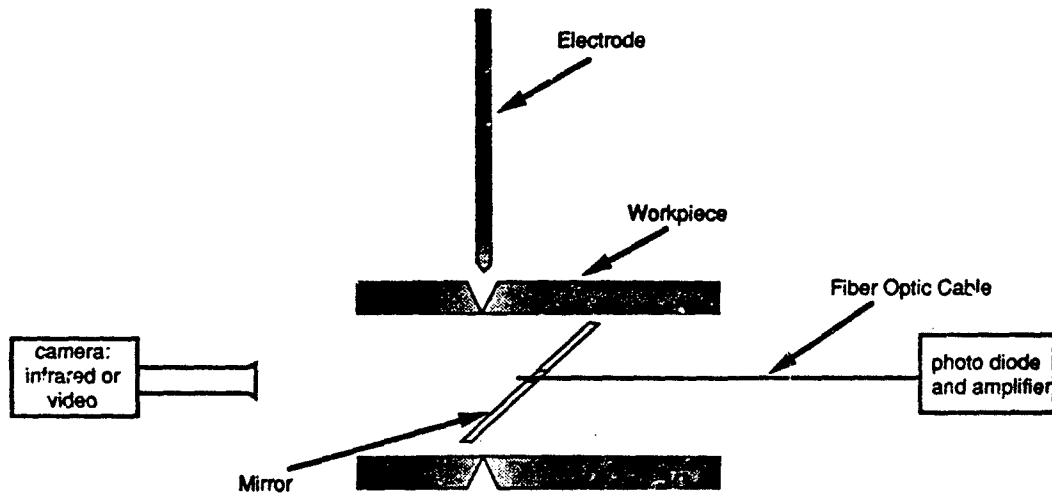


Figure 21. Effect of travel speed on the light reading

## ***The Nature of Underbead Light***

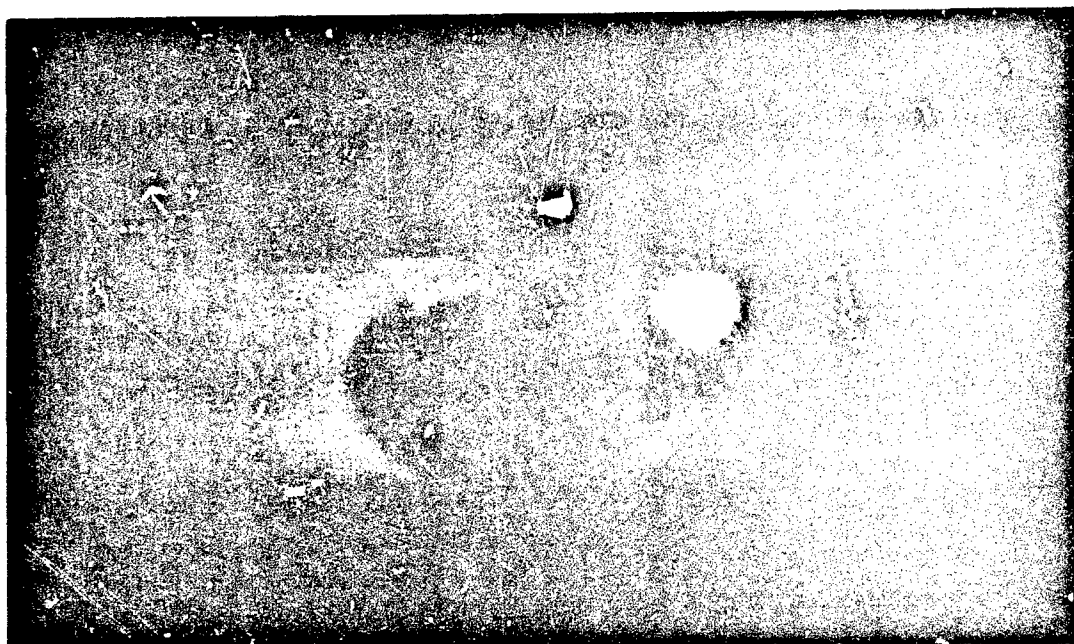
All of the above mentioned test welds were made on stainless steel. The original system utilized an opaque filter between the end of the fiber cable and the photo-diode to attenuate visible light, and pass infrared. This was done to remove ambient light from the penetration reading,\* and worked well until a new application arose for welding on carbon steel. A large difference was observed in the relationship between backside radiation and penetration for the two different steels. In order to understand this difference an infrared imaging system was set up, as shown in Figure 22, to determine what the sensor was actually seeing. The infrared images for two welds made on the two different steels, but with identical weld parameters are shown in Figures 23 and 24. Note that for the carbon steel weld, a much greater portion of the back-side radiation is coming from the area surrounding the fusion zone than for the stainless steel weld. Figure 25 shows the image from a regular video camera on the same carbon steel. Note that the visible underbead radiation is concentrated in the weld puddle—and thus for controlling weld underbead width, visible radiation is a better feedback parameter than infrared, yet for partial penetration welds, infrared is more significant. For this reason, the opaque filter was removed to allow all available light to pass on to the photo-diode.



**Figure 22. Set-up for monitoring input to fiber optic sensor**

\* It was later discovered that the ambient radiation read by the sensor was negligible compared to the radiation (both visible and infrared) coming from the back side of the weld. (Unless, of course, the ambient light was aimed directly at the sensor or fiber cable.)

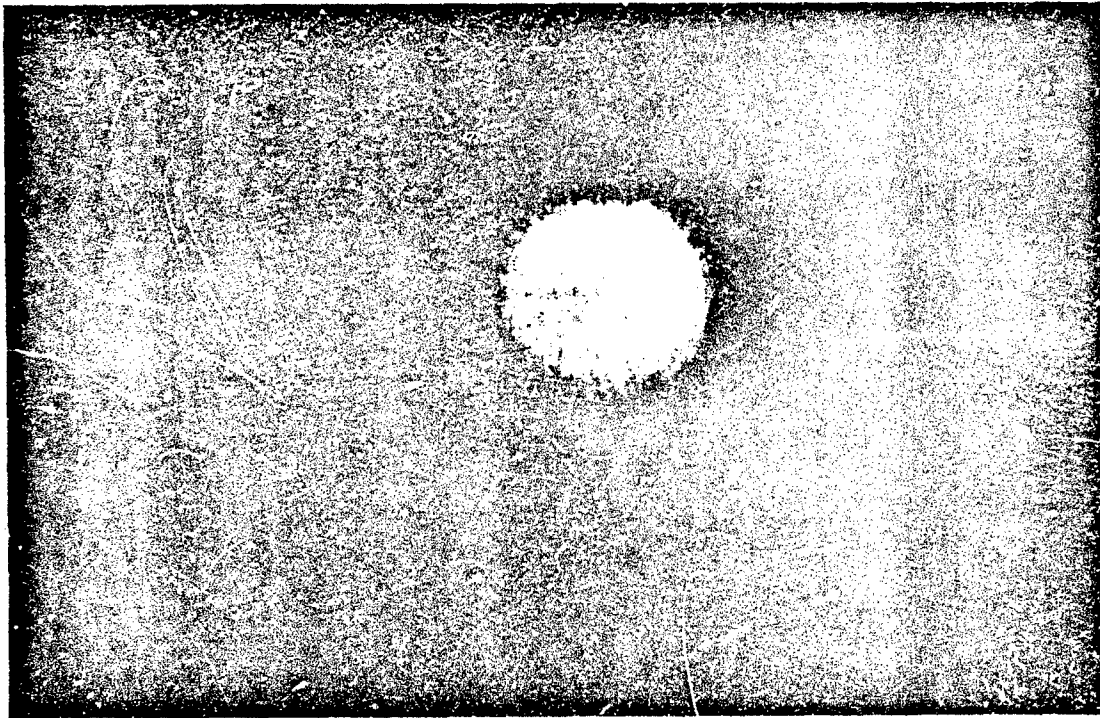




**Figure 23. Infrared video image of stainless steel weld**



**Figure 24. Infrared video image of carbon steel weld**



**Figure 25. Visible video image of carbon steel weld**

### ***Conclusions and Future Work***

Overall, the back-side radiation feedback system worked well in reducing the process sensitivity to changing weld parameters and disturbances. It has been tested with travel speeds ranging from 1.5 to 6 inches per minute (0.64 to 2.54 mm/s) and with +100% to -50% step changes in part thickness. It also compensates for sharp discontinuities in heat sinking and arc length. Furthermore, the process was found to be reasonably insensitive to fiber-optic cable alignment and position (as long as the cable is not aimed directly at the weld).

The next step will be to use the feedback system for welding actual pressure vessels. This will require penetration control for not only the root pass but also the fill passes. Arc welding systems are inherently noisy (electrically), and are notorious for causing digital electronic equipment to "crash". To eliminate the possibility of the system "crashing" during a weld, the prototype controller was implemented in analog hardware. An electrically shielded personal computer will be used in future work to implement the control laws. This will facilitate multipass weld control and more accurate compensation for variations in travel speed. It will also make the system more flexible and "user friendly". Eventually the user will be able to specify the part geometry, material composition and desired penetration for the root and fill passes and then use the computer to calculate the corresponding set points that will be needed to make the entire part. It will also be necessary to determine the effects of other disturbances to the system. Specifically: what would be the effects of variations in wire feed rate, material composition, surface preparation, joint geometry, cleanliness, and electrode angle and composition.

Many of the problems encountered in welding are related to variations in temperature caused by changes in energy input, heat sinking, misplacement of energy source, etc. This feedback control technique has the potential to reduce or eliminate a number of these and other problems because it tends to maintain the fusion zone at a constant size and temperature. However, additional studies are required to determine what effect the control technique will have on internal voids, the propensity for cracking, cold shunts, and other welding problems.

### **Acknowledgments**

There are many people who have contributed to this work. The author wishes to thank Dr. Isaac Horowitz of The University of California at Davis who developed "Quantitative Feedback Theory" (QFT)—which made this design both practical and understandable. Modeling and imaging expertise was provided by Lee A. Bertram, William S. Winters and Elizabeth A. Fuchs. Technical assistance was provided by Rich H. Campiotti, Anthony E. Chavez and Dean R. Williams—and a special thanks to Antonio J. De Sousa who spent many hours making and evaluating the welds. The contributions of all these people are sincerely appreciated. This investigation was carried out at Sandia National Laboratories in Livermore, CA. The support of the United States Department of Energy under contract DE-AC04-76DP00789 is gratefully acknowledged.

# **Pinch Weld Quality Control** **Using** **Quantitative Feedback Theory**

**Anthony E. Bentley**

*Process Development and Fabrication Division*

Sandia National Laboratories, Livermore, California

## **Abstract**

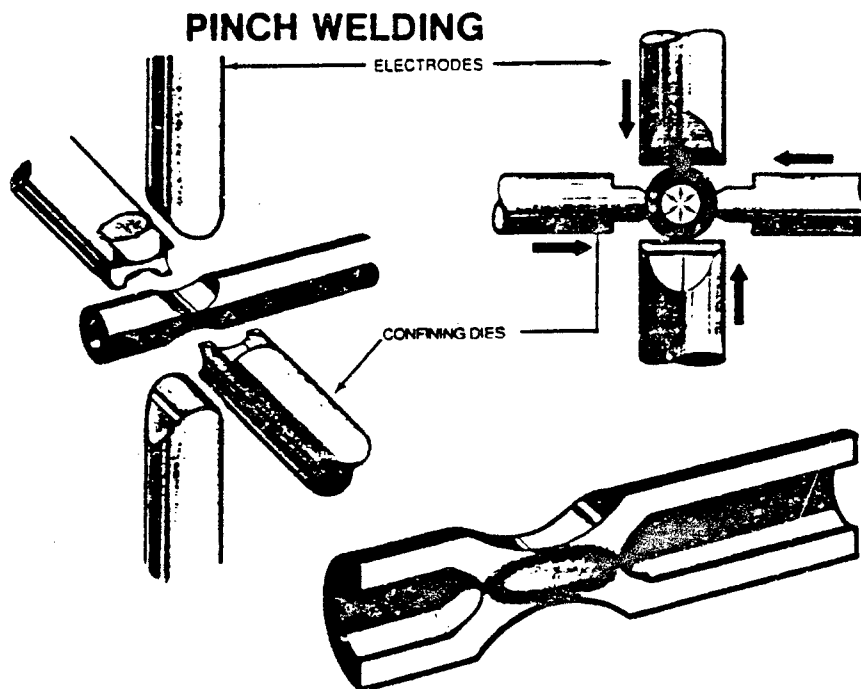
A system based on electrode displacement feedback is developed that greatly improves quality control of the pinch welding process. A correlation between weld quality and electrode displacement is established for constant force. The system is capable of producing repeatable welds of consistent thickness (and thus consistent quality), with wide variations in weld parameters. This is the first time feedback control has been successfully applied to pinch welding. *Quantitative Feedback Theory* (QFT) was used to design the control laws.

## **Introduction**

Pinch welding is a resistance welding process used to seal stainless steel tubes. It is the last step in the fabrication of complicated pressure vessels that must be highly reliable. Since there are currently no nondestructive evaluation techniques available to completely verify weld quality, the welds must be cut open and evaluated under the microscope. However, total bond length and the shape of the end regions at the interface can be determined (non-destructively) *after* a weld is made, from an x-ray radiograph. Weld quality can be estimated from this information. If the total bond length does not significantly exceed 0.1 inch or the shape of the end regions show excessive extrusion, the entire assembly must be discarded. Since there is often no possibility of rework, quality control is of paramount concern.

The weld (illustrated in Figure 1) is made by passing a high current through the part to be welded. Prior to the flow of current, a large force (typically one thousand pounds) is applied by the welding electrodes to the tube. Because of the resistance in the steel, current flowing across the tube generates heat. The combination of elevated temperature and electrode force causes the tube to collapse, and a metallurgical bond develops at the surfaces originally on the inside diameter of the tubes<sup>1</sup>. The resulting weld quality is a complicated function that depends on a number of weld and tubing parameters, the most significant of which are: current, weld duration and force.

Modern pinch welding equipment operates under the direction of a welding operator who determines proper machine settings based on the results of narrow experimental parameter searches. These tests are expensive even for statistically designed experiments. During the parameter selection process, welded tubes are slit longitudinally, etched (to enhance grain boundaries) and classified as to the amount of grain growth across the interface (among other things). An ideal weld interface (class 1 bond) is shown at 500X in Figure 2a along with the more typical interface (class 2) in Figure 2b. Poor quality welds are either class 3 or 4 (also shown in Figure 2.) Along the weld interface there typically exists bond sections of all four classes (with class 3 or 4 at the ends of the weld and class 1 or 2 in the middle).

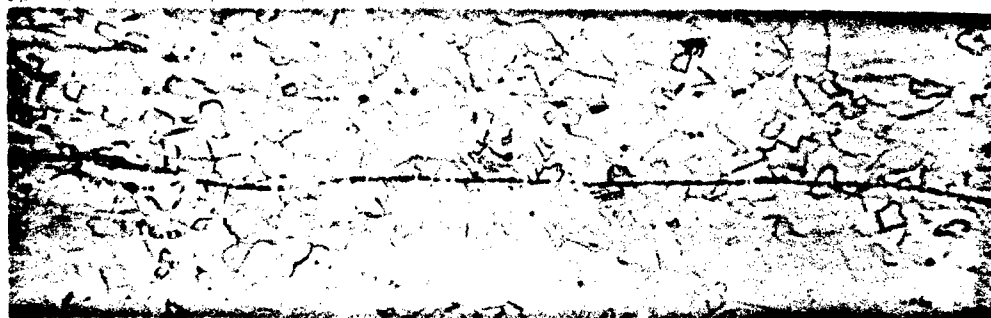


**Figure 1. Schematic illustration of Pinch welding**

1. T. R. Bieler, J. R. Spingarn, W. Jorgenson, "Voltage Drop and Temperature Measurements During Tube Closure by Resistance Welding", Report #SAND82-8024. Sandia National Laboratories, Livermore, CA, July 1982.



a. Class 1: Interface not visible when etched—grain growth across interface.



b. Class 2: Discontinuous interface visible—grain growth across interface.



c. Class 3: Continuous interface when etched—faintly visible unetched.



d. Class 4: Interface clearly visible unetched condition—no grain growth.

**Figure 2. Photomicrographs (500X) for evaluating pinch weld bond quality. Specimens etched in electrolytic oxalic acid.**

The challenge associated with quality control of pinch welding is the large amount of uncertainty in the relationship between weld quality and weld parameters. Prototype pinch welds are developed at Department of Energy design laboratories, but weld parameters cannot be successfully transferred to the production agencies because of the difficulty in calibrating development welding equipment with production equipment. Furthermore, calibration between production welders involves a tedious process of making welds, measuring the current, and adjusting the placement of power cables until all equipment receive the proper amount of weld current. (See Figures 3 and 4.)

Once a system is properly calibrated, factors such as electrode wear and oxidation on the tubes to be welded, can cause the relationship between weld parameters and bond quality to shift over time. Figure 5 shows the longitudinal cross-sections for two different welds made on the same pinch welder with the same control parameters. The second weld was made approximately one year after the first. Although all of the input parameters were identical (within measurement uncertainty), the resulting quality was dramatically different. From these figures it is clear that there are large variations in weld quality for constant weld parameters from machine-to-machine, and over time. In addition, weld current is difficult to control due to power surges and dips created by other high-power equipment on the same circuit and is also difficult to accurately measure because of its non-sinusoidal, large magnitude.

Once the weld parameters have been selected dimensional characteristics of the weld such as bond length, can be estimated through nondestructive examination with X-rays or ultrasound. However, the only way to completely determine pinch weld quality is the above mentioned microstructure evaluation. Production welds are randomly sampled and destructively tested to *infer* weld quality of the unsectioned parts. While these methods have allowed the production facilities to successfully produce high quality products over the past thirty years, they do not **improve** quality, but simply **inspect** quality, and in the process add tremendous cost to the product.

The goal of this work is to reduce the need for post weld inspection by implementing automatic, real-time quality control. That is, by utilizing feedback control, weld quality variation can be minimized to the point that inspection becomes unnecessary. Achieving this requires sensor systems capable of accessing weld quality in real-time. Although several methods have been investigated for real time quality assessment and feedback control of other resistance welding processes, none are directly applicable to pinch welding<sup>2</sup>. However, recent tests at Sandia demonstrated a correlation between pinch weld quality and electrode displacement during the weld, and suggested that displacement could be used as a quality measurement for feedback control. The objective of the study reported herein was to more clearly define the correlation between electrode displacement and weld quality, and develop a feedback control system to produce pinch welds of consistent weld quality, with wide variations in input power.

---

2. C. W. Pretzel and A. G. Beattie, "Acoustic Emission Characterization of Pinch Welds", Report #SAND85-8890, Sandia National Laboratories, Livermore, CA, May 1986.

## Tuning Process

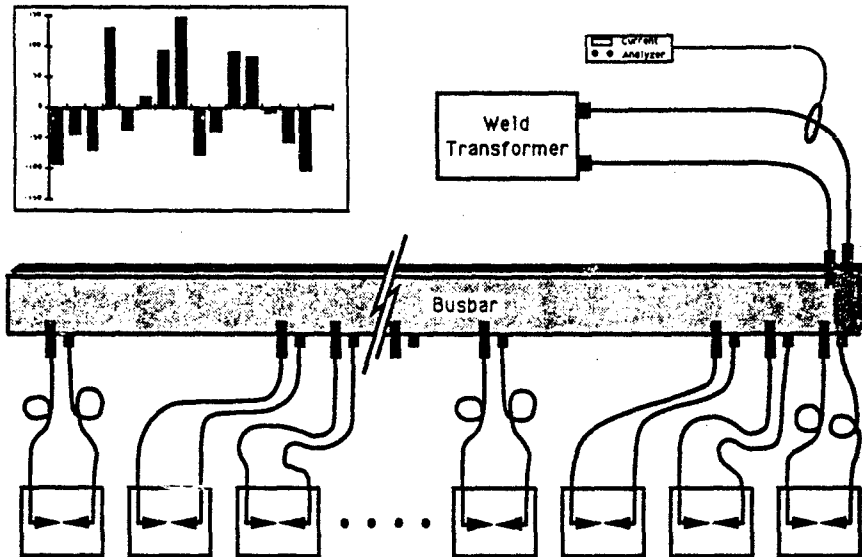


Figure 3. Production floor layout of pinch welding equipment.

## Current Variance Room A

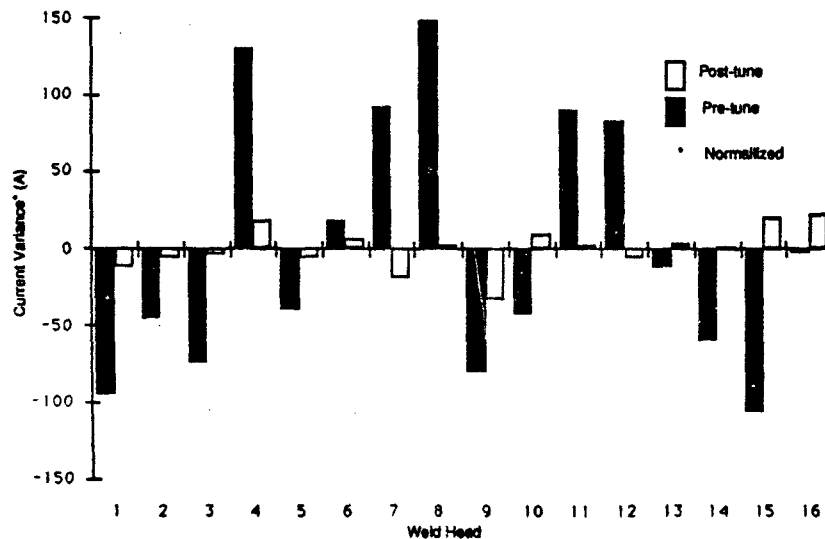
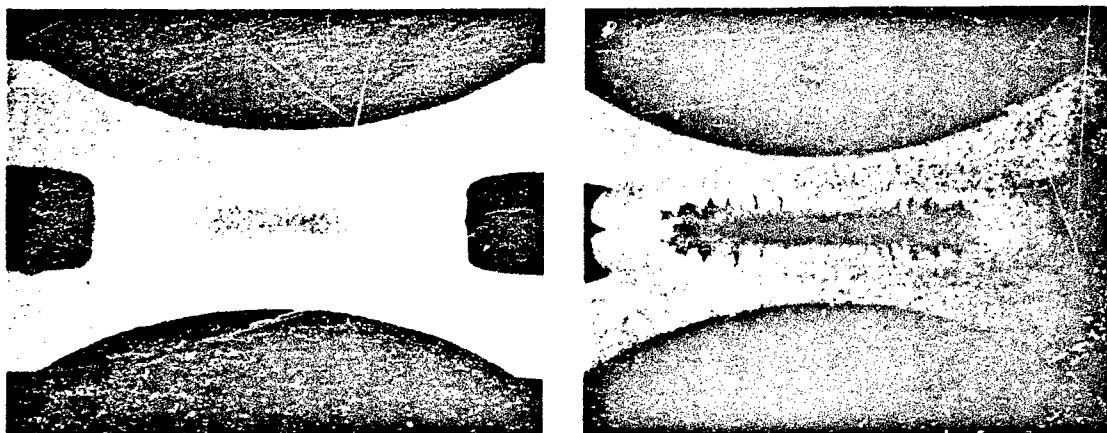


Figure 4. Machine-to-machine current variation—before and after tuning.





**Figure 5. Two pinch welds made with identical parameter settings. (14X)**

### ***Experimental Procedures***

A typical electrode displacement curve for a nominal weld is shown in Figure 6 superimposed with the current waveform used to make the weld. Weld time is specified in cycles—meaning the number of 60 Hz current cycles used to make the weld. The amount of current is controlled by modulating the duty-cycle of the 60 Hz current wave. The duty-cycle is specified in units of "percent heat". That is, a 50 percent heat setting delivers half of the available power to the part. (See Figure 7\*.) Weld current is therefore a function of the primary line voltage and the percent heat setting.

At the commencement of this study, welds of ideal quality were produced with the following parameters: primary voltage of 240 volts (rms), a heat setting of 45 percent, weld duration of 12 cycles and 900 pounds force. The above settings will hereafter be referred to as the nominal settings, and the weld produced by these settings, the nominal weld. A new controller was purchased for the welder that allowed the percent heat and weld duration to be externally controlled in real time. After the new controller was installed the heat setting required to make the nominal weld changed to 36 percent, later it changed to 40, and finally returned to 45 percent. The reasons for these shifts have not yet been determined but their effects can be eliminated through the feedback control technique described in this paper.

---

\* Note: Figure 7 shows the fire pulses delivered to the SCR's to initiate current flow. The SCR's are turned off when the current through the SCR's crosses zero. Since the voltage and current are out-of-phase, (with the voltage leading the current) the SCR's continue to conduct current for a short time after the voltage has crossed zero.

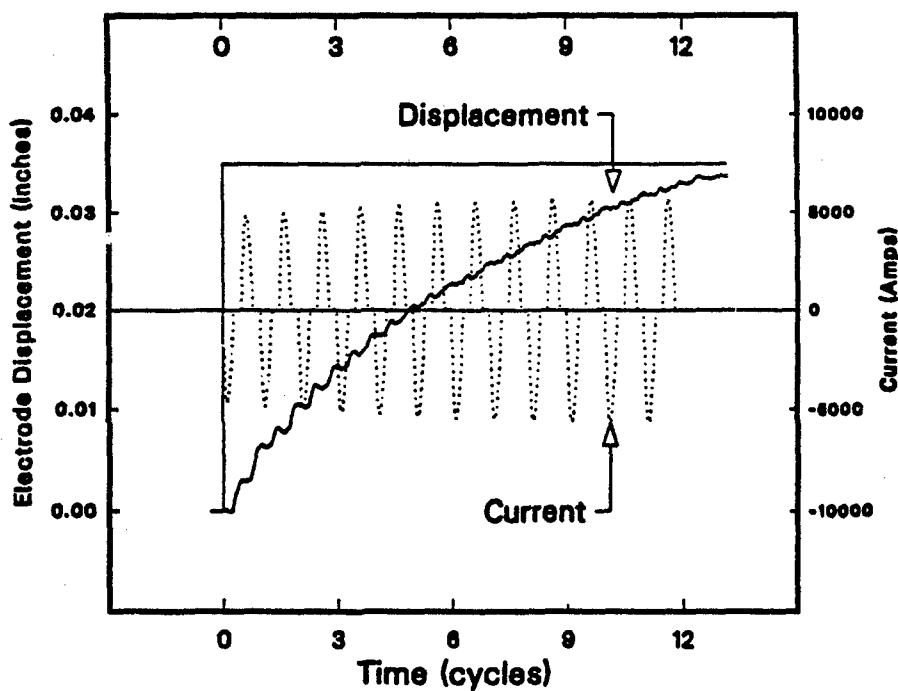


Figure 6. Pinch weld input (current) and output (displacement) curves.

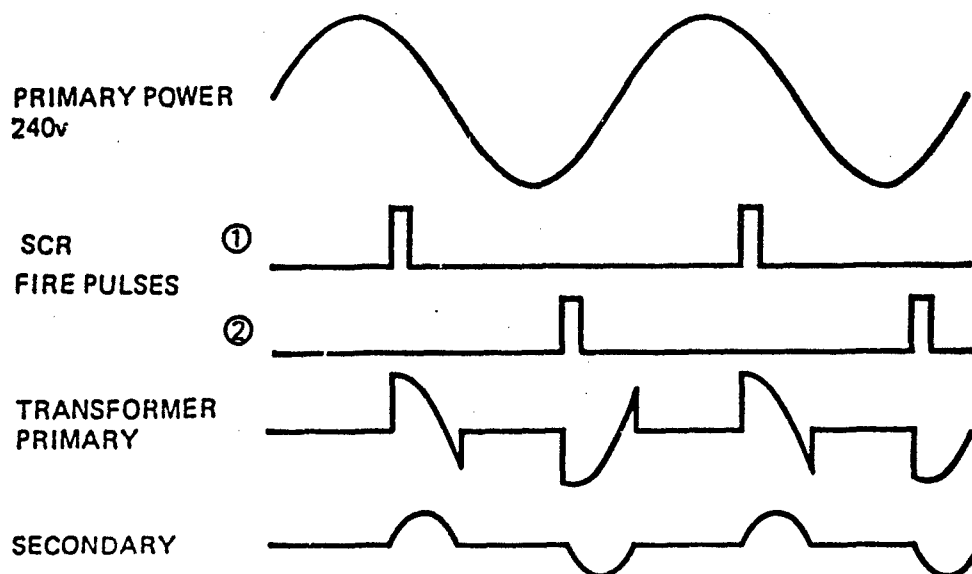


Figure 7. Percent heat control scheme used in pinch welding.

The open-loop sensitivity of weld quality to each of the above welding parameters was assessed in the following manner: A series of 52 pinch welds were made, with variations in voltage, percent heat, and force. The welds were examined using radiography and metallography to discover that in order to produce welds of consistent bond quality the voltage had to be held constant to  $\pm 0.75$  percent, the percent heat constant to  $\pm 1.5$  percent and the electrode force to  $\pm 3.5$  percent of the nominal settings.

Twenty one welds were made at nominal voltage, time and force settings, but the percent heat was varied in equal increments from -22% to +22% of the nominal. The electrode displacement curve for each weld was recorded on a storage scope and the final displacement values were found to vary linearly with percent heat. The welds were then cut open, and classified into four classes of bond quality along the length of the bond. The specification requires a minimum of one tenth of an inch in Class I or II bond to be acceptable. Figure 8 shows the bond quality data for the 21 welds as a function of electrode displacement. Five of the displacement curves are shown in Figure 9. The five welds in Figure 9 have been numbered for future reference. Also shown on Figure 9 are the ranges of acceptable and not acceptable welds based on weld geometry. The unacceptable welds are broken up into two categories: hot and cold.

Cold welds do not have enough heat to produce a quality bond of sufficient length, creating a potential for the weld to eventually leak. Conversely, hot welds have too much heating causing excessive melting to occur. As shown in Figure 10, there is an upper limit in bond length when expulsion may occur (when molten metal is ejected from the weld interface into the tube). Figures 10a through 10e show the metallographic cross-sections of each of the welds represented on the displacement graph of Figure 9. The weld in Figure 10f was made with slightly less heat than weld 10e, and had less displacement, yet showed expulsion. Thus the midpoint of the two acceptance limits shown in Figure 8 was chosen for the ideal (or nominal) pinch weld.

Another series of twenty two welds was made with nominal percent heat, time and force, but the primary line voltage was varied  $\pm 12\%$  of the nominal. This produced a family of curves identical to that of Figure 9. Finally, another set of 9 welds were made at nominal percent heat, voltage and time, but the electrode force was varied. These welds showed that the electrode force could be varied  $\pm 18\%$  of the nominal and still produce welds of acceptable quality. Furthermore the displacement curves of all 9 welds fit comfortably into the "good" range of final displacement values. (See Figure 11.) Also note that the welds with high force (corresponding with a high displacement) are the coldest welds, and the low force, low displacement welds are the hottest of the welds.

The weld quality vs. displacement correlation is shifted when the electrode force is varied—hence a single-input single-output displacement feedback system would not be able to account for variations in both current and force at the same time. However, this is not of great concern since the weld quality was found to be less sensitive to variations in force (for the range used in this study) when compared to variations in percent heat or line voltage. That is, at the nominal settings, the electrode force must vary 7 percent from the nominal before any noticeable changes occur in the geometry of the weld, while the percent heat need only vary 3 percent, and the primary voltage 1.5 percent before effecting the weld geometry.

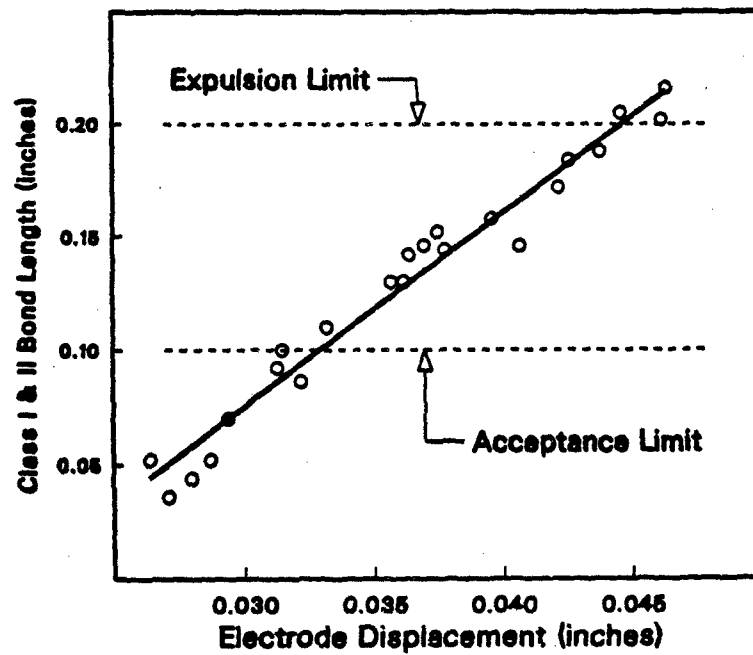


Figure 8. Pinch weld bond quality Vs. Displacement

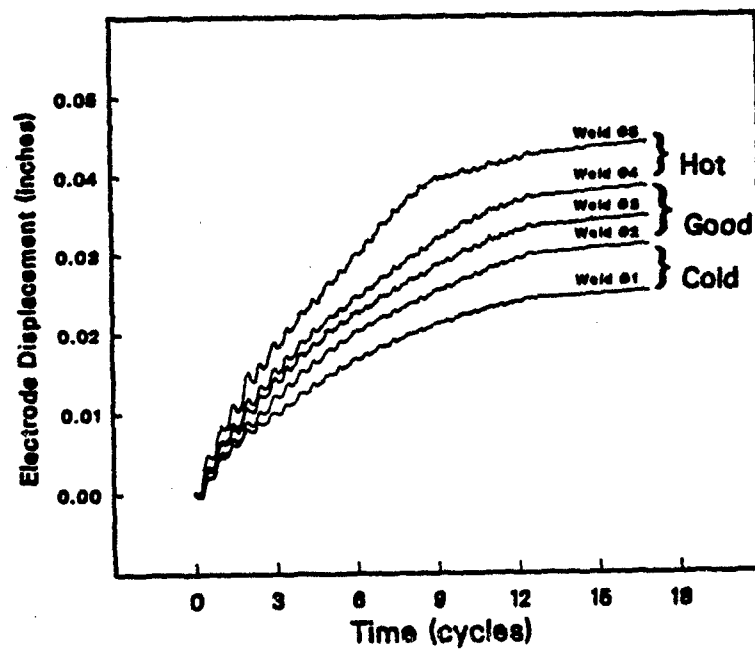
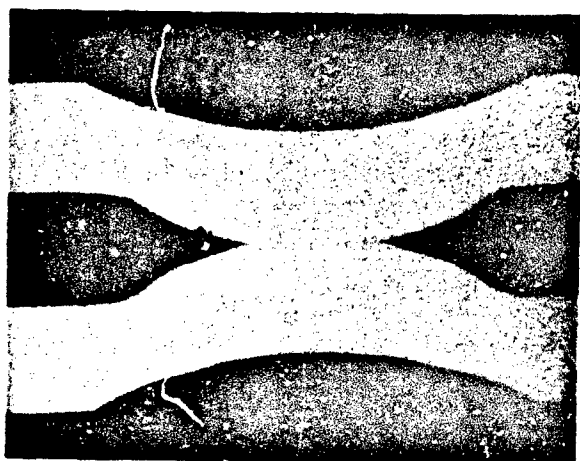
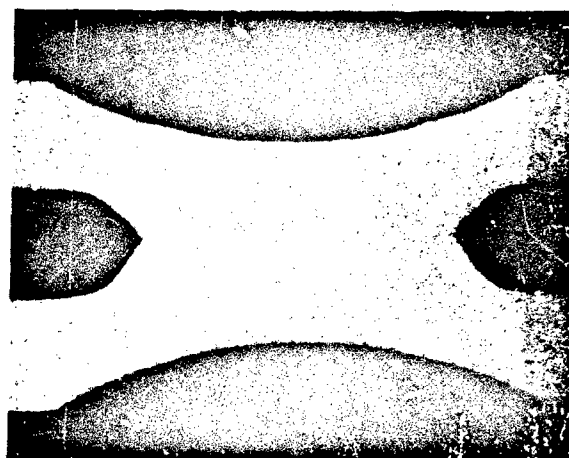


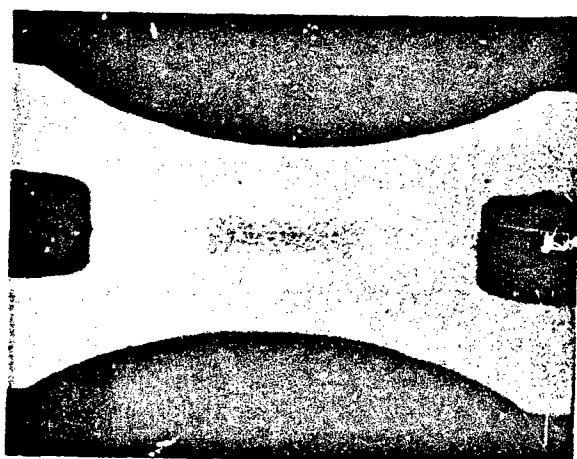
Figure 9. Pinch weld electrode displacement curves



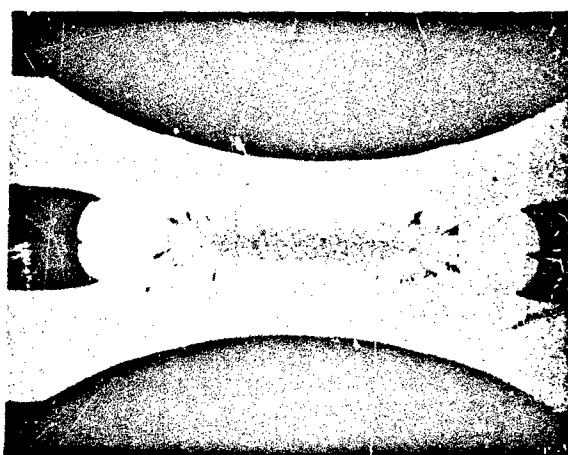
(a) Weld # 1



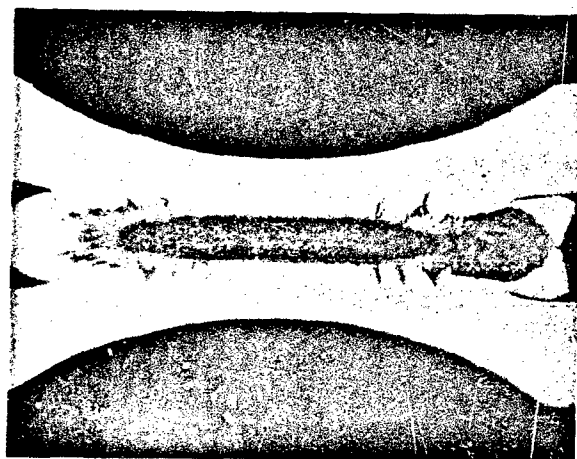
(b) Weld #2



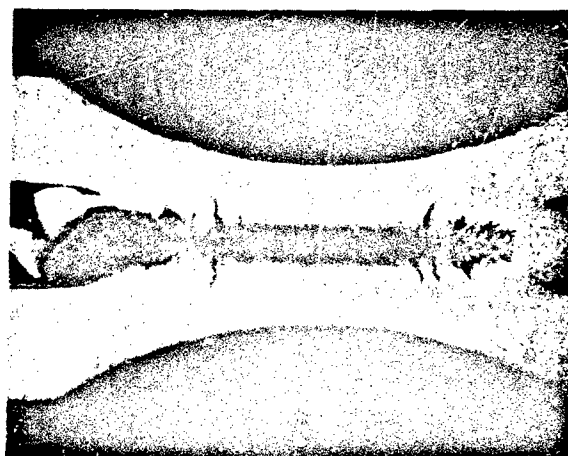
(c) Weld # 3 (nominal)



(d) weld #4



(e) Weld # 5



(f) Hot weld with Expulsion

Figure 10. Longitudinal cross sections for each weld in Figure 9 (14X)

Therefore the control system designed in this paper does not compensate for variations in electrode force, however, it does measure electrode force, and waits for it to reach the preset value before starting the weld, thus ensuring that all welds are initiated at the correct force. The pinch welder used in this study uses a pneumatic force system and is therefore extremely slow in response time. Because of the inherently slow response, electrode force does not change significantly during the course of the weld, even if the force has not yet reached steady-state. Since most pinch welds only last two tenths of a second, and the force system has a response time on the order of seconds, the force can be adequately controlled, (assuming that the input air pressure is set to overshoot it's nominal value by some moderate amount) simply by waiting for the force to reach the preset value before applying the weld current.

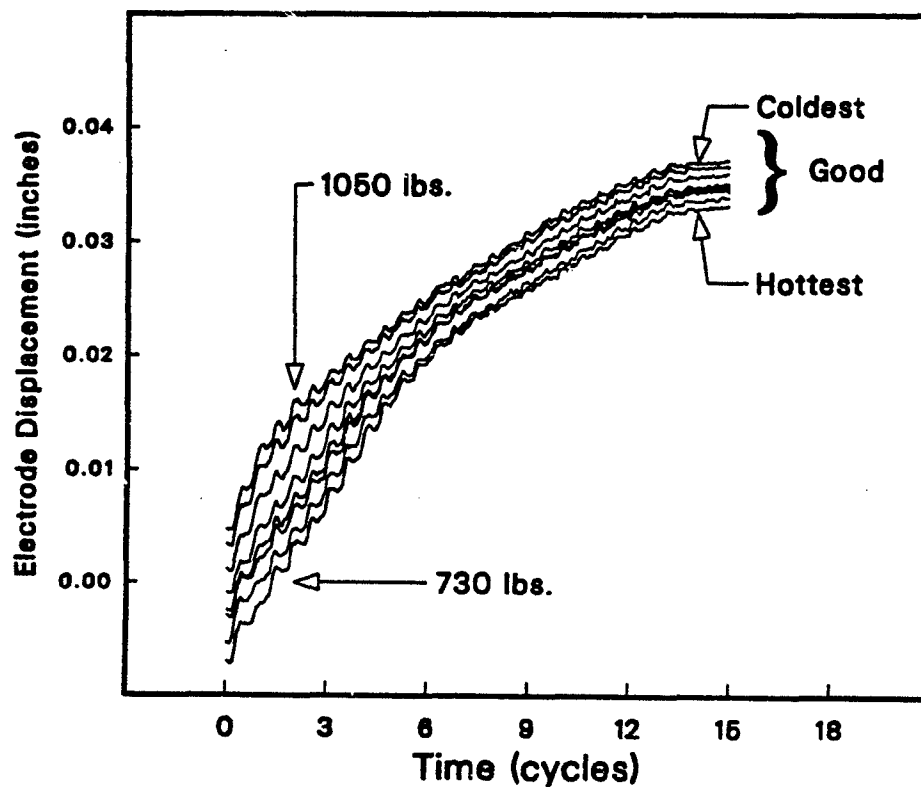
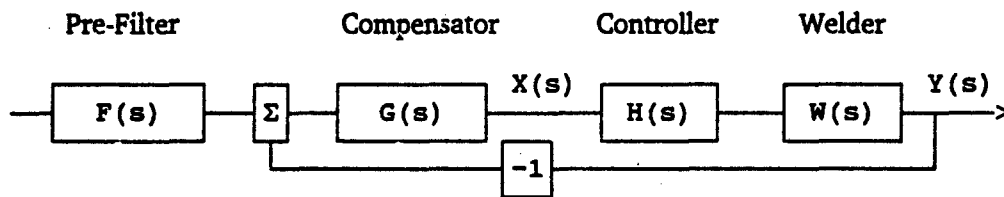


Figure 11. Pinch weld displacement curves Vs. electrode force

## Process Characterisation

A simplified block diagram of the control system is shown below in Figure 12. The elements in the diagram are shown as functions in 's'—implying the use of Laplace transforms. Laplace domain system analysis greatly simplifies the design of feedback systems, but it assumes linearity, and a quick observation of the input-output waveforms of Figure 6, reveals that the welding system is highly nonlinear. However, it has been shown that frequency domain techniques can be successfully applied to a large class of nonlinear, uncertain plants<sup>3-4</sup>.



**Figure 12. Block diagram of feedback system**

The next task was to determine the transfer functions for each of the components in Figure 12. In this configuration, the feedback loop is used to reduce the process sensitivity to parameter variations. Thus  $G(s)$  must be designed so that the closed-loop system reduces the uncertainty to acceptable levels. However, this will also change the bandwidth of the system. Both a compensator and pre-filter must be used in order to independently control bandwidth (time response) and sensitivity<sup>5</sup>. Therefore  $F(s)$  must be designed to provide the desired time response for the over-all closed-loop system (ideally, this would be the same as the nominal weld #3 shown in Figure 9).

The weld controller  $H(s)$ , controls the triggering of the SCR's which provide current to the weld transformer, as shown in Figure 7. The outputs of the controller are the SCR firing pulses, while the input is the percent heat control signal  $X(s)$ . Varying only the percent heat while holding all other inputs constant, reduces the system to a single-input/single-output system and the transfer function becomes:  $P(s) = Y(s)/X(s)$ , where:  $Y(s)$  is the Laplace transform of the displacement,  $X(s)$  is the Laplace transform of the percent heat signal, and  $P(s) = H(s) \cdot W(s)$ . All other inputs are considered to be process disturbances—which add uncertainty to the system equation.

3. I. Horowitz, M. Sidi, "Synthesis of Feedback Systems With Large Plant Ignorance for Prescribed Time Domain Tolerances", *International Journal of Control*, Vol. 16, pp 287-309, 1972.
4. I. Horowitz, "Synthesis of Feedback Systems With Nonlinear Time-varying Uncertain Plants to Satisfy Quantitative Performance Specifications", *Proceedings of IEEE*, Vol. 64, No. 1, Jan. 1976.
5. I. Horowitz, "Notes for course EEC152", University of California, Davis, Department of Electrical Engineering and Computer Science, Fall 1988.

Since any wave form can be modeled as a sum of sinusoids and exponentials, The welding system (here after referred to as the "plant")  $P(s)$ , was characterized as follows: The displacement data for the nominal weld was read into a spreadsheet program, and time domain equations were manually generated by the author, to fit the output (displacement) data. This produced the following model of the output for the nominal weld as a function of time:

$$y(t) \approx y_1(t) + y_2(t) + y_3(t) + y_4(t) \quad (1)$$

Where:

$$y_1(t) = 0.361 (1 + 0.2 e^{-86t} - 1.2 e^{-14t})$$

$$y_2(t) = -0.02 e^{-3t} \text{Sine}(14t)$$

$$y_3(t) = 0.02 e^{-6t} \text{Sine}(33t + 45^\circ)$$

$$y_4(t) = -0.03 e^{-50t} \text{Sine}(100t + 135^\circ)$$

The plot of the above equation (lite) along with the actual displacement data (heavy line) is shown in Figure 13a. The difference between the actual and model data is also plotted on the same graph in heavy line. Notice the decaying sine wave is basically all that is in the actual data that is not included in the model. This damped wave has a frequency of 120 Hz and is due to thermal expansion and contraction in the tube being welded, produced by the 60 Hz driving current. Each time a current pulse is delivered to the tube it begins to expand slightly, and between pulses the tube continues to collapse. The final component to the output was  $y_5(t) = 0.009 e^{-8t} \text{Sine}(2\pi ft)$  ( $f=120$  Hz).

The resulting plot is shown in Figure 13b. The remaining difference between the model and actual data was considered to be noise, since it was undamped and consisted of higher harmonics of 60 Hz (that is, 180 Hz, 240 Hz, 300 Hz, etcetera).

Transforming  $y(t)$  into the Laplace domain yields:

$$Y(s) \approx Y_1(s) + Y_2(s) + Y_3(s) + Y_4(s) + Y_5(s) \quad (2)$$

Where:

$$Y_1(s) = \frac{435}{s(s+14)(s+86)}$$

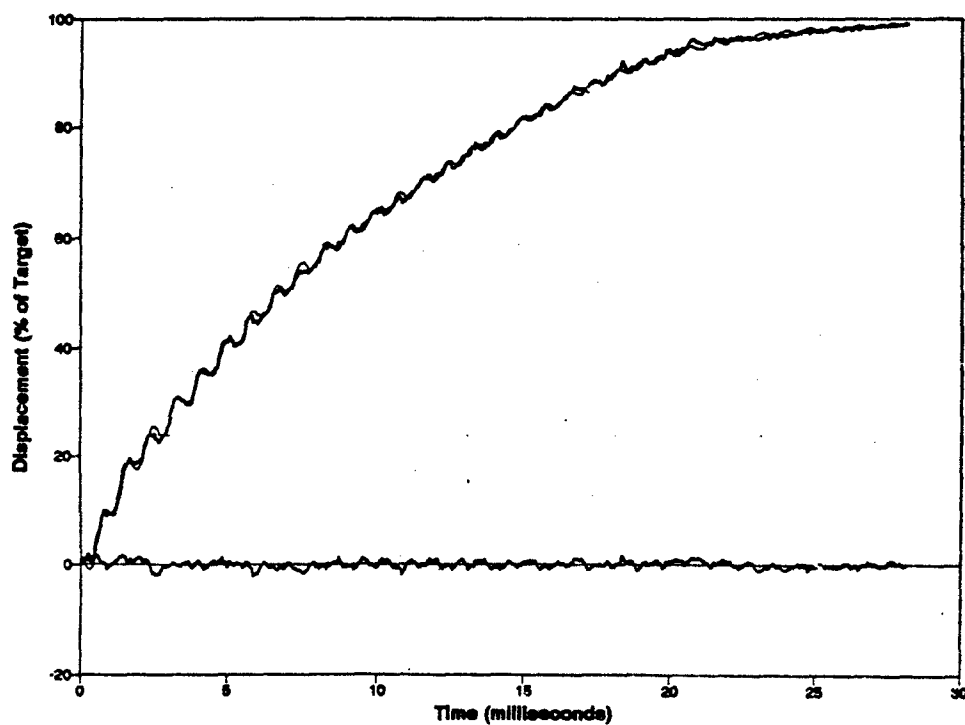
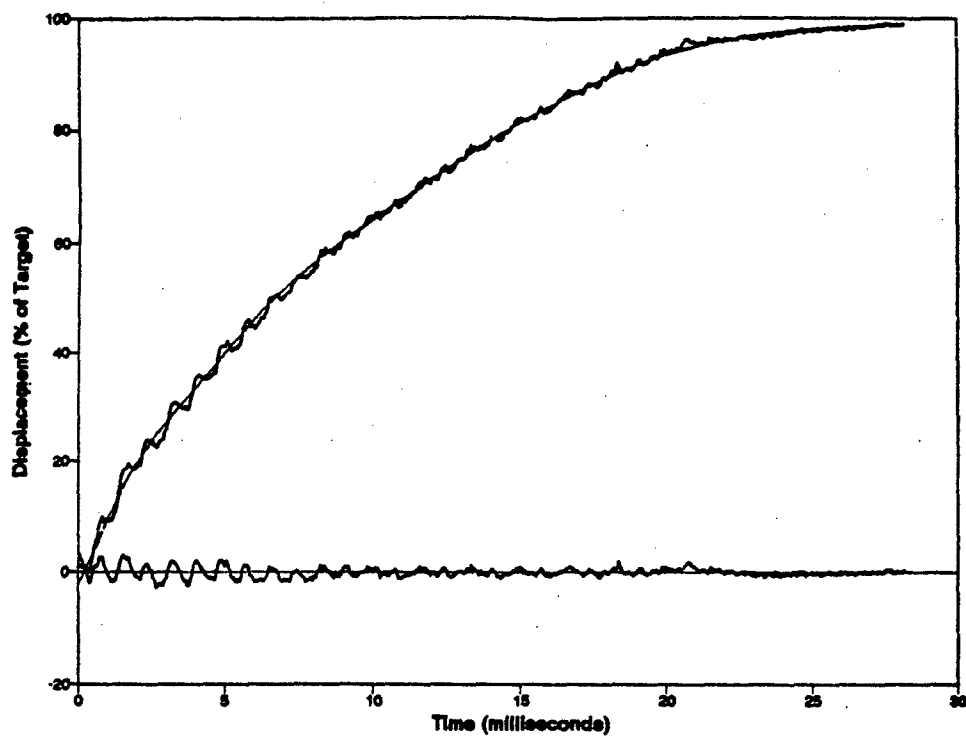
$$Y_2(s) = \frac{-0.3}{(s+3)^2 + 14^2}$$

$$Y_3(s) = \frac{0.013s + 0.5}{(s+6)^2 + 33^2}$$

$$Y_4(s) = \frac{-0.022s + 1.1}{(s+50)^2 + 100^2}$$

$$Y_5(s) = \frac{0.009s + 0.1}{(s+8)^2 + 760^2}$$





**Figure 13. Displacement curve of nominal weld—actual and model data.**

The input to the welder was a step function (since the data gathered was made at constant input parameter settings—that is the percent heat, voltage, and force were not varied once the weld had begun). Therefore the transfer function  $W(s)$  is simply the output  $Y(s)$  divided by the Laplace transform of the input step function. Since the Laplace transform of the unit step is  $1/s$ , then  $W(s) = Y(s) / (1/s) = s \cdot Y(s)$ .

The controller  $H(s)$  provides a digital input signal for external control of percent heat. Since the SCR's can only be fired once every half-cycle, the welding system cannot change percent heat more often than 8 milliseconds—the controller will not respond to the control signal  $X(s)$  between pulses. This was characterized as time delay of 11 milliseconds. (The actual time delay ranges from 2 to 11 milliseconds depending on when a change in  $X(s)$  occurs relative to the timing of the SCR pulses.) Thus we have:

$$P(s) = W(s) \cdot H(s) = s \cdot Y(s) \cdot e^{-s\tau} \quad \text{Where: } \tau = 11 \text{ milliseconds (3)}$$

This process was repeated for all five of the displacement curves shown in Figure 9 and similar equations were derived for each. These five equations now constitute a set of plant transfer functions, that span the range of uncertainty in the welding system. The goal of this project is to design one compensator,  $G(s)$  and one pre-filter,  $F(s)$  that will produce good welds for any plant in the set. That is: at any time the weld may "take on" the characteristics of any one of the plants in the set, and the feedback system must adjust the percent heat to arrive at the desired displacement.

Plotting the *magnitude* and *phase* of equation 3 for  $s = j\omega$  (where  $j = \sqrt{-1}$  and  $\omega = 2\pi f$ ) as a function of frequency  $\omega$ , produces a Bode plot. The *magnitude* portion of the Bode plots of each of the five welds are shown in Figure 14. Note that up until about 30 radians per second, the five curves are fairly "well behaved"—that is, they do not cross each other, and one can differentiate between the five curves easily. The magnitude for each of the welds ends up with a final roll-off of -20 dB per decade, while the phase ends up at  $-450^\circ$  (before addition of the above time delay). This is because all of the equations have a pair of complex zeros in the right half side of the  $s$ -plane. (This was not obvious from the equations, since they were expressed as sums of partial fractions rather than as a product of zeros over a common denominator.) This complex pair of zeros is a result of  $Y_5(s)$ —the term containing the 120 Hz. oscillation.

It has been shown that if a system is minimum-phase (no zeros in the right half of the  $s$ -plane), then the range of closed-loop uncertainty can be controlled by placing bounds on the *magnitude* of the frequency response without restrictions on the phase.<sup>6</sup> Although the plant is non-minimum phase, the right-half-plane zeros have little effect on the Bode plot for the frequency range of interest, (zero to about 100 radians per second) and the above simplification can also apply to this design.

---

6. I. Horowitz, *Synthesis of Feedback Systems*, Academic Press, Orlando, FL, 1963.

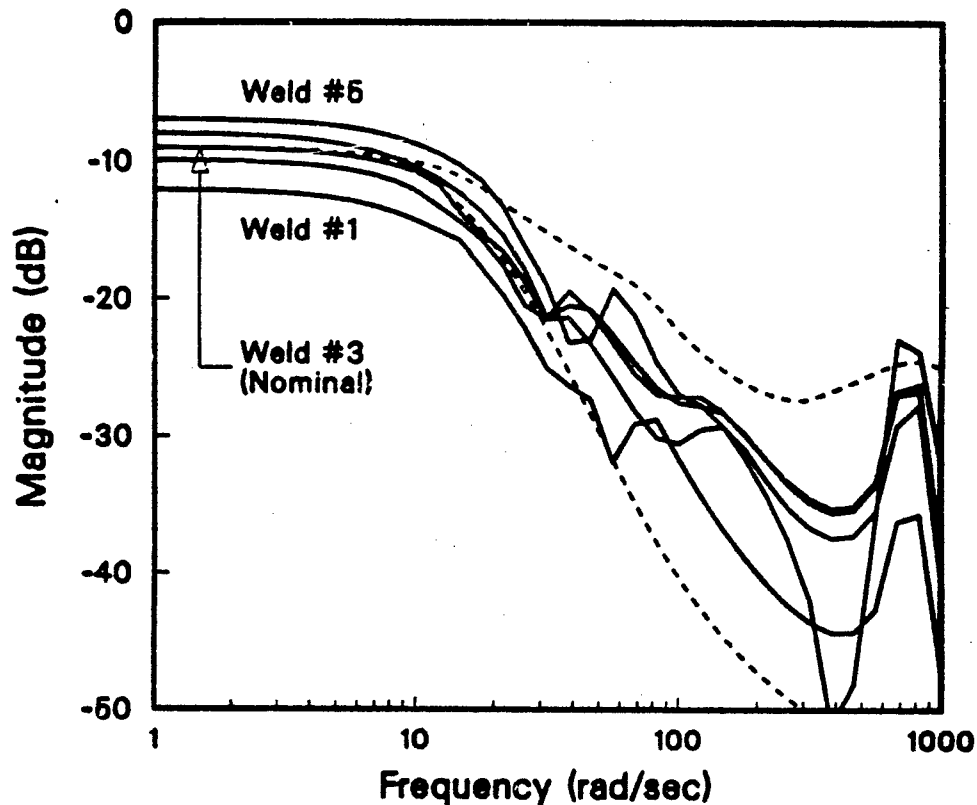


Figure 14. Frequency response of the welds in Figure 9.

Thus, by insuring that the magnitude of the closed-loop transfer function follows that of the nominal in Figure 14, the time-domain responses are forced to follow the output of the nominal weld shown in Figure 9. Since the displacement curves of weld numbers 2, 3 and 4 were all produced by acceptable welds, we will assume that any displacement curve whose frequency response lies between that of welds number 2 and 4 (at least for frequencies lower than 30 radians per second) will also produce an acceptable weld regardless of the phase characteristics of that weld. Ideally we would like all displacement curves to exactly follow the nominal, however some tolerance is required for a finite bandwidth system. Figure 14 also shows the frequency *bounds* used for the design of the compensator. The bounds (shown in dashed lines) closely follow the nominal weld for frequencies less than 3, then gradually open up. If there exists a compensator  $G(s)$  and a pre-filter  $F(s)$  that *maps* all of the five plant transfer functions to lie within the bounds shown in Figure 14, then the resulting welds should produce displacement curves that will lie well within the good region bounded by weld numbers 2 and 4 of Figure 9, and the final displacement values will match that of the nominal weld.

### Design Procedure

The width of the bounds in Figure 14 will hereafter be referred to as  $\Delta B(\omega)$ , and is a function of frequency. The purpose of the feedback loop is to reduce the uncertainty in the system so that  $\Delta |T(\omega)| < \Delta B(\omega)$  for all  $\omega$ , where  $T = L / (1 + L)$  and  $L(j\omega) = G(j\omega) \cdot P(j\omega)$ —That is, the range of the closed-loop transfer functions must be smaller than the range or width of the bounds in Figure 14. Since  $P(s)$  is fixed,  $G(s)$  must provide the necessary compensation to ensure that the closed-loop system meets the above condition for all plants in the set at all frequencies. The Nichols chart is the ideal tool for designing  $G(s)$  to the above specifications.

Plotting the frequency information for the five plants in Nichols chart form (Phase Vs. Magnitude) for a discrete set of frequencies between 1 and 100 radians per second, gives the set of plant "templates" shown in Figure 15. These templates give a quantitative measure of the amount of plant uncertainty at each frequency. For each frequency, there are five points plotted (one for each plant in the set), and they are connected by straight lines. It is assumed that any plant not represented by one of the five plant equations, but within the range of plant uncertainty, would fall somewhere in the area bounded by the lines connecting the five points.

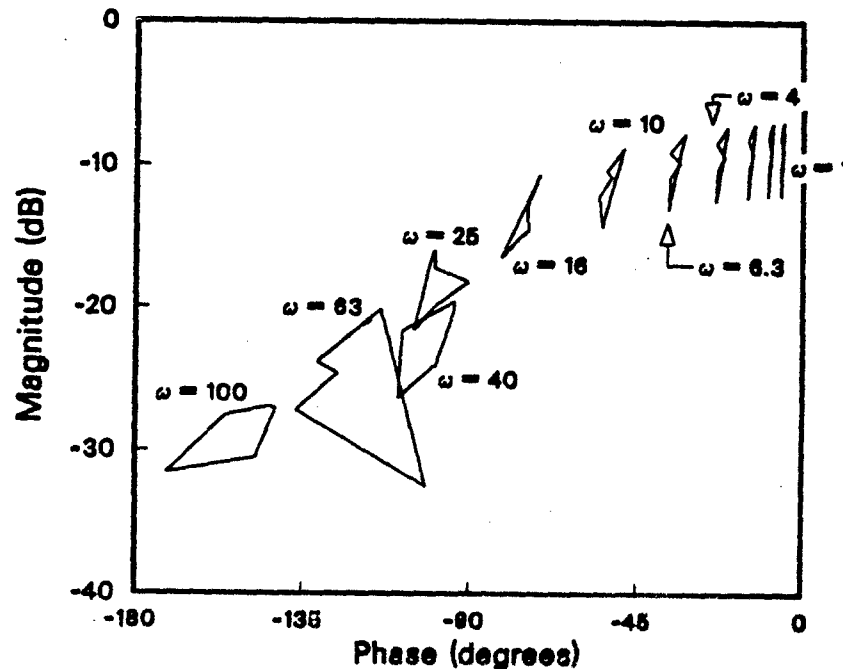


Figure 15. Plant templates for  $\omega = 1$  to 100 radians per second

These plant templates can then be printed on transparent paper, and superimposed onto a Nichols chart of the same scale. This allows the designer to read the magnitude range of the closed-loop transfer function  $\Delta|T(\omega)|$  directly from the Nichols chart. Any compensation added to the system from  $G(s)$  will affect all plants equally, and will thus translate the plant template to another location on the Nichols chart. Therefore, by moving the template over the range of the Nichols chart, the designer can accommodate all plants simultaneously and determine bounds for the compensator  $G(s)$ , which if satisfied, will guarantee that  $\Delta|T(\omega)|$  for the closed-loop system, will satisfy the bounds  $\Delta B(\omega)$ . Also, stability bounds can be derived from the Nichols chart, by insuring that  $T(\omega)$  is less than some value  $\gamma$  for all frequencies. Since  $\gamma$  is also related to the amount of overshoot in the output response, it was decided to design for  $\gamma=0$ —thus allowing for no overshoot at all. This was done because the electrode displacement is only controllable in the positive direction. That is: current applied to the tube can only cause the tube to collapse—there is no mechanism for causing the tube to re-expand. Therefore, because of this non-linearity (which was not included in the process characterization), overshoot in displacement can not be compensated for, and must be minimized.

Figure 16 shows (in dashed lines) the Nichols chart bounds for the nominal open-loop transfer function. If the bounds are satisfied for the nominal case, then the frequency bounds in Figure 14 will be satisfied for all plants in the set. Figure 16 also shows (in solid line) the "trajectory" of the uncompensated nominal plant  $P_n(j\omega)$  as the frequency is varied from 1 to 150 radians per second. Clearly the uncompensated system violates the low frequency bounds, and would thus have large steady-state errors. Raising the gain to reduce steady state error (without adding compensation) would drive the process unstable. Therefore the compensator  $G(s)$  must not only have a large gain, but must provide the necessary phase lead to stabilize the closed-loop system, and meet the design specifications. Figure 16 also shows (in solid line) the trajectory of the compensated nominal plant  $L_n(j\omega)$  where:  $L_n(s) = G(s) \cdot P_n(s)$ . The compensated system meets the bounds comfortably. The compensator  $G(s)$  is shown below:

$$G(s) = \frac{1600(s^2 + 27s + 19^2)(s + 32)^2}{s(s^2 + 25s + 25^2)(s + 126)^2} \quad (4)$$

Figures 17 and 18 show the Bode plots of  $G(s)$  and  $L_n(s)$  respectfully. Figure 19 shows the Bode plots of the closed loop system for all plants in the set along with the bounds of Figure 14. The purpose of the pre-filter  $F(s)$  is to "shape" the closed-loop responses to achieve the desired bandwidth—that is, to cause the closed-loop responses to "fit" inside the bounds of Figure 14—and thus meet the time-domain specifications on the output response. Ideally we want all outputs to match that of the nominal weld, and so the nominal weld transfer function  $P_n(s)$  is included in  $F(s)$ . This design of  $F(s)$  deviates somewhat from the classical QFT design method and is best explained later on in the paper by detailing its operation in the complete control system. The pre-filter  $F(s)$  is shown below, and the pre-filtered closed-loop transfer functions are plotted in Figure 20.

$$F(s) = P_n(s) + 1/G(s) \quad (5)$$

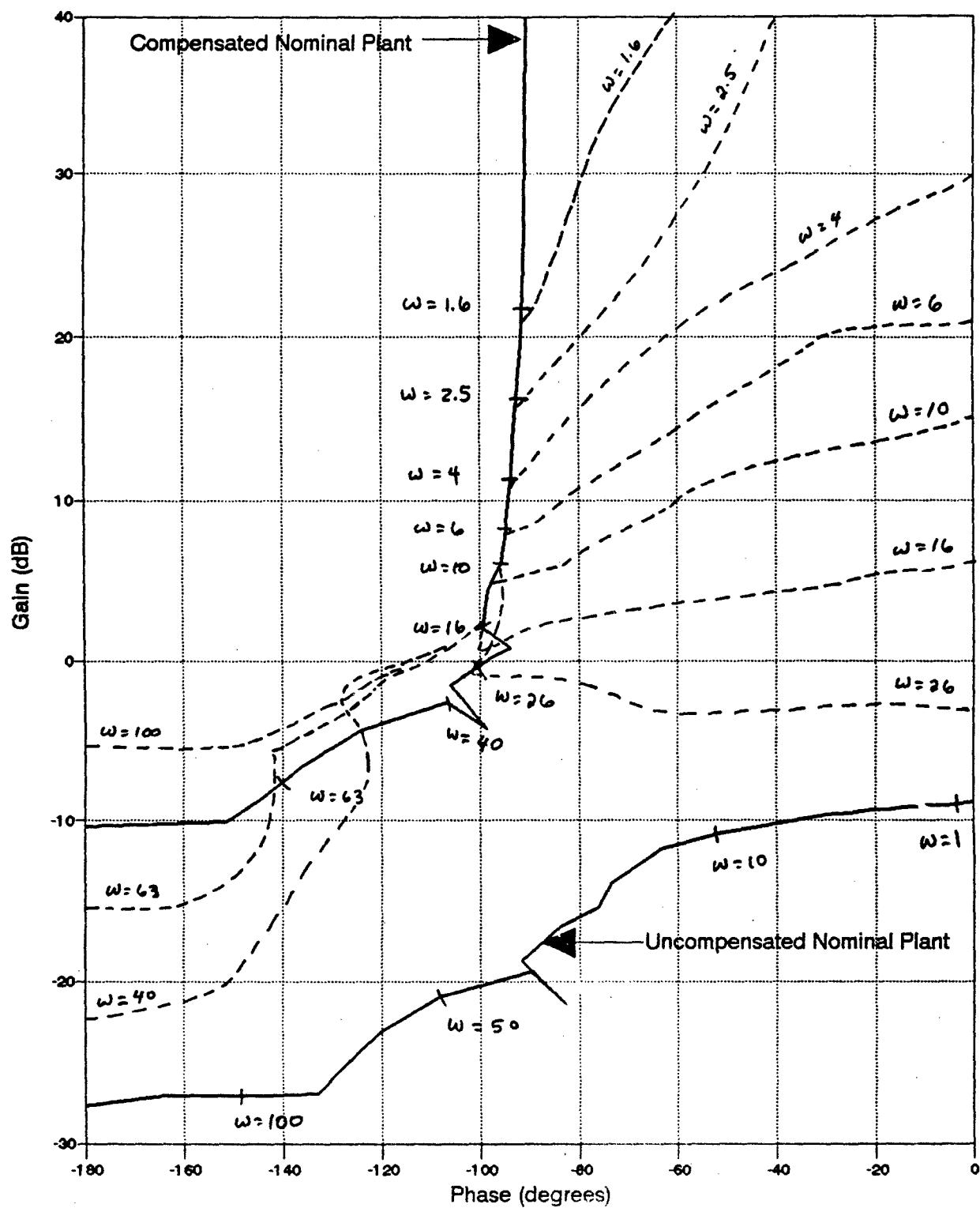


Figure 16. Nichols plot of  $P_n(j\omega)$  and  $L_n(j\omega)$  with the bounds on  $L_n(j\omega)$

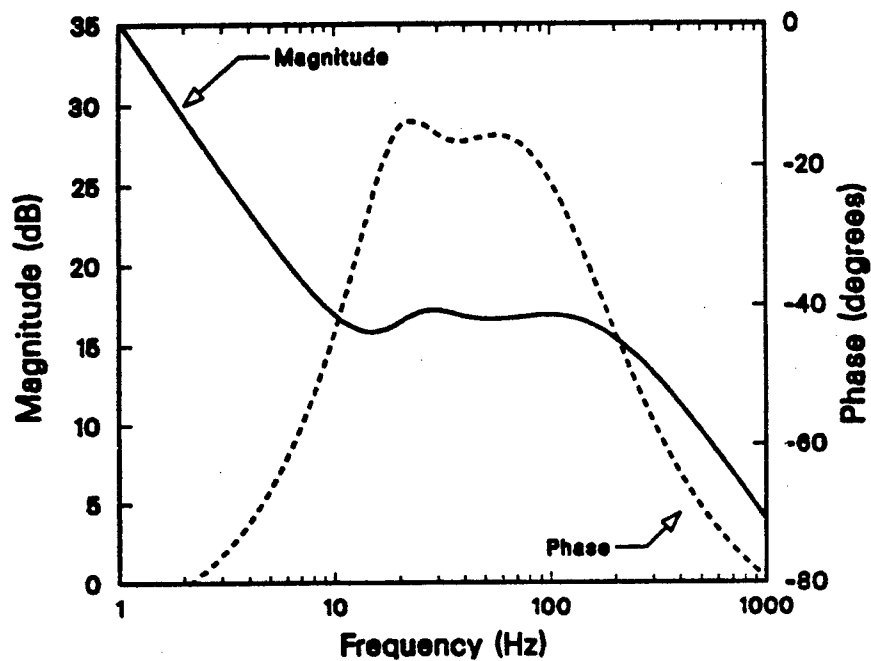


Figure 17. Bode plot of compensator  $G(s)$

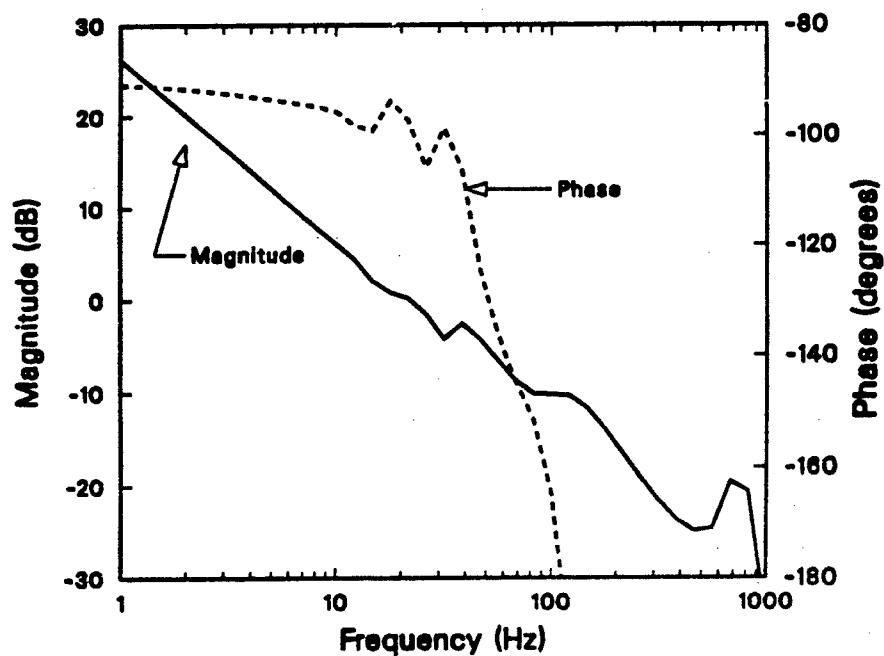


Figure 18. Bode plot of nominal loop transmission  $L_n(s)$

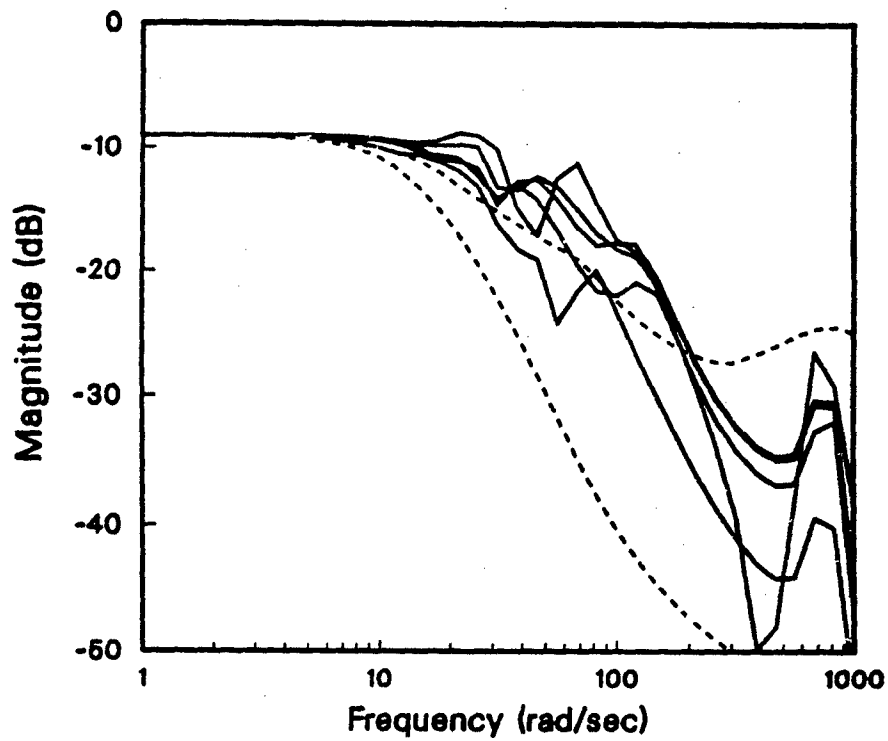


Figure 19. Bode Plot of closed-loop system  $L(s) / [ 1 + L(s) ]$

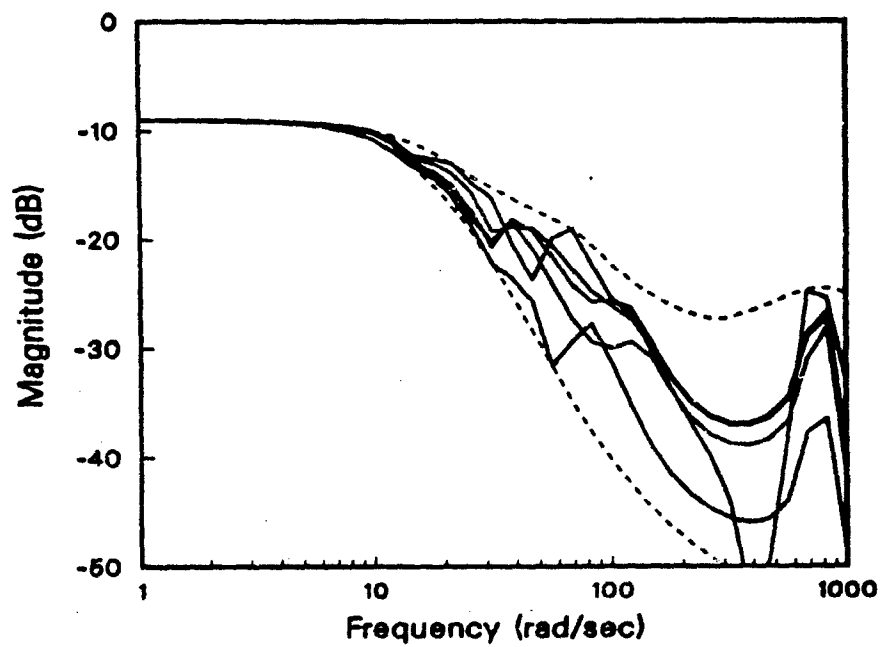


Figure 20. Pre-filtered, closed-loop system  $F(s) \cdot L(s) / [ 1 + L(s) ]$



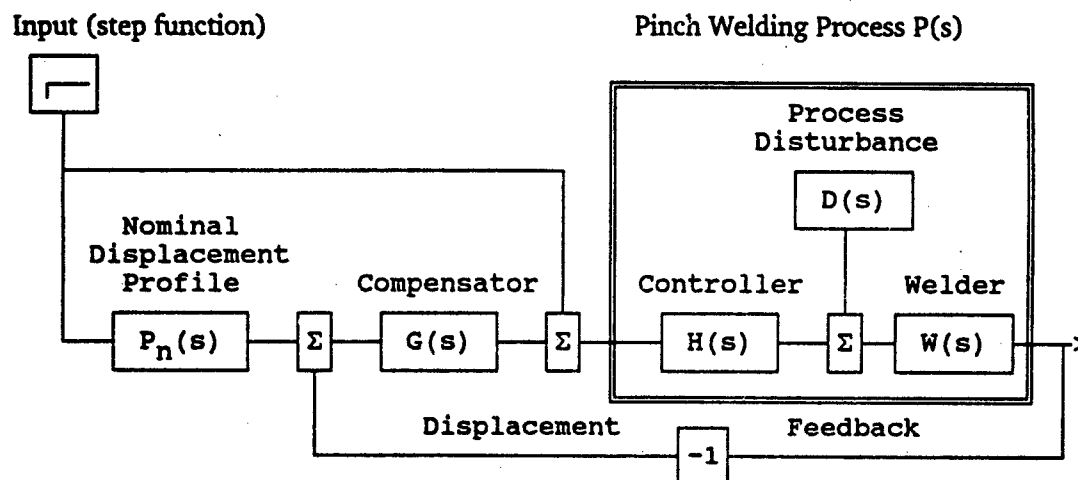


Figure 21. Block diagram of expanded control system

### Experimental Results

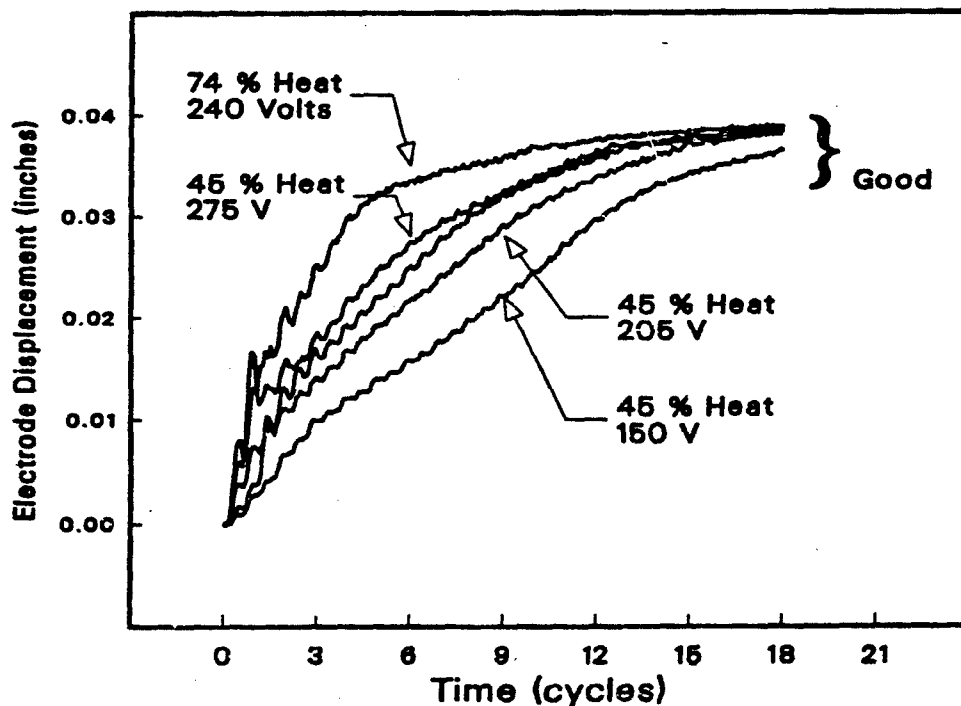
Applying equation 5 to the block diagram of Figure 12 and rearranging yields the feedback/feed-forward structure shown in Figure 21. Note that the welding process  $P(s)$  has been expanded to include unknown process disturbances, and that  $F(s)$  has been realized with the equation of the nominal weld  $P_n(s)$  and a feed-forward signal.

The control system was implemented in software on a personal computer. It works as follows: The welding operator selects the desired weld parameters (percent heat, primary line voltage and electrode force) and starts the welding sequence as they would if there were no feedback system connected. Once started, the controller opens a valve allowing pressurized air to enter the pneumatic cylinders which intern apply force to the electrodes. As the pressure builds, the electrode force is monitored by the computer. When the force reaches the preset value, the computer initiates the weld with a step function input to the controller. This starts the weld current flowing at the operator specified percent heat. The electrode displacement is measured and compared to the nominal displacement profile to become the error signal. If the welding process is responding nominally, then the error signal will be small and the compensator will not change the specified percent heat. However, when process disturbances change the behavior of the welding process, the compensated error signal adds an offset to the controller input signal, changing the percent heat. The duration of the weld is also shortened or increased as needed to drive the displacement to the specified value. When no disturbances are present the system responds the same as it did without feedback.

Note, the computer has no knowledge of the primary line voltage nor the operator specified percent heat—corrections to the percent heat are made solely on the displacement error signal. An obvious improvement to the robustness of the process would be to give the computer access to the percent heat and primary line voltage settings and use that knowledge to modify the operator specified percent heat in order to further compensate for improper settings. However, in order to fully test the feedback capability of the system, the voltage and percent heat settings were left as unknowns to the computer, and were varied to simulate the process disturbances  $D(s)$  shown in Figure 21. The final application would, however, incorporate the above improvement.

The system was tested, and found capable of controlling the final displacement to  $\pm 1.5$  percent. However, after cross-sectioning the welds an interesting observation was made: although the final displacement values for all welds was that of the nominal weld (weld number 3 in Figure 9), the weld geometry was closer to that of weld number 2 in Figure 10. Although all welds were of acceptable bond quality, it was hoped that the geometry would be closer to the ideal. The reason for this shift in the quality vs. displacement correlation is currently unknown, but it is suspected that it is related to electrode wear, since the electrodes were changed between the time of the preliminary experiments and the final system tests—however, this cannot be fully verified since the old electrodes were discarded. To correct for this shift, the nominal weld profile was scaled up to obtain a larger final displacement.

The system had no trouble compensating for input voltages ranging from the nominal of 240 volts down to 205 and up to 275 volts. Encouraged by these results, the system was tested for disturbances well beyond the region of weld uncertainty used for the design, to include welds made at such extremes as 150 volts-46% heat and 240 volts-74% heat. Electrode displacement traces for these welds are shown in Figure 22\*, and the corresponding metallographic cross-sections in Figure 23.

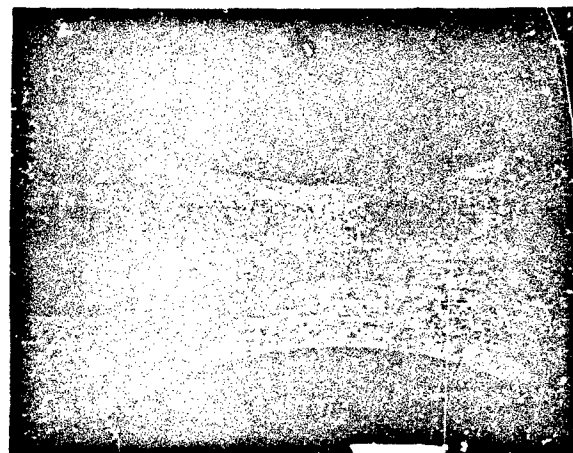


**Figure 22. Closed-loop displacement traces w/wide variations in power**

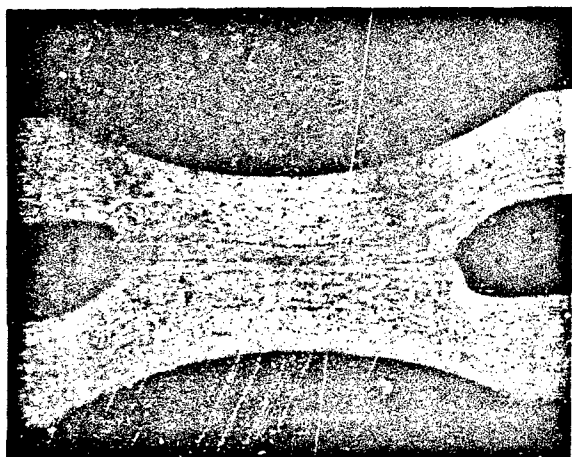
\* The 150 volt-46% heat weld continued past the time shown in Figure 22 until it reached the correct final value after about 24 current cycles.



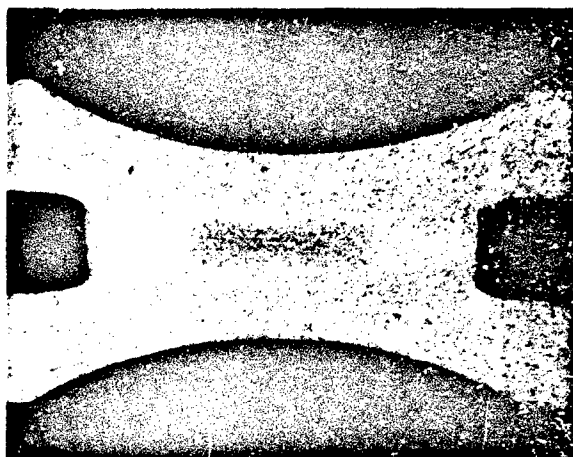
150 Volts



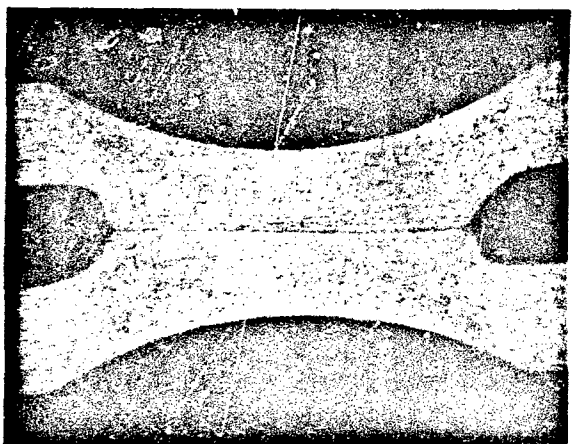
205 Volts



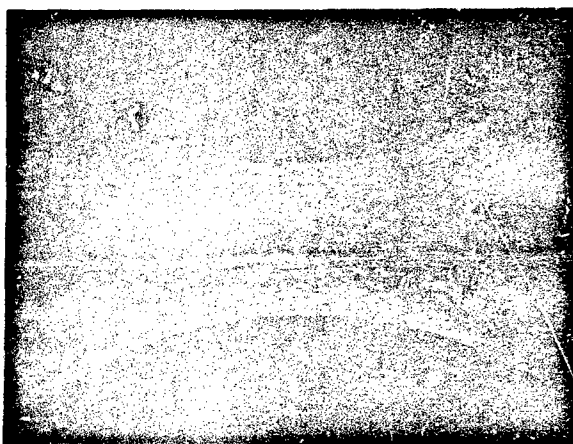
240 Volts



(Nominal)



275 Volts



74% Heat

**Figure 23. Metallography of Figure 22 welds—plus nominal (at 14X)**

All of the welds in Figure 23 were acceptable with around 150 thousandths of an inch of high quality bond, while such variations in weld parameters without feedback, would have caused disastrous effects on weld quality. (See Figure 24.) In order to further test the system, welds were made with several different combinations of line voltage and percent heat as shown in figure 25. The input voltage was varied from 144 to 275 volts, and the percent heat all the way from 5 to 99%. In each case the controller was able to bring the final displacements to the correct value. Figure 25 graphically illustrates this decrease in sensitivity, by showing the regions of allowed variation in voltage and percent heat for consistent bond quality. This is shown for both with and without feedback. Welds made with feedback but outside the parameter space shown in Figure 25 can still produce acceptable welds, but fall slightly under (or over) the desired displacement and corresponding bond quality. The system could not be tested above 275 volts because of a limitation on the input transformer, and therefore the portion of Figure 25 that is above 275 volts is a projection.

### **Conclusions and Future Work**

Overall, the feedback system worked extremely well in reducing the process sensitivity to weld input power through the use of displacement feedback. Displacement was accurately controlled and bond quality maintained, with -40 to +15 percent variations in primary line voltage and with  $\pm 80\%$  disturbances in percent heat. The next step will be to determine the effects of other disturbances to the system and the ability of a displacement based control system to compensate for them. Specifically: assess what would be the effects of variations in tube hardness, geometry, cleanliness, electrode wear and alignment, etcetera. Finally, the design will be adapted into a multiple input, multiple output system to compensate for all of the above added uncertainty, and also for variations in electrode force. Quantitative Feedback Theory has also been used to apply displacement feedback to the resistance upset welding process. The upset welding feedback system will be implemented and tested shortly. This promises to be even more rewarding than pinch welding and will find greater application throughout the welding industry.

### **Acknowledgments**

The author wishes to thank Dr. Isaac Horowitz of The University of California at Davis, who developed *Quantitative Feedback Theory* (QFT)—which made this project both practical, and understandable. In addition, the author wishes to thank: Lou N. Tallerico, Scot J. Marburger, Robert S. Arnot, Sam B. Johnson, Jay R. Spingarn, Rich H. Campiotti and Antonio J. DeSousa—a special thanks to Andy D. Gardea and Robert S. Arnot, who spent many hours to provide the metallography used throughout this study. The contributions of all are sincerely appreciated. This work was funded by the United States Department of Energy under contract DE-AC04-76DP00789.

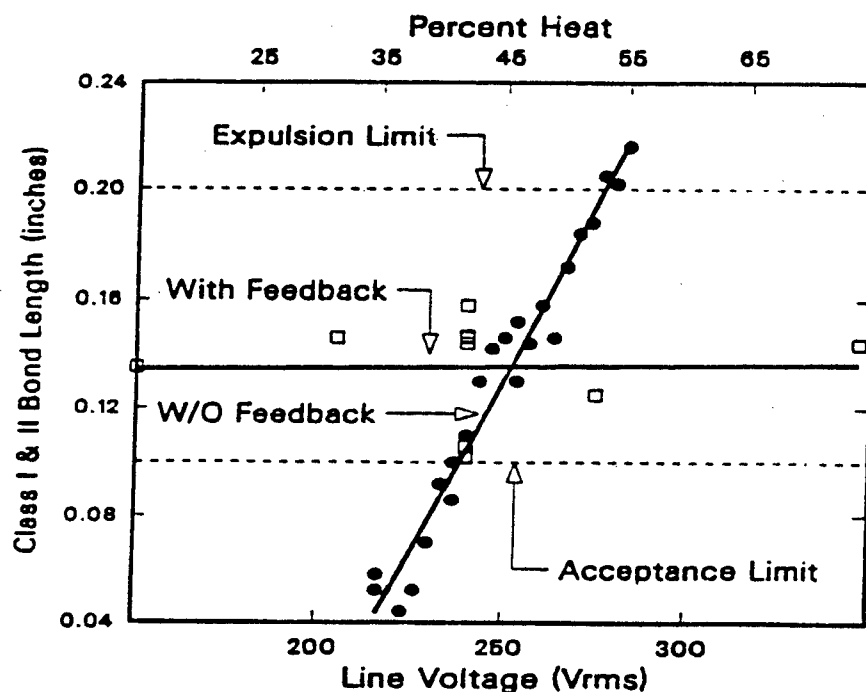


Figure 24. Bond quality vs. weld input with and without feedback control

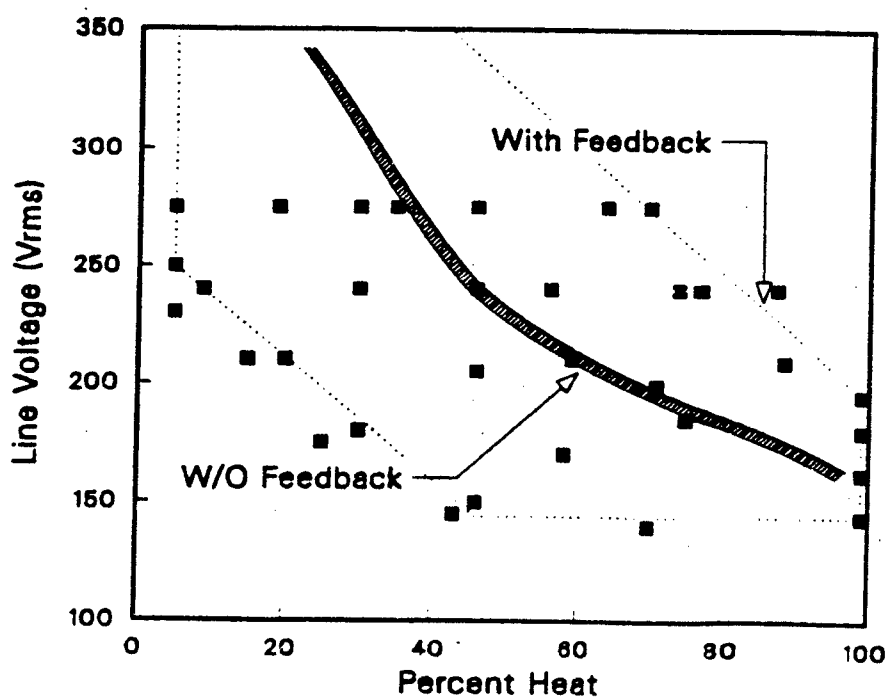


Figure 25. Input parameter space for consistent quality—w & w/o feedback

# STORAGE SIZE FROM PROCESS CONTROL BANDWIDTH SPECIFICATION AND THE OTHER WAY AROUND

by

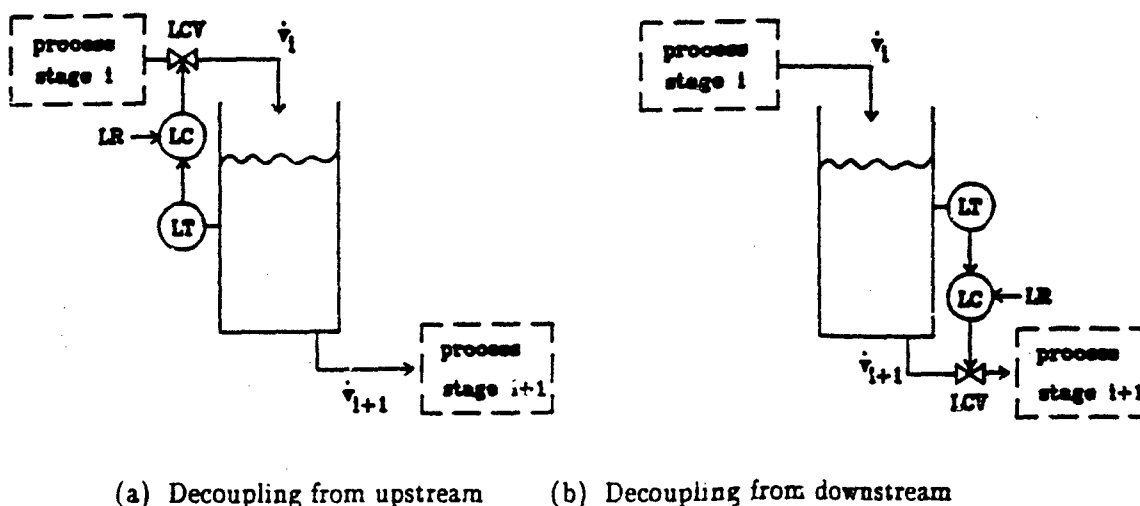
Dr Eduard Eitelberg

Professor & HoD, Department of Electrical & Control Engineering,  
University of Durban-Westville, Private Bag X54001,  
Durban 4000, South Africa

**Abstract:** Storage vessels are used extensively in the process industry for evening out process stream fluctuations between adjacent process stages. It is shown here quantitatively, that the product between vessel size and flow control bandwidth must be about four times the operating flow rate in order to simultaneously minimize intersection disturbances and avoid fluid escaping from the vessel. A higher value of this product either means unnecessary process disturbances or questionable investment for an oversized vessel. A lower value will lead to occasional spillages with the associated loss of production and potential environment pollution. This formula is extended to the safe operation of larger processing vessels by observing that the product between the reserve volume and the flow control bandwidth must be about twice the operating flow rate.

## 1. INTRODUCTION

Consider the typical arrangements of an evening tank control problem between two adjacent process stages in Figure 1.



**Figure 1:** Evening tank level control. LT = Level Transmitter/Sensor, LC = Level Controller, LCV = Level Control Valve, LR = Level Reference,  $\dot{v}_i$  = volumetric flow rate from stage i,  $\dot{v}_{i+1}$  = volumetric flow rate into stage i+1.

The control system configuration in Fig. 1a decouples the process stage  $i+1$  totally from  $\dot{v}_i$  fluctuations, if the tank hydrostatic pressure does not influence  $\dot{v}_{i+1}$ . The role of the control system is to avoid over- or underflowing of the storage tank despite the fluctuations (disturbances) in  $\dot{v}_{i+1}$ .

The control system configuration in Fig. 1b decouples the process stage  $i$  totally from  $\dot{v}_{i+1}$  fluctuations. The role of the control loop is to avoid over- or underflowing of the storage tank despite the fluctuations in  $\dot{v}_i$ .

## 2. MODELLING

Assume incompressible flows (without significant restriction for the validity of the general storage control analysis), then the volume  $V$  of the stored material is modelled by

$$\frac{dV}{dt} = \dot{v}_i - \dot{v}_{i+1} \quad (1)$$

Assume for simplicity vertical side walls of the tank, then the transmitted level signal can be scaled to represent the volume  $V$  directly. Hence, for the rest of this paper, we assume that LT signal represents the volume in the range of

$$0 \leq V \leq V_{\max} \quad (2)$$

$V_{\max}$  is the vessel size. Let us use  $v$  for the measured volume (level),  $u$  for the controlled variable ( $\dot{v}_i$  in case of Fig. 1a and  $\dot{v}_{i+1}$  in case of Fig. 1b) and  $d$  for the disturbance signal ( $\dot{v}_{i+1}$  in case of Fig. 1a and  $\dot{v}_i$  in case of Fig. 1b). Using the corresponding capital letters for Laplace transforms we obtain the transfer function models

$$Y = \frac{1}{s} (U - D) \quad (3a)$$

and

$$Y = -\frac{1}{s} (U - D) \quad (3b)$$

for Fig. 1a and 1b respectively. Since the only difference is in the sign of the integrator, we will continue with eq.(3a) (Fig. 1a).

## 3. CONTROL SYSTEM ANALYSIS

Denote the Level Controller transfer function with  $G_c(s)$ , the level (volume) reference with  $r$  ( $R$  in the Laplace domain), and the controller output to flow rate transfer function with  $G_v(s)$ . The resulting control block diagram is displayed in Figure 2.

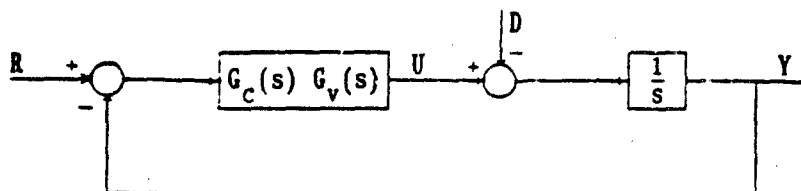


Figure 2: The 1 degree-of-freedom control problem.

Note that reference prefiltering is not considered here as we are solving a regulating problem.

The primary design aim is to avoid disturbing the flow rate  $U$  too much. The secondary objective is to achieve the first aim while keeping

$$0 < y < V_{\max} \quad (4)$$

That these objectives are contradictory and require a compromise is clear from the corresponding transfer functions:

$$\left. \frac{U}{D} \right|_{r=0} = T_u(s) = \frac{L(s)}{1 + L(s)} \quad (5)$$

and

$$\left. \frac{Y}{D} \right|_{r=0} = T_y(s) = -\frac{1}{s} \frac{1}{1 + L(s)} \quad (6)$$

with the loop transfer function

$$L(s) = G_c(s) G_v(s) \frac{1}{s} \quad (7)$$

Low gain and bandwidth  $T_u$  is achieved with low gain and bandwidth  $L$ . This, however, leads to high (low-frequency) gain in  $T_y$ .

With a reasonably practical controller design  $T_u$  will be just a low-pass system with unity low-frequency gain (or very close to it). Hence, the only sensible way to limit  $U$ -fluctuations is to limit  $T_u$ -bandwidth to, say,  $\Omega_u^*$ .  $\Omega_u^*$  may be determined (or limited) by the control system bandwidth in the process stage  $i$  of Fig. 1a.

If the  $\frac{L}{1+L}$  is designed with at least 2dB maximum "overshoot" between the gain and phase crossover frequencies then the frequency  $\Omega_u$  for the maximum value of  $\left| \frac{L}{1+L} \right|$  and the frequency  $\Omega_y$  for the maximum value of  $\left| \frac{1}{1+L} \right|$  are very close and (depending on the bandwidth definition) just a little less than  $\Omega_u^*$ . Also  $(\max \left| \frac{1}{1+L} \right| - \max \left| \frac{L}{1+L} \right|)$  is approximately 3 to 4 dB.



The above is based on the elementary comparison of reasonable designs on the background of Nichols and Inverse Nichols Charts and the assumption of little uncertainty between gain- and phase-crossover frequencies.

The author of this paper is not aware of any storage control situation where a P, or PI controller with some low-passing of the level transmitter signal would not yield satisfactory results, because  $G_v$  is essentially a gain for all frequencies up to  $\Omega_u$ . The uncertainty of  $G_v$  can be made very small with the help of valve positioners or with fast local flow feedback loops (not shown in Fig. 1). If this (additional) instrumentation is considered too expensive for an application then the standard QFT design of Horowitz should be used, although designers with a little loop shaping experience can just as well use the highest gain of  $G_v$  as the worst case for high frequency and the lowest gain of  $G_v$  as the worst case for low frequency loop shaping. The lowest gain of  $G_v$  is relevant for the storage size calculations, although it can lead to some overdesign.

#### 4. STORAGE SIZE

Now we are in the position to present a general Bode magnitude plot for

$$|T_y| = \left| \frac{1}{s} \right| \left| \frac{1}{1+L} \right| \quad (8)$$

in Figure 3, where the initial  $20 \frac{dB}{dec}$  roll-up is due to a P-controller ( $G_c(s) = K_P$ ) and  $40 \frac{dB}{dec}$  is due to a PI controller ( $G_c(s) = K_P(1 + \frac{\Omega_I}{s})$ ). The "overshoot" of  $\Delta$  dB is due to additional loop dynamics, such as transmitter signal filtering.

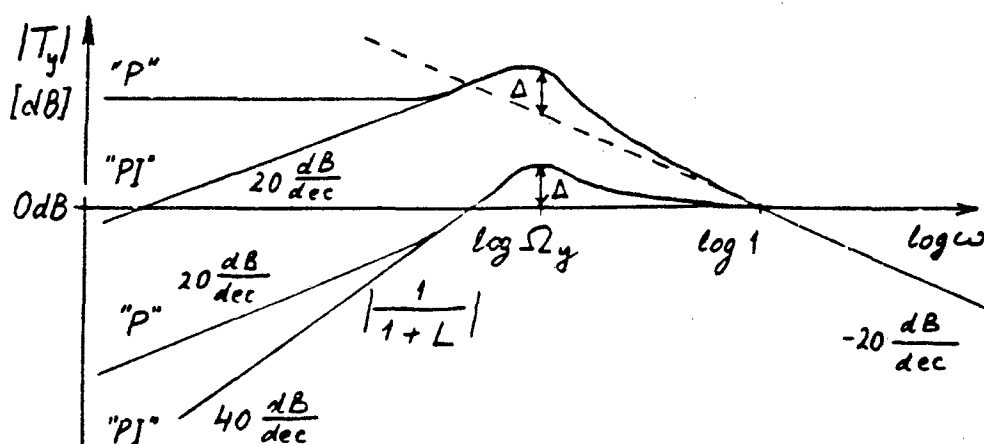


Figure 3: Typical  $|T_y|$  due to P and PI controllers, usually  $3dB < \Delta < 6dB$ .

One could now take the measured power spectral density  $P_d$  of  $D$  and demand that the standard deviation of  $y$  be for example 3 times less than  $\frac{1}{2} V_{\max}$  (for  $r = \frac{1}{2} V_{\max}$ ):

$$V_{\max} = 6\sigma_y = 6 \sqrt{\frac{1}{\pi} \int_0^{\infty} |T_y|^2 P_d d\omega} \quad (9)$$

For white noise  $D$  we can calculate approximately

$$V_{\max} = \begin{cases} 6\sqrt{P_d} / \sqrt{\pi\Omega_y} & \text{for "D" controller} \\ 6\sqrt{P_d} / \sqrt{3\pi\Omega_y} & \text{for "PI" controller} \end{cases} \quad (10)$$

Another computationally useful situation arises when  $d$  has occasional flow rate step disturbances of the magnitude  $\delta$ . These step changes will cause maximum volume deviations from  $r$  roughly equal to

$$\delta_V = |T_y(\Omega_y)| \delta \quad (11)$$

In my experience the actual value is less than the above  $\delta_V$  but not by much — see the example in section 7. Hence, eq. (11) is a worst case boundary.

From Fig. 3, approximately:

$$|T_y(\Omega_y)| = \frac{10^{\Delta/20}}{\Omega_y} \quad (12)$$

With  $3\text{dB} < \Delta < 6\text{dB}$ ,  $1.4 < 10^{\Delta/20} < 2$ . Using the larger value, we obtain for the maximum volume deviation from eq. (11)

$$\delta_{V\max} = \frac{2\delta}{\Omega_y} \quad (13)$$

and, with  $r = \frac{1}{2} V_{\max}$ , the storage tank size is given as

$$V_{\max} = \frac{4\delta}{\Omega_y} \quad (14)$$

where  $V_{\max}$  is the storage tank volume,  $\delta$  is upper bound for flow rate step disturbances and  $\Omega_y (= \Omega_u)$  is essentially the disturbance bandwidth transmitted from the tank into the stage  $i$  (stage  $i+1$  in Fig. 1b). Obviously, the control system of stage  $i$  must have at least the same bandwidth in order to counteract this disturbance.

In badly regulated or maintained processes sinusoidal disturbances can be observed. This case is covered exactly by the above equations (11) to (14), when  $\delta$  is the disturbance amplitude and  $\Omega_y$  is the disturbance frequency. If the disturbance frequency is not equal to  $\Omega_y$  then a smaller volume  $V_{\max}$  is needed than indicated by eq. (14).

Returning to eq. (10), we observe that the "P" controller case is more demanding on the storage size than the "PI" controller case, so let us consider the former further.

A noise can be considered white only if its bandwidth is larger than the bandwidth of the concerned system – in this case  $\Omega_y$ . That means, in the time domain, this noise has a standard deviation  $\sigma_d$  described by the inequality

$$\sigma_d > \sqrt{P_d \Omega_y / \pi} \quad (15)$$

Physically, this standard deviation cannot be greater than one sixth of the maximum flow rate  $\dot{v}_{\max}$  in case of approximately normally distributed flow fluctuations. Using a slightly exaggerated bound

$$\sigma_d < \frac{1}{3} \dot{v}_{\max} \quad (16)$$

yields with eqs. (15) and (10)

$$V_{\max} < \frac{2 \dot{v}_{\max}}{\Omega_y} \quad (17)$$

On the other hand, the maximum possible step disturbance  $\delta$  in eq. (14) is given by

$$\delta \leq \dot{v}_{\max} \quad (18)$$

Whence

$$V_{\max} \leq \frac{4 \dot{v}_{\max}}{\Omega_y} \quad (19)$$

Comparing equations (17) and (19) shows that in the worst case design we should be guided by the step disturbance considerations according to

$$V_{\max} \Omega_y = 4 \dot{v}_{\max} \quad (20)$$

## 5. UNSYMMETRICAL USAGE OF EVENING TANKS

Most well engineered systems operate the flow rates close to their maximum possible values, so that positive step disturbances in  $d$  can only have very small magnitudes. Hence the maximum possible step disturbance is bounded by

$$\delta < \max \dot{v}_{i+1} \quad (21a)$$

for Fig. 1a and

$$\delta < \max \dot{v}_i \quad (21b)$$

for Fig 1b. Usually  $\max \dot{v}_{i+1} = \max \dot{v}_i = \dot{v}_{\max}$ .

Correspondingly, a symmetrical  $r = \frac{1}{2} V_{\max}$  does not make sense. Rather, one should use an unsymmetrical reference, e.g.  $r$  close to 0 for Fig. 1a and  $r$  close to  $V_{\max}$  for Fig. 1b.

Under these conditions a smaller storage capacity is required – approximately equal to the maximum volume disturbance in eq. (13). Hence eq. (20) can be replaced by

$$V_{\max} \Omega_y = 2 \dot{v}_{\max} \quad (22)$$

There is a caution however: starting-up of the plant with this design must be slow, otherwise large magnitude positive steps in  $\dot{v}$  may be caused.

## 6. OPERATION OF LARGE PROCESSING VESSELS

As opposed to evening tanks, most processing vessel sizes are much greater than  $V_{\max}$  in equation (20) – due to residence time calculations, or having to be able to store for example 24 hours of process stream, and so forth. In these cases the spare volume for regulating purposes is  $V_{\max} - r$  and equation (20) must be modified to

$$\delta V_{\max} \Omega_y = 2 \dot{v}_{\max} \quad (23a)$$

with

$$\delta V_{\max} = V_{\max} - r \quad (23b)$$

In case of the processing vessels, keeping the vessel level undisturbed (not merely between 0 and  $V_{\max}$ ) may be the primary objective with flow disturbance reduction being of secondary importance. Therefore, an integral controller gets preference over the proportional controller.

## 7. A HYPOTHETICAL CALCULATION EXAMPLE

In a hypothetical process plant with very realistic data poisonous fluids are pumped from a production stage,  $i$ , into a chemical treatment stage,  $i+1$ , at a full load operating rate of  $2 \text{ m}^3/\text{min}$ . A clarifying tank of  $150 \text{ m}^3$  is used as in Fig. 1a. In order to obtain a sufficient clarification efficiency (residence time) the "level" reference is set close to the maximum tank capacity:

$$r = 130 \text{ m}^3 \quad (24)$$

Assuming  $G_v = 1$ , what is the "slowest" filtered PI controller needed to avoid spilling poisonous fluids (into a nearby river)?

The worst case disturbance is caused by blocking the treatment stage  $i+1$ :

The maximum allowable level deviation is

$$\delta V_{\max} = V_{\max} - r = 20 \text{ m}^3 \quad (26)$$

Hence from eq. (23)

$$\Omega_y = \frac{2\delta}{\delta V_{\max}} = 0.2 \frac{\text{rad}}{\text{min}} \quad (27)$$

Let us use for simplicity a first order low-pass filter with the corner frequency of  $\omega_F$ , then

$$G_c(s) = K_P \left(1 + \frac{\Omega_I}{s}\right) \frac{1}{1 + s/\omega_F} \quad (28)$$

Using elementary loop shaping considerations we can choose

$$\omega_F = 1.25\Omega_y = 0.25 \frac{\text{rad}}{\text{min}} \quad (29)$$

Then  $K_P$  is determined approximately from the requirement of

$$\frac{1}{\left|1 + \frac{K_P}{s(1 + s/0.25)}\right|} \leq 3 \text{ dB} \quad (30)$$

on the Inverse Nichols Chart in Fig. 4 (L' leaving some phase reserve for low frequency lag) yielding

$$K_P = 0.15 \quad (31)$$

The choice of 3dB in eq. (30) is motivated by the desire to avoid oscillatory behaviour in the disturbance transfer function  $T_u$ .

Lastly  $\Omega_I$  is chosen so that  $|T_u|$  is less than 3dB. Hence

$$\Omega_I = 0.02 \frac{\text{rad}}{\text{min}} \quad (32)$$

or smaller suffices.

Figure 5 shows simulated step responses of volume and vessel inflow  $\dot{v}_i$ . Notice that with respect to the step disturbance we have a spare volume overdiseign by about 40%. Nevertheless I would not change the right hand side of eq. (23a) to  $1.4 \dot{v}_{\max}$ . Any tighter design should be based on a detailed (simulation) study and signed approval of the responsible process engineer with the full knowledge of possible consequences.

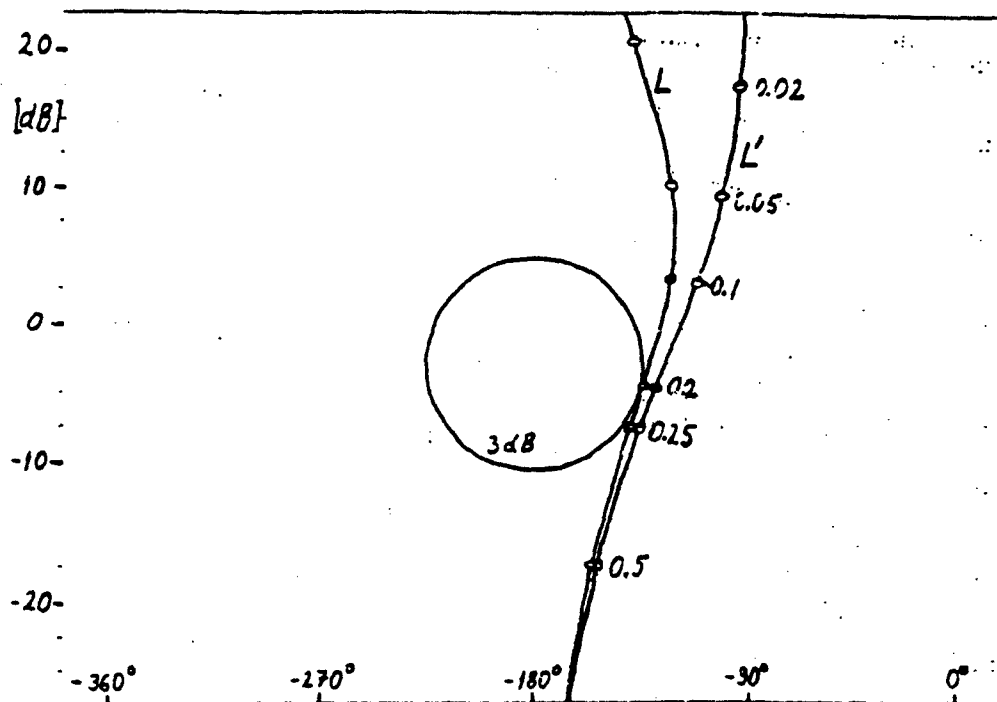


Figure 4: Inverse Nichols Chart for  $L' = 0.15/[s(1+s/0.25)]$  and  $L = 0.15(1+0.02/s)/[s(1+s/0.25)]$ .

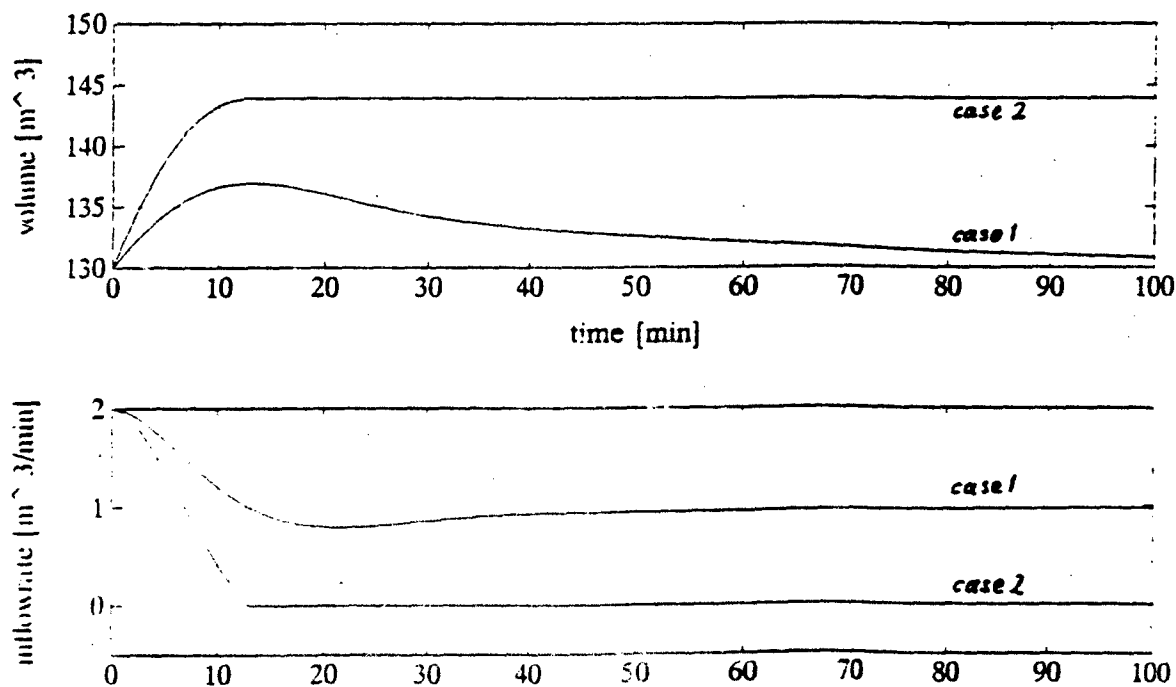


Figure 5: Response of the tank volume to 50% flow reduction in  $\dot{v}_{i+1}$  from  $2 \text{ m}^3/\text{min}$  (case 1) and to total blocking of stage  $i+1$  (case 2). Note that case 2 leads to controller saturation. Design as in Fig. 4.

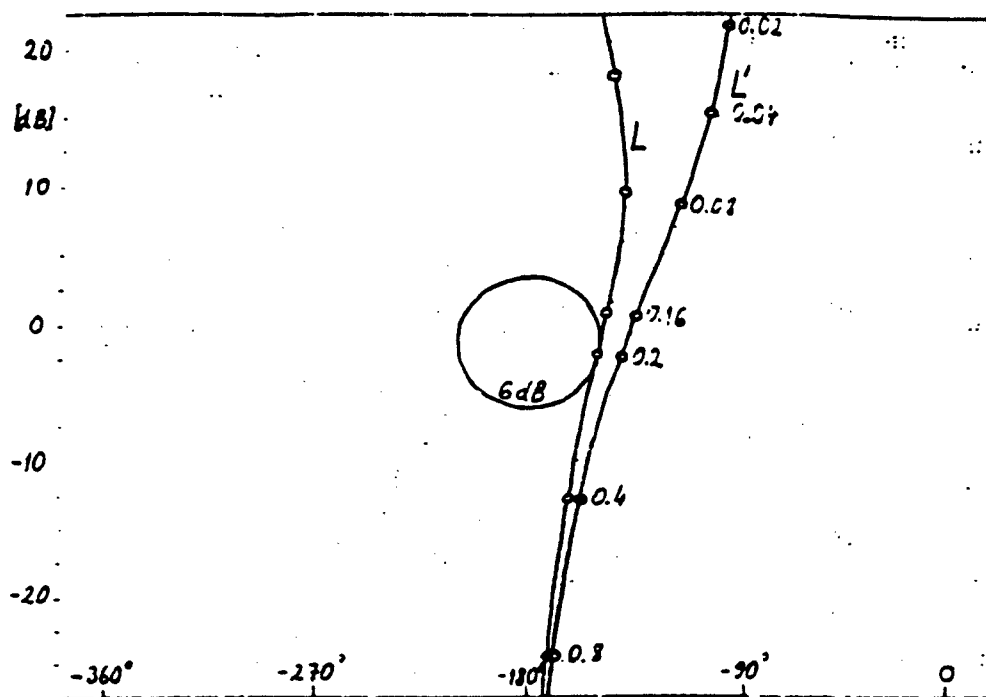
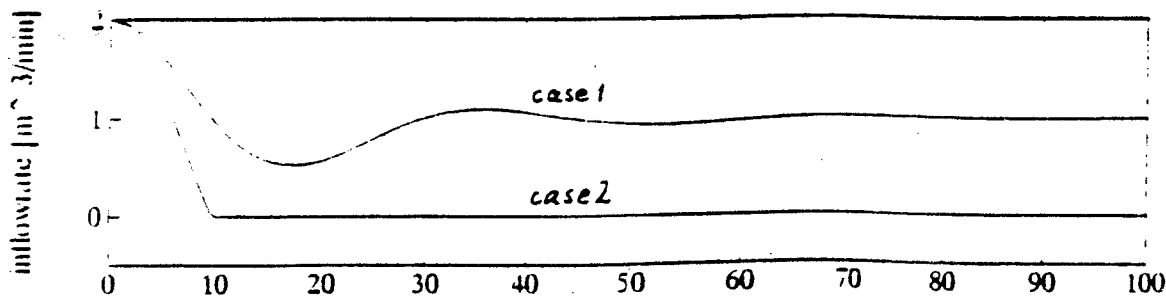
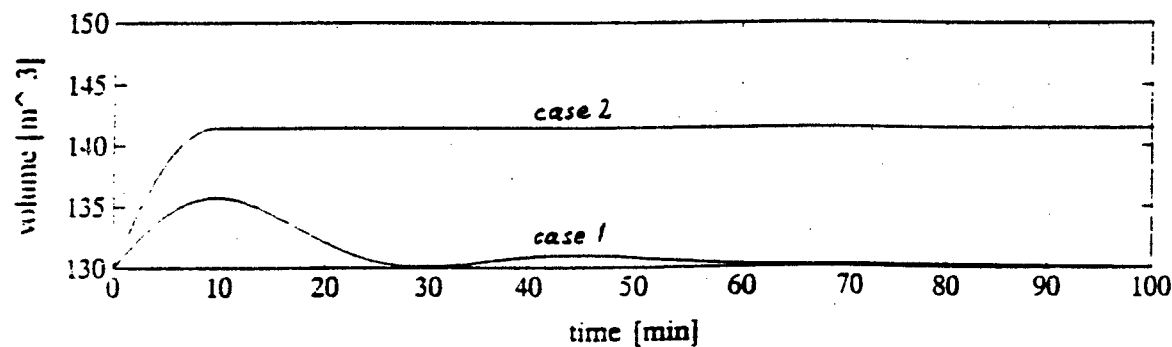


Figure 6: Inverse Nichols Chart for  $L' = 0.25/[s(1+s/0.16)]$  and  $L = 0.25(1+0.035/s)/[s(1+s/0.16)]$  for second design according to eq. (33).



For demonstrative purposes this design is repeated by allowing 6dB in eq. (30), instead of 3dB. The parameters

$$\omega_F = 0.16 \quad (33a)$$

$$K_P = 0.25 \quad (33b)$$

$$\Omega_I = 0.035 \quad (33c)$$

yield now the loop transfer functions  $L'$  and  $L$  as shown in Figure 6. The corresponding simulated step responses are shown in Figure 7.

## 8. CONCLUSION

It has been shown quantitatively here that the product between the reserve volume  $\delta_{Vmax}$  and the level control bandwidth  $\Omega_y$  must be twice the maximum process flow rate  $\dot{v}_{max}$  for safe operation of the vessel and for minimizing disturbance coupling between the process sections up- and down-stream from the vessel.

## 9. ACKNOWLEDGEMENT

The help of Dr. Edward Boje is acknowledged in derivation of equation (10) in particular and in shaping many control engineering ideas in general.



## QFT and Robust Process Control

P. S. V. NATARAJ

Systems and Control Group  
Department of Electrical Engineering  
Indian Institute of Technology  
Bombay - 400 076, INDIA

### Abstract

This paper presents a survey of the QFT-based robust controller synthesis work done at the Indian Institute of Technology, Bombay, in the area of chemical process control. The control problems considered are representative of those found in chemical and petroleum industries and fall into the following classes: lumped linear SISO multiple loop (1), lumped linear MIMO (3), lumped nonlinear SISO (2), lumped nonlinear MIMO (1) and distributed linear SISO (2). Specifically, problems concerning the following have been investigated: cascade of five continuous stirred tank reactors (CSTRs), 2x2 high purity binary distillation column, 2x2 fluidized bed catalytic cracking unit, 3x3 continuous distillation column with sidestreams, isothermal nonlinear CSTR with second order reaction kinetics, exothermic nonlinear CSTR with exotic dynamics (strong parametric sensitivity and ignition/extinction behaviour), isothermal fixed bed catalytic reactor with axial dispersion (distributed system with pseudo-homogenous catalysis) and heat equation. In every case, QFT procedures have been used to synthesize feedback systems that satisfy the performance specifications despite the considerable plant parameter uncertainty.

### Introduction

In the last three decades, QFT has been used to successfully design feedback systems for many an application drawn from the aeronautical and electrical fields. It seems to us that QFT's capabilities have, however, hardly been tapped by process control specialists. Motivated by the paucity of the process control applications of QFT, the control group at the Indian Institute of Technology, Bombay, set forth to explore the power and capabilities of QFT in tackling some typical control problems found in the chemical and petrochemical industries. This paper surveys the problems solved by the group in this area during the last one year. Detailed results are available in the theses and reports cited under the references.

A total of 9 problems falling into various classes have been successfully solved. The specific problems with the corresponding problem classes are listed in Table 1. In Section 2, a short description of each problem is given. Section 3 contains the concluding remarks along with a summary of very recent activities in this area.

## 2. Problems Solved Using QFT

### 2.1 Linear Plants

**Problem-1 (SISO) :** The system is a battery of five continuous stirred tank reactors (CSTRs) in each of which a first order irreversible reaction occurs. The first CSTR has a cooling coil through which the coolant flows. The problem is to control the concentration in the last CSTR using the coolant flow rate, despite feed concentration disturbances and the very large ( $\pm 100\%$ ) uncertainty in several basic reactor parameters. The performance specs are given in Table 2.

For the given uncertainty and performance specs, the standard SISO QFT procedure [Horowitz and Sidi, 1972] yields a design that gives large sensor noise amplification at the plant input. Using the design perspective procedure [Horowitz and Wang, 1979], a 5-cascaded multiple-loop feedback system giving significant reductions in sensor noise amplification (peak reduced by a factor of 4), is synthesized.

**Problem-2 (MIMO):** The 3x3 distillation column with sidestreams model is taken from Ray [1981]. By manipulating the rates of the distillate and two sidestreams, the product purities in these streams are to be controlled, according to the specs given in Table 2. A basically non-interacting system (BNIS) is desired, i.e. the closed-loop system is to be a decoupled one. All the 12 parameters occurring in the elements of Ray's transfer function model are assigned  $\pm 10\%$  uncertainty.

The third MIMO QFT technique [Horowitz, 1979] is used to successfully synthesize a 2-matrix-DOF feedback system.

**Problem-3 (MIMO):** Catalytic cracking is a very important process in the petroleum industry. Mostly, fluidized bed catalytic crackers (FCC) are used to carry out the cracking process. In our problem, the controlled variables are taken as the regenerator temperature and amount of carbon on the regenerated catalyst, with the air rate and catalyst circulation rate as the manipulated variables. A linear five state FCC model [Denn, 1986] is first reduced to a second order model using the balanced truncation procedure [Moore, 1981]. All ten parameters of the corresponding transfer function matrix elements are then assigned  $\pm 5\%$  uncertainty. Again, a BNIS system is desired, with the specs given in Table 2. The third MIMO QFT technique is adopted here too, to solve the problem. The design is found to be satisfactory even for the original five state model of Denn.

**Problem-4 (MIMO):** A 2x2 ill-conditioned high purity distillation column model has been analyzed in the  $H^\infty$ /SSV framework by Skogestad et al [1988]. Although a similar example (an extra time delay is present) is solved using QFT by Yaniv and Barlev [1990], for our own experience concerning directionality problems, Skogestad's model is persisted with and solved using the fourth MIMO QFT technique [Yaniv and Horowitz, 1986]. The performance specs are those of Yaniv and Barlev (see Table 2).

## 2.2 Nonlinear Plants

**Problem 5 (SISO):** Eaton and Rawlings [1990] give a nonlinear model of an isothermal CSTR with second order reaction kinetics. The plant input and output are the flowrate and reactant concentration. Disturbances are due to changes in operating temperature of the reactor. Assuming  $\pm 27\%$  uncertainty in the feed concentration, a two-DOF feedback system consisting of LTI controller and prefilter elements, is synthesized using the nonlinear QFT technique of Horowitz [1976]. The design is specific to a 0.05 step in reactor concentration setpoint. The specified performance levels (see Table 2) are attained even with a slowly time-varying feed concentration (not originally a part of the problem statement).

**Problem-6 (SISO):** An exothermic CSTR is usually a much more difficult candidate to control than its isothermal counterpart. The exothermic model discussed extensively by Uppal et al. [1974] exhibits exotic dynamics such as strong parametric sensitivity and ignition/extinction behaviour, over a range of parameter values. For this problem, the controlled and manipulated variables are chosen as the reactor and coolant temperatures, respectively. Disturbances in the feed temperature in turn affect the reactor temperature. Three dimensionless reactor parameters (dimensionless heat of reaction, Damkohler number, and dimensionless cooling rate) are assigned uncertainties ranging from  $\pm 12.5\%$  to  $\pm 40\%$ . The specified command input is a unit step in the dimensionless reactor temperature. The nonlinear QFT technique of Horowitz [1976] is used for synthesis.

**Problem-7 (MIMO):** The design example is the 2x2 MIMO version of that in problem 6. The controlled variables are the reactor temperature and concentration, while the manipulated variables are the coolant temperature and feed rate. Uncertainty is assigned to the same three reactor parameters mentioned above, and the plant set again includes a case having an unstable steady state. The nonlinear MIMO QFT design procedure used is quite similar to that presented by Yaniv [1991].

## 2.3 Linear Distributed Plants

**Problem-8 (SISO):** Chemical processes involving solid catalysts are usually carried out in fixed bed reactors. Some examples of such processes are ammonia, sulfuric acid, and methanol synthesis, hydrocracking, and polymerization. If axial mixing effects are important, the reactor is typically described by a second order p.d.e. with Danckwert's boundary conditions. The chosen process is a slightly modified version of the vapor phase ethylene hydration example given by Smith [1981]. It is required to synthesize a one-point feedback loop located half-way down the reactor ( $x = 0.5$ ), with the measured and manipulated variables as the ethylene concentration at  $x = 0.6$  and the reactant velocity, respectively. Only sensitivity reduction at point  $x = 0.6$  is sought (the same spec is given in Table 2).

A localized feedback loop is successfully synthesized using the one-point feedback approach of Keleman et al. [1989].

**Problem-9 (SISO):** The distributed plant given by the heat equation is taken from Keleman et al. [1989]. However, instead of only one feedback loop placed at  $x_{o1} = \pi/2$  by Keleman et al., an additional loop is placed at  $x_{o2} = 2\pi/3$ . The synthesis procedure [Hegde, 1992] yields a closed-loop system having much less sensitivity.

Let the heat equation be written as  $\bar{p} = hp$ , where  $p$  is the partial differential operator and  $h$  is an uncertain real parameter. For  $h \in [0.15, 1.5]$ , a one-point feedback loop is synthesized, as per the procedure suggested by Keleman et al.

The sensitivity specs for both cases discussed above, are given in Table 2.

### 3. Concluding Remarks

The above problems have been solved by graduate students using an IBM-compatible PC/AT-386 and a PC/AT. Most of the effort has gone into development of software in the MATLAB environment. However, the whole software is yet to be integrated into a suite of QFT programs. In passing, some useful routines developed for the following purposes, are mentioned :

- \* Find  $L_{opt}$  using interactive-graphics [Gera and Horowitz, 1980].
- \* Find LTIE plant from the operating records [Golubev and Horowitz, 1982].
- \* Fit a rational transfer function to frequency response data.
- \* Fit a 2-D rational transfer function using optimization (useful in DPS).
- \* Find the Laplace and inverse Laplace transforms, numerically.
- \* Perform equilibration/trade-offs between channels (MIMO QFT) [Horowitz and Sidi, 1980].

At the time of final submission of this paper, seven more linear SISO (NMP) problems have been solved. Specifically, the systems are: steam-water heat-exchanger, shell and tube heat-exchanger, furnace, catalytic reactor, blending process and distillation column (2 SISO loops). Additionally, two non-linear SISO problems - pH control and problem 5 pertaining to the isothermal reactor but with nominal plant cancellation network, have also been tackled. Two linear MIMO (NMP) systems: a distillation column with vapor recompression and a FCC unit, are currently under design investigations.

### Abbreviations

BNIS : Basically non-interacting system  
 Concn. : Concentration  
 Dist. : Disturbance  
 Recirc. : Recirculation  
 Reg. : Regenerator  
 Rej. : Rejection

Resp. : Response  
Specs : Specifications  
Temp. : Temperature

#### References

- Denn, M.M., 1986, *Process Modeling*, Longman Scientific and Technical Publications, Essex.
- Eaton, J.W. and Rawlings, J.B., 1990, Feedback Control of Chemical Processes Using On-Line Optimization Techniques, *Comp. & Chem. Engg.*, 14, 469-479.
- Gera, A. and Horowitz, I., 1980, Optimization of the Loop Transfer Function, *Int. J. Control*, 31, 389-398.
- Golubev, B. and Horowitz, I., 1982, Plant Rational Transfer Approximation from Input-Output Data, *Int. J. Control*, 36, 711-723.
- Hegde, M.D., 1992, *Synthesis for Sensitivity Reduction in Linear Distributed Systems*, M.Tech. Thesis, Indian Institute of Technology, Bombay, 400076, India.
- Horowitz, I., 1976, Synthesis of Feedback Systems with Nonlinear Time Varying Uncertain Plants to Satisfy Quantitative Performance Specifications, *Proc. IEEE*, 64, 123.
- Horowitz, I., 1979, Quantitative Synthesis of Uncertain Multiple Input-Output Feedback Systems, *Int. J. Control*, 30, 81-106.
- Horowitz, I. and Sidi, M., 1972, Synthesis of Feedback System with Large Plant Ignorance for Prescribed Time-Domain Tolerances, *Int. J. Control*, 16, 287-309.
- Horowitz, I. and Sidi, M., 1980, Practical Design of Feedback Systems with Uncertain Multivariable Plants, *Int. J. Sys. Sci.*, 19, 851-875.
- Horowitz, I. and Wang, T.S., 1979, Quantitative Synthesis of Multiple-Loop Feedback System with Large Uncertainty, *Int. J. Sys. Sci.*, 10, 1235-1268.
- Joshi, J.B., 1992, *Synthesis of Multivariable Feedback Systems for Performane Robustness*, M.Tech. Thesis, Indian Institute of Technology, Bombay, 400076, India.
- Kamat, U.J., 1992, *Synthesis of Feedback Systems for Uncertain Nonlinear Chemical Reactors*, M.Tech. Thesis, Indian Institute of Technology, Bombay, 400076, India.
- Kamat, U.J. and Nataraj, P.S.V., 1991, Quantitative Synthesis of Feedback System for an Uncertain Nonlinear Chemical Reactor System, submitted.

Kelemen, M., Kannai, Y. and Horowitz, I., 1989, One-Point Feedback Approach to Distributed Linear Systems, *Int. J. Control*, 49, 969-980.

Kundergi, R., 1991, *Design of Feedback Controllers for Uncertain Systems*, M.Tech. Mini-Project Report, Indian Institute of Technology, Bombay, 400076, India.

Moore, B.C., 1981, Principal Component Analysis in Linear Systems: Controllability, Observability and Model Reduction, *IEEE Trans. Automat. Contr.*, 25, 17-31.

Nagarkar, V.R. and Nataraj, P.S.V., 1992, Synthesis of a Multiple-Loop Feedback System for a Cascade of Reactors with Large Parameter Uncertainty. Submitted.

Narayanan, R., 1991, *Study of a QFT-Based Algorithm for Robust Control of a MIMO Plant*, M.Tech. Seminar Report, Indian Institute of Technology, Bombay, 400076, India.

Ray, W.H., 1981, *Advanced Process Control*, McGraw-Hill, New York.

Skogestad, S., Morari, M. and Doyle, J.C., 1988, Robust Control of Ill-Conditioned Plants: High-Purity Distillation, *IEEE Trans. Automat. Contr.*, 33, 1092-1105.

Smith, J.M., 1981, *Chemical Engineering Kinetics*, Third Edition, McGraw-Hill, New York.

Uppal, A., Ray, W.H. and Poore, A.B., 1971, On The Dynamic Behaviour Of Continuous Stirred Tank Reactors, *Chem. Engng. Sci.*, 29, 967.

Yaniv, O., 1991, Robust Design of MIMO Feedback Systems Having an Uncertain Non-Linear Plant, *Int. J. Control*, 53, 1283-1294.

Yaniv, O. and Barlev, N., 1990, Robust Non-Iterative Synthesis of Ill-Conditioned Plants, *Proc. American Control Conf.*

**Table 1 : Problems Successfully Tackled Using Various  
QFT Techniques, at IIT Bombay**

Problem No.	System	Problem Class	QFT Technique	Reference
1	Cascade of 5 CSTRs	Lumped, LTI, SISO, MP, Multiple-loop (six-DOF)	Multiple-loop design perspective [Horowitz and Wang, 1979]	[Nagarkar and Nataraj, 1992]
2	Distillation column with sidestreams [Ray, 1981]	Lumped, LTI, 3x3 MIMO, MP (2-matrix-DOF)	Third MIMO QFT [Horowitz, 1979]	[Joshi, 1992]
3	Fluidized bed catalytic cracker [Denn, 1980]	Lumped, LTI, 2x2 MIMO, MP (2-matrix-DOF)	Third MIMO QFT [Horowitz, 1979]	[Joshi, 1992]
4	High purity distillation column [Skogested et al, 1990]	Lumped, LTI, 2x2 MIMO, MP (2-matrix-DOF)	Fourth MIMO QFT [Yaniv and Horowitz, 1986]	[Narayanan, 1992]
5	Isothermal CSTR [Eaton & Rawlings, 1990]	Lumped, non-linear, SISO (2-DOF)	Nonlinear QFT [Horowitz, 1976]	[Kamat and Nataraj, 1992]
6	Exothermic CSTR [Uppal et al, 1974]	Lumped, non-linear, SISO (2-DOF)	Nonlinear QFT [Horowitz, 1976]	[Kundergi, 1991]
7	Exothermic CSTR [Uppal et al, 1974]	Lumped, non-linear, 2x2 MIMO (2-DOF)	Nonlinear MIMO QFT Algorithm Similar to that in [Yaniv, 1991]	[Kamat, 1992]
8	Isothermic-fixed-bed catalytic reactor [Smith, 1981]	Distributed, linear SISO (2-DOF)	One-point feed-back [Keleman et al., 1989]	[Hegde, 1992]
9	Heat equation [Keleman et al, 1989]	Distributed, linear SISO (2-DOF)	Two point feedback	[Hegde, 1992]

Table 2 : Performance Specifications for Various Problems

Problem No	Tracking				Dist. peak magnitude	Gain-phase margins	Remarks
	$T_u$ or $T_{iiu}$ $\zeta$	$\omega_n$	$T_L$ or $T_{iiL}$ $\zeta$	$\omega_n$			
1	0.45	5.00 $\times 10^{-3}$	1.25	5.00 $\times 10^{-3}$	$\leq 0.0428$ to a 20% step $t_p \sim 4000$	4.8 dB, 42°	
2	0.44	0.057	1.25	0.057	$\leq 2.3$ dB	5 dB, 45°	For BNIC, $ T_{ij}  \leq 0.2$
3	0.44	8.4 $\times 10^{-4}$	1.25	8.4 $\times 10^{-4}$	"	"	For BNIC, $ T_{ij}  \leq 0.2 \forall \omega$
4	See remarks				"	"	For a step in $r_i$ . $y_i(t) \geq 90\%$ for $t > 30$ min. Also, $y_i(t) \leq 50\%$ , $j \neq i$ . Steady state offset=0
5	0.45	1.48 $\times 10^{-3}$	1.25	1.48 $\times 10^{-3}$	"	"	Designed for a step in concentration setpoint of magnitude 0.05.
6	0.45	7.5	0.8	4	"	"	Designed for a unit step in dimensionless reactor temperature. Normalized time used.
7	0.44	8.5	0.8	4	"	"	For BNIC, $ T_{ij}  \leq .01 \forall \omega$ and $t_s \leq 2.5$ . Designed for a 30% step in reactor temperature and 1% step in reactor concentration. Normalized time used.



Table 2 (continued)

Problem No	Tracking				Dist. peak mag- tude	Gain- phase margins	Remarks
	$T_u$ or $\zeta$	$T_{iiu}$ or $\omega_n$	$T_L$ or $\zeta$	$T_{iil}$ or $\omega_n$			
8	Not considered				$ T_{x,x}(j\omega) $ $\leq 0.7 P_{x,x}(j\omega) $ for $\omega \in [0, 4]$	4.8dB, 42°	$x_i=0, x=0.6, x_o=0.5$ Notation as in Keleman et al [1990]
9(a)	Not considered				$ T_{x,x} $ $\leq 0.9 P_{x,x} $ for $\omega \in [0, 1.5]$	3.0dB, 20°	$x_i=\pi/4, x=\pi/4$ $x_{o1}=\pi/2, x_{o2}=2\pi/3.$
(b)	Not considered				$ T_{x,x} $ $\leq 0.8 P_{x,x} $ for $\omega \in [0, 1.6]$	4.8dB, 42°	$x_i=\pi/4, x=\pi/3,$ $x_o=\pi/2$

Table 3 : Additional Information Concerning Design Problems

Problem No.	Uncertainty		Controlled variable(s)	Manipulated variable(s)	Disturbance variable(s)	Performance specs on
	No. of parameters	Amount				
1	6	$\pm 100\%$	Reactor concn. (5th CSTR)	Coolant rate (1st CSTR)	Feed conc.	Tracking and dist. rej.
2	12	$\pm 10\%$	Distillate & side-streams' concn.	Distillate & side-streams' flowrates	-	Tracking & peak dist. resp. (BNIS)
3	10	$\pm 5\%$	Reg. temp. & carbon on reg. catalyst	Air rate & catalyst recirc. rate	-	-do-
4	3	$\pm 20\%$ $\pm 2\%$	Distillate & bottoms concn.	Reflux rate & vapor boilup	-	-do-
5	1	$\pm 27\%$	Reactor concn.	Feedrate	Reactor temp.	0.05 step in reactor concn. & peak dist. resp.
6	3	$\pm 12.5\%$ $\pm 40\%$ $\pm 40\%$	Reactor temp.	Coolant temp.	Feed temp.	Unit step in dimensionless reactor concn. & peak dist. resp.
7	3	$\pm 6.6\%$ $\pm 25\%$ $\pm 25\%$	Reactor temp. & Reactor concn.	Feedrate and Coolant rate	Feed temp.	30% step in reactor temp. 1% step in reactor concn (BNIS)
8	Nil	-	Reactor concn. at $x_0 = 0.5$	Feed velocity	Feed conc.	Sensitivity reduction
9(a)	Nil	-	Temp. at $x_0 = \pi/2$ , $2\pi/3$	Heat input	Heat losses	Sensitivity reduction
(b)	1	$\pm 82\%$	Temp. at $x_0 = \pi/2$	Heat input	Heat losses	Sensitivity reduction

# **QFT-Like Design of an Idle Speed Controller for an Uncertain Fuel Injected Engine**

Stephen J. Rober \*  
Stephen J. Koffman \*  
Matthew A. Franchek +

School of Mechanical Engineering  
Purdue University  
West Lafayette, IN 47907

## **Abstract**

Idle speed control of a V-6 fuel injected engine is presented as a feasibility study of a QFT-like design approach. The engine model is linearized about two operating conditions: i) loaded and ii) unloaded where the latter model is the least stable. The control objective is to maintain idle speed within a small tolerance despite uncertain torque demands imposed by various auto accessories. In the interest of fuel efficiency, idle air valve setting and ignition timing are the control inputs where each experiences an induction-to-power delay. Furthermore, each manipulated variable is limited by its hardware, i.e. saturation and bandwidth.

## **I. Introduction**

Combustion engines used in transportation account for approximately 2/3 of the fossil fuel usage in the US. In fact, over a nineteen year study the EPA determined that the automobile sector was the only group of combustion users whose emissions of pollutants has grown to over 144% of its 1970 estimates. With an increasing concern of the non-renewable resource depletion and the global greenhouse effect, an urgent need exists to increase engine efficiency while reducing pollution emissions. This need was emphasized recently (08 May 1992) by the United Nations where 143 nations debated an emissions control treaty.

This study focuses on increasing engine speed efficiency and reducing engine emissions. In particular, the idle speed of an engine is usually inflated so as to provide acceptable power in the face of uncertain torque demands required by the accessories. As a result, engine efficiency decreases while emission levels increase. In contrast, the objective of this work is to significantly lower the idle speed of an unloaded engine by providing it with self-regulation capability. Although this approach is not new to auto manufacturers, the simplicity of the proposed feedback configurations obtained from the following QFT-like design methodology is extremely attractive.

## **II. Review of Design Method**

The design methodology employed in this application was developed by Jayasuriya and Franchek [1]-[4] and has much in common with Quantitative Feedback Theory (QFT) [5]. This method is well suited for MISO systems, as it takes full advantage of all inputs to maintain the output rather than forcing diagonal dominance of a "squared" plant. Forcing diagonal dominance reduces loop interactions, which can be counter productive.

---

\* Graduate Student, School of Mechanical Engineering, Purdue University

+ Assistant Professor, School of Mechanical Engineering, Purdue University; author to whom all correspondence should be sent

The MISO method consists of sequential loop closures where the controller for each closed loop is designed such that the specified bounds on the system output and control effort are satisfied. While the approach also allows internal state specifications, this application is restricted to satisfying only the constraints for the output and control variables. Furthermore, the target transfer functions [1] - [4] will be chosen as constant values of the saturation/performance levels of the variables, and bandwidth constraints will be explicitly incorporated during loop shaping.

Figure 1 shows a block diagram of a generic MISO system.

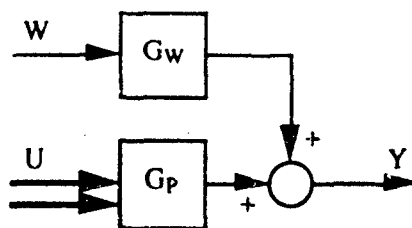


Figure 1 - Block Diagram of Generic MISO System

The first design decision to be made is which loop should be closed first. The logical approach is to first close the loop with the faster dynamics/smaller time delay and then subsequently close loops with slower dynamics/greater time delays. For clarity, subscripts in the following descriptions will indicate the order of loop closure.

The first loop is closed using a controller  $G_{C1}(s)$  in the forward path and unity feedback, and the closed loop transfer functions are written for disturbance-to-output  $\frac{Y(s)}{W(s)}$  and disturbance-to-control effort  $\frac{U_1(s)}{W(s)}$  with the currently unknown controller transfer function being included as  $G_{C1}(s)$ .

Using these transfer functions, the time domain constraints are enforced by the satisfying the following frequency domain inequalities:

$$y_{MAX} \geq \left| \frac{Y(j\omega)}{W(j\omega)} \right| \alpha = F_1(L_1(j\omega)) \quad (1)$$

$$u_{1 MAX} \geq \left| \frac{U_1(j\omega)}{W(j\omega)} \right| \alpha = F_2(L_1(j\omega)) \quad (2)$$

where  $\alpha$  is the magnitude of the step disturbance,  $y_{MAX}$  is the largest tolerable deviation, and  $u_{1 MAX}$  is the saturation level of the control effort in loop 1. A widely held belief in QFT as well as this technique is that satisfaction of frequency domain bounds implies satisfaction of the related time domain bounds. While this is not mathematically rigorous, experience has shown it to be valid for most physical systems.

Equations (1) and (2) are functions of the unknown loop transmission function  $L_1(j\omega)$ . These equations give both lower and upper bounds on the magnitude of  $L_1(j\omega)$  for each frequency  $\omega$ . For a given frequency, as the phase angle is changed, equations (1) and (2) trace lower and upper boundaries on the phase-gain plane. For a set of frequencies chosen by the designer, these phase-gain boundaries for each frequency are displayed on the Nichols chart and delineate regions where

the loop transmission function  $L_1(j\omega)$  must lie. The design is completed by loop shaping  $L_1(j\omega)$  to these regions. In this sense, the approach is much like QFT [5].

If the dynamics of  $G_{P1}(j\omega)$  are certain, a loop transmission function can be fitted to any portion of these regions using a controller  $G_{C1}(j\omega)$ . For uncertain MISO systems, this design procedure is altered. At a given frequency, an uncertain plant will occupy a region (template) on the Nichols chart instead of a single point as for the certain plant. The necessary design modification is to make sure that the entire template at a certain frequency completely lies within the boundaries for that frequency.

To facilitate this design process, a nominal plant  $L_{10}$  is selected from the plant set and marked on each template. At each design frequency, the corresponding template is moved around the Nichols chart to find the acceptable design region. As the template for a frequency is moved along the border of the region for this frequency, the path the nominal plant  $L_{10}$  makes is marked as the design boundary for the nominal plant.

Thus, by guaranteeing that the nominal plant stays within the new boundaries, the uncertain plant will satisfy the design specifications. A controller is found by loop shaping the nominal plant. This procedure works well for the first loop closure, but becomes increasingly more difficult for subsequent loop closures as the number of boundary conditions increase and uncertainty from plants of previous loops enters into the design bounds. This problem is explicitly discussed in Section IV in context of the design example.

Now the second loop is closed with a controller  $G_{C2}(s)$  and unity feedback. The resulting transfer functions are written for disturbance-to-output  $\frac{Y(s)}{W(s)}$ , disturbance-to-control effort of loop 1  $\frac{U_1(s)}{W(s)}$ , and disturbance-to-control effort of loop 2  $\frac{U_2(s)}{W(s)}$ . Note that another constraining equation is introduced to bound the control effort  $u_2(t)$ , i.e.

$$y_{MAX} \geq \left| \frac{Y(j\omega)}{W(j\omega)} \right| \alpha = F_3(L_2(j\omega)) \quad (3)$$

$$u_{1 MAX} \geq \left| \frac{U_1(j\omega)}{W(j\omega)} \right| \alpha = F_4(L_2(j\omega)) \quad (4)$$

$$u_{2 MAX} \geq \left| \frac{U_2(j\omega)}{W(j\omega)} \right| \alpha = F_5(L_2(j\omega)) \quad (5)$$

where  $\alpha$ ,  $y_{MAX}$ , and  $u_{1 MAX}$  are as before and  $u_{2 MAX}$  is the saturated value of the control effort for loop 2. Note that the transfer functions in (3) and (4) are different from those in (1) and (2) since the dynamics of loop 1 are included here. In an analogous manner that the controller for the first loop was designed, a controller for the second loop is designed here. This process is repeated for further loops with each loop closure adding another constraint equation and altering the previous constraining equations.

### III. Engine Model

The system for this case study is the V-6 engine represented by the block diagram (Williams, et al., 1988) shown in Figure 2.

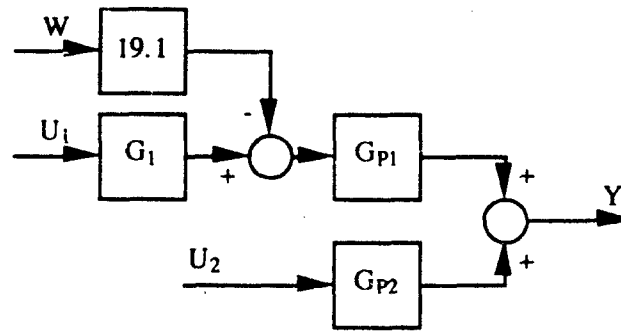


Figure 2 - Linearized Model of Uncompensated Engine

In Figure 2,  $w(t)$  is the disturbance torque,  $u_1(t)$  is the spark advance,  $u_2(t)$  is the idle air valve setting, and  $y(t)$  is the engine speed variation.

The plants  $G_1$ ,  $G_{p1}$ , and  $G_{p2}$  are defined as

$$G_1(s) = 15.9e^{-0.04s}$$

$$G_{p1}(s) = \frac{s + a}{s^2 + bs + c}, \quad a \in [3, 3.5], \quad b \in [2.2, 2.4], \quad c \in [5.62, 12]$$

$$G_{p2}(s) = \frac{de^{-0.16s}}{s^2 + fs + g}, \quad d \in [9, 12], \quad f \in [2, 2.2], \quad g \in [4.6, 10].$$

The gain of 19.1 on the disturbance represents the gearing ratio of an air conditioner compressor.

Unlike the model in Williams, et al., the parameters of the engine transfer functions are allowed to vary in the indicated intervals. These intervals account for the loaded and unloaded operating conditions of the engine.

The objective of a control design for this system is to reject a step disturbance of 10 Nm while ensuring that the speed variation  $y(t)$  is less than 20 rpm. The spark advance  $u_1(t)$  must be less than 20 points and the idle air valve setting  $u_2(t)$  must be less than 1000 points. The term 'point' is a measure of angular displacement. Also at steady state the spark advance must return to zero to ensure minimal engine emissions.

#### IV. Design of Controller and Simulation Results

This section describes the synthesis of an idle speed controller for the V-6 engine described in Section III using the technique described in Section II. Step responses for the compensated system are performed to verify the design.

##### *Design of Controller $G_{C1}$*

The spark advance-to-speed variation loop is the first loop to be closed since it has the smallest induction-to-power delay. Figure 3 shows the feedback structure for this loop closure.

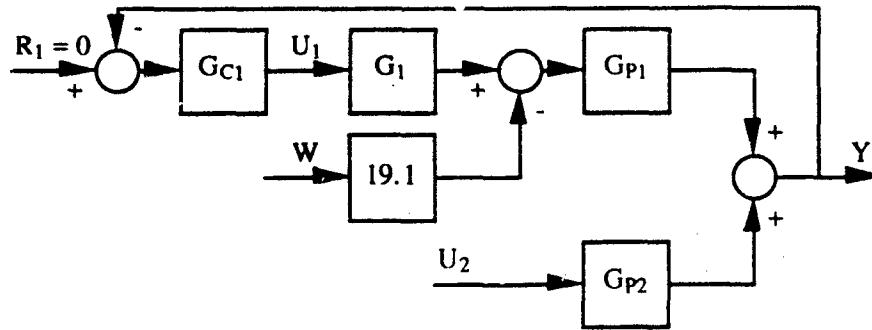


Figure 3 - Engine Model with a Controller in Loop 1 (Spark Advance)

The resulting transfer functions are:

$$\frac{Y(s)}{W(s)} = \frac{-19.1 G_{P1}(s)}{1 + G_{P1}(s) G_{C1}(s) G_1(s)} \quad (6)$$

$$\frac{U_1(s)}{W(s)} = \frac{19.1 G_{P1}(s) G_{C1}(s)}{1 + G_{P1}(s) G_{C1}(s) G_1(s)} \quad (7)$$

For a disturbance of 10 Nm, speed variation  $y(t)$  is to be less than 20 rpm and spark advance  $u_1(t)$  is to be less than 20 points. This is achieved by using (1) and (2) of Section II in the following form:

$$10.0 \left| \frac{-19.1 G_{P1}(j\omega)}{1 + G_{P1}(j\omega) G_{C1}(j\omega) G_1(j\omega)} \right| \leq 20.0 \quad (8)$$

$$10.0 \left| \frac{19.1 G_{P1}(j\omega) G_{C1}(j\omega)}{1 + G_{P1}(j\omega) G_{C1}(j\omega) G_1(j\omega)} \right| \leq 20.0 \quad (9)$$

These may be written as:

$$\left| \frac{1}{1 + L_1(j\omega)} \right| \leq \frac{20.0}{(10.0) (19.1) |G_{P1}(j\omega)|} \quad (10)$$

$$\left| \frac{L_1(j\omega)}{1 + L_1(j\omega)} \right| \leq \frac{20.0 |G_1(j\omega)|}{(10.0) (19.1)} \quad (11)$$

where  $L_1(s) = G_{P1}(s) G_{C1}(s) G_1(s)$ .

Inequalities (10) and (11) are interpreted as constraints on the closed loop sensitivity and transfer function, respectively. Such interpretations are useful when verifying that a computerized search is giving correct results.

In Section II, the procedure for finding the boundaries on the Nichols chart was explained. This procedure involved finding the templates for the uncertain dynamics and using them to plot the boundaries for the design frequencies. Since template generation can be computational intensive, Franchek and Jayasuriya [3] use Kharitonov polynomials for both the numerator and denominator of the plant transfer function to bound the templates. The bound for each template is a rectangle defined

by the minimum and maximum magnitude and phase. This approach will make the design conservative by taking into account a larger template than will actually exist. In contrast, this work grids the parameter space to develop "discrete" templates of the plant variations. These discrete templates are generated by selecting several values from each parameter interval. Using all combinations of these values the discrete templates are produced. Then the discrete templates are normalized by subtracting out the dB gain and phase of the point produced by the nominal plant.

Figure 4 shows such a normalized discrete template for the first loop for  $\omega = 1.0$  rad/s.

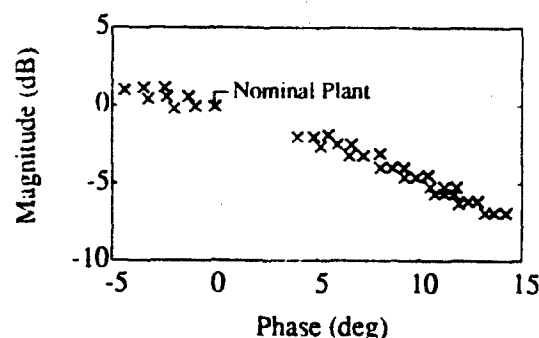


Figure 4 - Normalized Template for Loop 1 ( $\omega = 1.0$  rad/s)

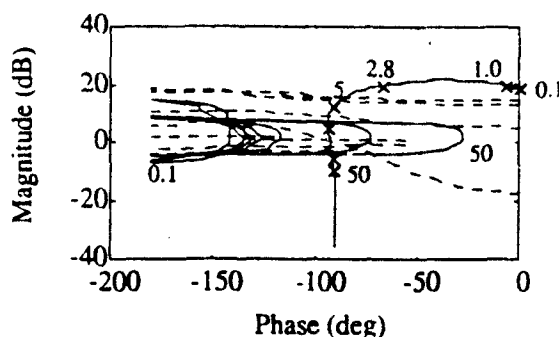


Figure 5 - Boundaries for Loop 1 and Uncompensated Nominal Plant

For a fixed frequency, the normalized discrete template is shifted in phase and gain until each point of the template satisfies the constraint (either (10) or (11), since each one has a separate search dedicated to it). Note that the shifting is done by first selecting a phase and then stepping through gain. The template starts out violating the constraint, and once an open loop (phase, gain) point is found that satisfies the constraint, this point is recorded as being on the boundary. A new phase is then selected and the process is repeated. For boundaries that are multiple-valued with respect to phase, the search process is reversed such that a magnitude is selected and phase is changed until a boundary point is found. This ensures that the entire boundary will be found rather than a branch of it when doing a simple search. Of course, the original scheme works when the boundaries are multiple-valued with respect to gain. Figure 5 shows the boundaries with the minimum phase portion of the nominal loop transmission superimposed.

The nominal loop transmission  $L_{10}(s) = G_{P10}(s) G_1(s) G_{C1}(s)$  was arbitrarily chosen as having the plant with the smallest parameters, i.e.

$$G_{P10}(s) = \frac{s + 3}{s^2 + 2.2s + 5.62}$$

The nonminimum phase portion,  $e^{-0.04s}$ , of the nominal loop transmission function is "absorbed" into the calculations for the bounds defined in (10) and (11). This can be seen in Figure 5 as the horizontal elongation of the boundaries within the  $\pm 10$  dB gain strip. Therefore, the boundaries are generated for and the loop shaping is done on the minimum phase portion of  $L_{10}$ . The dashed boundaries of Figure 5 are generated by equation (10) and the solid boundaries are generated by (11). Figure 6 shows the compensated loop for the first loop closure.



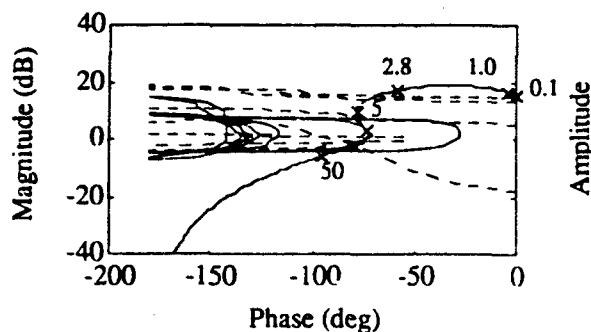


Figure 6 - Boundaries and Compensated Nominal Plant for Loop 1

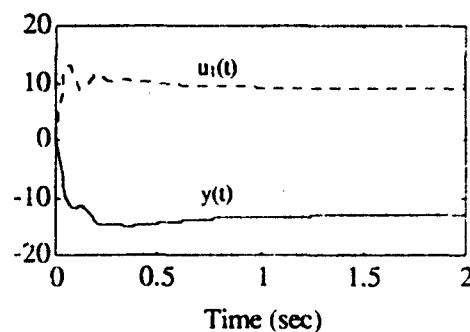


Figure 7 - Time Response for Compensated Loop 1 (Nominal Plant)

Since satisfaction of the performance boundaries does not guarantee good transient behavior nor stability, a lead controller is added to shift the loop to the left in the frequency range of 10 rad/s to 30 rad/s such that suitable phase and gain margins are achieved. An additional first-order roll-off was added to suppress noise transmission. The final compensator for loop 1 is

$$G_{C1}(s) = \frac{0.7 \left( \frac{s}{11.5} + 1 \right)}{\left( \frac{s}{34.6} + 1 \right) \left( \frac{s}{100} + 1 \right)}$$

The bandwidth of this controller is 55 rad/s.

Figure 7 shows the nominal response of the system for the first loop closure to a 10 Nm step disturbance. Clearly, the speed variation and spark advance are well within their limits of 20 rpm and 20 points, respectively.

#### Design of Controller $G_{C2}$

Figure 8 shows the block diagram of the system with the second loop (idle air valve) closed.

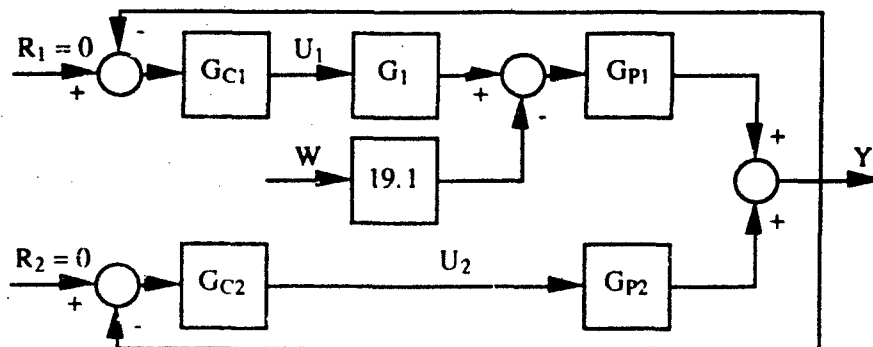


Figure 8 - Engine Model with Controllers in Loop 1 (Spark Advance) and Loop 2 (Idle Air Valve)

In addition to the constraints for the first loop (spark advance  $u_1(t)$  less than 20 points and speed variation  $y(t)$  less than 20 rpm), the constraint of the idle air valve setting  $u_2(t)$  less than 1000 points is added. Therefore, from equations (3), (4), and (5) the following inequalities must be satisfied:

$$10.0 \left| \frac{-19.1 G_{P1}(j\omega)}{1 + G_{P2}(j\omega) G_{C2}(j\omega) + G_{P1}(j\omega) G_{C1}(j\omega) G_1(j\omega)} \right| \leq 20.0 \quad (12)$$

$$10.0 \left| \frac{19.1 G_{P1}(j\omega) G_{C1}(j\omega)}{1 + G_{P2}(j\omega) G_{C2}(j\omega) + G_{P1}(j\omega) G_{C1}(j\omega) G_1(j\omega)} \right| \leq 20.0 \quad (13)$$

$$10.0 \left| \frac{19.1 G_{P1}(j\omega) G_{C2}(j\omega)}{1 + G_{P2}(j\omega) G_{C2}(j\omega) + G_{P1}(j\omega) G_{C1}(j\omega) G_1(j\omega)} \right| \leq 1000.0 \quad (14)$$

Note that the uncertainty from loop 1 is present in the bounds for loop 2. This "uncertainty interaction" can be dealt with by rewriting the inequalities as:

$$\left| \frac{1}{1 + G_L(j\omega) L_2(j\omega)} \right| \leq \frac{20.0}{(19.1) (10.0) |G_{P1}(j\omega) G_L(j\omega)|} \quad (15)$$

$$\left| \frac{1}{1 + G_L(j\omega) L_2(j\omega)} \right| \leq \frac{20.0}{(19.1) (10.0) |G_{P1}(j\omega) G_L(j\omega) G_{C1}(j\omega)|} \quad (16)$$

$$\left| \frac{G_L(j\omega) L_2(j\omega)}{1 + G_L(j\omega) L_2(j\omega)} \right| \leq \frac{1000.0 L_2(j\omega)}{(19.1) (10.0) |G_{P1}(j\omega) G_{C2}(j\omega)|} \quad (17)$$

where

$$G_L(s) = \frac{1}{1 + L_1(s)}$$

$$L_1(s) = G_{P1}(s) G_{C1}(s) G_1(s)$$

$$L_2(s) = G_{P2}(s) G_{C2}(s).$$

Now the product  $G_L(s)L_2(s)$  can be regarded as the uncertain loop transmission function for loop 2, and the controller can be found by loop shaping on the minimum phase portion of this "new" transmission function. That is to say that  $G_L(s)L_2(s)$  is used to form the templates for loop 2, while equations (15) - (17) are used to generate the boundaries. It should be noted that (15) and (16) differ only by a factor of  $\frac{1}{|G_{C1}(j\omega)|}$ . As a result, one boundary will dominate over the other boundary,

depending on the magnitude of  $G_{C1}(j\omega)$ . If the conditions of the dominant boundary are met, then the condition of the other boundary is met automatically.

For this loop, the bounds are not constant; they change values depending upon the point of the template being used, i.e. the bound depends on the uncertainty point under consideration. Since 36 discrete points are used to represent  $G_{P1}(s)$  and  $G_{P2}(s)$ , there are now  $36^2$  points (Figure 9) in the discrete template  $G_L(s)L_2(s)$ , thereby substantially increasing the number of points that need to be checked during each iteration of the search algorithm. By inspection, it would be possible to reduce the number of discrete points on the template. Because of the proximity of many of the points to each other, the calculations for many of the points are redundant.

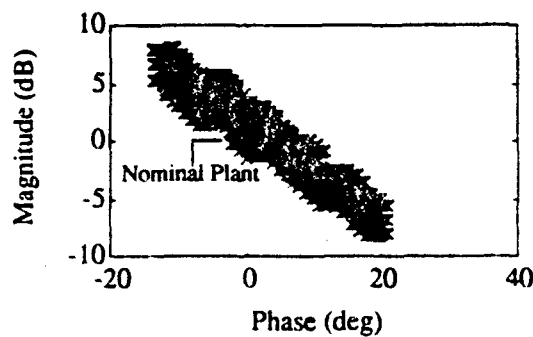


Figure 9 - Template for Loop 2  
( $\omega = 1.0$  rad/s)

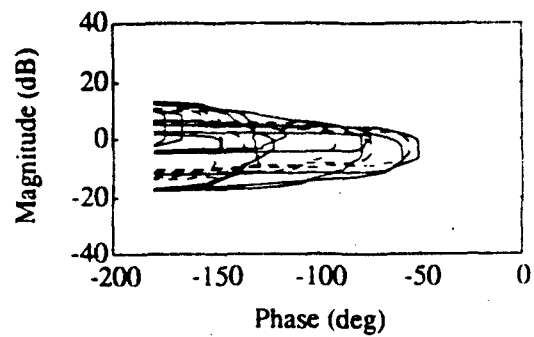


Figure 10 - Boundaries For Loop 2

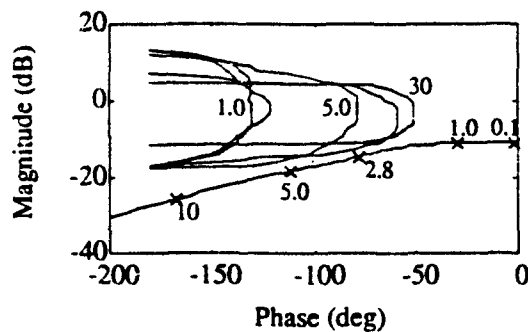


Figure 11 - Boundaries from (15) and Uncompensated Nominal Plant for Loop 2

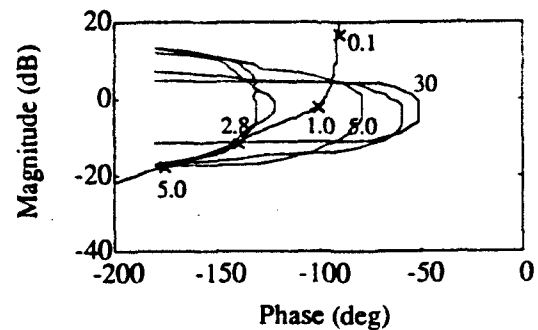


Figure 12 - Boundaries and Compensated Nominal Plant for Loop 2

Figure 10 shows the boundaries generated by (15) - (17). The solid lines represent (15), the dashed lines represent (16) and (17). It can be seen that the boundaries of (16) and (17) lie within the boundaries generated by (15); therefore, the boundaries generated by (15) are used in the design process. Figure 11 shows the boundaries generated by (15) and the nominal loop transmission for  $G_L L_{20}$ . As with  $L_{10}$ ,  $G_L L_{20}$  is chosen to represent the lowest values of the uncertainty parameters of  $G_{p1}(s)$  and  $G_{p2}(s)$ .

Since full rejection of the step disturbance is required at steady state, an integrator is added to  $G_{C2}(s)$  with a small amount of gain. To complete the design, a lead controller is added to avoid the low frequency boundaries. The final compensator is

$$G_{C2}(s) = \frac{2.5 \left( \frac{s}{1.75} + 1 \right)}{s \left( \frac{s}{5.1} + 1 \right)}$$

The bandwidth for this controller is 6 rad/s.

Figure 12 shows the compensated loop transmission for  $G_L L_{20}$ . Figure 13 shows the system response for the nominal plants  $G_{p1}(s)$  and  $G_{p2}(s)$  when a 10 Nm step disturbance is applied.

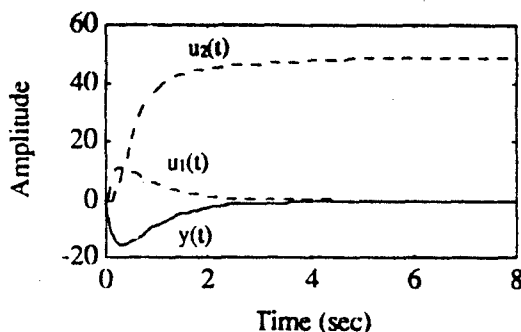


Figure 13 - Time Response of Compensated System (Nominal Plant)

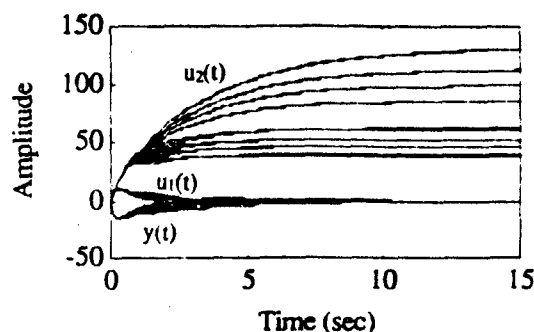


Figure 14 - Time Response of Compensated System (Full Range of Uncertainty)

Figure 14 shows the system response for the family of plants  $G_{p1}(s)$  and  $G_{p2}(s)$  when a 10 Nm step disturbance is applied. Clearly the performance bounds of 20 rpm for speed variation, 20 points for spark advance, and 1000 points for idle air valve setting are satisfied for the uncertain engine.

## V. Conclusions

The purpose of this work was to present a feasibility study of a QFT-like technique applied to an engine idling problem. Using this technique, a fixed controller was found to be adequate for loaded and unloaded operating conditions of the engine.

While the design technique proved quite powerful for the two inputs / one output V-6 engine idle speed control system design, the technique becomes increasingly more computationally intensive for MISO systems with more inputs and uncertain parameters. As the number of inputs increase, the number of boundary conditions increase. This is generally not a problem since one of the boundary conditions will be the most restrictive and hence will be the limiting factor in the design. Since parametric uncertainty from previous loops propagates to later loops, the number of template and search calculations increase combinatorically. Thus, the number of points from each parameter interval should be judiciously chosen to accurately represent the templates while keeping template and search calculations to a minimum.

This technique is based upon satisfying frequency domain constraints such that corresponding time domain constraints are met. While the transition from time domain to frequency domain is based upon conjecture, the premise holds for this application.

## References

- [1] Jayasuriya, S. and Franchek M.A., "Frequency Domain Design for Prespecified State and Control Constraints under Persistent Bounded Disturbances," *Proceedings of the IEEE Conference in Decision and Control*, Austin, TX 1988.
- [2] Franchek, M.A., Jayasuriya, S., and Rabins, M.J., "Controller Synthesis for Maximizing Disturbance Bounds in Linear Uncertain Systems," *Proceedings of the IFAC 11th Triennial World Congress*, Tallinn, Estonia, USSR, 1990, pp. 217-222.

- [3] Franchek, M.A. and Jayasuriya, S., "Frequency Domain Synthesis of an Idle Speed Control System for a Fuel Injected Engine," *Robust Control of Mechanical Systems: Theory and Applications*, ASME, DSC-Vol. 27, 1991, pp. 27-32.
- [4] Jayasuriya, S. and Franchek, M.A., "A Frequency Domain Design for MISO Regulation Systems Having Hard Time Domain Constraints," *Journal of Dynamic Systems Measurement, and Control*, 1992, (in review).
- [5] Horowitz, I.M. and Sidi, M., "Synthesis of Feedback Systems with Large Plant Ignorance for Prescribed Time-Domain Tolerances," *International Journal of Control*, Vol. 16, Feb. 1972, pp. 187-309.
- [6] Williams, S.J., Hrovat, D., Davey, C., Maclay, D., Crevel, J.W., and Chen, L.F., "Idle Speed Control Design Using an H-Infinity Approach," *Proceedings of 1989 American Control Conference*, Pittsburgh, PA, June 1989, pp. 1950-1956.

# APPLYING QFT TO BENCHMARK PROBLEMS

BAZVINE and R.J.WYNNE

Department of Engineering

University of Manchester

Oxford Road,

Manchester M13 9PL, U.K.

## Abstract :

Many papers have been published on the application of the QFT method to various problems. Although QFT is recognized by a large group in the control community as a robust control system design technique not many true comparisons have been made with other techniques. In order to make comparisons, in our view, it is necessary to find a common environment to implement various techniques, and to find common and reliable examples based on real systems. The aim of this paper is to pave the way for such comparisons by introducing a QFT toolbox which runs in the Matlab environment and using this to provide solutions to two of the IFAC benchmark problems. Since implementations of other robust control system design techniques are also available in Matlab e.g.  $H^\infty$ , the techniques can be compared directly using the same benchmark problems.

In this paper a brief description of the QFT toolbox is given and then the application of the technique to a missile autopilot and a hydraulic positioning system are discussed.

## INTRODUCTION :

Quantitative Feedback Theory has proved to be a valuable tool for robust control system design for systems with structured and unstructured uncertainty. The basic design method is well documented and many publications are available on both the theoretical and practical aspects of the technique (Astrom, 1988), (Horowitz, 1963, 1972, 1973 and 1982), (Sidi, 1976). Some more recent developments are discussed in (Yaniv, 1986) and (Thompson, 1990).

One aspect of the QFT method which has not received much attention in the literature and is addressed by this paper, is the implementation of the technique in a suitable computer environment.

A further aim of this paper is to show, using two benchmark problems, that most of the complexity of the QFT technique, due to the lengthy procedures of calculating various frequency boundaries, can be easily handled by a computer program. This approach enables the designer to focus on the more challenging aspects of the design procedure, namely the compensator design. The design of the compensator, or the loop controller, requires shaping of the loop function. This requires a certain amount of skill and experience. However, it is shown that for a certain class of systems the loop shaping procedure can be

greatly simplified using the computer software developed.

The final aim of this paper is to produce solutions to standard benchmark problems in order to allow comparisons to be made with those obtained using other robust control system design techniques in the future.

The organisation of the paper is as follows :

Section 2 is a description of the structure of the new Matlab toolbox. Section 3 contains the formulation and solution to the benchmark problems, a discussion and conclusions follow. Appendices A and B contain the original benchmark problems as published by IFAC.

## 2 - MATLAB QFT TOOLBOX :

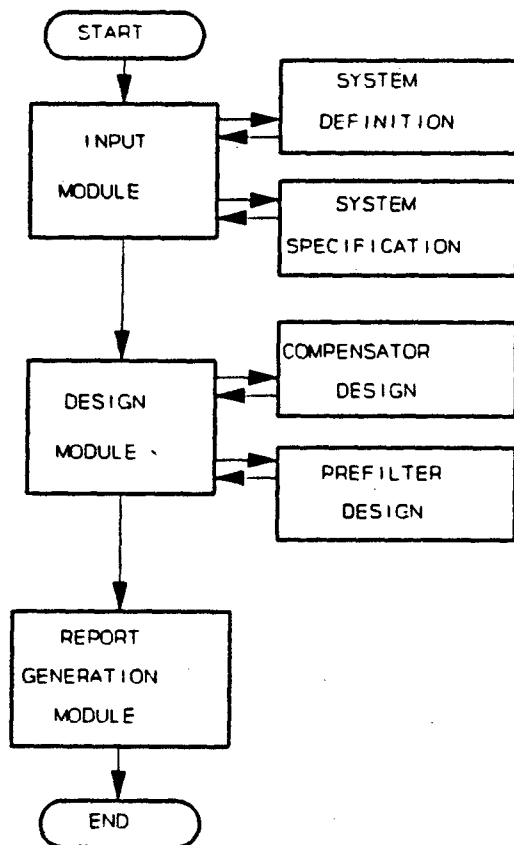


Fig. 1 - Structure of the QFT Toolbox

design procedure described in (Horowitz, 1982). The software is based on three modules; input, design and report generation (see Fig. 1).

### 2.1 - Input/System Definition Module:

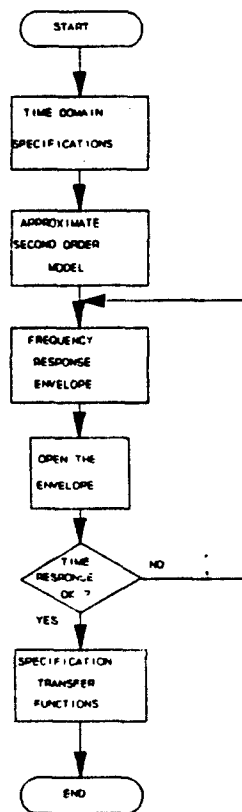
This module deals with the specification part of the design process. These include various transfer functions representing the uncertainty in the plant characteristics also the required rise time, maximum overshoot and settling time of the closed-loop system. The aim at this stage is to define the acceptable

The computer aided design package based on the Quantitative Feedback Theory (QFT), has been designed to provide a tool to deal with the problem of control system design for real systems where performance tolerances are tight and models have significant degrees of uncertainty. MATLAB has been used as the working environment for the QFT package which adds to the extensive collection of compatible programmes and toolboxes already available for other design procedures. The suitability of the modular structure of the QFT approach for computer implementation is shown in Fig. 1.

The Quantitative Feedback design procedure which has been described in the control literature can be implemented by hand calculations and graphical techniques. However, there is a significant amount of cut and try involved and the generation of the frequency boundaries is sufficiently tedious to deter all but the most persistent of designers from exploring the benefits of the technique. Thus a computer aided design package is essential. A package has been previously developed for a VAX (Astrom and co-workers, 1988), but the intention here was to initially investigate a solution within an environment familiar to most control engineers.

The software package to implement the design technique is based on Matlab. This was chosen as the software environment due to its wide acceptance within the control community and the extensive tools already available within Matlab. The structure of the package follows the five step

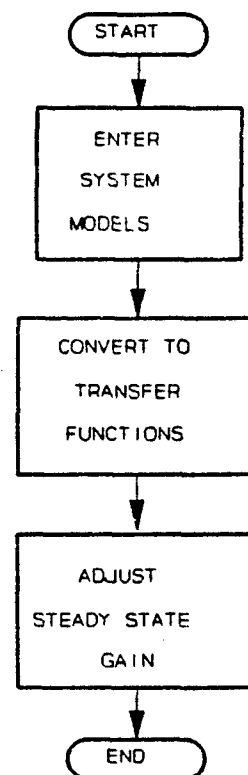
bounds on the performance in the time domain. The next stage is to translate the time domain bounds into the frequency domain. This process takes place inside a loop and is repeated until the time domain specification envelope corresponds as closely as required to the frequency domain specification envelope (see Fig. 3).



**Fig. 3**  
**Specification**

The next stage in the procedure involves the task of determining the trial frequencies and the "high frequency". This is done by plotting the required closed-loop frequency response envelope together with the frequency response of all plant transfer functions. The "high frequency" and the trial frequencies are chosen by the user. Some experience is required to select the most suitable values.

The variation of the frequency envelope defined by the specification at each trial frequency is chosen as the maximum allowable variation of the gain of the closed-loop transfer function at that frequency. The maximum allowable closed-loop gain and the open-loop plant gain variations at infinite frequency are also defined inside the input module. The final stage of the input module involves the generation of the plant templates. These are then passed to the design module.



**Fig. 2**  
**Data Definition**

## 2.2 - Design Module:

The design of the prefilter and the loop compensator is carried out independently within separate procedures which greatly simplifies the software design.

### 2.2.1 - The Compensator Design Module:

This module handles the majority of the stages in the design procedure (see Fig. 4). The first task is a search on the Nichols chart to find the frequency boundaries corresponding to each trial frequency. This is done by a process of moving each template up and down along lines of constant phase to find the point where the template fits inside the M-circles corresponding to the allowable closed-loop variation previously specified. The points are joined for each template to form a frequency boundary. Having found the frequency boundaries at low and medium frequencies, it is then necessary to define the high frequency boundary. This is done by combining the high frequency gain variation and closed-loop resonant peak.

Once all the boundaries have been computed the next stage is the design of the compensator. There are basically two approaches that can be used to design the loop transmission or the loop function, and thus determine a suitable compensator.

There is the general approach which is widely used. This starts from the nominal plant to which lead and lag elements are added sequentially to satisfy the frequency boundaries. If required, complex poles are added at high frequencies to improve the roll-off rate of the loop function. This approach has proved to



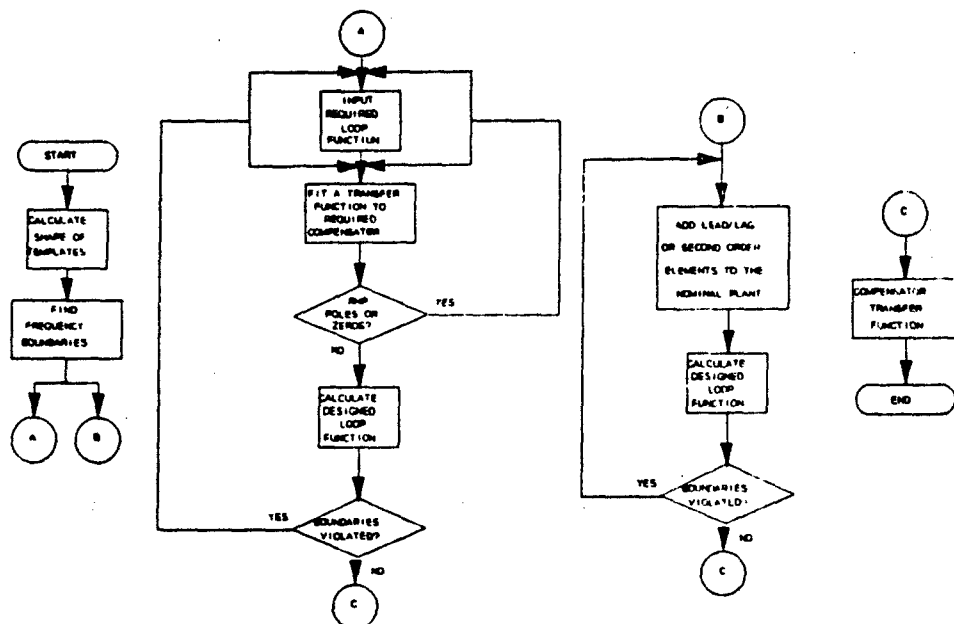


Fig. 4 - The Structure of the Compensator Design Module

work for most classes of systems but is not necessarily the quickest way to arrive at the solution.

A second approach, which is available for loop function design in the QFT toolbox, is one which is particularly suitable for computer implementation but its use is restricted to a certain class of problems. If the loop function of a system has no resonances or anti-resonances, that is to say the loop function is smooth on the Nichols chart then to arrive at a Quantitative design of a stable minimum phase rational compensator two conditions must be satisfied ;

- the loop function must satisfy all the frequency boundaries,
- the loop function must satisfy Bode's gain-phase relationship.

If these criteria are satisfied the QFT toolbox allows the user to select points on or above each frequency boundary at the trial frequencies. These points are checked using Bode's gain-phase relationship. A valid solution is one which passes through all the points without violating the boundaries.

To design the compensator, the frequency characteristics of the nominal plant are subtracted from the frequency characteristics of the defined loop function. Reshaping of the loop function may be necessary at this point. The reshaping is carried out inside a loop and continues until the gain and phase of the compensator are compatible according to Bode's gain-phase relationship. The structure of the compensator is then determined using a least squares transfer function fit to the data (Levy,1959;Sanathanan and Koerner,1963). This procedure is repeated until a solution is found which satisfies the stability, sensitivity and disturbance rejection requirements. Such a solution is returned to the design module to be used in the prefilter design.

### 2.2.2 - The Prefilter Design Module:

The gain plots of the compensated system define an envelope which must now be manipulated to fit

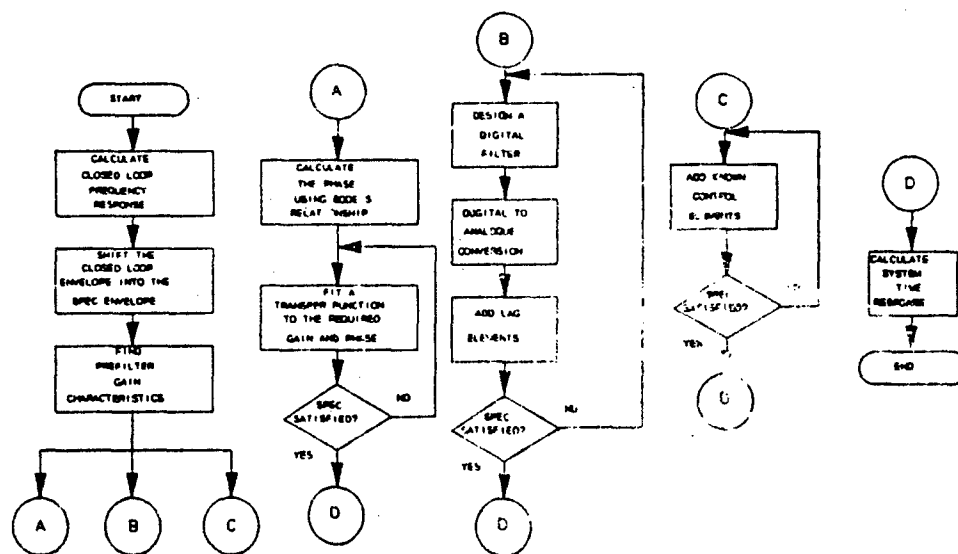


Fig. 5 - The Structure of the Prefilter Design Module

inside the specified design envelope. This is achieved by means of the prefilter. The task of prefilter design is therefore equivalent to finding a filter with some pre-specified gain characteristics.

The gain characteristics of the prefilter are found by translating the midpoint of the closed-loop envelope onto the midpoint of the specification envelope, the amount of translation being the required characteristics. The phase characteristics are not known, but can be obtained from the gain information since for any real filter there is a unique relationship between the gain and phase.

An alternative approach, also used here, is to design a digital filter to fit the required gain characteristics. This can then be transformed to an equivalent analogue transfer function. The required prefilter gain characteristics are displayed and the user is prompted for the order of the numerator and denominator of the digital filter to be found. A conversion is then carried out and the frequency response of the resulting analogue filter is compared to the required gain characteristics of the prefilter. The user is then given the choice to accept the design, to redesign, or to reshape the existing design by adding lag elements at chosen frequencies. The last option is included because during the digital to analogue conversion stage accuracy is lost at frequencies close to the sampling frequency. This problem can usually be solved by adding a lag element at a frequency between quarter to half the sampling frequency. The design procedure is completed by displaying the actual and the required prefilter frequency characteristics. The results are then returned to the main program.

### 2.3 - Report Generation Module:

This module produces graphical representations of the various stages of the design procedure. Several plots are generated and saved for later processing. The plots which can be generated are;

- The Nichols chart, with the frequency boundaries and the selected loop transmission and the nominal frequency response superimposed.
- The magnitude plot of the specification envelope and the designed system envelope for all plant conditions.
- The step response of all plant transfer functions.

- The controller output for a step change at the plant input.
- The step response of the discretized system for selected sampling intervals.
- The controller output of the discretized system for a step change at the input with various sampling times.

### 3 - APPLICATION TO THE BENCHMARK PROBLEMS :

In this section the application of the QFT to two benchmark problems published by the International Federation of Automatic Control is discussed. Both problems were solved using the Matlab QFT toolbox. Both problems are based on SISO systems and have a degree of uncertainty associated with them. The problems are published in a report entitled 'Benchmark problems for control system design' prepared by the IFAC Theory Committee in May 1990. The intention of this report is to provide problems which can be solved various techniques. Thus the relative merits of each technique can be compared.

#### 3.1 - Missile Control System :

The original problem specification can be found in the IFAC report (section 3). The formulation of the problem and the specification are in a form suitable for quantitative design. A minimum amount of work is required to find transfer functions from the state space formulation and to obtain a suitable step response envelope from the specifications.

There are eight flight conditions which produce eight transfer functions as follows ;

$$P_1(s) = \frac{17277 s^2 + 22655 s + 7.283e+06}{s^3 + 191.3 s^2 + 316.4 s + 12211}$$

$$P_2(s) = \frac{14261 s^2 + 19713 s + 1.148e+07}{s^3 + 191 s^2 + 325.2 s + 24650}$$

$$P_3(s) = \frac{53854 s^2 + 2.806e+05 s + 1.019e+08}{s^3 + 193 s^2 + 1183 s + 1.179e+05}$$

$$P_4(s) = \frac{47595 s^2 + 1.825e+05 s + 1.358e+08}{s^3 + 193.5 s^2 + 1316 s + 1.241e+05}$$

$$P_5(s) = \frac{76562 s^2 + 3.888e+05 s + 4.494e+08}{s^3 + 194.3 s^2 + 1882 s + 2.036e+05}$$

$$P_6(s) = \frac{14522 s^2 + 57621 s + 5.788e+06}{s^3 + 196 s^2 + 1248 s + 18849}$$

$$P_7(s) = \frac{12116 s^2 + 9260 s + 9.195e+06}{s^3 + 191 s^2 + 353.3 s + 31058}$$

$$P_0(s) = \frac{22306 s^2 + 16439 s + 2.132e+07}{s^3 + 191 s^2 + 414.3 s + 42608}$$

As it can be seen from Fig. 6 the model has very high gain and relatively high bandwidth. However the main difficulty of the design process is to deal with resonance in the presence of model uncertainty as the resonant frequency changes for every flight condition. It is not possible to reduce the gain in the presence of the resonances as this would violate the universal high frequency boundary, also known as the U-contour.

Simple attenuation of the resonance peak does not work either since an additional 90 degrees of phase lag is introduced for every 20 dB per decade attenuation which shifts the loop function further into the U-contour.

A possible design for the loop function is shown in Fig. 7. This was achieved by initially selecting suitable control elements to reduce the effect of the resonances and then using the direct design procedure to place the loop function on the frequency boundaries. All the frequency boundaries are satisfied and hence this is one possible solution. The roll-off rate of the loop function can further be improved by adding a simple lag element at roughly the break frequency of the open loop system, which results in the loop function shown in Fig. 8. The loop compensator required to produce such a loop function has the frequency characteristic shown in Fig. 9. The transfer functions of the loop compensator for each design is given below ;

$$G_1(s) = \frac{0.0002 s^4 + 0.05431 s^3 + 1.424 s^2 + 9.918 s + 25.48}{0.000456 s^4 + 0.1912 s^3 + 24.56 s^2 + 1000 s}$$

$$G_2(s) = \frac{0.0002 s^4 + 0.05431 s^3 + 1.424 s^2 + 9.918 s + 25.48}{4e-9 s^5 + 0.0004 s^4 + 0.1914 s^3 + 24.57 s^2 + 1000 s}$$

The loop compensator reduces the uncertainty of the closed loop system sufficiently so that the closed-loop frequency response fits inside the specification bounds as shown in Fig. 10. A simple prefilter then shifts the closed-loop frequency response into the specification envelope as shown in Fig. 11. The required prefilter has the following transfer function ;

$$F(s) = \frac{1}{0.00025 s^3 + 0.0125 s^2 + 0.2 s + 1}$$

In this design the specification bounds have been selected to be very relaxed at frequencies above 100 rad/s (Fig. 11). This was done to reduce the open-loop bandwidth and hence reduce the cost of feedback. Note that the compensator reduces the high bandwidth of the system.

The step responses of the system transfer functions at the eight flight conditions are shown in Fig. 12. A settling time of about 1 second was chosen to be adequate. The control effort required for such a response is shown in Fig. 13. Note that the controller output is multiplied by  $10^{-3}$  and hence it is very small in magnitude.

### 3.2 - Hydraulic Positioning System :

The original problem is given in The IFAC report (section 3). This is different from the missile

problem in two aspects. Firstly a parameter range is specified for the state space formulation of the problem. The parameters can have any value within their range independently of each other. Secondly the system is non-minimum phase. The first problem was to find the extreme values of the parameters that specify a maximum and minimum bound for the size of the transfer functions. The second problem was found not to limit the performance as much as expected since the right half plane zeros were far from the origin of the complex plane. Six transfer function were obtained as follows with frequency characteristics shown in Fig. 14;

$$\begin{aligned}
 P_1(s) &= \frac{9.37e-14 s^2 + 5.821e-11 s + 8650}{s^3 + 1.045 s^2 + 90824 s} \\
 P_2(s) &= \frac{-1.705e-13 s^2 - 5.821e-11 s + 6712}{s^3 + 297.2 s^2 + 80018 s} \\
 P_3(s) &= \frac{-4.547e-13 s^2 - 1.746e-10 s + 2709}{s^3 + 1116 s^2 + 48518 s} \\
 P_4(s) &= \frac{-4.263e-14 s^2 + 2.183e-11 s + 5352}{s^3 + 16.77 s^2 + 57552 s} \\
 P_5(s) &= \frac{-2 e-13 s^2 + 16256}{s^3 + 1200 s^2 + 2.917e+05 s} \\
 P_6(s) &= \frac{1 e-15 s^2 - 1 e-11 s + 1442}{s^3 + 0.2121 s^2 + 15137 s}
 \end{aligned}$$

Fig. 14. shows that the system becomes highly underdamped for certain values in the parameter range. The main difficulty with this problem was that the gain of the plant was too small to achieve a fast response. However the gain could not be increased because of the existence of the resonance peak. The other interesting point about the plant was that the plant templates grew in width as the frequency increased up to the resonant frequency indicating large variation of phase around the resonance region as shown in Fig. 15.

A possible design for the loop function is shown in Fig. 16. All the boundaries are satisfied and the loop function has a good roll-off rate at high frequency. Fig. 17 shows the same design at higher frequencies indicating clearly the existence of the resonance in the nominal plant and the loop function.

The compensator characteristics for this design are shown in Fig. 18. The compensator has the following transfer function ;

$$G(s) = \frac{1.057 s^2 + 52.74 s + 47.2}{2.06 e-05 s^4 + 0.00198 s^3 + 0.07285 s^2 + 1.08 s + 1}$$

The amplitude characteristics of the closed-loop system are shown in Fig. 19. It can be seen that the resonance peak of some plant transfer functions violate the specification bounds. The addition of a

simple prefilter attenuates the resonance peaks. Since all the frequency boundaries are satisfied it is possible to fit the closed-loop frequency response entirely inside the specification bounds. However, this will result in a more complicated structure for the prefilter and was found to have little effect on the step response of the system due to the low gain in the resonance region. Fig. 20 shows the system response and the specification bound for the final design. The prefilter is required to provide limited high frequency attenuation and the following transfer function is adequate;

$$F(s) = \frac{1}{0.02s + 1}$$

Fig. 21, 22 and 23 show the step response, controller output and the response to a step disturbance at the output of the system transfer functions respectively.

#### 4 - DISCUSSION AND CONCLUSIONS :

The QFT toolbox has been implemented on a PC-AT, PC-486 and IIP Workstation. The open architecture of Matlab makes the transition between the different platforms and versions of Matlab very easy. The controller designs for this paper were implemented on a PC-486 running Matlab-386.

There are some problems with numerical errors when dealing with high order plants and controllers, however when such problems occur external, numerically more robust routines can be called from within Matlab and the results imported into Matlab for analysis and graphical representation. Such problems were not encountered in this paper.

Both of the benchmark problems described in this paper precluded the use of the direct design of the compensator alone, the resonances and also the non-minimum phase characteristics of the hydraulic system required a combination of the general sequential procedure and the direct loop shaping approach. However, this is very easily implemented within the toolbox and the designer can readily see the implications of the selected elements on the loop function in relation to the frequency boundaries. The design discussed in a previous paper (Azvine and Wynne, 1991) was concerned with a controller for an aero engine for a commercial aircraft. This yielded a loop function which satisfies the two criteria established earlier and hence the compensator could be determined by fitting an appropriate transfer function in this case. The order of the transfer function and hence the controller could be determined by the designer, provided the resulting loop function satisfies the frequency boundaries. Thus a direct design of the compensator was possible in that case.

The two controllers which result from the design procedure applied to the benchmark problems, are both of relatively high order in relation to the plant dynamics. However, to meet the design specifications, given the relative complexity of the system dynamics it was necessary to implement such high order controllers. In the case of the missile system the additional high frequency lag element was introduced to reduce the control effort. The effect of this was easily assessed using the toolbox and is one of the most useful features of the QFT method; the designer is 'in control' of the design at each stage. The trade-offs between control effort, the cost of feedback and the achievable level of output are transparent throughout the design. Thus it also allows the designer to make value judgements about increasing the complexity of the controller to improve the performance of the closed-loop system.

In both of the designs implemented here the specifications are slightly violated Fig 12 and 21. However, in both cases it was decided that the increased complexity of the controller together with the added control effort was not justified for such marginal improvements in performance. This approach to design is familiar to most engineers who are used to finding a solution which meets the specification whilst operating within financial (cost) constraints.

The evidence in the UK is that industry is still predominantly concerned with SISO systems. The H<sup>∞</sup>

approach is being demonstrated to industrialists as a SISO design tool. However, the benchmark problems used here provide a mechanism for evaluating the design procedures and together with the new Matlab toolbox enable the evaluation of QFT in relation to other methods to be made within a common environment.

## 5 - REFERENCES :

- Astrom, K.J., P.O.Gutman, I.Horowitz, L.Neuman and O.Yaniv (1988). Robust feedback control design : the Horowitz method. Lecture notes presented at workshop prior to the 27th IEEE Conference on Decision and Control, Dec. 6, Austin, Texas.
- Azvine, B. and Wynne, R.J. 1991. Implementing the QFT method in the MATLAB environment. 5th IFAC/MACS symposium on CAD in control systems, 15-17 July, Swansea, U.K.
- Horowitz, I. 1982. Quantitative Feedback theory. IEE Proc., Vol. 129, Part D, No. 6, November.
- Horowitz, I.M. (1963). Synthesis of feedback systems. Academic Press. Chap. 6, pp. 267-295.
- Horowitz, I. and M.Sidi (1972). Synthesis of feedback systems with large plant ignorance for prescribed time domain tolerances. International Journal of Control. vol. 16, no. 2, pp. 287-309.
- Horowitz, I. (1973). Optimum loop transfer function in single-loop minimum-phase feedback systems. Int. J. Control 18, pp. 97-113.
- Horowitz, I. and M.Sidi (1973). Synthesis of cascaded multi-loop feedback systems with large plant parameter ignorance. Automatica, vol. 9, pp. 589-596.
- Levy, E.C. (1959). "Complex curve fitting", IRE Trans. , AC4, pp. 37-43.
- Sanathanan, C. and J.Koerner (1963). Transfer function synthesis as a ratio of two polynomials. IEE Trans. Autom. Control, AC-8, pp. 56-58.
- Sidi, M. (1976). Feedback synthesis with plant ignorance, non-minimum phase, and time domain tolerances. Automatica, vol. 12, pp. 265-271.
- Thompson, D.F. and O.D.I.Nwokah (1990). Frequency response specifications and sensitivity functions in quantitative feedback theory. Proceedings of The American Control Conference, pp. 599-604
- Yaniv, O. and I.Horowitz (1986). A Quantitative design method for mimo linear feedback systems having uncertain plants. Int. J. Control, Vol. 43, No. 2, pp. 401-421.

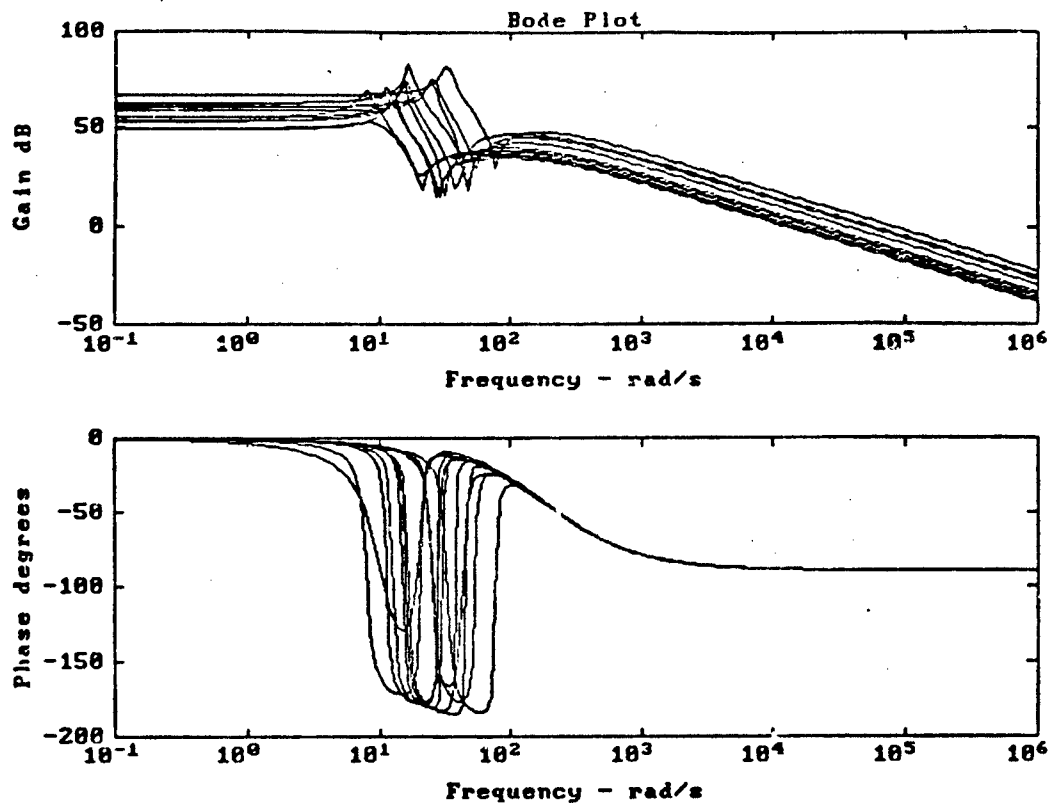


Fig. 6 - Open-loop Frequency Response of the Missile

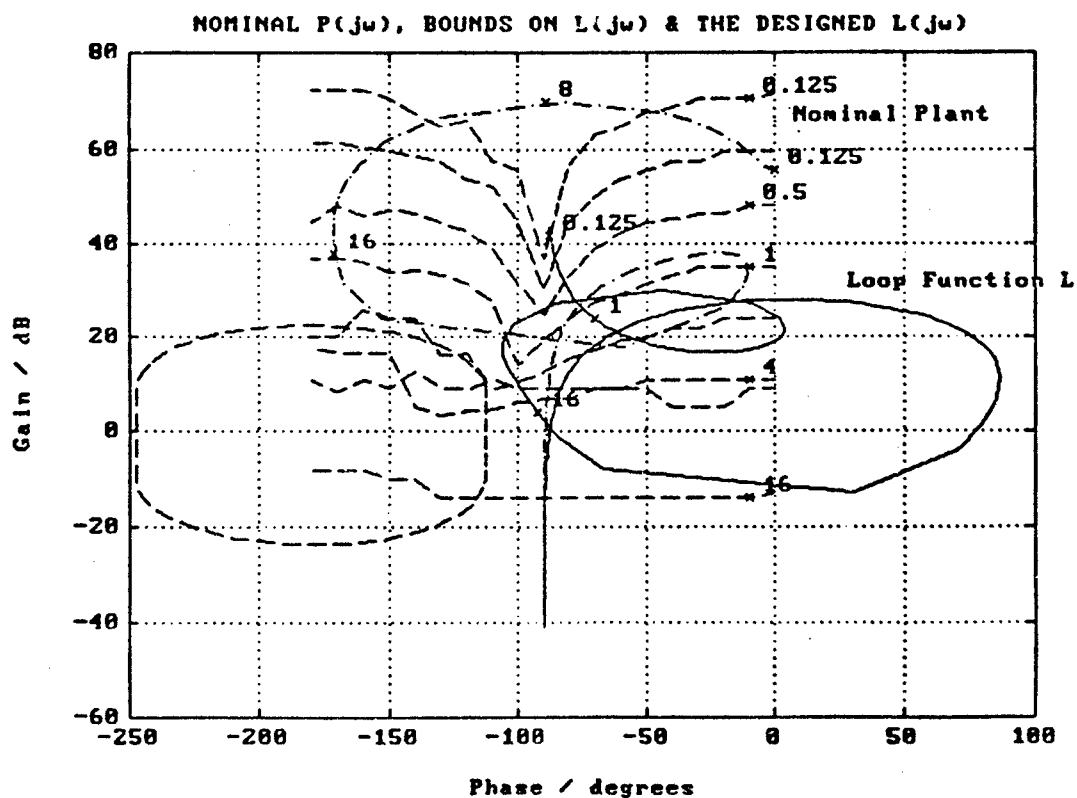


Fig. 7 - Loop Function on the Nichols Chart



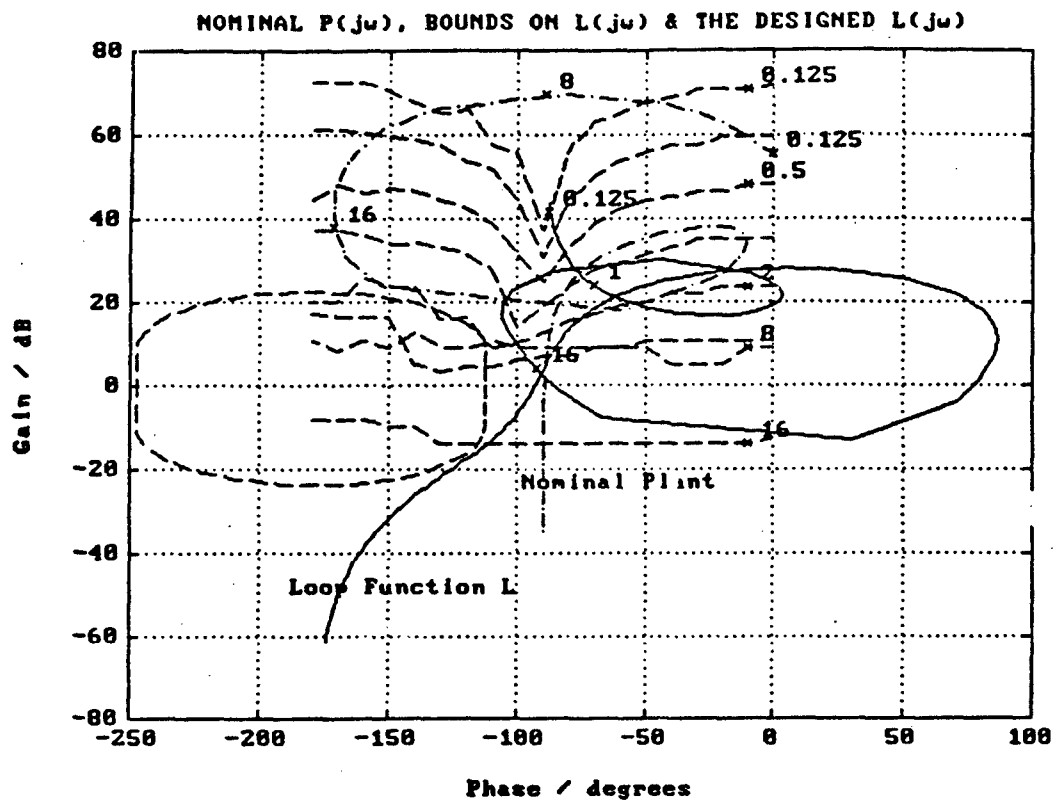


Fig. 8 - Improved Loop Function for the Missile Auto Pilot

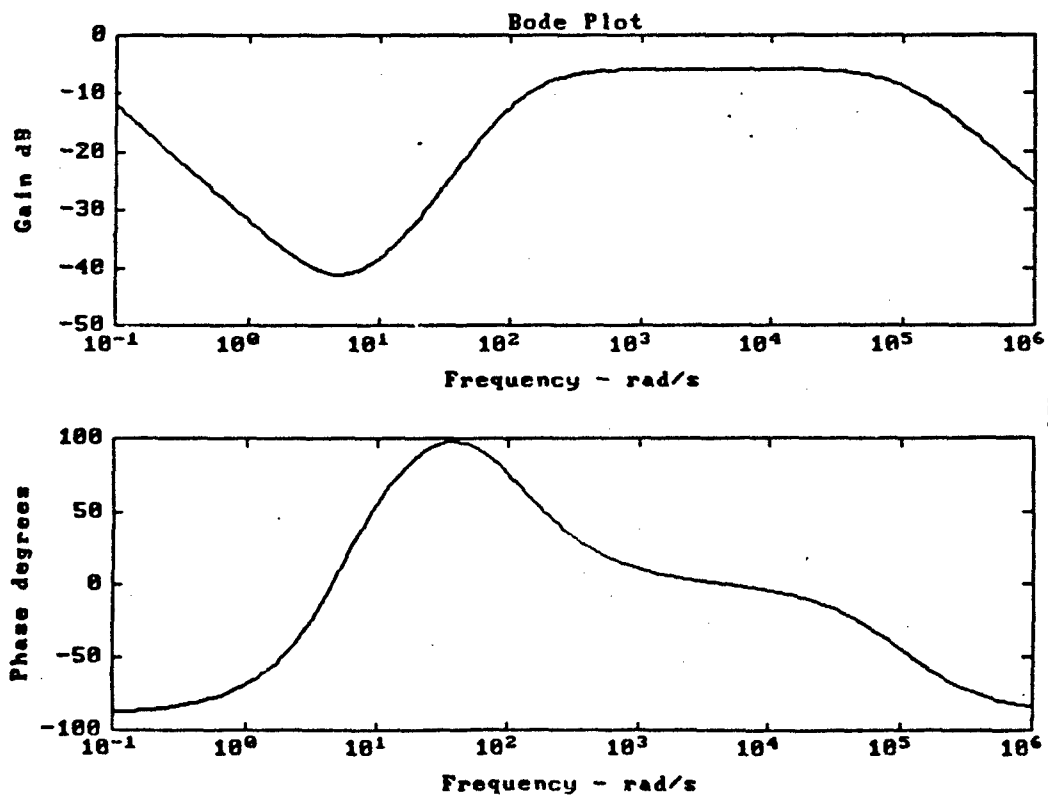


Fig. 9 - The Frequency Characteristics of the Compensator

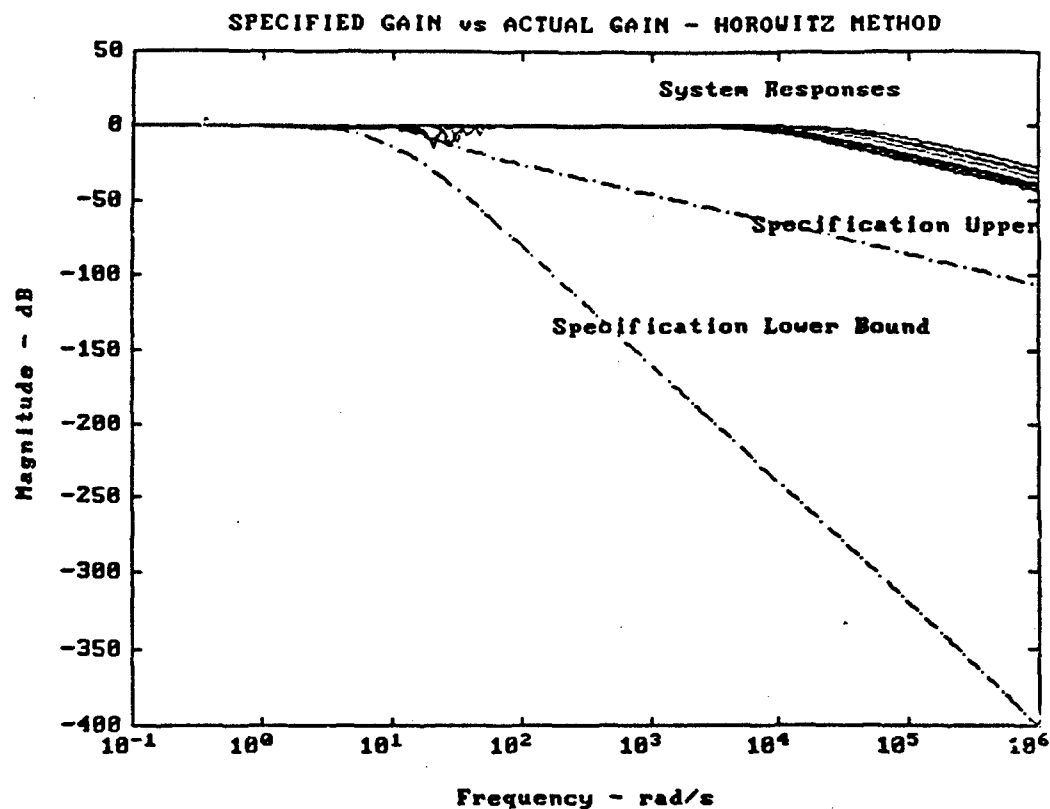


Fig. 10 - Closed-loop System Amplitude without the Prefilter

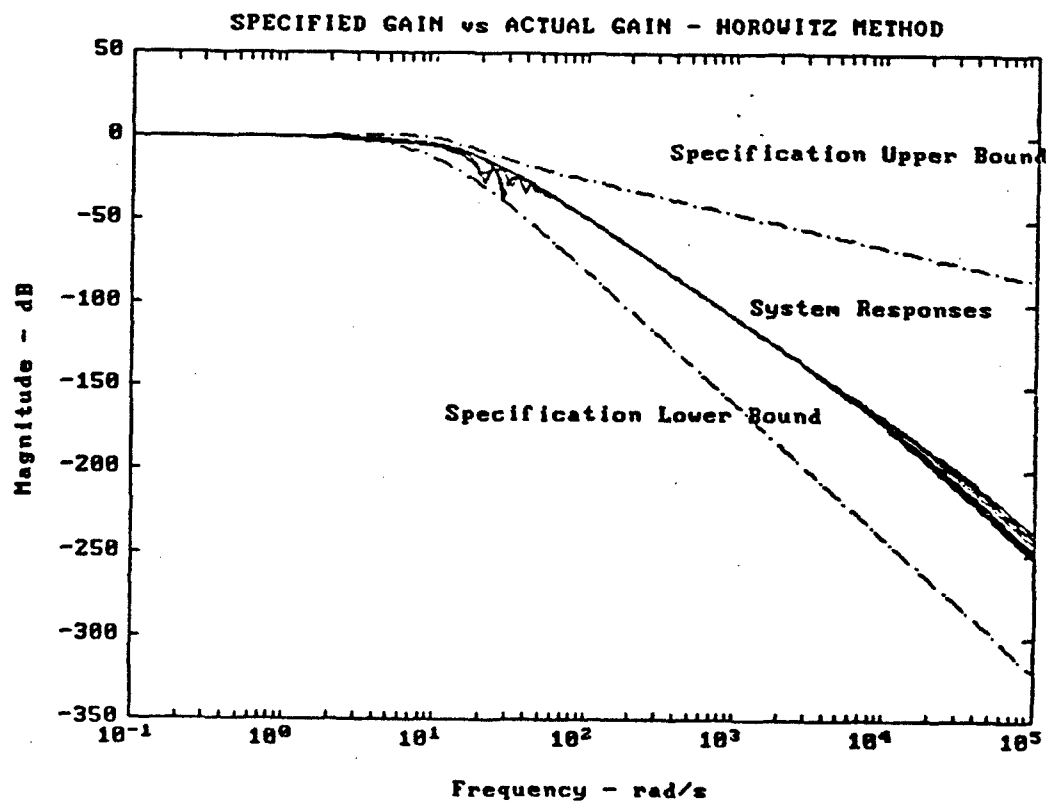


Fig. 11 - System Responses and the Specification Lines

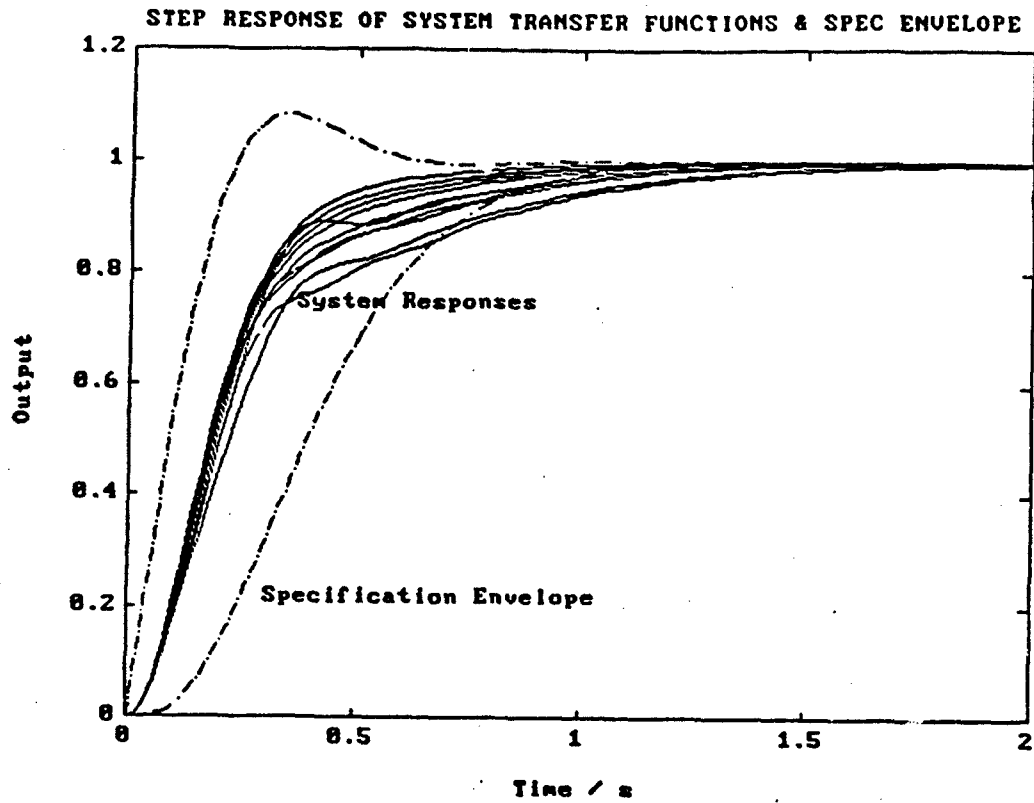


Fig. 12 - Step Response of the Closed-loop System

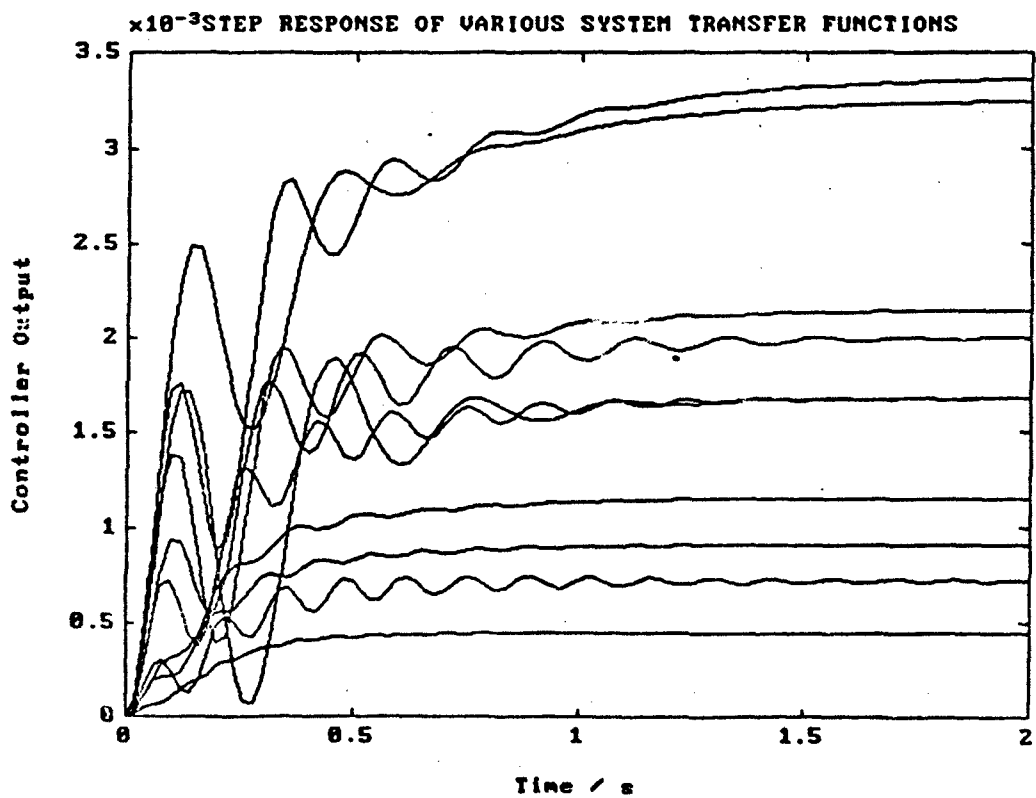


Fig. 13 - Controller Output for an Input Step Change

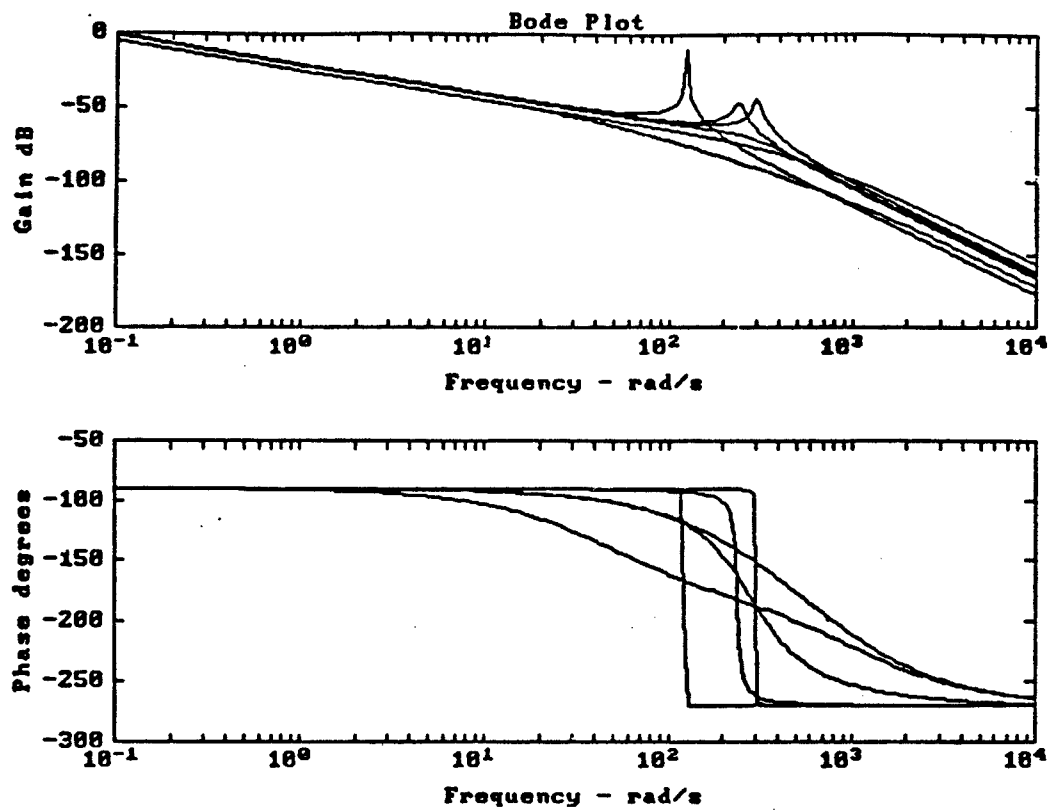


Fig. 14 - Bode Plot of the Hydraulic System

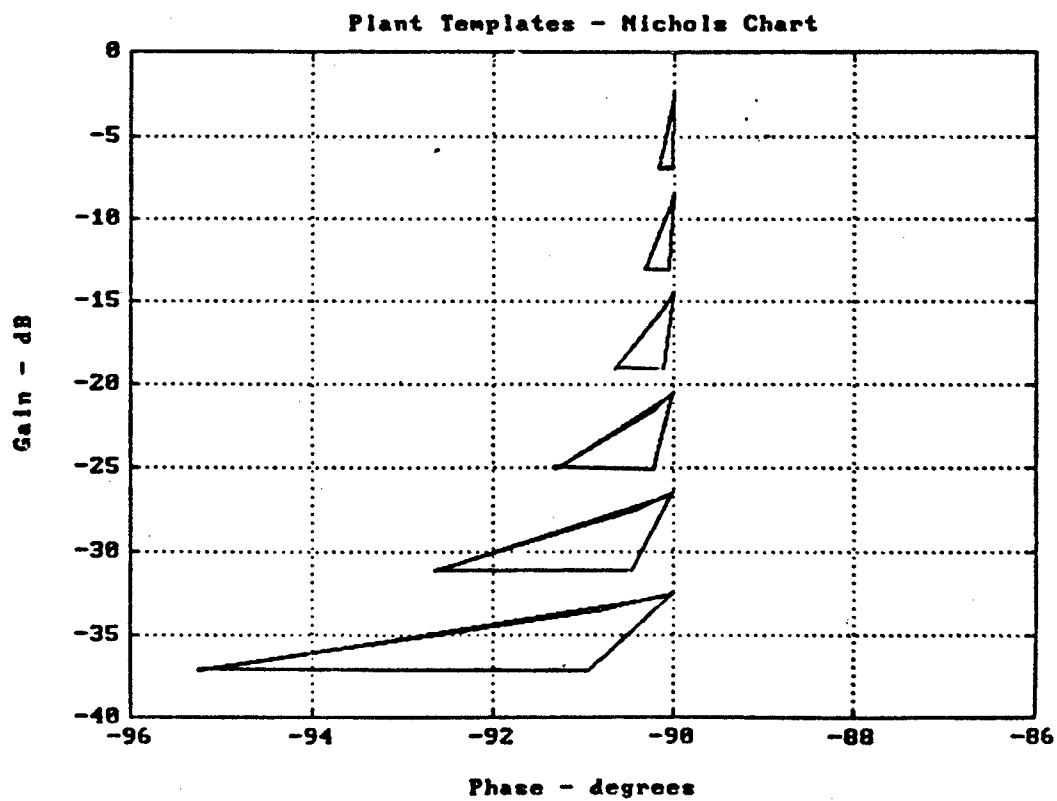


Fig. 15 - Plant Templates at the Trial Frequencies

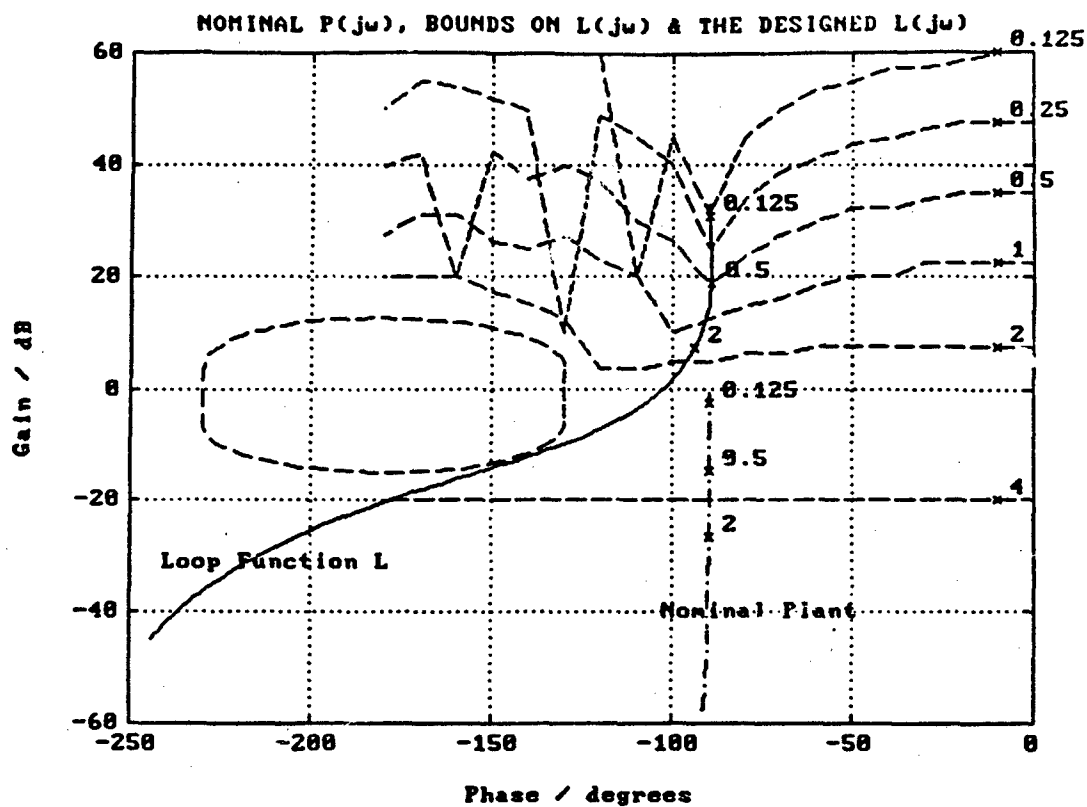


Fig. 16 - Loop Function on the Nichols Chart

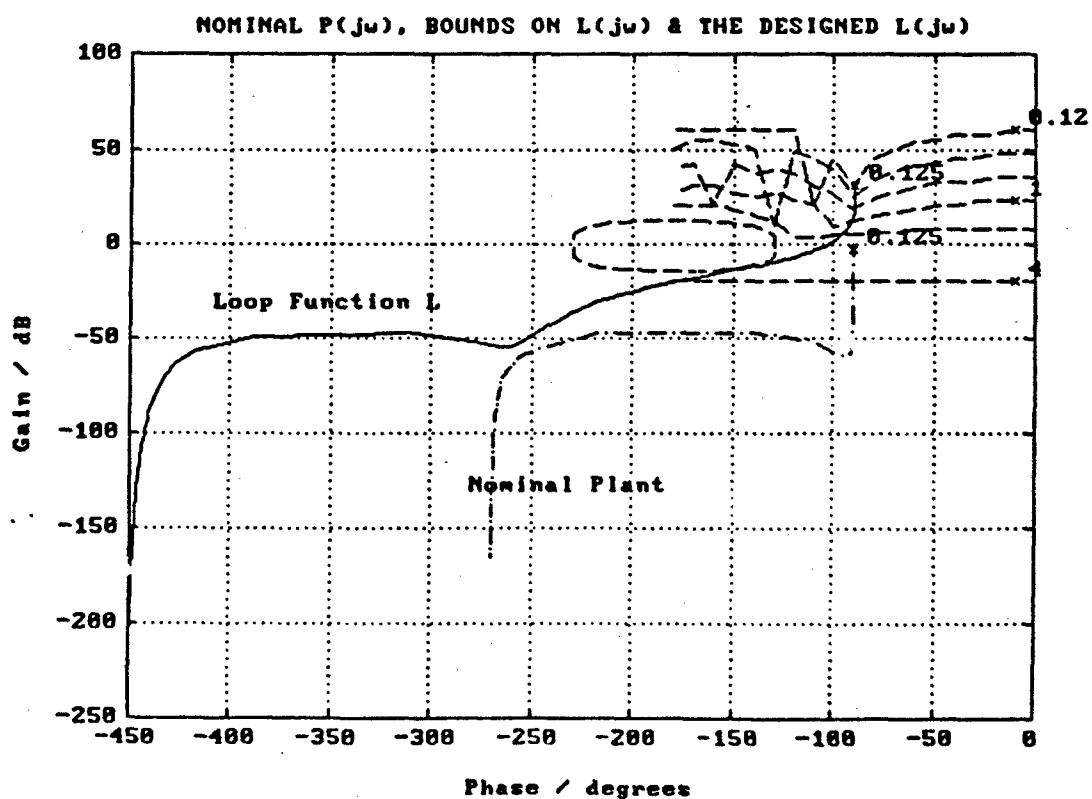


Fig. 17 - Loop Function at High Frequencies

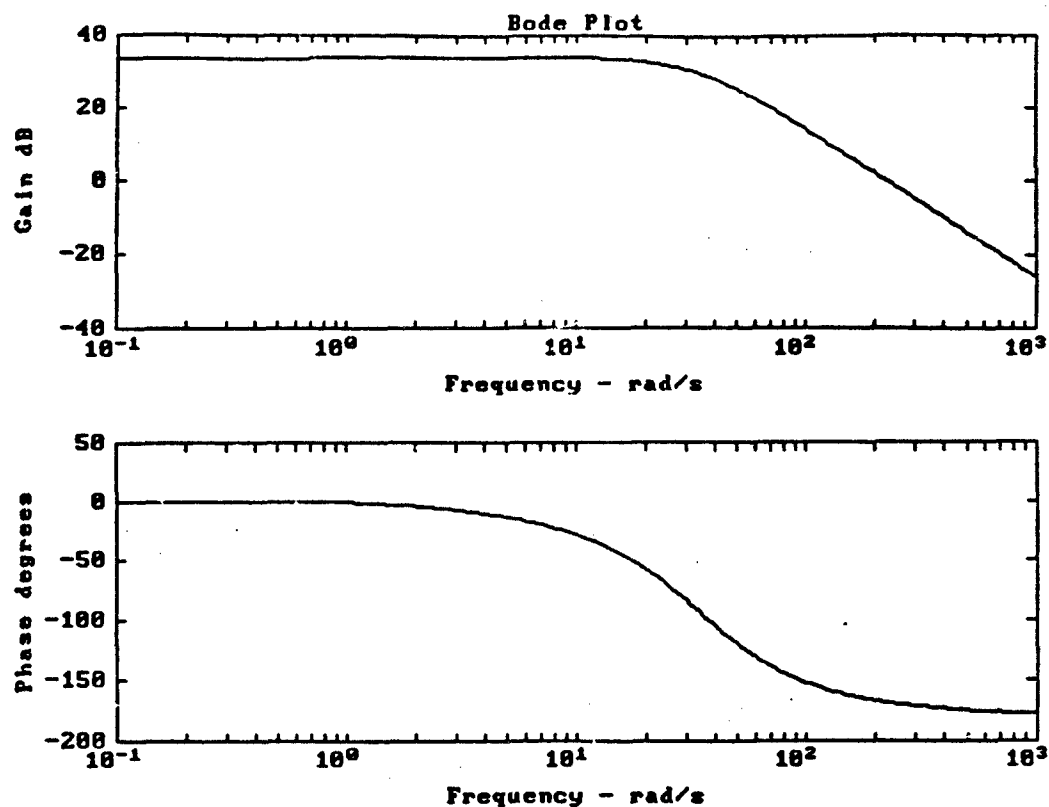


Fig. 18 - Frequency Characteristics of the Compensator

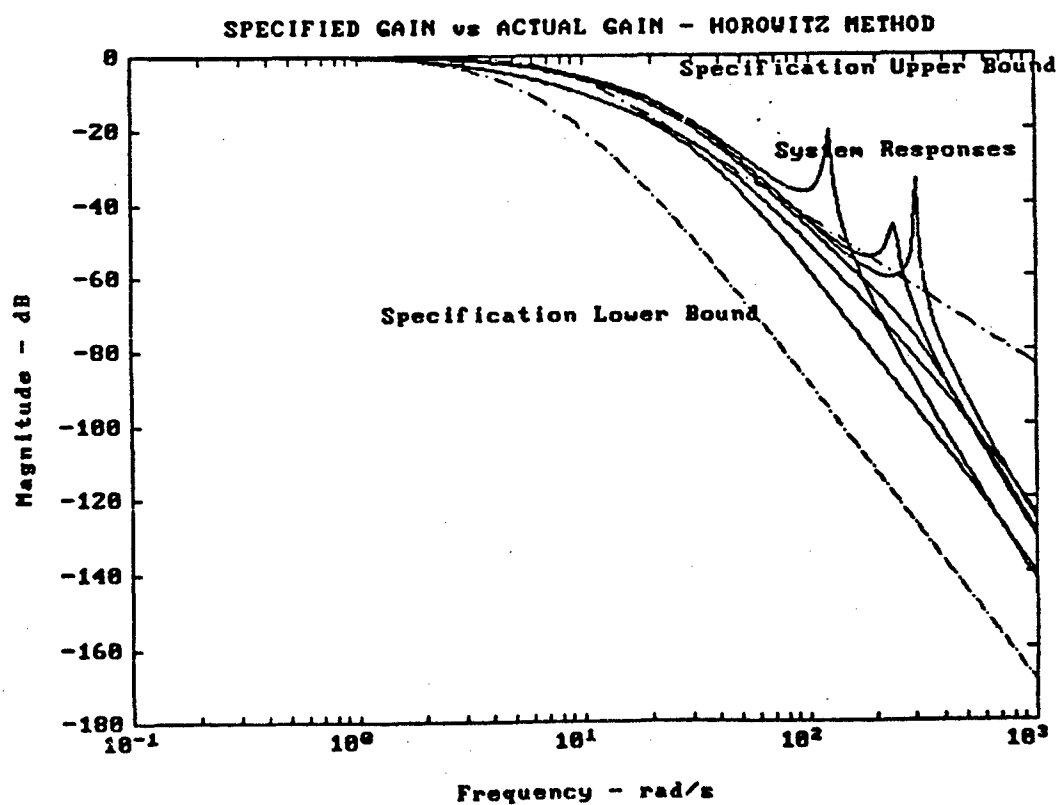


Fig. 19 - Closed-loop System Gain without the Prefilter

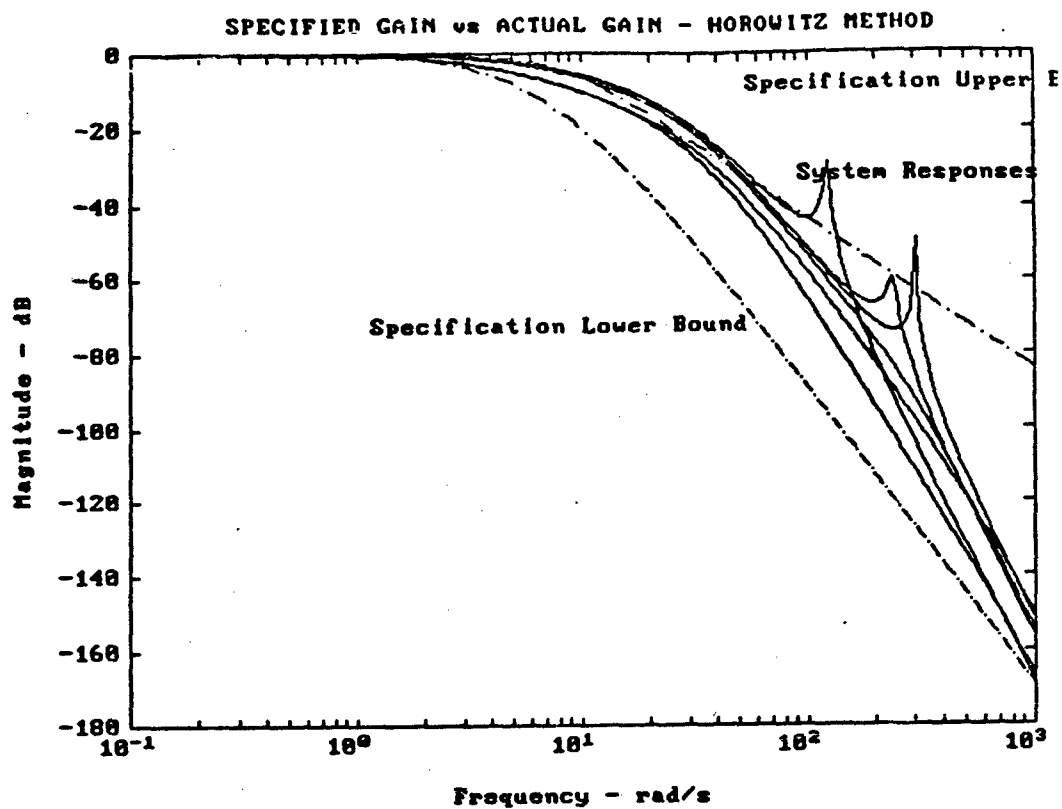


Fig. 20 - Closed-loop System Gain with the Prefilter

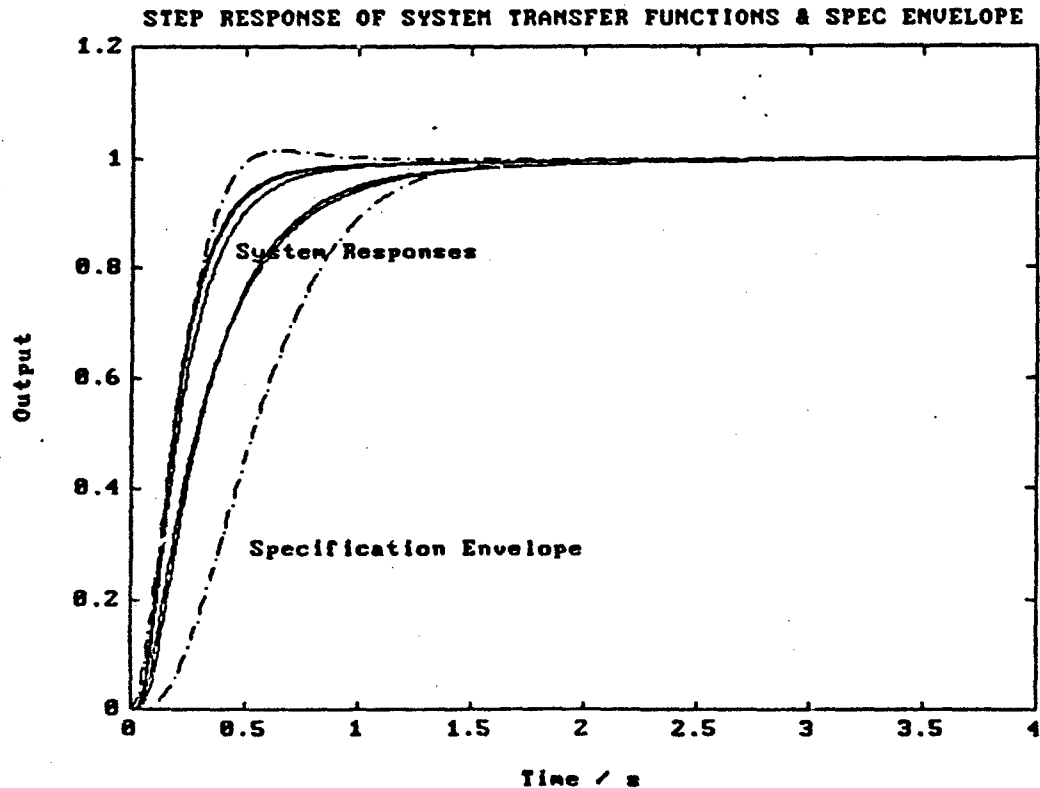


Fig. 21 - Output Response for a Step Change at the Input

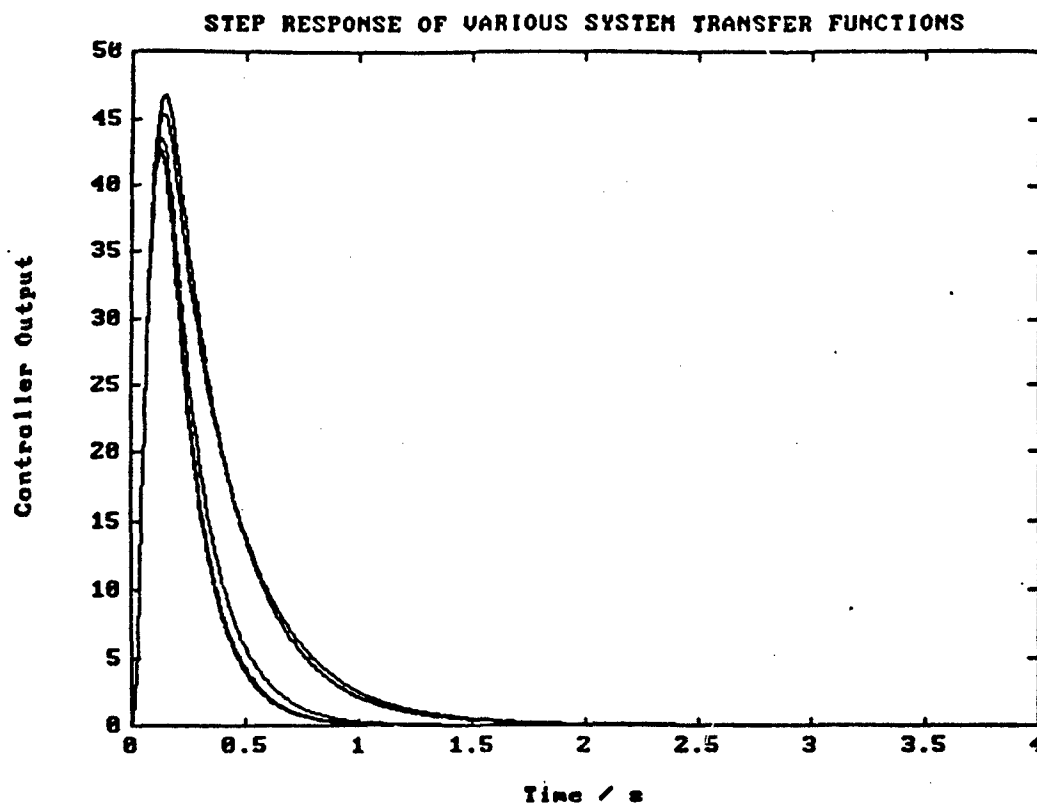


Fig. 22 - Controller Output for a Step Change at the Input

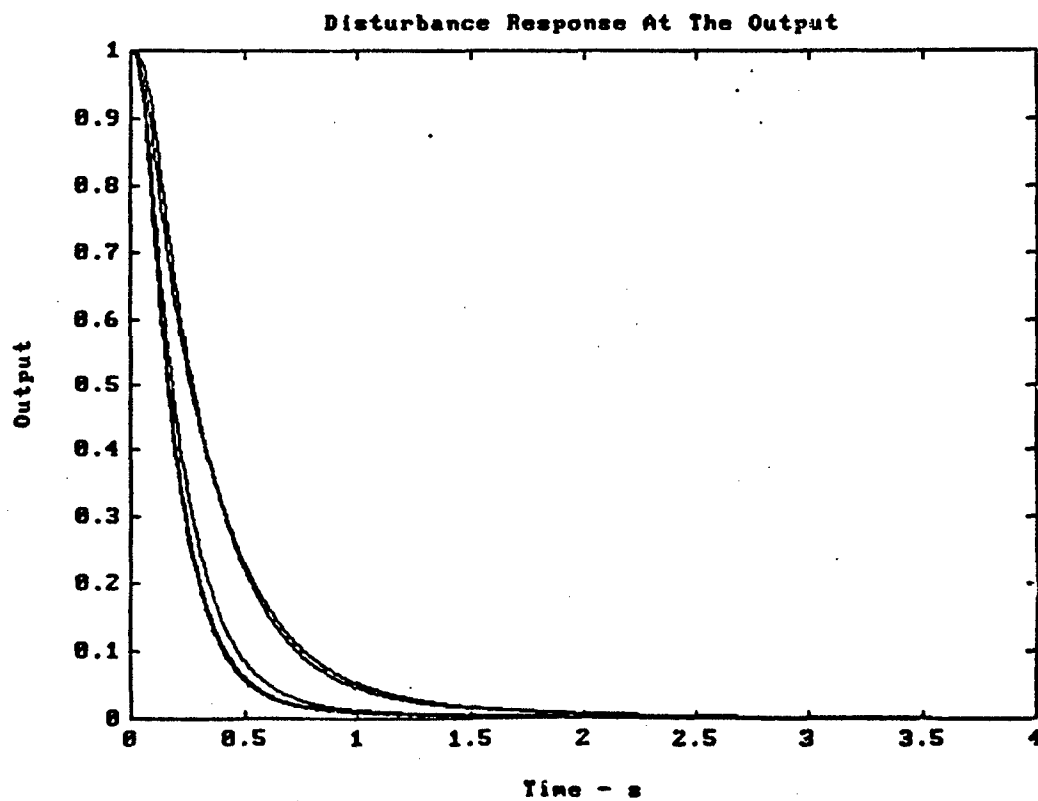


Fig. 23 - Output Response to a Step Disturbance



## GENERAL SENSITIVITY EXPRESSIONS FOR MIMO SYSTEMS.

C. Verde

Instituto de Ingenieria-UNAM

PB 70-472, COYOACAN 04510 D, F MEXICO

FAX: (525)-5483044

Email: VERDE@UNAMVM1.BITNET

**Abstract:** This paper presents a synthesis technique for time invariant, linear multi-input multi-output feedback control in the frequency domain. The technique handles stability, performance and robustness aspects of the design in the framework of the Quantitative Feedback Theory, QFT. In particular, it is suggested to transform the  $n$  square MIMO systems to  $n$  SISO systems, and to use the standard QFT procedure for SISO system with additional constraints which depends on the cross-coupling effects of the multiple loops. To illustrate the basis of the procedure one detailed example is given.

### I. INTRODUCTION

The most common systematic way to examine the frequency response of MIMO systems for the feedback scheme shown in Fig. 1 is today the singular values decomposition (Doyle and Stein, 1981), although they can not be used to obtain systems phase information and it is impossible to analyze the individual responses associated with particular pairs of reference  $r_i$  and output  $y_j$ . Moreover, assuming a  $n \times n$  MIMO system it is not easy to include direct bandwidth specifications and sensitivity constraints for each channel of the system.

On the other hand, in pioneering work by Rosenbrock (1969), the frequency response analysis and design for MIMO systems are done with the aid of the diagonal dominance concept, but in some process control as in the flight control problem this idea can not be easily used because of the strong interaction between loops.

Other alternative which was reported for the case of 2-input, 2-output systems by Sponer (1966) in the Germany literature is to seek a equivalence between the MIMO feedback system and single loops or channels in such way that the cross-coupling effects appear in the transfer function of the single loop and the rest of the inputs effect is considered as disturbance in the equivalent SISO feedback scheme. The main obstacles for analysis and design with this simple idea and with the Rosenbrock's approach, in the sixties, were the drawn package facilities and computation requirements; however these problems have today disappeared. This fact from engineer point of view has revitalized the classic frequency response approaches for MIMO systems. Therefore a

considerable effort is expended in developing feedback control system design approaches for MIMO systems which are generalizations of classical frequency response approach.

However most of the above mentioned ideas for MIMO systems problems assumed well known plants and deals with the design of feedback schemes for a nominal model which gives the desired system response. A serious disadvantages of this philosophy is the ignoring of the most important reason for the use of feedback, namely the reduction of sensitivity to parameter variations. As Horowitz (1991) remarks in the absence of this factor and of disturbances, there is hardly a justification for the use of a feedback structure. Moreover in the MIMO case, the return difference matrix of the feedback loop it is not unique because it is dependent on the break point of the loop and therefore, the demonstrated analogy between the sensitivity functions to disturbance and to plant parameter variations for SISO system (see Frank 1978) is not validated.

On the other hand the Quantitative Feedback Theory (QFT) proposed by Horowitz (1963) for SISO has been recognized to be an effective design approach for dealing with significant parametric uncertainties in the SISO case. However in the particular case of MIMO systems with strong cross-coupling effects between loops, it is not clear how to tackle, at the same time, the interaction and uncertainty problems in a systematic handy manner. The  $n^2$  scalar loop transmissions for a  $n \times n$  system together with the  $n^2$  scalar uncertain plant transfer functions complicate the analysis and design because there exists  $n^4$  scalar expressions for the sensitivity functions, which are extremely intermixed and which has to be analyzed to study the general sensitivity behavior of the MIMO system. Horowitz et al (1976 and 1979) published various approaches trying to reduce the MIMO uncertainty problem to equivalence SISO uncertainty problems. However a dominant design approach by QFT for MIMO system is not now recognized. In particular I. Horowitz (1991) has made some important remarks in his recently survey of QFT about constraints and problems in the MIMO case.

On the other hand recently O'Reilly et al (1991) has proposed a new framework called Individual Channel Design (ICD) to analyze and design MIMO systems with 2-inputs and 2-outputs taking into account the interaction effects between loops, and using simple classical tools for SISO systems, like Nyquist and Bode plots. The main contribution of the work of O'Reilly et al (1991) is the characterization of the cross-coupled effect of the MIMO system by a complex function called Multivariable Structure Function which allows us to write the transmission of each channel for the MIMO system in a very general compact form.

These two ideas have motivated this paper wherein the generic patterns for the  $n^2$  SISO systems which are equivalent to the two degree of freedom feedback MIMO system of Fig. 1 are presented. In particular it is shown by these equivalent relations that a generic pattern of the Horowitz's sensitivity,

$$H_{p_{ij}}^{k1} := \frac{\Delta t_{k1}/t_{k1}}{\Delta p_{ij}/p_{ij}}, \text{ exists for each element } t_{k1} \text{ of the closed loop transfer}$$

matrix with respect to the plant elements  $p_{ij}$  for  $i=1, \dots, n$  and  $j=1, \dots, n$ . These  $n^2$  transfer functions allow us to complement both approaches, the ICD and the QFT, to analyze and design controller for MIMO systems. It is proposed to cope with the controller design for MIMO systems first analyzing the  $n$  equivalent SISO problems with uncertainty in the framework of the ICD and second introducing the sensitivity functions and robustness specifications as new constraints in the well known QFT approach for SISO systems design. This proposition allows us to introduce directly the  $n^2$  sensitivity function for each closed loop transfer functions  $t_{ii}$  in the QFT approach and therefore the uncertainty effects in both gain and phase of the closed loop matrix  $T(s)$  can be straightforward analyzed using the classical control concepts in frequency domain.

This paper is organized as follows. In Section II, the analysis of multivariable systems using the Individual Channel Design is presented. Section III contains the details regarding the design technique. Section IV shows the simplicity of the design on the basis of an 2-input 2-output system, and the paper is concluded in Section V

## II MULTIVARIABLE CONTROL ANALYSIS

Consider the  $n \times n$  linear time invariant multivariable feedback system configuration with two degree of freedom of Fig. 1. in which  $P(s)$  corresponds to the transfer matrix of the plant with elements  $p_{ij}$ ,  $G(s)$  is a dynamic controller with elements  $g_{ij}$  and the matrix  $F(s)$  corresponds to a pre-filter. Then, the transfer matrix of the closed loop system is given by

$$T(s) = (I + L(s))^{-1} L(s) F(s) \quad (1)$$

where  $L(s) \triangleq P(s)G(s)$  is the open loop system matrix.

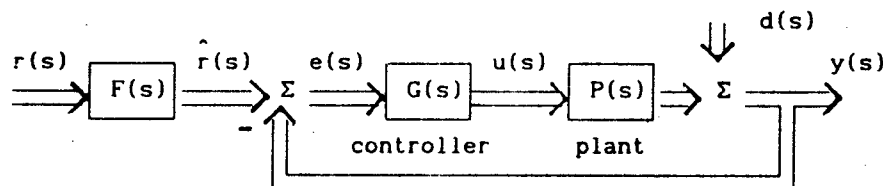


Fig. 1 Two degree of freedom multivariable feedback system

The variable  $s$  is up now dropped whenever confusion not arise as a consequence. To determine the general expressions for the elements  $t_{ii}$  of matrix  $T$ , (1) in term of plant  $P$ , pre-filter  $F$  and controller  $G$ , first the MIMO system is transformed, without loss of generality, in  $n$  SISO equivalent channels. Then the input-output pair  $(r_i, y_i)$  is defining the  $i$ th channel, and the effects of the remaining references  $r_j$  for  $j \neq i$  and perturbation vector  $d$

are assumed as global disturbances for the channel  $i$ . Therefore, the block diagram of the multivariable system, Fig. 1, assuming a diagonal pre-filter  $F$  can be modified as it is shown in Fig. 2 where the constant matrix  $A_i$  is given by

$$A_i = I_n - v_i v_i^T \in \mathbb{R}^{n \times n} \quad (2)$$

with  $I_n$  the identity matrix,  $v_i \in \mathbb{R}^n$  the unit vector  $i$ , the constant matrix  $M$  is given by

$$M_i = I_n - v_i v_i^T \in \mathbb{R}^{n \times n} \quad (3)$$

and the  $f_i$  corresponds to the transfer function of the diagonal element  $i$  of the prefilter  $F$ .

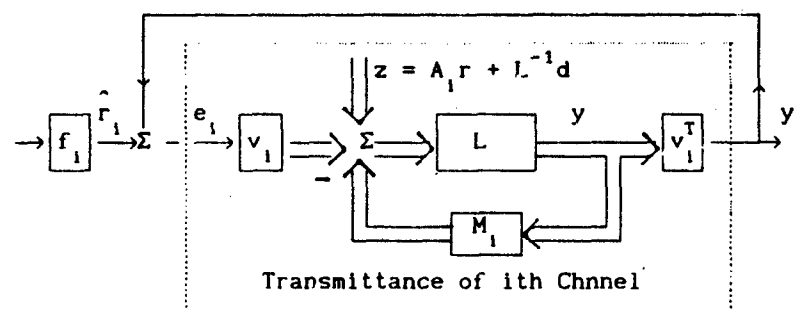


Fig. 2 Equivalence SISO feedback system

Analyzing the inner loop in Fig. 2, it is seen that the scalar transmittance or direct trajectory of channel  $i$ , has the general form

$$gt_i \triangleq y_i / e_i = v_i^T (I_n + L A_i)^{-1} L v_i \quad (4)$$

Then, defining  $R^i \triangleq (I + L A_i)$  and substituting the unit vector  $v_i$  and the product  $L v_i$  into eq. (4), the diagram of Fig. 2 can be redrawn as

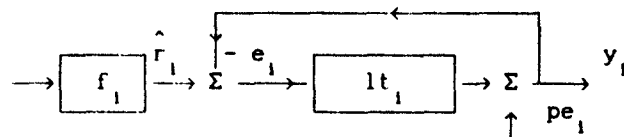


Fig. 3 Equivalent monovariabile system for  $i$ th Channel

with open loop transmittance

$$lt_1 = v_1^T (R^1)^{-1} lv_1 \quad (5)$$

$lv_1$  the column vector  $l$  of the open loop matrix  $L$  and the corresponding perturbation signal given by

$$pe_1 \triangleq v_1^T (R^1)^{-1} (L A_1 r + d) \quad (6)$$

Moreover the closed loop transfer function  $t_{11}$ , is reduced to

$$t_{11} = f_1 lt_1 / (1 + lt_1) \quad (7)$$

Therefore, the  $n$ -input  $n$ -output multivariable systems can be analyzed as  $n$  single loops, in which each individual channel is enclosed within a feedback loop trajectory  $gt_1$  and the signal perturbation,  $p_1$ , which is given by the inputs interaction through channels and disturbance effects. In order to abbreviate the presentation, it is assumed that the pair (actuator  $u_1$ , output variable  $y_1$ ) has been appropriately assigned. This assignment problem has been well addressed by various authors like, O'Reilly (1991), Horowitz (1976), Skelton (1985); therefore, a diagonal controller can be considered for simplicity

$$G \triangleq \text{diag}[g_1, g_2, \dots, g_n] \quad (8)$$

Then, the matrix  $R^1$  is reduced to

$$R^1 = \begin{bmatrix} 1+p_{1,1}g_1 \dots p_{1,1-1}g_{1-1} & 0 & p_{1,1+1}g_{1+1} & \dots & p_{1,n}g_n \\ \vdots & \vdots & \vdots & \ddots & \vdots \\ p_{1-1,1}g_1 \dots 1+p_{1-1,1-1}g_{1-1} & 0 & p_{1-1,1+1}g_{1+1} & \dots & p_{1-1,n}g_n \\ p_{1,1}g_1 & \dots & p_{1,1-1}g_{1-1} & 1 & p_{1,1+1}g_{1+1} & \dots & p_{1,n}g_n \\ p_{1+1,1}g_1 \dots p_{1+1,1-1}g_{1-1} & 0 & 1+p_{1+1,1+1}g_{1+1} & \dots & p_{1+1,n}g_n \\ \vdots & \vdots & \vdots & \ddots & \vdots \\ p_{n,1}g_1 & \dots & p_{n,1-1}g_{1-1} & 0 & p_{n,1+1}g_{1+1} & \dots & 1+p_{n,n}g_n \end{bmatrix} \quad (9)$$

Consequently defining the principal transfer function  $h_1$  as

$$h_i \triangleq g_i p_{ii} / (1 + g_i p_{ii}) \quad (10)$$

which corresponds to the closed loop transfer function of channel  $i$  neglecting the interaction between loops, the matrix  $R^i$  can be replaced by the product

$$R^i = Q^i \text{diag}[p_1 \dots p_{i-1} \quad 1 \quad p_{i+1} \dots p_n] \quad (11)$$

$$\text{with } Q^i = \begin{bmatrix} \frac{p_{1,1}}{h_1} & \dots & p_{1,i-1} & 0 & p_{1,i+1} & \dots & p_{1,n} \\ \vdots & & \vdots & \vdots & \vdots & & \vdots \\ p_{i-1,1} & \dots & \frac{p_{i-1,i-1}}{h_{i-1}} & 0 & p_{i-1,i+1} & \dots & p_{i-1,n} \\ p_{i,1} & \dots & p_{i,i-1} & 1 & p_{i,i+1} & \dots & p_{i,n} \\ p_{i+1,1} & \dots & p_{i+1,i-1} & 0 & \frac{p_{i+1,i+1}}{h_{i+1}} & \dots & p_{i+1,n} \\ \vdots & & \vdots & \vdots & \vdots & & \vdots \\ p_{n,1} & \dots & p_{n,i-1} & 0 & p_{n,i+1} & \dots & \frac{p_{n,n}}{h_n} \end{bmatrix} \quad (12)$$

Taking into account that matrix  $Q^i$  has a unit vector in the  $i$ th column and using the notation

$$\text{cofactor } m_{ij} = M_{ij} \quad (13)$$

for matrix cofactors, the channel transmittance expression  $1t_i$ , (4), is reduced, after some algebraic manipulation, to the generic form

$$1t_i = \frac{g_i}{Q_{ii}^i} [Q_{11}^i \dots Q_{ii}^i \dots Q_{nn}^i] \begin{bmatrix} p_{11} \\ \vdots \\ p_{ni} \end{bmatrix} = \frac{g_i}{Q_{ii}^i} [p_{ii} Q_{ii}^i + \sum_{\substack{j=1 \\ j \neq i}}^n Q_{ji}^i p_{ji}] \quad (14)$$

Since, the term into the bracket of eq. (14) corresponds to the determinant of the matrix

$$PH^i \triangleq \begin{bmatrix} p_{1,1} & p_{1,1} & \cdots & p_{1,n-1} & p_{1,n} \\ p_{1,1} & \frac{p_{1,1}}{h_1} & \cdots & p_{1,n-1} & p_{2,n} \\ \vdots & \vdots & \ddots & \vdots & \vdots \\ p_{n-1,1} & p_{n-1,1} & \cdots & \frac{p_{n-1,n-1}}{h_{n-1,n-1}} & p_{n-1,n} \\ p_{n,1} & p_{n,2} & \cdots & p_{n,1} & \frac{p_{n,n}}{h_n} \end{bmatrix} \quad (15)$$

and the cofactor  $Q_{11}^i = PH_{11}^i$ , then the direct trajectory of the channel  $lt_1$ , (14), takes the compact form

$$lt_1 = g_1 \det(PH^i) / PH_{11}^i \quad (16)$$

To obtain a similar pattern for the transfer function  $lt_1$  as the reported by O'Reilly (1991) for 2-input and 2-output, the  $PH^i$  is divided into submatrices according to

$$PH^i = \begin{bmatrix} p_{11} & P_{12}^i \\ P_{21}^i & P_{22}^i \end{bmatrix} \quad (17)$$

with  $p_{11}$  an scalar,  $P_{12}^i$  a row vector,  $P_{21}^i$  a column vector, and  $P_{22}^i$  a square matrix of appropriate dimensions. Then, using the Shur's formula and determinant properties, the channel transmittance, (16), can be written by

$$lt_1 = g_1 p_{11} (1 - p_{11}^{-1} P_{12}^i (P_{22}^i)^{-1} P_{21}^i) \triangleq g_1 p_{11} (1 - \chi_1) \quad (18)$$

where the rational function  $\chi_1$ , called by O'Reilly et al (1991) the multivariable structure function (MSF), is reduced to

$$\chi_1 \triangleq p_{11}^{-1} P_{12}^i (P_{22}^i)^{-1} P_{21}^i \quad (19)$$

This complex function  $\chi_1$  characterizes the cross-coupling effects in the loop 1 for all frequencies and depends on plant elements  $p_{kj}$  for  $k$  and  $j$  different from  $i$ , and principal transmittance  $h_j$ , (9), which is a function of the controller  $g_j$  and diagonal term  $p_{jj}$  for  $j \neq i$ .

It is important to note that expression (18) has the same pattern for all channels. The channel transmittances are obtained permuting rows and columns in  $PH^1$ .

Similar, the perturbation  $pe_i$  can be expressed in term of the matrix  $PH^1$ , obtaining the relation

$$pe_i = \sum_{j=1}^n \frac{p_{ij} [1 - (p_{ij})^{-1} Pr_j^1 (Pm_j^1)^{-1} Pc_j^1] h_j}{p_{jj} [1 - (p_{jj})^{-1} Pr_j^1 (Pm_j^1)^{-1} Pc_j^1]} (r_j - d_j) + d_i \quad (20)$$

where  $Pm_j^1$  is a  $n-2 \times n-2$  matrix formed eliminating both first and kth columns and rows of the general matrix  $PH^1$ , (15),  $Pr_j^1$  is a  $n-2$  row vector formed eliminating both first and kth component of the kth row of the general matrix  $PH^1$  and finally  $Pc_j^1$  is a column vector of dimension  $n-2$  formed eliminating first and kth component of the kth column of the matrix  $PH^1$ .

Finally, in order to characterize completely the SISO channel structure, the sensitivity functions of the closed loop with respect to a large parameter variation  $\Delta p_{ij}$  of the plant for all  $i$  and  $j$  are sought. In other words, the Horowitz's Sensitivity Function (Horowitz, 1963)

$$H_{p_{kj}} = \frac{t_{ii} \Delta t_{ii} / t_{ii}}{\Delta p_{kj} / p_{kj}} \quad (21)$$

for each element of the actual closed loop transfer matrix,  $t_{ii}$ , with respect to the actual plant elements,  $p_{ij}$ , for  $i=1, \dots, n$  and  $j=1, \dots, n$  has to be calculated. Taking into account the particular form of the closed loop transfer function  $t_{ii}$ , (9), and the pattern for the open loop  $lt_i$ , (18), the Horowitz's Sensitivity Function is reduced, after algebraic manipulations, to the general expression

$$H_{p_{kj}} = H_{lt_i} \frac{t_{ii}}{lt_i} f_i \frac{p_{kj}}{g_i p_{ii} (1 - \chi_i)} \frac{\Delta t_i}{\Delta p_{ij}} \quad (22)$$

Moreover, this expression can be reduced, depending on the considered element with variation, to the following three patterns



$$H_{p_{11}}^{t_{11}} = f_1 \frac{1}{(1 + lt_1^o)(1 - \chi_1)} \quad (23a)$$

$$H_{p_{jj}}^{t_{11}} = f_1 \frac{-h_j \chi_1}{(1 + lt_1^o)(1 - \chi_1)} \quad \text{for } i \neq j \quad (23b)$$

$$H_{p_{k1}}^{t_{11}} = f_1 \frac{-\chi_1}{(1 + lt_1^o)(1 - \chi_1)} \quad \text{for } k \neq 1 \quad (23c)$$

It is to remark that these expressions for the channel sensitivity allow us to analyze the effect of all parameter variations  $\Delta p_{jk}$  in the system without assuming a particular structure, like the multiplicative or additive uncertainty proposed by Doyle (1981).

From equation (18) and set (23), it can be observed that the term  $(1 - \chi_1)$  is playing a very important role in both performance and sensitivity of channel 1. In particular, if the magnitude of MSF  $\chi_1$  is near one at some frequency  $\omega_0$ , the channel 1 absorbs this frequency since the open loop transmission  $lt_1$ , (18) is practically zero. As consequence the feedback can not properly work at  $\omega_0$  and the channel can not attenuate disturbances with frequency component  $\omega_0$ . This fact can be reconfirmed looking the expressions (23). If  $\chi_1$  tends to one, since the three sensitivity expressions have the term  $(1 - \chi_1)$  as factor in the denominator, the sensitivity becomes then huge or infinite in the limit. On the contrary if the MSF  $\chi_1$  is near zero at some frequency  $\omega_0$ , the channel transmittance  $lt_1$  is approximately equal to  $g_1 p_{11}$ . This means, the cross-coupling loops do not modify strongly the channel behavior at this frequency. As consequence the sensitivity of the channel is given by the channel sensitivity neglecting interaction effect. Again this fact is validated by the channel sensitivity expressions (23). If  $\chi_1$  is near zero the first equation (23a) corresponds to the sensitivity of the standard single loop  $lt_1$  and the rest of the sensitivity values are near zero.

### III DESIGN PROCEDURE

The above presented expressions for the MIMO system are generics and do not depend on the method to design the controller  $g_1$ . However an apparent obstacle of this framework is that the loop transmission of the channel,  $lt_1$ , is dependent on the controller  $g_1$  and on the rest of  $g_j$  for  $j=1, \dots, n$  through the

transfer functions  $h_j$ . Therefore the ability to shape  $l_{t_1}$  only changing the controller  $g_1$ , as the standard QFT for SISO system recommends, can not be directly applied. Every time that the shape of the plot  $l_{t_1}$  is modified by the controller  $g_1$ , the shapes of the others  $l_{t_j}$  for  $j \neq 1$  are also modified. This disadvantage can be overcome extending the O'Reilly's procedure for 2-input and 2-output in the following way.

Since the prefilter  $F$  does not modify the shape of the open loop  $l_{t_1}$ , it is assumed at this moment the identity matrix without loss of generality.

Out of the bandwidth specifications, the designer can begin the procedure redefining the channels according to their bandwidths by (in) increasing order. In other words, channel 1 is associated to the lowest bandwidth and channel  $n$  to the highest bandwidth channel.

On the other hand, the bandwidth of the MIMO system has a very nice general property which can be summarized as follows (Verde, 1991).

Assuming the polar plot of the MSF  $\chi_1$  not near one, the bandwidth  $BW_{t_1}$  of the closed loop channel 1 is bound by the respective bandwidth  $BW_{h_1}$  of closed loop channel 1 in which the loops interaction effect is neglected. In other words the speed of a channel with cross-coupling between loops, depends only on the bandwidth of the respective channel neglecting interaction. Therefore the cross-coupling loops do not affect strongly the bandwidth of the channel.

Now the channels reassignment according to their bandwidths and the bound property of the channels speeds enable us to shape one by one the open loop  $l_{t_1}$  for each of the  $n$  SISO channels in the following iterative way. The design technique is based on the manipulation of both open loop transfer functions with and without cross-coupling interaction at high and low frequency regions. Specifically the gap between high and low frequency depends on the channel under consideration. However it is to remark that the narrower the gap between channels is, the greater the iteration number will be to yield a satisfactory design.

In the first stage, it is assumed that all the channels, excepts the first, have very great bandwidths. As consequence the complex function  $h_i$  for  $i \neq 1$  can be approximated to one and the only unknown function in the open loop equation (18) of channel 1 is the controller  $g_1$ . Thus, the QFT design for SISO system on  $g_1$  can always proceed on the basis of a known bounds of bandwidth, sensitivity constraint and stability margins for channel one. Since the controller  $g_1$  through the transfer function  $h_1$  can introduce transmission zeros in the MIMO system, it is necessary to test during the QFT procedure that this does not occur. A simple graphic procedure is indicated below which can be straightforward implemented for this purpose.

Taking into account that the zeros of the function  $(1-\chi_1)$  assuming  $h_j=1$  correspond to the transmission zeros of the MIMO system (see O'Reilly, 1991), it is proposed, similarly to Nyquist criterion, to use the calculus of residues for checking the lack of new RHPZ produced by the controller  $g_1$  in the function  $(1-\chi_1)$ . Therefore, it is only necessary to verify that the number of net clockwise encirclements of the point  $(1,0)$  of the polar plots of  $\chi_1$  assuming infinite bandwidths (i. e.  $h_j=1$ ) is held during the adjusting of the controllers by the QFT.

Once the channel 1 design for  $g_1$  is completed, the channel 2 design can then be adjusted by the QFT on the basis of known transfer function  $h_1$ , bandwidth specification, sensitivity constraint, stability margins for channel 2 and  $h_j=1$  for the rest of the channels in the open loop equation (18). Again the absence of new RHPZ in the system by  $g_2$  has to be verified. Of course the graphics method suggested for this purpose can again be used.

The above described design philosophy can be implemented in an iterative procedure for each element of the controller.

#### IV EXAMPLE

The following academic 2-input, 2-output example illustrates the basis of the above described ideas. Consider the plant transfer matrix

$$P = \frac{1}{\Delta} \begin{bmatrix} 117 & 30.1 \\ -10.7 & -10.3 \\ -0.671 \pm 2.25j & -1.21 \pm 5.35j \\ -1.14 - 1.05j & -0.650 \pm 2.24j \\ -0.130 & -0.028 \pm 0.005j \\ -0.00316 & \end{bmatrix} \quad (24)$$

$$\Delta \begin{bmatrix} 14.07 & 28.5 \\ -11.5 & -10.3 \\ -0.6572 \pm 2.19j & -0.658 \pm 2.24j \\ -0.523 & -0.784 \\ -0.033 \pm 0.003j & -0.028 \pm 0.001j \end{bmatrix}$$

where the following convention for a polynomial  $p$  of order  $n$  with zeros  $a_1, a_2, a_n$  and gain  $k$  has been used

$$p = k(s+a_1)(s+a_2)(s+a_n) \dots (s+a_n) = [k \mid -a_1 \mid -a_2 \mid \dots \mid -a_n]^T \quad (25)$$

the system characteristic equation is given by

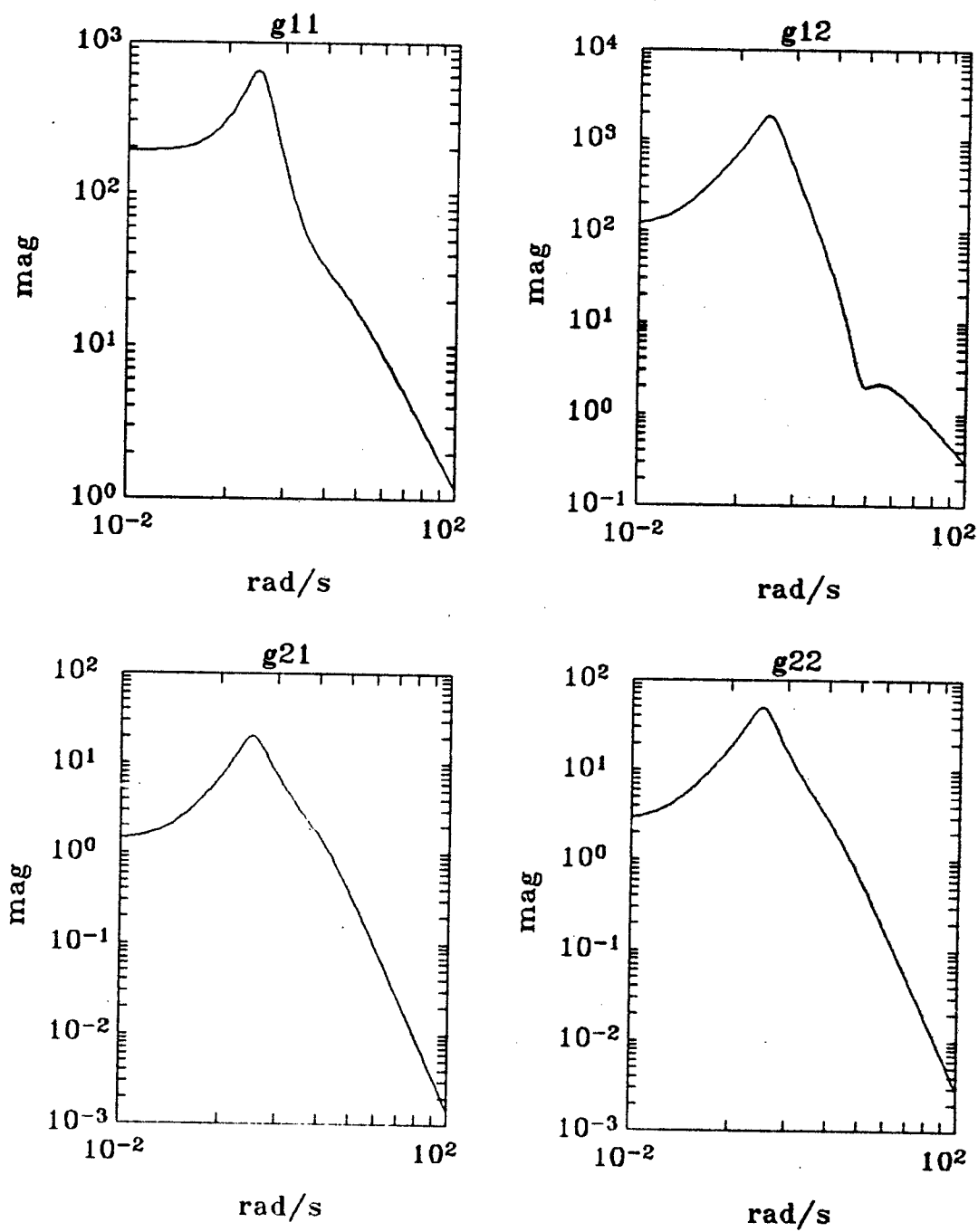


Fig. 4 Frequency response of the MIMO plant

$$\Delta = [1 \mid -10.5 \mid -3.19 \mid -0.653 \pm 2.25j \mid 0.133 \pm 0.376j \mid -0.405 \mid -0.003]^T \quad (26)$$

and set of finite zeros  $TZ = \{-10, -0.65 \pm 2.2j\}$ .

Assume typical frequency domain design specifications like the following set.

- 1) Zero steady state error in response to a unit step change in both outputs.
- 2) Bandwidth for output one less than 1 rad/s.
- 3) Bandwidth for output approximately 5 rad/s.
- 4) The system must be robust for plant uncertainty below 1 rad/s.
- 5) The effect of the controller inputs in the outputs decoupled as much as possible (i.e. the closed loop transfer functions  $t_{12}$  and  $t_{21}$  near zero).

First the analysis of the open loop system structure system using the ICD tools is done. It can be observed from the Fig. 4 where the frequency response of the plant is presented that the system is not diagonal dominant even at low frequency.

Assuming initially infinite bandwidth for the two channels, (i.e.  $h_1=1$  and  $h_2=1$ ) the polar plot of the complex function MSF  $\chi_1=\chi_2$  of the Fig. 5 allows then us to determine the frequency range in which the system is stronger coupled and very sensitive according the ICD framework. Two facts can be observed. The MSF polar plot is far way from 0 indicating that the structure is coupled, at low frequency and the plot is near 1 at low frequencies which implies a lacking of structure robustness at frequencies below 0.2 rad/s. Moreover to avoid the introduction of new RHPZ in the channels by the controllers  $g_1$  and  $g_2$ , these must be designed in such way that the two encirclements of the MSF  $\chi_1$  and  $\chi_2$  to the point (1,0) are maintained.

In order to achieve the steady state error the following structure with integral action for both controllers  $g_1$  and  $g_2$  is obviously proposed.

$$g_1 = \frac{k_1(s + a_1)}{s(s + b_1)}$$

Specifically first the controller  $g_1$  is adjusted shaping the open loop transfer function  $lt_1$  with  $h_2=1$  by the standard SISO QFT procedure. In this case the particular specifications are bandwidth less than 1 rad/s, uncertainty compensation for frequencies below 1 rad/s and the MSF  $\chi_2$  plot as near as possible to zero, maintaining the two encirclements to the point (1,0).

The Fig. 6 shows the behavior of channel 1 with the designed controller. It is to note from the frequency response of  $h_1$  and  $t_{11}$  the likeness between both

bandwidths.

Once the controller  $g_1$  is determined, the controller  $g_2$  must be designed by the QFT on the basis of the a known  $h_1$  in the open loop transfer function  $lt_2$ , taking into account specifications 3, 4, and 5 and maintaining the two encirclements to the point (1,0) of the MSF  $\chi_1$ .

After the two controller has been independently determined, the design is verify; if all the specifications are not satisfied, the controllers has to be redesigned but now taking the transfer functions  $h_1$  and  $h_2$  obtained previously. The Fig 7 shows the response of channel 1 and 2 after four iterations for the controllers redesign.

The Figs 8 and 9 show the sensitivity functions for the diagonal elements of the closed loop transfer functions. It is from the sensitivity that the robustness requirements are met.

## V CONCLUSION

This paper presents a method for MIMO system design which uses the advantages of the QFT procedure based on SISO system. The basic idea consists to consider a MIMO system as n equivalent SISO system where the cross-couplings effects are already introduced in the transfer functions via the Multivariable Structure Function proposed by O'Reilly et al (1991). It is emphasized that this is an introductory paper and many issues remain to be explored in future work.

## REFERENCES

- Doyle C. J. & Stein G., 1991. Multivariable Feedback Design: Concepts for Classical/Modern Synthesis. *IEEE Trans Auto Control*. AC-26 February.
- Frank P. 1978. Introduction to System Sensitivity Theory. *Academic Press*.
- Horowitz I. 1963. Synthesis of Feedback Systems. *Academic Press*.
- Horowitz I., 1991. Invited paper. Survey of quantitative feedback theory (QFT). *Int. J. Control*, Vol. 53. No.2, 255-291.
- Horowitz I., 1979. Quantitative synthesis of uncertain multiple input-output feedback system. *Int. J. Control*, Vol. 30, No.1, 81-106.
- O'Reilly J. & Leithead W., 1991. Multivariable Control by Individual Channel Design. *Int J. Control*, Vol. 53. No.7.
- Rosenbrock H. H., 1969. Design of Multivariable control system using the

Inverse Nyquist array. *Proc. IEE-D*, vol 116, 1929-1936.

Shaked U., Horowitz I. & Golde S., 1976, Synthesis of Multivariable, Basically Non-Interacting Systems With Significant Plant Uncertainty. *Automatica*, 12, 61-71.

Sponer J., 1968. Zur Messung exakt entkoppelter und nichtentkoppelter Zweifachregelungen. *MSR-9*, Dec, GDR. 438-445.

Verde C., 1992. Bounds on Bandwidth for MIMO Systems. Proceedings of American Control Conference. Chicago, IL. 22-26 June.

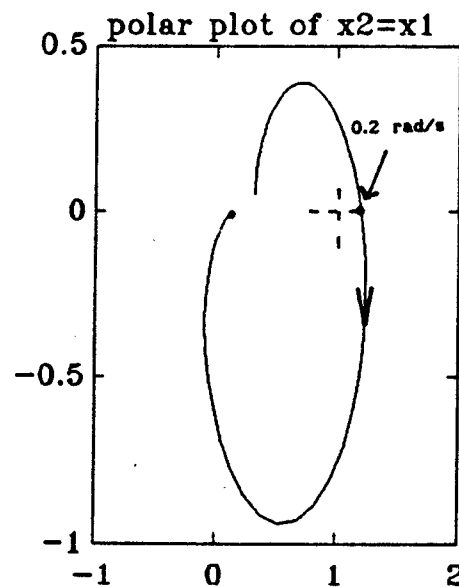


Fig. 5 Polar Plot of the Multivariable Structure Function  $x_1 = x_2$

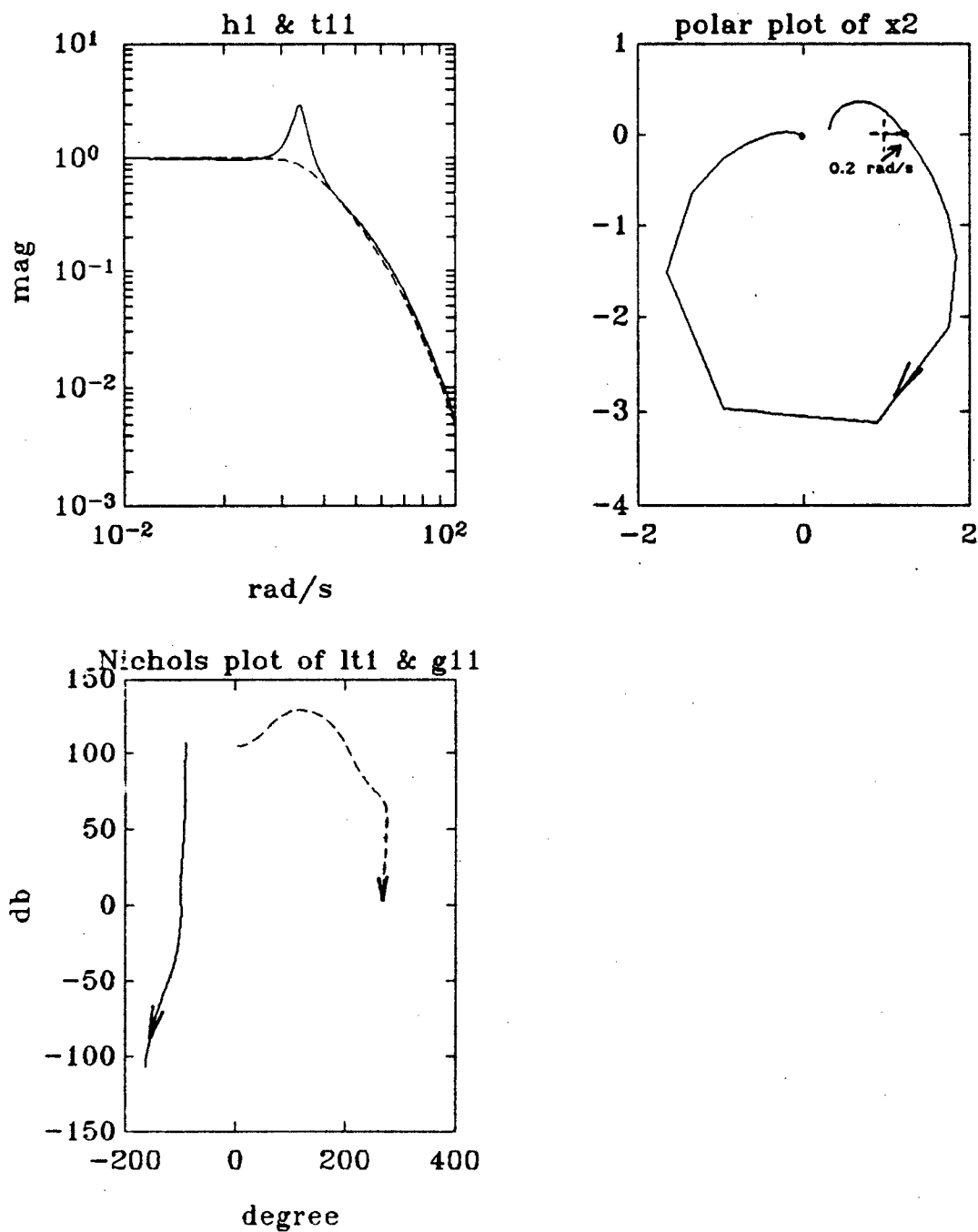


Fig. 6 Frequency response of channel 1 assuming  $h_2=1$ .

- a) Closed loop response with and without interaction effects
- b) Multivariable Structure Function  $\chi_2$  with  $h_1 \neq 1$
- c) Open loop response with and without interaction effects



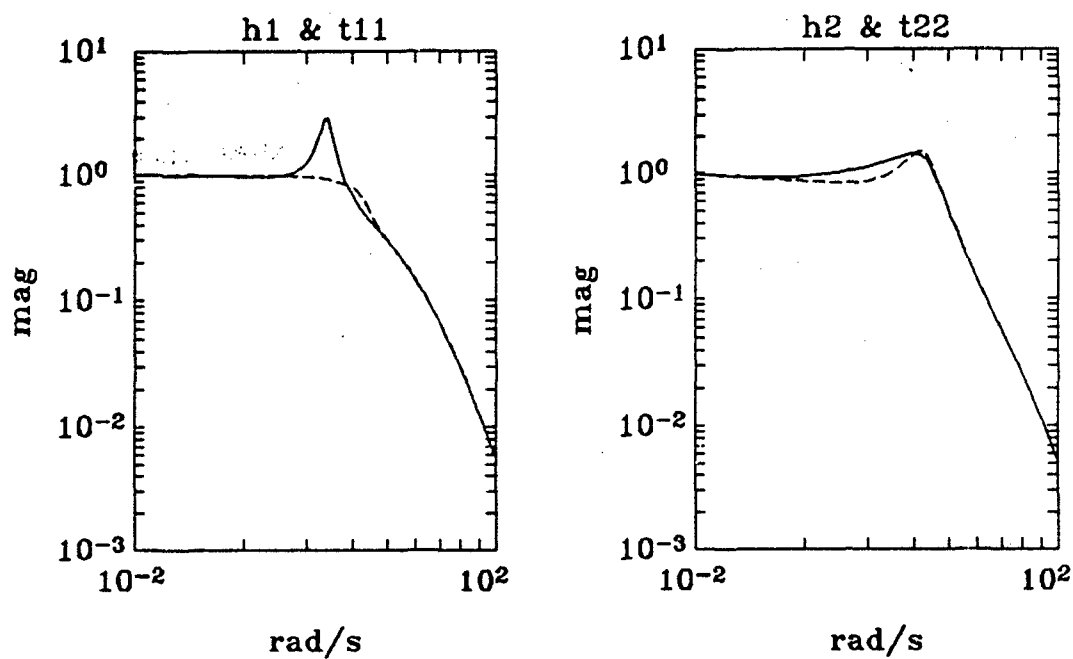


Fig. 7 Frequency response of the closed loops with and without interaction effects. a) Channel 1; b) Channel 2

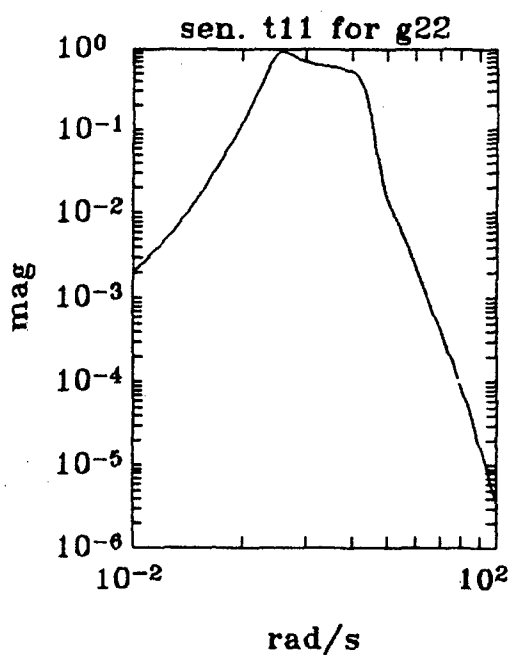
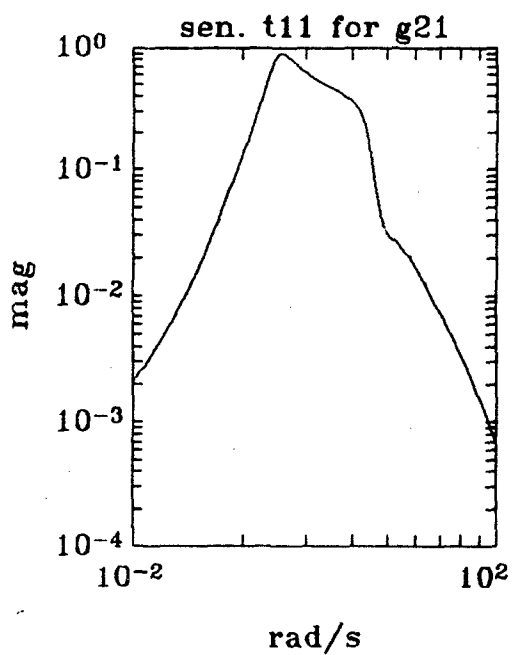
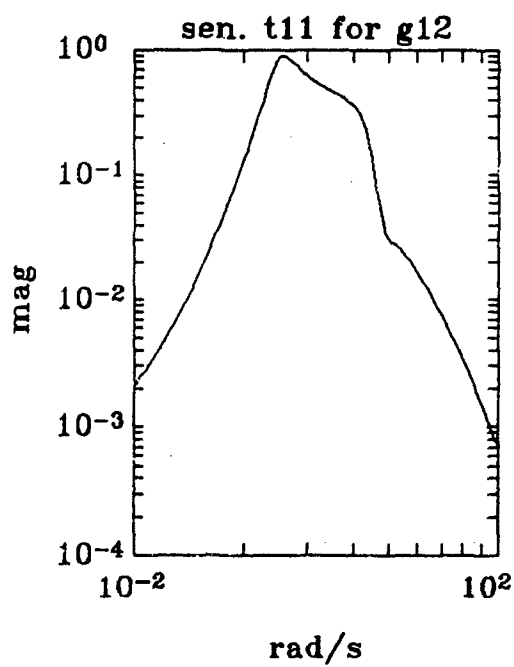
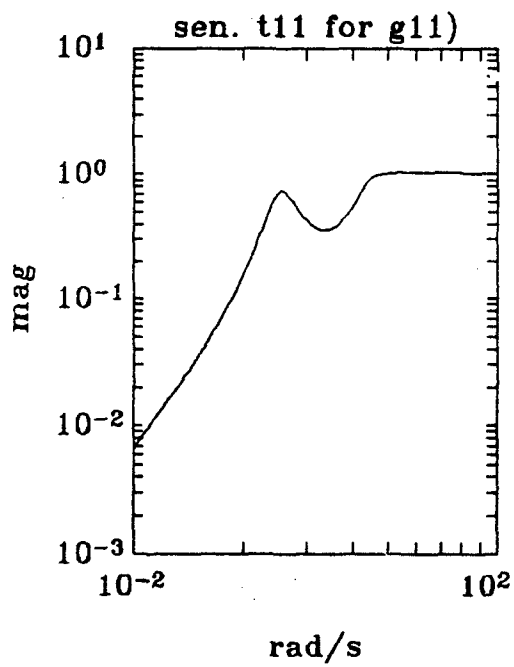


Fig. 8 Sensitivity functions for closed loop 1

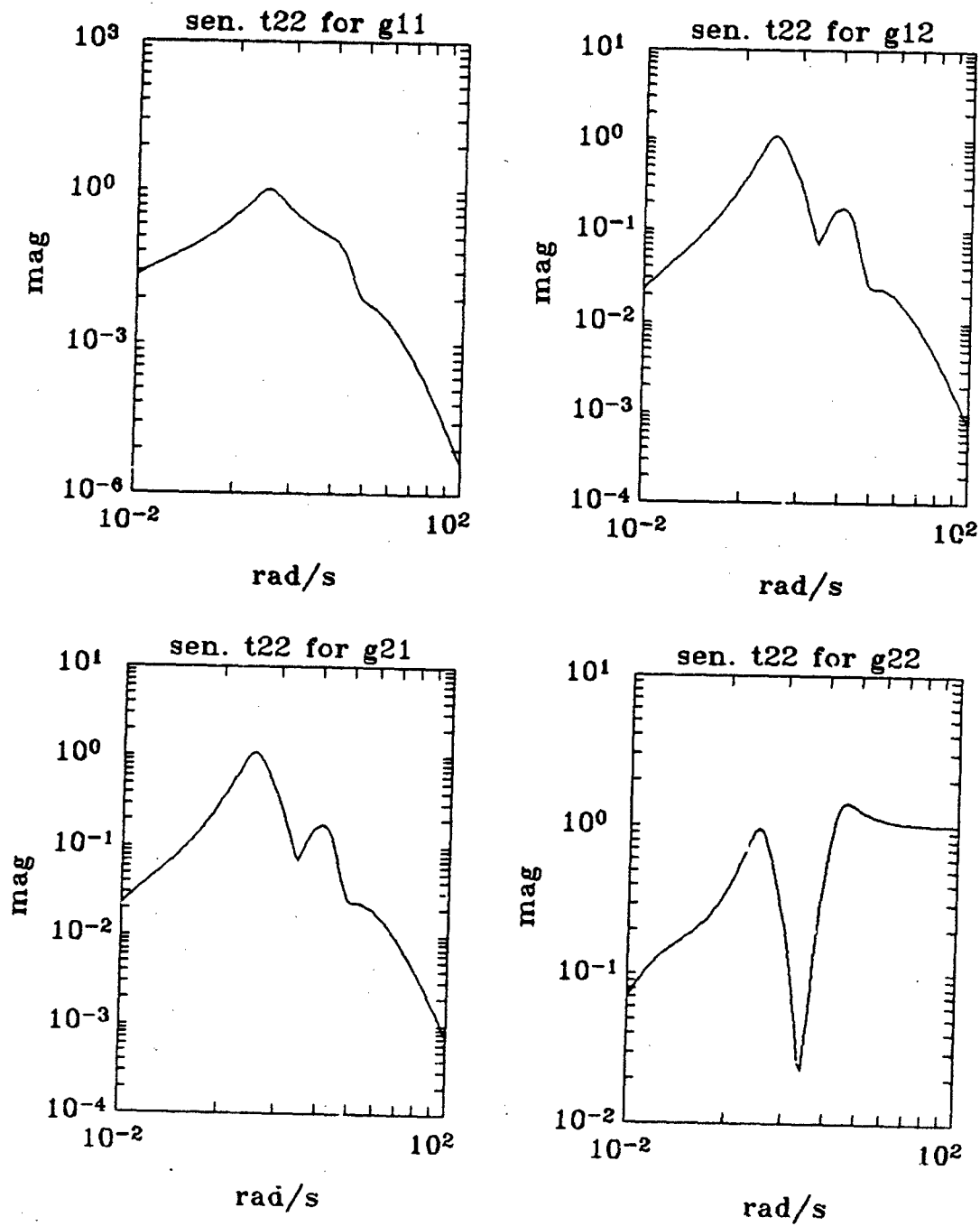


Fig. 9 Sensitivity functions for closed loop 2

# A MIMO P.M. SYSTEM SYNTHESIS THEORY WITH PLANT UNCERTAINTIES

Jui-Lin Lai\*\*      and      Bor-Chyun Wang\*

## 1. ABSTRACT

This paper investigates a linear time invariant system with serious plant uncertainties. The Quantitative Feedback Theory (Q.F.T.) synthesis technique is successfully to solve such an feedback problem. And the plant modification feedback system has been developed to save the "cost of feedback" under a tolerable signal level range. For a MIMO system, the "cost of feedback" is more serious in the QFT design, so it is very useful to consider the P.M. loop. In this paper, the M.I.M.O. multiple loops system design with P.M. loop is developed. A systematic design procedure is derived and numerical examples are illustrated. It is concluded that the "cost of feedback" is largely reduced in the MIMO multiple loop P.M. system.

## 2. INTRODUCTION

The more use of a feedback configuration around the uncertain plant, suffices to scare it into docile behavior. In 1972, I.M. Horowitz and M. Sidi [1] have introduced a design method Q.F.T. (Quantitative Feedback Theory) to solve the uncertainties in a plant even they are large. It is known that a feedback control loop can improve the sensitivity of parameter uncertainty and the effect of disturbance. By using a 2 D.O.F. feedback structure in Fig.1, this synthesis theory will design a controller  $G(s)$  to assure the sensitivity of system within a prescribed quantity which is the difference between A & B in Fig.2. The prefilter  $F(s)$  will make the frequency response of the system be bounded within the design specification (Fig.2). The problem had extended to more than two degree-of-freedom

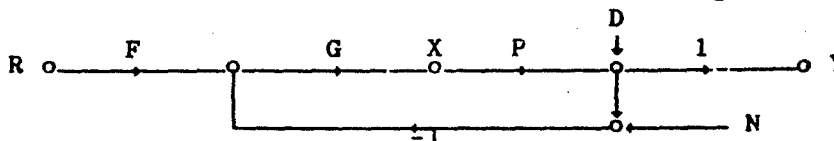


Fig. 1 2 D.O.F. system structure  
system [2,3], such as multiple-loop system [4], and plant modification P.M. structure system [5,6]. On the other hand, the single loop MIMO problem had developed in old method [10], improved method [7,9] and EDA method [11].

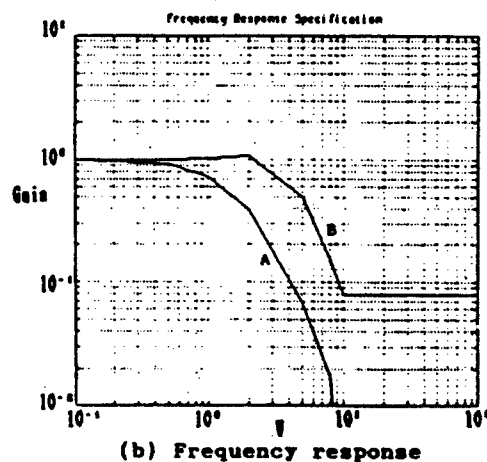
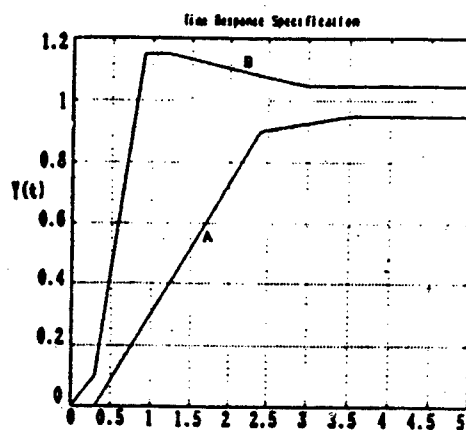
For a heavy uncertained plant, the "cost of feedback",  
C.O.F.  $\equiv$  noise response at plant input  
 $= X_i / N_i$  (refer Fig.16)

\* Institute of Control Engineering, National Chiao-Tung University, and Chung-Shan Institute of Science and technology, Taiwan, R.O.C..

\*\* Institute of Control Engineering, National Chiao-Tung University, and Department of Electronic Engineering, Lien-Ho Junior college, Taiwan, R.O.C..

usually high in order to satisfy the required system performance. In this case, both single-loop and multiple-loop MIMO designs cannot solve the problem. In this paper a MIMO P.M. system which allows feedback into the intermediate points of a cascaded plant, is discussed. Since the design degree of freedom is increased, then the C.O.F. can be reduced and the problem is solved. The P.M. system induces plant output signal level variation. This polynomial is restricted by a constraint in this paper.

Section 3 is dealing with the statement of the problem. In section 4, we will explore Signal Level problem, reviews some problems in P.M. structure system, and present the results which shows the sensor noise effect is reduced. Section 5 illustrates the system structure. In section 6, a M.I.M.O. system will be examined and 2-loop P.M. system will be successfully applied to the MIMO synthesis technique with numerical examples. The discussion about the observation of disturbance response, and sensor noise response on corresponding output point will be included in section 7. Section 8 is the conclusion of the present paper and some suggestions for the further work. Finally, some datum are listed in Appendix. In this paper, the P.M. loop is allowed in the MIMO system to improve the "C.O.F.".



(a) Time response  
Fig. 2 System specification

### 3. PROBLEM STATEMENT

There is given an  $n \times n$  linear time invariant plant with  $m$  cascaded section,  $P^a, P^b, \dots, P^m$  (all  $n \times n$  matrices). The  $n$  outputs of each section, may be measured and the data can be used for feedback purposes, the command input vector  $R$  may also be measured. There are  $m+1$  degrees of freedoms, ie,  $m+1$  independent matrices in NPM system.  $F, G^a, \dots, G^m$  in figure 3 are  $n \times n$  of compensating transfer functions to be chosen. There are assigned tolerances on these  $n^2$  elements of the overall system transfer function  $T$  in the form of  $n^2$  acceptable sets.

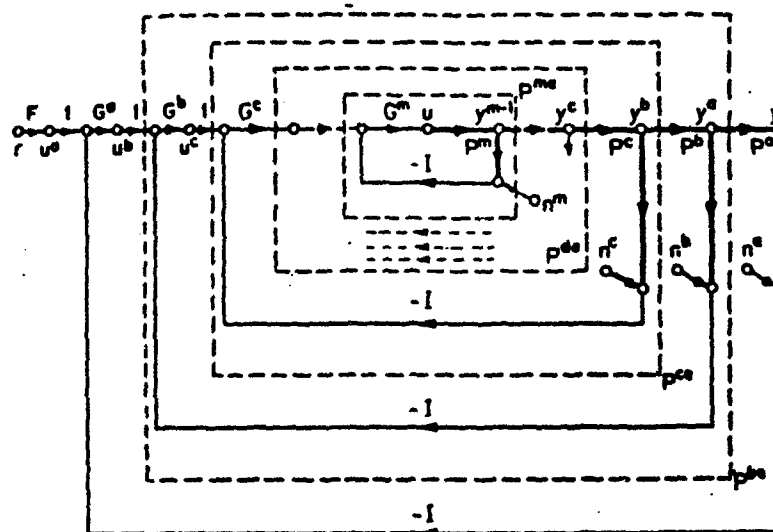


Fig. 3 feedback structure around m loop MIMO system

If the P.M. loop is allowed, the matrix degrees of freedom is drastically increased to  $(n+1)*m/2+1$  (figure 4). In P.M. system, if we draw all loops in one side of the cascaded plant  $p^m p^{m-1} \dots p^c p^b p^a$ , there are no loop crossing over, this is called no cross loop P.M. system (Fig.5). The D.O.F. is  $2*m$ . Even in the NCPM case, the cost of freedom is largely reduced. But one must careful that the tolerable signal level variation constraint must be considered.

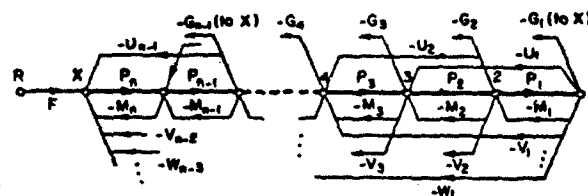


Fig. 4 P.M. feedback structure

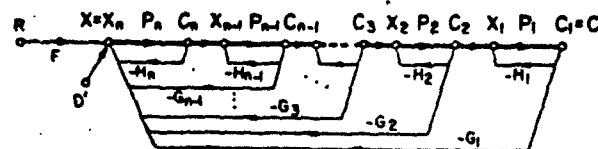


Fig. 5 NCPM feedback structure

#### 4. SIGNAL LEVEL CONSIDERATION IN PLANT MODIFICATION SYSTEM

Consider a single input single output (S.I.S.O.) system, where the plant consists of  $m$  cascading sections, see figure 6, with a required maximum output signal level  $C_1(s)$ . The signal

level at the input of  $P^a$  is:

$$C_{2s} = X_1 = \frac{C_1}{P^a}, \quad (1)$$

where  $C_{2s}$  is the output of  $P^b$ . This relation will not be changed in the NPM cascaded multiple-loop feedback structure in which all feedback path return to the input of plant  $P^m$ .

$$C_{ms} = X_{(m-1)} = \frac{C_1}{P^a P^b P^c \dots P^{m-1}} \quad (2)$$

Suppose a feedback loop is put around plant  $P^a$  with compensator  $H(s)$  in figure 6(b).

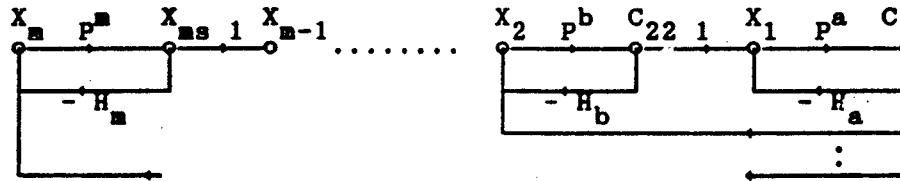
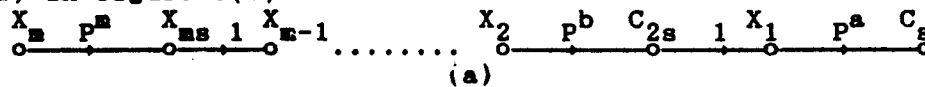


Fig. 6 (a) a cascaded plant system  
(b) adding a P.M. loop system

The signal at  $X_1$  is still  $C_1/P^a$ , but

$$\begin{aligned} C_{22} &= X_1 + H_a C_1 = C_1/P^a + H_a C_1 = (1 + H_a P^a) C_1/P^a \\ &= (1 + H_a P^a) X_1 = (1 + H_a P^a) C_{2s} \end{aligned} \quad (3)$$

For the same required signal level of  $C_1$ , adding an P.M. inner loop, the resulting signal level of  $C_{22}$  equals to  $C_{2s}$  multiplied by  $(1 + H_a P^a)$ . The plant  $P^a$  appears to modification and the system is called a P.M. system. It is conceivable that this level of  $C_{22}$  may be so much larger than  $C_{2s}$ , so  $P^b$  may have to handle this large signal level. If the 'feedback expert' is working together with the 'plant expert' in design of the plant itself, then the trade-off in such significant plant modification may be seriously considered. In the case of an existing plant, a P.M. design method must keep the increase of the plant input signal within a tolerance range [4]. The 2 loop P.M. system structure is shown in figure 7(b). In addition, the insight obtained from a synthesis procedure is very useful for those cases, and the feedback expert is called to help the plant expert in the actual plant designed [4].

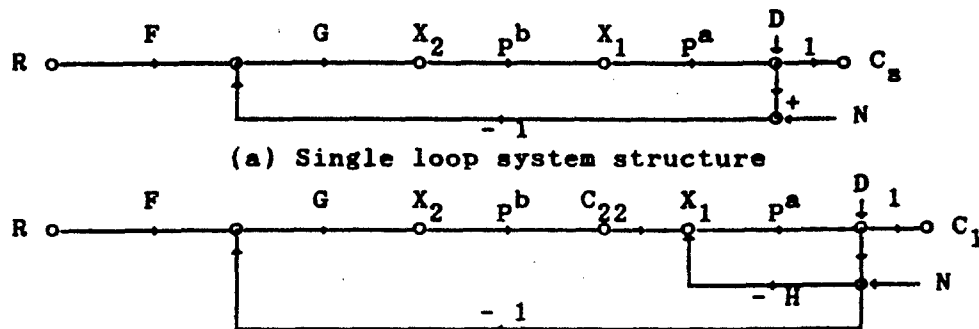


Fig. 7 (b) The P.M. 2-loop system structure.

In order to follow the same design notation as in a non-P.M. cascaded system design [1,8], let  $L_{on} = G p_n^b p_{en}^a$ ; where

$p_{en}^a = \frac{p^a}{1 + L_{an}}$ ,  $L_{an} = H p^a$  in nominal plant case. For the sake of the signification signal level variation due to  $L_a$ , it is impractical to let  $L_a$  cope completely with the uncertainty in  $p^a$ . The P.M. design theory is developed by base on individual an sidering the frequency spectrum [4,5]. While the uncertainty in the low frequency range, the control signals be dominated, so it is take care of by the outer loop  $L_o$ . But  $L_o$  handle the uncertainty only  $p^b$  in high frequency range, thus the UHWP region be determined by the variation due to  $p^b$ . The inner loop  $L_a$  cannot handle all the uncertaunties of  $p^a$ , ie,  $\Delta|p_e^a|$  may be not equal to zero, so the outer loop  $L_o$  must have some overdesign to make up the difference. Since the uncertainty in  $p_e^a$  is compatible with  $L_o$  and it's  $\alpha$  allow for  $p_e^a$  uncertainty, then  $L_o$  can be designed as a highly economical loop in terms of bandwidth.

#### 4.1 Signal Level Variation ratio (SLVR) and $\rho$

The signal level ( S.L.) problem is the basic one in the plant modification system design. SLVR is defined with respect to a single loop design for the same plant (figure 7(a)). The maximum output signal level is :

$$|C_s(j\omega)|_{\max} = |R F(j\omega)| \left| \frac{L_s(j\omega)}{1 + L_s(j\omega)} \right|_{\max}, \quad (4)$$

and the maximum signal level at the output of  $p^b$  is :

$$|C_{2s}(j\omega)|_{\max} = |R F(j\omega)| \left| \frac{L_s(j\omega)}{p_a(j\omega)[1 + L_s(j\omega)]} \right|_{\max}. \quad (5)$$



The ratio :

$$r_s(j\omega) = \frac{|C_{2s}(j\omega)|}{|C_s(j\omega)|} \max_{\tau} \quad (6)$$

Similarly, in P.M. 2 loop system (figure 7(b))

$$|C_1(j\omega)| \max_{\tau} = |R F(j\omega)| \left| \frac{L_o(j\omega)}{1 + L_o(j\omega)} \right| \max_{\tau} \quad (7)$$

$$|C_{22}(j\omega)| \max_{\tau} = |R F(j\omega)| \left| \frac{L_o(j\omega)}{P_{ae}(j\omega)[1 + L_o(j\omega)]} \right| \max_{\tau} \quad (8)$$

$$r_2(j\omega) \max_{\tau} = \frac{|C_{22}(j\omega)|}{|C_1(j\omega)|} \max_{\tau} \quad (9)$$

The signal level variation ratio (SLVR)  $\rho$  is defined to be :

$$\rho(j\omega) = \frac{|C_{22}| \max}{|C_{2s}| \max} = \frac{r_2}{r_s} = \frac{|C_1| \max}{|C_s| \max} \quad (10)$$

The P.M. system synthesis theory is restricted to the R.M.S. signal level, not to peak values. That is, this synthesis theory is based on the amount of signal level variation  $Q$  defined by :

$$Q = \frac{\int_0^{\infty} |C_{22}(w)|_{\max}^2 dw}{\int_0^{\infty} |C_{2s}(w)|_{\max}^2 dw} \quad (11)$$

#### 4.2 Division of the Frequency Spectrum

According to the single loop design result (Fig. 8), the frequency range is divided into 5 distinct parts (where both the h.f uncertainty of  $P^a$  and  $P^b$  are 14 db).

- (1) The very low frequency range  $R_1 = [0, w_1]$  is the range of  $|L_s(j\omega)| \geq 25$  db over the entire plant parameter space. In this range in P.M. synthesis the inner loops are not used to help the outer loop  $L_o$ , ie, in  $R_1$ ,  $L_{sn} \approx L_{on}$ , where  $L_{sn}$  and  $L_{on}$  designed the nominal loop transmission.
- (2) Middle frequency range  $R_2 = [W_1, W_2]$  defined by -14 db  $\leq |L_s(j\omega)| \leq 25$  db, where -14 db is due to  $P^b$ .
- (3) High frequency range I  $R_3 = [W_2, W_3]$  defined by -28 db  $\leq |L_s(j\omega)| \leq -14$  db, where -24 db is due to  $P^a + P^b$ .
- (4) High frequency range II  $R_4 = [W_3, W_4]$  where  $W_4 = 10 \times W_3$ .
- (5) The very high frequency range  $R_5 = [W_4, \infty]$ .

It is helpful for interpretation of SLVR in different frequency range, in order to develop the design procedures of the P.M. inner loop  $L_i$ .

#### 4.3 Relation between SLVR $\rho$ and $|1 + L_{an}|$

If the maximum output over  $P$  in figures 7(a) and 7(b) should be the same, i.e.,  $|C_1|_{\max} = |C_s|_{\max}$ . By inspection of Equation 3,  $(1 + P^a H)$  is an important factor and it is useful to relate Loci of constant  $|1 + P^a H|$  to  $P^a H$  on the Nichol's Chart. Let  $L_a = P^a H$ ;  $\ell = 1/L_a$  and  $z = \frac{1}{1 + L_a}$  then

$\ell = \frac{1}{1 + 1/\ell} = \frac{\ell}{1 + \ell}$ . The relation between  $z$  and  $\ell$  gives the conversional Loci of constant  $z$  magnitude on the Nichol's Chart, so the relation of  $|1 + L_a|$  with respect to  $L_a$  is the reversed Nichol's plot, obtained by changing the sign of constant magnitude curves. We will develop a subroutine under 'MATLAB' control program to plot this Loci, expression in Fig. 9. Those Loci is a very usefully tool in the P.M. system design.

Our design philosophy is to make  $L_a$  as small as possible in  $R_1$ , in order that the minimum signal level of  $C_{22}$  be very closely equal to that of  $C_{2s}$ . This is because that the control signal level is the highest in this low frequency, so that even small precent changes could lead to large absolute differences. In the high frequency ranges, where the signal level is not important, only centrate in the reduction of the sensor noise effect. The details are illurstrated by a numerical example.

#### 4.4 Numerical Example

Example 1 : 2 loop with P.M. system (Fig. 7(b))

Plant :  $P = p^a p^b$

where  $p^a = \frac{K}{s}$  ;  $p^b = \frac{M}{s + a}$

Plant uncertainties:  $1 \leq K \leq 5$  ;  $1 \leq M \leq 5$  ;  $.1 \leq a \leq 2$

Perfomance specification : shown in figure 2

disturbance response :  $\left| \frac{C}{D} \right| = \gamma \leq 2.3 \text{ db}$

Restriction on signal level :  $Q \leq 1.05$  for step input.

The step by step design procedures for any SISO 2 -loop P.M. system are follows :

Step.1. : Choose an acceptable curve of  $|1 + L_a^*|$  ( see figure 10 ) from a given value of permitted  $C_{22}$  power increase  $Q$  as defined in Equation 11, where  
\* indicates the perminary design in the  $\ell.f.$

Step.2. : Determine the bounds  $B_{L_a}^*$  on the inner loop  $L_a = P^a H$  and design  $L_a^*$  in the  $\ell.f$  range  $R_1, R_2$  (figure 11).

Step.3. : Determine the template of  $P^b P_e^a$ , where  $P_e^a = P^a / (1 + L_a^*)$ . Find the bounds  $B_{L_o}(w)$  on the outer loop, in order to satisfy the design specification on  $T(jw)$  (figure 12).

Step.4. : Design the outer loop  $L_o$  from the bounds  $B_{L_o}(w)$ .

Fixed  $L_o$ , using  $L_o = G P^b P_e^a$  to find the corresponding bounds  $B_{L_a}(w)$  in c.f  $R_3, R_4, R_5$  range, such that  $L_o$  is still satisfied  $T(jw)$  (figure 13).

Step.5. : Completion of the design of the inner loop  $L_a$  which satisfies both  $B_{L_a}^*(w)$  and  $B_{L_a}(w)$ .

From a given  $Q$  ( $Q \leq 1.05$  in this example) and base on Equation 11,  $|1 + L_{an}(w)|$  can be selected to satisfy specification from  $Q$ . In 1978, Bor-Chyun Wang had discussed this problem [5], and obtained a set of datum about the relation of  $Q$  and the corresponding value of  $|1 + L_{an}|$ . This example, we use the result for 'CASE-C', as figure 9 and figure 10 bounds on  $|1 + L_{an}|$ . According to figure 10 the bound of  $L_{an}^*$  is shown in figure 11 with resulting  $L_{an}^*$ .

For pedagogic reason, it is better to understand the nature of  $L_a$  in  $R_1, R_2$  before considering how to derive  $|1 + L_{an}(w)|$  from  $Q$ . The nature of  $L_{an}$  is decisively influenced by the nature of non P.M. cascaded loop design. Recall that in the c.f range ( $R_1, R_2$ ), there is little demand on  $L_a$ , the bounds are upper ones. The resulting power variation  $Q$  was defined to be the ratio of area under the curves  $|C_{22}|_{\max}^2$  and  $|C_{2s}|_{\max}^2$  (figure 17), which gives  $Q = 0.9885$  in this example, and satisfies the specification  $Q \leq 1.05$ .

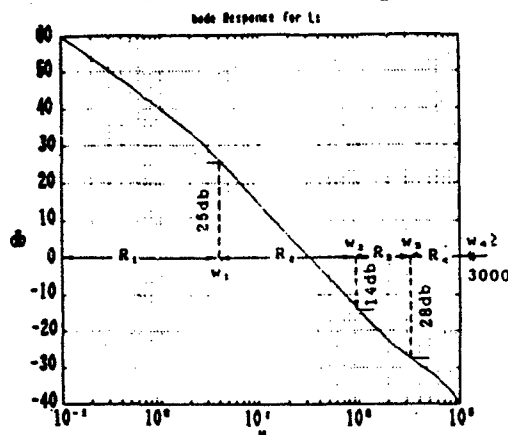


Fig. 8 Division of the frequency spectrum

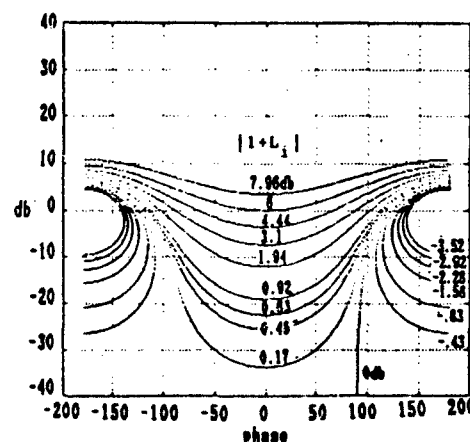


Fig. 9 Loci of constant  $|1+L_1|$  on  $L_1$  Nichol-Chart

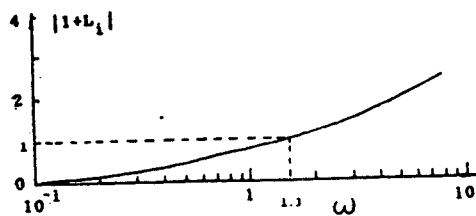


Fig. 10 Bound on  $|1+L_i|$  in the low frequency

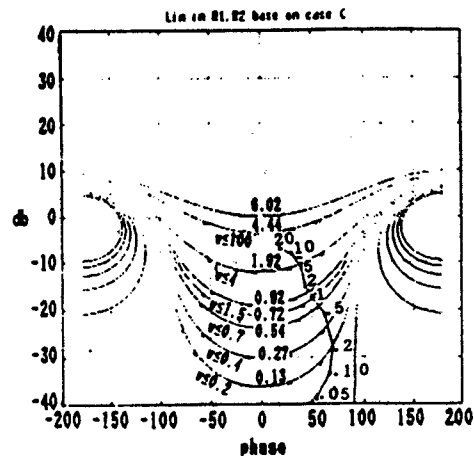


Fig. 11 Bound of  $L_{an}^*$  and design  $L_{an}^*$

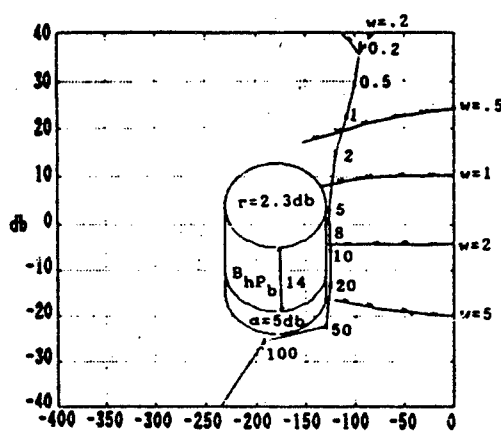


Fig. 12 The bound of  $L_{on}$  and design  $L_{on}$

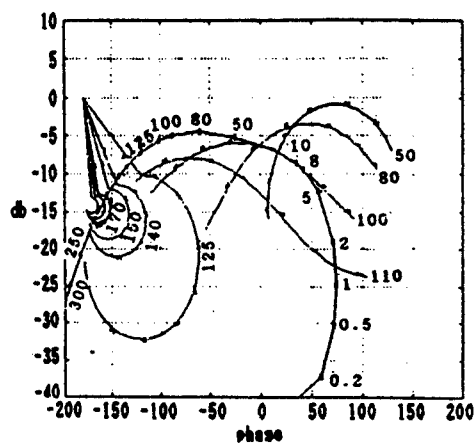


Fig. 13 The bound of  $L_{an}^*$  and design  $L_{an}^*$

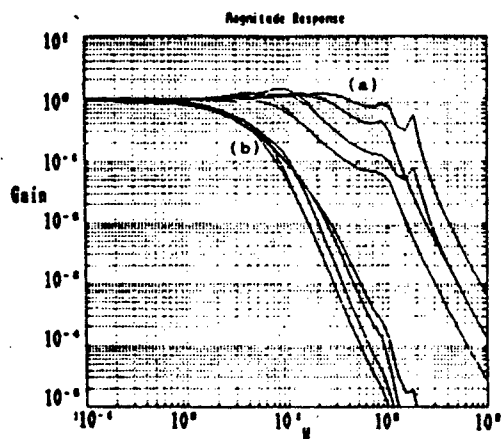


Fig. 14 Frequency response  
(a) without prefilter  
(b) with prefilter

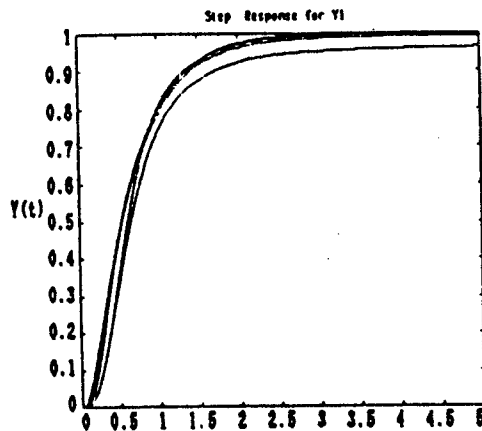


Fig. 15 Time response

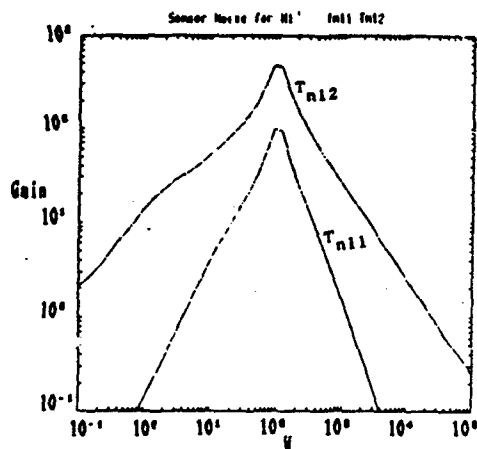


Fig. 16 Sensor noise effect

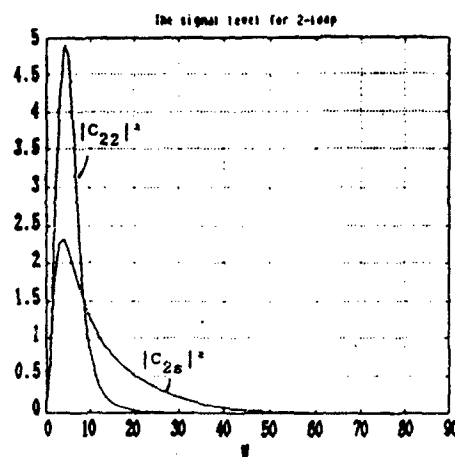


Fig. 17 The signal level for  $C_{22}$  and  $C_{2s}$

#### 4.5 Noise Consideration

Observe the noise response in the h.f range for output sensor noise  $N$ .

\* single-loop system :

$$T_n = \frac{X_2}{N} \approx \frac{-L}{p^a p^b} \quad (12)$$

\* 2-loop P.M. system :

$$T_n^2 = \frac{X_2}{N} \approx \frac{-L_o}{p^a p^b} \quad (13)$$

The details of numerical examples for single loop system, 2-loop NPM cascaded loops system and 3-loop P.M. system are enclosed in [4,6]. Here, one may ask, for a 2-section cascaded plant 2 loop system, why choose the P.M. system instead of NPM system. One of the reason is that only single sensor at  $C_1$  is available in a practical system. So the 2 loop NPM is not existed. On the other hand, both sensors are available, the noise power ratio (NPR)  $W_i$  is a good index to indicate which structure is suggested. The Noise Power Ratio (N.P.R)  $W_i$  is defined as the ratio of total noise power in the cascaded 2-loop non P.M. system to that a 2-loop P.M. system [5].

#### 5. SYSTEM STRUCTURE

The MIMO P.M. multiple loop system is shown in figure 18.

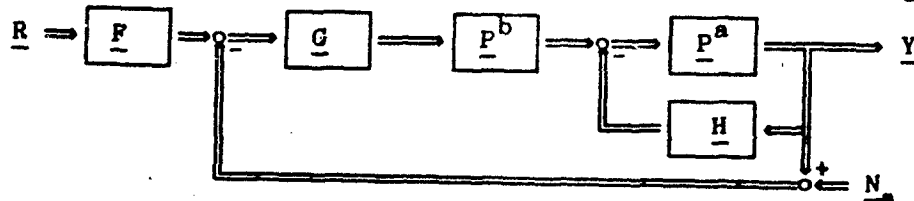
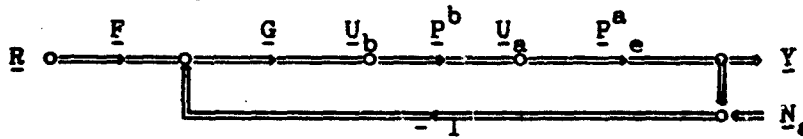


Fig. 18 2-loop MIMO P.M. structure



Concerning the uncertainties of plant  $\underline{P}^a$  is coped within two loops, the inner loop do very small contribution at h.f range. Hence the  $4|P_e^a|$  can not equal zero in the h.f range, so the UHWB region for outer loop  $L_o$  is not only depending on the variation of the  $P^b$  but also depending on  $4P_e^a$ .

## 7. NUMERICAL EXAMPLES

Plant :  $\underline{P} = \underline{P}^a \underline{P}^b$

$$\text{where } \underline{P}^a = \begin{bmatrix} \frac{k_{11}}{s} & \frac{k_{12}}{s+a} \\ \frac{k_{21}}{s} & \frac{k_{22}}{s+a} \end{bmatrix} ; \quad \underline{P}^b = \begin{bmatrix} \frac{m_{11}}{s+a} & \frac{m_{12}}{s+a} \\ \frac{m_{21}}{s} & \frac{m_{22}}{s} \end{bmatrix}$$

Plant uncertainties:  $1 \leq k_{11} \leq 3 ; .2 \leq k_{12} \leq .4$

$$.2 \leq k_{21} \leq .5 ; 2 \leq k_{22} \leq 3$$

$$1 \leq m_{11} \leq 2 ; .1 \leq m_{12} \leq .2$$

$$.1 \leq m_{21} \leq .5 ; .5 \leq m_{22} \leq 1$$

$$.1 \leq a \leq 2 ;$$

performance specification: the specification of  $t_{11}$  and  $t_{22}$

are shown in figure 2, and

$$|t_{12}(j\omega)| \leq -20 \text{ db}, |t_{21}(j\omega)| \leq -20 \text{ db}$$

Disturbance response :  $|\frac{L_i}{1+L_i}| = \gamma \leq 2.3 \text{ db}, i=1,2.$

Three case are considered:

(i) Single-loop MIMO system.

Example 2:

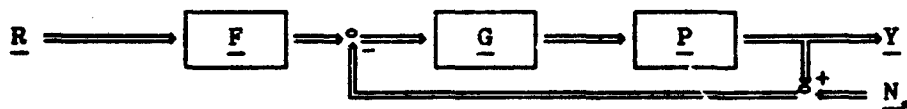


Fig. 21 MIMO feedback system

First, to find the  $\underline{Q}$  matrix depend on the plant  $\underline{P}$

$$\underline{Q} = \begin{bmatrix} \frac{B_{11}}{s(s+a)} & \frac{B_{12}}{s(s+a)} \\ \frac{B_{21}}{s(s+a)} & \frac{B_{22}}{s(s+a)} \end{bmatrix} = \begin{bmatrix} q_{11} & q_{12} \\ q_{21} & q_{22} \end{bmatrix}$$

where  $B_{11} = A/x_{22} ; B_{12} = A/x_{12} ; B_{21} = A/x_{21} ; B_{22} = A/x_{11} ;$

$$A = x_{11}x_{22} - x_{12}x_{21} ;$$

$$x_{11} = k_{11}m_{11} + k_{12}m_{21} ; x_{12} = k_{11}m_{12} + k_{12}m_{22} ;$$

$$x_{21} = k_{21}m_{11} + k_{22}m_{21} ; x_{22} = k_{21}m_{12} + k_{22}m_{22}.$$

The "basically non-interacting" (BNIC) loop will be builded in the  $t_{12}$  and  $t_{21}$ , and reject the unwanted output  $y_{12}$  and  $y_{21}$  due to the inputs  $r_2$  and  $r_1$ , so that,  $f_{12}$  and  $f_{21}$  are set to be zero. The  $L_1$  outer loop design:

There are two kinds of performance tolerancers. In the BNIC  $t_{ij}$  terms is denoted as a D-type specification, and the interacting  $t_{ij}$  terms are denoted as a A-type and B-type specifications.

There will obtain the specification in following :

$$D_{12} \text{ spec. : } \left| \frac{1}{1+L_1} \right| \leq \frac{b_{12}}{b_{22}} \left| \frac{q_{12}}{q_{11}} \right| = \frac{1}{10} \frac{q_{12}}{b_{22}} \left| \frac{q_{12}}{q_{11}} \right|$$

$$B_{11} \text{ spec. : } \left| \frac{1}{1+L_1} \right| \leq \frac{r_{d12}}{b_{21}} \left| \frac{q_{12}}{q_{11}} \right| = 10 r_{d12} \left| \frac{q_{12}}{q_{11}} \right|$$

$$A_{11} \text{ spec. : } \Delta \left| \frac{L_1}{1+L_1} \right| \leq \frac{b'_{11}}{a'_{11}}$$

For  $D_{12}$  specification, take the worst case, find  $\left| \frac{q_{12}}{q_{11}} \right|_{\min}$  with all others known elements, the D bounded can be plotted on the Nichol's Chart. Base on this result be able to find the value of  $r_{d12}$  and the A, B specifications can be solved, also,

plot the a,b bound on the Nichol's Chart, is shown in Fig. 22. Accordance A, B and D bounds to find the bounded of  $L_{10}$  and designed  $L_{10}$ , is shown in the figure 23(a). Similarity, we can find the bounds of  $L_{20}$  and designed  $L_{20}$  in figure 23(b). The system response of frequency domain in the figure 24. Therefore, those time responses of  $t_{11}$ ,  $t_{12}$ ,  $t_{21}$  and  $t_{22}$  will be bounded within the specification are shown in the figures 25. Finally, the sensor noise effect is express in the figure 26.

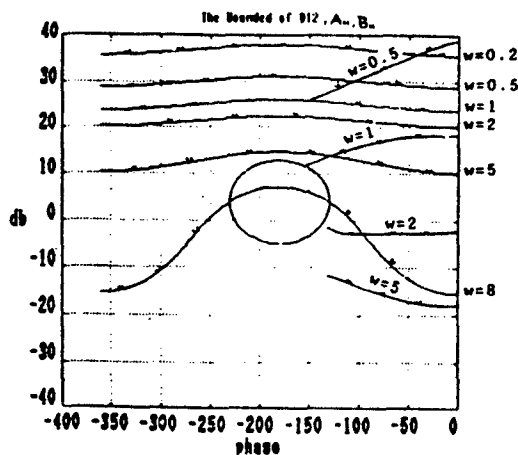


Fig. 22 The bounds of  $D_{12}$ ,  $A_{11}$  and  $B_{11}$



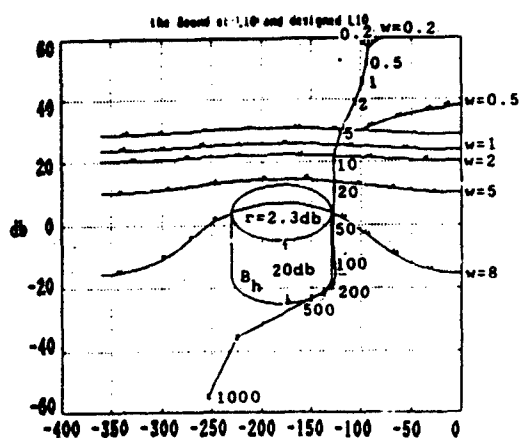


Fig. 23 (a) The bound of  $L_{1n}$  and design  $L_{1n}$

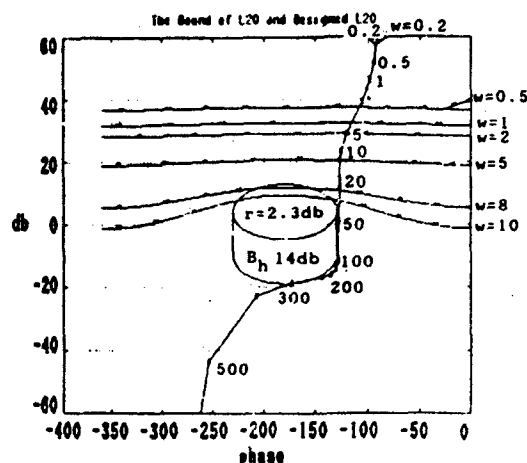


Fig. 23 (b) The bound of  $L_{2n}$  and design  $L_{2n}$

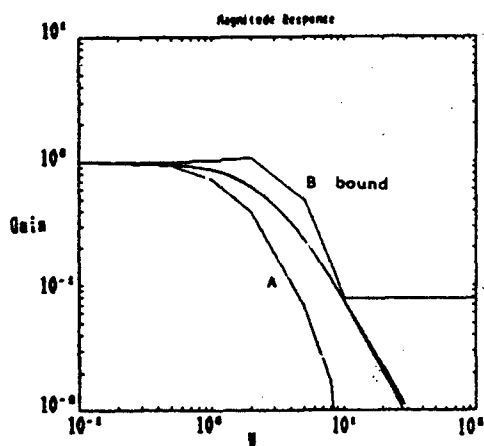


Fig. 24 (a) Frequency response for  $L_1$

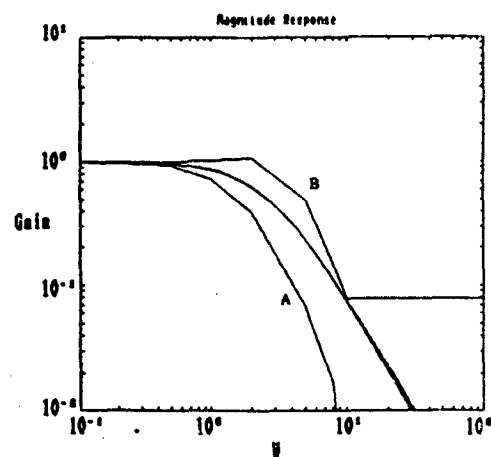


Fig. 24 (b) Frequency response for  $L_2$

99.04.14 - 10:26:14

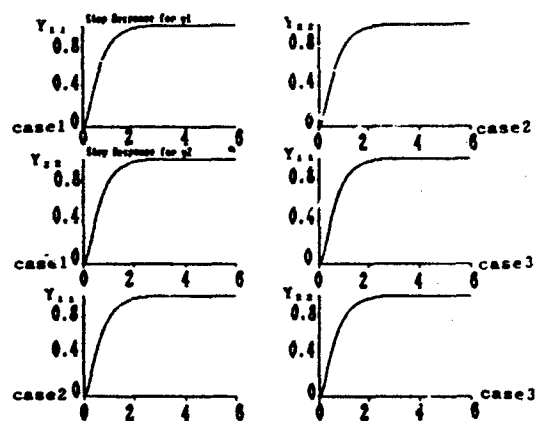


Fig. 25 (a) Step response for  $Y_{11}$  and  $Y_{22}$

99.04.15 - 02:48:30

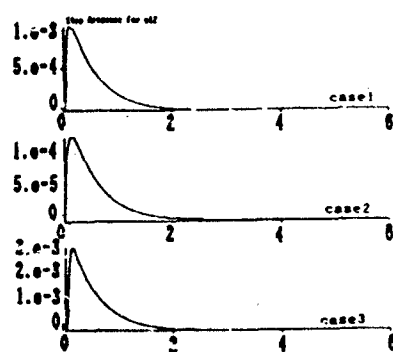


Fig. 25 (b) Step response for  $Y_{12}$

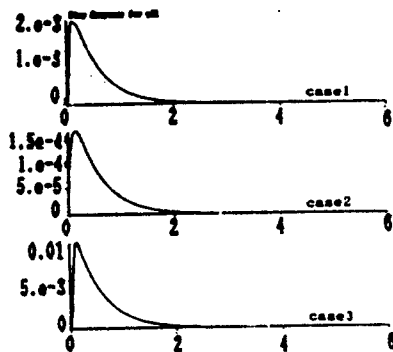


Fig. 25 (c) Step response for  $Y_{21}$

	$k_{11}$	$k_{12}$	$k_{21}$	$k_{22}$	$m_{11}$	$m_{12}$	$m_{21}$	$m_{22}$	$a$
Case 1	1	.2	.3	.2	1	.1	.1	.5	.1
Case 2	3	.2	.2	.3	2	.1	.1	1	.1
Case 3	1	.4	.5	.2	1	.2	.5	.5	2

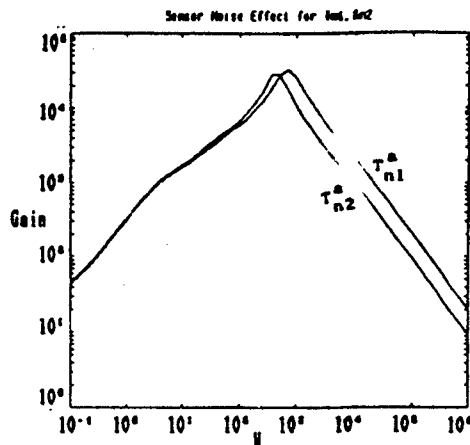


Fig. 26 Sensor noise

(ii) 2-loop non P.M. system  
Example 3:

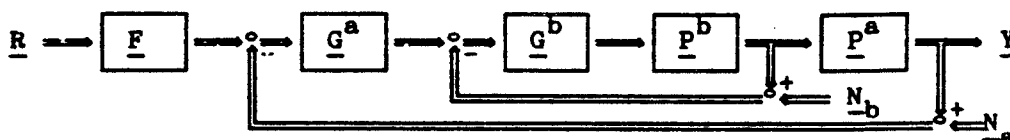


Fig. 27 2-loop MIMO feedback structure

A single loop design is used to demonstrate the advantage of multiple loop design. When design outer loop will remain 5 db safety margin for the bounded in the h.f range. The outer loop  $L_{10}$  and  $L_{20}$  will be designed that like to the case(i), where results are shown in figures 28 to 30. Details are in [12].

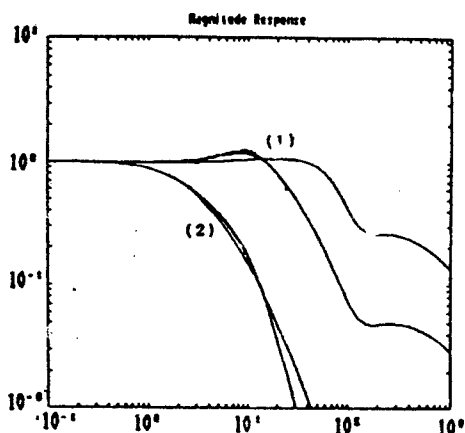


Fig. 28 (a) Frequency response of  $Y_{11}$   
(1) without prefilter  
(2) with prefilter

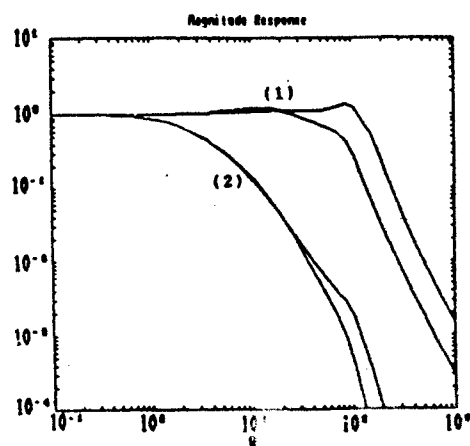


Fig. 28 (b) Frequency response of  $Y_{22}$   
(1) without prefilter  
(2) with prefilter

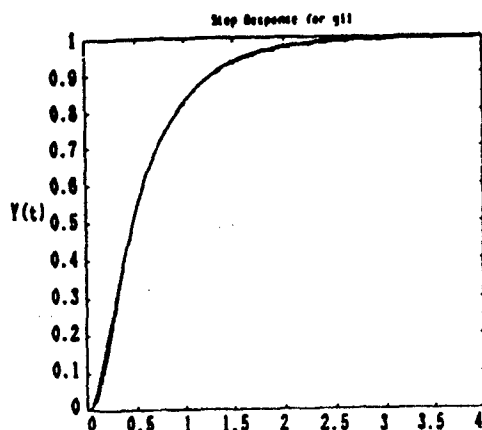


Fig. 29 (a) Step response for  $Y_{11}$

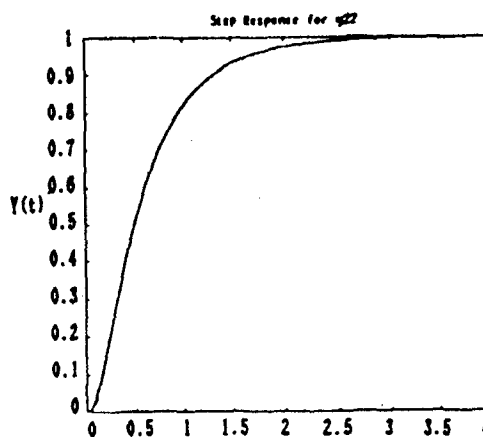


Fig. 29 (b) Step response for  $Y_{22}$

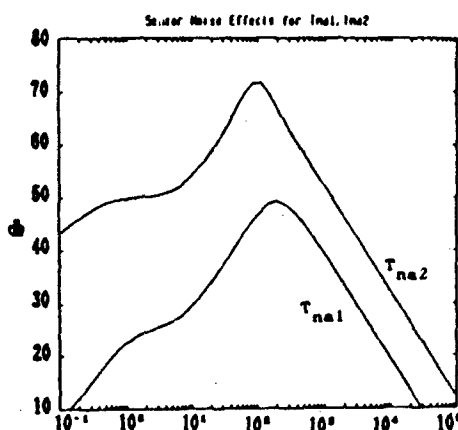


Fig. 30 (a) Sensor noise for  $N_a$

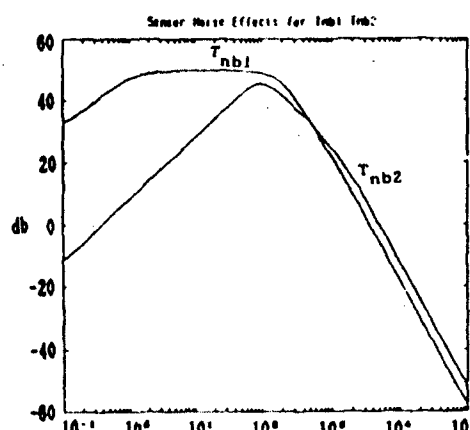


Fig. 30 (b) Sensor noise for  $N_b$

(iii) 2-loop P.M. MIMO system  
Example 4 : (figure 18)

Since here is a P.M. system, one more specification is required the restriction on signal level :  $Q \leq 1.05$  for unit step input. The design steps are shown in figures 31 to 33. Recover from  $Q$  matrix to  $P$  matrix structure, which system schematic detail present in figure 19, the really results in the system responses is in figure 34 by simulations. From figure 35 it will be found the steady state response of disturbance  $D$  input always converge to near zero, so this system will show the capability of disturbance rejection. The figures 36 and 37 are appear the relation of signal level variation ratio for loop 1 and loop 2. Base on the equation 11 to calculate the values of  $Q$ , that are 0.96 and 1.2. For a sensor noise problem, the effects of sensor noise is shown in figure 38, we will find that the 'cost of feedback' be reduced by P.M. loop, which is much economical than single loop system. Given a White - Noise at  $N$ , the responses at the plant inputs  $y_{12}$  and  $y_{22}$ , are shown in the figure 39. By inspection of figure 38, it is obviously that the noise response at h.f range is significantly reduced which is unanimous with figure 39.

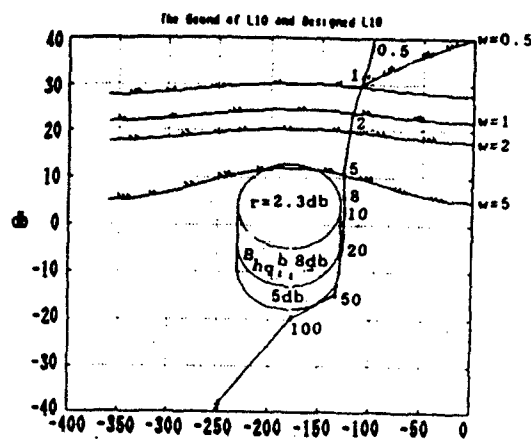


Fig. 31 (a) The bound of  $L_{1n}$  and design  $L_{1n}$

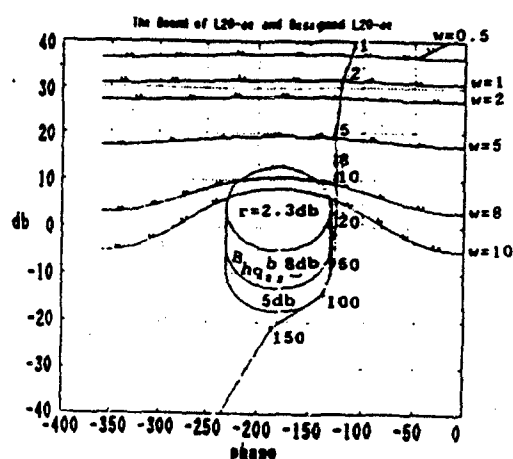


Fig. 31 (b) The bound of  $L_{2n}$  and design  $L_{2n}$

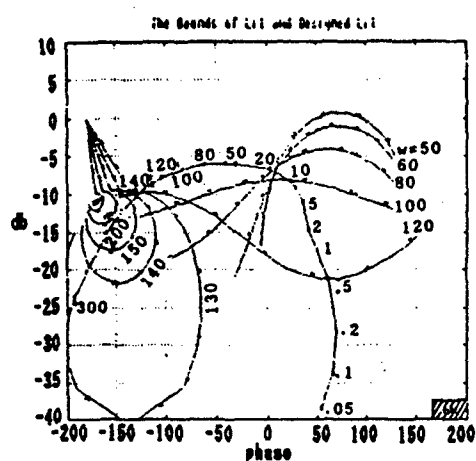


Fig. 32 (a) The bound of  $L_{1n}$  and design  $L_{1n}$

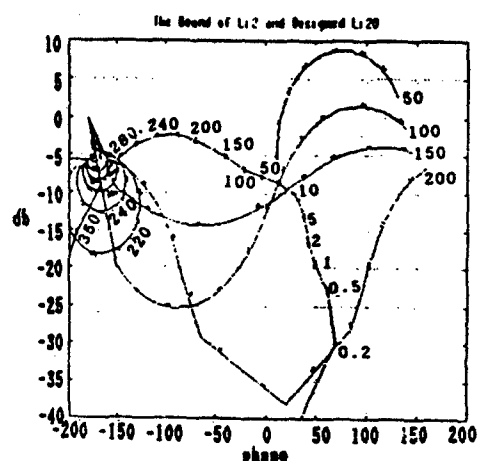


Fig. 32 (b) The bound of  $L_{2n}$  and design  $L_{2n}$

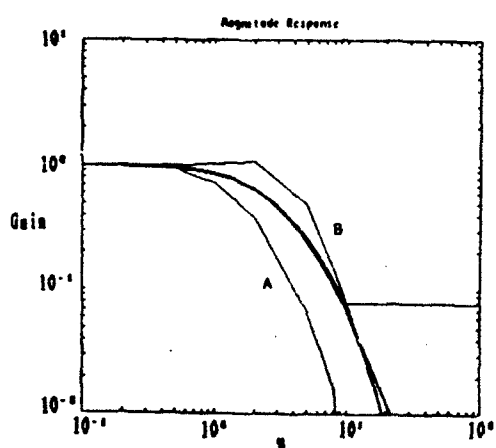


Fig. 33 (a) Frequency response for  $L_1$

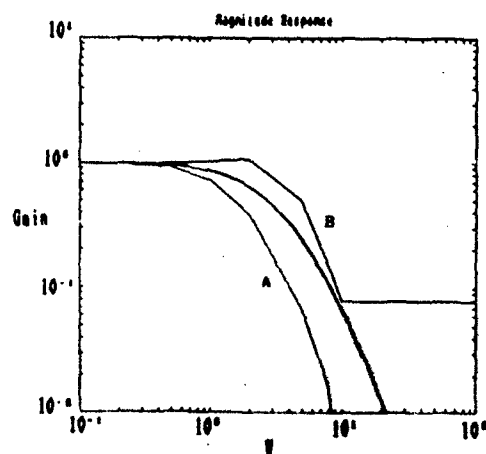


Fig. 33 (b) Frequency response for  $L_2$

00.03.20 - 00:47:36

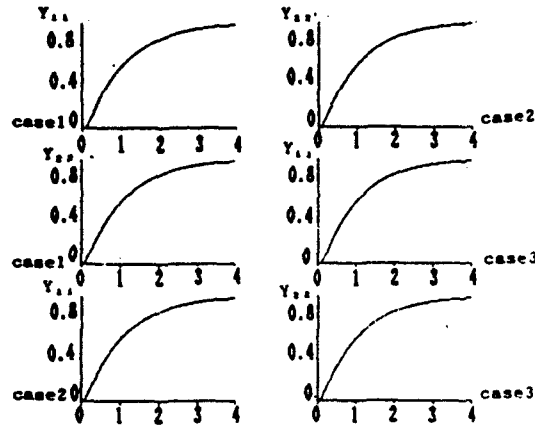


Fig. 34 (a) Step response for  $Y_{11}$  and  $Y_{22}$

00.03.20 - 00:37:37

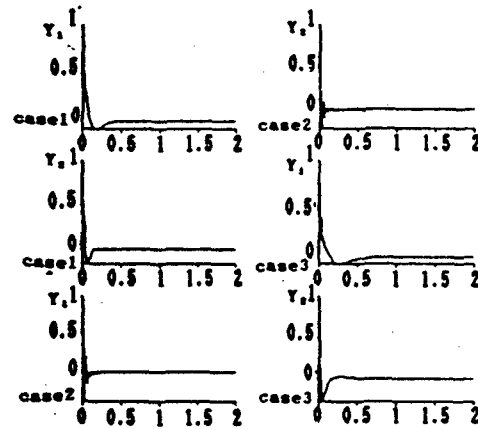


Fig. 35 Disturbance rejection response

00.00.20 - 10:41:16

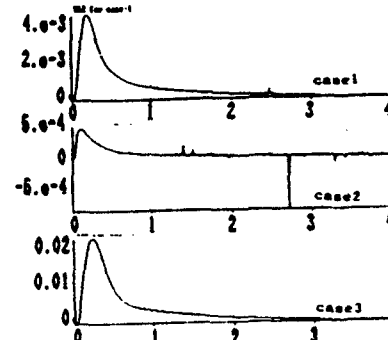


Fig. 34 (b) Step response for  $Y_{12}$

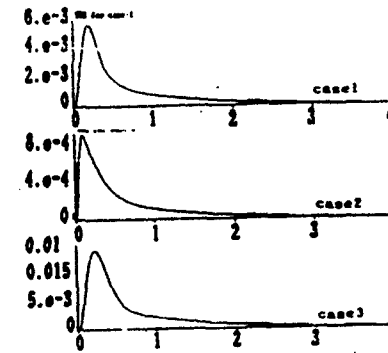


Fig. 34 (c) Step response for  $Y_{21}$

	$k_{11}$	$k_{12}$	$k_{21}$	$k_{22}$	$m_{11}$	$m_{12}$	$m_{21}$	$m_{22}$	$a$
Case 1	1	.2	.2	2	1	.1	.1	.5	.1
Case 2	3	.2	.2	3	2	.1	.1	.1	.1
Case 3	1	.4	.5	2	1	.2	.5	.5	2

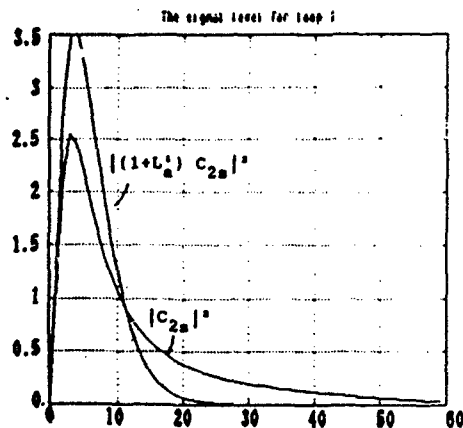


Fig. 36 The signal level for  $C_{2s}^1$  and  $C_{22}^1$

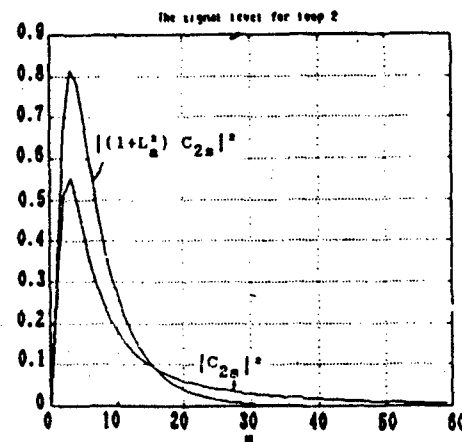


Fig. 37 The signal level for  $C_{2s}^2$  and  $C_{22}^2$

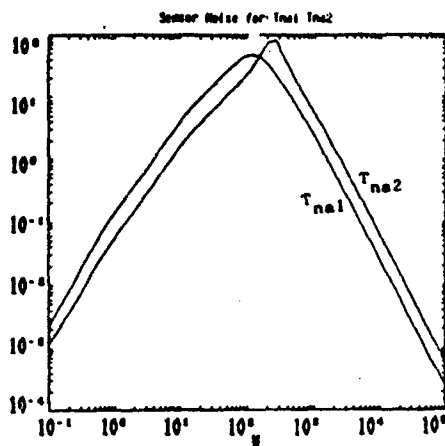


Fig. 38 (a) Sensor noise for  $N_a$

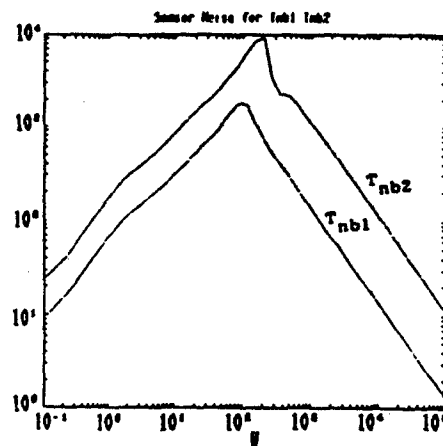


Fig. 38 (b) Sensor noise for  $N_b$

90.04.00 - 02:30:59

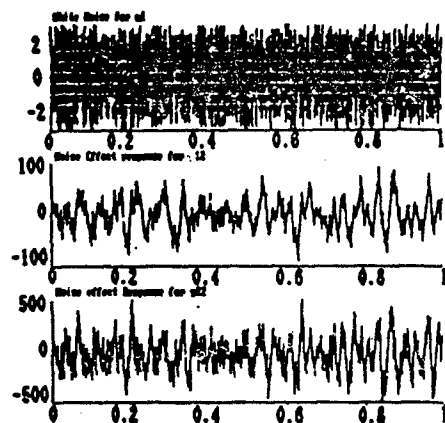


Fig. 39 Noise effect for plant input

## 8. CONCLUSIONS

The QFT synthesis method is the most effective tool for system design with large parameter uncertainties in the MIMO plant. For a multiple loop P.M. system, the feedback signal is able to feed back into intermediate point of the plant. In the QFT, P.M. MIMO synthesis process, we have the following conclusions:

- (1) The optimization of the design should be accomplished with respect to  $\alpha_i$  ( $i$  th loop overdensity) by trade-off between the outer ( $i$  th) loop and the inner  $((i-1)$  th) loop for a  $n$ -loop system.
- (2) The fixed point theorem will ensure the solution of equivalent MISO system satisfy the MIMO cascade  $m$ -loop system.
- (3) In this paper, we use equivalent single loops to design the system, produces overdensity in the second loop. If the improve method of MIMO is applied to the second loop, the overdensity may be improved. However the method of design may become complex in the MIMO multiple loop P.M. system.

- (4) The P.M. MIMO structure still permits greater reduction in the cost of feedback even consider the bandwidth increasing due to its signal level.
- (5) The signal level problem is important in P.M. design to prevent the saturation of the internal plant output.
- In summary the permission of adopting P.M. loop will largely increase the number of total loops in the overall system. So the cost of feedback can be largely reduced.

#### REFERENCE

- [1] Horowitz, I. and Sidi, M., 1973, Automatica, 9, 589.
- [2] Horowitz, I., Neumann, L. and Yaniv, O., 1985, Int. J. control, 42, 273.
- [3] Horowitz, I. and Sidi, M., 1980, Int. J. Systems Sci., 11, 851.
- [4] Horowitz, I. and Wang, B.C., 1979, Int. J. Control, 30, 837.
- [5] Wang, B.C., "Synthesis of multiple loop feedback system with plant modification", 1978, University of Colorado, ph. D. thesis.
- [6] Lee, W.L., "Application and improvement of a nonlinear element in plant modification synthesis", 1988, National Chiao Tung University, Master thesis.
- [7] Horowitz, I. and Yaniv, O., 1985, Int. J. Control, 42, 305.
- [8] Horowitz, I. and Wang, T.S., 1979, Int. J. Control, 29, 645.
- [9] Horowitz, I., 1982, Int. J. Control, 36, 977.
- [10] Horowitz, I., Neumann, L. and Yaniv, O., 1985, Int. J. Control, 42, 273.
- [11] Chen, C.M. and Wang, B.C., 1990, Control-Theory and Advanced Technology (Japan), 6, 257.
- [12] Lai, J.L., "A MIMO -P.M. system synthesis theory with plant uncertainties", 1990, National Chiao Tung University, Master thesis, Taiwan, R.O.C..

#### APPENDIX

##### Rational Function of Numerical Example

- (1) 2-loop P.M. SISO system: (example -1)

$$L_{on} = \frac{15 \times (s + 6)(s + 40) \times 40 \times 10000}{240}$$

$$L_{an} = \frac{s(s + 2)(s + 20)(s^2 + 50s + 10000)}{0.5 \times (s + 3)(30s + 1) \times 12000 \times 400}$$

$$F = \frac{12}{(s + 2)(s + 6)}$$

- (2) Single loop MIMO system: (example - 2)

$$L_{1n} = \frac{200 \times (s + 15)(s + 130) \times 250 \times 500000}{1950}$$

$$L_{2n} = \frac{s(s + 5)(s + 50)(s^2 + 600s + 500000)}{200 \times (s + 15)(s + 120) \times 250 \times 200000}$$

$$F_{11} = \frac{10}{(s + 2)(s + 5)}$$

$$F_{22} = \frac{8}{(s + 2)(s + 4)}$$

(3) 2-loop non P.M. MIMO system: (example - 3)

$$L_{1n}^{ae} = \frac{15 \times (s + 8) \times 40000}{s(s + 1)(s^2 + 320s + 40000)}$$

$$L_{2n}^{ae} = \frac{24 \times (s + 8) \times 10000}{s(s + 0.3)(s^2 + 100s + 10000)}$$

$$L_{1n}^b = \frac{10000 \times 1000}{(s^2 + 130s + 10000)(s + 1000)}$$

$$L_{2n}^b = \frac{10000 \times 1000}{(s^2 + 130s + 10000)(s + 1000)}$$

$$F_{11} = \frac{100}{(s + 2)(s + 5)(s + 10)}$$

$$F_{22} = \frac{100}{(s + 2)(s + 5)(s + 10)}$$

(4) 2-loop P.M. MIMO system: (example - 4)

$$L_{1n}^{ae} = \frac{(s + 6)(s + 40) \times 80666}{s(s + 2)(s + 40)(s^2 + 80s + 12100)}$$

$$L_{2n}^{ae} = \frac{(s + 6)(s + 40) \times 666667}{s(s + 2)(s + 20)(s^2 + 200s + 40000)}$$

$$L_{1n}^a = \frac{0.5 \times (s + 3)(30s + 1) \times 4800000}{(s + 9)(30s + 25)(s^2 + 150s + 16000)(s + 300)}$$

$$L_{2n}^a = \frac{0.5 \times (s + 3)(30s + 1) \times 60000 \times 500}{(s + 9)(30s + 25)(s^2 + 120s + 60000)(s + 500)}$$

$$F_{11} = \frac{100}{(s + 2)(s + 5)(s + 10)}$$

$$F_{22} = \frac{100}{(s + 2)(s + 5)(s + 10)}$$



# A MIMO UNCERTAIN SYSTEM WITH NONLINEAR COMPENSATOR

Ruey-Chung Chu\*

Bor-Chyun Wang\*\*

## ABSTRACT

The quantitative feedback theory(QFT) design technique has been successfully applied to solve the multiple-input multiple-output(MIMO) uncertainty problem. But there is no any literature studying how to apply special compensator to reduce the cost of feedback in the MIMO design approach. In MIMO uncertain system design, although the improved method can reduce the inherent overdesign, but the cost of feedback (COF) is still high in case of a large uncertain plant. In this paper, a nonlinear element called "Clegg Integrator" (CI) is introduced as part of the compensator in the design. It is concluded that the "cost of feedback", i.e. effect of sensor noise, is further improved.

Four types of structure with C.I. element placed in different location are used to illustrate and to compare the quantitative improvement of the COF by numerical examples. The result gives the control designer a more flexible choice in the MIMO system.

## 1 Introduction

There is an equipment which has the ability to achieve objectives. It is denoted as the plant. Here, the values of plant parameters are not known precisely, but the ranges of their values are known. In 1972, I. M. Horowitz and M. Sidi [1] have presented a design method — QFT to solve the single (or multiple) - input single - output( SISO or MISO ) single loop system (Fig.1). A MIMO system [4] can be designed by a set of MISO equivalent single loop systems with a similar structure as in Figure 1.

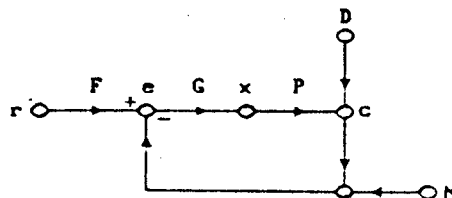


Figure 1. A two-degree-of-freedom structure.

\* Dept. of Control Eng. , National Chiao - Tung University , Taiwan, Republic of China.

\*\* Chung - Shan Institute of Science and Technology , Taiwan , Republic of China.

This paper is devoted to find controllers and prefil-  
ters to statisfy assigned performance tolerances in a MIMO  
system. The design approach for each loop of the MIMO system  
is identical to that for the MISO single loop approach. By  
using Schauder's fixed point theory [4], an uncertain MIMO  
problem can be converted into separated single-loop problems.  
The solutions to these single-loop problems are guaranteed to  
solve the original MIMO problem. The COF in MIMO system is a  
very important factor to indicate the goodness of the closed  
loop design. For a large parameter variation plant, the COF  
usually high, so the sensor noise effect is seriouise. Sometim-  
es the COF is so large, it even saturating the input signal at  
the plant input, so the overall system fail to operate. The  
Clegg Integrator (CI), can effectively reduce the COF in SISO  
[2] and PM [9] system. Therefore, in this paper, the nonlinear  
compensator is first tried to improve the COF in a MIMO sys-  
tem. It is successful to develop a step by step design method  
for a nonlinear compensator in the MIMO uncertain system. It  
is also proved that it can effectively reduce the COF. Since  
the frequency response method is not applicable for a system  
containing nonlinear element, so in this paper, the real time  
simulation is adpoted to prove the design result. In the foll-  
owing paragraph, both MIMO old [4] and improved [7] methods  
are considered.

A quick review of the QFT is in section 2. Section 3  
presents the characteristic of a C.I. element. Section 4 illu-  
strates the structure of systems which are discussed in this  
paper. The synthesis of MIMO system by nonlinear compensator  
is shown in section 5. For the purpose of easy comparison, the  
same numerical example in section 2 is used in the MIMO NL  
design for each structure. Conclusions and discussion are in-  
cluded in section 7. Finally, rational functions of numerical  
examples are listed in the appendix.

## 2. Review of QFT in MIMO System

### 2.1 MIMO Compensation

The basic MIMO compensation structure for a  $2 \times 2$  MIMO  
system is shown in Figure 2, where  $\underline{P}$  is the uncertain plant  
matrix,  $\underline{G}$  is a diagonal compensator matrix, and  $\underline{F}$  is

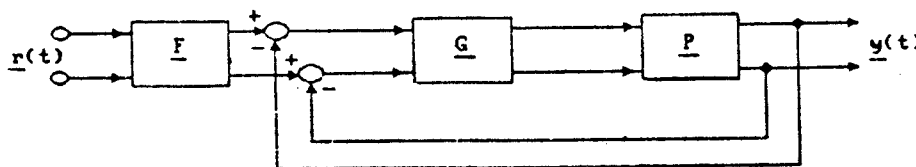


Figure 2 MIMO control structure ( $2 \times 2$  system).

a prefilter matrix. The non-diagonal  $\underline{G}$  is not considered in this paper. These matrices are defined as follows:

$$\underline{P} = \begin{bmatrix} p_{11} & p_{12} \\ p_{21} & p_{22} \end{bmatrix}, \quad \underline{G} = \begin{bmatrix} g_1 & 0 \\ 0 & g_2 \end{bmatrix},$$

$$\underline{F} = \begin{bmatrix} f_{11} & f_{12} \\ f_{21} & f_{22} \end{bmatrix}. \quad (2-1)$$

The signal flow graph of a 2x2 MIMO system is shown in Figure 3. There are four closed-loop system transfer functions  $t_{ij}(s)$  relating the output  $y_i(s)$  to the input  $r_j(s)$ , i.e.,  $y_i(s) = t_{ij}(s)r_j(s)$ . Therefore, there are also four sets of acceptable regions  $\tau_{ij}(s)$ . If we design the compensator matrix  $\underline{G}$ , and the prefilter matrix  $\underline{F}$  according to these bounds, then  $t_{ij}(s) \in \tau_{ij}(s)$ .

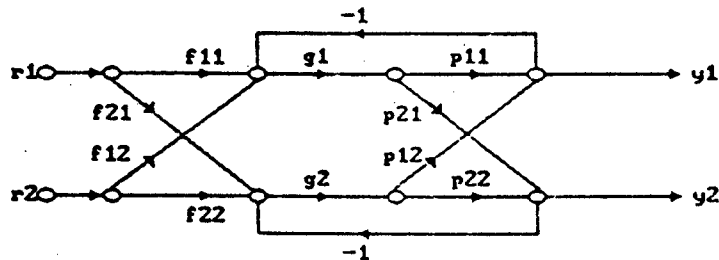


Figure 3 Two-by-two MIMO system scheme.

From Figure 2, the system control ratio relating  $\underline{y}$  to  $\underline{r}$  is,

$$\underline{T} = [\underline{I} + \underline{P}\underline{G}]^{-1} \underline{P}\underline{G}\underline{F}. \quad (2-2)$$

If  $\underline{P}$  is nonsingular, let

$$\underline{P}^{-1} = \begin{bmatrix} p_{11}^* & p_{12}^* \\ p_{21}^* & p_{22}^* \end{bmatrix}. \quad (2-3)$$

The four effective plant transfer functions are formed as

$$q_{ij} \equiv 1/p_{ij}^* = \det \underline{P} / \text{Adj } \underline{P}. \quad (2-4)$$

We obtain the following equations for a unit impulse input,

$$y_{11} = \frac{q_{11}}{1 + g_1 q_{11}} (g_1 f_{11} - \frac{t_{21}}{q_{12}}), \quad (2-5a)$$

$$y_{12} = \frac{q_{11}}{1 + g_1 q_{11}} (g_1 f_{12} - \frac{t_{22}}{q_{12}}), \quad (2-5b)$$

$$y_{21} = \frac{q_{22}}{1 + g_2 q_{22}} (g_2 f_{21} - \frac{t_{11}}{q_{21}}), \quad (2-5c)$$

$$y_{22} = \frac{q_{22}}{1+g_2 q_{22}} (g_2 f_{22} - \frac{t_{12}}{q_{21}}) . \quad (2-5d)$$

Figure 4 shows the four equivalent MISO loops.

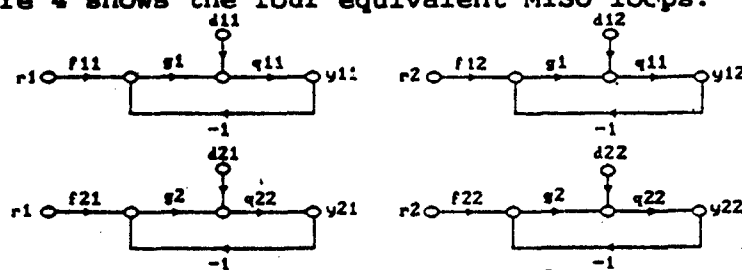


Figure 4 Effective MISO loops.

If all of these MISO problem are solved, there exists a fixed point, then  $y_{ij}(s)$  may be replaced by a  $t_{ij}(s)$ . We can rewrite the above expressions as,

$$t_{ij} = t_{rj} + t_{d_{ij}} , \quad (2-6)$$

where

$$t_{rj} = f_{ij} \frac{L_1}{1+L_1} , \quad (2-7)$$

$$t_{d_{ij}} = \frac{q_{11} d_{ij}}{1+L_1} , \quad (2-8)$$

$$L_1 = g_1 q_{11} . \quad (2-9)$$

When the response of an output,  $y_i$ , due to an input,  $r_j$ , is ideally zero, then the  $y_{ij}$  loop is called a basically non-interacting (BNIC) loop. The design specification of BNIC loop is

$$|1/(1+L_1)| \leq |b_{ij}/q_{11} d_{ij}| = \frac{b_{ij}}{\left| \frac{q_{11}}{q_{1k}} \right| b_{kj}} , \quad k \neq i, \quad (2-10)$$

and it is denoted as a D-type specification, specifically  $D_{ij}$ .

The specification on the interacting loop is

$$a_{ij}(w) \leq |t_{rj}(jw) + t_{d_{ij}}(jw)| \leq b_{ij}(w) , \quad (2-11)$$

where  $a_{ij}(w)$  and  $b_{ij}(w)$  are the lower and upper bounds of the design specifications for the interacting loop. We obtain A-type and B-type specifications.

$$A \quad |L_1/(1+L_1)| \leq b'_{ij}/a'_{ij} , \quad (2-12)$$

$$|1/(1+L_1)| \leq \frac{r_{d_{ij}}}{\left| \frac{q_{11}}{q_{1k}} \right| b_{kj}} , \quad k \neq i . \quad (2-13)$$

Equation ( 2-12 ) is denoted as  $A_{ij}$ , and equation ( 2-13 ) is

denoted as  $B_{1j}$ .  $B_{1j}$  is almost the same as  $D_{1j}$  except that  $\tau_{d_{1j}}$  is not known.

Equilibrium exists when it is impossible to reduce the burden on any  $L_1$ , without increasing it on some other  $L_j$ . This results in only one column of the equivalent MISO systems being dominant. Note that the above discussion is at a fixed  $w$  value. It may be that there are different columns dominating at different  $w$  values. However, after equilibrium is reached, it may be desirable to sacrifice one loop for the sake of another. This involves "tradeoffs" between the different loops. These tradeoffs always make it harder on one loop when reduction is accomplished in another.

## 2.2. Improved Design Technique

The improved design technique can reduce the inherent overdesign. Since the old method in section 2.1 does not consider the correlation between the  $t_{1j}$  of the system, but it is considered when the improved method is used to design the second and subsequent loop.

Assume that loop one has been designed by using the method one. Thus  $L_1$  and  $f_{1j}$  are given, and general equations are shown as,

$$t_{1j} = \frac{f_{1j}L_1 + d_{1j}q_{11}}{1 + L_1}, \quad (2-14)$$

$$t_{2j} = \frac{f_{2j}L_2 + d_{2j}q_{22}}{1 + L_2}, \quad (2-15)$$

$$\text{where } L_1 = g_1q_{11}, \quad L_2 = g_2q_{22}, \quad (2-16 \text{ a,b})$$

$$d_{1j} = -t_{2j}/q_{12}, \quad d_{2j} = -t_{1j}/q_{21}, \quad j=1,2. \quad (2-17 \text{ a,b})$$

Substituting equation (2-14) into equation (2-15) yields,

$$t_{2j} = \frac{f_{2j}L_{2e} + d_{2je}}{1 + L_{2e}}, \quad (2-18)$$

where

$$L_{2e} = \frac{g_2q_{22}(1 + L_1)}{1 - \tau_{12} + L_1} = g_2q_{22e}, \quad (2-19)$$

$$\tau_{12} = \frac{p_{12}p_{21}}{p_{11}p_{22}} = \frac{q_{11}q_{22}}{q_{12}q_{21}}, \quad (2-20)$$

$$q_{22e} = \frac{q_{22}(1 + L_1)}{1 - \tau_{12} + L_1}, \quad (2-21)$$

$$d_{2je} = \frac{g_1f_{1j}p_{21}(1 - \tau_{12})}{1 - \tau_{12} + L_1}. \quad (2-22)$$

Using equation (2-18) through equation (2-22), the elements  $L_{2e}$  and  $f_{2j}$  can be designed to meet the desired tolerances.

### 3. Nonlinear Compensation

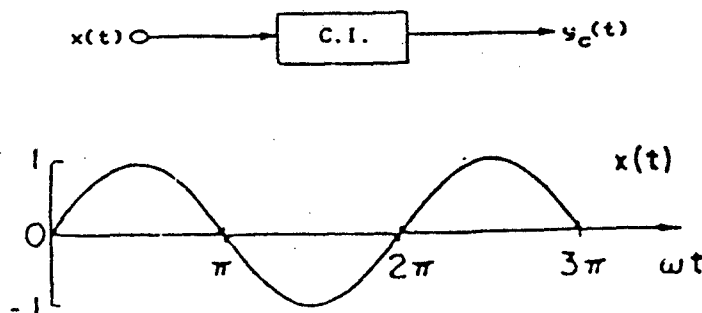
#### 3.1 Introduction of the Clegg Integrator

The crucial limiting factor in linear design is that the rate of attenuation of  $|L|$  can not be increased due to fixed magnitude - phase relationship, so that  $|L| > |P|$  over a large frequency range, in problems with large uncertainty in the plant high-frequency gain factor.

One is led to consider the use of a nonlinear element whose describing function  $D(j\omega)$  has a smaller phase lag than that of a linear element with the same magnitude characteristic. Such an element as part of  $L$  would seem to permit a faster attenuation of the nonlinear  $|L_d(j\omega)|$  than is possible in a linear  $|L(j\omega)|$ . The Clegg Integrator is an integrator which resets to zero at zero crossing of the input, and is an ordinary integrator between zero crossings. Its response to a sinusoidal input is shown in Figure 5 with the describing function,

$$D(j\omega) = \frac{1.62 \exp(-j38^\circ)}{\omega} = \left(\frac{1.62}{j\omega}\right) \exp(j52^\circ). \quad (3-1)$$

$D(j\omega)$  has the same magnitude characteristic as an integrator of gain 1.62, but its phase lag, at all frequencies, is  $52^\circ$  less than that of the linear integrator. Hence, it appears that the equivalent  $|L(j\omega)|$  containing the C.I., may be decreased at a rate  $(180 - \theta_m + 52)/(180 - \theta_m)$  faster than that of a purely linear  $L(j\omega)$ , where  $\theta_m$  is the phasemargin of system.



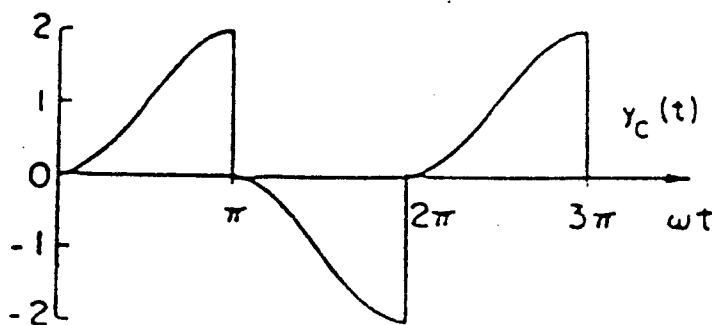


Figure 5 Sinusoidal response of Clegg Integrator.

### 3.2 Characterization of C.I. for Synthesis Purpose

It is difficult that characterization of the non-linear element is directly used for quantitative synthesis. Thus, a general characterization must be derived for quantitative synthesis.

Let  $0 < t_1 < t_2 < \dots < t_n$  be the zero crossings of  $x(t)$ , the input to the C.I. . Then  $y_C(t)$ , the output of the C.I. , with  $t_0=0$ , is

$$y_C(t) = \int_{t_1}^t x(\tau) d\tau = \int_0^t x(\tau) d\tau - \sum_{k=1}^1 \int_{t_{k-1}}^{t_k} x(\tau) d\tau, \quad (3-2)$$

where

$$t_1 \leq t < t_{i+1}, \quad i=0,1,\dots,n-1, \quad t_0=0.$$

However,

$$y_C(t_{k-}) = \int_{t_{k-1}}^{t_k} x(\tau) d\tau \equiv y_k. \quad (3-3)$$

Hence,

$$y_C(t) = \int_0^t [x(\tau) - \sum_{k=1}^1 y_k \delta(\tau - t_k)] d\tau. \quad (3-4)$$

valid for the entire interval, and assuming that the last zero crossing is at  $t_n$ . Thus the C.I. can be replaced by a linear integrator and a train of impulses as an additional input, the strength of the impulse at  $t_{k+}$  being obtained from the output of the C.I. at  $t_{k-}$ . The equivalent representation of C.I. is shown in Figure 6.

The above representation is suitable for analysis, but the real problem is to exploit it for synthesis. Hence it is necessary to turn to specific problem classes, that of step response being considered in this paper, and replacing G

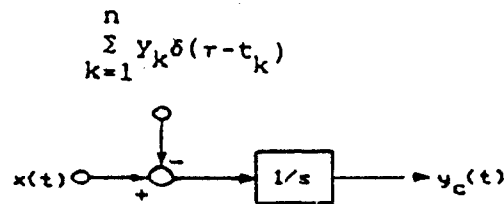


Figure 6 Equivalent representation of C.I. .

of Figure 1 by Figure 7, with F temporarily taken as 1.

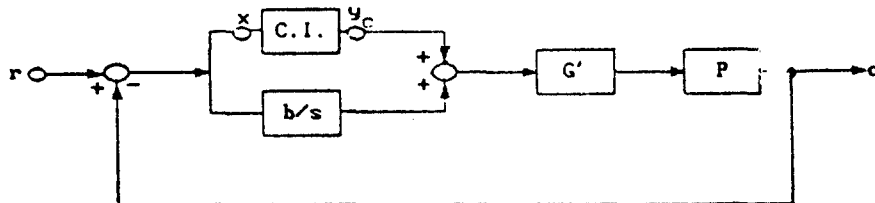


Figure 7 A nonlinear compensation control system.

Now, we consider a typical linear system which is shown in Figure 8, and its step response  $c_o(t)$  with overshoot is shown in Figure 9. When  $x=0$ ,  $c=c_o$ , and the system transfer function is given by,

$$T(s) = \frac{C_o(s)}{R(s)} = \frac{w_n^2}{s^2 + 2\xi w_n s + w_n^2} \quad (3-5)$$

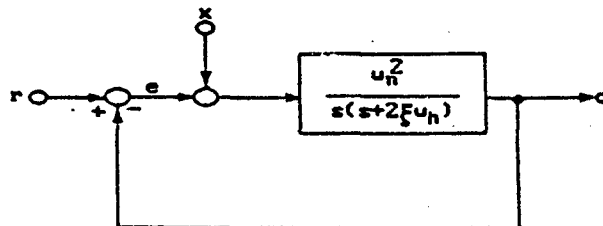


Figure 8 Second - order model.

If  $r(t) = u(t)$ , then

$$c_o(t) = 1 - \exp(-\xi w_n t) \left[ \cos(w_n \sqrt{1 - \xi^2} t) + \frac{\xi}{\sqrt{1 - \xi^2}} \sin(w_n \sqrt{1 - \xi^2} t) \right] \quad (3-6)$$

Assume  $c_o(t) = 1$  when  $t = t_1$ , then  $e(t) = r(t) - c_o(t) = 0$ . The first



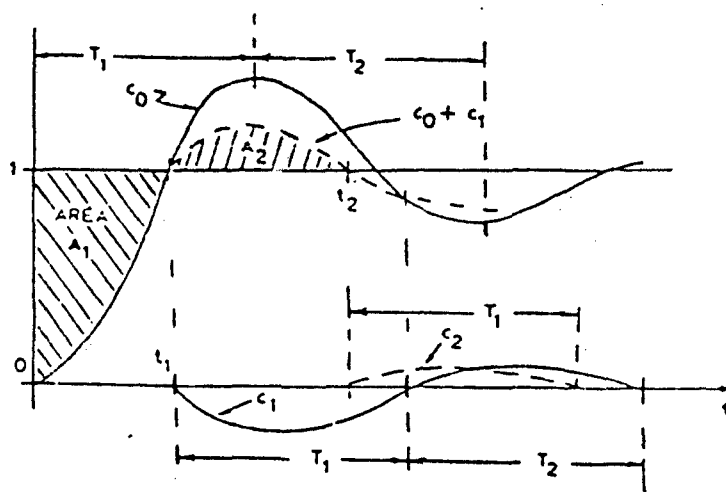


Figure 9 Derivation of nonlinear step response from that of equivalent linear system.

reset of C.I. occurs at  $t_1$ . From equation (3-6), we obtain

$$t_1 = \frac{\pi - \cos^{-1} \xi}{w_n \sqrt{1 - \xi^2}} \quad (3-7)$$

Assume that the maximum overshoot of  $c_0(t)$  occurs at  $t_m$ , so

$$\dot{c}_0(t_m) = 0 \Rightarrow t_m = \frac{\pi}{w_n \sqrt{1 - \xi^2}} \quad (3-8)$$

The area  $A_1$  is given by,

$$A_1 = \int_0^{t_1} [1 - c_0(t)] dt = \frac{1}{w_n} \exp(-\xi(\pi - \cos^{-1} \xi) / \sqrt{1 - \xi^2}) \times [1 + 2\xi \exp(\xi(\pi - \cos^{-1} \xi) / \sqrt{1 - \xi^2})] \quad (3-9)$$

The system output response to a unit impulse at a point  $x$  in Figure 7 is simply  $c_1 = -T/(1+b)$ . Now,  $x(t) = A_1 \delta(t - t_1)$ , so  $c_1 = -[A_1 T/(1+b)] \delta(t - t_1)$ .

Hence

$$\begin{aligned} -\frac{b+1}{A_1} c_1 &= \mathcal{L}^{-1} \left[ \frac{w_n^2}{s^2 + 2\xi w_n s + w_n^2} \right] \\ &= \frac{w_n}{\sqrt{1 - \xi^2}} \exp(-\xi w_n t) \sin(w_n \sqrt{1 - \xi^2} t) \quad (3-10) \end{aligned}$$

Substituting equations (3-7, 8) into equation (3-10), we obtain  $c_1(t_m - t_1)$

$$= -\frac{1}{b+1} \exp(-\xi \pi / \sqrt{1 - \xi^2}) [1 + 2\xi \exp(\xi(\pi - \cos^{-1} \xi) / \sqrt{1 - \xi^2})] \quad (3-11)$$

Substituting equation (3-8) into equation (3-6), we obtain

$$c_o(t_m) = 1 + \exp(-\xi\pi/\sqrt{1-\xi^2}) . \quad (3-12)$$

The maximum overshoot is found to be,

$$\begin{aligned} M_n(\xi, b) &= c_o(t_m) + c_1(t_m - t_1) - 1 \\ &= \frac{1}{b+1} \exp(-\xi\pi/\sqrt{1-\xi^2}) \{b - 2\xi \exp[\xi(\pi - \cos^{-1}\xi)/\sqrt{1-\xi^2}]\} \\ &= \{b - 2\xi \exp[\xi(\pi - \cos^{-1}\xi)/\sqrt{1-\xi^2}]\} \frac{M_1}{1+b} , \end{aligned} \quad (3-13)$$

where

$$M_1 = \exp(-\pi\xi/\sqrt{1-\xi^2}) , \quad (3-14)$$

is the maximum overshoot in the linear design with same value of  $\xi$ , and  $1/s$  in place of the C.I. .

It is seen from equation (3-13) that the nonlinear step response is actually improved if the associated linear response has significant overshoot. On the other hand, if there is no overshoot on the step response, there is no reset action at all and the nonlinear response is identical with the linear. If the linear response has only small overshoot which causes reset, so the resulting  $c_1$  then dominates between  $t_1$  and  $t_2$ , causing undershoot. Clearly, the worst case is for a critically damped step response, and using the second - order response function as a model the value of  $A_1$  is found to be  $2/w_n$ , if  $w_n$  is the natural frequency. Hence, equation (3-10) becomes,

$$-\frac{b+1}{A_1} c_1 = \mathcal{L}^{-1} \left[ \frac{w_n^2}{(s + w_n)^2} \right] = w_n^2 t \exp(-w_n t) . \quad (3-15)$$

Premultiplying both sides of equation (3-15) by  $A_1/(b+1)$  yields,

$$c_1 = \frac{-2w_n t}{b+1} \exp(-w_n t) . \quad (3-16)$$

We would like to find a maximum value of  $c_1$ , so let  $\dot{c}_1(t_x) = 0$ . It is easy to obtain  $t_x = 1/w_n$ , and to substitute it into equation (3-16), so  $|c_1|_{\max} = 0.736/(b+1)$ . Hence the peak undershoot is,

$$u_p = \frac{0.736}{b+1} . \quad (3-17)$$

Hence,  $b$  must be chosen such that the undershoot satisfies the system tolerances. Such a tolerance on undershoot becomes a necessary part of the design specifications for nonlinear design. In practice,  $F$  being low-pass which can decrease undershoot because the area  $A_1$  in Figure 9 is decreased such that  $c_1$  is decreased also.

#### 4. Structure of the System

The MIMO system is shown in Fig. 10, where  $p_{ij}$  is the element of the uncertainty plant matrix  $P$ ,  $f_{11}$  and  $f_{22}$  are prefilters and  $g_1$ ,  $g_2$  are compensators.  $d_1$ ,  $d_2$  are step-disturbance inputs and  $N_1$ ,  $N_2$  are white-noise inputs. In this paper, compensators are not limited to be linear. There are four cases: (1) both  $g_1$  and  $g_2$  are linear designs, (2)  $g_1$  is nonlinear design and  $g_2$  is linear design, (3) both  $g_1$  and  $g_2$  are nonlinear designs, (4)  $g_1$  is linear design and  $g_2$  is nonlinear design. Their results are shown in section 5 and section 6 respectively.

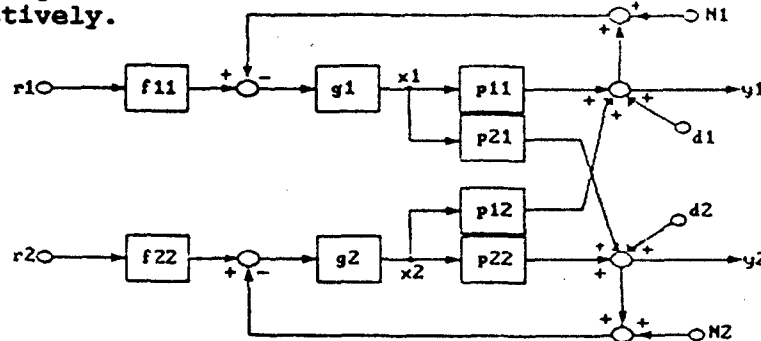


Figure 10 Block diagram of linear system.

#### 5. Synthesis of the MIMO System by Nonlinear Compensator

Take example 1 from section 6 to explain the design technique by using C.I. element for MIMO control system. The loop two is designed by using the improved method.

From equations (3-13, 14), we know the overshoot in the nonlinear system with a C.I. element is less than in the equivalent linear system. The value of  $f_{n1}$  (non-linear) can therefore be smaller than that of  $f_1$  (linear) for the same overshoot  $M_n = M_1$  of equations (3-13, 14). We obtain

$$\gamma = \max_w \left| \frac{w_n^2}{(w_n^2 - w^2) + j2f_w w} \right| \text{ from equation (3-5) and } |L/(1+L)| \leq \gamma.$$

Let  $d\gamma/dw$  be zero, then  $w = w_n(1 - 2f^2)^{1/2}$ ,

hence,

$$\gamma = \frac{1}{2F\sqrt{1-F^2}} \quad (3-18)$$

We use equations (3-13,14) to find  $f_{n1}$  and substitute it into equation (3-18) to find  $\gamma_{n1}$ . Hence  $\gamma_{n1}$  can be larger than  $\gamma_1$  of an equivalent linear design, so that  $\theta_m(\text{linear}) > \theta_m(\text{non-linear})$ , where  $\theta_m$  is the phase margin of system.

Since,

$$M_1 = \exp(-\pi F / \sqrt{1-F^2}) = 17\%.$$

and,

maximum undershoot = 20% = 0.736/(1+b),  
so we obtain  $f_1=0.5$  and  $b=2.7$ . Substituting these values into equation (3-13), we obtain  $f_{n1} = 0.3$ . From equation(3-18), we obtain  $\gamma_{n1} = 5\text{dB}$ . The specification of disturbance response becomes  $|L_1/(1+L_1)| \leq 5 \text{ dB}$ .

The design procedures are as follows:

- Step.1. : Find bounds on  $L_{1no} = g_{1n}q_{11o}$  to satisfy the performance specifications and the disturbance specification  $\left| \frac{L_{1n}}{1+L_{1n}} \right| \leq 5 \text{ dB}$ .
- Step.2. : Design the loop transmission function  $L_{1no}$ , as shown in Figure 12.
- Step.3. : Design the prefilter  $f_{11n}$  by shaping the frequency response of  $\left| \frac{L_{1n}}{1+L_{1n}} \right|$  to satisfy the specification, as shown in Figure 13.
- Step.4. : Find bounds on  $L_{2eno} = g_{2n}q_{22eno}$  to satisfy the performance specifications and the disturbance response  $\left| \frac{L_{2en}}{1+L_{2en}} \right| \leq 2.3 \text{ dB}$ .
- Step.5. : Design the loop transmission function  $L_{2eno}$ , as shown in Figure 14.
- Step.6. : Design the prefilter  $f_{22n}$  such that the frequency response of  $\left| \frac{f_{22n}L_{2en}}{1+L_{2en}} \right|$  meets the specification, as shown in Figure 15.

## 6. Numerical Examples

### Example 1.

All parameters and specifications are the same for examples 1-4 except maximum overshoot and maximum undershoot specifications are useful at examples 1, 3 and 4.

Plant :

$$P = P_2 P_1 = \begin{bmatrix} P_{11} & P_{12} \\ P_{21} & P_{22} \end{bmatrix},$$

$$P_1 = \begin{bmatrix} \frac{M_{11}}{s+a} & \frac{M_{12}}{s+a} \\ \frac{M_{21}}{s} & \frac{M_{22}}{s} \end{bmatrix}, \quad P_2 = \begin{bmatrix} \frac{K_{11}}{s} & \frac{K_{12}}{s+a} \\ \frac{K_{21}}{s} & \frac{K_{22}}{s+a} \end{bmatrix}.$$

Plant uncertainty :  $0.1 \leq a \leq 2$ ,  $1.4 \leq K_{11} \leq 2$ ,  
 $0.2 \leq K_{12} \leq 0.4$ ,  $0.2 \leq K_{21} \leq 0.3$   
 $1.96 \leq K_{22} \leq 2$ ,  $0.7 \leq M_{11} \leq 2$   
 $0.1 \leq M_{12} \leq 0.2$ ,  $0.1 \leq M_{21} \leq 0.2$   
 $0.5 \leq M_{22} \leq 1$

Performance specifications : the specifications of time domain and frequency domain on  $|t_{11}(j\omega)|$  and  $|t_{22}(j\omega)|$  are shown in Figure 2.1,  $|t_{12}(j\omega)| \leq -20\text{dB}$ , and  $|t_{21}(j\omega)| \leq -20\text{dB}$ .

Disturbance response :  $|L_1/(1+L_1)| \leq 2.3 \text{ dB}$ .

Maximum overshoot : 17%.

Maximum undershoot : 20%.

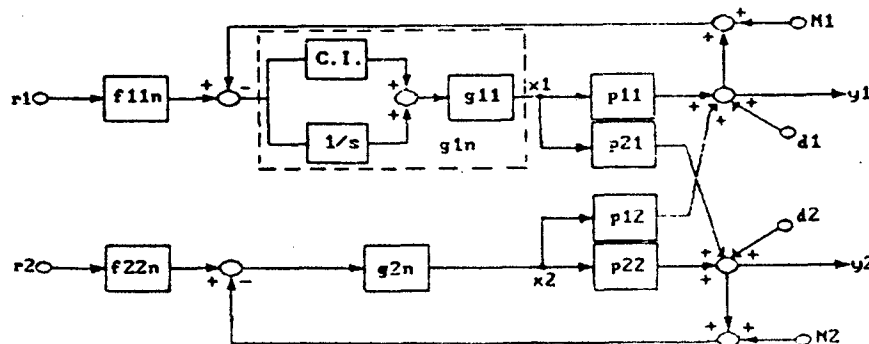


Figure 11 MIMO control system with nonlinear design in loop  $L_1$ .

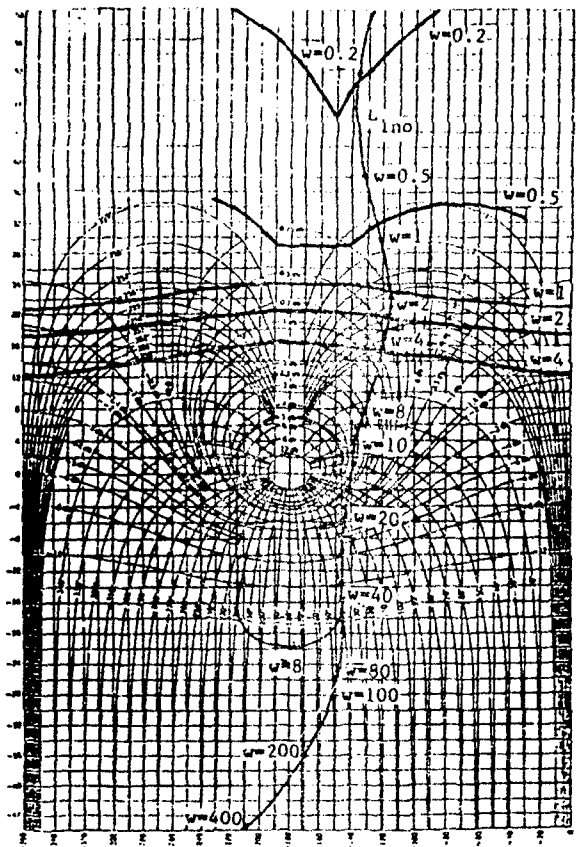


Figure 12 Bounds on  $L_{no}$  and nominal loop transmission  $L_{ino}$ .

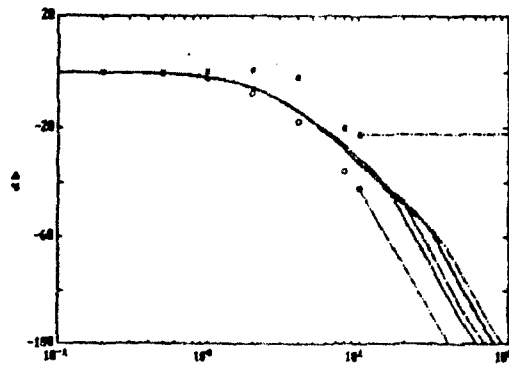


Figure 13 Frequency response of  $\left| \frac{f_{1n} L_{1n}}{1 + L_{1n}} \right|$ .

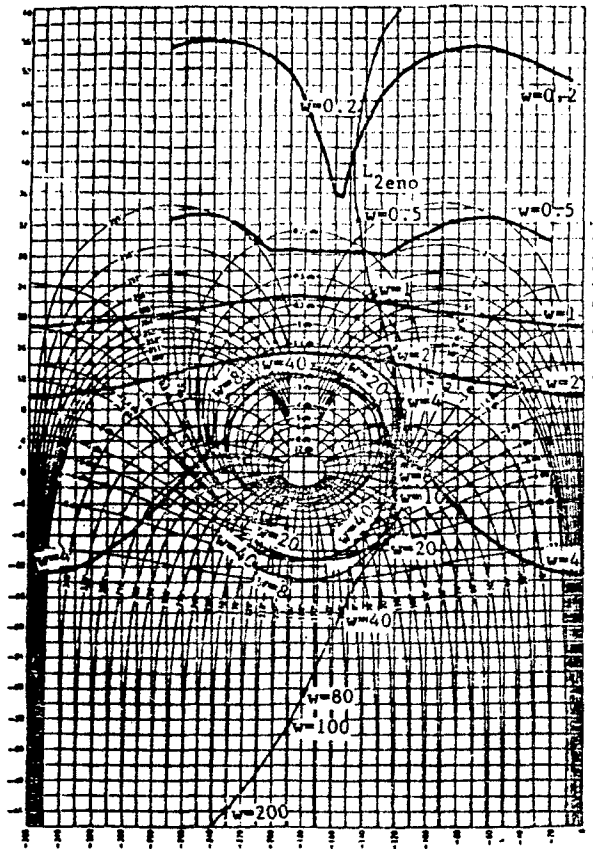


Figure 14 Bounds on  $L_{2_{eno}}$  and nominal loop transmission  $L_{2_{eno}}$ .

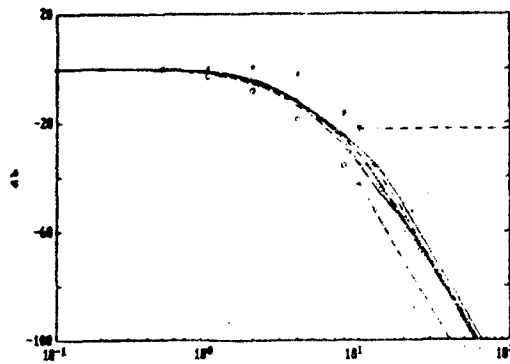


Figure 15 Frequency response of  $\left| \frac{f_{22n} L_{2en}}{1 + L_{2en}} \right|$ .

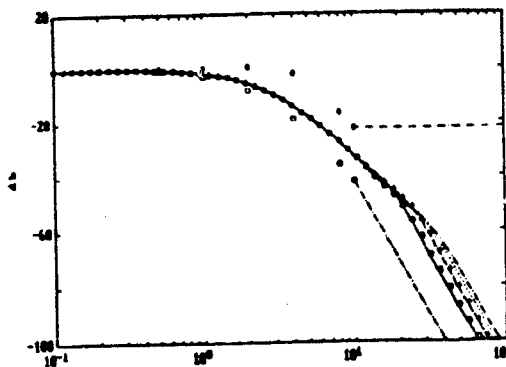


Figure 16 (a) Frequency response of  $t_{11}$ .

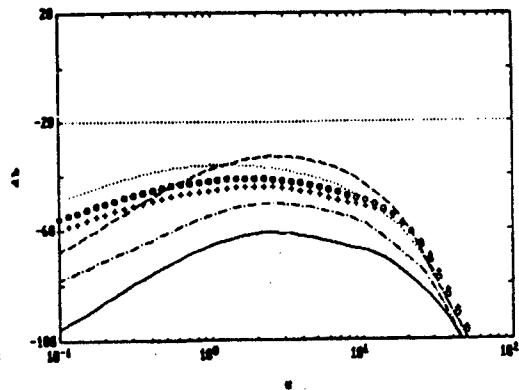


Figure 16 (b) Frequency response of  $t_{12}$ .

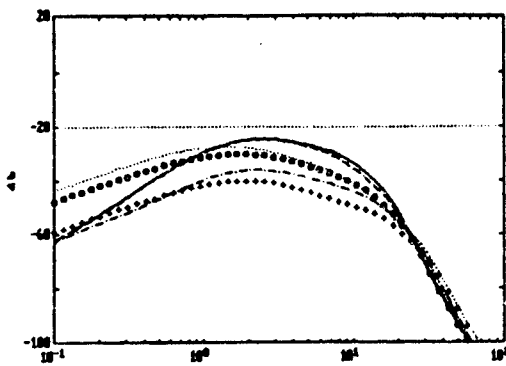


Figure 16 (c) Frequency response of  $t_{21}$ .

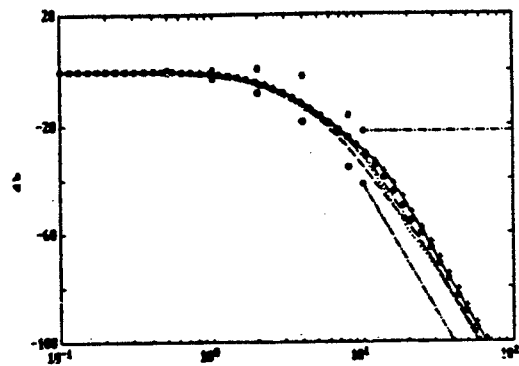


Figure 16 (d) Frequency response of  $t_{22}$ .

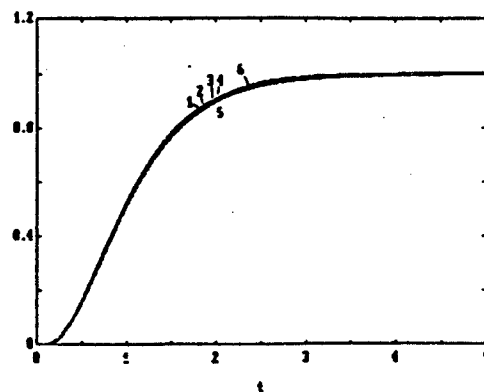


Figure 17 (a) Time response of  $y_{11}$ .

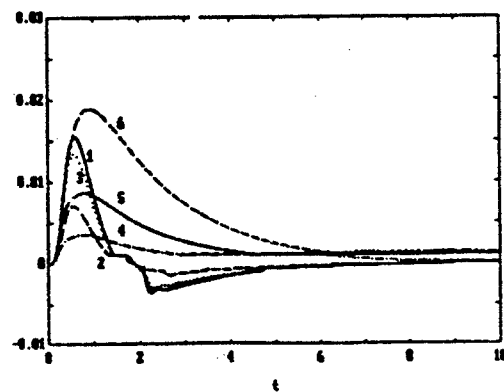


Figure 17 (b) Time response of  $y_{12}$ .



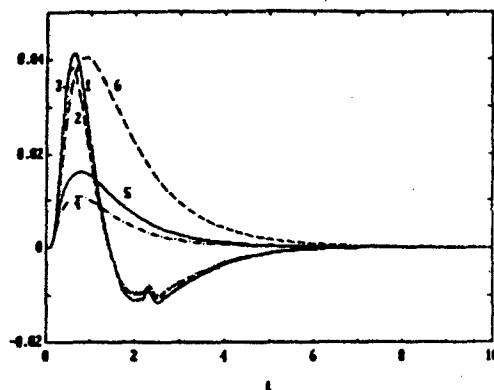


Figure 17 (c) Time response of  $y_{21}$ .

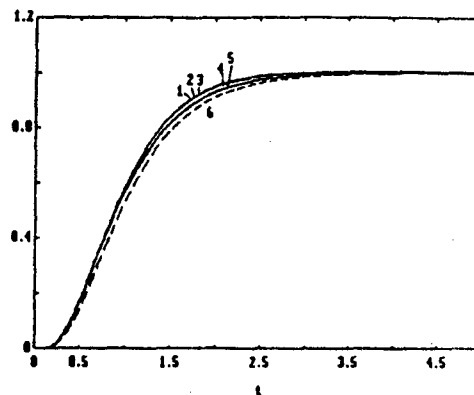


Figure 17 (d) Time response of  $y_{22}$ .

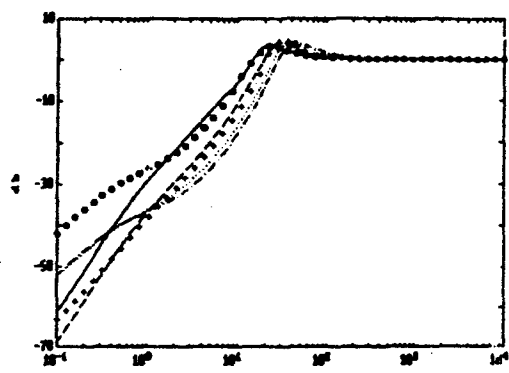


Figure 18 (a) Frequency response of  $y_1$  to step disturbance input  $d_1$ .

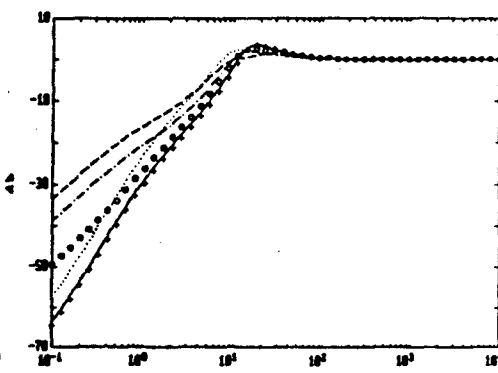


Figure 18 (b) Frequency response of  $y_2$  to step disturbance input  $d_2$ .

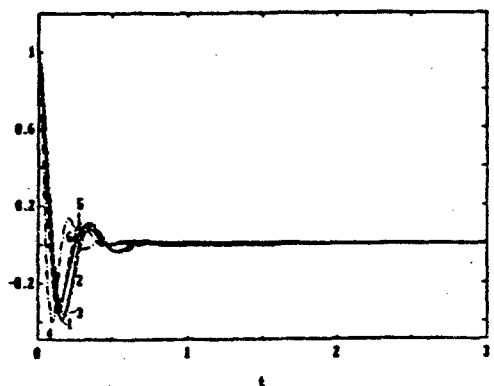


Figure 19 (a) Time response of step-disturbance output  $y_{11}$ .

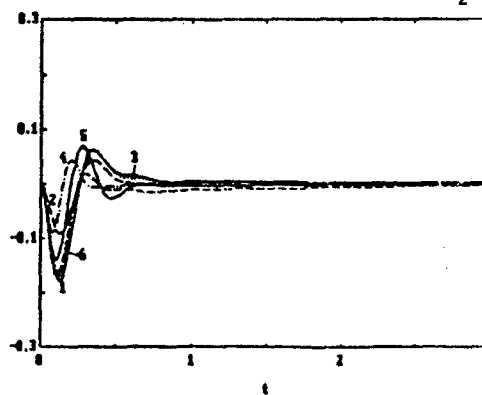


Figure 19 (b) Time response of step-disturbance output  $y_{12}$ .

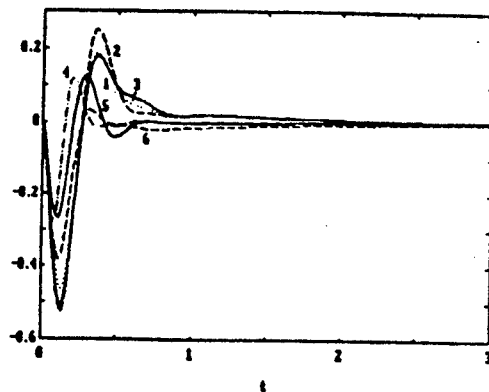


Figure 19 (c) Time response of step-disturbance output  $v_{21}$ .

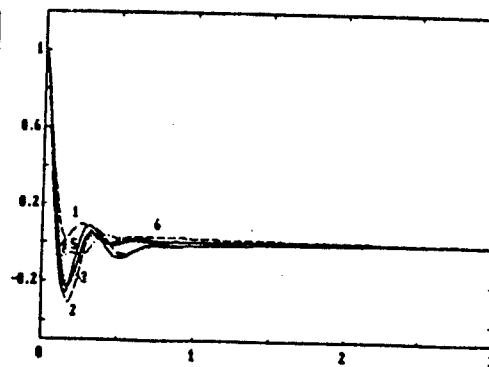


Figure 19 (d) Time response of step-disturbance output  $y_{22}$ .

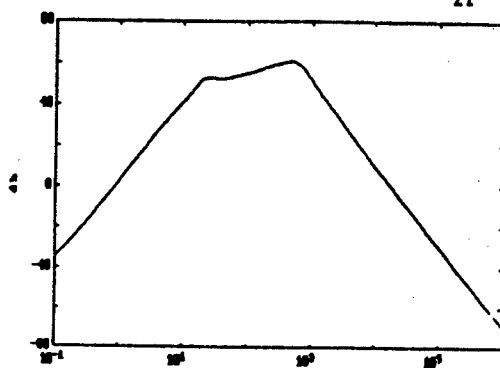


Figure 20 (a) Frequency response of  $T_{N1}$ .

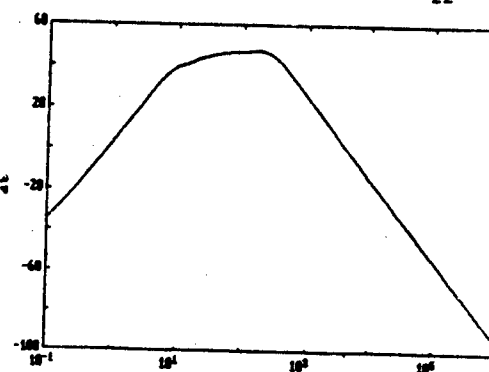


Figure 20 (b) Frequency response of  $T_{N2}$ .

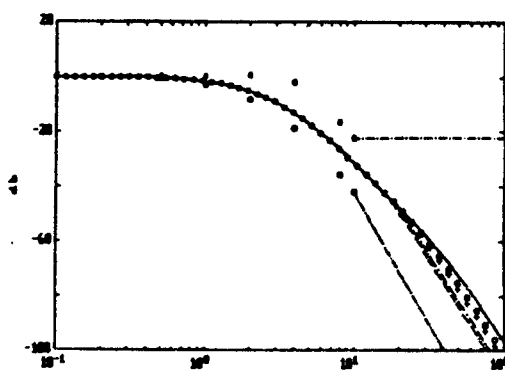


Figure 21 (a) Frequency response of  $t_{11}$ .

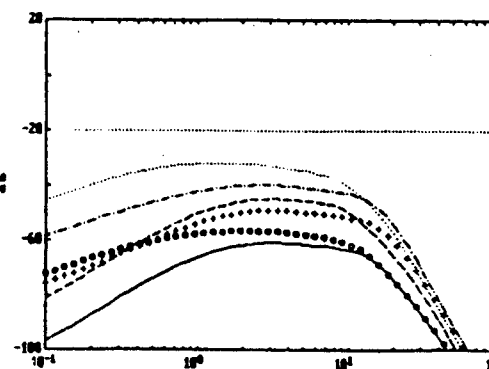


Figure 21 (b) Frequency response of  $t_{12}$ .

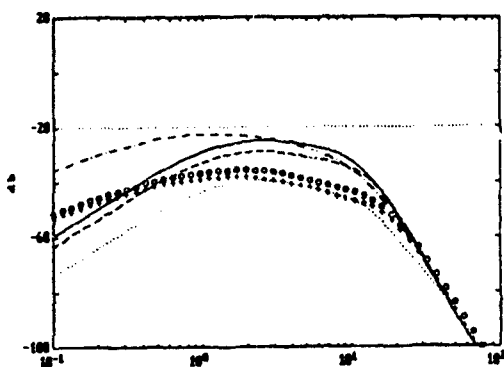


Figure 21 (c) Frequency response of  $t_{21}$ .

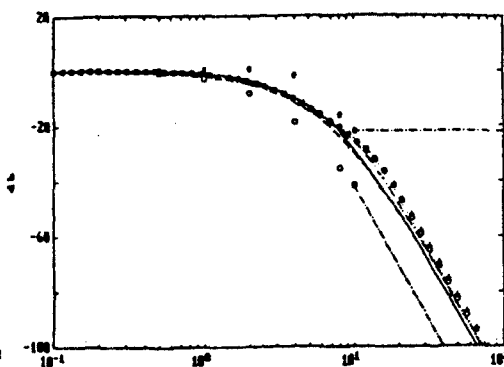


Figure 21 (d) Frequency response of  $t_{22}$ .

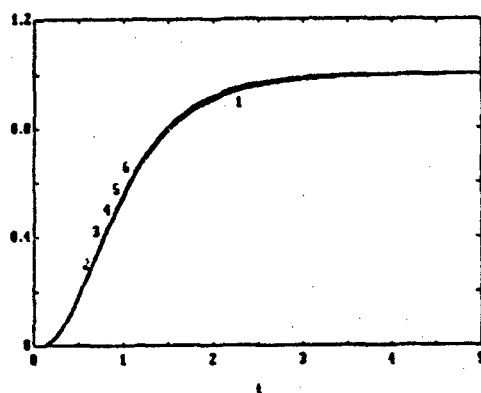


Figure 22 (a) Time response of  $y_{11}$ .

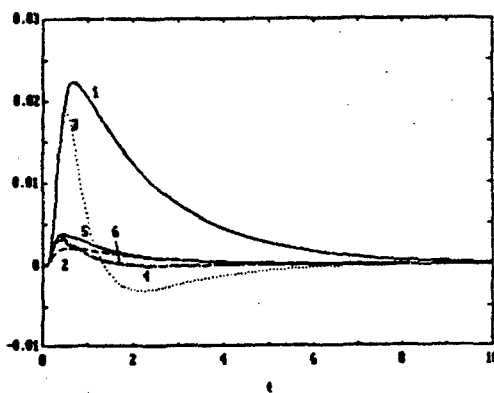


Figure 22 (b) Time response of  $y_{12}$ .

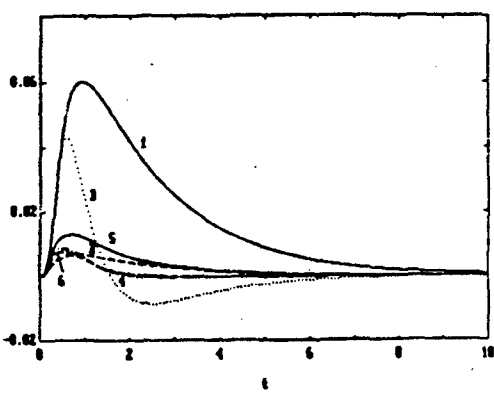


Figure 22 (c) Time response of  $y_{21}$ .

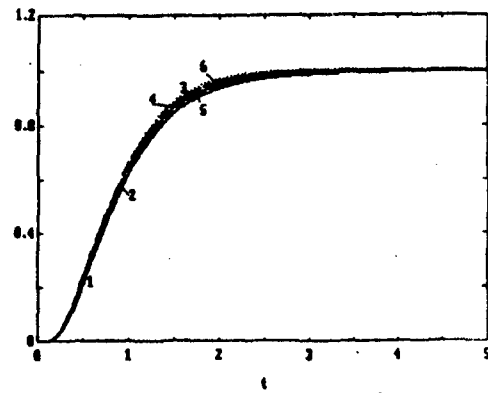


Figure 22 (d) Time response of  $y_{22}$ .

The frequency responses of  $t_{11}$ ,  $t_{12}$ ,  $t_{21}$  and  $t_{22}$  are shown in Figure 16 (a) - (d) and their time responses are presented in Figure 17 (a)-(d). The frequency responses  $y_1$  and  $y_2$  with respect to step-disturbance input, are shown in Figure 18 (a)-(b) respectively. The time responses  $y_{11}$ ,  $y_{12}$ ,  $y_{21}$  and  $y_{22}$  with respect to step - disturbance input, are shown in Figure 19 (a)-(d). The noise responses,  $T_{N1}$  and  $T_{N2}$ , are shown in Figure 20 (a)-(b). It is concluded that the system responses all meet the design specifications from above results.

#### Example 2.(Figure 10)

The frequency responses of  $t_{11}$ ,  $t_{12}$ ,  $t_{21}$  and  $t_{22}$  are shown in Figure 21 (a)-(d) respectively. The step responses of  $y_{11}$ ,  $y_{12}$ ,  $y_{21}$  and  $y_{22}$  are shown in Figure 22 (a)-(d).

#### Example 3.

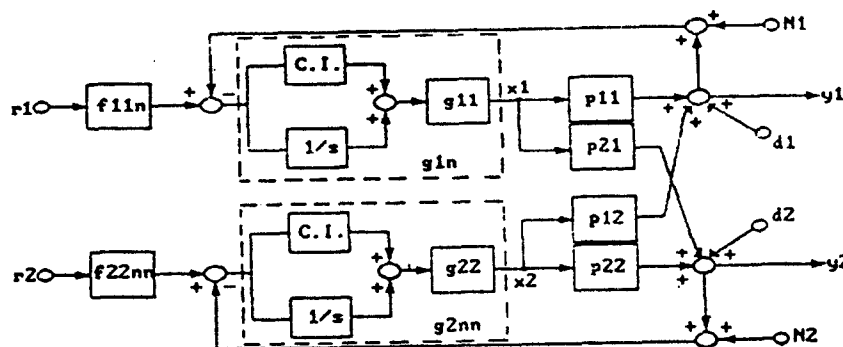


Figure 23 MIMO control system with nonlinear design in loop  $L_1$  and  $L_2$ .

The frequency responses of  $t_{11}$ ,  $t_{12}$ ,  $t_{21}$  and  $t_{22}$  are shown in Figure 24 (a)-(d) and their time responses are presented in Figure 25 (a)-(d).

#### Example 4.

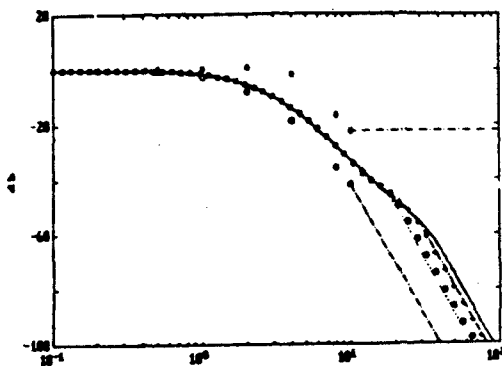


Figure 24 (a) Frequency response of  $t_{11}$ .

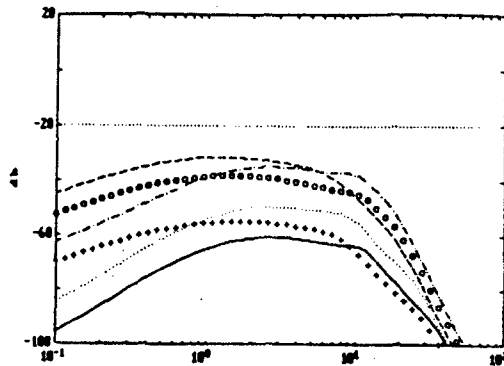


Figure 24 (b) Frequency response of  $t_{12}$ .

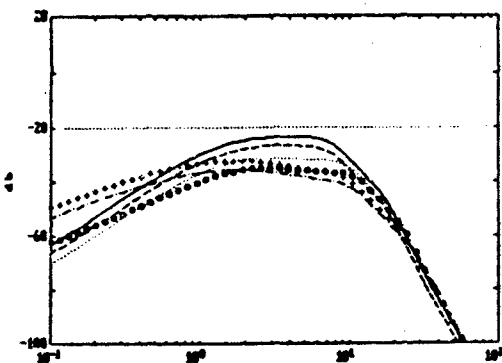


Figure 24 (c) Frequency response of  $t_{21}$ .

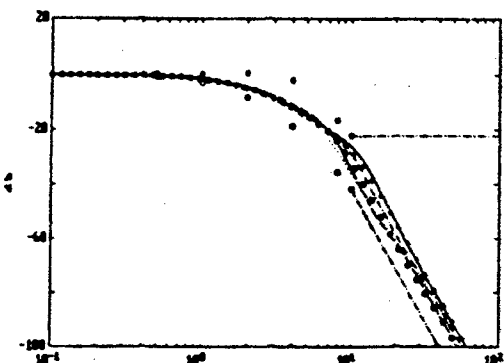


Figure 24 (d) Frequency response of  $t_{22}$ .

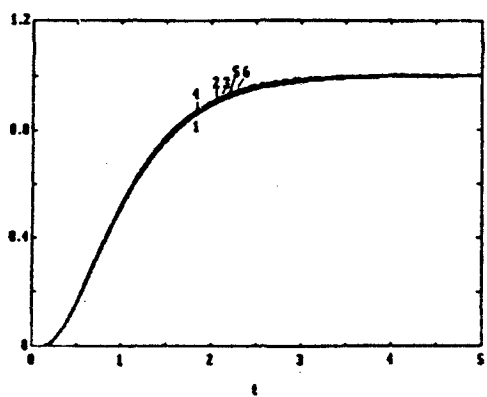


Figure 25 (a) Time response of  $y_{11}$ .

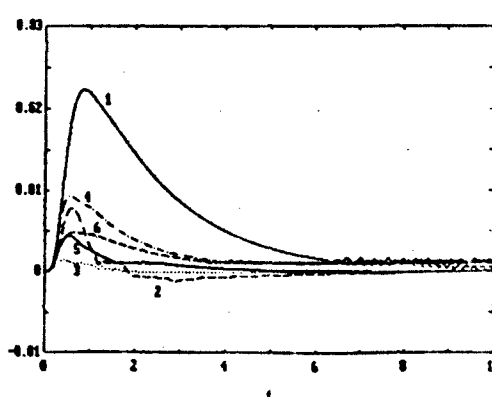


Figure 25 (b) Time response of  $y_{12}$ .

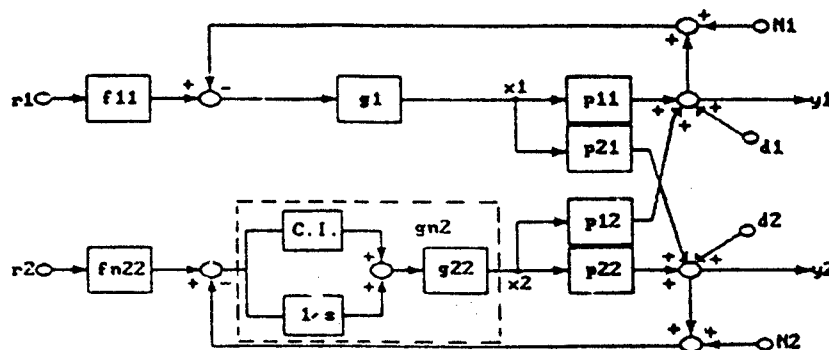


Figure 26 MIMO control system with nonlinear design in loop  $L_2$

The frequency responses of  $t_{11}$ ,  $t_{12}$ ,  $t_{21}$  and  $t_{22}$  are shown in Figure 27 (a)-(d) and their time responses are presented in Figure 28 (a) - (d). Comparison of frequency responses of  $T_{N1}(s)$  and  $T_{N2}(s)$  for four cases, are shown in Figure 29 (a)-(b). The noise time responses of  $T_{N1}(s)$  and  $T_{N2}(s)$  produced by zero-mean sensor white noise are shown in Figure 30 (a)-(h).

## 7. Conclusions

This paper uses the improved MIMO design technique and a nonlinear element, C.I., to design a MIMO system to meet desired performance tolerances and to reduce the cost of feedback. From numerical examples, we obtain the following conclusions :

- (1) The MIMO improved method can certainly reduce the inherent overdesign, and the C.I. element can further reduce the cost of feedback.
- (2) The response of nonlinear system to command input is almost exactly that of a linear system designed for the same specifications, but the coupling of system is nonlinear.
- (3) It is robustness of design such that the system response is insensitive to variation of plant parameters and disturbance. So, the nonlinear compensator can be successfully

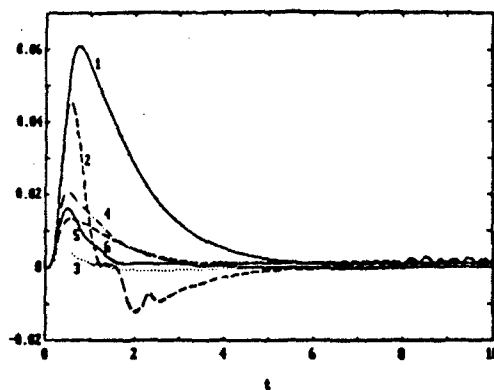


Figure 25 (c) Time response of  $y_{21}$ .

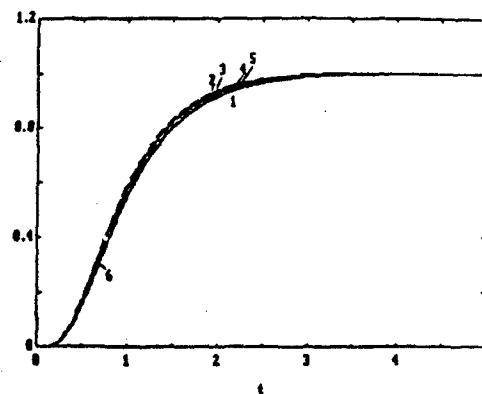


Figure 25 (d) Time response of  $y_{22}$ .

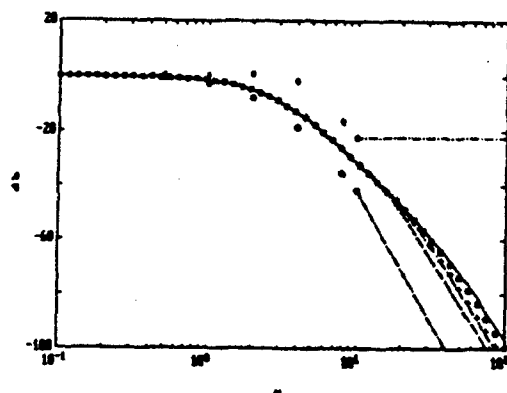


Figure 27 (a) Frequency response of  $t_{11}$ .

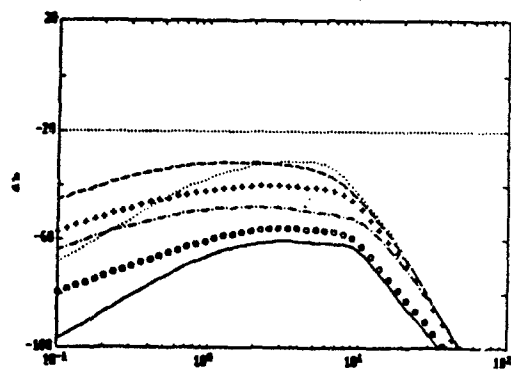


Figure 27 (b) Frequency response of  $t_{12}$ .

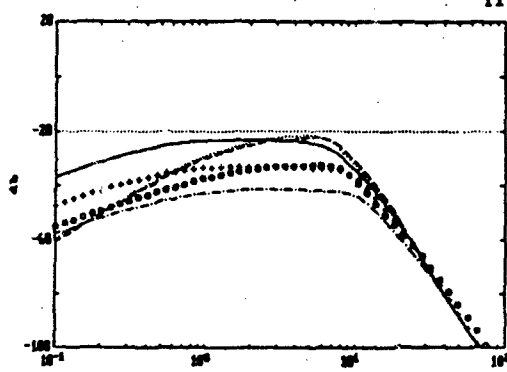


Figure 27 (c) Frequency response of  $t_{21}$ .

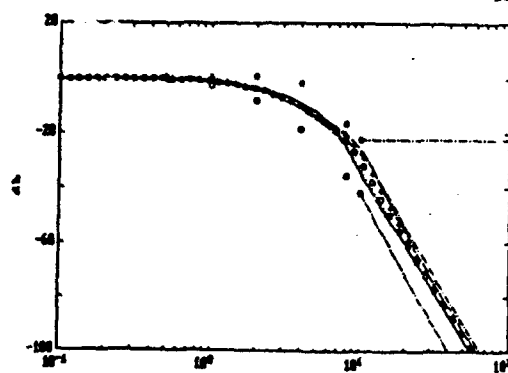


Figure 27 (d) Frequency response of  $t_{22}$ .

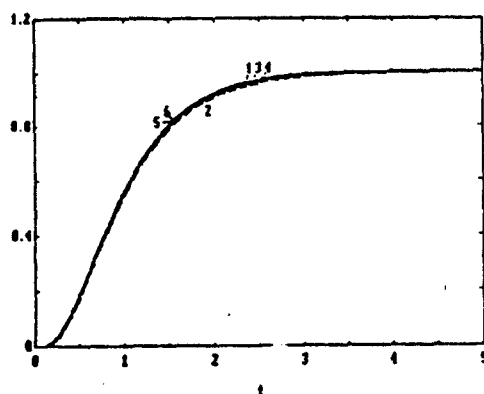


Figure 28 (a) Time response of  $y_{11}$ .

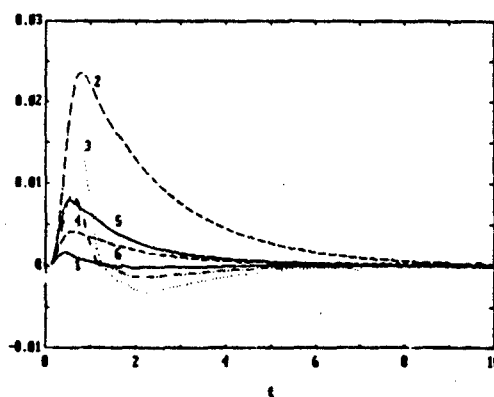


Figure 28 (b) Time response of  $y_{12}$ .

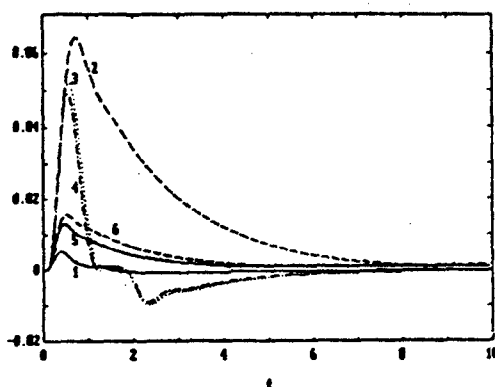


Figure 28 (c) Time response of  $y_{21}$ .

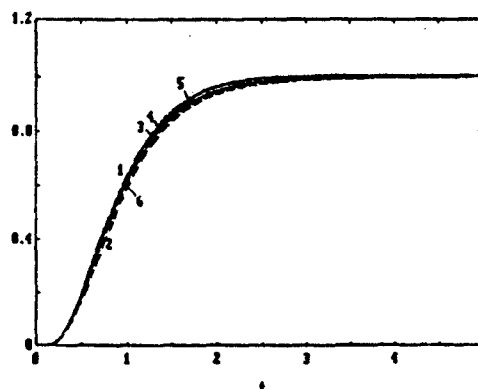


Figure 28 (d) Time response of  $y_{22}$ .

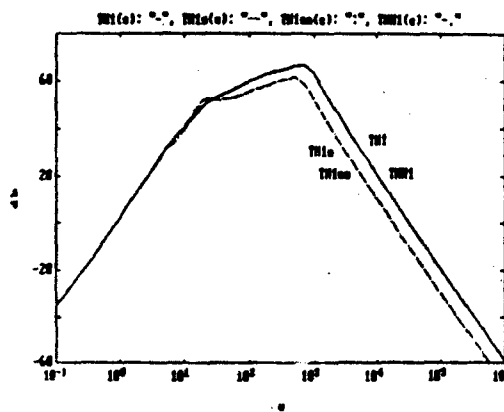


Figure 29 (a) Comparison of frequency response of  $T_{11}$ .

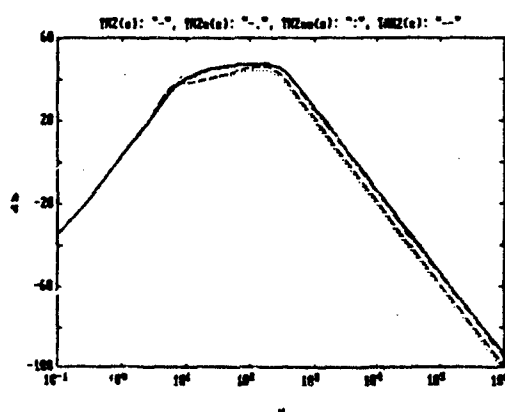


Figure 29 (b) Comparison of frequency response of  $T_{12}$ .



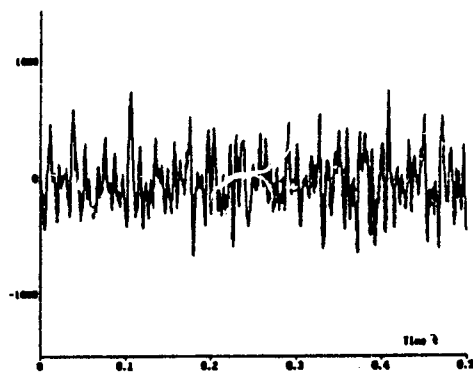


Figure 30 (a) Sensor noise of  $T_{N1}$  (case 1).

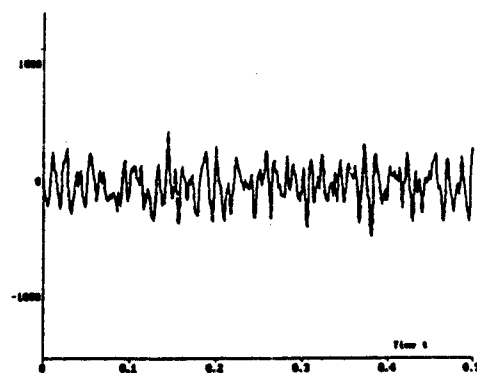


Figure 30 (b) Sensor noise of  $T_{N1}$  (case 2).

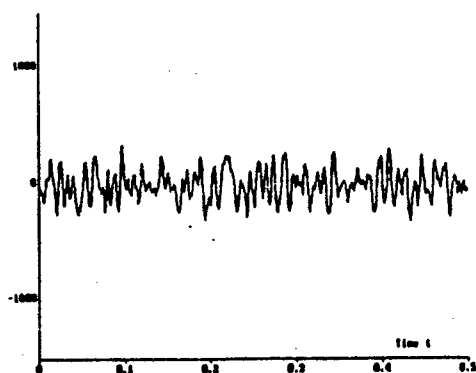


Figure 30 (c) Sensor noise of  $T_{N1}$  (case 3).

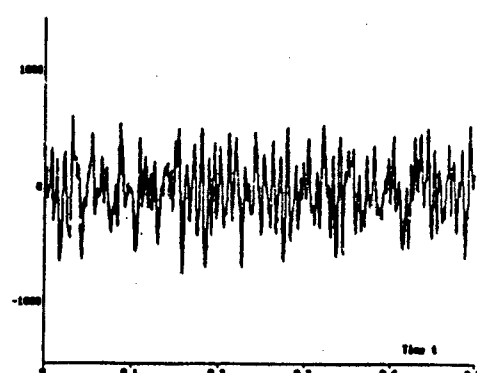


Figure 30 (d) Sensor noise of  $T_{N1}$  (case 4).

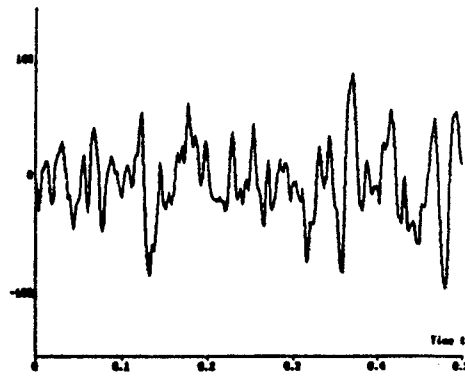
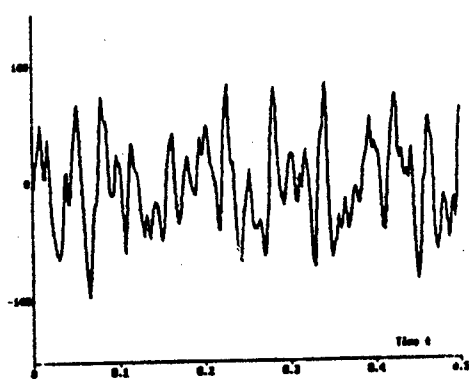


Figure 30 (e) Sensor noise of  $T_{N2}$  (case 1). Figure 30 (f) Sensor noise of  $T_{N2}$  (case 2).

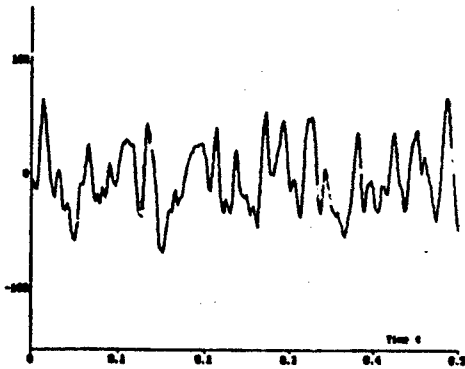
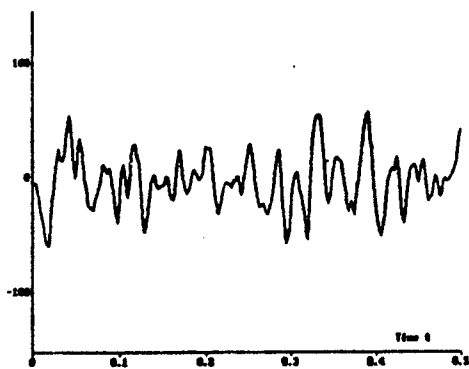


Figure 30 (g) Sensor noise of  $T_{N2}$  (case 3). Figure 30 (h) Sensor noise of  $T_{N2}$  (case 4).

adopted in the MIMO system.

- (4) Considering loop two, the reduction of cost of feedback is not evident whether the loop one is nonlinear design or not. On the other hand, if the C.I. element is placed within the compensator of loop two, the cost of feedback can be more reduced.

#### REFERENCES

- [1] Horowitz, I. , and Sidi, M., 1972, Int. J. Control, 16, 287.
- [2] Krishnan, K. R. , and Horowitz, I., 1974, Int. J. Control, 689, 19.
- [3] Clegg, J. C., 1958, Trans. A. I. E. E. Part II, Appl. Ind.
- [4] Horowitz, I., 1979, Int. J. Control, 30, 81.
- [5] Horowitz, I., and Loecher, Clayton, 1981, Int. J. Control, 33, 677.
- [6] Horowitz, I. , and Sidi, M. , 1980, Int. J. Systems SCI., 11, 851.
- [7] Horowitz, I., 1982, Int. J. Control, 36, 977.
- [8] Gelb, A., and Vander Velde, W. E., 1968, Multiple - Input Describing Functions and Nonlinear System Design, McGraw-Hill.
- [9] Wang, B. C. , and Lee, W. L. , 1992, SICE'92 in Kumamoto, Japan, ES12-6.

# APPENDIX

## Rational Functions of Numerical Examples

### I. Example 1

$$g_{1n}(s) = \frac{325925926(s+0.6)(s+45)}{(s+8)(s+150)(s^2+480s+600^2)}$$

$$f_{11n}(s) = \frac{24}{(s+2)(s+3)(s+4)}$$

$$g_{2n}(s) = \frac{18789903(s+1)(s+21)}{(s+9)(s+45)(s^2+336s+280^2)}$$

$$f_{22n}(s) = \frac{30}{(s+2.5)(s+3)(s+4)}$$

### II. Example 2

$$g_1(s) = \frac{1062901961(s+0.6)(s+20)}{(s+6)(s+154)(s^2+640s+800^2)}$$

$$f_{11}(s) = \frac{30}{(s+2)(s+3)(s+5)}$$

$$g_2(s) = \frac{21581502(s+0.62)(s+20)}{(s+8)(s+4)(s^2+390s+300^2)}$$

$$f_{22}(s) = \frac{55.5}{(s+2.5)(s+3)(s+7.4)}$$

### III. Example 3

$$g_{1n}(s) = \frac{325925926(s+0.6)(s+45)}{(s+8)(s+150)(s^2+480s+600^2)}$$

$$f_{11n}(s) = \frac{24}{(s+2)(s+3)(s+4)}$$

$$g_{2nn}(s) = \frac{9061842(s+1)(s+22)}{(s+5)(s+52)(s^2+259s+240^2)}$$

$$f_{22nn}(s) = \frac{32}{(s+2)(s+4)^2}$$

### IV. Example 4

$$g_1(s) = \frac{1062901961(s+0.6)(s+20)}{(s+6)(s+154)(s^2+640s+800^2)}$$

$$f_{11}(s) = \frac{30}{(s+2)(s+3)(s+5)}$$

$$g_{n2}(s) = \frac{11200000(s+0.6)(s+18)}{(s+3.5)(s+60)(s^2+264s+240^2)}$$

$$f_{n22}(s) = \frac{36}{(s+3)^2(s+4)}$$

April 27, 1992

**Direct Quantitative Feedback Theory Design for  
Multi-Input Multi-Output Systems<sup>1</sup>**

**Myoung Soo Park<sup>2</sup>   Yossi Chait<sup>3</sup>   Julie Rodrigues<sup>4</sup>  
Mechanical Engineering Department  
University of Massachusetts  
Amherst, MA 01003**

**ABSTRACT**

There are several Quantitative Feedback Theory methods that can be applied to multi-input multi-output systems. These methods, without exception, are based on inversion of the plant and the controller, and hence cannot be directly applied to non-square plants.

This paper proposes a sequential, multi-input multi-output Quantitative Feedback Theory method that is based on direct design. The new method features a new concept that unifies the treatment of square and non-square plants. The method and the concept are presented in detail for the disturbance rejection problem of a square plant. It is shown to be mathematically equivalent to the inversion based method. Because the new method is applicable to non-square plants, it should be considered a natural extension of present, sequential, multi-input multi-output Quantitative Feedback Theory methods.

---

<sup>1</sup>Research supported by NSF grant (No. MSS 8920628). This support is greatly appreciated.

<sup>2</sup>Ph.D. research assistant.

<sup>3</sup>Assistant professor.

<sup>4</sup>Undergraduate research assistant.

## NOMENCLATURE

- $m$  : The number of plant outputs.
- $n$  : The number of plant inputs.
- $P$  : An  $m$  by  $n$  matrix;  $P = \{p_{ij}\}$ ,  $i=1, \dots, m$ ,  $j=1, \dots, n$ .
- $P_{ij}$  : A submatrix formed by eliminating the  $i^{\text{th}}$  row and  $j^{\text{th}}$  column of the matrix  $P$ .
- $P^T$  : The transpose of the matrix  $P$ .
- $P^{-1}$  : The inverse of the matrix  $P$ .
- $\alpha_{ij}^P$  : The cofactor of the element  $P_{ij}$  in a matrix  $P$ ;  $\alpha_{ij}^P = (-1)^{i+j} (\Delta P)$ .
- $\Delta P$  : Determinant of the matrix  $P$ .

## 1. INTRODUCTION

Consider a linear time invariant (LTI), multi-input multi-output (MIMO), uncertain plant (shown in Fig. 1). To reflect uncertainty in the plant,  $P(s) \in \rho$ , where  $\rho$  is a set of LTI transfer function matrices. The control design problem considered in this paper is to find a controller  $G(s)$  to meet certain performance specifications on the closed-loop transmission from the disturbance  $D(s)$  to the output  $Y(s)$  and guarantee robust stability.

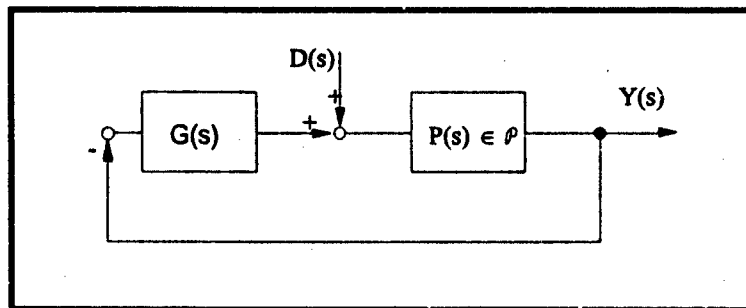


Figure 1: The feedback system

Several methods have been developed for design of such a controller within the framework of Quantitative Feedback Theory (QFT). One similarity among these methods is that they all involve inversion of a square plant and a square controller (Shaked *et al.* 1976, Horowitz 1979, Horowitz and Sidi 1980, Horowitz and Loecher 1981, Horowitz 1982 a, Horowitz 1982 b, Horowitz *et al* 1985, Horowitz and Yaniv 1985, Yaniv and Horowitz 1986). Because of this inversion, these methods cannot be used for a non-square plant. It should be noted that Horowitz (1963, §10) investigated the non-square plant problem by considering inversion of the return difference,  $I + PG$ . For the more outputs than inputs case, Horowitz suggested to augment the plant with zeros as necessary to obtain a square plant. For the more inputs than outputs case, Horowitz suggested that the designer eliminate certain rows from the plant in order to square it (e.g., rows that are highly coupled to others). Noteworthy is the recent results by Nwokah and his co-workers (Nwokah *et al.* 1990, Perez *et al.* 1991). In these works, key developments from the "British" frequency domain methods are extended to a class of uncertain plants within the general spirit of QFT. These results are fundamentally different from present QFT methods for the following reasons: (1) they do not involve plant inversion, (2) they involve of a certain degree of conservatism in cases of

parametric uncertainty; and (3) the closed-loop specifications are given in terms of the diagonal elements and a certain degree of interaction.

The objective of this paper is to develop a new QFT design method based on a unified treatment of the general  $m \times n$  MIMO plant. Naturally, this can be made possible only if the method does not involve inversion of the plant and of the controller. The underlying concept used to develop this method is presented in detail using a disturbance rejection problem with a square plant ( $m=n$ ). The applicability of this concept to non-square plants will become clear from the presentation in this paper, and further details will be the topic of future papers.

This paper is organized as follows. Section 2 describes the feedback control problem. In Section 3.1, we first describe the present QFT sequential method for the disturbance rejection problem. In Section 3.2, the new QFT method is presented, where a recursive equation is derived for a square plant. In Sections 3.3-3.4, we compare the two methods and show they are mathematically equivalent. Finally, in Sections 4-5 we discuss the problem of robust stability and application to a non-square plant, respectively.

## 2. STATEMENT OF THE CONTROL PROBLEM

Consider the feedback system shown in Fig. 1. The plant transfer function matrix (TFM) is  $P(s) = [p_{ij}]$ , where  $P(s) \in \rho$ ,  $\rho$  is a set of LTI transfer function matrices. The uncertainty can be of any type, e.g., parametric, additive, multiplicative or others. The TFM from the disturbance to the output is described by  $Y(s) = (I + P(s)G(s))^{-1} P(s)D(s)$ . Denote the transfer function  $D(s)$  to  $Y(s)$  by  $T(s)$ ,

$$T(s) = (I + P(s)G(s))^{-1} P(s) \quad (1)$$

The control objective is to design the controller,  $G(s)$ , that satisfies the following performance specification

$$|t_{ij}(j\omega)| \leq \beta_{ij}(\omega) \begin{cases} i=1,2,\dots,m \\ j=1,2,\dots,n \end{cases}$$

In addition, the closed loop system must be robustly stable.

## 3. QFT DESIGN

In this section, we present the concept underlying the derivation of our new method. For several reasons we consider here only square plants, i.e.  $m=n$ . These reasons are: the complete presentation has been divided to several standard length papers and the need to compare to present QFT methods that deal only with square plants. For comparison purposes, we begin by briefly reviewing the present MIMO QFT sequential method. Throughout the paper we use the brief notation of  $P$  for  $P(s)$  (where possible), and:

$$P = \{p_{ij}\}, T = \{t_{ij}\} \text{ and } G = \text{diag}[g_1, g_2, \dots, g_n] \quad \begin{cases} i=1,2,\dots,n \\ j=1,2,\dots,n \end{cases}$$

The main idea in the present MIMO QFT method is to solve the feedback problem in  $n$  sequential steps. At the  $i^{\text{th}}$  step, one derives from Eq. (1) the appropriate relations for  $t_{ij}$  in terms of the single controller  $g_i$ . QFT bounds on this  $g_i$  are then obtained to simultaneously satisfy the specifications on the closed-loop transfer functions in the  $i^{\text{th}}$  channel,  $t_{ij}$ ,  $j=1,2,\dots,n$ . Subsequently, the designer proceeds sequentially to synthesize

in a similar manner the remaining controllers. The new method presented in this paper employs this same idea of sequential design.

### 3.1 The Present QFT Method

Assume that the plant inverse exists. The present QFT involves inversion of the transfer function (PG). Using such inversion, Eq. (1) can be written as

$$(I+G^{-1}P^{-1})T = G^{-1} \quad (2)$$

Using the notation  $P^{-1}=\{q_{ij}\}$ , expand Eq. (2) as follows

$$\begin{pmatrix} 1+q_{11}/g_1 & q_{12}/g_1 & \cdot & q_{1n}/g_1 \\ q_{21}/g_2 & 1+q_{22}/g_2 & \cdot & q_{2n}/g_2 \\ \cdot & \cdot & \cdot & \cdot \\ \cdot & \cdot & \cdot & \cdot \\ q_{n1}/g_n & \cdot & \cdot & 1+q_{nn}/g_n \end{pmatrix} \begin{pmatrix} t_{11} & \cdot & t_{1n} \\ \cdot & \cdot & \cdot \\ \cdot & \cdot & \cdot \\ \cdot & \cdot & \cdot \\ t_{n1} & \cdot & t_{nn} \end{pmatrix} = \begin{pmatrix} 1/g_1 & 0 & \cdot & \cdot & 0 \\ 0 & 1/g_2 & 0 & \cdot & 0 \\ \cdot & \cdot & \cdot & \cdot & \cdot \\ \cdot & \cdot & \cdot & \cdot & \cdot \\ 0 & \cdot & \cdot & 0 & 1/g_n \end{pmatrix}$$

Using Gauss elimination (Strang 1980), the TFM  $I+(PG)^{-1}$  is transformed into an upper diagonal matrix. The final result of this process is

$$\begin{pmatrix} 1+q_{11}/g_1 & q_{12}/g_1 & \cdot & \cdot & q_{1n}/g_1 \\ 0 & 1+q_{22}^2/g_2 & \cdot & \cdot & q_{2n}^2/g_2 \\ \cdot & \cdot & \cdot & \cdot & \cdot \\ 0 & \cdot & 0 & 1+q_{(n-1)(n-1)}^{n-1}/g_{(n-1)} & q_{(n-1)n}^{(n-1)}/g_{(n-1)} \\ 0 & \cdot & \cdot & 0 & 1+q_{nn}^n/g_n \end{pmatrix} \begin{pmatrix} t_{11} & \cdot & t_{1n} \\ \cdot & \cdot & \cdot \\ \cdot & \cdot & \cdot \\ \cdot & \cdot & \cdot \\ t_{n1} & \cdot & t_{nn} \end{pmatrix} = \begin{pmatrix} c_{11}/g_1 & 0 & 0 & \cdot & \cdot & 0 \\ c_{21}/g_2 & c_{22}/g_2 & 0 & \cdot & \cdot & 0 \\ \cdot & \cdot & \cdot & \cdot & \cdot & \cdot \\ c_{(n-1)1}/g_{(n-1)} & \cdot & \cdot & c_{(n-1)(n-2)}/g_{(n-1)} & c_{(n-1)(n-1)}/g_{(n-1)} & 0 \\ c_{n1}/g_n & \cdot & \cdot & \cdot & c_{n(n-1)}/g_n & c_{nn}/g_n \end{pmatrix} \quad (3)$$

where  $q_{ij}^1=q_{ij}$  and

$$q_{mj}^m = q_{mj}^1 - \sum_{i=1}^{m-1} \frac{q_{mi}^i q_{ij}^i}{(g_i + q_{ii}^i)}, \quad m=2,3,\dots,n$$

and



$$c_{mj} = \begin{cases} -\sum_{i=1}^{m-1} \frac{q_{mi}^i c_{ij}}{g_i + q_{ii}^i} & \text{when } m > j, \text{ where } m = 2, 3, \dots, n \text{ and } j = 2, 3, \dots, n-1 \\ 0 & \text{when } m < j \\ 1 & \text{when } m = j \end{cases}$$

After several algebraic manipulations, one can derive the relations for  $t_{ij}$  in terms of  $q_{ij}$ ,  $g_i$  and  $t_{ij}$ ,  $i \neq j$ . The following is the final relations for  $t_{ij}$  (Chait and Park, 1992)

$$|t_{ij}| = \left| \frac{c_{ij} - \sum_{k=i+1}^n (q_{ik}^i t_{kj})}{g_i + q_{ii}^i} \right| \leq \beta_{ij}(\omega) \quad (4)$$

### 3.2 The New QFT Method

The new QFT method employs the same sequential design principle used in the present method. However, the new method does not require explicit inversion of the TFM (PG). In contrast to Eq. (2), the new method utilizes the following equation

$$(I + P G)T = P, \quad (5)$$

that can be rearranged to

$$(P G)T = P - T. \quad (6)$$

Expand Eq. (6) as follows

$$\begin{pmatrix} p_{11}g_1 & p_{12}g_2 & \dots & p_{1n}g_n \\ p_{21}g_1 & p_{22}g_2 & \dots & p_{2n}g_n \\ \vdots & \vdots & \ddots & \vdots \\ p_{n1}g_1 & p_{n2}g_2 & \dots & p_{nn}g_n \end{pmatrix} \begin{pmatrix} t_{11} & t_{12} & \dots & t_{1n} \\ t_{21} & t_{22} & \dots & t_{2n} \\ \vdots & \vdots & \ddots & \vdots \\ t_{n1} & t_{n2} & \dots & t_{nn} \end{pmatrix} = \begin{pmatrix} p_{11} - t_{11} & p_{12} - t_{12} & \dots & p_{1n} - t_{1n} \\ p_{21} - t_{21} & p_{22} - t_{22} & \dots & p_{2n} - t_{2n} \\ \vdots & \vdots & \ddots & \vdots \\ p_{n1} - t_{n1} & p_{n2} - t_{n2} & \dots & p_{nn} - t_{nn} \end{pmatrix} \quad (7)$$

Now, consider Eq. (7) for the  $K^{\text{th}}$  column only

$$\begin{pmatrix} p_{11}g_1 & p_{12}g_2 & \dots & p_{1n}g_n \\ p_{21}g_1 & p_{22}g_2 & \dots & p_{2n}g_n \\ \vdots & \vdots & \ddots & \vdots \\ p_{n1}g_1 & p_{n2}g_2 & \dots & p_{nn}g_n \end{pmatrix} \begin{pmatrix} t_{1K} \\ t_{2K} \\ \vdots \\ t_{nK} \end{pmatrix} = \begin{pmatrix} p_{1K} - t_{1K} \\ p_{2K} - t_{2K} \\ \vdots \\ p_{nK} - t_{nK} \end{pmatrix}$$

Since the controller  $G$  is diagonal, the above can be written in a compact form

$$P \text{diag}[g_1, g_2, \dots, g_n] [t_{1K} \ t_{2K} \ \dots \ t_{nK}]^T = P \text{diag}[t_{1K} \ t_{2K} \ \dots \ t_{nK}] [g_1, g_2, \dots, g_n]^T.$$

That is

$$\begin{pmatrix} P_{11}t_{1K} & P_{12}t_{2K} & \cdots & P_{1n}t_{nK} \\ P_{21}t_{1K} & P_{22}t_{2K} & \cdots & P_{2n}t_{nK} \\ \vdots & \vdots & \ddots & \vdots \\ P_{n1}t_{1K} & P_{n2}t_{2K} & \cdots & P_{nn}t_{nK} \end{pmatrix} \begin{pmatrix} g_1 \\ g_2 \\ \vdots \\ g_n \end{pmatrix} = \begin{pmatrix} P_{1K}-t_{1K} \\ P_{2K}-t_{2K} \\ \vdots \\ P_{nK}-t_{nK} \end{pmatrix} \quad (8)$$

In Eq.(8), there are  $n$  equations and  $n$  unknown (the  $g_i$ 's). This system of equations can be solved directly for any  $g_i$  using LU decomposition or Cramer's rule. Of course, a necessary condition for such procedure is that the inverse of the plant  $P$  exists.

The concept underlying the new method can now be presented. Denote Eq. (8) in a compact form by  $Ax = b$ . For simplicity of notation, it is assumed here that the sequential procedure starts from  $i=1$  and proceeds in order to  $i=n$ . If necessary, Eq. (8) should be first permuted to allow this sequence. As is done in the present method, we derive relations for  $t_{ij}$  in terms of the single controller,  $g_i$ . The sequential procedure for deriving these relations is outlined in Table 1.

Step	Procedure
1	Replace the $i^{\text{th}}$ element in the vector $b$ by $p_{iK}$
2	Replace the $i^{\text{th}}$ element in the vector $x$ by $t_{iK}$
3	Replace the $i^{\text{th}}$ column in $A$ matrix by the column $[p_{1i}g_i \ p_{2i}g_i \ \cdots \ p_{(i-1)i}g_i \ (1+p_{ii}g_i) \ p_{(i+1)i}g_i \ \cdots \ p_{ni}g_i]^T$
4	Using Cramer's rule, derive for $t_{iK}$
5	Repeat Steps 1-4 for the $(i+1)^{\text{th}}$ element while preserving previous replacements

Table 1. The procedure for deriving  $t_{iK}$  relations

Using the procedure in Table 1, at the  $i^{\text{th}}$  step, we have

$$\begin{pmatrix} 1+p_{1i}g_i & p_{12}g_2 & \cdots & p_{1i}g_i & \cdots & p_{1n}t_{nK} \\ p_{21}g_1 & 1+p_{22}g_2 & \cdots & p_{2i}g_i & \cdots & p_{2n}t_{nK} \\ \vdots & \vdots & \ddots & \vdots & \ddots & \vdots \\ p_{i1}g_1 & p_{i2}g_2 & \cdots & 1+p_{ii}g_i & \cdots & p_{in}t_{nK} \\ p_{(i+1)1}g_1 & p_{(i+1)2}g_2 & \cdots & p_{(i+1)i}g_i & \cdots & p_{(i+1)n}t_{nK} \\ \vdots & \vdots & \ddots & \vdots & \ddots & \vdots \\ p_{n1}g_1 & p_{n2}g_2 & \cdots & p_{ni}g_i & \cdots & p_{nn}t_{nK} \end{pmatrix} \begin{pmatrix} t_{1K} \\ t_{2K} \\ \vdots \\ t_{iK} \\ g_{(i+1)} \\ \vdots \\ g_n \end{pmatrix} = \begin{pmatrix} p_{1K} \\ p_{2K} \\ \vdots \\ p_{iK} \\ p_{(i+1)K} - t_{(i+1)K} \\ \vdots \\ p_{nK} - t_{nK} \end{pmatrix} \quad (9)$$

From Eq. (9), the relations for  $t_{iK}$  can be easily obtained by using Cramer's rule as follows (Strang 1980). Denote the above equation in a compact form as  $By = c$ , where  $B=[b_1 \ b_2 \ \cdots \ b_i \ \cdots \ b_n]$  and  $b_i$  is the  $i^{\text{th}}$  column vector. Application of Cramer's rule gives

$$t_{ik} = \frac{\Delta[b_1 \ b_2 \ \dots \ b_{(i-1)} \ c \ b_{(i+1)} \ \dots \ b_n]}{\Delta B} \quad (10)$$

The matrix B can be written as a product of two matrices,  $B = M N$ , where M and N are defined by

$$M = \begin{pmatrix} 1+p_{11}g_1 & p_{12}g_2 & \cdot & p_{1i}g_i & \cdot & p_{1n} \\ p_{21}g_1 & 1+p_{22}g_2 & \cdot & p_{2i}g_i & \cdot & p_{2n} \\ \cdot & \cdot & \cdot & \cdot & \cdot & \cdot \\ p_{i1}g_1 & p_{i2}g_2 & \cdot & 1+p_{ii}g_i & \cdot & p_{in} \\ p_{(i+1)1}g_1 & p_{(i+1)2}g_2 & \cdot & p_{(i+1)i}g_i & \cdot & p_{(i+1)n} \\ \cdot & \cdot & \cdot & \cdot & \cdot & \cdot \\ p_{n1}g_1 & p_{n2}g_2 & \cdot & p_{ni}g_i & \cdot & p_{nn} \end{pmatrix}$$

$$N = \text{diag}[1, 1, \dots, 1, t_{(i+1)k}, \dots, t_{nk}]$$

To compute  $\Delta B = \Delta(MN) = \Delta M \Delta N$ , since

$$\Delta N = \prod_{i=i+1}^n t_{ik}$$

let us consider the matrix M. Since the controllers  $[g_1, \dots, g_{(i-1)}]$  were already designed in the previous (i-1) steps, the first (i-1) columns of the matrix M can be written as follows

$$M = \begin{pmatrix} p_{11}^1 & p_{12}^2 & \cdot & p_{1i}g_i & \cdot & p_{1n} \\ p_{21}^1 & p_{22}^2 & \cdot & p_{2i}g_i & \cdot & p_{2n} \\ \cdot & \cdot & \cdot & \cdot & \cdot & \cdot \\ p_{i1}^1 & p_{i2}^2 & \cdot & 1+p_{ii}g_i & \cdot & p_{in} \\ \cdot & \cdot & \cdot & \cdot & \cdot & \cdot \\ p_{n1}^1 & p_{n2}^2 & \cdot & p_{ni}g_i & \cdot & p_{nn} \end{pmatrix}$$

where

$$p_{ij}^j = \begin{cases} 1+p_{ii}g_i & i=j \\ p_{ij}g_j & i \neq j \end{cases}$$

Next, define a matrix  $L^i$  as follows

$$L^i = \begin{pmatrix} p_{11}^1 & p_{12}^2 & \cdot & p_{1i} & \cdot & p_{1n} \\ p_{21}^1 & p_{22}^2 & \cdot & p_{2i} & \cdot & p_{2n} \\ \cdot & \cdot & \cdot & \cdot & \cdot & \cdot \\ p_{ni}^1 & p_{n2}^2 & \cdot & p_{ni} & \cdot & p_{nn} \end{pmatrix}$$

and hence

$$\Delta M = \Delta L^i g_i + \alpha_{ii}^{L^i}$$

Finally, the denominator of Eq. (10) has the form

$$\Delta B = (\Delta L^i g_i + \alpha_{ii}^{L^i}) \prod_{i=1}^n t_{ik}. \quad (11)$$

Next, we turn our attention to the numerator in Eq. (10). The matrix in the numerator in Eq. (10) can also be written as the product of two matrices, VW, where

$$V = \begin{pmatrix} p_{11}^1 & p_{12}^2 & \cdot & p_{1K} & \cdot & p_{1n} \\ p_{21}^1 & p_{22}^2 & \cdot & p_{2K} & \cdot & p_{2n} \\ \cdot & \cdot & \cdot & \cdot & \cdot & \cdot \\ p_{i1}^1 & p_{i2}^2 & \cdot & p_{iK} & \cdot & p_{in} \\ \cdot & \cdot & \cdot & \cdot & \cdot & \cdot \\ p_{n1}^1 & p_{n2}^2 & \cdot & p_{nK} & \cdot & p_{nn} \end{pmatrix}$$

$$W = \text{diag}[1, 1, \dots, 1, t_{(i+1)K}, \dots, t_{nK}].$$

Expanding  $\Delta[b_1 \dots b_{(i-1)} \text{ c } b_{(i+1)} \dots b_n] = \Delta(VW) = \Delta V \Delta W$ , where

$$\Delta V = \sum_{k=1}^n \{p_{kk} \alpha_{ki}^{L^i}\} - \sum_{k=i+1}^n \{t_{kK} \alpha_{ki}^{L^i}\},$$

and

$$\Delta W = \prod_{i=i+1}^n t_{iK}$$

yields the final form for the numerator of Eq. (10)

$$\Delta[b_1 \cdots b_{(i-1)} \text{ c } b_{(i+1)} \cdots b_n] = \left[ \sum_{k=1}^n \{p_{kk} \alpha_{ki}^{L^i}\} - \sum_{k=i+1}^n \{t_{kk} \alpha_{ki}^{L^i}\} \right] \prod_{i=i+1}^n t_{iK} \quad (12)$$

Because the numerator and the denominator of Eq. (10) have a common term, Eq. (10) becomes

$$t_{iK} = \frac{\sum_{k=1}^n \{p_{kk} \alpha_{ki}^{L^i}\} - \sum_{k=i+1}^n \{t_{kk} \alpha_{ki}^{L^i}\}}{\Delta L^i g_i + \alpha_{ii}^{L^i}} \quad (13)$$

Note that

$$\sum_{k=1}^n \{p_{kk} \alpha_{ki}^{L^i}\} = \begin{cases} \Delta L^i & K=i \\ 0 & K \neq i \end{cases}$$

The structure of Eq. (13) is similar to that obtained in present MIMO QFT sequential methods. This implies that QFT bounds for  $g_i$  can be computed using the approach suggested in these methods (e.g., see Chait and Park, 1992). Roughly speaking, at each step we derive QFT bounds for  $g_i$  using the relations for  $t_{ik}$ ,  $k=1, \dots, n$ , and their closed-loop specifications,  $\beta_{ik}$ .

### 3.3 A Comparison Between Present QFT and New QFT Methods

Now that we have presented the relations for  $t_{11}$ ,  $t_{12}$ ,  $\dots$ ,  $t_{1n}$  in Sections 3.1 (present method) and 3.2. (new method), we will prove that both methods are mathematically equivalent for this special case of square plants ( $n=m$ ). Consider Eq. (13) for  $n=2$  and  $i=1$ . In this case,  $\Delta L^i = \Delta P$  and  $\alpha_{k1}^{L^i} = \alpha_{k1}$ . Hence,

$$t_{1K} = \frac{\sum_{k=1}^n \{p_{kk} \alpha_{k1}\} - \sum_{k=2}^n \{t_{kk} \alpha_{k1}\}}{\Delta P g_1 + \alpha_{11}} \quad (14)$$

By definition

$$\frac{\alpha_{ji}}{\Delta P} = \frac{(-1)^{j+i} (\Delta P_{ji})}{\Delta P} = \frac{\text{Adj } P_{ij}}{\Delta P} = q_{ij}$$

Divide each term on the right hand side of Eq. (13) by  $\Delta P$

$$t_{1K} = \frac{\frac{\sum_{k=1}^n \{p_{kK} \alpha_{k1}\}}{\Delta P} - \frac{\sum_{k=2}^n \{\alpha_{k1} t_{kK}\}}{\Delta P}}{\frac{\alpha_{11}}{\Delta P} + g_1}.$$

Using the definition of  $q_{ij}$ , the denominator is simplified to  $q_{11} + g_1$ , while in the numerator we obtain

$$\frac{\sum_{k=2}^n \{\alpha_{k1} t_{kK}\}}{\Delta P} = \sum_{k=2}^n \{q_{1k} t_{kK}\}.$$

For  $K=1$ ,  $t_{11}$  can be written as

$$t_{11} = \frac{1 - \sum_{k=2}^n \{q_{1k} t_{k1}\}}{q_{11} + g_1}$$

and for  $K>1$ ,  $t_{1K}$  becomes

$$t_{1K} = \frac{-\sum_{k=2}^n \{q_{1k} t_{kK}\}}{q_{11} + g_1}.$$

Therefore, we have shown that for the special case of square plants, both methods (present & new) yield a closed-loop relations the first step that are mathematically equivalent. Although the relations for the next steps are not shown here, the equivalency holds for any step in the sequential procedure.

### 3.4 Examples

As an illustrative example, let us compare the two methods with the case of two inputs and two outputs. Given  $n=m=2$ , we have

$$P = \begin{pmatrix} p_{11} & p_{12} \\ p_{21} & p_{22} \end{pmatrix} \quad T = \begin{pmatrix} t_{11} & t_{12} \\ t_{21} & t_{22} \end{pmatrix} \quad G = \begin{pmatrix} g_1 & 0 \\ 0 & g_2 \end{pmatrix}.$$

#### (i) Present QFT method

Using the definition of  $q_{ij}$ ,

$$Q = \begin{pmatrix} \frac{p_{22}}{\Delta P} & \frac{-p_{12}}{\Delta P} \\ \frac{-p_{21}}{\Delta P} & \frac{p_{11}}{\Delta P} \end{pmatrix}$$

where  $\Delta P = p_{11}p_{22} - p_{12}p_{21}$ .

Substitute these expressions into Eq. (4)

$$t_{11} = \frac{1 - q_{12} t_{21}}{g_1 + q_{11}} = \frac{p_{11} p_{22} - p_{12} p_{21} + p_{12} t_{21}}{(p_{11}p_{22} - p_{12} p_{21}) g_1 + p_{22}}$$

and

$$t_{12} = \frac{-q_{12} t_{22}}{g_1 + q_{11}} = \frac{p_{12} t_{22}}{(p_{11}p_{22} - p_{12} p_{21}) g_1 + p_{22}}$$

For the second step, Eq. (4) gives

$$t_{21} = \frac{p_{21}}{(p_{11}p_{22} - p_{12} p_{21}) g_1 g_2 + p_{11} g_1 + p_{22} g_2 + 1}$$

and

$$t_{22} = \frac{(p_{11}p_{22} - p_{12} p_{21}) g_1 + p_{22}}{(p_{11}p_{22} - p_{12} p_{21}) g_1 g_2 + p_{11} g_1 + p_{22} g_2 + 1}$$

(ii) The new QFT method

For the first step ( $i=1$ ), we use Eq. (14) to derive  $t_{11}$  and  $t_{12}$ . The cofactors and the  $\Delta P$  in Eq. (14) are

$$\alpha_{11} = p_{22},$$

$$\alpha_{21} = -p_{12},$$

$$\Delta P = p_{11} p_{22} - p_{12} p_{21}.$$

Substitute these expressions into Eq. (14),

$$t_{11} = \frac{p_{11} p_{22} - p_{12} p_{21} + p_{12} t_{21}}{(p_{11}p_{22} - p_{12} p_{21}) g_1 + p_{22}}$$

and

$$t_{12} = \frac{p_{12} t_{22}}{(p_{11}p_{22} - p_{12} p_{21}) g_1 + p_{22}}.$$

For the second step, Eq. (14) is used to obtain

$$t_{21} = \frac{p_{21}}{(p_{11}p_{22} - p_{12} p_{21}) g_1 g_2 + p_{11} g_1 + p_{22} g_2 + 1}$$

and

$$t_{22} = \frac{(p_{11}p_{22} - p_{12} p_{21}) g_1 + p_{22}}{(p_{11}p_{22} - p_{12} p_{21}) g_1 g_2 + p_{11} g_1 + p_{22} g_2 + 1}.$$

Therefore, we have shown equivalency between the present and new methods for the two input/output case.

Next, we present the specific equations for the three input/output case using the new method. For  $i=1$ , the procedure in Table 1 gives

$$\begin{pmatrix} 1+p_{11}g_1 & p_{12}t_{2K} & p_{13}t_{3K} \\ p_{21}g_1 & p_{22}t_{2K} & p_{23}t_{3K} \\ p_{31}g_1 & p_{32}t_{2K} & p_{33}t_{3K} \end{pmatrix} \begin{pmatrix} t_{1K} \\ g_2 \\ g_3 \end{pmatrix} = \begin{pmatrix} p_{1K} \\ p_{2K} - t_{2K} \\ p_{3K} - t_{3K} \end{pmatrix}$$

Using Eq. (13),  $\Delta L^1 = \Delta P$ , and

$$t_{1K} = \frac{p_{1K}\alpha_{11} + p_{2K}\alpha_{21} + p_{3K}\alpha_{31} - t_{2K}\alpha_{21} - t_{3K}\alpha_{31}}{\Delta P g_1 + \alpha_{11}}.$$

For the second step ( $i=2$ ), the procedure in Table 1 gives

$$\begin{pmatrix} 1+p_{11}g_1 & p_{12}g_2 & p_{13}t_{3K} \\ p_{21}g_1 & 1+p_{22}g_2 & p_{23}t_{3K} \\ p_{31}g_1 & p_{32}g_2 & p_{33}t_{3K} \end{pmatrix} \begin{pmatrix} t_{1K} \\ t_{2K} \\ g_3 \end{pmatrix} = \begin{pmatrix} p_{1K} \\ p_{2K} \\ p_{3K} - t_{3K} \end{pmatrix}.$$

$$\Delta L^2 = \begin{pmatrix} p_{11}^1 & p_{12} & p_{13} \\ p_{21}^1 & p_{22} & p_{23} \\ p_{31}^1 & p_{32} & p_{33} \end{pmatrix}$$

Application of Eq. (13) yields



$$t_{2K} = \frac{p_{1K}\alpha_{12}^{L^1} + p_{2K}\alpha_{22}^{L^1} + p_{3K}\alpha_{32}^{L^1} - t_{3K}\alpha_{32}^{L^1}}{\Delta L^2 g_2 + \alpha_{22}^{L^1}}$$

$$= \frac{g_1(p_{1K}\alpha_{12} + p_{2K}\alpha_{22} + p_{3K}\alpha_{32} + t_{3K}\alpha_{32}) + p_{2K}p_{33} - p_{3K}p_{23} + t_{3K}p_{23}}{g_2(g_1\Delta P + \alpha_{11}) + g_1\alpha_{22} + p_{33}}$$

Finally, for the last step ( $i=3$ ), using procedure in Table 1,

$$\begin{pmatrix} 1+p_{11}g_1 & p_{12}g_2 & p_{13}g_3 \\ p_{21}g_1 & 1+p_{22}g_2 & p_{23}g_3 \\ p_{31}g_1 & p_{32}g_2 & p_{33}g_3 \end{pmatrix} \begin{pmatrix} t_{1K} \\ t_{2K} \\ t_{3K} \end{pmatrix} = \begin{pmatrix} p_{1K} \\ p_{2K} \\ p_{3K} \end{pmatrix}$$

and apply Eq. (13) with

$$\Delta L^3 = \begin{pmatrix} p_{11}^1 & p_{12}^2 & p_{13} \\ p_{21}^1 & p_{22}^2 & p_{23} \\ p_{31}^1 & p_{32}^2 & p_{33} \end{pmatrix}$$

$$t_{3K} = \frac{p_{1K}\alpha_{13}^{L^1} + p_{2K}\alpha_{23}^{L^1} + p_{3K}\alpha_{33}^{L^1}}{\Delta L^3 g_3 + \alpha_{33}^{L^1}}$$

$$= \frac{g_1g_2(p_{1K}\alpha_{13} + p_{2K}\alpha_{23} + p_{3K}\alpha_{33}) + g_1(p_{3K}p_{11} - p_{1K}p_{31}) + g_2(p_{3K}p_{22} - p_{2K}p_{32}) + p_{3K}}{g_3(g_1g_2\Delta P + g_2\alpha_{11} + g_1\alpha_{22} + p_{33}) + g_1g_2\alpha_{33} + p_{11}g_1 + p_{22}g_2 + 1}$$

#### 4. STABILITY

Robust stability of the control system shown in Fig. 1 is related to sequential design of the return difference  $I+PG$ . The present QFT sequential procedure for closed-loop robust stability (e.g. Yaniv and Horowitz 1986, Chait 1991, Chait and Park, 1992) follows closely the one suggested by Mayne (1973, 1979) for fixed systems. This, in fact, allows QFT methods to readily make use of related results on stability, interaction and integrity of feedback systems with decentralized design (Mayne 1973, 1979). Nwokah, in recent works has been making an explicit use of the similarities between the "British" and the QFT frequency domain design methods (e.g., Nwokah et al. 1990).

#### 5. NON-SQUARE PLANTS

The new method developed in this paper considers square and non-square plants in a unified manner. This is because it focuses on the return different  $I+PG$  which is always a square MTF regardless of the dimensions of  $P$  and  $G$  (recall, present MIMO QFT methods involve  $1+G^{-1}P^{-1}$ ). Therefore, the new concept introduced for deriving  $t_{ij}$  relations for computing bounds at each design step (as outlined in Table 1) is also

applicable for the non-square case. Details of the new method applied to the non-square case and for other MIMO feedback problems will be presented in future papers.

## 6. CONCLUSIONS

A new direct Quantitative Feedback Theory Design method for multi-input multi-output systems has been developed. It was shown that the direct QFT design method is mathematically equivalent with the present QFT method that involves plant and controller inversion. However, the underlying concept used to derive the direct QFT method is also applicable to a non-square MIMO system.

## 7. REFERENCES

- Chait, Y., 1991, Robust internal stability in multi input/output Quantitative Feedback Theory, *Procs. CDC Conf.*, 2970-2971.
- Chait, Y., and Park, M. S., 1992, Disturbance Rejection in Flexible Structures via the Quantitative Feedback Theory. *AIAA J. of Guidance and Control*, submitted.
- Horowitz, I., 1963, *Synthesis of Feedback Systems* (New York: Wiley Interscience).
- Horowitz, I., 1979, Quantitative Synthesis of Uncertain Multiple Input-output Feedback System. *International Journal of Control*, 30, 81-106.
- Horowitz, I., and Sidi, M., 1980, Practical design of feedback systems with uncertain multivariable plants. *International Journal of Control*, 11(7), 851-875.
- Horowitz, I., and Loecher, C., 1981, Design of a 3 x 3 multivariable feedback system with large plant uncertainty. *International Journal of Control*, 33(4), 677-699.
- Horowitz, I., 1982 a, Improved design technique for uncertain multi-input-multi-output feedback systems. *International Journal of Control*, 36(6), 977-988.
- Horowitz, I., 1982 b, Uncertain multiple-input-multiple-output systems with internal variable feedback. *International Journal of Control*, 36(6), 989-1009.
- Horowitz, I., Neumann, L. and Yaniv, O., 1985, Quantitative synthesis of uncertain cascaded multiple-input multiple-output feedback systems. *International Journal of Control*, 42(2), 273-303.
- Horowitz, I., and Yaniv, O., 1985, Quantitative cascaded multiple-input multiple-output synthesis by an improved method. *International Journal of Control*, 42(2), 305-431.
- Mayne, D.Q., 1973, The design of linear multivariable systems, *Automatica*, 9, 201-207.
- Mayne, D.Q., 1979, Sequential design of linear multivariable systems, *Procs. IEE*, 126, 568-572.
- Nwokah, O.D.I., Thompson, D.F., and Perez, R.A., 1990, On some existence conditions for QFT controllers, *Recent Developments in Quantitative feedback Theory*, ASME DSC-Vol. 24, Ed. Nwokah, O.D.I., 1-9.
- Perez, R. A., Nwokah O.D.I, and Thompson, D.F., 1991, Almost decoupling quantitative feedback theory, *1991 American Control Conference*, Vol. 2, 2001-2006.
- Shaked, U., Horowitz, I., and Golde, S., 1976, Synthesis of multivariable basically non-interacting systems with significant plant uncertainty. *Automatica*, 12, 61-71.
- Strang, G., 1980, *Linear Algebra and Its Applications*, 2nd Ed., (New York: Academic Press).
- Yaniv, O., and Horowitz, I., 1986, A quantitative design method for MIMO linear feedback systems having uncertain plants. *International Journal of Control*, 43, 402-421.

# QFT Design of Earthquake Simulator Machines

Allen J. Clark\*  
MTS Systems Corporation  
14000 Technology Drive  
Eden Prairie, Minnesota 55344-2290

## Abstract

One commonly used type of earthquake simulator machine is the servohydraulically actuated specimen platform or shaking table. High accuracy servocontrol of such machines is very difficult because of the large load impedance uncertainty of the specimen (large amplitude tests to catastrophic failure). It is also difficult because of the basic nonlinear nature of large amplitude servovalve-actuator force and velocity characteristics. Another problem is the requirement to control the system through multiple resonances of the machine itself, in addition to the specimen's dynamic characteristics. The process of developing mathematical models suitable for applying QFT techniques to the earthquake simulator machine problem, and the results of that application will be discussed.

---

\*Applications Specialist, Advanced Technology Development

# A Model Reference Quantitative Feedback Design Theory and Aircraft Engine Application

Chin-Horng Yau\*, Joseph E. Gallagher<sup>+</sup> and Osita D.I. Nwokah\*\*

School of Mechanical Engineering  
Purdue University  
West Lafayette, IN 47907-1288

May 12, 1992

## ABSTRACT

A new decentralized robust control design framework, model reference quantitative feedback design (MRQFD), is developed for the design of the MIMO parametric uncertain control systems. An internal model reference loop is proposed to obtain the achievement of generalized diagonal dominance (GDD) and the reduction of uncertainty in the resultant compensated internal loop system. Based on non-negative matrix theory, a useful design guide is derived to achieve the GDD condition for the internal model reference loop. Then a sensitivity-based quantitative feedback design (QFD) method is developed and used to solve the resulting series of single loop QFD problems. The MIMO quantitative specifications are guaranteed to be satisfied by the proposed design framework for largely uncertain systems. A successful application to the design of a robust multivariable controller for the Allison PD-514 aircraft turbine engine is presented to demonstrate the effectiveness of the methodology developed here.

---

\* Ph.D. Candidate. <sup>+</sup> Graduate student.

\*\* Professor.

## 1. INTRODUCTION

Over the last decade a steady and growing research effort has been invested into the robustness aspects of multivariable control system design (see for example, Dorato and Yedavalli, 1990 and references cited therein). In particular, the familiar classical concepts of gain and phase margin have been generalized to the multivariable case (Postlethwaite et al., 1981), whilst concepts such as Bode's sensitivity function (Bode, 1945) have been introduced into multivariable system design in the form of the spectral norm of the return difference matrix (Doyle and Stein, 1981). The majority of the research effort has been devoted to the systems that are assumed to have unstructured uncertainty. This allows such problem to be transformed into a form where the small gain theory (Desoer and Vidyasagar, 1975; Zames, 1981) and powerful recent mathematical techniques from functional analysis and operator theory (Francis, 1987; Doyle et al., 1989) can be successfully employed for system analysis and synthesis. However many problems of practical interest appear as models with both large parametric uncertainty and high frequency non-parametric uncertainty. Typical examples include flight control and turbomachinery control over a flight envelope parametrized by power level, height and mach number, as well as general automotive engine control systems. All these problems yield a collection of linear time-invariant models obtained by linearization of a parametrically dependent nonlinear differential equation set about a finite number of different operating points. This problem class is often endowed with hard stability and performance constraints such as on rise time and overshoot. It is important to keep in mind that for practical control engineers the control design process is interactive, which involves an interplay between customer specification, almost always quantitatively described, uncertain plant characteristics, and the multivariable feedback design process itself (O'Reilly and Leithead, 1991). The quantitative feedback design (QFD) robust control methodology for multiple input multiple output (MIMO) systems introduced by Horowitz (Horowitz, 1979; 1991) is perhaps the only known technique that considers large parametric uncertainty and quantitative performance requirements. The Horowitz's MIMO QFD method, using Schauder's fixed point theory, requires an  $n \times n$  time solution for the elements of the closed loop transfer matrix. The downside is that the method though useful and transparent in the hands of an experienced control engineer has not until recently lent itself easily to formal mathematization as in the more recent paradigms such as  $H^\infty$  control and  $\mu$  synthesis.

Here we present a systematic methodology: a model reference quantitative feedback design (MRQFD) theory, for the design of robust decentralized controllers for MIMO uncertain systems. Kidd (1984) has proposed a linear model reference feedback system, combined with direct Nyquist array (DNA) design techniques (Rosenbrock, 1974), to extend the DNA techniques to multivariable uncertain systems. One of our efforts is to develop a useful systematic design procedure, based on non-negative matrix theory, to achieve generalized diagonal dominance for parametric multivariable uncertain systems within the model reference concept. The theory of non-negative matrices plays a key role in assuring that the internal model reference loop system satisfies the  $H$ -matrix condition, that is, generalized diagonally dominant, over the frequency range of interest (Berman and Plemmons, 1979; Nwokah, 1988). A sensitivity based QFD method is then developed and used to solve the resultant robust control problem for each loop of the generalized diagonally dominant uncertain system. The QFD method proposed here ensures that satisfaction of the QFD specifications for each individual channel is guaranteed to satisfy the MIMO quantitative

specification. A successful application to the design of a robust multivariable controller for the Allison PD-514 aircraft turbine engine is presented to demonstrate the effectiveness of the methodology developed here.

## 2. MODEL REFERENCE QUANTITATIVE FEEDBACK DESIGN

### 2.1 The 3 Degree-of-freedom Feedback Structure

Consider the three degree-of-freedom multivariable feedback structure shown in Figure 1. The  $n$ -dimensional signals  $r(s)$ ,  $w(s)$ ,  $e(s)$ ,  $u(s)$ ,  $d(s)$ ,  $y(s)$ , and  $n(s)$  represent command input, filtered command input, error signal, control input, external disturbance, controlled output and sensor noise respectively. The matrices  $G(\alpha, s)$ ,  $K_a(s)$ ,  $H_m(s)$ ,  $K(s)$ , and  $F(s)$  are all  $n \times n$  rational transfer matrices.  $G(\alpha, s)$  is the parametric uncertain plant with real parameter vector  $\alpha$  being a member of a compact parameter space  $\Omega$ .  $K_a(s)$ ,  $H_m(s)$ ,  $K(s)$ , and  $F(s)$  are respectively the internal loop controller, the reference model, the outer loop controller, and prefilter matrix. The transfer matrices  $K_a(s)$ ,  $H_m(s)$ ,  $K(s)$  and  $F(s)$  have the additional property of being diagonal.

The internal model reference loop (IMRL) can be redrawn as shown in Figure 2. Let the reference model  $H_m(s)$  be described by a transfer matrix with the same pole-zero structure as the plant transfer matrix  $G(\alpha, s)$ ,  $\forall \alpha \in \Omega$ . Suppose an internal loop controller  $K_a(s)$  is chosen such that the resulting transfer matrix between  $u(s)$  and  $y(s)$ ,  $H_a(\alpha, s)$ , behaving dynamically as the reference model  $H_m(s)$ . Then, the resultant control design problem leads to a two degree-of-freedom (DOF) feedback structure as shown in Figure 3. Such a structure is similar to the standard two DOF control structure, which was advocated by Horowitz (1963) and is now very popular in the control community. However, in Figure 3, the transfer matrix  $H_a(\alpha, s)$  is compensated to be in generalized diagonal dominance (GDD) condition, which is a key feature that distinguishes over formulation from the standard 2-DOF structure. As shown in the work of Yau and Nwokah (1991), due to the GDD condition of  $H_a(\alpha, s)$ , the resulting 2-DOF control design is much easier than those in the classical MIMO QFT method (Horowitz, 1979) and the sequential MIMO QFT method (Yaniv and Horowitz, 1986).

The internal model reference loop can be also used in connection with the Nyquist array method (Rosenbrock, 1974). Actually, the work here is motivated by Kidd (1984) on the extension of the Nyquist array method to uncertain systems with the internal model reference concept.

### 2.2 The Feedback Control Specifications

The closed loop transfer matrix for Figure 3 can be given as:

$$T(\alpha, s) = [I + H_a(\alpha, s)K(s)]^{-1} H_a(\alpha, s)K(s)F(s) \quad (2.1)$$

and the MIMO quantitative design specification would be formally stated as follows:

- (1)  $T(\alpha, s)$  is stable for every  $\alpha \in \Omega$ ,

$$(2) \quad |t_{ii}(\alpha, j\omega) - t_i^0(j\omega)| \leq \mu_i(\omega), \quad \forall \omega \geq 0, \quad i=1,2,\dots,n, \quad \forall \alpha \in \Omega,$$

$$(3) \quad |t_{ij}(\alpha, j\omega)| \leq \gamma_{ij}(\omega), \quad i \neq j, \quad i,j=1,2,\dots,n, \quad \forall \alpha \in \Omega,$$

$$(4) \quad \sum_{i=1, i \neq j}^n \gamma_{ij}(\omega) < \min_{\alpha} |t_{ii}(\alpha, \omega)|, \quad i=1,2,\dots,n, \quad \forall \alpha \in \Omega,$$

$$(5) \quad \left| \frac{1}{1 + L^i(\alpha, j\omega)} \right| \leq m_i(\omega), \quad i=1,2,\dots,n, \quad \forall \alpha \in \Omega.$$

where  $L^i(\alpha, j\omega)$  is the  $i$ -th diagonal entry of  $H_s(\alpha, s)K(s)$ , with  $\mu_i(\omega)$  and  $\gamma_{ij}(\omega)$  being prespecified performance bounds, and  $t_i^0(j\omega)$  representing the target tracking response. Condition (1) is a robust stability requirement, while (2)-(4) are quantitative robust performance criteria. Condition (5) is a disturbance attenuation criterion. Note that condition (4) is a formal statement that the closed loop specification matrices  $T(j\omega)$  satisfies a diagonal dominance criterion (Rosenbrock, 1974). This condition, suggested by Nwokah (1988), provides a link between the Nyquist array method (Rosenbrock, 1974) and Horowitz's MIMO QFT method (Horowitz, 1991).

### 3. THE INTERNAL MODEL REFERENCE LOOP (IMRL)

#### 3.1 Model Matching Problem

As shown in Figure 2, the transfer matrix between  $u(s)$  and  $y(s)$ ,  $H_s(\alpha, s)$  may be written as

$$H_s(\alpha, s) = [I + G(\alpha, s)K_s(s)]^{-1} G(\alpha, s) [I + K_s(s)H_m(s)]. \quad (3.1)$$

In particular,  $H_m$  can be chosen to be equal to  $G_D$  where  $G_D$  is the diagonal elements of  $G(\alpha_0, s)$  for a specific parameter vector  $\alpha_0 \in \Omega$  (this choice of  $H_m$  may be arbitrary). The output error vector, between the reference model and the plant is given by

$$e_s(s) = y_m(s) - y(s), \quad (3.2)$$

and the error vector  $e_s$  is related to the input vector  $u$  by the transfer matrix equation

$$\begin{aligned} e_s(s) &= [I + G(\alpha, s)K_s(s)]^{-1} [H_m(s) - G(\alpha, s)]u(s) \\ &= [I + G(\alpha, s)K_s(s)]^{-1} G(\alpha, s) \cdot G^{-1}(\alpha, s) [H_m(s) - G(\alpha, s)]u(s) \end{aligned} \quad (3.3)$$

Define



$$S_s(\alpha, s) := [I + G(\alpha, s)K_s(s)]^{-1},$$

$$H_2(\alpha, s) := [I + G(\alpha, s)K_s(s)]^{-1} G(\alpha, s),$$

$$\Delta_s(\alpha, s) := H_m(s) - G(\alpha, s), \text{ and}$$

$$\Delta_m(\alpha, s) := G^{-1}(\alpha, s) [H_m(s) - G(\alpha, s)].$$

where  $S_s(\alpha, s)$ ,  $H_2(\alpha, s)$ ,  $\Delta_s(\alpha, s)$ , and  $\Delta_m(\alpha, s)$  are respectively the sensitivity function of the IMRL system, the closed loop transfer matrix of the  $H_2$  subsystem, the model error, and the relative model error. Hence, from (3.3), we have

$$e_s(s) = S_s(\alpha, s) \Delta_s(\alpha, s) u(s) = H_2(\alpha, s) \Delta_m(\alpha, s) u(s). \quad (3.4)$$

Internal stability requires that the error vector  $e_s(s)$  be bounded for all bounded input  $u(s)$ . Thus, the matching criterion can be represented as

$$\|S_s(\alpha, j\omega) \Delta_s(\alpha, s)\| = \|H_2(\alpha, j\omega) \Delta_m(\alpha, s)\| \leq \varepsilon(\omega), \quad \forall \omega \in [0, \infty), \quad \forall \alpha \in \Omega. \quad (3.5)$$

where  $\varepsilon(\omega)$  is the desired bound for the error vector  $e_s(j\omega)$  for all bounded  $\|u(j\omega)\|$ .

(3.5) is certainly satisfied if  $\Delta_s(\alpha, s) \rightarrow 0$  (or equivalently,  $\Delta_m \rightarrow 0$ ),  $\forall \omega \in [0, \infty)$ , and  $\forall \alpha \in \Omega$ . It is noted that  $\Delta_s \rightarrow 0$  implies that  $G(\alpha, j\omega) \rightarrow H_m(j\omega)$ . The model error  $\Delta_s$  and the relative model error  $\Delta_m$  are fixed when a parametric uncertain plant  $G(\alpha, s)$ ,  $\alpha \in \Omega$  is given and the reference model  $H_m(s)$  is selected.

Suppose that  $\Delta_s(\alpha, j\omega)$  and  $\Delta_m(\alpha, j\omega)$  are real stable transfer function matrices for every  $\alpha \in \Omega$  and  $u(s)$  is the set of input signals 2-norm bounded by unity. If  $H_2(\alpha, s)$  is diagonally internally stabilizable by the internal loop controller  $K_s(s)$ , then we may utilize the  $H_\infty$  norm (Francis, 1987) to rewrite (3.5) as

$$\max_{\alpha \in \Omega} \frac{1}{\varepsilon} \|S_s(\alpha, s) \Delta_s(\alpha, s)\|_\infty \leq 1, \text{ or} \quad (3.6)$$

$$\max_{\alpha \in \Omega} \frac{1}{\varepsilon} \|H_2(\alpha, s) \Delta_m(\alpha, s)\|_\infty \leq 1. \quad (3.7)$$

Note that (3.6) is a weighted sensitivity  $H_\infty$  optimization problem. Let

$$\delta_s(j\omega) := \max_{\alpha \in \Omega} \|\Delta_s(\alpha, j\omega)\|.$$

Thus, for the purpose of the design, we may rewrite (3.6) as

$$\max_{\alpha \in \Omega} \|S_s(\alpha, j\omega)\|_\infty \leq \frac{\varepsilon}{\delta_s}. \quad (3.8)$$

Observing equation (3.1), we know that if

$$\|I + G(\alpha, j\omega)K_a(j\omega)\| \gg 1 \quad \text{and} \quad \|I + K_a(j\omega)H_m(j\omega)\| \gg 1 \\ \forall \omega \in [0, \infty), \quad \forall \alpha \in \Omega, \quad (3.9)$$

then  $\|H_a(j\omega)\| \rightarrow \|H_m(j\omega)\|$ . Therefore, if a sufficiently high gain controller  $K_a(s)$  is allowed to be applied to the IMRL system, then  $H_a(\alpha, s)$  will approach the reference model  $H_m(s)$ . By (3.8), it is equivalent to asking the sensitivity function to be sufficiently small for the error vector  $e_a(j\omega)$  to be very small in norm.

We also may decompose  $H_a(\alpha, s)$  as the following

$$H_a(\alpha, s) = H_m(s) + H_a(\alpha, s) - H_m(s) \\ = [I + (H_a(\alpha, s) - H_m(s))H_m^{-1}(s)]H_m(s)$$

and let

$$M_a(\alpha, s) := (H_a(\alpha, s) - H_m(s))H_m^{-1}(s).$$

Note that the condition (3.9) would equivalently make  $M_a(\alpha, s)$  sufficiently small, that is,  $\|M_a\| \ll 1$  for every  $\omega$ , and every  $\alpha \in \Omega$ , which provides a foundation of the diagonal stabilizability for  $H_a(\alpha, s)$  and will be discussed later.

However, in practice there is likely to be some frequency above which equation (3.9) is not satisfied. This agrees with the fundamental understanding that the benefits of feedback in reducing sensitivity to parameter uncertainty is restricted to a low frequency region, normally up to the bandwidth of the system (Horowitz, 1963; Freudenberg and Looze, 1988).

As discussed previously, it is assumed that the variations or uncertainty in the plant parameters are known to lie within certain range, that is, the compact parameter set  $\Omega$  is known a priori. The internal loop controller,  $K_a(s)$ , is then determined such that the modulus of the diagonal elements of the plant transfer function matrix equals the modulus of the reference model transfer function matrix over the desired range. The off-diagonal entries of the reference model transfer function matrix are chosen to be zero, since this then tends to reduce interaction within the resulting compensated system. For the case of the diagonal reference model considered here, this corresponds to making the system  $H_a(\alpha, s)$  diagonally dominant or generalized diagonally dominant, i.e. H-matrix condition, over the frequency range of interest for every  $\alpha \in \Omega$ .

### 3.2 The Pole-Zero Characteristics of the IMRL

For simplicity, the notations  $s$  and  $\alpha$  will be omitted in the appropriate places without confusion in the following discussions. From Figure 2,

$$y = (I + GK_a)^{-1} G(I + K_a H_m)u = H_2 H_1 u = H_a u \quad (3.10)$$

where

$$H_a = H_2 H_1, \quad H_1 = I + K_a H_m, \quad H_2 = (I + GK_a)^{-1} G.$$

In general, since the selection (if possible) of the matrices  $H_m(s)$  and  $K_a(s)$  are under the control of the designer, the subsystem  $H_1$  may be assumed to be stable, and therefore the stability of the overall inner loop system depends only on the stability of the subsystem  $H_2$ . If the open loop plant transfer function matrix has unstable poles, then the plant may be stabilized by the appropriate choice of a stable controller matrix  $K_a(s)$ . It has been shown (Kidd, 1984; Yau and Nwokah, 1991) that the pole-zero characteristics of the IMRL system have the following relation.

$$\det[H_a] = \frac{Z_{H_1} Z_G}{P_{H_m} P_{H_2}}, \quad (3.11)$$

where  $Z_{H_1}$  and  $Z_G$  are the transmission zero polynomials of  $H_1$  and  $G$ , and  $P_{H_m}$  and  $P_{H_2}$  are the pole polynomials of  $H_m$  and  $H_2$  respectively.

Hence, it can be seen that the transmission zeros of the IMRL system are the set of transmission zeros of the plant plus the set of transmission zeros of the subsystem  $H_1$ . The poles of the system  $H_a$  are the set of poles of the reference model plus the set of closed loop poles of the subsystem  $H_2$ . Suppose  $H_m$  and  $G$  have the same number of unstable poles. Suppose further that  $H_a$  and  $H_m$  have the same number of unstable poles. Then, it is implied by (3.11) that  $H_2$  should be stable. Therefore, if  $G$  is minimum phase and high gain diagonal stabilizable, then  $H_2$  is high gain stabilizable. If  $Z_{H_1}$  and  $P_{H_2}$  are both Hurwitz, then  $H_a$  and  $G$  as well as  $H_m$  have the same number of unstable poles. Write  $G(\alpha, s) = [I + (G(\alpha, s) - H_m(s)) H_m^{-1}(s)] H_m(s)$ , and define

$$M_{G0}(\alpha, s) = (G(\alpha, s) - H_m(s)) H_m^{-1}(s), \quad (3.12)$$

then we have  $G(\alpha, s) = (I + M_{G0}(\alpha, s)) H_m(s)$ . Therefore

$$I + GK_a = I + (I + M_{G0}) H_m K_a = [I + M_{G0} H_m K_a (I + H_m K_a)^{-1}] (I + H_m K_a). \quad (3.13)$$

Define  $T_m(s) = H_m K_a (I + H_m K_a)^{-1}$ . Then (3.13) leads to

$$I + GK_a = (I + M_{G0} T_m) (I + H_m K_a). \quad (3.14)$$

It is noted that the stability of  $T_m$  is implied by the stability of  $I + H_m K_a$  (that is,  $H_1$ ). Suppose that  $M_{G0}(\alpha, s)$  is a non-singular perturbation of the nominal plant  $H_m(s)$  for every  $\alpha$ . Hence by Rouché's Theorem (Rosenbrock, 1974), the stability of  $I + G(\alpha, s) K_a(s)$  is implied by the stability of  $I + H_m(s) K_a(s)$  together with the condition of the spectral radius of  $M_{G0}(\alpha, s) T_m(s)$  being less than one,  $\rho(M_{G0} T_m) < 1$ , for every  $\alpha$  and for every  $s$ .

From the analysis of the IMRL presented above, it is clear that such a system possesses characteristics that can be used in the design of feedback control systems for multivariable plants subject to parametric uncertainty. If a sufficient feedback gain is applied to the subsystem  $H_2$ , then the plant poles can be moved sufficiently leftward in the  $s$ -plane such that the dominant response is that of the reference model. Hence  $K_a(s)$  should be chosen to robustly stabilize  $G(\alpha, s)$ . The conditions for robust diagonal stability will be discussed in the next section.

### 3.3 Conditions of Robust Diagonal Stabilizability

As discussed previously, the basic idea of the IMRL system is to choose the internal loop controller  $K_a(s)$  such that  $H_a(\alpha, s)$  is restricted strongly near  $H_m(s)$  for every  $\alpha \in \Omega$ . Then we stabilize  $H_m(s)$  by choice of an outer loop controller  $K(s)$  in the resulting 2-DOF design as described in section 2 such that  $H_a(\alpha, s)$  is also stabilized for every  $\alpha \in \Omega$ . From the analysis of the IMRL system, it is noted that the existence of an IMRL diagonal controller,  $K_a(s)$ , is strongly dependent on the feasibility of robust diagonal stabilizability. Here we first present some easily computable existence conditions for robust diagonal stabilization. Let  $G(\alpha, s)$ ,  $\alpha \in \Omega$  be an  $n \times n$  uncertain plant matrix set and  $D_N$  be the usual Nyquist contour. Then, by the Nyquist hodograph of an element of the matrix  $G(\alpha, s)$ , we shall mean the fuzzy Nyquist diagram generated by the union of the value sets (or templates, Horowitz, 1991) of the said element of  $G(\alpha, s)$  as  $s$  transverse  $D_N$ , and  $\alpha$  ranges over  $\Omega$ . Write

$$G = G_D + G_C = [I + G_C G_D^{-1}] \cdot G_D, \quad \forall \alpha \in \Omega,$$

where  $G_D = \text{diag}(g_{11}, g_{22}, \dots, g_{nn})$ , and  $G_C$  is the matrix of the off-diagonal elements of  $G$ , with zero diagonal elements. Define the interaction matrix of  $G$  as:

$$M_G = G_C \cdot G_D^{-1}, \quad \forall \alpha \in \Omega.$$

Then  $\det G = \det [I + M_G] \cdot \det G_D$ .

**Theorem 3.1 :** The transfer matrix  $G(\alpha, s)$  is robustly internally diagonally stabilizable on  $\Omega$  if and only if

- (i) Each  $g_{ii}(\alpha, s)$  is robustly internally stabilizable by some  $k_{ii}(s)$ , for  $i=1, 2, \dots, n$ .
- (ii)  $Z_{M_G}(\alpha) - P_{M_G}(\alpha) = 0$ , where  $Z_{M_G}(\alpha)$  and  $P_{M_G}(\alpha)$  are respectively the number of zeros and poles of  $\det [I + M_G]$  contained in  $C_{+e}$  for every  $\alpha \in \Omega$ . Or equivalently, the Nyquist hodograph of  $\det G(\alpha, j\omega) [\prod_{i=1}^n g_{ii}(\alpha, j\omega)]^{-1}$  neither touches nor encloses the origin for all  $\alpha \in \Omega$ .
- (iii)  $\det G(\alpha, s)$  and  $\det G_D(\alpha, s)$  (that is,  $\prod_{i=1}^n g_{ii}(\alpha, s)$ ) have the same number of unstable poles in  $C_{+e}$  for every  $\alpha$ .

**Proof :** By the principle of argument and the generalized Nyquist stability criterion, the proof can be established straightforwardly. A slight modification of Perez et al.(1991) would also give the proof.

Let  $\{G(\alpha, s)\}$  be the open-loop plant transfer matrix family and let  $\{G(\alpha, \infty)\}$  be the corresponding family of the high-frequency plant-gain matrices of  $\{G(\alpha, s)\}$ , where  $\{G(\alpha, \infty)\} = \{G(\alpha, s) : |s| \rightarrow \infty\}$ . A necessary condition for the existence of a fixed diagonal robust stabilizing controller for the family  $\{G(\alpha, s)\}$  is that for every nominal  $G(\alpha_0, \infty)$  and every other  $G(\alpha, \infty)$  in  $\{G(\alpha, \infty)\}$ ,  $\det G(\alpha, \infty) (\det G(\alpha_0, \infty))^{-1} > 0$ . The essence of this condition was noted by Horowitz (1963) a long time ago, but has recently been reinvestigated (see for example, Kwakernaak, 1982; Nwokah and Thompson, 1989 and references cited therein). It has been shown (Nwokah, 1988) that all the known necessary conditions for robust stabilizability were equivalent to

the *topological path connectedness* of the high-frequency plant-gain family  $\{G(\alpha, \infty)\}$ .

In the framework of the IMRL system, if  $G(\alpha, s)$  is high gain stabilizable, then both GDD of  $H_1(\alpha, s)$  and stabilization of  $H_2(\alpha, s)$  are feasible. For single-input single-output systems, the root locus technique is a powerful tool giving a significant insight upon the behavior of a feedback control system with adjustable gain. An extended tool, multivariable root locus technique, has been introduced to multivariable systems (Owens, 1978; MacFarlane, 1979). It is clear that for MIMO systems the finite eigenvalues of the closed loop system approach the transmission zeros of the open loop system whereas the asymptotes of the remaining poles are again symmetrically distributed within the complex plane. Since for uncertain plants the right-half plane plant zeros are not exactly known and cannot be compensated for by unstable compensator poles, the plant zeros must lie in the left-half complex plane. Furthermore, the asymptotes can be adjusted by means of the controller so as to point to stable pole positions *only if* there are at most two poles more than plant zeros, or equivalently,  $G(\alpha, s)$  has uniform rank  $r \leq 2$  for every  $\alpha \in \Omega$  (Owens, 1978).

The conditions for robustly diagonal stabilization are stated in the following theorem.

**Theorem 3.2:** The sufficient conditions for the existence of a fixed, diagonal, proper, stable, and minimum-phase controller  $K_a(s)$  such that  $H_2(\alpha, s) = [I + G(\alpha, s)K_a(s)]^{-1}G(\alpha, s)$  is asymptotically stable for every  $\alpha \in \Omega$  are as following:

- (i) Each plant in  $\{G(\alpha, s)\}$  arises from a stabilizable and detectable system;
- (ii) The number of transmission zeros of each  $G(\alpha, s)$  in  $\{G(\alpha, s)\}$  is the same, and furthermore every transmission zero is in a bounded region of the left-half complex plane;
- (iii) Each plant is a nonsingular perturbation of the nominal plant and has uniform rank  $r \leq 2$ ;
- (iv) There exists a fixed positive diagonal matrix  $D$  such that for each plant the matrix  $\Pi_\infty D$  has all its eigenvalues in a bounded region of the right-half complex plane for every  $\alpha \in \Omega$ , where  $\Pi_\infty = \lim_{|s| \rightarrow \infty} G(\alpha, s) \cdot G(\alpha_0, s)^{-1}$ .

**Proof:** The proof can be obtained from Kwakernaak (1982) by changing the square matrix therein with the positive diagonal matrix in condition (iv) presented here.

The minimum-phase condition and uniform rank limitation are required to guarantee high gain stability. However, in the real world, it is impossible to have infinitely high gain due to the bandwidth consideration. The IMRL system can also be applied to non-minimum phase systems if the number of non-minimum phase transmission zeros is the same for every plant in  $\{G(\alpha, s)\}$  and only a reasonable level of gain is required for GDD achievement, that is, the feedback would not push the closed loop poles to the unstable transmission zeros. The application of the design methodology to a MIMO aircraft engine control problem presented in this paper is indeed a successful demonstration of the IMRL scheme being applied to a non-minimum phase multivariable system.

## 4. ACHIEVMENT OF GENERALIZED DIAGONAL DOMINANCE

### 4.1 Preliminaries

Here we present a brief summary of relevant non-negative matrix theory. Let  $R$ ,  $C$  and  $P$  represent respectively the set of real numbers, complex numbers and non-negative numbers. If  $S$  is any set, then  $M_{m,n}(S)$  represents the set of  $m \times n$  matrices with entries from the set  $S$ . The comparison matrix  $M(Z)$  of a complex matrix  $Z \in M_{n,n}(C)$  is defined by:  $m_{kk} = |z_{kk}|$ ,  $k=1,2,\dots,n$ , and  $m_{k\ell} = -|z_{k\ell}|$  for  $k \neq \ell$ ,  $k, \ell=1,2,\dots,n$ .

**Definition 4.1** (Berman and Plemmons, 1979) : A matrix  $A \in M_{n,n}(R)$  is called non-negative (denoted:  $A \geq 0$ ) if all the elements of  $A$  are non-negative ( $a_{ij} \geq 0$  for  $i=1,2,\dots,n$ ;  $j=1,2,\dots,n$ ). We say that  $A \geq B$  if  $A-B \geq 0$ .

**Definition 4.2** (Rosenbrock, 1974) : A matrix  $Z \in M_{n,n}(C)$  is said to be diagonally dominant if either:

- (i)  $|z_{kk}| > \sum_{\ell=1, \ell \neq k}^n |z_{k\ell}|$ , (row dominance), or
- (ii)  $|z_{kk}| > \sum_{\ell=1, \ell \neq k}^n |z_{\ell k}|$ , (column dominance)

**Definition 4.3** (Berman and Plemmons, 1979) : A matrix  $Z \in M_{n,n}(R)$  is called an M-matrix if the diagonal elements are non-negative, the off-diagonal elements are non-positive and principal minors are positive.

**Definition 4.4** (Ostrowski, 1937) : A matrix  $Z \in M_{n,n}(C)$  is called H-matrix if  $M(Z)$  is an M-matrix.

**Definition 4.5** (Fan, 1967) : A matrix  $Z \in M_{n,n}(C)$  is irreducible if there does not exist a permutation matrix  $P \in M_{n,n}(P)$  such that

$$PZP^{-1} = \begin{bmatrix} \bar{Z}_{11} & \bar{Z}_{12} \\ 0 & \bar{Z}_{22} \end{bmatrix}$$

where  $\bar{Z}_{11}$  and  $\bar{Z}_{22}$  are square submatrices.

A real matrix  $A \in M_{n,n}(P)$  is said to dominate a complex matrix  $Z \in M_{n,n}(C)$  if  $a_{k\ell} \geq |z_{k\ell}|$ ,  $k, \ell=1,2,\dots,n$ . Next the famous theorem of Perron and Frobenius on the spectral properties of non-negative matrices is stated.

**Theorem 4.1** : Suppose  $A \in M_{n,n}(P)$  is irreducible. Then there exist an eigenvalue  $\lambda_0$  of  $A$  (called the Perron-Frobenius eigenvalue) such that

- (i)  $\lambda_0 \in \mathbb{R}$ , and  $\lambda_0 > 0$ ;
- (ii) with  $\lambda_0$  can be associated positive left and right eigenvectors;
- (iii)  $\lambda_0 \geq |\lambda|$  for every other eigenvalue  $\lambda$  of  $A$ ;
- (iv) the eigenvectors associated with  $\lambda_0$  are unique to constant multipliers;
- (v) if  $0 \leq B \leq A$  and  $\beta$  is an eigenvalue of  $B$ , then  $|\beta| \leq \lambda_0$ ; moreover,  $|\beta| = \lambda_0$  implies  $B=A$ ; and,
- (vi)  $\lambda_0$  is a simple root of the characteristic equation of  $A$ .

The Perron root of a non-negative irreducible matrix is the maximum eigenvalue of the matrix. By Theorem 4.1, this eigenvalue is real and non-negative.

**Definition 4.6 :** A matrix  $A \in M_{n,n}(\mathbb{C})$  is generalized row diagonally dominant if there exists an  $x \in \mathbb{R}^n$ ,  $x > 0$  such that

$$|a_{ii}| x_i > \sum_{j=1, j \neq i}^n |a_{ij}| x_j \quad \text{for } i=1,2,\dots,n.$$

A matrix  $A \in M_{n,n}(\mathbb{C})$  is generalized column diagonally dominant if there exists a  $x \in \mathbb{R}^n$ ,  $x > 0$  such that

$$|a_{ii}| x_i > \sum_{j=1, j \neq i}^n |a_{ji}| x_j \quad \text{for } i=1,2,\dots,n.$$

Let  $Z \in M_{n,n}(\mathbb{C})$ , write

$$Z = D + C = [I + CD^{-1}]D, \quad (4.1)$$

where  $D = \text{diag}(z_{11}, z_{22}, \dots, z_{nn})$ , and  $C$  is the matrix of the off-diagonal elements of  $Z$ , with zero diagonal elements. Define the interaction matrix of  $Z$  as  $M = CD^{-1}$ .

**Theorem 4.2 :** For an irreducible matrix  $Z \in M_{n,n}(\mathbb{C})$ , the following are equivalent:

- (i)  $M = CD^{-1}$  has perron root  $\lambda_0 < 1$ .
- (ii)  $Z$  is generalized row diagonal dominant.
- (iii) There exists a diagonal  $Q > 0$  such that  $Q^{-1}ZQ$  is row dominant.
- (iv)  $Z$  is generalized column diagonal dominant.
- (v) There exist a diagonal  $\bar{Q} > 0$  such that  $\bar{Q}Z\bar{Q}^{-1}$  is column dominant.
- (vi)  $Z$  is an H-matrix.

*Proof :* The proof can be obtained with a slight modification of Limebeer(1982).

**Corollary 4.2 (Nwokah, 1978) :** If  $Z \in M_{n,n}(\mathbb{C})$ , then its eigenvalues are contained in the union of

the discs

$$|\lambda - z_{ii}| \leq \lambda_0 |z_{ii}|, \text{ for } i = 1, 2, \dots, n. \quad (4.2)$$

where  $\lambda_0$  is the perron root of  $M = CD^{-1}$ .

#### 4.2 Generalized Diagonal Dominance of The IMRL

Consider a MIMO system, with a diagonal reference model denoted by

$$H_m = \text{diag}(h_{m1}, \dots, h_{mn}), \quad (4.3)$$

a diagonal compensator denoted by

$$K_s = \text{diag}(k_{s1}, \dots, k_{sn}), \quad (4.4)$$

and with the inner loop system denoted by the transfer-function matrix equation

$$H_s = (I + GK_s)^{-1} G(I + K_s H_m). \quad (4.5)$$

Let

$$H_1 = I + K_s H_m, \text{ and } H_2 = (I + GK_s)^{-1} G. \quad (4.6)$$

Since  $K_s$  and  $H_m$  are diagonal matrices,  $H_1$  is a diagonal matrix, and hence is already an H-matrix. Since the product of an H-matrix with a diagonal matrix with non-zero diagonal elements also gives another H-matrix, it follows that  $H_s$  is an H-matrix *if and only if*  $H_2$  is an H-matrix (Fiedler and Patk, 1962). Hence it is sufficient for  $H_2$  to be an H-matrix in order for  $H_s$  to be generalised diagonally dominant. The inverse transfer matrix  $\hat{H}_2$  is given by

$$H_2^{-1} := \hat{H}_2 = \hat{G} + K_s. \quad (4.7)$$

Let  $B = (b_{kq})$  and  $W = \text{diag}(w_1, w_2, \dots, w_m)$ , where  $b_{kk} = 0$  for  $1 \leq k \leq m$ ,  $b_{kq} = |\hat{h}_{2kq}|$  for  $k \neq q$ ,  $k, q = 1, 2, \dots, m$ , and  $w_k = |\hat{h}_{2kk}|$  for  $1 \leq k \leq m$ . Write  $\lambda_0 = \lambda_0(BW^{-1})$  for the Perron root (maximum eigenvalue) of  $BW^{-1}$ . Then from Theorem 4.2,  $\hat{H}_2$  being an H-matrix is equivalent to the condition  $\lambda_0 < 1$ .

By Gershgorin's theorem (Rosenbrock, 1974) and Corollary 4.2, it follows that if:

$$\lambda_0 = |\hat{h}_{kk}|^{-1} \sum_{q=1, q \neq k}^n |\hat{h}_{kq}| < 1, \quad k = 1, 2, \dots, n, \quad (4.8)$$

then  $\hat{H}_2$  is an H-matrix. Hence, for design purposes, we can let

$$\lambda_0 |\hat{h}_{kk}| \geq \sum_{q=1, q \neq k}^n |\hat{h}_{kq}|, \quad k = 1, 2, \dots, n, \quad (4.9)$$

and  $\lambda_0 < 1$ , to guarantee that  $\hat{H}_2$  is an H-matrix. We state the result as the following Lemma.

**Lemma 4.1:** If  $|k_{si} + \hat{g}_{ii}| \geq \frac{1}{\lambda_0} \sum_{j=1, j \neq i}^n |\hat{g}_{ij}|$ , for  $i = 1, 2, \dots, n$ , and  $\lambda_0 < 1$ , then  $\hat{H}_2$  is an H-matrix.



*Proof:* Since  $\hat{H}_2 = K_a + \hat{G}$ , the lemma is a direct result of the above discussion.

For design purposes, the main concern is designing a controller  $K_a(s)$  to make  $\hat{H}_2$  an H-matrix. Thus, by Lemma 4.1 and the property of norms

$$|k_{ii} + \hat{g}_{ii}| \geq |k_{ii}| - |\hat{g}_{ii}|, \quad (4.10)$$

we obtain a bound on  $k_{ii}$  to insure diagonal dominance:

$$|k_{ii}| \geq |\hat{g}_{ii}| + \frac{1}{\lambda_0} \sum_{j=1, j \neq i}^n |\hat{g}_{ij}|. \quad (4.11)$$

The above result provides a guide to the design of the controller  $K_a$  to make  $\hat{H}_2$  an H-matrix. However, of particular importance is the design of the controller  $K_a$  which makes the inner loop transfer matrix  $H_e$  an H-matrix.

From the definition in equations (4.1), we have

$$Z = (I + M) D. \quad (4.12)$$

Taking inverse in (4.12) gives:

$$Z^{-1} = \hat{Z} = D^{-1} (I + M)^{-1}. \quad (4.13)$$

Since D is diagonal, asking  $(I + M)^{-1}$  to be an H-matrix is equivalent to making  $\hat{Z}$  an H-matrix. We therefore need to provide conditions, which guarantee that Z is an H-matrix whenever  $\hat{Z}$  is an H-matrix. By the properties of non-negative matrices (Berman and Plemmons, 1979), it is clear that  $\lambda_0(T) < 1$  if and only if  $(I - T)^{-1}$  exists and

$$(I - T)^{-1} = \sum_{k=0}^{\infty} T^k < \infty. \quad (4.14)$$

Let  $\lambda_0 = \lambda_0(M) < 1$ , then the eigenvalue problem  $Mx = \lambda_0(M)x$  has a positive solution x. Such an x exists by the Perron-Frobenius theorem. Thus

$$(I + M)x = [1 + \lambda_0]x, \quad x > 0, \quad (4.15)$$

implies that

$$\begin{aligned} (I + M)^{-1}x &= \frac{1}{1 + \lambda_0}x \\ &= \left[ I + \sum_{k=1}^{\infty} (-1)^k M^k \right] x \\ &= (I + \bar{M})x, \end{aligned} \quad (4.16)$$

where  $\bar{M} = \sum_{k=1}^{\infty} (-1)^k M^k$ . Due to the fact that  $\lambda_0 < 1$ , then

$$\begin{aligned}
\frac{1}{1+\lambda_0} &= 1 - \lambda_0 + \lambda_0^2 - \lambda_0^3 + \lambda_0^4 - \dots \\
&< 1 + \lambda_0 + \lambda_0^2 + \lambda_0^3 + \lambda_0^4 + \dots \\
&= \frac{1}{1-\lambda_0} \quad (\text{since } 0 < \lambda_0 < 1).
\end{aligned} \tag{4.17}$$

Hence

$$(I + \tilde{M})x = \frac{1}{1+\lambda_0}x \leq \frac{1}{1-\lambda_0}x. \tag{4.18}$$

Therefore, for  $I + \tilde{M}$  to be an H-matrix, we need  $\lambda_0(\tilde{M}) < 1$ , i.e. the Perron root of  $\tilde{M}$  less than 1, or  $\frac{1}{1-\lambda_0} - 1 < 1$ , which implies  $\lambda_0(M) < \frac{1}{2}$ . Hence we state:

**Lemma 4.2 :** Let  $Z \in M_m(\mathbb{C})$  have the interaction matrix  $M = CD^{-1}$ , with perron root  $\lambda_0(M) = \lambda_0(CD^{-1})$ . Suppose  $\lambda_0(M) < \frac{1}{2}$ , then  $Z$  and  $Z^{-1}$  are both H-matrices.

Combining Lemma 4.1 and Lemma 4.2, we obtain the main result of this section as follows:

**Theorem 4.3 :** In the internal model reference loop system proposed in Figure 2, if

$$|k_{ii}| \geq \frac{1}{\lambda_0} \sum_{j=1, j \neq i}^n |\hat{g}_{ij}| + |\hat{g}_{ii}|, \quad i=1, 2, \dots, n, \quad \forall s \in D_N,$$

and  $\lambda_0 < \frac{1}{2}$ , then  $H_s = H_2 H_1$  is an H-matrix for all  $s$  on  $D_N$ .

### 4.3 GDD for Parametric Uncertain Systems

Consider the IMRL system with the parametric uncertain plant  $G(\alpha, s)$  as shown in Figure 2. The output vector is related to the input vector by the following transfer matrix.

$$H_s(\alpha, s) = (I + G(\alpha, s)K_s)^{-1} G(\alpha, s) (I + K_s H_m) \tag{4.19}$$

Let

$$H_2(\alpha, s) = (I + G(\alpha, s)K_s)^{-1} G(\alpha, s) \tag{4.20}$$

The main purpose in this section is to make  $H_2(\alpha, s)$  GDD for every member of  $G(\alpha, s)$  in the parameter set  $\alpha \in \Omega$ . Equivalently, we need to insure that  $H_2(\alpha, s)$  is GDD for every plant member. Taking inverses in (4.20), we have

$$\hat{H}_2(\alpha, s) = K_s(\alpha, s) + \hat{G}(\alpha, s) \tag{4.21}$$

Write

$$W(\alpha, s) = \hat{H}_2(\alpha, s) \quad (4.22)$$

Let  $W_0(s)$  be the majorant transfer matrix of  $W(\alpha, s)$ , which is defined as follows

$$|w_{ii}^0| = \min_{\alpha \in \Omega} |w_{ii}(\alpha, s)|, \quad i = 1, 2, \dots, n; \text{ and} \quad (4.23)$$

$$|w_{ij}^0| = \max_{\alpha \in \Omega} |w_{ij}(\alpha, s)|, \quad i \neq j, \quad i = 1, 2, \dots, n. \quad (4.24)$$

Define

$$D_0(s) = \text{diag}(|w_{ii}^0(s)|), \quad (4.25)$$

and

$$C_0(s) = C_{ij}^0(s) = \begin{cases} 0, & i = j \\ |w_{ij}^0(s)|, & i \neq j, \quad i, j = 1, 2, \dots, n. \end{cases} \quad (4.26)$$

The majorant matrices are most easily obtained from the QFD uncertainty templates (Horowitz, 1979). Let the interaction index  $\lambda_m(s)$  of  $W_0(s)$  be the majorant interaction index of  $W(\alpha, s)$ , and let  $\lambda_0(\alpha, s)$  be the interaction index of  $W(\alpha, s) \forall \alpha \in \Omega$ .

**Lemma 4.3:**  $\lambda_m(s) \geq \lambda_0(\alpha, s)$  for all  $\alpha \in \Omega$ , where  $\lambda_0(\alpha, s)$  is the Perron root of  $W(\alpha, s)$ .

*Proof:* This follows the fact that the Perron root of an irreducible non-negative matrix is a continuous and monotonic function of the matrix elements (Seneta, 1973).

Suppose  $W(\alpha, s)$  is generalized diagonally dominant for all  $\alpha \in \Omega$  at every  $s$  considered, i.e.  $\lambda_0(\alpha, s) < 1$  for every  $s$ , or the slightly stronger condition arising from Lemma 3.3,  $\lambda_m(s) < 1$  for all  $s$ . We note here that  $\lambda_0(s)$  can be made less than 1 at every  $s$  by suitable choice of  $K_*(s)$ .

Let

$$|g_{ii}^0(s)| = \min_{\alpha \in \Omega} |\hat{g}_{ii}(\alpha, s)|, \quad i = 1, 2, \dots, n; \text{ and} \quad (4.27)$$

$$|g_{ij}^0(s)| = \max_{\alpha \in \Omega} |\hat{g}_{ij}(\alpha, s)|, \quad i, j = 1, 2, \dots, n. \quad (4.28)$$

Parallel to Lemma 4.1, we can have the following Lemma for uncertain systems.

**Lemma 4.4:** If  $|k_{ii}(s)| \geq |g_{ii}^0(s)| + \frac{1}{\lambda_m(s)} \sum_{j=1, j \neq i}^n |g_{ij}^0(s)|$ ,  $i=1, 2, \dots, n$ , for all  $s \in D_N$ , and  $\lambda_m < 1$ , then  $\hat{H}_2(\alpha, s)$  is an H-matrix for all  $\alpha \in \Omega$ , and for all  $s$  considered.

Similarly, we have a parallel version of Theorem 4.3 for parametric uncertain systems.

**Theorem 4.4:** If  $|k_{ii}(s)| \geq |g_{ii}^0(s)| + \frac{1}{\lambda_m(s)} \sum_{j=1, j \neq i}^n |g_{ij}^0(s)|$ ,  $i=1, 2, \dots, n$ , for all  $s \in D_N$ , and  $\lambda_m < \frac{1}{2}$ , then  $H_*(\alpha, s) = H_2(\alpha, s) H_1$  is an H-matrix, for all  $\alpha \in \Omega$ , and at every  $s$  considered.

In fact, if  $|k_{ai}(s)|$  is very large then  $H_a(\alpha, s)$  will approach  $H_m(s)$ , which is the very idea for the model reference feedback system proposed here. By Theorem 4.4, we can find  $k_{ai}(s)$ ,  $i=1, 2, \dots, n$ , at every frequency such that Theorem 4.4 is satisfied. Our recommendation is to make  $\lambda_m < 0.2$  (Araki et al., 1981).

## 5. INDIVIDUAL CHANNEL DESIGN WITH QFD METHOD

Once a reasonable level of diagonal dominance has been achieved ( $\lambda_0 \leq 0.2$ ) over the set  $\Omega$ , we can use single loop QFD design methodology for the design of each loop of the MIMO system. The QFD problem can be posed as a formal sensitivity constrained optimization problem which reduces to the problem statements in  $H^\infty$  control when the hard performance constraints and parametric uncertainty descriptions are relaxed. Details of the sensitivity-based QFD are provided in Nwokah et al. (1992).

Suppose there is given an ideal target closed loop transmission function  $T_b^0(s)$  and an ideal disturbance response transfer function  $T_b^0(s)$  for the resulting  $i$ -th single loop channel obtained by the internal model reference loop method developed in the last section. The QFD problem is to find (if possible) an admissible pair of strictly proper, real rational, and stable functions  $\{k_i(s), f_i(s)\}$  in the two degree-of-freedom feedback arrangement, which is shown in Figure 3, such that the following conditions are satisfied with some measure of optimality (for various individual channels  $i, i=1, 2, \dots, n$ ):

- (i) robust stability:  $T^i(\alpha, s)$  is stable,  $\forall \alpha \in \Omega$ ,
- (ii) robust performance:  $\max_{\alpha \in \Omega} |T^i(\alpha, s) - T_b^0(s)| \leq \delta_T^i(s), \forall s$ ,
- (iii) disturbance attenuation:  $\max_{\alpha \in \Omega} |T_b^i(s)| \leq |T_b^0(s)| = \delta_b^i(s), \forall s$

where  $\delta_T^i(s) \geq 0$  and  $\delta_b^i(s) \geq 0$  are specified a priori, and

$$T^i(\alpha, s) = H^i(\alpha, s) \cdot f_i(s), \quad T_b^i(s) = H_b^i \cdot f_i(s)$$

$$H^i(\alpha, s) = \frac{L^i(\alpha, s)}{1 + L^i(\alpha, s)}, \quad H_b^i(s) = \frac{L_b^i(s)}{1 + L_b^i(s)}$$

$$S^i(\alpha, s) = \frac{1}{1 + L^i(\alpha, s)}, \quad S_b^i(s) = \frac{1}{1 + L_b^i(s)}$$

$$L^i(\alpha, s) = h_a^i(\alpha, s) \cdot k_i(s), \quad L_b^i(s) = h_{a0}^i(s) \cdot k_i(s)$$

under the constraint that  $k_i(s)$  is an internally stabilizing controller for the plant set  $\{h_a^i(s)\}$ .

After appropriate algebraic manipulations, we can obtain the equivalent descriptions for conditions (i) to (iii) in terms of sensitivity function constraints. Furthermore by suitable choice of the real rational stable weighting functions  $W^i(s)$  and  $V^i(s)$ , the following equivalent  $H^\infty$  minimization problem for the QFD optimization problem can be set up (Nwokah et al., 1992):

$$\min_{k_i \in K} \sup_{\omega} \left\{ \|W^i S^i\|_\infty + \|V^i H^i\|_\infty \right\} < 1. \quad (5.1)$$

Alternatively we can solve the simpler  $H^\infty$  problem (Chiang and Safanov, 1988):

$$\min_{k_i \in K} \left\| \frac{W^i S^i}{V^i H^i} \right\|_\infty = \mu_i. \quad (5.2)$$

Indeed  $\mu_i < 1/\sqrt{2}$  is a sufficient condition for the original  $H^\infty$  to be solved (Francis, 1987). Once  $k_i$  is determined, we draw the graph of  $L_0 = h_{z0}^i k_i$  on the Nichols chart. This forms the initializing loop transmission function for the QFD optimization algorithm. On the same Nichols chart are superimposed the standard QFD performance and stability boundaries. Then the QFD optimization routine strives to reduce the gain-bandwidth area of loop transmission function by moving  $L_0$  towards the boundaries at every frequency, as the work done by Thompson and Nwokah (1991). If the exact target function  $T_h(s)$  is the required performance, we can go further to design a prefilter  $f_i(s)$  making the closed loop system satisfy the quantitative specifications.

## 6. AN AIRCRAFT ENGINE APPLICATION

The application of the developed MRQFD method to the design of a robust controller for the Allison PD-514 aircraft turbine engine is presented in this section. The PD-514 is a low-bypass-ratio, twin-spool, axial flow turbofan aircraft engine with augmenter as shown in Figure 4. The PD-514 has two control inputs, namely, fuel flow and exit nozzle area, which are used to control the output of thrust and total air flow.

The objective of the multivariable engine controller design is to provide stable performance, and to improve the engine thrust response by providing fast response with no overshoot, and zero steady-state error over the flight envelope. Also, the control system is required to be robust in achieving desired performance despite uncertainty.

The performance of aircraft engines can be modelled accurately through aerothermodynamic relations. The result of this modelling process is a set of highly nonlinear differential equations. However, the resulting models are too complex to be used in controller design. Therefore, in order to simplify the controller design process, the performance of the engine is linearized about an operating point, which is defined by altitude, mach number, and power lever angle (PLA) or throttle setting of the aircraft. The modelling process is then repeated for a number of operating points in order to define the performance over the entire flight envelope. The resulting linear models introduce structured uncertainty due to parameter variations between models. Unstructured uncertainty is also present in the form of unmodelled dynamics, unmodelled parameter variations,

and measurement errors.

The modelling process of the PD-514 is described in the work of Gallagher (1992). The models of the PD-514 are originally obtained in state-space form. In order to apply the MRQFD method to the control system design, the models are transformed to the form of transfer matrix representation. The flight envelope including forty seven operating points is shown in Figure 5. Here, a robust decentralized controller is designed for a set of thirty seven operating points of the PD-514 engine. The number of the non-minimum phase transmission zeros is the same for all these thirty seven operating points.

The input-output relationship may be written as:

$$y = G(\alpha, s) u \quad (6.1)$$

where

$$u = \begin{bmatrix} u_1 \\ u_2 \end{bmatrix} = \begin{bmatrix} \text{fuel flow} \\ \text{nozzle area} \end{bmatrix}, \quad y = \begin{bmatrix} y_1 \\ y_2 \end{bmatrix} = \begin{bmatrix} \text{thrust} \\ \text{air flow} \end{bmatrix}$$

and

$$G(\alpha, s) = \begin{bmatrix} g_{11} & g_{12} \\ g_{21} & g_{22} \end{bmatrix} \quad (6.2)$$

The transfer function for each entry of  $G(\alpha, s)$  may be represented as follows.

$$g_{ij} = \frac{k_{ij}(s+z_{ij}^1)(s+z_{ij}^2)}{(s+p_{ij}^1)(s+p_{ij}^2)}, \quad i, j=1,2.$$

The values of  $k_{ij}$ ,  $z_{ij}^1$ ,  $z_{ij}^2$ ,  $p_{ij}^1$ , and  $p_{ij}^2$ ,  $i, j=1,2$  for different operating points were given in Gallagher (1992). Figure 6 contains the Nyquist arrays for the thirty seven operating points. In Figure 6, the uncertainty of the system is represented by the spread of the Nyquist plots for a single channel. In this application, the thrust/fuel flow ( $g_{11}$ ) channel shows the most uncertainty, and the air flow/fuel flow ( $g_{21}$ ) the least. Figure 7 shows that the interaction indices are not less than one for every operating point, that is, the system is not robust GDD.

The first step in the controller design is the selection of an appropriate reference model  $H_m(s)$ . The reference model was obtained by taking the 'center of gravity' of the transfer matrix set, and neglecting its off-diagonal elements. This produces the transfer matrix:

$$H_m(s) = \begin{bmatrix} \frac{-0.1371(s+4.2407)(s-11.1867)}{(s+3.1340)(s+4.2407)} & 0 \\ 0 & \frac{0.1891(s+3.134)(s+10.7487)}{(s+3.1340)(s+4.2407)} \end{bmatrix} \quad (6.3)$$

Then from Theorem 4.4, and letting  $\lambda_m = 0.2$ , we may generate the design bounds for the internal

loop controller  $K_a(s)$ . Figure 8 shows the design bounds of  $k_{a1}(s)$  and  $k_{a2}(s)$  for the thirty seven operating points. Implementation of the internal loop controller

$$K_a(s) = \begin{bmatrix} \frac{20(\frac{s}{3.28}+1)}{(\frac{s}{50}+1)} & 0 \\ 0 & \frac{40(\frac{s}{8.51}+1)}{(\frac{s}{5}+1)} \end{bmatrix} \quad (6.4)$$

into the IMRL of Figure 2 results in the Nyquist arrays in Figure 9. This figure shows that the uncertainty is significantly reduced and the system is generalized diagonally dominant. Figure 10 is a plot of the interaction indices (Perron root) for the compensated inner loop,  $H_a(\alpha, s)$ , which also shows that the system is now sufficiently GDD, since  $\lambda_m < 0.2$  for most of the operating points considered as suggested in Section 4. Now that the system is sufficiently GDD, the single loop QFD method as described in Section 5 may be applied for the design of each individual loop.

The initial step of the QFD problem is the description of the desired performance of the system. Figure 11 shows the upper and lower time response bounds for thrust/fuel flow channel and the corresponding frequency response for the upper ( $T_u$ ), lower ( $T_l$ ), and nominal ( $T_0$ ) performance bounds. Also, the maximum disturbance response was selected as 2 (6 dB) and the relative stability margin was selected as 1.25 (1.94 dB). The normalized plant uncertainty  $\delta_{H_a}$  was obtained from the Bode diagram of the plants for the compensated inner loop transfer function. The constraint for the sensitivity function,  $M_1(\omega)$ , is thus obtained as described in Section 5. Figure 12 shows that the desired time response bounds and their corresponding frequency response bounds of the second channel (air flow/nozzle area). The required maximum disturbance response and relative stability margin for the second channel is the same as the first channel. Thus, we also obtain the sensitivity function constraint  $M_2(\omega)$  for channel two.

Now, we may apply the QFD technique for designing the outer loop controller  $k_1(s)$  and  $k_2(s)$ . If necessary, we may go further to design the prefilters  $f_1(s)$  and  $f_2(s)$ . The outer loop controller is designed to be

$$K(s) = \begin{bmatrix} \frac{388.2(s+4.3)(s+10.0)}{s(s+11.8)(s+30)(s+10.0)} & 0 \\ 0 & \frac{507.0(s+40)}{s(s+13.0)^2} \end{bmatrix} \quad (6.5)$$

The compensated loop transmission function and the performance boundaries in the Nichols chart are shown in Figure 13 for channel one and in Figure 14 for channel two. The thrust response to a unit step input of fuel flow is shown in Figure 15 for four typical operating points. This response satisfies the design requirements so it is not necessary to go further to design prefilter  $f_1(s)$ . Notice that the reverse reaction near  $t=0$  is due to the effect of the existence of one nonminimum phase

zero in the resulting closed loop transfer matrix. The air flow response to a unit step input of nozzle area is shown in Figure 16, which shows that the desired performance requirement is satisfied by the designed control system. Hence, it is not necessary to design the prefilter for the channel two either.

## 7. CONCLUSIONS

In this paper we have introduced a new methodology: model reference quantitative feedback design, for the design of the MIMO parametric uncertain control systems. If sufficient feedback gain for a MIMO uncertain system is allowed, we may achieve robust generalized diagonal dominance and uncertainty reduction with the model reference concepts. The design guides for obtaining generalized diagonal dominance condition, that is, H-matrix, have been derived for the parametric uncertain multivariable systems. Since the quantitative specifications for uncertainty and performance are of practical importance, a sensitivity based QFD method has been developed and been used for each individual channel so as to obtain a robust controller which made the closed loop system satisfy the MIMO quantitative specifications.

The developed MRQFD method has been successfully applied to the design of a robust decentralized controller for the Allison PD-514 aircraft turbine engine. This application demonstrated the effectiveness of the proposed method for practical applications. Although further nonlinear optimization techniques may be applied to obtain the optimal controller gain-bandwidth area, it was not done here. Nevertheless, it was shown that the designed controllers gave a very good result in stability and performance robustness.

## ACKNOWLEDGMENT

The authors wish to thank R. Davies and D. Veiey for their work on the design of the internal loop controller in Section 6.

## REFERENCES

- Araki, M., B. Kondo, and K. Yamamoto, 1981, "GG-pseudo-band Method for the Design of Multivariable Control Systems," *8th IFAC Triennial World Congress*, Kyoto, Japan, pp. 393-398.
- Berman, A. and R.J. Plemmons, 1979, *Nonnegative matrices in the mathematics sciences*. Academic Press, New York.
- Bode, H.W., 1945, *Network Analysis and Feedback Amplifier Design*, Van Nostrand, New York.
- Chiang, R.Y. and M.G. Safanov, 1988, *Robust-Control Toolbox for the MATLAB™*, South Natick, MA: The Mathworks Inc.
- Desoer, C. A., and M. Vidyasagar, 1975, *Feedback Systems: Input-Output Properties*, Academic Press, New York.
- Dorato, P. and R. Yedavail, 1990, *Recent Advances in Robust Control* IEEE Press, New York.
- Doyle, J.C. and G. Stein, 1981, "Multivariable Feedback Design: Concepts for a Classical/Modern



- Synthesis," *IEEE Transaction of Automatic Control*, AC-26, pp. 4-16.
- Doyle, J.C., K. Glover, P.P. Khargonekar, and B.A. Francis, 1989, "State-Space Solutions to Standard  $H_2$  and  $H_\infty$  Control Problem," *IEEE Transaction of Automatic Control*, AC-34, pp. 831-847.
- Fan, K., 1967 "Subadditive Functions on a Distributive Lattice and an Extension of Sza'sz's Inequality," *Journal of Mathematic Analysis and Applications* 18, pp. 262-268.
- Fielder, M. and V. Ptak, 1962, "On Matrices with Non-positive Off Diagonal Elements and Positive Principal Minors," *Czechoslovak Math. J.* 87, pp. 382-400.
- Freudenberg, J.S. and D.P. Looze, 1988, *Frequency Domain Properties of Scalar and Multivariable Feedback Systems*, Lecture Notes in Control and Information Sciences 104, Springer-Verlag, New York.
- Francis, B.A., 1987, *A Course in  $H^\infty$  Control Theory*, vol. 88 Lecture Notes in Control and Information Sciences, Springer-Verlag, Berlin, West Germany.
- Gallagher, J.E., 1992, *Quantitative Feedback Design of a Robust Control System for an Aircraft Engine*, M.S. Thesis, School of Mechanical Engineering, Purdue University, May 1992.
- Horowitz, I.M., 1963, *Synthesis of feedback systems*, Academic Press, Orlando, FL.
- Horowitz, I.M., 1979, "Quantitative Synthesis of Uncertain Multiple Input-output Feedback Systems," *International Journal of Control*, 30, pp. 81-106.
- Horowitz, I.M., 1991, "Survey of Quantitative Feedback Theory," *International Journal of Control*, 53, pp. 255-291.
- Kidd, P.T., 1984, "Extension of the Nyquist Array Technique to Uncertain Multivariable Systems Subject to External Disturbances," *International Journal of Control*, 40, pp. 875-901.
- Limebeer, D.J.N., 1982, "The Application of Generalized Diagonal Dominance to Linear System Stability Theory," *International Journal of Control*, 36, pp. 185-212.
- MacFarlane, A.G.J., 1979, *Frequency-response Methods in Control Systems*, IEEE Press, New York.
- Nwokah, O.D.I., 1978, "Estimates for the Inverse of a Matrix and Bounds for Eigenvalues," *Linear Algebra and Its Applications*, 22, pp. 283-291.
- Nwokah, O.D.I., 1988, "Strong Robustness in Multivariable Systems," *IEEE Conference on Decision and Control*, Austin, TX.
- Nwokah, O.D.I. and D.F. Thompson, 1989, "Algebraic and Topological Aspects of Quantitative Feedback Theory," *International Journal of Control*, 50, pp. 1057-1069.
- Nwokah, O.D.I., S. Jayasuriya, and Y. Chait, 1992, "Parametric Robust Control by Quantitative Feedback Theory," *AIAA Journal of Guidance, Control and Dynamics*, 15, pp. 207-214.
- O'Reilly, J. and W.E. Leithead, 1991, "Multivariable Control by 'Individual Channel Design'," *International Journal of Control*, 54, pp. 1-46.
- Ostrowski A., 1937, "Über die determinatem Überwiegender Hauptdiagonale," *Comment. Math. Helv.* 10, pp. 69-96.
- Owens, D.H., 1978, *Feedback and Multivariable Systems*, IEE Control Engineering Series 7, London.
- Perez, R.A., O.D.I. Nwokah, and D.F. Thompson, 1991, "Almost Decoupling by Quantitative Feedback Theory," *Proceedings of American Control Conference*, Boston, MA, 1991.
- Postlethwaite, I., J.E. Edmunds, and A.G.J. MacFarlane, 1981, "Principal Gains and Principal Phases in the Analysis of Linear Multivariable Feedback Systems," *IEEE Transaction of Automatic Control*, AC-26, pp. 32-46.
- Rosenbrock, H.H., 1974 *Computer-aided Control System Design*, Academic Press, New York.
- Seneta, E., 1973, *Non-negative Matrices*, John Wiley, New York.
- Thompson D.F. and O.D.I. Nwokah, 1991, "Analytic Loop Shaping Method in Quantitative Feedback Theory," *Proceedings of ASME Winter Annual Meeting*, Atlanta, GA.
- Yaniv, O. and I.M. Horowitz, 1986, "A Quantitative Design Method for MIMO Linear Feedback Systems Having Uncertain Plants," *International Journal on Control*, 43, pp. 401-421.
- Yau, C.H., and O.D.I. Nwokah, 1991, "A Model Reference Quantitative Feedback Design Theory," *Proceedings of ASME Winter Annual Meeting*, DSC-VOL.27, Atlanta, GA, December 1-6.

Zames, G., 1981. "Feedback and Optimal Sensitivity: Model Reference Transformation, Multiplicative Semi Norms, and Approximate Inverses," *IEEE Transaction of Automatic Control*, AC-26, pp. 301-320.

## LIST OF FIGURE CAPTIONS

- Figure 1: The 3-DOF multivariable feedback structure.
- Figure 2: The internal model reference loop.
- Figure 3: Two degree-of-freedom feedback system.
- Figure 4: The Pd-514 aircraft turbine engine.
- Figure 5: The flight envelope for the PD-514.
- Figure 6: The Nyquist arrays of the original plant for the thirty seven operating points.
- Figure 7: The interaction indices of the original plant.
- Figure 8: The design bounds for the internal loop controller  $k_{a1}(s)$  and  $k_{a2}(s)$ .
- Figure 9: The Nyquist arrays for the compensated IMRL system  $H_a(\alpha, s)$ .
- Figure 10: The interaction indices for the compensated IMRL system  $H_a(\alpha, s)$ .
- Figure 11: (a) The desired time response bounds for the first channel (thrust/fuel).  
(b) The corresponding desired frequency response bounds for the first channel.
- Figure 12: (a) The desired time response bounds for the second channel (air flow/nozzle area).  
(b) The corresponding desired frequency response bounds for the second channel.
- Figure 13: The QFD Nichols chart with the compensated loop transmission function and the performance boundaries for the first channel.
- Figure 14: The QFD Nichols chart with the compensated loop transmission function and the performance boundaries for the second channel.
- Figure 15: The closed loop thrust response to a unit step input of fuel flow.
- Figure 16: The closed loop air flow response to a unit step input of nozzle area.

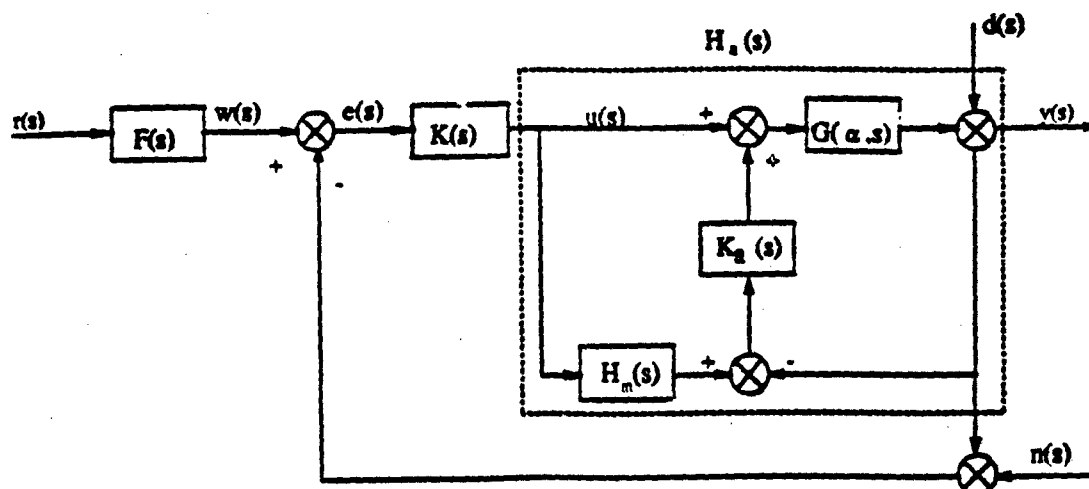


Figure 1: The 3-DOF multivariable feedback structure.

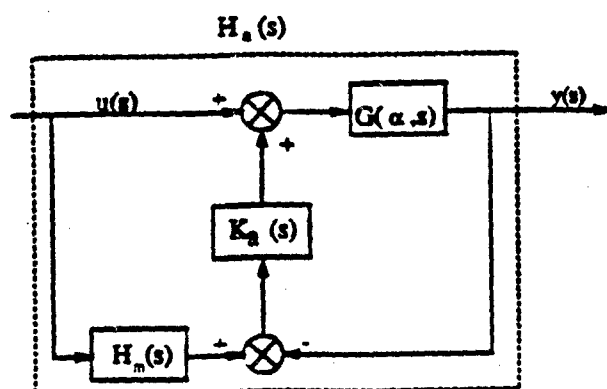


Figure 2: The internal model reference loop.

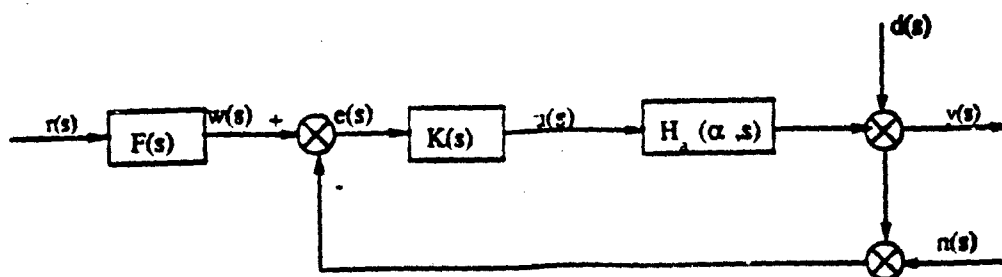


Figure 3: Two degree-of-freedom feedback system.

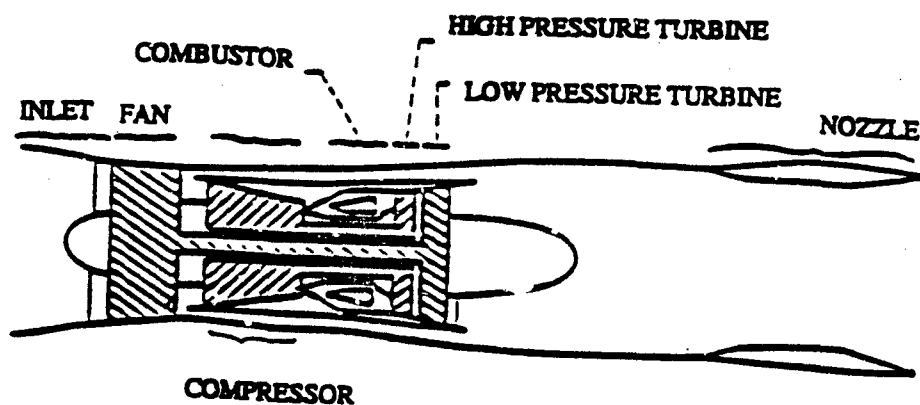


Figure 4: The Pd-514 aircraft turbine engine.

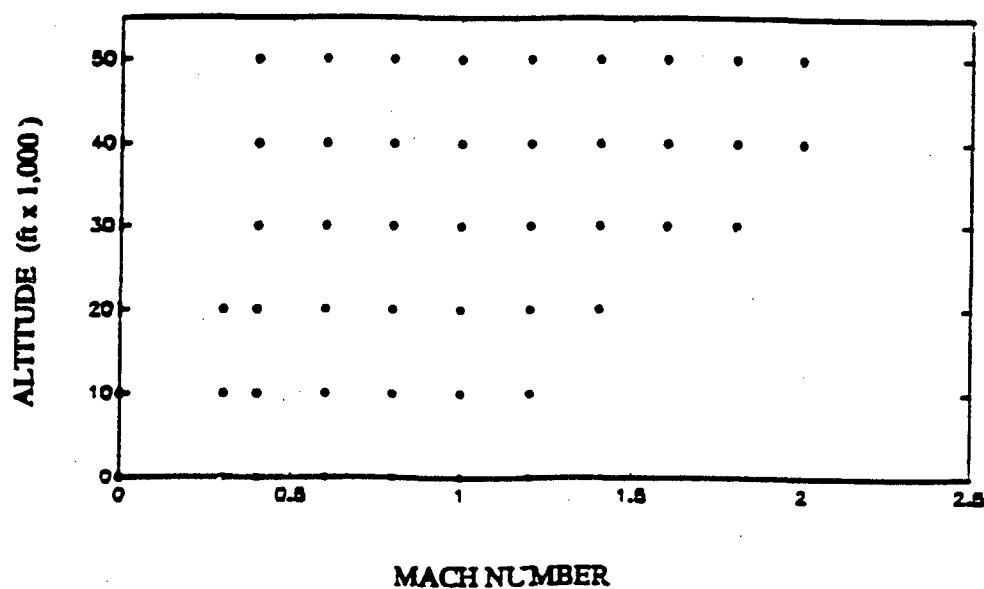


Figure 5: The flight envelope for the PD-514.

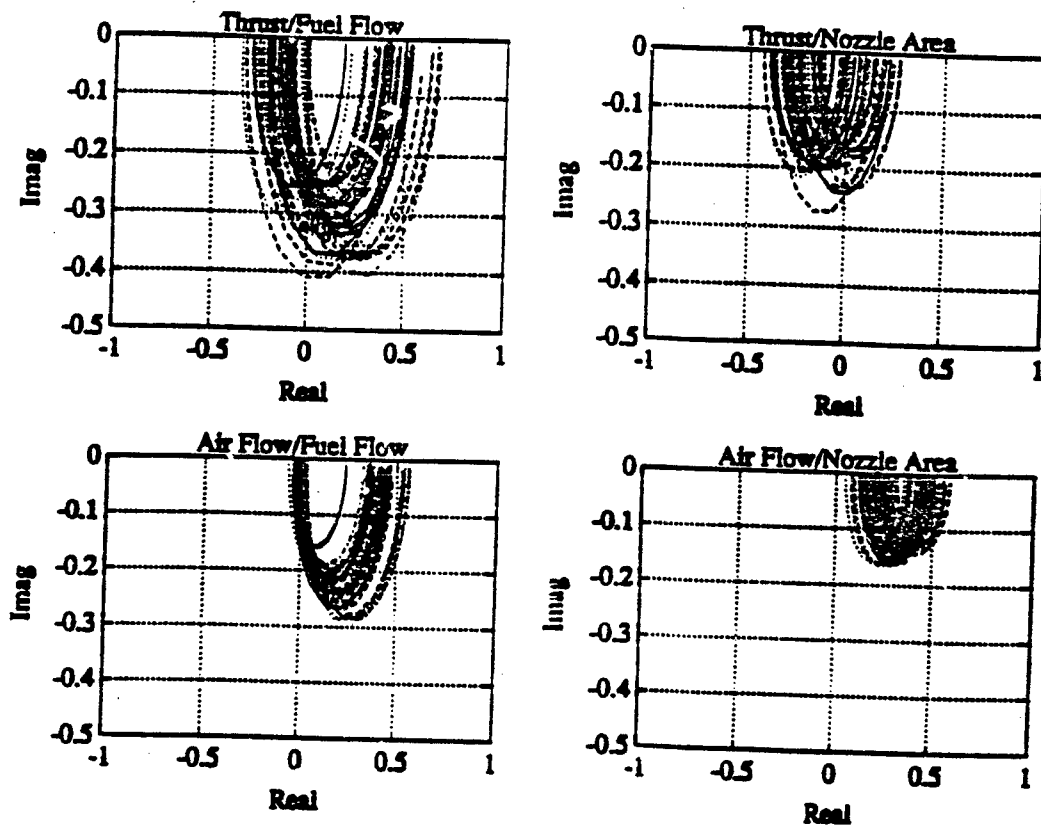


Figure 6: The Nyquist arrays of the original plant for the thirty seven operating points.

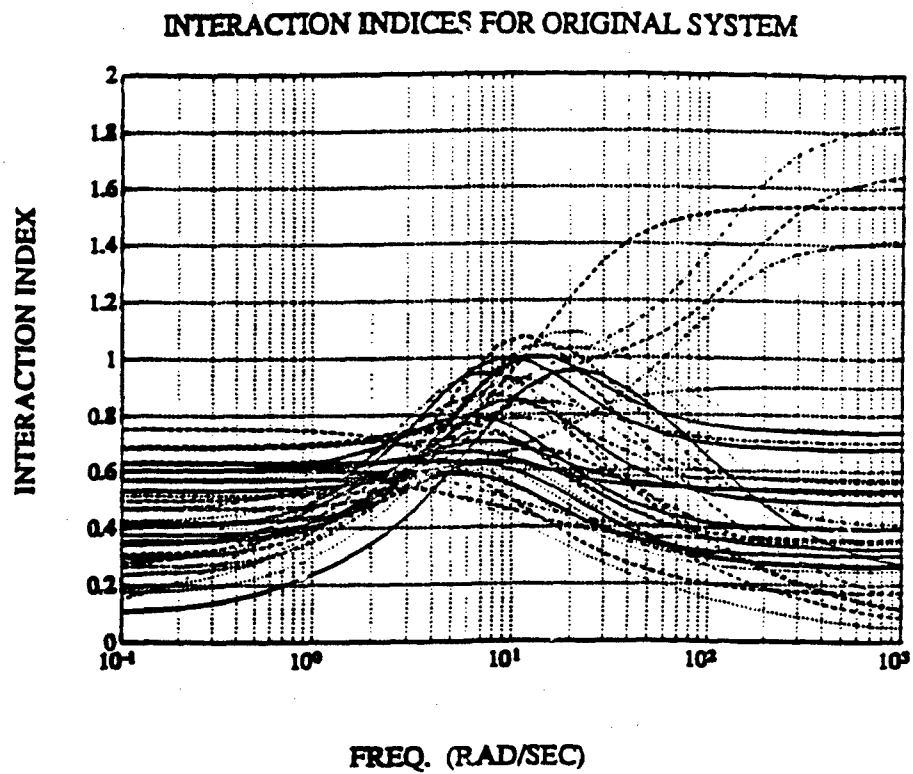
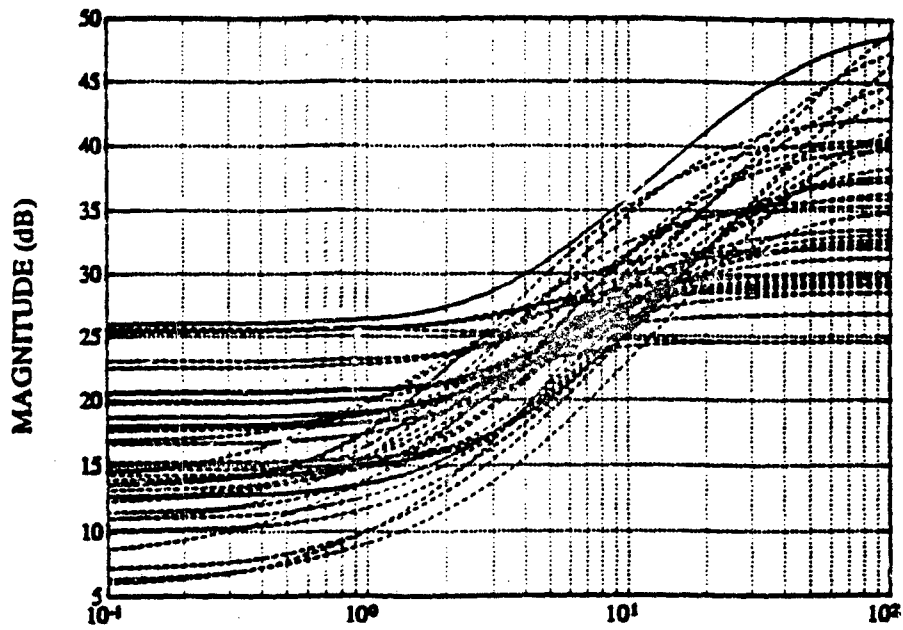
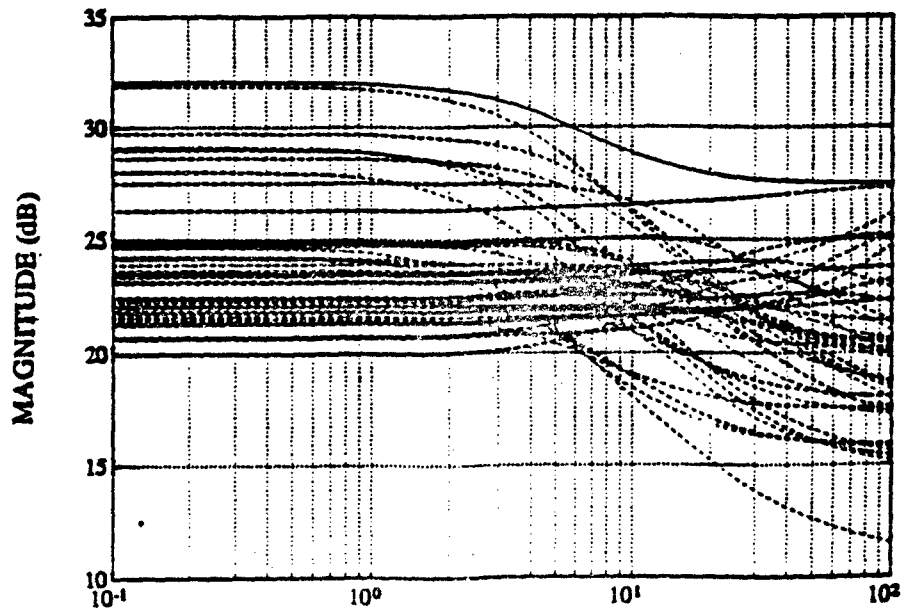


Figure 7: The interaction indices of the original plant.

DESIGN BOUND FOR  $K_{a1}(s)$



DESIGN BOUND FOR  $K_{a2}(s)$



FREQ. (RAD/SEC)



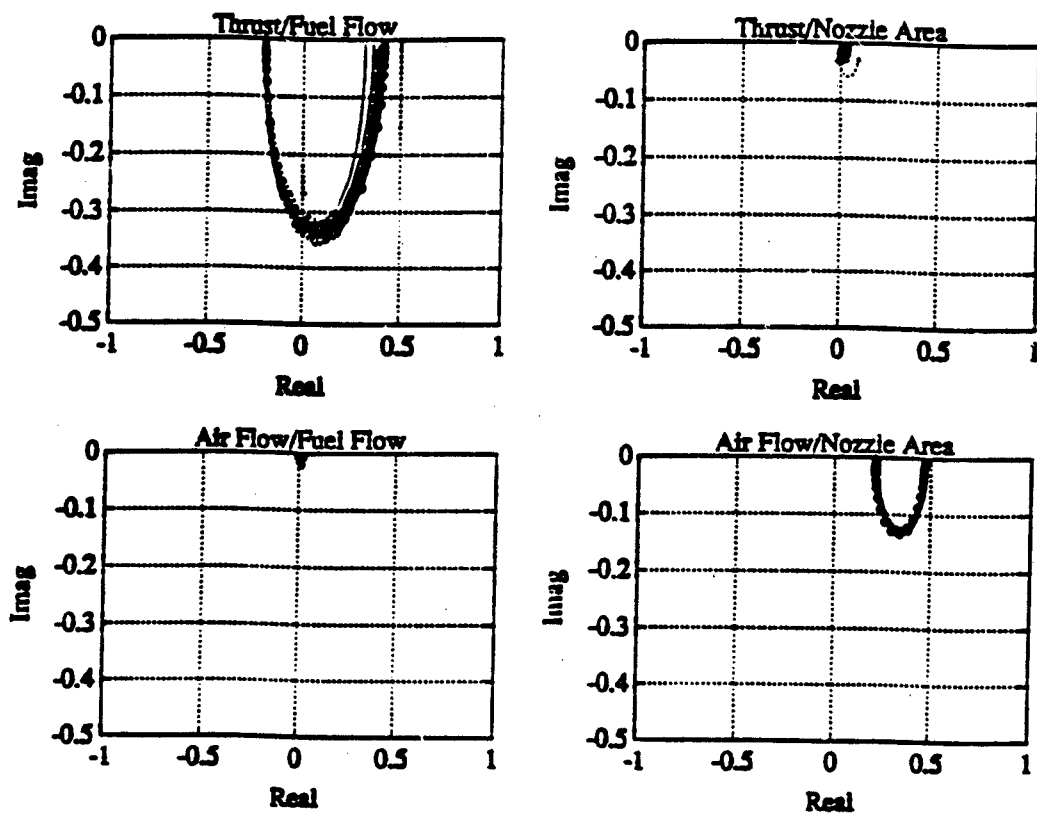


Figure 9: The Nyquist arrays for the compensated IMRL system  $H_1(\alpha, s)$ .

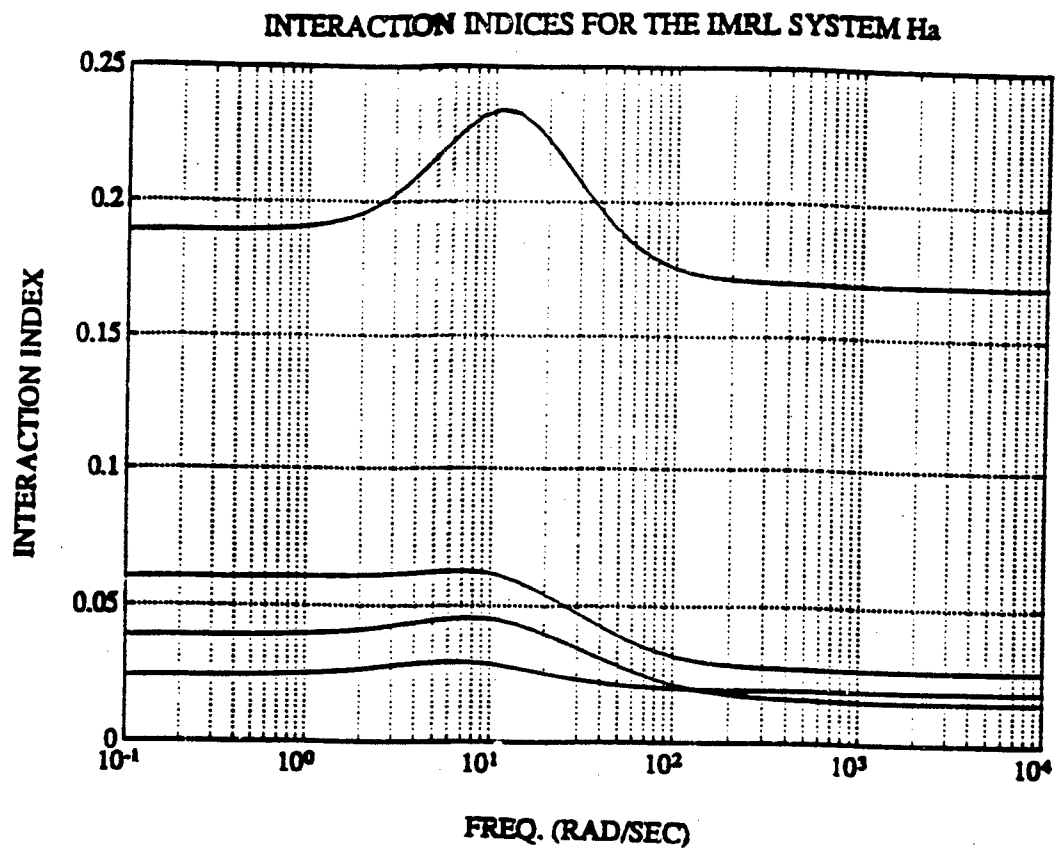


Figure 10: The interaction indices for the compensated IMRL system  $H_a(\alpha, s)$ .

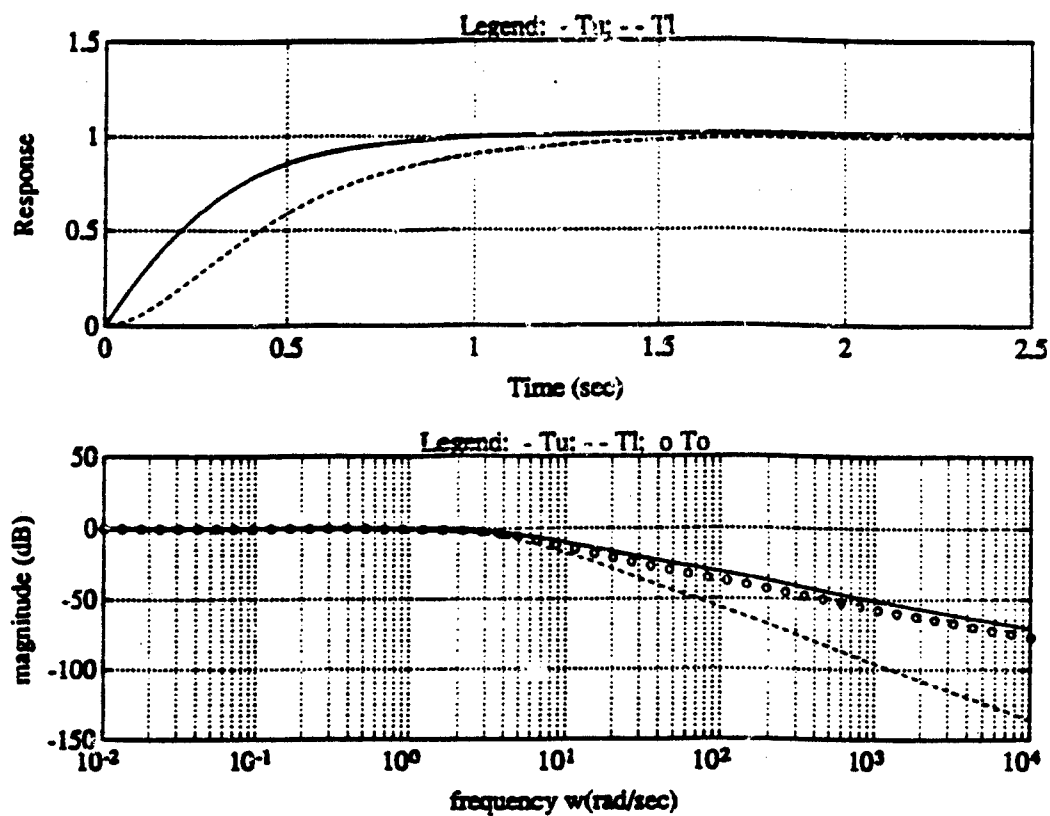


Figure 11: (a) The desired time response bounds for the first channel (thrust/fuel).  
 (b) The corresponding desired frequency response bounds for the first channel.

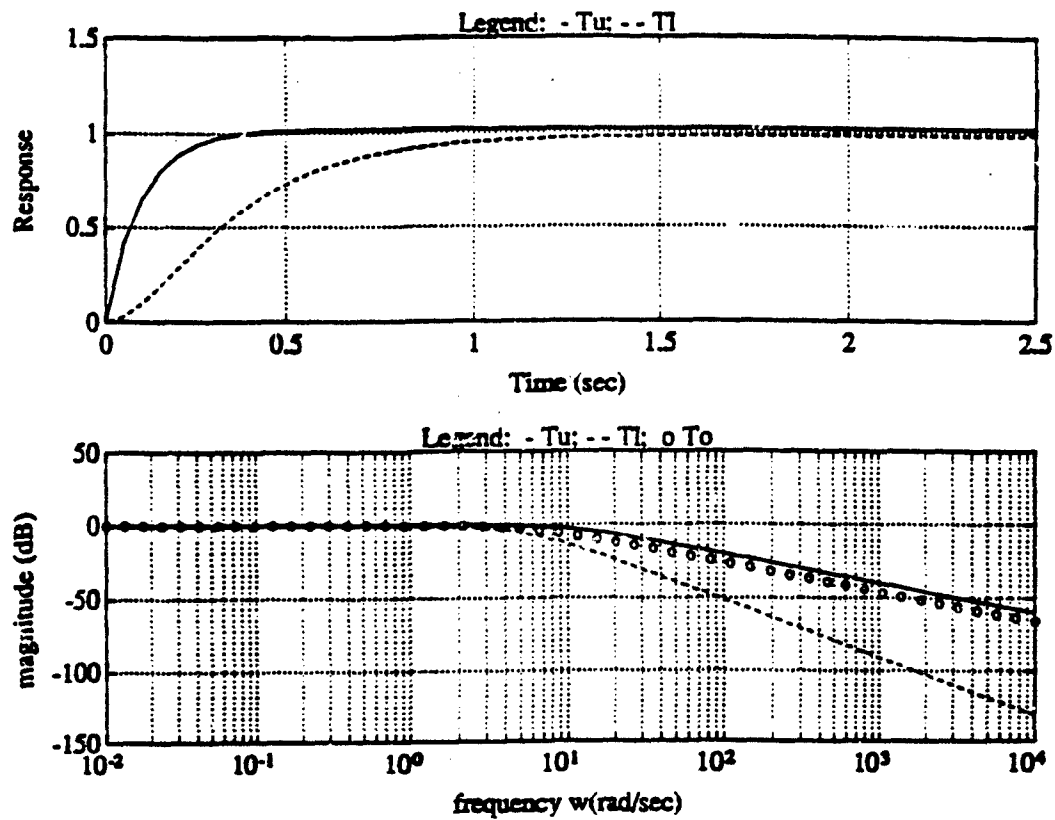


Figure 12: (a) The desired time response bounds for the second channel (air flow/nozzle area).  
 (b) The corresponding desired frequency response bounds for the second channel.

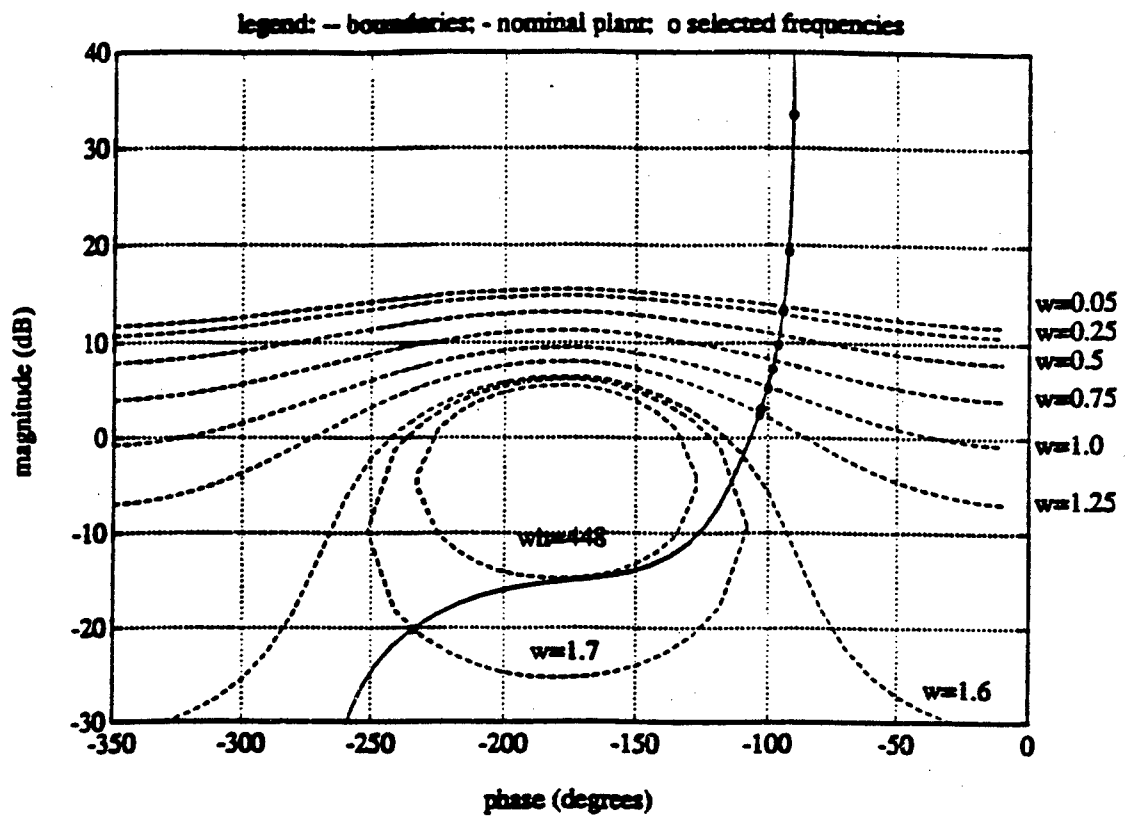


Figure 13: The QFD Nichols chart with the compensated loop transmission function and the performance boundaries for the first channel.

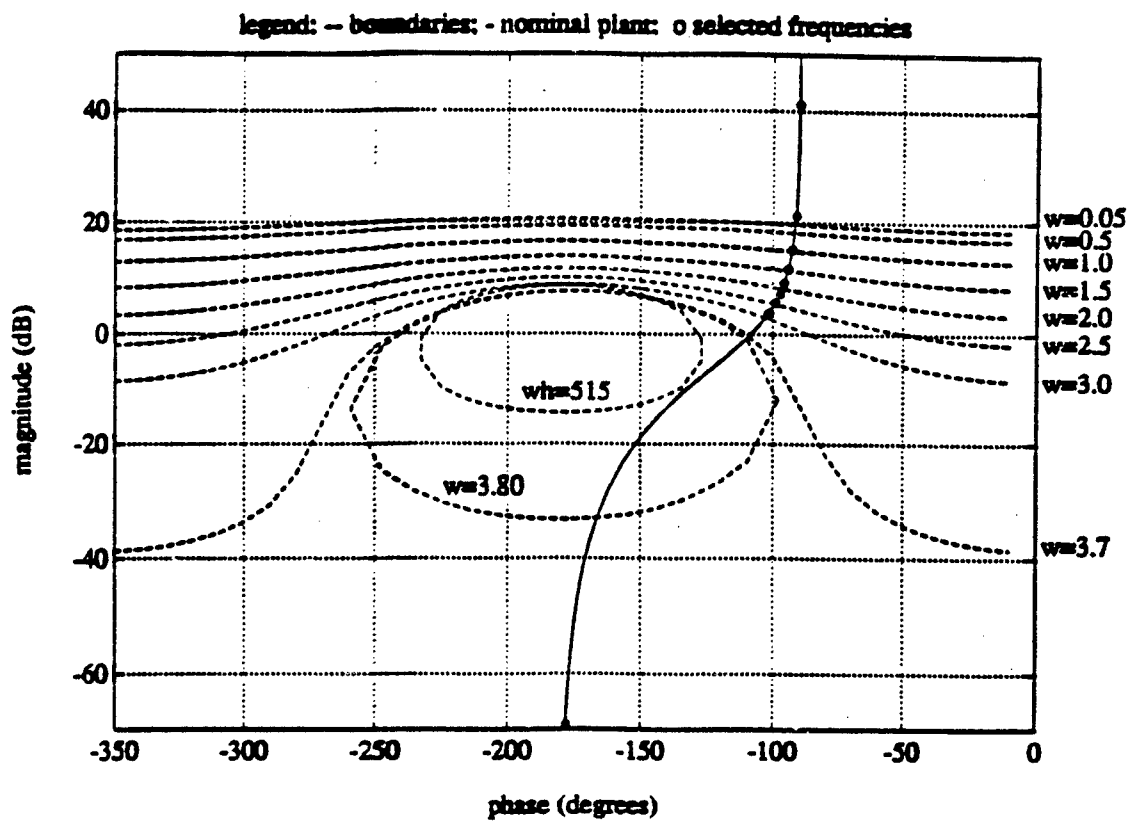


Figure 14: The QFD Nichols chart with the compensated loop transmission function and the performance boundaries for the second channel.

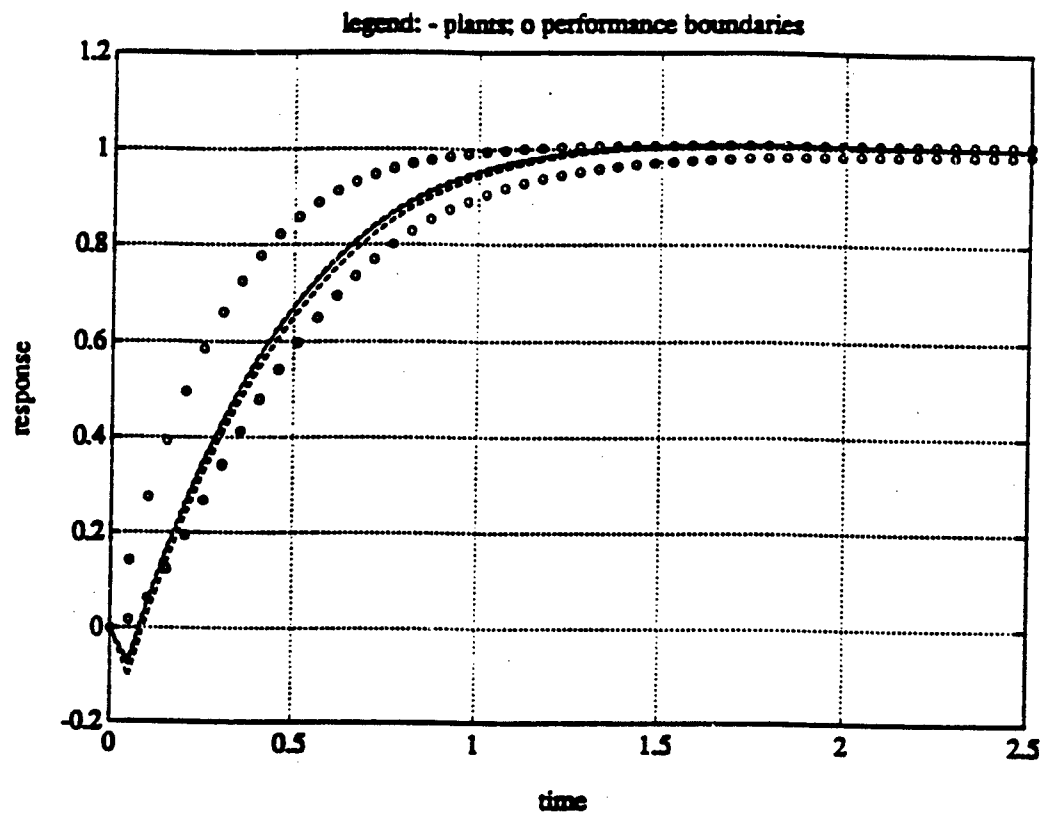


Figure 15: The closed loop thrust response to a unit step input of fuel flow.

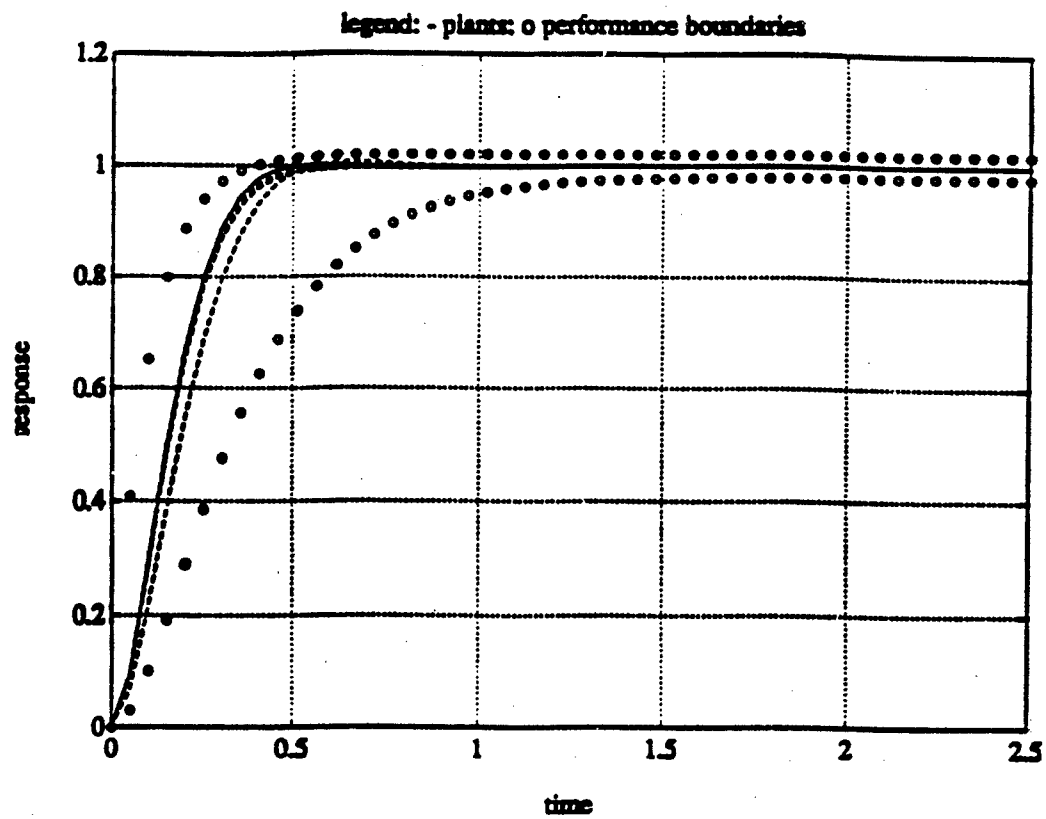


Figure 16: The closed loop air flow response to a unit step input of nozzle area.



# Control System Design for Parametric Uncertainty\*

L.H. Keel

Center of Excellence in Information Systems

Tennessee State University

330 Tenth Avenue North

Nashville, TN 37203-3401

S.P. Bhattacharyya

Department of Electrical Engineering

Texas A&M University

College Station, TX 77843

## ABSTRACT

This paper introduces some recently developed frequency domain design techniques that are effective in the design of control systems that are robust under parametric uncertainty. We have extended the well known classical control tools (i.e., Nyquist plot, Bode plot, and Nichols chart) developed for a fixed plant to the domain of uncertain interval plants. Using this new family of plots, classical control design techniques can be used to design robust control systems. The technique is illustrated by examples.

## 1. INTRODUCTION

Control under parametric uncertainty is a problem of longstanding interest and many useful results have been developed in the QFT school of thought ([1]) as well as the parameter plane approach ([2] and see references in [3]). There appeared a renewed interest in this area following the discovery in 1978 of Kharitonov's Theorem for interval polynomials [4]. Despite its elegance this result could not be directly applied to

---

\*This research was supported in part by NASA Grant NAG-1863 and NSF Grant ECS-8914357

control systems due to the severe restriction in Kharitonov's Theorem that requires independent perturbations of the coefficients of the polynomial. A breakthrough was made by Chapellat and Bhattacharyya in their 1989 paper (CB Theorem) which lifted this limitation. This paper introduced the notion of interval plants, namely a family of plants consisting of a ratio of interval polynomials, and dealt with the problem of determining the robust stability of an interval plant contained in a control loop with a fixed controller. The CB Theorem gives Kharitonov-like results for this problem by constructing certain one parameter segments, called CB segments [5], which completely and nonconservatively characterize the robust stability of such interval control systems. This novel result has also been extended to show that the worst case  $H^\infty$  stability margin of an interval control system occurs on one of these CB segments [6].

Despite these developments, this area has mainly concentrated on analysis problems and still suffers from a lack of effective design methodologies. The present paper is an attempt to show that classical control design methods can indeed be coupled with the above results to develop controller design strategies for robustness under parametric uncertainty. This is done here by developing robust versions of the simple and powerful graphical tools such as Nyquist plot, Bode plots, and Nichols Chart. We show that these extended plots can be precisely constructed from the CB segments. Moreover extremal classical stability margins occur on these segments. Consequently, one can achieve complete frequency domain information about this important class of systems and apply this to the controller design problem. This is demonstrated in the paper and illustrated by an example.

The paper is organized as follows: We first give a brief summary of the essential results on parametric robust stability and control. In section 3, we give procedures for constructing various envelopes that contain the entire frequency response of the interval system. Section 4 discusses the problem of extremal gain and phase margins of the family, and a simple method of computing these margins are given in Section 5. Using these frequency envelopes, lead-lag compensation is attempted by examining the band of crossover frequencies, much as in classical control for fixed systems. Illustrative examples are included. Finally, some concluding remarks are given.

## 2. PRELIMINARIES

Consider the feedback system shown in Figure 1 with

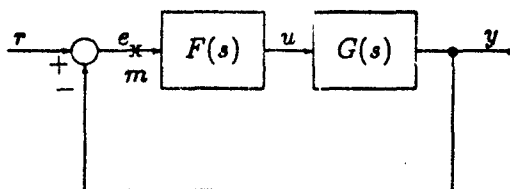


Figure 1. Feedback System

$$F(s) := \frac{F_1(s)}{F_2(s)} \quad G(s) := \frac{N(s)}{D(s)}. \quad (2.1)$$

We suppose that  $N(s)$  and  $D(s)$  lie in uncertainty sets described by

$$\begin{aligned} N(s) &:= n_0 + n_1 s + n_2 s^2 + n_3 s^3 + \dots + n_{p-1} s^{p-1} + n_p s^p \\ D(s) &:= d_0 + d_1 s + d_2 s^2 + d_3 s^3 + \dots + d_{p-1} s^{p-1} + d_p s^p \end{aligned} \quad (2.2)$$

where

$$n_i \in [n_i^-, n_i^+] \text{ and } d_i \in [d_i^-, d_i^+], \text{ for } i \in \{0, 1, \dots, p\} := p \quad (2.3)$$

and  $F_1(s)$  and  $F_2(s)$  are fixed polynomials in  $s$ . Let us define the interval polynomials

$$\begin{aligned} \mathcal{N}(s) &:= \{N(s) \mid n_0 + n_1 s + n_2 s^2 + \dots + n_p s^p, n_i \in [n_i^-, n_i^+], i \in p\} \\ \mathcal{D}(s) &:= \{D(s) \mid d_0 + d_1 s + d_2 s^2 + \dots + d_p s^p, d_i \in [d_i^-, d_i^+], i \in p\} \end{aligned} \quad (2.4)$$

and the corresponding interval system consisting of the set of transfer functions:

$$\mathcal{G}(s) := \left\{ \frac{N(s)}{D(s)} \mid (N(s), D(s)) \in (\mathcal{N}(s) \times \mathcal{D}(s)) \right\}. \quad (2.5)$$

Let the Kharitonov polynomials associated with  $\mathcal{N}(s)$  and  $\mathcal{D}(s)$  be respectively:

$$\begin{aligned} K_n^1(s) &:= n_0^- + n_1^- s + n_2^+ s^2 + n_3^+ s^3 + n_4^- s^4 + n_5^- s^5 + \dots \\ K_n^2(s) &:= n_0^- + n_1^+ s + n_2^+ s^2 + n_3^- s^3 + n_4^- s^4 + n_5^+ s^5 + \dots \\ K_n^3(s) &:= n_0^+ + n_1^- s + n_2^- s^2 + n_3^+ s^3 + n_4^+ s^4 + n_5^- s^5 + \dots \\ K_n^4(s) &:= n_0^+ + n_1^+ s + n_2^- s^2 + n_3^- s^3 + n_4^+ s^4 + n_5^+ s^5 + \dots \end{aligned} \quad (2.6)$$

and

$$\begin{aligned} K_d^1(s) &:= d_0^- + d_1^- s + d_2^+ s^2 + d_3^+ s^3 + d_4^- s^4 + d_5^- s^5 + \dots \\ K_d^2(s) &:= d_0^- + d_1^+ s + d_2^+ s^2 + d_3^- s^3 + d_4^- s^4 + d_5^+ s^5 + \dots \\ K_d^3(s) &:= d_0^+ + d_1^- s + d_2^- s^2 + d_3^+ s^3 + d_4^+ s^4 + d_5^- s^5 + \dots \\ K_d^4(s) &:= d_0^+ + d_1^+ s + d_2^- s^2 + d_3^- s^3 + d_4^+ s^4 + d_5^+ s^5 + \dots \end{aligned} \quad (2.7)$$

We write

$$\mathcal{K}_N(s) := \{K_n^1(s), K_n^2(s), K_n^3(s), K_n^4(s)\} \quad (2.8)$$

$$\mathcal{K}_D(s) := \{K_d^1(s), K_d^2(s), K_d^3(s), K_d^4(s)\} \quad (2.9)$$

and also define the set of line segments joining appropriate pairs of Kharitonov polynomials.

$$\begin{aligned} \lambda K_n^i(s) + (1 - \lambda) K_n^j(s), \quad \text{for } \lambda \in [0, 1], (i, j) \in \{(1, 2), (1, 3), (2, 4), (3, 4)\} \\ \lambda K_d^i(s) + (1 - \lambda) K_d^j(s), \quad \text{for } \lambda \in [0, 1], (i, j) \in \{(1, 2), (1, 3), (2, 4), (3, 4)\} \end{aligned}$$

We call these Kharitonov segments and denote the segment sets associated with  $\mathcal{D}(s)$  and  $\mathcal{N}(s)$  respectively as,

$$\mathcal{S}_D(s) :=$$

$$\left[ \lambda K_d^i(s) + (1 - \lambda) K_d^j(s) \mid \lambda \in [0, 1], (i, j) \in \{(1, 2), (1, 3), (2, 4), (3, 4)\} \right] \quad (2.10)$$

and

$$S_N(s) :=$$

$$\left[ \mu K_n^i(s) + (1 - \mu) K_n^j(s) \mid \mu \in [0, 1], (i, j) \in \{(1, 2), (1, 3), (2, 4), (3, 4)\} \right]. \quad (2.11)$$

We now consider the uncertainty set  $\mathcal{N}(s) \times \mathcal{D}(s)$  and introduce the set of segments introduced by Chapellat Bhattacharyya [7].

$$(\mathcal{N}(s) \times \mathcal{D}(s))_{CB} := \{(N(s) \times D(s)) \mid$$

$$N(s) \in \mathcal{K}_N(s), D(s) \in \mathcal{S}_D(s), \text{ or } N(s) \in S_N(s), D(s) \in \mathcal{K}_D(s)\}. \quad (2.12)$$

The characteristic polynomial of the system is denoted as

$$\Pi(s) = D_g(s)D(s) + N_g(s)N(s) \quad (2.13)$$

Similarly the characteristic polynomial  $\Pi(s)$  ranges over the corresponding uncertainty set denoted by

$$\Pi(s) = \{F_2(s)D(s) + F_1(s)N(s) : (N(s), D(s)) \in \mathcal{N}(s) \times \mathcal{D}(s)\}. \quad (2.14)$$

We now introduce the CB subset of the family of interval systems  $G(s)$ :

$$G_{CB}(s) := \left\{ \frac{N(s)}{D(s)} : (N(s), D(s)) \in (\mathcal{N}(s) \times \mathcal{D}(s))_{CB} \right\}. \quad (2.15)$$

These subsets will play a central role in all the results to be developed later. We note that each element of  $G_{CB}(s)$  is a one parameter of transfer functions and there are at most 32 such distinct elements. Referring to the control system in Figure 1, the following transfer functions are of interest in analysis and design problems:

$$\frac{y(s)}{u(s)} = G(s) \quad \frac{u(s)}{e(s)} = F(s) \quad (2.16)$$

$$T^o(s) := \frac{y(s)}{e(s)} = G(s)F(s) \quad (2.17)$$

$$T^v(s) := \frac{y(s)}{r(s)} = \frac{G(s)F(s)}{1 + G(s)F(s)} \quad (2.18)$$

$$T^e(s) := \frac{e(s)}{r(s)} = \frac{1}{1 + G(s)F(s)} \quad (2.19)$$

$$T^u(s) := \frac{u(s)}{r(s)} = \frac{F(s)}{1 + G(s)F(s)}. \quad (2.20)$$

As  $G(s)$  ranges over the uncertainty set  $G(s)$  (equivalently,  $(N(s), D(s))$  ranges over  $\mathcal{N}(s) \times \mathcal{D}(s)$ ) the transfer functions  $T^o(s)$ ,  $T^v(s)$ ,  $T^u(s)$ ,  $T^e(s)$  range over corresponding uncertainty sets  $T^o(s)$ ,  $T^v(s)$ ,  $T^u(s)$ , and  $T^e(s)$ , respectively. In other words,

$$T^o(s) := \{F(s)G(s) : G(s) \in G(s)\} \quad (2.21)$$

$$\mathbf{T}^v(s) := \left\{ \frac{F(s)G(s)}{1 + F(s)G(s)} : G(s) \in \mathbf{G}(s) \right\} \quad (2.22)$$

$$\mathbf{T}^u(s) := \left\{ \frac{F(s)}{1 + F(s)G(s)} : G(s) \in \mathbf{G}(s) \right\} \quad (2.23)$$

$$\mathbf{T}^e(s) := \left\{ \frac{1}{1 + F(s)G(s)} : G(s) \in \mathbf{G}(s) \right\}. \quad (2.24)$$

The CB subsets of the transfer function sets (2.21) - (2.24) and the polynomial set (2.14) are also introduced:

$$\mathbf{T}_{CB}^o(s) := \{F(s)G(s) : G(s) \in \mathbf{G}_{CB}(s)\} \quad (2.25)$$

$$\mathbf{T}_{CB}^v(s) := \left\{ \frac{F(s)G(s)}{1 + F(s)G(s)} : G(s) \in \mathbf{G}_{CB}(s) \right\} \quad (2.26)$$

$$\mathbf{T}_{CB}^u(s) := \left\{ \frac{F(s)}{1 + F(s)G(s)} : G(s) \in \mathbf{G}_{CB}(s) \right\} \quad (2.27)$$

$$\mathbf{T}_{CB}^e(s) := \left\{ \frac{1}{1 + F(s)G(s)} : G(s) \in \mathbf{G}_{CB}(s) \right\} \quad (2.28)$$

and

$$\Pi_{CB}(s) := \{F_2(s)D(s) + F_1(s)N(s) : (N(s), D(s)) \in (\mathcal{N}(s) \times \mathcal{D}(s))_{CB}\} \quad (2.29)$$

In the paper we shall deal with the complex plane image of each of the above sets evaluated at  $s = j\omega$ . We denote each of these two dimensional sets in the complex plane by replacing  $s$  in the corresponding argument by  $\omega$ . Thus, for example,

$$\Pi(\omega) := \{\Pi(s) : s = j\omega\} \quad (2.30)$$

and

$$\mathbf{T}_{CB}^v(\omega) := \{\mathbf{T}_{CB}^v(s) : s = j\omega\} \quad (2.31)$$

The Nyquist plot of a set of functions (or polynomials)  $\mathbf{T}(s)$  is denoted by  $\mathbf{T}$ :

$$\mathbf{T} := \cup_{0 \leq \omega < \infty} \mathbf{T}(\omega) \quad (2.32)$$

The boundary of a set  $S$  is denoted  $\partial S$ .

The control system of Figure 1 is stable for fixed  $F(s)$  and  $G(s)$  if the characteristic polynomial

$$\Pi(s) = F_2(s)D(s) + F_1(s)N(s) \quad (2.33)$$

is Hurwitz, i.e. has all its  $n = q + \text{degree}[D(s)]$  roots in the open left half of the complex plane. The system is robustly stable if and only if each polynomial in  $\Pi(s)$  is of degree  $n$  (degree  $D(s)$  remains invariant and equal to  $q$  as  $D(s)$  ranges over  $\mathcal{D}(s)$ ) and every polynomial in  $\Pi(s)$  is Hurwitz.

The following important result was provided in Chapellat and Bhattacharyya [7].

**Theorem 1. (CB Theorem)** *The control system of Figure 1 is stable for all  $G(s) \in \mathbf{G}(s)$  if and only if it is stable for all  $G(s) \in \mathbf{G}_{CB}(s)$ .*

The above Theorem gives a constructive solution to the problem of checking robust stability by reducing it to a problem of checking a set of (at most) 32 root locus problems. In the following sections we point out that these segments also suffice to characterize the Nyquist and Bode bands and Nichols chart templates of interval systems. This quantitative information is useful for developing robust controller designs.

### 3. CONSTRUCTION OF FREQUENCY ENVELOPES

In this section, we develop three important frequency domain design tools.

#### 3.1. Bode Magnitude and Phase Envelopes

For any function say,  $T(s)$  let  $\mu_T(\omega) := |T(j\omega)|$  and  $\phi_T(\omega) := \angle T(j\omega)$  denote the magnitude and phase evaluated at  $s = j\omega$ . If  $T(s)$  denotes a set of functions we let the extremal values of magnitude and phase at a given frequency be defined as follows:

$$\begin{aligned}\bar{\mu}_T(\omega) &:= \sup_{T(j\omega)} |T(j\omega)| \\ \underline{\mu}_T(\omega) &:= \inf_{T(j\omega)} |T(j\omega)|.\end{aligned}\tag{3.1}$$

Similarly

$$\begin{aligned}\bar{\phi}_T(\omega) &:= \sup_{T(j\omega)} \angle T(j\omega) \\ \underline{\phi}_T(\omega) &:= \inf_{T(j\omega)} \angle T(j\omega).\end{aligned}\tag{3.2}$$

Suppose that  $G(s)$  is an interval family as in (2.5). Our objective is to compute

$$\bar{\mu}_G(\omega), \quad \underline{\mu}_G(\omega)\tag{3.3}$$

and

$$\bar{\phi}_G(\omega), \quad \underline{\phi}_G(\omega).\tag{3.4}$$

We begin with the following two simple lemmas.

**Lemma 1.** *Let  $A$  be a closed polygon in the complex plane, and "a" be an arbitrary point in  $A$ . Let  $V_A$  be the set of vertices and  $E_A$  be the set of edges of  $A$ . Then the following statements are true.*

- 1)  $\max_A |a| = \max_{V_A} |a|$
- 2)  $\min_A |a| = \min_{E_A} |a|$

**Lemma 2.** Let  $A$  and  $B$  be disjoint closed polygons in the complex plane, and " $a$ " and " $b$ " be arbitrary points on  $A$  and  $B$ , respectively. Let  $V_A$  and  $V_B$  be the sets of vertices and let  $E_A$  and  $E_B$  be the sets of edges of  $A$  and  $B$ , respectively. Then the following statements are true.

$$1) \quad \max_{A \times B} \{ \angle a - \angle b \} = \max_{V_A \times V_B} \{ \angle a - \angle b \}$$

$$2) \quad \min_{A \times B} \{ \angle a - \angle b \} = \min_{V_A \times V_B} \{ \angle a - \angle b \}$$

Proofs of the above two lemmas are obvious from geometric considerations.

Let  $\mathcal{N}(\omega)$  denote the complex plane image of the set of polynomials  $N(s) \in \mathcal{N}(s)$  evaluated at  $s = j\omega$ . Similar definitions hold for  $\mathcal{D}(\omega)$ ,  $\mathcal{S}_\mathcal{N}(\omega)$  and  $\mathcal{S}_\mathcal{D}(\omega)$ .  $\mathcal{N}(\omega)$  is bounded by the set of Kharitonov segments  $\mathcal{S}_\mathcal{N}(\omega)$ . Similarly,  $\mathcal{D}(\omega)$  is bounded by the set  $\mathcal{S}_\mathcal{D}(\omega)$ . These facts along with Lemmas 1 and 2 lead to the following results. Before we state Theorem 2, let us define the following sets.

$$\mathbf{G}(\omega) := \{ G(j\omega) = \frac{N(j\omega)}{D(j\omega)} \mid N(j\omega) \in \mathcal{N}(\omega), D(j\omega) \in \mathcal{D}(\omega) \} \quad (3.5)$$

$$\bar{\mathbf{G}}_{CB}(\omega) := \{ G(j\omega) = \frac{N(j\omega)}{D(j\omega)} \mid N(j\omega) \in \mathcal{K}_\mathcal{N}(\omega), D(j\omega) \in \mathcal{S}_\mathcal{D}(\omega) \} \quad (3.6)$$

$$\underline{\mathbf{G}}_{CB}(\omega) := \{ G(j\omega) = \frac{N(j\omega)}{D(j\omega)} \mid N(j\omega) \in \mathcal{S}_\mathcal{N}(\omega), D(j\omega) \in \mathcal{K}_\mathcal{D}(\omega) \}. \quad (3.7)$$

**Theorem 2.** For every frequency  $\omega \geq 0$ ,

$$\begin{aligned} \bar{\mu}_{\mathbf{G}}(\omega) &= \bar{\mu}_{\bar{\mathbf{G}}_{CB}}(\omega) \\ \underline{\mu}_{\mathbf{G}}(\omega) &= \underline{\mu}_{\underline{\mathbf{G}}_{CB}}(\omega) \end{aligned}$$

Let us also define the set of systems constructed from Kharitonov vertices as follows:

$$\mathbf{G}_\mathcal{K}(\omega) := \{ G(j\omega) = \frac{N(j\omega)}{D(j\omega)} \mid N(j\omega) \in \mathcal{K}_\mathcal{N}(\omega), D(j\omega) \in \mathcal{K}_\mathcal{D}(\omega) \}. \quad (3.8)$$

**Theorem 3.** For every frequency  $\omega \geq 0$ ,

$$\begin{aligned} \bar{\phi}_{\mathbf{G}}(\omega) &= \bar{\phi}_{\mathbf{G}_\mathcal{K}}(\omega) \\ \underline{\phi}_{\mathbf{G}}(\omega) &= \underline{\phi}_{\mathbf{G}_\mathcal{K}}(\omega) \end{aligned}$$

Using the above extremal properties it is possible to evaluate the Bode magnitude and phase envelopes of interval transfer functions. Let us consider the family of transfer functions

$$\mathbf{P}(s) := \{ P(s) \mid G(s)F(s), G(s) \in \mathbf{G}(s) \}. \quad (3.9)$$

Since  $F(s)$  is fixed,

$$\begin{aligned}\bar{\mu}_P(\omega) &= |F(j\omega)| \bar{\mu}_G(\omega) \\ \underline{\mu}_P(\omega) &= |F(j\omega)| \underline{\mu}_G(\omega).\end{aligned}\quad (3.10)$$

Similarly,

$$\begin{aligned}\bar{\phi}_P(\omega) &= \angle F(j\omega) + \bar{\phi}_G(\omega) \\ \underline{\phi}_P(\omega) &= \angle F(j\omega) + \underline{\phi}_G(\omega).\end{aligned}\quad (3.11)$$

These relations are sufficient to construct the Bode magnitude and phase envelopes.

### 3.2. Nyquist Envelope

We further investigate the extremal frequency domain properties of the transfer functions which occur in the configuration given in Figure 1.

**Theorem 4.** *For every  $\omega \geq 0$ ,*

$$\partial G(\omega) \subset G_{CB}(\omega) \quad (3.12)$$

$$\partial T^o(\omega) \subset T_{CB}^o(\omega) \quad (3.13)$$

$$\partial T^v(\omega) \subset T_{CB}^v(\omega) \quad (3.14)$$

$$\partial T^u(\omega) \subset T_{CB}^u(\omega) \quad (3.15)$$

$$\partial T^e(\omega) \subset T_{CB}^e(\omega) \quad (3.16)$$

The proof of this theorem may be developed from geometric arguments and is omitted here. This result shows that at every  $\omega \geq 0$  the image set of each transfer function in (2.21) - (2.24) is bounded by the corresponding image set of the CB segments.

From the theorem 4, we obtain the following corollary which deals with the Nyquist plots of each of the transfer functions in (2.21) - (2.24).

**Corollary 1.** *The Nyquist plots of each of the transfer function sets  $T^o(s)$ ,  $T^v(s)$ ,  $T^u(s)$ , and  $T^e(s)$  are bounded by their corresponding CB subsets:*

$$\partial T^o \subset T_{CB}^o \quad (3.17)$$

$$\partial T^v \subset T_{CB}^v \quad (3.18)$$

$$\partial T^u \subset T_{CB}^u \quad (3.19)$$

$$\partial T^e \subset T_{CB}^e \quad (3.20)$$

This result has many important implications in control system design and will be explored in the next section.



### 3.3. Nichols Chart Template

Using the magnitude and phase data obtained to generate Bode envelopes, it is straight forward to construct Nichols Chart templates. At each fixed frequency the magnitude and phase have certain ranges, the corresponding rectangle is created on the magnitude vs phase plane. As frequency moves from zero to  $\infty$ , different sizes of rectangles are created. Finally, the Nichols Chart Envelope consists of the collection of all these rectangles. An illustrative example is given showing more detail.

*Remark 1.* For a fixed system, all of the above three frequency plots provide the same information. However, for the case of interval systems, it is important to note that neither Bode nor Nichols chart envelopes provide as accurate information as the Nyquist envelope does. It is due to the fact that in general different parameter values provide extremal values of magnitude and phase envelopes.

## 4. EXTREMAL GAIN AND PHASE MARGINS FOR INTERVAL CONTROL SYSTEMS

If a fixed closed loop system is stable we can determine its gain margin  $\gamma$  as follows:

$$\gamma^+(G(s), F(s)) := \max \left\{ \bar{K} : F_2(s)D(s) + KF_1(s)N(s) \right. \\ \left. \text{is Hurwitz for } K \in [1, \bar{K}] \right\} \quad (4.1)$$

$$\gamma^-(G(s), F(s)) := \max \left\{ \underline{K} : F_2(s)D(s) + \frac{1}{K}F_1(s)N(s) \right. \\ \left. \text{is Hurwitz for } K \in [\underline{K}, 1] \right\} \quad (4.2)$$

Similarly the phase margin  $\phi$  is defined as follows:

$$\phi^+(G(s), F(s)) := \max \left\{ \bar{\phi} : F_2(s)D(s) + e^{j\phi}F_1(s)N(s) \right. \\ \left. \text{is Hurwitz for } \phi \in [0, \bar{\phi}] \right\} \quad (4.3)$$

$$\phi^-(G(s), F(s)) := \max \left\{ \underline{\phi} : F_2(s)D(s) + e^{-j\phi}F_1(s)N(s) \right. \\ \left. \text{is Hurwitz for } \phi \in [0, \underline{\phi}] \right\} \quad (4.4)$$

Note that  $\gamma^+$ ,  $\gamma^-$ ,  $\phi^+$ , and  $\phi^-$  are uniquely determined when  $F(s)$  and  $G(s)$  are fixed.

We now state some fundamental results on the extremal gain and phase margins over the uncertainty set  $\mathcal{N}(s) \times \mathcal{D}(s)$ .

**Theorem 5.** Suppose that the closed loop system shown in Figure 1 is robustly stable, i.e. stable for all  $G(s) \in \mathcal{G}(s)$ . Then

$$\max_{G(s) \in \mathcal{G}(s)} \gamma^\pm = \max_{G(s) \in \mathcal{G}_{CB}(s)} \gamma^\pm \quad (4.5)$$

$$\max_{G(s) \in \mathcal{G}(s)} \phi^\pm = \max_{G(s) \in \mathcal{G}_{CB}(s)} \phi^\pm \quad (4.6)$$

and

$$\min_{G(s) \in G(s)} \gamma^{\pm} = \min_{G(s) \in G_{CB}(s)} \gamma^{\pm} \quad (4.7)$$

$$\min_{F(s) \in G(s)} \phi^{\pm} = \min_{G(s) \in G_{CB}(s)} \phi^{\pm} \quad (4.8)$$

**Proof.** It is obvious that the extremal gain and phase margins occur on the boundaries of the set of Nyquist plots of  $F(s)G(s)$  for all  $G(s) \in G(s)$ . From the theorem 4 and corollary 1, the Nyquist envelopes are contained in the the set of Nyquist plots of  $F(s)G(s)$  for  $G(s) \in G_{CB}(s)$ . Therefore, computing extremal gain and phase margins of  $F(s)G(s)$  over  $G(s) \in G_{CB}(s)$  is identical to determining these margins over  $G(s) \in G(s)$ . Q.E.D.

## 5. ANALYTICAL COMPUTATION OF EXTREMAL GAIN AND PHASE MARGINS

In this section, we consider an analytical way to compute extremal (i.e., both maximum and minimum) gain and phase margins. As discussed earlier, the extremal gain and phase margins are the minimum and maximum values of extremal margins of individual segment systems of the form

$$\left\{ \frac{K_n^i(s)}{S_d^k(s, \lambda)} \mid \lambda \in [0, 1] \right\} \quad \text{or} \quad \left\{ \frac{S_n^i(s, \lambda)}{K_d^k(s)} \mid \lambda \in [0, 1] \right\} \quad (5.1)$$

over  $(i, k) \in \{(1, 2, 3, 4) \times (1, 2, 3, 4)\}$ . Therefore, in this section, we develop simple techniques to compute the extremal gain and phase margins over a single segment system. This technique is useful when the designer wants to know which member of the system among the family provides the extremal (minimum or maximum) margin. The particular member is determined by the corresponding value of  $\lambda$ . Hence, the problem is reduced to choose the optimal value of  $\lambda \in [0, 1]$  so that the corresponding fixed system has the minimum or maximum stability margin.

Now Let us consider the following segment system for convenience.

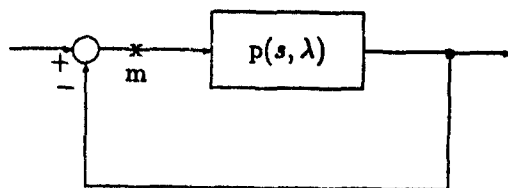


Figure 2. Segment System

with

$$p(j\omega, \lambda) = \frac{p_o(j\omega)}{p_1(j\omega) + \lambda p_2(j\omega)}$$

where  $p_0(s)$ ,  $p_1(s)$ , and  $p_2(s)$  are fixed polynomials in  $s$ , and  $\lambda \in [0, 1]$ .

The problem of computing the extremal gain and phase margins at the loop breaking point "m" over a single segment system is described as follows. Let us denote

$$(\Lambda \times \Omega) := \{(\lambda, \omega) \mid \angle p(j\omega, \lambda) = 180^\circ, \lambda \in [0, 1]\} \quad (5.2)$$

and

$$\bar{\mu}_p := \max_{(\Lambda \times \Omega)} |p(j\omega, \lambda)| \quad (5.3)$$

$$\underline{\mu}_p := \min_{(\Lambda \times \Omega)} |p(j\omega, \lambda)| \quad (5.4)$$

$$\bar{\phi}_p := \max_{(\Lambda \times \Omega)} \angle p(j\omega, \lambda) \quad (5.5)$$

$$\underline{\phi}_p := \min_{(\Lambda \times \Omega)} \angle p(j\omega, \lambda). \quad (5.6)$$

Then

$$\text{maximum gain margin over } p(s): \quad \bar{\rho} := \frac{1}{\underline{\mu}_p} \quad (5.7)$$

$$\text{minimum gain margin over } p(s): \quad \underline{\rho} := \frac{1}{\bar{\mu}_p} \quad (5.8)$$

$$\text{maximum phase margin over } p(s): \quad \bar{\theta} := \bar{\phi}_p - 180^\circ \quad (5.9)$$

$$\text{minimum phase margin over } p(s): \quad \underline{\theta} := \underline{\phi}_p - 180^\circ. \quad (5.10)$$

Similar definitions can be made for the case of gain margins less than 1.

As seen in eqs. (5.7) - (5.10), the problem of computing the extremal gain or phase margin over the segment system is a two parameter optimization problem. This can be reduced to a simple one parameter problem as follows. Write

$$p_i(j\omega) := p_{iR}(\omega) + jp_{iI}(\omega)$$

Then

$$\begin{aligned} p(j\omega, \lambda) &= \frac{p_0(j\omega)}{p_1(j\omega) + \lambda p_2(j\omega)} \\ &= \frac{p_{0R}(\omega) + jp_{0I}(\omega)}{[p_{1R}(\omega) + \lambda p_{2R}(\omega)] + j[p_{1I}(\omega) + \lambda p_{2I}(\omega)]} \\ &= \frac{p_{0R}(\omega)p_{1R}(\omega) + p_{0I}(\omega)p_{1I}(\omega) + \lambda[p_{0R}(\omega)p_{2R}(\omega) + p_{0I}(\omega)p_{2I}(\omega)]}{\underbrace{[p_{1R}(\omega) + \lambda p_{2R}(\omega)]^2 + [p_{1I}(\omega) + \lambda p_{2I}(\omega)]^2}_{\text{Re}\{p(j\omega, \lambda)\}}} \\ &\quad + j \frac{p_{0I}(\omega)p_{1R}(\omega) - p_{0R}(\omega)p_{1I}(\omega) + \lambda[p_{0I}(\omega)p_{2R}(\omega) - p_{0R}(\omega)p_{2I}(\omega)]}{\underbrace{[p_{1R}(\omega) + \lambda p_{2R}(\omega)]^2 + [p_{1I}(\omega) + \lambda p_{2I}(\omega)]^2}_{\text{Im}\{p(j\omega, \lambda)\}}} \quad (5.11) \end{aligned}$$

In order to determine the gain margin, we set

$$\angle p(j\omega, \lambda) = 180^\circ \quad (5.12)$$

which implies

$$\operatorname{Im}\{p(j\omega, \lambda)\} = 0. \quad (5.13)$$

Note that (5.13) will be satisfied when  $\angle p(j\omega, \lambda) = 0^\circ$  or  $180^\circ$ . We exclude frequencies  $\omega$  for which  $\angle p(j\omega, \lambda) = 0^\circ$ . From eqs. (5.13) and (5.11), we have

$$\begin{aligned} \operatorname{Im}\{p(j\omega, \lambda)\} &= [p_{0I}(\omega)p_{1R}(\omega) - p_{0R}(\omega)p_{1I}(\omega)] + \lambda[p_{0I}(\omega)p_{2R}(\omega) - p_{0R}(\omega)p_{2I}(\omega)] \\ &= 0 \end{aligned} \quad (5.14)$$

equivalently

$$\lambda(\omega) = \frac{p_{0R}(\omega)p_{1I}(\omega) - p_{0I}(\omega)p_{1R}(\omega)}{p_{0I}(\omega)p_{2R}(\omega) - p_{0R}(\omega)p_{2I}(\omega)}. \quad (5.15)$$

From this representation, we can easily conclude that instead of searching over both  $\omega \in [0, \infty)$  and  $\lambda \in [0, 1]$ , searching only selected ranges of  $\omega$  that satisfy  $\lambda \in [0, 1]$  is enough. Thus, we let

$$\begin{aligned} \lambda(\omega) &= \frac{p_{0R}(\omega)p_{1I}(\omega) - p_{0I}(\omega)p_{1R}(\omega)}{p_{0I}(\omega)p_{2R}(\omega) - p_{0R}(\omega)p_{2I}(\omega)} \\ &= 0 \text{ or } 1. \end{aligned} \quad (5.16)$$

Without loss of generality, we have

$$\begin{aligned} \text{for } \lambda = 1 & \quad p_{0R}(\omega)p_{1I}(\omega) - p_{0I}(\omega)p_{1R}(\omega) - p_{0I}(\omega)p_{2R}(\omega) + p_{0R}(\omega)p_{2I}(\omega) = 0 \\ \text{for } \lambda = 0 & \quad p_{0R}(\omega)p_{1I}(\omega) - p_{0I}(\omega)p_{1R}(\omega) = 0 \end{aligned} \quad (5.17)$$

The valid ranges of  $\omega$  with respect to the condition  $\lambda \in [0, 1]$  can be easily determined from the roots of the above two equations. Thus, the problem posed in eqs. (5.7) and (5.8) is reduced to selection of maximum and minimum magnitudes over the magnitudes evaluated over the admissible ranges of  $\omega$  determined from the roots of eq. (5.17). Furthermore, the optimal value  $\lambda^*$ , equivalently optimal values of parameters over the segment system, can also be easily determined by substituting  $\omega^*$  that corresponds to the maximum gain margin into eq. (5.15).

If the segment system is of the form

$$p(s, \lambda) := \frac{p_1(s) + \lambda p_2(s)}{p_0(s)},$$

one can follow a similar procedure to determine the extremal margins and the corresponding optimal systems over the segment system. Similar procedures can also be applied for computing extremal phase margins over a single segment. This is easily derived by replacing the condition (5.12) by

$$|p(j\omega, \lambda)| = 1 \quad (5.18)$$

## 6. EXAMPLE: LEAD-LAG COMPENSATION

In this section, we give an example of lead - lag compensation design utilizing the developments described above. Let us consider the interval plant

$$G(s) = \frac{a_0}{b_3 s^3 + b_2 s^2 + b_1 s}$$

where its coefficients are bounded by the given intervals as follows:

$$\begin{array}{ll} a_0 \in [4, 6] & b_3 \in [.4, .6] \\ & b_2 \in [1.4, 1.6] \\ & b_1 \in [.8, 1.2] \end{array}$$

The objective of the design is to achieve that the entire family of systems has the phase margin at least  $30^\circ$  and gain margin at least 20dB.

With the lag compensator

$$C_1(s) = \frac{21.2766s + 1}{280.505s + 1}$$

we have achieved approximately  $35^\circ$  of guaranteed phase margin and 10dB of guaranteed gain margin.

With the additional lead compensator

$$C_2(s) = \frac{s + .4}{s + 2.5}$$

we have achieved approximately  $55^\circ$  of guaranteed phase margin and 22dB of guaranteed gain margin. Therefore, the controller is

$$C(s) = \frac{21.2766s + 1}{280.505s + 1} \frac{s + .4}{s + 2.5}$$

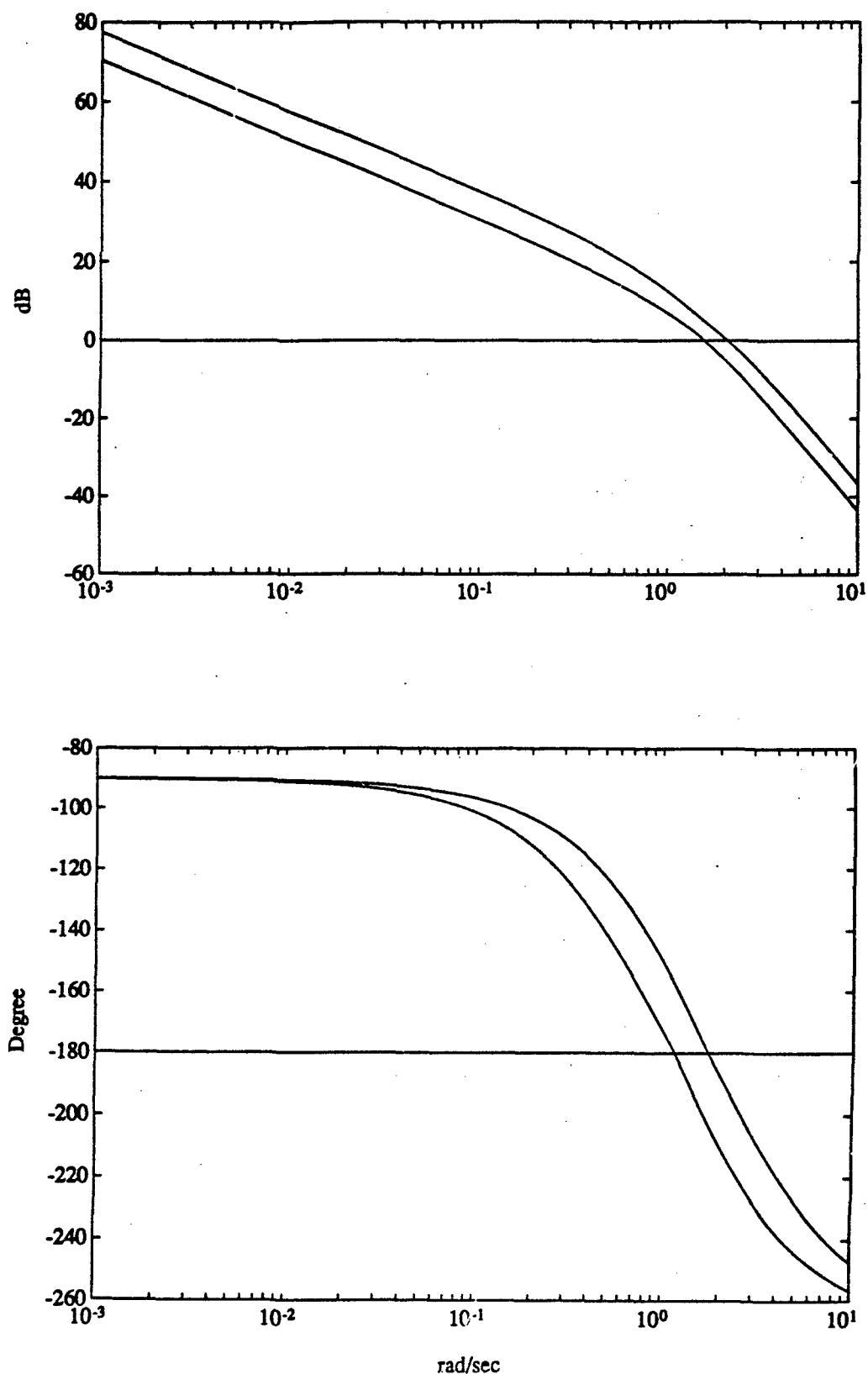
Figure 3 shows Bode envelopes of the uncompensated system  $G(s)$  Figures 4 and 5 show Bode envelopes of the lag compensated system and the lag-lead compensated system, respectively. Figure 6 has been constructed to show changes of frequency responses of uncompensated and compensated systems. Figures 7, 8, and 9 show the Nyquist envelopes, and Figures 10, 11, and 12 show the Nichols charts of the respective systems.

## 7. CONCLUDING REMARKS

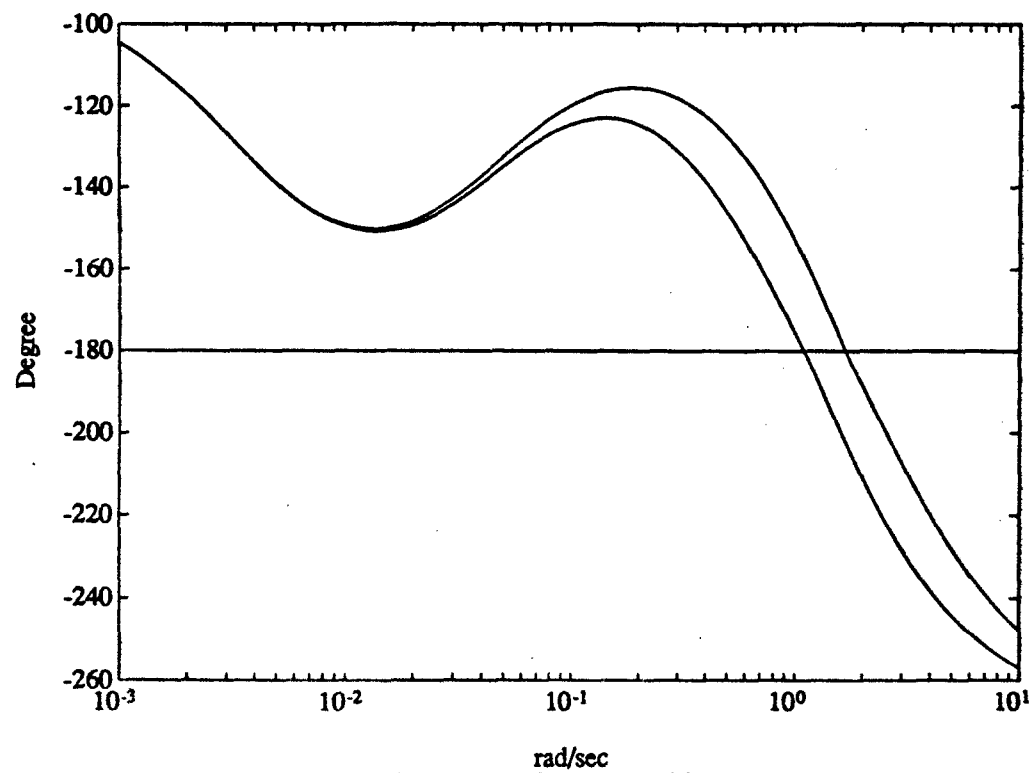
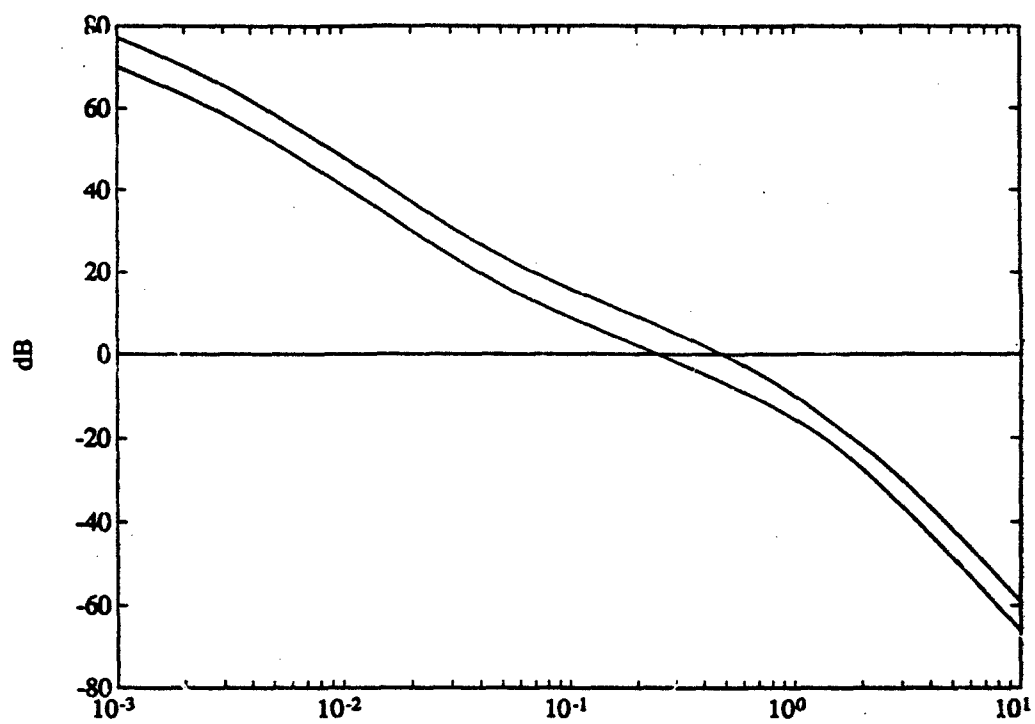
The new results given here characterize the entire frequency domain design information needed for interval systems. Using this development we also showed that basically all frequency domain based classical control design and analysis techniques can be applied to interval uncertain systems.

## REFERENCES

- [1] I. Horowitz, "A survey of quantitative feedback theory," *International Journal of Control*, vol. 53, pp. 255 - 291, 1991
- [2] D. D. Šiljak, *Nonlinear Systems: Parametric Analysis and Design*. New York: Wiley, 1969.
- [3] D. D. Šiljak, "Parameter space methods for robust control design: a guided tour," *IEEE Transactions on Automatic Control*, vol. AC - 34, pp. 674 - 688, July 1989.
- [4] V. L. Kharitonov, "Asymptotic stability of an equilibrium position of a family of systems of linear differential equations," *Differential Uravnen*, vol. 14, pp. 2086 - 2088, 1978.
- [5] S. P. Bhattacharyya, "Robust parametric stability: the role of the CB segments," in *Control of Uncertain Dynamic Systems*, (L. H. Keel and S. P. Bhattacharyya, eds.), Littleton, MA: CRC Press, September 1991.
- [6] H. Chapellat, M. Dahleh, and S. P. Bhattacharyya, "Robust stability under structured and unstructured perturbations," *IEEE Transactions on Automatic Control*, vol. AC - 35, pp. 1100 - 1108, October 1990.
- [7] H. Chapellat and S. P. Bhattacharyya, "A generalization of Kharitonov's theorem: robust stability of interval plants," *IEEE Transactions on Automatic Control*, vol. AC - 34, pp. 306 - 311, March 1989.

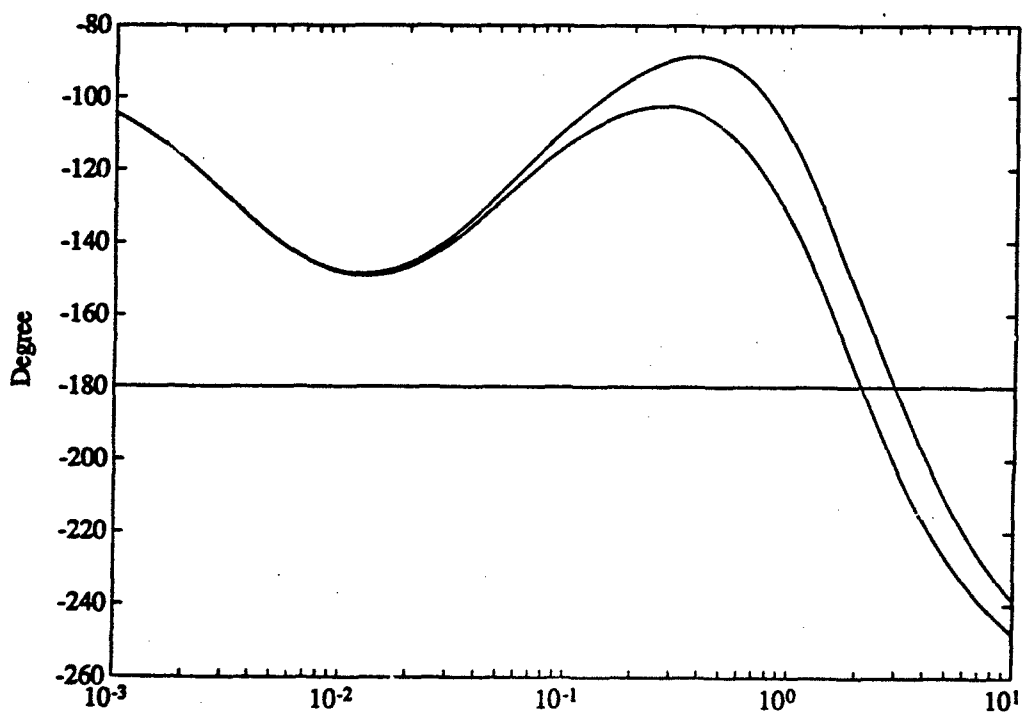
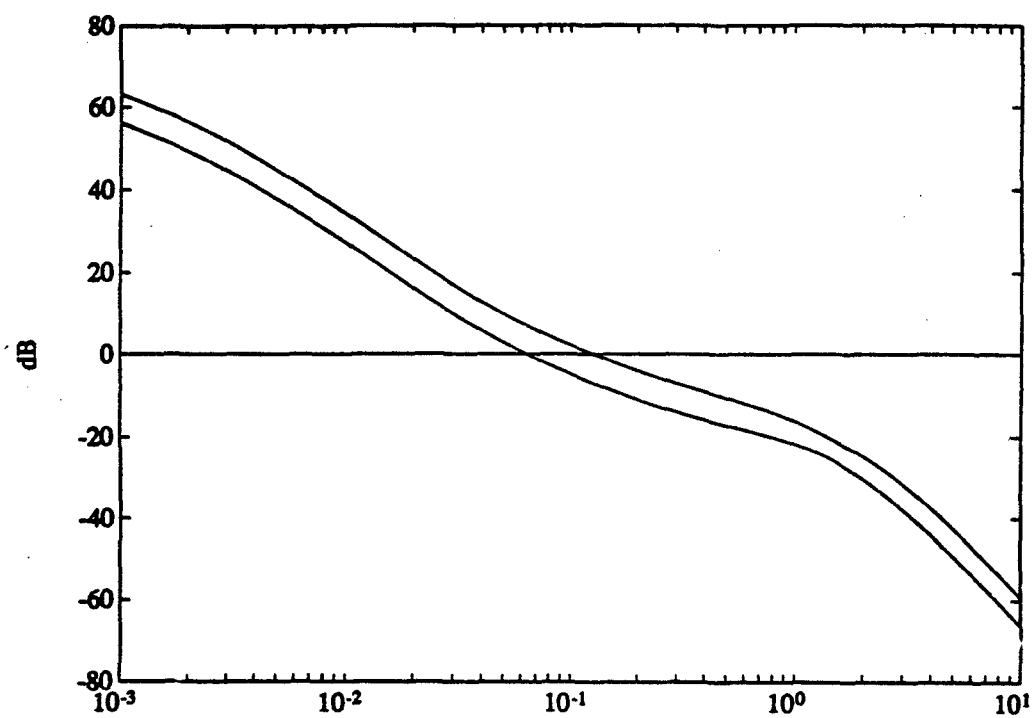


rad/sec  
Figure 3. Uncompensated System

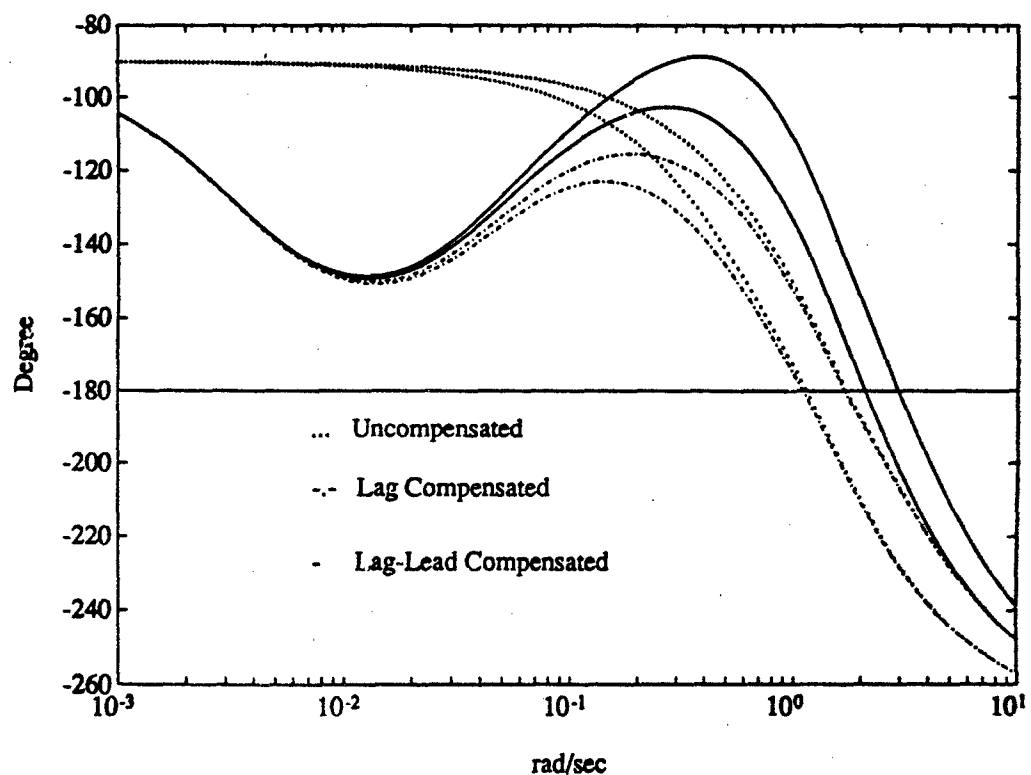
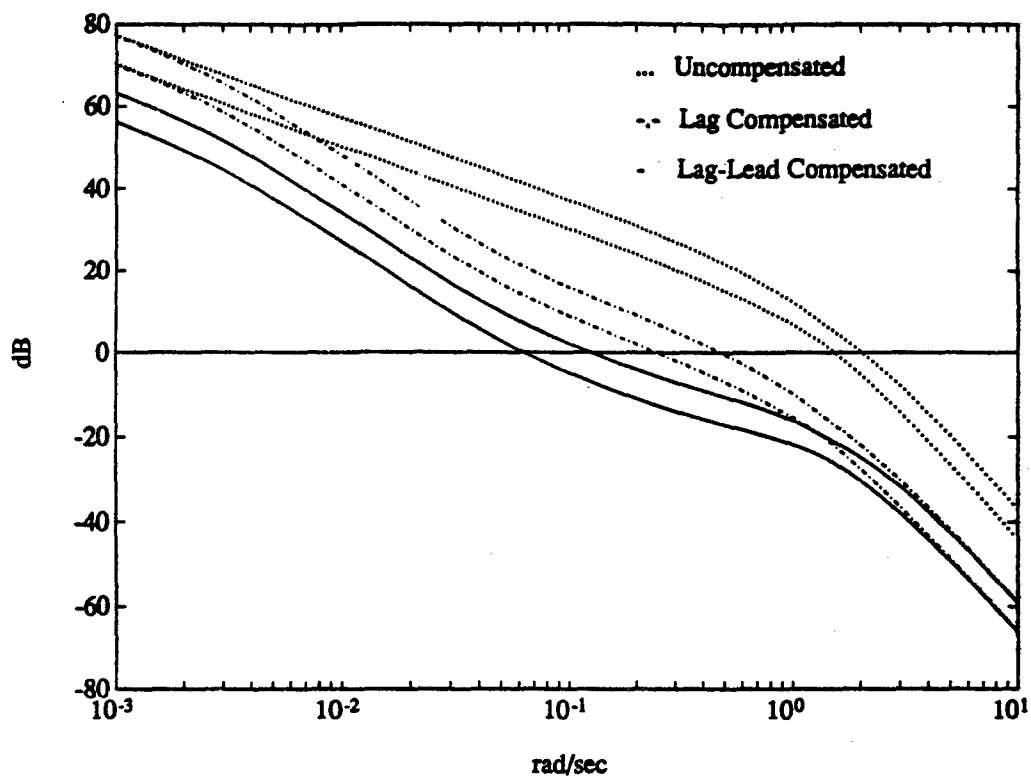


rad/sec  
Figure 4. Lag Compensated System  
450





rad/sec  
Figure 5. Lag-Lead Compensated System  
451



rad/sec  
Figure 6.  
452

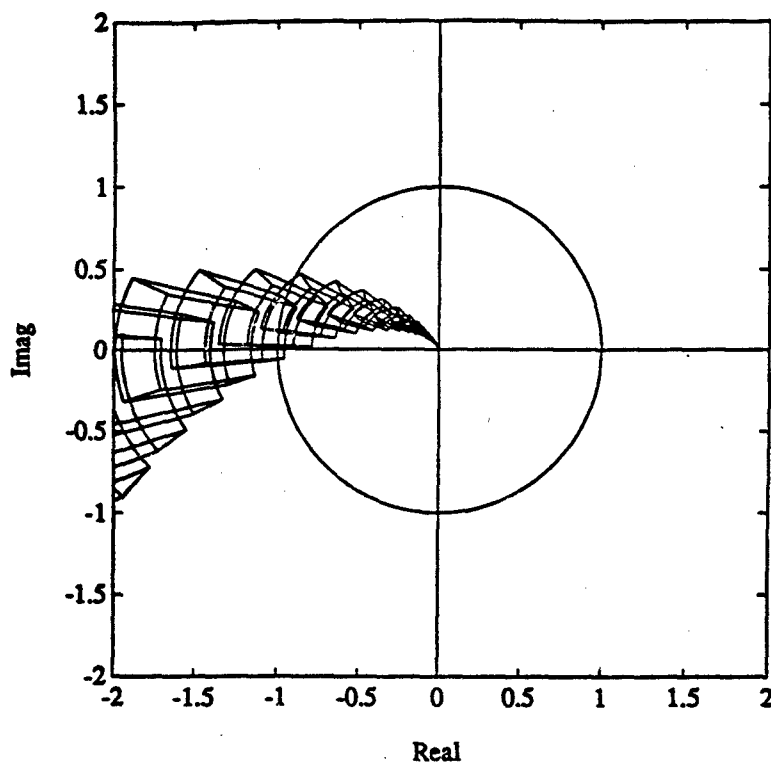


Figure 7. Uncompensated System

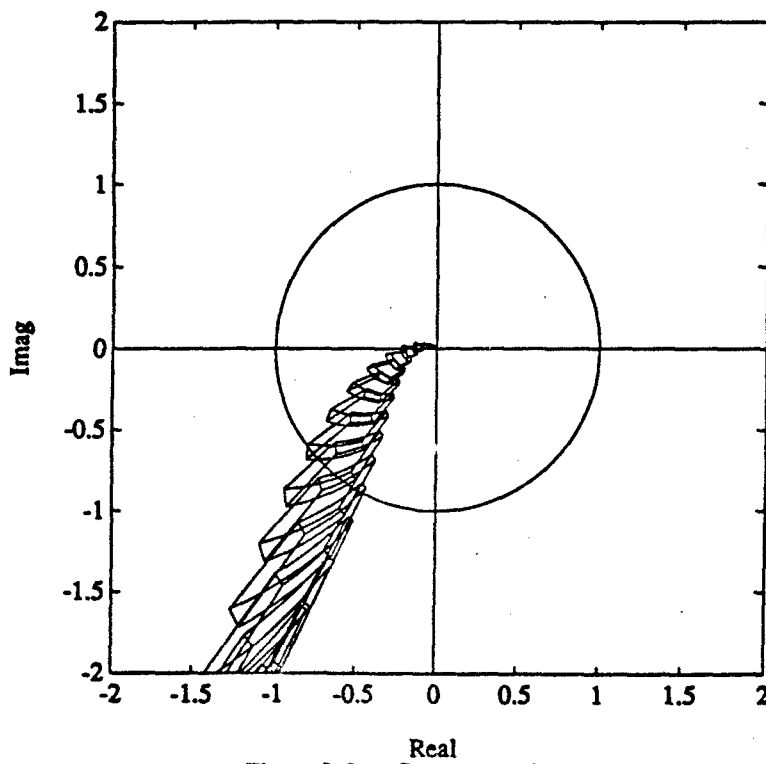


Figure 8. Lag Compensated System

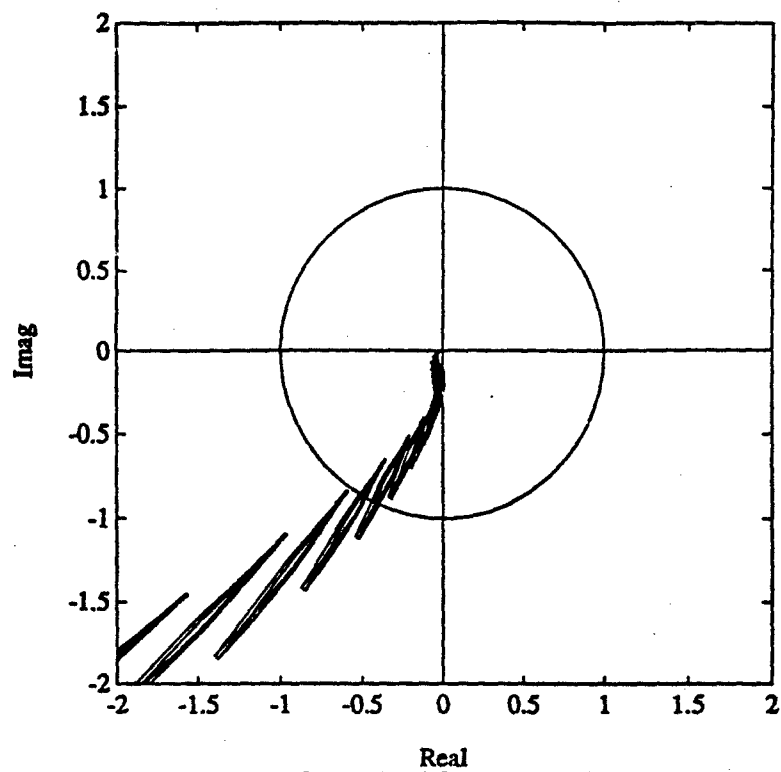


Figure 9. Lag-Lead Compensated System

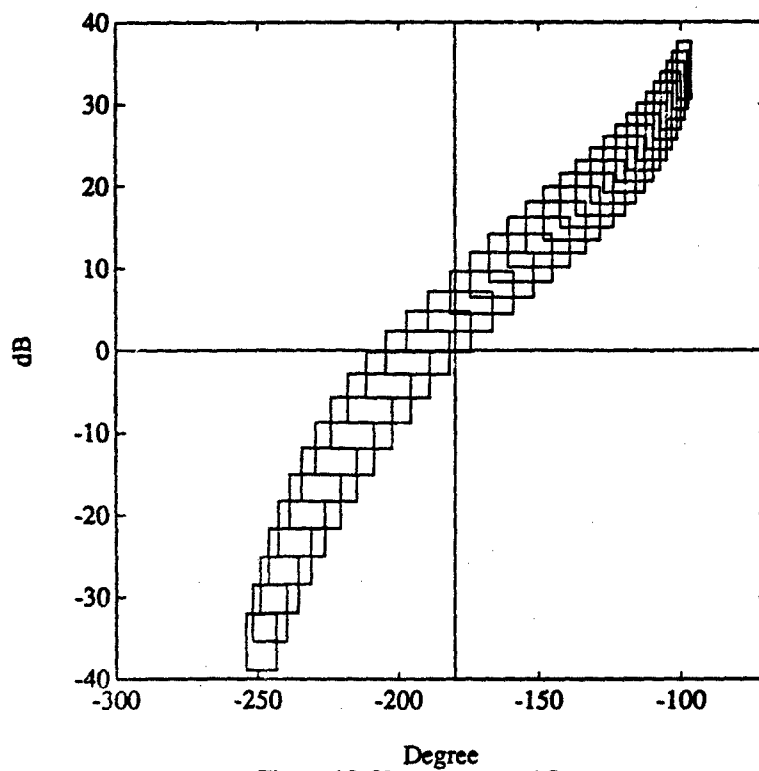


Figure 10. Uncompensated System

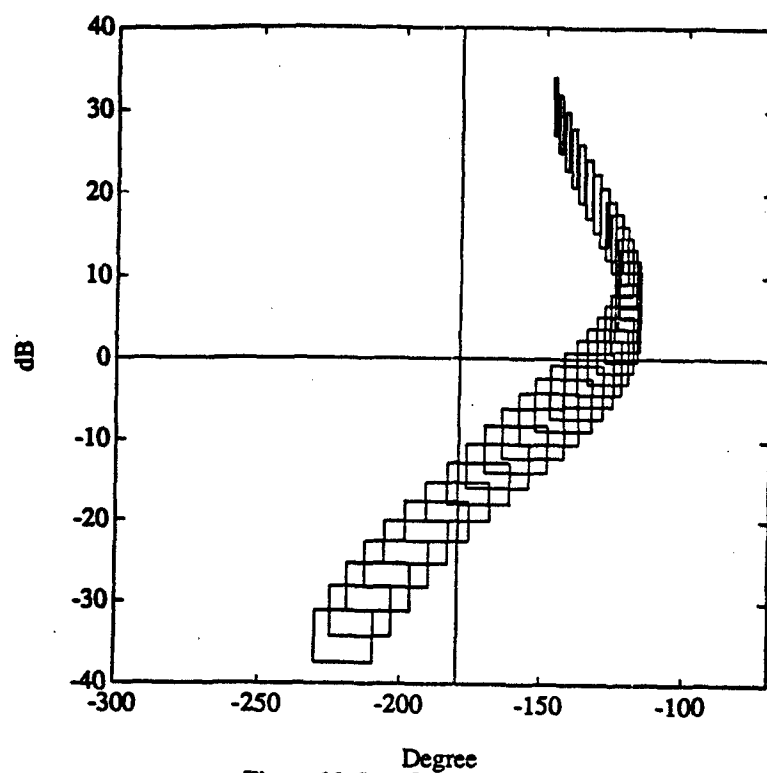


Figure 11. Lag Compensated System

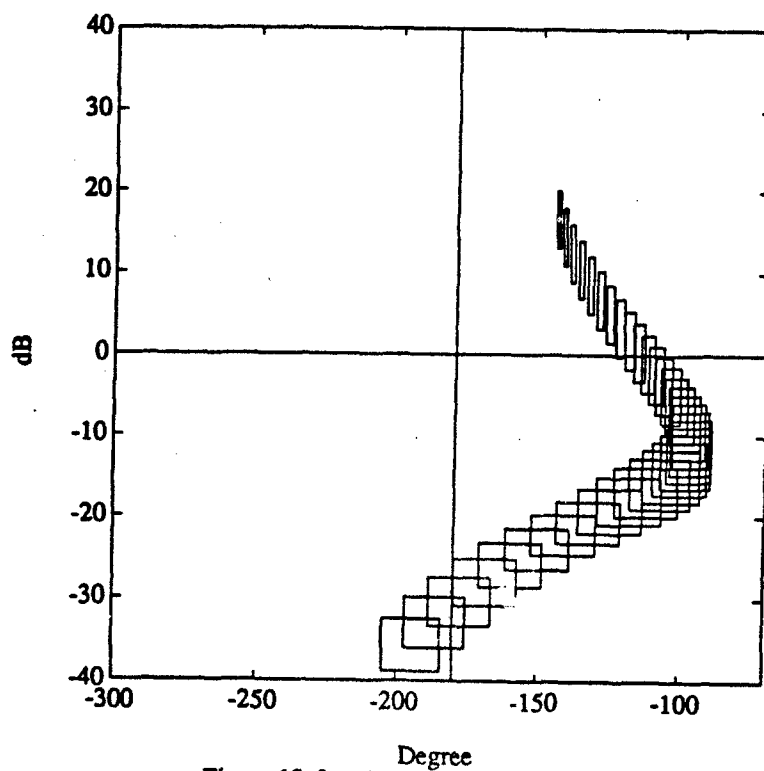


Figure 12. Lag-Lead Compensated Systems

**THIS PAGE INTENTIONALLY LEFT BLANK**

# DESIGN OF FEEDBACK SYSTEMS USING KHARITONOV'S SEGMENTS IN QUANTITATIVE FEEDBACK THEORY

I.J.FIALHO, V.PANDE and P.S.V.NATARAJ\*

Systems and Control Group  
Department of Electrical Engineering  
Indian Institute of Technology  
Powai, Bombay - 400 076  
INDIA

## ABSTRACT

The approach of Quantitative Feedback Theory (QFT) for robust control, has been receiving increasing attention lately. The basic QFT technique comprises of these four steps : template generation, derivation of the bounds on loop transmission, determination of an appropriate loop transmission function and the synthesis of the pre-filter. The usual 'gridding' method of template generation has a great deal of subjectivity, is potentially risky as crucial points may not be considered, and worst of all, becomes computationally untractable with increasing number of uncertain parameters. As such, this method has been severely criticized (Doyle 1986). In this paper, we deal with the problem of obtaining the bounds on the loop transmission function, for plants with parameters varying independently in prescribed intervals. A technique for calculating the bounds in loop transmission is developed, after suitably extending some recent results concerning the role of Kharitonov segments in robust stability analysis (Chapellat et al. 1990). The developments reported here should be viewed as a first attempt to use robust stability results based on the Kharitonov approach to benefit the synthesis procedure of QFT for achieving robust performance.

## 1. INTRODUCTION

Quantitative Feedback Theory, pioneered by Horowitz (Horowitz 1991), is one of the few approaches for synthesis of feedback systems for plants with significant parameter and disturbance uncertainty. The design is quantitative in the sense that it is intimately related to the sizes of the uncertainty sets and the level of performance desired. QFT has been under development since 1959 and can currently handle several problem classes involving large parameter uncertainty: SISO and MIMO linear and non linear, lumped and distributed, output and internal variable feedback, time invariant and time varying plants, etc..

Consider a lumped minimum phase (MP) single-input single-output (SISO) linear time invariant (LTI) plant  $g(s)$  in a two-degree-of-freedom feedback structure shown in Fig.1. Suppose the uncertain parameters of  $g(s)$  vary independently in prescribed ranges to give a set of plants  $G = \{g\}$ . Despite the uncertainty in the plant parameters, it is required that the following be

satisfied by choosing LTI rational strictly proper  $c(s)$  and  $f(s)$ ,  
 $\forall \omega, \forall g \in G$ :

$$0 < |A(j\omega)| \leq |T_r(j\omega)| \leq |B(j\omega)| \quad (1a)$$

$$\left| \frac{1}{1 + g(j\omega)c(j\omega)} \right| \leq \mu \quad (1b)$$

where  $T_r(s) = \frac{y(s)}{r(s)}$ , and  $A(s)$ ,  $B(s)$  are stable MP transfer functions.

Since we shall consider only MP plants, the above magnitude specifications are sufficient. Specification (1a) refers to the tracking properties of the closed loop system, while specification (1b) captures the extra stability (gain-phase) margins usually desired by the designer. Note that  $G$  can include unstable plants as well.

With the specifications (1) given in the frequency domain, the QFT design procedure consists of the following basic steps (Mcrowitz and Sidi 1972)

- (a) Computation of the set of values  $\{g(j\omega_i)\}$  to give the plant template  $T_p \{g(j\omega_i)\}$  in the Nichols plane for some selected  $\omega_i$  values.
- (b) Using  $T_p \{g(j\omega_i)\}$ , derivation of the bounds  $B(\omega_i)$  in the Nichols plane, on the nominal loop transmission  $L_o = cg_o$ , where  $g_o$  is the nominal plant.
- (c) Determination of a (sub optimal)  $L_o$  that satisfies the bounds  $B(\omega_i)$  and has a pre-assigned pole-zero excess.
- (d) Synthesis of a pre-filter  $f(s)$ .

Since the plant parameters vary in continuous sets, in practice, approximate plant templates  $T_{pa} \{g(j\omega_i)\}$  are generated in step (a) and used in step (b) to obtain the



approximate bounds  $B_a(\omega_i)$  on  $L_o(j\omega_i)$ . Several methods exist for the purpose (East 1981, 1982, Bailey et al. 1988). The most widely used technique, according to (Yaniv and Horowitz 1987), is as follows. For each uncertain parameter, the minimum, mean, and maximum values are picked, i.e. a grid of 3 points is made, and  $T_{pa} \left\{ g(j\omega_i) \right\}$  is generated for all possible parameter combinations using the picked values.

The above 'gridding' technique, however, leaves much to be desired, at least on two major issues. Firstly, 'gridding' is highly subjective in nature, with the burden on the designer to judiciously select the number and location of the grid points. Even with fine grids it is potentially risky as there is no guarantee that all the critical points of  $T_p$  (critical for obtaining  $B(\omega_i)$ ) are actually present in  $T_{pa}$ . Secondly, the procedure can run into severe computational problems on most departmental workstations, possibly precluding the use of the QFT technique itself. This is because, at each  $\omega$ , one considers  $m^p$  plants, where  $m$  is the number of grid points and  $p$  is the number of uncertain parameters. Should  $(m,p)$  be large, the quantum of computation becomes tremendous. For example, if  $p=15$  and one used the 3 point grid technique, then, at each  $\omega$ ,  $3^{15}$  plants are to be considered. Again, if the parameter variations are large,  $m=3$  might be grossly inadequate, with possibly at least an occasional example demanding  $m \approx 10$ . Clearly, if QFT is to be used in such situations, alternatives to this strategy of a 'brute force global search' (Fan et al. 1991) are needed.

In this paper, we propose, for the case of SISO LTI MP plants with independent parameter uncertainty, an efficient technique for generating the bounds  $B_a(\omega_i)$  on  $L_o$ . The proposed technique is free from subjectivity, takes into account all key parameter combinations, and yields practically the exact bounds on  $L_o$ . Another significant feature is that this is achieved with a tremendous saving in computations (over that required for the gridding technique) for cases where the number of uncertain parameters and/or the parameter variations are large. The technique is developed by extending recent results of the Kharitonov approach to robust stabilization (Chapellat et al. 1990).

This paper is organized as follows: Section 2 contains a brief overview of the Kharitonov approach, together with an important lemma that will be needed in the sequel. The proposed technique is developed in section 3. In section 4, an example to demonstrate the technique is presented. Finally, section 5 contains the conclusions and scope for further research.

## 2 THE KHARITONOV APPROACH TO ROBUST STABILIZATION

In this section, we first briefly review some important concepts of Kharitonov polynomials (Kharitonov 1978), and then give an important lemma that will be needed in the development to follow.

Consider a real polynomial  $p(s)$ . Let  $p^{\text{even}}(s)$  and  $p^{\text{odd}}(s)$  be the even and odd parts of  $p(s)$ , respectively. That is,

$$p(s) = \underbrace{p_0 + p_2 s^2 + p_4 s^4 + \dots}_{p^{\text{even}}(s)} + \underbrace{p_1 s + p_3 s^3 + p_5 s^5 + \dots}_{p^{\text{odd}}(s)} \quad (2.1a)$$

We also have

$$p^{\text{even}}(\omega) = p^{\text{even}}(j\omega) = p_0 - p_2 \omega^2 + p_4 \omega^4 - \dots \quad (2.1b)$$

$$p^{\text{odd}}(\omega) = \frac{p^{\text{odd}}(j\omega)}{j\omega} = p_1 - p_3 \omega^2 + p_5 \omega^4 - \dots$$

Now consider a family  $F$  of real interval polynomials:

$$p(s) = p_0 + p_1 s + \dots + p_{n-1} s^{n-1} + p_n s^n \quad (2.2)$$

where

$$p_0 \in [x_0, y_0], p_1 \in [x_1, y_1], \dots, p_n \in [x_n, y_n], \quad (2.3)$$

Associated with the interval polynomial  $p(s)$  are four Kharitonov polynomials defined as follows:

$$K_F^1(s) = x_0 + x_1 s + y_2 s^2 + y_3 s^3 + x_4 s^4 + x_5 s^5 + y_6 s^6 + \dots \quad (2.4.1)$$

$$K_F^2(s) = x_0 + y_1 s + y_2 s^2 + x_3 s^3 + x_4 s^4 + y_5 s^5 + y_6 s^6 + \dots \quad (2.4.2)$$

$$K_F^3(s) = y_0 + x_1 s + x_2 s^2 + y_3 s^3 + y_4 s^4 + x_5 s^5 + x_6 s^6 + \dots \quad (2.4.3)$$

$$K_F^4(s) = y_0 + y_1 s + x_2 s^2 + x_3 s^3 + y_4 s^4 + y_5 s^5 + x_6 s^6 + \dots \quad (2.4.4)$$

We next consider the family G of SISO plants :

$$g(s) = \frac{n(s)}{d(s)} \quad (2.5)$$

Here,  $n(s)$  belongs to a family of real interval polynomials N, and  $d(s)$  belongs to a family of real interval polynomials D, as defined below

$$N = \left\{ n(s) \mid n(s) = n_0 + n_1 s + \dots + n_p s^p \right. \\ \left. \text{where } n_i \in [\alpha_i, \beta_i], \forall i = 0, \dots, p \right\} \quad (2.6)$$

$$D = \left\{ d(s) \mid d(s) = d_0 + d_1 s + \dots + d_q s^q \right. \\ \left. \text{where } d_i \in [\gamma_i, \delta_i], \forall i = 0, \dots, q \right\} \quad (2.7)$$

Let  $K_N$  be the set of four Kharitonov polynomials associated with N. Further, let  $KK_N$  be the subset of N consisting of the four following line segments

$$\begin{aligned} & \left[ K_N^1(s), K_N^2(s) \right] ; \quad \left[ K_N^1(s), K_N^3(s) \right] \\ & \left[ K_N^2(s), K_N^4(s) \right] ; \quad \left[ K_N^3(s), K_N^4(s) \right] \end{aligned} \quad (2.8)$$

These are called the four Kharitonov segments associated with N. By line segment  $\left[ K_N^1(s), K_N^2(s) \right]$ , we mean of course all convex combinations of the form

$$(1 - \lambda) K_N^1(s) + \lambda K_N^2(s)$$

The subsets  $K_D$  and  $KK_D$  of D are similarly defined. Finally, let  $G_{KK}$  be the subset of G defined by

$$G_K = \left[ \frac{n(s)}{d(s)} \in G : \left[ n(s) \in K_N \text{ and } d(s) \in K_D \right] \right. \\ \left. \text{or } \left[ n(s) \in K'_N \text{ and } d(s) \in K'_D \right] \right] \quad (2.9)$$

Thus,  $G_K$  contains at most 32 one parameter families of rational functions. These are known as the 'Kharitonov segments'.

Before proceeding further, we state the following two lemmas.

Lemma 2.1 (Chapellat et al. 1990)

Let  $g(s) = n(s)/d(s)$  be a proper (real or complex) rational function in  $H_\infty(C_+)$ , with  $\deg(d(s)) = q$ , then  $\|g\|_\infty < 1$  iff

- 1)  $|n_q| < |d_q|$
- 2)  $d(s) + e^{j\theta} n(s)$  is Hurwitz for all  $\theta \in [0, 2\pi)$ .

Lemma 2.2 (Chapellat et al. 1990)

Let  $Q(s)$  and  $R(s)$  be two arbitrary but fixed complex polynomials and consider the family  $P$  of polynomials

$$Q(s)n(s) + R(s)d(s), \quad n(s) \in N, d(s) \in D.$$

Then, all polynomials in  $P$  are Hurwitz stable iff it is the case when  $n(s), d(s)$  are such that  $n(s)/d(s) \in G_K$ .

We now prove an important lemma that is of fundamental importance in the sequel.

Lemma 2.3

Let  $g(s) = n(s)/d(s) \in G$ , be a family of strictly proper stable MP plants, such that  $n(s)$  and  $d(s)$  have fixed degrees. Let  $A(s)$  and  $B(s)$  be stable MP transfer functions such that  $A(s)/B(s)$  is proper. Then, if  $c$  is a stabilizing controller,

$$\Delta \text{Lm} |g c (1 + gc)^{-1}| < \text{Lm} |B(j\omega)| - \text{Lm} |A(j\omega)| \quad \forall \omega, \forall g \in G$$

iff

$$\Delta \text{Lm} |g c (1 + gc)^{-1}| < \text{Lm} |B(j\omega)| - \text{Lm} |A(j\omega)| \quad \forall \omega, \forall g \in G_K$$

(Lm denotes the log magnitude, in decibels)

Proof: We equivalently have to prove the following

$$\begin{aligned} \text{Lm} \left| \frac{g_1 c}{1 + g_1 c} \right| - \text{Lm} \left| \frac{g_2 c}{1 + g_2 c} \right| &< \text{Lm} |B(j\omega)| - \text{Lm} |A(j\omega)| \\ &\forall g_1, g_2 \in G, \forall \omega \\ \text{iff} \\ \text{Lm} \left| \frac{g_1 c}{1 + g_1 c} \right| - \text{Lm} \left| \frac{g_2 c}{1 + g_2 c} \right| &< \text{Lm} |B(j\omega)| - \text{Lm} |A(j\omega)| \\ &\forall g_1, g_2 \in G_K, \forall \omega \end{aligned} \quad (2.10)$$

Eliminating Lm in the above expressions, we have to show that

$$\begin{aligned} \left| \frac{g_1 c(1 + g_2 c)}{g_2 c(1 + g_1 c)} \right| &< \left| \frac{B(j\omega)}{A(j\omega)} \right| \quad \forall g_1, g_2 \in G, \forall \omega \\ \text{iff} \\ \left| \frac{g_1 c(1 + g_2 c)}{g_2 c(1 + g_1 c)} \right| &< \left| \frac{B(j\omega)}{A(j\omega)} \right| \quad \forall g_1, g_2 \in G_K, \forall \omega \end{aligned} \quad (2.11)$$

Multiplying across by  $|A(j\omega)/B(j\omega)|$ , and from the definition of the  $\|\cdot\|_\infty$ , we have to prove that

$$\begin{aligned} \left\| \frac{Ag_1 c(1 + g_2 c)}{Bg_2 c(1 + g_1 c)} \right\|_\infty &< 1 \quad \forall g_1, g_2 \in G, \\ \text{iff} \\ \left\| \frac{Ag_1 c(1 + g_2 c)}{Bg_2 c(1 + g_1 c)} \right\|_\infty &< 1 \quad \forall g_1, g_2 \in G_K \end{aligned} \quad (2.12)$$

Let  $A = n_a/d_a$ ,  $B = n_b/d_b$ ,  $C = n_c/d_c$ ,  $g_1 = n_1/d_1$ ,  $g_2 = n_2/d_2$ .

Then, we can write

$$\frac{Ag_1 c(1 + g_2 c)}{Bg_2 c(1 + g_1 c)} = \frac{d_b n_a n_1 n_c d_2 d_c + d_b n_a n_1 n_c n_2 n_c}{n_b d_a n_2 n_c d_1 d_c + n_b d_a n_2 n_c n_1 n_c} \quad (2.14)$$

If Part : We start by noting that

$$\left\| \frac{Ag_1c(1 + g_2c)}{Bg_2c(1 + g_1c)} \right\|_\infty < 1, \quad \forall g_1, g_2 \in G_K$$

iff

$$a) |n_q| < |d_q|, \quad \forall g_1, g_2 \in G_K \quad (2.15)$$

$$b) (n_b d_a n_2 n_c d_1 d_c + n_b d_a n_2 n_c n_1 n_c) + e^{j\theta} (d_b n_a n_1 n_c d_2 d_c + d_b n_a n_1 n_c n_2 n_c)$$

$$\text{is Hurwitz } \forall \theta \in [0, 2\pi), \quad \forall g_1, g_2 \in G_K. \quad (2.16)$$

Consider (2.16) which can be rewritten as

$$n_1 (n_b d_a n_2 n_c n_c + e^{j\theta} d_b n_a n_c d_2 d_c + e^{j\theta} d_b n_a n_c n_2 n_c) + d_1 (n_b d_a n_2 n_c d_c)$$

is Hurwitz  $\forall \theta \in [0, 2\pi), \quad \forall g_1, g_2 \in G_K.$  (2.17)

From Lemma 2.2, it is seen that (2.17) is equivalent to

$$n_1 (n_b d_a n_2 n_c n_c + e^{j\theta} d_b n_a n_c d_2 d_c + e^{j\theta} d_b n_a n_c n_2 n_c) + d_1 (n_b d_a n_2 n_c d_c)$$

is Hurwitz  $\forall \theta \in [0, 2\pi), \quad \forall g_1 \in G, g_2 \in G_K.$  (2.18)

Now, (2.18) can be rewritten as

$$n_2 (n_b d_a n_c d_1 d_c + n_b d_a n_c n_1 n_c + e^{j\theta} d_b n_a n_1 n_c n_c) + d_2 (e^{j\theta} d_b n_a n_1 n_c d_c)$$

is Hurwitz  $\forall \theta \in [0, 2\pi), \quad \forall g_1 \in G, g_2 \in G_K,$  (2.19)

so that, by invoking Lemma 2.2 once more, we have

$$n_2 (n_b d_a n_c d_1 d_c + n_b d_a n_c n_1 n_c + e^{j\theta} d_b n_a n_1 n_c n_c) + d_2 (e^{j\theta} d_b n_a n_1 n_c d_c)$$

is Hurwitz  $\forall \theta \in [0, 2\pi), \quad \forall g_1 \in G, g_2 \in G.$  (2.20)

We also note the following

$$|n_q| < |d_q|, \quad \forall g_1, g_2 \in G_K \quad \text{iff} \quad |n_q| < |d_q|, \quad \forall g_1, g_2 \in G. \quad (2.21)$$

Thus, from (2.20), (2.21) and Lemma 2.1, we can conclude that

$$\left\| \frac{Ag_1c(1+g_2c)}{Bg_2c(1+g_1c)} \right\|_{\infty} < 1 \quad \forall g_1, g_2 \in G$$

which is what was required to be proved.

Only if part : the proof is obvious as  $G_{KK}$  is a subset of  $G$ .

□

On similar lines, it can be proved that

$$| (1 + gc)^{-1} | \leq \mu \quad \forall \omega, \forall g \in G_{KK}$$

iff

$$| (1 + gc)^{-1} | \leq \mu \quad \forall \omega, \forall g \in G$$

Therefore, if a controller  $c(s)$  is synthesised so that the performance specifications are satisfied for all  $g \in G_{KK}$ , then they are also be satisfied for all  $g \in G$ .

### 3. TEMPLATE GENERATION

As has been discussed earlier, template generation is the main computational bottleneck in QFT design procedures, especially in cases where the number of uncertain parameters and/or their range of variation is large. In the light of Lemma 2.3, it is seen that the design specifications i.e. (1a) and (1b) are satisfied for all  $g \in G$  iff they are satisfied for all  $g \in G_{KK}$ . The important and interesting implication of this lemma is that the whole QFT design procedure can now be carried out using only the subset  $G_{KK}$  of the entire uncertain set  $G$ . A real rational proper stabilizing controller  $c(s)$  and prefilter  $f(s)$  can be designed so that the design specification are satisfied for all  $g \in G_{KK}$ . Lemma 2.3 assures us that the specifications will be satisfied for all  $g \in G$ .

More specifically and importantly, the template  $T_{pa} \{g(j\omega_i)\}$  at any  $\omega_i$ , can be now generated by considering a maximum of 32 parameter families, namely, the Kharitonov segments. At any frequency  $\omega_i$ , the parameter  $\lambda$  is varied in discrete steps (the number of steps depending on the accuracy desired) in the interval  $[0, 1]$  and the resulting template is used to evaluate the bounds  $B(\omega_i)$ . The consequent reduction in computations is tremendous.

Firstly, the number of Kharitonov segments is at a maximum, 32, and this is independent of the number of uncertain parameters, their range of variation, and the system order. In many cases (as in the example in Section 4) the number of segments is much less. Secondly, the choice of a very fine grid for  $\lambda \in [0, 1]$ , say 100 points, does not render this method computationally untractable, as would have been the case in the 'brute force' method. We illustrate this through the following example. Let  $p = 5$ , and  $m = 100$ , say, due to the fact that the range of variation of the parameters is rather high. Then, by the brute force method, at every frequency  $\omega_i$ , the number of computations is  $10^{10}$ . Varying  $\lambda$  in  $[0, 1]$  in steps of 0.01 i.e. 100 points, results in a maximum of 3200 computations at every frequency  $\omega_i$ . Thus, very accurate results may be sought without the fear of excessive computations.

It is thus readily appreciated that the method of template generation proposed above results in significant computation reductions in QFT. It is also seen that this reduction becomes more and more significant as the number of uncertain parameters and/or their range of variation increases. At this point a few remarks are in order.

**Remark 3.1 :** The case of dependent parameter variation can also be considered, using the proposed method. The results may however be overly conservative.

**Remark 3.2 :** The proof of Lemma 2.3 will go through without the restriction on the poles of the plant. The restriction on the zeros of the plant i.e. that the plant zeros must lie in the L.H.P., is necessary. In other words, the above Lemma holds for unstable plants which have no R.H.P. zeros. However, we shall show later that Lemma 2.3 holds under much weaker assumptions.

We now illustrate the theory with an example.

#### 4 ILLUSTRATION OF THE PROPOSED METHOD

In this section, we solve an example to illustrate the method outlined in the previous section. We consider the design example solved in (Horowitz and Sidi 1972). Here

$$g(s) = \frac{K}{s(s+a)} \quad (4.1)$$

$$K \in [1, 100], a \in [1, 10]$$

For this example, the Kharitonov polynomials for the numerator and denominator are



$$K_N^1(s) = K_N^2(s) = 1 \quad (4.2.a)$$

$$K_N^3(s) = K_N^4(s) = 100 \quad (4.2.b)$$

$$K_D^1(s) = K_D^3(s) = s + s^2 \quad (4.2.c)$$

$$K_D^2(s) = K_D^4(s) = 10s + s^2 \quad (4.2.d)$$

We thus have four Kharitonov segments which are formed as described in Section 2. Using these four segments, and by varying  $\lambda$  in the interval  $[0,1]$  in steps of 0.2, the approximate template  $T_{pa} \left\{ g(j\omega_i) \right\}$  is generated for  $\omega = 2, 5$  and 15 rad/sec. This is shown in Fig. 2 for  $\omega = 2$ . Also shown in this figure is the corresponding template generated by the 'brute force' method. It is seen that the template generated by the Kharitonov segments completely encloses the latter. Using the specifications given in (Horowitz and Sidi 1972) the bounds on the nominal loop transmission  $L_o(j\omega_i)$  i.e.  $B(\omega_i)$ , are also calculated by both the methods. These are tabulated in Table 1. It is readily seen that the bounds obtained by both the methods are exactly the same.

## 5. CONCLUSIONS AND SCOPE FOR FURTHER WORK

In this paper we have presented a method that helps to reduce the computational burden associated with template generation in QFT. The proposed method is based on concepts from Kharitonov polynomials developed in (Chapellat et al. 1990). Only SISO plants with independent parametric uncertainty are discussed in this paper. The case of dependent uncertainty can also be handled, but the results may be overly conservative and lead to severe over design. A future paper will explore methods of handling the dependent case in a non-conservative fashion. A natural off-shoot of this will be the extension of the proposed method to MIMO QFT and this will indeed represent a significant contribution to this design procedure. We thus hope that this work will go a long way in making QFT a viable method of controller design.

## REFERENCES

- Bailey, F.N., Panzer, D. and Gu, G., 1988, International Journal of Control, Vol 48, No 5, p 1787.
- Chapellat, H., Dahleh, M. and Bhattacharyya, S.P., 1990, IEEE Transactions on Automatic Control, Vol AC-35, No 10, p 1100.
- Doyle, J.C., 1986, Quantitative Feedback Theory (QFT) and Robust Control,

Proc. of the American Control Conference, p 1691.

East, D.J., 1981, International Journal of Control, Vol 34, p 731.

East, D.J., 1982, International Journal of Control, Vol 35, p 891.

Fan, M.K.H., Tits, A.L. and Doyle, J.C., 1991, IEEE Transactions on Automatic Control, Vol AC-36, No 1, p 25.

Horowitz, I.M., 1991, International Journal of Control, Vol 53, No 2, p 255.

Horowitz, I.M. and Sidi, M., 1972, International Journal of Control, Vol 16, No 2, p 287.

Kharitonov, V.L., 1978, Differential Uravnen, 14, p 2086.

Yaniv, O. and Horowitz, I.M., 1987, International Journal of Control, Vol 46, No 3, p 945.

TABLE 1: Bounds on the nominal loop transmission

Freq rad/sec	Phase angle (deg)	Bounds on the nominal loop transmission $L_0$ in dB					
		$\phi = -30$	$\phi = -60$	$\phi = -90$	$\phi = -120$	$\phi = -150$	$\phi = -165$
$\omega_1$ 1	Brute force method	5.875	3.375	2.1875	1.935	8.562	10.340
	Proposed method	5.875	3.375	2.1875	1.935	8.562	10.340
$\omega_2$ 2	Brute force method	-2.3468	-4.000	-5.500	-6.500	-2.687	5.453
	Proposed method	-2.3468	-4.000	-5.5005	-6.500	-2.687	15.453
$\omega_3$ 5	Brute force method	-9.125	-10.093	-11.109	-10.750	-8.234	1.310
	Proposed method	-9.125	-10.093	-11.109	-10.750	-8.234	1.310
$\omega_4$ 10	Brute force method	-20.125	-20.750	-20.820	-19.640	-15.340	-10.980
	Proposed method	-20.125	-20.750	-20.820	-19.640	-15.340	-10.980
$\omega_5$ 30	Brute force method	-33.000	-32.625	-31.375	-29.625	-24.980	-19.320
	Proposed method	-33.000	-32.625	-31.375	-29.625	-24.980	-19.320

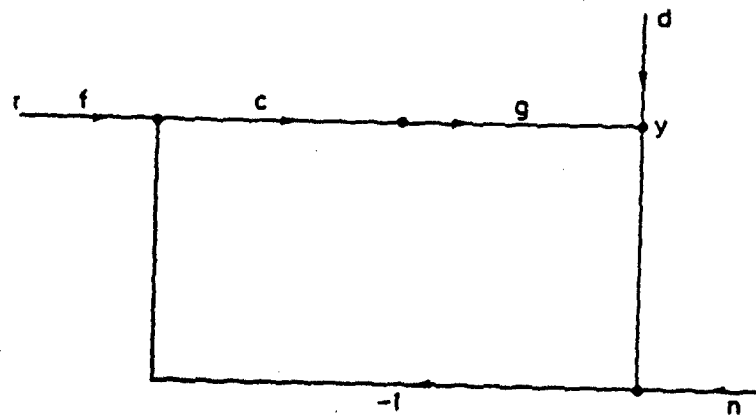


Fig. 1

Two-degree-of-freedom feedback structure.

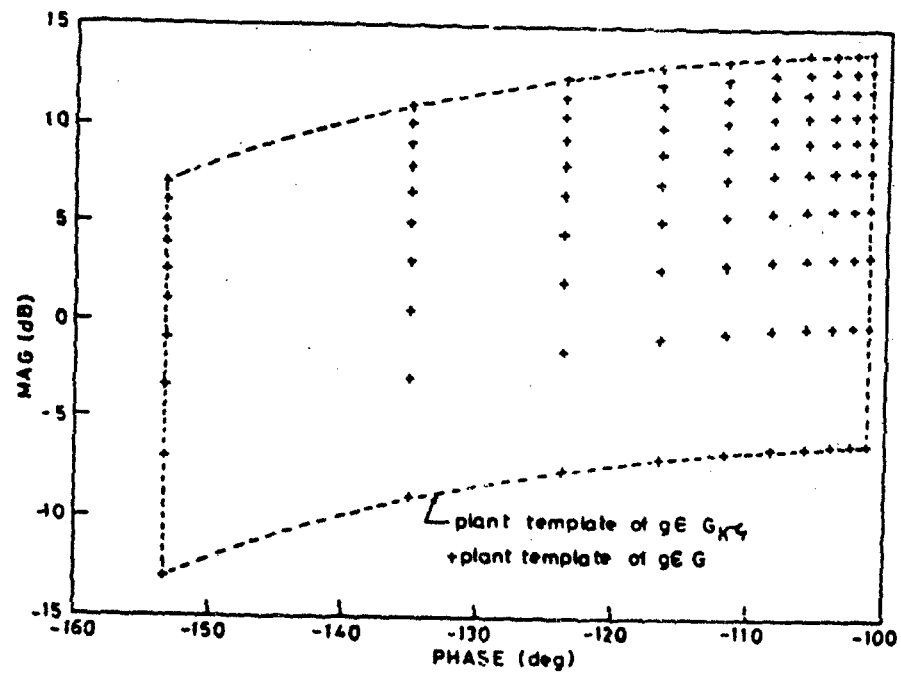


Fig. 2

Plant template at  $\omega = 2$  rad/sec.

QFT and Irrational Transfer Functions:  
The Design of Feedback for Distributed-Parameter Structures

M. McCormick\*

J.W. Brewer\*\*

M. Hafez\*\*

Department of Mechanical, Aeronautical, and Materials Engineering  
Bainer Hall  
University of California,  
Davis, CA 95616 USA  
Feb 1992

\* Graduate Student

\*\* Professor

Abstract: In this paper, we consider the direct application of QFT to a controlled object that is described by a partial differential equation. In particular, we are interested in distributed mechanical systems described by various versions of the "beam" equation. It is demonstrated that QFT can be applied directly, without resorting to simplifications such as the use of a finite-state, state-variable approximation during the design phase.

The price that one pays for not working with a finite-state approximation is that the transfer function is an irrational function of the complex frequency,  $s$ .

The advantage of working directly with the irrational transfer function is that one obtains a more accurate estimate of stability margins and other high-frequency (post cross-over) effects such as bandwidth constraint violations.

We demonstrate that the irrational transfer function offers no special difficulty in the selection of compensators in the usual QFT-manner. The Laplace transform is applied to the partial differential equation and to the boundary conditions. The result is a system of equations that can be solved for the transfer function. For that purpose, a symbolic manipulator, such as MATHEMATICA, is invaluable. Of course the result of a symbolic manipulator must be verified in some way and we describe methods for that purpose.

Unstructured uncertainty is accounted for in every design method, including QFT. In the standard QFT procedure, an "internal" damping is imposed in the form of a maximum M-circle that must not be penetrated by any of the templates. This is done to provide sufficient damping to a disturbance response but an important side benefit is that this M-circle constraint imposes a gain and phase margin on the closed loop.

The nature of this uncertainty in the case of distributed mechanical models is explored in our paper. Certainly, the damping characteristics as well as other high-frequency effects ignored in, say, the Euler beam equation are examples of this unstructured uncertainty. Preliminary verification of the design with simulation offers some problems and we explore the use of finite difference.

# Nomenclature

- A - cross-sectional area
- c - a shear-stress constant,  $\sigma = c\partial\epsilon/\partial t$
- $c_s \pm cI$
- $C_k$  - arbitrary constants
- E - modulus of elasticity
- $f_k(x,s)$  - irrational transfer-function parameters
- $G_c(s)$  - cascade compensator
- h - height of a cross-section
- I - cross-sectional moment of inertia
- ITF - irrational transfer function
- k - curvature
- $K_k(x,s)$  - arbitrary constants
- L - length of the beam
- $m_e$  - the mass of the effector or the load at the end of the beam
- $M_s$  - shear-stress moment
- $M_b(x,t)$  - mechanical moment
- PDE - partial differential equation
- P(s) - precompensator
- s - the Laplace variable
- t - time
- T(x,t) - kinetic energy
- u(x,t) - the linear displacement of the center line of the beam from its undeformed center-line position defined by the hub angle
- V(x,t) - potential energy
- x - axial position
- y(x,t) - transverse displacement: the linear, arc length, displacement of the center line of the beam from its initial "at rest" position
- $\epsilon$  - strain
- $\theta(t)$  - the hub rotation angle corresponding to the rigid body rotation of the beam
- $\lambda(x,s)$  - eigenvalue of the Laplace-transformed beam equations
- $\Lambda(x,s)$  - a transfer-function parameter that characterizes the nature of the damping in the beam
- $\rho$  - mass density
- $\sigma$  - shear stress
- $\tau(t)$  - torque, the manipulated input

## 1. Introduction

The modeling of linear elastic beams has been the object of study for decades and is associated with some of the most prominent names in applied mathematics. Of course, a model is the basis for control system design. Most often, these models take the form of a partial differential equation (a "PDE").

The most common method of transforming the partial differential equation into a form usable in feedback design is to obtain an infinite-series solution, an eigenfunction expansion (Chait et al, 1990; Margolis, 1976). This approach, also known as "modal modeling", is based on obtaining the eigenfunctions for the partial differential equation of the system. Each eigenfunction is associated with a natural frequency of the continuous media. To allow for computation and manipulation, these infinite eigenfunction expansions are truncated at a finite number of terms. The accuracy of the model improves with the number of frequencies included. At times, it is necessary to include a large number of eigenfunctions in order to accurately predict the high frequency behavior of continuous media.

While the eigenfunctions are well known for some of the more familiar PDEs, it can be a difficult mathematical problem to obtain the eigenfunctions in only slightly more complicated situations. For example, when damping effects are accounted for, the basic PDE is a non-self-adjoint operator and the solution of the eigenfunctions of the adjoint equation must be obtained as well as the eigenfunctions in order to obtain the required orthogonality conditions. For this reason, proponents of modal models will often resort to approximate, ad-hoc methods of describing effects such as damping in the beam.

One wonders if these approximations and heuristics are really necessary? If high frequency control (fast response time) of the beam is to be designed, it seems prudent to create a more accurate high frequency model of the beam. If the stability margins are to be true measures of our factors of safety against unmodeled dynamics, matters must not be confounded by errors due to mathematical approximations. Also, consideration of the bandwidth constraints require model accuracy in the higher frequency range.

It is proposed that high frequency (and also low frequency) control of an elastic beam can be achieved by using the Quantitative Feedback Theory (QFT) method proposed by Isaac Horowitz. This is because the PDE model can be used



directly in this context without resorting to a detailed eigenfunction analysis or without resorting to approximations, ad-hoc or otherwise.

Our primary contribution is to delineate all details of a computer-aided design procedure which includes the use of an irrational (transcendental) transfer function. Section 2 delineates the manner in which the transfer function is obtained from the underlying partial differential equation (the "PDE"). For any complexity at all a computer aid, a symbolic manipulator, must be used to make the necessary manipulations. It is demonstrated in Section 2 that modal models are useful for checking the accuracy of computer-aided algebra in those extreme cases where the modal model is easily obtained. Other types of checks are described there as well.

Section 3 is an example design, an application of QFT to the design of a beam subject to shear-stress damping. A damping coefficient and the load mass are the uncertain parameters in this example. Many interesting aspects of the dynamic model are highlighted and the manner in which some of these features limit the performance of the closed loop is described.

Section 4 is a summary section which concludes with some suggestions for future research.

## 2. The Bernoulli-Euler Beam PDE

We have in mind the beam pictured in Figure 2.1. The intention is to treat an example suggestive of applications to robot design or to the design of a space-structure component.

This beam acts in a horizontal plane and is assumed to be stiff with respect to any motion out of the plane. This permits us to ignore gravity and the interaction of the dynamics associated with torsion and vertical bending. It is further assumed that the beam is stiff with respect to axial forces and centripetal acceleration is negligible (Harn, 1991, 207).

Another major assumption in the formation of this first model of the beam is that the shear and rotary-inertia forces are small and will be ignored. Timenshenko states that "both corrections are unimportant if the wave length of the transverse vibrations is large in comparison with the dimensions of the cross section." (Timenshenko, 1953, 329). An initial assumption is that there is no damping present in the beam. A PDE which includes damping effects is presented in Section 2.4

The beam is a continuous "pinned-free" system of length  $L$ . A torque,

" $\tau(t)$ ", is input to the body through a hub at the pinned end and the beam is free to rotate around the center of the hub. The hub is assumed to be massless and of negligible radius. The free end of the beam is rigidly attached to a point mass of mass " $m_e$ " which has no rotational inertia. We refer to this mass, alternatively, as the "end-effector" or the "load".

The beam has a cross-sectional area of " $A$ ", density " $\rho$ ", modulus of elasticity " $E$ ", and cross-sectional moment of inertia about the vertical axis " $I$ " all of which are assumed to be constant with respect to time " $t$ " and axial position " $x$ ".

" $\theta(t)$ " is the hub rotation angle corresponding to the rigid-body rotation of the beam and  $u(x,t)$  is the linear displacement of the center line of the beam from its undeformed center-line position defined by the hub angle.  $u(x,t)$  is assumed to be within the elastic range of the beam and sufficiently small so that the change in axial distance  $x$ , due to beam bending, is negligible. These assumptions lead to the approximation that  $u(x,t)$  is approximately equivalent to the arc length traversed by the beam due to its dynamic behavior. " $y(x,t)$ " denotes the linear, arc length, displacement of the center line of the beam from its initial "at rest" position.

Using these definitions and assumptions (Cetinkunt, 1990, p429, Korlov, 1990, p9),  $y(x,t)$ , the transverse displacement of any point along the beam, is given by:

$$y(x,t) = u(x,t) + x \cdot \theta(t) \quad (2.1)$$

The total energy of the beam can be characterized by its potential energy,  $V(t)$ , and its kinetic energy,  $T(t)$  (Meirovitch, 1990, p270, Centinkunt, 1990, p430). The kinetic energy of the system is expressed by

$$T(t) = \frac{1}{2} \int_0^L \rho A \left[ \frac{\partial y(x,t)}{\partial t} \right]^2 dx + \frac{1}{2} m_e \left[ \frac{\partial y(x=L,t)}{\partial t} \right]^2 \quad (2.2)$$

The system potential energy, wholly made up of the energy stored by the strain present in the beam, can be expressed by

$$V(t) = \frac{1}{2} \int_0^L EI \left[ \frac{\partial^2 y(x,t)}{\partial x^2} \right]^2 dx \quad (2.3)$$

The virtual work associated with the non-conservative forces acting on the system is

$$\delta W(t) = \tau \left[ \frac{\partial y(x=0,t)}{\partial x} \right] \quad (2.4)$$

Applying Hamilton's principle to these three equations we can obtain the

differential equation of motion for the system and its boundary conditions. The equation of motion is equivalent to the familiar "Bernoulli-Euler Equation" for a flexible beam,

$$EI \frac{\partial^4 y(x,t)}{\partial x^4} + \rho A \frac{\partial^2 y(x,t)}{\partial t^2} = 0 \quad (2.5)$$

Substitute (2.1) to obtain the more common form of the beam equation:

$$EI \frac{\partial^4 u(x,t)}{\partial x^4} + \rho A \frac{\partial^2 u(x,t)}{\partial t^2} = -\rho A \frac{\partial^2 [x \theta(t)]}{\partial t^2} \quad (2.6)$$

Here,  $u(x,t)$  is measured with respect to the centerline of the beam that is rotating with a non-constant angular acceleration. This angular acceleration,  $\alpha$ , produces a transverse acceleration in the beam of  $a(x,t) = -x\alpha$ . " $\alpha$ " is equal to  $\partial^2 \theta / \partial t^2$ , so the right side of Equation 2.6 is interpreted as the summation of forces acting in the rotating reference frame. Note that all of these equations, including the beam equation, are based upon neglecting the axial forces (centripetal acceleration, Coriolis forces, etc.) in the system.

## 2.1 The PDE Models of Elastic Beams and Stability Margins

The Bernoulli-Euler equation is commonly used to describe the motion of a beam at low frequencies. That is because we neglect in the derivation the rotational inertial of a differential element as well as the shear forces acting in the beam. This results in small errors at low frequencies, however these errors become magnified at higher frequencies. This is because at high frequencies, the transverse displacements become heavily damped and the shear forces and rotary inertia become more prominent.

The famous Timoshenko PDE, is a model of a beam which includes the effect of these forces; however, even this more comprehensive model breaks down at even higher frequencies (Crandall, 1968, 347). That is to say, and this is important,

*Any PDE model of the elastic beam will involve modeling uncertainties at the high frequencies. This is the nature of mathematical modeling: We cannot expect that all possible mechanical degrees-of-freedom are represented.* (2.7)

These uncertainties demonstrate the need for stability margins in our feedback compensator design.

## 2.2 The Boundary Conditions

The following four boundary conditions are obtained by Hamilton's principle

$$y(x=0,t) = 0 \quad (2.8)$$

The end of the beam is pinned, so there can be no translation at this point for any value of time.

From static-beam analysis, we know that the bending moment of a beam is related to its change in slope by:

$$\frac{\partial^2 y(x,t)}{\partial^2 x} = - \frac{M_0}{EI} \quad (2.9)$$

where  $M_0$  is the moment at the point where the slope is evaluated. We can use this relationship at  $x = 0$  where the bending moment is known to be the torque input to the beam to get,

$$\frac{\partial^2 y(x=0,t)}{\partial^2 x} = - \frac{\tau}{EI} \quad (2.10)$$

The end mass is assumed to be a point mass, so there is no rotary torsion acting at the free end. This gives us the equation:

$$\frac{\partial^2 y(x=L,t)}{\partial^2 x} = 0 \quad (2.11)$$

The fourth boundary equation is:

$$EI \frac{\partial^3 y(x=L,t)}{\partial^3 x} = m_0 \frac{\partial^2 y(x=L,t)}{\partial t^2} \quad (2.12)$$

$m_0$  is the value of the point mass. The first term is the shearing force exerted on the end mass by the beam and the second term is the end mass times its acceleration. Note that the derivative on the right side of (2.12) is the acceleration of the end of the beam in inertial space so (2.12) is obtained by applying Newton's second law to the point mass at the end of the beam.

### 2.3 The Transfer Function and MATHEMATICA

In this section, The Bernoulli-Euler equation (2.6) is used with the four side conditions (2.8,10-12) to obtain the transfer function for our dynamic model. We perform a Laplace transform on (2.6,8,10-12). This leads to obtaining the transfer function of the output,  $\mathcal{L}[y(x=L,t)]$  to the input torque,  $\mathcal{L}[\tau(t)]$ . In this way the frequency response is obtained by setting  $s = j\omega$ .

The advantage of this procedure is that it does not require any approximations such as the truncation of an infinite series.

Transform Equation 2.5 to obtain:

$$EI \frac{d^4 y(x,s)}{dx^4} + \rho A s^2 y(x,s) = 0 \quad (2.13)$$

Assume that  $y(x,s) = \exp(\lambda x)$  is the general solution to (2.13) and substitute to find

$$\lambda^4 = - \frac{\rho A s^2}{EI} \quad (2.14)$$

Thus, there are four distinct solutions for

$$\lambda = \pm \Lambda e^{(\pm j\pi/4)} \quad (2.15)$$

$$\Lambda = \left[ -\frac{\rho A s^2}{EI} \right]^{1/4} \quad (2.16)$$

The general solution to equation (2.13) can now be expressed as:

$$y(x,s) = C_1 \exp(\lambda_1 x) + C_2 \exp(\lambda_2 x) + C_3 \exp(\lambda_3 x) + C_4 \exp(\lambda_4 x) \quad (2.17)$$

We rearrange (2.17) in the usual way to obtain  $y(x,s)$  in terms of trigonometric functions:

$$y(x,s) = K_1 \exp(\Lambda x/\sqrt{2}) \sin(\Lambda x/\sqrt{2}) + K_2 \exp(\Lambda x/\sqrt{2}) \cos(\Lambda x/\sqrt{2}) + \\ K_3 \exp(-\Lambda x/\sqrt{2}) \sin(\Lambda x/\sqrt{2}) + K_4 \exp(-\Lambda x/\sqrt{2}) \cos(\Lambda x/\sqrt{2}) \quad (2.18)$$

To solve for the four unknown parameters,  $K_1$ - $K_4$ , we must use the Laplace transform on the boundary conditions: The four boundary equations (2.6,8-10) become:

$$y(x=0,s) = 0 \quad (2.19)$$

$$\frac{d^2 y(x=0,s)}{dx^2} = -\frac{\tau(s)}{EI} \quad (2.20)$$

$$\frac{d^2 y(x=L,s)}{dx^2} = 0 \quad (2.21)$$

$$EI \frac{d^2 y(x=L,s)}{dx^2} = m_e s^2 y(x=L,s) \quad (2.22)$$

Equations 2-10 through 2-13 can be solved by hand without complicated mathematic manipulations, but the process is tedious due to the number of terms involved. To minimize the possibility of mathematical errors, the software MATHEMATICA, a symbolic manipulator, was used to solve the set of five equations (2.18-22) for the unknown constants,  $K_1$  through  $K_4$ . The resulting values are complicated, page long, functions of  $s$ ,  $s^2$ ,  $e^s$ ,  $\sin(s)$  and  $\cos(s)$  as well as the physical parameters ( $E$ ,  $I$ , etc.) of the system, multiplied by the input torque (McCormick, 1992):

$$K_k = f_k(s, \text{physical parameters}) \cdot \tau(s) \quad (2.23)$$

The transfer function between the angular displacement of any point on the center line of the beam and the torque input can then be explicitly and exactly stated as:

$$y(x,s)/\tau(s) = f_1 \exp(\Lambda x/\sqrt{2}) \sin(\Lambda x/\sqrt{2}) + f_2 \exp(\Lambda x/\sqrt{2}) \cos(\Lambda x/\sqrt{2}) + \\ f_3 \exp(-\Lambda x/\sqrt{2}) \sin(\Lambda x/\sqrt{2}) + f_4 \exp(-\Lambda x/\sqrt{2}) \cos(\Lambda x/\sqrt{2}) \quad (2.24)$$

This transfer function is "irrational", clearly not the simple ratio of

polynomials. At this point, we can substitute  $s = j\omega$  and obtain the frequency response.

Although this frequency-domain solution to the beam equation is an accurate manipulation of the underlying PDE and side condition, and of great value for QFT design, other mathematical devices must be used to obtain the motion of the beam in the time domain. This problem of obtaining the time domain responses is addressed further in Section 2.5.

#### 2.4 An Improved Model With Structural Damping

Damping is most often neglected when dealing with a flexible beam because its effect is small and its origins are not always well-understood. Obviously, the beam is a damped system, because the common experience is that oscillations decay in time. However, a universally accepted theory for how this damping occurs is an area of current research.

Humar (1990, p639) argues that damping in the beam can be represented by a viscous external damping force on the beam and an internal resistance to strain. Viscous damping from the environment can be added in by appending the term of  $c_v \partial y(x,t)/\partial t$  to the left hand side of (2.5). " $c_v$ " represents the environmental viscous damping constant per unit length. This constant may vary from zero (in a vacuum) to small values (in air) and, at times, to significant values (under water).

The Laplace transformation of this term converts it to  $c_v s y(x,s)$ . This value can be combined with  $\rho A s^2 y(x,s)$  (2.13) to obtain  $[c_v s + \rho A s^2] y(x,s)$ . The effect is to change the value of " $\Lambda$ " in (2.16). In this paper we choose to ignore viscous damping because its effect will be dependent upon the beam's working environment and is not intrinsic to the beam itself. Clearly, this term will be important in some applications.

Humar describes another form of damping: "resistance to internal strain will depend on the strain rate,  $\partial \epsilon / \partial t$ ." (Humar, 1990, p639). This strain produces a stress that has the value  $\sigma = c \partial \epsilon / \partial t$ . The constant, " $c$ ", is the damping coefficient associated with this internal shear stress and, in this study, it is assumed to be constant over the body. This stress varies linearly across the beam cross-section of height  $h$  and produces a moment

$$M_z = \int_A \sigma h \, dA \quad (2.25)$$

Thus,

$$M_s = \int_A c \frac{\partial(hk)}{\partial t} dA \quad (2.26)$$

where  $\epsilon = h \cdot k$  and the curvature,  $k$ , is defined by

$$k = \frac{\partial^2 y(x,t)}{\partial x^2} \quad (2.27)$$

Humar puts all this together to demonstrate that the PDE becomes

$$EI \frac{\partial^4 y(x,t)}{\partial x^4} + cI \frac{\partial^3 y(x,t)}{\partial t \partial x^2} + \rho A \frac{\partial^2 y(x,t)}{\partial t^2} = 0 \quad (2.28)$$

We refer to the damping term as a "shear-stress damping".

Use the Laplace transform so that (2.28) becomes

$$[EI + cIs] \frac{d^4 y(x,s)}{dx^4} + \rho A s^2 y(x,s) = 0 \quad (2.29)$$

The solution to this equation is the same as for (2.13), however the coefficient " $\Lambda$ " becomes

$$\Lambda = \left[ \frac{-\rho A s^2}{EI + cIs} \right]^{1/4} \quad (2.30)$$

The inclusion of shear-stress damping changes only the value of  $\Lambda$  and no other parameter so we include or exclude the effect of damping by merely selecting one form or the other of this coefficient.

Similarly, the effect of viscous damping, characterized by " $c_v$ " is added or deleted from our model by including or excluding terms from the most general form for  $\Lambda$ :

$$\Lambda = \left[ \frac{-\rho A s^2 + c_v s}{EI + cIs} \right]^{1/4} \quad (2.30)$$

To summarize this section, we choose to neglect the effects of viscous damping ( $c_v = 0$ ) but to include the effects of shear-stress damping. We characterize this damping by the constant

$$c_s = cI \quad (2.31)$$

As seems common in the discussion of damping, there is no generally agreed-upon value for  $c_s$  so it is a candidate uncertain parameter in the QFT design process. More explicitly, Equations (2.24) and (2.30) are our model of the damped beam for the QFT-compensator design. In this way, we produce an accurate frequency-domain model, as accurate as the modeling assumptions themselves. Of course, since modeling assumptions inevitably exclude some high-frequency mechanical effects, stability margins are still called for.

With this model in hand, we turn to the important matter of feedback control system design.

### 3. Application of QFT to the Design of Feedback Control of an Elastic Beam

The first step in the QFT compensation procedure is to express the plant in terms of a transfer function relating the input torque and the output angular displacement of the end mass. The elastic-beam, irrational transfer function (ITF) derived in Section 2 is

$$y(x,s)/\tau(s) = f_1 \exp(\Lambda x/\sqrt{2}) \sin(\Lambda x/\sqrt{2}) + f_2 \exp(\Lambda x/\sqrt{2}) \cos(\Lambda x/\sqrt{2}) + f_3 \exp(-\Lambda x/\sqrt{2}) \sin(\Lambda x/\sqrt{2}) + f_4 \exp(-\Lambda x/\sqrt{2}) \cos(\Lambda x/\sqrt{2}) \quad (3.1)$$

where

$$\Lambda = \left[ \frac{-\rho A s^2}{EI + c_s s} \right]^{1/4} \quad (3.2)$$

Where  $f_1$  through  $f_4$  are complicated, page long, functions of the Laplace variable  $s$  and the system parameters (McCormick, 1992, see his appendix).

By setting  $x = L$  (the length of the beam) an irrational transfer function relating the input torque to the angular displacement is obtained. This irrational transfer function poses no obstacle to the QFT design process because it is possible to obtain the magnitude and phase of the irrational transfer function,  $y/\tau$ , by letting  $s = j\omega$  for a range of  $\omega$ .

#### 3.1 Magnitude and Phase of the Undamped Beam Model

The problem with assigning the chore of algebraic manipulation to a symbolic manipulator is that the designer must have some way of checking all facets of this computer-aided process. As a preliminary check on this computer-derived, irrational transfer-function model, the magnitude and phase plots are developed for an undamped system ( $c_s = 0$ ). It is possible to develop a six-dynamic-mode model to verify these plots since the eigenfunctions are well known in that extreme and special case.

This is not to say that the derivation of the modal model does not involve significant complications (McCormick, 1992). The modal model, as well as the irrational transfer function model are not trivial to express in a computer calculation. (In fact, it was necessary to check both of these complex models with a simpler two-dynamic-mode modal model.) The Bode plots obtained from the ITF model corresponds precisely to the Bode plots obtained from modal analysis. These plots are presented in Figures 3.1 and 3.2.

It can be seen from the magnitude plot (Fig. 3.1) that the two models agree in magnitude up to the seventh resonance, where the accuracy of the modal model breaks down. This is expected because the modal model was developed using only



six dynamic modes. At 5000 rad/sec the ITF model exhibits an odd jump in magnitude. Our speculation is that this effect is due to computational errors but, fortunately, these errors occur in a frequency range well beyond that examined in this paper.

Both magnitude curves display the general form expected for this type of a system. Because the system is based on a torque input and a position output, an overall slope of -40 db/decade is expected on the magnitude curve: We expect the transfer function will behave something like  $C/s^2$ . In addition, we expect the system will have resonant frequencies easily related to the modal eigenvalues. Also, since we are studying a continuous model, there will be an ever-increasing density of these resonances at the higher frequencies.

While the general form of the magnitude plots agree with what is anticipated, the phase plots exhibit more intriguing characteristics. There are also some of the usual glitches that must be dealt with in any use of software-derived phase values. (In our case, phase was most often calculated using the all-purpose MATLAB.)

Software is often unintentionally programmed to make certain counter-intuitive choices about the folding of phase functions; for example, the choices programmed into software where deciding whether to add multiples of 360 degrees to the phase values calculated from an arctangent subroutine. This sort of problem is exemplified in Figure (3.2) by the +180 to -180 degree jumps in the ITF phase curve. The magnitude curve in this same frequency range displays an average slope of -40 db so it is expected that the phase of the system should be -180 degrees at low frequencies. It is important to resolve these curious matters.

Some of the confusing aspects in Figure (3.2) are resolved by redrawing the phase curves to match the slope of the magnitude curve resolves. Also, it is true that the MATLAB software will not always make a choice consistent with what we know of such things where the phase curves is discontinuous by 180 or 360 degrees. (We found that a ITF which includes damping will not be as prone to these unfortunate choices of phase change, but not this is not completely the case.)

A guide which aids us to explain and resolve the oddities of the phase curve is the pole-zero diagram of the modal-model. The poles and zeros of the six-mode model are shown in Figure (3.3). First of all, notice that the zeros

appear in mirror-image pairs, mirror images about the imaginary axis. The poles are pure imaginary and a few zeros are real but most appear as complex conjugate pairs. The large number of nonminimum-phase zeros is consistent with the observations of others in their study of dynamic structures: Safanov observes that, "non-located control systems are always non-minimum phase above some finite frequency." (Safanov, 1989, p2530).

The effect of the minimum phase/non-minimum phase zero mirroring is more easily visualized by expressing the poles and zeros in terms of their natural frequencies as in Figure (3.4). Here the ordinate is a number, actually a name, arbitrarily assigned to the pole or zero beginning at low frequency and proceeding to the higher frequencies. The very-low frequency slope of the magnitude curve is -40 db/decade but there is a set of complex conjugate poles at 55 rad/sec. These conjugate poles create a resonance in the magnitude plot (refer to Figure 3.1) and would, ordinarily, decrease the slope of the magnitude curve to -80 db/decade except that this set of poles is closely followed by a set of real, mirror-image zeros at 60 rad/sec. These zeros add 40 db/decade to the magnitude curve and, in this way, maintain the average slope of the graph at -40 db/decade.

These poles (at 55 rad/sec) are undamped (refer to Fig. 3.3) so they should produce an abrupt shift of -180 degrees in the phase diagram. Figure 3-2 shows this phase jump to be from -180 to -360 degrees. The system zeros do not affect the phase diagram because the minimum phase zero shifts the phase +90 degrees and the non-minimum phase zero shifts the phase -90 degrees: These phase shifts cancel each other out.

The next set of poles occurs at 200 rad/sec, followed by a set of zeros at 300 rad/sec. The same analysis applies except that the MATLAB phase plot shown in Figure 3-2 does not correctly assign the direction of the jump and the phase is indicated as  $-360 + 180 = -180$  degrees instead of  $-360 - 180 = -540$  degrees. At 500 rad/sec the phase should decrease to -720 degrees because of the presence of another set of poles. Obviously, the software is returning the phase modulo  $2\pi$ .

The phase curves are corrected by hand and that procedure is carried out over the entire frequency range and the resulting correct phase plot appears as Figure 3.5.

Incidentally, the mirror-image zeros have no effect on the phase curve

throughout the frequency range and that fact has a strong influence on the ability of a designer to compensate the system to achieve a high crossover frequency. This is especially true where one accepts the natural constraint that only stable compensators can be used (it would be special embarrassment to have a control actuator disassemble an expensive device merely because the feedback signal is temporarily lost or shut down!). Also, the corrected phase decreases rapidly with increasing frequency. This rapid decrease in phase also has a strong influence on high frequency compensation and that point is addressed in Section 3.5.

The primary conclusion here is that in the special case of an undamped beam, the case for which the eigenfunctions are well-known, it is verified that the MATHEMATICA-derived, ITF provides the correct results. This encourages us to investigate the more interesting cases.

### 3.2 Magnitude and Phase of the Damped Beam Model

We expect that the addition of damping (see equation (3.2)) should create magnitude and phase plots similar to those of Section 3.1 in the case of small values of  $c_s$ . The Bode plots for that case met those expectations.

The Bode plots for a relatively large damping ratio of  $c_s = 0.10$  are shown in Figures 3.6 and 3.7. The comparison with the undamped case is instructive. First notice that the resonant peaks in the magnitude plot have been diminished, especially at the higher frequencies.

Another more surprising result is that the addition of the damping term is seen to decrease the average slope of the magnitude curve with increasing frequency. This is an oddity and needs some interpretation. The explanation is that the relative positions of certain low-frequency poles and zeros are interchanged. The damping reduces the natural frequency of certain complex poles while there is no similar effect on the natural frequency of the nearby zeros. As the damping is internal to the system, no change in the zeros is expected. The slope of the magnitude plot is seen to decrease, due to this effect, from -40 db/decade to -100 db/decade over the frequency interval shown.

The damped ITF model displays a roughly similar drop-off in phase as is the case for the undamped case. However, the abruptness of the phase shifts have been lessened and result is smoother phase transitions. We observe no obvious discrepancies with theory in the Bode diagram of the the damped ITF.

### 3.3 QFT With the Damped ITF Model

Quantitative feedback theory has several characteristics that make it ideal for control of a flexible beam. Being a frequency domain technique, QFT enables the use of the PDE/ITF model for the beam. This enables the inclusion of shear damping (and viscous damping if desired) in the model. It also permits the designer to utilize a more precise high-frequency model without approximating a large number of modes. In this way, better values are obtained for stability margins and for the transmissions of sensor noise or disturbance to the controlled variable,  $r(t)$ .

As indicated in Section 2, there are many ways of representing a damped beam. The most common models are the Bernoulli-Euler and Timoshenko models. Both of these PDE can be derived only by neglecting certain high-frequency effects. The Timoshenko beam is accurate for a wider range of frequencies but at the cost of more complexity. In fact, all beam PDEs should be associated with uncertainty at some high frequencies. This simple fact obligates the designer to include stability margins in the compensation design. The QFT provides these margins through the usage of a peak modulus,  $M_p$  in the design process. Although the more common way to think of the  $M_p$  requirement is that it is included in order to provide an "internal damping-ratio", a damping in the feedback loop in response to any spurious disturbance signal.

The uncertainty of the value of the shear-stress damping coefficient is another beam effect that encourages the use of QFT. This damping coefficient takes on some value within a relatively large range:

$$0.01 \leq c_s \leq 0.10 \quad (3.3)$$

Perhaps the most interesting reason for applying QFT to a damped beam system is that the damped beam system is most accurately represented by an irrational transfer function (ITF). The irrationality of the plant transfer function poses no special problem in the application of QFT because QFT is based in the frequency domain. Since QFT is a frequency-domain procedure, it brings out very interesting high-frequency behavior of the ITF. The process brings insight into the manner in which the high frequency behavior of the ITF affects stability and eventually limits the speed of response.

A minor adjustment should be made in the QFT procedure as presented by Horowitz to permit the use of the ITF model. Horowitz assumes that the plant model is a rational transfer function and uses this assumption to obtain a

"universal high-frequency" template, a straight vertical line on the Nichols chart at high frequencies. This assumption is invalid for this ITF system. The minor adjustment is to require that templates remain outside the  $M_0$ -circle in the Nichols chart. This stricture is imposed in the same manner for high frequency templates as it is for low frequencies.

Still another reason for applying a frequency-domain procedure such as QFT to a damped beam is that this beam system possesses right half-plane zeros. Blind use of other procedures such as observer-based design can result in effective compensators with poles in the right half plane. This will happen anywhere the closed-loop poles are arbitrarily placed at too high a bandwidth. (That is the price one pays for turning over a design to blind calculation.) As we have demonstrated, the irrational transfer function does possess right half-plane zeros, and QFT makes it obvious how these zeros constrain our ability to achieve a stable compensation scheme.

The uncertain QFT parameters chosen for this system are the end mass,  $m_e$ , and the beam shear-damping coefficient  $c_s$ . An uncertain end mass was chosen to represent what might happen, say, if the beam is a robot arm used to move many different loads of different mass. The beam damping coefficient seems an ideal candidate for uncertainty because its exact value is unknown and not always measurable. All the other physical parameters were chosen to remain constant.

The Nichols chart of the uncompensated plant is shown for the four extreme parameter variations in Fig. 3.8. Note that all versions of the uncompensated systems pass near the 0 db, 180 degree point at low frequencies and are, therefore, near the stability limit. It can also be seen that at high frequencies ( $\omega > 40$  rad/sec), the phase is rapidly decreasing while the magnitude is relatively constant. The rapid decrease of phase is due to the increasing density of pole pairings and the magnitude is not decreasing rapidly because of the minimum/non-minimum zero mirrorings.

First, we make a useful observation: Care should be exerted when choosing the QFT nominal point for the ITF model. The resonances in the system cause abrupt rises in the magnitude curve over narrow ranges of frequencies. The uncertain parameters are associated with large changes in the resonant frequencies. Because the templates are found for a relatively small number of discrete frequencies and for discrete parameter values, some of the abrupt

risers in magnitude are not always represented in an arbitrarily-selected, finite set of templates. A wise choice of the nominal point can reduce the need for including an inordinate number of frequencies and reduce frustration and confusion.

To prevent these resonances from making the system response unstable, the most unstable values of parameters ( $m_s = 1.0$ ,  $c_s = 0.01$ ) were chosen for the nominal point. If the compensated system is stable for this, "worst case", set of parameter values, the system likely will be stable for all of the other allowable parameter variations.

### 3.4 Compensation for a Low Cross-Over Frequency

To test this application of the QFT procedure, modest design requirements are specified in the first example. The step response is specified to have a settling time of 10.0 seconds, an overshoot less than 10%, a steady state error of less than 2%, a phase margin of 60 degrees and a gain margin of greater than 6 db (these margins corresponds to  $M_p = 1$ ). These requirements are used in the QFT procedure to produce the boundaries on the Nichols chart shown in Figure 3.9.

Also represented in Figure 3.9 is the partially compensated (with cascade compensator only) nominal point plant. Following the usual QFT procedure the system is fully compensated using the following cascade compensator

$$G_c(s) = \frac{5.5 \times 10^6}{(s/1000+1)(s/20+1)(s/50+1)}$$

and the precompensator

$$P(s) = \frac{81}{(s/3+1)^4}$$

Because the plant model used in the IFT design procedure is an irrational transfer function, a finite-difference approximation of the PDE (2.28) is used to represent the plant for the time domain simulations. To be consistent with this finite difference approximation, the models of the cascade compensator and precompensator must be converted from transfer function representations to discrete-time models where the time steps are dictated by the finite difference simulations. Only in this way can the step response of the fully compensated system be obtained. This closed-loop simulation has many interesting aspects (McCormick, 1992) but that is not a major topic of concern in this paper.

The closed-loop responses, obtained in this way for the given ranges of parameter variation, are shown in Figure 3.10.

It can be seen from this figure that the design requirements are met for all of the allowable parameter variations. It was found that the effect of variation in the shear-stress damping coefficient has a minimal effect on the closed-loop step response of the compensated system whereas the end mass variations plays a more influential role (McCormick, 1992). The indication in Figure 3.10 is that QFT is a promising method for obtaining closed-loop control for continuous, ITF models when the specified crossover frequency is relatively low.

### 3.5 Compensation for a Higher Cross-Over Frequency

In Section 3.4, it is demonstrated that frequency-domain design methods are a reasonable procedure for the damped beam when sufficiently low crossover frequencies are acceptable. It is human and useful to wonder about the limits to which one may push the performance of a feedback design. In this section we make such a consideration without regard to the possibility that some other factor, say the structural strength of the beam, might be the limiting factor in high-speed control.

Figure (3.11) shows the range of magnitude and phase variations in the uncompensated plant. Discrete frequencies are marked on the chart, as well as the boundary for  $m_e = 1.0$ .

If only the worst-case set of parameter values is considered ( $m_e = 1.0$ ,  $c_s = 0.01$ ), the phase is seen to decrease much more quickly than expected by examination of the slope of the magnitude curve. This is due to the non-minimum phase zeros present in the system model. The number of these zeros increase with frequency, so the effect will become more pronounced as frequency increases. To illustrate all this, notice that in the first decade of non-minimum phase zeros (40 to 400 rad/sec) the phase loss is more than -300 degrees and the magnitude loss remains -40 db/decade.

If attention is restricted to stable feedback compensators, the addition of zeros to the compensator seems desirable. Each minimum phase zero in the compensator would raise the system phase +90 degrees. However, it would also raise the slope of the gain +20 db/decade. The gain must be below 0 db for crossover to occur and the average slope of the beam magnitude curve is -40 db/decade. This means that the number of excess zeros over poles in the compensator located before crossover can only be one.

To insure stability, the compensated plant must not have a phase of  $-180 \pm$

$(360 \cdot n)$  degrees before crossover (" $n$ " is any integer). The plant is seen to have a phase of  $-180$  degrees at low frequency, so a low frequency zero must be present in the feedback compensator to make the response stable. This raises the average slope of the magnitude to  $-20$  db/decade between 40 and 400 rad/sec.

The same kind of compensation is not possible at higher frequencies. It was demonstrated, numerically, in Section 3.2 that damping smoothes out the phase variations but decreases the slope of the magnitude curve with increasing frequency. If the uncompensated plant had a even more-negative gain slope, it would be easier to compensate the system for higher frequencies. Physically adding damping to the beam would lower this slope, however it would equally well lower the phase response.

Due to the fact that the phase starts at  $-180$  degrees and drops off increasingly fast while the magnitude stays near a steady slope of  $-40$  db/decade, no stable compensation scheme exists to achieve a stable high-frequency crossover. It is impossible to achieve a transient response faster than some fundamental limit for the damped beam system by measuring only the end deflection and controlling the input torque.

This result may have some physical justification. After all, the fundamental PDE (2.28) will only admit finite wave speeds, there will be a physical delay before a signal,  $r(t)$ , at the hub can be transmitted to the effector.

The situation gets even worse when parameter variations are included in the design. It can be demonstrated that the variations in phase due to parameter variation in the beam-effector system are as much as  $170^\circ$  for a particular frequency (McCormick, 1992). Also, as the frequency of the increases, these phase variations increase. However, the magnitude variation does not increase with frequency. It is this increase in phase variation, that controls the design of compensation for crossover. The large phase variations in phase at a fixed frequency are the result of the changes in the relative positions of poles and zeros which, in turn, are caused by the parameter variations.

Incidentally, this sort of thing has been observed by others, Safanov noted a similar phenomenon in his study: "...small variations in...system parameters can result in the interchanging of poles and zeros...producing phase errors of up to  $-360$  degrees." (Safanov, 1989, p2531). These phase errors induced by parameter variations further limit the possible rise time of the system.



The variations in phase make the QFT templates "wider" in the horizontal (phase) direction for a given frequency on the Nichols chart. As the phase will sometimes vary between  $-180$  to  $+180$  degrees at crossover (phase margin of zero) a total phase variation of  $360$  degrees can occur at crossover. This restricts the permissible positions in the nominal plant phase to  $360^\circ$  less the variation in phase at the crossover frequency. As long as the phase variation is less than  $360$  degrees, this presents only an added difficulty to the designer in the form of a lessened phase margin. Above the frequency where the phase variation becomes greater than  $360$  degrees, stable crossover is unobtainable. As the phase variation is increasing with frequency, it will eventually exceed  $360$  degrees.

Because parameter variation, and the interaction between system phase and magnitude is at the heart of QFT, it is a good choice for the feedback design of the damped beam system. For high frequency crossovers, use of QFT provides an insight as to how the phase drives the design and eventually limits the response time.

Of course, the case where an unstable compensator is feasible presents other possibilities and opportunities.

#### 4. Conclusions and Suggestions for Future Research

The focus of this paper is a structural-beam system, with a torque input at one end of a beam and the transverse displacement of an end mass as output. It is demonstrated that this system has very interesting feedback control properties that are easily visualized and understood through the application of Isaac Horowitz's quantitative feedback theory.

QFT is very useful in the compensation design because it permits the use of an irrational transfer function describing the motion of the beam as governed by its partial differential equation. It is this type of transfer function that would obtain directly from a PDE model without approximation. This means that any high-frequency inaccuracies are the result only of the modeling process itself. The use of an ITF is seen to pose no difficulty in the QFT design process.

The price that one pays for the use of ITF is that the algebraic manipulations are considerable but these are easily resolved using a symbolic manipulator such as MATHEMATICA. The modal-approximation methods used by other investigators still play an important role in the procedure we recommend:

These models represent extreme and special cases where there is sufficient accuracy to serve as a check to the results of symbolic manipulation of ITF. It would seem that use of our method opens-up the door to the use of far more accurate modeling in the form of complex PDE models. This can only improve, say, the design of very fast response-time control. In turn, this will mean that we can have more confidence in stability margins and in the estimates of any bandwidth problem.

For example, we demonstrate in this paper the use of ITF to rigorously include the effects of shear-stress damping or environmental viscous damping in the plant model.

The shear stress damping is seen to have a large effect on the state representation of the ITF. This seems to be due to the fact that this factor can interchange the relative location of various poles and zeros of ITF. Therefore it is desirable that this damping is included in the plant model with as much accuracy as possible. QFT offers the designer the unique ability to model the plant with high accuracy, at all frequencies, for a large range of shear stress damping coefficients.

The trade off between transient response time and closed-loop stability is the most important constraint governing the control of a damped flexible beam. This constraint becomes more demanding as frequency increases. This trade off is at the heart of QFT design, a procedure developed to minimize the bandwidth necessary for meeting a specified transient response.

We expanded the interpretation of the "internal damping ratio" specification proposed by Horowitz. By specifying a peak modulus,  $M_p$ , QFT design not only provides closed-loop damping to plant disturbances, it also insures stability margins. These margins are required in our example because of the unavoidable approximations of the modeling process itself.

We investigated the ultimate limits of feedback design, limits associated by requiring that the cascade compensator not include right half-plane poles. Through the accurate high frequency representation of the damped beam system allowed by ITF, the speed of transient closed-loop responses are seen to be limited by consideration of stability: We demonstrated that it is impossible, with minimum phase compensation, to achieve a stable, very high crossover frequency for the damped beam system. This is in accordance with other current research on continuous systems (Safanov, '89, p2531). We expect to show that

all this is related to the finite wave speed implicit in dynamic beam equations.

Further research in this area will employ even more accurate irrational transfer function models of damped continuous structures. Even, we expect, systems of PDEs. Our paper indicates that such interesting high frequency behavior will be encountered in that way. We have established that QFT should prove to be an excellent compensation design for these advanced ITF models.

Finally, we recognize that another limitation of using computer-aided ITF modeling is that finite difference or finite element methods must be employed to verify closed-loop designs. The designer who adopts our procedure will be committed to further development of these numerical tools.

References:

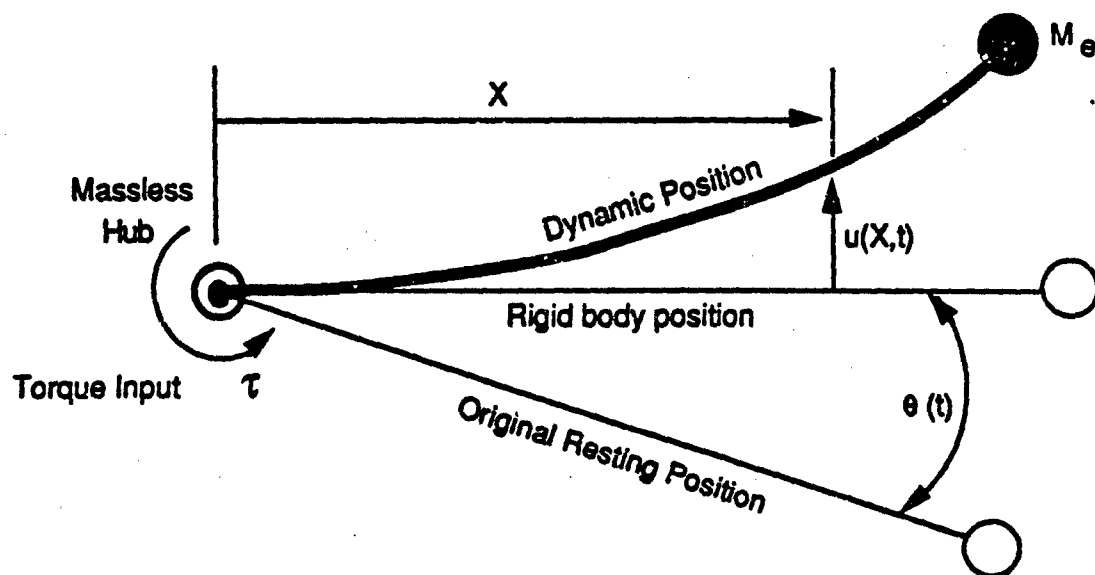
- Cetinkung S. and S. Wu, (1990) "Tip Control of a Flexible One-Arm Robot with Predictive Adaptive Output Feedback Implemented with a Lattice Filter Parameter Identifier" Computers and Structures - An International Journal, v36, n3
- Chait, T. and M. Miklavcic, C.R. Maccluer and C.J. Radcliffe, (1990) "A Natural Modal Expansion for the Flexible Robot Arm Problem Via a Self-Adjoint Formulation" IEEE Transactions on Robotics and Automation, v6, n5
- Crandall, S. and D. Karnopp, Kurtz, and Pridmore-Brown (1968) Dynamics of Mechanical and Electromechanical Systems. McGraw-Hill, Inc., New York, NY
- Doyle, J.C. (1986) "Quantitative Feedback Theory (QFT) and Robust Control" American Control Conference
- Harn, Y.P. and E. Polak, (1991) "Proportional-Plus-Multiintegral Stabilizing Compensators for a Class of MIMO feedback Systems With Infinite Dimensional Plants" IEEE Transactions on Automatic Control, v 36, no 2
- Harris, C.M. (1988) Shock & Vibration Handbook, Third Edition, McGraw-Hill, Inc., New York, NY
- Horowitz, I. and M. Sidi, (1972) "Synthesis of Feedback Systems with Large Plant Ignorance for Prescribed Time Domain Tolerances" International Journal of Control, v16
- Horowitz, I. (1991) "Survey of Quantitative Feedback Theory (QFT)" International Journal of Control, Taylor & Francis Ltd., London;, v53, n2
- Humar, J.L. (1990) Dynamics of Structures, Prentice-Hall, Inc., Englewood Cliffs, New Jersey
- Karnopp, D. and D. Margolis, and R. Rosenberg, (1990) System Dynamics - A Unified Approach, Second Edition, John Wiley & Sons, Inc., New York, NY.
- Korlov, V.V. and Y.H. Chen, (1990) "Controller Design Robust to Frequency Variation in a One-Link Flexible Robot Arm" Journal of Dynamic Systems, Measurement and Control, v111, n1
- Margolis, D. (1976) "Finite Mode Bond Graph Representation of Vehicle-Guideway Interaction Problems" Journal of The Franklin Institute, v302, n01
- Meirovitch, L. (1990) Dynamics and Control of Structures, John Wiley & Sons, Inc., New York, NY
- McCormick, M.P. (1992) Control of a Flexible Damped Beam by Applying Quantitative Feedback Theory to an Irrational Transfer Function M.S. Thesis, Dept. of Mechanical, Aeronautical, and Materials Engineering, University of California, Davis, CA
- Popov, E. P. (1968) Introduction to Mechanics of Solids, Prentice-Hall, Inc.,

Englewood Cliffs, New Jersey

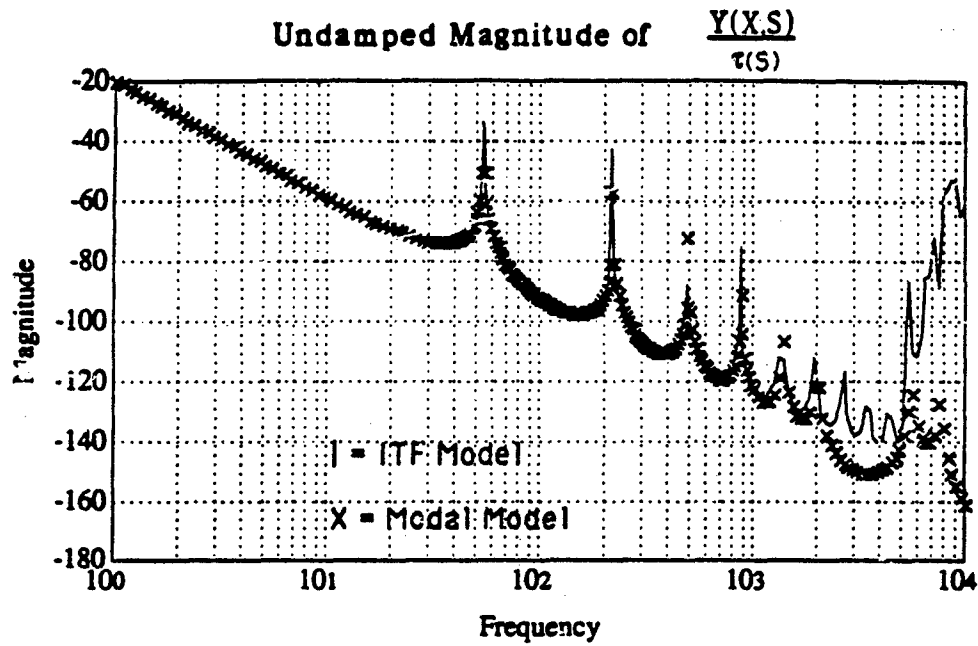
Safanov M.G. and H. Flasher, (1989) "Modeling and Robustness Issues in Control Design for Flexible Structures" American Control Conference, v3

Timenshenko, S.P. (1958) "The Transverse Vibrations of Bars of Uniform Cross-Sections" Philosophical Magazine, pp 125-131, 1922, (from The Collected Papers of Stephen P. Timenshenko, McGraw-Hill, Inc., New York, NY, 1958)

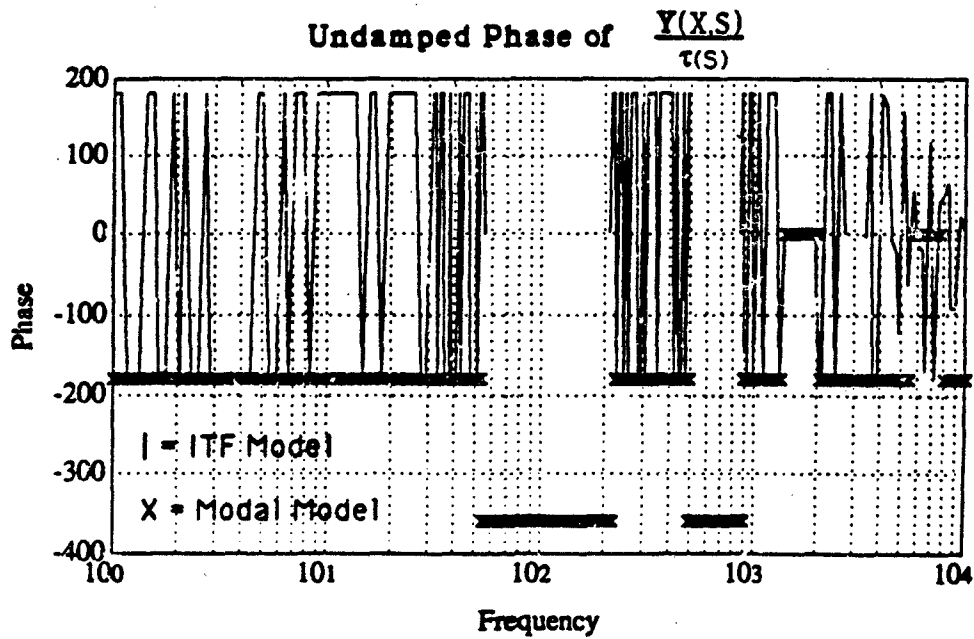
Figure 2-1

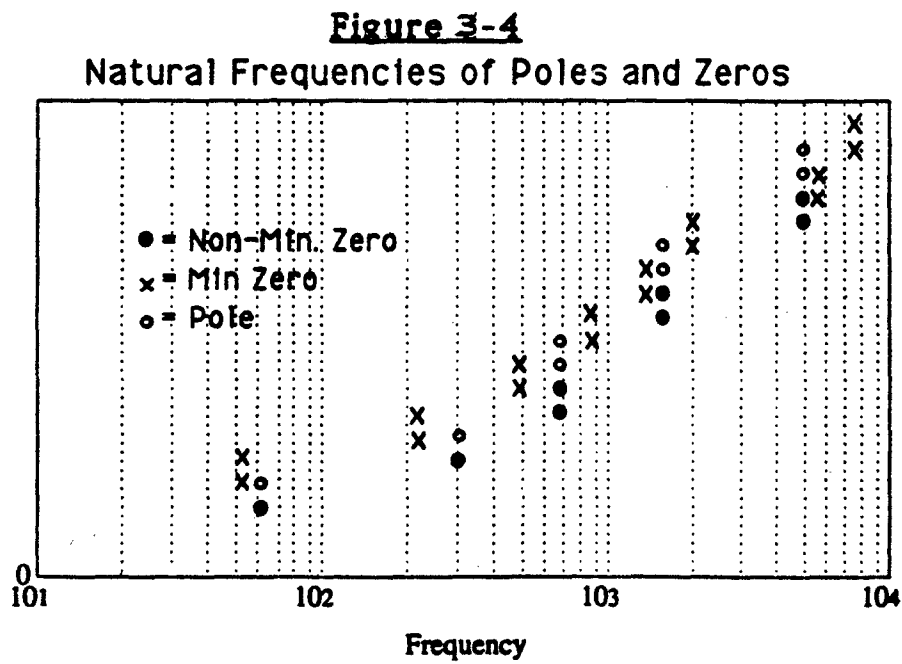
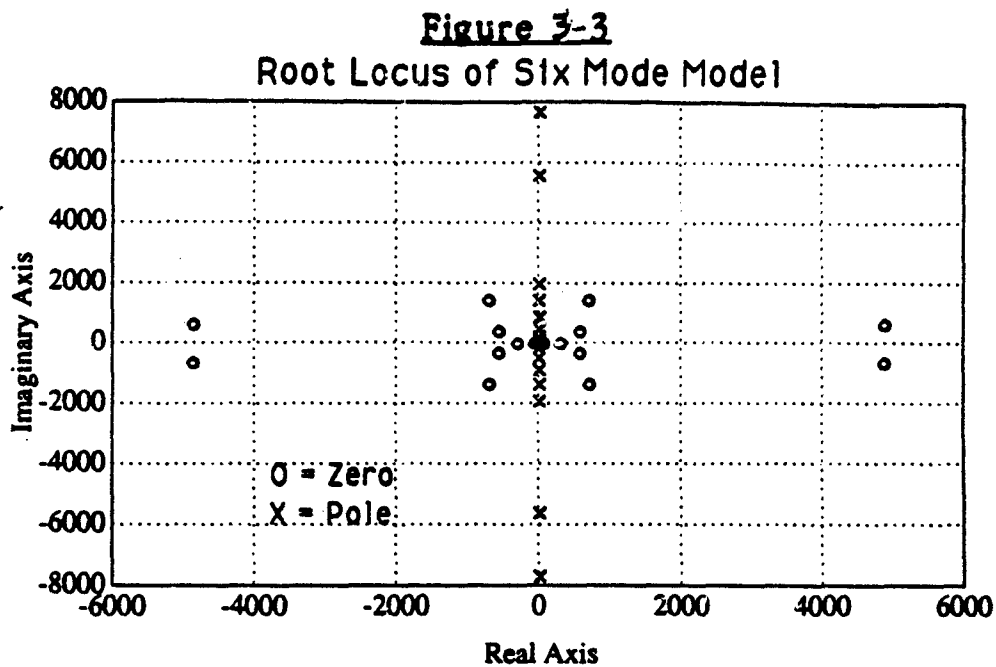


**Figure 3-1**



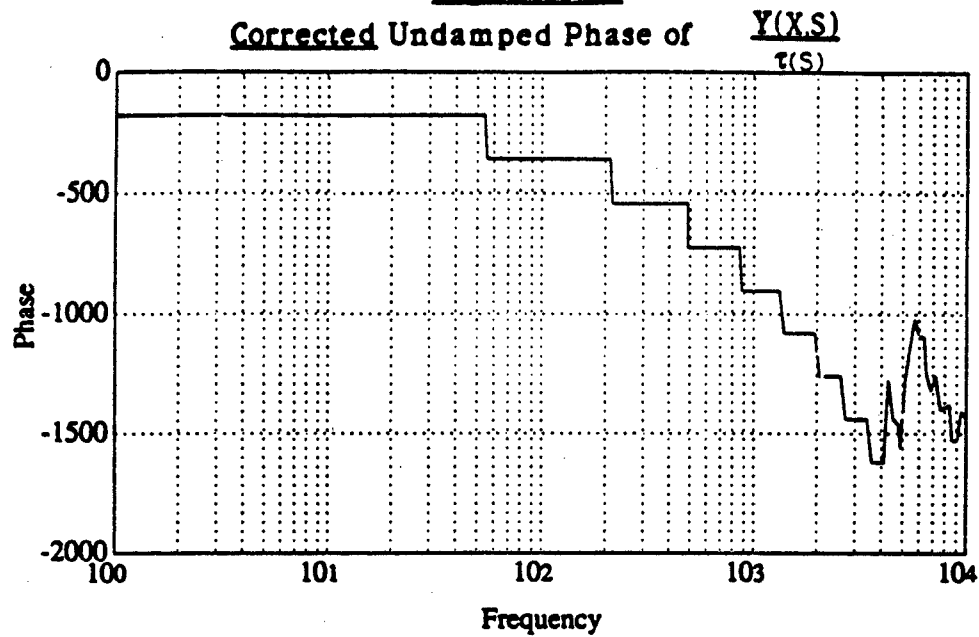
**Figure 3-2**



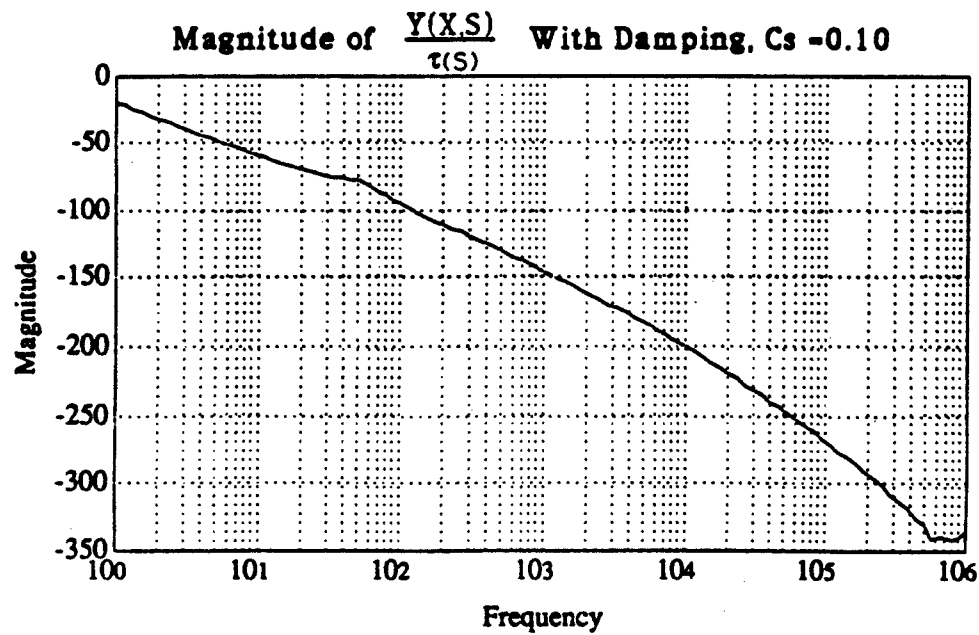




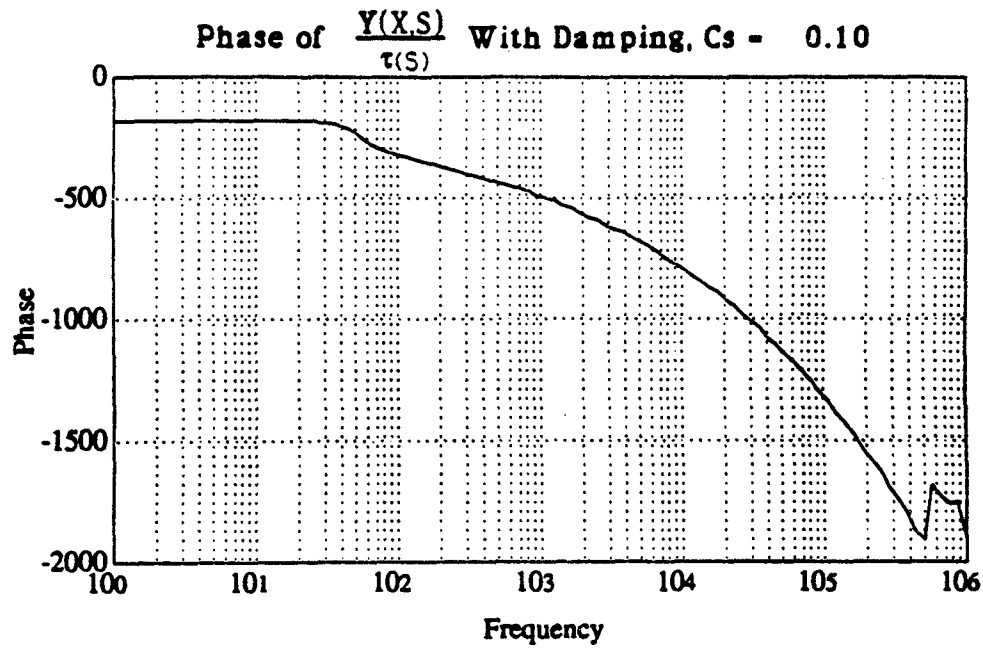
**Figure 3-5**



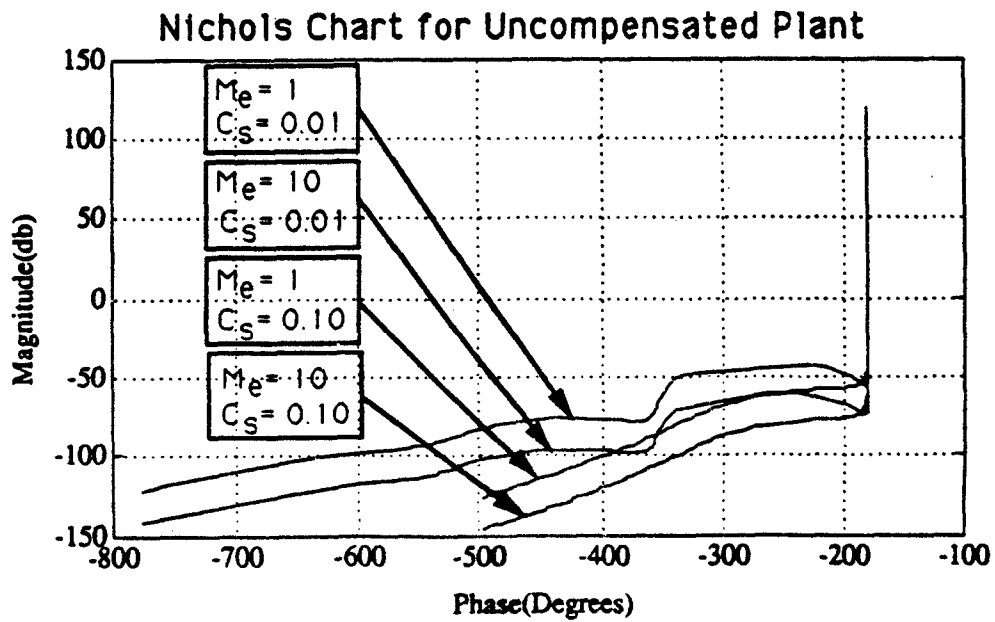
**Figure 3-6**



**Figure 3-7**

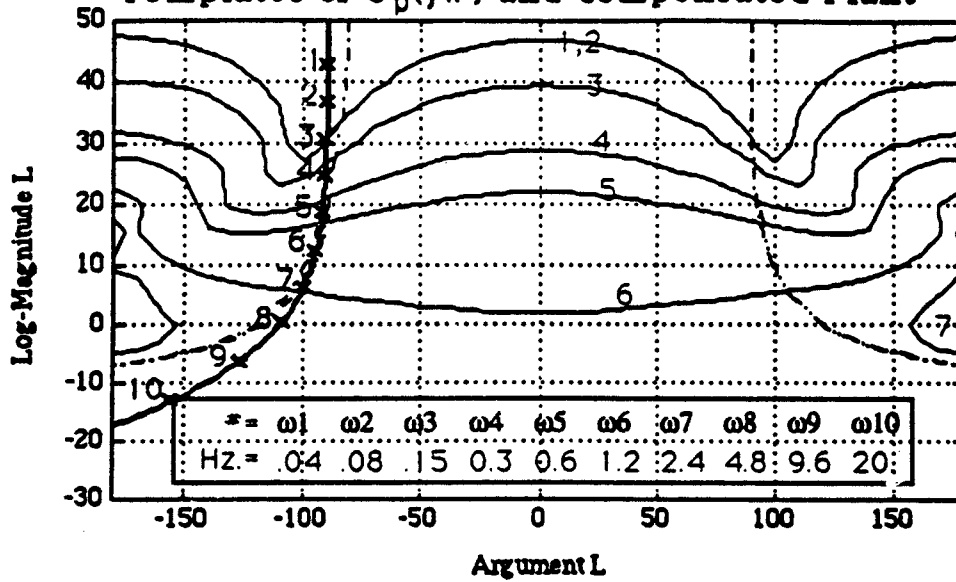


**Figure 3-8**



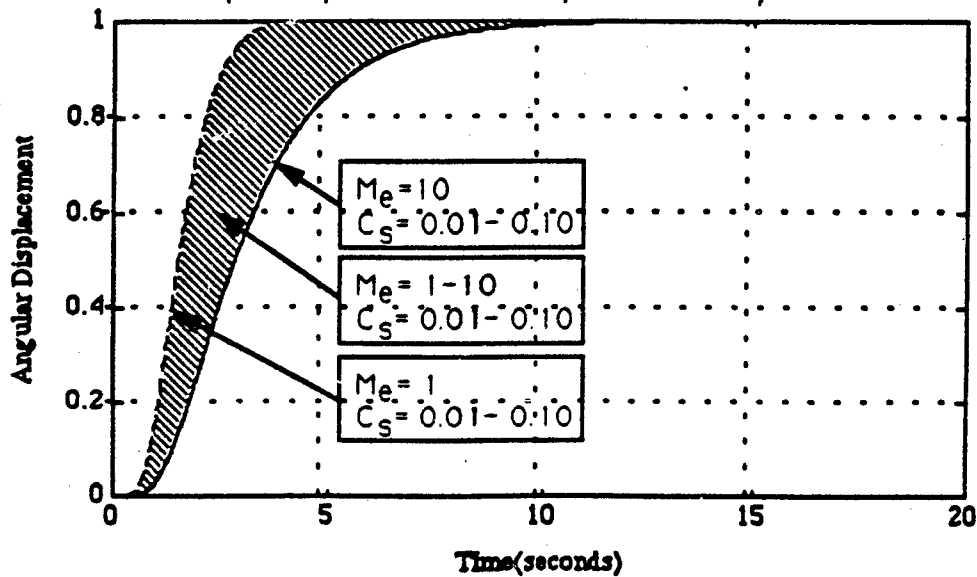
**Figure 3-9**

**Templates of  $G_p(j\omega)$  and Compensated Plant**



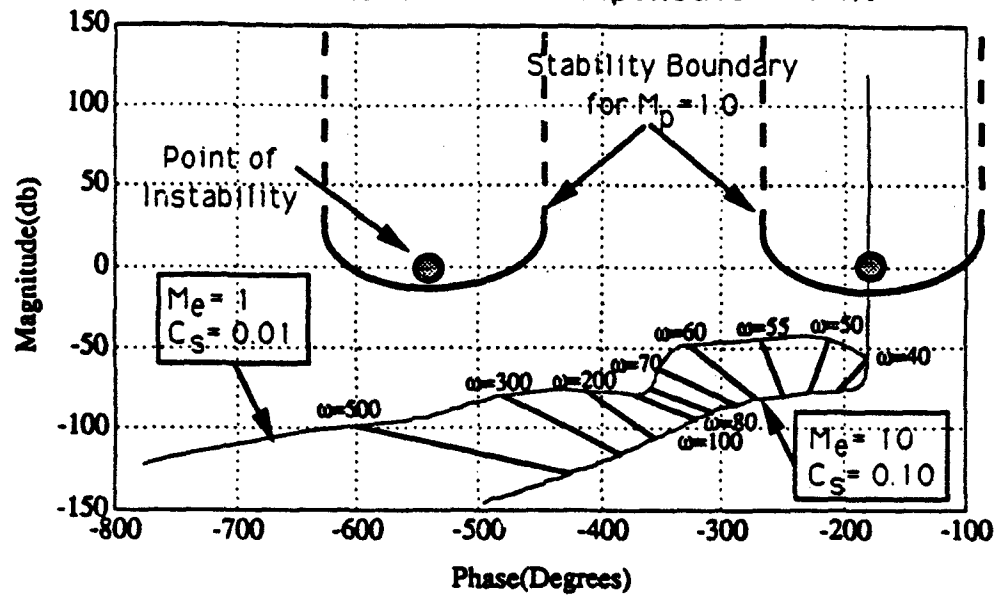
**Figure 3-10**

**Step Response of Compensated System**



**Figure 3-11**

**Nichols Chart for Uncompensated Plant**



**STABILITY OF QUANTITATIVE FEEDBACK DESIGNS AND THE  
EXISTENCE OF ROBUST QFT CONTROLLERS**

By

Suhada Jayasuriya<sup>†</sup> and Yongdong Zhao<sup>‡</sup>  
Department of Mechanical Engineering  
Texas A&M University  
College Station, TX 77843

<sup>†</sup> Professor

<sup>‡</sup> Graduate Student

This material is based upon work supported by the National Science Foundation  
under NSF Grant No. MSS-9114562.

## ABSTRACT

Quantitative Feedback Theory (QFT) has received much criticism for a lack of clearly stated mathematical results to support its claims. Considered in this paper are two important fundamental questions: (i) whether or not a QFT design is robustly stable, and (ii) does a robust stabilizer exist. Both these are precursors for synthesizing controllers for performance robustness. Necessary and sufficient conditions are given to resolve unambiguously the question of robust stability in SISO systems which in fact confirms that a properly executed QFT design is automatically robustly stable. This Nyquist type stability result is based on the so called zero exclusion principle and is applicable to a very large class of problems under some simple continuity assumptions. In particular, the class of uncertain plants include those in which there are no right half plane pole-zero cancellations over all plant uncertainties. A sufficiency condition for a robust stabilizer to exist is derived from the well known Nevanlinna-Pick theory in classical analysis. Essentially the same condition may be used to answer the question of existence of a QFT controller for the general robust performance problem. These existence results are based on an upper bound on the nominal sensitivity function. Also considered is QFT design for a special class of interval plants in which only the poles and the d.c. gain are assumed uncertain. The latter problem lends itself to certain explicit computations that considerably simplifies the QFT design problem.

## I. INTRODUCTION

Quantitative Feedback Theory (QFT) developed by Horowitz (1963, 1991) is known to be a very effective design tool. The classic multiple-input single-output QFT problem considers the synthesis of a fixed controller for a plant family  $p \in \mathcal{P}$  so that its output  $y(t) \in \mathcal{A}_{rd}$ , where  $\mathcal{A}_{rd}$  is an acceptable output set in response to command inputs  $r \in \mathcal{R}$  and disturbances  $d \in \mathcal{D} \forall p \in \mathcal{P}$ . The design technique essentially consists of obtaining a set of bounds on a nominal loop transfer function which are then used to guide the shaping of the nominal loop transfer function. If one is able to shape such a nominal loop transfer function then that is accepted as a QFT solution to the problem. The many different QFT examples that appear in the literature in fact suggest and seem to confirm that there is no problem with stability or satisfaction of the assumed frequency domain equivalents of the time domain specifications (However, the original time domain specifications may not be completely satisfied) by all  $p \in \mathcal{P}$ . One basic question with the QFT method is how does one know apriori whether a suitable loop transfer function may be found. Unfortunately, this question is not an easy one to answer. One may in fact ask the more basic question of whether the plant family at least can be stabilized. The latter is obviously necessary to even have a chance of finding a QFT controller for the robust performance problem. The issue of stability is one of many criticisms of QFT by Doyle (1986).

In particular, Doyle (1986) raised the question of whether or not a QFT controller exists for the simple two element plant families

$$\mathcal{P} = \left\{ \frac{1}{1 \pm s} \right\} \quad \text{or} \quad \mathcal{P} = \left\{ \frac{\pm 1}{1 - s} \right\}$$

for which it is well known that no proper LTI controllers exist for simultaneously stabilizing both plants in each two element family. Subsequently, Yaniv and Horowitz

(1987) responded that QFT never claimed that controllers could be found for the above families. In Horowitz (1991) a more complete answer was given to the question. However, it was not stated as a direct robust stabilization result but instead it was stated in the context of arbitrarily large feedback benefits (ALFB). In this paper we ontext of arbitrarily large feedback benefits (ALFB). In this paper we will address the question directly from a robust stabilization view point and in a sense restate a fact that has been known to specialists of QFT.

Clearly, it is useful to know apriori exactly what type of linear uncertain plants may be robustly stabilized. We show that the class of uncertain plants can be quite general and will include the possibility of zeros and/or poles both crossing the imaginary axis from the left half plane to the right half plane and *vice versa*, subjected to the constraint that there are no right half plane pole-zero cancellations. We give two necessary conditions to determine whether a plant family is robustly stabilizable. We also give a sufficient condition to determine whether such a controller exists. The latter condition is derived using the Nevanlinna-Pick theory of classical analysis. The sufficiency test reduces to (i) determining whether a certain proper, rational, stable interpolation function can be determined to interpolate some fixed complex numbers at the unstable poles and non-minimum phase zeros of the nominal plant and whether its  $\infty$ -norm is smaller than the estimatable infimum of the amplitude of a specially constructed plant family over all frequencies. Based on the latter result an existence condition for the general QFT performance robustness question is also given by viewing the problem as a sensitivity constrained optimization problem.

Another problem studied in this paper is the design of a stabilizing controller for a class of interval plants in which the zeros are fixed but the poles are allowed



to be uncertain. A simple necessary and sufficient test for robust stabilization is derived for this class of problems. The analysis result reduces to a question of determining whether or not a specially constructed polar plot intersects the unit box placed around the complex plane origin. As for synthesis we show that a set of frequency domain forbidden regions for a nominal loop transfer function can be explicitly determined for this family by computing at most four points at each frequency upto a finite frequency. In particular the forbidden regions appear as parallelograms in the complex plane. The final step of course is the loop shaping and one may proceed with this last step if the answer to the existence question is affirmative. Also developed in the paper is how the general QFT problem may be solved for this special class of interval plants. The latter is done by posing the QFT problem as a sensitivity constrained optimization problem as is done in Nwokah, et al. (1992).

The paper is organized as follows. In section II a necessary and sufficient result is stated along with two necessary conditions, all for robust stabilization. Developed in section III is a sufficiency test for robust stabilizability based on the Nevanlinna-Pick interpolation theory. In section IV we formulate the robust stabilization problem for a special class of interval plants with fixed zeros and uncertain poles and give a necessary and sufficient test for robust stability. Also included is a discussion of how robust performance is incorporated in the synthesis problem. Examples illustrating the key results are in section V. The conclusions are in section VI.

## II. ROBUST STABILIZATION

Consider the classic unity negative feedback, multiple-input single-output 2 dof feedback configuration where the interval plant family is described by the strictly

proper transfer function:

$$P(s, \alpha) = \frac{P_1(s, \alpha)}{P_o(s, \alpha)}, \quad (1)$$

and the proper compensator transfer function is:

$$G(s) = \frac{Q_1(s)}{Q_o(s)}. \quad (2)$$

Here,  $\alpha \in \Psi \subset \mathbb{R}^r$  denotes the uncertain parameter vector and

$$\begin{aligned} P_1(s, \alpha) &= p_{1m}(\alpha)s^m + \dots + p_{10}(\alpha), \\ P_o(s, \alpha) &= p_{on}(\alpha)s^n + \dots + p_{o0}(\alpha) \end{aligned} \quad (3)$$

with  $m \leq n$ .

The closed loop transfer function of the system is

$$\frac{P(s, \alpha)G(s)}{1 + P(s, \alpha)G(s)}, \quad \alpha \in \Psi,$$

whose characteristic polynomial is therefore

$$\delta(s, \alpha) \stackrel{\text{def}}{=} Q_o(s)P_o(s, \alpha) + Q_1(s)P_1(s, \alpha). \quad (4)$$

Since  $P(s, \alpha)$  is strictly proper and  $G(s)$  is proper, the coefficient of the highest order term in  $\delta(s, \alpha)$  is

$$p_{on}q_{on}.$$

where  $q_{on}$  is the coefficient of the highest degree term in  $Q_o(s)$ . When dealing with the problem of robust stabilization, we assume that the uncertain plant description does not allow a change in plant order. i.e., it is assumed that

$$p_{on}q_{on} \neq 0,$$

or equivalently, we assume that

$$0 \notin p_{on}(\Psi).$$

**Remark:** Note that the above restriction does not prevent one from allowing pole-zero cancellation for some arbitrary  $\alpha_1 \in \Psi$ . If there are such pole-zero cancellations we simply assume that there are common factors in the characteristic polynomial.

Consequently, the following reasonable assumptions about the plant family are made.

**Assumptions:**

- (i)  $\Psi$  is a compact set
- (ii)  $p_{0j}(\alpha)$ ,  $j = 0, \dots, n$ ,  $p_{1k}(\alpha)$ ,  $k = 0, \dots, m$ , are continuous with respect to  $\alpha$
- (iii)  $0 \notin p_{0n}(\Psi)$

Denoting,

$$\delta_1(j\omega, p) \stackrel{\text{def}}{=} 1 + \frac{Q_1(j\omega)P_1(j\omega, \alpha)}{Q_0(j\omega)P_0(j\omega, \alpha)}, \quad (5)$$

we have the following modified "Zero Exclusion Principle" (Anagnost et al. [1989]) in terms of  $\delta_1$ .

**LEMMA 2.1.**  $G(s)$  stabilizes the whole interval plant  $P(s, \alpha)$  if and only if:

- (i) there exists an  $\alpha_0 \in \Psi$  such that  $G(s)$  stabilizes  $P(s, \alpha_0)$ ,
- (ii)  $0 \notin \delta_1(j\omega, \Psi)$ , for all  $\omega \in [0, \infty]$  and
- (iii) there are no imaginary axis pole-zero cancellations in  $\frac{Q_1(j\omega)P_1(j\omega, \alpha)}{Q_0(j\omega)P_0(j\omega, \alpha)}$ .

**Proof:** First we prove sufficiency by contradiction. Suppose that  $G(s)$  cannot stabilize  $P(s, \alpha)$  for all  $\alpha \in \Psi$ . Then we have at least one parameter vector, say  $\alpha_1$ , such that  $\delta(s, \alpha)$  is unstable. Note that all the zeros of  $\delta(s, \alpha)$  are continuous functions of the parameter  $\alpha$ . Let  $s_1(\alpha)$  be a zero of  $\delta(s, \alpha)$  with a positive real part for  $\alpha = \alpha_1$ , i.e.,

$$\text{Re } s_1(\alpha_1) > 0.$$

Define

$$\alpha(\mu) = (1 - \mu)\alpha_1 + \mu\alpha_0,$$

then we have

$$\alpha(0) = \alpha_1, \quad \alpha(1) = \alpha_o.$$

Clearly,  $\operatorname{Re} s_1(\alpha(\mu))$  is continuous with respect to  $\mu$  and since

$$\operatorname{Re} s_1(\alpha(0)) = \operatorname{Re} s_1(\alpha_1) > 0$$

$$\operatorname{Re} s_1(\alpha(1)) = \operatorname{Re} s_1(\alpha_o) < 0$$

there exists a constant  $\mu_o \in (0, 1)$  such that

$$\operatorname{Re} s_1(\alpha(\mu_o)) = 0$$

In other words, we have a pure imaginary number

$$s_1(\alpha(\mu_o)) = j\omega_o, \quad \omega_o \in [0, \infty).$$

Hence, by the definition of  $s_1(\alpha)$  we have

$$\delta(j\omega_o, \alpha(\mu_o)) = 0.$$

But,

$$\delta(j\omega_o, \alpha(\mu_o)) = P_o(j\omega_o, \mu_o)Q_o(j\omega_o)\delta_1(j\omega_o, \alpha(\mu_o))$$

from which it follows that either  $P_o(j\omega_o, \mu_o)Q_o(j\omega_o) = 0$  or  $\delta_1(j\omega_o, \alpha(\mu_o)) = 0$ . We also know from the definition of  $\delta(s, \alpha)$  in (4) that if the condition  $P_o(j\omega_o, \mu_o)Q_o(j\omega_o) = 0$  is true then  $P_1(j\omega_o, \mu_o)Q_1(j\omega_o) = 0$  must also be true. But these two conditions cannot hold simultaneously because of condition (iii). Therefore,

$$\delta_1(j\omega_o, \alpha(\mu_o)) = 0,$$

which contradicts (ii). Consequently, the interval plant is stabilized by  $G(s)$ . The proof of necessity is obvious.  $\square$

The following corollary gives a simple necessary condition for robust stability .

**COROLLARY 2.1.** If there are closed right half plane pole-zero cancellations in the loop transfer function  $\frac{P_o Q_1}{P_o Q_o}$  then the closed loop family can not be stable.

**Proof:** The imaginary axis pole-zero cancellation case is already covered by Lemma 2.1. For the case of right half plane pole-zero cancellation suppose there is a pole zero cancellation at  $s = a > 0$  for some  $\alpha_k \in \Psi$ , then the closed loop characteristic equation becomes

$$\delta(s, \alpha_k) = (s - a)\bar{\delta}(s, \alpha_k)$$

and the closed loop system has a right half plane pole at  $s = a > 0$ .

□

**QFT Methodology:** In the QFT problem formulation one considers the loop transfer function

$$L(s, \alpha) = L_o(s) \frac{P(s, \alpha)}{P_o(s)}$$

where

$$L_o(s) = G(s) \frac{P_1^o(s)}{P_o^o(s)}$$

and

$$P_o(s) = \frac{P_1^o(s)}{P_o^o(s)} .$$

Here,

$$P_1^o(s) = p_{1m}(\alpha_o)s^m + \dots + p_{1o}(\alpha_o)$$

$$P_o^o(s) = p_{on}(\alpha_o)s^n + \dots + p_{oo}(\alpha_o)$$

With the nominal loop transfer function  $L_o(s)$  defined as above, by lemma 2.1 the robust stability problem is reduced to determining whether or not  $L_o(s)$  is stable

and

$$\delta_1(j\omega, \alpha) = 1 + L_o(j\omega) \frac{P(j\omega, \alpha)}{P_o(j\omega)} \neq 0 \quad \forall \alpha \in \Psi \text{ and } \omega \in [0, \infty]. \quad (6)$$

It is clear from Eqn. (6) that  $\delta_1(j\omega, \alpha) = 0$ , if and only if  $L_o \frac{P(j\omega, \alpha)}{P_o(j\omega)} = -1$  which is true if and only if the polar plot  $L_o(j\omega)$  intersects the value set  $\left\{ -\frac{P_o(s)}{P(s, \alpha)} \right\}_{s=j\omega}$ . From this observation we can give an obvious necessary condition for robust stability as follows:

Since,  $L_o(s)$  is usually strictly proper (in QFT it is always true), we have

$$\lim_{\omega \rightarrow \infty} L_o(j\omega) = 0$$

Thus a necessary condition for robust stability is stated in corollary 2.2 below.

**COROLLARY 2.2.** The plant family  $P(s, \alpha)$  cannot be stabilized if  $0 \in \left\{ -\frac{P_o(s)}{P(s, \alpha)} \right\}_{s=j\infty}$

□

**Remark:** It is worth recalling that in a typical QFT design one imposes a constraint on the maximum closed loop gain  $\left| \frac{L}{1+L} \right|$  which is equivalent to a condition of the form  $\left| 1 + L_o \frac{P}{P_o}(j\omega) \right| \geq \beta > 0$ . So clearly, if the latter condition holds the robust stability condition  $\delta_1(j\omega, \alpha) \neq 0$  holds since  $|\delta_1(j\omega, \alpha)| > 0$ .

Next, we will state a necessary condition for robust stability in terms of the d.c. gain of the nominal loop transfer function  $L_o(s)$ . The latter condition will impose a special structural constraint on  $L_o(s)$ .

**LEMMA 2.2.** When  $L_o(0)$  is finite (i.e.,  $L_o(s)$  does not have any poles at the origin), and  $\left\{ \frac{P_o(s)}{P(s, \alpha)} \right\}_{s=j\infty} > 0$  the plant family  $P(s, \alpha)$  can be stabilized only if  $L_o(0) > \inf_{\alpha \in \Psi} \left\{ -\frac{P_o(0)}{P(0, \alpha)} \right\}$ , if  $n_o^*$  is even, or  $L_o(0) < \sup_{\alpha \in \Psi} \left\{ -\frac{P_o(0)}{P(0, \alpha)} \right\}$ , if  $n_o^*$  is odd. Here  $n_o^*$  is the number of unstable poles of the nominal loop transfer function  $L_o(s)$ .

**Proof:** Consider the closed loop characteristic equation

$$\delta_1(s, \alpha) = 1 + L_o(s) \frac{P(s, \alpha)}{P_o(s)}$$

The zeros of  $\delta_1(s, \alpha)$  are the same as zeros of  $\Lambda(s, \alpha) = \frac{P_o(s)}{P(s, \alpha)} + L_o(s)$ .

From the Nyquist stability criterion the zeros of  $\Lambda(s, \alpha)$  all lie in the open left half plane if and only if the Nyquist plot of  $\frac{P_o(s)}{P(s, \alpha)} + L_o(s)$  encircles the origin  $n_u^\alpha$  times in a counter-clockwise direction. Since, we know  $\frac{P_o(s)}{P(s, \alpha)}(j\infty) > 0$ , it follows that if  $n_u^\alpha$  is even (odd), then  $\frac{P_o(0)}{P(0, \alpha)} + L_o(0) > 0$  ( $< 0$ ) to have an even (odd) number of encirclements of the origin by  $\Lambda(j\omega, \alpha)$ .

Consequently,

$$L_o(0) > \inf_{\alpha \in \mathcal{V}} \left\{ -\frac{P_o(0)}{P(0, \alpha)} \right\} \quad \text{for } n_u^\alpha \text{ even}$$

$$L_o(0) < \sup_{\alpha \in \mathcal{V}} \left\{ -\frac{P_o(0)}{P(0, \alpha)} \right\} \quad \text{for } n_u^\alpha \text{ odd}$$

□

**Remark:** Note that the case  $\frac{P_o(s)}{P(s, \alpha)}(j\infty) < 0$  can be handled in a similar manner. In this case the necessary condition of lemma 2.2 becomes

$$L_o(0) < \sup_{\alpha \in \mathcal{V}} \left\{ -\frac{P_o(0)}{P(0, \alpha)} \right\} \quad \text{for } n_u^\alpha \text{ even}$$

$$L_o(0) > \inf_{\alpha \in \mathcal{V}} \left\{ -\frac{P_o(0)}{P(0, \alpha)} \right\} \quad \text{for } n_u^\alpha \text{ odd}$$

Next, we turn to the case where the uncertain plant family forms a countable set. The results developed above can all be applied in such a case by enlarging the family to be a subset of an infinite family. However, such a characterization does not provide a conclusive answer as is illustrated below.

Consider the two, two element families  $\mathcal{P}_1 = \left\{ \frac{1}{1 \pm s} \right\}$  and  $\mathcal{P}_2 = \left\{ \frac{\pm 1}{1-s} \right\}$  that are well known to be non-stabilizable by proper LTI compensation (Doyle [1986]). If

we want to use the above results then we must pose the question as follows: Can the plant families

$$\hat{\mathcal{P}}_1 = \left\{ \frac{1}{1+as} \right\} \quad a \in [-1, 1]$$

and

$$\hat{\mathcal{P}}_2 = \left\{ \frac{b}{1-s} \right\} \quad b \in [-1, 1].$$

be robustly stabilized? Note that the two element families are now embedded in two infinite families. With these enlarged families if we try to use the basic stability results of lemma 2.1 and/or corollary 2.2 we run into some difficulties. The plant family  $\hat{\mathcal{P}}_1$  does not even satisfy the basic assumptions of lemma 2.1 thus making it impossible to conclude anything about the stability of the two plant family  $\mathcal{P}_1$ . However, the second enlarged family satisfies the basic assumptions of plant family and  $\frac{\hat{\mathcal{P}}_2}{\hat{P}_\infty} = \frac{b}{b_\infty}$  is an interval that includes the origin. Hence, from corollary 2.2 it follows that the plant family  $\hat{\mathcal{P}}_2$  cannot be robustly stabilized. However, the latter conclusion does not imply that the two plant family  $\mathcal{P}_2$  cannot be robustly stabilized. One of the difficulties in using the results developed thus far is the fact that the two plant sets are not dense where as our previous results require the uncertain plant family to be a dense set.

#### Robust Stabilization of a Denumerable Plant Family:

Consider the plant family  $\mathcal{P} = \{p_1, p_2, \dots, p_k\}$  and let  $L_o(s) + \frac{P_s}{P}$  be the closed loop characteristic polynomial with  $P_o, P \in \mathcal{P}$  and  $L_o(s)$  the nominal loop transfer function. In this case it is not necessary that corollary 2.2 holds. In fact the plant family  $\mathcal{P}$ , can have elements for which  $\rho^+(\infty) = \frac{P_o(\infty)}{P(\infty)} > 0$  and others for which  $\rho^-(\infty) = \frac{P_o(\infty)}{P(\infty)} < 0$  and still be stabilizable. Here,  $\rho(s) = \frac{P_o(s)}{P(s)}$ . Define the two families  $\mathcal{P}^+$  and  $\mathcal{P}^-$  as follows:

$$\mathcal{P} = \mathcal{P}^+ \cup \mathcal{P}^-$$



where

$$\mathcal{P}^+ = \{p_i \in \mathcal{P} \mid \frac{P_o}{p}(\infty) > 0\}$$

$$\mathcal{P}^- = \{p_i \in \mathcal{P} \mid \frac{P_o}{p}(\infty) < 0\}$$

If  $L_o(s)$  is chosen strictly proper with no poles at the origin, then  $L_o(\infty) = 0$  and  $[L_o(s) + \frac{P_o(s)}{P(s,o)}]_{s=\infty} = \rho(\infty)$ . From the Nyquist stability criterion it therefore follows that the sign of  $[L_o(s) + \frac{P_o}{P}]_{s=0}$  should necessarily be positive (negative) if  $\rho > 0$  ( $\rho < 0$ ) and the number of unstable poles of  $L_o(s)$  is even (odd) so that the encirclement condition is satisfied. Hence, we have the following necessary condition when the number of unstable poles of  $L_o(s)$  is even.

$$L_o(0) + \rho^+(0) > 0, \text{ and } L_o(0) + \rho^-(0) < 0$$

i.e.,

$$-\rho^-(0) > L_o(0) > -\rho^+(0)$$

Similarly, when the number of unstable poles of  $L_o(s)$  is odd we have the following necessary condition:

$$-\rho^-(0) < L_o(0) < -\rho^+(0)$$

Following the above discussion we can now state a necessary condition for robust stabilizability of a denumerable plant family in theorem 2.1.

**THEOREM 2.1.** If  $L_o(s)$  has no poles at the origin, then the plant family  $\mathcal{P}$  is robustly stabilizable only if

- (i)  $-\rho^-(0) > L_o(0) > -\rho^+(0)$  when  $L_o(s)$  has an even number of right half plane poles, or
- (ii)  $-\rho^-(0) < L_o(0) < -\rho^+(0)$  when  $L_o(s)$  has an odd number of right half plane poles.

□

With the above theorem it can now be verified that the two, two plant, families  $\mathcal{P}_1$  and  $\mathcal{P}_2$  cannot be robustly stabilized with an LTI compensator. For  $\mathcal{P}_1$  we have,  $\rho^+(0) = 1$  and  $\rho^-(0) = 1$  with  $P_o(s) = \frac{1}{1+s}$ . From theorem 2.1 we require that  $-1 > L_o(0) > -1$ , no matter how many right half plane poles are included in  $L_o(s)$ , which is impossible to satisfy. Hence, the family  $\mathcal{P}_1$  cannot be robustly stabilized. For the family  $\mathcal{P}_2$  we have,  $\rho^+(0) = -1$  and  $\rho^-(0) = 1$  with  $P_o(s) = \frac{1}{1-s}$ . From theorem 2.1 we require that either  $-1 > L_o(0) > 1$  or  $-1 < L_o(0) < 1$ , depending on whether  $L_o(s)$  has an even or odd number of right half plane poles and is impossible to satisfy. Hence the family  $\mathcal{P}_2$  cannot be robustly stabilized.

### III. EXISTENCE OF QFT CONTROLLERS

In this section we state a sufficiency condition for the existence of a controller for robust stabilization. The result is based on the well known Nevanlinna-Pick interpolation theory. The classic Nevanlinna-Pick (NP) Problem can be stated as follows:

**Nevanlinna-Pick Problem:** Let  $a_i, b_i, i = 1, \dots, m$  be complex numbers such that  $\text{Re}(a_i) > 0$  and  $|b_i| \leq 1$  with  $a_i \neq a_j$ , when  $i \neq j$ . The NP interpolation problem is to determine an analytic function  $f(z)$ , if one exists, so that

$$f(a_i) = b_i, i = 1, \dots, m, \quad \text{and} \quad \|f\|_\infty \leq 1$$

It is well known that the above NP problem is solvable if and only if a special matrix  $\Lambda$  called the Pick matrix formed with the interpolating points is positive semi-definite. The Pick matrix is defined as

$$\Lambda = \begin{bmatrix} \frac{1-b_1\bar{b}_1}{a_1+\bar{a}_1} & \dots & \frac{1-b_1\bar{b}_m}{a_1+\bar{a}_m} \\ \dots & \dots & \dots \\ \frac{1-b_m\bar{b}_1}{a_m+\bar{a}_1} & \dots & \frac{1-b_m\bar{b}_m}{a_m+\bar{a}_m} \end{bmatrix}$$

Now, we state a slight variation (considered by Khargonekar and Tannenbaum (1985)) of the classic NP problem where  $b_i$ 's are allowed to be any where in the complex plane. By choosing a real parameter  $\gamma \geq 0$  one can look for an analytic function  $f_\gamma(z)$  such that  $f_\gamma(a_i) = \gamma b_i$ ,  $i = 1, \dots, m$ . The maximum  $\gamma$ ,  $\gamma_{max}$  such that for each  $\gamma \leq \gamma_{max}$ ,  $f_\gamma$  exists can be computed as follows:

Define

$$A = \begin{bmatrix} \frac{1}{a_1+d_1} & \dots & \frac{1}{a_1+d_m} \\ \dots & \dots & \dots \\ \frac{1}{a_m+d_1} & \dots & \frac{1}{a_m+d_m} \end{bmatrix} \quad (7)$$

$$B = \begin{bmatrix} \frac{b_1 \bar{d}_1}{a_1+d_1} & \dots & \frac{b_1 \bar{d}_m}{a_1+d_m} \\ \dots & \dots & \dots \\ \frac{b_m \bar{d}_1}{a_m+d_1} & \dots & \frac{b_m \bar{d}_m}{a_m+d_m} \end{bmatrix} \quad (8)$$

If at least one of the  $b_i \neq 0$ , then

$$\gamma_{max} = \frac{1}{\sqrt{\lambda_{max}}}$$

where  $\lambda_{max}$  is the largest eigenvalue of  $A^{-1}B$ .

With the above results we are now ready to address the question of existence of a robustly stabilizing controller. Recall, from section II above that the uncertain family can be robustly stabilized if and only if an  $L_o(s)$  can be found such that it stabilizes the nominal plant and  $1 + L_o(j\omega) \frac{P(j\omega, \alpha)}{P_o(j\omega)} \neq 0 \forall \omega \in [0, \infty]$ . We will first state the following lemma which characterizes among internally stabilizing  $G$ 's the one yielding

$$\min_G \left| \frac{1}{1 + L_o(j\omega)} \right| \forall \omega \in [0, \infty]$$

**LEMMA 3.1.** Let  $P_o = \frac{N}{M}$  be a coprime factorization of the nominal plant  $P_o$  over  $\text{RH}^\infty$  the set of all stable, proper, real-rational functions and let  $X, Y$  be two

functions in  $\text{RH}^\infty$  satisfying the equation

$$NX + MY = 1.$$

Then

$$\gamma_{\min} = \min_{G \text{ stabilizing}} \left\| \frac{1}{1 + L_o(j\omega)} \right\|_\infty$$

is given by

$$\frac{1}{\sqrt{\lambda_{\max}}}$$

where  $\lambda_{\max}$  is the largest eigenvalue of  $A^{-1}B$  with matrices  $A$  and  $B$  defined as in (7) and (8) with

$$a_i = z_i^*$$

and

$$b_i = MY(z_i^*)$$

where  $z_i^*$  are the right half plane zeros of  $MN$ .

**Proof:** It is well known that all internally stabilizing controllers for  $P_o$  can be characterized as

$$\left\{ \frac{X + MQ}{Y - NQ} : Q \in \text{RH}^\infty \right\}.$$

Consequently,

$$\begin{aligned} \frac{1}{1 + L_o} &= \frac{1}{1 + \frac{N}{M} \left( \frac{X + MQ}{Y - NQ} \right)} \\ &= MY - MNQ \end{aligned}$$

Now, define

$$S_o(s) = \frac{1}{\gamma} (MY - MNQ).$$

Next we can pose the following NP interpolation problem: Find a stable  $S_o$  such that the following interpolation conditions are satisfied

$$S_o(z_i^*) = \frac{1}{\gamma} MY(z_i^*), \quad i = 1, \dots, m$$

where  $z_i^*$ ,  $i = 1, \dots, m$  are the zeros of  $MN$  including those at  $\infty$  needed to assure a strictly proper controller if needed.

It can be easily seen that if  $S_o$  is stable that  $Q$  is also stable. (Notice that if  $Q$  were unstable then for  $S_o$  to be stable the unstable poles of  $Q$  must cancel some of the right half plane zeros of  $MN$ . But if the interpolation conditions are satisfied then  $MNQ(z_i^*) = 0$  implying that there should not be any cancellation of right half plane zeros of  $MN$  by unstable poles of  $Q$ . Hence, it follows that  $Q$  must be stable.)

The Pick matrix associated with the above NP problem is

$$\Lambda = A - \gamma^{-2}B$$

with  $A$  and  $B$  as defined in (7) and (8). Therefore  $\gamma_{\max}$  for which the NP problem is solvable is given by  $\frac{1}{\sqrt{\lambda_{\max}}}$  where  $\lambda_{\max}$  is the largest eigenvalue of  $A^{-1}B$ .  $\square$

Now we will state the following sufficiency theorem for the existence of a robustly stabilizing controller.

**THEOREM 3.1.** If  $\inf_{\omega \in [0, \infty]} \inf_{\alpha \in \Psi} \left| \frac{P(j\omega, \alpha)}{P(j\omega, \alpha) - P_o(j\omega)} \right| > \gamma_{\min}$  then there exists a stabilizing controller for the entire family  $P(s, \alpha)$ ,  $\alpha \in \Psi$ .

**Proof:** Suppose  $L_o(s)$  stabilizes the nominal plant  $P_o(s)$ . From lemma 2.1 if in addition  $1 + L(j\omega, \alpha) \neq 0$ ,  $\forall \omega \in [0, \infty]$ ,  $\alpha \in \Psi$  then the closed loop family is stable.

The  $\omega$ 's at which  $1 + L$  is zero are characterized by  $L = -1$  or  $L_o = -\frac{P_o}{P}$ . But  $L_o = -\frac{P_o}{P}$  is equivalent to

$$\frac{1}{1 + L_o} = \frac{P}{P - P_o}$$

Hence, if  $\frac{1}{1 + L_o} \neq \frac{P}{P - P_o}$  then  $1 + L \neq 0$  and the entire uncertain family is robustly stable.

Consequently, the family of plants is robustly stable if

$$\left| \frac{1}{1+L_o} \right| \neq \left| \frac{P}{P-P_o} \right| \quad (9)$$

Note that

$$\left| \frac{P}{P-P_o}(j\omega) \right| \in [\mu, \infty]$$

since  $P_o \in P$ . Let  $\mu_{\min} = \inf_{\omega \in [0, \infty]} \mu$ . Then it is sufficient that  $\left\| \frac{1}{1+L_o} \right\|_{\infty} < \mu_{\min}$  to assure the condition stipulated in (9).  $\square$

**Remark:**

1. Note that the above existence condition can never be satisfied (i) if there are uncertain zeros of  $P(s, \alpha)$  that cross from the left half plane to the right half plane and *vice versa* or (ii) fixed zeros on the imaginary axis. This is so because  $\mu = 0$  at some frequencies and some  $\alpha \in \Psi$ .
2. It can be easily seen that the necessary and sufficient condition that  $\frac{1}{1+L_o} \neq \frac{P}{P-P_o}$  requires the intersection of two complex functions. The sufficiency condition of theorem 3.1 is simply based on the magnitude. So it is not difficult to see that even if the magnitude condition is violated there still may exist a stabilizing controller for the plant family.
3. If the nominal plant  $P_o$  is chosen to lie in the interior of the plant family  $P$  at each frequency, then  $\frac{P}{P-P_o}$  will cover all phase angles in  $[0, 2\pi]$ .
4. Since  $\frac{P}{P-P_o}$  is proper the infinite frequency interval  $[0, \infty]$  may be replaced by the finite range  $[0, \omega_c]$  where  $\omega_c$  is such that  $\left| \frac{P}{P-P_o} \right|_{j\omega \geq \omega_c} \approx \left| \frac{P}{P-P_o} \right|_{j\infty}$

Now, we state a corollary of theorem 3.1 for the existence of a QFT controller for performance robustness. Suppose the QFT problem is formulated as a sensitivity

constrained optimization problem as in Nwokah et al. (1992) and let

$$\inf_{\omega \in (0, \infty)} \left| \frac{1}{1 + L_o} \right| = \mu_P.$$

**COROLLARY 3.1.** If  $\gamma_{\min} < \mu_P$  and the plant family satisfies the conditions of lemma 2.1 then there exists a QFT controller satisfying the robust performance specifications characterized by  $\mu_P$ .

**Proof:** Obvious.

#### IV. A SPECIAL CASE

In this section we study the robust stabilization and the performance robustness of an interval family in which the uncertainty is only in the pole locations. Hence, the zeros of the plant family are assumed fixed. For this special case we show that the robust stabilization problem reduces to determining a nominal loop transfer function  $L_o(s)$  that stabilizes the nominal plant which simultaneously avoids certain forbidden regions that can be explicitly computed simply by locating four points in the complex plane at each frequency. Then we show how an output disturbance rejection requirement can be handled. Finally we show that if there are QFT type tracking specifications that the synthesis problem can be reduced to a sensitivity constrained optimization problem which in turn can be solved using the previous output disturbance rejection synthesis procedure.

Consider the interval plant family

$$P(s, p) = \frac{P_1(s)}{P_o(s, p)}, \quad (10)$$

and the proper compensator transfer function

$$G(s) = \frac{Q_1(s)}{Q_o(s)} \quad (11)$$

We assume that all the uncertainties occur only in the denominator of  $P(s, p)$ ,

i.e.:

$$P_o(s, p) = \sum_{i=0}^{n_o} p_i s^i, \quad p_i \in [\alpha_i, \beta_i], \quad i = 0, \dots, n_o. \quad (12)$$

Let

$$P_1(s) = \sum_{i=0}^{n_1} p_{1i} s^i,$$

and

$$Q_i(s) = \sum_{j=0}^{m_i} q_{ij} s^j, \quad i = 0, 1, \quad (13)$$

$$m_o \geq m_1.$$

Denote

$$p \stackrel{\text{def}}{=} (p_0 \dots p_{n_o})^T \in R^{(n_o+1)}, \quad (14)$$

$$\Psi \stackrel{\text{def}}{=} [\alpha_o, \beta_o] \times \dots \times [\alpha_{n_o}, \beta_{n_o}]. \quad (15)$$

The closed loop characteristic polynomial is given by

$$\delta(s, p) = Q_o(s)P_o(s, p) + Q_1(s)P_1(s). \quad (16)$$

Without loss of any generality, in the following discussion we suppose that

$$0 < \alpha_{n_o} \leq \beta_{n_o}. \quad (17)$$

Now, we turn to consider the conditions under which  $\delta(j\omega, p) \neq 0$  for all  $\omega$ .

First by denoting

$$\delta_1(j\omega, p) = P_o(j\omega, p) + \frac{Q_1(j\omega)}{Q_o(j\omega)} P_1(j\omega) \quad (18)$$

we can state the following modified "Zero Exclusion Principle" in terms of  $\delta_1$ .

**LEMMA 4.1.**  $G(s)$  stabilizes the whole interval family  $P(s, p)$  if and only if:

(i) there exists a  $p_o \in \Psi$  such that  $G(s)$  stabilizes  $P(s, p_o)$ ,



(ii)  $0 \notin \delta_1(j\omega, p)$ ,  $p \in \Psi$ , for all  $\omega \in [0, \infty]$  if  $Q_o(0) \neq 0$  and for  $\omega \in (0, \infty]$  if  $Q_o(0) = 0$ .

**Proof:** Assume that the compensator  $G(s)$  is selected to have no imaginary axis poles except at the origin. So we can assume that  $Q_o(j\omega) \neq 0$  for  $\omega \neq 0$  from which it follows that

$$0 \notin \delta(j\omega, \Psi) \text{ for } \omega \geq 0$$

if and only if

$$0 \notin \delta_1(j\omega, \Psi)$$

in the case of  $Q_o(0) \neq 0$ . Now consider the case  $Q_o(0) = 0$ . In this case,

$$\delta(0, \Psi) = Q_1(0)P_1(0) \neq 0$$

because

$$Q_1(0) \neq 0, \quad P_1(0) \neq 0$$

otherwise there is an unstable pole and zero cancellation. So the requirement

$$0 \notin \delta(0, \Psi)$$

is automatically satisfied and we only need to check whether  $0 \notin \delta(j\omega, \Psi)$  for  $\omega > 0$ , which is equivalent to  $0 \notin \delta_1(j\omega, \Psi)$ ,  $\omega > 0$ .  $\square$  Using lemma 3.1, we can concentrate our discussion on the case  $Q_o(0) \neq 0$  and consider  $\delta_1(j\omega, p)$  instead of  $\delta(j\omega, p)$ .

For the polynomial  $P_o(j\omega, p)$ , we can define its odd and even parts as follows:

$$\begin{aligned} P_o^o(\omega, p) &= p_1\omega - p_3\omega^3 + p_5\omega^5 \dots, \\ P_o^e(\omega, p) &= p_o - p_2\omega^2 + p_4\omega^4 \dots. \end{aligned} \quad (19)$$

Then we have

$$P_o(j\omega, p) = P_o^e(\omega, p) + jP_o^o(\omega, p). \quad (20)$$

We now define the following polynomials to facilitate the description of our first result of this section.

**DEFINITION 4.1**

$$\begin{aligned}
 P_o^{eM}(\omega) &= \beta_o - \alpha_2\omega^2 + \beta_4\omega^4 \dots, \\
 P_o^{em}(\omega) &= \alpha_o - \beta_2\omega^2 + \alpha_4\omega^4 \dots, \\
 P_o^{eM}(\omega) &= \beta_1\omega - \alpha_3\omega^3 + \beta_5\omega^5 \dots, \\
 P_o^{em}(\omega) &= \alpha_1\omega - \beta_3\omega^3 + \alpha_5\omega^5 \dots,
 \end{aligned} \tag{21}$$

$$\Delta P_o^e(j\omega) = \frac{1}{2}(P_o^{eM} - P_o^{em}),$$

$$\Delta P_o^o(j\omega) = \frac{1}{2}(P_o^{oM} - P_o^{om}),$$

$$\bar{P}_o^e(\omega) = \frac{1}{2}(P_o^{eM} + P_o^{em}),$$

$$\bar{P}_o^o(\omega) = \frac{1}{2}(P_o^{oM} + P_o^{om}),$$

$$\bar{P}_o(j\omega) = \bar{P}_o^e(\omega) + j\bar{P}_o^o(\omega).$$

Clearly for each fixed  $\omega$ , and  $\forall p \in \Psi$ , we have

$$\begin{aligned}
 P_o^{em}(\omega) &\leq P_o^e(\omega, p) \leq P_o^{eM}(\omega) \\
 P_o^{om}(\omega) &\leq P_o^o(\omega, p) \leq P_o^{oM}(\omega).
 \end{aligned} \tag{22}$$

Note that the parameters appearing in  $P_i^e(\omega)$  do not appear in  $P_i^o(\omega)$ , and vice versa. Thus we have two real numbers  $\lambda_1, \lambda_2$  with  $|\lambda_1| \leq 1$  and  $\lambda_2 \leq 1$  such that

$$P_o^e(\omega, p) = \Delta P_o^e(\omega)\lambda_1 + \bar{P}_o^e(\omega), \tag{23}$$

$$P_o^o(\omega, p) = \Delta P_o^o(\omega)\lambda_2 + \bar{P}_o^o(\omega).$$

On the other hand, for an arbitrary pair of  $\lambda_1, \lambda_2$  with

$$|\lambda_1| \leq 1, |\lambda_2| \leq 1,$$

there exists at least one parameter  $p \in \Psi$  such that (23) holds. This is because:

(i)

$$P_o^{pm}(\omega) \leq \Delta P_o^e(\omega)\lambda_1 + \bar{P}_o^e(\omega) \leq P_o^{eM}(\omega),$$

$$P_o^{pm}(\omega) \leq \Delta P_o^e(\omega)\lambda_2 + \bar{P}_o^e(\omega) \leq P_o^{eM}(\omega),$$

(ii) For each fixed  $\omega$ ,  $P_o^e(\omega, p)$  and  $\bar{P}_o^e(\omega, p)$  are continuous functions of parameter  $p$ ,  $P_o^{eM}(\omega)$  (or  $P_o^{pm}(\omega)$ ) and  $P_o^{eM}(\omega)$  (or  $P_o^{pm}(\omega)$ ) are their respective reachable maximum values (or minimum values). It follows from the Mean Value Theorem of continuous functions that there exists at least one parameter  $p \in \Psi$  satisfying (23). Therefore for each fixed frequency  $\omega$ ,

$$P_o(j\omega, \Psi) = \Delta P_o^e(\omega)\lambda_1 + j\Delta P_o^e(\omega)\lambda_2 + \bar{P}_o(j\omega),$$

$$|\lambda_i| \leq 1, i = 1, 2.$$

And

$$\begin{aligned} \delta_1(j\omega, \Psi) &= P_o(j\omega, \Psi) + P_1 \frac{Q_1}{Q_o} \\ &= \Delta P_o^e \lambda_1 + j\Delta P_o^e \lambda_2 + \bar{P}_o + P_1 \frac{Q_1}{Q_o} \\ &= \Delta P_o^e \lambda_1 + j\Delta P_o^e \lambda_2 + \bar{P}_o \left(1 + \frac{P_1 Q_1}{\bar{P}_o Q_o}\right), \end{aligned}$$

$$|\lambda_i| \leq 1, i = 1, 2.$$

Denote

$$L_o(j\omega) = \frac{P_1(j\omega)Q_1(j\omega)}{\bar{P}_o(j\omega)Q_o(j\omega)} \quad (24)$$

as the nominal loop transfer function with the nominal plant  $\frac{P_0}{P_0}$  and let  $u(\omega)$  and  $v(\omega)$  be the real and imaginary parts, respectively, of  $L_0(j\omega)$ , i.e.

$$L_0(j\omega) = u(\omega) + jv(\omega). \quad (25)$$

For a fixed frequency  $\omega$ , by substituting (25) into (24), we have

$$\begin{aligned} \delta_1(j\omega, \Psi) &= \Delta P_0^* \lambda_1 + j \Delta P_0^* \lambda_2 + \bar{P}_0^* (1 + u) - \bar{P}_0^* v + j(\bar{P}_0^* u + \bar{P}_0^* v) \\ &= \Delta P_0^* \left( \lambda_1 + \frac{\bar{P}_0^*}{\Delta P_0^*} u - \frac{\bar{P}_0^*}{\Delta P_0^*} v + \frac{\bar{P}_0^*}{\Delta P_0^*} \right) + j \Delta P_0^* \left( \lambda_2 + \frac{\bar{P}_0^*}{\Delta P_0^*} u + \frac{\bar{P}_0^*}{\Delta P_0^*} v \right), \\ |\lambda_i| &\leq 1, i = 1, 2. \end{aligned}$$

Denote

$$\begin{aligned} K_1(\omega) &= \frac{\bar{P}_0^*}{\Delta P_0^*} u - \frac{\bar{P}_0^*}{\Delta P_0^*} v + \frac{\bar{P}_0^*}{\Delta P_0^*} \\ K_2(\omega) &= \frac{\bar{P}_0^*}{\Delta P_0^*} u + \frac{\bar{P}_0^*}{\Delta P_0^*} v \end{aligned} \quad (26)$$

and define a box around the origin

$$B \stackrel{\text{def}}{=} \{(\lambda_1 + j\lambda_2) \in R^2, ; |\lambda_i| \leq 1, i = 1, 2.\} \quad (27)$$

Based on the above definitions and discussion, we will now state the following Lemma.

**LEMMA 4.2.** For each fixed  $\omega$ ,

$$\delta_1(j\omega, \Psi) = \{ (\Delta P_0^* (\lambda_1 + K_1(\omega)) + j\omega \Delta P_0^* (\lambda_2 + K_2(\omega))); (\lambda_1, \lambda_2) \in B \}. \quad (28)$$

□

With the criterion function  $K(\omega)$  defined as follows:

$$K(\omega) \stackrel{\text{def}}{=} K_1(\omega) + jK_2(\omega). \quad (29)$$

we can state the first main result of this section given next.

**THEOREM 4.1.** Let  $G(s)$  be the compensator, and  $L_o(s) = G(s) \frac{P_o(s)}{P_o(s)}$ , the nominal loop transfer function. The fixed compensator  $G(s)$  stabilizes the interval plant family  $P(s, p)$  if and only if:

- (i)  $L_o(j\omega)$  satisfies the Nyquist stability criterion and
- (ii) the plot of  $K(\omega)$  does not intersect the box B.

**Proof:** From Lemma 4.1, we only need to show that under conditions (ii),  $0 \notin \delta_1(j\omega, \Psi)$  for all  $\omega \in [0, \infty)$ . In fact, for a fixed  $\omega$ , there is a  $p \in \Psi$  such that  $\delta_1(j\omega, p) = 0$  if and only if there exists  $(\lambda_1 + j\lambda_2) \in B$  such that

$$\lambda_1 + K_1(\omega) = 0, \text{ and } \lambda_2 + K_2(\omega) = 0,$$

because both  $\Delta P_o^*$  and  $\Delta P_o^*$  are positive. And from Lemma 4.2 it follows that for each fixed  $\omega$ ,  $0 \notin \delta_1(j\omega, \Psi)$  if and only if one of the following inequalities holds:

$$|K_1(\omega)| > 1, \text{ or } |K_2(\omega)| > 1.$$

This is equivalent to the plot of the criterion function  $K(\omega)$  not intersecting B and the proof of the theorem is thus complete.  $\square$

#### IV.1 Synthesis for Robust Stabilization:

Theorem 4.1 is an effective tool for synthesizing a robustly stabilizing compensator  $G(s)$ . The essential idea is to use classical loop shaping to avoid certain forbidden regions for the loop transfer function  $L_o(s)$  corresponding to the nominal plant  $\frac{P_o(s)}{P_o(s)}$ . In particular, we can use Eqns. (24) and (25) together with the condition that  $|K_1| > 1$ , or  $|K_2| > 1$  to get constraints on  $u(\omega)$  and  $v(\omega)$ , the real and imaginary parts of  $L_o(j\omega)$ , which can then be used to shape the latter function. The

forbidden region for the nominal loop transfer function,  $L_o(j\omega)$ , at each frequency, is defined by the constraints

$$|K_1| \leq 1 \quad \text{and} \quad |K_2| \leq 1.$$

First of all we need to express  $u$  and  $v$  in terms of  $K_1$  and  $K_2$ . To that end denote

$$A(\omega) = \frac{1}{|\bar{P}_o^*|} \begin{bmatrix} \bar{P}_o^* \Delta P_o^* & \bar{P}_o^* \Delta P_o^* \\ -\bar{P}_o^* \Delta P_o^* & \bar{P}_o^* \Delta P_o^* \end{bmatrix}, \quad (30)$$

$$b(\omega) = \frac{1}{|\bar{P}_o^*|} \begin{bmatrix} -(\bar{P}_o^*)^2 \\ \bar{P}_o^* \bar{P}_o^* \end{bmatrix}. \quad (31)$$

By solving  $u$  and  $v$  from equation (26) with the above definitions, we have

$$\begin{bmatrix} u(\omega) \\ v(\omega) \end{bmatrix} = A(\omega) \begin{bmatrix} K_1 \\ K_2 \end{bmatrix} + b(\omega). \quad (32)$$

Therefore the forbidden region for  $L_o(j\omega)$  in the  $u$ - $v$  plane is given as follows:

$$\Pi_\omega = \{u + vj; \begin{bmatrix} u \\ v \end{bmatrix} = A(\omega) \begin{bmatrix} K_1 \\ K_2 \end{bmatrix} + b(\omega), |K_i| \leq 1, i = 1, 2\}. \quad (33)$$

By denoting the four points

$$\pi_\omega(1, 1) = A(\omega) \begin{bmatrix} 1 \\ 1 \end{bmatrix} + b(\omega),$$

$$\pi_\omega(1, -1) = A(\omega) \begin{bmatrix} 1 \\ -1 \end{bmatrix} + b(\omega),$$

$$\pi_\omega(-1, 1) = A(\omega) \begin{bmatrix} -1 \\ 1 \end{bmatrix} + b(\omega),$$

$$\pi_\omega(-1, -1) = A(\omega) \begin{bmatrix} -1 \\ -1 \end{bmatrix} + b(\omega)$$

it is easy to see that  $\Pi_\omega$  is a parallelogram with the above four points as its vertices. The above discussion together with theorem 4.1 leads to the following theorem.

**THEOREM 4.2.** Let  $L_o(j\omega)$  be the loop transfer function corresponding to the nominal plant  $\frac{A}{P_o}$ . The compensator  $G = \frac{L_o}{P_o}$  stabilizes the whole interval plant family if and only if:

(i)  $L_o(j\omega)$  satisfies the Nyquist stability criterion and

(ii) for each frequency  $\omega \in [0, \infty]$ ,  $L_o(j\omega) \notin \Pi_\omega$ . □

Note that by the definitions in (30) and (31), there are two constant matrices  $A_\infty \in R^{2 \times 2}$  and  $b_\infty \in R^2$  such that

$$\lim_{\omega \rightarrow \infty} A(\omega) = A_\infty, \quad \lim_{\omega \rightarrow \infty} b(\omega) = b_\infty.$$

Consequently, during synthesis, we only need to select a specified frequency  $\omega_c$  such that

$$A(\omega) \approx A_\infty, \quad b(\omega) \approx b_\infty$$

for  $\omega \geq \omega_c$ . Therefore during loop shaping  $L_o(j\omega)$ , instead of checking whether or not

$$L_o(j\omega) \notin \Pi_\omega$$

for all  $\omega \in [0, \infty)$ , we only need to check

$$L_o(j\omega) \notin \Pi_\omega, \quad \omega \in [0, \omega_c),$$

and

$$L_o(j\omega) \notin \Pi_\infty, \quad \omega \in [\omega_c, \infty).$$

Since the nominal plant  $\frac{A}{P_o}$  is strictly proper from corollary 2.2 a necessary condition for robust stabilization is that

$$0 \notin \Pi_\infty.$$

**IV.2. Disturbance rejection:**

In addition to stabilization, suppose we also want to attain the following disturbance rejection specification:

$$|T_{yd}(j\omega, \Psi)| \leq r(\omega), \quad \omega \in [0, \omega_d], \quad (34)$$

where  $T_{yd}$  is the closed loop transfer function from a disturbance input at the output to the output,  $\omega_d$  is a specified frequency such that the frequency band of the disturbance is included in  $[0, \omega_d]$ . It is easy to see that

$$T_{yd}(j\omega, \Psi) = \frac{1}{1 + \frac{P_1 Q_1}{P_o(j\omega, \Psi) Q_o}} = \frac{P_o(j\omega, \Psi)}{\frac{P_1 Q_1}{Q_o} + P_o(j\omega, \Psi)}. \quad (35)$$

By recalling (24), (25) and (26), for each frequency  $\omega$ , we have

$$\frac{Q_1 P_1}{Q_o} + P_o(j\omega, \Psi) = \Delta P_o^*(\lambda_1 + K_1(\omega)) + j\Delta P_o^*(\lambda_2 + K_2(\omega)),$$

$$|\lambda_i| \leq 1, \quad i = 1, 2.$$

Thus

$$\left| \frac{Q_1 P_1}{Q_o} + P_o(j\omega, \Psi) \right| = \sqrt{(\Delta P_o^*)^2(\lambda_1 + K_1)^2 + (\Delta P_o^*)^2(\lambda_2 + K_2)^2}. \quad (36)$$

Moreover from (20)

$$\begin{aligned} |P_o(j\omega, \Psi)| &= \sqrt{(\bar{P}_o^* + \Delta P_o^* \lambda_1)^2 + (\bar{P}_o^* + \Delta P_o^* \lambda_2)^2} \\ &\leq \sup_{\Psi} \sqrt{(|\bar{P}_o^*| + \Delta P_o^*)^2 + (|\bar{P}_o^*| + \Delta P_o^*)^2} \\ &\triangleq \sigma(\omega), \end{aligned} \quad (37)$$

which renders

$$|T_{yd}(j\omega, \Psi)| \leq \frac{\sigma(\omega)}{\sqrt{(\Delta P_o^*)^2(\lambda_1 + K_1)^2 + (\Delta P_o^*)^2(\lambda_2 + K_2)^2}}. \quad (38)$$

Hence, a sufficient condition for (34) to hold is

$$\frac{\sigma(\omega)}{\sqrt{(\Delta P_o^*)^2(K_1 + \lambda_1)^2 + (\Delta P_o^*)^2(K_2 + \lambda_2)^2}} \leq r(\omega). \quad (39)$$



It can be easily verified that the forbidden region inside which inequality (39) is violated, denoted  $D_\omega$ , consists of all points  $(K_1, K_2)$  satisfying

$$\frac{\sigma(\omega)}{\sqrt{(\Delta P_\sigma^2)^2(K_1 + \lambda_1)^2 + (\Delta P_\sigma^2)^2(K_2 + \lambda_2)^2}} > r(\omega),$$

or equivalently

$$\frac{(K_1 + \lambda_1)^2}{\left(\frac{\sigma}{r\Delta P_\sigma^2}\right)^2} + \frac{(K_2 + \lambda_2)^2}{\left(\frac{\sigma}{r\Delta P_\sigma^2}\right)^2} < 1, \quad (40)$$

$$|\lambda_i| \leq 1, \quad i = 1, 2.$$

The boundary of  $D_\omega$  is the envelope of the following family of ellipses:

$$\frac{(K_1 + \lambda_1)^2}{\left(\frac{\sigma}{r\Delta P_\sigma^2}\right)^2} + \frac{(K_2 + \lambda_2)^2}{\left(\frac{\sigma}{r\Delta P_\sigma^2}\right)^2} = 1$$

with the center  $(\lambda_1, \lambda_2)$  moving within  $B$ . In order to estimate  $D_\omega$ , define a rectangle around the origin in the  $(K_1 - K_2)$  plane as follows:

$$E_\omega = \{(K_1, K_2); |K_1| \leq 1 + \frac{\sigma}{r\Delta P_\sigma^2}, |K_2| \leq 1 + \frac{\sigma}{r\Delta P_\sigma^2}\}. \quad (41)$$

Then

$$D_\omega \in E_\omega$$

and the boundary of  $D_\omega$  coincides with that of  $E_\omega$  except around the four corners. Their relation is illustrated in Fig. 1. From (32) and (41), we can easily construct the forbidden region in the  $u - v$  plane by considering inequality (39) at each frequency. Denote

$$\Psi_\omega = \{u + vj; \begin{bmatrix} u \\ v \end{bmatrix} = A(\omega) \begin{bmatrix} K_1 \\ K_2 \end{bmatrix} + b(\omega), (K_1, K_2) \in E_\omega\}, \quad (42)$$

and define four points as

$$\psi_\omega(1, 1) = A(\omega) \begin{bmatrix} 1 + \frac{\sigma}{r\Delta P_\sigma^2} \\ 1 + \frac{\sigma}{r\Delta P_\sigma^2} \end{bmatrix} + b(\omega),$$

$$\psi_{\omega}(1, -1) = A(\omega) \begin{bmatrix} 1 + \frac{\sigma}{r\Delta P_0^2} \\ -1 - \frac{\sigma}{r\Delta P_0^2} \end{bmatrix} + b(\omega),$$

$$\psi_{\omega}(-1, 1) = A(\omega) \begin{bmatrix} -1 - \frac{\sigma}{r\Delta P_0^2} \\ 1 + \frac{\sigma}{r\Delta P_0^2} \end{bmatrix} + b(\omega),$$

$$\psi_{\omega}(-1, -1) = A(\omega) \begin{bmatrix} -1 - \frac{\sigma}{r\Delta P_0^2} \\ -1 - \frac{\sigma}{r\Delta P_0^2} \end{bmatrix} + b(\omega).$$

Then  $\Psi_{\omega}$  is nothing more than the parallelogram having the above four points as its vertices. It follows from the fact that  $B \in E_{\omega}$  that

$$\Pi_{\omega} \in \Psi_{\omega}. \quad (43)$$

Now we can state the following lemma.

**LEMMA 4.3.** If  $L_o(j\omega) \notin \Psi_{\omega}$ , then

$$|T_{yd}(j\omega, P)| \leq r.$$

**Proof:**

$$L(j\omega) \notin \Psi_{\omega}$$

means that

$$(K_1(\omega), K_2(\omega)) \notin E_{\omega}.$$

and it follows that (39) and (34) both hold.  $\square$

Now, we can state the main result of this section by assuming without loss of any generality that  $\omega_d < \omega_c$ .

**THEOREM 4.3** Let  $L_o(j\omega)$  be the loop transfer function of the nominal plant  $\frac{B}{P_o}$ . The compensator  $G = \frac{L_c}{P_c}$  stabilizes the whole interval plant family and satisfies the disturbance rejection specification given in (34) if:

- (i)  $L_o(j\omega)$  satisfies the Nyquist stability criterion
- (ii) for each frequency  $\omega \in [0, \omega_d]$ ,  $L_o(j\omega) \notin \Psi_{\omega}$ .

(iii) for each frequency  $\omega \in (\omega_d, \omega_c)$ ,  $L(j\omega) \notin \Pi_\omega$ .

(iv) for each frequency  $\omega \in [\omega_c, \infty)$ ,  $L(j\omega) \notin \Pi_\infty$ . □

**Remark:** Note that in the above formulation of the disturbance rejection problem some conservativeness is introduced through the bound developed in (34). This simplification is utilized here mainly for deriving an explicit form the forbidden regions. Moreover such simplification may provide a reasonable answer to the existence question as was discussed previously in section III.

#### IV.3 The General QFT Synthesis Problem:

The goal of the general QFT synthesis problem is to determine an admissible pair of strictly proper, rational and preferably stable transfer functions  $(G(s), F(s))$  in the classic two degree of freedom arrangement shown in Fig. 2 such that the following conditions are satisfied and the bandwidth of the compensator  $G$  is minimized.

1.  $T(s, p) = \frac{G(s)P(s, p)}{1 + G(s)P(s, p)}$ , is stable  $\forall p \in \Psi$ .

2.  $\max_{p \in \Psi} |T(s, p) - T(s, p_0)| \leq \delta_T(s)$ ,  $\forall s$

3.  $\max_{p \in \Psi} |T_d(s, p)| \leq r(s)$ ,  $\forall s$

where  $\delta_T(s)$  and  $r(s)$  are the prespecified QFT performance requirements and  $T_d$  is a transfer function from a disturbance to the output.

The above design requirements can be converted into a sensitivity constrained optimization problem as follows. First note that we can write

$$\frac{T(s, p) - T(s, p_0)}{T(s, p_0)} = \frac{P(s, p) - P(s, p_0)}{(1 + G(s)P(s, p))}$$

Denoting  $T_0(s) = T(s, p_0)$  and  $S(s, p) = \frac{1}{1 + L(s, p)}$  with  $L(s, p) = G(s)P(s, p)$  we get

$$\max_{p \in \Psi} |T(s, p) - T_0(s)| = \max_{p \in \Psi} \left| T_0(s) S(s, p) \frac{P(s, p) - P(s, p_0)}{P(s, p_0)} \right|, \forall s$$

and the tracking constraint reduces to:

$$\max_{p \in \mathcal{P}} |S(j\omega, p)| \leq \sup_{p \in \mathcal{P}} \frac{\delta_T(j\omega)}{T_o(j\omega) \left( \frac{P(s, p) - P(s, p_o)}{P(s, p_o)} \right)} = \delta_t(\omega), \quad \forall \omega \in [0, \infty].$$

The disturbance rejection requirements can also be reduced (see Nwokah et al. [1992] for details) to a constraint of the form  $|S(j\omega, p)| \leq \delta_d(\omega)$  leading to the following sufficient condition. The QFT specifications will be satisfied if

$$\max_{p \in \mathcal{P}} |S(j\omega, p)| \leq \min \{ \delta_t, \delta_d(\omega) \}, \quad \forall \omega \in [0, \infty]$$

Now notice that  $T_{yd}(j\omega, p)$  defined in section 4.3 above is the same as the sensitivity function  $S(j\omega, p)$  and the QFT performance requirements reduce exactly to the same problem which can be solved using theorem 4.3.

## V. EXAMPLES

In order to illustrate the above results, we consider the following two examples.

Example 1. Let the uncertain plant be:

$$P(s, p) = \frac{1}{p_1 s^2 + p_2 s + p_3}, \quad G(s) = \frac{2}{s + 1.5},$$

where

$$p_1 \in [1 \ 2], \quad p_2 \in [2 \ 3], \quad p_3 \in [-1 \ 0].$$

Thus we have

$$P_o(s, p) = p_1 s^2 + p_2 s + p_3, \quad P_1(s, p) = 1, \quad Q_o(s) = s + 1.5, \quad Q_1 = 2,$$

It follows from a simple computation that:

$$\Delta P_o^*(\omega) = \frac{\omega^2 + 1}{2}, \quad \Delta P_o^* = \frac{\omega}{2},$$

$$\bar{P}_o^* = -\frac{3\omega^2 + 1}{2}, \quad \bar{P}_o^* = \frac{5\omega}{2},$$

$$\bar{P}_o = -\frac{1}{2}(3\omega^2 + 1) + \frac{5}{2}\omega j.$$

The criterion function  $K(\omega)$  here is:

$$K(\omega) = \frac{2}{\omega^2 + 1} \left( \frac{3}{\omega^2 + 2.25} - \frac{3\omega^2 + 1}{2} \right) + j \left( 5 - \frac{4}{\omega^2 + 2.25} \right)$$

$$L_o(j\omega) = -\frac{4}{(3\omega^2 + 1 - 5\omega j)(1.5 + \omega j)}$$

The plots of  $K(\omega)$  and  $L_o(j\omega)$  shown in Fig. 3 confirm that  $P(s,p)$  is stabilized by  $G(s)$ .

Example 2. Now we apply theorem 4.2 to the same system for the purpose of illustrating synthesis. From a simple computation, we have

$$A(\omega) = \frac{1}{(3\omega^2 + 1)^2 + 25\omega^2} \begin{bmatrix} -(\omega^2 + 1)(3\omega^2 + 1) & 5\omega^2 \\ -5\omega(\omega^2 + 1) & -\omega(3\omega^2 + 1) \end{bmatrix},$$

$$b(\omega) = \frac{1}{(3\omega^2 + 1)^2 + 25\omega^2} \begin{bmatrix} -(3\omega^2 + 1)^2 \\ -5\omega(3\omega^2 + 1) \end{bmatrix}.$$

It is easy to see that

$$A_\infty = \begin{bmatrix} -\frac{1}{3} & 0 \\ 0 & 0 \end{bmatrix},$$

$$b_\infty = \begin{bmatrix} -1 \\ 0 \end{bmatrix}.$$

In this case we can set

$$\omega_c = 20.$$

Several forbidden regions obtained for frequencies  $\omega = 0, 0.1, 1, 5, 20$ , are shown in Fig. 4. Theoretically, although an infinite number of forbidden regions must be

sketched, in practice a finite number can be chosen as was done in this example. The next step is to loop shape a suitable nominal loop transfer function. Since the nominal plant

$$\frac{P_1}{P_0} = \frac{2}{3s^2 + 5s - 1}$$

has one unstable pole the synthesized loop transfer function must encircle the point  $(-1,0)$  once and should not penetrate the corresponding forbidden region at the chosen frequencies. The compensator  $\frac{2}{s+1.5}$  will work as was shown in the first example. In a real design situation one must evaluate the compensator chosen, by invoking theorem 4.1. This last step will especially be important if only a small number of frequencies were considered to generate the forbidden regions.

## VI. CONCLUSION

A necessary and sufficient theorem was given for robust stabilization of a general family of interval plants. Also given were three necessary conditions for robust stabilization when the plant family is dense and when it is not. A sufficiency theorem based on the Nevanlinna-Pick interpolation theory was given for the existence of a stabilizing controller for an uncertain plant family. Also developed in the paper are some simple criteria for solving the QFT problem when the plant family is characterized as an interval family with fixed zeros and uncertain poles. As a key contribution of this paper we have formalized mathematically and in fact justified a number of claims made in the QFT methodology. We have also provided some simple sufficiency conditions for determining whether a QFT controller exists. Our current research is aimed at determining more sharply stated existence results. In any event we believe the existence results given here to be the first of its kind.

## REFERENCES

- [1] J. Anagnost, C. Desoer and R. Minnichelli, "Generalized Nyquist Tests for Robust Stability: Frequency Domain Generalizations of Kharitonov's Theorem," in *Robustness in Identification and Control*, (M. Milanese, R. Tempo and A. Vicino, eds), pp. 79-96, NY:plenum, 1989.
- [2] J.C. Doyle, "Quantitative Feedback Theory (QFT) and Robust Control," *Proceedings of the 1986 Automatic Control Conference*, Seattle, WA, June 1986.
- [3] I.M. Horowitz, "*Synthesis of Feedback Systems*," Academic Press, New York, 1963.
- [4] I.M. Horowitz, "Survey of Quantitative Feedback Theory," *International Journal of Control*, 1991.
- [5] I.M. Horowitz, "Quantitative Feedback Theory- Reply to Doyle's Criticisms," *Proceedings of the 1987 Automatic Control Conference*, Minneapolis, MN, June 1987.
- [6] P. Khargonekar, and A. Tannenbaum, "Non-Euclidean Metrics and Robust Stabilization of Systems with Parameter Uncertainty," *IEEE Trans. on Auto. Contr.*, Vol. AC-30, no. 10, pp. 1005-1013, October 1985.
- [7] O.D.I. Nwokah, S. Jayasuriya, and Y. Chait, "Parametric Robust Control by Quantitative Feedback Theory," *AIAA Journal of Guidance and Control*, 1992.

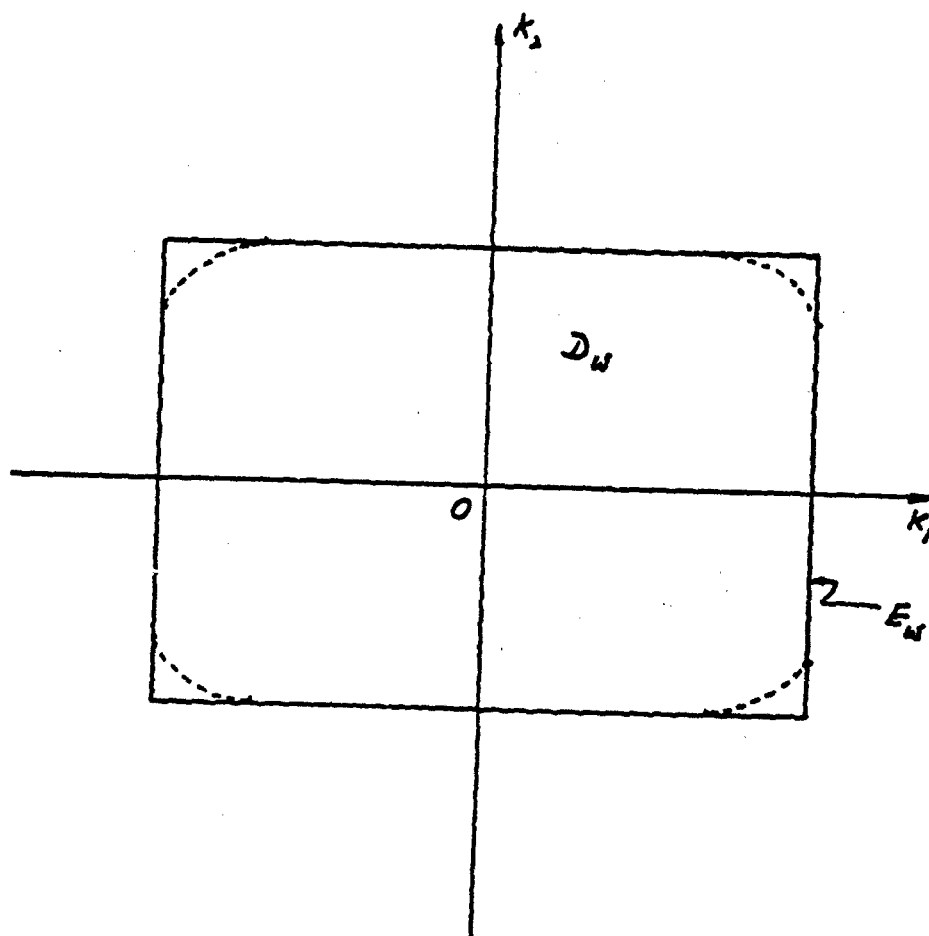


Figure 1. Forbidden region for disturbance rejection



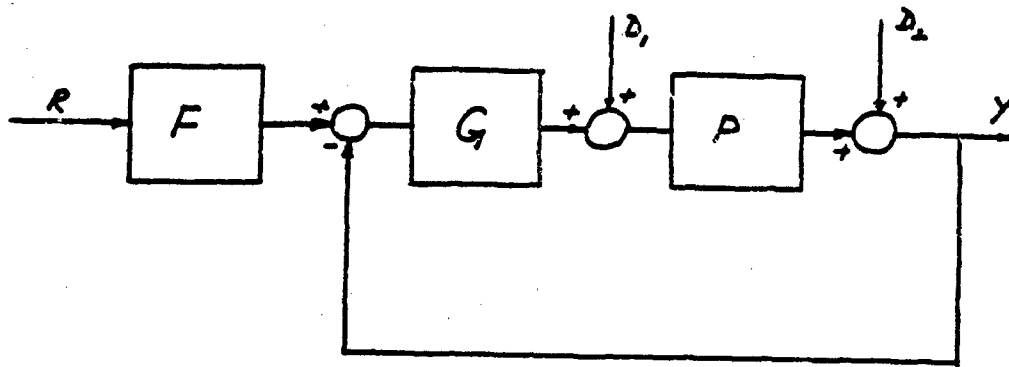


Figure 2. Two degree of freedom configuration

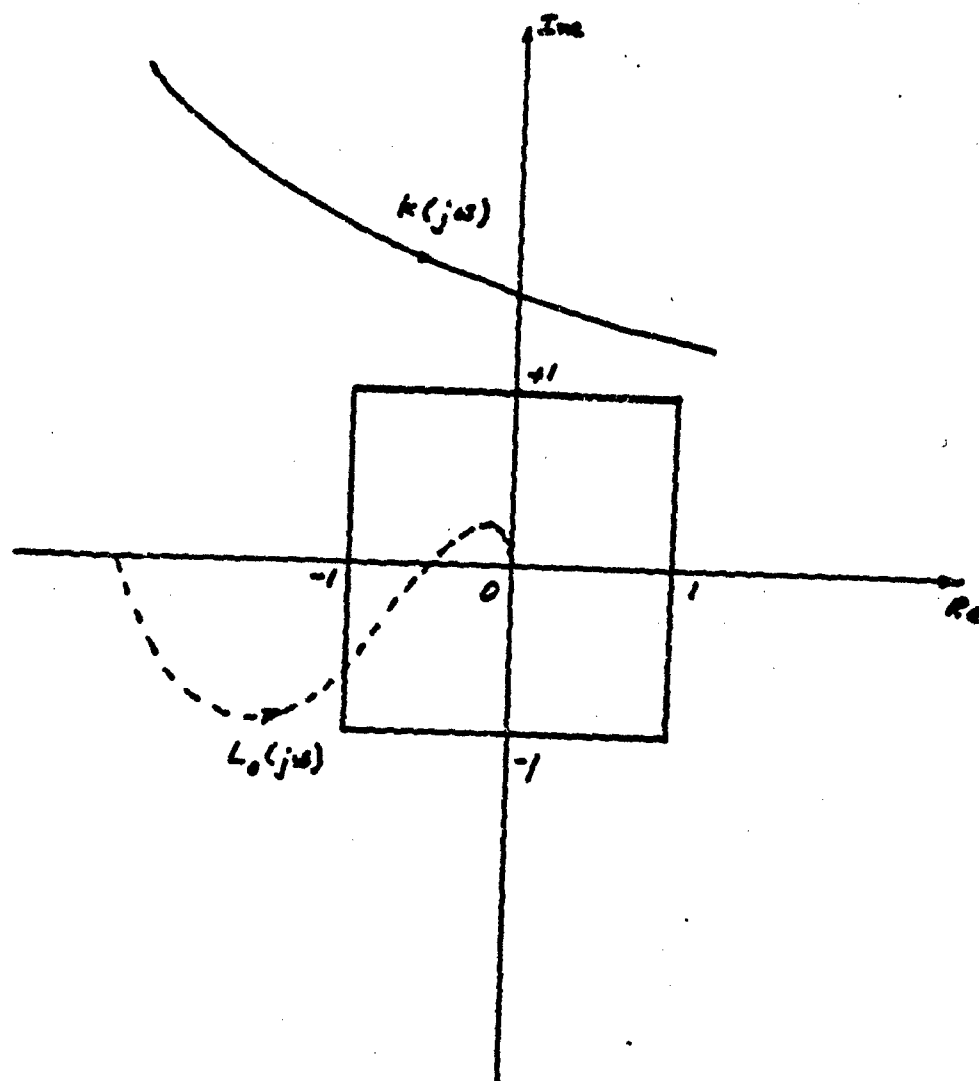


Figure 3. Plot of  $K(j\omega)$  and  $L_o(j\omega)$

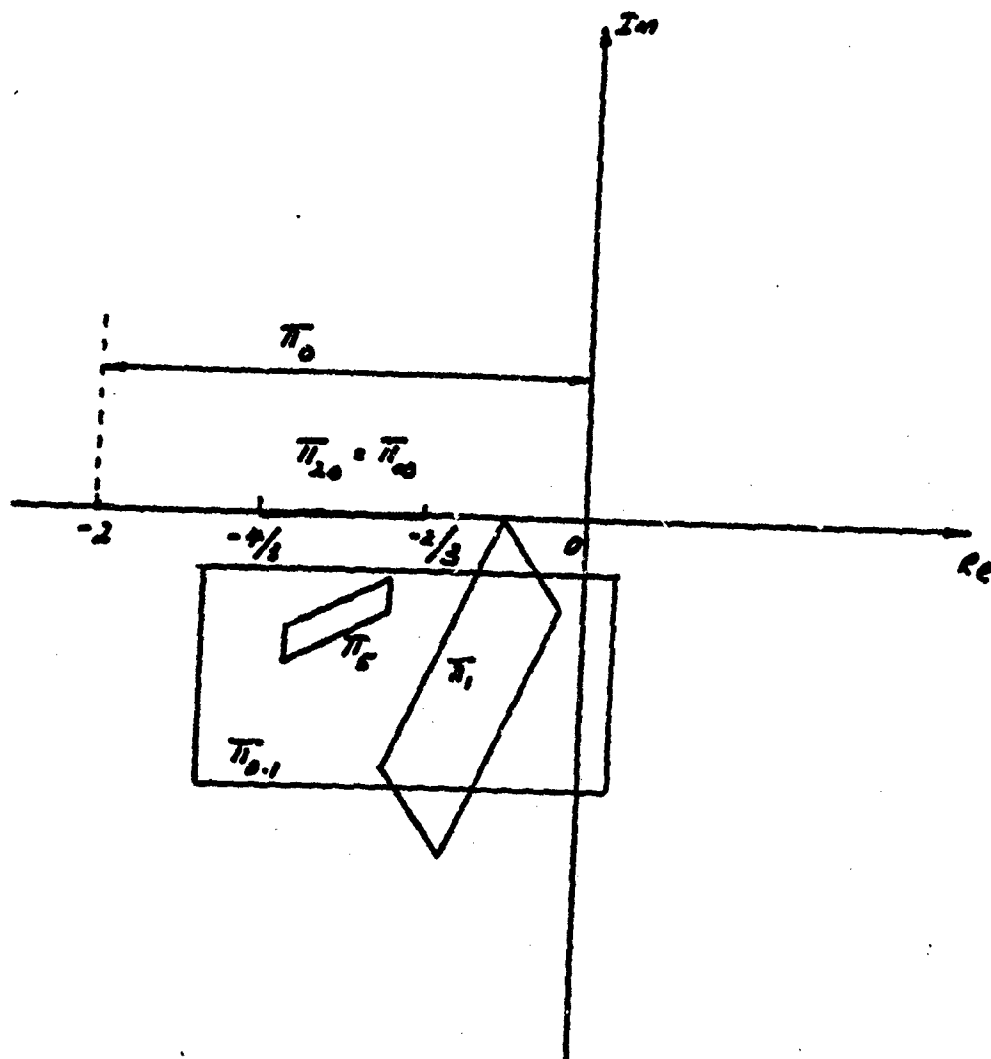


Figure 4. The forbidden regions for  $L_o(j\omega)$  at  $\omega = 0, 0.1, 1, 5, 20$ , and  $\infty$

# Quantitative Design of a Class of Nonlinear Systems with Parameter Uncertainty

S. Oldak\*, C. Baril\* and P.O. Gutman\*

## Abstract

This paper considers the case in which a linear time invariant (LTI) but uncertain plant suffers from nonlinearities  $y = n(x)$  which can be expressed as  $y = K_n x + \eta(x)$ ,  $|\eta(x)| \leq M$ , with  $K_n$  a possibly uncertain scalar. This covers a large and very important class of nonlinearities encountered in practice such as friction, backlash, dead zone and quantization.

Quantitative design techniques are presented for this class for the satisfaction of specifications in the frequency domain. Special attention is paid to the avoidance of limit cycles using describing function theory, although the design method is also amenable of application using other stability criteria such as the circle criteria. Numerical examples are developed illustrating the design procedure.

---

\*Lowdermilk Faculty of Agricultural Engineering, Technion - Israel Institute of Technology, Haifa 32000, Israel

## 1 Introduction

In Quantitative Feedback Theory (QFT) or the Horowitz method, there are three quantitative design techniques for the practical design of feedback control systems with nonlinear uncertain plants [Horowitz 1991]. In the first one [Horowitz 1976], it has been shown that the uncertain nonlinear plant  $w$  can be replaced for design purposes by a linear time invariant (LTI) set of equivalent plants with respect to a set  $\mathcal{A} = \{a\}$  of acceptable system responses. Then, the system can be designed as done in the case of LTI plants with parameter uncertainty.

In the second approach [Horowitz 1982], the uncertain nonlinear plant is substituted by an uncertain LTI set of plants with a set of disturbances at its input. The resulting disturbance set is generally a function of the specified set of acceptable outputs  $\mathcal{A} = \{a\}$ . It was shown that these techniques can be applied to a large class of plants, and that LTI compensation results in the system output  $c \in \mathcal{A}$  despite parameter uncertainty in  $w$ .

The third technique achieves satisfactory performance for LTI plants suffering from amplitude saturation [Horowitz 1983] and from amplitude and rate saturation [Horowitz 1984]. A special case is treated when the LTI plant is unstable [Horowitz and Liao 1986].

This paper presents a fourth technique, applicable to a special class of systems. In this group all the elements of the plant are assumed to be LTI, possibly uncertain, but suffering from the liabilities of a finite number of nonlinearities  $y = n(x)$  which can be expressed as  $y = K_n x + \eta(x)$ ,  $|\eta(x)| \leq M$ , with  $K_n$  a possibly uncertain scalar. Many of the most common nonlinearities are included in this class, such as Coulomb friction, backlash, dead zone and quantization. The characteristics of some of them are illustrated in figure 1. The effects of these nonlinearities have been studied in the last four decades with special dedication [Oldenburger 1956, Brandenburg et al. 1986, Brandenburg, Schafer 1989], since they appear in any servomechanism such as a robot or a machine tool, and they can seriously impair their performance. However the main emphasis has been on the avoidance of limit cycles, and not on specified performance. Moreover it was assumed that all the parameters of the plant are perfectly known, which is not a practical assumption.

In the technique presented in this paper these limitations are overcome. For a large class of problems quantitative design allows the satisfaction of frequency domain specifications despite parameter uncertainty and the presence of nonlinearities. The technique also leads a transparent way of understanding why in some cases limit cycles cannot be avoided and/or arbitrary specifications cannot be achieved. Design examples are given illustrating the design procedure.

## 2 The Design Procedure

Assume that the plant is composed of LTI elements with possibly uncertain parameters, and one nonlinearity of the form  $y = n(x) = K_n x + \eta(x)$ ,  $|\eta(x)| \leq M$ . A good estimate of the effect of this nonlinear element on the system output can be obtained substituting it with  $K_n$ , and adding at its output a "worst case" disturbance. The obtained model is illustrated in figure 2. This approximation has been used for a long time [Aizerman 1963, Peschon 1965, Netushil 1987], but only for analysis; here it will be employed for synthesis.

The effect of any disturbance  $d(t)$  on the closed loop system output is given by

$$c_d(t) = \int_0^t c_s(\tau) d(t - \tau) d\tau$$

where  $c_s(t)$  represents the system output when the disturbance is an impulse. By the construction of the model of figure 2, it is known that  $|d(t)| \leq M$ , so assuming that the final design will be stable, an upper bound of its effect can be found:

$$\begin{aligned} |c_d(t)| &= \left| \int_0^t c_s(\tau) d(t - \tau) d\tau \right| \leq \int_0^t |c_s(\tau)| |d(t - \tau)| d\tau \\ &\leq M \int_0^t |c_s(\tau)| d\tau \end{aligned} \quad (1)$$

Note that this bound is valid even when the system is in a limit cycle mode [Peschon 1965].

Upper bound (1) indicates that the "worst effect" of any nonlinearity, in the specified class, is determined by the system impulse disturbance response. Note that after all the nonlinearities have been substituted using the model of figure 2, and subject to limit cycle avoidance, the design problem becomes that of an uncertain LTI plant with disturbances for which QFT has available design techniques. In the design examples of the following sections it will be shown how the disturbance problems are obtained in a heuristic way from bound (1). This can be done considering a specific time domain model for  $c_s(t)$  and translating to frequency domain. QFT will not be reviewed here since several surveys with a thorough description can be found in the literature [Horowitz, Sidi 1972, Horowitz 1991, Dazzo, Houpis 1988, Gutman et al. 1988].

### 2.1 Example 1

The system of this example is shown in figure 3 embedded in a two degrees of freedom structure. This system can represent a single loop servomechanism in which an electrical or hydraulic motor drives a load through a gear train with backlash [Brandenburg et al. 1986, Brandenburg, Schafer 1989, Thomas 1956]. Notice that backlash is equivalent to a deadzone in the compliant gear train.

The objective of the design is to control  $\theta_m$  despite backlash and plant parameter uncertainty. In this example

$$\Theta_{ref} = \frac{1}{s}; \quad P_1 = \frac{1}{s(J_m s + B_m)}; \quad P_2 = \frac{1}{s(J_l s + B_l)} \quad (2)$$

with

$$K_m \in 0.041[1, 1.2]; \quad K_l \in 4.8[0.85, 1]; \quad B_m \in 0.0032[1, 20] \\ B_l \in 0.00275[0.4, 1]; \quad J_l = 0.0015; \quad J_m = 63.9 \times 10^{-6}$$

and  $b = 0.2$  is the backlash or equivalent deadzone parameter.

The design equations are found substituting the backlash block in figure 3 with the model in figure 2. This gives  $M = b = 0.2$ , and  $K_n = 1$ . With  $I$  given in figure 3, the open loop transmission is defined as

$$L = GP$$

with

$$P = \frac{\Theta_m}{I} = \frac{K_m P_1}{1 + \frac{K_l P_1}{1 + K_l P_2}} \quad (3)$$

The effects of the equivalent disturbance and the command input are considered separately. The system output for a command input  $\theta_{ref}$  is

$$\Theta_m = \frac{FL\Theta_{ref}}{1 + L} = T\Theta_{ref} \quad (4)$$

where  $T$  is defined as the closed loop command impulse response of the system. Specifications on  $T$  hence take the form

$$a(\omega) \leq |T(j\omega)| \leq b(\omega)$$

such as those shown in figure 4 with dotted lines for this example. These specifications can be obtained by the translation of corresponding ones in the time domain [Horowitz 1991, Dazzo, Houpis 1988, Gutman et al. 1988]. The corresponding requirement on  $L(s)$  is

$$\Delta \log \left| \frac{L}{1 + L} \right| \leq \left( \frac{b}{a} \right)_{db} \quad (5)$$

The system output for a disturbance  $D(s)$  is given by

$$\Theta_m(s) = \frac{DW}{1 + L} = ZD \quad (6)$$

with  $W = \frac{\Theta_m}{D} \Big|_{G(s)=0}$ . Thus for the disturbance effect, the frequency domain specifications are of the form

$$|Z(j\omega)| = \left| \frac{W}{1 + L}(j\omega) \right| \leq b_d(\omega) \quad (7)$$

In this example

$$W = -\frac{K_I P_1}{1 + K_I(P_1 + P_2)}$$

To obtain  $b_d(\omega)$  consider expression (6). In order to get small steady state values of the nonlinearity effect, at low frequencies  $|L(j\omega)| \gg 1$  so

$$\frac{\Theta_m}{D} \approx \frac{W}{GP} = -\frac{K_I}{GK_m(1 + K_I P_2)}$$

A Bode plot of  $\frac{W}{P}$  shows that  $\frac{\Theta_m}{D}$  suffers from a resonance peak unless  $G$  is capable of eliminating it. Figure 5 shows the resulting Bode plot of equation (6) when a "smooth"  $G$  is used in the design. In practice it is not desirable to cancel the resonance peak, since this cannot be done exactly, and a very small drift in  $G$  might result in abrupt phase and magnitude changes in  $L(s)$ . The presence of the resonance peak means that the disturbance step response of the closed loop system will be of a very oscillatory but damped nature. A reasonable approximation of this behavior is

$$\theta_{m_s}(t) = c_s(t) \approx K_c e^{-at} \sin \omega_0 t$$

where  $c_s$  denotes the closed loop step disturbance response, then we choose

$$b_d(\omega) = \left| \frac{K_c \omega_0 \omega}{(j\omega + a)^2 + \omega_0^2} \right| \quad (8)$$

Specifications must be set on the maximum effect of the nonlinearity on the system output. In this example  $|c_d(t)| \leq 0.1 = MU$  is chosen as the specification, with  $U = \int_0^t |c_s(\tau)| d\tau$ , and  $M = b$ . Since  $M = 0.2$ ,  $U \leq 0.5$  is sought for all  $t$ . Since it is known that the resonance will occur approximately at  $\omega_0 = 53$  rad/sec, this value is used in equation (8), and from figure 4,  $a = 5$  rad/sec is chosen, since this is approximately the required bandwidth of the closed loop system. Finally  $K_c = 0.07$  is found from simulations of (8) in such a way that  $U = 0.5$  is satisfied by model (8). The resulting  $b_d(\omega)$  is plotted in figure 5.

Limit cycles will be regarded as undesirable in this paper, so the system will be examined to determine whether they can be avoided. The describing function method can be used for this purpose [Gelb, Vander Velde 1968]. Although this technique is only approximate and has some failures, valuable results can be obtained in many servomechanisms if there is enough low pass filtering in the system linear parts [Brandenburg et al. 1986, Brandenburg, Schafer 1989]. Alternatively other stability criteria such as the circle criteria can be used as discussed in section 4. To determine when limit cycle solutions can be avoided, substitute the deadzone nonlinearity by its sinusoidal describing function  $N_0$  and compute the open loop transmission. To avoid limit cycles it is required that (see figure 3) [Gelb, Vander Velde 1968]

$$L_n = GP_n = G \frac{K_m P_1}{1 + \frac{N_0 K_I P_1}{1 + N_0 K_I P_2}} \neq -1 \quad (9)$$



where the subscript  $n$  is used to indicate that describing function is being used. This same requirement could have been obtained computing the loop transmission around the nonlinearity.

It can be seen, e.g. in the Nichols chart, that requirement (9) is equivalent to demand

$$\left| \frac{L_n}{1 + L_n} \right| < \infty \quad (10)$$

which can easily be imposed by obtaining templates of  $P_n$ , and using these to get bounds. This is done similarly as is done for relative stability requirements such as

$$\left| \frac{L}{1 + L} \right| \leq \gamma \text{ db} \quad (11)$$

which must also be imposed.  $\gamma = 3$  db will be used in this example. Note that to obtain the template of  $P_n$ ,  $N_0$  is considered as an uncertain parameter varying over all its possible values. For deadzone [Gelb, Vander Velde 1968]  $0 < N_0 < 1$ . It is convenient at this point to choose a nominal point such that  $L_{n_0} = L_0$ , and the design of the loop transmission can be carried out on a single chart. This is accomplished here having  $N_{0_0} = 1$  at the nominal, and an arbitrary set of nonlinear model parameters. Note that the nominal point can be chosen outside the actual ranges of parameters, so this procedure is general even if  $L$  and  $L_n$  have no common point. We arbitrarily chose  $K_{m_0} = 0.041$ ,  $K_{l_0} = 4.08$ ,  $B_{m_0} = 0.0032$  and  $B_{l_0} = 0.0011$ . Figure 6 shows some of the resulting templates of  $P_n$ .

From here on, the design proceeds as in usual QFT design. Only the most dominant bounds, shown in figure 7, on  $L_0$  given by constraints (5), (7), (10) and (11) are considered.

The next step is to design an  $L_0$  that satisfies these bounds. This is done with special care in this example since, aside from the resonance already found,  $P$  has one antiresonance. This antiresonance cannot be eliminated exactly by compensator  $G$  for the same reasons given above for the resonance, so a "smooth"  $G$  is designed with the peaks of  $P_0$  appearing in  $L_0$  in figure 7.

$$G = \frac{23000(1 + s/3000)(1 + s/2.5 \times 10^4)}{(1 + s/2.5 \times 10^4 + s^2/(2.5 \times 10^4)^2)^2}$$

Note from equation (6) that at low frequencies ( $|L(j\omega)| \gg 1$ ),  $|Z(j\omega)| \rightarrow 0$  as  $\omega \rightarrow 0$  even when  $G(s)$  is of type zero, and for this reason an integrator was not added to the compensator. The prefilter is designed accordingly

$$F = \frac{1}{(1 + s/10)(1 + 1.4s/5 + s^2/25)}$$

The resulting values of  $|T(j\omega)|$  for several design parameters are simulated in figure 4 using equation (4) and with  $K_n = 1$  substituting the nonlinearity. Similarly

$|Z(j\omega)|$  from equation (6) is shown in figure 5. The values of  $U(t) = \int_0^t |c_\delta(\tau)| d\tau$  are shown in figure 8 for different plant parameter combinations. Finally the system is simulated in time domain with the dead zone in place. The step responses, shown in figure 9, are satisfactory. When the nonlinearity is substituted by the model of figure 2, and the equivalent disturbance has a non zero steady state value, linear analysis gives that  $\theta_l$  has a non zero steady state value. As seen in figure 9 this is also the case in the simulations. It can also be observed from these simulations that the effect of the nonlinearity is hardly noticed at the system output  $\theta_m$ . The main reason is that since  $G$  does not eliminate the resonance-antiresonance pair of the plant, the loop transmission  $L$  in figure 7 is designed with more gain than demanded by the specifications for a wide frequency range so that the system can be stabilized. This overdesign can also be observed in figure 5 where the specification is oversatisfied for most of the frequency range. Another reason is that upper bound (1) is conservative tending to some overdesign.

## 2.2 Example 2

In this example we consider the same plant as in Example 1, but in figure 3 we assume that the measurement feedback is obtained from  $\theta_l$  instead of  $\theta_m$ . We now show that limit cycles cannot be avoided. For this compute

$$P_n = \frac{\Theta_l}{I} = \frac{\frac{K_l K_m P_1 P_2 N_0}{1 + N_0 K_l P_2}}{1 + \frac{P_1 N_0 K_l}{1 + N_0 K_l P_2}}$$

with  $N_0$  the describing function of deadzone. Since for deadzone  $0 < N_0 < 1$  the template of  $P_n$  grows to  $-\infty$  db as  $N_0 \rightarrow 0$ . Bounds satisfying constraint (10), will consequently delimits a region which includes the  $-180^\circ$  line for  $|L| < 1$  in the Nichols chart. Consequently any practical design of  $L_0$ , with an excess of more than two poles over zeros, must cross these bounds and limit cycles must be sustained. A similar but more obscure treatment to this case was given in [Thomas 1956].

A similar argument can be used to show that limit cycles cannot be avoided with linear feedback compensators when the feedback measurement is obtained from both  $\theta_l$  and  $\theta_m$  in a cascaded configuration. This suggests the possibility that only nonlinear feedback compensation might be able to deal with limit cycle avoidance in this setting.

## 2.3 Example 3

In this example we consider a similar system as above, only that now backlash is negligible and the main nonlinear effects are a result of dry friction (modelled as an ideal relay) as shown in figure 10. The block diagram of figure 10 is a representation of the laboratory prototype of figure 11. This is a position servomechanism where a DC current controlled motor drives a flexible arm. The ensemble is placed on a moving

platform which oscillates at an angular velocity  $\dot{\theta}_0$  producing a disturbance torque acting via the shaft friction. The motor bearings and additional bearings along the shaft produce the friction torque. Two measurement sensors are needed to obtain the position of the shaft with respect to a fixed reference (one for the shaft and the other for the platform positions), and two potentiometers were used here. Note that this is not a command input problem as in Examples 1 and 2, but a regulator problem where the objective is to set an upper bound of the effect of the disturbance  $\dot{\theta}_0$  on the system output (motor shaft position)  $\theta_m$ .

Transfer functions  $P_1$  and  $P_2$  are defined as in (2) and  $P$  in (3) only that now the parameter ranges are

$$K_m \in 0.041[1, 1.2]; \quad K_l \in 4.8[0.85, 1]; \quad B_m \in 0.0032[0.01, 0.3] \\ B_l \in 0.00275[0.1, 0.3]; \quad J_l = 0.0015; \quad J_m = 63.9 \times 10^{-6}$$

The maximum friction parameter value (maximum saturation level of the ideal relay) is  $F_d = 10$ .

Note that the viscous friction parameter  $B_m$  is very small, so in figure 10,  $x_1(t) + x_2(t) \approx x_1(t)$  for reasonable  $|\dot{\theta}_0|$ . Therefore it will be assumed that the external disturbance  $\dot{\theta}_0$  acts exclusively on the nonlinearity input. When we replace the friction block by the model of figure 2 we have here (see figure 1d)  $K_n = 0$  and  $|d(t)| \leq F_d = 10$ . The transfer function from the equivalent disturbance to the system output is

$$Z(s) = \frac{\Theta_m}{D(s)} = \frac{W}{1 + L}$$

with  $W = \frac{\Theta_m}{D(s)} \Big|_{G(s)=0} = \frac{P}{K_m}$  and  $L = GP$ .

The time domain specifications are  $|\theta_m(t)| \leq 11F_d$  at all  $t$ , and when  $d(t)$  is a step the signal should be under 0.25% of the step amplitude for  $t > 2\text{sec}$  with zero steady state error when  $t \rightarrow \infty$ . The translation of these specifications to frequency domain is done observing that when  $\omega \rightarrow 0$ ,  $|L(j\omega)| \gg 1$  and  $Z(j\omega) \approx \frac{1}{GK_m}$ . So if  $G$  has enough bandwidth a non-oscillatory time domain response can be specified. The zero steady state error requirement imposes an integrator in  $G$  which will appear as a zero at the origin at low frequencies in  $Z$ . The settling time requirement suggests a term of the form  $e^{-3t}$ . Then at low frequencies we have that  $|Z(j\omega)| \approx \frac{K's}{(1+s/3)}$  with  $K'$  a constant. When  $\omega \rightarrow \infty$ ,  $Z(j\omega) \approx W = \frac{P}{K_m}$  and it is observed that  $\left| \frac{P}{K_m} \right|_{\max} < \frac{K''}{(1+s/300)^2}$ , with  $K''$  another constant. From these considerations let

$$b_d(\omega) = \left| \frac{K_c s}{(1 + s/3)(1 + s/300)^2} \right|_{s=j\omega} \quad (12)$$

To determine a suitable value for  $K_c$  we now take into account constraint (1), and numerically we find the value that makes  $U = \int_0^\infty |c_s(\tau)| d\tau \leq 11$ . In this example we

found that  $K_c = 2$  satisfies with the equality sign. Then the frequency specification in this example is that  $|Z(j\omega)| \leq b_d(\omega)$ , shown in figure 12.

To study limit cycle avoidance, the nonlinearity is substituted by its sinusoidal describing function. For the ideal relay  $0 < N_0 < \infty$  [Gelb, Vander Velde 1968]. The associated plant is

$$P_n = \frac{K_m P_{1n}}{1 + \frac{K_i P_{1n}}{1 + K_i P_2}}$$

where

$$P_{1n} = \frac{1}{s(1 + J_m s + B_m + N_0)}$$

The condition for limit cycle avoidance is  $L_n = GP_n \neq -1$ , but instead of using requirement (10) here the more conservative

$$\left| \frac{L_n}{1 + L_n} \right| < 20\text{db}$$

is imposed. Figure 13 shows the resulting bounds on  $L_0$  for the avoidance of limit cycles together with the final design. It is seen that there are no special problems in avoiding these bounds. The nominal point used is  $K_{m0} = 0.041$ ,  $K_{i0} = 4.8$ ,  $B_{m0} = 0.00096$  and  $B_{i0} = 0.000825$ ,  $N_{00} = 1$ .

A relative stability requirement (11) must also be imposed on  $L_0$ .  $\gamma = 6\text{db}$  is used here. The Nichols chart bounds imposed by this specification and (12) are shown in figure 14 where also  $L_0$  is shaped to satisfy the constraints. The resulting compensator is

$$G(s) = \frac{12(s/1.15 + 1)(s/10 + 1)(s/100 + 1)(s^2/280^2 + 1.4s/280 + 1)(s^2/300^2 + 1.4s/300 + 1)}{s(s/50 + 1)(s^2/56.6^2 + 0.01s/56.6 + 1)(s^2/260^2 + 0.6s/260 + 1)(s^2/280^2 + 0.7s/280 + 1)}$$

The magnitude Bode plots of the closed loop system are shown in figure 12. Figure 15 shows the time domain responses of the experimental prototype for an oscillatory  $\theta_0$ . Compensator  $G(s)$  is implemented digitally in a PC-XT computer with a Metrabyte A/D-D/A converter. The translation to  $z$  domain was done using a ramp invariant discretization [Hanselmann 1987] with

$$G(z) = \frac{30.37z^8 - 46.52z^7 + 4.109z^6 + 18.25z^5 - 7.261z^4 + 1.245z^3 - 0.053z^2 + 0.0054z - 0.0015}{z^8 - 2.47z^7 + 3.153z^6 - 2.475z^5 + 0.9903z^4 - 0.236z^3 + 0.042z^2 - 0.0045z + 0.0003}$$

The sampling frequency is 50Hz and the software is written in Turbo Pascal. A pre-sampling filter is also hardware added between the prototype and the computer

$$H = \frac{1}{s^2/150^2 + 1.4s/150 + 1}$$

Figure 15 also shows the simulated responses. It is seen that there is good agreement between the theoretical and the practical results, and that they both oversatisfy the time domain specification with  $|\theta_m(t)| < 40 < 110$ , the reason being that there is overdesign at various frequencies in figures 12 and 14.

### 3 Multiple Nonlinearities

The case of multiple nonlinearities in the plant is treated identically as before [Peschon 1965]. We assume that all the elements of the plant are LTI except for  $m$  nonlinearities  $y_i = K_n x_i + \eta_i(x_i)$ ,  $|\eta_i(x_i)| \leq M_i$ ,  $i = 1 \dots m$ .

Describing function theory can also be used in this case, when there is enough LTI low pass filtering between each of the nonlinearities [Gelb, Vander Velde 1968]. Now the possibly complex amplitudes of the describing functions of each nonlinearity are interrelated by their interconnections with the LTI elements. Thus it is possible to find templates of  $P_n$  and bounds  $B(\omega)$  due to requirement (10). The dependence of the describing function values on each other might make this procedure difficult. One simplification is to consider each nonlinearity as an independent uncertain parameter (see [Brandenburg, Schafer 1989] for example), which will however result in more uncertainty in the template of  $P_n$  than inherently needed.

The effect of each nonlinearity on the system output must be specified  $|c_d(t)|$  and translated to frequency domain giving specifications  $b_{d_i}(\omega)$ ,  $i = 1, \dots, m$ , with the sensitivity requirements obtained by substituting each nonlinearity with the model of figure 2. Only the most dominant constraints are considered on a Nichols chart, otherwise the procedure is as in the single nonlinearity case.

### 4 Use of the circle criterion

The circle criterion [Hsu, Meyer 1968] can also be used for assuring that the final design is free from limit cycle solutions. Its advantage is that is exact, as opposed to the describing function method which is approximate. For simplicity, only the most general nonlinearity case will be considered here, including time varying and hysteresis elements, and only one nonlinearity is allowed in the system. Extensions can be done to more restrictive classes which will result in less stringent stability bounds. In any case, the circle criteria, being a sufficient condition on stability, is more demanding than the describing function method.

Let  $x(t)$  and  $y(t)$  be the input and the output of the nonlinearity respectively. For the application of the circle criteria, it will be demanded that

$$a \leq \frac{y(t)}{x(t)} \leq b$$

for all  $t$ , with  $0 < a < b \leq \infty$ . Note that this class excludes nonlinearities such as the backlash hysteresis from figure 1e. An additional restriction is that when  $b = \infty$ , every bounded  $x(t)$  results in  $y(t)$  bounded.

Denote  $L_c(s)$  as the linear loop transmission around the nonlinearity.  $L_c(s)$  is assumed to be stable, otherwise see [Hsu, Meyer 1968].

The circle criterion states that a sufficient condition for the avoidance of limit cycles is that

$$\left| \frac{\frac{a+b}{2} L_c(s)}{1 + \frac{a+b}{2} L_c(s)} \right| < \left| \frac{b+a}{b-a} \right| \quad (13)$$

which can be easily checked in the Nichols chart when  $L = L_c(s)$ , using the templates of  $P$ .

In the more general case, when  $L \neq L_c(s)$  (i.e. it is not possible to write  $L_c = GL'_c(s)$  with  $L'_c$  independent of  $G$ ), a computer program can be set to find bounds on  $G(s)$ , by means of a nonlinear search procedure. These bounds define regions in the logarithmic gain-phase plane where condition (13) is satisfied. Then, bounds obtained for the nominal loop transmission  $L_0 = GP_0$  can also be translated to bounds on  $G(s) = \frac{L_0}{P_0}$ . Compensator  $G(s)$  is shaped directly using the most dominant bounds.

Note that the circle criteria is also a sufficient condition for square integrable ( $L_2$ ) stability if the inputs belong to the  $L_2$  class [Atherton 1984].

## Conclusions

This paper has presented a quantitative design procedure for a very important class of nonlinearities. Its main contribution is that it provides a novel way to translate the effect of these nonlinearities on the system output to frequency domain. Thanks to QFT which provides pointwise design in the frequency domain, it has been shown how this technique can lead to the transparent design of a loop transmission and prefilter that satisfy specifications and avoid limit cycle solutions. Worth emphasizing are its simplicity, and its wide application to many practical problems.

The main disadvantage of this method is that the disturbance bound  $b_d$  used for the design is conservative. This is because the rate of variation of the equivalent disturbance in the nonlinearity model is not taken into account in the design. Another important limitation is that when describing function is used for limit cycle determination, although the design procedure is simplified, there are doubts about the validity of the analysis. The circle criterion can be used instead, but in general, the design becomes more complicated and the system bandwidth may increase.

It was shown in various practical examples that the introduced method can give valuable insight and good results.

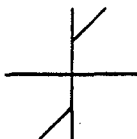
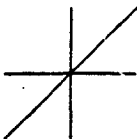
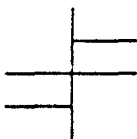
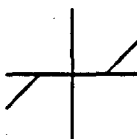
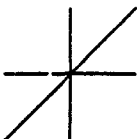
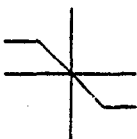
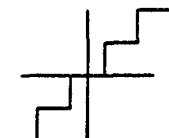
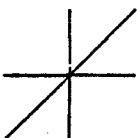

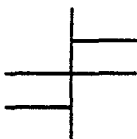
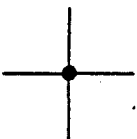
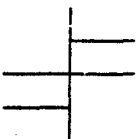
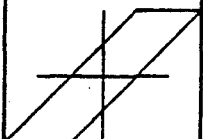
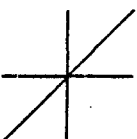
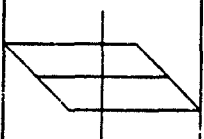
## References

- [Aizerman 1963] Aizerman M.A., "Theory of Automatic Control", Addison-Wesley, 1963.

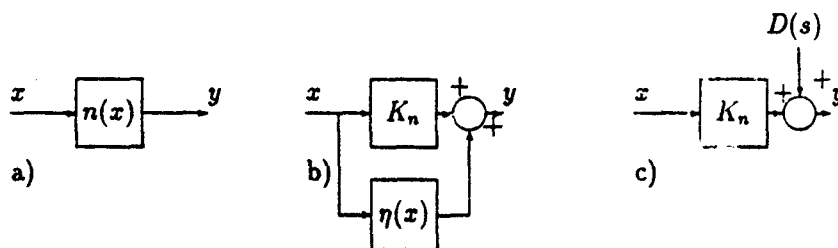
- [Atherton 1984] D.P. Atherton, "Stability of Nonlinear Systems", Research Studies Press, 1984.
- [Brandenburg et al. 1986] G. Brandenburg, H. Unger, A. Wagenpfeil, "Stability Problems of a Speed-Controlled Drive in an elastic System with backlash and Corrective measures by a Load Observer", *Proc. of the Int. Conference on Electrical Machines*, Munchen, 1986.
- [Brandenburg, Schafer 1989] G. Brandenburg, U. Schafer, "Adaptive Compensation of Simultaneously Acting Backlash and Coulomb Friction in Elastic Two-Mass Systems of Robots and Machine Tools" *Proc. of the IEEE Int. Conf. on Cont. and Applications*, Jerusalem, 1989
- [Canudas et al. 1987] C. Canudas, K.J. Astrom, K. Braun; "Adaptive Friction Compensation in DC-Motor Drives", *IEEE Journal of Robotics and Automation*, Vol. RA-3, No. 6, December, 1987, pp. 681-685.
- [Dazzo, Houpis 1988] J.J. D'azzo, C.H. Houpis, "Linear Control System Analysis and Design, Conventional and Modern", McGraw-Hill, 1988
- [Gelb, Vander Velde 1968] A. Gelb and W.E. Vander Velde, "Multiple Input Describing Functions and Nonlinear System Design" McGraw Hill, 1968
- [Gutman et al. 1988] P.O. Gutman, H. Levin, L. Neumann, T. Sprecher, E. Venezia; "Robust and Adaptive Control of a Beam Deflector", *IEEE Trans. on Aut. Cont.*, VI. 33, No. 7, 1988, pp. 610-619.
- [Hanselmann 1987] . Hanselmann, "Implementation of Digital Controllers - A Survey", *Automatica*, Vol. 23, No. 1, ,1987, pp. 7-32.
- [Horowitz, Sidi 1972] I. Horowitz, M. Sidi; "Synthesis of Feedback Systems with Large Plant Uncertainty for Prescribed Time Domain Tolerances", *Int. J. of Control*, 16, 1972, pp. 287-309.
- [Horowitz 1976] I. Horowitz, "Synthesis of feedback systems with non-linear time-varying uncertain plants to satisfy quantitative performance specifications", *Proc. of the IEEE*, 64, 1976, pp. 123-130.

- [Horowitz, Sidi 1980] I. Horowitz, M. Sidi, "Practical design of feedback systems with uncertain multivariable plants", *Int. J. of Systems Sci.*, 11, No. 7, 1980, pp. 851-875.
- [Horowitz, Loecher 1981] I. Horowitz, C. Loecher, "Design of a  $3 \times 3$  multivariable feedback system with large plant uncertainty" *Int. J. of Control*, 33, No. 4, 1981, pp. 677-699.
- [Horowitz 1982] I. Horowitz, "Feedback systems with non-linear uncertain plants", *Int. J. Control*, 36, No. 1, 1982, pp. 155-171.
- [Horowitz 1983] I. Horowitz, "A synthesis theory for a class of saturating systems", *Int. J. Control*, 38, 1983, pp. 169-187.
- [Horowitz 1984] I. Horowitz, "Feedback systems with rate and amplitude limiting", *Int. J. Control*, 40, 1984, pp. 1215-1229.
- [Horowitz and Liao 1986] I. Horowitz, Y.K. Liao, "Quantitative nonlinear compensation design for saturating unstable uncertain plants", *Int. J. Control*, 44, 1984, pp. 1137-1146.
- [Horowitz 1991] I. Horowitz, "Survey of quantitative feedback theory", *Int. J. Control*, 53, No. 2, 1991, pp. 255-291.
- [Hsu, Meyer 1968] J. Hsu, A. Meyer; "Modern Control Principles and Applications", Mc-Graw Hill Book Co., USA, 1968.
- [Netushil 1987] A. Netushil, "Teoría del Mando Automático", Ed. Mir, Moscow, (in Spanish), 1987
- [Oldak, Gutman 1992] S. Oldak, P.O. Gutman, "Self Oscillating Adaptive Design of Systems with Dry Friction and Significant Parameter Uncertainty", *Submitted for publication to Int. Journal of Adaptive Control and Signal Processing*, 1992
- [Oldenburger 1956] R. Oldenburger, "Frequency Response", The American Society of Mechanical Engineers, The MacMillan Co., New York, 1956
- [Peschon 1965] J. Peschon, "Disciplines and Techniques of Systems Control", Blansdel Publishing Co., New York, 1965
- [Thomas 1956] C.H. Thomas, "Stability Characteristics of Closed-Loop Systems with Dead Band", in [Oldenburger 1956].

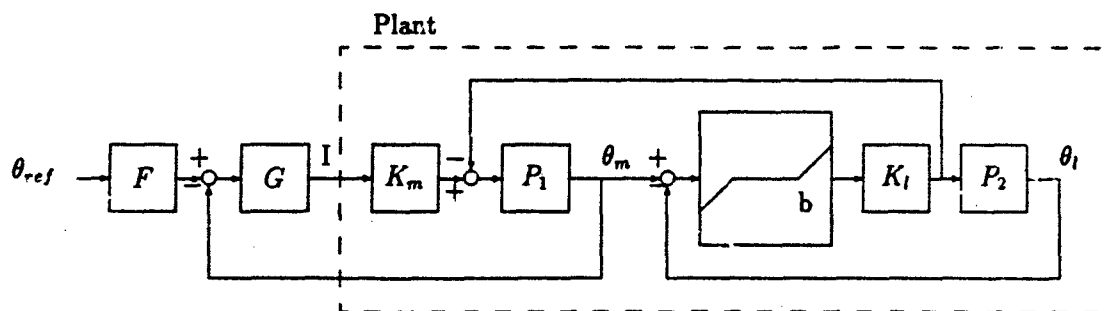


Name	$n(x)$	$K_n x$	$\eta(x)$
a) Preload			
b) Dead Zone			
c) Quantization			
d) Dry Friction			
e) Backlash			

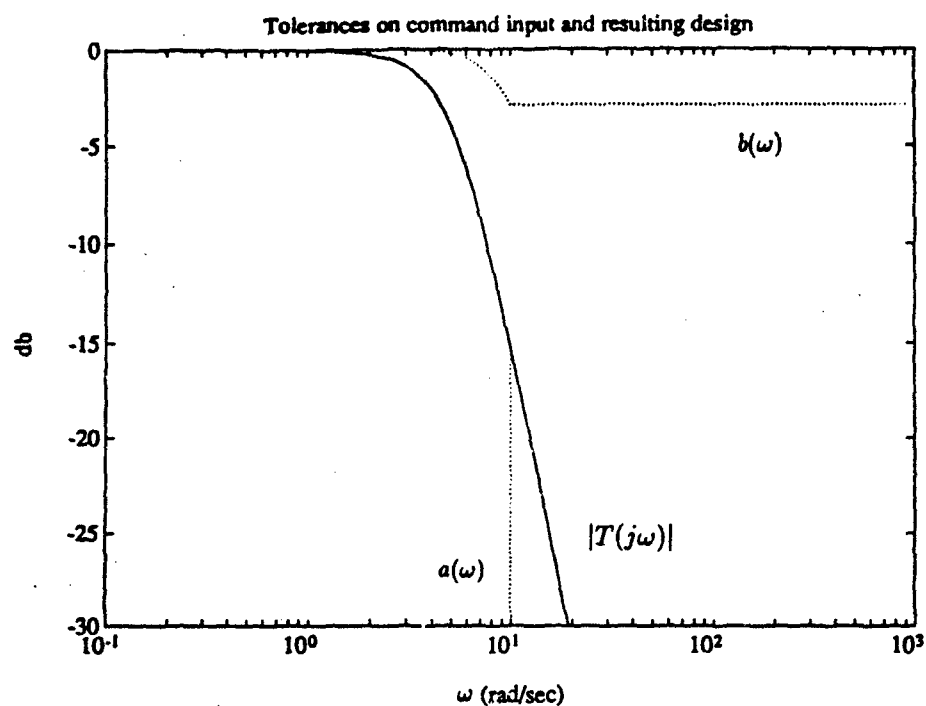
• **Figure 1** Some members of the class of nonlinearities  $y = n(x) = K_n x + \eta(x)$ ,  $|\eta(x)| \leq M$ .



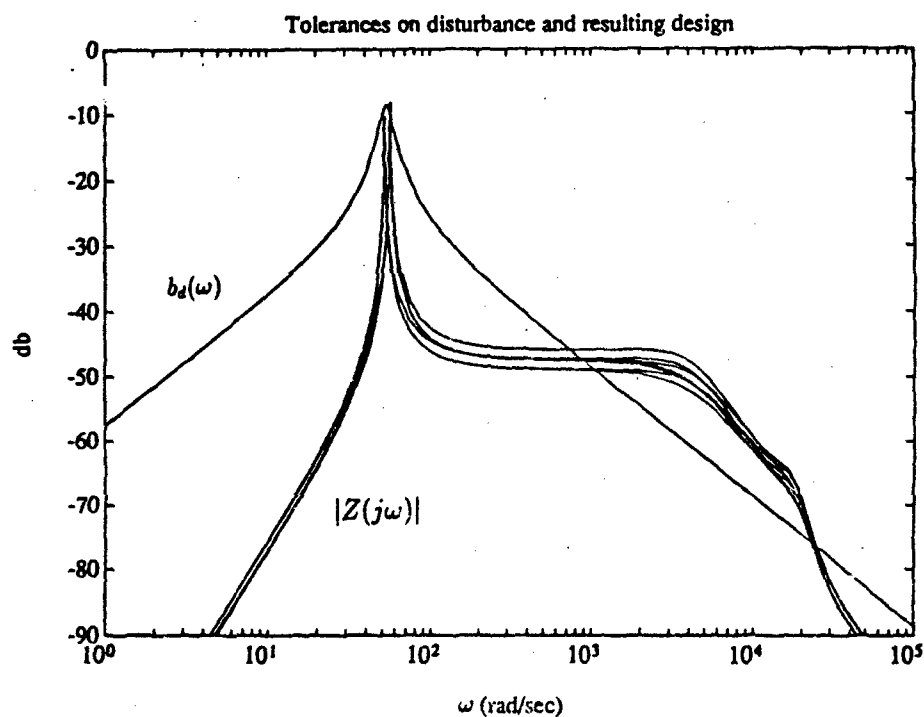
- **Figure 2** Model obtained from a nonlinearity  $y = n(x) = K_n x + \eta(x)$ ,  $|\eta(x)| \leq M$ . a, b) are exact representations of the nonlinearity. c) Approximate model of the nonlinearity, note that  $|d(t)| \leq M$ .



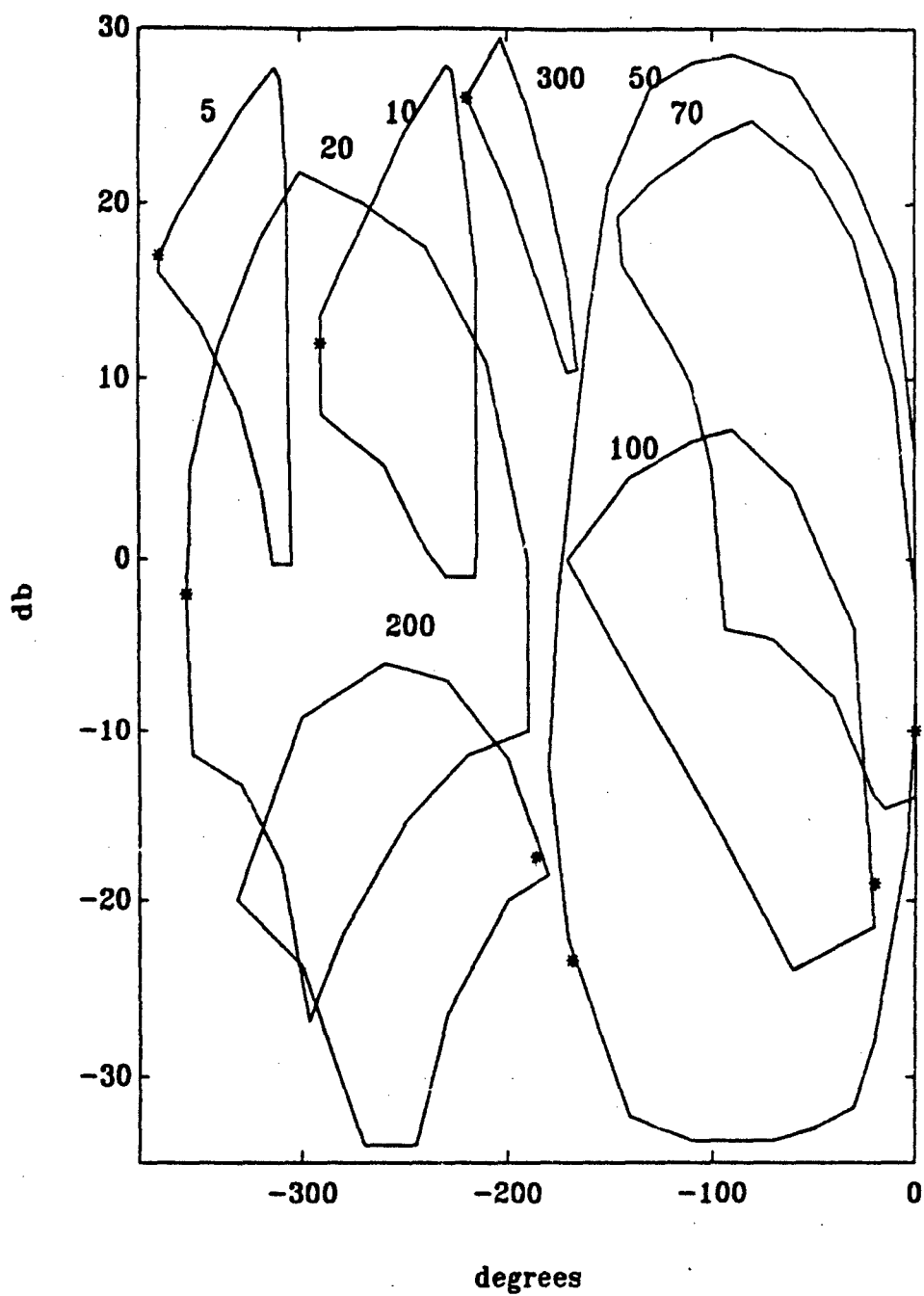
- **Figure 3** Closed loop system of Example 1.



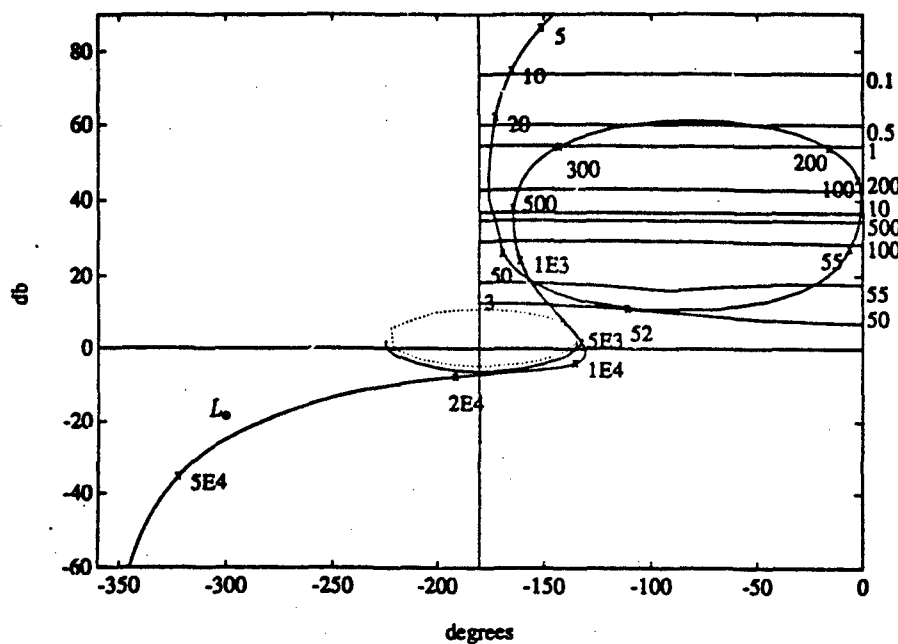
• Figure 4 Closed loop tolerances  $a(\omega) \leq |T(j\omega)| \leq b(\omega)$  and resulting design for Example 1.



• Figure 5 Closed loop tolerances on the maximum nonlinearity effect on the system output,  $|Z(j\omega)| \leq b_d(\omega)$  and resulting design for Example 1.

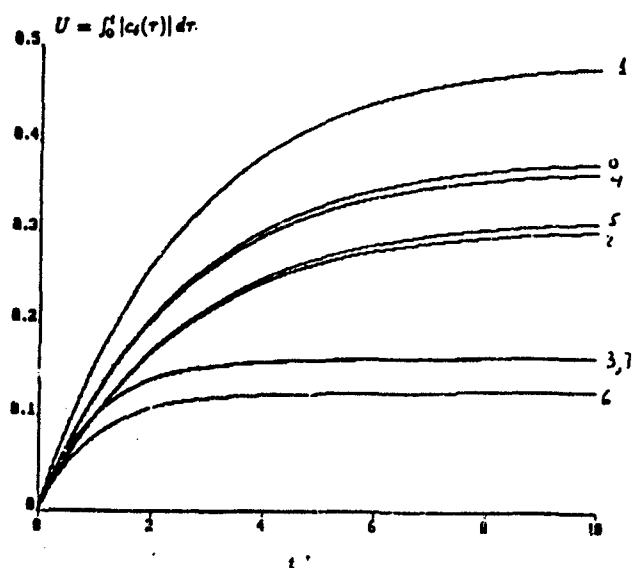


• **Figure 6** Some templates of  $P_n$  as a function of frequency [rad/sec] in Example 1 for the avoidance of limit cycles. The frequency is marked next to the templates, the nominal point denoted with \*.

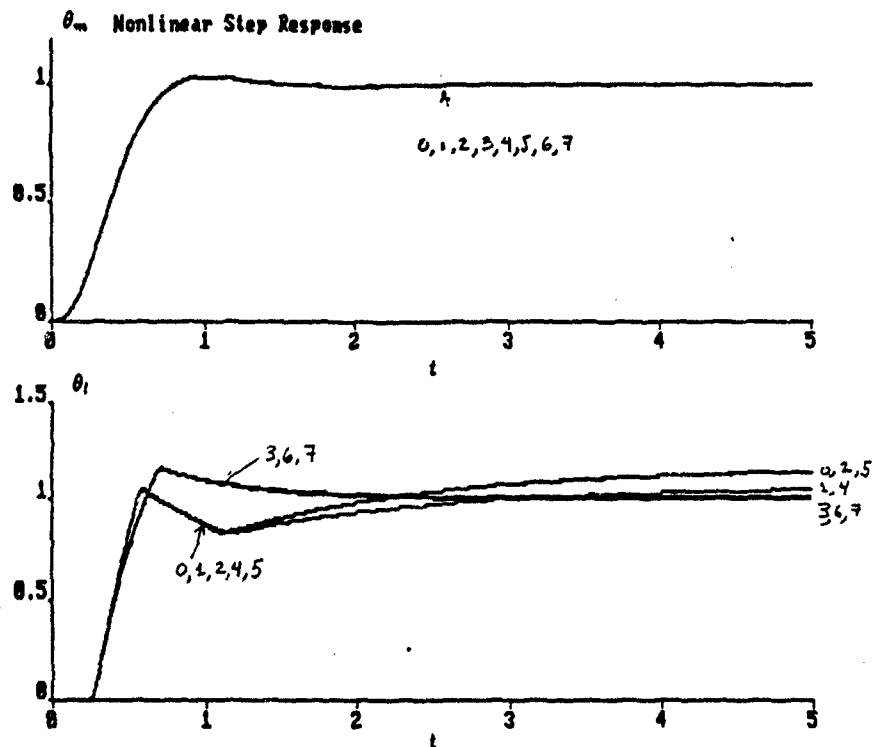


• Figure 7 Nichols chart with the most dominant bounds and design of  $L_0$  for Example 1.

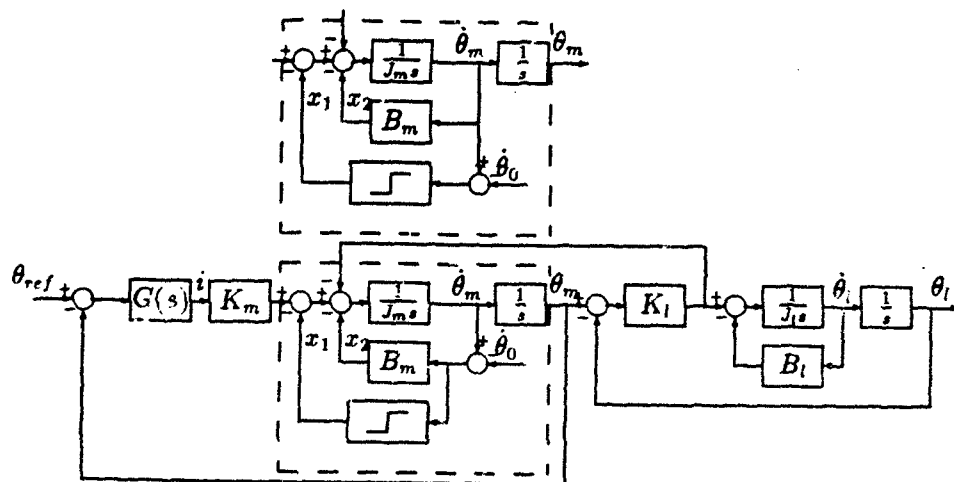
Case	$K_m$	$K_l$	$B_m$	$B_l$
0	0.041	4.08	0.0032	0.0011
1	0.041	4.8	0.0032	0.0011
2	0.0492	4.08	0.0032	0.0011
3	0.0492	4.8	0.0032	0.00275
4	0.041	4.08	0.064	0.0011
5	0.0492	4.08	0.064	0.0011
6	0.0492	4.08	0.064	0.00275
7	0.0492	4.8	0.064	0.00275



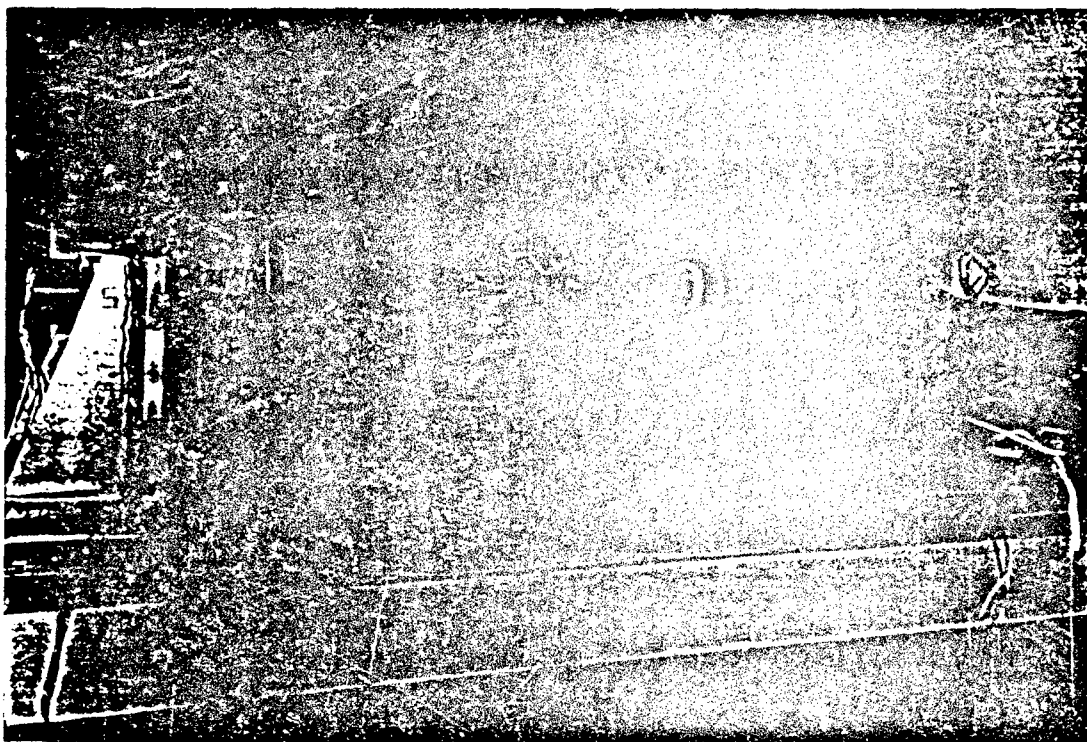
• Figure 8 Resulting values of  $U(t) = \int_0^t |c_s(\tau)| d\tau$  for different plant parameter combinations.



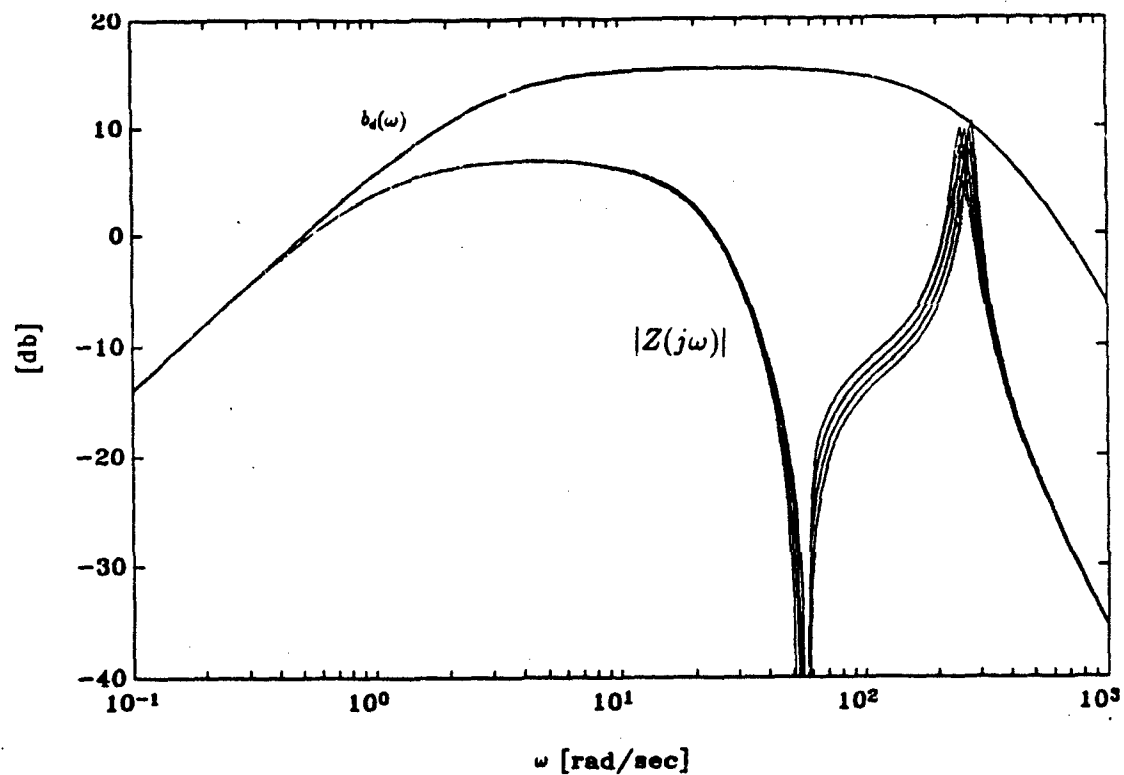
• Figure 9 Step responses of the system of Example 1.



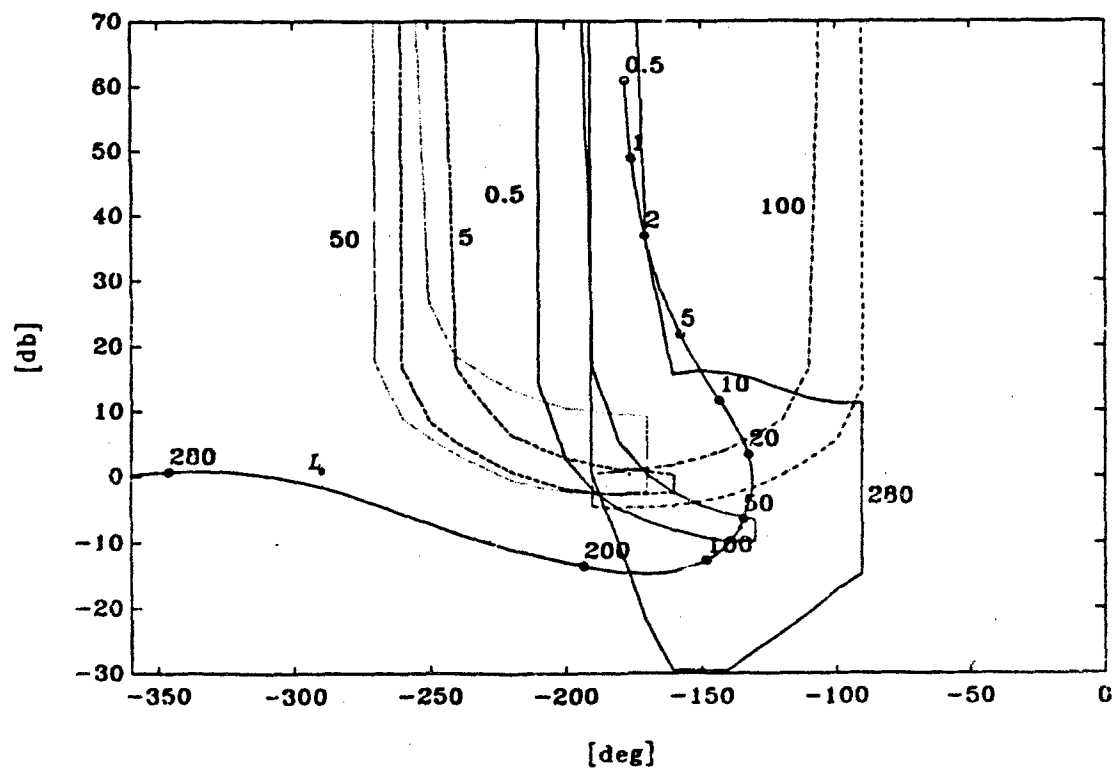
• Figure 10 Block diagram of a 2-mass system with dry friction. The block in the upper part of the diagram is the model used for disturbance attenuation design.



• Figure 11 DC motor position servo prototype of Example 3.

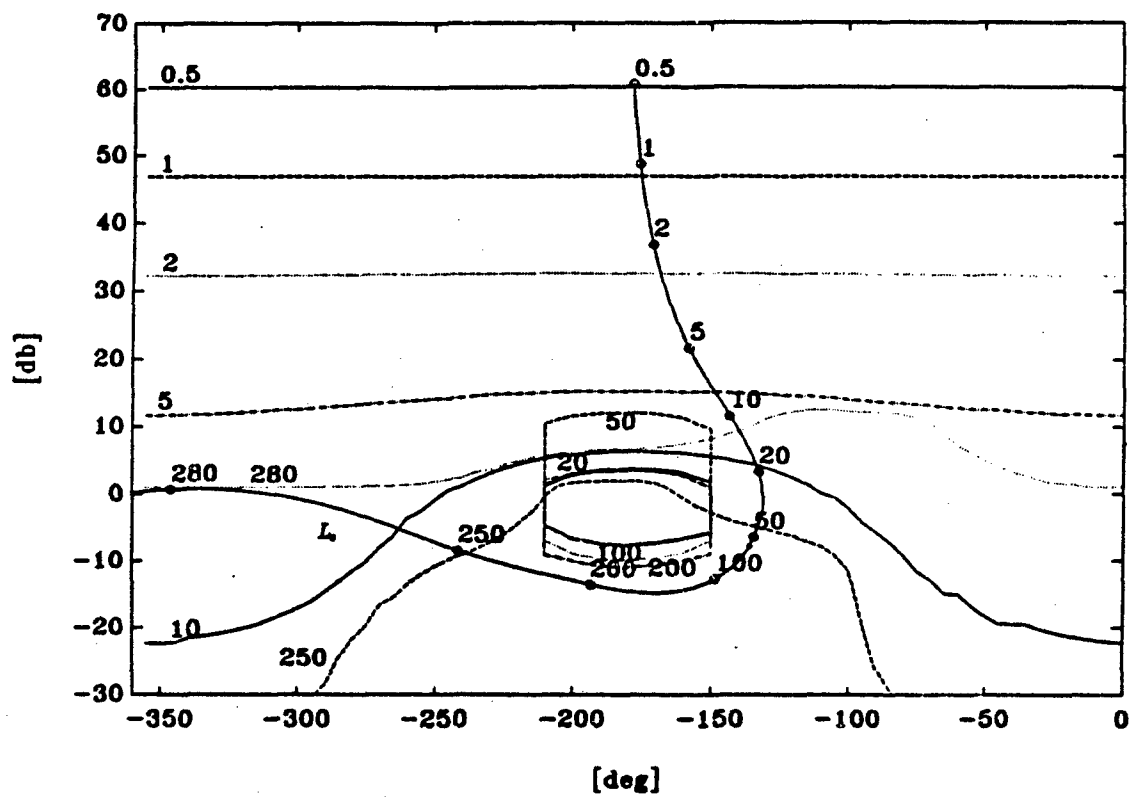


• **Figure 12** Closed loop frequency domain specification and magnitude Bode plot of  $|Z(j\omega)|$  in Example 3.

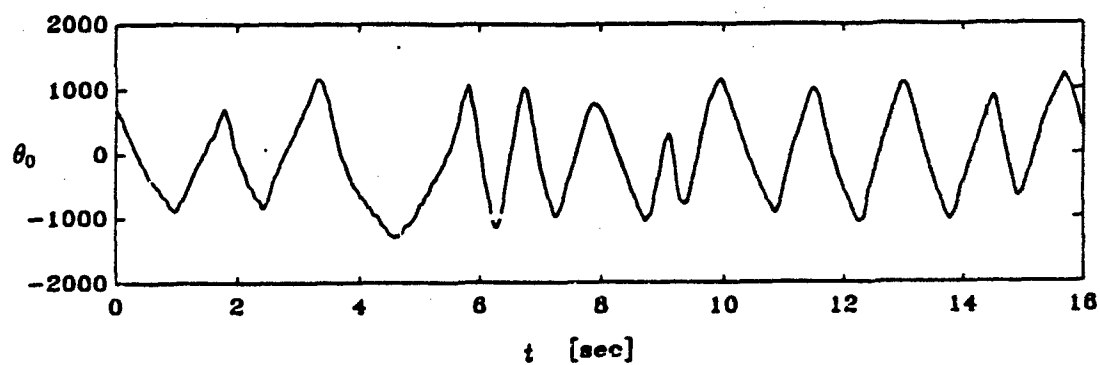
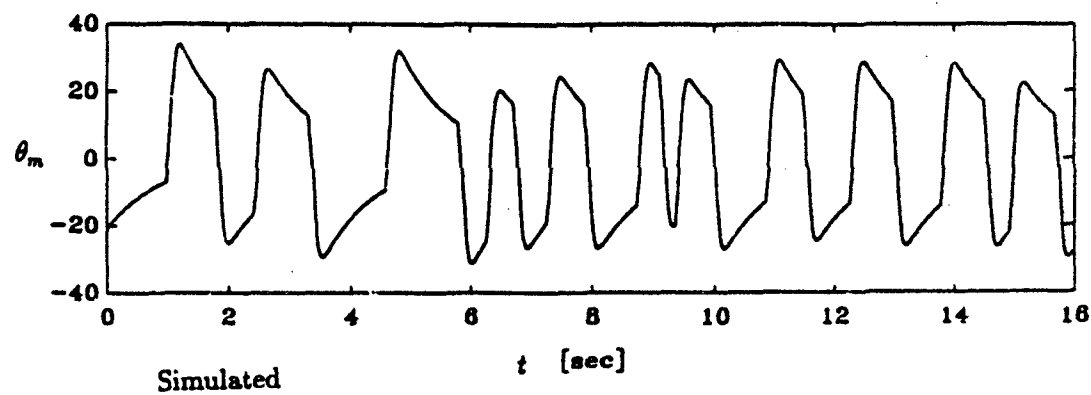
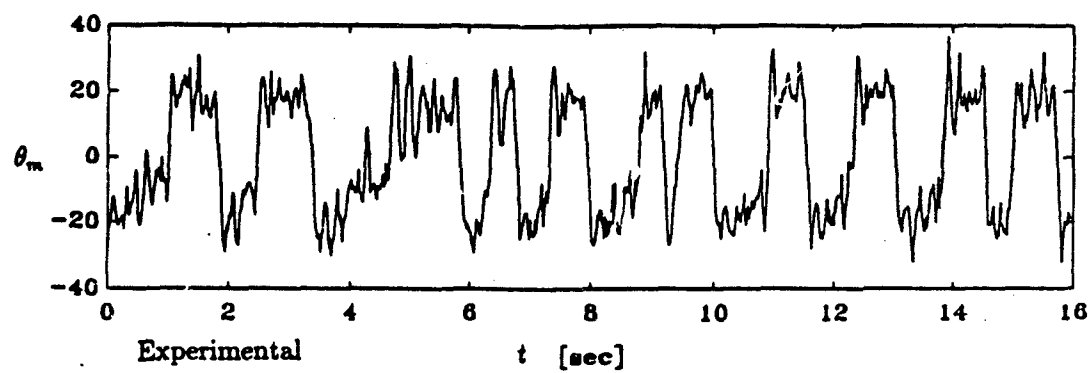


• **Figure 13** Bounds on  $L_0$  for the avoidance of limit cycles, and final design.





• Figure 14 Nichols Chart with stability and disturbance attenuation bounds for the design of  $L_0$  in Example 3.



• Figure 15 Experimental and simulated time domain responses of the laboratory DC position servo system.

# THE LOOP GAIN-PHASE SHAPING DESIGN PROGRAMS\*

F. N. Bailey<sup>+</sup>  
C.-H. Hui<sup>++</sup>  
A. Punyko<sup>+</sup>

## 1. INTRODUCTION

The Loop Gain-Phase Shaping Design Programs (LGPSDP) are a series of programs for computer aided design of SISO control systems using the method of loop gain-phase shaping (LGPS) developed by I. Horowitz, et. al. [1,2]. At present the LGPSDP series includes programs for 1) generating process uncertainty templates (TEMP21 and TEMP30), 2) generating gain performance boundaries (PBOUND20), 3) generating phase performance boundaries (TBOUND10), 4) generating stability boundaries (SBOUND11) and 5) fitting a rational function to given gain-phase boundaries (LOOP20). All of these programs were developed at the Department of Electrical Engineering of the University of Minnesota.

The LGPSDP programs are graphics oriented with the user entering data on a graphics display appropriate to the problem and obtaining results as graphics displays of templates, boundaries, etc. Programs in the LGPSDP series use file formats that are Matlab compatible so that further processing or display in the Matlab environment is easily accomplished.

All programs in the LGPSDP series runs under DOS on IBM PC/AT and PS/2 or compatible computers with Enhanced Graphic Adapter (EGA) or Video Graphics Array (VGA) graphics. Since some of the algorithms are computation intensive, a math coprocessor (80x87) is strongly recommended.

## 2. THE TEMPLATE PROGRAMS (TEMP21 and TEMP30)

The Template Programs allows the user to generate and save process uncertainty templates describing gain-phase variations of process transfer functions having uncertain coefficients. Generated templates are saved in the .TPL format for use in the Gain or Phase Performance Boundary Programs (PBOUND20 or TBOUND10).

Conceptually, the process uncertainty template  $Q(\omega)$  describes, at frequency  $\omega$ , the gain and phase variations that occurs in a transfer function due to specified parameter uncertainty. Given a transfer function

$$P(s; \alpha) = \frac{\sum_i b_i(\alpha) s^i}{\sum_j a_j(\alpha) s^j} \quad (1)$$

with the parameter vector  $\alpha \in A \subset \mathbb{R}$  and nominal parameter values  $\alpha_0$ , the template  $Q(\omega)$  describes a region in the N-plane (Nichols plot) or C-plane (Nyquist plot) occupied by the complex values of  $P(j\omega; \alpha)$  as  $\alpha$  varies in  $A$ . The template nominal point  $q$  is the value  $P(j\omega; \alpha_0)$ . For a detailed discussion of templates and their computation see [3].

\* This work was supported in part by a grant from The US-Spain Joint Committee for Scientific and Technological Cooperation under Project No. CCB 8504018

<sup>+</sup> Department of Electrical Engineering, University of Minnesota, 200 Union St. SE, Minneapolis, MN, 55455 USA

<sup>++</sup> The DSP Control Group, 4600 Pentagon Pk. Suite 100, Edina, MN, 55435 USA

## 2.1 PROGRAM OPERATION

The Template Program requires the input of a process model in the transfer function form shown in (1). Uncertain coefficients in the numerator and denominator polynomial must be expressed as affine functions of a set of parameters  $\alpha_1, \alpha_2, \dots, \alpha_q$  whose nominal values and ranges of variation are specified by the user.

At the beginning the user is asked to choose a procedure for entering the parametric transfer function (1). This function can be entered from a file (with a .TRF extension) or defined at the keyboard using a built-in transfer function entry subroutine. User defined transfer functions can be saved and saved transfer functions can be edited after entry. They are stored in a user specified file name with a .TRF extension. Next the user is asked to supply a template frequency and other data appropriate to the problem.

For each user specified frequency  $\omega$ , the program generates points on the boundary of the template  $Q(\omega)$ . This template boundary can be displayed in either the N-plane (Nichols format) or the C-plane (Nyquist format).

## 2.2 ALGORITHMS

The TEMP21 program uses a special fast algorithm described in [4]. While this algorithm is very fast it assumes that parameter variations in the numerator are independent of those in the denominator. In some cases this is acceptable while in others it leads to considerable over estimation of template size. The TEMP30 program uses another algorithm described in [5] that circumvents this assumption at the price of additional complexity and template generation time.

## 2.3 COMMENTS AND LIMITATIONS

Both of the template programs described above have the following limitations (for further detail see [3]):

- a. Uncertainty in polynomial coefficients can only be specified as affine functions of the uncertain parameters. More complex relations must be reduced to this form.
- b. Parameter variation ranges may not cross zero.
- c. The transfer function may not have poles or zeros at the user specified template frequencies for any parameter values in the specified ranges. (If poles or zeros are detected at template frequencies, a warning is given and the resulting template may be unreliable.)

## 3. THE GAIN PERFORMANCE BOUNDARY PROGRAM

The Gain Performance Boundary Program allows the user to generate and save gain performance boundaries using process uncertainty templates and closed loop system gain performance specifications. The templates must be LGPSDP files in the .TPL format generated by TEMP21, TEMP30 or equivalent programs. Generated boundaries can be saved in the .PBD format for use in the fitting program LOOP20.

Conceptually, a gain performance boundary describes a region (in the N-plane or C-plane) that the nominal open loop gain function  $L_o(j\omega)$  must avoid to meet closed loop gain performance specifications. A gain performance boundary is obtained by moving a process uncertainty template over the M-contours (closed loop gain contours) of a Nichols Chart. Given a template  $Q(\omega)$ , with its nominal point  $q$  located at the N-plane point  $(g, \phi)$ , there is an associated total closed loop gain variation  $\delta M(g, \phi)$  (as indicated by the M-contours) over the entire template. Given a closed loop gain performance specification  $\delta T(\omega)$ , the gain performance set  $B_{gp}(\omega)$  represents the set of all location of the template [as indicated by the  $(g, \phi)$  location of its nominal point  $q$ ] such that  $\delta M \geq \delta T(\omega)$ . The gain performance boundary  $\partial B_{gp}(\omega)$  is the boundary of this set.

### 3.1 PROGRAM OPERATION

The program initially requests the file name of a template. Here the user may enter a complete template LGFSDP file name or ask for a display of all .TPL files in the current directory. The program then asks for the desired value of the closed loop gain performance specification  $\delta T$ .

The gain performance boundary  $\partial B_{pg}(\omega)$  is located by a search procedure similar to the manual procedure described in [2]. For a fixed phase location  $\phi_i$  of the template nominal point  $q$ , the total closed loop gain variation over the template  $Q(\omega)$ , with nominal point located at  $(g, \phi_1)$ , is  $\delta M(g, \phi_1)$ . The search for the intersection of the boundary  $\partial B_{pg}(\omega)$  with the N-plane set  $\phi = \phi_i$  involves finding the roots  $g^*(\phi_i)$  of the nonlinear relation

$$\delta M(g, \phi_i) - \delta T(\omega) = 0 \quad (2)$$

For each  $\phi_i$ , the roots  $g^*(\phi_i)$  of (2) define points of the boundary  $\partial B_{pg}(\omega)$  lying on the line  $\phi = \phi_i$ . Thus the N-plane curve  $g^*(\phi)$ , for  $\phi \in [-180^\circ, 180^\circ]$ , describes the entire boundary in the  $(g, \phi)$ -plane. Typically there is only one root for each  $\phi$ , but multiple roots are possible as  $\partial B_{pg}(\omega)$  can be multiple valued along lines of constant  $\phi$ .

To begin a boundary search the user selects "Search a Phase Range" in the program menu. The user is then asked to enter data which specifies the search parameters. Search results are plotted in a Nichols plot. Searches can be varied and repeated as desired. A sequence of search results can be combined to reveal the entire gain performance boundary.

A useful tool in guiding searches is the Cross Section Plot. A cross section plot is a plot of the magnitude  $\delta M(g, \phi)$  vs.  $g$  for a fixed  $\phi$ . A line of magnitude  $\delta T$  is also plotted on the cross section plot. By noting intersections of the  $\delta M(g, \phi)$  curve with the  $\delta T$  line one can readily locate all points on  $\partial B_{pg}(\omega)$  at the specified value of  $\phi$  and thus easily identify multiple valued regions in the boundary.

### 3.2 ALGORITHM

The program uses a modified bisection algorithm to find the roots  $g^*$  of (2). The algorithm iterates on  $g$  until  $\delta M(g, \phi) - \delta T(\omega) < \epsilon$ . When possible, convergence of the algorithm is accelerated by using extrapolation over  $\phi$  to obtain an initial estimate of  $g^*$ . The iteration convergence parameter  $\epsilon$  is initially set to 0.01 but can be changed by the user. Smaller values of  $\epsilon$  lead to smoother boundaries at the cost of longer execution times.

### 3.3 COMMENTS AND LIMITATIONS

The gain performance boundary program does not automatically find boundaries: it provides a tool for user directed boundary search. The user should be aware of the following limitations:

- Each search finds only one branch of a boundary. If the boundary is multiple valued then additional searches must be used to find other branches. This may require careful starting of the search near the area of interest, small phase steps, small gain steps and/or adjustment of the convergence parameter.
- The algorithm searches only the boundary of the template to find  $\delta M$ . For large templates located so that the point (0dB, -180°) is inside the template this can produce incorrect results.
- Since the M-contours become very large in the vicinity of the (0dB, -180°) point, the search algorithm or the cross section generation algorithm may produce strange results when the template boundary is near this point.
- Since the M-contours are compressed in the region where  $g \ll 0$ dB, the value of the convergence parameter may have to be reduced to obtain accurate results in this region.

#### 4. THE PHASE PERFORMANCE BOUNDARY PROGRAM

The Phase Performance Boundary Program allows the user to generate and save phase performance boundaries using process uncertainty templates and closed loop system phase performance specifications. (Phase performance robustness is important in robust multi-axis coordinated motion. For additional details see [6].) The templates must be in the .TPL format generated by the TEMP21 or TEMP30 programs. Generated boundaries can be saved in the .TBD format for use in the fitting program LOOP20.

Conceptually, a phase performance boundary describes a region (in the N-plane or  $\mathbb{C}$ -plane) that the nominal open loop gain function  $L_o(j\omega)$  must avoid to meet closed loop phase performance specification. A phase performance boundary is obtained by moving a process uncertainty template over the P-contours (closed loop phase contours) of a Nichols Chart. Given a template  $Q(\omega)$ , with its nominal point  $q$  located at the N-plane point  $(g, \phi)$ , there is an associated total closed loop phase variation  $\delta P(g, \phi)$  (as indicated by the P-contours) over the entire template. Given a closed loop phase performance specification  $\delta\theta(\omega)$ , the phase performance set  $B_{pp}(\omega)$  represents the set of all locations of the template [as indicated by the  $(g, \phi)$  location of its nominal point  $q$ ] such that  $\delta P \geq \delta\theta(\omega)$ . The phase performance boundary  $\partial B_{pp}(\omega)$  is the boundary of this set.

##### 4.1 PROGRAM OPERATION

The operation of the phase performance boundary program is essentially identical to the operation of the gain performance boundary program described above. The program initially requests the name of a template file and the closed loop phase performance specification  $\delta\theta$ . The search for the phase performance boundary is carried out as indicated in the discussion of the gain performance boundary program.

#### 5. THE STABILITY BOUNDARY PROGRAM (SBOUND11)

The Stability Boundary Program allows the user to generate and save high frequency stability boundaries using process uncertainty information. Generated boundaries can be saved in the .SBD format for use in the fitting program LOOP20.

Conceptually, a stability set  $B_s(\omega)$  describes a region (in the N-plane or the  $\mathbb{C}$ -plane) that the nominal loop gain function  $L_o(j\omega)$  must avoid to obtain prescribed stability or relative stability specifications. The stability boundary  $\partial B_s(\omega)$  is the boundary of this set. Here we are limited to generation of high frequency stability boundaries - those most commonly of interest in application.

Two types of high frequency stability boundaries are generated by SBOUND11: (1) parametric uncertainty stability boundaries based on M-contour specifications of relative stability with high frequency process uncertainty template offsets (gain only) and (2) mixed uncertainty stability boundaries based on M-contour specifications of relative stability with frequency dependent mixed uncertainty offsets (gain and phase). For a discussion of (2) see [7].

##### 5.1 PROGRAM OPERATION

The program initially displays a Nichols Plot showing several M-contours and then requests a user choice of one of the two types of stability boundaries.

If the first type is selected the user must specify relative stability by selecting an M-contour and then specify the gain variation parameters of the relevant high frequency parametric uncertainty template. No frequency information is required.

If the second type is selected the user must enter the frequency, select an M-contour specifying relative stability and then specify the gain and phase dimensions of the mixed uncertainty template. This process can be repeated at several frequencies.

In both cases the resulting user generated stability boundaries can be displayed in the N-plane or the  $\mathbb{C}$ -plane.

## 6. THE LOOP GAIN PROGRAM

The Loop Gain Program allows the user to generate nominal loop gain functions  $L_o(j\omega)$  meeting given robust performance and robust stability specifications using performance boundaries and stability boundaries generated with PBOUND20, TBOUND10 and SBOUND11. The performance boundaries must be in the .PBD format generated by the PBOUND20 program or the .TBD format generated by the TBOUND10 program. The stability boundaries must be in the .SBD format generated by the SBOUND11 program. Gain vs. frequency and phase vs. frequency data (Bode plot format) describing the chosen nominal loop gain function can be saved in a .LGN file for further processing.

Conceptually, a nominal loop gain function is obtained by fitting a rational function to constraints given by:

- 1) the desired system type (type 0,1,etc.) and, for type 0 systems, the loop gain at  $\omega = 0$ ,
- 2) performance and stability boundaries obtained from specifications and process uncertainty templates,
- 3) the required high frequency phase (determined by the loop pole excess).

Given these constraints the Loop Gain Program provides a graphical environment for finding feasible nominal loop gain functions with minimum bandwidth.

### 6.1 PROGRAM OPERATION

The program begins by asking the user to enter data describing the problem design constraints (i.e., performance and stability boundaries). The user entered performance and stability boundaries are then displayed in a Nichols Plot (N-plane) Window of the LOOP20 Workspace and the Main Menu is presented. A Scratch Window is available to the right of the Nichols Plot Window for the entry of gain/frequency data describing trial loop gain functions.

The basic loop gain-phase shaping design procedure involves an iteration of the following two design steps:

- 1) the user enters new gain/frequency data or edits existing gain/frequency data in the Scratch Window, and
- 2) the programs computes and plots the associated gain-phase plot (over the displayed performance and stability boundaries) in the Nichols Plot Window.

To accomplish this second step the program interpolates additional gain-frequency points between the entered data points and then computes the minimum phase, phase/frequency data using the Bode integral [8].

Thru iteration of this man-machine editing/plotting cycle the user can "learn" how to fit a minimum bandwidth loop gain function to the problem performance and stability boundary constraints.

#### The LOOP20 Workspace

The Nichols Window is used to display boundaries, trial loop gain functions and user defined transfer functions in standard Nichols format. Displayed boundaries are marked by their frequencies when appropriate. When gain-phase plots of trial loop gain functions are displayed, small crosses are used to relate specific gain-frequency points in the Scratch Window to those on the associated gain-phase plot.

The Scratch Window displays gain-frequency data points entered by the user. Gain is indicated using the gain scale inherited from the Nichols Window while frequency is explicitly marked next to each data point. To facilitate editing and learning in the design process the user can store and display three uniquely colored columns of gain-frequency data in the Scratch Window. The gain-phase plots associated with these columns can be simultaneously displayed and identified

by color. Several gain/frequency data editing commands (e.g., interpolate points, block move in gain or frequency, slope change) are provided to facilitate the shaping of a loop gain function to fit the constraints.

## 6.2 ALGORITHMS

The generation of the gain-phase plot from the gain-frequency data is a three step operation. First the gain-frequency data is extrapolated on each end for 1.5 decades using the initial and final slopes. Second, five additional points are interpolated between each point in the gain/frequency data set using a third order spline. Finally, the minimum phase, phase-frequency data is calculated using the Bode integral theorem (a Hilbert transform) which relates the minimum phase of a rational function to the gain frequency data. The specific form of the Bode integral used is given in [8].

## 6.3 COMMENTS AND LIMITATIONS

Understanding the use of the various LOOP20 editing functions requires some careful thinking about the relations between gain and (minimum) phase in a rational function. As a start the user should note that when the slope of the gain-frequency plot is constant the minimum phase is constant and has a value of  $4.5m$  degrees, where  $m$  is the slope of the gain-frequency plot in dB/decade.

## 7. AN EXAMPLE - DC MOTOR WITH UNCERTAIN LOAD

The following example (extracted from [9]) illustrates the application of the the above CAD tools to a simple robust control system design problem.

### Problem Statement

The goal here is the design of a robust controller for a speed control system where the load on the motor can vary over a wide range of values.

### Process Model

A DC motor with an inertial load  $J_L$  can be modelled by the transfer function

$$P(s;J_L) := \frac{\omega_L(s)}{e(s)} = \frac{K_m}{(LJ_m + LJ_L)s^2 + (RJ_m + RJ_L)s + K_m^2} \quad (3)$$

where  $\omega_L$  is the motor shaft speed and  $e$  is the motor armature voltage. Reasonable parameter values for this transfer function are (in SI units):

$$\begin{aligned} L &= 2.2E-3 \\ R &= 0.4 \end{aligned}$$

$$\begin{aligned} K_m &= 0.2 \\ J_m &= 1.4E-3 \end{aligned}$$

We will assume that the load moment of inertia  $J_L$  varies in the interval  $J = [0.05J_m, 10J_m]$  and take  $J_L = J_m$  as the nominal value. That is, we define  $\alpha = J_L$  and take  $\alpha_0 = J_m$ .

### Performance Specifications

The performance goal of interest here is to have the motor shaft speed  $\omega_L$  track a speed reference signal  $r$ . Typical frequency domain specifications for the closed loop tracking transfer function  $T(s) := \omega_L(s)/r(s)$  are given below.



$$|T(j\omega)| = \begin{cases} 0 \pm 0.05 \text{ dB} & \text{for } \omega \leq 10 \text{ rps} \\ 0 \pm 0.2 \text{ dB} & \text{for } 10 < \omega \leq 100 \text{ rps} \\ -20 \pm 2.0 \text{ dB} & \text{for } \omega = 300 \text{ rps} \\ -40 \pm 20 \text{ dB} & \text{for } \omega > 10^4 \text{ rps} \end{cases} \quad (4)$$

We will require that these closed loop performance specifications be met for all  $J_L$  in the interval  $J$ .

#### Stability Specifications

For simplicity, we have chosen the relative stability specification by specifying a gain-phase margin region corresponding to the 5dB M-contour on the Nichols Chart. This corresponds to a gain margin of about 4 dB and phase margin of about 35°. In addition, we require that this gain-phase margin should be robust with respect to variations of  $J_L$  in the interval  $J$ .

#### Additional Specifications

For disturbance rejection we will require the  $L_o(j\omega)$  be type 1 (i.e., one pole at  $s = 0$ ). We will also assume that the compensator has a one pole excess [giving an overall pole excess of three in the nominal loop gain function  $L_o(j\omega)$ ].

#### The LGPS Solution

We begin the LGPS solution by plotting the process uncertainty templates  $Q(\omega)$  for  $P(s; J_L)$  at several frequencies. These templates are shown in Fig. 1. Note that since  $P(s; J_L)$  has only one independent parameter these templates are one-dimensional. In addition, since  $P(s; J_L)$  has independent parameter variations in numerator and denominator and these variations are affine in the uncertain parameter  $J_L$  [see (3)], then the templates obtained with TEMP21 are exact [3].

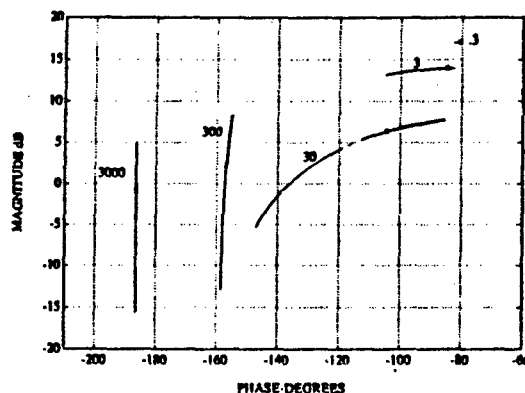


Fig. 1 Process Uncertainty Templates  $Q(\omega)$  for  $\omega = 0.3, 3.0, 30, 300$ , and  $3000$ . (Template nominal point locations are indicated by a "+".)

The second step in the LGPS design process is to compute and plot the performance and stability boundaries at appropriated frequencies. Performance boundaries are obtained by entering the templates plus the  $\delta T$  specification given in (4) in the performance boundary program (PBOUND20). The resulting performance boundaries are shown in Fig. 2.

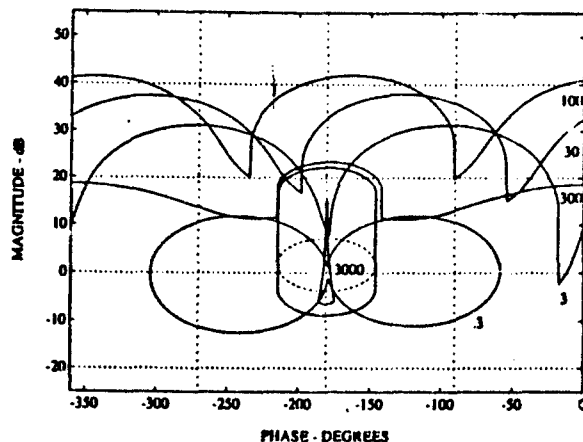


Fig. 2 Performance and Stability Boundaries  
(Frequencies Marked on the Boundaries)

The relevant high frequency stability boundary is obtained by combining the stability specification (i.e., the 5dB M-contour) with the high frequency process uncertainty template ( $\omega = 3000$  in Fig. 1) in the stability boundary program (SBOUND11). This boundary is the closed region encircling the  $(-180^\circ, 0\text{dB})$  point shown in Fig. 2. (The use of the high frequency stability boundary is based on the assumption that the process uncertainty template has become a vertical line at frequencies where the gain-phase plot of the nominal loop gain function  $L_o(j\omega)$  is passing near the stability boundary. It can be seen in Fig. 3 that this assumption is indeed justified. In general more complex stability boundaries may be required.) Note that the performance boundary for  $\omega = 3000$  lies entirely inside the stability boundary and is thus irrelevant to further LGFS design steps.

The fourth step is to fit a minimum bandwidth loop gain function to the performance and stability boundaries using the loop gain fitting program LOOP20. Assuming one excess pole in the compensator [i.e.,  $\arg\{L_o\}$  goes to  $-270^\circ$  as  $\omega$  goes to  $\infty$ ] we fit a nominal loop gain function to the performance and stability boundaries as shown in Fig. 3.

At this point we have the frequency response description of a rational  $L_o(j\omega)$  that satisfies the design constraints. That is, at each of the specified frequencies  $\omega_i$ , the nominal loop gain function  $L_o(j\omega_i)$  satisfies the constraint implied by its respective performance boundary  $\partial B_p(\omega_i)$ . A traditional Bode plot description of  $L_o(j\omega)$  is shown in Fig. 4.

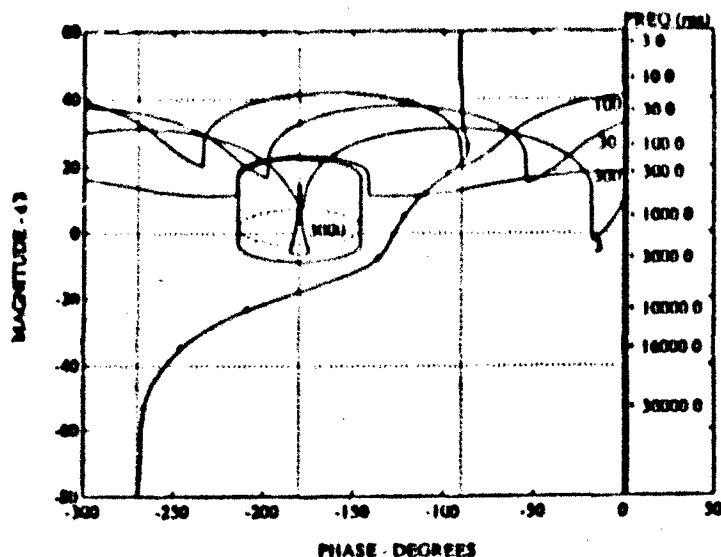


Fig. 3 An LGPS Solution to the Example.  
( $\omega = 0.3$  Boundary Omitted)

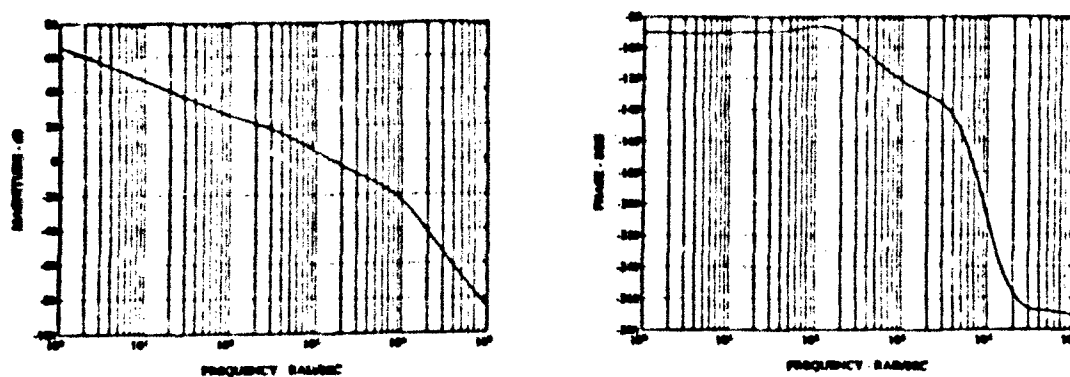


Fig. 4 Bode Plot of  $L_o(j\omega)$ .

Finding a solution that not only satisfies the constraints but also minimizes the loop gain and bandwidth requires additional work with the LOOP20 software.

## 8. CONCLUSION

The LGPSDP series gives a complete solution to the classical QFT robust control problem in a wide range of situations. It can handle specifications on closed gain, phase and disturbance rejection. The templates generated by TEMP21 and TEMP30 assume only parametric uncertainty but obvious modifications for mixed uncertainty are possible (e.g. see [7]). The weakest link in the procedure is the fitting process treated by LOOP20. Additional work in this area appears to be of major importance.

## 9. REFERENCES

- [1] Horowitz, I., Synthesis of Feedback Systems, Academic Press, 1963.
- [2] Horowitz, I. and M. Sidi, "Synthesis of Feedback Systems with Large Plant Ignorance for Prescribed Time-Domain Tolerances", Int. Jour. Control, 16, 2, 287-309, 1972.
- [3] Bailey, F. N., D. Panzer, and G. Gu, "Two Algorithms for Frequency Domain Design of Robust Control Systems", Int. Jour. of Control, 48, 5, 1787-1806, November, 1988.
- [4] Bailey, F. N. and C.-H. Hui, "A Fast Algorithm for Computing Parametric Rational Functions", IEEE Trans. Aut. Cont., Sept. 1989.
- [5] Fu, M., "Computing the Frequency Response of Linear Systems with Parametric Perturbations", Syst. and Cont. Ltrs., 15, 45-62, 1990.
- [6] Bailey, F. N. and M. Kallel, "Loop Gain-Phase Shaping Techniques For Robust Coordinated Motion Control", Proc. ACC, June 1992.
- [7] Bailey, F. N. and J. C. Cockburn, "Loop Gain-Phase Shaping Design of SISO Robust Controllers Having Mixed Uncertainty", Proc. ACC, June 1991.
- [8] Shinnars, Stanley M., Modern Control System Theory and Application (2nd Ed.), Addison-Wesley, 1978.
- [9] Bailey, F. N. and C.-H. Hui, "Loop Gain-Phase Shaping for Single-Input-Single-Output Robust Controllers", IEEE Control Systems Magazine, 11, 1, 93-101, Jan. 1991.

## Development of an Analog MIMO QFT CAD Package

by

Richard R. Sating, I. M. Horowitz, C. H. Houppis  
Air Force Institute of Technology

### 1 Overview of Multivariable Control Problem

A CAD package is developed as a design tool for applying the Quantitative Feedback Theory (QFT) design technique to multivariable control systems involving uncertain continuous time MIMO plants which are free from outside disturbances. A MIMO uncertain square plant  $P_e$  with  $m$  inputs and  $m$  outputs is to be controlled by use of a diagonal compensator  $G$  and a diagonal prefilter  $F$  in the feedback structure shown in Fig. 1 such that the closed loop system meets stability and performance specifications.

A flight control system is utilized to illustrate this MIMO QFT CAD package. The plant model  $P$  to be controlled is in general constituted by four component parts. A block diagram showing the placement of the aircraft plant model  $P_{CONT}$ , the actuator dynamics  $T_{ACT}$ , the sensor dynamics  $T_{SENS}$ , and the sensor gain matrix  $W_{SENS}$  is shown in Fig. 2. The plant  $P$  of dimension  $m \times l$  is, in general, not square. Since QFT requires a square plant then the square  $m \times m$  plant  $P_e$  is formed from the non-square  $m \times l$  plant  $P$  by use of the  $l \times m$  weighting matrix  $W$  as shown in the block diagram in Fig. 3.

### 2 Implementation of the MIMO QFT CAD Package [1]

Several platforms are considered for use in implementing the MIMO QFT CAD package, including Matlab, MATRIXx, Control-C, Mathematica, Macsyma, and the 'C' language. Mathematica is chosen as the platform for the CAD package due to its high numeric precision and symbolic capability. Additional features include the interactive front end, portability, and cost. The shortfall in execution speed associated with interpreted execution is remedied by exporting computationally demanding tasks to 'C' subroutines, while the absence of control tools is addressed by developing the needed resources.

### 3 Loading Plant Data (see block 1 in Fig. 5)

The plant models may be entered manually or if they are available on a disk they can be loaded directly, that is, automated loading of each aircraft plant matrix  $P_{CONT}$  is implemented to eliminate the need for manual data entry. Once loaded, transfer function elements of  $P_{CONT}$  can be listed in factored form or plotted on a Bode plot.

Often, each plant model has associated with it a unique set of parameters. The CAD package allows the designer to define a set of parameters associated with the plant models. For an aircraft model, the set of parameters may include vehicle altitude, Mach number, and angle of attack. The designer may then specify the values of these parameters along with a comment to be stored along with each plant model loaded.

### 4 Actuator and Sensor Models (see block 2 in Fig. 5)

Dynamics of each actuator  $T_{ACT}(s)$  and sensor  $T_{SENS}(s)$  used to control the plant is defined by a deterministic LTI transfer function. The block diagram in Fig. 2 illustrates the use of actuators and sensors.

### 5 Sensor Gain Matrix (see block 3 in Fig. 5)

In some instances, a subset of plant outputs or a linear combination of plant outputs are to be controlled. In these cases, the designer can specify the appropriate sensor gain matrix  $W_{SENS}$ . An entry is accepted for each matrix element, in the format of a coefficient form or factored form polynomial, where the coefficients, poles, zeros, and gain can be constants or a function of plant parameter values defined when the plant models are loaded. Constants may be used as elements of  $W_{SENS}$  by using transfer functions with no poles or zeros but with the desired gains.

### 6 Weighting Matrix (see blocks 4, 5, and 6 in Fig. 5)

A block diagram illustrating the insertion of the weighting matrix  $W$  to form  $P_e$  is shown in Fig. 3. The elements of  $W$  are defined by the designer in the same manner as for  $W_{SENS}$ . When the plant matrix is not a square matrix of desired dimensions, the weighting matrix  $W$  is selected to achieve a square  $m \times m$  effective plant  $P_e$ . When more plant inputs are available than required for control purposes, the weighting matrix provides additional degrees of freedom in the blending of plant inputs used to control the system. In these cases it is desirable that the selected  $W$  yield minimum-phase effective plants  $(q_{ij})_l$  for all plant cases  $l = 1, \dots, J$ . The Binet-Cauchy Theorem is applied to determine whether a minimum-phase  $P_e$  is achievable. In some multivariable control problems, the degree of uncertainty in the system to be controlled may render impossible a successful design. Thus for some of these cases, gain scheduling may be utilized to affect a QFT design.

## 7 Formation of Effective Plant Models (see blocks 7 and 8 in Fig. 5)

For each plant case  $l$ , the weighting matrix and sensor gain matrix, whose elements may be functions of plant parameters, are evaluated using the plant parameter values associated with the plant model

$$\underline{W}_l = \underline{W}(\text{param}_1, \text{param}_2, \dots, \text{param}_p) \begin{cases} \text{param}_1 = \text{paramVal}_1 \\ \text{param}_2 = \text{paramVal}_2 \\ \vdots \\ \text{param}_p = \text{paramVal}_p \end{cases} \quad (1)$$

$$\underline{W}_{\text{SENS}_l} = \underline{W}_{\text{SENS}}(\text{param}_1, \text{param}_2, \dots, \text{param}_p) \begin{cases} \text{param}_1 = \text{paramVal}_1 \\ \text{param}_2 = \text{paramVal}_2 \\ \vdots \\ \text{param}_p = \text{paramVal}_p \end{cases} \quad (2)$$

Each effective plant is then formed from its component parts:

$$\underline{P}_{e_l} = \{p_{ij}\}_l = \underline{P}_l \cdot \underline{W}_l = (\underline{W}_{\text{SENS}_l} \cdot \underline{T}_{\text{SENS}_l} \cdot \underline{P}_{\text{CONT}_l} \cdot \underline{T}_{\text{ACT}_l}) \cdot \underline{W}_l \quad (3)$$

When  $\underline{P}_{e_l}$  is formed, a common denominator  $(\underline{P}_{e_{\text{den}}})_l$  is factored out of each  $p_{ij}$  yielding the expression:

$$\underline{P}_{e_l} = \left( \frac{1}{(\underline{P}_{e_{\text{den}}})_l} \right) \cdot (\underline{P}_{e_{\text{num}}})_l \quad (4)$$

and where the elements of the matrix  $(\underline{P}_{e_{\text{num}}})_l$  are polynomials in factored form.

The effective plant matrix  $\underline{P}_{e_l}$  must be full rank and have diagonal elements which have the same sign for all plant cases as  $\omega \rightarrow \infty$ . The CAD package allows the sign of the  $m$  diagonal plants to be examined for the  $J$  plant cases as  $\omega \rightarrow \infty$  in table form. The CAD package also allows the designer to list the determinant of  $\underline{P}_e$ , one plant case at a time. A non-zero determinant is indicative of full rank. The numerator factors of the determinant, which are zeros of the  $q_{ij}$  (see Sec. 8), are examined as well. Thus, these determinants determine the minimum- or non-minimum-phase character of the effective plants. If any  $\underline{P}_{e_l}$  is unacceptable based on the above criteria, the weighting matrix can be revised,  $\underline{P}_{e_l}$  recomputed, and the tests applied once again.

## 8 Inverse of $\underline{P}_e$ (see blocks 9 and 10 in Fig. 5)

The polynomial matrix inverse is performed using the Mathematica Inverse function:

$$\underline{P}_e^{-1} = \frac{\text{adj} \underline{P}_e}{\det \underline{P}_e} = \{p_{ij}^*\} = \underline{P}_{e_{\text{den}}} \cdot \underline{P}_{e_{\text{num}}}^{-1} \quad (5)$$

The effective plants are then formed by inverting the elements  $p_{ij}^*$ :

$$\underline{Q} = \frac{\det \underline{P}_e}{\text{adj} \underline{P}_e} = \{q_{ij}\} = \left\{ \frac{1}{p_{ij}^*} \right\} \quad (6)$$

The  $\underline{Q}$  matrix elements become the effective plants of the MISO loops. By the principle of superposition, each MISO loop transmission consists of both a tracking and a disturbance component. When using a diagonal prefilter, only the diagonal MISO loops have a transfer function component due to tracking:

$$t_{ij} = t_r + t_d \quad (7)$$

Off-diagonal loops, with  $f_{ij} = 0$  and  $i \neq j$ , have a transfer function component due to disturbance only:

$$t_{ij} = t_{d_{ij}} \quad \text{where } i \neq j \quad (8)$$

Expressions for tracking and disturbance transfer function components of the  $(i,j)$  MISO loop are given:

$$(t_r)_l = f_{ij} \left[ \frac{g_i(q_{ii})_l}{1 + g_i(q_{ii})_l} \right] = f_{ij} \left[ \frac{(L_i)_l}{1 + (L_i)_l} \right] \quad (9)$$

$$(t_{d_{ij}})_l = \frac{(d_{ij})_l (q_{ii})_l}{1 + g_i(q_{ii})_l} = \frac{(d_{ij})_l (q_{ii})_l}{1 + (L_i)_l} \quad (10)$$

where the index  $l$  specifies one of the  $J$  LTI plants, i.e.,  $l = 1, 2, \dots, J$ , and where  $L_i = g_i q_{ii}$ .

The disturbance input, a function of all other controlled outputs, can be expressed by the equation:

$$d_{ij} = - \sum_{k=1, k \neq i}^m \frac{t_{kj}}{q_{ik}} \quad (11)$$

The  $\underline{Q}$  matrix elements are then tested to verify that the condition of diagonal dominance is satisfied. If diagonal dominance holds for all plant cases, then a QFT Method 1 design can be attempted. Otherwise, a QFT Method 2

(improved method) design must be attempted. If the results of this test are not satisfactory, then the choice of weighting matrix can be modified, and the  $Q$  matrix recomputed.

Additional tools for examining the effective plants  $q_u$  of the  $Q$  matrix set include a Bode plot function and a transfer function display subroutine. The Bode plot for a  $Q$  matrix element can be displayed for a specified plant case or for all  $J$  plant cases together. The Bode plot for the set of  $J$  plant cases is useful for displaying the variation in effective plant transmission as an aid in selecting template frequencies. Also, the CAD package allows the  $Q$  matrix transfer function elements to be displayed in factored form for any selected plant case.

To reduce the order of the  $Q$  matrix transfer functions the package performs automatic cancellation, cancelling nearly identical pole-zero pairs based on a user specified ratio of the distance between the pole-zero pair to the distance of the zero from the origin in both the right-half and left-half plane.

#### 9 Improved Method (see blocks 13 and 14 in Fig. 5)

The improved method, also known as QFT Method 2, takes into account any correlation between the uncertainty in the designed MISO loops and the next row of MISO loops for which a design is to be attempted. The standard approach of QFT Method 1 assumes worst case conditions and does not take this design information into account.

The improved method requires the derivation of the effective  $q$  plant transfer function for the next channel to be designed, i.e., for a  $2 \times 2$  system in which the compensator for channel 1 has been designed and  $L_1$  is known:

$$q_{22} = \frac{q_{22}(1+L_1)}{1 - \eta_{12} + L_1} \quad \text{where} \quad \eta_{12} = \frac{p_{12} p_{21}}{p_{11} p_{22}} \quad (12)$$

The improved method CAD routines currently address a  $2 \times 2$  MIMO problem only.

#### 10 Templates (see block 15 in Fig. 5)

The CAD package requires the designer to specify the template frequencies for which the templates are generated. The set of templates, one for each template frequency, are then generated to represent the uncertainty in the effective plant  $q_u$ , and a chart of templates is displayed.

A plant template outlines the range of uncertainty in the frequency domain on the NC of a plant transfer function for a specific frequency. The template for  $\omega = \omega_i$  is formed by first plotting the frequency domain transmission at  $\omega = \omega_i$  for each of the  $J$  plant cases, then enclosing the set of plant points with an outline. The outline is analogous to a rubber band stretched around a set of nails representing the template points.

#### 11 Choice of Nominal Plant (see block 16 in Fig. 5)

The CAD package allows the designer to display a plot of numbered plant cases for a user specified template frequency. The designer chooses the nominal plant from the set of  $J$  effective plants. A chart of templates is then displayed with the selected nominal point emphasized. While any plant case can be chosen, it is an accepted practice to select, whenever possible, a plant case which exists at the lower left corner for all frequencies for which the templates are obtained. If the choice of nominal plant is not satisfactory, another choice may be selected.

Once a nominal plant case is chosen, the templates are shifted such that the nominal point of each template is located at (0 deg, 0 dB) on the NC. This can be done because only the location of the plants points relative to each other on the template is of importance when generating bounds. The template can then be shifted on the NC such that the nominal plant is at a desired location by adding the coordinates of the desired location to the coordinates of all plant points. In this way, the template can be conveniently placed at any desired location on the NC.

#### 12 Specifications (see block 11 in Fig. 5)

##### 12.1 Stability Specifications

A stability margin is specified for each row of MISO loops. The stability margin may be specified in terms of the gain margin  $g_m$ , the phase margin angle  $\gamma$ , or the corresponding  $M_L$  contour. Any of these three specifications can be determined from any of the others. Only the  $M_L$  contour stability specification is stored in memory.

##### 12.2 Performance Specifications

Frequency domain performance specifications are defined in the form of LTI transfer functions.

For the diagonal MISO loops upper and lower bounds are specified:

$$a_{ii} \leq |t_{ii}| \leq b_{ii} \quad \text{for } i = 1, 2, \dots, J \quad (13)$$

For the off-diagonal MISO loops an upper bound is specified:

$$|t_{ij}| \leq b_{ij} \quad \text{for } i = 1, 2, \dots, J \quad (14)$$

### 12.3 Gamma Bound Specifications

The improved method requires the derivation of the effective  $q$  plant transfer function, ie. Eq. (12). By proper design of the compensator  $g_1$ , new RHP poles will not be introduced in  $q_{22e}$ . By requiring the magnitude of the denominator of Eq. (12) be larger than a small value  $k$ , sign changes in the denominator are prevented and new RHP poles are not introduced:

$$k \leq |1 - \gamma_{12} + L_1| \quad (15)$$

For the case in which  $g_2$  is designed first, the requirement on channel 2 is:

$$k \leq |1 - \gamma_{21} + L_2| \quad (16)$$

A unique minimum value  $k$  is specified by the designer for each of the  $m$  channels.

### 13 Bounds on the NC (see block 17 in Fig. 5)

For a given row  $i$  of MISO loops, for a template frequency  $\omega = \omega_i$ , several bounds may be included in the set plotted on the NC. These bounds include a stability bound, a tracking bound, a disturbance bound for each off-diagonal MISO loop, and a gamma bound when using the improved method. This set of bounds can be replaced by a single composite bound before beginning a design.

#### 13.1 Stability Bounds

A stability bound is plotted for each template. The stability bounds constrain the maximum closed-loop transmission with unity gain prefilter to have a bounded magnitude:

$$\left| \frac{g_i(q_{ii})}{1 + g_i(q_{ii})} \right| \leq M_L \quad \text{for } i = 1, 2, \dots, J \quad (17)$$

The bound is plotted for a given frequency by plotting the path of the nominal point while traversing the  $M_L$  contour with the template generated for that frequency. The software must be able to determine the point of tangency on the outline of the template and the location of the template, when tangent at that point, as the  $M_L$  contour is traversed. To accomplish this task, an equation is derived which gives the NC magnitude  $M$  to which a template point at the NC phase angle  $\phi$  must be shifted to be in contact with the  $M_L$  contour. The use of this equation to plot points on the stability bound is then discussed.

For a given test point on the outline of the template, located at a given angle  $\phi$  on the NC, an equation is derived for the NC magnitude  $M$  at which this point is in contact with the  $M_L$  contour. The derivation begins with the requirement that the magnitude of the closed loop transmission be equal to the magnitude  $M_m$  associated with the  $M_L$  contour for the open loop transmission  $L$  where  $M_m = 10^{M_L/20}$  and where  $M_L$  is given in Decibels:

$$M_m = \left| \frac{L}{1 + L} \right| \quad (18)$$

Taking the magnitude of the numerator and denominator, with  $L = M e^{j\phi}$  and solving for  $M$  yields:

$$M = \frac{-\cos(\phi) \pm \sqrt{\cos^2(\phi) - (1 - M_m^2)}}{(1 - M_m^2)} \quad (19)$$

Next, the range of angles of the  $M_L$  contour over which real solutions for  $M$  exist is derived. This range is then used to determine the range of angles over which the stability bound exists. The angle range of the  $M_L$  contour is:

$$\phi_{M_m \min} \leq \phi \leq \phi_{M_m \max} \quad (20)$$

Where:

$$\phi_{M_m \min} = +\cos^{-1} \left( \frac{-\sqrt{1 - M_m^2}}{1} \right) - 360^\circ \quad (21a)$$

$$\phi_{M_m \max} = -\cos^{-1} \left( \frac{-\sqrt{1 - M_m^2}}{1} \right) \quad (21b)$$

To plot a pair of points on the stability bound, the template is placed on the NC with the nominal point located at the NC phase angle at which the bound point is to be plotted. To locate the point of tangency above the  $M_L$  contour, the outline of the template is searched by applying Eq. (19). The point on the template which requires the highest template placement on the NC to bring the template into contact with the  $M_L$  contour is the point of tangency. The location of the nominal point when the template is in contact with and above the  $M_L$  contour at the point of tangency will be a point on the upper portion of the stability bound contour. To locate the point of tangency below the  $M_L$  contour, the template border is searched again. The point on the template border which requires the lowest template placement on the NC to bring the template into contact with the  $M_L$  contour is the point of tangency. The



location of the nominal point when the template is in contact with and below the  $M_L$  contour at the point of tangency will be a point on the lower portion of the stability bound contour. The above procedure is carried out with the template nominal positioned at a set of angles over which the stability bound exists to generate the points used to plot the stability bound.

### 13.2 Disturbance Bounds

Disturbance bounds are plotted for each template, one for each off-diagonal MISO loop in the row of MISO loops for which the compensator is to be designed. Each disturbance bound is generated based on the constraint:

$$t_{ij} = d_{ij} \left[ \frac{q_{ii}}{1 + L_i} \right] \leq b_{ij} \quad \text{for } i \neq j \quad (22)$$

Where the disturbance is a function of all other controlled outputs:

$$d_{ij} = - \sum_{k=1, k \neq i}^m \frac{t_{kj}}{q_{ik}} \quad (23)$$

The specifications dictate that  $d_{ij}$  is less than an upper bound for each plant case  $l$  in the set of  $J$  plants:

$$(|d_{ij}|_{\max})_l = \sum_{k=1, k \neq i}^m \frac{|b_{kj}|}{|q_{ikl}|} \quad (24)$$

The most extreme upper bound on  $d_{ij}$  for all the  $J$  plant cases is then:

$$|d_{ij}|_{\max} = [ (|d_{ij}|_{\max})_l ]_{\max \text{ over } l} \quad (25)$$

Based on Eqs. (22) and (25) a lower bound can be placed on  $|1 + L_i|$

$$|1 + L_i| \geq \frac{|d_{ij}|_{\max} |q_{ii}|}{|b_{ij}|} \quad (26)$$

By substituting  $L_i = \frac{1}{m}$  Eq. (26) can be transformed such that the bound is plotted on the inverse NC:

$$\frac{m}{1 + m} \leq \frac{|b_{ij}|}{|q_{ii}| |d_{ij}|_{\max}} \quad (27)$$

Simplifying by using the symbol  $M_D$  to designate the inverse NC constant magnitude contour:

$$\left| \frac{m}{1 + m} \right| \leq M_D \quad \text{where } M_D = \frac{|b_{ij}|}{|q_{ii}| |d_{ij}|_{\max}} \quad (28)$$

In general,  $M_D$  is different for different plant cases since  $q_{ii}$  is different for different plant cases. From this point forward the inverse NC constant magnitude contour will be referred to as the  $M_D$  contour. An equation is derived which gives the NC magnitude to which a template point located at the NC phase angle  $\phi$  must be shifted to be in contact with the specified  $M_D$  contour. The equation is then used to plot points on the disturbance bound.

The derivation begins with the requirement on  $m$ :

$$\left| \frac{m}{1 + m} \right| \leq M_D \quad (29)$$

Taking the magnitude of the left-hand-side, with  $m = M_{inv} e^{j\phi_{inv}}$  at  $\omega = \omega_i$  and solving for  $M_{inv}$  yields:

$$M_{inv} = \frac{-\cos(\phi_{inv}) \pm \sqrt{\cos^2(\phi_{inv}) - (1 - M_D^2)}}{(1 - M_D^2)} \quad (30)$$

This requirement applies to  $m = (gq_{ii})^{-1}$ , not to  $L_i = gq_{ii}$ , as desired. By making the substitution  $M = M_{inv}^{-1}$  and  $\phi = -\phi_{inv}$ , the solution is now written to apply to  $L_i$ , where  $L_i = M e^{j\phi}$ .

For the case of  $M_D < 1$ , one solution exists for a given value of  $\phi$  on the NC, corresponding to the single point of contact, at that angle, with the  $M_D$  contour which runs across the NC:

$$M = \frac{(1 - M_D^2)}{-\cos(\phi) + \sqrt{\cos^2(\phi) - (1 - M_D^2)}} \quad \text{for } M_D < 1 \quad (31)$$

A disturbance bound generated using an  $M_D$  contour with  $M_D < 1$  is an open bound contour running across the entire angle range of the NC.

For the case of  $M_D > 1$ , two solutions exist over a limited range of angles on the NC:

$$M = \frac{(1 - M_D^2)}{\cos(\varphi) + \sqrt{\cos^2(\varphi) - (1 - M_D^2)}} \quad \text{for } M_D > 1 \quad (32)$$

This case is analogous to the pair of solutions obtained when using Eq. (19) to plot stability bounds. The derivation of the range of angles for which the solutions exist is then carried out:

$$\varphi_{D_{\min}} \leq \varphi \leq \varphi_{D_{\max}} \quad (33)$$

Where

$$\varphi_{D_{\min}} = +\cos^{-1} \left( \frac{\sqrt{1 - M_D^2}}{1} \right) - 360^\circ \quad (34a)$$

$$\varphi_{D_{\max}} = -\cos^{-1} \left( \frac{\sqrt{1 - M_D^2}}{1} \right) \quad (34b)$$

A disturbance bound generated using an  $M_D$  contour, with  $M_D > 1$ , is a closed contour on the NC. For the case of  $M_D = 1$  a small value can be added to  $M_D$  allowing it to be handled as if  $M_D > 1$ .

To plot a point on the disturbance bound, the template is placed on the NC with the nominal point at the NC angle at which the bound point is to be plotted. The template outline is then searched to locate the point which results in the most restrictive bound point using the same algorithm used to plot stability bounds. For  $M_D > 1$  two searches using Eq. (32) are implemented, determining the most restrictive upper and lower disturbance bound points at the NC angle at which the bound points are plotted. For  $M_D < 1$  one search using Eq. (31) is implemented to determine the most restrictive bound point at the NC angle at which bound point is plotted. The quantity  $M_D$  is re-evaluated based on  $q_{ii}$  for each template point examined by the search routine to take into account correlation between the right hand side and left-hand side of Eq. (27) due to correlation between  $q_{ii}$  and  $m = L_i^{-1}$  among the  $J$  plant cases. Using the above procedure the bound is plotted across the range of angles for which it exists.

### 13.3 Gamma Bounds

Gamma bounds are generated based on Eq. (35), for each template, where the compensator for row  $j$  is to be designed after the compensator for row  $i$  of the MISO loops. It is desired that the magnitude of the denominator of the effective plant  $q_{22}$ , calculated using the improved method, not be smaller than a specified minimum value despite plant uncertainty:

$$|1 + g_{ii} - \gamma_{ij}| \geq k \quad (35)$$

Equation (35) is used to derive the equations used to plot gamma bounds on  $L_{40}$ . It is shown that for  $|1 - \gamma_{ij}| > k$  there exists a range of angles  $\varphi_{G_{\min}} \leq \varphi \leq \varphi_{G_{\max}}$  in which a range of transmission magnitudes  $M_a(\varphi) \leq M \leq M_b(\varphi)$  are not acceptable where  $L_4 = Me^{j\varphi}$ . For this case a closed gamma bound exists on the NC over a limited range of angles. It is also shown that for  $|1 - \gamma_{ij}| < k$  a range of magnitudes  $0 \leq M \leq M_b(\varphi)$  are not acceptable at any given  $\varphi$  where  $L_4 = Me^{j\varphi}$ . For this case an open gamma bound runs across the length of the NC.

Assuming for a moment that  $\gamma_{ij}$  is fixed, the range limits of the transmission magnitude  $M_a(\varphi)$  and  $M_b(\varphi)$  are derived in terms of the transmission phase angle  $\varphi$  beginning with the inequality:

$$|1 - \gamma_{ij} + L_4| \geq k \quad (36)$$

The bound on  $L_4$  for  $\omega = \omega_0$  exists where the inequality is about to be violated:

$$|1 - \gamma_{ij} + L_4| = k \quad (37)$$

Substituting  $1 - \gamma_{ij} = \alpha_1 + j\alpha_2$  and  $L_4 = Me^{j\varphi}$  and solving for  $M$  yields two solutions for  $M$ , the range limits  $M_a(\varphi)$  and  $M_b(\varphi)$ :

$$M_a(\varphi) = -[\alpha_1 \cos(\varphi) + \alpha_2 \sin(\varphi)] - \sqrt{[\alpha_1 \cos(\varphi) + \alpha_2 \sin(\varphi)]^2 - (\alpha_1^2 + \alpha_2^2 - k^2)} \quad (38a)$$

$$M_b(\varphi) = -[\alpha_1 \cos(\varphi) + \alpha_2 \sin(\varphi)] + \sqrt{[\alpha_1 \cos(\varphi) + \alpha_2 \sin(\varphi)]^2 - (\alpha_1^2 + \alpha_2^2 - k^2)} \quad (38b)$$

Solutions exist for angles at which the discriminant is non-negative:

$$[\alpha_1 \cos(\varphi) + \alpha_2 \sin(\varphi)]^2 - (\alpha_1^2 + \alpha_2^2 - k^2) \geq 0 \quad (39)$$

Since this transcendental equation cannot be solved for  $\varphi$ , an iterative search is used to determine the range  $\varphi_{G_{\min}} \leq \varphi \leq \varphi_{G_{\max}}$  for which solutions for  $M_a(\varphi)$  and  $M_b(\varphi)$  exist when  $|1 - \gamma_{ij}| > k$ .

Initially, it is assumed that gamma is fixed. To plot a point on the gamma bound, the template is placed on the NC with the nominal point at the NC angle at which the bound point is to be plotted. The template outline is then searched to locate the point which results in the most restrictive bound point using the same algorithm used to plot stability bounds. For  $|1-\gamma_{ij}| > k$  two searches are implemented using Eq. (38a) and (38b) to determine the upper and lower bound points at each NC angle for which the closed gamma bound contour is plotted. For  $|1-\gamma_{ij}| < k$  one search is implemented using Eq. (38b) to determine the upper bound point at each NC angle for which the bound is plotted. Using the above procedure the gamma bound is plotted across the range of angles for which it exists.

An additional consideration which must be taken into account is the fact that a different gamma exists for each plant case. This variation is handled by the CAD package by generating a gamma bound for each value of gamma, one for each of the J plant cases. The value of gamma is held constant when generating each gamma bound. A composite bound is then formed from the set of J gamma bounds. (composite bounds are discussed in Sec. 13.5)

#### 13.4 Tracking Bounds

Tracking bounds are used to insure that the variation in closed loop frequency domain transmission  $t_{ij}$  of the diagonal MISO loop does not exceed the variation  $\delta_R$  permitted by the performance specs. The variation in the closed loop transmission of the diagonal MISO loop results from both uncertainty in the response due to tracking and from the presence of the disturbance input:

$$t_{ij} = t_{\tau_i} + t_{d_{ij}} \quad (40)$$

where  $t_{\tau_i}$  and  $t_{d_{ij}}$  are given by Eqs. (9) and (10).

A portion of the permitted variation  $\delta_R$  of the total response  $t_{ij}$  is therefore allocated to the transmission due to disturbance  $t_{d_{ij}}$  resulting in a reduced range of variation  $\delta_R'$  for the transmission due to tracking  $t_{\tau_i}$ . Because the relationship between  $t_{\tau_i}$  and  $t_{d_{ij}}$  is additive, the permitted variation is represented in terms of magnitude rather than log magnitude when allocating for disturbance:

$$\Delta \tau_{\tau_i} = 10^{(\delta_R/20)} \quad (41)$$

$$\Delta \tau_{\tau_i}' = 10^{(\delta_R'/20)} \quad (42)$$

By allocating the portion  $2\tau_{d_{ij}}$  to disturbance, the permitted variation in closed loop transmission is reduced to  $\Delta \tau_{\tau_i}'$ , as shown in Fig. 4.

The permitted closed loop variation in tracking is now:

$$\Delta \tau_{\tau_i}' = \Delta \tau_{\tau_i} - 2\tau_{d_{ij}} \quad (43)$$

The performance tolerances for the closed loop transmission  $t_{\tau_i}$  then become:

$$a_{ii}' = a_{ii} + \tau_{d_{ij}} \quad (44)$$

$$b_{ii}' = b_{ii} - \tau_{d_{ij}} \quad (45)$$

And the requirement on the closed loop transmission becomes:

$$a_{ii}' \leq |t_{\tau_i}| \leq b_{ii}' \quad (46)$$

With this disturbance allocation the method discussed in Sec. 13.2 can be used to determine the point on the disturbance bound on  $L_i$  at a given frequency. From Eq. (26) the constraint on  $L_i$  for  $b_{ij} = \tau_{d_{ij}}$  is:

$$|1 + L_i| \geq \frac{|k_{ii}|_{\max} |k_{ji}|}{|\tau_{d_{ij}}|} \quad (47)$$

with  $|k_{ii}|_{\max}$  defined by Eq. (25) with  $i = j$ .

The constraint on  $L_i$  used to determine a point on the tracking bound is:

$$\text{Lm}(T_{R_{\max}}) - \text{Lm}(T_{R_{\min}}) \leq \delta_R' \quad (48)$$

where  $\delta_R' = \text{Lm}(\Delta \tau_{\tau_i}') = \text{Lm}(\Delta \tau_{\tau_i} - 2\tau_{d_{ij}})$  and where the transmission with unity gain prefilter  $T_R$  is:

$$T_R = \left| \frac{L_i}{1 + L_i} \right| \quad (49)$$

The CAD package uses an iterative search to determine the value of  $\tau_{d_{ij}}$  for which Eqs. (47) and (49) place the same restriction on  $L_i$ ; this is the value of  $\tau_{d_{ij}}$  for which the least restrictive composite bound point on  $L_i$  will be generated. Because points on the the disturbance bound are identical to those on the allocated tracking bound for the value of  $\tau_{d_{ij}}$  thus chosen, only points on the tracking bound are plotted on the NC. In general the value of  $\tau_{d_{ij}}$

is unique at each  $\omega = \omega_i$  and for each phase angle  $\phi$  at which the bound point is plotted. Once a value of  $\tau_{d_i}$  is available at a given phase angle  $\phi$ ,  $\delta R'$  can be calculated and a point on the tracking bound can be plotted.

To plot a point on the tracking bound, the template for  $\omega = \omega_i$  is placed on the NC with the nominal point located at the NC angle  $\phi$  at which the bound point is to be plotted. The template is then moved up or down as needed until the difference between the largest ( $TR_{max}$ ) and smallest ( $TR_{min}$ ) closed loop transmissions  $T_R$ , as determined by the template outline, is equal to  $\delta R'$  in Decibels:

$$Lm(TR_{max}) - Lm(TR_{min}) = \delta R' \quad (50)$$

The position of the nominal point when Eq. (50) is satisfied is the point on the tracking bound. To generate the entire bound, this procedure is repeated for the range of angles of the NC, using a unique  $\tau_{d_i}$  at each phase angle. By constraining  $I_{d_i}$  to be above the bound, the actual variation in  $t_{ij}$  will be less than  $\delta R$ .

### 13.5 Composite Bounds

A set of composite bounds is formed based on any or all of the tracking, stability, disturbance, and gamma bounds. The composite bound for a given frequency is formed by retaining the most restrictive portion of the bounds for the given frequency for which the composite bound is formed. The procedure used to generate the composite bound hides the line segment of any bound whose endpoints lie entirely within the forbidden regions of any other bounds. For a tracking bound, which is a single contour running across the NC, the forbidden region is the area on the NC below the bound. For a stability bound, the forbidden region is the region enclosed by the bound on the NC. Disturbance and gamma bounds likewise have forbidden regions associated with them. A line segment included on the composite bound may extend into a forbidden region, resulting in rough breaks at the points of intersection. This is the price paid for the simplicity of this method of generating a composite bound.

### 14 Compensator Design (see block 18 in Fig. 5)

The compensator is designed to satisfy design specifications for the entire row of MISO loops in which the compensator is used. Since  $L_{io} = g_{iijio}$  is the same for all MISO loops in a given row, bounds for all MISO loops are plotted together on the NC. The compensator design is therefore performed for an entire row of MISO loops using a single design iteration based on composite bounds plotted on the NC.

The CAD package makes a Bode plot, a Nichols plot with bounds, and a factored form listing of  $L_{io} = g_{iijio}$  available to the designer. On both plots, the bound frequencies are marked on the loop transmission using colored markers. On the NC, all bounds are plotted in color to match the color of the markers on the loop transmission. The designer must be sure the colored markers do not violate bounds of matching color. The Bode plot must be used to read off the frequencies associated with the colored markers, when used in place of frequency labels on the NC. The Bode plot is also useful for noting the frequency associated with features of interest on  $L_{io}$ .

The CAD package allows the open loop transmission to be shaped by adding, deleting, or modifying the poles and zeros of the compensator and by allowing adjustment of the gain. After any change to the poles and zeros, the gain is automatically adjusted such that the loop transmission is relatively unaffected at frequencies much less than that associated with the modified pole or zero. This allows the designer to "bend" the loop transmission on the NC at successively higher frequencies until an acceptable loop shape is obtained. An updated listing, in factored form, of the compensator poles, zeros, and gain is displayed after any of these changes is made. Both real and complex poles and zeros may be added to the compensator. Complex poles and zeros are displayed as a natural frequency and a zeta. The designer can add complex poles and zeros in the form displayed or as complex numbers.

The designer may terminate the loop shaping process by saving the compensator or may abort the design changes before returning to the CAD package menu system. If saved, the compensator can be further modified by again executing the "Design Compensator" option. In addition, the designer may save the NC or the Bode plot to a postscript file at any time. Once the designer has obtained a satisfactory compensator design, and the design has been saved, then the prefilter can be designed.

### 15 Prefilter Design (see block 19 in Fig. 5)

The proper design of the compensator guarantees that the variation in closed loop transmission due to uncertainty for  $t_{ij}$  is acceptable, but does not guarantee that the transmission is within the upper and lower performance tolerances  $a_{ij}$  and  $b_{ij}$ . The prefilter is therefore required to shift the closed loop transmission  $t_{ij}$  such that it satisfies the upper and lower performance tolerances.

The prefilter design begins with the determination of  $TR_{max}$  and  $TR_{min}$ , the maximum and minimum closed loop transmission due to tracking  $T_R$  with unity gain prefilter, respectively, at each template frequency  $\omega_i$  using Eq. (49).

These quantities are obtained at each  $\omega_i$  by placing the template for  $\omega_i$  on the NC with the nominal point at the location of  $L_{i0} = g_i q_{i0}$  for  $\omega = \omega_i$ . The search subroutine used for generating the tracking bounds is then used to search the perimeter of the template for the maximum and minimum closed loop transmissions  $TR_{\max}$  and  $TR_{\min}$ .

As is the case for tracking bounds on the NC, a portion of the permitted range of variation of  $t_{ij}$  is allocated to the disturbance. With the compensator design in hand, the maximum transmission due to disturbance  $|t_{d_{ij}}|$  is determined by maximizing Eq. (10) over the plant cases  $i = 1, 2, \dots, J$  where  $f_{ij} = 1$  and  $(d_{ij})_l = |d_{ij}|_{\max}$  from Eq. (25) with  $i = j$ . Because the phase of  $t_{d_{ij}}$  is unknown, the most extreme case is assumed; the maximum and minimum limits on the range of variation of  $t_{ij}$  must each be made more restrictive by the magnitude of the disturbance, as illustrated in Fig. 4. The tolerances on  $t_i$  become:

$$b_{ii}' = b_{ii} - |t_{d_{ii}}| \quad (51a)$$

$$a_{ii}' = a_{ii} + |t_{d_{ii}}| \quad (51b)$$

Finally, the filter bounds on the nominal  $t_i$  are computed as follows:

$$Lm(b_{ii}') = Lm(TR_{\min}) \quad (52a)$$

$$Lm(a_{ii}') = Lm(TR_{\max}) \quad (52b)$$

These upper and lower bounds cover only the range of frequencies covered by the templates. The CAD package extends this frequency range one decade higher and one decade lower based on the values of  $TR_{\min}$  and  $TR_{\max}$  obtained by minimizing or maximizing  $TR$  over the plant cases. Templates on the NC are not used to compute these values since no templates are generated in the frequency range into which the bounds are to be extended.

Once the bounds are plotted on the Bode plot, a prefilter is synthesized such that the Bode plot lies between these two bounds and satisfies  $t_{ii}(s) = 1$  in the limit as  $s \rightarrow 0$ . Once the design is complete, the designer may either save or abort changes made to the prefilter. If the design is saved, the design process can be continued on yet another row of MISO loops, until all compensators and prefilters have been designed.

#### 16 Simulation (see block 21 in Fig. 5)

The CAD package provides two tests to verify that the completed MIMO design meets the stability and performance specifications for the  $J$  plant cases. The first test allows the designer to verify that the stability specifications have been satisfied by plotting an array of the  $J$  open loop MISO loop transmissions  $(L_i)_l = g_i(q_{ii})_l$  for a given row of MISO loops  $i$  for all plant cases  $l = 1, 2, \dots, J$  along with the  $M_L$  contour. If no open loop transmission violates the  $M_L$  contour, then the stability specifications are satisfied for row  $i$  of the MISO loops.

The second test allows the designer to verify by inspection that performance specifications placed on the closed loop system have been met over the frequency range of interest by plotting an  $m \times m$  array of Bode magnitude plots, one Bode plot for each element  $t_{ij}$  of the closed loop transfer function matrix  $\underline{T}$ . For each diagonal  $t_{ii}$ ,  $J$  Bode magnitude plots are plotted along with the performance bounds  $a_{ii}$  and  $b_{ii}$ . For each off-diagonal  $t_{ij}$ ,  $J$  Bode magnitude plots are plotted along with the performance bound  $b_{ij}$ . The  $m \times m$  closed loop transfer function matrix  $\underline{T}$ , whose elements  $t_{ij}$  are the transmissions plotted on the Bode plots, is formed for the  $J$  plant cases based on the equation:

$$\underline{T} = [\underline{I} + \underline{P}\underline{G}]^{-1} \underline{P}\underline{G}\underline{F} \quad (53)$$

where  $\underline{I}$  is the identity matrix, and  $\underline{P}$ ,  $\underline{F}$ , and  $\underline{G}$  are the  $m \times m$  plant matrix, diagonal prefilter matrix, and diagonal compensator matrix, respectively.

For the third test, the completed design is saved to a MATRIXx readable file and a System-Build model created. The designer can then insert nonlinear dynamics such as saturation and hysteresis. The model is then simulated to verify that the time domain figures of merit specifications are satisfied.

#### 17 Summary

An analog MIMO QFT CAD package has been developed based on Mathematica which automates the design procedure, including problem setup, equivalent plant formation, compensator and prefilter design, and design validation for  $m \times m$  MIMO systems. Routines have been added to perform an improved method design for  $2 \times 2$  systems. This CAD package is being extended to handle analog or discrete systems and  $3 \times 3$  improved method designs.

#### 18 References

- [1] Sating, Richard R., Development of an Analog MIMO QFT CAD Package. MS thesis, School of Engineering, Air Force Institute of Technology (AU), Wright-Patterson AFB OH, June 1992.

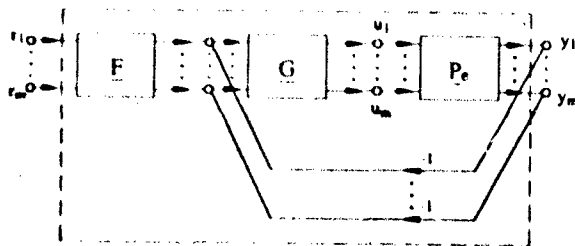


Fig. 1 MIMO QFT controller block diagram

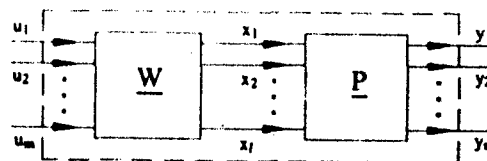


Fig. 3 Formation of square effective plant  $P_e$

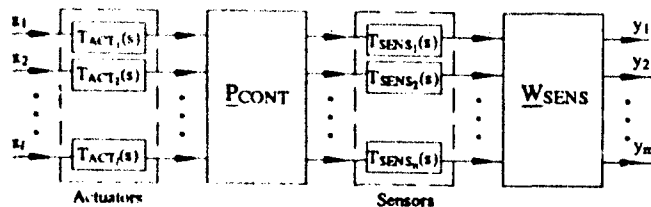


Fig. 2 Components of the Plant  $P$

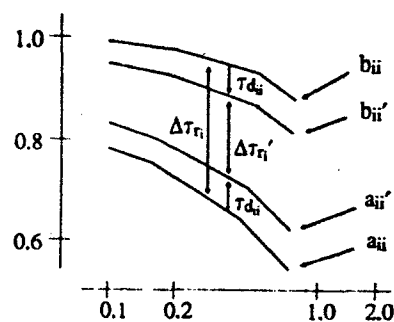


Fig. 4 Allocation for disturbance

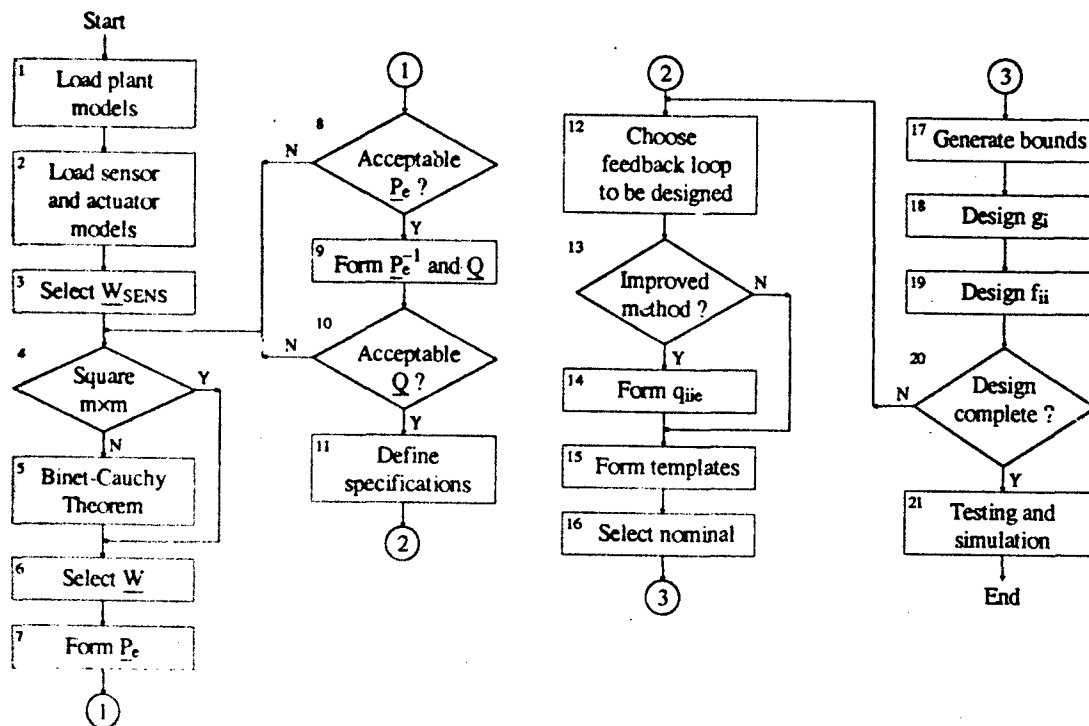


Fig. 5 Flowchart for MIMO QFT CAD Package

# MULTIPLE INPUT SINGLE OUTPUT QFT CAD USER MANUAL

ODED YANIV\*

## Abstract

This user manual describes how to use a user friendly CAD program to find feedback structures for a multiple-input single-output (MISO) linear time-invariant plant. The CAD program is based on the Horowitz frequency domain design method for uncertain feedback systems [2] that appears in the literature under the name Quantitative Feedback Theory (QFT). The package includes discrete and continuous design, loop shape environment, optimization option and linear and nonlinear simulations. A mouse can be used for all design options.

## 1 Introduction

The design process, for both analog and digital control systems, follows the following steps: (1) The designer defines the plant (usually a set of possible plants), output performance tolerances due to tracking input and/or disturbances, and margin performance (an option that transfer the plant into Z-Domain is included); (2) The package translates the data of step (1) into bounds; (3) A user friendly environment to perform Loop Shaping to satisfy the bounds is executed (discrete and continuous options are included); (4) The designer defines an optimization criterion and gets an optimal solution; (5) Prefilter design; (6) Closed loop simulations including choice of the nonlinear elements: saturation of the plant input and its dead zone, stiction and friction, choice of where the input is (tracking, plant input plant output and sensor output) choice of the input (step, sine square wave and an input from a file; and (7) Closed loop analysis.

In Section 2 the MISO problems which the package solves are defined. Section 2 shows some figures for several examples.

This user friendly package is an excellent environment for control engineers as well as control students. After a short practice an engineer can find an optimal practical control law to a problem containing sampling time, delays, plant uncertainty etc. and can easily study their effect on the solution. Students who like to practice the QFT technique can use this package to quickly learn about loop shaping in continuous and discrete domains. nonminimum phase systems, sampling time and its effect on the solution, uncertainty and its effect on the controller bandwidth, gain scheduling and any plant parameter scheduling and its effect on the controller bandwidth, closed loop performance and its effect on the controller bandwidth and tradeoff among all these parameters.

The package uses the same notations which appears in the text book of D'Azzo and Houpis [1].

---

\*Faculty of Engineering, E.E.-Systems, Tel-Aviv University, Tel-Aviv 69 978, Israel.

## 2 The Problems That The Package Solves

QFT is an engineering design tool devoted to practical design of feedback control systems. It is based on the assumption that feedback is needed only because of plant and/or disturbance uncertainty, which then leads to the following problem: There is given an open loop set of plants  $\mathcal{P} = \{P\}$  and a set of acceptable plant tracking input output relations  $\mathcal{T}_R$ . Also there is given a set of acceptable disturbance input output relations  $\mathcal{T}_D$ . The problem is to find a linear time invariant controller and prefilter of Fig. 1.1 such that: The transfer function from the prefilter input to the plant output ( $Y/R$ ) is a member of the acceptable set  $\mathcal{T}_R$ , and the transfer function from the disturbance  $D_1$  ( $D_2$ ) to the plant output  $Y/D_1$  ( $Y/D_2$ ) is a member of the acceptable set  $\mathcal{T}_D$  for all  $P \in \mathcal{P}$ . In the next sections these problems are defined quantitatively

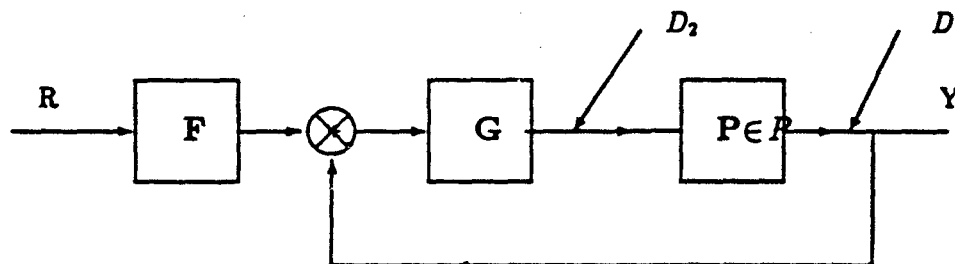


Figure 1: Schematic representation of a MISO feedback system

as implemented in the CAD package.

### 2.1 For Tracking Specification

There is given a set  $\mathcal{P} = \{P_j\}$ ,  $j = 1, \dots, J$ , where  $J$  is the number of linear time invariant SISO plants. The plant is embedded in a two degree-of-freedom feedback structure described schematically in Fig. 1.2. The closed loop system, from input  $R$  to output  $Y$  is plant sensitive.

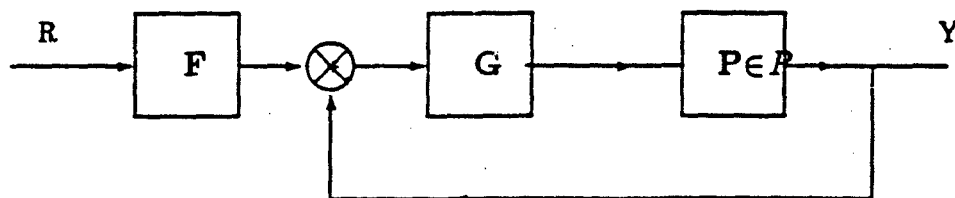


Figure 2: Schematic representation of a tracking feedback structure

There are given bounds on this sensitivity in the form of two functions of the frequency  $\omega$ ,  $B_U(\omega)$  and  $B_L(\omega)$ . The modelling of a desired  $B_U$  and  $B_L$  for a specified problem is discussed in [1, sections 21.4 and 12.2]. See an example in Fig. 1.3. The problem is to find the controller  $G$  and prefilter  $F$  of Fig. 1.2 such that the closed loop transfer function.



$$T_R(j\omega) = \frac{GP_j F}{1 + GP_j} \quad (1)$$

satisfies for all  $P \in P_j$ :

$$B_L(\omega) \leq |T_R(j\omega)| \leq B_U(\omega) \quad (2)$$

the distance from the  $-1 + 0j$  point constraint:

$$|1 + GP_j| \geq s \text{ i.e. } |1/(1 + GP_j)| \leq 1/s \quad (3)$$

and the constraint on the closed loop damping ratio [1 section 21.11]

$$\left| \frac{GP_j}{1 + GP_j} \right| \leq \gamma \quad (4)$$

where  $s \leq 1$  is a chosen parameter. The greater  $s$  is, the smaller the steady state sinusoidal error for a stated sinusoidal input [1, Sec. 9.2]. The gain margin  $\alpha$  and phase margin  $\gamma$  (see definition in [1, Sec. 8.18] including Log magnitude and phase diagram and polar plots of  $GP$  showing the gain margin  $\alpha$  and phase margin  $\gamma$  for open loop stable as well as open loop unstable systems [1, Fig. 8.40]) are related to  $s$  as follows: The gain margin  $\alpha$  is  $(1 - s)^{-1}$  and the phase margin is  $180^\circ - 2\cos^{-1}(s/2)$ . For example  $s = 0.5$  gives 6dB gain margin and  $30^\circ$  phase margin, which gives by equation 3

$$|1 + GP| \geq -6dB \quad (5)$$

The parameter ' $\gamma$ ' limits the maximum value of  $|GP_j/(1 + GP_j)|$ . For a second order system it also determines the minimum damping [1 section 9.3]

## 2.2 For Disturbance Rejection Specifications $D_1$ and $D_2$

There is given a set  $\mathcal{P}$  of linear time invariant single-input single output plants. The plant is embedded in a single degree-of-freedom feedback structure described schematically in Fig. 1.4. There is given an upper bound  $|M_D(j\omega)|$  on the magnitude of the control ratio from the disturbance input  $D_1$  ( $D_2$ ) to the plant output  $T_{D_1}$  ( $T_{D_2}$ ). See a typical example in Fig. 1.5. The problem is to find a controller  $G$  such that one of the following two options for disturbance rejection specifications is satisfied:

Option 1

$$T_{D_1}(j\omega) = \frac{P}{1 + GP} \quad (6)$$

satisfies for all  $P \in P_j$

$$|T_{D_1}(j\omega)| \leq |M_D(j\omega)| \quad (7)$$

Option 2

$$T_{D_2}(j\omega) = \frac{1}{1 + GP} \quad (8)$$

satisfies for all  $P \in P_j$

$$|T_{D_2}(j\omega)| \leq |M_D(j\omega)| \quad (9)$$

In both options the distance from the  $-1 + 0j$  point constraint should satisfy:

$$|1 + GP| \geq s \quad (10)$$

and the constraint on the closed loop damping ratio [1 section 21.11]

$$\left| \frac{GP_j}{1+GP_j} \right| \leq \gamma \quad (11)$$

where  $\gamma \leq 1$  is a chosen parameter which replaces the gain and phase margin, see equation 3. Guidelines for calculating  $|M_D(j\omega)|$  are given in [1 section 12.8].  $\gamma \geq 1$  limits the maximum value of  $|GP_j/(1+GP_j)|$ . For a second order system it also determines the minimum damping. For guidelines on choosing  $\gamma$ , see [1 section 9.3]

### 2.3 For Both Disturbance and Tracking Specifications

The problem described now is an integration of the two problems given in the two previous sections. There is given a set  $\mathcal{P} = \{P_j\}$  of linear time invariant MISO plants. The plant is embedded in a two degree-of-freedom feedback structure described schematically in Fig. 1.6. The closed loop system, from input R to output Y is plant sensitive. There are given bounds on this sensitivity in the form of two functions of  $\omega$ ,  $B_U(\omega)$  and  $B_L(\omega)$ , see Fig. 1.3. Similarly there is given an upper bound on the transfer function from the disturbance input to the plant output in the form of a function  $|M_D(j\omega)|$ , see Fig. 1.5. The problem is to find the controller G and prefilter F of Fig. 1.6 such that the closed loop satisfies the following three conditions for all  $P \in \mathcal{P}$ :

Condition 1: This condition is for tracking specifications. The transfer function from the prefilter input to the plant output.

$$T_R(j\omega) = \frac{GPF}{1+GP} \quad (12)$$

should satisfy:

$$B_L(\omega) \leq |T_R(j\omega)| \leq B_U(\omega) \quad (13)$$

Condition 2: This condition is for disturbance rejection specifications. Two options exists.

- Option 1: The transfer function from the disturbance input to the plant output  $T_{D_1}$

$$T_{D_1}(j\omega) = \frac{P}{1+GP} \quad (14)$$

satisfies:

$$|T_{D_1}(j\omega)| \leq |M_D(j\omega)| \quad (15)$$

- Option 2: The transfer function from the disturbance input to the plant output  $T_{D_2}$

$$T_{D_2}(j\omega) = \frac{1}{1+GP} \quad (16)$$

satisfies:

$$|T_{D_2}(j\omega)| \leq |M_D(j\omega)| \quad (17)$$

Condition 3: The distance from the  $-1 + 0j$  point constraint  $\gamma \leq 1$

$$|1+GP| \geq \gamma \quad (18)$$

and the constraint on the closed loop damping ratio [1 section 21.11]

$$\left| \frac{GP_j}{1+GP_j} \right| \leq \gamma \quad (19)$$

where  $\gamma \leq 1$  is a chosen parameter which replaces the gain and phase margin, see equation 3, and  $\gamma \geq 1$  limits the maximum value of  $|GP_j/(1+GP_j)|$ . For a second order system it also determines the minimum damping. Guidelines for choosing  $\gamma$ , see [1 section 9.3]

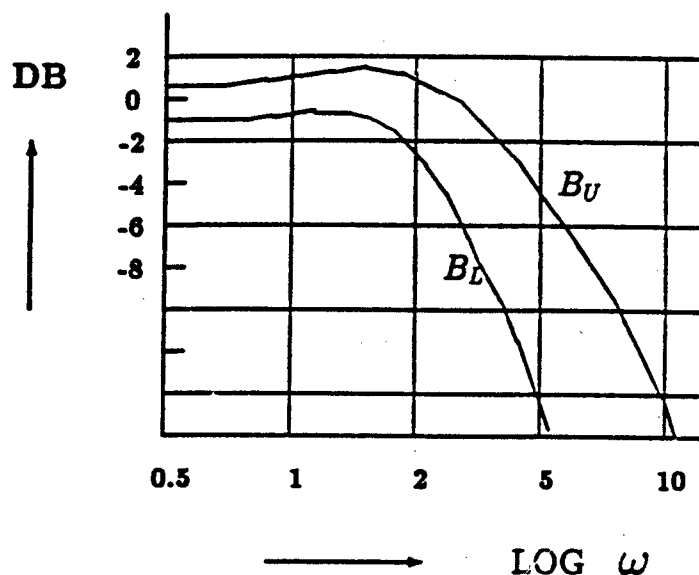


Figure 3: Typical closed loop tracking specifications

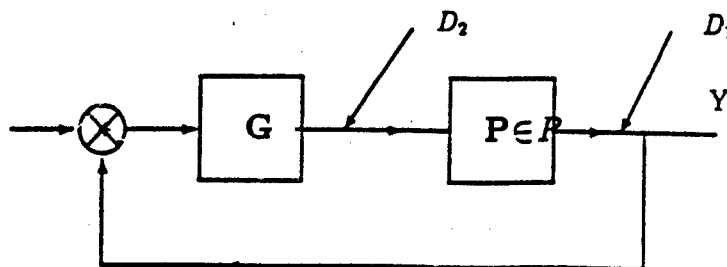


Figure 4: A disturbance rejection feedback structure

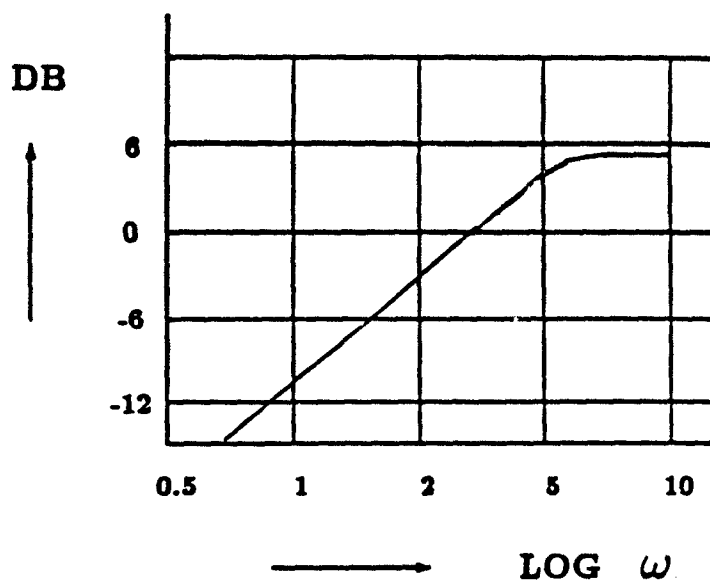


Figure 5: Typical disturbance rejection specifications

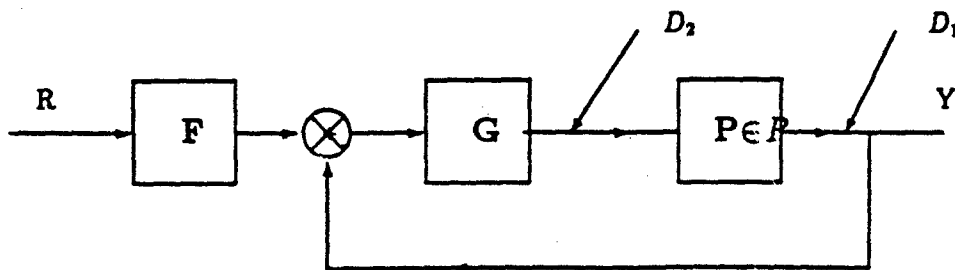
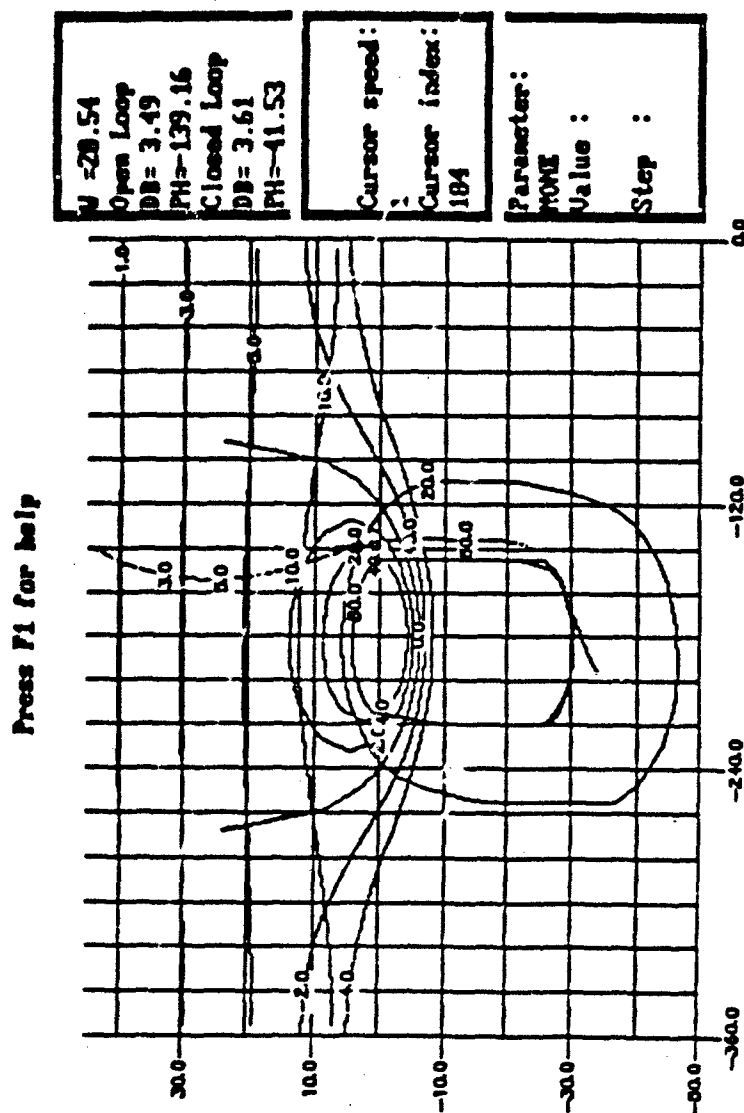


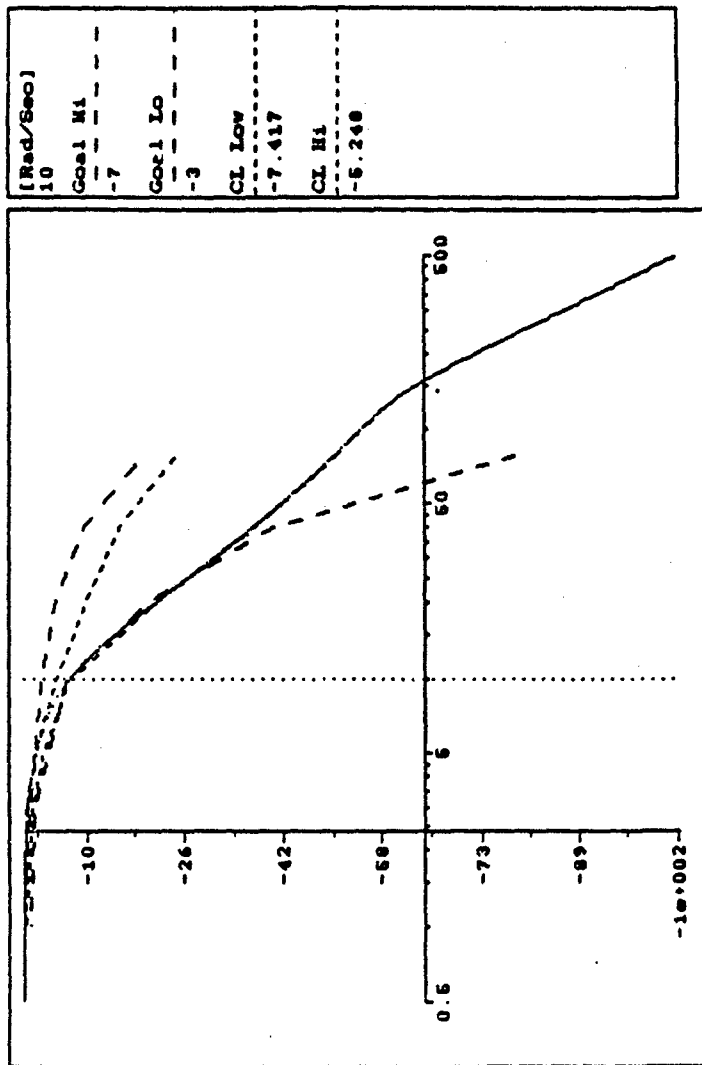
Figure 6: Schematic representation of a MISO feedback system

### 3 Examples

The following figures (7-9) shows the loop shape environment with all its options which includes cursor for reading the open and closed loop values. Bode plot of the maximum and minimum tracking transfer functions and one option of the simulations.



down end esc home left right s-tab tab up Ginput



-) (- or (sec)



TIME
0.5
Max value
0.9482
Min value
0.887

## References

- [1] J. J. D'Asso and C. H. Houptis, "Linear Control System Analysis and Design Conventional and Modern", McGraw-Hill, 1988.
- [2] Horowitz, I., "Synthesis of Feedback Systems With Large Plant Ignorance for Prescribed Time-Domain Tolerances", Int. J. Control, Vol. 16, No. 2, p. 287-309, 1972.



# Object-Oriented Design and Programming of a QFT CAD Environment

W. E. Bell, R. L. Ewing, I. M. Horowitz, G. B. Lamont, F. L. Trevino  
Department of Electrical and Computer Engineering  
Air Force Institute of Technology  
Wright-Patterson, Air Force Base, Ohio 45433  
lamont@aft.af.mil

## Abstract

The use of Quantitative Feedback Theory (QFT) has developed from a number of design and synthesis perspectives in order to achieve robust stability, robust tracking and robust gain and phase margins. Various models include multiple-input single-output (MISO) and multiple-input multiple-output (MIMO) feedback systems with continuous and discrete controllers. QFT's potential in solving real-world control problems requires extensive computer-aided design (CAD) facilities. Such a capability is required since considerable numerical and symbolic manipulation is employed in developing a robust controller for systems with plant parameter uncertainties and additive disturbances.

The objective of this paper is to discuss the general development of a computer-aided control system design (CACSD) package with emphasis on a QFT tool box. The design and implementation of such a software system is approached from an object-oriented point-of-view for ease of software maintenance and expansion.

Part I of the paper discusses the concept of object-oriented software design and programming. Part II deals with applying this discipline to the creation of a general CACSD package. Part III deals specifically with the development of the associated QFT CAD toolbox.

## PART I: Object-Oriented Software Design and Programming

In the software development process, the objective is to develop a high level design and then to decompose this design into lower level modules until reaching the primitive level (implementation/coding). Two software design approaches to decomposition are *functional* and *object-oriented design* (OOD). Most packages today are modular and are written using functional programming techniques. A *functional program* is a collection of tasks which the computer program sequentially executes, operating on data in the way each line instructs. Tasks are usually modularised into functional procedures (subroutines). Operations are processed through a hierarchical structure of procedures until the program is completed. An *object-oriented* (OO) program is also modular except the modules are objects instead of procedures. Objects contain both data and procedures that operate on that data. OO programs are not sequential in nature but are event-driven. An event is, for example, a user selecting a command from a menu object. The menu object contains an *event-handler* that sends appropriate messages to the other objects in the program instructing them as to what function the user has asked to be performed. Each object operates on its own data in order to achieve that function. Thus, the main difference between OO programs and functional programs can be viewed as nouns doing verbs (objects responding to messages) instead of verbs acting on nouns (sequential statements performing functions on stored data).

This part of the paper explains what is involved in applying OOD concepts. Section 1 gives a firm basis in definitions of terms used in the OOD process. Section 2 describes the OOD process. Section 3 introduces the specific OO environment of Borland Turbo Pascal 6.0 Turbo Vision[1] (the OO programming language used in this CACSD implementation). Sections 4 and 5 give the advantages and disadvantages of OOD over functional design. And finally Section 6 presents a summary of benefits in using OOD for reliability, maintenance and user interface within currently evolving engineering software packages, such as ICECAP-PC[2, 3].

### 1 Terminology

In order to understand OOD, the reader needs a comprehensive understanding of the terms used in the OOD process[4, 5]. This section is a dictionary and discussion of the terms used in this paper.

#### 1.1 Abstract Data Types

Examples of data types can include integers, characters, and boolean variables along with their associated operations. A more formal method of defining data types is the concept of *abstract data types* (ADT). By formal definition, an ADT is a *three-tuple*,  $(D, F, A)$ , where  $D$  represents the domains of the data type,  $F$  the functions (services, procedures, methods or functions) on the data type, and  $A$  is a set of axioms (first-order predicate calculus) that encode the desired semantics of the operations[6]. An ADT is an encapsulated data structure with its associated functions. An explicit enumeration of the axioms is usually not included since testing is employed to validate the functions. The ADT state by definition is the value of the data structure variable. The ADT data and functions provide the interface to the user and their implementation is not visible (interface). The invisibility of an ADT's state and the separation of its interface component from its implementation are the distinguishing features which separate an ADT from a simple data type such as an integer. The ADT provides the fundamental basis for the OO concept of an *object* and a *class*.

#### 1.2 Object

All computer programs operate on structured data sets. Typical data structures are stacks, queues, arrays and records. An *object* is an entity that contains both attributes and services that operate on the attributes. In CACSD OO development, a typical object may be a matrix, polynomial or transfer function with its associated procedures for manipulation (eigenvalues, roots, time response, etc.).

An object is implemented in a computer program by three main parts: its attributes, an event handler, and services. The *attributes* are the data types the object maintains and is stored in the computer's memory under the object's name. The *event handler* is a listing of messages to which the object can respond and the services the object should enact if the corresponding message is received. The *services* are executable procedures that operate on the object's attributes and send messages to other objects. Their counterpart in functional programming would be subroutines.

### 1.3 Class

A *class* is a higher level of abstraction than an object, that is, a set of objects can share the common structure and common behavior of a class. A class is defined as a collection (set) of services and a collection of attributes. The class must also have a name. The class interface consists of *public* (visible) elements, *private* (invisible) elements, and *protected* (visible only to subclasses) elements. When the attributes and services can be accessed by other objects, they are visible outside the object. If they can not be accessed by another object, then the attributes and services are defined as invisible, i.e., *information hiding*. In selecting a class, the criteria includes reusability, complexity (time and space), and attributes. This definition represents the general ADT concept as previously presented in terms of data and functions (services).

An object is by definition an *instantiation* or *instance* of a class. The object has all the attributes and services of its class. The object *state*, which only changes through invocation of the services, consists of the associated attribute values or instance variables. Although each object has its own unique state, the services are identical in all objects instantiated from the same class. So while a class defines services and attributes, classes do not contain any real data until they are instantiated existence as an object. Objects from the same class, therefore, share the same services but not the same instantiated variables! A class is a template for an object. An object is an instance of an ADT with the added property of method inheritance.

*Class inheritance* is a relationship among classes whereby one class shares the structure and behavior defined in one or more other classes. Under instantiation, unique data variables are created for the object, but the class services are used for the object services. The instantiated object can also have its own unique services or modify the ones it inherits.

An inheritance hierarchy of classes is a tree structure that permits any class in the tree to inherit and operate using any service or attributes in a class higher in the tree. The utility of this inheritance is that once a class has been fully written and tested, it never needs to be modified again. These same capabilities can be used by future objects by simply declaring them to be instantiations of the first object's class. This vastly simplifies the process of software development and maintenance using OOD.

Inheritance defines the structure and capabilities of a class while instantiation defines lines of ownership and control of actual data. The two concepts are quite different and understanding this difference is key to understanding object-oriented analysis, design and programming.

### 1.4 Object-Oriented Analysis (OOA), Design (OOD) & Programming (OOP)

*OOA* is an OO approach to problem requirements definition[7]. *OOA* attempts to identify the classes and objects that model the application context. *Domain analysis* attempts to identify the classes and objects that are common to all applications within a specified domain such as CACSD. *Partitioning* of classes in this process can be quite difficult in general. Approaches to partitioning include categorization, clustering and prototyping. *Categorization* of group entities is based upon properties or characteristics that form a predefined category. *Clustering* refers to grouping entities according to some high level description such as name. *Prototyping* refers to the predefining of a prototypical type for a class of objects. Other objects are members of that class if they resemble this type.

*OOD* is a design methodology using *OOA* decomposition. The *OOD* process consists of identifying the classes and objects from the *OOA* level of abstraction, identifying in detail the attributes and services of each class and object, identifying in more detail the relationships between objects, defining message connections

(event handlers), and implementing object modules. There is in general no unique optimal OOD in any given application.

*OOD* is a programming technique coding collections of objects. Evaluation of implemented objects (or classes) can be done using standard programming discipline metrics such as object coupling, cohesion, sufficiency, completeness and primitiveness. *Coupling* refers to the relationships between objects, *cohesion* refers to the relationship between internal object constructs. *Sufficiency* and *completeness* refer to the object having enough of all possible behaviors so as to be useful. *Primitiveness* refers to when a desired program behavior can be implemented by not accessing invisible structures of an object. The chosen computer language should have the proper OO constructs of classes and objects. Examples include Ada, C++, Smalltalk and TurboVision which vary in their OO constructs.

OOD notation can be expressed in a set of hierarchical graphs: class diagrams, state transition diagrams and object diagrams. Although not enumerated here, specific icons can be associated with the characteristics of each diagram[4]. A *class diagram* presents each class and its relationship with other classes. The dynamic behavior of the class is represented by a *state transition diagram* which portrays the transition from state to state as caused by an event handler as well as the actions resulting from a state change. The *object diagram* presents each object and its relationship to others. Since objects are created and destroyed during program execution, the object diagram represents the dynamics of the object. Object diagrams are prototypical classifications. By construction, class and object diagram development document the logical design of the system.

## 2 OOD Process

This section presents a practical approach to applying the OOD process to software development. OOD allows the software engineer to take advantage of three important software design concepts: abstraction, information hiding, and modularity. The process of OOD begins with OOA. First, a paragraph is written in plain English language that describes the objective of the computer program. Classes/objects are extracted from the paragraph by underlining the nouns in the sentences. *Attributes of objects* are extracted by underlining the adjectives of the sentence and grouping them with their associated objects (nouns they modify). *Services* are identified by underlining all the verbs, verb phrases, and predicates in the sentences. *Attributes of the services* are found by underlining all the adverbs and grouping them with their associated services (verbs they modify)[7]. Each grouping of attributes and services is identified using categorization, clustering or prototyping.

A modified methodology[7] involves the following steps:

- 1 Define the problem to be solved
- 2 Decompose the problem into classes/objects
- 3 Determine each object's required attributes
- 4 Determine each object's required services
- 5 Determine interfaces between attributes and services
- 6 Determine a parent-child hierarchy related to the attributes and services (classes/objects)
- 7 Determine inheritance relationships related to attributes and services (classes)
- 8 Create a user-interface object (message connections/event handlers)
- 9 Create each object

The first four steps are achieved as in the OOA phase. There exist many techniques for iteratively applying these four steps further down levels of abstraction until finally arriving at the primitive level. At this lowest level the objects required to solve the problem are obvious, as are the services they need to perform, and the associated attributes they need to use.

Step 5, determining interfaces between objects and services, is done by determining how each object depends on the others. From this it can be determined what messages each object needs to send to the other

objects. Event-handling routines are designed for each object, so they can perform the desired services when the message is received.

The next two steps (6 & 7) are related and display one of the advantages of OOP at the implementation level. The objects that have services and attributes in common are grouped into classes. These classes can be completely separate from one another, or they may have common attributes or common services. Whenever possible, blocks of code should not be repeated, so if the classes have common attributes and services, then these common attributes and services are grouped into a class of their own, and the original classes are made children of that new class. This class may not make sense as an object in itself and there may never be an object who is a direct instantiation of it, but its children would have "tighter code" since they have this "library" of ready-made services to use.

Step 8 creates an interface object which can serve as the system interface between the human user and the internal objects. This interface object contains the overall event-handling service as well as most of the file and screen I/O.

The final step is to pick a particular language and implement the design in code[8]. The next section describes such a language.

### 3 Borland Turbo Vision

Borland<sub>TM</sub> provides an excellent pre-defined object library in its Turbo Vision[1] package available with Turbo Pascal V 6.0 and Turbo C++. The Turbo Vision object library provides a predefined framework to develop OO windowing applications and OO interfaces including:

1. Multiple, resizable, overlapping OO windows  
(handy for viewing the same function on multiple planes such as x, y and w)
2. Mouse support
3. Drop-down menus and dialogue boxes for user input
4. Buttons, scroll bars, checkbox boxes and radio buttons
5. Standardised event handling for keyboard and mouse events

Experience with Turbo Vision has shown that while it presents an intense learning curve, time spent learning it is worthwhile. One word of caution: if the decision is made to build an application with Turbo Vision, the entire project should be built using Turbo Vision objects and standards. Attempting to mix standard functional code with Turbo Vision objects can create memory conflicts. Another point to note is that Turbo Vision programs are not portable between platforms; Turbo Vision programs are limited to MS-DOS computers.

Turbo Vision consists of a class diagram (PART II, Table 1) of predefined class types that provide a basic user interface. The term "family tree" is used to indicate the inheritance lines of each class.

The root class of Turbo Vision is TObject. TObject has no ancestors and is extremely limited functionally. It has a constructor (Constructor INIT), a destructor (Destructor DONE), and a service (Procedure FREE) that disposes of the instantiated class (object) and frees its memory. TObject has six child classes, among whom is TView. TView is of primary importance because its children provide the user interface.

TView is the parent to all classes which can write to the screen. The Turbo Vision standard is that all screen writes be accomplished via the TView.Draw service. While it is possible to use the standard Pascal write and writeln statements, it violates the Turbo Vision standard and their use is strongly discouraged. The writeln and readln statements employed for user input are replaced by dialogue boxes which are descendants of TView. TView has another important property; it is the lowest class on the tree that is capable of message transmission and reception. Thus, any class that needs to communicate with other classes should be a descendant of TView whether or not they are visible to the user on the screen. All the "workhorse" type classes in Turbo Vision are made descendants of TView. For example, a matrix object, a polynomial object, or a transfer function object should all be instantiations of TView descendants. TView has several descendants,

such as TApplication, TDialog, TDesktop, TMenuBar, and TStatusLine. The following discussion is limited to these classes as they are of primary importance. For further information, the Borland Turbo Vision Guide[1] that comes with Turbo Pascal V 6.0 is highly recommended.

The focal point of any Turbo Vision program is always an instantiation of TApplication which the programmer must define. Furthermore, there should be only one TApplication object for any given program. This object owns via instantiation all other objects, handles all message dispatching, communicates directly with the main menu, manages idle times, and processes computer errors.

Descendants of TDialog provide pop-up dialogue boxes for user input. Dialogue boxes contain radio buttons, check boxes, list boxes, and input lines. *Radio buttons* are input devices that allow the user to choose only one item among a palette of options. *Check boxes* are input devices that allow the user to choose any combination of items among a palette of options. *List boxes* provide a list of items to choose from, such as files on disk or directories. *Input lines* provide text entry of a string variables. Each of these (radio buttons, check boxes, list boxes and input lines) are descendants of TView. Each can be instantiated into a descendant of a TDialog object. Many fine examples are given in the Turbo Vision Guide[1].

Other classes are TDesktop, TMenuBar, and TStatusLine. TDesktop is simply the background view upon which all other visible views appear. TMenuBar is the menu bar object that displays and controls drop down menus. TStatusLine provides a bottom frame to display and control shortcut keystrokes and other useful information such as remaining heap size.

Event Handling is always a big design concern in OOP. In Turbo Vision, all events are represented via a TEvent type record. TEvent is a record that identifies the type of event that has occurred. While, all events are not commands, all commands are events. For example, the movement of a mouse pointer is not a command; however, it is an event. All Turbo Vision classes have event handlers to process TEvent records; however, the descendant of TApplication is the highest level for all event-handling.

Turbo Vision provides several tools to relieve the software engineer of many mundane chores of interface design while allowing all the benefits of programming in a typical high-level language. Execution speed, numerical precision, and mathematical algorithms are all designed with far greater control and efficiency than could ever be attained by developing our own language interpreter like commercial control system packages often do. Once the initial obstacle of learning OOD, OOP and the Turbo Vision toolbox are mastered, building applications becomes quick and effective.

## 4 Advantages of OOP

The following opinions were formed from specific experiences after modifying and debugging the functional version of ICECAP-PC (a CACSD package) and then having translated it into OO code. While the experiences discussed here are based upon a specific package, they can certainly (based on discussion found in current literature of similar design projects) be generalised.

*File I/O Abstraction:* A typical danger spot in functional programming is opening a data file in one section of the code and then closing it (or forgetting to close it, or hitting some conditional branching statement that bypasses its closing) in some later section of code. In OOP, a database-type object is used which is the only object in the program that can get and save data from files. Therefore, only one OPEN/CLOSE command pair is used for the entire program.

*User I/O Abstraction:* An advantage of the user interface object is that it abstracts the programmer from having to worry about any user I/O during the writing of the mathematical code, etc. One object deals with user requests and translates the requests into event messages to be sent to the "workhorse" objects. Likewise, the same object returns the workhorse answers to the user in some screen format. Thus the workhorse object need only contain code for the algorithms to convert the input into the correct output.

*Object Abstraction:* The software engineer can design at the highest level of abstraction listing the upper level tasks that need to be done to solve the problem assuming that some object can do each task. Then one moves down one level of abstraction and takes each task and decomposes down into subtasks assuming some object (or service) can do each subtask. This is done down to the primitive/coding level. Debugging is

decomposed the same way. The software engineer looks at the input and output of the highest level object. If it is wrong, the input and output of each of the objects in the next level down is examined. Only the object with an incorrect input/output pair must be further decomposed. Because each object is thus self-contained, it makes maintenance very simple.

**Smaller Code:** After the main classes in the program are fully defined in terms of what attributes and services they need, inheritance is used to decrease the size of the code. A Library class can be defined that becomes the parent of all the main workhorse classes. This Library class contains all the services that the workhorse classes hold in common. This means that each of the separate classes are smaller because they can globally access the services they inherited from their parent Library. Library might contain services to decipher user textual input, to work with data files, and other general purpose type services. The classes could also be made smaller by the creation of a math library class. This class might contain services to do common mathematical functions.

**Productivity:** Because the object library from Borland Turbo Vision was available, productivity was found to be much higher than would be typically expected in software development. The functional version of ICECAP-PC was not complete in the human factors engineering area because only so much time could be devoted to menuing systems and output screen formatting and context sensitive help screens. Using the professionally packaged class library of Turbo Vision, the software engineer is able to focus almost completely on CACSD algorithms and let the commercial package take care of user I/O. Because of this, the authors have been able to work on expanding ICECAP-PC's CACSD toolboxes beyond that which could otherwise have been accomplished. Furthermore, later researchers should be able to go even farther since the overhead of porting the ICECAP-PC subroutines into an OO environment has already been accomplished.

**Reliability:** OOP disciplines produce more reliable code due to modular debugging and use of existing objects that have been debugged through years of use. In the case of ICECAP-PC, the benefits of two worlds have been inherited. At the upper level, the program has its I/O based on a commercially produced and tested package (Turbo Vision). At the primitive level, the object services are based on the basic control system algorithms from ICECAP-PC (developed since 1977 and used by a large student body). After the OO program had been tested at all levels of abstraction, new objects could be added to the existing reliable code with a high degree of confidence in the reliability of the CACSD package as a whole.

**Maintainability:** The same OOP disciplines produce more maintainable code due to the self-sufficiency of objects. Proper OOP techniques avoid the use of global variables and low functional independence which often plagues functional program modules. If each object is compiled (relatively) separately and it responds with expected output responses to test inputs, then it does not display the undesirable dependence qualities of low *cohesion* or high *coupling* with some other object.

This paper claims that following proper OOP disciplines results in highly *cohesive* code, because each object is functionally bound to operate on its data alone. Of course, while objects higher on the parent-child tree own more data, they still perform only one higher level function. The higher level object is made up of smaller objects who are each functionally bound to operate on their more specific piece of the data. This recurses down through the object tree until the primitive level is reached. At this lowest level, very cohesive services (subroutines) are written.

In the same way, following proper OOP disciplines results in low *coupling* between objects, because each object is again functionally bound to operate on its data alone. High external and common coupling is avoided by only having a single object which is able to access the central data file. Furthermore, high *content* coupling is rendered almost impossible in OOP because it is not possible (without trying very hard) to branch into a service located in another object or into a service located inside the same object. However, in order to save some code, the use of limited *control* coupling (using global flags to control how some objects respond) has been found to be useful. In the strictest sense, using these global flags do break the rules of OOP.

## 5 Disadvantages of OOP

Only two disadvantages with using OOP have been experienced, neither of which are directly related to OOP itself. The first can be attributed to learning a new programming language and learning a new way of thinking about algorithms to solve problems. The second can be attributed to the decision to operate within an MS-DOS environment.

Any time a new programming syntax must be adopted, there is a learning curve that must be overcome. With OOP this is doubly true, because not only must the syntax of Turbo Vision, or some other OO language package, be learned, but the software engineer's thinking process must change. Humans typically think in functional terms. Therefore, the transition into OOP is not as intuitively easy as using functional programming techniques.

Any time code is developed within the MS-DOS environment, limitations are placed on how much memory room is available for use by the program. A stack cannot be larger than 64K, variable declarations cannot be larger than 64K, and the compiled program and heap space (dynamic variable space) cannot exceed 640K. The 640K barrier can be overcome in Turbo Pascal by breaking the compiled code into overlay units, but even then each unit cannot be larger than 64K and must be able to be compiled to some extent separately from the other units. These memory restrictions place some limit on how closely one can follow the generally accepted rules of OOP.

Ideally, the objects required to solve the current problem should all be allowed to remain in memory at once. Due to heap limitations, several large objects cannot be instantiated in the heap at once. This forces the use of *common data coupling* or *temporal* and *procedural* cohesion in order not to lose data when one object's data memory locations must be released for use by the next object. The solution is to keep compiled object code as small as possible. Also the size of code inherited from an object's parents must be monitored. If an object's local code is 64K, but it inherits 30K of services from its parent, then it is too large to be used as a Turbo Pascal overlay unit. Because of this tradeoff between heap size and object size, it has been found necessary to break the rules of OOP by using compiled units that are not objects, but are "global procedure libraries".

Use of these global variables, control flags, and procedures is done very cautiously and only when absolutely necessary. Eventually, as more clever ways of defining the objects in ICECAP-PC are found, this "fast-prototyping" answer is to be replaced with more reliable and proper OO code.

## 6 Summary of Object-Oriented Approach

Object-oriented design and programming has grown to a standard practice because of various benefits over functional design and programming. Such advantages include the reuse of existing software components, more maintainable systems, reduction of developmental risk, and use of OOP language constructs. Disadvantages include the higher cost of development and possible performance degradation due to message passing, the multi-layer abstraction, hierarchy of classes, and associated memory and execution overhead.

The OO approach generally results in smaller systems because of reusable subsystems and thus the OO system are more amenable to providing an economic framework for evolution. The original ICECAP-PC was developed using the functional design approach as were its predecessors. The new OO version of ICECAP-PC provides for better reliability, maintenance and user interface.

As has been introduced in this part of the paper and is further discussed in Part II, it has been found that OOP seems to offer new opportunities in the design of engineering packages. Specifically it has been found that a commercially packaged object toolkit like Borland's Turbo Vision abstracts the software engineer from the concerns of user interface and allows concentration on the mathematical algorithms and instruction within the CACSD package.



## PART II: An Object-Oriented CAD Environment

CACSD software development is an inherently complex process because of (1) the multitude of mathematical operations and capabilities required and (2) the variety of requirements posed by the end users (control students and control engineers).

Relatively new, and growing rapidly, is the use of object-oriented design (OOD) and programming (OOP) techniques as presented in PART I. While the software engineering community has embraced this technique with open arms, other engineering disciplines, control systems engineering inclusive, have been slow to adopt this technology. The purpose of Part II is to discuss the object-oriented ICECAP-PC Release 10 project now underway at the Air Force Institute of Technology.

### 1 Scope of Effort

Since 1977, graduate students [9, 10, 11, 12, 13, 14, 15, 16] at the Air Force Institute of Technology (AFIT), have contributed to the development of the Interactive Control Engineering Computer Analysis Package (ICECAP) program. In 1985, ICECAP-PC[17], a Pascal version of the mainframe program using structured and functional design techniques was tailored to the personal computer. This Pascal version of ICECAP-PC has gone through various design revisions with current research involving the object-oriented (OO) redesign using the interface definition of Turbo Vision[1]. ICECAP-PC is a public domain CACSD tool targeted for educational use. This is not meant to imply deficient capabilities. Rather, every effort is made to ensure that ICECAP-PC Release 10 is mathematically correct, rich in capability, and both easy and quick to use from a user's perspective. The purpose is simply to challenge the state-of-the-art in CACSD software design. The new ICECAP-PC is easier to use, more accurate, faster, leaner, more capable, and more robust than prior versions.

### 2 Design Goals

The first priority is to provide a CACSD environment to perform basic control system analysis functions such as polynomial and matrix manipulations, and time and frequency domain analysis with a user-friendly interface including graphical presentations, help, and macro facilities. These exist already in the current functional version of ICECAP-PC. In addition to improving these, the following are to be provided:

- A context sensitive help facility.
- A "systems build" capability to design a control system graphically in block diagram form.
- An improved user programmable macro language.
- An improved root finding capability.
- A nonlinear simulation capability.
- An improved MISO and MIMO QFT toolbox (continuous and discrete systems)
- An improved report generating facility.
- A Database Metadata Dictionary

Providing a new user interface using proven human factors engineering (HFE) concepts is also a top priority. This interface should be both intuitive and powerful to satisfy both the novice that normally uses menus as currently employed in ICECAP-PC and the professional who wants direct access to the underlying algorithms. This interface includes single-stroke menu selection, MatLab/MatrixX type data input with direct entry of complex numbers, one-stroke shortcut keys to circumvent novitiate menu levels, and a macro facility for system programming.

## 2.1 CASE Environment

Besides OOP, another new technology revolutionising the software design process is computer-aided software engineering (CASE). CASE provides an integrated set of tools which increases productivity and empowers the production of more reliable and more maintainable code. The desire for ICECAP-PC to inherit all the benefits of CASE was the basis for using the Turbo Pascal 6.0 Turbo Vision OO environment. The Turbo Pascal 6.0 Compiler, Profiler, Debugger, Make, and Touch tools provide limited CASE environment. The Turbo Vision tools force the OO discipline upon the code. Thus the claim is made that OOD coupled with an integrated programming environment like Turbo Pascal 6.0 is, indeed, a CASE environment[8].

The advantages of developing ICECAP-PC in a CASE environment have been extensive. Most of these advantages have already been discussed in Part I of this paper: better file I/O handling, better user I/O, better code design, better debugging, smaller code size, increased productivity, more reliable code, and more easily maintainable code. One of the largest benefits of the newest CASE environments is the concept of automatic code generation. The user describes the desired flowchart of functions, and the CASE tool writes reliable code. Turbo Vision offers a similar capability in the form of precompiled libraries of objects. It has been said that 80% of code development is spent on user interface overhead, but Turbo Vision already has all the mouse support and menuing system support and windowing support any CACSD package requires.

## 2.2 Interface

The Interface for ICECAP-PC is a menu-driven, mouse-supported interactive system. Simple drop-down window menus form the main command interface and replace the command line and menu system of the previous version. All drop-down menus are activated using the mouse or single keystrokes. The user enters the data in a MatLab/MatrixX style input line. Furthermore, the input line has a history buffer and all prior entries can be recalled and edited. While general commands are processed with drop-down menus, the user interacts with dialog boxes to provide specific instructions. Mathematical operations also use dialog boxes. Hot keys add additional speed to the command entry process.

The main menu consists of only three levels at its deepest point. The user does not have to descend through several levels of menus to get to the desired function. The "Tools" menu option replaces the main menu with the specified toolbox main menu. The QFT toolbox and its menu are discussed in Part III of this paper.

## 3 ICECAP-PC Structure

ICECAP-PC has ten predefined matrices, ten predefined polynomials, and ten predefined transfer functions. All matrices, polynomials and transfer functions share a common data type and are located in a single disk file.

While other data types are used for program control, using a unified data structure was found to provide enough similarity between matrices, polynomials and transfer functions to make them children of the same parent, thus greatly saving program code size and memory.

The following paragraphs describe the classes used to implement ICECAP-PC. The relationship of the ICECAP-PC classes are explained to be children of classes in Turbo Vision. Table 1 shows the class structure of ICECAP-PC. All ICECAP specific classes are denoted with an asterisk.

TIceMain, a child of TApplication, is the main program class. The main job of TIceMain is to process events from the main menu, from shortcut keys and messages from other classes. Additionally, it processes background tasks, such as updating the screen buffer and the heap viewer, during idle periods. IceMain is the instantiation of TIceMain and owns all other classes through instantiation.

TViewInterior is an important class that owns all the I/O devices. It owns the view screen and is the sole class in ICECAP-PC that is allowed to write to it.

TLibrary is the parent class to TMacro, TMatrix, TTransFunc, and TQFT. By defining this service in TLibrary and making TMatrix, TTransFunc, TMacro and TQFT children of TLibrary, the Parseline service

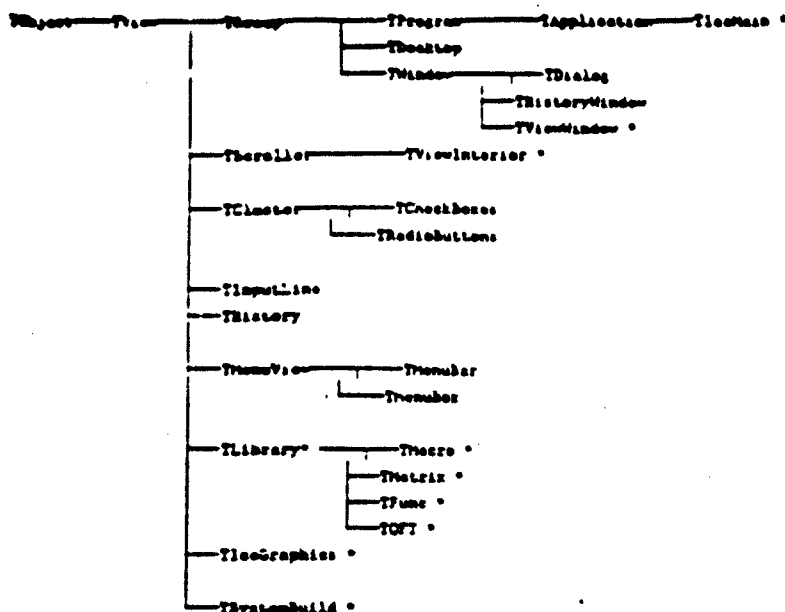


Table 1: Complete Family Tree Structure of ICECAP-PC

is inherited by all four classes, thus reducing the overall code size. TLibrary has two other services that merit mention, specifically the only two services in ICECAP-PC that are allowed to access data on disk are TLibrary.RetrieveData and TLibrary.StoreData. This prevents the common error of leaving data files open thus making the program vulnerable to a crash. These two services open the file, read/write the data, close the file and send the variable to the caller.

Children of TLibrary are TMacro, TMatrix, TTransFunc, and TQFT. TMacro provides the macro language capability for ICECAP-PC. TMatrix is the class responsible for all matrix operations. TTransFunc is the class responsible for all transfer function and polynomial operations. TQFT is the class responsible for the QFT implementation.

As is discussed in Part I of this paper, the most difficult step in OOD is defining the objects. When the viewpoint of the lowest level of abstraction is taken, it would seem logical to the strictest OO designer that each polynomial and matrix and transfer function should be an object. Then when the user asks for a frequency response of the open loop transfer function (OLTF), the OLTF object would draw a frequency response of itself on the screen. However, when the viewpoint of the OO software engineer is taken, it becomes more logical to think of some nebulous transfer function object that owns each of the individual transfer function data records. When the user asks for two transfer functions to be added together, the transfer function object services carry out the task. How could two objects add themselves to each other? There would have to be some owning object who could simultaneously access both their individual data records. The ICECAP-PC data structure has been designed using the latter implementation viewpoint.

Using the idea of not having each polynomial or matrix be its own object and having an overall Polynomial and Matrix object, these parental objects are called Toolboxes. The current toolboxes within ICECAP-PC are the transfer function/polynomial toolbox, the matrix toolbox, the macro toolbox, the nonlinear toolbox, the system build toolbox, the database toolbox, the digital signal processing (DSP) toolbox, and the Quantitative Feedback Theory (QFT) toolbox. Each toolbox can be thought of as a major division of the program which the user would use to solve a given problem. The functions of each of the toolboxes are described briefly. Other toolboxes are in development.

The transfer function/polynomial toolbox within ICECAP-PC provides the basic building block mathematical algorithms necessary to design control systems using conventional (as opposed to modern) control techniques. The toolbox is composed of objects of one class called TTransFunc. This class contains all

the services required to manipulate polynomials and transfer functions (ratio of polynomials). There are polynomial services such as adding, subtracting, multiplying, defining, modifying, etc. There are transfer functions services for forming closed loop transfer functions, finding time equations, taking partial fraction expansions, and transforming into state matrices, etc.

The *matrix toolbox* within ICECAP-PC provides the basic building block mathematical algorithms necessary to design control systems using modern (as opposed to conventional) control techniques. The toolbox is composed of objects of one class called TMatrix. This class contains all the services required to manipulate matrices. There are basic matrix services such as adding, subtracting, multiplying and advanced services such as eigenvalues, controllability, observability, etc.

The *macro toolbox* within ICECAP-PC provides a batch language which allows automatic performance of program operation. The toolbox is composed of objects of one class called TMacro. This class contains all the services required to edit macro files, translate macro files into program input commands, and provide user interface during macro file execution.

The *nonlinear toolbox* within ICECAP-PC provides the capability for nonlinear simulation of system transfer functions. The toolbox is composed of objects of one class called TNonLinear. This class contains all the services required for nonlinear simulation modeling. The services include support for both semi-automatic and interactive linearisation of nonlinear systems.

The *system build toolbox* within ICECAP-PC provides the ability to construct system transfer functions from icon representations of gains, filters, nonlinearities, time delays, frequency response, etc. The toolbox is composed of objects of one class called TSysBuild. This class contains all the services needed for the graphical user interface as well as program control to generate the necessary commands to generate the transfer function described by the icon representation.

The *database toolbox* within ICECAP-PC provides all the data storage and retrieval functions as well as data interrelation functions. The toolbox is composed of objects of one class called TDataBase. This class contains all the services required to control data flow between the program and disk files. It also contains the class level applications which maintain relational information tables between data items known as the Database Metadata Dictionary.

The *DSP toolbox* within ICECAP-PC provides a no-frills ability to perform some limited digital signal processing (DSP) technology demonstrations. The toolbox is composed of objects of one class called TDSP. This class contains all the services required to do convolutions, fourier transforms, complex phaser rotation, and signal aliasing.

Graphical representation of time/frequency data is provided by the *Graphics toolbox* using the Graphics class. User modification of matrix/polynomial objects within the Graphics object, requires an interactive interface such as function keys, cursor controls, or a mouse. Implementation of this interactive environment involves the mapping of a graphical object into memory, and enabling the image to be moved by cursor control without conflicting with other graphical objects. Within each interactive graphic display environment, the user is able to drag an image across the screen. When this image moves, it does not disturb the pixels underneath the image.

The *QFT toolbox* within ICECAP-PC provides the basic building block mathematical algorithms necessary to design control systems using QFT control techniques. The toolbox is composed of objects of one class called TQFT. This class contains all the services required to define tracking and disturbance specifications, enter plant variations to manipulate transfer function matrices, enter disturbance models, generate plant templates, generate bounds, design a nominal loop transmission, generate a controller, design a filter, simulate responses, and generate a comprehensive report.

## 4 Testing and Validation

Perhaps the most important aspect of a CACSD package to the engineering user is its ability to give correct answers. While ICECAP-PC can in no way claim the level of testing and validation done on a commercial package, certain disciplines have been strictly adhered to during the code development. ICECAP-PC has

been tested and validated throughout the coding stage using black box testing, white box testing, and its macro language toolbox.

Black box testing is the process of looking at the CACSD package as a black box which accepts inputs and produces outputs. The tester does not care how the package arrived at the outputs, as long as they are the correct outputs for the inputs given. As each service was created within ICECAP-PC, a page of all possible input patterns was constructed as well. When the service was completely coded, each input was applied to it and the output was checked for correctness.

White box testing is the process of looking at the internal algorithms within the CACSD package. The tester provides an input to a service or object and then traces through the program code one step at a time examining all the variable states and how they are affected as the algorithm progresses toward the output. During white box testing the code is tested for both robustness and efficiency (in terms of memory use, execution time, and other machine-oriented parameters).

The macro language facility within ICECAP-PC is used to its fullest during the testing phase especially during black box testing. The pages and pages of test conditions are programmed into macro files which are available with the ICECAP-PC source code. This saves the tester much time during the many iterations of running examples, finding errors, correcting the code, and rerunning the same examples until they run correctly. This also guarantees correct and repeatable inputs to the program during testing.

## 5 Object-Oriented CAD Summary

The new ICECAP-PC has benefited greatly from the use of OO technology. OOP has made the use of memory more efficient in both the heap space and the stack. The user interface has been improved in both ease of issuing commands and context sensitive help and error messages for the commands. Furthermore, the forced modularity discipline of the object structure has produced more reliable, efficient, and maintainable code.

As in any CACSD package, successful design depends on clean, efficient, and mathematically correct numerical methodology. Thus it is incumbent on the CACSD designer to carefully choose the algorithm, and to seek ways to improve the accuracy of the math foundation. One of the principle goals of the ICECAP-PC project is to take a careful look at the underlying math routines and find ways to improve them.

Taken as a whole, the OO ICECAP-PC is a much sturdier base upon which to develop the QFT CAD toolbox described in Part III of this paper.

### Part III: An Object-Oriented QFT CAD Environment

Quantitative Feedback Theory (QFT) quantitatively formulates various factors in the form of sets (a)  $T_R = \{T_R\}$  of acceptable command or tracking input-output relations (b)  $T_D = \{T_D\}$  of acceptable disturbance input-output relations, and (c) a set  $\mathcal{P} = \{P\}$  of possible plants. The object is to guarantee that the realized control ratio  $T_R = Y/R$  is a member of  $T_R$  and  $T_D = Y/D$  is a member of  $T_D$ , for all  $P$  in  $\mathcal{P}$ . That is, various bounds are specified *a priori* for acceptable performance in regard to each transfer function relationship [18, 19, 20, 21, 22].

QFT methods have been developed for both linear and nonlinear, time-invariant and time-varying, continuous and sampled-data, uncertain multiple-input single-output (MISO) and multiple-input multiple-output (MIMO) plants, as well as for output and internal variable feedback models and distributed systems.

The QFT frequency-domain technique involves  $s$ ,  $z$  and  $w$  domain transformations of the specifications and variable plants. Most of the QFT design steps have been automated in CAD packages [10, 2, 3]. Using an OO approach in this ICECAP-PC toolbox, the various QFT objects presented in the following discussion are associated with various services. The OO window interface guides the user step by step through the QFT MISO phases (specifications, plant models, disturbance models, templates construction, loop transmission generation, filter generation, simulation and reporting). In the MIMO QFT CAD process, transfer function matrix manipulation is provided as discussed in the following section.

## 1 MIMO QFT Synthesis Approach

The QFT MIMO synthesis problem [23, 24] is converted into a number of MISO single-loop feedback problems in which parameter uncertainty, external disturbances, and performance tolerances are derived from the original MIMO problem. The combined solutions to these MISO single-loop problems achieve the desired performance for the MIMO plant. The basic approach is a point-wise frequency domain MISO synthesis technique. The state-space model representation for a LTI MIMO system is:

$$\dot{x}(t) = Ax(t) + Bu(t) \quad (1)$$

$$y(t) = Cx(t) \quad (2)$$

where  $x$  is an  $m$  vector,  $y$  is an  $n$  vector and  $u$  is an  $r$  vector.  $A$ ,  $B$ , and  $C$  are constant matrices of the proper dimension. The plant transfer-function matrix  $P(s)$  is defined as

$$P(s) = C[sI - A]^{-1}B \quad (3)$$

This plant matrix  $P(s) = [p_{ij}(s)]$  is a member of the set  $\mathcal{P} = \{P(s)\}$  of possible plant matrices which are functions of the uncertainty in the plant parameters. The plant matrices are entered and, as appropriate, so are the sensor and actuator matrices. If the equivalent plant matrix  $P_e$  resulting from the three matrices is not square, a weighting matrix  $W$  can be used to form an effective square plant. An interactive dialog provides the user with the ability to iteratively generate  $W$ .

In CACSD practice, one of three explicit methods can be used. One method is based upon the physical modeling of various plants representing the variety of possible plants. The second includes the selection of only a finite set of  $P$  matrices, representing the extreme boundaries of plant pole/zero uncertainty. The third considers the variations in plant coefficients by considering a preselected number of plants to represent the maximum variations. A convex hull is then closed around these plants to derive the minimum number of plant models to represent the variation.

An  $m \times m$  MIMO closed-loop system can be represented by three  $m \times m$  matrices,  $F$ ,  $G$ , and  $P$  as shown in FIG 1. There are  $m^2$  closed-loop system transfer functions  $t_{ij}(s)$  (transmissions) contained within its system transmission matrix or system tracking matrix.  $T_R(s) = \{t_{ij}(s)\}$ , relates the outputs  $y_i(s)$  to the inputs  $r_j(s)$ , that is,  $y_i(s) = t_{ij}(s)r_j(s)$ . In a quantitative problem statement there are tolerance bounds

on each  $t_{ij}(s)$ , giving a set of  $m^2$  acceptable regions  $r_{ij}(s)$  which are to be specified in the design, thus  $t_{ij}(s) \in r_{ij}(s)$  and  $T(s) = \{r_{ij}(s)\}$ . These regions can also be directly given in the frequency domain.

Based upon FIG 1 The following system equations can be written:  $y = Px$ ,  $x = Gu$ ,  $u = v - y$ ,  $v = Fr$ .

In these equations  $G(s)$  is the matrix of compensator transfer functions and is often simplified so that it is diagonal.  $F(s)$  is the matrix of prefilter transfer functions which may also be a diagonal matrix. The combination of these equations yields a 2 degree-of-freedom feedback structure:

$$y = [I + PG]^{-1} PGF r \quad (4)$$

where the system tracking control ratio relating  $r$  to  $y$  is

$$T_R = [I + PG]^{-1} PGF \quad (5)$$

The disturbance model is given as

$$T_D \equiv [I + PG]^{-1} P = \{d_{ij}\} \quad (6)$$

The MIMO design objective is to determine a  $F$  and  $G$  for all plants in  $\mathcal{P}$  such that

- the closed-loop control ratio of Eq. 5 is stable "stability"
- the norm of  $t_{ij}(\omega)$  is bounded;  $\alpha_{ij}(\omega) \leq |t_{ij}(\omega)| \leq b_{ij}(\omega)$  for  $\omega \leq \omega_0$  "closed-loop performance"
- the disturbance Eq. 6 is bounded by  $\alpha_p(\omega) > 0$  "disturbance rejection"

## 2 MISO Equivalents for a MIMO System

A linear mapping from a MIMO system structure results in  $m^2$  MISO equivalent systems, each with two inputs and one output. One input is designated as a "desired" tracking input and the other as a "disturbance" input. To develop this mapping consider the inverse of the plant matrix represented by:

$$P^{-1} = \begin{bmatrix} p_{11}^* & p_{12}^* & \dots & p_{1m}^* \\ p_{21}^* & p_{22}^* & \dots & p_{2m}^* \\ \vdots & \vdots & \ddots & \vdots \\ p_{m1}^* & p_{m2}^* & \dots & p_{mm}^* \end{bmatrix} \quad (7)$$

The  $m^2$  effective plant transfer functions are formed by defining

$$q_{ij} \equiv 1/p_{ij}^* = [\det P / \text{adj} P]_{ij} \quad (8)$$

where  $\det P$  reflects a minimum phase transfer function model. A  $Q$  matrix is defined as:

$$Q \equiv \begin{bmatrix} q_{11} & q_{12} & \dots & q_{1m} \\ q_{21} & q_{22} & \dots & q_{2m} \\ \vdots & \vdots & \ddots & \vdots \\ q_{m1} & q_{m2} & \dots & q_{mm} \end{bmatrix} = \begin{bmatrix} 1/p_{11}^* & 1/p_{12}^* & \dots & 1/p_{1m}^* \\ 1/p_{21}^* & 1/p_{22}^* & \dots & 1/p_{2m}^* \\ \vdots & \vdots & \ddots & \vdots \\ 1/p_{m1}^* & 1/p_{m2}^* & \dots & 1/p_{mm}^* \end{bmatrix} \quad (9)$$

where  $P = [p_{ij}]$ ,  $P^{-1} = [p_{ij}^*] = [1/q_{ij}]$ , and  $Q = [q_{ij}] = [1/p_{ij}^*]$ . The matrix  $P^{-1}$  is partitioned to form

$$P^{-1} = [p_{ij}^*] = [1/q_{ij}] = A + B \quad (10)$$

where  $A = \{\lambda_{ii}\}$  is the diagonal part and  $B = \{b_{ij}\}$  is the off-diagonal component of  $P^{-1}$ . Thus,  $\lambda_{ii} = 1/q_{ii} = p_{ii}^*$ ,  $b_{ii} = 0$ , and  $b_{ij} = 1/q_{ij} = p_{ij}^*$  for  $i \neq j$ . Premultiplying Eq. (5) by  $P^{-1}[I + PG]$  yields, using Eq. (10),

$$T_R = [A + G]^{-1}[GF - BT] \quad (11)$$

Each of the  $m^2$  matrix elements on the right side of Eq. (11) can be interpreted as a MISO problem. This fixed point mapping is described by defining  $Y(T_R)$  as:

$$Y(T_R) \equiv [A + G]^{-1}[GF - BT] \quad (12)$$

where  $G = \{g_{ii}\}$  is assumed to be diagonal and each member of  $T_R$  is from the acceptable set  $\mathcal{T}_R$ . If this mapping has a fixed point, i.e.,  $T_R \in \mathcal{T}_R$  such that  $Y(T_R) = T_R$ , then this  $T_R$  is a solution of Eq. (11).

The control ratios for the desired tracking of the inputs by the corresponding outputs for each feedback loop of Eq. (12) have the form

$$y_{ii} = w_{ii}(v_{ij} + d_{ij}) = y_r + y_{d,i} \quad (13)$$

where  $w_{ii} = q_{ii}/(1 + g_{ii}q_{ii})$  and  $v_{ij} = g_{ij}f_{ij}$ . The interaction between the loops has the form

$$d_{ij} = - \sum_{k \neq i} \left[ \frac{t_{kj}}{q_{ik}} \right] \quad k = 1, 2, \dots, m \quad (14)$$

and appears as a "disturbance" input in each of the feedback loops. As mentioned previously regarding the MIMO weighting matrix, the various diagonal transfer functions can be modified as a function of the off diagonal terms above and to their left. This results in a more complex but better model. The modeling objective is to generate a  $Q$  with diagonal dominance. The disturbance MISO input although minimised is still retained in the model.

Eq. (13) represents the control ratio of the  $i$ th MISO system. The transfer function  $w_{ii}v_{ij}$  relates the "desired"  $i$ th output to the  $j$ th input  $r_j$  and the transfer function  $w_{ii}d_{ij}$  relates the  $i$ th output to the  $j$ th "disturbance" input  $d_{ij}$ . Defining the loop transmission  $L_i$  for each of these loops, an additional design objective can be included that states:

$$|1 + L_i(\omega)| \geq m_i(\omega) \text{ for all } i \text{ and all plants "stability margin performance"}$$

For nonlinear systems a similar ploy is used in that the nonlinear components of the system equations are modeled as disturbances. The QFT controller is designed based upon the linear component and the bounds of the disturbances. Simulation of the controller system is then accomplished using the nonlinear structure explicitly.

### 3 MISO Performance Models

To synthesise [23, 24, 25, 26, 6] a QFT MISO design, the model control ratio can be generated based upon the system's performance specifications in the time domain using the individual MISO models. For a minimum phase continuous structure of FIG 3, the MISO control ratios for tracking and for disturbance rejection are, respectively,

$$T_R(s) \equiv \frac{F(s)G(s)P(s)}{1 + G(s)P(s)} = \frac{F(s)L(s)}{1 + L(s)} (\text{Tracking}) \quad (15)$$

$$T_{L1}(s) \equiv \frac{P(s)}{1 + G(s)P(s)} = \frac{P(s)}{1 + L(s)} (\text{Plant Disturbance}) \quad (16)$$

$$T_{D1}(s) \equiv \frac{1}{1 + G(s)P(s)} = \frac{1}{1 + L(s)} (\text{Measure Disturbance}) \quad (17)$$



where  $L(s) \equiv G(s)P(s)$  is defined as the loop transmission. A fourth transfer function,  $T$ , can also be defined:

$$T(s) \equiv \frac{G(s)P(s)}{1 + G(s)P(s)} = \frac{T_R(s)}{F(s)} \quad (18)$$

which is used to define additional performance requirements.

FIG 2 represents the feedback structure which is generic in nature for continuous and discrete systems. The previous equations can be modified for a discrete feedback block diagram using a multiplicative zero-order hold (ZOH Operator). The ICECAP-PC user's manual contains QFT flowcharts for the continuous and discrete design processes. For sampled-data systems, two QFT approaches exist. The first transfers the sampled-data system into the  $s$ -domain. From this plant with an integrated zero-order-hold structure, the mapping  $z = e^{sT}$  is used to transfer to the frequency domain. The standard QFT techniques are then employed in the frequency domain [21]. The second method uses the QFT frequency domain design techniques that have been highly developed for the  $s$  domain which can also be applied in the  $w$  domain. The condition for this application is that the pertinent  $s$ ,  $z$  and  $w$  plane modeling relationships, based on the Tustin approximation, are valid for low sampling frequencies [19]. An example is now used to illustrate the various phases of the QFT design process.

### 3.1 Design Example

A QFT MISO system is designed using the control system of FIG 3, with  $r(t) = d_2(t) = u_{-1}(t)$  to meet the following example time-domain specifications:

Tracking Specification:  $T_R$

$T_{RU}$ : Second Order System with Peak Overshoot ( $M_p$ ) of 1.3 and settling time ( $t_s$ ) of 1.65

$T_{RL}$ : Second Order System overdamped system with a settling time ( $t_s$ ) of 1.65

From these two tracking specifications the appropriate values of  $a_{ij}(\omega)$  and  $b_{ij}(\omega)$  can be determined to bound  $T_R$ . FIG 3 and 4 represent the generic time and frequency responses for the tracking specifications. For the stability margin bounds,  $|1 + L_i| \geq m_i(\omega)$ .

Disturbance Bound Specification:

$|T_D| \leq \alpha_p(\omega) = |c(t_p)_{max}| = 0.1$  for all  $\omega$

Phase Margin Angle:  $\gamma = 40^\circ$

These specifications can be initially defined in the frequency domain by defining a finite set of magnitude values vs frequency.

The example's second-order model is

$$P_k(s) = (ka)/(s(s+a))$$

$$\text{where } 2 \leq a \leq 10, 1 \leq k \leq 5, k = 1, 2, \dots, J$$

where  $J$  is the number of uncertain plants and the variation of  $a$  and  $k$  describe the region of uncertainty.

Observe that the phase margin and gain margin performance requirements can also be incorporated as the following bound where  $b_{ij} \equiv \delta_R$ :

$$|T(\omega)| \leq \delta_R(\omega) \quad (19)$$

and the tracking bound as

$$|T_{RU}(\omega) - T_{RL}(\omega)| \leq \delta_R(\omega) \quad (20)$$

These tracking specifications are based upon satisfying some or all of the step forcing function figures of merit for underdamped ( $M_p, t_p, t_s, t_r, K_m$ ) and overdamped ( $t_s, t_r, K_m$ ) responses for a simple second-order system.

The upper and lower tracking MISO models are normally second order systems since the designer must meet the given time-domain unit-step performance specifications ( $M_p, t_p, t_s$ , and  $t_r$ ). This design process is recursive. First  $T_{RU}(j\omega)$  and  $T_{RL}(j\omega)$  are determined and then the  $(|T_{RU}(j\omega)| - |T_{RL}(j\omega)|)$  difference must increase with frequency in order to achieve a satisfactory controller. Thus  $T_{RU}(j\omega)$  and  $T_{RL}(j\omega)$  are

modified without changing the desired performance characteristics by modifying  $T_{RL}$  with a negative real pole which is chosen as close to the origin as possible without affecting this original time response.

For minimum-phase plants, only the tolerance on  $|T_R(j\omega_i)|$  need be satisfied for a satisfactory design. For nonminimum-phase plants, tolerances on  $\angle T_R(j\omega_i)$  must also be specified and satisfied in the design process. It is desirable to synthesise the control ratios corresponding to the upper and lower bounds  $T_{RU}$  and  $T_{RL}$ , respectively, so that  $\delta_R(j\omega_i)$  increases as  $\omega_i$  increases above the 0 dB crossing frequency of  $T_{RU}$ . This characteristic of  $\delta_R(j\omega_i)$  simplifies the process of synthesising a loop transmission  $L_o(s) = G(s)P_o(s)$ , where  $P_o(s)$  is the selected nominal plant transfer function.

The Bode plots are generated from the time responses  $y(t)_U$  and  $y(t)_L$  and represent the upper bound  $B_U$  and lower bounds  $B_L$ , respectively, of the specifications in the frequency domain. As mentioned previously, the specifications can be directly defined in the frequency domain, and thus the generation of time-domain specifications is not required.

The templates are constructed next from CAD generated plots. The  $B_R(j\omega_i)$ ,  $B_D(j\omega_i)$ , and  $B_{mo}(j\omega_i)$  bounds and  $B'_h$ ,  $B_h$ , and  $B_L$  contours are then obtained. The optimal loop transmission transfer function  $L_{mo}(w)$  and the prefilter  $F(w)$  are synthesised. The following sections present a summary of the details.

### 3.2 Template Generation

The simplest QFT disturbance rejection model considered is  $T_D(s) = Y(s)/D(s) = \alpha_p$ , a constant (the maximum magnitude of the output based upon a unit step disturbance input).

To characterise the plant model variations, consider the log-magnitude (Lm) of Eq. (15):

$$\text{Lm } T_R = \text{Lm } F + \text{Lm } \left[ \frac{L}{1+L} \right] \quad (21)$$

The change in  $T_R$  due to the uncertainty in  $P$  is

$$\Delta(\text{Lm } T_R) = \text{Lm } T_R - \text{Lm } F = \text{Lm } \left[ \frac{L}{1+L} \right] \quad (22)$$

By the proper design of  $L = L_o$  and  $F$ , this change in  $T_R$  is restricted so that the actual value of  $\text{Lm } T_R$  always lies between  $B_U$  and  $B_L$ . Synthesising  $L_o$  requires the generation of templates. These templates for various values of  $\omega_i$  over a specified frequency range characterise the variation of the plant uncertainty, as described by the  $J$  plant transfer functions. Selecting the frequency range for the templates generally requires the selection of three frequency values, no less than an octave apart, up to approximately the -12 dB value of the  $B_U$  plot. In addition, for a Type 0 plant [18] select  $\omega_x = 0$  and for a Type 1 or higher-order plants select  $\omega_x \neq 0$ . Automatic or interactive generation of these bounds is permitted. A nominal plant is also selected at this time. Graphical and tabular template data can be displayed for evaluation.

### 3.3 High-Frequency Boundary

The specifications on system performance in the frequency domain identify a minimum damping ratio  $\zeta$  for the dominant roots of the closed-loop system which becomes a bound on the value of  $M_m$ . On the Nichols chart, this bound on  $M_m = M_L$  establishes a region which must not be penetrated by the template of  $L(j\omega)$  for all  $\omega$ . The boundary of this region is referred to as the universal high-frequency boundary (UHFB) or the U-contour, because this becomes the dominating constraint on  $L(j\omega)$  as  $\omega$  approaches  $\infty$ . Therefore, the top portion of the M-contour on the Nichols chart, which corresponds to the value of the selected value of  $M_L$ , becomes part of the U-contour.

For a large problem class, the limiting value of the plant transfer function approaches

$$\lim_{\omega \rightarrow \infty} [P(j\omega)] = \frac{K}{\omega^n} \quad (23)$$

where  $\eta$  represents the excess of poles over zeros of  $P(s)$ . The plant template, for this problem class, approaches a vertical line of length equal to

$$\Delta \equiv \lim_{\omega \rightarrow \infty} [\text{Lm}P_{\max} - \text{Lm}P_{\min}] \quad (24)$$

$$= \text{Lm}K_{\max} - \text{Lm}K_{\min} = VdB \quad (25)$$

If the nominal plant is chosen at  $K = K_{\min}$ , then the constraint  $M_L$  gives a boundary which approaches the U-contour of FIG 5.

### 3.4 Tracking, Disturbance and Stability Margin Bounds

The determination of the tracking  $B_R(j\omega_i)$  bounds, the disturbance  $B_D(j\omega_i)$  bounds and the stability margin bounds are required in order to yield the optimal composite bounds  $B_o(j\omega_i)$  on  $L_o(j\omega_i)$ . The solution for  $B_R(j\omega_i)$  requires that the actual  $\Delta T_R(j\omega_i)$  be  $\leq \delta_R(j\omega_i)$ . Thus it is necessary to determine the resulting constraint, or bound,  $B_R(j\omega_i)$  on  $L(j\omega_i)$ . The procedure is to pick a nominal plant  $P_o(s)$  and to derive the bounds, by use of the templates, on the resulting nominal transfer function  $L_o(s) = G(s)P_o(s)$ . In ICECAP-PC, the process is automated. However, the user can observe the bound generation for a specific angle and frequency on the Nichols chart. The user can also move the templates under key/mouse input on the Nichols chart for manual bound generation. The disturbance bounds  $B_D(j\omega_i)$  can be determined in a similar manner [2, 3].

For CAD generation of  $B_R(j\omega)$  and  $B_D(j\omega)$ , the above process is automated given the plant variations with the ZOH, disturbance models, specifications and the selection of a nominal plant  $P_o$ . In particular, the minimum and maximum values of  $\text{Lm}M$  for each plant template at  $j\omega_i$  are found for a given angle ( $0 \geq$  and  $\leq 2\pi$ ) over the range 0 to  $-180$  degrees ( $5^\circ$  increments) such that their max-min difference is  $\leq \delta_R(j\omega_i)$ . If a template for a specific plant becomes tangent to the  $M_L$  contour, the angle iteration stops since entering this region would violate the  $T_R(j\omega_i)$  specifications. The process for generating  $B_R$  is iterated for  $\omega_i$  over the specified frequency bandwidth with values an octave apart. This is the basic technique that was employed in the ICECAP-QFT software in 1985 [10]. A modified approach [19] for finding the bounds is to manipulate the form of  $T_R(\omega) \leq \delta_R(\omega)$  from Eq. 25 into an inequality equation, vary the phase angle  $\theta$  of  $G(j\omega_i)$  and  $\omega_i$  over the same ranges as above along with the variations of the plant, and solve for the max and min values of  $|G(j\omega_i)|$  for each  $\theta$ . Both algorithms essentially solve the same inequality and thus provide an automated process for generating the bounds  $B_R(j\omega_i)$ . The same process can be employed to find the bounds for  $B_D(j\omega_i)$  and any other bounds. Numerical consideration must be given to implementing either of these techniques for sampled-data systems, especially if the computations are done in the  $s$ -plane frequency domain [19].

The composite  $B_o(j\omega_i)$  bound for the loop transmission is composed of those portions of each respective bound  $B_R(j\omega_i)$ ,  $B_D(j\omega_i)$  and stability margin bound that have the largest relative values (a union of the various bounds). To synthesise  $L_o(j\omega_i)$ , it must lie on or just outside the bound  $B_o(j\omega_i)$  for each  $\omega_i$ . This process of generating  $B_o$  is implemented in the QFT Toolbox.

### 3.5 Synthesizing a Nominal Loop Transmission

The loop shaping or synthesising of  $L_o(j\omega)$  is shown by the dashed curve in the Nichols chart of FIG 6. A point such as  $L_o(j2)$  must be on or above  $B_o(j2)$ . Further, in order to satisfy the specifications,  $L_o(j\omega)$  cannot violate the U-contour. In this example a reasonable  $L_o(j\omega)$  closely follows the U-contour up to  $\omega = 40$  and must stay below it. Synthesising an  $L_o(s)$  which satisfies the above specifications involves constructing a rational function (more poles than zeros).  $L_o(j\omega)$  is built up rational term-by-term (loop shaping) to remain on or just outside the U-contour in the Nichols chart. A graphical interface is provided for determining a rational loop transmission with minimum bandwidth. Various interactive and automated loop-shaping processes have been proposed [27, 28]. ICECAP-PC provides a number of interactive and automated techniques for generating  $L_o$ .

### 3.6 Filter Design, Simulation and Reporting

The design of the prefilter requires the positioning of  $L_m [T(j\omega)]$  within the frequency domain specifications. The magnitude of the frequency response must lie within the bounds  $B_U$  and  $B_L$ . By use of straight-line approximations  $F(s)$  is synthesised so that  $L_m F(j\omega)$  lies within the time domain boundaries. ICECAP-PC provides a table and a bode plot for help in defining the MISO filter transfer function. Simulation of the overall control system can now validate the design.

Simulation is accomplished by observing the step response (tracking) in the time domain and the frequency response over the band of interest for all plant variations and disturbance bounds. For nonlinear system simulation, nonlinear equation solvers are used in ICECAP-PC. If the resulting simulation does not validate the design specifications, the user can return to the appropriate phase and modify the design and continue the QFT design process.

Since the QFT process involves considerable computation and data processing, CACSD files are stored for each phase and combined under program control to generate a rough text report of QFT data to which the student or control engineer can add prose in order to generate a report.

## 4 Conclusions

The development of an object-oriented CACSD quantitative feedback design package requires extensive data and symbolic manipulation. The use of computer-aided packages for performing some of these manipulations is straight forward using tables and equations, yet the synthesis of the loop transmission  $L_0$  is still an interactive process.

The generation of an OOD and OOP CACSD package such as ICECAP-PC permits ease of extension and testing for such techniques as QFT. Use of this QFT OO CAD package with graphical interfacing promotes ease of data manipulation and permits evolution of numerous compensator designs. ICECAP-PC is a continuing cooperative development project and available free of charge for MS/DOS environments from the authors.

## References

- [1] *Turbo Pascal Version 6.0: Turbo Vision Guide*. Scotts Valley CA: Borland International, Inc., 1990.
- [2] W. E. Bell, "An object oriented computer aided design (cad) for conventional control system analysis," Master's thesis, Air Force Institute of Technology, December 1992.
- [3] F. L. Trevino, "Object oriented cad for modern control system analysis," Master's thesis, Air Force Institute of Technology, Dec 1992.
- [4] G. Booch, *Object-Oriented Design with Applications*. Redwood City CA: Benjamin/Cummings Pub Co., 1991.
- [5] P. Coad and E. Yourdan, *Object-Oriented Analysis*. Englewood Cliffs NJ: Yourdan Press, 1991.
- [6] I. M. Horowitz and M. Sidi, "Synthesis of feedback systems with large plant ignorance for prescribed time-domain tolerances," *Int. J. Control*, vol. 16, pp. 287-309, 1972.
- [7] R. S. Pressman, *Software Engineering: A Practitioner's Approach*. New York: McGraw-Hill, 2nd edition ed., 1987.
- [8] E. J. Chikofsky, "Software development: Computer-aided software engineering (case)," in *IEEE Computer Society Press Technology Series*, Washington D.C.: IEEE Computer Society Press, 1989.
- [9] A. T. Arnold, "Further development of an interactive control engineering computer analysis package (icecap) for discrete and continuous systems," Master's thesis, Air Force Institute of Technology, December 1986.

- [10] S. H. Cole, "A computer-aided design package for quantitative feedback theory," Master's thesis, Air Force Institute of Technology, December 1986.
- [11] C. J. Gembarowski, "Development of an interactive control engineering computer analysis package (icecap) for discrete and continuous systems," Master's thesis, Air Force Institute of Technology, Dec 1982.
- [12] S. J. Larimer, "An interactive computer-aided design program for digital and continuous control system analysis and synthesis," Master's thesis, Air Force Institute of Technology, Mar 1978.
- [13] G. T. Logan, "Development of an interactive computer aided design program for digital and continuous control system analysis and synthesis," Master's thesis, Air Force Institute of Technology, Mar 1982.
- [14] C. Narathong, "A modern control theory enhancement tool to an interactive control engineering computer analysis package (icecap)," Master's thesis, Air Force Institute of Technology, Dec 1983.
- [15] M. A. Travis, "Interactive computer graphics for system analysis," Master's thesis, Air Force Institute of Technology, Dec 1983.
- [16] R. E. Wilson, "Continued development of an interactive control engineering computer analysis package (icecap) for discrete and continuous systems," Master's thesis, Air Force Institute of Technology, Dec 1983.
- [17] S. K. Mashiko and G. C. Tarczynski, "Development of a computer-aided design package for control system design and analysis for a personal computer (icecap)," Master's thesis, Air Force Institute of Technology, Dec 1985.
- [18] J. J. D'Azso and C. H. Houpis, *Linear Control System Analysis and Design: Conventional and Modern*. New York, New York: McGraw-Hill Book Company, second edition ed., 1981.
- [19] D. C. H. Houpis, "Quantitative feedback theory technique for designing multivariable control systems," Tech. Rep. AFWAL-TR-86-3107, Wright-Patterson Air Force Base, Dayton, Ohio, 1986.
- [20] C. H. Houpis, "Overview of quantitative feedback theory (qft): part i," in *ASME Winter Meeting, Dallas, Texas*, Dec 1990.
- [21] C. H. Houpis and G. B. Lamont, *Digital Control Systems (Theory, Hardware, Software)*. New York, New York: McGraw Hill Book Company, 2nd ed., 1992.
- [22] G. Lamont, "Overview of quantitative feedback theory (qft): part ii," in *ASME Winter Meeting, Dallas, Texas*, Dec 1990.
- [23] J. Coucoules, "Study of the effects of discretising quantitative feedback theory analog control system designs," Master's thesis, Air Force Institute of Technology, Dec 1985.
- [24] I. M. Horowitz, "Improved design technique for uncertain multiple-input, multiple-output feedback systems," *International Journal of Control*, no. 4, pp. 677-699, 1981.
- [25] I. M. Horowitz and O. Yaniv, "Quantitative cascaded multiple-input, multiple-output synthesis by an improved method," *International Journal of Control*, vol. 42, no. 2, pp. 305-311, 1985.
- [26] I. M. Horowitz and Y. K. Liao, "Quantitative feedback design for sampled-data systems." Class Notes. Dept. of Applied Mathematics Weismann Institute of Science, Israel, and Dept. of Electrical Engineering, University of Colorado, Boulder.
- [27] F. N. Bailey and C.-H. Hui, "Loop gain-phase shaping for single-input single-output robust controllers," *IEEE Control Systems Magazine*, vol. 11, pp. 93-101, January 1991.
- [28] D. F. Thompson, *Optimal and Sub-Optimal Loop Shaping in Quantitative Feedback Theory*. PhD thesis, Purdue University, August 1990.

Figure 1: QFT Feedback Structure (MIMO)

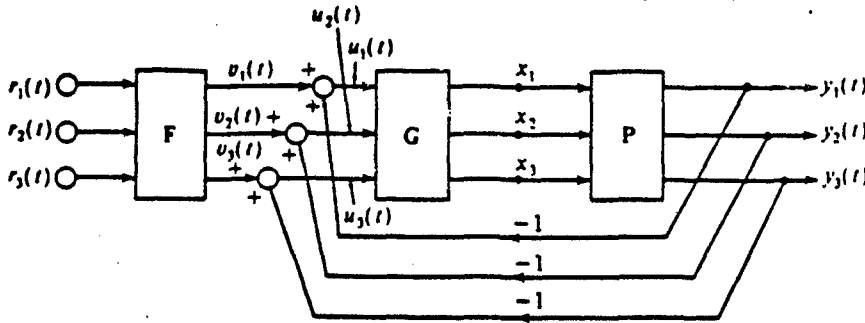


Figure 2: Discrete Feedback Structure

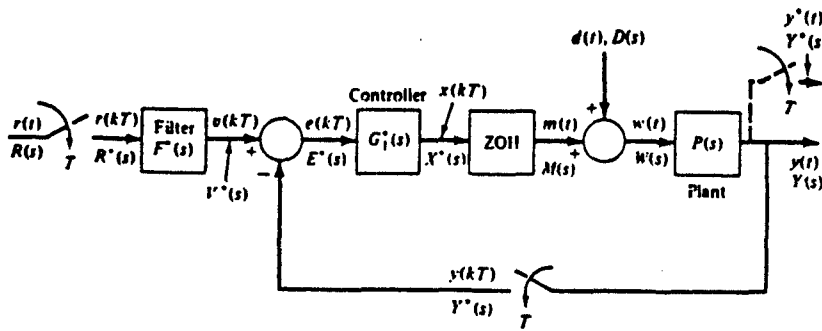


Figure 3: Tracking Time Response

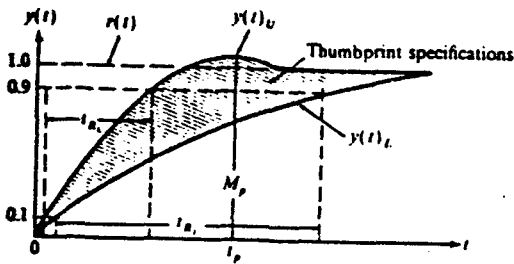


Figure 4: Bode Plot of Tracking Bounds

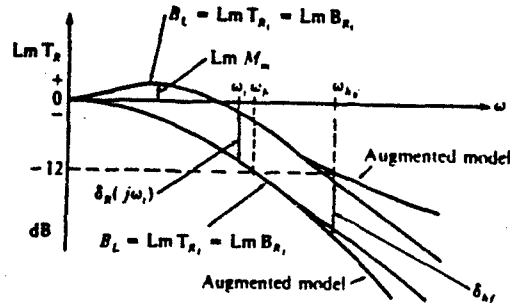


Figure 5: U-Contour

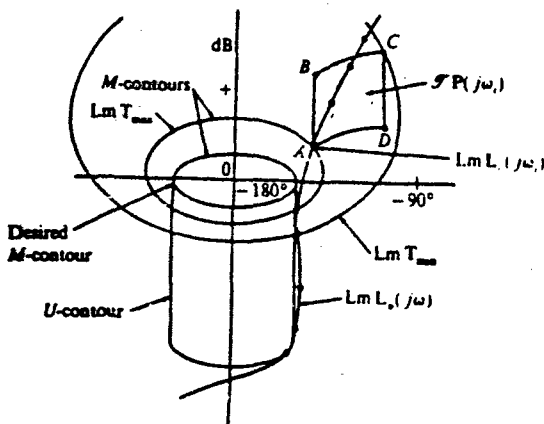


Figure 6: Controller Synthesis (Loop Shaping)

